

---

# **IONIC LIQUIDS: THEORY, PROPERTIES, NEW APPROACHES**

---

Edited by **Alexander Kokorin**

**INTECHWEB.ORG**

## **Ionic Liquids: Theory, Properties, New Approaches**

Edited by Alexander Kokorin

### **Published by InTech**

Janeza Trdine 9, 51000 Rijeka, Croatia

### **Copyright © 2011 InTech**

All chapters are Open Access articles distributed under the Creative Commons Non Commercial Share Alike Attribution 3.0 license, which permits to copy, distribute, transmit, and adapt the work in any medium, so long as the original work is properly cited. After this work has been published by InTech, authors have the right to republish it, in whole or part, in any publication of which they are the author, and to make other personal use of the work. Any republication, referencing or personal use of the work must explicitly identify the original source.

Statements and opinions expressed in the chapters are these of the individual contributors and not necessarily those of the editors or publisher. No responsibility is accepted for the accuracy of information contained in the published articles. The publisher assumes no responsibility for any damage or injury to persons or property arising out of the use of any materials, instructions, methods or ideas contained in the book.

**Publishing Process Manager** Ana Nikolic

**Technical Editor** Teodora Smiljanic

**Cover Designer** Martina Sirotic

**Image Copyright** Ragne Kabanova, 2010. Used under license from Shutterstock.com

First published February, 2011

Printed in India

A free online edition of this book is available at [www.intechopen.com](http://www.intechopen.com)

Additional hard copies can be obtained from [orders@intechweb.org](mailto:orders@intechweb.org)

Ionic Liquids: Theory, Properties, New Approaches, Edited by Alexander Kokorin

p. cm.

ISBN 978-953-307-349-1



**INTECH** OPEN ACCESS  
PUBLISHER

**INTECH** open

**free** online editions of InTech  
Books and Journals can be found at  
**[www.intechopen.com](http://www.intechopen.com)**



---

# Contents

---

## **Preface IX**

### **Part 1 Material Characterizations (Physico-Chemical Properties) 1**

- Chapter 1 **Thermodynamic Properties of Ionic Liquids - Measurements and Predictions - 3**  
Zhi-Cheng Tan, Urs Welz-Biermann, Pei-Fang Yan,  
Qing-Shan Liu and Da-Wei Fang
- Chapter 2 **Thermal Properties of Ionic Liquids and Ionanofluids 37**  
A.P.C. Ribeiro, S. I. C. Vieira, J. M. França,  
C. S. Queirós, E. Langa, M. J. V. Lourenço,  
S. M. S. Murshed and C. A. Nieto de Castro
- Chapter 3 **Physico-Chemical Properties of Task-Specific Ionic Liquids 61**  
Luís C. Branco, Gonçalo V.S.M. Carrera, João Aires-de-Sousa,  
Ignacio Lopez Martin, Raquel Frade and Carlos A.M. Afonso
- Chapter 4 **Physicochemical Properties of Ionic Liquids Containing N-alkylamine-Silver(I) Complex Cations or Protic N-alkylaminium Cations 95**  
Masayasu Iida and Hua Er
- Chapter 5 **Physical Properties of Binary Mixtures of ILs with Water and Ethanol. A Review. 111**  
Oscar Cabeza, Sandra García-Garabal, Luisa Segade,  
Montserrat Domínguez-Pérez, Esther Rilo and Luis M. Varela
- Chapter 6 **Photochromism in Ionic Liquids. Theory and Applications 137**  
Fernando Pina and Luís C. Branco
- Chapter 7 **Dynamic Heterogeneity in Room-Temperature Ionic Liquids 167**  
Daun Jeong, Daekeon Kim, M. Y. Choi,  
Hyung J. Kim and YounJoon Jung

Chapter 8	<b>Peculiarities of Intramolecular Motions in Ionic Liquids</b>	<b>183</b>
	Alexander I. Kokorin	
Chapter 9	<b>Atom Substitution Effects in Ionic Liquids: A Microscopic View by Femtosecond Raman-Induced Kerr Effect Spectroscopy</b>	<b>201</b>
	Hideaki Shirota and Hiroki Fukazawa	
Chapter 10	<b>Interactions between Organic Compounds and Ionic Liquids. Selectivity and Capacity Characteristics of Ionic Liquids</b>	<b>225</b>
	Fabrice Mutelet and Jean-Noël Jaubert	
Chapter 11	<b>Nonaqueous Microemulsions Containing Ionic Liquids – Properties and Applications</b>	<b>245</b>
	Oliver Zech, Agnes Harrar, and Werner Kunz	
Chapter 12	<b>H/D Effects of Water in Room Temperature Ionic Liquids</b>	<b>271</b>
	Hiroshi Abe and Yukihiko Yoshimura	
<b>Part 2</b>	<b>Physical Simulations (Theory and Modelling)</b>	<b>301</b>
Chapter 13	<b>Using Molecular Modelling Tools to Understand the Thermodynamic Behaviour of Ionic Liquids</b>	<b>303</b>
	Lourdes F. Vega, Oriol Vilaseca, Edoardo Valente, Jordi S. Andreu, Fèlix Llorell, and Rosa M. Marcos	
Chapter 14	<b>Self-Consistent Mean-Field Theory for Room-Temperature Ionic Liquids</b>	<b>329</b>
	Yansen Lauw and Frans Leermakers	
Chapter 15	<b>Pseudolattice Theory of Ionic Liquids</b>	<b>347</b>
	L. M. Varela, J. Carrete, M. García, J. R. Rodríguez, L.J. Gallego, M. Turmine and O. Cabeza	
Chapter 16	<b>Ionic Liquids as Designer Solvents for the Synthesis of Metal Nanoparticles</b>	<b>367</b>
	Vipul Bansal and Suresh K. Bhargava	
Chapter 17	<b>Evaluation of Mobility, Diffusion Coefficient and Density of Charge Carriers in Ionic Liquids and Novel Electrolytes Based on a New Model for Dielectric Response</b>	<b>383</b>
	T.M.W.J. Bandara and B.-E. Mellander	
<b>Part 3</b>	<b>Nanomaterials</b>	<b>407</b>
Chapter 18	<b>Aggregates in Ionic Liquids and Applications Thereof</b>	<b>409</b>
	J. D. Marty and N. Lauth de Viguerie	

- Chapter 19 **Supramolecular Structures in the Presence of Ionic Liquids 427**  
Xinghai Shen, Qingde Chen, Jingjing Zhang and Pei Fu
- Chapter 20 **Formation of Complexes in RTIL and Ion Separations 483**  
Konstantin Popov, Andrei Vendilo, Igor Pletnev, Marja Lajunen, Hannu Rönkkömäki and Lauri H.J. Lajunen
- Chapter 21 **The Design of Nanoscale Inorganic Materials with Controlled Size and Morphology by Ionic Liquids 511**  
Elaheh Kowsari
- Chapter 22 **Synthesis of Novel Nanoparticle - Nanocarbon Conjugates Using Plasma in Ionic Liquid 533**  
Toshiro Kaneko and Rikizo Hatakeyama
- Chapter 23 **Nanoparticle Preparation in Room-Temperature Ionic Liquid under Vacuum Condition 549**  
Tetsuya Tsuda, Akihito Imanishi, Tsukasa Torimoto and Susumu Kuwabata
- Part 4 Academic Technologies (New Technological Approaches) 565**
- Chapter 24 **Perspectives of Ionic Liquids Applications for Clean Oilfield Technologies 567**  
Rafael Martínez-Palou and Patricia Flores Sánchez
- Chapter 25 **Ionic Liquid Based Electrolytes for Dye-Sensitized Solar Cells 631**  
Chuan-Pei Lee, Po-Yen Chen and Kuo-Chuan Ho
- Chapter 26 **Quaternary Ammonium and Phosphonium Ionic Liquids in Chemical and Environmental Engineering 657**  
Anja Stojanovic, Cornelia Morgenbesser, Daniel Kogelnig, Regina Krachler and Bernhard K. Keppler
- Chapter 27 **Ionic Liquids within Microfluidic Devices 681**  
Marina Cvjetko and Polona Žnidaršič-Plazl
- Chapter 28 **Ionic Liquids: Methods of Degradation and Recovery 701**  
E.M. Siedlecka, M. Czerwicka, J. Neumann, P. Stepnowski, J.F. Fernández and J. Thöming
- Chapter 29 **Progress in Paramagnetic Ionic Liquids 723**  
Yukihiro Yoshida and Gunzi Saito



---

## Preface

---

During the last 30 years, the Ionic Liquids (ILs) became one of the most interesting and rapidly developing areas of modern physical chemistry, technologies and engineering, including constructing new devices for various applications. Further development of this field depends on R&D in ILs chemistry and revealing new perspective practical approaches. Because of the ILs importance and advantages, this book reviews in detail and compiles information on some important physico-chemical properties of ILs and new practical possibilities in 29 chapters gathered in 4 parts. This is the first book of a series of forthcoming publications on this field by this publisher. This volume covers some aspects of synthesis, isolation, production, properties and applications, modification, the analysis methods and modeling to reveal the structures and properties of some room temperature ILs, as well as their new possible applications. This book will be of help to many scientists: chemists, physicists, biologists, technologists and other experts in a variety of disciplines, both academic and industrial, as well as to students and PhD students. It may be also suitable for teaching, and help promote the progress in ILs development.

**Prof. Dr. Alexander Kokorin**  
N.Semenov Institute of Chemical Physics RAS,  
Moscow  
Russian Federation





## **Part 1**

### **Material Characterizations (Physico-Chemical Properties)**



# Thermodynamic Properties of Ionic Liquids - Measurements and Predictions -

Zhi-Cheng Tan, Urs Welz-Biermann, Pei-Fang Yan,  
Qing-Shan Liu and Da-Wei Fang

*China Ionic Liquid Laboratory and Thermochemistry Laboratory  
Dalian Institute of Chemical Physics, Chinese Academy of Sciences, Dalian 116023,  
China*

## 1. Introduction

Research of ionic liquids (ILs) is one of the most rapidly growing fields in the past years, focusing on the ultimate aim of large scale industrial applications. Due to their unique tunable properties, such as negligible vapor pressure at room temperature, stable liquid phase over a wide temperature range and thermal stability at high temperatures, ionic liquids are creating an continuously growing interest to use them in synthesis and catalysis as well as extraction processes for the reduction of the amount of volatile organic solvents (VOSs) used in industry.

For the general understanding of these materials it is of importance to develop characterization techniques to determine their thermodynamic and physicochemical properties as well as predict properties of unknown Ionic Liquids to optimize their performance and to increase their potential future application areas.

Our laboratory in cooperation with several national and international academic and industrial partners is contributing to these efforts by the establishment of various dedicated characterization techniques (like activity coefficient measurements using GC technology) as well as determination of thermodynamic and physicochemical properties from a continuously growing portfolio of (functionalized) ionic liquids. Based on the received property data we published several papers related to the adjacent prediction of properties (like molar enthalpy of vaporization, parachor, interstice volume, interstice fractions, thermal expansion coefficient, standard entropy etc.). Additionally our laboratory created and launched a new most comprehensive Ionic Liquid property data base--delphi-IL.([www.delphil.net](http://www.delphil.net)). This fast growing collections of IL data will support researchers in the field to find and evaluate potential materials for their applications and hence decrease the time for new developments.

In this chapter we introduce the following techniques, summarize recent published results completed by our own investigations:

1. Activity coefficient measurements using GC technique,
2. Thermodynamic properties determined by adiabatic calorimetry and thermal analysis (DSC, TG-DTG).
3. Estimation and prediction of physicochemical properties of ILs based on experimental density and surface tension data.

### 1.1 Activity coefficient measurements using GC technique

For the use of Ionic Liquids as solvents it is very important to know about their interaction with different solutes. Activity coefficients at infinite dilution of a solute  $i$  ( $\gamma_i^\infty$ ) can be used to quantify the volatility of the solute as well as to provide information on the intermolecular energy between solvent and solute. Values of  $\gamma_i^\infty$  are also important for evaluating the potential uses of ILs in liquid-liquid extraction and extractive distillation. Since ILs have a negligible vapor pressure, the gas-liquid chromatography (GLC) using the ionic liquid as stationary phase, is the most suitable method for measuring activity coefficients at infinite dilution  $\gamma_i^\infty$ .

A large number of studies on the activity coefficients at infinite dilution  $\gamma_i^\infty$  of organic solvents in different ILs have been reported in the past decade. In this section, we first introduce the experimental techniques used to measure the activity coefficients at infinite dilution,  $\gamma_i^\infty$ ; then describe our results of  $\gamma_i^\infty$  and compare them with literature data. Most results of these studies have been published since 2000. Finally, we discuss the separation problems of hexane/benzene and cyclohexane/benzene by use of ILs based on the results of  $\gamma_i^\infty$ .

### 1.2 Thermodynamic properties determined by adiabatic calorimetry and thermal analysis techniques (DSC and TG-DTG)

Thermodynamic properties of ionic liquids, such as heat capacity  $C_{p,m}$ , glass transition temperature  $T_g$ , melting temperature  $T_m$ , thermal decomposition temperature  $T_d$ , enthalpy and entropy of phase transitions are important data for the basic understanding of these materials and their application in academia and industry. These thermodynamic properties can be determined using adiabatic calorimetry and thermal analysis techniques (DSC, TG-DTG).

Our laboratory in cooperation with the thermochemistry laboratory at the Dalian Institute of Chemical Physics has a long history in the development and set up of specialized adiabatic calorimetric apparatus and the determination of the above listed thermodynamic properties of Ionic Liquids.

In this section, we introduce the required experimental techniques, the specific adiabatic calorimeter established in our laboratory, and describe our recently published results of thermodynamic property measurements for some typical ionic liquids.

### 1.3 Estimation and prediction of physicochemical properties of ILs based on experimental density and surface tension data.

More and more publications have reported the physicochemical properties of some ILs, but the overall amount of property data measured by experimental methods are still not fulfilling the requirements for their broad application, especially, due to the lack of data of IL homologues which would be helpful to improve the selection of more appropriate test candidates for different applications. A recently developed technical approach- based on the experimental data of densities and surface tensions of small number of ionic liquids - enables estimation and prediction of density, surface tension, molecular volume, molar volume, parachor, interstice volume, interstice fractions, thermal expansion coefficient, standard entropy, lattice energy and molar enthalpy of vaporization of their homologues.

In this section, we introduce the theoretical models for the prediction of additional physicochemical property data and describe our recently published results for three imidazolium-based ionic liquid homologues,  $[C_n\text{mim}][\text{EtSO}_4]$ ,  $[C_n\text{mim}][\text{OcSO}_4]$  and  $[C_n\text{mim}][\text{NTf}_2]$  ( $n=1-6$ ).

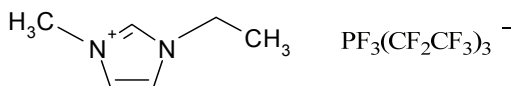
## 2. Activity coefficient measurements using GC technique

### 2.1 Introduction

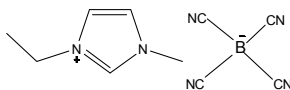
Ionic Liquids (ILs) are often called designer solvents or task specific ionic liquids (TSILs) because of their possible tailoring to fulfil technological demands of various applications. IL properties can be significantly adjusted by tailoring their anion and/or cation structures.<sup>1</sup> Due to their unique properties such as nonflammability, wide liquid range, stability at high temperatures, and negligible vapor pressure, ionic liquids created interest to use them in separation process as potential green replacement for conventional volatile, flammable and toxic organic solvents. Therefore it is very important to know their interaction with different solutes. Activity coefficients at infinite dilution of a solute  $i$  ( $\gamma_i^\infty$ ) can be used to quantify the volatility of the solute as well as to provide information on the intermolecular energy between solvent and solute.<sup>2,3</sup>

Since ILs have a negligible vapor pressure, the gas-liquid chromatography (GLC) using the ionic liquid as stationary phase is the most suitable method for measuring activity coefficients at infinite dilution  $\gamma_i^\infty$ . Experimental  $\gamma_i^\infty$  data provide useful information about the interaction between the solvent (IL) and solute. Disubstituted imidazolium based ionic liquids are a class of very promising extraction and separation reagents, being reported in various publications. Most of this research work is based on anions like  $[\text{BF}_4]^-$ ,<sup>4-8</sup>  $[\text{PF}_6]^-$ ,<sup>9</sup>  $[\text{N}(\text{CF}_3\text{SO}_2)_2]^-$ ,<sup>10-14</sup>  $[\text{Br}]^-$ ,<sup>15</sup>  $[\text{Cl}]^-$ ,<sup>16</sup>  $[\text{CF}_3\text{SO}_3]^-$ ,<sup>17-19</sup>  $[\text{SCN}]^-$ ,<sup>20,21</sup>  $[\text{MDEGSO}_4]^-$ ,<sup>22</sup>  $[\text{FeCl}_4]^-$ ,<sup>23</sup> and  $[\text{CoBr}_4]^-$ .<sup>24</sup> In separation processes property of the extractant is very important, namely its selectivity  $S_{ij}^\infty$  which can be directly calculated from activity coefficients at infinite dilution for different separation processes. Until now  $[\text{BMIM}][\text{SCN}]$  and  $[\text{EMIM}][\text{SCN}]$  showed much higher  $S_{ij}^\infty$  ( $i$  = hexane,  $j$  = benzene) values compared to other ILs due to their small anion  $[\text{SCN}]^-$ .

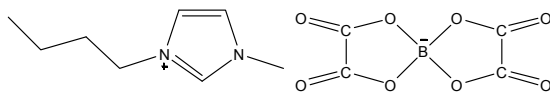
In order to expand our knowledge about the nature of ILs, the influence of the anion structure on the thermodynamic properties of the disubstituted imidazolium based ionic liquid with  $[\text{FAP}]^-$ ,<sup>25</sup>  $[\text{TCB}]^-$ ,<sup>26</sup> and bis(oxalato)borate  $[\text{BOB}]^-$ ,<sup>27</sup> Anions were studied in our work. Structures of investigated ILs are presented below:



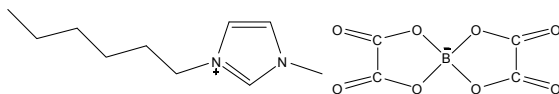
1-Ethyl-3-methylimidazolium tris(pentafluoroethyl)trifluorophosphate  $[\text{EMIM}][\text{FAP}]$



1-Ethyl-3-methylimidazolium tetracyanoborate  $[\text{EMIM}][\text{TCB}]$



1-Butyl-3-methylimidazolium bis(oxalato)borate [BMIM][BOB]



1-Hexyl-3-methyl-imidazolium bis(oxalato)borate [HMIM][BOB]

## 2.2 General techniques

### 2.2.1 Pre-processing

The purity of ILs was checked by  $^1\text{H}$  NMR,  $^{13}\text{C}$  NMR and  $^{11}\text{B}$  NMR spectroscopy. The water content was determined by Karl-Fischer titration, and were found to be less than 100 ppm. Before use, the support material and ILs were subjected to vacuum treatment with heating to remove traces of adsorbed moisture.

### 2.2.2 Experimental procedure

The GC column used in the experiment were constructed of stainless steel with length of 2 m and an inner diameter of 2 mm. Dichloromethane or methanol can be used as solvent to coat ILs onto the solid support 101 AW (80/100 mesh) by a rotary evaporator to ensure the homogeneous spread of the IL onto the surface of support. The solid support was weighed before and after the coating process. To avoid possible residual adsorption effects of the solutes on the solid support, the amount of ionic liquids ([EMIM][FAP], [EMIM][TCB], [BMIM][BOB] and [HMIM][BOB]) were all about 30.00 mass percent of the support material. Experiments were performed on a GC-7900 gas chromatograph apparatus, supplied by Shanghai Techcomp Limited Company in China equipped with a heated on-column injector and a flame ionization detector. The carrier gas flow rate was determined using a GL-102B Digital bubble/liquid flow meter with an uncertainty of  $\pm 0.1 \text{ cm}^3 \text{ min}^{-1}$ , which was placed at the outlet of the column. The carrier gas flow rate was adjusted to obtain adequate retention times. The pressure drop ( $P_i - P_o$ ) varied between (35 and 150) kPa depending on the flow rate of the carrier gas. The pressure drop was measured by a pressure transducer implemented in the GC with an uncertainty of  $\pm 0.1 \text{ kPa}$ . The atmospheric pressure was measured using a membrane manometer with an uncertainty of  $\pm 0.2 \text{ kPa}$ . Solute injection volumes ranged from 0.1  $\mu\text{l}$  to 0.3  $\mu\text{l}$  and were considered to be at infinite dilution on the column. The injector and detector temperature were kept at 473K and 523K respectively during all experiments. The temperature of the oven was measured with a Pt100 probe and controlled to within 0.1 K. The GLC technique and equipment was tested for the system hexane in hexadecane as stationary phase at 298 K, and the results were within 2.0 % of the literature values<sup>28</sup>.

The uncertainty of  $\gamma_i^\infty$  values may be obtained from the law of propagation of errors. The following measured parameters exhibit uncertainties which must be taken into account in the error calculations with their corresponding standard deviations: the adjusted retention time  $t_{R'}$ ,  $\pm 0.01 \text{ min}$ ; the flow rate of the carrier gas,  $\pm 0.1 \text{ cm}^3 \cdot \text{min}^{-1}$ ; mass of the stationary phase,  $\pm 0.05\%$ ; the inlet pressure,  $\pm 0.1 \text{ KPa}$ , outlet pressure,  $\pm 0.2 \text{ KPa}$ ; the temperature of the oven,  $\pm 0.1 \text{ K}$ . The main source of uncertainty in the calculation of the net retention

volume is the determination of the mass of the stationary phase. The estimated uncertainty in determining the net retention volume  $V_N$  is about  $\pm 2\%$ . Taking into account that thermodynamic parameters are also subject to an error, the resulting uncertainty in the  $\gamma_i^\infty$  values is about  $\pm 4\%$ .

### 2.3 Theoretical basis

The equation developed by Everett<sup>29</sup> and Cruickshank et al<sup>30</sup> was used in this work to calculate the  $\gamma_i^\infty$  of solutes in the ionic liquid

$$\ln \gamma_{13}^\infty = \ln \left( \frac{n_3 RT}{V_N P_1^*} \right) - \frac{P_1^* B_{11} - V_1^*}{RT} + \frac{P_o J (2B_{12} - V_1^\infty)}{RT} \quad (1)$$

where  $V_N$  is the standardized retention volume of the solute,  $P_o$  is the outlet pressure,  $n_3$  is the number of moles of the ionic liquid on the column packing,  $T$  is the column temperature,  $P_1^*$  is the saturated vapour pressure of the solute at temperature  $T$ ,  $B_{11}$  is the second virial coefficient of the pure solute,  $V_1^*$  is the molar volume of the solute,  $V_1^\infty$  is the partial molar volume of the solute at infinite dilution in the solvent (assumed as the same as  $V_1^*$ ) and  $B_{12}$  (where 2 refers to the carrier gas, nitrogen) is the cross second virial coefficient of the solute and the carrier gas. The values of  $B_{11}$  and  $B_{12}$  were calculated using the McGlashan and Potter equation<sup>31</sup>

$$\frac{B}{V_c} = 0.430 - 0.886 \left( \frac{T_c}{T} \right) - 0.694 \left( \frac{T_c}{T} \right)^2 - 0.0375(n-1) \left( \frac{T_c}{T} \right)^{4.5} \quad (2)$$

where  $n$  refers to the number of carbon atoms of the solute. Using the Hudson and McCoubrey combining rules,<sup>32,33</sup>  $V_{12}^c$  and  $T_{12}^c$  were calculated from the critical properties of the pure component.

The net retention volume  $V_N$  was calculated with the following usual relationship

$$V_N = J \cdot U_o \cdot (t_r - t_g) \cdot \frac{T_{col}}{T_f} \left( 1 - \frac{P_{ow}}{P_o} \right) \quad (3)$$

where  $t_r$  is the retention time,  $t_g$  is the dead time,  $U_o$  is the flow rate, measured by digital bubble/liquid flow meter,  $T_{col}$  is the column temperature,  $T_f$  is flowmeter temperature,  $P_{ow}$  is saturation vapor pressure of water at  $T_f$  and  $P_o$  is the pressure at the column outlet.

The factor  $J$  appearing in eqs 1 and 3 corrects for the influence of the pressure drop along the column and is given by following equation<sup>34</sup>

$$J = \frac{3}{2} \cdot \frac{(P_i/P_o)^2 - 1}{(P_i/P_o)^3 - 1} \quad (4)$$

where  $P_i$  and  $P_o$  are the inlet and the outlet pressure of the GC column, respectively.

The vapor pressure values were calculated using the Antoine equation and constants were taken from the literature.<sup>35</sup> Critical data and ionization energies used in the calculation of  $T_{12}^c$ , were obtained from literature.<sup>35-37</sup>

### 2.4 Results and discussion

The values of  $\gamma_i^\infty$  of different solutes (alkanes, cycloalkanes, 1-alkenes, 1-alkynes, benzene, alkylbenzenes, and alcohols) in the ionic liquids [EMIM][FAP], [EMIM][TCB], [BMIM][BOB] and [HMIM][BOB] obtained at several temperatures were listed in table 1-4.

The activity coefficients of the linear alkanes, 1-alkenes, 1-alkynes, alkylbenzenes, and alkanols increase with increasing chain length. This is also a typical behaviour for other measured ionic liquids based on methylimidazolium cation. High values of  $\gamma_i^\infty$  signify very small interactions between solute and solvent. The values of  $\gamma_i^\infty$  for alkenes and cycloalkanes are similar for the same carbon number. The cyclic structure of cycloalkanes reduces the value of  $\gamma_i^\infty$  in comparison to the corresponding linear alkane. The values of  $\gamma_i^\infty$  for alkenes are lower than those for alkanes for the same carbon number. This is caused by interaction of double bonding in alkenes with the polar ionic liquid. Alkynes, aromatic hydrocarbons and alkanols have smaller values of  $\gamma_i^\infty$  than alkanes, cycloalkanes, and alkenes which are revealed by stronger interactions between solvent and solute. This is the result of interactions between the triple bond in alkynes, six  $\pi$ -delocalized electrons in aromatics and polar group in alkanols with the polar cation and anion of the ionic liquid. For alkanes, 1-alkenes, 1-alkynes and alkanols values of  $\gamma_i^\infty$  decrease with increasing temperature. For the rest of the investigated solutes, benzene and alkylbenzenes values of  $\gamma_i^\infty$  change a little with increasing temperature.

By comparing Table 3 and 4, we can see that lengthening the alkane chain on the imidazolium (for the ILs with the [BOB] anion) causes a decrease in  $\gamma_i^\infty$  of the same solute (e.g. heptane, octane, benzene, 1-hexene) in the IL at the same temperature. This means that the imidazolium-based ILs with long alkyl chain reveals stronger interactions with solutes. This is also a typical behaviour for other measured ionic liquids based on methylimidazolium cations. Table 5 lists the  $\gamma_i^\infty$  for some solutes in 1-hexyl-3-methylimidazolium bis(trifluoromethanesulfonato)amide [HMIM][NTf<sub>2</sub>],<sup>10</sup> 1-butyl-3-methylimidazolium bis(trifluoromethanesulfonato)amide [BMIM][NTf<sub>2</sub>],<sup>38</sup> 1-hexyl-3-methylimidazolium thiocyanate [HMIM][SCN],<sup>39</sup> 1-butyl-3-methylimidazolium thiocyanate [BMIM][SCN],<sup>20</sup> 1-ethyl-3-methylimidazolium thiocyanate [EMIM][SCN],<sup>21</sup> 1-octyl-3-methylimidazolium tetrafluoroborate [OMIM][BF<sub>4</sub>],<sup>7</sup> 1-butyl-3-methylimidazolium tetrafluoroborate [BMIM][BF<sub>4</sub>],<sup>40</sup> 1-ethyl-3-methylimidazolium tetrafluoroborate [EMIM][BF<sub>4</sub>],<sup>4</sup> 1-hexyl-3-methylimidazolium trifluoromethanesulfonate [HMIM][CF<sub>3</sub>SO<sub>3</sub>],<sup>17</sup> and 1-butyl-3-methylimidazolium trifluoromethanesulfonate [BMIM][CF<sub>3</sub>SO<sub>3</sub>]<sup>19,41</sup> at  $T=298.15$  K.

These data listed in Table 5 demonstrate a significant influence of the alkyl chain of ionic liquids based on methylimidazolium cation on the  $\gamma_i^\infty$  values. From table 5 we can also see that the activity coefficients and intermolecular interactions of different solutes in ILs are very much dependent on the chemical structure of the cation and anion.

The selectivity at infinite dilution for the ionic liquid which indicated suitability of a solvent for separating mixtures of components  $i$  and  $j$  by extraction was given by<sup>28</sup>

$$S_{ij}^\infty = \frac{\gamma_{i3}^\infty}{\gamma_{j3}^\infty} \quad (6)$$

Table 5 also summarizes the selectivities for the separation of hexane/benzene, cyclohexane/benzene, and hexane/hexene mixtures at  $T=298.15$  K, which were calculated from the  $\gamma_i^\infty$  values for the ILs under study and collected from literature. As presented in table 5, the trend in  $S_{ij}^\infty$  values depends on the number of carbon atoms in the alkyl groups attached to the cation, most of the ILs with shorter alkyl chain have higher  $S_{ij}^\infty$  values while those with longer alkyl chain have smaller  $S_{ij}^\infty$  values, e.g., [OMIM][BF<sub>4</sub>], 9 carbon atoms,  $S_{ij}^\infty$  ( $i$  = hexane,  $j$  = benzene) = 10.4,  $S_{ij}^\infty$  ( $i$  = cyclohexane,  $j$  = benzene) = 6.8; [BMIM][BF<sub>4</sub>], 5 carbon atoms,  $S_{ij}^\infty$  ( $i$  = hexane,  $j$  = benzene) = 37.3,  $S_{ij}^\infty$  ( $i$  = cyclohexane,  $j$  = benzene) = 19.7;



[EMIM][BF<sub>4</sub>], 3 carbon atoms,  $S_{ij}^{\infty}$  ( $i$  = hexane,  $j$  = benzene) = 49.5,  $S_{ij}^{\infty}$  ( $i$  = cyclohexane,  $j$  = benzene) = 38.9. An anion with smaller carbon atoms (or no carbon atoms) tends to have a higher selectivity value, e.g., [BMIM][SCN], [HMIM][SCN] and [EMIM][SCN] because of the small anion [SCN], all of them have much higher  $S_{ij}^{\infty}$  ( $i$  = hexane,  $j$  = benzene) values than the other ILs listed in Table 5. The above trends indicate that the size of the alkyl chain on both the cation and anion plays a important role in selectivity values.

## 2.5 Conclusions

Activity coefficients at infinite dilution for various solutes (alkanes, cycloalkanes, 1-alkenes, 1-alkynes, benzene, alkylbenzenes, and alcohols) in the ionic liquids [EMIM][FAP], [EMIM][TCB], [BMIM][BOB] and [HMIM][BOB] were measured at different temperatures

Solute( $i$ )	313 K	323 K	333 K	343 K	353 K	364 K
Pentane	4.44(313.1)	3.59(322.9)	2.87(333.6)	2.36(343.5)	2.01(353.5)	
Hexane	10.14(313.1)	8.15(322.9)	6.47(333.6)	5.24(343.5)	4.38(353.5)	
Heptane	19.72(313.1)	16.27(322.9)	13.00(333.6)	10.61(343.5)	8.75(353.5)	
Octane	33.30(313.1)	28.33(322.9)	23.35(333.6)	19.47(343.5)	16.14(353.5)	
Nonane	49.35(313.1)	42.85(322.9)	36.04(333.6)	31.80(343.5)	27.02(353.5)	
Cyclohexane	9.47(313.1)	7.98(322.9)	6.58(333.6)	5.52(343.5)	4.71(353.5)	
Methyl cyclohexane	13.71(313.1)	11.75(322.9)	9.91(333.6)	8.40(343.5)	7.21(353.5)	
1-Hexene	6.66(312.8)	5.49(323.6)	4.64(333.5)	3.93(343.6)	3.34(353.6)	
1-Octene	18.84(312.8)	16.39(323.6)	14.76(333.5)	12.89(343.6)	11.11(353.6)	
1-Decene	37.62(312.8)	34.74(323.6)	32.40(333.5)	29.46(343.6)	26.71(353.6)	
1-Pentyne	2.46(313.6)	2.26(322.7)	1.99(333.5)	1.82(343.4)	1.67(353.3)	
1-Hexyne	4.18(313.6)	3.87(322.7)	3.52(333.5)	3.26(343.4)	2.94(353.3)	
1-Heptyne	6.46(313.6)	6.11(322.7)	5.67(333.5)	5.29(343.4)	4.82(353.3)	
1-Octyne	9.53(313.6)	9.12(322.7)	8.65(333.5)	8.08(343.4)	7.52(353.3)	
Benzene <sup>b</sup>	1.06(313.1)	1.09(322.9)	1.15(333.1)	1.11(343.5)	1.10(353.3)	1.09(363.9)
Toluene <sup>b</sup>	1.54(313.1)	1.59(322.9)	1.69(333.1)	1.66(343.5)	1.66(353.3)	1.66(363.9)
Ethylbenzene <sup>b</sup>	2.40(313.1)	2.48(322.9)	2.63(333.1)	2.55(343.5)	2.54(353.3)	2.51(363.9)
o-Xylene <sup>b</sup>	2.14(313.1)	2.20(322.9)	2.35(333.1)	2.30(343.5)	2.30(353.3)	2.29(363.9)
m-Xylene <sup>b</sup>	2.29(313.1)	2.37(322.9)	2.53(333.1)	2.47(343.5)	2.47(353.3)	2.46(363.9)
p-Xylene <sup>b</sup>	2.37(313.1)	2.44(322.9)	2.60(333.1)	2.55(343.5)	2.54(353.3)	2.53(363.9)
Methanol	2.65(313.6)	2.29(322.7)	2.02(333.5)	1.73(343.4)	1.51(353.3)	
Ethanol	3.29(313.6)	2.86(322.7)	2.44(333.5)	2.17(343.4)	1.88(353.3)	
1-Propanol	4.46(313.6)	3.87(322.7)	3.35(333.5)	2.92(343.4)	2.59(353.3)	

<sup>a</sup> Measured experimental temperatures are given in parentheses. <sup>b</sup> Values are measured in the temperature interval 313 to 364 K.

Table 1. Experimental activity coefficients at infinite dilution,  $\gamma_i^{\infty}$  for various solutes in the ionic liquid 1-Ethyl-3-methylimidazolium tris(pentafluoroethyl)trifluorophosphate at temperatures 313 to 364 K<sup>a</sup>

using GLC method. This result shows the influence of the cation's alkyl chain length on the  $\gamma_i^\infty$  and  $S_{ij}^\infty$  values. For the separation of aliphatic hydrocarbons from aromatic hydrocarbons, the ionic liquids tested in our work show moderate value of selectivity. The results summarized in Table 5 demonstrate a significant influence of the structure of anion and cation in the ionic liquids on the  $\gamma_i^\infty$  values and selectivity.

Solute( <i>i</i> )	303 K	313 K	323 K	333 K	343 K
Pentane	10.26 (302.8)	8.21 (313.4)	7.05 (323.1)	5.92 (332.8)	4.88 (343.4)
Hexane	20.97 (302.8)	17.40 (313.4)	15.07 (323.1)	12.51 (332.8)	10.29 (343.4)
Heptane	37.62 (302.8)	32.19 (313.4)	28.13 (323.1)	23.82 (332.8)	19.85 (343.4)
Octane	58.88 (302.8)	52.45 (313.4)	46.72 (323.1)	40.73 (332.8)	34.94 (343.4)
Nonane	85.01 (302.8)	78.07 (313.4)	70.83 (323.1)	63.53 (332.8)	55.31 (343.4)
Cyclohexane	13.82 (302.8)	12.44 (313.4)	11.20 (323.1)	9.85 (332.8)	8.64 (343.4)
Methyl cyclohexane	20.72 (302.8)	18.86 (313.4)	16.94 (323.1)	15.15 (332.8)	13.29 (343.4)
1-Hexene	11.28 (303.5)	9.74 (313.2)	8.39 (323.3)	7.35 (333.1)	6.27 (343.1)
1-Octene	30.05 (303.5)	26.84 (313.2)	24.00 (323.3)	21.53 (333.1)	18.97 (343.1)
1-Decene	60.51 (303.5)	55.95 (313.2)	51.53 (323.3)	47.75 (333.1)	43.43 (343.1)
1-Pentyne	2.72 (303.5)	2.61 (313.3)	2.50 (323.3)	2.38 (333.1)	2.29 (343.1)
1-Hexyne	4.18 (303.5)	4.04 (313.3)	3.92 (323.3)	3.77 (333.1)	3.58 (343.1)
1-Heptyne	6.33 (303.5)	6.15 (313.3)	5.97 (323.3)	5.78 (333.1)	5.59 (342.8)
1-Octyne	9.64 (303.5)	9.42 (313.3)	9.11 (323.3)	8.84 (333.1)	8.58 (342.8)
Benzene	1.31 (303.6)	1.31 (313.3)	1.34 (323.2)	1.31 (333.3)	1.30 (343.2)
Toluene	1.90 (303.6)	1.92 (313.2)	1.98 (323.1)	1.94 (333.2)	1.92 (343.3)
Ethylbenzene	3.00 (303.6)	3.00 (313.2)	3.05 (323.1)	2.97 (333.2)	2.92 (343.3)
o-Xylene	2.49 (303.6)	2.53 (313.3)	2.58 (323.2)	2.56 (333.2)	2.54 (343.1)
m-Xylene	2.92 (303.6)	2.99 (313.2)	3.03 (323.2)	3.01 (333.1)	2.99 (343.1)
p-Xylene	2.78 (303.7)	2.85 (313.2)	2.87 (323.2)	2.85 (333.3)	2.84 (343.2)
Methanol	1.13 (303.5)	1.05 (313.3)	0.97 (323.3)	0.91 (333.1)	0.85 (343.1)
Ethanol	1.64 (303.5)	1.50 (313.3)	1.37 (323.3)	1.27 (333.1)	1.16 (343.1)
1-Propanol	2.12 (303.5)	1.92 (313.3)	1.74 (323.3)	1.60 (333.1)	1.46 (343.1)

<sup>a</sup> Measured experimental temperatures are given in parentheses.

Table 2. Experimental activity coefficients at infinite dilution  $\gamma_i^\infty$  for various solutes in the ionic liquid [EMIM][TCB] at different temperatures<sup>a</sup>.

Solute( <i>i</i> )	308 K	318 K	328 K	338 K	348 K
Pentane	9.11(307.8)	6.63(317.6)	5.12(328.2)	4.02(338.5)	3.23(347.7)
Hexane	27.60 (307.8)	19.18(317.7)	12.98(328.3)	9.61(338.5)	7.55(347.7)
Heptane	57.79 (307.9)	41.52 (317.6)	30.05 (328.3)	21.99 (338.5)	17.08 (347.7)
Octane	116.45(307.9)	85.74 (317.6)	62.78(328.2)	45.70(338.5)	35.48(347.7)
Nonane	194.07(307.9)	151.69 (317.6)	116.00(328.3)	87.18(338.5)	67.62(347.7)
Cyclohexane	25.44(307.8)	18.52(317.8)	13.93(328.3)	10.63(338.6)	8.52(347.6)
Methyl cyclohexane	42.37 (307.9)	31.05(317.7)	23.24(328.3)	17.76(338.6)	14.05(347.6)
1-Hexene	17.21(307.6)	12.74(317.6)	9.42(327.8)	7.80(337.7)	6.03(347.8)
1-Octene	65.85(307.6)	50.10(317.7)	39.00(327.8)	32.23(337.7)	24.95(347.8)
1-Decene	144.01(307.6)	119.05(317.7)	100.48(327.7)	87.99(337.8)	72.49(347.9)
1-Pentyne	5.49(307.8)	4.36(317.5)	3.55(327.6)	2.96(337.7)	2.47(347.8)
1-Hexyne	9.30(307.8)	7.73(317.5)	6.38(327.6)	5.43(337.7)	4.71(347.7)
1-Heptyne	14.34(307.8)	12.29(317.5)	10.52(327.7)	9.17(337.7)	7.96(347.8)
1-Octyne	21.35(307.8)	18.74(317.5)	16.31(327.7)	14.49(337.7)	12.71(347.8)
Benzene	3.29 (307.8)	3.06(317.5)	2.70(328.2)	2.48(338.5)	2.29(348.5)
Toluene	5.31(307.8)	4.71(317.5)	4.36(328.2)	3.93(338.5)	3.68(348.5)
Ethylbenzene	8.40(307.7)	7.49(317.5)	6.89(328.2)	6.22(338.4)	5.85(348.5)
o-Xylene	7.08(307.8)	6.43(317.5)	5.94(328.3)	5.50(338.4)	5.09(348.5)
m-Xylene	8.35(307.8)	7.56(317.6)	6.96(328.4)	6.33(338.4)	5.91(348.4)
p-Xylene	8.40(307.8)	7.48(317.6)	6.81(328.4)	6.33(338.4)	5.86(348.4)
Methanol	1.94(307.7)	1.73(317.5)	1.51(327.5)	1.34(337.7)	1.18(347.8)
Ethanol	3.40(307.7)	2.90(317.5)	2.48(327.6)	2.14(337.7)	1.83(347.8)
1-Propanol	4.75(307.8)	4.03(317.5)	3.40(327.6)	2.93(337.7)	2.50(347.8)

<sup>a</sup> Measured experimental temperatures are given in parentheses.

Table 3. Experimental activity coefficients at infinite dilution  $\gamma_i^\infty$  for various solutes in the ionic liquid [BMIM][BOB] at different temperatures<sup>a</sup>.

Solute( <i>i</i> )	308 K	318 K	328 K	338 K	348 K
Pentane	8.31(308.0)	6.89(318.2)	5.46(328.2)	4.52(338.4)	3.88(348.4)
Hexane	19.10(308.3)	15.72(318.1)	12.35(328.2)	10.18(338.3)	8.58(348.4)
Heptane	36.20(308.6)	30.89(318.2)	24.46(328.3)	20.42(338.5)	17.39(348.5)
Octane	59.37(308.5)	51.87(318.1)	43.48(328.2)	37.22(338.4)	31.84(348.6)
Nonane	89.28(308.3)	79.96(318.1)	69.05(328.2)	60.60(338.4)	53.04(348.4)
Cyclohexane	15.64(308.4)	13.18(318.1)	11.28(328.2)	9.52(338.5)	8.41(348.5)
Methyl cyclohexane	23.46(308.4)	19.90(318.1)	17.12(328.3)	15.07(338.3)	13.03(348.5)
1-Hexene	11.35(308.3)	8.97(318.2)	7.21(328.3)	5.91(338.3)	4.91(348.6)
1-Octene	30.22(308.3)	25.63(318.2)	21.88(328.3)	18.70(338.3)	16.01(348.4)
1-Decene	57.09(308.3)	51.64(318.1)	46.15(328.2)	40.86(338.4)	37.03(348.3)
1-Pentyne	5.17(308.4)	4.67(318.3)	4.14(328.2)	3.73(338.3)	3.28(348.3)
1-Hexyne	7.87(308.4)	7.27(318.3)	6.61(328.3)	6.10(338.3)	5.52(348.3)
1-Heptyne	11.49(308.4)	10.86(318.3)	10.13(328.2)	9.41(338.4)	8.96(348.3)
1-Octyne	16.18(308.6)	15.41(318.3)	14.58(328.3)	13.75(338.5)	13.01(348.3)
Benzene	2.20(308.0)	1.98(318.2)	1.87(328.4)	1.73(338.5)	1.63(348.5)
Toluene	3.15(308.1)	2.99(318.1)	2.79(328.4)	2.65(338.5)	2.48(348.5)
Ethylbenzene	4.75(308.2)	4.42(318.2)	4.18(328.4)	3.90(338.5)	3.65(348.5)
o-Xylene	4.14(308.3)	3.91(318.3)	3.71(328.4)	3.49(338.4)	3.27(348.6)
m-Xylene	4.69(308.4)	4.44(318.3)	4.17(328.5)	3.95(338.4)	3.69(348.6)
p-Xylene	4.71(308.4)	4.43(318.3)	4.23(328.5)	3.95(338.4)	3.71(348.6)
Methanol	1.59(308.3)	1.43(318.1)	1.26(328.5)	1.14(337.5)	1.01(347.6)
Ethanol	2.43(308.3)	2.15(318.1)	1.85(328.5)	1.64(337.5)	1.41(347.7)
1-Propanol	3.08(308.3)	2.70(318.1)	2.27(328.5)	1.99(337.5)	1.70(347.7)

<sup>a</sup> Measured experimental temperatures are given in parentheses.

Table 4. Experimental activity coefficients at infinite dilution  $\gamma_i^\infty$  for various solutes in the ionic liquid [HMIM][BOB] at different temperatures<sup>a</sup>.

Ionic liquids	$\gamma_i^\infty$ (298.15 K)				Selectivity $S_{ij}^\infty$ values		
	Hexane	Cyclohexane	1-Hexene	Benzene	(a)	(b)	(c)
[HMIM][BOB]	24.42 <sup>a</sup>	18.78 <sup>a</sup>	14.40 <sup>a</sup>	2.37 <sup>a</sup>	10.3 <sup>b</sup>	7.9 <sup>b</sup>	1.7 <sup>b</sup>
[BMIM][BOB]	39.39 <sup>a</sup>	34.30 <sup>a</sup>	23.01 <sup>a</sup>	3.67 <sup>a</sup>	10.7 <sup>b</sup>	9.3 <sup>b</sup>	1.7 <sup>b</sup>
[HMIM][NTf <sub>2</sub> ] <sup>c</sup>	8.2 <sup>a</sup> (298K)	5.8 <sup>a</sup> (298K)	4.6 <sup>a</sup> (298K)	0.78 <sup>a</sup> (298K)	10.5 <sup>b</sup> (298K)	7.4 <sup>b</sup> (298K)	1.8 <sup>b</sup> (298K)
[BMIM][NTf <sub>2</sub> ] <sup>d</sup>	15.4 <sup>a</sup> (298K)	9.32 <sup>a</sup> (298K)	7.67 <sup>a</sup> (298K)	0.88 <sup>a</sup> (298K)	17.5 <sup>b</sup> (298K)	10.6 <sup>b</sup> (298K)	2.0 <sup>b</sup> (298K)
[HMIM][SCN] <sup>e</sup>	/	28.2	28.7	1.91	/	14.8	/
[BMIM][SCN] <sup>f</sup>	226	62.3	61.6	2.13	106.1	29.3	3.7
[EMIM][SCN] <sup>g</sup>	327	113.9	104.5	3.43	95.4	33.2	3.1
[OMIM][BF <sub>4</sub> ] <sup>h</sup>	12.4 <sup>a</sup> (298K)	8.06 <sup>a</sup> (298K)	7.06 <sup>a</sup> (298K)	1.19 <sup>a</sup> (298K)	10.4 <sup>b</sup> (298K)	6.8 <sup>b</sup> (298K)	1.8 <sup>b</sup> (298K)
[BMIM][BF <sub>4</sub> ] <sup>i</sup>	64.1 <sup>a</sup>	33.9 <sup>a</sup>	/	1.72 <sup>a</sup>	37.3 <sup>b</sup>	19.7 <sup>b</sup>	/
[EMIM][BF <sub>4</sub> ] <sup>j</sup>	106.9 <sup>a</sup>	84.03 <sup>a</sup>	/	2.16 <sup>a</sup>	49.5 <sup>b</sup>	38.9 <sup>b</sup>	/
[HMIM][CF <sub>3</sub> SO <sub>3</sub> ] <sup>k</sup>	21.45 <sup>a</sup>	11.04 <sup>a</sup>	/	1.412 <sup>a</sup>	15.2 <sup>b</sup>	7.8 <sup>b</sup>	/
[BMIM][CF <sub>3</sub> SO <sub>3</sub> ] <sup>l</sup>	39.2 <sup>a</sup>	23.1 <sup>a</sup>	/	1.8 <sup>a</sup>	21.8 <sup>b</sup>	12.8 <sup>b</sup>	/
[BMIM][CF <sub>3</sub> SO <sub>3</sub> ] <sup>m</sup>	41.6	20.6	17.6	1.55	26.8	13.3	2.4

<sup>a</sup> Extrapolated values, <sup>b</sup> Calculated from the extrapolated values, <sup>c</sup> Ref.[10], <sup>d</sup> Ref.[38], <sup>e</sup> Ref.[39], <sup>f</sup> Ref.[20], <sup>g</sup> Ref.[21], <sup>h</sup> Ref.[7], <sup>i</sup> Ref.[40], <sup>j</sup> Ref.[4], <sup>k</sup> Ref.[17], <sup>l</sup> Ref.[19], <sup>m</sup> Ref.[41].

Table 5. Values of  $\gamma_i^\infty$  at  $T = 298\text{K}$  and selectivity values  $S_{ij}^\infty$  at infinite dilution for different separation problems: (a) hexane/ benzene, b) cyclohexane/ benzene, (c) hexane/1-hexene.

## 2.6 References

- [1] Visser, A. E.; Rogers, R. D. Room-Temperature Ionic Liquids: New Solvents for *f*-element Separations and Associated Solution Chemistry. *J. Solid State Chem.* 2003, 171, 109–113.
- [2] Dohnal, V.; Horakova, I. A New Variant of the Rayleigh Distillation Method for the Determination of Limiting Activity Coefficients. *Fluid Phase Equilib.* 1991, 68, 73-185.
- [3] Letcher, T. M.; Jerman, P. Activity Coefficients of Cyclohexane +*n*-Alkane Mixtures. *J. Chem. Thermodyn.* 1976, 8, 127-131.
- [4] Ge, M.-L.; Wang, L.-S.; Wu, J.-S.; Zhou, Q. Activity Coefficients at Infinite Dilution of Organic Solutes in 1-Ethyl-3-methylimidazolium Tetrafluoroborate Using Gas-Liquid Chromatography. *J. Chem. Eng. Data* 2008, 53, 1970–1974.
- [5] Mutelet, F.; Jaubert, J.-N. Measurement of Activity Coefficients at Infinite Dilution in 1-Hexadecyl-3-methylimidazolium Tetrafluoroborate Ionic Liquid. *J. Chem. Thermodyn.* 2007, 39, 1144-1150.
- [6] Zhou, Q.; Wang, L.-S.; Wu, J.-S.; Li, M.-Y. Activity Coefficients at Infinite Dilution of Polar Solutes in 1-Butyl-3-methylimidazolium Tetrafluoroborate Using Gas-Liquid Chromatography. *J. Chem. Eng. Data* 2007, 52, 131–134.
- [7] Heintz, A.; Verevkin, S. P. Thermodynamic Properties of Mixtures Containing Ionic Liquids. 6. Activity Coefficients at Infinite Dilution of Hydrocarbons, Alcohols, Esters, and Aldehydes in 1-Methyl-3-octyl-imidazolium Tetrafluoroborate Using Gas-Liquid Chromatography. *J. Chem. Eng. Data* 2005, 50, 1515–1519.
- [8] Letcher, T. M.; Soko, B.; Reddy, P. Determination of Activity Coefficients at Infinite Dilution of Solutes in the Ionic Liquid 1-Hexyl-3-methylimidazolium

- Tetrafluoroborate Using Gas-Liquid Chromatography at the Temperatures 298.15 K and 323.15 K. *J. Chem. Eng. Data* 2003, 48, 1587-1590.
- [9] Letcher, T. M.; Soko, B.; Ramjugernath, D. Activity Coefficients at Infinite Dilution of Organic Solutes in 1-Hexyl-3-methylimidazolium Hexafluorophosphate from Gas-Liquid Chromatography. *J. Chem. Eng. Data* 2003, 48, 708-711.
- [10] Heintz, A.; Verevkin, S. P. Thermodynamic Properties of Mixtures Containing Ionic Liquids. 8. Activity Coefficients at Infinite Dilution of Hydrocarbons, Alcohols, Esters, and Aldehydes in 1-Hexyl-3-Methylimidazolium Bis(trifluoromethylsulfonyl)-Imide Using Gas-Liquid Chromatography. *J. Chem. Eng. Data* 2006, 51, 434-437.
- [11] Deenadayalu, N.; Letcher, T. M.; Reddy, P. Determination of Activity Coefficients at Infinite Dilution of Polar and Nonpolar Solutes in the Ionic Liquid 1-Ethyl-3-methylimidazolium Bis(trifluoromethylsulfonyl)Imide Using Gas-Liquid Chromatography at the Temperature 303.15 or 318.15 K. *J. Chem. Eng. Data* 2005, 50, 105-108.
- [12] Letcher, T. M.; Marciniak, A.; Marciniak, M.; Domanska, U. Activity Coefficients at Infinite Dilution Measurements for Organic Solutes in the Ionic Liquid 1-Hexyl-3-methyl-imidazolium Bis(trifluoromethylsulfonyl)-Imide Using G.L.C. at  $T = (298.15, 313.15, \text{ and } 333.15) \text{ K}$ . *J. Chem. Thermodyn.* 2005, 37, 1327-1331.
- [13] Krummen, M.; Wasserscheid, P.; Gmehling, J. Measurement of Activity Coefficients at Infinite Dilution in Ionic Liquids Using the Dilutor Technique. *J. Chem. Eng. Data* 2002, 47, 1411-1417.
- [14] Heintz, A.; Kulikov, D. V.; Verevkin, S. P. Thermodynamic Properties of Mixtures Containing Ionic Liquids. 2. Activity Coefficients at Infinite Dilution of Hydrocarbons and Polar Solutes in 1-Methyl-3-ethyl-imidazolium Bis(trifluoromethyl-sulfonyl) Amide and in 1,2-Dimethyl-3-ethyl-imidazolium Bis(trifluoromethyl-sulfonyl) Amide Using Gas-Liquid Chromatography. *J. Chem. Eng. Data* 2002, 47, 894-899.
- [15] Mutelet, F.; Jaubert, J.-N.; Rogalski, M.; Boukherissa, M.; Dicko, A. Thermodynamic Properties of Mixtures Containing Ionic Liquids: Activity Coefficients at Infinite Dilution of Organic Compounds in 1-Propyl Boronic Acid-3-Alkylimidazolium Bromide and 1-Propenyl-3-alkylimidazolium Bromide Using Inverse Gas Chromatography. *J. Chem. Eng. Data* 2006, 51, 1274-1279.
- [16] David, W.; Letcher, T. M.; Ramjugernath, D.; Raal, J. D. Activity Coefficients of Hydrocarbon Solutes at Infinite Dilution in the Ionic Liquid, 1-Methyl-3-octylimidazolium Chloride from Gas-Liquid Chromatography. *J. Chem. Thermodyn.* 2003, 35, 1335-1341.
- [17] Yang, X.-J.; Wu, J.-S.; Ge, M.-L.; Wang, L.-S.; Li, M.-Y. Activity Coefficients at Infinite Dilution of Alkanes, Alkenes, and Alkyl benzenes in 1-Hexyl-3-methylimidazolium Trifluoromethanesulfonate Using Gas-Liquid Chromatography. *J. Chem. Eng. Data* 2008, 53, 1220-1222.
- [18] Ge, M.-L.; Wang, L.-S. Activity Coefficients at Infinite Dilution of Polar Solutes in 1-Butyl-3-methylimidazolium Trifluoromethanesulfonate Using Gas-Liquid Chromatography. *J. Chem. Eng. Data* 2008, 53, 846-849.
- [19] Ge, M.-L.; Wang, L.-S.; Li, M.-Y.; Wu, J.-S. Activity Coefficients at Infinite Dilution of Alkanes, Alkenes, and Alkyl Benzenes in 1-Butyl-3-methylimidazolium

- Trifluoromethanesulfonate Using Gas-Liquid Chromatography. *J. Chem. Eng. Data* 2007, 52, 2257–2260.
- [20] Domanska, U.; Laskowska, M. Measurements of Activity Coefficients at Infinite Dilution of Aliphatic and Aromatic Hydrocarbons, Alcohols, Thiophene, Tetrahydrofuran, MTBE, and Water in Ionic Liquid [BMIM][SCN] using GLC. *J. Chem. Thermodyn.* 2009, 41, 645–650.
- [21] Domanska, U.; Marciniak, A. Measurements of Activity Coefficients at Infinite Dilution of Aromatic and Aliphatic Hydrocarbons, Alcohols, and Water in the new Ionic Liquid [EMIM][SCN] using GLC. *J. Chem. Thermodyn.* 2008, 40, 860–866.
- [22] Deenadayalu, N.; Thango, S. H.; Letcher, T. M.; Ramjugernath, D. Measurement of Activity Coefficients at Infinite Dilution Using Polar and Non-polar Solutes in the Ionic Liquid 1-Methyl-3-octyl-imidazolium Diethyleneglycolmonomethylethersulfate at  $T = (288.15, 298.15, \text{ and } 313.15) \text{ K}$ . *J. Chem. Thermodyn.* 2006, 38, 542–546.
- [23] Kozlova, S. A.; Verevkin, S. P.; Heintz, A.; Peppel, T.; Kockerling, M. Activity Coefficients at Infinite Dilution of Hydrocarbons, Alkylbenzenes, and Alcohols in the Paramagnetic Ionic Liquid 1-Butyl-3-methyl-imidazolium Tetrachloridoferrate(III) using Gas-Liquid Chromatography. *J. Chem. Thermodyn.* 2009, 41, 330–333.
- [24] Kozlova, S. A.; Verevkin, S. P.; Heintz, A. Paramagnetic Ionic Liquid 1-Butyl-3-methylimidazolium Tetrabromidocobaltate (II): Activity Coefficients at Infinite Dilution of Organic Solutes and Crystal Structure. *J. Chem. Eng. Data* 2009, 54, 1524–1528.
- [25] Yan P.-F.; Yang M.; Liu X.-M.; Liu Q.-S.; Tan Z.-C.; Welz-Biermann, U. Activity Coefficients at Infinite Dilution of Organic Solutes in 1-Ethyl-3-methylimidazolium Tris(pentafluoroethyl)trifluorophosphate [EMIM][FAP] Using Gas-Liquid Chromatography. *J. Chem. Eng. Data* 2010, 55, 2444–2450.
- [26] Yan P.-F.; Yang M.; Liu X.-M.; Wang C.; Tan Z.-C.; Welz-Biermann, U. Activity coefficients at infinite dilution of organic solutes in the ionic liquid 1-ethyl-3-methylimidazolium tetracyanoborate [EMIM][TCB] using gas-liquid Chromatography. *J. Chem. Thermodyn.* 2010, 42, 817–822.
- [27] Yan P.-F.; Yang M.; Li C.-P.; Liu X.-M.; Tan Z.-C.; Welz-Biermann, U. Gas-liquid chromatography measurements of activity coefficients at infinite dilution of hydrocarbons and alkanols in 1-alkyl-3-methylimidazolium bis(oxalato)borate. *Fluid Phase Equilib.* 2010, 298, 287–292.
- [28] Tiegs, D.; Gmehling, J.; Medina, A.; Soares, M.; Bastos, J.; Alessi, P.; Kikic, I. *DECHEMA Chemistry Data Series IX, Part 1*, DECHEMA: Frankfurt/Main, 1986.
- [29] Everett, D. H. Effects of Gas Imperfections on GLC Measurements. *Trans. Faraday Soc.* 1965, 61, 1637–1645.
- [30] Cruickshank, A. J. B.; Windsor, M. L.; Young, C. L. The Use of Gas-Liquid Chromatography to Determine Activity Coefficients and Second Virial Coefficients of Mixtures. *Proc. R. Soc.* 1966, A295, 259–270.
- [31] McGlashan, M. L.; Potter, D. J. B. *Proc. R. Soc.* 1951, 267, 448–456.
- [32] Hudson, G. H.; McCoubrey, J. C. Intermolecular Forces between unlike Molecules. *Trans. Faraday Soc.* 1960, 56, 761–771.

- [33] Cruickshank, A. J. B.; Windsor, M. L.; Young, C. L. Prediction of Second Virial Coefficients of Mixtures from the Principle of Corresponding States. *Trans. Faraday Soc.* 1966, 62, 2341-2347.
- [34] Grant, D. W. *Gas-Liquid Chromatography*; van Nostrand Reinhold Company: London, 1971.
- [35] Design Institute for Physical Properties, Sponsored by AIChE, *DIPPR Project 801- Full Version*; Design Institute for Physical Property Data/AIChE, 2005. Online version available at:  
<http://www.knovel.com/knovel2/Toc.jsp?BookID=1187&VerticalID=0>.
- [36] Yaws, C. L. *Yaws' Handbook of Thermodynamic and Physical Properties of Chemical Compounds*, Knovel, 2003, online version available at:  
<http://www.knovel.com/knovel2/Toc.jsp?BookID=667&VerticalID=0>.
- [37] Dean, J. A. *Lange's Handbook of Chemistry*, 15th Edition, McGraw-Hill, 1999, online version available at:  
<http://www.knovel.com/knovel2/Toc.jsp?BookID=47&VerticalID=0>.
- [38] Heintz, A.; Casa's, L. M.; Nesterov, I. A.; Emeyanenko, V. N.; Verevkin, S. P. Thermodynamic Properties of Mixtures Containing Ionic Liquids. 5. Activity Coefficients at Infinite Dilution of Hydrocarbons, Alcohols, Esters, and Aldehydes in 1-Methyl-3-butylimidazolium Bis(trifluoromethylsulfonyl) Imide Using Gas-Liquid Chromatography. *J. Chem. Eng. Data* 2005, 50, 1510-1514.
- [39] Domanska, U.; Marciniak, A.; Krolikowska, M.; Arasimowicz, M. Activity Coefficients at Infinite Dilution Measurements for Organic Solutes and Water in the Ionic Liquid 1-Hexyl-3-methylimidazolium Thiocyanate. *J. Chem. Eng. Data* Doi: 10.1021/je900890u.
- [40] Zhou, Q.; Wang, L.-S. Activity Coefficients at Infinite Dilution of Alkanes, Alkenes, and Alkyl benzenes in 1-Butyl-3-methylimidazolium Tetrafluoroborate Using Gas-Liquid Chromatography. *J. Chem. Eng. Data* 2006, 51, 1698-1701.
- [41] Domanska, U.; Marciniak, A. Activity Coefficients at Infinite Dilution, Measurements for Organic Solutes and Water in the Ionic Liquid 1-Butyl-3-methylimidazolium Trifluoromethanesulfonate. *J. Phys. Chem. B* 2008, 112, 11100-11105.

### 3. Thermodynamic properties of Alkyl Pyridinium Bromide Ionic Liquids determined by Adiabatic Calorimetry and Thermal Analysis

#### 3.1 Introduction

Ionic liquids are attracting increasing attention in many fields including organic chemistry,<sup>1-4</sup> electrochemistry,<sup>2, 5, 6</sup> catalysis,<sup>7-9</sup> physical chemistry and engineering<sup>10-14</sup> with their special physical and chemical properties, such as low vapor pressure, low inflammability, high inherent conductivities, thermal stability, liquidity over a wide temperature range, easy recycling, and being a good solvent for a wide variety of organic and inorganic chemical compounds. The physicochemical properties of an ionic liquid vary greatly depending on the molecular structure, e.g., miscibility with water and organic solvents, melting point, and viscosity.<sup>15-17</sup> Besides, ionic liquids are "designable" as structural modifications in both the cation and anion permit the possibility to design task-specific applications when the ionic liquid contain a specific functionality covalently incorporated in either the cation or anion.<sup>4</sup> Alkyl pyridinium bromide ionic liquids, which are easy to synthesize and purify, are one of them and show good perspective in the applications of extraction and separation processes, synthetic chemistry, catalysis and materials science.<sup>18-20</sup>



However, most scientists focus on the synthesis and application of ionic liquids while few researchers put their efforts on the fundamental thermodynamic studies.<sup>10, 20-23</sup> As far as we know, the thermodynamic properties of ionic liquids, such as heat capacity  $C_{p,m}$ , glass transition temperature  $T_g$ , melting temperature  $T_m$ , thermal decomposition temperature  $T_{decomp}$ , enthalpy and entropy of phase transitions are important properties that reflect the structures and stabilities of compounds but rarely reported till now.

In the present study, two ionic liquids 1-ethylpyridinium bromide (EPBr, CAS NO. 1906-79-2) and 1-propylpyridinium bromide (PPBr, CAS NO. 873-71-2) were prepared and the structures were characterized by  $^1\text{H-NMR}$ . The thermodynamic properties of EPBr and PPBr were studied with adiabatic calorimetry (AC) and thermogravimetric analysis (TG-DTG). The phase change behaviour and thermodynamic properties were compared and estimated in the series alkyl pyridinium bromide ionic liquids, which were very important in industry and their application application.

## 3.2 Experimental section

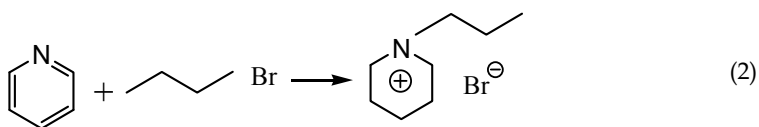
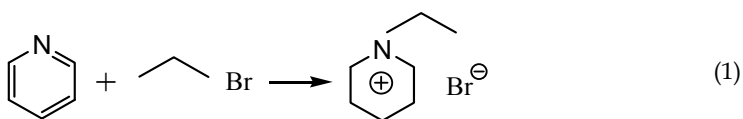
### 3.2.1 Materials

All reagents were of commercial origin with purities >99.5%. 1-bromopropane (AR grade, Sinopharm Chemical Reagent Co., China), pyridine and 1-bromoethane (AR grade, Tianjin Damao Chemical Reagent Co., China) were distilled before use. After absorbing the water by molecular sieves, ethyl acetate (AR grade, Tianjin Kemiou Chemical Reagent Co., China) and acetonitrile (AR grade, Tianjin Fengchuan Chemical Reagent Co., China) were distilled and used in synthesis process.

### 3.2.2 Preparation of EPBr and PPBr ILs

Pyridine (1mol) was placed in a 500 ml round-bottomed flask and stirred, and 1-bromoethane or 1-bromopropane (1.1mol) was added dropwise into the flask at 70 °C. A slight excess of the 1-bromoethyl or 1-bromopropane was used to guarantee the consumption of pyridine. Ethyl acetate (80 ml) was added to reduce the viscosity of the mixture, which was left to stir under reflux at 70 °C for 48 h. The halide salt separated as a second phase from the ethyl acetate. Excess of ethyl acetate were removed by decantation.

The following reaction equations 1 and 2 gave the reaction scheme:



The products were recrystallized from acetonitrile. The volume of acetonitrile used for the recrystallization were approximately half of the halide salt. Acetonitrile was then decanted after crystallization, this step was repeated twice. After the third cycle, the remaining acetonitrile and 1-bromoethane or 1-bromopropane were removed under reduced pressure using rotary evaporator at 70 °C, and the bromide salts were finally dried in high vacuum at 70 °C.

### 3.2.3 $^1\text{H}$ -NMR of EPBr and PPBr ILs

The  $^1\text{H}$ -NMR spectra were recorded on a Bruker-400Hz spectrometer and chemical shifts were reported in ppm using DMSO as an internal standard.

### 3.2.4 Adiabatic Calorimetry (AC).

Heat capacity measurements were carried out in a high-precision automated adiabatic calorimeter<sup>24-26</sup> which was established by Thermochemistry Laboratory of Dalian Institute of Chemical Physics, Chinese Academy of Sciences in PR China. The schematic diagram of the adiabatic calorimeter is shown in Figure 1.

To verify the reliability of the adiabatic calorimeter, the molar heat capacities of Standard Reference Material 720, Synthetic Sapphire ( $\alpha\text{-Al}_2\text{O}_3$ ) were measured. The deviations of our experimental results from the recommended values by NIST<sup>27</sup> were within  $\pm 0.1\%$  in the temperature range of 80-400 K.

### 3.2.5 Thermogravimetric Analysis (TGA)

The TG measurements of the sample were carried out by a thermogravimetric analyzer (Model: TGA/SDTA 851e, Mettler Toledo, USA) under  $\text{N}_2$  with a flow rate of  $40 \text{ ml}\cdot\text{min}^{-1}$  at the heating rate of  $10 \text{ K}\cdot\text{min}^{-1}$  from 300 to 580 K, respectively. The sample about 10-15 mg was filled into alumina crucible without pressing.

## 2.3 Results and discussion

### 2.3.1 $^1\text{H}$ -NMR of EPBr and PPBr ILs

The  $^1\text{H}$ -NMR spectra  $\delta_{\text{H}}$  (400 MHz, DMSO) of two ILs were listed in Table 1. Analysis of EPBr and PPBr by  $^1\text{H}$ -NMR resulting in spectra is in good agreement with the literature<sup>28</sup> and does not show any impurities.

### 3.3.2 Low-temperature heat capacity

Experimental molar heat capacities of two ILs measured by the adiabatic calorimeter over the experimental temperature range are listed in Table 2 and plotted in Figure 2, respectively.

From Figure 2.a.(EPBR), a smoothed curve with no endothermic or exothermic peaks was observed from the liquid nitrogen temperature to 380 K, which indicated that the sample was thermostable in this temperature range. From 380 K to 400 K, a sharply endothermic peak corresponding to a melting process was observed with the peak temperature 391.31 K. The melting process was repeated twice and the melting temperature was determined to be  $391.31 \pm 0.28 \text{ K}$  according to the two experimental results.

The values of experimental heat capacities can be fitted to the following polynomial equations with least square method:<sup>29</sup>

Before the fusion (8 -380 K),

$$C_{p,m}^0 / \text{J}\cdot\text{K}^{-1}\cdot\text{mol}^{-1} = 160.770 + 120.380x + 43.911x^2 - 74.730x^3 - 119.630x^4 + 78.756x^5 - 118.390x^6 \quad (3)$$

After the fusion (395 - 410 K),

$$C_{p,m}^0 / \text{J}\cdot\text{K}^{-1}\cdot\text{mol}^{-1} = 294.630 + 5.947x \quad (4)$$

where  $x$  is the reduced temperature;  $x = [T - (T_{\max} + T_{\min}) / 2] / [(T_{\max} - T_{\min}) / 2]$ ;  $T$ , the experimental temperature;  $T_{\max}$  and  $T_{\min}$ , the upper and lower limit in the temperature region. The correlation coefficient of the fitting  $r^2 = 0.9981$  and  $0.9955$  corresponding to equation 3 and 4, respectively.

However, from Figure 2.b.(BPBR), an endothermic step corresponding to a glass transition occurred with the glass transition temperature  $T_g = 171.595$  K. A sharply endothermic peak corresponding to a melting process was observed with the peak temperature  $342.83$  K. The melting process was repeated twice and the melting temperature was determined to be  $342.83 \pm 0.69$  K according to the two experimental results.

Similarly, the values of experimental heat capacities were fitted to the following polynomial equations with least square method:

Before the glass transition (78 -165 K),

$$C_{p,m}^0 / \text{J}\cdot\text{K}^{-1}\cdot\text{mol}^{-1} = 109.490 + 28.801x + 1.571x^2 - 9.155x^3 - 10.402x^4 + 7.121x^5 - 7.845x^6 \quad (5)$$

After glass transition and before fusion (180 -315 K),

$$C_{p,m}^0 / \text{J}\cdot\text{K}^{-1}\cdot\text{mol}^{-1} = 204.590 + 66.960x + 19.987x^2 + 4.091x^3 + 19.909x^4 + 27.504x^5 + 9.812x^6 \quad (6)$$

After fusion (355-400 K),

$$C_{p,m}^0 / \text{J}\cdot\text{K}^{-1}\cdot\text{mol}^{-1} = 310.530 + 8.712x + 3.097x^2 - 0.713x^3 - 6.183x^4 + 0.471x^5 + 3.554x^6 \quad (7)$$

The correlation coefficient of the fitting is  $r^2 = 0.9996, 0.9999, 0.9995$  corresponding to equation 5, 6, 7, respectively.

### 3.3.3 Thermodynamic functions

The thermodynamic functions ( $H_T^0 - H_{298.15}^0$ ) and ( $S_T^0 - S_{298.15}^0$ ) of the two ILs relative to the reference temperature  $298.15$  K were calculated in the experimental temperature range with an interval of  $5$  K, using the polynomial equations of heat capacity and thermodynamic relationships as follows:

For EPBr,

Before melting,

$$H_T^0 - H_{298.15}^0 = \int_{298.15}^T C_{p,m}^0(s) dT \quad (8)$$

$$S_T^0 - S_{298.15}^0 = \int_{298.15}^T \frac{C_{p,m}^0(s)}{T} dT \quad (9)$$

After melting,

$$H_T^0 - H_{298.15}^0 = \int_{298.15}^{T_i} C_{p,m}^0(s) dT + \Delta_{fus} H_m^0 + \int_{T_f}^T C_{p,m}^0(l) dT \quad (10)$$

$$S_T^0 - S_{298.15}^0 = \int_{298.15}^{T_i} \left[ \frac{C_{p,m}^0(s)}{T} \right] dT + \frac{\Delta_{fus} H_m^0}{T_m} + \int_{T_f}^T \left[ \frac{C_{p,m}^0(l)}{T} \right] dT \quad (11)$$

where  $T_i$  is the temperature at which the solid-liquid phase transition started;  $T_f$  is the temperature at which the solid-liquid phase transition ended;  $\Delta_{fus} H_m^0$  is the standard molar enthalpy of fusion;  $T_m$  is the temperature of solid-liquid phase transition.

For PPBr, the calculation of thermodynamic functions is the same with EPBr before and after the melting. Moreover, the glass transition was included in the calculation. The standard thermodynamic functions  $H_T^0 - H_{298.15}^0$ ,  $S_T^0 - S_{298.15}^0$ , of the two ILs, are listed in Table 3.

### 3.3.4 The thermostability tested by TG-DTG

The TG-DTG curves shown in Figure 3 indicated that the mass loss of EPBr was completed in a single step. The sample keeps thermostable below 470 K. It begins to lose weight at about 480 K, reaches the maximum rate of weight loss at 541.229 K and completely loses its weight when the temperature reaches 575 K. Similar one-step decomposition process occurs for PPBr beginning at about 460 K and finishing at about 570 K while the peak temperature of decomposition is 536.021K.

### 3.3.5 Comparison and estimation of thermodynamic properties for alkyl pyridinium bromide ionic liquids

According to experimental data in section 3.3-3.4, the thermodynamic properties as well as the structure of EPBr and PPBr were compared and estimated as follows:

- Molar heat capacity  $C_{p,m}(\text{EPBr}) < C_{p,m}(\text{PPBr})$  reveals that EPBr has lower lattice energy than PPBr in low temperature due to shorter carbon chain in pyridinium cation of EPBr. This rule may be applicable in the alkyl pyridinium halide family and will be verified in our further research work:  $C_{p,m}(\text{EPX}) < C_{p,m}(\text{PPX}) < C_{p,m}(\text{BPX})$ ; X stands for Cl, Br, I.
- Melting temperature  $T_m(\text{EPBr}) > T_m(\text{PPBr})$  and phase transition enthalpy  $\Delta H_m(\text{EPBr}) > \Delta H_m(\text{PPBr})$  are possibly because of the fact that the H- $\pi$  bond effects of pyridinium cation played the major role in ionic compounds.<sup>30</sup> The more methylene group added in the cation, the more steric hindrance strengthened which results in decrease of the melting temperature and enthalpy.
- Thermal decomposition temperature  $T_d(\text{EPBr}) > T_d(\text{PPBr})$  indicates that EPBr is more thermostable than PPBr which is favorable in practical applications for EPBr.

## 3.4 Conclusions

Two ionic liquids 1-ethylpyridinium bromide (EPBr) and 1-propylpyridinium bromide (PPBr) were prepared and characterized. The structure and purity were verified by <sup>1</sup>H-NMR. The thermodynamic properties of EPBr and PPBr were studied with adiabatic calorimetry (AC) and thermogravimetric analysis (TG-DTG). The phase change behaviour and thermodynamic properties were compared and estimated in a series of alkyl pyridinium bromide ionic liquids. Results indicate that EPBr has higher melting and thermal decomposition temperature, phase transition enthalpy and entropy but lower heat capacity than PPBr due to the different molecular structures.

EPBr			PPBr		
Chemical shift	Hydrogen number	Radical	Chemical shift	Hydrogen number	Radical
1.529~1.566 (t)	3	CH <sub>3</sub>	0.861~0.905 (m)	3	CH <sub>3</sub>
/	/	/	1.906~01.997(m)	2	-CH <sub>2</sub> -
4.636 ~4.69 (q)	2	-CH <sub>2</sub> -	4.593 ~4.629(t)	2	-CH <sub>2</sub> -
8.160~8.193 (t)	2	C(3,5)H	8.173~8.208 (t)	2	C(3,5)H
8.594~8.63(m)	1	C(4)H	8.616~8.655 (q)	1	C(4)H
9.147-9.163 (d)	2	C(2,6)H	9.144-9.158 (d)	2	C(2,6)H

Table 1. The <sup>1</sup>H NMR spectrum  $\delta_H$  (400 MHz, DMSO) of EPBr and PPBr

$T$	$C_{p,m}$	$T$	$C_{p,m}$	$T$	$C_{p,m}$
K	J·K <sup>-1</sup> ·mol <sup>-1</sup>	K	J·K <sup>-1</sup> ·mol <sup>-1</sup>	K	J·K <sup>-1</sup> ·mol <sup>-1</sup>
EPBr					
77.657	76.37	167.830	120.1	293.984	211.1
78.910	76.76	170.492	121.8	296.941	213.4
80.835	77.37	173.132	123.5	299.903	215.8
82.735	77.98	175.742	125.1	302.846	218.2
84.596	78.61	178.330	126.8	305.833	220.6
86.427	79.23	180.889	128.5	308.861	223.0
88.247	79.87	184.399	130.8	311.872	225.5
90.064	80.53	188.087	133.2	314.867	227.9
91.831	81.18	190.997	135.2	317.847	230.4
93.600	81.84	193.889	137.1	320.809	232.8
95.319	82.50	196.797	139.1	323.753	235.3
97.043	83.18	199.725	141.1	326.680	237.7
98.712	83.84	202.635	143.1	329.637	239.7
100.356	84.51	205.562	145.1	332.620	241.7
102.007	85.19	208.506	147.2	335.578	244.3
103.584	85.85	211.429	149.2	338.514	246.8
105.159	86.52	214.368	151.3	341.443	248.3
106.748	87.20	217.323	153.4	344.374	250.9
108.294	87.88	220.256	155.5	347.145	253.4
109.824	88.56	223.219	157.6	350.716	255.1
111.334	89.24	226.300	159.8	353.930	257.2
112.825	89.92	229.327	162.0	356.934	259.4
114.310	90.61	230.295	162.7	359.924	263.8
115.777	91.29	233.046	164.7	362.891	268.3
117.254	91.99	235.996	166.9	365.830	274.9
118.706	92.68	239.019	169.1	368.779	283.7
120.141	93.38	242.710	171.8	371.726	294.8
122.451	94.51	246.377	174.5	374.657	311.8
125.457	96.01	249.319	176.7	377.584	336.2
128.389	97.50	252.303	179.0	381.896	383.3

131.317	99.03	255.273	181.2	384.471	518.9
134.260	100.6	258.223	183.4	386.772	880.6
137.187	102.2	261.164	185.6	388.702	1385
140.095	103.8	264.144	187.9	390.114	2426
142.990	105.4	267.165	190.2	391.059	2913
145.862	107.0	270.171	192.5	393.468	368.3
148.691	108.6	273.161	194.8	397.309	290.8
151.509	110.2	276.142	197.1	400.484	292.6
154.275	111.9	279.102	199.4	403.532	295.6
157.015	113.5	282.050	201.7	406.667	298.0
159.741	115.1	285.031	204.0	409.650	300.3
162.457	116.8	288.045	206.4		
165.147	118.5	291.028	208.7		
<b>PPBr</b>					
78.023	81.93	150.821	126.5	278.727	242.3
79.011	82.58	152.964	127.4	281.695	246.8
80.509	83.51	155.094	128.5	284.662	251.8
81.987	84.05	157.212	129.6	287.618	257.7
83.448	85.09	159.316	131.0	290.563	264.1
84.877	85.97	161.411	132.2	293.520	270.1
86.291	87.20	163.494	133.4	296.504	277.0
87.683	88.42	165.562	135.0	299.478	286.4
89.059	89.68	167.612	137.0	302.426	295.6
90.419	90.18	169.627	140.7	305.368	306.0
91.759	90.61	171.595	146.1	308.308	318.8
93.086	91.64	173.525	150.0	311.222	333.0
94.399	92.72	175.436	152.2	314.133	350.3
95.699	93.54	177.336	153.9	317.045	371.4
96.985	94.26	179.229	155.2	319.893	396.1
98.259	95.12	181.811	157.4	322.596	425.8
99.522	95.89	184.960	159.3	325.158	460.4
100.773	96.75	187.964	160.7	327.559	500.2
102.016	97.24	190.976	162.2	329.799	547.5
103.246	97.66	193.999	163.8	331.870	602.5
104.467	98.77	197.005	165.7	333.775	666.6
105.680	99.93	200.025	167.7	335.515	740.5
106.884	100.3	203.068	169.2	337.098	826.3
108.077	100.8	206.105	170.4	338.540	921.4
109.263	101.9	209.166	172.4	339.842	1029
110.443	102.3	212.232	174.1	341.032	1133
111.612	102.7	215.267	176.7	342.146	1156
112.773	103.7	218.270	179.2	343.563	753.9
113.931	104.5	221.226	182.0	345.633	464.8
115.078	105.1	224.186	184.1	348.293	353.8
116.220	105.4	227.228	186.9	351.393	301.7
117.354	106.1	230.236	189.0	354.574	302.4
118.482	107.0	233.079	192.1	357.586	303.4

119.602	108.0	235.879	193.9	360.598	304.5
121.367	109.6	238.705	196.9	363.600	305.8
123.762	111.6	242.272	199.5	366.595	306.9
126.132	113.2	245.916	202.6	369.613	307.8
128.476	114.7	248.905	205.8	372.656	308.6
130.800	116.1	251.877	208.6	376.372	310.4
133.098	117.4	254.857	211.8	379.412	311.2
135.379	118.5	257.855	215.2	382.441	312.5
137.636	119.5	260.823	218.3	385.470	313.9
139.877	120.7	263.802	221.6	388.488	315.1
142.099	121.8	266.790	225.1	391.504	316.3
144.303	123.0	269.785	229.3	394.600	317.4
146.491	124.2	272.790	233.3	397.710	318.5
148.663	125.5	275.759	238.0		

Table 2. Experimental molar heat capacities of EPBr and PPBr

$T$ K	$C_{p,m}$ J·K <sup>-1</sup> ·mol <sup>-1</sup>	$H_T - H_{298.15}$ kJ·mol <sup>-1</sup>	$S_T - S_{298.15}$ J·K <sup>-1</sup> ·mol <sup>-1</sup>	$C_{p,m}$ J·K <sup>-1</sup> ·mol <sup>-1</sup>	$H_T - H_{298.15}$ kJ·mol <sup>-1</sup>	$S_T - S_{298.15}$ J·K <sup>-1</sup> ·mol <sup>-1</sup>
/	EPBr			PPBr		
80	78.73	-30.09	-162.1	83.06	-34.44	-183.7
85	78.71	-29.69	-157.4	86.46	-34.02	-178.6
90	79.54	-29.30	-152.9	89.79	-33.58	-173.5
95	81.03	-28.90	-148.5	92.97	-33.12	-168.6
100	83.04	-28.49	-144.2	96.03	-32.65	-163.7
105	85.40	-28.07	-140.0	99.04	-32.16	-159.0
110	88.03	-27.63	-136.0	102.1	-31.66	-154.3
115	90.81	-27.19	-132.0	105.2	-31.14	-149.7
120	93.70	-26.73	-128.1	108.5	-30.61	-145.1
125	96.62	-26.25	-124.2	111.8	-30.06	-140.6
130	99.54	-25.76	-120.4	115.1	-29.49	-136.2
135	102.4	-25.25	-116.6	118.2	-28.91	-131.8
140	105.3	-24.73	-112.9	121.1	-28.31	-127.4
145	108.1	-24.20	-109.2	123.7	-27.70	-123.1
150	110.9	-23.65	-105.5	126.0	-27.07	-118.9
155	113.6	-23.09	-101.9	128.3	-26.44	-114.7
160	116.4	-22.52	-98.22	131.1	-25.79	-110.6
165	119.1	-21.93	-94.62	135.3	-25.12	-106.5
170	121.8	-21.33	-91.03	Glass transition		
175	124.6	-20.71	-87.46	/	/	/
180	127.4	-20.08	-83.90	155.7	-23.96	-99.99
185	130.3	-19.44	-80.36	158.6	-23.18	-95.66
190	133.3	-18.78	-76.83	161.4	-22.38	-91.38
195	136.4	-18.10	-73.30	164.3	-21.56	-87.15
200	139.6	-17.41	-69.79	167.3	-20.73	-82.96

205	143.0	-16.71	-66.28	170.4	-19.89	-78.79
210	146.4	-15.98	-62.77	173.6	-19.03	-74.65
215	150.0	-15.24	-59.27	177.0	-18.15	-70.53
220	153.8	-14.48	-55.76	180.6	-17.26	-66.42
225	157.6	-13.70	-52.25	184.5	-16.35	-62.31
230	161.6	-12.91	-48.73	188.6	-15.41	-58.21
235	165.6	-12.09	-45.21	192.9	-14.46	-54.11
240	169.7	-11.25	-41.68	197.4	-13.49	-50.00
245	173.9	-10.39	-38.14	202.1	-12.49	-45.88
250	178.1	-9.511	-34.59	207.1	-11.46	-41.75
255	182.3	-8.610	-31.04	212.3	-10.42	-37.60
260	186.5	-7.688	-27.47	217.7	-9.341	-33.43
265	190.6	-6.745	-23.89	223.5	-8.238	-29.22
270	194.7	-5.781	-20.30	229.7	-7.105	-24.99
275	198.7	-4.798	-16.71	236.4	-5.940	-20.72
280	202.5	-3.795	-13.10	243.8	-4.740	-16.39
285	206.2	-2.773	-9.496	252.3	-3.500	-12.00
290	209.8	-1.733	-5.886	262.2	-2.215	-7.532
295	213.3	-0.675	-2.275	273.9	-0.876	-2.953
298.15	215.3	0.000	0.000	282.4	0.000	0.000
300	216.6	0.400	1.335	288.0	0.528	1.764
305	219.7	1.490	4.943	305.2	2.009	6.661
310	222.9	2.597	8.545	326.5	3.587	11.79
315	225.9	3.719	12.14	352.9	5.283	17.22
320	229.1	4.856	15.73	Phase transition		
325	232.3	6.010	19.32	/	/	/
330	235.8	7.180	22.90	/	/	/
335	239.6	8.368	26.48	/	/	/
340	244.0	9.577	30.07	/	/	/
345	249.0	10.81	33.67	/	/	/
350	255.0	12.07	37.29	/	/	/
355	262.2	13.36	40.96	302.5	16.98	51.22
360	270.9	14.69	44.68	304.4	18.50	55.46
365	281.4	16.07	48.47	306.3	20.02	59.67
370	294.1	17.51	52.38	307.9	21.56	63.85
375	309.4	19.02	56.42	309.6	23.10	68.00
380	327.8	20.61	60.65	311.5	24.65	72.11
385	Phase transition			313.7	26.22	76.20
390	/	/	/	315.7	27.79	80.26
395	288.7	33.16	92.83	317.5	29.37	84.29
400	292.6	34.61	96.49	319.5	30.97	88.30
405	296.6	36.09	100.2			
410	300.6	37.58	103.8			

Table 3. Smoothed heat capacities and thermodynamic functions of EPr and PPr.



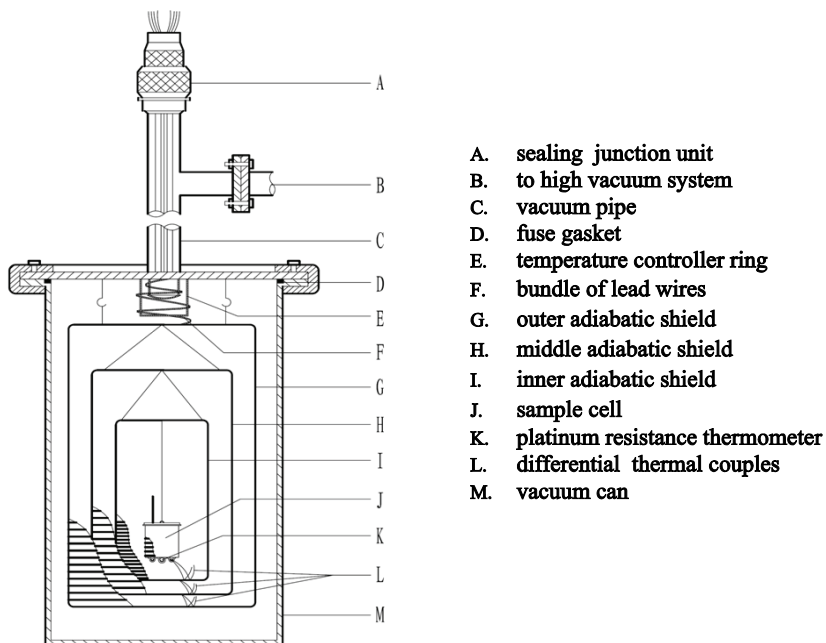


Fig. 1. A. Schematic diagram of main body of the adiabatic calorimeter

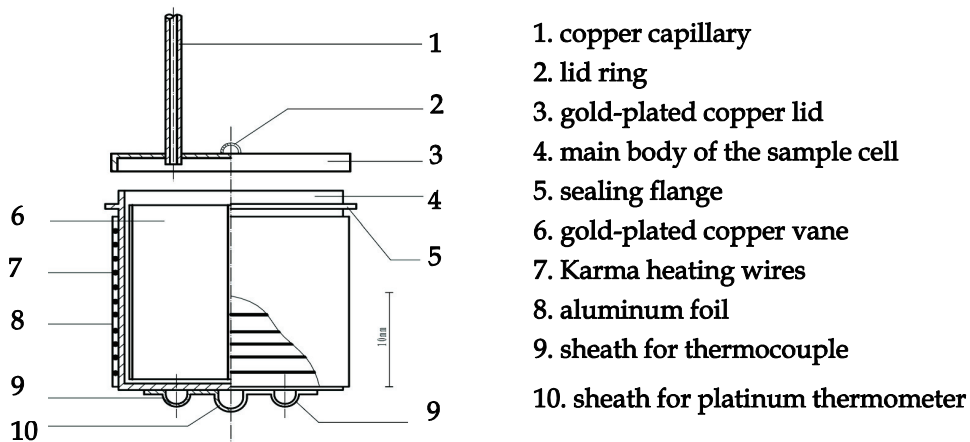


Fig. 1. B. Schematic diagram of sample cell of the adiabatic calorimeter

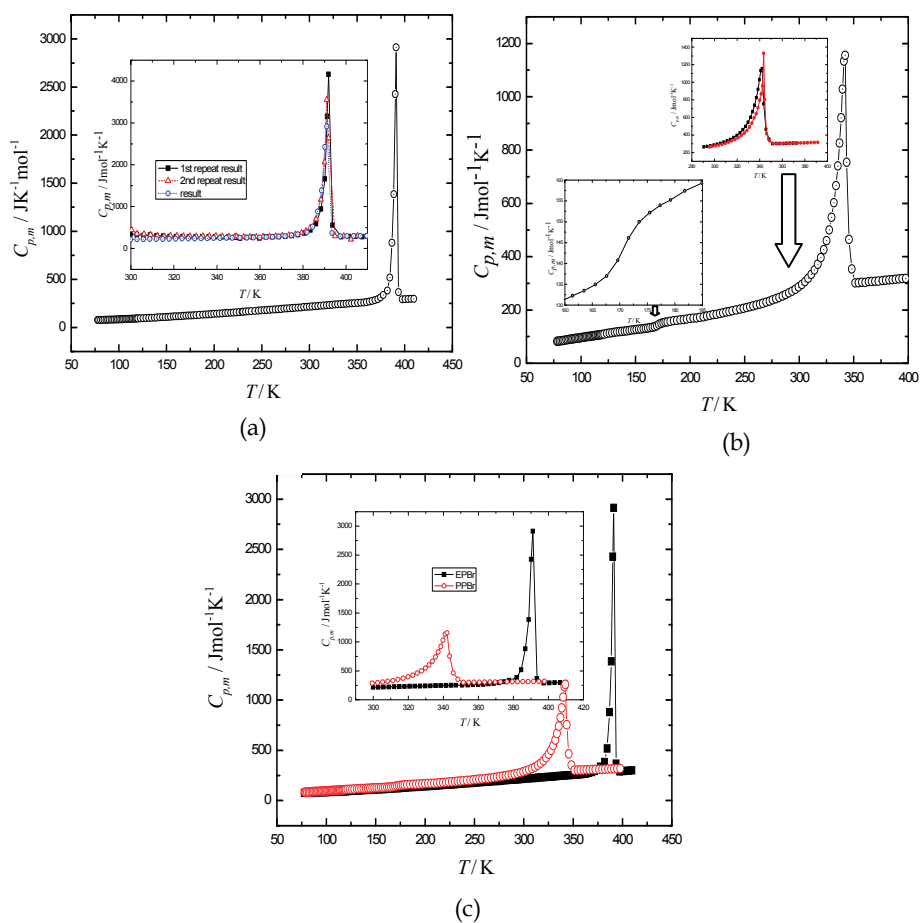


Fig. 2. Experimental molar heat capacity  $C_{p,m}$  as a function of temperature (a) EPBr; (b) PPBr; (c) Comparison from 300 to 400 K

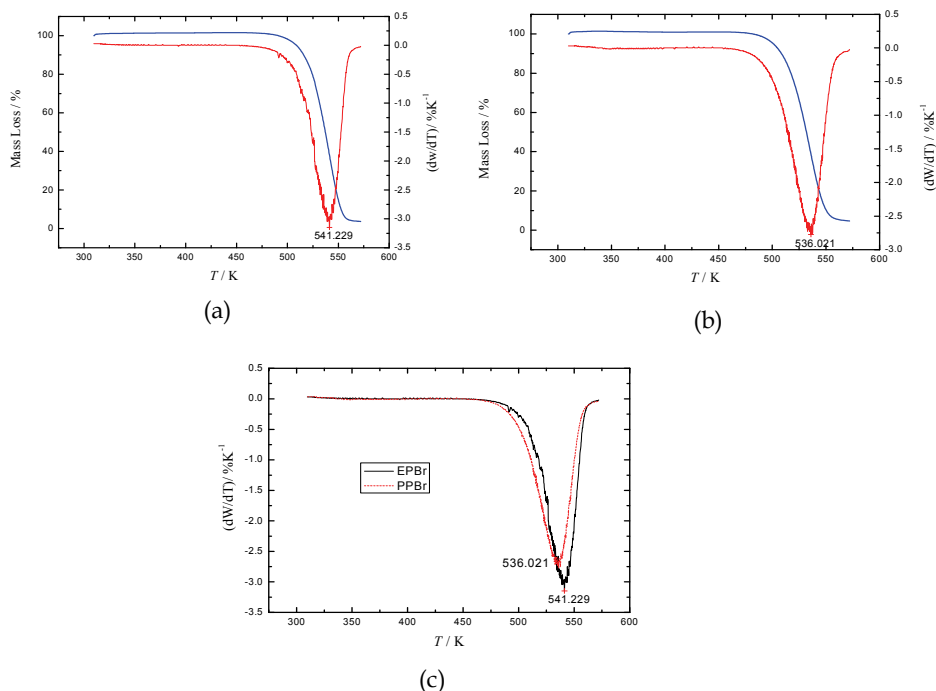


Fig. 3. TG-DTG curves under high purity nitrogen.(a) EPBr; (b) PPBr; (c) DTG curves of two ILS

### 3.5 References

- [1] Earle M.J.; Seddon, K.R. Ionic liquids. *Pure Appl. Chem.*, 2000, 72, 1391-1398.
- [2] Rogers, R.D.; Seddon, K.R. Eds. ACS Symposium Series 818, American Chemical Society: Washington, DC, 2002.
- [3] Rogers, R.D., Seddon, K.R., Eds. ACS Symposium Series 856, American Chemical Society: Washington, DC, 2003, Chapter 12.
- [4] Ikegami S.; Hamamoto H. *Chem. Rev.*, 2009, 109, 583-593.
- [5] Tu, W.W.; Lei, J.P.; Ju, H.X. *Chem-Eur. J.*, 2009, 15, 779-784.
- [6] Xu, H.; Xiong, H.Y.; Zeng, Q.X.; Jia, L.; Wang, Y.; Wang, S.F. *Electrochem. Commun.*, 2009, 11, 286-289.
- [7] Parvulescu, V.I.; Hardacre, C. *Chem. Rev.*, 2007, 107, 2615-2665.
- [8] Singh, M.; Singh, R.S.; Banerjee, U.C. *J. Mol. Catal. B-Enzym.*, 2009, 56, 294-299.
- [9] Karout, A.; Pierre, A.C. *Catal. Commun.*, 2009, 10, 359-361.
- [10] Verevkin, S.P.; Kozlova, S.A.; Emel'yanenko, V. N.; Goodrich, P.; Hardacre, C. *J. Phys. Chem. A*, 2008, 112, 11273-11282.
- [11] Lassegues, J.C.; Grondin, J.; Aupetit, C.; Johansson, P. *J. Phys. Chem. A*, 2009, 113 (1), 305-314.
- [12] Chang, T.M.; Dang, L.X. *J. Phys. Chem. A*, 2009, 113 (10), 2127-2135.

- [13] Hayamizu, K.; Tsuzuki, S. Seki, S. *J. Phys. Chem. A*, 2008, 112 (47), 12027-12036.
- [14] Oxley, J.D.; Prozorov, T. Suslick, K.S. *J. Am. Chem. Soc.*, 2003, 125 (37), 11138-11139.
- [15] Sobota, M.; Dohnal, V.; Vrbka, P. *J. Phys. Chem. B*, 2009, 113, 4323-4332.
- [16] Tong, J.; Liu, Q. S.; Wei, G.; Yang, J. Z. *J. Phys. Chem. B*, 2007, 111, 3197-3200.
- [17] Tong, J.; Liu, Q. S.; Wei, G. X.; Fang, D. W.; Yang, J. Z. *J. Phys. Chem. B*, 2008, 112, 4381-4386.
- [18] Lopes, J.N.C.; Padua, A.A.H. *J. Phys. Chem. B*, 2006, 110, 19586-19592.
- [19] Pham, T.P.T, Cho, C.W.; Jeon, C.O.; Chung, Y.J.; Lee, M.W.; Yun, Y.S. *Environ. Sci. Technol.*, 2009, 43, 516-521.
- [20] Jacob, M. C.; Mark, J. M.; JaNeille, K. D.; Jessica, L. A.; Joan, F. B. *J. Chem. Thermodynamics*, 2005, 37, 559-568.
- [21] Tong, J.; Liu, Q. S.; Peng, Z.; Yang, J. Z. *J. Chem. Eng. Data*, 2007, 52, 1497-1500.
- [22] Tong, J.; Liu, Q. S.; Wei, G.; Yang, J. Z. *J. Chem. Eng. Data*, 2009, 54, 1110-1114.
- [23] Del Popolo, M. G.; Mullan, C. L.; Holbrey, J. D.; Hardacre, C.; Ballone, P. *J. Am. Chem. Soc.*, 2008, 130, 7032-7041.
- [24] Tong, B.; Tan, Z.C.; Shi, Q.; Li, Y.S.; Yue, D.T.; Wang, S.X. *Thermochimi. Acta*, 2007, 457, 20-26.
- [25] Tong, B.; Tan, Z.C.; Zhang, J.N.; Wang, S.X. *J. Therm. Anal. Calorim.*, 2009, 95, 469-475, 2009
- [26] Tan, Z.C.; Shi, Q.; Liu, B.P.; Zhang, H.T. *J. Therm. Anal. Calorim.*, 2008, 92, 367-374.
- [27] Archer, D.G. *J. Phys. Chem. Ref. Data*. 1993, 22, 1411-1453.
- [28] Katritzky, A.R.; Dega-Szafran, Z. *Magn. Reson. Chem.*, 1989, 27, 1090-1093.
- [29] Tong, B.; Tan, Z.C.; Lv, X.C.; Sun, L.X.; Xu, F.; Shi, Q.; Li, Y.S. *J. Therm. Anal. Calorim.*, 2007, 90, 217-221.
- [30] Jiang, D.; Wang Y.Y.; Liu, J.; Dai, L.Y. *Chinese Chem. Lett.* 2007, 5, 371-375.

## 4. Estimation and prediction of physicochemical properties of imidazolium-based ionic liquids

### 4.1 Introduction

The physicochemical properties of ionic liquids (ILs) at 298.15 K could be estimated and predicted in terms of empirical and semi-empirical equations, as well as the interstice model theory. In the present study, the properties of molecular volume, density, standard molar entropy, lattice energy, surface tension, parachor, molar enthalpy of vaporization, interstice volume, interstice fractions, thermal expansion coefficient were discussed. These properties first were estimated through the data of experimental density and surface tension for 1-ethyl-3-methylimidazolium ethylsulfate ([C<sub>2</sub>mim][EtSO<sub>4</sub>]), 1-butyl-3-methylimidazolium octylsulfate ([C<sub>4</sub>mim][OcSO<sub>4</sub>]) and 1-ethyl-3-methylimidazolium bis(trifluoromethanesulfonato)amide ([C<sub>2</sub>mim][NTf<sub>2</sub>]). The properties of molecular volume and parachor of the three homologues imidazolium-based ILs [C<sub>n</sub>mim][EtSO<sub>4</sub>], [C<sub>n</sub>mim][OcSO<sub>4</sub>] and [C<sub>n</sub>mim][NTf<sub>2</sub>] (*n*=1-6) were predicted, and then, the density and surface tension were obtained. Other properties were also calculated using the obtained density and surface tension values. The predicted density was compared to the experimental values for [C<sub>4</sub>mim][NTf<sub>2</sub>] and [C<sub>2</sub>mim][OcSO<sub>4</sub>], which shows that the deviation between experimental and predicted data are within the experimental error. Finally, we compared the values of molar enthalpy of vaporization estimated by Kabo's empirical equation with those predicted by Verevkin's simple rule for [C<sub>2</sub>mim][EtSO<sub>4</sub>],

[C<sub>4</sub>mim][O<sub>3</sub>SO<sub>4</sub>], [C<sub>2</sub>mim][NTf<sub>2</sub>], [C<sub>4</sub>mim][NTf<sub>2</sub>], *N*-butyltrimethylammonium bis(trifluoromethanesulfonato)amide [N<sub>4111</sub>][NTf<sub>2</sub>], *N*-methyltrioctylammonium bis(trifluoromethanesulfonato)amide ([N<sub>8881</sub>][NTf<sub>2</sub>]) and *N*-octyl-3-methylpyridinium tetrafluoroborate ([m<sub>3</sub>opy][BF<sub>4</sub>]), and found that the values obtained by these two equations are in good agreement with each other. Therefore, we suggest that the molar enthalpy of vaporization of ILs can be predicted by Verevkin's simple rule when experimental data for density and surface tension are not available.

ILs as organic salts, often exhibits interesting properties such as low melting points, good solvation properties and non-volatility, which are required both by industrial and scientific communities for their broad application range as electrolytes in batteries and supercapacitors<sup>[1-2]</sup>, reaction media in nanoscience<sup>[3]</sup>, physical chemistry<sup>[4-5]</sup> and many other areas. Therefore, the data of physicochemical properties of ILs are of fundamental for their future application and valuable for an insight into the origins of their unique behavior. Recently, more and more publications reported the experimental physicochemical properties of various ILs <sup>[6-15]</sup>. Although there is a significant amount of data related to imidazolium-based ILs, properties of homologue of [C<sub>*n*</sub>mim][EtSO<sub>4</sub>], [C<sub>*n*</sub>mim][O<sub>3</sub>SO<sub>4</sub>] and [C<sub>*n*</sub>mim][NTf<sub>2</sub>] (*n*=1-6) covered in this research are still limited <sup>[16-17]</sup>. Hence, we estimated various physicochemical properties of [C<sub>2</sub>mim][EtSO<sub>4</sub>], [C<sub>4</sub>mim][O<sub>3</sub>SO<sub>4</sub>], and [C<sub>2</sub>mim][NTf<sub>2</sub>] by using their experimental density and surface tension data. In the next step, the physicochemical properties of their homologues [C<sub>*n*</sub>mim][EtSO<sub>4</sub>], [C<sub>*n*</sub>mim][O<sub>3</sub>SO<sub>4</sub>] and [C<sub>*n*</sub>mim][NTf<sub>2</sub>] (*n*=1-6) were predicted from the estimated values of their molecular volume and parachor. In the present study, the ionic liquid cations are 1-alkyl-3-methylimidazolium [C<sub>*n*</sub>mim]<sup>+</sup>, tetra-alkyl ammonium [TAA]<sup>+</sup>, *N*-octyl-3-methylpyridinium [m<sub>3</sub>opy]<sup>+</sup>; the anions of the ILs are ethylsulfate [EtSO<sub>4</sub>]<sup>-</sup>, octylsulfate [O<sub>3</sub>SO<sub>4</sub>]<sup>-</sup>, bis(trifluoromethanesulfato)amide [NTf<sub>2</sub>]<sup>-</sup> and Tetrafluoroborate [BF<sub>4</sub>]<sup>-</sup>.

## 4.2 Volumetric, entropy and lattice energy

The molecular volume,  $V_m$ , can be calculated from experimental density using the following equation:

$$V_m = M / (N \rho) \quad (1)$$

where  $M$  is molar mass,  $\rho$  is density and  $N$  is Avogadro's constant.

According to Glasser's theory<sup>[18]</sup>, the standard molar entropy could be estimated from the equation:

$$S^0(298.15 \text{ K}) = 1246.5 V_m + 29.5 \quad (2)$$

where  $V_m$  is the molecular volume.

The lattice energy,  $U_{\text{POT}}$ , was estimated according to the following equation <sup>[18]</sup>:

$$U_{\text{POT}}(298.15 \text{ K}) = 1981.2 (\rho / M)^{1/3} + 103.8 \quad (3)$$

where  $M$  is molar mass and  $\rho$  is density.

The contribution methylene (-CH<sub>2</sub>-) group to the molecular volume is 0.0272 nm<sup>3</sup> for [C<sub>*n*</sub>mim][BF<sub>4</sub>]<sup>[18]</sup>, 0.0282 nm<sup>3</sup> for [C<sub>*n*</sub>mim][NTf<sub>2</sub>]<sup>[18]</sup>, 0.0270 nm<sup>3</sup> for [C<sub>*n*</sub>mim][AlCl<sub>4</sub>]<sup>[15]</sup> and 0.0278 nm<sup>3</sup> for [C<sub>*n*</sub>mim][Ala]<sup>[14]</sup>. Due to the similar values of the contribution per -CH<sub>2</sub>- to the molecular volume, the group of methylene in the alkyl chains of the imidazolium-based ILs could be considered to have the similar chemical environment. Hence, the mean value of

the contribution can be calculated to be  $0.0275 \text{ nm}^3$ , the physicochemical properties (density, standard entropy, lattice energy) of the homologues of  $[\text{C}_n\text{mim}][\text{EtSO}_4]$  and  $[\text{C}_n\text{mim}][\text{OcSO}_4]$  ( $n=1-6$ ) could be predicted. Using the value  $0.0282 \text{ nm}^3$  for the contribution per  $-\text{CH}_2-$  to the molecular volume for the homologues of  $[\text{C}_n\text{mim}][\text{NTf}_2]$ <sup>[18]</sup> ( $n=1-6$ ), the physicochemical properties of all IL homologues can be predicted. The calculated density value  $1.4381 \text{ g cm}^{-3}$  for  $[\text{C}_4\text{mim}][\text{NTf}_2]$  is in good agreement with the experimental values  $1.4366$ <sup>[6]</sup>,  $1.43410$  and  $1.43573 \text{ g cm}^{-3}$ <sup>[19]</sup>. The predicted density value  $1.0881 \text{ g cm}^{-3}$  for  $[\text{C}_2\text{mim}][\text{OcSO}_4]$  is also in good agreement with the experimental value of  $1.0942 \text{ g cm}^{-3}$ <sup>[20]</sup>.

All of the estimated and predicted physicochemical property data are listed in Tables 1–3. Based on the plotting,  $S^\theta$ , against the number of the carbons,  $n$ , in the alkyl chain of the ILs (see Fig. 1), the contribution per methylene group to the standard entropy,  $S^\theta$ , was calculated to be  $35.1 \text{ J K}^{-1} \text{ mol}^{-1}$  for  $[\text{C}_n\text{mim}][\text{NTf}_2]$ ,  $34.3 \text{ J K}^{-1} \text{ mol}^{-1}$  for  $[\text{C}_n\text{mim}][\text{EtSO}_4]$  and  $34.3 \text{ J K}^{-1} \text{ mol}^{-1}$  for  $[\text{C}_n\text{mim}][\text{OcSO}_4]$ . The above calculated values are in good agreement with the literature values of  $35.1 \text{ J K}^{-1} \text{ mol}^{-1}$  for  $[\text{C}_n\text{mim}][\text{NTf}_2]$ <sup>[18]</sup>,  $33.9 \text{ J K}^{-1} \text{ mol}^{-1}$  for  $[\text{C}_n\text{mim}][\text{BF}_4]$ <sup>[18]</sup>,  $33.7 \text{ J K}^{-1} \text{ mol}^{-1}$  for  $[\text{C}_n\text{mim}][\text{AlCl}_4]$ <sup>[15]</sup> and  $34.6 \text{ J K}^{-1} \text{ mol}^{-1}$  for  $[\text{C}_n\text{mim}][\text{Ala}]$ <sup>[14]</sup>. According to these various values for the contribution per methylene group to the standard entropy in the homologue series with different anions, it could be concluded that these contributions are relatively similar for all imidazolium-based ILs.

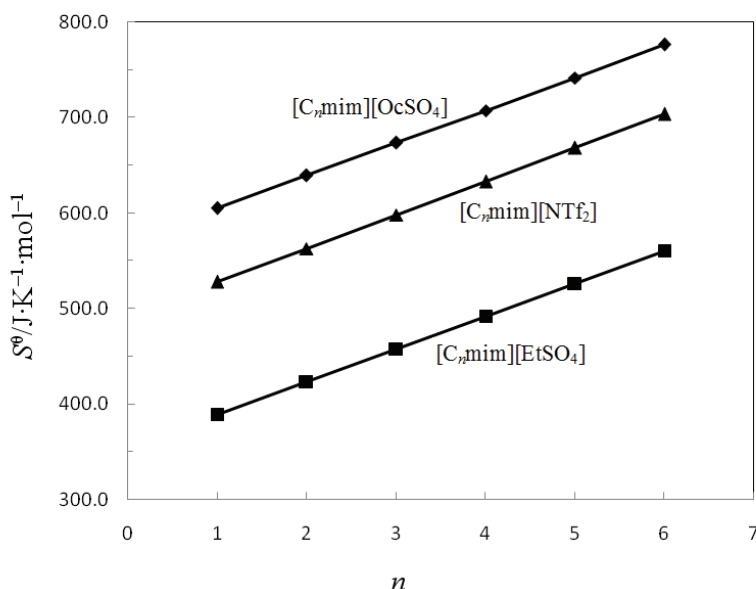


Fig. 1. Plots of  $S^\theta$  against the number of the carbon ( $n$ ), in the alkyl chain of the ILs at 298.15 K  
 —◆—  $S^\theta = 570.7 + 34.27n$ ,  $R = 0.9999$  for  $[\text{C}_n\text{mim}][\text{OcSO}_4]$ ;  
 —▲—  $S^\theta = 492.7 + 35.14n$ ,  $R = 0.9999$  for  $[\text{C}_n\text{mim}][\text{NTf}_2]$ ;  
 —■—  $S^\theta = 355.2 + 34.29n$ ,  $R = 0.9999$  for  $[\text{C}_n\text{mim}][\text{EtSO}_4]$

### 4.3 Parachors and Molar enthalpy of vaporization

The parachor,  $P$ , was estimated from the following equation<sup>[21]</sup>:

$$P=(M\gamma^{1/4})/\rho \quad (4)$$

where  $M$  is molar mass,  $\rho$  is the density and  $\gamma$  is the surface tension.

According to literature [15], the contribution per methylene ( $-\text{CH}_2-$ ) group to parachor is 31.1. The values of parachor for the homologue series of the imidazolium-based ILs  $[\text{C}_n\text{mim}][\text{EtSO}_4]$ ,  $[\text{C}_n\text{mim}][\text{OcSO}_4]$  and  $[\text{C}_n\text{mim}][\text{NTf}_2]$  ( $n = 1-6$ ) were predicted.

The values of molar enthalpy of vaporization were estimated in terms of Kabo's empirical equation [22]:

$$\Delta_g H_m^\theta(298.15 \text{ K})=0.01121(\gamma V^{2/3} N^{1/3})+2.4 \quad (5)$$

where  $V$  is molar volume,  $\gamma$  is the surface tension and  $N$  is the Avogadro's constant.

According to Eq.(4), the surface tension can be calculated from predicted density and parachor data. The calculated value  $31.71 \text{ mJ} \cdot \text{m}^{-2}$  for the surface tension of  $[\text{C}_4\text{mim}][\text{NTf}_2]$  is in good agreement with the experimental value  $32.80 \text{ mJ} \cdot \text{m}^{-2}$  [6]. The molar enthalpy of vaporization,  $\Delta_g H_m^\theta$ , then can be obtained based on the predicted density and surface tension data.

All of these data are listed in Tables 1–3 and 5.

The plots of density,  $\rho$ , and surface tension,  $\gamma$ , against the number of carbon,  $n$ , in alkyl chain of ILs at 298.15 K are shown in Fig. 2 and 3.

From the Figs. 2 and 3, it can be seen that as for density:  $[\text{C}_n\text{mim}][\text{NTf}_2] > [\text{C}_n\text{mim}][\text{EtSO}_4] > [\text{C}_n\text{mim}][\text{OcSO}_4]$  and as for surface tension:  $[\text{C}_n\text{mim}][\text{EtSO}_4] > [\text{C}_n\text{mim}][\text{NTf}_2] > [\text{C}_n\text{mim}][\text{OcSO}_4]$ .

#### 4.4 Interstice model theory

According to the interstice model[23-24] the interstice volume,  $V$ , could be estimated by classical statistical mechanics:

$$V = 0.6791(k_b T / \gamma)^{3/2} \quad (6)$$

where  $k_b$  is the Boltzmann constant,  $T$  is the thermodynamic temperature and  $\gamma$  is the surface tension of ILs.

The molar volume of ionic liquids,  $V$ , consists of the inherent volume,  $V_i$ , and the volume of the interstices; whereas the molar volume of the interstice is  $\sum v = 2Nv$ :

$$V = V_i + 2Nv \quad (7)$$

If the expansion volume of IL only results from the expansion of the interstices when the temperature increase, then, the thermal expansion coefficient,  $\alpha$ , can be predicted from the interstice model:

$$\alpha = (1/V)(\partial V / \partial T)_p = 3Nv / VT \quad (8)$$

All data obtained by this estimation and prediction are listed in Tables 1–3.

The prediction and estimation values in Tables 1–3 of the thermal expansion coefficients are good agreement with experimental values. It also can be noticed that the values of interstice fractions,  $\sum v / V$ , differentiate only about 10–15% for all ILs studied in the present research and these values are in good agreement with the values of volume expansion resulted in the process from solid to liquid state for the majority of materials. Therefore the interstice model is applicable and the interstice model theory can be used to the thermal expansion coefficient of imidazolium-based ILs.

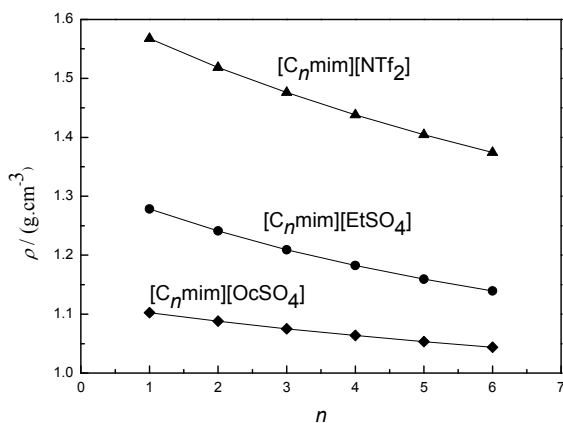


Fig. 2. Plot of density ( $\rho$ ) against  $n$  ( $n=1-6$ ) at 298.15 K

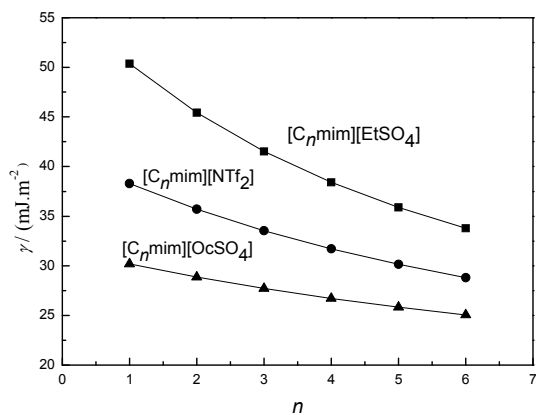


Fig. 3. Plots of surface tension ( $\gamma$ ) against  $n$  ( $n=1-6$ ) at 298.15 K

IL	$V_m$ nm <sup>3</sup>	$\rho$ g cm <sup>-3</sup>	$S^\theta$ J · K <sup>-1</sup> mol <sup>-1</sup>	$U_{POT}$ kJ mol <sup>-1</sup>	$V$ cm <sup>3</sup> mol <sup>-1</sup>	$p$
[C <sub>1</sub> mim][EtSO <sub>4</sub> ] <sup>b</sup>	0.2880	1.2784	389.5	459	173.9	463.2
[C <sub>2</sub> mim][EtSO <sub>4</sub> ] <sup>a</sup>	0.3163	1.2411 <sup>[6]</sup>	423.7	448	190.4	494.3
[C <sub>3</sub> mim][EtSO <sub>4</sub> ] <sup>b</sup>	0.3438	1.2094	458.0	439	207.0	525.4
[C <sub>4</sub> mim][EtSO <sub>4</sub> ] <sup>b</sup>	0.3713	1.1826	492.3	430	223.5	556.5
[C <sub>5</sub> mim][EtSO <sub>4</sub> ] <sup>b</sup>	0.3988	1.1593	526.6	423	240.1	587.6
[C <sub>6</sub> mim][EtSO <sub>4</sub> ] <sup>b</sup>	0.4263	1.1393	560.9	416	256.6	618.7



IL	$\frac{\Delta_{lg}H_m^0}{\text{kJ mol}^{-1}}$	$\frac{10^{24}V}{\text{cm}^3}$	$\frac{\sum V}{\text{cm}^3}$	$10^2 \sum V/V$	$\frac{10^4 \alpha}{\text{K}^{-1}}$	$\frac{\gamma}{\text{mJ m}^{-2}}$
[C <sub>1</sub> mim][EtSO <sub>4</sub> ] <sup>b</sup>	151.0	15.86	19.10	10.98	5.53	50.38
[C <sub>2</sub> mim][EtSO <sub>4</sub> ] <sup>a</sup>	144.7	18.52	22.30	11.71	5.89,5.58 <sup>[6]</sup>	45.44 <sup>[6]</sup>
[C <sub>3</sub> mim][EtSO <sub>4</sub> ] <sup>b</sup>	139.9	21.19	25.52	12.33	6.20	41.53
[C <sub>4</sub> mim][EtSO <sub>4</sub> ] <sup>b</sup>	136.3	23.82	28.68	12.83	6.45	38.42
[C <sub>5</sub> mim][EtSO <sub>4</sub> ] <sup>b</sup>	133.6	26.38	31.76	13.23	6.66	35.89
[C <sub>6</sub> mim][EtSO <sub>4</sub> ] <sup>b</sup>	131.5	28.89	34.78	13.55	6.82	33.78

<sup>a</sup> property data for this IL were estimated values; <sup>b</sup> property data for this IL were predicted values

Table 1. Estimated and predicted values of physicochemical properties of [C<sub>n</sub>mim][EtSO<sub>4</sub>] (n=1-6) at 298.15K

IL	$\frac{V_m}{\text{nm}^3}$	$\frac{\rho}{\text{g cm}^{-3}}$	$\frac{S^0}{\text{J K}^{-1} \text{mol}^{-1}}$	$\frac{U_{\text{POT}}}{\text{kJ mol}^{-1}}$	$\frac{V}{\text{cm}^3 \text{mol}^{-1}}$	$p$
[C <sub>1</sub> mim][NTf <sub>2</sub> ] <sup>b</sup>	0.3998	1.5676	527.9	422	240.7	598.7
[C <sub>2</sub> mim][NTf <sub>2</sub> ] <sup>a</sup>	0.4280	1.5187 <sup>[6]</sup>	563.0	415	257.7	629.8
[C <sub>3</sub> mim][NTf <sub>2</sub> ] <sup>b</sup>	0.4562	1.4759	598.2	409	274.6	660.9
[C <sub>4</sub> mim][NTf <sub>2</sub> ] <sup>b</sup>	0.4844	1.4381	633.3	403	291.6	692.0
[C <sub>4</sub> mim][NTf <sub>2</sub> ] <sup>a</sup>	0.4849	1.4366 <sup>[6]</sup>	633.9	402	291.9	698.6
[C <sub>4</sub> mim][NTf <sub>2</sub> ] <sup>a</sup>	0.4857	1.43410 <sup>[19]</sup>	635.0	402	292.4	
[C <sub>4</sub> mim][NTf <sub>2</sub> ] <sup>a</sup>	0.4852	1.43573 <sup>[19]</sup>	634.3	402	292.1	
[C <sub>5</sub> mim][NTf <sub>2</sub> ] <sup>b</sup>	0.5126	1.4044	668.5	397	308.6	723.1
[C <sub>6</sub> mim][NTf <sub>2</sub> ] <sup>b</sup>	0.5408	1.3743	703.6	392	325.6	754.2

IL	$\frac{\Delta_{lg}H_m^0}{\text{kJ mol}^{-1}}$	$\frac{10^{24}v}{\text{cm}^3}$	$\frac{\sum v}{\text{cm}^3}$	$10^2 \sum V/V$	$\frac{10^4 \alpha}{\text{K}^{-1}}$	$\frac{\gamma}{\text{mJ m}^{-2}}$
C <sub>1</sub> mim][NTf <sub>2</sub> ] <sup>b</sup>	142.6	23.94	28.82	11.98	6.02	38.29
C <sub>2</sub> mim][NTf <sub>2</sub> ] <sup>a</sup>	139.2	26.59	32.01	12.43	6.25,6.66 <sup>[6]</sup>	35.70 <sup>[6]</sup>
C <sub>3</sub> mim][NTf <sub>2</sub> ] <sup>b</sup>	136.5	29.20	35.16	12.80	6.44	33.54
C <sub>4</sub> mim][NTf <sub>2</sub> ] <sup>b</sup>	134.4	31.76	38.24	13.11	6.60	31.71
C <sub>4</sub> mim][NTf <sub>2</sub> ] <sup>a</sup>	139.0	30.19	36.35	12.45	6.27,6.73 <sup>[6]</sup>	32.80 <sup>[6]</sup>
[C <sub>4</sub> mim][NTf <sub>2</sub> ] <sup>a</sup>						
[C <sub>4</sub> mim][NTf <sub>2</sub> ] <sup>a</sup>						
C <sub>5</sub> mim][NTf <sub>2</sub> ] <sup>b</sup>	132.7	34.26	41.25	14.13	6.72	30.15
C <sub>6</sub> mim][NTf <sub>2</sub> ] <sup>b</sup>	131.4	36.70	44.18	14.32	6.83	28.80

<sup>a</sup> property data for this IL were estimated values; <sup>b</sup> property data for this IL were predicted values

Table 2. Estimated and predicted values of physicochemical properties of [C<sub>n</sub>mim][NTf<sub>2</sub>] (n=1-6) at 298.15 K

IL	$\frac{V_m}{\text{nm}^3}$	$\frac{\rho}{\text{g cm}^{-3}}$	$\frac{S^\theta}{\text{J K}^{-1} \text{mol}^{-1}}$	$\frac{U_{\text{pot}}}{\text{kJ mol}^{-1}}$	$\frac{V}{\text{cm}^3 \text{mol}^{-1}}$	$p$
[C <sub>1</sub> mim][OcSO <sub>4</sub> ] <sup>b</sup>	0.4617	1.1025	605.0	407	277.9	651.5
[C <sub>2</sub> mim][OcSO <sub>4</sub> ] <sup>b</sup>	0.4892	1.0881	639.3	402	294.5	682.6
[C <sub>2</sub> mim][OcSO <sub>4</sub> ] <sup>a</sup>	0.4866	1.0942 <sup>[20]</sup>	636.0	402	293.0	
[C <sub>3</sub> mim][OcSO <sub>4</sub> ] <sup>b</sup>	0.5167	1.0753	673.6	396	311.1	713.7
[C <sub>4</sub> mim][OcSO <sub>4</sub> ] <sup>a</sup>	0.5442	1.0638 <sup>[6]</sup>	707.8	391	327.6	744.8
[C <sub>5</sub> mim][OcSO <sub>4</sub> ] <sup>b</sup>	0.5717	1.0534	742.1	387	344.2	775.9
[C <sub>6</sub> mim][OcSO <sub>4</sub> ] <sup>b</sup>	0.5992	1.0439	776.4	382	360.7	807.0
IL	$\frac{\Delta_f H_m^\theta}{\text{kJ mol}^{-1}}$	$\frac{10^{24} V}{\text{cm}^3}$	$\frac{\sum V}{\text{cm}^3}$	$10^2 \sum V/V$	$\frac{10^4 \alpha}{\text{K}^{-1}}$	$\frac{\gamma}{\text{mJ m}^{-2}}$
[C <sub>1</sub> mim][OcSO <sub>4</sub> ] <sup>b</sup>	124.1	34.19	41.17	14.81	7.45	30.19
[C <sub>2</sub> mim][OcSO <sub>4</sub> ] <sup>b</sup>	123.3	36.58	44.05	14.96	7.52	28.86
[C <sub>2</sub> mim][OcSO <sub>4</sub> ] <sup>a</sup>						
[C <sub>3</sub> mim][OcSO <sub>4</sub> ] <sup>b</sup>	122.8	38.86	46.79	15.04	7.57	27.72
[C <sub>4</sub> mim][OcSO <sub>4</sub> ] <sup>a</sup>	122.6	41.09	49.47	15.10	7.59, 6.21 <sup>[6]</sup>	26.71 <sup>[6]</sup>
[C <sub>5</sub> mim][OcSO <sub>4</sub> ] <sup>b</sup>	122.5	43.20	52.02	15.11	7.60	25.83
[C <sub>6</sub> mim][OcSO <sub>4</sub> ] <sup>b</sup>	122.6	45.24	54.47	15.10	7.60	25.05

<sup>a</sup> property data for this IL were estimated values; <sup>b</sup> property data for this IL were predicted values

Table 3. Estimated and predicted values of the physicochemical properties of [C<sub>n</sub>mim][OcSO<sub>4</sub>] (*n*=1-6) at 298.15 K

#### 4.5 Prediction of enthalpy of vaporization

Recently, Verevkin<sup>[25]</sup> has published an article titled “Predicting Enthalpy of Vaporization of Ionic Liquids: A Simple Rule for a Complex Property” in which he predicted molar enthalpy of vaporization of ILs by a simple rule in case of lack of experimental data. He proposed following simple rule:

$$\Delta_f H_m^\theta(\text{IL}) = \sum n_i \Delta H_i + \sum n_j \Delta H_j \quad (9)$$

where  $\Delta H_i$  is the contribution of the *i*th element,  $n_i$  is the number of the element of the *i*th type in ILs,  $\Delta H_j$  is the contribution of the *j*th structural correction and  $n_j$  is the number of the element of the *j*th structural correction in ILs. The parameters<sup>25</sup> for predicting the molar enthalpy of vaporization of ILs are listed in Table 4.

Verevkin pointed out that “a special structural correction could be also necessary for quaternary ammonium based ILs”<sup>[25]</sup>. Herein, the structure of the quaternary ammonium cation is regarded to be the ring of imidazolium cation, therefore, their structural correction parameter is  $\Delta H = 27.1 \text{ kJ mol}^{-1}$ . The predicted data are listed in Table 5. From this table, the values of the molar enthalpy of vaporization,  $\Delta_f H_m^\theta$ , predicted by Eq. (9) are in good agreement with the values estimated by Eq. (5) except for C<sub>4</sub>mim[OcSO<sub>4</sub>]. This is because that the Eq. (5) is valid mainly for ILs [C<sub>n</sub>mim][NTf<sub>2</sub>]. Indeed, the assumption to consider the quaternary ammonium cation as a ring system needs further confirmation.

Parameter (kJ mol <sup>-1</sup> )	Value	Parameter (kJ mol <sup>-1</sup> )	Value
$\Delta H_C$	2.5	$\Delta H_P$	4.1
$\Delta H_N$	26.3	$\Delta H_S$	-8.2
$\Delta H_O$	23.6	$\Delta H_{CF_3}$	-63.1
$\Delta H_B$	23.0	$\Delta H_{ring}$	27.1
$\Delta H_F$	13.7		

Table 4. Parameters for predicting the enthalpy of vaporization of ILs at 298.15 K<sup>[25]</sup>

ILs	$\frac{\rho}{\text{g cm}^{-3}}$	$\frac{\gamma}{\text{mJ m}^{-2}}$	$\frac{\Delta_g H_m^0}{\text{kJ mol}^{-1,a}}$	$\frac{\Delta_g H_m^0}{\text{kJ mol}^{-1,b}}$
[C <sub>2</sub> mim][EtSO <sub>4</sub> ]	1.2411 <sup>[6]</sup>	45.44 <sup>[6]</sup>	158.8	144.7
[C <sub>2</sub> mim][NTf <sub>2</sub> ]	1.5187 <sup>[6]</sup>	35.70 <sup>[6]</sup>	132.9	139.3
[C <sub>4</sub> mim][NTf <sub>2</sub> ]	1.4366 <sup>[6]</sup>	32.80 <sup>[6]</sup>	137.9	139.0
[C <sub>4</sub> mim][OcSO <sub>4</sub> ]	1.0638 <sup>[6]</sup>	26.71 <sup>[6]</sup>	178.8	122.5
[N <sub>4111</sub> ][NTf <sub>2</sub> ]	1.3940 <sup>[6]</sup>	32.46 <sup>[6]</sup>	136.2	135.3
[N <sub>8881</sub> ][NTf <sub>2</sub> ]	1.1046 <sup>[6]</sup>	27.93 <sup>[6]</sup>	181.2	187.8
[m <sub>3</sub> opy][BF <sub>4</sub> ]	1.0945 <sup>[8]</sup>	36.51 <sup>[8]</sup>	166.2	167.4

<sup>a</sup> data predicted from Eq.(9); <sup>b</sup> data estimated from Eq.(5)

Table 5. The values of the molar enthalpy of vaporization of ILs at 298.15 K

#### 4.6 Conclusions

The physicochemical properties (molecular volume, molar volume, parachor, interstice volume, interstice fractions, thermal expansion coefficient, standard entropy, lattice energy and molar enthalpy of vaporization) of [C<sub>2</sub>mim][EtSO<sub>4</sub>], [C<sub>4</sub>mim][OcSO<sub>4</sub>] and [C<sub>2</sub>mim][NTf<sub>2</sub>] were estimated by using their experimental data of density and surface tension. Based on the estimated data of the molecular volume and parachor, the physicochemical properties (density, surface tension and all of the properties mentioned above) for their homologue series [C<sub>*n*</sub>mim][EtSO<sub>4</sub>], [C<sub>*n*</sub>mim][OcSO<sub>4</sub>] and [C<sub>*n*</sub>mim][NTf<sub>2</sub>] (*n*=1-6) were predicted.

We compared the values of molar enthalpy of vaporization for [C<sub>2</sub>mim][EtSO<sub>4</sub>], [C<sub>4</sub>mim][OcSO<sub>4</sub>], [C<sub>2</sub>mim][NTf<sub>2</sub>], [C<sub>4</sub>mim][NTf<sub>2</sub>], [N<sub>4111</sub>][NTf<sub>2</sub>], [N<sub>8881</sub>][NTf<sub>2</sub>] and [m<sub>3</sub>opy][BF<sub>4</sub>], estimated by Kabo's empirical equation with those predicted by Verevkin's simple rule, and found that the values calculated in terms of the two approaches are in good agreement with each other. Hence, it is suggested that the molar enthalpy of vaporization of ILs could be estimated in terms of Verevkin's simple rule when the experimental data is not available.

#### 4.6 Acknowledgement

The authors gratefully acknowledge the National Nature Science Foundation of China for providing financial support to carry out the studies under the Grant NSFC No 21073189, 21003068, 21071073.

## 4.7 References

- [1] Tsunashima, K.; Sugiya, M. *Electrochem. Commun.*, 2007, 9: 2353
- [2] Seki, S.; Kobayashi, Y.; Miyashiro, H.; Ohno, Y.; Usami, A.; Mita, Y.; Watanabe, M.; Terada, N. *Chem. Commun.*, 2006, 544
- [3] Itoh, H.; Naka, K.; Chujo, Y. *J. Am. Chem. Soc.*, 2004, 126: 3026
- [4] Du, Z.; Yu, Y. L.; Wang, J. H. *Chem. Eur. J.*, 2007, 13: 2130
- [5] Endres, F.; Abedin, S. Z. E. *Phys. Chem. Chem. Phys.*, 2006, 8: 2101
- [6] Wandschneider, A.; Lehmann, J. K.; Heintz, A. *J. Chem. Eng. Data*, 2008, 53: 596
- [7] Bandres, I.; Giner, B.; Artigas, H.; Lafuente, C.; Royo, F. M. *J. Chem. Eng. Data*, 2009, 54: 236
- [8] Sun, J.; Forsyth, M.; MacFarlane, D. R. *J. Phys. Chem. B*, 1998, 102: 8858
- [9] Tokuda, H.; Hayamizu, K.; Ishii, K.; Susan, M. A. B. H.; Watanabe, M. *J. Phys. Chem. B*, 2004, 108: 16593
- [10] Tokuda, H.; Ishii, K.; Susan, M. A. B. H.; Tsuzuki, S.; Hayamizu, K.; Watanabe, M. *J. Phys. Chem. B*, 2006, 110: 2833
- [11] Bandrés, I.; Giner, B.; Artigas, H.; Royo, F. M.; Lafuente, C. *J. Phys. Chem. B*, 2008, 112: 3077
- [12] Tong, J.; Liu, Q. S.; Guan, W.; Yang, J. Z. *J. Phys. Chem. B*, 2007, 111: 3197
- [13] Tong, J.; Liu, Q. S.; Zhang, P.; Yang, J. Z. *J. Chem. Eng. Data*, 2007, 52: 1497
- [14] Fang, D. W.; Guan, W.; Tong, J.; Wang, Z. W.; Yang, J. Z. *J. Phys. Chem. B*, 2008, 112: 7499
- [15] Tong, J.; Liu, Q. S.; Xu, W. G.; Fang, D. W.; Yang, J. Z. *J. Phys. Chem. B*, 2008, 112: 4381
- [16] Fernández, A.; Torrecilla, J. S.; García, J.; Rodríguez, F. *J. Chem. Eng. Data*, 2007, 52: 1979
- [17] Fernández, A.; García, J.; Torrecilla, J. S.; Oliet, M.; Rodríguez, F. *J. Chem. Eng. Data*, 2008, 53: 1518
- [18] Glasser, L. *Thermochim. Acta*, 2004, 421: 87
- [19] Troncoso, J.; Cerdeirina, C. A.; Sanmamed, Y. A.; Romani, L.; Rebelo, L. P. N. *J. Chem. Eng. Data*, 2006, 51: 1856
- [20] Hasse, B.; Lehmann, J.; Assenbaum, D.; Wasserscheid, P.; Leipertz, A.; Froba, A. P. *J. Chem. Eng. Data*, 2009, 54: 2576
- [21] Deetlefs, M.; Seddon, K. R.; Shara, M. *Phys. Chem. Chem. Phys.*, 2006, 8: 642
- [22] Zaitsau, D. H.; Kabo, G. J.; Strechan, A. A.; Paulechka, Y. U.; Tschersich, A.; Verevkin, S. P.; Heintz, A. *J. Phys. Chem. A*, 2006, 110: 7303.
- [23] Yang, J. Z.; Lu, X. M.; Gui, J. S.; Xu, W. G. *Green Chem.*, 2004, 6: 541
- [24] Zhang, Q. G.; Yang, J. Z.; Lu, X. M.; Gui, J. S.; Huang, M. *Fluid Phase Equilib.*, 2004, 226: 207
- [25] Verevkin, S. P. *Angew. Chem. Int. Edit.*, 2008, 47: 5071

# Thermal Properties of Ionic Liquids and Ionanofluids

A.P.C. Ribeiro, S. I. C. Vieira, J. M. França, C. S. Queirós, E. Langa,  
M. J. V. Lourenço, S. M. S. Murshed and C. A. Nieto de Castro  
*Faculdade de Ciências da Universidade de Lisboa  
Portugal*

## 1. Introduction

The current world economy and energy situation demands the search for alternative energies to conventional fuels, the optimization of current energy technologies, and the search for new and clean working fluids. In the field of heat transfer, all current liquid coolants used at low and moderate temperatures exhibit very poor thermal conductivity and heat storage capacities, as the classical equipments for heat transfer use working fluids that were developed, tested and applied in a world of positive economical growth. In contrast, the uses of chemical technologies today are considered unsustainable. Although increased heat transfer can be achieved creating turbulence, increasing surface area and so on, ultimately the transfer will still be limited by the low thermal conductivity of the conventional fluids. Therefore, there is a need for new and efficient heat transfer liquids that can meet the cooling challenges for advanced devices as well as energy conversion for domestic and industrial applications.

Ionic liquids (IL) have proven to be safe and sustainable alternatives for many applications in industry and chemical manufacturing. Their success arises mainly from their thermophysical and phase-equilibria properties, and the versatility of their synthesis, manageable to be tailored for a given application. Their solvent properties as well as their heat transfer or heat storage and surface properties make this class of fluids possible to use in a high plethora of applications (Earle & Seddon, 2007; Nieto de Castro & Santos, 2007). Other advantages of ionic liquids include high ionic conductivity, high chemical and thermal stabilities, negligible vapor pressure and an ability to dissolve a wide range of inorganic and organic compounds. Due to all of these fascinating characteristics they have been investigated extensively as alternatives to molecular solvents for liquid phase reactions (Wasserscheid & Welton, 2007; Pârvulescu & Hardacre, 2007). Ionic liquids are of great interest to scientists as well as chemical companies, not only because of their interesting properties, but also for their actual and potential applications in the chemical process industries. In the past, the values of their thermophysical properties found to have significant effect on the design of physico-chemical processing and reaction units, influencing directly the design parameters and performance of equipments like heat exchangers, distillation columns and reactors (França et al., 2009). Their thermophysical properties justify the replacement of several of the chemical processes now under exploitation, and some of the solvents used, because they can, in certain conditions, be

considered as green solvents. However the optimal technological design of green processes requires the characterization of the ionic liquids used, namely their thermodynamic, transport and dielectric properties.

Thermophysical properties data of ionic liquids, that we can trust, not only because the samples are well purified and characterized, but also because the uncertainty of the data is well discussed, are needed for several applications and for the design of chemical plants. They can be obtained from experimental measurements, predictive or estimation techniques. Although there were some interesting developments in this last area, by using group contribution methods, the calculation of the thermophysical properties of ionic liquids with more or less theoretical based schemes is still very difficult, but useful for some properties (Gardas & Coutinho, 2009). Experiment, although not yet perfect, is still our main source of information. Recently, our group has reported few works (França et al., 2009; Nieto de Castro et al., 2010; Nunes et al., 2010) where experimental data on thermophysical properties of numerous ionic liquids are presented besides analyzing details of the situation of the values of these thermophysical properties, measurement methods and uncertainty as well as their potential applications including as heat transfer fluids.

The screening of all possibilities revealed in a recent review article (Murshed et al., 2008a) lead us to use nanofluids with ionic liquid as base fluids. Considering the fact that solid materials or particles, namely nanoparticles or carbon nanotubes (CNTs) have orders of magnitude higher thermal conductivity at room temperature than the base fluids, it has been shown that the thermal conductivity of fluids containing suspended particles (metallic, non-metallic) could be significantly higher than the base fluids (Murshed et al., 2008a). With this classical idea and applying nanotechnology to heat transfer, Steve Choi from Argonne National Laboratory of USA (Choi, 1995) coined the term "*nanofluid*" to designate a new class of heat transfer fluids which is formed by the dispersion of nanometer sized solid particles, rods or tubes in traditional heat transfer fluids such as water, ethylene glycol, and engine oil. From the investigations performed thereafter, nanofluids were found to have higher thermal conductivity and thermal diffusivity than those of the base fluids (Murshed et al., 2005, 2006 & 2008a). The suspensions or emulsions are stable and Newtonian, and these nanofluids have been proposed as 21st century heat transfer agents for cooling devices which respond more efficiently to the challenges of great heat loads, higher power engines and brighter optical devices, increased transportation, micromechanics, instrumentation, HVAC (heating, ventilating and air-conditioning) and medical applications (Das et al., 2006; Murshed et al., 2008a). Some researchers already considered these nanofluids to be the cooling media of the future (Das, 2006). Although significant progress has been made, variability and controversies in the heat transfer characteristics (Kebllinski et al., 2008; Murshed et al., 2009) still exist which may be the result from the synthesis of the nanofluids being quite delicate. In fact, a nanofluid does not necessarily mean a simple mixture of nanoparticles and a liquid and the techniques used by different authors are sometimes ill-defined (Das, 2006; Murshed et al., 2008a).

Previous studies in nanofluids have used common liquids such as water, ethylene glycol or oils. No innovation has been made so far in the base fluids, until the work of (Nieto de Castro et al., 2010) where results for the thermal conductivity of several ionic liquids containing CNTs are presented. In addition to aforementioned advantages and applications, these liquids are also currently under intense study for chemical and materials processing, as environmentally friendly solvents and reaction fluids ("green" solvents) (Wasserscheid & Welton, 2007; Earle & Seddon, 2000; Nunes et al., 2010). These fluids are generally non-

flammable and non-volatile under ambient conditions and their thermophysical properties, being compatible with the requisites of heat transfer fluids, can be fine-tuned by their structure and tailored to satisfy the specific application requirements. According to the American National Renewable Energy Laboratory there have been no major developments in the field of thermal energy storage systems in the 1990's and the discovery of ionic liquids systems qualifies them as viable thermal fluids, a fact that is supported by recent applications as thermal fluids (Holbrey, 2007; França et al., 2009).

The discovery that carbon nanotubes and room-temperature ionic liquids can be blended to form gels that may be used to make novel electronic devices, coating materials, and antistatic materials, opens a completely new field (Fukushima et al., 2003; Fukushima & Aida, 2007). Blends or emulsions of ionic liquids with nanomaterials, mostly nanocarbons (tubes, fullerenes, and spheres) are termed as *Bucky gels*. The possibility of using ionic liquids containing dispersed nanoparticles with specific functionalization, for example single-walled nanotubes (SWCNTs), multi-walled nanotubes (MWCNTs) and fullerenes (C60, C80, etc.), opens the door to many potential applications. The use of nanoparticles as heat transfer enhancer allows us to associate small quantities of different types of nanomaterials to ionic liquids (i.e. ionanofluids), which are highly flexible such that they can be designed (target-oriented) in terms of molecular structure, to achieve the desired properties necessary to accomplish a given job. Complex systems based on nanomaterials and common solvents such as nanofluids proved to have thermophysical properties that can revolutionize the actual utilization of heat transfer fluids and heat storage cycles. This is mainly due to the existence of thermal conductivity enhancements derived from the presence of additional mechanisms of heat transfer, in comparison with the base solvent.

If nanoparticulates in any shapes and structures (e.g., spheres, cylinder or tubes) are dissolved or mixed as a thermally stable suspension in ionic liquids, "bucky gels" termed as "Ionanofluids" are formed. These ionanofluids have recently been found to have enhanced thermal conductivity ranging from 2 to 35%, and heat capacity compared to their base ionic liquids (Nieto de Castro et al., 2010; Ribeiro et al., 2010). Since these ionanofluids have fascinating features such as high thermal conductivity, high volumetric heat capacity and are non-volatile, they can potentially be used as novel heat transfer fluids.

Another fascinating area of application of the ionanofluids is their use in the development of new pigments for solar paint coatings, with high solar absorbance and the same thermal emissivity when compared with the base paint (Vieira et al., 2010), having a color different from black, with high importance in solar energy thermal conversion for architectural use. Preliminary work performed by this group, using carbon nanotubes, [C<sub>6</sub>mim][PF<sub>6</sub>] and crystal violet, showed a net gain in the paint efficiency ( $a_s/\epsilon_T$ ) of 0.45 to 0.57.

The purpose of this chapter is to present and analyze the most important thermal properties for an optimal technological design of process plants, namely thermal conductivity and heat capacity of ionic liquids and ionanofluids, from experimental data to molecular modeling of heat transfer and storage in these types of systems. Ionic liquids based on C<sub>n</sub>mim cations and (CF<sub>3</sub>SO<sub>2</sub>)<sub>2</sub>N, BF<sub>4</sub>, PF<sub>6</sub> anions are used to illustrate the most important behaviors. The thermal conductivity and specific heat capacity data of several ionic liquids including 1-hexyl-3-methylimidazolium tetrafluoroborate, [C<sub>6</sub>mim][BF<sub>4</sub>], 1-butyl-3-methylimidazolium hexafluorophosphate, [C<sub>4</sub>mim][PF<sub>6</sub>], 1-hexyl-3-methylimidazolium hexafluorophosphate, [C<sub>6</sub>mim][PF<sub>6</sub>], 1-butyl-3-methylimidazolium trifluoromethanesulfonate, [C<sub>4</sub>mim][CF<sub>3</sub>SO<sub>3</sub>] and 1-butyl-1-methylpyrrolidinium bis((trifluoromethyl)sulfonyl)imide, [C<sub>4</sub>mpyr][[(CF<sub>3</sub>SO<sub>2</sub>)<sub>2</sub>N] and multi-walled carbon nanotubes (MWCNTs) ionanofluids as a

function of temperature are presented and discussed in this chapter. New results on the application of natural nanomaterials in heat transfer and storage are also presented.

## 2. Sample preparation and characterization

All ionic liquids used were synthesized and purified following the procedure given elsewhere (Bonhote et al., 1996; Holbrey et al., 2001). They were prepared through metathesis reactions from the appropriate  $[C_n\text{mim}]\text{Cl}$ . Prior to use samples were extensively washed using distilled water and dried overnight at 70 °C under high vacuum (0.1 Pa). Sample ionic liquids were analyzed by  $^1\text{H}$  and  $^{13}\text{C}$  NMR and elemental analysis. The water content was measured using Coulometric Karl-Fisher titration (Metrohm 831) before and after each measurement. In all cases, the water mass fraction was found to be less than 0.0002. The halide content of ionic liquids was determined using suppressed ion chromatography as described in (Villagran et al., 2004) and all ionic liquids had a chloride mass fraction of less than  $5 \cdot 10^{-6}$ , unless otherwise stated.

The carbon nanotubes used were Baytubes® C150 HP of Multi-Walled Carbon Nanotubes (MWCNTs) from Bayer Material Science (Germany). According to Bayer Material Science, the specifications of MWCNTs are given in Table 1. Baytubes® are produced from a high-yielding catalytic process based on chemical vapor deposition. The process yields easy to handle agglomerates with high apparent density. The optimized process results in a high degree of purity (low concentration of residual catalyst and absence of free amorphous carbon). Baytubes® are agglomerates of multi-wall carbon nanotubes with small outer diameters, narrow diameter distribution, and an ultra-high aspect ratio (length-to-diameter ratio). They show excellent tensile strength and E-modulus, as well as exceptional thermal and electrical conductivities. Aida and co-workers (Fukushima et al., 2003; Fukushima & Aida, 2007) found that imidazolium-ion-based ionic liquids were excellent dispersants for CNTs forming physical gels. Similar techniques were followed in this study to obtain very stable emulsions for 0.5 to 3% (w/w) loadings of MWCNTs (Sonicator Sonics & Materials, Model VC50) in various ionic liquids.

Property	Value	Unit	Method
C-Purity	> 99	%	Elementary analysis
Free amorphous carbon	Not detectable	%	TEM
Number of walls	3-15	-	TEM
Outer mean diameter	13-16	nm	TEM
Outer diameter distribution	5-20	nm	TEM
Inner mean diameter	4	nm	TEM
Inner diameter distribution	2-6	nm	TEM
Length	1-10	$\mu\text{m}$	SEM
Bulk density	140-230	$\text{kg}\cdot\text{m}^{-3}$	EN ISO 60

Table 1. Specifications of Baytubes® product used

Figure 1 shows the ionanofluid for  $[C_4\text{mim}][(\text{CF}_3\text{SO}_2)_2\text{N}]+0.5\%(\text{w/w})$  MWCNTs. The liquid is black, coloured by the Baytubes®, and viscous. The gel is stable but special care is to be taken in its production.





Fig. 1. Filling a thermal conductivity cell with the ionanofluid  $[\text{C}_4\text{mim}][(\text{CF}_3\text{SO}_2)_2\text{N}] + 0.5\%(\text{w/w})$  MWCNTs.

### 3. Experimental details

In this study, a KD2 Pro Thermal Properties Analyzer (Labcell Ltd., UK) was used to measure the thermal conductivity of sample fluids. The measurement principle of KD2 is based on the transient hot-wire technique. Instead of using a bare wire, an electrically isolated thermal probe coated with a thin coating of an insulator is used as the ionic liquids are electrically conducting liquids (Ramires et al., 1994; Chen et al., 2008; Nunes et al., 2010). The thermal probe of this KD2 analyzer has 1.3 mm diameter and 60 mm length and contains both the heating element and thermoresistor. This probe should be inserted into the sample vertically, rather than horizontally, to minimize the possibility of inducing convection. The measurement is made by heating the probe within the sample while simultaneously monitoring the temperature change of the probe. A microprocessor connected to the probe is used to control the heating rate and to measure the temperature change data. The thermal conductivity is then calculated based on a parameter-corrected version of the transient temperature model given by Carslaw and Jaeger (Carslaw & Jaeger, 1959) for an infinite line heat source with constant heat output and zero mass in an infinite medium. For this model to accurately describe the physical behavior of a system, the heat source must closely approximate an infinitely long and as thin as possible wire. This KD2 analyzer used the solutions for a heated cylindrical source with a non-negligible radius and finite length as described by Kuitenberg and co-workers (Kuitenberg et al., 1993). Both models give good fit to the temperature data but differ slightly in value of the fitting parameters and these differences can be accounted for by the careful calibration allowing

the former (simpler also) model to be widely used and it has been employed herein (Chen et al., 2008). Before and after analysis of the sample liquids, the meter was calibrated using water and a standard sample of glycerol of known thermal conductivity. Approximately 15 cm<sup>3</sup> of the sample to be analyzed was sealed in a glass sample vial. The probe was inserted vertically into the sample via a purpose-made port in the lid of the vial. The sealed vial was then fully immersed in a temperature-controlled water bath (Grant GD120) which allowed equilibrating at the desired temperature of the test sample. Once the sample reached the required temperature, a further 15 min was allowed to pass before carrying out the measurement to ensure complete temperature equilibration and stability. At least four measurements were taken at each temperature, with a delay of at least 15 min between each measurement, to ensure reproducibility. More details about the measurement procedure can be found in a work (Ge et al., 2007) where KD2 Pro device was also used to measure thermal conductivity of several ionic liquids. Based on the standard deviations of experimental and calibration data, the uncertainty of the thermal conductivity and temperature measurements were estimated to be  $\pm 0.005 \text{ W m}^{-1} \text{ K}^{-1}$  and  $\pm 1 \text{ K}$ , respectively. On the other hand, the heat capacity measurements were performed with a differential scanning calorimeter (DSC-111, Setaram, France) which was calibrated in enthalpy (Joule effect) and temperature following the procedure described by (Nieto de Castro et al., 2000; ; Lourenço et al., 2006). This calorimeter is a heat-flux DSC which operates based on the Tian-Calvet principle and uses a cylinder type measuring system composed by two sintered alumina cylinder tubes. These tubes are set parallel to each other in the heating furnace. The sensing part of this calorimeter is the central portion of the cylinders and thermocouple-carrying heat-flux transducers (thermopiles) are wrapped around this central portion. The heat flow can then be measured by the temperature changes in these transducers. Details of the experimental procedure and calibration of this DSC can be found elsewhere (Nieto de Castro et al., 2000; Lourenco et al., 2006) and will not be elaborated here. In this study, the melting temperatures of Hg, Ga, In, Sn, Pb and Zn were used to calibrate the temperature as indicated in the instrument user manual and the heat of fusion of these metals was used to assess the calibration uncertainty due to the Joule effect. Table 2 shows the reference materials used, their origin and purity, as well as the recommended values for the enthalpies and temperatures of fusion. Calibration materials used were chosen from the published references as well as from the Certified Reference Materials Certificate (CRMC) – LGC (UK). Results obtained for the melting (fusion) temperatures and fusion enthalpies of the Hg, Ga, In, and Sn are shown in Table 3. The uncertainty in the enthalpy measurements was found to be of the order of 1%, while the temperature measurements agree within 0.1 K with the standard values, except for mercury, where data only at 2 K min<sup>-1</sup> was determined. The heat capacity was obtained using closed stainless steel crucibles, by continuous method-standard zone, with a scanning rate of 2 K min<sup>-1</sup> (Setaram SETSOFT 2000, Version 3.0). The mass of the samples was confirmed after each run to check any possible weight losses. The heat capacity was determined from the total energy detected by the calorimeter i.e.  $(Q_P)_{\text{meas}}$ , the calibration constant,  $K$ , and the scanning rate  $\beta$  using the following equation:

$$C_P = \frac{(Q_P)_{\text{meas}}}{K \cdot \beta} \quad (1)$$

Reference Material	Origin	Purity (%)	$T_{fus}/K$	$\Delta_{fus}H_m / J\ mol^{-1}$	Reference
Hg	BDH	> 99.999	$234.29 \pm 0.01$	$2295.3 \pm 0.8$	(Sabbah et al., 1999)
Ga	Alfa Chemicals	99.999	302.915 $302.92 \pm 0.02$	$5569 \pm 50$ $5590 \pm 40$	(Thomas, 1990) (Chase, 1998)
In	LGC 2601	99.999	$429.76 \pm 0.02$	$3296 \pm 9$	CRMC
Sn	LGC 2609	99.999	$505.07 \pm 0.02$	$7187 \pm 4$	CRMC
Pb	LGC 2608	99.996	$600.62 \pm 0.02$	$4756 \pm 11$	CRMC
Zn	LGC 2611	99.996	$692.68 \pm 0.02$	$7103 \pm 31$	CRMC

Table 2. Reference materials used for the temperature calibration

	Hg (Bi-distilled)	Ga	In	Sn
$(\Delta_{fus}H)_{std} / J\ mol^{-1}$	$2295.3 \pm 0.8$ (Sabbah et al., 1999; Chase, 1998)	$5569 \pm 60$ (Sabbah et al., 1999) $5590 \pm 40$ (Chase, 1998)	$3296 \pm 9$	$7187 \pm 4$
$(\Delta_{fus}H)_{exp} / J\ mol^{-1}$	$2268 \pm 33$	$5568 \pm 71$	$3249 \pm 35$	$7083 \pm 74$
$T_{std} / K$	$234.29 \pm 0.01$ (Thomas, 1990; Sabbah et al., 1999)	$302.92 \pm 0.02$ (Chase, 1998), 302.915 (Thomas, 1990)	$429.76 \pm 0.02$	$505.07 \pm 0.02$
$T_{exp} / K$	$233.58 \pm 0.19$ (at 2 K min <sup>-1</sup> )  -	-  $303.08 \pm 0.29^a$	$429.68 \pm 0.07$  $429.66 \pm 0.02^a$	$505.01 \pm 0.07$  $505.16 \pm 0.15^a$

<sup>a</sup> Extrapolation to zero scanning rate

Table 3. Comparison between the temperature and enthalpy of fusion of mercury, gallium, indium (LGC 2601) and tin (LGC 2609).

After calibration, the measurement technique of specific heat of sample fluids composed of a double experiment performing two nearly identical runs—one with the two cells without sample and the other with the sample in one of the cells. In this way, any differences between the two crucibles are eliminated from the final signal to be used in equation (1). The uncertainty of the heat capacity determinations is found to be better than 1.5% at a 95% confidence level. It is noted that according to the ISO definition, a coverage factor  $k=2$  is used and in order to obtain the accuracy value it must be divided by 2 (Sampaio & Nieto de Castro, 1998). We have checked the accuracy of the measurements by measuring the heat capacity of certified reference material sapphire (NIST SRM-707), between room temperature and 430 K, and found deviations of less than 1.5 % with an average absolute deviation (AAD) of 0.68%.

## 4. Results and discussions

### 4.1 Thermal conductivity of ionic liquids and ionanofluids

The thermal conductivity of [C<sub>6</sub>mim][BF<sub>4</sub>], [C<sub>4</sub>mim][PF<sub>6</sub>], [C<sub>6</sub>mim][PF<sub>6</sub>], [C<sub>4</sub>mim][CF<sub>3</sub>SO<sub>3</sub>], and [C<sub>4</sub>mpyrr][(CF<sub>3</sub>SO<sub>2</sub>)<sub>2</sub>N] were measured for various temperature ranging from 293 K to 353 K and at 0.1 MPa. Figure 2 shows the results obtained from this study. It can be seen that the thermal conductivity variation with temperature is linear and that no data point departs from linearity by more than  $\pm 0.6\%$ . A linear correlation used to fit the results is expressed by equation (2). Table 4 depicts the coefficients of regression for equation (2) and the root mean square deviations of the fits. The variance of the fits do not exceed 0.48 mW m<sup>-1</sup> K<sup>-1</sup>, about 0.3%.

$$\lambda(W \cdot m^{-1} \cdot K^{-1}) = a_1 + a_2(T / K) \quad (2)$$

Few similar studies from literature on ionic liquids are also reported here as their results are compared with the present results. Using the transient short-hot-wire method with an uncertainty of 2-4% (Tomida et al., 2007) measured the thermal conductivity of [C<sub>4</sub>mim][PF<sub>6</sub>], and [C<sub>6</sub>mim][PF<sub>6</sub>] from temperature between 294 K and 335 K and at pressure up to 20 MPa. Their samples were synthesized, dried by heating in a vacuum and purified by adsorbing the impurities onto activated charcoal. Therein, the water content after the measurements was found to be in the range 70-90 ppm. (Ge et al., 2007) reported measurements for [C<sub>4</sub>mpyrr][(CF<sub>3</sub>SO<sub>2</sub>)<sub>2</sub>N] and [C<sub>4</sub>mim][CF<sub>3</sub>SO<sub>3</sub>] using the same instrument presented in this work, with an estimated uncertainty of  $\pm 0.005 W m^{-1} K^{-1}$ . The water content was found to be less than 80 ppm and the chloride mass fraction was less than  $5 \cdot 10^{-6}$ .

Ionic Liquids and Ionanofluids	$a_1 \pm \sigma_{a1}$ / W m <sup>-1</sup> K <sup>-1</sup>	$10^4(a_2 \pm \sigma_{a2})$ / W m <sup>-1</sup> K <sup>-2</sup>	$\sigma$ / W m <sup>-1</sup> K <sup>-1</sup>
[C <sub>6</sub> mim][BF <sub>4</sub> ]	0.19379 $\pm$ 0.00179	-1.214 $\pm$ 0.053	0.00029
[C <sub>4</sub> mim][CF <sub>3</sub> SO <sub>3</sub> ]	0.16149 $\pm$ 0.00248	-0.679 $\pm$ 0.077	0.00041
[C <sub>4</sub> mpyrr][(CF <sub>3</sub> SO <sub>2</sub> ) <sub>2</sub> N]	0.12699 $\pm$ 0.00313	-0.300 $\pm$ 0.100	0.00032
[C <sub>4</sub> mim][PF <sub>6</sub> ]	0.15784 $\pm$ 0.00253	-0.429 $\pm$ 0.078	0.00041
[C <sub>6</sub> mim][PF <sub>6</sub> ]	0.16279 $\pm$ 0.00292	-0.714 $\pm$ 0.090	0.00048
[C <sub>6</sub> mim][BF <sub>4</sub> ] + MWCNT	0.17631 $\pm$ 0.00179	-0.357 $\pm$ 0.006	0.00029
[C <sub>4</sub> mim][CF <sub>3</sub> SO <sub>3</sub> ] + MWCNT	0.16310 $\pm$ 0.00200	-0.321 $\pm$ 0.006	0.00032
[C <sub>4</sub> mpyrr][(CF <sub>3</sub> SO <sub>2</sub> ) <sub>2</sub> N] + MWCNT	0.13279 $\pm$ 0.00313	-0.300 $\pm$ 0.010	0.00032
[C <sub>4</sub> mim][PF <sub>6</sub> ] + MWCNT	0.16501 $\pm$ 0.00372	-0.500 $\pm$ 0.115	0.00061
[C <sub>6</sub> mim][PF <sub>6</sub> ] + MWCNT	0.15844 $\pm$ 0.00179	-0.500 $\pm$ 0.055	0.00029

Table 4. Coefficients of equation (2) for ionic liquids and ionanofluids (1wt.% of MWCNTs)

Figure 3 demonstrates the deviations of our data as well as data from literature from equation (2). It can be seen that none of our data point deviated from the linear fitting by more than 0.5%. In addition, the deviations from our fits of the data from (Ge et al., 2007) for [C<sub>4</sub>mpyrr][(CF<sub>3</sub>SO<sub>2</sub>)<sub>2</sub>N] and [C<sub>4</sub>mim][CF<sub>3</sub>SO<sub>3</sub>], and by (Tomida et al., 2007) for [C<sub>4</sub>mim][PF<sub>6</sub>], and [C<sub>6</sub>mim][PF<sub>6</sub>], obtained using a bare platinum wire are also shown in Figure 3. In all cases, the data agree within the errors associated with the methods used. It can also be seen that both sets of literature data (Ge et al., 2007; Tomida et al., 2007) are slightly higher than those of our data which may be associated with higher purity samples

utilized in the present study. (Ge et al., 2007) showed that small levels of water or halide, which are common impurities from the synthesis of ionic liquids, both increase the thermal conductivity of ionic liquids.

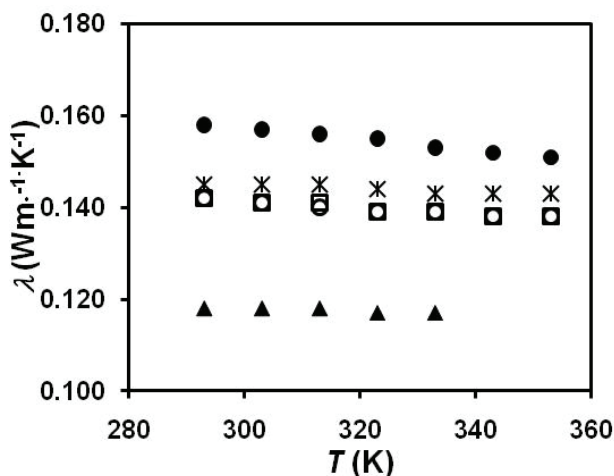


Fig. 2. Thermal conductivity of ionic liquids as a function of temperature (legends: ● - [C₆mim][BF₄]; ○ - [C₄mim][CF₃SO₃]; ▲ - [C₄mpyrr][(CF₃SO₂)₂N]; \* - [C₄mim][PF₆]; □ - [C₆mim][PF₆]).

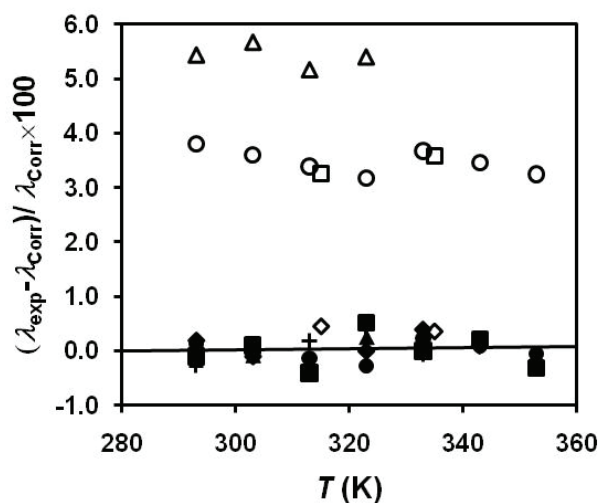


Fig. 3. Deviations between our data and other data from equation (2), as a function of temperature (legends: ● - [C₆mim][BF₄]; + - [C₄mim][CF₃SO₃]; ▲ - [C₄mpyrr][(CF₃SO₂)₂N]; ◆ - [C₄mim][PF₆]; ■ - [C₆mim][PF₆]; △ - [C₄mpyrr][(CF₃SO₂)₂N] from (Ge et al., 2007); ○ - [C₄mim][CF₃SO₃] from (Ge et al., 2007); ◇ - [C₄mim][PF₆] from (Tomida et al., 2007); □ - [C₆mim][PF₆] from (Tomida et al., 2007)).

The thermal conductivities of the ionanofluids produced by dispersing MWCNTs in  $[\text{C}_6\text{mim}][\text{BF}_4]$ ,  $[\text{C}_4\text{mim}][\text{PF}_6]$ ,  $[\text{C}_6\text{mim}][\text{PF}_6]$ ,  $[\text{C}_4\text{mim}][\text{CF}_3\text{SO}_3]$  and  $[\text{C}_4\text{mpyr}][(\text{CF}_3\text{SO}_2)_2\text{N}]$  were measured at various temperatures between 293 K and 353 K and at 0.1 MPa. Thermal conductivity data obtained for these new ionanofluids are presented. Figure 4 shows the measured thermal conductivity of various ionanofluids as a function of temperature and at constant concentration of MWCNTs (1 wt. %). Some of the ionanofluids show a temperature dependent enhancement ( $[\text{C}_6\text{mim}][\text{BF}_4]$  and  $[\text{C}_4\text{mim}][\text{CF}_3\text{SO}_3]$ ), while the remaining ionanofluids demonstrate a constant increase (5% for  $[\text{C}_4\text{mpyr}][(\text{CF}_3\text{SO}_2)_2\text{N}]$ , 3.4% for  $[\text{C}_4\text{mim}][\text{PF}_6]$ , and 1.8% for  $[\text{C}_6\text{mim}][\text{PF}_6]$ ). Like ionic liquids, the thermal conductivity variation is linear with temperature and that no data point departs from linearity by more than  $\pm 0.25\%$ . The coefficients of regression for equation (2) and the root mean square deviations of the fits are given in Table 4.

Results of temperature-dependent thermal conductivity enhancements of these ionanofluids ( $\lambda_{\text{ionanofluids}}/\lambda_{\text{IL}}$ ) are also presented in Figure 5. The natures of the enhancements of thermal conductivity of these ionanofluids are somewhat similar to previously reported enhancements for other nanofluids (Murshed et al, 2008a). In general, ionanofluids containing  $[\text{PF}_6]^-$  based ionic liquids have the smallest enhancement in thermal conductivity whilst those based on  $[\text{C}_6\text{mim}][\text{BF}_4]$  had the largest (9% on average) change. No smooth dependence on the cations or anions was found. Similar dependency was also recently observed for the  $[\text{C}_n\text{mim}]^+$ -based ionic liquids in another study by our group (Ribeiro et al., 2010).

The interpretation of the thermal conductivity enhancement in particle suspensions such as nanofluids has been the object of many publications, since the pioneering work of Maxwell (Maxwell, 1891). This Maxwell's model was developed for millimeter and micrometer sized particles suspended in liquids, and the ratio between the thermal conductivity of the nanofluid and that of the base fluid,  $\lambda_{\text{NF}}/\lambda_{\text{BF}}$ , was found to depend on the thermal conductivity of both phases (solid and liquid) and on the volume fraction of the solid. This model, adapted for the ionanofluids is given as

$$\frac{\lambda_{\text{NF}}}{\lambda_{\text{IL}}} = \frac{\lambda_{\text{CNT}} + 2\lambda_{\text{IL}} + 2\phi_{\text{CNT}}(\lambda_{\text{CNT}} - \lambda_{\text{IL}})}{\lambda_{\text{CNT}} + 2\lambda_{\text{IL}} - \phi_{\text{CNT}}(\lambda_{\text{CNT}} - \lambda_{\text{IL}})} \quad (4)$$

where  $\lambda_{\text{NF}}$ ,  $\lambda_{\text{IL}}$ ,  $\lambda_{\text{CNT}}$  are, the thermal conductivity of nanofluid, ionic liquid, and carbon nanotubes (CNT), respectively.  $\phi_{\text{CNT}}$  is the volume fraction of CNTs.

In order to incorporate the shape of the particles (e.g. cylinders) and the interaction between the particles, extensions of this Maxwell model were later developed by (Hamilton and Crosser, 1962) and (Hui et al., 1999). However, these classical models were found to be unable to accurately predict the anomalously high thermal conductivity of nanofluids (Murshed et al., 2008a). Thus, researchers have proposed several mechanisms to explain this phenomenon. For example, (Kebllinski et al., 2002) systematized the four different mechanisms for heat transfer to explain these enhancements, namely (i) Brownian motion of the nanoparticles (ii) liquid layering at the liquid/particle interphase, (iii) the nature of the heat transport in the nanoparticles and (iv) the effect of nanoparticle clustering. From the analysis made in an exhaustive review paper on nanofluids (Murshed et al., 2008a) and other publications cited, therein, it is our belief that the effect of the particle surface chemistry and the structure of the interphase particle/fluid are the major mechanisms responsible for the unexpected enhancement in nanofluids.

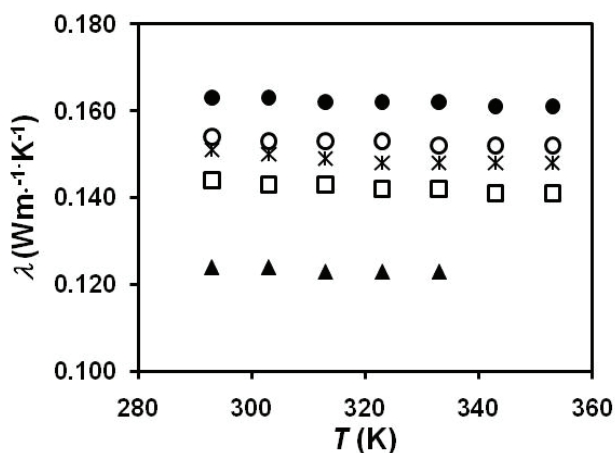


Fig. 4. Thermal conductivity of ionanofluids as a function of temperature for 1 wt% loading of MWCNTs (legends: ● - [C<sub>6</sub>mim][BF<sub>4</sub>] + MWCNTs; ○ - [C<sub>4</sub>mim][CF<sub>3</sub>SO<sub>3</sub>] + MWCNTs; ▲ - [C<sub>4</sub>mpyrr][(CF<sub>3</sub>SO<sub>2</sub>)<sub>2</sub>N] + MWCNTs; \* - [C<sub>4</sub>mim][PF<sub>6</sub>] + MWCNTs; □ - [C<sub>6</sub>mim][PF<sub>6</sub>] + MWCNTs)

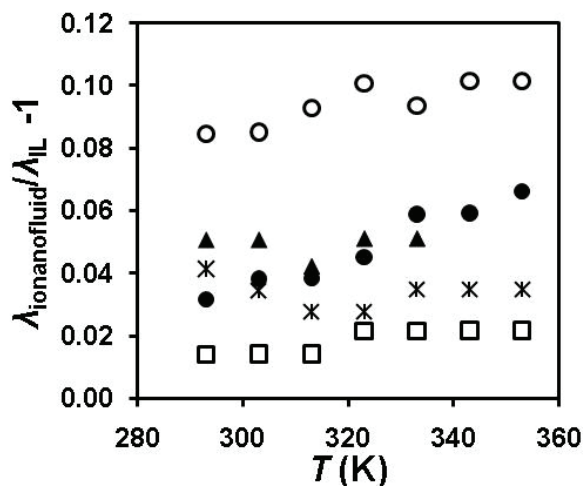


Fig. 5. Thermal conductivity enhancement in the ionanofluids with a loading of 1 wt% of MWCNTs (legends : ● - [C<sub>6</sub>mim][BF<sub>4</sub>] + MWCNTs; ○ - [C<sub>4</sub>mim][CF<sub>3</sub>SO<sub>3</sub>] + MWCNTs; ▲ - [C<sub>4</sub>mpyrr][(CF<sub>3</sub>SO<sub>2</sub>)<sub>2</sub>N] + MWCNTs; \* - [C<sub>4</sub>mim][PF<sub>6</sub>] + MWCNTs; □ - [C<sub>6</sub>mim][PF<sub>6</sub>] + MWCNTs)

Incorporating some of the key mechanisms, Murshed and co-workers (Leong et al., 2006; Murshed et al., 2008b) solved the heat transfer equation for spherical and infinitely long cylinders for three-phase systems (particle, interfacial layer and base fluids) and developed two models for the effective thermal conductivity of nanofluids containing spherical and

cylindrical nanoparticles. Besides particle concentration and thermal conductivity of each phase, these models take into account the effect of particle size, and interfacial nanolayer between particle and the base fluids. The thermophysical properties of the interfacial layer are considered to be different from those of the bulk liquid and of the solid particles. In this study, one of these models for cylindrical particles (Murshed et al., 2008b) was used for the determination of the effective thermal conductivity of ionanofluids containing CNTs in various ionic liquids. The model is expressed as

$$\lambda_{NF} = \frac{(\lambda_{CNT} - \lambda_{Int})\phi_{CNT}\lambda_{Int}\left[2\gamma_1^2 - \gamma^2 + 1\right] + (\lambda_{CNT} + 2\lambda_{Int})\gamma_1^2\left[\phi_{CNT}\gamma^2(\lambda_{Int} - \lambda_{LI}) + \lambda_{LI}\right]}{\gamma_1^2(\lambda_{CNT} + 2\lambda_{Int}) - (\lambda_{CNT} - \lambda_{Int})\phi_{CNT}\left[\gamma_1^2 + \gamma^2 - 1\right]} \quad (5)$$

where

$$\gamma = 1 + \frac{h}{a} \quad \text{and} \quad \gamma_1 = 1 + \frac{2h}{a} \quad (6)$$

In these equations (5) and (6),  $\lambda_{IP}$  is the thermal conductivity of the interphase,  $a$  is the radius of the cylinder and  $h$  the thickness of the interfacial layer (nanolayer at the CNT-IL interface). It should be noted that there is no exact theoretical model to determine  $h$ ; however, (Murshed et al., 2008b) showed that this parameter is not critical and in the present calculations we used  $h \approx 2$  nm as used by (Murshed et al., 2008b) for CNTs-nanofluids. In addition, as no values of  $\lambda_{IP}$  exist for IL/CNTs systems, we have used  $\lambda_{IP}$  as an adjustable parameter, keeping in mind that its value will be, in principle, intermediate between the values of  $\lambda_{IL}$  and  $\lambda_{CNT}$ . (Murshed et al., 2008b) found  $\lambda_{IP} = 60 \lambda_{IL}$  for ethylene glycol/CNTs nanofluids.

Table 5 shows the results obtained for the ionanofluids studied. It also compares the experimentally observed enhancement ( $\lambda_{NF}/\lambda_{IL}-1$ ) with the values predicted from Maxwell model (Maxwell, 1891) and Murshed et al.'s model (Murshed et al., 2008b). In the prediction, an average value of  $a = 7.5$  nm was used for the MWCNTs and a value of  $\lambda_{CNT} = 2000 \text{ W m}^{-1} \text{ K}^{-1}$  (Choi et al., 2001) was assumed, as no other information regarding the value for the Baytubes® exists. Calculations were performed for 293 K, as the temperature dependence of the thermal conductivity of both the ionic liquids and the ionanofluids is small. Values for the density of the ionic liquids were obtained from the ILThermo database (NIST Standard Reference Database #147). The limiting value of Maxwell model, for volume fractions that oscillate between 0.6 and 0.7 is approximately 1.2, depending also slightly of the thermal conductivity of the ionic liquid. As equation (4) is the limiting value of equation (5), applying equation (5) to these systems, values of  $\lambda_{IP}=0$ , and  $h=0$  were obtained, and it predicts a value of the thermal conductivity enhancement greater than found for all the systems studied. Only for systems where the enhancement is of the order of 20% or greater can the theory describe the effect of the thermal conductivity of the interface solid/liquid, as found for  $[\text{C}_4\text{mim}][(\text{CF}_3\text{SO}_2)_2\text{N}]$  (Ribeiro et al., 2010).

In terms of volume, we have occupancy of 6% of the nanotubes. This might suggest that the ionanofluids consist the same type of nanostructural organization found by (Lopes & Padua, 2006) using molecular dynamics simulations for  $[\text{C}_n\text{mim}][(\text{CF}_3\text{SO}_2)_2\text{N}]$  and  $[\text{C}_n\text{mim}][\text{PF}_6]$  ionic liquids. They reported that for ionic liquids with alkyl chains where  $n \geq 4$ , aggregation of the alkyl chains into nonpolar domains was observed. This creates a tridimensional



Base Ionic Liquid	$\rho / \text{kg m}^{-3}$	$\lambda_{\text{IL}} / \text{W m}^{-1} \text{K}^{-1}$	$w_{\text{CNT}}$	$\phi_{\text{CNT}}$	$\lambda_{\text{NF}} / \lambda_{\text{IL}} - 1$		
					Experimental	Eq. (4)	Eq. (5)
[C <sub>6</sub> mim][BF <sub>4</sub> ]	1148	0.158	0.01	0.0590	0.048	0.19	0.19
[C <sub>4</sub> mim][CF <sub>3</sub> SO <sub>3</sub> ]	1306	0.142	0.01	0.0666	0.094	0.21	0.22
[C <sub>4</sub> mpyrr][[(CF <sub>3</sub> SO <sub>2</sub> ) <sub>2</sub> N]	1454	0.118	0.01	0.0735	0.049	0.24	0.25
[C <sub>4</sub> mim][PF <sub>6</sub> ]	1372	0.145	0.01	0.0697	0.034	0.22	0.23
[C <sub>6</sub> mim][PF <sub>6</sub> ]	1298	0.142	0.01	0.0662	0.018	0.21	0.22

Table 5. Thermal conductivity enhancement in the ionanofluids studied ( $T=293 \text{ K}$ )

network of ionic channels formed by the anions and the imidazolium rings of the cations and provides evidence of microphase separation between polar and non-polar domains within the liquid phase structure. The CNTs dispersed in the ionic liquid are likely to interact preferentially with the non polar domains associated with the alkyl chains, therefore creating microclusters that will enhance the heat transfer. However, as the length of the nanotubes (commonly 1-10  $\mu\text{m}$ ) is significant, the structure of the ionanofluids is likely to be different compared with that of the base fluid.

The enhanced thermal conductivity of the ionanofluids is consistent with previous studies involving metal nanoparticles in molecular solvents such as water or ethylene glycol (Choi et al., 2001; Murshed et al., 2008b). The strong interaction between the ionic liquid and CNTs has been demonstrated by (Fukushima et al., 2003; Fukushima & Aida, 2007) wherein the ionanofluids containing highly exfoliated CNT bundles were found to be less entangled after mixing. These bundles form a network structure that will indeed increase the thermal conductivity (an effect similar to aggregation) by creating privileged paths for heat conduction.

## 4.2 Heat capacity of ionic liquids and ionanofluids

Measurements of the heat capacity were performed at 0.1 MPa, and temperatures between 308 and 423 K and the results obtained for [C<sub>4</sub>mim][BF<sub>4</sub>] and [C<sub>4</sub>mim][PF<sub>6</sub>] ionic liquids are presented in Table 6. The experimental values were fitted as a function of temperature with the polynomial given as.

$$C_P (\text{J} \cdot \text{mol}^{-1} \cdot \text{K}^{-1}) = b_1 + b_2 (T / \text{K}) + b_3 (T / \text{K})^2 \quad (7)$$

Table 7 shows the coefficients of regression for equation (7) and the root mean square deviations associated with the fits for [C<sub>4</sub>mim][BF<sub>4</sub>] and [C<sub>4</sub>mim][PF<sub>6</sub>]. While the variance for [C<sub>4</sub>mim][BF<sub>4</sub>] is 0.914  $\text{J mol}^{-1} \text{K}^{-1}$ , approximately 0.3 %, the variance for [C<sub>4</sub>mim][PF<sub>6</sub>] is 1.29  $\text{J mol}^{-1} \text{K}^{-1}$ , approximately 0.3 %. Figure 6 shows the variation of heat capacity with temperature, together with the results obtained by various research groups (Rebelo et al., 2004; Kim et al., 2004; Fredlake et al., 2004; Waliszewski et al., 2005; Van Valkenburg et al., 2005; Garcia-Miaja et al., 2008 & 2009). All these data were obtained with DSC. A wide variation between the datasets of up to 20 % at room temperature is observed. This situation is very uncommon in calorimetry; however it is known that, apart from differences in sample purity, the DSC used must be well calibrated and this may explain the scatter of data.

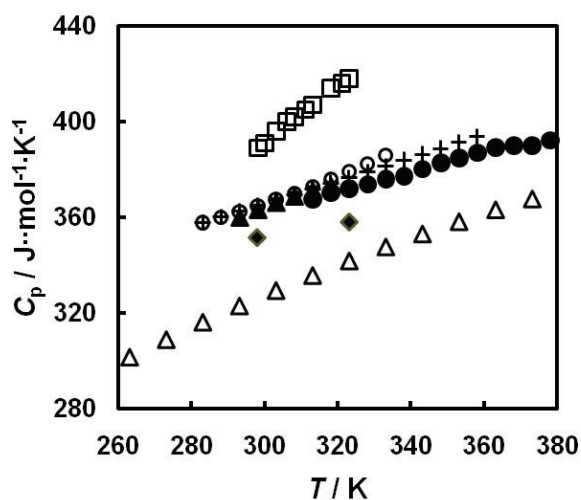
Figure 7 shows the variation of heat capacity with temperature together with the results obtained from various research groups (Holbrey et al., 2003; Kabo et al., 2004; Fredlake et al.,

T/K	$C_p / \text{J mol}^{-1} \text{K}^{-1}$	
	$[\text{C}_4\text{mim}][\text{BF}_4]$	$[\text{C}_4\text{mim}][\text{PF}_6]$
308.16	367.26	410.64
318.16	370.39	417.74
328.22	373.73	423.43
338.19	377.15	429.11
348.25	382.69	436.22
358.25	386.99	441.90
368.17	390.00	444.74
378.20	392.18	450.43
388.20	395.28	457.53
398.20	397.93	463.21
408.16	403.88	470.32
418.19	404.98	473.16
423.22	406.62	474.58

Table 6. Heat capacity of  $[\text{C}_4\text{mim}][\text{BF}_4]$  and  $[\text{C}_4\text{mim}][\text{PF}_6]$  as a function of temperature

Ionic Liquid	$b_1 \pm \sigma_{b1}$ / $\text{J mol}^{-1} \text{K}^{-1}$	$b_2 \pm \sigma_{b2}$ / $\text{J mol}^{-1} \text{K}^{-2}$	$10^4 (b_3 \pm \sigma_{b3})$ / $\text{J mol}^{-1} \text{K}^{-3}$	$\sigma$ / $\text{J mol}^{-1} \text{K}^{-1}$
$[\text{C}_4\text{mim}][\text{BF}_4]$	$177.989 \pm 23.134$	$0.80054 \pm 0.12732$	$-6.1596 \pm 1.7393$	0.9140
$[\text{C}_4\text{mim}][\text{PF}_6]$	$182.288 \pm 32.828$	$0.87307 \pm 0.18067$	$-4.2115 \pm 2.4681$	1.2933

Table 7. Coefficients of equation (7)

Fig. 6. Comparison of present results and data obtained from literature for heat capacity of  $[\text{C}_4\text{mim}][\text{BF}_4]$  as a function of temperature (legends: ● - Present work; ○ - Rebelo et al., 2004; □ - Kim et al., 2004; ◆ - Fredlake et al., 2004; + - Waliszewski et al., 2005; △ - Van Valkenburg et al., 2005; \* - Garcia-Miaja et al., 2008; ▲ - Garcia-Miaja et al., 2009)

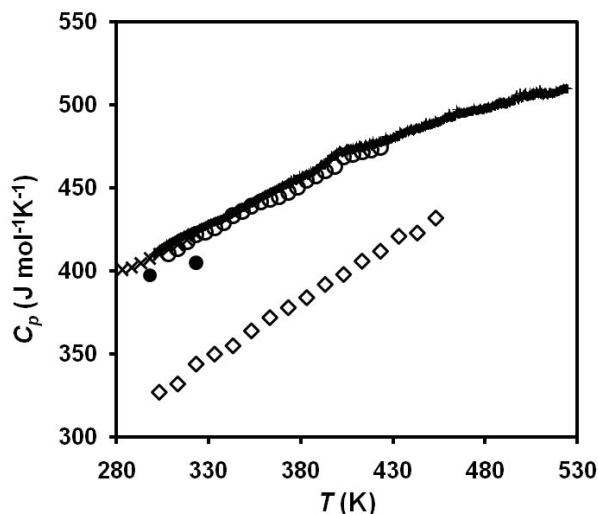


Fig. 7. Comparison of present heat capacity data of  $[C_4mim][PF_6]$  with results from literature as a function of temperature (legends:  $\circ$  - Present work;  $\diamond$  - Holbrey et al., 2003;  $+$  - Kabo et al., 2004;  $\bullet$  - Fredlake et al., 2004;  $\times$  - Troncoso et al., 2006)

2004; Troncoso et al., 2006). With the exception of the data reported by Kabo and co-workers (Kabo et al., 2004) which were obtained using a heat bridge calorimeter, all the remaining data were obtained using DSC. Our data agrees with the data of (Troncoso et al., 2006) between 0.4 and 0.6% and with (Kabo et al., 2004) between 0.8% and 1.2%. Results with deviations greater than  $\pm 2\%$  are not included. Although data reported in this study are slightly lower, these variations are within the expected uncertainty of the data in all cases. In contrast, the data reported by (Fredlake et al., 2004) and especially those reported by (Holbrey et al., 2003) are much lower than our data with the latter data showing deviations of up to -20%.

The possible use of ionic liquids as heat transfer fluids, for heat exchange in chemical plants and solar thermal power generation, from cryogenic temperatures up to 200 °C, is based on the values of heat capacity per unit volume, very low vapor pressures, wide liquid ranges, thermal stability (some can be used at temperatures up to 500 °C) has been discussed (Holbrey et al., 2003), and its comparison with the properties of synthetic compounds (based on hydrocarbons, polyaromatics and siloxanes), showed that common imidazolinium systems have higher heat capacities per unit volume than two high performance commercial thermal fluids, Paratherm HE<sup>®</sup> and Dowtherm MX<sup>™</sup>, in all the applicable temperature range. This analysis was complemented (França et al., 2009; Nieto de Castro, 2010a) for several ionic liquids and Syltherm 800<sup>™</sup>, Syltherm HF<sup>™</sup> and Dowtherm A<sup>™</sup> (trademarks of Dow Chemical Company, USA) as well as Paratherm HE<sup>®</sup> (registered mark of Paratherm Corporation). Figure 8 demonstrates the results obtained for various ionic liquids such as  $[C_4mim][(CF_3SO_2)_2N]$ ,  $[C_2mim][C_2H_5SO_4]$ ,  $[C_4mim][dca]$  and  $[Aliquat\ 336^{®}\text{-derived}][dca]$  together with data for several commercial heat transfer fluids. It is clear that the heat capacities per unit

volume ( $\rho C_p$ ) of these ionic liquids are 20-40% higher than those of commercial heat transfer fluids in the temperature range studied. The same happens with other ionic liquids (França et al., 2009). These results are highly promising if we use these biodegradable and green ionic liquids in ionanofluids for their numerous potential applications.

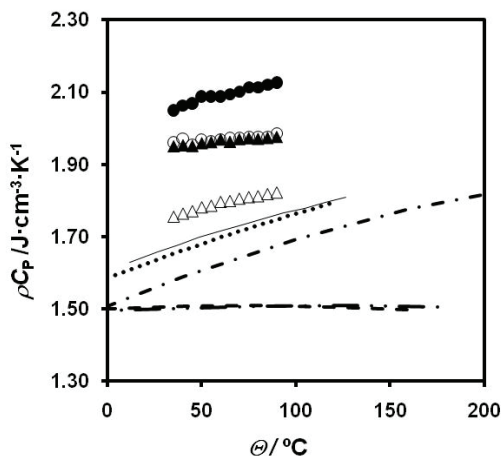


Fig. 8. Temperature-dependent heat capacity per unit volume for the ionic liquids and several heat transfer fluids (legend: ▲ - [C<sub>4</sub>mim][CF<sub>3</sub>SO<sub>2</sub>]<sub>2</sub>N; ● - [C<sub>2</sub>mim][C<sub>2</sub>H<sub>5</sub>SO<sub>4</sub>]; ○ - [C<sub>4</sub>mim][dca]; △ - [Aliquat 336<sup>®</sup>-derived][dca]; ---Syltherm800<sup>™</sup>; ---- Syltherm HF<sup>™</sup>; — Dowtherm A<sup>™</sup>; --- Dowtherm MX<sup>™</sup>; ..... Paratherm HE<sup>®</sup>). Data for the heat transfer fluids are obtained from their Material Safety Data Sheets which are available on-line.

The heat capacity of [C<sub>4</sub>mim][PF<sub>6</sub>]-based ionanofluid was measured for two different concentrations of MWCNTs (1 wt.% and 1.5 wt.%) and the results are shown in Figure 9. The results are very surprising, as a large maximum in the heat capacity as a function of temperature is found compared with the bulk ionic liquid. Interestingly, around temperature between 350 to 375K, a jump in heat capacity of ionanofluids was observed (Figure 9) and the reason for such behavior is not known at this moment. Similar data has not been reported previously for nanofluids. Figure 10 depicts the heat capacity enhancement of ionanofluids ( $C_{P,NF}$ ) over base ionic liquid ( $C_{P,IL}$ ) i.e.  $C_{P,NF}/C_{P,IL}-1$  as a function of temperature. The maximum enhancement observed, shaped as a dome as in critical behavior in pure fluids and near immiscibility critical end points, is clear and shows a peak of 8% compared with the bulk liquid irrespective of the CNT loading. Some noise, within the accuracy of the measurements, is found at the lower and higher temperatures. Further investigations using other ionic liquids and the application of phenomenological theories of criticality are to be performed in order to understand the interactions involved in these systems and to examine whether the aggregation phenomena or nanostructural organization exhibited are important in the mechanisms of the effects observed.

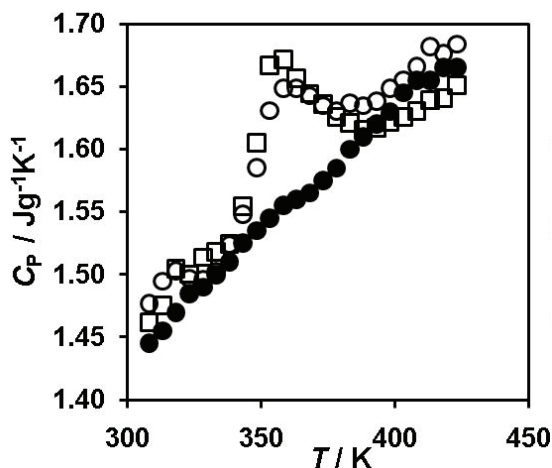


Fig. 9. Heat capacity of  $[\text{C}_4\text{mim}][\text{PF}_6]$ -based ionanofluid for two different MWCNTs loadings as a function of temperature (legends: ● -  $[\text{C}_4\text{mim}][\text{PF}_6]$ ; □ -  $[\text{C}_4\text{mim}][\text{PF}_6]$  + 1 wt% of MWCNTs; ○ -  $[\text{C}_4\text{mim}][\text{PF}_6]$  + 1.5 wt% of MWCNTs). The data are expressed in mass units as the molecular weight of the MWCNTs is not known.

## 5. Natural nanomaterials and their potential in ionanofluids

Natural nanomaterials open a completely new field in heat transfer as they have unusual thermal properties derived from its structure. It is in principle possible to use natural products from the biosphere, marine or plant origin, to be used as heat transfer enhancers. There is a plethora of materials, all renewable and biodegradable that can be tested and their thermal properties are to be determined. From the present knowledge some of them are already applied in domestic application like cherry stones and grape seeds, whereby several minutes of heating in a microwave oven can be sufficient to heat a fleece bag of these seeds to 70°C and let it last for several hours at 50°C, a self kept warming pillow. This result is quite surprising and can only be explained by the structure of the cherry stones.

Figure 11 presents FEG-SEM images obtained from a JEOL JSM-7001F equipment for cherry stone bits, produced by grinding the cherry stones down to grains of 200  $\mu\text{m}$  average diameter, with four different magnifications i.e., 200x, 650x, 1400x and 7500x (also shown on images) (Queirós, 2010). The structure of the surface and of the pores is completely visible. It is very clear that the surface of the material has micropores (dimensions around 10  $\mu\text{m}$ ), but these micropores have nanopores smaller than 1  $\mu\text{m}$ , like ice cream cone shape. These pores can not only trap gases inside and increase the thermal conductivity and the heat capacity, but also they can accommodate ionic liquid molecules (Kaviani, 1995), producing a very complex, but efficient, heat transfer interface in an ionanofluid.

The heat capacity data of these cherry stones and other fruit seeds (natural micro and nanomaterials), shells and pits, are shown, as a function of temperature, in Figure 12. These include walnut and hazelnut shells, annona (custard apple) fruit seeds, peach pits and olive stones (Queirós, 2010). The plot shows that the heat capacity of all samples increases up to a maximum between 350 and 370 K, decreasing then to very small values (around 1  $\text{Jg}^{-1}\text{K}^{-1}$ ).

Remembering that the heat capacity of liquid water is around  $4 \text{ Jg}^{-1}\text{K}^{-1}$ , it can be seen that the maximum values can be as great as  $10 \text{ Jg}^{-1}\text{K}^{-1}$  (walnut shell) or  $9.4 \text{ Jg}^{-1}\text{K}^{-1}$  (cherry stone), the lowest value being obtained for the olive stone ( $4.3 \text{ Jg}^{-1}\text{K}^{-1}$ ). The shape of the curves is the

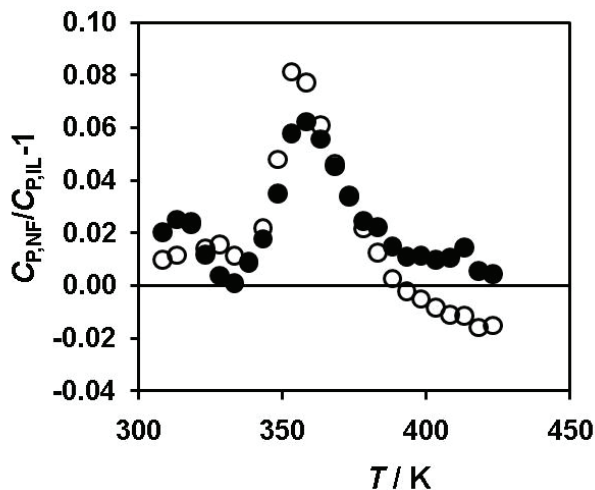


Fig. 10. Heat capacity enhancement of  $[\text{C}_4\text{mim}][\text{PF}_6]$ -based ionic liquid for two different MWCNTs loadings as a function of temperature (legends:  $\square$  -  $[\text{C}_4\text{mim}][\text{PF}_6]$  + 1 wt% MWCNTs;  $\circ$  -  $[\text{C}_4\text{mim}][\text{PF}_6]$  + 1.5 wt% MWCNTs)

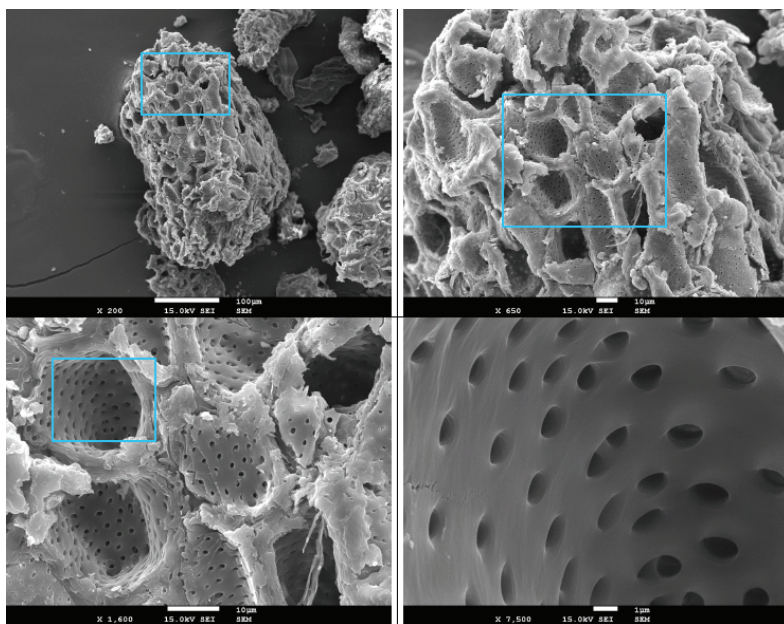


Fig. 11. FEG-SEM images of cherry stones bits for different magnifications (Queirós, 2010).

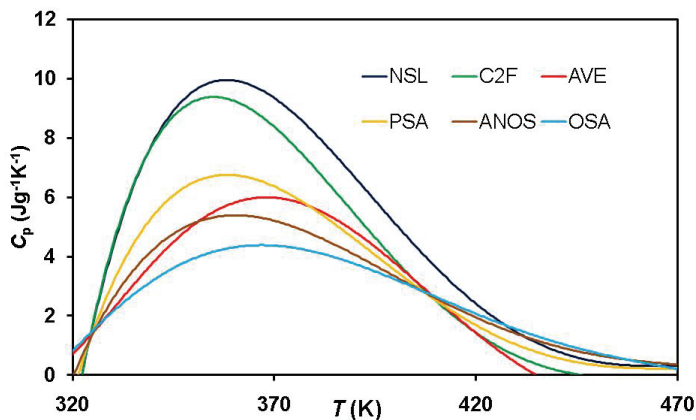


Fig. 12. Temperature-dependent heat capacity of several fruit seeds (legend: NSL – walnut shell; AVE – hazelnut shell; C2F – cherry stones; ANOS – annona fruit seed; PSA – peach pit; OSA – olive stone).

same, and the change in the temperature of the maximum is very small (10 K), facts that seem to demonstrate that the structure of these materials is similar, although the absolute capacity to store heat changes from material to material. Keeping in mind that the densities of these materials vary between 0.7 and 1.1 gcm<sup>-3</sup>, the heat storage density or the heat capacity per unit volume ( $\rho C_p$ ) can vary between 2.9 and 11 Jcm<sup>-3</sup>K<sup>-1</sup>, a factor of 2 to 6 greater than common heat transfer oils and 1.5 to 5.5 greater than ionic liquids (França et al, 2009). These values suggest that ionanofluids based on these nanomaterials are excellent heat storage and transfer fluids and that ionanofluids can replace the existing aliphatic, aromatic and silicone oils used in the industry, as biodegradable, non-toxic and more efficient in terms of heat transfer load and capacity, namely for microchannel heat exchangers.

## 6. Conclusions

In this chapter, thermal conductivity and heat capacity of several ionic liquids and MWCNTs-ionanofluids as a function of temperature are presented and analyzed. The thermal conductivity data obtained have an uncertainty of 3-5% and, where available, are in good agreement with the available reported data. Present data for the heat capacity of ionic liquids also agree well with published data and have an estimated uncertainty of 1%. In the case of ionanofluids, the data are completely new and cannot be compared with other data. Moderate enhancements of thermal conductivity (between 2 and 9%) were observed for the ionanofluids in comparison with the base ionic liquids and the thermal conductivity showed a weak dependence on temperature.

Present results on specific heat capacity of ionic liquids agree well with the best values obtained with adiabatic calorimetry and DSC measurements from literature. For heat capacity of ionanofluids, an enhancement of up to 8% was found for C<sub>4</sub>mim][PF<sub>6</sub>] with both 1 wt% and 1.5 wt% of MWCNTs, a phenomena found for the first time for nanofluids.

The behavior of these ionanofluids together with the specific behavior of ionic liquids studied suggest the existence of nanocluster formation and preferred paths for heat transfer and storage, a fact that will be the subject of further studies.

The mass production of ionic liquids has not yet been attained; however, when it should, we would be able to replace actual non-biodegradable and environmental harmful heat transfer fluids. In addition, due to their increased heat storage capacity as compared with traditional heat transfer fluids, they have the potential to use in shell and tube heat exchangers, and in other small capacity heat exchangers like micro-channels.

In addition, the use of natural and therefore recyclable and biodegradable nanomaterials, that can replace the CNT's, can provide a great change in the field, due to its big heat capacity, as shown with the results presented for fruit seeds.

With the fascinating features of ionanofluids such as high thermal conductivity, high heat storage capacity and non-volatile nature, they can potentially be used as novel heat transfer fluids. Nonetheless, besides studying thermal conductivity measurement, more experimental and theoretical investigations on heat capacity and viscosity of ionanofluids are imperative in order to exploit their potential applications in numerous important fields.

## 7. Acknowledgments

This work was partially financed by FCT - Fundação para a Ciência e Tecnologia, Portugal, through project EQU-FTT-104614-2008. APCR and SICV would like to thank FCT for PhD grants SFRH/BD/ 39940/2007 and SFRH/BD/64974/2009 and EL is grateful to FCT for a post-doctoral grant SFRH/BPD/42035/2007.

## 8. References

- Bonhote, P., Dias, A., Papageorgiou, N., Kalyanasundaram, K. & Gratzel, M. (1996). Hydrophobic, highly conductive ambient-temperature molten salts. *Inorganic Chemistry*, Vol. 35, No. 5, pp. 1168-1178.
- Carslaw, H. S. & Jaeger, J. C. (1959). *Conduction of Heat in Solids*. Oxford University Press, London.
- Chase, M. W. (1998). *NIST-JANAF Thermochemical Tables (Journal of Physical Chemistry Reference Data Monograph)*. 4th Ed., American Institute of Physics, USA.
- Chen, H., He, Y., Zhu, J., Alias, H., Ding, Y., Nancarrow, P., Hardacre, C., Rooney, D. & Tan, C. (2008). Rheological and heat transfer behaviour of the ionic liquid, [C(4)mim][NTf<sub>2</sub>]. *International Journal of Heat and Fluid Flow*, Vol. 29, pp.149-155.
- Choi, S. U. S. (1995). Enhancing thermal conductivity of fluids with nanoparticles. *ASME FED*, Vol. 231, pp. 99-105.
- Choi, S. U. S., Zhang, Z., Yu, W., Lockwood, F. & Grulke, E. (2001). Anomalous thermal conductivity enhancement in nanotube suspensions. *Applied Physics Letters*, Vol. 79, No. 14, pp. 2252-2254.
- Das, S., Choi, S. U. S. & Patel, H. (2006). Heat transfer in nanofluids - A review. *Heat Transfer Engineering*, Vol. 27, pp.3-19.
- Das, S. K. (2006). Nanofluids - the cooling medium of the future. *Heat Transfer Engineering*, Vol. 27, pp. 1-2.
- Earle, M. & Seddon, K. (2007). Ionic liquids. Green solvents for the future. *Pure and Applied Chemistry*, Vol. 72, pp.1391-1398.



- França, J., Nieto de Castro, C. A., Lopes, M. L. M. & V. Nunes, V. (2009). Influence of thermophysical properties of ionic liquids in chemical process design. *Journal of Chemical Engineering Data*, Vol. 54, pp.2569-2575.
- Fredlake, C., Crosthwaite, J., Hert, D., Aki, S. & Brennecke, J. (2004). Thermophysical properties of imidazolium-based ionic liquids. *Journal of Chemical and Engineering Data*, Vol. 49, No.4, pp. 954-964.
- Fukushima, T., Kosaka, A., Ishimura, Y., Yamamoto, T., Takigawa, T., Ishii, N. & Aida, T. (2003). Molecular ordering of organic molten salts triggered by single-walled carbon nanotubes. *Science*, Vol. 300, pp. 2072-2074.
- Fukushima, T. & Aida, T. (2007). Ionic liquids for soft functional materials with carbon nanotubes. *Chemistry-A European Journal*, Vol. 13, No.18, pp. 5048-5058.
- Garcia-Miaja, G., Troncoso, J. & Romani, L. (2008). Excess properties for binary systems ionic liquid plus ethanol: Experimental results and theoretical description using the ERAS model. *Fluid Phase Equilibria*, Vol. 274, No.1-2, pp.59-67.
- Garcia-Miaja, G., Troncoso, J. & Romani, L. (2009). Excess molar properties for binary systems of alkylimidazolium-based ionic liquids plus nitromethane. Experimental results and ERAS-model calculations. *Journal of Chemical Thermodynamics*, Vol. 41, No. 3, pp. 334-341.
- Gardas, R. L. & Coutinho, J. A. P. (2009). Group contribution methods for the prediction of thermophysical and transport properties of ionic liquids. *AIChE Journal*, Vol. 55, pp.1274-1290.
- Ge, R., Hardacre, C., Nancarrow, P. & Rooney, D. (2007). Thermal conductivities of ionic liquids over the temperature range from 293 K to 353 K. *Journal of Chemical and Engineering Data*, Vol. 52, No. 5, pp. 1819-1823.
- Hamilton, R. & Crosser, O. (1962). Thermal Conductivity of Heterogeneous 2-Component Systems. *Industrial & Engineering Chemistry Fundamentals*, Vol. 1, No. 3, 187-191.
- Holbrey, J., Seddon, K. & Wareing, R. (2001). A simple colorimetric method for the quality control of 1-alkyl-3-methylimidazolium ionic liquid precursors. *Green Chemistry*, Vol. 3, No. 1, pp.33-36.
- Holbrey, J., Reichert, W., Reddy, R. & Rogers, R. (2003). Heat capacities of ionic liquids and their applications as thermal fluids. *Ionic Liquids as Green Solvents: Progress and Prospects*, Vol. 856, pp.121-133.
- Holbrey, J. (2007). Heat capacities of common ionic liquids- Potential applications as thermal fluids?. *Chimica Oggi-Chemistry Today*, Vol. 25, No. 6, pp. 24-26.
- Hui, P., Zhang, X., Markworth, A. & Stroud, D. (1999). Thermal conductivity of graded composites: Numerical simulations and an effective medium approximation. *Journal of Materials Science*, Vol. 34, No. 22, pp. 5497-5503.
- Kabo, G., Blokhin, A., Paulechka, Y., Kabo, A., Shymanovich, M. & Magee, J. (2004). Thermodynamic properties of 1-butyl-3-methylimidazolium hexafluorophosphate in the condensed state. *Journal of Chemical and Engineering Data*, Vol. 49, No.3, pp. 453-461.
- Kaviani, M. (1995). *Principles of Heat Transfer in Porous Media*. Springer-Verlag New York Inc.
- Kebilinski, P., Phillpot, S., Choi, S. & Eastman, J. (2002). Mechanisms of heat flow in suspensions of nano-sized particles (nanofluids). *International Journal of Heat and Mass Transfer*, Vol.45, No.4, pp.855-863.

- Keblinski, P., Prasher, R. & Eapen, J. (2008). Thermal conductance of nanofluids: is the controversy over? *Journal of Nanoparticle Research*, Vol. 10, No. 7, pp. 1089-1097.
- Kim, K., Shin, B., Lee, H. & Ziegler, F. (2004). Refractive index and heat capacity of 1-butyl-3-methylimidazolium bromide and 1-butyl-3-methylimidazolium tetrafluoroborate, and vapor pressure of binary systems for 1-butyl-3-methylimidazolium bromide plus trifluoroethanol and 1-butyl-3-methylimidazolium tetrafluoroborate plus trifluoroethanol. *Fluid Phase Equilibria*, Vol. 218, No. 2, pp. 215-220.
- Kluitenberg, G., Ham, J. & Bristow, K. (1993). Error analysis of the heat pulse method for measuring soil volumetric heat-capacity. *Soil Science Society of America Journal*, Vol. 57, No.6, pp.1444-1451.
- Leong, K. C., Yang, C. & Murshed, S. M. S. (2006). A model for the thermal conductivity of nanofluids - the effect of interfacial layer. *Journal of Nanoparticle Research*, Vol. 8, No.2, pp.245-254.
- Lopes, J. & Padua, A. (2006). Nanostructural organization in ionic liquids. *Journal of Physical Chemistry B*, Vol. 110, No. 7, pp. 3330-3335.
- Lourenço, M. J. V., Santos, F. J. V., Ramires, M. L. V. & Nieto de Castro, C. A. (2006). Isobaric specific heat capacity of water and aqueous cesium chloride solutions for temperatures between 298 K and 370 K at  $p=0.1$  MPa. *Journal of Chemical Thermodynamics*, Vol. 38, No. 8, pp. 970-974.
- Maxwell, J. C. (1891). *A Treatise on Electricity and Magnetism*. Clarendon Press, Oxford, UK.
- Murshed, S. M. S., Leong, K. C. & Yang, C. (2005). Enhanced thermal conductivity of  $\text{TiO}_2$ -water based nanofluids. *International Journal of Thermal Sciences*, Vol. 44, pp. 367-373.
- Murshed, S. M. S., Leong, K. C. & Yang, C. (2006). Determination of the effective thermal diffusivity of nanofluids by the double hot-wire technique. *Journal of Physics D: Applied Physics*, Vol. 39, pp.5316-5322.
- Murshed, S. M. S., Leong, K. C. & Yang, C. (2008a). Thermophysical and electrokinetic properties of nanofluids - A critical review. *Applied Thermal Engineering*, Vol. 28, No.17-18, pp. 2109-2125.
- Murshed, S. M. S., Leong, K. C. & Yang, C. (2008b). Investigations of thermal conductivity and viscosity of nanofluids. *International Journal of Thermal Sciences*, Vol. 47, No.5, pp.560-568.
- Murshed, S. M. S. (2009). Comment and correction on “ thermal conductance of nanofluids: is the controversy over?”. *Journal of Nanoparticle Research*, Vol. 11, pp.511-512.
- Nieto de Castro, C. A., Lourenço, M. J. V. & Sampaio, M. O. (2000). Calibration of a DSC: its importance for the traceability and uncertainty of thermal measurements. *Thermochimica Acta*, Vol. 347, pp. 85-91.
- Nieto de Castro, C.A. & Santos, F. J. V. (2007). Measurement of ionic liquids properties - Are we doing it well?. *Chimica Oggi-Chemistry Today*, Vol. 25, pp.20-23.
- Nieto de Castro, C. A., Lourenço, M. J. V., Ribeiro, A. P. C., Langa, E., Vieira, S. I. C., Goodrich, P. & Hardacre, C. (2010). Thermal properties of ionic liquids and ionic nanofluids of imidazolium and pyrrolidinium liquids. *Journal of Chemical Engineering Data*, Vol. 55, pp.653-661.

- Nieto de Castro, C. A., Langa, E., Morais, A. L., Matos Lopes, M. L., Lourenço, M. J. V., Santos, F. J. V., Santos, M. S. C. C. S., Lopes, J. S. L., Veiga, H. I. M., Macatrão, M., Esperança, J. M. S. S., Rebelo, L. P. N., Marques, C. S., Afonso, C. A. M. (2010a). Studies on the density, heat capacity, surface tension and infinite dilution diffusion with the ionic liquids  $[C_4mim][NTf_2]$ ,  $[C_4mim][dca]$ ,  $[C_2mim][EtOSO_3]$  and  $[aliquat][dca]$ . *Fluid Phase Equilibria*, Vol. 294, pp.157-179.
- Nunes, V. M. B.; Lourenço, M. J. V., Santos, F. J. V., Matos Lopes, M. L. S. & Nieto de Castro, C. A. (2010). Accurate measurements of physico-chemical properties on ionic liquids and molten salts, In: *Ionic Liquids and Molten Salts: Never the Twain*, Seddon, K. R. & Gaune-Escard, M., (Eds.), pp. 229-263, John Wiley, USA.
- Pârvulescu, V.I. & Hardacre, C. (2007). Catalysis in ionic liquids. *Chemical Reviews*, Vol. 106, No. 6, pp. 2615-2665.
- Phomkong, W., Srzednicki, G. & Driscoll, R. H. (2006). Thermophysical Properties of Stone Fruit. *Drying Technology*, Vol. 24, pp. 195-200
- Queirós, C. S. "Study on the use of waste fruit as new heat absorbing materials", MSc Thesis in Technological Chemistry, FCUL, 2010.
- Ramires, M. L. V., Nieto de Castro, C. A., Fareleira, J. & Wakeham, W. A. (1994). Thermal-conductivity of aqueous sodium-chloride solutions. *Journal of Chemical and Engineering Data*, Vol. 39, pp. 186-190.
- Rebelo, L., Najdanovic-Visak, V., Visak, Z., da Ponte, M., Szydłowski, J., Cerdeirina, C., Troncoso, J., Romani, L., Esperança, J., Guedes, H. & de Sousa, H. (2004). A detailed thermodynamic analysis of  $[C(4)mim][BF_4]$  plus water as a case study to model ionic liquid aqueous solutions. *Green Chemistry*, Vol. 6, No. 8, pp. 369-381.
- Ribeiro, A. P. C., Goodrich, P., Hardacre, C., Lourenço, M. J. V., & Nieto de Castro (2010). Thermal conductivity of ionic liquids with carbon nanotubes (IoNanofluids). *To be submitted*.
- Sabbah, R., An, X., Chickos, J., Leitão, M., Roux, M. & Torres, L. (1999). Reference materials for calorimetry and differential thermal analysis. *Thermochimica Acta*, Vol. 331, No. 2, pp.93-204.
- Sampaio, M. O. & Nieto de Castro, C. A. (1998). Heat capacity of liquid terpenes. *Fluid Phase Equilibria*, Vol. 150-151, pp. 789-796.
- Thomas, H. P. (1990). The international temperature scale of 1990 (ITS-90). *BIPM: Metrologia*, Vol. 27, pp 3-10.
- Tomida, D., Kenmochi, S., Tsukada, T., Qiao, K. & Yokoyama, C. (2007). Thermal conductivities of  $[bmim][PF_6]$ ,  $[hmim][PF_6]$ , and  $[omim][PF_6]$  from 294 to 335 K at pressures up to 20 MPa. *International Journal of Thermophysics*, Vol. 28, No. 4, pp. 1147-1160.
- Troncoso, J., Cerdeirina, C., Sanmamed, Y., Romani, L. & Rebelo, L. (2006). Thermodynamic properties of imidazolium-based ionic liquids: densities, heat capacities, and enthalpies of fusion of  $[bmim][PF_6]$  and  $[bmim][NTf_2]$ . *Journal of Chemical and Engineering Data*, VI. 51, No.5, pp. 1856-1859.
- Van Valkenburg, M., Vaughn, R., Williams, M. & Wilkes, J. (2005). Thermochemistry of ionic liquid heat-transfer fluids. *Thermochimica Acta*, Vol. 425, No. 1-2, pp. 181-188.

- Vieira, S. I. C., Lourenço, M. J. V., Maia Alves, J., Nieto de Castro, C. A. (2010). Using ionic liquids and CNT's (IoNanoFluids) in pigment development. *Pigments and Dyes*, to be submitted.
- Villagran, C., Deetlefs, M., Pitner, W. & Hardacre, C. (2004). Quantification of halide in ionic liquids using ion chromatography. *Analytical Chemistry*, Vol. 76, pp.2118-2123.
- Waliszewski, D., Stepniak, I., Piekarski, H. & Lewandowski, A. (2005). Heat capacities of ionic liquids and their heats of solution in molecular liquids. *Thermochimica Acta*, Vol. 433, No. 1-2, pp. 149-152.
- Wasserscheid, P. & Welton, T. (2007). *Ionic Liquids in Synthesis*, Wiley-VCH: Weinheim, Germany.

# Physico-Chemical Properties of Task-Specific Ionic Liquids

Luís C. Branco<sup>1</sup>, Gonçalo V.S.M. Carrera<sup>1</sup>, João Aires-de-Sousa<sup>1</sup>,  
Ignacio Lopez Martin<sup>2</sup>, Raquel Frade<sup>3</sup> and Carlos A.M. Afonso<sup>3</sup>

<sup>1</sup>REQUIMTE, Departamento de Química, Faculdade de Ciências e Tecnologia,  
Universidade Nova de Lisboa, Campus da Caparica, 2829-516 Caparica

<sup>2</sup>Departamento de Química Orgánica, Universidad de Extremadura, Cáceres E-10071,

<sup>3</sup>CQFM, Centro de Química-Física Molecular, IN - Institute of Nanosciences and  
Nanotechnology, Instituto Superior Técnico, 1049-001 Lisboa,

<sup>1,3</sup>Portugal

<sup>2</sup>Spain

## 1. Introduction

Ionic liquids (ILs) are currently defined as organic salts that melt at or below 100 °C. Even though, they have been first described as early as the 1910s[1], only in the last 20 years the interest from both academia and industry has been gained significant impact. This recent interest is mainly due of their environmental friendly characteristics as green alternative for traditional volatile organic solvents (VOCs) and because of their wide range of physicochemical properties. There are a large number of organic cations and anions that can be combined to form different ionic liquids, and this is one of the most important features of these compounds.

ILs have been also described with some peculiar properties such as their high conductivity, variable range of density and viscosity values, tuneable polarity and solubility as well as their high thermal and chemical stability.[2]

In this chapter will be discussed some relevant physico-chemical properties of ILs particularly melting point, density, viscosity and toxicity.

The number of different cations readily obtained is very large only by modification of the substituents of these families of organic cations particularly for imidazolium, pyridinium, ammonium, phosphonium and guanidinium units. In last decades, ILs based on methylimidazolium cations have been the most studied and applied in several research topics. Anions, on the other hand, can be of either organic or inorganic nature. Overall, the number of possible ionic liquids is estimated around  $10^{18}$ , whereas the number of traditional solvents widely used in industry accounts for a few hundred.

The reported experimental procedures in order to synthesize and purify different types of methylimidazolium ILs is significantly higher compared with other cation families.

Depending of cation/anion combinations, the physico-chemical properties of ILs will be changed. Looking for the large number of possible combinations the development of novel

functional compounds designated as Task-Specific Ionic Liquids (TSILs) has been a remarkable issue.[3]

The purification process of ILs is a relevant step of synthetic methodologies because all of the physico-chemical properties reported in this chapter are moderate to high sensitive to the presence of impurities.

The presence of water or halogen ions (e.g. chloride, bromide or iodide) impurities are frequently considered as the reason of remarkable discrepancies of some properties in particular viscosity, density or conductivity.[4]

In the literature is frequent to find differences of viscosity or density for the same ionic liquid measured in similar experimental conditions. This fact is mainly observed for ILs more hygroscopic.

The possibility to develop alternative synthetic methods that can avoid the presence of some impurities have been recently described.[5] In the same line several greener methodologies using for example no-solvent reaction media, microwave and ultra-sonification systems have been reported.[6] Different purification methods are also described on the literature according the type of impurities and their desired applications.

It's already possible to develop TSILs with at least one peculiar physico-chemical property such as high-dense ILs[7], high thermal ILs[8], large conductivity ILs[9], high or low-viscous ILs[10] and non-toxic or biodegradable ILs.[11] For example, high-dense ILs have been prepared on the lab by introduction of heavy elements (e.g. iodo, bromo or fluor) in the cation combined with fluoride based anions. These TSILs are relevant as energetic materials.[12] High to low-viscous ILs can be useful depending the further applications. For some organic or bioorganic transformations and chemical engineering applications the viscosity values of ILs is a crucial parameter. Large conductivity allows that ILs can be used as alternative electrolytes or relevant materials for electrochemical processes.[13] Non-toxic and biodegradable ILs have been recently applied in biological and pharmaceutical research areas.[14]

In experimental point of view is difficult to design novel functional materials as task-specific ionic liquids without any additional help from prediction or theoretical methods. These methods can orientated the synthetic strategies and avoid the long and expensive ILs synthesis.

ILs can be considered complex molecules containing cation and anion units with polar and apolar domains, which allow their use in a high range of tasks but at the same time restrict the physico-chemical properties prediction, simply by looking to the structure of the compounds. In order to circumvent this problem, the construction of models more or less complex and specific is required.

The **melting point** is the primal property in the definition of an ionic liquid, establishing the lowest temperature from it can be obtained the liquid state. Because the importance of this property several models were constructed such as computational, chemoinformatic linear and non-linear, group contribution equation, physico-chemical equations based and empirical methods. Melting point has been described as a complex property based not only in the intermolecular forces but also in the arrangement of the crystal lattice. Considering the attempts made so far, when more general models are required two different situations might happen, or there is a decrease of the predictive ability or more complex models are required considering the number of parameters involved and the complexity of the algorithm. Despite some limitations of current models is possible to discover new room

temperature ionic liquids with relatively simple models. The most studied families of ILs are based on imidazolium, pyridinium, ammonium and guanidinium cations.

**Density** is another important physico-chemical property based essentially in the mass of the elements of the compound and their inter-molecular forces. The complexity of this property is lower than the melting point, but in order to have quantitative values, several models were constructed using empirical, group contribution, linear and quantum mechanic methods. The obtained predictions are generally accurate.

Some recent efforts to predict the polarity of ionic liquids were performed.[15] This property illustrates the complexity of ionic liquids.

Other properties as viscosity and toxicity are also focused in this chapter. The prediction of these properties is important in order to obtain ionic liquids for specific applications. Because of the reliability of the experimental data, standardization of conditions and time of establishment of the property limited their predictions.

Modelling ionic liquids lacks behind experimental measures, since for a model to be built, reliable experimental data are needed. Stringent protocols need to be implemented in order to obtain sound physicochemical data. Only then robust models can be developed.

## 2. Melting point

Despite the description of the first ionic liquid (ethylammonium nitrate) by Walden in 1914, the field of low temperature melting salts remained a rarity for decades.[16] In the 1970s and 1980s the moisture sensitive chloroaluminate imidazolium ionic liquids attracted the interest of electrochemists.[17] The most important features for this new class of ionic liquids becoming common use were their air and moisture stabilities.

For many important applications of ILs a low melting temperature is desirable. It is known that large non-symmetric ions with a high degree of conformational freedom and diffused univalent charge drop the melting point. Yet, this rule-of-thumb falls short for the rational design of ionic liquids.

The main reasons for developing tools to predict ILs properties are their tuneable nature, this is to say, the prospect of finding an IL exhibiting certain physical-chemical-biological property. And then the enormous number of possible cation-anion combinations, which makes unrealistic synthesising all of them to check for their properties.

Nevertheless, modelling the melting temperature,  $T_m$  of ionic liquids faces some difficulties. First, the reliability of available experimental data related with the discrepancies in the publication of melting point values for the same ILs. Moreover, conformational freedom can lead to glass formation and polymorphism.[18] These downsides probably account for the limit of accuracy attained when predicting the melting points of ILs.

There are two main ways of modelling ILs.

- i. Quantitative Structure-Property Relationships (QSPR)
- ii. Theoretical quantum chemical calculations.

Pros, cons, and examples of these two different approaches will be discussed herein.

### 2.1 Quantitative Structure-Property Relationships

QSPR modelling is based on the idea that all the information related to a molecule can be derived from its chemical nature by means of parameters that encode or describe different molecular features, and these parameters, or descriptors, can be correlated to a particular property (QSPR) or activity (QSAR) chemical or biochemical, the so-called figure of merit.

In other words the goal of a QSPR is to find a function that predicts any molecular property/activity, using information solely derived from the chemical structure.[19]

$$\text{Property} = F(\text{structure}) = F(\cdot)$$

$$F(\cdot) = g\{f_E[f_R(\cdot)]\} \quad (1)$$

Where  $f_R$  is the molecular representation;  $f_E$  contains the structural encoding descriptors; and  $g$  represents the mapping function. The input domain of  $F$  is then the global information that characterises the molecules, and the output domain is typically a set of numbers quantifying the property of interest.

$f_R$ : the molecular representation can be substantiated by means of SMILES notation, H-depleted graphs, geometrical representations, and by quantum-mechanical optimised structures.

$f_E$ : to encode the structure, descriptors can be produced in different ways, in particular:

- a. based on molecular properties using experimental quantities as descriptors. In this approach the feature representation of the molecule is realised through several characteristic experimental properties (solvatochromic parameters). In this case the limitation lies mainly on the fact that a given set of experimental values is required for each compound. This is the method employed to derive Kamlet-Taft parameters (Linear Solvation Energy Relationship, LSER).
- b. Based on group contributions. Relies on the idea that a molecule acts as a number of fragments (atoms, bonds, moieties,...) independently contributing to the investigated property, usually by an additive scheme. Yet, many of these methods are of questionable accuracy and have limited applicability due to the oversimplification of the molecular structure representation.[2]
- c. Based on structural molecular descriptors. Molecular descriptors such as topological indices, quantum-chemical, geometrical, and electrostatic descriptors and so forth, are used to encode molecular features. This approach can take advantage of full, realistic representation of the molecules if descriptors are derived from quantum chemical geometry optimisations, especially those carried out at *ab initio* level.

$g$ : The mapping function can be based on linear or non-linear methods, such as multivariate statistics, standard regression analyses, genetic algorithm regression models and artificial neural networks. Linear methods are more easily interpretable, and conclusions on the mechanisms of action can eventually be derived. Non-linear methods, on the other hand, yield more accurate models, yet difficult to understand in physical terms.

## 2.2 Theoretical quantum chemical calculations

In this approach, the thermodynamic parameters associated to the fusion process are computed, for an appropriate Born-Fajans-Haber cycle, using quantum-mechanical calculations. Unlike the QSPR models, this methodology requires little or no experimental data.[21]

## 2.3 Reports on modelling melting point for ionic liquids

The first models to predict the  $T_m$  of ionic liquids were developed by Katritzky *et al.* in 2002. Two separate studies were reported for pyridinium,[22] and benzyliimidazolium bromides.[23] Melting point data were withdrawn from the Beilstein database and ranged



from 30 to 370 °C. A total of 126 pyridiniums and 149 benzyliimidazoliums were modelled, respectively.

For the pyridinium cations, a six-descriptor equation with a reasonably good correlation is developed for the prediction of the melting temperatures by means of a CODESSA built-in heuristic regression model.

The descriptors most significant to the model are related to the coordination ability of the cation, to electrostatic intermolecular interactions, and to the conformational and rotational degrees of freedom in solid and liquid phases.

For the benzyliimidazolium cations, best multi-linear regression yielded a five-parameter correlation able to predict the melting point of this class of compounds. The descriptors involved in the correlations reflect directly both the intermolecular interactions and the influence of intramolecular electronic effects on those interactions. Prediction studies using the same type of methodology have been reported for other families of potential ILs. Trohalaki *et al.* built separate models for thirteen bromides, thirteen nitrates, and seven nitrocyanamide salts of 1,2,4-triazolium cations.[24] Novelty is related with the application of Quantum-Chemical RHF/6-31G\*\* theory for computing the optimised structures of the melts in the gas phase. Then CODESSA was used to derive the model by best multi-linear regression or heuristic method. These authors pointed out the necessity for designing specific descriptors for ILs. Similarly, using CODESSA and semi-empirical AM1 calculations in order to optimise the geometries, Zhang *et al.* estimated the  $T_m$  for two separate families of dialkylimidazolium (nineteen tetrafluoroborate anions and twenty nine hexafluorophosphate anions) cations.[25] They concluded that the descriptors involved in the models (three and five, respectively) reflect both intermolecular and intramolecular interactions.

Eike, Brennecke, and Maginn[26] applied a genetic function with the Cerius2 package to model the same pyridinium bromides previously reported,[22] and 109 ammonium or choline-based bromides. In all cases, five-descriptor correlations were calculated, showing that asymmetry due to one or two moderately long chains (e.g. n-octyl chains) with two or three shorter chains (e.g. n-butyl) should be favourable. In addition, branching on the longer chains is predicted to be beneficial as long as two or more bonds separate branch points.

In 2005, Aires-de-Sousa and Carrera[27] reported the use of non-linear methods, namely decision trees and neural networks, for the modelling of the set of 126 pyridinium bromides first modelled by Katritzky group. Descriptors were calculated with DRAGON[28] (since then the program has been updated, and the webpage has moved to [http://www.taletе.mi.it/products/dragon\\_description.htm](http://www.taletе.mi.it/products/dragon_description.htm)) and PETRA[29] programs on 3D models computed with CORINA.[3] These non-linear methods are highly flexible and capable of accounting for multiple mechanisms of action, whereas linear methods are more rigid. Thus, in comparison with previous studies, comparable  $R^2$  (as high as 0.933) and RMS (as low as 12.61 °C) were attained. Furthermore, the quality of the predictions can be improved by using an ensemble of trees, i.e. a decision forest. Decision trees and neural networks thus constitute suitable methodologies for modelling purposes.

In 2007 Varnek *et al.*[31] published a comprehensive study testing the performance of different linear and non-linear machine learning methods in performing QSPR modelling. A large set of 717 nitrogen-containing cations, all paired with bromide anions, was studied, as well as subsets of it. Descriptors were used from different types such as molecular fragments, E-state indices, and various molecular features. The authors concluded that the most efficient method-descriptors combination depends on the data set used. Overall, there

is a slight preference of non-linear SVM (support vector machines), AsNN (associative neural networks), and BPNN (back propagation neural networks) over other methods, such as modified partial least-squares analysis and multiple linear regression analysis, no matter what descriptors, of those tested, are used.

In 2009, Liu *et al.* modelled, once again, the groups of melts previously studied by different groups, in which the influence of the anion is ignored, it being the same (bromide) in all cases. Descriptors were calculated with CODESSA, and the sole novelty of this piece of work is the use of a Projection Pursuit Regression (PPR) to derive the model, along with CODESSA built-in Heuristic Method (HM), preceded by Principal Component Analysis (PCA). The authors concluded that PPR performed better than HM.

In 2010, Yan *et al.*[32] reported models for small sets of thirty imidazolium bromides, of 20 imidazolium chlorides, and for the merger of both. Only cationic structures of these ILs were optimised, by means of Hyperchem[33] software and MOPAC program.[34] QSAR module of Materials Studio software and Genetic Algorithm (GA) programs[35] were employed to calculate and select the structure descriptors of ILs. Then, the prediction models correlating the selected structure descriptors and melting points of ILs were set up by using the multiple linear regressions (MLR) method and the back-propagation artificial neural network (BP ANN) method, separately. The authors concluded that ANN shows higher prediction precision than MLR, and that this might denote a non-linear relationship between the cationic structure and the melting point.

A different way of encoding the structure consists of using chemical graphs as input for a recursive neural network (RNN). The RNN automatically encodes the structural information depending on the computational problem at hand.[36] Again, the influence of the anion was overlooked, for this methodology was applied to a set of ILs based on pyridinium bromide.

López-Martin *et al.*[37] reported the first study in which both ions were taken into account to build up a model for predicting the melting point of ILs. Their unique approach consists of optimising the geometries of both ions separately, by means of semi-empirical AM1 calculations; then descriptors are derived with CODESSA for each ion, and finally ion descriptors are paired up for each ionic liquid to develop a model by means of partial least squares analysis. Advantage was taken from the fact that CODESSA provides a variety of constitutional, topological, geometrical, electrostatic, thermodynamic, and quantum-chemical descriptors. The correlation was high for a group of 62 different imidazolium units, encompassing 22 different cations and 11 different anions. Interestingly, the model selects three descriptors related to the structural regions in the imidazolium cation that are important for determining the melting point: the charge-rich region, at 4 Å, localised on the imidazolium ring; the symmetry-breaking region, at 5.5 Å, that decreases the melting point; and from 12 Å onwards the hydrophobic region that increases  $T_m$  due to Van der Waals interactions.

Subsequently, Torrecilla *et al.*[38] extended the scope of this approach to a larger and more diverse group of imidazolium cations. Moreover, the methodology was improved by introducing *ab initio* Hartree-Fock calculations to obtain the minimised ion geometries, and optimising an artificial neural network to build up the prediction model, that rendered a regression coefficient of 0.99 and a mean  $P$ -value of 0.92 (with a mean prediction error of 1.3 %). Sifting a pool of *ca.* 700 descriptors for each ionic liquid by means of linear statistics analyses produced a pool of nine descriptors for the cations and five descriptors for the

anions as being most influential. These are the sole descriptors that were subsequently used in the modelling.

Interestingly, Carrera *et al.*[39] developed a QSPR for the  $T_m$  of 101 guanidinium salts, which encompassed four different anions ( $\text{Cl}^-$ ,  $\text{Br}^-$ ,  $\text{I}^-$ , and  $\text{BPh}_4^-$ ), by means of counter-propagation neural networks, and then synthesised and successfully checked the melting point of six suitable low-melting ILs according to the model. Furthermore, the authors included twelve new descriptors, among a total of 92, purposely designed to encode certain features of the guanidinium cations. Typical absolute errors of 20 °C do not change if anionic families are considered individually.

Molecular dynamics and Monte Carlo simulations have been used in the last decade to model ionic liquids.[4] Most of these simulations are classical as opposed to quantum mechanical; the interactions between chemical species are modelled by empirical force fields, hence, the quality of these simulations is strongly dependent on the intermolecular potential employed. It has been proven that it is possible to find force fields accurate enough to describe ILs.[41] Long and large simulations using *ab initio* are impractical, however, *ab initio* molecular dynamics (AIMD) are somewhat less computer demanding and provide an accurate picture of ion-ion interactions of the liquid state, by combining electronic structure calculations with conventional Molecular Dynamic (MD) methods.

Several reviews have been published that can help to gain insight into the details of molecular modelling.[42]

Thompson and Alavi studied the melting of ILs [emim][PF<sub>6</sub>],[43] and 1-*n*-butyl-4-amino-1,2,4-triazolium bromide[44] by means of molecular dynamics simulations using the force field of Lopes *et al.*[45] If homogeneous nucleation is the sole mechanism to initiate melting, superheating will occur, and direct heating MD simulations of a solid without an interface also show this effect, yielding values for  $T_m$  20 to 30% larger than the experimental melting points. The superheating effect can be eliminated by simulating a system with a solid-liquid interface, and void defects are introduced in the lattice in order to eliminate the free-energy barrier for the interface formation. Calculated  $T_m$  values were 10% higher than experimental ones. However, the downside of this procedure is that it requires more than 500 molecules and long simulation times.

Maginn and Jayaraman computed the melting point of two polymorph crystals of the IL [bmim][Cl] using a thermodynamic integration-based atomistic simulation method[46] (The absolute errors were in the range of 30 to 50 °C).[47]

As early as 2003, Singer *et al.* applied *ab initio* calculations to investigate the relationship between the computed structure and the melting point of three dialkylimidazolium halides.[48] Two levels of computation implemented in Gaussian98 (HF and MP2) with a variety of basis sets, including diffuse functions were used in order to optimise several stable conformers for each cation. Gross trends relating interaction energy and melting point were found, suggesting that more than one factor contributes to the melting point behaviour of these ILs. Interaction energy is defined as the difference between the energy of the ionic system ( $E_{AX}$ ) and the sum of the energies of purely cationic ( $E_{A^+}$ ) and anionic ( $E_{X^-}$ ) species.

$$E(\text{kJ} \cdot \text{mol}^{-1}) = 2625.5 [E_{AX}(\text{au}) - E_{A^+}(\text{au}) + E_{X^-}(\text{au})] \quad (2)$$

Moreover, optimised structures have been well-correlated with solid X-ray geometries. Recently, Li *et al.*[49] reported a similar study on the correlation between the interaction

energy and the melting point of thirty aminoacid based ILs. A density functional theory (DFT) method with 6-3111++G(d,p) basis set was used with Gaussian 03 package.

In previous report Katsyuba *et al.*[50] applied DFT methods alongside vibrational spectroscopy for the study of several imidazolium ILs molecular structure. Unlike Li *et al.* showed a correlation between molecular structure and the melting point, without involving the energy of interaction.

Another way of prediction of the melting point of ILs is employed by Krossing *et al.*[21] where they used an appropriate Born-Fajans-Cycle,  $\Delta_{fus}G$  is estimated applying the principles of Volume-Based Thermodynamics (VBT) and simple quantum chemical calculations in combination with available experimental data. Each ion geometry was optimised in the gas phase at the (RI)-BP86/SV(P) level using TURBOMOLE.[51] The free energies of solvation were calculated using COSMO.[52]

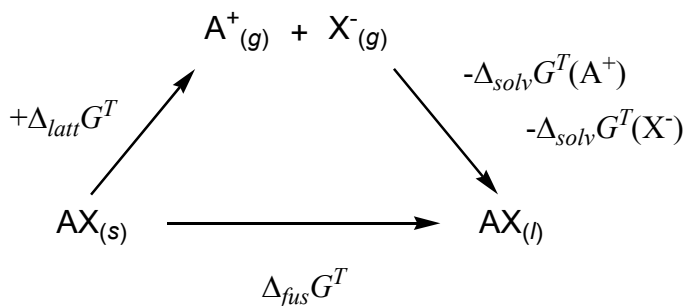


Fig. 1. Born-Fajans-Haber cycle for the assessment of the melting (fusion) of a binary salt (at T) from lattice (latt) and solvation (solv) energies.

Fourteen salts were investigated, and  $T_m$  could be predicted with good accuracy in most cases. It is possible to obtain a clear indication whether a given ion pair is suitable as an IL within 2 to 4 h. However, this approach is difficult to use for purely theoretical predictions, since for an exact estimation of the free energy of fusion, both its intercept and slope have to be known with great accuracy.

Krossing *et al.*[53] present another methodology for predicting  $T_m$  that needs no experimental data. Moreover, only single ions are used as input, thus avoiding lengthy, computer demanding calculation of ion pairs. Average error is 36.4 °C. Implementing the methodology by using COSMO-RS interaction enthalpies reduces the error to 24.5 °C. Optimisations were carried out with TURBOMOLE v5.10[54] and then COSMO. This methodology is an adaptation and refinement of Yalkowsky and Zhao method for neutral organic molecules.[55] Interestingly, the model includes the influence of both ions in the salt and needs only three 'descriptors' to achieve similar results to existing QSPR studies.

## 2.4 Measuring melting point of ionic liquids

The knowledge of the  $T_m$  of an ionic liquid is important to determine its low-end operating range. Modelling the melting point of ILs faces some problems. It is necessary to know some experimental values in order to develop QSPR models, but for some ILs several  $T_m$  values are reported.[31] This can have to do with the occurrence of polymorphs or, sometimes, with poor quality measurements due to, by instance, the presence of impurities.

Furthermore, in some cases only glass transition temperatures have been determined, and these values should be avoided for the model.

The NIST ionic liquid database provide with accurate, reliable data, yet only a small number of values are available so far.[56]

Test samples must be, as pure as possible and, in any case, parameters of purity should be measured and reported, such as water content, halide impurity, and other arising typically from the synthetic procedure.

In the recent years, several reports on determination of  $T_m$  of ionic liquids have appeared. Yet abundant other values have been measured earlier, sometimes only for in-house use, some other available in databases.[57]

Brennecke *et al.* measured the melting points of several ILs, including pyridinium, imidazolium, and ammonium cations. Melting points were measured by Differential Scanning Calorimetry (DSC). Commercial samples (>98 % purity) and some synthesised on purpose were dried *in situ* several times, if needed, until result remained constant. For some of the ILs studied, only  $T_g$  was detected.[58]

Xu *et al* reported  $T_m$  or  $T_g$  of chiral-amine functionalised ILs. DSC showed that all compounds studied had melting points of glass transitions between -49 to 145 °C. Samples were cooled to -70 to -100 °C, then heated at a 10 °C/min rate. Compounds were synthesised in 95 to 97 % purity and characterised by usual  $^1\text{H}$ , and  $^{13}\text{C}$  NMR, FTIR and HRMS techniques, yet no means of further purification were reported.[59]

ILs based on aminoacid derivative anions have been studied by different groups, and their  $T_m$  or  $T_g$  were reported.[6] Typically, these samples were dried under vacuum at moderate to high temperatures (40 to 80 °C) for 24-48h, and purity were checked by  $^1\text{H}$  and  $^{13}\text{C}$  NMR. In the report of Hardacre *et al.* water contents, as determined by Karl-Fischer titration, were reported. These authors also reported the DSC heating and cooling cycle rates of 10 and 5 K min<sup>-1</sup>, respectively. Heating and cooling cycles were repeated during four cycles to ensure reproducibility (uncertainty was determined to be 0.01 K).

Physical-chemical properties of pyrrolidinium ILs have been reviewed by Domańska[61] while new hydrophobic pyridinium-based ILs have been reported by Papaiconomou *et al.*[62] (for some ILs both  $T_g$  and  $T_m$  could be determined by DSC, 10 °C/min rate).

A pool of 53 amidinium based potential ILs were synthesised by Dechambenoit *et al.* For some of them the melting point was reported, and it was found that only a few of them qualified as ILs.[63]

Gores *et al.* studied nine different ILs (pyrrolidinium and imidazolium) and they gave a clear report of the purification and experimental measurement of the transition points at very low heating and cooling temperatures. All ILs were dried under high vacuum (10<sup>-3</sup> Pa) and, if necessary, high temperature (up to 333 K). They were checked by  $^1\text{H}$ ,  $^{13}\text{C}$ ,  $^{11}\text{B}$ , and  $^{19}\text{F}$  NMR. Water content was determined by Karl-Fischer titration. Every sample was cooled down and heated up for at least seven to twenty times for reproducibility, at cooling and heating rates ranging from 2.5 to 30 K h<sup>-1</sup>.

### 3. Density

Density ( $\rho$ ) is a fundamental property in all the materials and is defined by the mass per volume unit:

$$\rho = \frac{m}{v} \quad (3)$$

Density values are currently expressed in  $\text{Kg.m}^{-3}$  (or  $\text{g.cm}^{-3}$ ) as S.I. units. This property reflects the interactions and the distance between the chemical structures defining the applicability of a substance in daily life situations as permitting that an iceberg or a ship floats.

The relevance of this property have been reported in different correlation studies between the structure of a compound with its density. In n-alkanes, it was observed that density increases with the increment of the number of carbon atoms in the alkyl chain, other observation concerns to the higher density of cyclic n-alkanes comparing with linear equivalents.[64] In the case of more complex molecules is more complicated to obtain a direct correlation between the structure of the compound and the density. ILs are examples of very complex molecules with a wide range of applications. Looking for the high number of possible combinations between cation and anions, it's important to develop prediction or estimation methodologies for density parameters instead the experimental preparation of the IL (with the required density simply by trial an error, sparing time and money).

### 3.1 Relationship between structure and density

In order to establish relationships between the structure of the ionic liquid and density, several attempts were performed with differential degrees of complexity, range of applicability and methodology used. Experimental studies regarding specific classes of ILs are important in order to create detailed databases as well as to establish some relationships and validate other methodologies.

Water and halides are important contaminants for experimental measurements of the density, it's already known that the presence of these impurities generally leads to a decrease of the measured value of density.[65]

The most studied family of ILs is based on imidazolium[66] cation. Ammonium[67], phosphonium[68] and guanidinium[69] based ILs were also studied. It was observed that the increase of alkyl chain in 1-alkyl-3-methylimidazolium provokes a correspondent decrease on density values as described by Esperança et al[68] and Gardas[70] et al. Both independent studies reported a constant augment of the molar volume of the salt per each two  $-\text{CH}_2-$  groups ( $34.4 \text{ cm}^3.\text{mol}^{-1}$  and  $33.88 \text{ cm}^3.\text{mol}^{-1}$ , respectively). This progressive augment of molar volume leads to the decrease of density. In another study was observed that the presence of fluorine in the structure of the IL (as cation or anion) provokes an increment of density.[71] Other halogens (e.g. iodine and bromide) increases significantly the density values [72] The presence of pentafluorosulfane ( $-\text{SF}_5$ ) in the cation structure will lead to an increase of density and a reduced melting point.[73] An additional observation is related with the higher densities for aromatic cations than aliphatic ones mainly due their  $\pi$ - $\pi$  interactions which can reduce the inter-molecular distances. The presence of nitrile[74] and hydroxyl[75] groups in the cation normally increase the density. The symmetry and the presence of cyclic units are characteristics that increase the density values which have been related with the reduction of conformational and rotational degrees of freedom and consequent reducing of the free volume between structures. The presence of alkyl ether functional groups for imidazolium based ILs provokes higher densities than n-alkyl substituted equivalents.[76] Many studies have reported that the anion also influences significantly the value of density, the increment of the number of fluorine atoms in the anion generally will lead to higher densities:  $[\text{CH}_3\text{SO}_3]^- \approx [\text{BF}_4]^- < [\text{CF}_3\text{CO}_2]^- < [\text{CF}_3\text{SO}_3]^- < [\text{PF}_6]^- < [\text{NTf}_2]^-$ . The presence of heavy elements on the anion structure increases significantly the

density (e.g. oxypentafluorotungstate anion,  $[\text{WOF}_5]^-$ ). [77] With the support of experimental studies is possible to find the density value of a certain compound. But the accurate quantitative prediction of density is only determine using predictive tools.

One of the first attempts about ILs density predictions was performed by Deetlefs et al. [78] They described two different methods: a) one is based on the equation proposed by Macleod [79] that correlate the density and the surface tension (Equation 3); b) the other is based in the value of refractive index  $R_I$ , molar refractivity  $R_M$  and molar mass of the compound  $M$  through the relationship of Lorentz-Lorenz (Equation 4):

$$R_M = \frac{M}{\rho} \left( \frac{R_I^2 - 1}{R_I^2 + 2} \right) \quad (4)$$

The molar refractivity  $R_M$  is obtained by the addition of tabulated values of structural fragments. With both methods was possible to attain  $R^2$  of 0.999 and 0.998, respectively, for a set of nine ILs.

Differently Ye and Shreeve [80] determine the volume of ILs through the tabulated volumes of cation and anion, crystallographic data and simplified relation between the volume of the salt and the volume of cation and anion:

$$V_{\text{salt}} = V_{\text{cation}} + V_{\text{anion}} \quad (5)$$

This method permitted the density prediction of 35 RTILs based on imidazolium cation with a medium absolute error (MAE) of 0.02 g.cm<sup>-3</sup>. More recently the same authors [81] propose a correction (to the previous method [81]) of  $-8 \text{ \AA}^3$  to  $-\text{NH}_2$  groups in certain chemical environments in order to predict the density of energetic materials.

Gardas et al [82] extended the method of Ye and Shreeve [81] by the introduction of a range of temperatures and pressures using the following equation:

$$\rho = \frac{W}{N V_0 (a + bT + cP)} \quad (6)$$

where  $V_0$  is the molecular volume at the reference temperature ( $T_0$ ) and pressure ( $P_0$ ). The coefficients  $a$ ,  $b$  and  $c$  can be obtained by fitting this equation to experimental data.  $N$  is the Avogadro number and  $W$  the molecular weight.

In a different study, Trohalaki et al [83] used heuristic methods based in several linear regressions to obtain the density of triazolium bromides, the descriptors were used in order to represent the degree of electrostatic interaction and the relation between the surface charge associated to hydrogen bridges and the total surface.

Valderrama et al [84] reported a semi-empirical linear model based on empirical parameters and boiling points that can help for the determination of ILs density values at different temperatures. This model permits that the obtained prediction has 98% of probability with a deviation lower than 10%.

The same author [85] used artificial neural-networks and group contribution method (based on the mass of selected fragments) to calculate the density of several families of the ILs at several temperatures. With this model was obtained an absolute average deviation of 0.26% for a prediction set of 83 points.

Qiao et al[86] used group contribution method based on the addition of selected fragments with the value associated to a specific fragment depending on the localization of the group. All the fragments are accounted in a linear fashion. The method is able to estimate densities of several families of ILs at different temperatures and pressures (the average relative error obtained is 0.88%).

Lazzús[87] predicted the density of several families of ionic ILs using 11 descriptors and polynomial equation. The value of density is predicted at several temperatures and pressures.

The same author[88], obtained a model based on artificial neural network with particle swarm optimization using as input the molar mass and the structure of the compound, represented by the abundance of defined fragments. This method was valid for imidazolium based ILs over a wide range of pressures and temperatures. Using a back propagation neural-network Lazzús[89] estimated the density of several families of ILs using as input the frequency or specific fragments, temperature, pressure and molar mass.

Wang et al[90] used a group contribution equation of state that embodies hard-sphere repulsion, dispersive attraction and ionic electrostatic interaction energy. According to the method each ionic liquid is divided into several groups representing the cation, anion and alkyl group substituents. The method was used to predict the density of imidazolium based ILs over a wide range of temperatures and pressures. The model was found to estimate accurately the densities of the different ILs with an average relative deviation of 0.63% for prediction set.

Palomar et al[91] using a more sophisticated methodology (quantum chemistry methodology called COSMO) were able to optimize the geometry of the salt and determined the different interactions between cation and anion and consequently the volume of the analysed salts. With this method was obtained the density of 40 imidazolium salts with a correlation of 0.995 as  $R^2$  comparing predicted and experimental values. This method is able to determine the distribution of sigma charges. In this distribution is found a zone of polar interactions and other zone of apolar interactions, and according of this distribution the observed densities were interpreted.

The same author[92] used back-propagation neural network associated to distribution of sigma charges determined by COSMO-RS in order to determine accurately the density of imidazolium salts. More recently,[93] the same group used a complex methodology to search the cation/anion pair that can lead to required values of the selected properties, including density. In the first step, the properties of interest are calculated based on back-propagation-neural network model associated to sigma charge distribution. In the second step, the calculated properties are used as input to determine the correspondent sigma distribution charge using an inverse neural network.

Preiss et al[94] used COSMO software to construct a cavity based on the optimized radius of each element of the salt. The volume of the cavity is the calculated volume of the structure from it can be easily determined the molar volume  $V_m$  and also the value of density. The value of  $V_m$  is used to determine relevant properties.

In Table 1 are represented the predicted and experimental densities of reference ILs illustrating the accuracy of one of the first methods[81] developed to predict densities at atmospheric pressure and at room temperature. This table can also be used as reference to find an ionic liquid with the target density.



Cation	Anion	Predicted $\rho$ g.cm <sup>-3</sup>	Experimental $\rho$ g.cm <sup>-3</sup>
<b>Imidazolium</b>			
MMIM	NTf <sub>2</sub>	1.558	1.559
EMIM	BF <sub>4</sub>	1.289	1.279
	NTf <sub>2</sub>	1.511	1.518
	OTf	1.389	1.390
	CF <sub>3</sub> CO <sub>2</sub>	1.284	1.285
	DCA	1.098	1.08
BMIM	BF <sub>4</sub>	1.207	1.208
	PF <sub>6</sub>	1.367	1.37
	NTf <sub>2</sub>	1.433	1.429
	OTf	1.304	1.30
	CF <sub>3</sub> CO <sub>2</sub>	1.211	1.209
	DCA	1.052	1.06
HMIM	BF <sub>4</sub>	1.149	1.148
	PF <sub>6</sub>	1.293	1.293
	NTf <sub>2</sub>	1.371	1.37
	OTf	1.242	1.24
OMIM	BF <sub>4</sub>	1.108	1.109
	PF <sub>6</sub>	1.236	1.237
	NTf <sub>2</sub>	1.320	1.32
	OTf	1.194	1.12
	DCA	0.995	1.0
C <sub>10</sub> MIM	BF <sub>4</sub>	1.075	1.072[95]
<b>Phosphonium</b>			
P <sub>6,6,6,14</sub>	BF <sub>4</sub>	0.929	0.94
	NTf <sub>2</sub>	1.062	1.07
	Cl	0.867	0.883
<b>Ammonium</b>			
N <sub>1,8,8,8</sub>	NTf <sub>2</sub>	1.109	1.11
	CF <sub>3</sub> CO <sub>2</sub>	0.961	0.97
N <sub>1,1,2,3</sub>	NTf <sub>2</sub>	1.406	1.41
<b>Pyridinium</b>			
N-C <sub>4</sub> Pyr	BF <sub>4</sub>	1.222	1.22
N-C <sub>6</sub> Pyr	BF <sub>4</sub>	1.161	1.16
<b>Pyrrolidinium</b>			
C <sub>1</sub> C <sub>4</sub> Pyrr	NTf <sub>2</sub>	1.400	1.40
	OTf	1.266	1.25
	DCA	1.020	1.02
C <sub>6</sub> C <sub>6</sub> Pyrr	NTf <sub>2</sub>	1.240	1.25
C <sub>1</sub> C <sub>8</sub> Pyrr	NTf <sub>2</sub>	1.296	1.29

Table 1. Predicted versus experimental density of reference ionic liquids, the predicted and experimental values were extracted from reference[81] unless otherwise stated.

### 3.2 Applications of task-specific ionic liquids based on density property

The range of applications where density plays a fundamental role is vast. Density is fundamental in several design problems in industry such as design of condensers, reboilers, liquid/liquid mixer settler units, determination of tower heights and dimensions of storage vessels. This property is also important in the context of inertial fluids used in navigation instruments as accelerometers and gyroscopes.[73]

Density values can also help for the determination of several thermodynamic and physico-chemical properties.

This property is useful to determine the efficiency of an energetic material, as explosives which are dependent of the pressure and velocity of detonation as well as of the specific density. With the density parameters is possible to determine the enthalpy of formation of a compound  $\Delta H^\circ$ :

$$\Delta H^\circ = \Delta H_{cation}^\circ + \Delta H_{anion}^\circ + \Delta H_{crystal\_lattice} \quad (7)$$

With  $\Delta H_{crystal\_lattice}$  being dependent on the value of density:

$$\Delta H_{crystal\_lattice} = 1981.2 \cdot \left( \sqrt[3]{\frac{M}{\rho}} \right) + 108.8 \quad (8)$$

where  $M$  is the molar mass. Other properties can be calculated with  $V_m$  as for example the standard entropy  $S^\circ$  according Glasser's theory[96]:

$$S^\circ = 1246.5 \cdot V_m + 29.5 \quad (9)$$

The coefficient of thermal expansion  $\alpha_P$  can also be determined with the knowledge of the variation of the volume with temperature according the equation 10:

$$\alpha_P = \left( \frac{1}{V} \right) \left( \frac{\partial V}{\partial T} \right)_P \quad (10)$$

Finally, the isothermic compressibility  $k_T$  can be obtained according equation 11:

$$k_T = -\frac{1}{V} \cdot \left( \frac{\partial V}{\partial P} \right) \quad (11)$$

This section described the relevance to establish a structure-property relationship between the structure of an ionic liquid and the value of density. According this relationship can be possible to find in straightforward manner the target ionic liquid for a given application.

## 4. Viscosity

Viscosity is a measure of a fluid's internal resistance to flow and may be thought of as a measure of fluid friction. Two different viscosity coefficients have been described, dynamic viscosity, the more usual one which is defined in Pascal-second (Pa.s, SI unit) or centipoises (cP, where 1 cP = 0.001 Pa.s) and kinematic viscosity that is the dynamic viscosity divided by the density (normally in  $m^2.s^{-1}$  or centistokes).

The viscosity parameters of fluids can be measured using viscosimeters when one flow condition is observed or rheometers for liquids with viscosities which vary with flow conditions.

It's already known that in the case of liquids, the additional forces between molecules become important. In liquids, viscosity is independent of pressure (except at very high pressure); and tends to change depending of variation of the temperature.[96] The dynamic viscosities of liquids are typically several orders of magnitude higher than dynamic viscosities of gases.

Viscosity is an important physical property of ionic liquids (ILs).

High viscosity values are useful for applications as lubricants[97] or engineering systems while low viscosity values is generally desired in order to use ILs as a solvent[98] (to minimize pumping costs and increase mass transfer rates). The viscosities of ILs are relatively high compared to those of common organic solvents. Organic solvents typically have room temperature viscosities ranging from 0.2 to 10 cP[99] whereas ILs display a broad range of room temperature viscosities, from 10 to greater than  $10^5$  cP.[100] The viscosities of ILs vary widely depending on the selection of organic cation and inorganic or organic anions.

In this context, in the case of ILs can be possible to tune the viscosity parameters according our desired application.

#### 4.1 Experimental viscosity ILs studies

Experimental data for viscosity of ILs is still narrow and limited to a few classes of well-researched ILs mainly based on metylimidazolium, ammonium, phosphonium, guanidinium, pyrrolidinium and pyridinium cations, among others. More viscosity data and better understanding of this property are required for developing ILs for a specific purpose, and if experimentally measured viscosity data are not available, theoretical or empirical methods must be used in order to establish if the viscosity are within acceptable limiting values defined in the design specifications.

Viscosity of an ionic liquid is dictated by a combination of electrostatics, van der Waals interactions, hydrogen bonding, and ion size and also polarizability, several studies of viscosity can provide information on its fundamental chemical characteristics. ILs based on metylimidazolium cations have been reported with values of viscosity larger according the increase of the length of substituted alkyl cation unit.[101] The ramifications in the alkyl chain seem to reduce the viscosity values of IL. The anion is focused as an important factor where the presence of polyfluor units is favorable in order to reduce the viscosities because the van der waals interactions are also reduced.[102] In this context, anions based on trifluoroacetate, tetrafluoroborate, trifluoromethanesulfonate and bistrifluoromethanesulfonylimide have been described as anions of ILs that promote lower viscosities.[103]

Another relevant factor that influence the viscosity values is related with the size and symmetry of the anion, for example in the case of imidazolium ILs was described that the increase of viscosity is:  $\text{Cl}^- > \text{PF}_6^- > \text{BF}_4^- > \text{NTf}_2^-$ . [104]

The viscosity frequently exhibits a pronounced temperature dependence, however, with values falling significantly upon modest increases in temperature.

Recently, Sanchez and co-workers[105] reported a detailed study about several physical properties of ILs such as viscosity, density and surface tension measured at atmospheric

pressure and at temperatures between (293 and 363) K. For viscosity studies were selected 13 commercial available RTILs based on imidazolium, pyridinium, and pyrrolidinium cations combined with dicyanamide, thiocyanate, methylsulfate, or tetrafluoroborate anions.

The viscosities of [BMIM][BF<sub>4</sub>], [OMIM][BF<sub>4</sub>], [BMIM][DCA], [BMPy][BF<sub>4</sub>], and [BMPy][DCA] decrease rapidly when the temperature is increased. The measured viscosities were higher for the liquids with pyridinium cation than those obtained for the imidazolium-based ILs. The reported viscosities are strongly influenced by the purity of ILs such as water or organic solvents content and halogen impurities. The different purity grade of ILs is one of the reasons about the significant discrepancies of viscosity values observed for the same ILs.

Marsh and co-workers[106] reported the first systematic study of the effect of impurities and additives (e.g., water, chloride, and co-solvents) on the physical properties of Room Temperature Ionic Liquids (RTILs). They concluded that the viscosity of mixtures was dependent mainly on the mole fraction of added molecular solvents and only to a lesser extent upon their identity, allowing viscosity changes during the course of a reaction to be entirely predictable. While the presence of chloride impurities, arising from the preparation of the ILs, increase viscosity dramatically. In general, the addition of co-solvents particularly reduces the viscosity, with the effect being stronger according the higher co-solvent dielectric constant. Torrecilla et al[107] described the effect of relative humidity (RH) of air on the water content, density, apparent molar volume, dynamic viscosity, and surface tension of the ionic liquid 1-ethyl-3-methylimidazolium ethylsulfate, [EMIM][EtSO<sub>4</sub>]. Viscosity measurements were conducted at a temperature of 298.15 K, at atmospheric pressure, and in a RH range of (0 to 100) %. As expected, the absorption of atmospheric moisture by the IL affects its chemical structure. Of the studied physical properties, viscosity exhibits the greatest sensitivity which decreases with increasing RH and water content of the IL.

The relevance of purity of the ILs is clearly observed in the case of halogen contamination (e.g. chloride). In order to illustrate the magnitude of the increase in viscosity with chloride content, known quantities of [C<sub>n</sub>mim]Cl were deliberately added to [C<sub>4-6</sub>mim][BF<sub>4</sub>] and to [C<sub>4-6</sub>mim][PF<sub>6</sub>]. In all cases, the viscosity increased dramatically with the concentration of chloride.

Takada et al[108] described the effect of adding an inorganic salt, lithium chloride, and water on the viscosity of an ionic liquid, 1-n-butyl-3-methylimidazolium chloride [BMIM][Cl], which was studied by shear stress measurements with a rheometer. The shear rate dependence of the viscosity showed shear thinning behavior, which implies that some structure should exist in the liquid and the structure should change at high shear rates. Addition of LiCl enhances the viscosity of [BMIM][Cl]. The increasing rate of the viscosity by addition of LiCl was about 10 times larger than in aqueous solution of LiCl. When water was added into [BMIM][Cl], the correspondent viscosity value decreased. The increasing rate of the viscosity by addition of LiCl for [BMIM][Cl] with about 5 wt % of water was almost the same as that for [BMIM][Cl], without addition of water.

Several studies have been reported in the literature about the viscosity behavior of methylimidazolium, pyridinium and pyrrolidinium as pure ILs or in binary mixture using water or organic solvents (IL + water or IL + organic solvent) at different temperatures and pressure values.[109]

A number of research groups have examined the introduction of an ether oxygen atom into the cations to lower viscosity for the resulting IL.[110]

Wu et al[111] described the preparation of tetraalkylammonium-based aminoacid ionic liquids that showed lower viscosity values compared with other ammonium ILs or examples of ILs with aminoacids as anions. It seems that in the case of combination of tetraethylammonium alanine is found the lowest viscosity of 81 mPa.s (alfa-alanine) and 132 mPa.s (beta-alanine). Anouti et al[112] also described examples of alkylammonium cation based protic acid ILs which were developed through a simple neutralization reaction between an amine (such as di-isopropylmethylamine, and di-isopropylethylamine) and a Brønsted acid, HX, where X is  $\text{HCOO}^-$ ,  $\text{CH}_3\text{COO}^-$ , or  $\text{HF}_2^-$ . Particularly relevant, the very low viscosities measured in the case of N-ethyl di-isopropyl formate (18 cP) and N-methyl di-isopropyl formate (24 cP) at 25 °C. More recent, Bond et al[113] reported a novel series of ILs based on S-alkyl thiolonium, S-alkyl thiotetrazolium and S-alkyl thiobenzolium cations combined with  $\text{NTf}_2$ , TfO, alkyl phosphate, Cl and  $\text{PF}_6$  as anions. The most part of these novel ILs are liquid at RT and have been presented as examples of low viscous RTILs (viscosity values between 36.9 to 222 mPa.s). Other examples of low viscous ILs have been recently reported by Matsumoto and co-workers[114] using perfluoroalkylborate with ether-oxygen units such as  $[\text{CF}_3\text{OCF}_2\text{CF}_2\text{BF}_3]^-$ . According the authors the viscosity of  $[\text{CF}_3\text{OCF}_2\text{CF}_2\text{BF}_3]^-$  based ILs was much lower than those of the corresponding  $[\text{C}_n\text{F}_{2n+1}\text{BF}_3]^-$  ( $n=3, 4$ ) based ILs even though the size and the shape of the three borate anions were close to each other.

## 4.2 Prediction viscosity ILs studies

The development of prediction methods for viscosity of ILs have been reported.[115] While much work has been devoted to the wide range of applications of ILs, the basic understanding and study of their structure-property relationships is of equivalent importance but has lagged behind. More specifically, studies on how the structure of the ions in the IL influences their physical properties are rare. Knowledge of the structure-property relationship is important for assessing the suitability of ILs for specific applications as well as the design of new ILs. Very few works have systematically studied the qualitative and/or quantitative relationships between the structures of ILs and their fundamental properties[116], such as melting point, viscosity, density, surface tension, thermal and electrochemical stability, solvent properties, and speed of sound. At present, however, data for many other physico-chemical properties of ionic liquids are in short supply, or too unreliable to allow similar structure-property relationship studies.[117]

In this context is relevant the Hunt publication[118] about the viscosity study of 1-Butyl-2,3-dimethyl-imidazolium-based ILs. Substitution for a methyl group at the 2-position of the imidazolium cation in order to form 1-butyl-2,3-dimethyl-imidazolium ( $[\text{BDMIM}]^+$ ) eliminates the main hydrogen-bonding interaction between the chloride anion and the imidazolium cation. Loss of this hydrogen bonding interaction could be expected to lead to a reduction in melting point and a decrease in viscosity; however the opposite is observed experimentally; melting points and viscosity both increased.

The prediction of the physico-chemical properties of an unknown ionic liquid will depend on understanding the fundamental molecular-level interactions that give rise to the observed physical and chemical properties. To obtain a deeper understanding of these interactions, the authors investigated the gas-phase ion pairs of a variety of ILs.[119] To give explanation why does a reduction in hydrogen bonding lead to an increase in viscosity values, they performed a study using *ab initio* quantum-chemical methods. The structure and hydrogen bonding of ion pairs ( $[\text{BDMIM}]^+$  and  $\text{Cl}^-$ ) were compared with those obtained

for the unsubstituted analogue [BMIM]Cl. After studies the authors hypothesized that the effects due to a loss in hydrogen bonding are outweighed by those due to a loss in entropy. The amount of disorder in the system can be reduced in two different ways: elimination of ion-pair conformers, which are stable for [BMIM]Cl but not in the case of IL [BDMIM]Cl, and an increase in the rotational barrier of the butyl chain, which limits free rotation as well as facilitates alkyl chain association. The reduction in entropy leads to greater ordering within the liquid increasing viscosity.

Many estimation methods for the viscosity of pure components and mixtures are available in recent literature.[119] The most useful viscosity estimation methods for complex molecules have been reported based on group contributions (e.g., the Orrick-Erbar method,[120] the Sastry-Rao method,[121] and the UNIFAC-VISCO method[122]), the corresponding states concept (e.g., Przesdziecki and Sridhar,[123] Chatterjee and Vasant,[124] Teja and Rice,[125] and Queimada et al.[126]) or the corresponding-states group-contribution (CSGC) method (e.g., Yinghua et al.[127]). Group contribution methods for the estimation of liquid viscosity usually employ some variation of temperature dependence proposed by de Guzman,[128] known as the Andrade equation.[129]

Coutinho et al[116] described the use of a group contribution method in order to estimate the viscosity of imidazolium, pyridinium, and pyrrolidinium based ILs containing hexafluorophosphate [PF<sub>6</sub>], tetrafluoroborate [BF<sub>4</sub>], bis(trifluoromethanesulfonyl) imide [Tf<sub>2</sub>N], chloride [Cl], acetate [CH<sub>3</sub>COO], methyl sulfate [MeSO<sub>4</sub>], ethyl sulfate [EtSO<sub>4</sub>], and trifluoromethanesulfonate [CF<sub>3</sub>SO<sub>3</sub>] anions, covering wide ranges of temperatures (293 to 393K) and viscosity values (4 to 21.000 cP). This method uses a group contribution technique[121] to estimate the A and B parameters in the following equation:

$$\ln \eta / \rho M = A + B/T \quad (12)$$

where  $\eta$  and  $\rho$  are the viscosity in cP units and density in g.cm<sup>-3</sup> units, respectively. M is the molecular weight and T is the absolute temperature.

For circa 500 data points of 29 ILs studied, an average percent deviation (MPD) of 7.7% with a maximum deviation smaller than 28% was observed (71.1% of the estimated viscosities presented deviations smaller than 10% of the experimental values while only 6.4% have deviations larger than 20%). The group contribution method allowed to evaluate the viscosity of new ILs in wide ranges of temperatures at atmospheric pressure and, as data for new groups of cations and anions became available, can be extended to a larger range of ILs. Zhao and co-workers[130] described two prediction methods for shear viscosity of the pure IL [bmim][PF<sub>6</sub>] at 300 K based on reverse non-equilibrium molecular dynamics and equilibrium molecular dynamics simulations respectively. The reverse non-equilibrium molecular dynamics approach has been suitable in order to study the shear viscosity of an ionic liquid of high viscosity. For the case of IL [bmim][PF<sub>6</sub>], the results are in agreement with computationally more demanding equilibrium MD simulations. The force field used produces a good agreement with experimental results, although the calculated viscosity is lower than the experimental value (25 to 40% depending on which experimental value selected as reference). However, these results are an improvement comparing with previous force fields methods which typically overestimated the viscosities of ILs by more than one order of magnitude.

Ghatee et al.[131] described a correlation study with two linear relations of viscosities of ILs. The first one presents the temperature dependence of imidazolium, pyridinium,

pyrrolidinium, quaternary ammonium, and nicotinium-based ILs with high accuracy. From the non-linear behaviour of fluidity, the following linear equation can fit the viscosity of different ILs:

$$(1/\eta)^\phi = a + bT, \quad (13)$$

where  $a$  and  $b$  are substance dependent constants and  $\phi$  is a characteristic exponent.

This equation fits the fluidity accurately and involves the exponent  $\phi = 0.30$  (the characteristic exponent enriched in the correlation applies universally to all ILs).[132]

The second one is a correlation of viscosity with surface tension involving the exponent  $\phi$ , and can fit ILs quite accurately.[133] These correlations have been used as an explanation about the mechanism which a viscous flow is influenced by the nature of the inter-molecular and inter-ionic interactions as well as by the particular structural packing characteristics of ILs.

The temperature dependence of viscosity is a phenomenon where the viscosity ( $\eta$ ) of a liquid decreases or equivalently its fluidity ( $\eta^{-1}$ ) increases with the temperature. Normally, the viscosity of a liquid is a non-linear function of temperature. (At low temperature values increases sharply, and at high temperatures approaches to a small value asymptotically).

Ribeiro et al[134] reported the use of molecular dynamics simulations (MDS) in order to evaluate the influence of alkoxy chain units on the viscosity of a Quaternary Ammonium Ionic Liquid. The MD simulations revealed differences on cation correlation between ILs N-ethyl-N,N-dimethyl-N-(2-methoxyethyl) ammonium bis(trifluoromethanesulfonyl)imide ( $[N_{2,1,1,2-OR}][NTf_2]$ ) and N-ethyl-N,N-dimethyl-N-butyl ammonium bis(trifluoromethanesulfonyl)imide ( $[N_{2,1,1,4}][NTf_2]$ ) beyond the more evident charge ordering effect, which determines the main features of the equilibrium structure of ILs. The key structural difference between these two systems is related with the ether function which for larger conformational freedom of the long chain, in spite of closer approach between the alkoxy chain proper to its higher polarity in comparison to the alkyl chain counterpart. Due to many van der Waals interactions between the long chains of neighbouring cations, there is significant aggregation between the chains within a rather apolar environment. The MD simulations also indicated that the decreases of viscosity, and increase of ionic conductivity, are not due to any change on ionic pairing in the case of ether functionalized ionic liquid. The relevant ether effect on the equilibrium structure is related with short-range cation-cation correlations; i.e., interactions between long alkyl chains in close contact are more effective than between the more flexible alkoxy chains. This explanation can justify the less viscosity values of IL  $[N_{2,1,1,2-OR}][NTf_2]$  than  $[N_{2,1,1,4}][NTf_2]$ .

Anion conformation of a low viscous RTIL 1-ethyl-3-methylimidazolium bis(trifluorosulfonyl)imide ( $[EMIM][NTf_2]$ ) has been studied by Raman spectra and theoretical DFT calculations by Ishiguro and co-workers.[135] Theoretical calculations involved the evaluation of the torsion potential energy surface (PES) with respect to the F-S-N-S dihedral angle and full geometry optimization followed by normal frequency analyses for the single  $NTf_2$  anions were carried out on the basis of Hartree-Fock (HF) theory, as well as density functional theory. They concluded that two possible conformers of the  $NTf_2$  anion coexist in equilibrium when in the liquid state. A stronger dipole-dipole interaction is thus expected for one of the conformers with EMIM cations, which might lead to the favourable formation of the conformer in the IL  $[EMIM][NTf_2]$  at 298 K.

A few theoretical and computational studies have already addressed in some detail the problem of viscosity in ILs.[136] However, a complete microscopic theory of viscosity is currently not available. It is a challenging task to accurately compute the viscosity of a complex system by means of simulation methods. For a system with high viscosity, it is extremely difficult to reach the hydrodynamic limit (zero wave number) where the experimental data is observed. This is because, in order to reach this limit, a very large simulation box is required. Traditional simulation methods normally used for shear viscosity of fluids fall into two categories: (a) the evaluation of the transverse-current autocorrelation function (TCAC) through equilibrium molecular dynamics (EMD) trajectories and (b) non-equilibrium molecular dynamics (NEMD) simulations that impose a periodic perturbation.[137] In recent work, Hess[138] compared most of the above methods by performing simulations of Lennard-Jones and water system. They concluded that the NEMD method using a periodic shear perturbation can be the best option.

Margulis and Hu[139] presented a detailed study about the response of IL 1-hexyl-3-methylimidazolium chloride ([C<sub>6</sub>MIM][Cl]) to external perturbations and the calculation of shear viscosity. It seems after analysis of all the techniques used for the authors that only the periodic perturbation method is feasible. Other methods have been described as useful in order to validate these systems of linear response theory. The very large simulations are still far from the hydrodynamic limit, the transport coefficients of shear viscosity extracted from them using the periodic perturbation method qualitatively agree with experimental data. Accurate knowledge of the long time behaviour of TCACs is important in order to calculate the coefficient of viscosity on the basis of equilibrium simulations. Because of the complex nature of the ILs, this requires very long runs on extremely large simulation boxes to reach the limit of zero  $k$  and infinite time. In contrast, these limits are easily reached for systems such as water on normal simulation boxes and standard run times.

Magin et al[140] described atomistic simulations studies about the dependence of the shear viscosity of [EMIM][NTf<sub>2</sub>] at specific temperature and water percentage. Atomistic simulations have proven helpful in order to understand the correlation between the physical properties of a fluid and its structure and composition. Yan et al[141] described for the first time the use of simulations to determine the viscosity of an ionic liquid. They computed the viscosity of 1-ethyl-3-methylimidazolium nitrate ([EMIM][NO<sub>3</sub>]) at 400 K from the momentum fluctuations in an equilibrium molecular dynamics (MD) simulation.[138] Using a fixed charge model, they found that the simulations yielded a viscosity that was about of 50% higher than the experimental value. The addition of electronic polarization parameters to the model, allowed a drop in the viscosity value of 7% comparing with experimental value. Looking for this observation the authors suggested that polarization parameters should be introduced properly in order to capture the charge screening that takes place in these liquids with a large effect on viscosity values.

Bhargava and Balasubramanian[142] carried out equilibrium MD simulations with a fixed charge model of 1,3-dimethylimidazolium chloride ([mmim][Cl]) at 425 K. Using a Green-Kubo expression (that is, the long-time integral of the stress-stress time correlation function) they obtained a viscosity for [mmim][Cl] that was about four times higher than the experimental value for [emim][Cl]. Apparently, there were no experimental data at this temperature for [mmim][Cl], but the authors assumed that the values would be similar to [emim][Cl].

Micaelo and co-workers[143] conducted MD simulations of [bmim][PF<sub>6</sub>] and [bmim][NO<sub>3</sub>] at temperatures ranging from 298 to 363 K.



Unlike the previous studies in which the viscosity was computed from integrating correlation functions obtained from equilibrium MD trajectories, a non-equilibrium periodic perturbation method[144] was used. In this method, the system is driven away from equilibrium by a spatially varying force and the velocity response is used to obtain the viscosity values.[145]

The shear viscosity  $\eta(\gamma)$  is defined according to the following constitutive equation

$$J_y = -\eta(\gamma)\delta v/\delta y \quad (14)$$

where  $J_y$  is the momentum flux along the (arbitrarily selected) Cartesian  $y$  direction and  $\gamma = \delta v/\delta y$  is the velocity gradient or shear rate ( $\gamma$ ).

Note that the dependence of the shear viscosity on shear rate has been explicitly noted. Alternatively, a non-equilibrium MD simulation can be conducted in which the response of the system to an external perturbation have been considered. The most widely used non-equilibrium approach for viscosity calculations is called "SLLOD" algorithm[146] in which a shear rate is imposed on the system and the resulting stress is computed. The shear viscosity is found at a given shear rate from where  $P_{ij}$  is an off-diagonal component of the stress tensor,  $i$  is the direction of flow caused by the imposed shear rate, and  $j$  is the direction normal to the flow. For the SLLOD algorithm, special "sliding brick" boundary conditions are also typically used, which require modification of the Ewald sum if charged systems are simulated.[147]

A non-equilibrium molecular dynamics procedure is used along with an established fixed charge force field. It is found that the simulations quantitatively capture the temperature dependence of the viscosity as well as the drop in viscosity that occurs with increasing water content. Using mixture viscosity models, the authors showed that the relative drop in viscosity with water content is actually less than the predicted values for an ideal system. This means that dissolved water is actually less effective at lowering the viscosity of these mixtures when compared to a solute obeying ideal mixing behaviour.

## 5. Toxicity

Several studies have been reported on the literature as an attempt to predict the effect of the ILs on aquatic and terrestrial environments as well as in humans. Different models have been used including aquatic organisms, aquatic and terrestrial plants, rat and human cell lines and enzymatic systems, for instance. All models allowed establishing some relations between the structure of the ions and cytotoxicity. Experimental data of several authors are in agreement with the increasing toxicity with the increasing of the alkyl chain length of the substituents in the case of methylimidazolium ([MIM]) cations[148] (Table 1). Methylimidazolium based ILs have been one of the most studied cations, but more recently some new classes have emerged, such as Pyrrolidinium ([Pyr]), Pyridinium ([Py]), Tetra-alkylammonium ( $[N_{x,y,w,z}]$ ) and Tetra-alkylphosphonium ( $[P_{x,y,w,z}]$ ). Toxicity of ammonium and phosphonium based ILs have also been demonstrated to increase significantly with the length of the substituent chains and in particular the case of ILs tri-*n*-octylmethylammonium ([Aliquat]) and tri-*n*-hexyl-tetradecylphosphonium ( $[P_{6,6,6,14}]$ ) are in general very toxic as demonstrated by Frade, R.F.M *et al.*[149] Same authors have also reported toxicity studies for the new ILs based on tetramethylguanidinium ([TMG]) and dimethylguanidinium ([DMG]) cations. For example the tetrabutyl-dimethylguanidinium tetrafluoroborate [(di-b)<sub>2</sub>dmg] [BF<sub>4</sub>] was classified as toxic for CaCo-2 cells while diethyl-dimethylguanidinium tetrafluoroborate [(eb)<sub>2</sub>dmg] [BF<sub>4</sub>] was not toxic.[151] This might be

due to the fact that these cations have a higher number of alkyl chains and therefore a slight increase in the number of carbons leads to a significant effect in the lipophilicity of the cation and as already reported this parameter and toxicity behaviour are closely related.[150] Besides [MIM] cations of short alkyl chains as well as other cations including [Pyr], [Py], [dmg] and tetrabutylammonium  $[N_{4,4,4,4}]$  have allowed the preparation of safe ILs to the CaCo-2 toxicity model.[151] Furthermore, the addition of functional groups on the cation such as ether or carboxylic groups have been incorporated in order to reduce significantly the toxicity (Table 2).[151] The first toxicological studies with ILs were not able to demonstrate an evident effect of the anion in toxicity behaviour, however the most common anions were based on inorganic structures such as halogens (e.g. bromide, [Br] or chloride, [Cl]), tetrafluoroborate ([BF<sub>4</sub>]) and hexafluorophosphate ([PF<sub>6</sub>]). Later a wider range of anions including organic structures were also tested such as dicyanamide ([DCA]), bis-(trifluoromethylsulfonyl)imide ([NTf<sub>2</sub>]), hexafluoroantimonate ([SbF<sub>6</sub>]), acesulfame ([ACS]) and saccharin ([SAC]) among others, which became clear that the type of anion can affect the overall toxicity of the ionic liquid (Table 2).[151] Cytotoxicity data of some representative ILs including different classes of cations and anions are shown in Table 2. Estimated values produced from modelling studies were also introduced for comparison. Experimental and estimated Log<sub>10</sub>EC<sub>50</sub> values were taken from several reported studies and were converted to EC<sub>50</sub> (concentration that reduces viability in about 50%).

CATION ALKYLIC CHAINS	<i>Vibrio fischeri</i> (experimental) ppm, μM, mg/L	<i>Vibrio fischeri</i> (estimated) μM, mg/L	IPC-81 (experimental) μM	IPC-81 (estimated) μM
<b>IMIDAZOLIUM IONIC LIQUIDS</b>				
[MMIM] <sup>+</sup>	[MeSO <sub>4</sub> ]- 57544	[MeSO <sub>4</sub> ]- 57544		
[EMIM] <sup>+</sup>	[Cl]- 35481 [EtSO <sub>4</sub> ]- <b>10471</b>	[Cl]- <b>36509</b> [EtSO <sub>4</sub> ]- <b>10447</b>	[CF <sub>3</sub> SO <sub>3</sub> ]- 12303 [BF <sub>4</sub> ]- 2754 [MeSO <sub>4</sub> ]- 8511 [PF <sub>6</sub> ]- 8318 [BBDB]-* 10 [BOB]-* 860	[CF <sub>3</sub> SO <sub>3</sub> ]- 12023 [BF <sub>4</sub> ]- 3090 [MeSO <sub>4</sub> ]- 8128 [PF <sub>6</sub> ]- 7244 [BBDB]- <u>13</u> [BOB]- <u>890</u>
[C <sub>2</sub> OHMIM] <sup>+</sup>			[NTf <sub>2</sub> ]- 5800	
[BMIM] <sup>+</sup>	[Cl]- 2500/5.12/891 [Br]- 1175/10.23 [BF <sub>4</sub> ]- 3500/3548 [DCA]- 977/4.68 [NTf <sub>2</sub> ]- 300/2.45 [PF <sub>6</sub> ]- 1175	[Cl]- <u>2.95</u> <b>855</b> [Br]- <b>1203</b> / <u>2.95</u> [BF <sub>4</sub> ]- <b>3753</b> [DCA]- <b>959</b> / <u>2.95</u> [NTf <sub>2</sub> ]- <u>0.56</u> [PF <sub>6</sub> ]- <b>1203</b>	[MeSO <sub>3</sub> ]- 3236 [NTf <sub>2</sub> ]- 500 [Cl]- 3548 [Br]- 2692 [BF <sub>4</sub> ]- 1318 [PF <sub>6</sub> ]- 1259 [DCA]- 1400 [SbF <sub>6</sub> ]- 180 [HSO <sub>4</sub> ]- 1700	[MeSO <sub>3</sub> ]- 3631 [Cl]- 3388/ <u>1489</u> [Br]- 3311/ <u>1489</u> [BF <sub>4</sub> ]- <u>1489</u> [PF <sub>6</sub> ]- <u>1489</u> ( <u>k<sub>0</sub>=4.67</u> ) [DCA]- <u>2900</u> [SbF <sub>6</sub> ]- <u>190</u> [HSO <sub>4</sub> ]- <u>1600</u>
[C <sub>3</sub> OMIM] <sup>+</sup>			[I]- 4000 [NTf <sub>2</sub> ]- 1600	

[C <sub>6</sub> MIM] <sup>+</sup>	[Br] <sup>-</sup> 6.46/0.03 [Cl] <sup>-</sup> 87 [PF <sub>6</sub> ] <sup>-</sup> 148 [BF <sub>4</sub> ] <sup>-</sup> 1514	[Br] <sup>-</sup> <b>6.43/0.35</b> [Cl] <sup>-</sup> <b>88</b> [PF <sub>6</sub> ] <sup>-</sup> <b>155</b> [BF <sub>4</sub> ] <sup>-</sup> <b>1511</b>	[Cl] <sup>-</sup> 708 [BF <sub>4</sub> ] <sup>-</sup> 955 [PF <sub>6</sub> ] <sup>-</sup> 813	[Cl] <sup>-</sup> <u>352</u> [BF <sub>4</sub> ] <sup>-</sup> <u>352</u> [PF <sub>6</sub> ] <sup>-</sup> <u>352</u> ( <u>k<sub>0</sub></u> =17.38)
[C <sub>8</sub> MIM] <sup>+</sup>	[Br] <sup>-</sup> 1.17/0.004 [Cl] <sup>-</sup> 15 [PF <sub>6</sub> ] <sup>-</sup> 9 [BF <sub>4</sub> ] <sup>-</sup> 26	[Br] <sup>-</sup> <b>1.17/0.089</b> [Cl] <sup>-</sup> <b>16</b> [PF <sub>6</sub> ] <sup>-</sup> <b>9.04</b> [BF <sub>4</sub> ] <sup>-</sup> <b>25</b>	[Cl] <sup>-</sup> 102	
[C <sub>10</sub> MIM] <sup>+</sup>	[Cl] <sup>-</sup> 3,16 [BF <sub>4</sub> ] <sup>-</sup> 0,66	[Cl] <sup>-</sup> <b>3,25</b> [BF <sub>4</sub> ] <sup>-</sup> <b>0,66</b>	[Cl] <sup>-</sup> 22 [Br] <sup>-</sup> 3.39 [BF <sub>4</sub> ] <sup>-</sup> 5.89 [PF <sub>6</sub> ] <sup>-</sup> 32	[Cl] <sup>-</sup> <u>20</u> [BF <sub>4</sub> ] <sup>-</sup> <u>20</u> [PF <sub>6</sub> ] <sup>-</sup> <u>20</u> ( <u>k<sub>0</sub></u> =234.42)
<b>PYRIDINIUM IONIC LIQUIDS</b>				
[C <sub>4</sub> Py] <sup>+</sup>	[Br] <sup>-</sup> 538 [Cl] <sup>-</sup> 437/2.57 [DCA] <sup>-</sup> 407/2.04	[Cl] <sup>-</sup> <b>432/1.35</b> [DCA] <sup>-</sup> <b>432/1.35</b>	[Br] <sup>-</sup> 8000/7043 [BF <sub>4</sub> ] <sup>-</sup> 1445	[Br] <sup>-</sup> <u>1871</u> [BF <sub>4</sub> ] <sup>-</sup> <u>1871</u> ( <u>k<sub>0</sub></u> =3.80)
[C <sub>3</sub> Opy] <sup>+</sup>			[Cl] <sup>-</sup> 2100 [NTf <sub>2</sub> ] <sup>-</sup> 1300	
[C <sub>4</sub> MPy] <sup>+</sup>	[DCA] <sup>-</sup> 98/0.46 [Br] <sup>-</sup> 130/0.56	[DCA] <sup>-</sup> <u>0.37</u> [Br] <sup>-</sup> <u>0.37</u>	[BF <sub>4</sub> ] <sup>-</sup> 1995	[BF <sub>4</sub> ] <sup>-</sup> <u>1279</u> ( <u>k<sub>0</sub></u> =5.37)
[C <sub>4</sub> MMPy] <sup>+</sup>	[DCA] <sup>-</sup> 56/0.24 [Br] <sup>-</sup> 119/0.49	[DCA] <sup>-</sup> <u>0.76</u> [Br] <sup>-</sup> <u>0.76</u>	[BF <sub>4</sub> ] <sup>-</sup> 1778	[BF <sub>4</sub> ] <sup>-</sup> <u>771</u> ( <u>k<sub>0</sub></u> =8.51)
[C <sub>6</sub> MPy] <sup>+</sup>	[Br] <sup>-</sup> 0.11	[Br] <sup>-</sup> <u>0.15</u>		
[C <sub>6</sub> MPy] <sup>+</sup>	[Br] <sup>-</sup> 1.77/0.006	[Br] <sup>-</sup> <u>0.003</u>		
<b>PYRROLIDINIUM IONIC LIQUIDS</b>				
[C <sub>4</sub> Pyr] <sup>+</sup>			[Br] <sup>-</sup> 5888	[Br] <sup>-</sup> 4266
[C <sub>2</sub> OHMPyr] <sup>+</sup>			[NTf <sub>2</sub> ] <sup>-</sup> 5200	
[C <sub>4</sub> MPyr] <sup>+</sup>			[Cl] <sup>-</sup> >20000 [Br] <sup>-</sup> 5888 [BF <sub>4</sub> ] <sup>-</sup> 794 [DCA] <sup>-</sup> 16982 [NTf <sub>2</sub> ] <sup>-</sup> 1000	[Br] <sup>-</sup> <u>1919</u> [BF <sub>4</sub> ] <sup>-</sup> <u>1919</u> ( <u>k<sub>0</sub></u> =3.72)
[C <sub>6</sub> MPyr] <sup>+</sup>	[Cl] <sup>-</sup> 977	[Cl] <sup>-</sup> <b>959</b>	[Cl] <sup>-</sup> 1479	[BF <sub>4</sub> ] <sup>-</sup> <u>420</u> ( <u>k<sub>0</sub></u> =14.79)
[C <sub>3</sub> OMPyr] <sup>+</sup>			[Cl] <sup>-</sup> 850 [NTf <sub>2</sub> ] <sup>-</sup> 1800	
<b>QUATERNARY AMMONIUM IONIC LIQUIDS</b>				
[N <sub>1,1,1,1</sub> ] <sup>+</sup>	[Br] <sup>-</sup> >100	[Br] <sup>-</sup> <u>234</u>		
[N <sub>4,4,4,4</sub> ] <sup>+</sup>	[Br] <sup>-</sup> 1.86	[Br] <sup>-</sup> <u>0.83</u>	[Br] <sup>-</sup> 178	
[N <sub>2,1,1,4</sub> ] <sup>+</sup>			[Cl] <sup>-</sup> > 20000	
[N <sub>2,1,1,2-OH</sub> ] <sup>+</sup>			[NTf <sub>2</sub> ] <sup>-</sup> 6300 [I] <sup>-</sup> > 20000	
[N <sub>2,1,1,2-OMe</sub> ] <sup>+</sup>			[Cl] <sup>-</sup> 3900 [NTf <sub>2</sub> ] <sup>-</sup> 6300	

QUATERNARY PHOSPHONIUM IONIC LIQUIDS				
[P <sub>4,4,4,4</sub> ] <sup>+</sup>	[Br] <sup>-</sup> 0.51	[Br] <sup>-</sup> 5.75	[Br] <sup>-</sup> 45.71	[BF <sub>4</sub> ] <sup>-</sup> 13.40 (k <sub>0</sub> =338.84)
QUINOLIDINIUM IONIC LIQUIDS				
[C <sub>4</sub> Qui] <sup>+</sup>			[Br] <sup>-</sup> 209 [BF <sub>4</sub> ] <sup>-</sup> 145	[Br] <sup>-</sup> 555 [BF <sub>4</sub> ] <sup>-</sup> 555 (k <sub>0</sub> =11.48)
[C <sub>8</sub> Qui] <sup>+</sup>			[BF <sub>4</sub> ] <sup>-</sup> 1.38	[BF <sub>4</sub> ] <sup>-</sup> 29.38 (k <sub>0</sub> =165.96)

\* [BBDB]- bis-[1,2-benzenodiolato(2-)] borate; [BOB]- bis-[oxalato(2-)]-borate

Table 2. Concentration of the ionic liquid that causes 50% decrease of viability (EC<sub>50</sub>) of two of the most currently applied models: the aquatic microorganism *Vibrio fischeri* and the leukemia rat cell line IPC-81. Some values are calculated experimentally whereas others are determined from quantitative structure-activity relationship models (estimated).

### 5.1 Prediction of ILs toxicity by quantitative structure-activity relationship (QSAR) modelling

Owing to the possibility of generating many thousands of new ILs, the prediction of their toxicity will be facilitated by the existence of quantitative structure-activity relationship (QSAR) methods. Therefore, several studies have already been performed by some groups with the attempt of establishing equations that correlate ionic liquid structure with their experimentally determined toxicity. Correlations are evaluated by statistical parameters and validated by comparison of predict and experimental values ILs that did not participate in the modelling. If the calculated data well-fits the experimental data, the equation will be successful; otherwise it will have to be optimized. For modelling several methods exist of different complexity, which are based on different mathematical functions and different computational algorithms. The first QSAR study correlating ILs structure and toxicity was published in 2004 by Ranke J. *et al.*[152] and they used a logistic model, which correlates the cell viability to the logarithm of the tested concentrations, and linear regression analysis performed with the R language and development for statistical computing. For these studies were selected ILs based on methyl and ethyl (R<sub>1</sub>) alkyl (R<sub>2</sub>) imidazolium (IMI) cations combined with [Cl], [Br], [BF<sub>4</sub>], [PF<sub>6</sub>] and para-toluenosulfonate ([pTsO]) anions and the regression analysis led to the following equations according of used toxicity model:

$$\text{Log}_{10}(\text{EC}_{50}) = (-0.69 \times nR_1) - (0.31 \times nR_2) + 5.24 \quad (r^2 = 0.9137) \quad (\text{IPC-81 leukemia cells})$$

$$\text{Log}_{10}(\text{EC}_{50}) = (-0.54 \times nR_2) + 6.92 \quad (r^2 = 0.988) \quad (\text{C6 glioma cells})$$

$$\text{Log}_{10}(\text{EC}_{50}) = (-0.66 \times nR_1) - (0.57 \times nR_2) + 6.65 \quad (r^2 = 0.93) \quad (\text{Vibrio fischeri}) \quad (15)$$

where  $nR_1$  and  $nR_2$  are the number of carbons of the substituent chains  $R_1$  and  $R_2$ , respectively, and  $\text{EC}_{50}$ , the concentration which induces 50% viability decrease.

The correlation coefficients ( $R^2$ ) demonstrated that the structural parameters and the  $\text{EC}_{50}$  values were well-correlated. The models showed that toxicity clearly increases with the length of the substituent chains, as seen in previous studies. In this case, the toxicity of the anion is not taking into account in the estimative of the ionic liquid toxicity.[1] Later, a similar equation (to equation 16) was obtained in an independent study with [MIM]-based

ILs, proofing the linearity of the variable  $\text{Log}_{10}\text{EC}_{50}$  and the alkyl chain length, for this type of cation combined with small anions such as  $[\text{Cl}]$ ,  $[\text{PF}_6]$ ,  $[\text{BF}_4]$  and  $[\text{Br}]$ . [153]

More recent, Couling D. J. *et al.* [154] published a QSAR study including other organic cations besides imidazolium such as pyridinium  $[\text{Py}]$ , tetra-alkylammonium  $[\text{N}_{x,y,w,z}]$  and tetra-alkylphosphonium  $[\text{P}_{x,y,w,z}]$ . The study involved four different parameters (descriptors); each of them were calculated with other parameters that can reflect the electrostatic and steric influences of individual atoms in the molecule, the partial positive (or negative) charges of cation (or anion), the solvent-accessible surface and the molecular structure. These descriptors were considered for both cation and anion separately and were used in order to generate correlations of the genetic function approximation (GFA) statistical method (which is an algorithm that provides multiple models rather than a single model as an attempt to generate the best fitting). Likewise, a different correlation was obtained for each toxicity model:

$$\text{Log}_{10}\text{EC}_{50}/\text{mmolL}^{-1} = 0.885055 + 1.90609 [\text{RNCG}] - 3.81771 [\text{Shadow-v}] - 1.13277 [\text{RPGC}^*] \\ (R^2=0.782) \text{ (Vibrio fischeri)} \quad (16)$$

where  $[\text{RNCG}]$  is the partial charge of the most negative atom divided by the total negative charge of the cation;  $[\text{RPGC}^*]$  is the partial charge of the most positive atom divided by the total positive charge of the anion; and  $[\text{Shadow-v}]$  is the ratio of the longest to the shortest side of the rectangle that envelops the molecular structure.

$$\text{Log}_{10}\text{LC}_{50}/\text{mmolL}^{-1} = 1.37806 - 3.62486[\text{DPSA}_3] - 1.50205[\text{S}_{\text{aasN}}] - \\ - 1.54858[\text{S}_{\text{aaCH}}] \quad (R^2=0.862) \text{ (Daphnia magna)} \quad (17)$$

where  $[\text{DPSA}_3]$  is the difference between the atomic charge weighted positive and negative solvent-accessible surface area;  $[\text{S}_{\text{aasN}}]$  is the sum of the E-state indices for all carbon atoms with 2 aromatic bonds and one hydrogen bond; and  $[\text{S}_{\text{aaCH}}]$  is the sum of the E-state indices for all carbon atoms with 2 aromatic bonds and one single bond.

These models suggest that ILs toxicity decreases with the increase of localized negative (or positive) charge in the anion (or cation), which means that anions with a single negative atom are likely less toxic or do not affect significantly toxicity which agrees with the study performed by Ranke *et al.* [154] From Table 2, it's possible to observe that the predicted data (values calculated with equation 16 and indicated in italic and underlined) do not vary significantly with the anion. These models also demonstrated the significantly toxicity increase with the number of alkyl chain unit of the aromatic carbons and the slightly increase with the number of nitrogen atoms having two aromatic bonds and one single bond. As result of these studies a toxicity trend was reported based on  $[\text{N}_{x,y,w,z}]$  (less toxic) <  $[\text{Py}]$  <  $[\text{IMI}]$  (more toxic). [156]

In 2004, Stolte S. *et al.* [155] build a different toxicity model using cytotoxicity data gather from studies including several anions and 1-alkyl-3-methylimidazolium cations (with ethyl, butyl and hexyl chains) and performed in the IPC-81 rat leukemia cell line. Firstly, intrinsic toxicity of the anions and cations were assessed assuming that sodium chloride and lithium chloride and, the chloride as anion, respectively, had no impact on toxicity behaviour. These studies revealed that only 10 anions from a total of 27 demonstrated considerable toxicity

having an anion effect ratio (AR) > 5 (AR is the ratio of the EC<sub>50</sub> value of the chloride containing reference ionic liquid and the EC<sub>50</sub> value measured for the same cation with a different anion). The model was build having in consideration the combinations with AR > 5 and assumed that toxicity of the ionic liquid was a sum of the intrinsic toxicities of the cation and the anion as separated entities (model of concentration addition). Non-linear least-squares method was fitted to the experimental data using the logistic model. In a presence of a sub-toxic stimulus, the linear logistic model parameterised by Van Ewijk and Hoekstra was used, instead. Calculations were done with the software library drift for the R language and environment for statistical computing. Model demonstrates that toxicity increases with the ions lipophilicity and susceptibility to hydrolytic cleavage, and that the model of concentration addition may be useful to predict the EC<sub>50</sub> values of not studied ILs.[157] As seen in Table 2, this model reflects the toxicity of the different anions (values double underlined) showing that toxicity may depend on the anion structure. Putting the data together, we may assume that the non evidence of anion toxicity in the earlier studies was due of the lower size and lipophilicity of selected anions.

Luis, P. *et al.*[156] have proposed a new QSAR model based on a novel group contribution method considering that the properties of a molecule is a result of the contributions of its atoms and/or fragments[9]. As a consequence, anions were grouped into three main descriptors (A<sub>1</sub> - [BF<sub>4</sub>], A<sub>2</sub> - [PF<sub>6</sub>], [Cl], [CH<sub>3</sub>SO<sub>4</sub>] and A<sub>3</sub> - [Br], [N(CN)<sub>2</sub>], [C<sub>2</sub>H<sub>3</sub>SO<sub>4</sub>]) while cations were classified in to three classes (imidazolium, [IM], [Py] and [Pyr]) giving origin to more three descriptors (C<sub>1</sub>, C<sub>2</sub> and C<sub>3</sub>) and the number of carbon atoms in the three alkyl chain substituents were also considered contributing to more new three descriptors (R, R<sub>1</sub> and R<sub>2</sub>). A dimensionless toxicity (Y\*) was calculated by the sum of each group of descriptors contributions, where A<sub>1/2/3</sub> and C<sub>1/2/3</sub> were counted as 0 or 1 if absent or present, respectively, and R, R<sub>1/2</sub> were counted as a number within the interval [0-10] for R, 1 or 2 for R<sub>1</sub> and 0, 1 or 2 for R<sub>2</sub> representing the number of carbon atoms in the alkyl chains. This dimensionless parameter was used to build the following equation, using multi-linear regression analysis and Polymath 5.0 software:

$$\text{Log}_{10}\text{EC}_{50}(\mu\text{M}) = 4.76 - (4.76+0.18) \times Y^* \text{ (Vibrio fischeri)} \quad (r^2=0.925) \quad (18)$$

The model shows that the lowest toxicity is confined to the [Pyr] cation following by [IM] and [Py] cations and reflects the effect of the anion. Predicted results fit well the experimental data (Table 2, values in bold).

Furthermore, an interesting model correlating lipophilicity (K<sub>0</sub>), determined by high performance liquid chromatography (HPLC), and toxicity was demonstrated to result in a linear model (Log<sub>10</sub>EC<sub>50</sub>(μM) versus Log<sub>10</sub>(K<sub>0</sub>)) of a great convenience.[150] The study was confined to the classes of cations [IM], [Py], [Pyr], [N<sub>x,y,w,z</sub>], [P<sub>x,y,w,z</sub>] and Quinolidinium [Qui] and produced the following equation:

$$\text{Log}_{10}(\text{EC}_{50}) = 3,91 - 1,1 \times \text{Log}_{10}(k_0) \quad (r^2=0,78) \quad (19)$$

where k<sub>0</sub> is the liphophilicity parameter calculated by HPLC.

The model does not take into account the anion effect and the differences between experimental and predicted data are still significant, especially for high k<sub>0</sub> and then this model should be applied only for k<sub>0</sub> <5.[150] Garcia-Lorenzo *et al.* (2008) has developed a

new a QSAR model using the Topological Sub-structural Molecular Design (TOPS-MODE) approach, which calculates the spectral moments of the fragments constituting each molecule.[157] The software used was the MODESLAB 1.5 software. Following this approach, the spectral moment is determined by the construction of a matrix where non-diagonal entries are ones or zeros if the corresponding bonds share one atom or not and diagonal entries describe several bond weights such as bond dipole moments, bond distance, partition coefficient, polar surface area, polarizability, Gasteiger-Marsilli atomic charges, van der Waals atomic radii and molar refractivity. Genetic algorithm was used to select the variables and its number and regression-based approach was used for the modelling. QSAR model determinates the total contribution to the toxicity of the different fragments of the molecule (P) by summing the different bond contributions ( $\mu_k$ ), being  $\mu_k$  defined as follows:

$$\mu_k^T(i) = b_{ii}(T)^k \quad (20)$$

corresponding  $\mu_k^T(i)$  to the bond  $i$  and  $b_{ii}(T)^k$  to the diagonal entries of the weighted E matrix being  $T$  the type of bond weight.

A large number of ILs based on the imidazolium cation and their  $\text{Log}_{10}\text{EC}_{50}$  in CaCo-2 model were used for this QSAR study. From the group of selected ILs, [MIM] cations with alkyl chains of 4 or 6 carbons or fluorobenzyl-3-methylimidazolium, 1-p-chlorobenzyl-3-methylimidazolium and 1-benzyl-3-methylimidazolium cations produced a similar impact on toxicity and were seen to influence negatively toxicity behaviour (increased  $\text{Log}_{10}\text{EC}_{50}$ ) compared with [MIM] with alkyl chains of 8 and 10 carbons that contributed positively to the toxicity (decreased  $\text{Log}_{10}\text{EC}_{50}$ ).[159] A positive contribution was seen for the anion chloride whereas methyl sulphate ( $[\text{MeSO}_4]$ ) and ethyl sulphate ( $[\text{EtSO}_4]$ ) contributed negatively for the toxicity.[159]

For the methods mentioned before, the computer is set to follow a number of instructions in order to solve the problem however it exists more complicated algorithms that can solve the problem by itself using several functions and at the same time adjusting certain parameters until solving the problem. Some more recent works have followed this approach named Neural Network. The network contains rows of processing elements (neurons) interconnected to each other. Independent variables are sent to the input neurons and the parameters, used to count the relative importance of each variable, are determined (weights) and then multiplied by the different variables, using an activation function, in the hidden neurons. This process can generate several components or descriptors but reduces the number of variables. The values determined for the different descriptors are transformed by a transfer function in the output neuron(s) and the output (calculated  $\text{Log}_{10}\text{EC}_{50}$ ) is generated. The weights have to be optimized (learning or training process) in order to generate the best fitting between experimental and calculated data (validation process). Information can travel only one way (from input to output) (feed-forward networks) or in both directions (feedback networks). Multilayer perception (MLP) functions, radial-basis (RB) functions and linear functions can be also used in the learning process. Torrecilla J. S. *et al.*[158] reported MLP functions as a better model than either linear models or RB models. They used a database of  $\text{Log}_{10}\text{EC}_{50}$  in IPC-81 cells and Acetyl cholinesterase enzyme (AChE) systems obtained from the literature and MATLAB version 7.01.24704 (R14). From 46

independent variables related with elemental composition and molecular weight of the ILs, 12 components were determined and multiplied by the weights using the function TrainBR (Bayesian regularization algorithm) as activation function and afterwards the sigmoid function for calculation of the output value. For the MLP model, the mean predictor error (MPE) and  $R^2$  were 3.9% (2.8%) and 0.982 (0.973) for the IPC-81 (AChE) system, respectively. Recently, a quantum-chemical-based guide was also established by Torrecilla J.S. *et al.* in order to predict cytotoxicity of ILs.[160] Molecular structures and surface charges under a conductor environment were determined independently for the cation and anion using the B3LYP/6-31++G\*\* computational level (Gaussian03 package) and the continuum solvation COSMO model using the BVP86/TZVP/DGA1 level of theory, respectively. The aim was to build a 3D distribution of polarization charges ( $\sigma$ ) of each molecule and to convert this data in to a surface composition function ( $\sigma$ -profile) by the COSMO term program, which was necessary to determine the molecular descriptor  $S_{\sigma\text{-profile}}$  (which measures the distribution of the polar electronic charge of a molecular structure on the polarity  $\sigma$  scale).  $S_{\sigma\text{-profile}}$  of a pure ionic liquid was defined as the sum of those  $S_{\sigma\text{-profile}}$  values of their independent ions (4 descriptors for cations and 6 descriptors for anions). Multi-linear regression relationships (MATLAB version 7.01.24704) were used to calculate and optimized the  $\text{Log}_{10}\text{EC}_{50}$  using toxicity data of a wide group of ILs in IPC-81 cells (86 ILs plus 15 ILs as validated sample). The sigmoid function was used as a transfer function and the activation function was based on the back-propagation (BP) algorithm. In order to design the best MLP model, the regression model selection (RMS) analysis was tested (SPSS software version 15.0.1). The MLP model presented an acceptable goodness of fit, with  $R^2 > 0.96$  and  $\text{MPE} < 5.7\%$ . The  $S_{\sigma\text{-profile}}$  of the cation located at the non-polar region was found to correlate with the lipophilicity parameter ( $\text{Log}K_0$ ) determined by HPLC by Ranke *et al.* and co-workers.[157] This neural network is able to demonstrate the lower toxicity of the imidazolium cations with oxygenated side chains as a result of the charge shift of the structure toward more polarized regions. Some of the estimated values can be seen in Table 2 and they are very close to the experimental values.

## 6. References

- [1] Walden, P.; *Bull. Acad. Impér. Sci. St. Pétersbourg*, 1914, 8, 405-422.
- [2] Rogers, R. D.; Seddon, K. R.; *Ionic Liquids as Green Solvents: Progress and Prospects*; American Chemical Society, 2003.
- [3] Davis, J. H. Jr.; *Chemistry Letters* 2004, 33, 9.
- [4] Wasserscheid, P.; Welton, T.; *Ionic Liquids in Synthesis*, 1st ed.; Wiley-VCH, 2002.
- [5] Stark, A.; Behrend, P.; Braun, O.; Müller, A.; Ranke, J.; Ondruschka, B.; Jastorff, B.; *Green Chem.* 2008, 10, 1152-116
- [6] Cravotto, G.; Gaudino, E. C.; Boffa, L.; Lévêque, J. M.; Estager, J.; Bonrath, Werner; *Molecules* 2008, 13, 149-156.
- [7] Ye, C.; Shreeve, J. M. *J. Org. Chem.* 2004, 69, 6511-6513.
- [8] Kulkarni, P. S.; Branco, L. C.; Crespo, J. G.; Nunes, M. C.; Raymundo, A.; Afonso, C. A. M.; *Chem. Eur. J.* 2007, 13, 8478.
- [9] Stoppa, A.; Zech, O.; Kunz, W.; Buchner, R.; *J. Chem. Eng. Data* 2010, 55, 1768-1773.



- [10] a) Zhou, Z.-B.; Matsumoto, H.; Tatsumi, K.; *Chem. Eur. J.* 2004, 10, 6581 – 6591. b) Wasserscheid, P.; Drieben-Hülscher, B.; van Hal, R.; Steffens, H. C.; Zimmermann, J.; *Chem. Commun.* 2003, 2038-2039.
- [11] a) Garcia, M. T.; Gathergood, N.; Scammells, P. J.; *Green Chem.* 2005, 7, 9-14. b) Carrera, G. V. S. M.; Frade, R. F. M.; Aires-de-Sousa, J.; Afonso, C. A. M.; Branco, L. C., *Tetrahedron*, 2010, in press (doi:10.1016/j.tet.2010.08.040).
- [12] Tao, G. H.; Huang, Y.; Boatz, J. A.; Shreeve, J. M.; *Chem. Eur. J.* 2008, 14, 11167-11173.
- [13] Buzzeeo, M. C.; Evans, R. G.; Compton, R. G.; *ChemPhysChem* 2004, 5, 1106-1120.
- [14] Hough, W. L.; Smiglak, M.; Rodríguez, H.; Swatłowski, R. P.; Spear, S. K.; Daly, D. T.; Pernak, J.; Grisel, J. E.; Carliss, R. D.; Soutullo, M. D.; Davis Jr, J. H.; Rogers, R. D.; *New J. Chem.* 2007, 31, 1429.
- [15] Reichardt, C.; *Green Chem.* 2005, 7, 339-351.
- [16] Hurley, F. H.; Wier, T. P., *J. Electrochem. Soc.* 1951, 98, 207-212.
- [17] Wilkes, J. S., et al., *Inorg. Chem.* 1982, 21, 1263-1264.
- [18] Holbrey, J. D., et al., *Chem. Commun.* 2003, 1636-1637.
- [19] Bernazzani, L., et al., *J. Chem. Inf. Model.* 2006, 46, 2030-2042.
- [20] Marrero, J.; Gani, R., *Fluid Phase Equilibria* 2001, 183-184, 183-208.
- [21] Krossing, I., et al., *J. Am. Chem. Soc.* 2006, 128, 13427-13434.
- [22] Katritzky, A. R., et al., *J. Chem. Inf. Comput. Sci.* 2002, 42, 71-74.
- [23] Katritzky, A. R., et al. *J. Chem. Inf. Comput. Sci.* 2002, 42, 225-231.
- [24] a) Trohalaki, S., et al., *Energy Fuels* 2005, 19, 279-284. b) Trohalaki, S.; Pachter, R., *QSAR Comb. Sci.* 2005, 24, 485-490.
- [25] Sun, N., et al., *Fluid Phase Equilibria* 2006, 246, 137-142.
- [26] Eike, D. M.; Brennecke, J. F.; Maginn, E. J., *Green Chem.* 2003, 5, 323-328.
- [27] Carrera, G.; Aires-de-Sousa, J., *Green Chem.* 2005, 7, 20-27.
- [28] Todeschini, R. and Consonni, V. *Handbook of molecular descriptors*. Weinheim : Wiley-VCH, 2000.
- [29] TORVS. PETRA. [Online] <http://www2.chemie.uni-erlangen.de/software/petra/>.
- [30] Networks, Molecular. CORINA. [Online] [http://www.molecularnetworks.com/online\\_demos/corina\\_demo](http://www.molecularnetworks.com/online_demos/corina_demo).
- [31] Varnek, A., et al., *J. Chem. Inf. Model.* 2007, 47, 1111-1122.
- [32] Yan, C., et al., *Fluid Phase Equilibria* 2010, 292, 104-109.
- [33] Hypercube, Inc. [Online] <http://www.hyper.com>.
- [34] Stewart, J. J. P. Program Package MOPAC2007. [Online] <http://www.mopac2007.com>.
- [35] Studio, Materials. QSAR/ Accelerys. San Diego, CA, USA : s.n., 2005.
- [36] Bini, R., et al., *Green Chem.* 2008, 10, 306-309.
- [37] López-Martin, I., et al. *ChemPhysChem* 2007, 8, 690-695.
- [38] Torrecilla, J. S., et al. *Phys. Chem. Chem. Phys.* 2008, 10, 5826-5831.
- [39] Carrera, G. V. S. M., et al., *Tetrahedron* 2008, 64, 2216-2224.
- [40] Bhargava, B. L.; Balasubramanian, S.; Klein, M. L., *Chem. Commun.* 2008, 3339-3351.
- [41] Lynden-Bell, R. M., et al., *Acc. Chem. Res.* 2007, 40, 1138-1145.
- [42] a) Pópolo, M. G. D., et al., *Acc. Chem. Res.*, 2007, 40, 1156-1164. b) Gomes, M. F. C., Lopes, J. N. C. and Pádua, A. A. H., *Topics in current Chemistry* 2010, 290, 161-183. c)

- Maginn, E. J., *Acc. Chem. Res.* 2007, 40, 1200-1207. d) Rebelo, L. P. N., et al., *Acc. Chem. Res.* 2007, 40, 1114-1121.
- [43] Alavi, S.; Thompson, D. L., *J. Chem. Phys.* 2005, 122, 154704-1/12.
- [44] Alavi, S.; Thompson, D. L., *J. Phys. Chem. B* 2005, 109, 18127-18134.
- [45] Lopes, J. N. C.; Deschamps, J.; Pádua, A. A. H., *J. Phys. Chem. B* 2004, 108, 2038-2047.
- [46] Eike, D. M.; Brennecke, J. F.; Maginn, E. J., *J. Chem. Phys.* 2005, 122, 014115-1/12.
- [47] Jayaraman, S.; Maginn, E. J., *J. Chem. Phys.* 2007, 127, 214504-1/14.
- [48] Turner, E. A.; Pye, C. C.; Singer, R. D., *J. Phys. Chem. A* 2003, 107, 2277-2288.
- [49] Li, W., et al., *Theochem-J. Mol. Struct.* 2010, 942, 19-25.
- [50] Katsyuba, S. A., et al., *J. Phys. Chem. A* 2007, 111, 352-370.
- [51] Turbomole. [Online] <http://www.turbomole.com>.
- [52] Klammt, A. COSMO-RS: from quantum chemistry to fluid phase thermodynamics and drug design. 1st ed. Amsterdam : Elsevier, 2005.
- [53] Preiss, U.; Bulut, S. and Krossing, I., *J. Phys. Chem. B*, 2010, in press (DOI:10.1021/jp104679m).
- [54] University of Karlsruhe. Turbomole v5.10. Turbomole GmbH. [Online] 2008. <http://www.turbomole.com>.
- [55] Zhao, L.; Yalkowsky, S. H., *Ind. Eng. Chem. Res.* 1999, 38, 3581-3584.
- [56] National Institute of Standards and Technology. Ionic Liquids Database- (ILThermo). NIST Standard Reference Database #147. [Online] 2006. <http://ilthermo.boulder.nist.gov>.
- [57] MDL Information Systems GmbH. The Beilstein Database. [Online] <http://www.beilstein.com>.
- [58] Crosthwaite, J. M., et al., *J. Chem. Thermodyn.* 2005, 559-568.
- [59] Luo, S.-P., et al., *Tetrahedron: Asymmetry* 2006, 17, 2028-2033.
- [60] a) Ohno, H.; Fukumoto, K., *Acc. Chem. Res.* 2007, 40, 1122-1129. b) Tao, G., et al., *Green Chem.* 2006, 8, 639-646. c) Gardas, R. L., et al., *J. Chem. Eng. Data* 2010, 55, 1505-1515.
- [61] Domańska, U., *Int. J. Mol. Sci.* 2010, 11, 1825-1841.
- [62] Papaiconomou, N., et al., *J. Chem. Eng. Data* 2010, 55, 1971-1978.
- [63] Dechambenoit, P., et al., *New J. Chem.* 2010, 34, 1184-1199.
- [64] Web page: <http://www.sigmaaldrich.com>. accessed at 04/08/2010.
- [65] Jacquemin, J.; Husson, P.; Mayer, V. ; Cibulka, I. ; *J. Chem. Eng. Data* 2007, 52, 2204-2211.
- [66] a) Esperança, J. M. S. S.; Visak, Z. P.; Plechkova, N. V.; Seddon, K. R.; Guedes, H. J. R.; Rebelo, L. P. N.; *J. Chem. Eng. Data* 2006, 51, 2009-2015. b) Schrekker, H. S.; Silva, D. O.; Gelesky, M. A.; Stracke, M. P.; Schrekker, C. M. L.; Gonçalves, R. S.; Dupont, J.; *J. Braz. Chem. Soc.* 2008, 19, 426-433.
- [67] Jacquemin, J.; Nancarrow, P.; Rooney, D. W.; Gomes, M. F. C.; Husson, P.; Majer, V.; Pádua, A. A. H.; Hardacre, C.; *J. Chem. Eng. Data* 2008, 53, 2133-2143.
- [68] Esperança, J. M. S. S.; Guedes, H. J. R.; Blesic, M.; Rebelo, L. P. N.; *J. Chem. Eng. Data* 2006, 51, 237-242.
- [69] Carrera, G. V. S. M.; Afonso, C. A. M.; Branco, L. C., *J. Chem. Eng. Data* 2010, 55, 609-615.
- [70] Gardas, R. L.; Freire, M. G.; Carvalho, P. J.; Marrucho, I. M.; Fonseca, I. M. A.; Ferreira, A. G. M.; Coutinho, J. A. P.; *J. Chem. Eng. Data* 2007, 52, 80-88.
- [71] Xue, H.; Shreeve, J. M.; *Eur. J. Inorg. Chem.* 2005, 2573-2580.

- [72] Ye, C.; Shreeve, J. M.; *J. Org. Chem.* 2004, 69, 6511-6513.
- [73] Gao, H.; Ye, C.; Winter, R. W.; Gard, G. L.; Sitzmann, M. E.; Shreeve, J. M.; *Eur. J. Inorg. Chem.* 2006, 3221-3226.
- [74] Zhao, D.; Fei, Z.; Scopelliti, R.; Dyson, P. J.; *Inorg. Chem.* 2004, 43, 2197-2205.
- [75] Greaves, T. L.; Weerawardena, A.; Fong, C.; Krodziewska, I.; Drummond, C. J.; *J. Phys. Chem. B* 2006, 110, 22479-22487.
- [76] Branco, L. C.; Rosa, J. N.; Ramos, J. J. M.; Afonso, C. A. M.; *Chem. Eur. J.* 2002, 8, 3671-3677.
- [77] Matsumoto, K.; Hagiwara, R.; *J. Fluorine Chem.* 2005, 126, 1095-1100.
- [78] Deetlefs, M.; Seddon, K. R.; Shara, M.; *Phys. Chem. Chem. Phys.* 2006, 8, 642-649.
- [79] Macleod, D. B.; *Trans Faraday Soc.* 1923, 19, 38-41.
- [80] Ye, C.; Shreeve, J. M.; *J. Phys. Chem. A* 2007, 111, 1456-1461.
- [81] Ye, C.; Shreeve, J. M.; *J. Chem. Eng. Data* 2008, 53, 520-524.
- [82] Gardas, R. L.; Coutinho, J. A. P.; *Fluid Phase Equilibria* 2008, 263, 26-32.
- [83] Trohalaky, S.; Pachter, R.; Drake, G. W.; Hawkins, T.; *Energy Fuels* 2005, 19, 279-284.
- [84] Valderrama, J. O.; Zarricueta, K.; *Fluid Phase Equilibria* 2009, 275, 145-151.
- [85] Valderrama, J. O.; Reátegui, A.; R. E. Rojas; *Ind. Eng. Chem. Res.* 2009, 48, 3254-3259.
- [86] Qiao, Y.; Ma, Y.; Huo, Y.; Ma, P.; Xia, S.; *J. Chem. Thermodynamics* 2010, 42, 852-855.
- [87] Lazzús, J. A.; *J. Phys. Org. Chem.* 2009, 22, 1193-1197.
- [88] Lazzús, J. A.; *Int. J. Thermophys.* 2009, 30, 883-909.
- [89] Lazzús, J. A.; *J. Taiwan Institute Chemical Engineers* 2009, 40, 213-232.
- [90] Wang, J.; Li, Z.; Li, C.; Wang, Z.; *Ind. Eng. Chem. Res.* 2010, 49, 4420-4425.
- [91] Palomar, J.; Ferro, V. R.; Torrecilla, J. S.; Rodríguez, F.; *Ind. Eng. Chem. Res.* 2007, 46, 6041-6048.
- [92] Palomar, J.; Torrecilla, J. S.; Ferro, V. R.; Rodríguez, F.; *Ind. Eng. Chem. Res.* 2008, 47, 4523-4532.
- [93] Palomar, J.; Torrecilla, J. S.; Ferro, V. R.; Rodríguez, F.; *Ind. Eng. Chem. Res.* 2009, 48, 2257-2265.
- [94] Preiss, U. P. R. M.; Slattery, J. M.; Krossing, I.; *Ind. Eng. Chem. Res.* 2009, 48, 2290-2296.
- [95] Glasser, L.; *Thermochim. Acta* 2004, 421, 87-93.
- [96] Pereiro, A. B.; Veiga, H. I. M.; Esperança, J. M. S. S.; Rodríguez, A.; *J. Chem. Thermodynamics* 2009, 41, 1419-1423.
- [97] Ye, C.; Liu, W.; Chen, Y.; Yu, L.; *Chem. Commun.* 2001, 2244-224.
- [98] (a) Welton, T.; *Chem. Rev.* 1999, 99, 2071-2084; (b) Dupont, J.; de Souza, R. F.; Suarez, P. A. Z.; *Chem. Rev.* 2002, 102, 3667-3691.
- [99] Riddick, J.A.; Bunger, W.B.; Sakano, T.K.; *Organic Solvents, Physical Properties and Method of Purification*, 4th ed., John Wiley & Sons, New York, 1986.
- [100] Bonhote, P.; Sias, A.-P.; Papageorgiou, N.; Kalyanasundaram, K.; Gratzel, M.; *Inorg. Chem.* 1996, 35, 1168-1178.
- [101] Zhou, Z.-B.; Matsumoto, H.; Tatsumi, K.; *Chem. Eur. J.* 2004, 10, 6581.
- [102] Zhou, Z.-B.; Matsumoto, H.; Tatsumi, K.; *Chem. Eur. J.* 2005, 11, 752.
- [103] Zhou, Z.-B.; Matsumoto, H.; Tatsumi, K.; *Chem. Eur. J.* 2006, 12, 2196.
- [104] Henderson, W. A., Jr.; Fox, D. M.; De Long, H. C.; Trulove, P. C.; *Chem. Commun.* 2006, 3708.

- [105] Sánchez, L.G.; Espel, J.E.; Onink, F.; Meindersma, G.W.; de Haan, A.B.; *J. Chem. Eng. Data* 2009, 54, 2803–2812.
- [106] Marsh, K.N.; Brenneck, J.F.; Chirico, R.D.; Frenkel, M.; Heintz, A.; Magee, J.W.; Peters, C.J.; Rebelo, L.P.N.; Seddon, K.R.; *Pure Appl. Chem.* 2009, 5, 781–790.
- [107] Torrecilla, J.S.; Rafione, T.; García, J.; Rodríguez, F.; *J. Chem. Eng. Data* 2008, 53, 923–928.
- [108] Takada, A.; Imaichi, K.; Kagawa, T.; Takahashi, Y.; *J. Phys. Chem. B* 2008, 112, 9660–9662.
- [109] Dománska, U.; Laskowska, M.; *J. Solution Chem.* 2009, 38, 779–799.
- [110] Rickert, P.G.; Antonio, M.R.; Firestone, M.A.; Kubatko, K. A.; Szreder, T.; Wishart, J.F.; Dietz, M. L.; *J. Phys. Chem. B* 2007, 111, 4685–4692.
- [111] Jiang, Y.-Y.; Wang, G.-N.; Zhou, Z.; Wu, Y.-T.; Geng, J.; Zhang; Z.-B.; *Chem. Commun.* 2008, 505–507.
- [112] Anouti, M.; Vigeant, A.; Jacquemin, J.; Brigouleix, C.; Lemordant, D.; *J. Chem. Thermodynamics* 2010, 42, 834–845.
- [113] Torriero, A. A. J.; Siriwardana, A. I.; Bond, A. M.; Burgar, I. M.; Dunlop, N. F.; Deacon, G. B.; MacFarlane, D. R.; *J. Phys. Chem. B* 2009, 113, 11222–11231.
- [114] Terasawa, N.; Tsuzuki, S.; Umecky, T.; Saito, Y.; Matsumoto, H.; *Chem. Commun.* 2010, 46, 1730–1732.
- [115] Gardas, R.L.; Coutinho, J.A.P.; *Fluid Phase Equilibria* 2008, 266, 195–201.
- [116] a) Katritzky, A.R.; Lomaka, A.; Petrukhin, R.; Jain, R.; Karelson, M.; Visser, A.E.; Rogers, R.D.; *J. Chem. Inf. Comp. Sci.* 2002, 42, 71–74. b) Deetlefs, M.; Seddon, K.R.; Shara, M.; *Phys. Chem. Chem. Phys.* 2006, 8, 642–649.
- [117] a) Zhang, S.J.; Sun, N.; He, X.Z.; Lu, X.M.; Zhang, X.P.; *J. Phys. Chem. Ref. Data* 2006, 35, 1475–1517. b) Tochigi, K.; H. Yamamoto, *J. Phys. Chem. C* 111 (2007) 15989–15994.
- [118] Hunt, P.A.; *J. Phys. Chem. B* 2007, 111, 4844–4853.
- [119] a) Monnery, W.D.; Svrcek, W.Y.; Mehrotra, A.K.; *Can. J. Chem. Eng.* 1995, 73, 3–40. b) Vesovic, V.; Wakeham, W.A.; *Chem. Eng. Sci.* 1989, 44, 2181–2189. c) Assael, M. J.; Dalaouti, N.K.; Metaxa, I.; *Fluid Phase Equilibria* 2002, 199, 237–247.
- [120] Reid, R.C.; Prausnitz, J.M.; Sherwood, T.K.; *The Properties of Gases and Liquids*, 4th ed., McGraw-Hill, New York, 1987.
- [121] Sastry, S.R.S.; Rao, K.K.; *Fluid Phase Equilibria* 2000, 175, 311–323.
- [122] Gastonbonhomme, Y.; Petrino, P.; Chevalier, J.L.; *Chem. Eng. Sci.* 1994, 49, 1799–1806.
- [123] Przedzicki, J.W.; Sridhar, T.; *AIChE J.* 1985, 31, 333–338.
- [124] Chatterjee, A.; Vasant, A.K.; *Chem. Ind.* 1982, 5, 375–380.
- [125] a) Teja, A.S.; Rice, P.; *Ind. Chem. Fund.* 1981, 20, 77–81. b) Teja, A.S.; Rice, P.; *Chem. Eng. Sci.* 1981, 36, 7–10.
- [126] a) Queimada, A.J.; Marrucho, I.M.; Coutinho, J.A.P.; Stenby, E.H.; *Int. J. Thermophys.* 2005, 26, 47–61. b) Queimada, A.J.; Rolo, L.I.; Caço, A.I.; Marrucho, I.M.; Stenby, E.H.; Coutinho, J.A.P.; *Fuel* 2006, 85, 874–877.
- [127] Yinghua, L.; Peisheng, M.; Ping, L.; *Fluid Phase Equilibria* 2002, 198, 123–130.
- [128] de Guzman, J.; *Anales Soc. Espan. Fis. Quim.* 1913, 11, 353–362.
- [129] Andrade, E.D.C.; *Nature* 1930, 125, 309–310.

- [130] Zhao, W.; Leroy, F.; Balasubramanian, S.; Müller-Plathe, F.; *J. Phys. Chem. B* 2008, 112, 8129–8133.
- [131] Ghatee, M.H.; Zare, M.; Zolghadr, A. R. Moosavi, F.; *Fluid Phase Equilibria* 2010, 291, 188–194.
- [132] Seddon, K.R.; Stark, A.; Torres, M.J.; *ACS Symp. Ser.* 2002, 819, 35–49.
- [133] Ghatee, M.H.; Zolghadr, A.R.; *Fluid Phase Equilibria* 2008, 263, 168–175.
- [134] Siqueira, L. J. A.; Ribeiro, M. C. C.; *J. Phys. Chem. B* 2009, 113, 1074–1079.
- [135] Fujii, K.; Seki, S.; Fukuda, S.; Kanzaki, R.; Takamuku, T.; Umebayashi, Y.; Ishiguro, S.; *J. Phys. Chem. B* 2007, 111, 12829–12833.
- [136] a) Yan, T. Y.; Burnham, C. J.; Del Popolo, M. G.; Voth, G. A. J.; *Phys. Chem. B* 2004, 108, 11877–11881. b) Urahata, S.; Ribeiro, M. J.; *Chem. Phys.* 2006, 124, 74513. Rey-Castro, C.; Vega, L.; *J. Phys. Chem. B* 2006, 110, 14426–14435.
- [137] a) Balucani, U.; Brodholt, J. P.; Jedlovsky, P.; Vallauri, R.; *Phys. Rev. E* 2000, 62, 2971–2973. b) Backer, J. A.; Lowe, C. P.; Hoefsloot, H. C. J.; Ledema, P. D.; *J. Chem. Phys.* 2005, 122, 154503.
- [138] Hess, B.; *J. Chem. Phys.* 2002, 116, 209–217.
- [139] Hu, Z.; Margulis, C. J.; *J. Phys. Chem. B* 2007, 111, 4705–4714.
- [140] Kelkar, M. S.; Maginn, E. J.; *J. Phys. Chem. B* 2007, 111, 4867–4876.
- [141] Yan, T. Y.; Burnham, C. J.; Del Pópolo, M. G.; Voth, G. A.; *J. Phys. Chem. B* 2004, 108, 11877.
- [142] Bhargava, B. L.; Balasubramanian, S. *J. Chem. Phys.* 2005, 123, 144505.
- [143] Micaelo, N. M.; Baptista, A. M.; Soares, C. M.; *J. Phys. Chem. B* 2006, 110, 14444.
- [144] Gosling, E. M.; McDonald, I. R.; Singer, K.; *Mol. Phys.* 1973, 26, 1475.
- [145] Ciccotti, G.; Jacucci, G.; McDonald, I. R.; *J. Stat. Phys.* 1979, 21, 1.
- [146] Evans, D. J.; Morriss, G. P.; *Statistical Mechanics of Nonequilibrium Liquids*; Academic Press: London, 1990.
- [147] Wheeler, D. R.; Fuller, N. G.; Rowley, R. L.; *Mol. Phys.* 1997, 92, 55.
- [148] Stolte, S.; Arning, J.; Bottin-Weber, U.; Muller, A.; Pitner, W. R.; Welz-Biermann, U.; Jastorff, B.; Ranke, J.; *Green Chem.* 2007, 9, 760–767.
- [149] a) Frade, R. F. M.; Matias, A.; Branco, L. C.; Afonso, C. A. M.; Duarte, C. M. M.; *Green Chem.* 2007, 9, 873–877. b) Frade, R. F. M.; Rosatella, A. A.; Marques, C. S.; Branco, L. C.; Kulkarni, P. S.; Mateus, N. M. M.; Afonso, C. A. M.; Duarte, C. M. M.; *Green Chem.* 2009, 11, 1660–1665.
- [150] Ranke, J.; Muller, A.; Bottin-Weber, U.; Stock, F.; Stolte, S.; Arning, J.; Stormann, R.; Jastorff, B.; *Ecotoxicol Environ Saf.* 2007, 67, 430–438.
- [151] a) Cho, C.; Pham, T. P. T.; Jeon, Y.; Yun, Y.; *Green Chem.* 2008, 10, 67–72. b) Matzke, M.; Stolte, S.; Thiele, K.; Jufferholz, T.; Arning, J.; Ranke, J.; Welz-Biermann, U.; Jastorff, B.; *Green Chem.* 2007, 9, 1198–1207.
- [152] Ranke, J.; Molter, K.; Stock, F.; Bottin-Weber, U.; Poczobutt, J.; Hoffmann, J.; Ondruschka, B.; Filser, J.; Jastorff, B.; *Ecotoxicol Environ Saf.* 2004, 58, 396–404.
- [153] Romero, A.; Santos, A.; Tojo, J.; Rodriguez, A.; *J. Hazard Mater.* 2008, 151, 268–273.
- [154] Couling, D. J.; Bernot, R. J.; Docherty, K. M.; Dixon, J. K.; Maginn, E. J.; *Green Chem.* 2006, 8, 82–90.

- [155] Stolte, S.; Arning, J.; Bottin-Weber, U.; Matzke, M.; Stock, F.; Thiele, K.; Uerdingen, M.; Welz-Biermann, U.; Jastorff, B.; Ranke, J.; *Green Chem.* 2006, 8, 621-629.
- [156] Luis, P.; Ortiz, I.; Aldaco, R.; Irabien, A.; *Ecotox Environ Safe* 2007, 67, 423-429.
- [157] A. Garcia-Lorenzo, E. Tojo, J. Tojo, M. Teijeira, F. J. Rodriguez-Berrocal, M. P. Gonzalez and V. S. Martinez-Zorzano, *Green Chem*, 2008, 10, 508-516.
- [158] Torrecilla, J. S.; Palomar, J.; Lemus, J.; Rodriguez, F.; *Green Chem.* 2010, 12, 123-134.

# Physicochemical Properties of Ionic Liquids Containing *N*-alkylamine-Silver(I) Complex Cations or Protic *N*-alkylaminium Cations

Masayasu Iida<sup>1</sup> and Hua Er<sup>2</sup>

<sup>1</sup>*Division of Materials Science, Graduate School of Humanities and Sciences, Nara Women's University, Kita-uoya-nishi-machi, Nara 630-8506,*

<sup>2</sup>*School of Chemistry and Chemical Engineering, Beifang Ethnic University, Ningxia 750021,*

<sup>1</sup>*Japan*

<sup>2</sup>*P. R. China*

## 1. Introduction

Metal-containing ionic liquids are expected to behave as functional materials that combine the unique properties of ionic liquids with additional magnetic, electric, catalytic or emission properties. (Abbott *et al.* 2008; Nockemann *et al.*, 2006, 2009; Scheeren *et al.*, 2006) Ionic liquids of metal complexes which contain metal ions in their molecular structures (metallo-ILs) are particularly applicable in many fields as task-specific soft materials with many possibilities for molecular design. (Lee *et al.*, 2004; Lin *et al.* , 2005; Binnemans, 2007) The first systematic studies of metallo-ILs have been performed for the mixtures of 1-ethylpyridinium bromide and aluminum(III) chloride (Hurley & Wier, 1951). Since then the halogenoaluminate(III) and the alkylhalogenoaluminate(III) ionic liquids have been the most extensively studied systems (Hussey, 1988). The conventional metallo-ILs can be formed by the complexation reactions of simple anionic species with neutral compounds such as:  $\text{AlCl}_3 + \text{EMICl} \rightarrow \text{EMI}^+\text{AlCl}_4^-$ , where  $\text{EMI}^+$  is 1-ethyl-3-methyl-imidazolium cation. These ionic liquids provide a useful extension to the range of solvents that are available for synthetic chemistry (Welton, 1999).

Numerous transition metal chlorides have been shown to form well-defined anionic complexes in basic haloaluminate ionic liquids. When transition metals are bound to neutral ligands in ILs to form transition-metal complex cations, the salts tend to have higher melting points compared with conventional ILs. (Lee *et al.*, 2004; Lin & Vasam, 2005) However, for such kinds of metallo-ILs there are potential applications in a wide range of fields due to their affinity for anionic surfaces which are present abundantly in nature (Israelachvili, 1992) and for carbon surfaces rich in  $\pi$ -electron density by virtue of cation- $\pi$  interactions. (Ma & Dougherty, 1997; Fukushima *et al.*, 2003; Zhang & Cui, 2009)

On the other hand, protic ionic liquids (PILs) have recently attracted attention for their variable proton activities (Yoshizawa *et al.*, 2003; Belieres & Angell, 2007; Angell *et al.*, 2007; Greaves & Drummond, 2008). Although the first room-temperature ionic liquid is ethylammonium nitrate (= EAN) which is the simplest PIL, a large part of the ILs hitherto

studied treats aprotic ILs (AILs). PILs generally have larger polarities and can dissolve metal salts to a larger extent than common AILs. Studies on PILs have been increasing and revealed the attractive features. PIL is also an interesting subset of ILs as follows. They generally form hydrogen-bonded networks, have larger polarity, and generally incorporate metal salts to a larger extent in comparison with AILs due to the more hydrophilic character. The PILs have advantages of potential application in organic synthesis, fuel cells, biological fields, and self-assembly media for amphiphiles. (Greaves, 2006, 2008)

In the present review, we refer to the systems of metallo-ILs having alkylamine or alkylethylenediamine ligands which are the structurally most simple and neutral amphiphilic ligands. Furthermore, alkylamines or alkylethylenediamines can provide protic ionic liquids. We here focus on the physicochemical properties of ionic liquids of *N*-alkylethylenediamines containing silver(I) ion or proton and compare the effects of alkylchains on the physicochemical properties between the silver(I)-ILs and the PILs. We emphasize the difference in the physicochemical properties between the alkylamines and alkylethylenediamines; the latter is more advantageous to incorporate metal ions to the polar domains in the ILs than the former.

## 2. Alkylammonium and metallo-alkylamine ionic liquids

The most extensively studied PIL is EAN, whose property is close to that of water. EAN also forms a strong hydrogen-bonded network structure and is miscible in water and other polar organic solvents. The alkylammonium PILs are solvents available for the self-organization of amphiphiles. Studies on the micellar formation in EAN for cationic surfactants (Evans *et al.*, 1982; Evans & Wennerström, 1999) revealed that the CMCs in EAN are about a factor of 5-10 higher than those in water and that the aggregation numbers are about a factor of 4 smaller. Self-organization of amphiphilic molecules in various solvents including EAN is explained on the basis of cohesive energy. The Gordon parameter (*G*) defined as  $\gamma/V_m^{1/3}$  [J/m<sup>3</sup>], where  $\gamma$  is the surface tension and the  $V_m$  molar volume, is a measure of cohesive energy density of solvents and therefore indicates the driving force for self-assembly. PILs composing of alkylammonium ions other than EAN have also been studied as self-assembly media for amphiphiles. (Greaves *et al.*, 2006, 2008) The *G* value decreases with an increase in the alkyl chain lengths and the driving force for aggregation also decreases. It has been clarified that the alkylammonium PILs are the solvents with the lowest *G* value (552 J/m<sup>3</sup>) which can still self-assemble amphiphiles.

The alkylamine-silver(I) cationic complexes with NO<sub>3</sub><sup>-</sup> and BF<sub>4</sub><sup>-</sup> have been prepared and it was found that they form liquid crystals having bilayer structure of a U-shaped geometry for the cations at near room temperature. (Albéniz *et al.*, 2000) Low melting points of this kind of the complexes are advantageous to form room-temperature ionic liquids using proper counter anions. The ionic liquids of [Ag(H<sub>2</sub>N-R)<sub>2</sub>](TFSA) and [Zn(H<sub>2</sub>N-R)<sub>4</sub>](TFSA)<sub>2</sub> (R = Methyl, Ethyl, Propyl, or *t*-Butyl; TFSA = bis(trifluoromethanesulfonyl)amide anion) have been first prepared (Huang *et al.*, 2006). These metallo-ILs have been utilized in the electrodepositions of silver and zinc, respectively, and have tunable specific functionalities as well as the physicochemical properties by changing both organic ligands and central metal ions.

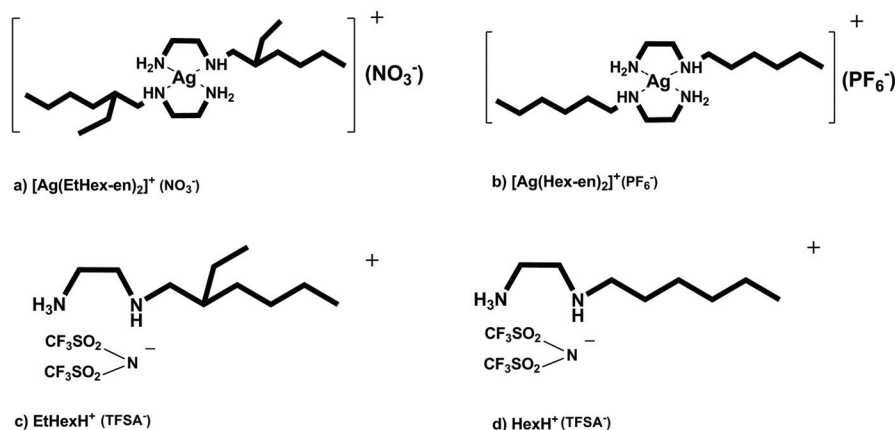
*N*-alkylethylenediamines have two amines and are more favorable for an incorporation of Lewis acids such as proton and transition metal ions into the ILs in comparison with *N*-alkylamines. Therefore, it is of interest to compare the IL systems containing protic *N*-



alkylethylenediaminium (PIL) with those containing metal(I) *N*-alkylethylenediamine complexes (metallo-IL).

### 3. Silver(I)-alkylethylenediamine ILs and alkylethylenediaminium PILs

Bis(*N*-alkylethylenediamine)silver(I) nitrates (alkyl = hexyl, octyl, dodecyl, and hexadecyl) have been prepared by our research group and the X-ray crystallographic analysis for the dodecyl complex has been performed. (Manna *et al.*, 2001; Iida *et al.*, 2004) These surfactants are structurally similar to gemini-type surfactants which have been extensively studied and showed a variety of aggregation phenomena due to multi-alkyl chains and bulky headgroup. (Zana & Xia, 2003) As the metallosurfactants have additional properties due to containing transition metals, multi-chained metallosurfactants are oriented to a wide range of potential applications such as metallomesogens, optoelectronic devices, magnetic resonance imaging, homogeneous catalysis, and nanoparticles. Physicochemical properties of *N*-alkylethylenediamine metal complexes in solution have been studied and it has been clarified that they behave as components of various aggregates in solution such as reverse micelles, microemulsions, and ionic liquid crystals. (Er *et al.*, 2003, 2007) It is characteristic that the W/O microemulsions (or reverse micelles) provided homogeneous and uniformly sized silver(0) or palladium(0) nanoparticles by the reaction with aqueous NaBH<sub>4</sub> solution. It was clarified that the dodecyl and octyl complexes form lyotropic or thermotropic liquid crystals. The octyl complex has a transition from the crystal to the thermotropic liquid crystal at 48 °C, whereas the hexyl complex is melt at 44 °C without a formation of liquid crystal.



Scheme 1. Room temperature ionic liquids containing alkylethylenediamines

From these low-melting points, room-temperature ionic liquids or room-temperature ionic liquid crystals are expected to form by properly controlling structural conditions.

#### 3.1 Formation of room-temperature ionic liquids of alkylethylenediamine silver(I) complexes

An introduction of ethyl-branch in the ligand or an exchange of the counter anion by PF<sub>6</sub> (Scheme 1) was very effective on lowering the melting point of [Ag(Hex-en)<sub>2</sub>]<sub>2</sub>NO<sub>3</sub>. The

complexes of  $[\text{Ag}(\text{EtHex-en})_2]\text{NO}_3$  ( $\text{EtHex-en}$  = 2-ethylhexylethylenediamine) and  $[\text{Ag}(\text{Hex-en})_2]\text{PF}_6$  were newly synthesized. The Hex-en and EtHex-en were prepared by the reactions between the alkylbromides and ethylenediamine (1:5 molar ratio) and then by the distillation under around 1 kPa. The EtHex complex was prepared by the reaction of  $\text{AgNO}_3$  with the ligand in 1: 1.9 molar ratio at 0 °C. The purities of the silver(I) complexes were confirmed by CHN elemental analyses and  $^{13}\text{C}$  NMR spectra. With considering the water content (determined by a Karl-Fisher titration), the elemental analyses gave satisfactory results.

The appearance of the EtHex-en complex at solid state (around - 60 °C) was pale-yellowish transparent, glassy, and the observation by polarizing microscopy (PM) clarified the solid to be isotropic, while the  $[\text{Ag}(\text{Hex-en})_2]\text{PF}_6$  was devitrified at solid state. The DSC curve (with Shimadzu DSC-50 attached LTC-50 apparatus for low-temperature measurements at a constant rate of 10 K  $\text{min}^{-1}$ ) for  $[\text{Ag}(\text{EtHex-en})_2]\text{NO}_3$  described in Fig. 1(a) shows that the glass transition at - 54 °C and small endothermic peak ( $\Delta H = - 1.5 \text{ kJ mol}^{-1}$ ) at - 30 °C were observed; the latter may be ascribed to the enthalpy relaxation. On the other hand,  $[\text{Ag}(\text{Hex-en})_2]\text{PF}_6$  shows a sharp and endothermic peak corresponding to 18 kJ  $\text{mol}^{-1}$  enthalpy change. (Fig. 1(b)) For comparison, DSC curves for  $[\text{Ag}(\text{Hex-en})_2]\text{NO}_3$  and  $[\text{Ag}(\text{oct-en})_2]\text{NO}_3$  are described together. (Figs. 1(c) and (d))

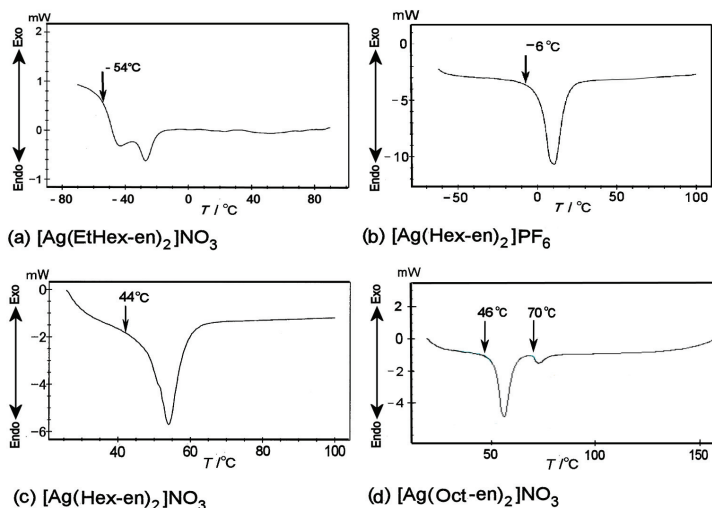


Fig. 1. DSC curves of (a)  $[\text{Ag}(\text{EtHex-en})_2]\text{NO}_3$  at - 80–200 °C, (b)  $[\text{Ag}(\text{Hex-en})_2]\text{PF}_6$  at - 80–200 °C, (c)  $[\text{Ag}(\text{Hex-en})_2]\text{NO}_3$  at 25–200 °C, and (d)  $[\text{Ag}(\text{Oct-en})_2]\text{NO}_3$  at 25–200 °C

The Hex-en complex of the nitrate shows the melting at 44 °C ( $\Delta H = - 34 \text{ kJ mol}^{-1}$ ) and the Oct-en complex of the nitrate ( $\Delta H = - 32 \text{ kJ mol}^{-1}$  for 46 °C and  $\Delta H = - 2.7 \text{ kJ mol}^{-1}$  for 70 °C) shows the formation of liquid crystals in the range of 46–70 °C. These DSC results show that the structural ordering in the solid state is in the order,  $[\text{Ag}(\text{oct-en})_2]\text{NO}_3 > [\text{Ag}(\text{Hex-en})_2]\text{NO}_3 > [\text{Ag}(\text{Hex-en})_2]\text{PF}_6 > [\text{Ag}(\text{EtHex-en})_2]\text{NO}_3$ .

The glassy structure of  $[\text{Ag}(\text{EtHex-en})_2]\text{NO}_3$  in the solid state was directly observed by wide angle X-ray diffraction (WAXD) in the range of  $2\theta = 10\text{--}60^\circ$ . The WAXD was measured with a 0.8 kW generator of  $\text{Cu}_{K\alpha}$  radiation (Panalytical X'Pert Pro). The samples were placed on a horizontal cell in vacuo and measured by using a reflection method. The WAXD profiles for

$[\text{Ag}(\text{EtHex-en})_2]\text{NO}_3$  and  $[\text{Ag}(\text{Hex-en})_2]\text{PF}_6$  at two temperatures ( $-58$  and  $25$  °C) are shown in Fig. 2(a) and 2(b), respectively. In both systems the profiles show amorphous structures, whereas the Hex-en complex is less amorphous than the EtHex-en complex and several sharp peaks additionally appear. The sharper peaks due to the crystalline portions appear more clearly in the Hex-en complex. This result explains the larger and simpler endothermic peak in the DSC curve for the Hex-en complex in comparison with the EtHex-en complex.

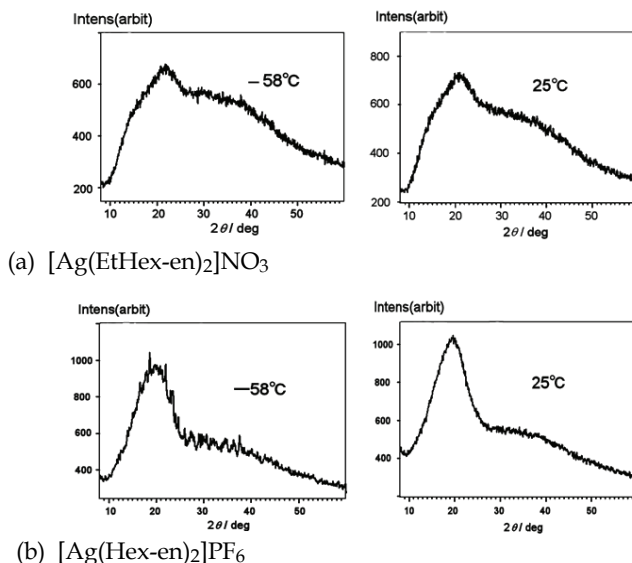


Fig. 2. WAXD profiles of (a)  $[\text{Ag}(\text{EtHex-en})_2]\text{NO}_3 \cdot 0.3\text{H}_2\text{O}$  and (b)  $[\text{Ag}(\text{Hex-en})_2]\text{PF}_6$  at  $-58$  and  $25$  °C.

Hydrophilic-hydrophobic balance of a molecule is an important factor governing a self-aggregation behavior both in neat state and in solution. Therefore, in order to consider the formation of ILs we examined the solubilities of the respective complexes in various solvents. All of the four complexes well dissolved (class 1) in acetone, dichloromethane, ethylacetate, and 1,4-dioxane. The differences in the solubilities for the complexes were seen in some solvents and the results are listed in Table 1. The hydrophobicities of  $\text{PF}_6^-$  and C8-alkyl chains clearly appeared in the cases of water and benzene, but the relationship is somewhat complicated in the other solvents.

	Water	Methanol	Ethanol	$\text{CHCl}_3$	Diethyl Ether	Benzene
$[\text{Ag}(\text{Hex-en})_2]\text{NO}_3$	1	1	1	2	3	3
$[\text{Ag}(\text{Hex-en})_2]\text{PF}_6$	3	1	1	3	3	1
$[\text{Ag}(\text{Oct-en})_2]\text{NO}_3$	3	3	3	2	2	1
$[\text{Ag}(\text{EtHex-en})_2]\text{NO}_3$	3	1	1	3	1	1

1:  $> 10\%$ ; 2:  $0.1\text{--}10\%$ ; 3:  $< 0.1\%$

Table 1. A classification of the solubilities of the bis (alkylethylenediamine)silver(I) complexes.

Dynamic properties of solutions are generally sensitive to the extent of the aggregation in the solution. Self-diffusions and electric conductivities are particularly important and fundamental in the studies on ionic liquid systems. (Tokuda *et al.*, 2004, 2005; Ueno *et al.*, 2010) As small amounts of water significantly affect the dynamic properties in the Ag-ILs, the self-diffusions of the silver complexes and water were measured with a change in the water content. The measurements were performed in the temperature range of 30 (or 40)–70 °C using  $^1\text{H}$  NMR PFG analysis with a JEOL FX-90 spectrometer operating at 90 MHz for the methylene-chain protons in the silver(I) complex. The diffusion coefficients as a function of temperature are given by Arrhenius plots in Fig. 3. Good linearities in the Arrhenius plots are obtained for the Hex-en complex (e), whereas the plots are curved for the EtHex systems at lower water content. Even in the case of the EtHex-en complex the linearities of the plots for both the complex and content water become better with an increase in the water content. Small diffusion coefficients of the EtHex complex at the lowest water content ( $W_0 = 0.3$ , Fig. 3 (a)(i)) mean the formation of strong self-assemblies of the complexes. The liquid at room temperature is regarded as a super-cooling liquid.

For the ILs the curvature of the Arrhenius plots are generally observed and the following Vogel-Tamman-Fulcher (VTF) equation (1) have been conveniently used to interpret the results.

$$D = D_0 \exp\left(-\frac{B}{T - T_0}\right) \quad (1)$$

where  $D_0$  and  $B$  are characteristic constants (VTF parameters) for a given system and a given property, and  $T_0$  is a reference temperature which should be the ideal glass transition temperature of the system independent of the studied property. In the present study, the data for the largest curvature system ( $[\text{Ag}(\text{EtHex-en})_2]\text{NO}_3$ ,  $W_0 = 0.3$ ) were used and the best fitting parameter of  $T_0$  was determined as 200 K. This value was used in the other systems to determine the other  $D_0$  and  $B$  parameters.

For the same  $T_0$  value (200 K), both the  $D_0$  and  $B$  values for  $[\text{Ag}(\text{EtHex-en})_2]\text{NO}_3$  were determined (Iida *et al.*, 2008); they decrease with an increase in the water content. As the  $B$  parameter is related with the apparent activation energy in the Arrhenius plot, the decrease with an increase in water is a reasonable result.

In the case of the Hex complex, the liquid is more fluid. The resultant diffusion coefficient is somewhat larger and the temperature dependency is smaller than the EtHex complex.

In relating with the self-diffusions, the electric conductivities for the two PILs were measured at  $25 \pm 1$  °C with a HORIBA B173, where 0.01 mol dm $^{-3}$  KCl aqueous solution at 25 °C ( $\kappa = 1.41$  mS cm $^{-1}$ ) was used as a standard. The electric conductivities were 31 and 74  $\mu\text{S cm}^{-1}$  for the  $[\text{Ag}(\text{EtHex-en})_2]\text{NO}_3$  and  $[\text{Ag}(\text{Hex-en})_2]\text{PF}_6$ , respectively. The larger electric conductivity for the Hex-en complex than that for the EtHex complex is consistent with the result of the self-diffusions. These very small values reflect the high viscosities. This type of ionic liquids is thus disadvantageous for an application to the field of electric conductivity.

A series of alkyethylenediamine-metal complexes form aggregates in solution such as microemulsions and lyotropic liquid crystals, and thus the present silver(I)-ILs are also expected to form organized nanostructures, which were investigated by small-angle X-ray scattering (SAXS). The SAXS was measured in the range  $2\theta = 1$ – $10^\circ$  at room temperature with a 15-kW generator of  $\text{Cu}_{K\alpha}$  radiation (RIGAKU RINT-TRIII). The sample was put in a 0.4-mm cell interposed by a 0.02-mm Mylar film. The SAXS profiles are given as plots of

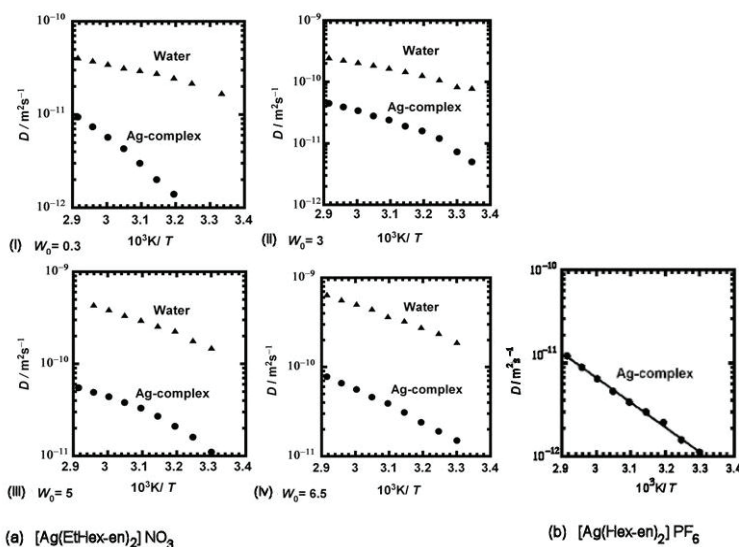


Fig. 3. Diffusion coefficients of the EtHex-en complex containing varying amounts of water (i-iv) and the Hex-en complex as a function of temperature shown as Arrhenius plots.

intensity versus  $q$  ( $4\pi\sin\theta/\lambda$ ), in which  $\lambda = 0.154$  nm. The SAXS profiles for the EtHex-en and Hex-en systems show a broad and large peak in a similar manner. Although the peak positions are almost the same of  $q = 3.2 \text{ nm}^{-1}$ , which corresponds to the close alkyl-chain lengths of 2.0 nm, the half-width of the peak for the EtHex-en complex is  $1.72^\circ$  while that for the Hex-en complex is  $2.47^\circ$ . This significant difference means that the nanostructure observed by SAXS is more ordered in the EtHex-en complex than in the Hex-en complex. The result of SAXS is in contrast to that of WAXD, which shows that the nearby structure around each molecule is less ordered and the system is more easily vitrified. The formation of nanostructure in ionic liquid system has also been clarified for alkylimidazolium systems. (for example, Lopes & Pauda, 2006)

The ordering of the nanostructure containing silver ions will be conveniently monitored by this heavy metal using TEM (Transmission Electron Microscope). The encapsulated silver ions in the nanodomains of ILs will be expected to behave as an appropriate probe. Furthermore, one of the characteristic features of ionic liquids is non-volatility, which may make possible to directly observe the nanostructures using TEM under high vacuum (around  $10^{-5}$  Pa). Especially, silver(I) ions in the Ag-ILs are able to be monitored assembled in the polar regions of the ILs nanostructure and are partially reduced to silver(0) by light or heat promoted by the ethylenediamine headgroup. We have thus studied the Ag-ILs by TEM from the following two viewpoints. One is the direct observation of the nanostructures of Ag-ILs for the neat Ag-ILs and the other is the formation of silver(0) nanoparticles on the basis of the nanodomains of Ag-ILs.

The TEM measurements were performed at ambient temperature on a Hitachi H-800 electron microscope operating at 200 kV. A specimen for the TEM measurements was prepared by spreading an ionic liquid or a small-drop silver(0) sol directly onto a standard 200-mesh copper grid (coated with a thin amorphous carbon film) and letting the dry

completely in air. The size distribution for the Ag(0) nanoparticles prepared from was derived from histograms for about 800 particles. A thin liquid film of the Ag-ILs was made by about twice dilution with diethylether.

Fig. 4 shows the TEM images for the two Ag-ILs. The image for  $[\text{Ag}(\text{EtHex-en})_2]\text{NO}_3$  (Fig. 4(a)) indicates that the hydrophilic (black) regions and hydrophobic alkyl-chain (white) regions are present in the liquid state and form organized structures, such as microemulsions. On the other hand, a similar TEM image for  $[\text{Ag}(\text{Hex-en})_2]\text{PF}_6$  (Fig. 4(b)) shows that the organized structure is less clear. These characteristics in the TEM images are consistent with the results of the half-widths in the SAXS profiles. A formation of nanostructure, such as a W/O microemulsion in the EtHex liquid is comparable to the W/O microemulsion or lyotropic liquid crystals composed of  $[\text{Ag}(\text{Oct-en})_2]\text{NO}_3$  (Oct-en = *N*-octylethylenediamine) or  $[\text{Ag}(\text{Dod-en})_2]\text{NO}_3$  (Dod-en = *N*-dodecylethylenediamine). (Iida *et al.*, 2004) The use of alkylethylenediamine silver(I) and palladium(II) complexes to create silver(0) or palladium(0) nanoparticles has been successfully performed for the  $[\text{Ag}(\text{Tetd-en})_2]\text{NO}_3$  (Tetd-en = *N*-tetradecylethylenediamine)/water/heptane or  $[\text{Pd}(\text{Oct-en})_2]\text{Cl}_2$ /water/chloroform microemulsion system. (Manna *et al.*, 2001; Iida *et al.*, 2002) In the present Ag-IL, the silver(I) ions are condensed in very limited nanoregions surrounded by the alkyl chains without organic solvents; this characteristic property suggests potential applications to effectively obtain silver(0) nanoparticles from the present ionic liquid system.

The reaction of neat Ag-ILs with aqueous  $\text{NaBH}_4$  solution was performed for  $[\text{Ag}(\text{EtHex-en})_2]\text{NO}_3$  and for  $[\text{Ag}(\text{Hex-en})_2]\text{PF}_6$ ; the following contrast results have been obtained. The reaction of the EtHex derivative gave a yellow sol with an absorption peak of 409 nm, whereas that of the Hex derivative gave only colorless solution with precipitates of bulk silver metal.

The formation of silver(0) colloidal sol by the reaction of Ag-ILs with aqueous  $\text{NaBH}_4$  solution was subtly dependent on the alkyl-chain of the silver complex. The TEM images of the sol obtained were observed under some conditions (water content or the excess ligand content) of the Ag-ILs and the results are described in Fig. 5. The Ag-IL system gave well-uniformed nanoparticles compared to the previously reported the Tetd-en complex microemulsion system in spite of the shorter alkyl-chain length. The difference in the nanostructures of the Ag-ILs between the silver complexes was observed by SAXS, and the TEM observation of the Ag-ILs clarified the significant difference in the organization of polar region where the silver ions are encapsulated. The slight difference in the molecular structure of the Ag-IL results in the contrast reaction with aqueous  $\text{NaBH}_4$  solution. This government of the delicate condition in the formation of the silver(0) nanoparticles is also observed in the other reaction conditions. The effect of the presence of small amounts of water on the formation of silver(0) nanoparticles was examined.

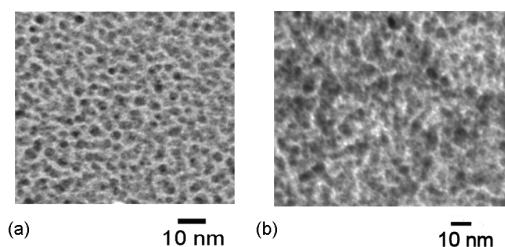


Fig. 4. TEM images of the direct observation of (a) $[\text{Ag}(\text{EtHex-en})_2]\text{NO}_3$  and (b) $[\text{Ag}(\text{Hex-en})_2]\text{PF}_6$  liquids.

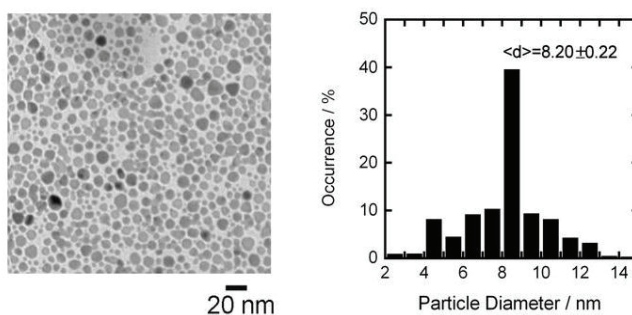


Fig. 5. TEM images and size distribution of silver(0) nanoparticles obtained by the reactions between the Ag-ILs and aqueous  $\text{NaBH}_4$  solution. neat  $[\text{Ag}(\text{EtHex-en})_2]\text{NO}_3$  ( $W_0 = 0.3$ )

Although the EtHex complex is sparingly soluble in water, this liquid incorporates a small amounts of water to form a transparent liquid. The EtHex complex was reacted with aqueous  $\text{NaBH}_4$  solution with varying  $W_0$  values. At higher water content, a similar deep-yellowish colloidal sol as for  $W_0 = 0.3$  was obtained and the resultant solution was observed by TEM after dried on the TEM grid. In the case of  $W_0 = 5$ , the sizes were somewhat larger and the distributions more polydispersed than those obtained from the liquid with  $W_0 = 0.3$ . This result may reflect the enlargement of the hydrophilic silver(I) domains with an increase in the water content. In order to stabilize the reversed-micellar structure in the  $[\text{Ag}(\text{EtHex-en})_2]\text{NO}_3$  liquid, the free ligand was added to the Ag-IL so that the ligand/silver molar ratio became 3:1. When this liquid was reacted with aqueous  $\text{NaBH}_4$  solution, the yellowish silver(0) sol was obtained as well. The TEM observation of the sol gave silver(0) nanoparticles having smaller sizes than in the neat system. This result indicates that the addition of the free ligand makes the hydrophilic core of Ag-IL smaller and stabilizes the reversed-micellar structure.

The characteristic difference in the reaction of the Ag-ILs with aqueous  $\text{NaBH}_4$  solution between  $[\text{Ag}(\text{EtHex-en})_2]\text{NO}_3$  and  $[\text{Ag}(\text{Hex-en})_2]\text{PF}_6$  was reflected in the ordering of the nanostructures of the Ag-ILs observed by the TEM images and the SAXS profiles.

### 3.2 Room-temperature PILs of alkylethylenediaminium coupled with TFSA anion.

As the silver(I) ion is a Lewis acid, a replacement of the silver(I) ion with proton may also have comparable properties of IL as well as PILs. (Scheme 1) The major structural differences between the Ag-ILs and the corresponding PIL are that the Ag-IL has a double-chain and the PIL has a single-chain, and that the latter can form hydrogen-bonding network structures.

Protic ionic liquids (PIL) composed of monoprotic alkylethylenediaminium (alkyl = hexyl and 2-ethylhexyl) cations coupled with bis(trifluoromethanesulfonyl)imide anion (= TFSA) at room temperature have been isolated. (Iida *et al.*, 2009) It is contrast that the monoprotic hexylethylenediaminium (= HexH)TFSA salt tends to be crystallized by cooling while the monoprotic 2-ethylhexylethylenediaminium (= EtHexH)TFSA salt assumed only a glassy state in the solid state. In the liquids, the HexH salt was more fluid than the EtHexH salt.

Protic ionic liquids (PILs) have recently attracted attention from a viewpoint of variable proton activities. PILs are generally more hydrophilic and dissolve metal salts to a larger extent than aprotic ionic liquids (AILs). Alkylethylene-diamines have two amines and have



larger affinity to Lewis acids compared to alkyl amines. Therefore, it is significant to investigate the ionic liquid systems of alkyl ethylenediamines in relation to an interaction with Lewis acids including transition metal ions. As shown in the previous section, alkyl-ethylenediamine silver(I) complexes provided room temperature ionic liquids and showed unique phase behavior. The silver(I) ionic liquids are, however, gradually decomposed by light and temperature and applications to wide fields are limited. As silver ion is a Lewis acid, the proton analogue is expected to form more hydrophilic ionic liquids than the Ag-ILs.

The following four PILs have been isolated: HexH(TFSA), diprotic hexylethylenediaminium bis(trifluoromethanesulfonyl)amide (= HexH<sub>2</sub>(TFSA)<sub>2</sub>), EtHexH(TFSA), diprotic 2-ethylhexylethylene-diaminium bis(tri-fluoromethanesulfonyl)amide (= EtHexH<sub>2</sub>(TFSA)<sub>2</sub>). Of these alkyl-diaminium TFSA salts, monoprotic HexH(TFSA) and EtHexH(TFSA) were liquids at room temperature and were less viscous than the diprotic salts; we have thus studied physical properties of the two monoprotic liquids of HexH(TFSA) and EtHexH(TFSA). We focused on a comparison of the properties between the 2-ethylhexyl and hexyl PILs based on the molecular structures.

Each PIL was prepared by the neutralizations of the alkyl ethylenediamines with HTFSA (supplied from Morita Chemicals) and then isolated by a repeat freeze-thaw method from diethyl ether solutions as a colorless (or pale yellowish) liquid. All of the ILs were dried under vacuum at room temperature for a day. The CHN elemental analyses were performed with Perkin Elmer model 2400II. With considering the following water content, the elemental analyses gave satisfactory results. The water contents were directly measured using a Karl-Fisher titration, which gave the molar ratios of water ( $W_0$ ) to the respective IL molecules as follows: 0.02 for HexH(TFSA), 0.02 for EtHexH(TFSA), 0.7 for HexH<sub>2</sub>(TFSA)<sub>2</sub>•H<sub>2</sub>O, and 0.9 for EtHexH<sub>2</sub>(TFSA)<sub>2</sub>•H<sub>2</sub>O. The PILs were somewhat hygroscopic and gradually absorbed moisture to have around 0.1–0.2 molar water content. The water content slightly affected dynamic properties such as self-diffusions and electric conductivities.

The densities were measured at 25 °C using a micropipette and the results were 1.41 g cm<sup>-3</sup> for HexH(TFSA) and 1.32 g cm<sup>-3</sup> for EtHexH(TFSA). The presence of the 2-ethyl branch will expand the assembled structure of the PIL and results in the lowering of the density.

As the diprotic chlorides for both the alkyl ethylenediamines were isolated as crystals, we determined the  $pK_a$  values by titration of both the diprotic chlorides (0.01 mol dm<sup>-3</sup>) with aqueous NaOH solutions at constant ionic strength (0.1 mol dm<sup>-3</sup>, with an addition of KCl). The  $pK_{a1}$  and  $pK_{a2}$  values obtained were 7.28 and 10.57 for Hex, and 7.30 and 10.42 for EtHex, respectively. As HTFSA is a super acid ( $pK_a = -4$  (MacFarlane *et al.*, 2006)), a relationship of  $\Delta(pK_a(\text{base}) - pK_a(\text{acid})) > 8$  for the monoprotic PILs holds well. That is, the transfer of the proton from the acid to the base was almost complete. (Nuthakki *et al.*, 2007; Greaves & Drummond, 2008)

The solubilities of HexH(TFSA) and EtHexH(TFSA) liquids in various solvents were tested and classified into three categories as follows. They were more than 10% (w/v) in methanol, ethanol, acetone, dichloromethane, ethyl acetate, chloroform, diethyl ether, and 1,4-dioxane, from 0.1% (w/v) to 10% (w/v) in water and benzene, and were less than 0.1% (w/v) in cyclohexane and hexane. Thus, the present PILs have moderate hydrophilic-hydrophobic balances. As these PILs have the same hydrophobic counter anion of TFSA, the difference in the hydrophilicity-hydrophobicity due to the alkyl chain of the cation was not clearly reflected in the solubilities of the PILs.



Melting was observed by DSC in the temperature range of  $-100$ – $150$  °C. The samples (3–5 mg) were placed in aluminum pans and run at a rate of  $10\text{ K min}^{-1}$  under nitrogen gas at a flow rate of  $20\text{ mL min}^{-1}$ . The results are described in Fig. 6. There is a contrast profile that for HexH(TFSA) a glass transition temperature ( $T_g$ ), a crystallization temperature ( $T_c$ ), and a melting point ( $T_m$ ) were observed while for EtHexH(TFSA) only a glass transition was observed. The larger trend of crystallization for HexH(TFSA) is analogous to that for the corresponding silver(I) complexes. In the latter case, the Hex salt showed a melting point where the enthalpy change ( $\Delta H = 9.4\text{ kJ mol}^{-1}$ ) was smaller than the general melting enthalpies, while for the EtHex salt the solid state was glassy and the glass transition was observed. Similar difference in the DSC profiles has been observed in the counterion and alkyl-chain effects on alkyl-ammonium salts. (Belieres & Angell, 2007) In the present PILs, however, the liquids are present at lower temperature and the difference in the alkyl chains is clearer than the alkyl-ammonium systems.

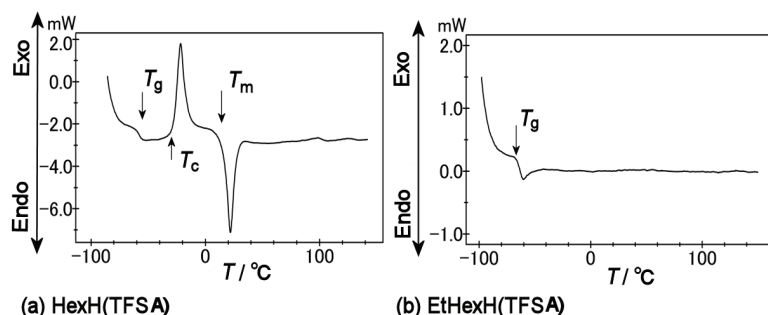


Fig. 6. DSC curves of (a) HexH(TFSA) at  $-80$ – $150$  °C and (b) EtHexH(TFSA) at  $-100$ – $150$  °C.

Wide-angle X-ray diffractions (WAXD) were measured at  $27$  °C and  $-120$  °C similarly to the methods for the Ag-ILs. The WAXD profiles for HexH(TFSA) and EtHexH(TFSA) at solid ( $-120$  °C) states are shown in Fig. 7. The profiles in the liquid states of both systems were close to that of EtHexH(TFSA) in the solid state at  $-120$  °C (Fig. 2 b)). On the other hand, HexH(TFSA) assumed an amorphous-based crystalline state at  $-120$  °C (Fig. 2(a)). The more ordered structure for the Hex silver(I) complex than for the EtHex silver(I) complex in

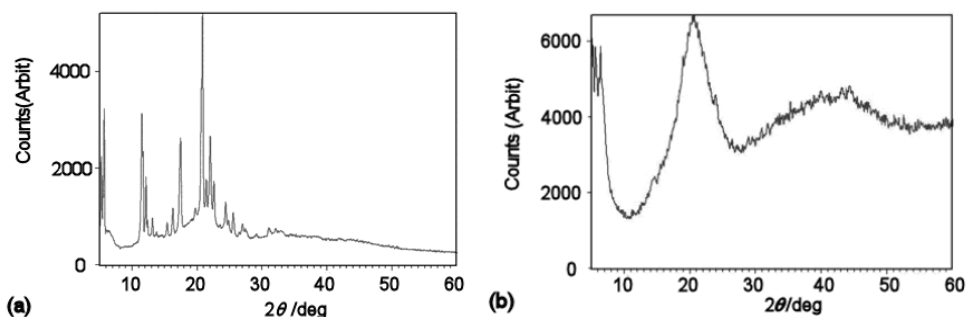


Fig. 7. WAXD profiles of (a) HexH(TFSA) at  $-120$  °C and (b) EtHexH(TFSA) at  $-120$  °C.

WAXD have been observed as described above. It is comparable that  $[\text{Ag}(\text{Hex-en})_2]\text{NO}_3$  is a crystal while  $[\text{Ag}(\text{EtHex-en})_2]\text{NO}_3$  is a viscous liquid at room temperature. The present WAXD explains the DSC profiles that HexH(TFSA) showed both glassy and melting transitions while EtHexH(TFSA) showed only a glassy transition. The introduction of 2-ethyl side-chain has a significant effect on disordering of the structures of the molecular assemblies for both the Ag-IL and the PIL. Thus the melting point of EtHexH(TFSA) was appreciably lowered and these ILs easily assume glassy states in solid.

The dynamic properties of the ILs were studied by the measurements of self-diffusions of the cations and the electric conductivities of the PILs. The measurements were followed by the above method. As both ILs are somewhat hygroscopic, the water content ( $W_0 = 0.01$ – $0.02$ ) of dried ILs was gradually changed to around  $W_0 = 0.2$  through the storage in a vial bottle for several days. We thus compared the self-diffusions of the cations in both the IL systems between  $W_0 = 0.02$  and  $0.2$ . Figure 8 shows Arrhenius plots for the self-diffusions in the range of  $25$ – $70$  °C. The result shows a better linearity even for the EtHex derivative compared to the Ag-ILs described above. This better linearity may be due to the TFSA anion which generally makes fluid ionic liquid systems. The self-diffusion coefficients for the HexH cation were slightly larger than those for the EtHexH cation. This trend is the same as that for the Ag-ILs. As the linearities of the Arrhenius plots were good, the apparent activation energies were obtained as follows. For the HexH and EtHexH cations, the apparent activation energies were  $46.3 \pm 0.8$  kJ mol $^{-1}$  and  $45.8 \pm 0.8$  kJ mol $^{-1}$ , respectively, at  $W_0 = 0.02$ . At higher water content ( $W_0 = 0.2$ ), the self-diffusions slightly increase and the difference between the HexH and EtHexH cations increases. Larger fluidity of the HexH cation was more clearly detected at  $W_0 = 0.2$ . The apparent activation energies were obtained for the HexH and EtHexH cations as  $41.6 \pm 0.9$  kJ mol $^{-1}$  and  $42.7 \pm 0.7$  kJ mol $^{-1}$ , respectively.

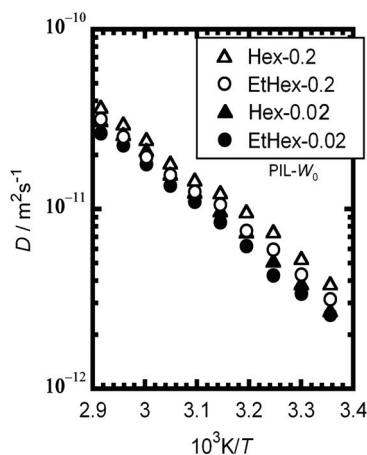


Fig. 8. Diffusion coefficients of HexH and EtHexH cations for  $W_0 = 0.02$  and  $0.2$ .

In relating with the self-diffusions, the electric conductivities for the two PILs were measured at  $25 \pm 1$  °C in a similar manner as for the Ag-ILs. The electric conductivities were  $250 \mu\text{S cm}^{-1}$  for HexH(TFSA) ( $W_0 = 0.02$ ) and  $210 \mu\text{S cm}^{-1}$  for EtHexH(TFSA) ( $W_0 = 0.02$ ). The absolute values of the electric conductivities of the PILs are much larger than those of the Ag-ILs due to both the smaller molecular interactions and the smaller molecular weights. The larger electric conductivity for the Hex PIL than that for the EtHex PIL is consistent with the result of the self-diffusions as observed for the Ag-ILs. Further consideration of the ionicity which can be estimated from the self-diffusions, electric conductivities, and densities (Tokuda, 2004, 2005; Ueno, 2010) will be discussed in a nearly publishing paper.

#### 4. Conclusion

There are particular meanings of the treatment of a series of bis(alkyl-en)metal complexes. As a development of the molecular structures of these silver(I) complexes offers a variety of molecular assemblies, the formation of ionic liquids can be regarded as one of the categories for various kinds of molecular assemblies. In the 2-ethylhexyl derivative of Ag-ILs, the organized nanostructures like W/O microemulsions are more effectively formed compared to the hexyl derivative. Uniformly-sized silver(0) nanoparticles were created by the reaction of the 2-ethylhexyl derivative with aqueous  $\text{NaBH}_4$  solution but the hexyl derivative did not give silver(0) colloids. Such a selectivity for the formation of silver(0) nanoparticles depending on the alkylchains and disuse of organic solvents are the advantages of the methodology using Ag-ILs for the synthesis of silver(0) nanoparticles.

A direct comparison of physicochemical properties between the Ag-ILs and PILs of alkylethylenediamines using the same counteranion is particularly important to understand the structural specificities in the formation of these unique ILs. Although the 2-ethylhexyl derivative of the Ag-IL forms more ordered nanostructures than the hexyl derivative and is advantageous to form silver(0) sols, in both the Ag-IL and PIL systems the former derivative tends to assume vitreous states. Wider alkyl-chain systems containing the same TFSA anion have been intensively studied and a comparison between the Ag-ILs and PILs has been performed to understand the structural effects of the cations on the physicochemical properties. The results will be published in near future.

#### 5. References

- Abbott, A. P.; Frisch, G. ; Ryder, K. S. (2008). Metal Complexation in Ionic Liquids. *Annu. Rep. Prog. Chem., Sect. A*, 104, 21-45.
- Albéniz, A. C. ; Barberá, J. ; Espinet, P. ; Lequerica, M. C.; Levelut, A. M. ; López-Marcos, K. J.; Serrano, J. L. (2000). Ionic Silver Amino Complexes Displaying Liquid Crystalline Behavior Close to Room Temperature. *Eur. J. Inorg. Chem.*, 133-138.
- Angell, C. A.; Byrne, C. A. N.; Belieres, J-P., (2007). Parallel Developments in Aprotic and Protic Ionic Liquids: Physical Chemistry and Applications. *Acc. Chem. Res.*, 40, 1228-1236.
- Belieres J. -P. ; Angell, C. A. (2007). Protic Ionic Liquids: Preparation, Characterization, and Proton Free Energy Level Preparation. *J. Phys. Chem., B*, 111, 4926-4937.

- Binnemans, K., (2007). Lanthanides and Actinides in Ionic Liquids, *Chem. Rev.* 107, 2592-2614.
- a) Er, H. ; Asaoka, N. ; Hisamatsu, N. ; Iida, M. ; Imae, T. (2003). Effects of Metal Counterion Interactions on the Percolation in Microemulsions Composed of Bis(N-octylethylenediamine)Metal(II) Complexes in Water/Benzene and Water/Chloroform Systems. *Colloids Surf, A.* 221, 119-129.
- b) Er, H. ; Ohkawa, S. ; Iida, M. (2007). Aggregation Behavior of Alkylethylenediamine Palladium(II) Complexes in Water and in Water/Organic Solvent Mixtures. *Colloids Surf, A.* 301, 189-198.
- a) Evans, D. F.; Yamauchi, A.; Roman, R.; Casassa, E. Z. (1982). Micelle Formation in Ethylammonium Nitrate, a Lowmelting Fused Salt. *J. Colloid Interface Sci.*, 88, 89-96.
- b) Evans, D. F.; Wennerström, H. (1999). *The Colloidal Domain*, 2<sup>nd</sup> ed, Wiley-VCH, New York.
- Fukushima, T.; Kosaka, A.; Ishimura, Y.; Yamamoto, T.; Takigawa, T.; Ishii, N. ; Aida, T., (2003). Molecular Ordering of Organic Molten Salts Triggered by Single-Walled Carbon Nanotubes. *Science*, 300, 2072-2074.
- a) Greaves, T. L. ; Weerawardena, A.; Fong, C. ; Krodziewska, I. ; Drummond, C. J. (2006). Protic Ionic Liquids: Solvents with Tunable Phase Behavior and Physicochemical Properties. *J. Phys. Chem. B*, 110, 22479-22487.
- b) Greaves, T. L.; Drummond, C. J. (2008). Protic Ionic Liquids: Properties and Applications. *Chem. Rev.*, 108, 206-237.
- c) Greaves, T. L.; Weerawardena, A. ; Krodziewska, I. ; Drummond, C. J. (2008). Protic Ionic Liquids: Physicochemical Properties and Behavior as Amphiphile Self-Assembly Solvents. (2008). *J. Phys. Chem. B*, 112, 896-905.
- Huang, J.-F.; Luo, H.; Dai, S. (2006). A New Strategy for Synthesis of Novel Classes of Room-Temperature Ionic Liquids Based on Complexation Reaction of Cations. *J. Electrochem. Soc.*, 153, 9-13.
- Hurley, F. H.; Weir, T. P. (1951). Electrodeposition of Metals from Fused Quaternary Ammonium Salts. *J. Electrochem. Soc.*, 98, 203-206.
- Hussey, C. L. (1988). Room Temperature Haloaluminate Ionic Liquids. Novel Solvents for Transition Metal Solution Chemistry. *Pure & Appl. Chem.*, 60, 1763-1772.
- a) Iida, M. ; Ohkawa, S. ; Er, H.; N. Asaoka, N. ; Yoshikawa, H. (2002). Formation of Palladium(0) Nanoparticles from a Microemulsion System Composed of Bis(N-octylethylenediamine) palladium(II) Chloride Complex. *Chem. Lett.*, 31, 1050-1051.
- b) Iida, M. ; Inoue, M. ; Tanase, T. ; Takeuchi, T. ; Sugibayashi, M. ; Ohta, K. (2004). Formation of Thermotropic and Lyotropic Liquid Crystals of Bis(N-alkylethylenediamine)silver(I) Nitrate. *Eur. J. Inorg. Chem.*, 3920-3929.
- c) Iida, M. ; Baba, C.; Inoue, M. ; Yoshida, H. ; Taguchi, E. ; Furusho, H. (2008). Novel Ionic Liquids of Bis(alkylethylenediamine)silver(I) Salts and the Formation of Silver(0) Nanoparticles from the Ionic Liquid System. *Chem. – Eur. J.*, 14, 5047-5056.
- d) Iida, M. ; Syouno, E. ; Kawakami, S. ; Hanai, M. (2009). Properties of Protic Ionic Liquids Composed of N-Hexylethylenediaminium and N-(2-

- Ethylhexyl)ethylenediaminium Cations with Bis(trifluoromethanesulfonyl)amide Anion. *Chem. Lett.* 38, 544-545.
- Israelachvili, J. N., "Intermolecular and Surface Forces," 2nd ed, (1992). Academic Press, London. Chaps. 12, 17, and 18.
- Lee, C. K. ; Hsu, K-M. ; Tsai, C-H. ; Lai, C. K. ; Lin I. J. B., (2004). Liquid Crystals of Silver Complexes Derived from Simple 1-alkylimidazoles, *Dalton Trans.*, 1120-1126.
- Lin, I. J. B.; Vasam, C. S., (2005). Metal-containing Ionic Liquids and Ionic Liquid Crystals Based on Imidazolium Moiety. *J. Orgnomet. Chem.*, 690, 3498-3512.
- Lopes, J. N. C. ; Pauda, A. A. H. (2006). Nanostructural Organization in Ionic Liquids. *J. Phys. Chem. B*, 110, 3330-3335.
- Ma, J. C. ; Dougherty, D. A. (1997). The Cation- $\pi$  Interaction. *Chem. Rev.* 97, 1303-1324.
- MacFarlane, D. R. ; Pringle, J. M. ; Johansson, K. M. ; Forsyth, S. A. ; Forsyth, M. (2006). Lewis Base Ionic Liquids. *Chem Comm*, 1905-1917.
- Manna, A.; Imae, T.; Iida, M. ; Hisamatsu, N. (2001). Formation of Silver Nanoparticles from a *N*-Hexadecylethylenediamine Silver Nitrate Complex. *Langmuir*, 17, 6000-6004.
- a) Nockemann, P. ; Thijs, B. ; Pittois, S. ; Thoen, J. ; Glorieux, C. ; Van Hecke, K. ; Van Meervelt, L. ; Kirchner, B. ; Binnemans, K. (2006). Task-Specific Ionic Liquid for Solubilizing Metal Oxides. *J. Phys. Chem. B*, 110, 20978-20992.
- b) Nockemann, P. ; Thijs, B. ; Lunstroot, K. ; Parac-Vogt, T. N. ; Görrler-Walrand, C. ; Binnemans, K. ; Van Hecke, K. ; Van Meervelt, L. ; Nikitenko, S. ; Daniels, J. ; Henning, C. ; Van Deun, R., (2009). Speciation of Rare-Earth Metal Complexes in Ionic Liquids: A multiple-Technique Approach. *Chem. -Eur. J.* 15, 1449-1461.
- Nuthakki, B. ; Greaves, T. L. ; Krodziewska, I. ; Weerawardena, A. ; Burgar, M. I. ; Mulder, R. J. ; Drummond, C. J. (2007). Protic Ionic Liquids and Ioncity. *Aust. J. Chem.*, 60, 21-28.
- Scheeren, C. W.; Machado, G. ; Teixeira, S. R. ; Morais, J. ; Domingos, J. B. ; Dupont, J. (2006). Synthesis and Characterization of Pt(0) Nanoparticles in Imidazolium Ionic Liquids, *J. Phys. Chem.(B)*, 110, 13011-13020.
- a) Tokuda, H.; Hayamizu, K. ; Ishii, K. ; Susan, M. A. B. H. ; Watanabe, M., (2004). Physicochemical Properties and Structures of Room Temperature Ionic Liquids. 1. Variation of Anionic Species. *J. Phys. Chem. B*, 108, 16593-16600.
- b) Tokuda, H. ; Hayamizu, K. ; Ishii, K. ; Susan, M. A. B. H. ; Watanabe, M., (2005). Physicochemical Properties and Structures of Room Temperature Ionic Liquids. 2. Variation of Alkyl Chain Length in Imidazolium Cation. *J. Phys. Chem. B*, 109, 6103-6110.
- Ueno, K.; Tokuda, H. ; Watanabe, M., (2010). Ioncity in Ionic Liquids: Correlation with Ionic Structure and Physicochemical Properties. *Phys. Chem. Chem. Phys.*, 12, 1649-16548,
- Welton, T. (1999). Room-Temperature Ionic Liquids. Solvents for Synthesis and Catalysis. *Chem. Rev.* 99, 2071-2083.
- Yoshizawa, M. ; Xu, W. ; Angell, C. A. (2003). Ionic Liquids by Proton Transfer: Vapor Pressure, Conductivity, and the Relevance of  $pK_a$  from Aqueous Solutions. *J. Am. Chem. Soc.*, 125, 15411-15419.
- Zana, R. ; Xia, J. (2003). *Gemini Surfactants*, Marcel Dekker, Inc., New York.

Zhang H. ; Cui, H. (2009). Synthesis and Characterization of Functionalized Ionic Liquid-Stabilized Metal (Gold and Platinum) Nanoparticles and Metal Nanoparticle/Carbon Nanotube Hybrids. *Langmuir*, 25, 2604-2612.

# Physical Properties of Binary Mixtures of ILs with Water and Ethanol. A Review.

Oscar Cabeza, Sandra García-Garabal, Luisa Segade,  
Montserrat Domínguez-Pérez, Esther Rilo and Luis M. Varela<sup>1</sup>

*Universidade da Coruña*

<sup>1</sup>*Universidade de Santiago de Compostela  
Spain*

## 1. Introduction

The interest on ionic liquids (ILs) began in the present century, because these compounds have many physico-chemical interesting properties to be one of the most promising new materials family for the development of the novel Green Chemical industry, where generated pollution would be negligible (Rogers & Seddon, 2002; Rogers et al., 2002). To develop the novel green processes in the chemical industry using ILs it is necessary to know and to understand the physical properties of the fluids to be used, both pure ILs as mixed with other solvents (Rogers & Seddon, 2005; Danek, 2006). This last is particularly important to develop one of the most promising uses of the ILs, as electrolytes for lithium batteries, dye-sensitized solar cells (DSSC) and electrochemical processes (as deposition or metal recovery) (Ohno, 2005; Brennecke et al., 2007). Electrolytes are materials with free ions, which can move transporting electrical charge. They can be solid, liquid or even gaseous, but the most interesting for the chemical industries are liquid or gel. The use of a pure liquid as electrolyte is not very common, because the optimum efficiency in the charge transport process is given by a mixture of different substances, as it is well known for molten salt electrolytes (Danek, 2006). Furthermore, pure ILs have the problem of being very viscous at room temperature, and hence its electrical conductivity is relatively low. If we heat the IL those problems are minimized, because viscosity reduces and electrical conductivity increases, both exponentially. Usually pure ILs have a boiling temperature high enough to allow warming, although decomposition temperature is usually much lower (not higher than 400 K) (Rogers & Seddon, 2002). A much cheaper alternative to decrease viscosity and to increase electrical conductivity of the ionic liquid is to make a solution using a solvent. Thus, while viscosity decreases exponentially with the solvent molar fraction, electrical conductivity increases more than 10 times for a given IL + solvent concentration (Seddon et al., 2000). This last behaviour have been observed in aqueous solutions of metal salts, as aluminium halogen ones (Vila et al., 2005) and indicates that the increase of mobility of the IL ions is higher than the decrease of ion concentration when solvent is added, up to an optimum content.

In spite of its interest, the measurement of the physical properties of IL mixtures begins in the present decade, and before 2005 the amount of papers published about it was scarce (Marsh et al., 2004). From that year the publication rhythm increased a lot, as can be

observed in the references included in this chapter, which majority were published in the last five years. Furthermore its evident applied interest, from the theoretical point of view the study of the physical properties of IL mixtures has contributed to the development of the first theoretical models to explain the ionic structure of the IL ions and the electrical transport mechanisms (Malhan et al., 2007; Varela et al., 2009; Woodward & Harris, 2010). The most promising one is the Bahe-Varela theory, which supposes a pseudo-lattice in the IL formed by the anions and cations, which do not allow the free movement of the ions, but they will hop from one pseudo-lattice position to another free contiguous if they have enough energy (Bahe, 1972; Varela et al., 1997). The presence of some solvent molecules will not break the ionic structure, because the solvent molecules will place in the free space among ions. When the solvent quantity is increased their molecules cannot accommodate and destroy the pseudo-lattice, resulting in a structural phase transition (Varela et al., 2009). See the chapter entitled *Pseudolattice theory of ionic liquids* by L.M. Varela et al., in this same book

In this work we perform a review of the many experimental measurements published in literature about IL + solvent mixtures for different physical magnitudes. Among all measured systems published in the literature (more than 200) we have chosen those reporting data for mixtures of any IL with water or ethanol as solvents. These are those solvents we work in our own laboratory and also they are the most used by researchers, mainly because they are the most promising for applications. The range of physical properties analysed includes density (which gives information about volumetric properties), refractive index (which gives information about ionic interactions), viscosity (the most common transport property studied), electrical conductivity (the key magnitude for electrolyte applications) and surface tension (to know the surface interactions and its composition). We will include in the study all data published using as mean reference the IL thermo webpage, updated in May of 2010, where all experimental physicochemical data is saved for the pure compounds and for binary and ternary mixtures (<http://ilthermo.boulder.nist.gov/ILThermo/mainmenu.uix>).

This work is organized in chapters, each of them dedicated to the different physical magnitudes revised here. The data published for the different IL families at 298.15 K will be plotted in graphs and commented the IL and/or solvent influence in the magnitude value. If there are published different measured values for the same mixture and magnitude we will discuss them. Also, a study about the temperature influence in each magnitude for a single mixture will be also given. Finally we will relate the measured values for density and refractive index, in one hand, and for viscosity and electrical conductivity in the other.

## 2. Chemical compounds

The mixtures of IL + water or + ethanol presented include majority of commercial ILs miscible with water or ethanol in a broad range of concentrations. There are some ILs miscible in both solvents, other do not mix with one of them, and many of them are not miscible with any of the two solvents (obviously this last will not be considered in this work). In any case, the IL mixtures measured up to now are a small part of all the millions of ILs that can be synthesized. The ILs cation presented include: 1-alkyl-3-methyl imidazolium, with the alkyl chain being methyl (dMIM), ethyl (EMIM), butyl (BMIM), octyl (OMIM); also the similar cation 1-alkyl-2,3-dimethyl imidazolium, with the alkyl chain being propyl (PdMIM) or butyl (BdMIM). Some pyridinium based cations are reported, the 1-alkyl-pyridinium with the alkyl chain being ethyl (EPy) or butyl (BPy); and the 1-butyl-4-methyl pyridinium (BMPy). Ammonium and phosphonium based ILs are not miscible in water or ethanol (Galan et al., 2003; Huddleston et



al., 2001). The anions reported here include halogens as chlorine (Cl), bromine (Br) and perchlorate (pCl); alkyl sulphates, as methyl sulphate (MS) and ethyl sulphate (ES). Also we report data for ILs with anion dicyanamide (dCy), tricyanamide (tCy) and tricyanomethane (tCyM); trifluoromethanesulfonate (OTf), bis(trifluoromethylsulfonyl)imide (NTf<sub>2</sub>), nitrate (NO<sub>3</sub>), hexafluoro phosphate (PF<sub>6</sub>), and the most popular, the tetrafluoro borate (BF<sub>4</sub>). Obviously, not all possible combinations of anions and cations have been reported, but here we present mixtures of more than 25 different ILs with water and/or ethanol. All details about compounds and experimental techniques are in the corresponding reference.

### 3. Density

Density,  $\rho$ , is defined as the mass per unit volume at constant temperature and pressure, so the unit for density is kg/m<sup>3</sup>. Density for ILs decreases with temperature in their liquid range and increases with pressure, both linearly (Gardas et al., 2007; Rilo et al., 2010c). The reciprocal value of density is the specific volume, which is usually referred as the molar volume,  $V_m$ , calculated from density and the molar mass value,  $M$ ,

$$V_m = \frac{M}{\rho} \quad (1)$$

When studying binary mixtures, the ideal behaviour is defined using the molar volume instead density, and so the excess molar volume,  $V_m^E$ , is defined as:

$$V_m^E = V_m - V_m^{id} = V_m - (x_1 V_{m1} + x_2 V_{m2}) \quad (2)$$

where  $x_i$  and  $V_{mi}$  are the molar fraction and the molar volume of the pure compound  $i$ , respectively. In the case of IL mixtures with water and ethanol the excess molar volume is very small (lower than a 1% of the  $V_m$  value in all range of concentrations), and so mixtures are quasi ideal (Rilo et al., 2009).

#### 3.1 Discussion of results

In the following four figures we will plot density data of all mixtures IL + water at 298.15 K reported in literature versus the molar fraction of the corresponding IL,  $x_{IL}$ . If more than one author have published the same system, we include only one of them (except discrepancies between both sets of data were important). The source of each set of data is included in the corresponding figure. Thus, in Figure 1 we plot density vs. IL molar fraction for aqueous mixtures of five imidazolium (Rilo et al., 2009; Malhan et al., 2007; Ge et al., 2009) and the only two pyridinium based ILs (Ortega et al., 2008; Mokhatarani et al., 2009b), all of them with BF<sub>4</sub> as common anion. Other authors also measured some of those systems, but results are very similar (Zhou et al., 2006; Zhang et al., 2006; Wu et al., 2009). The behaviour is very similar for all of the systems with BF<sub>4</sub> anion, and the absolute value decreases with the cation size. In Figure 2 we plot BMIM, HMIM and OMIM-Cl aqueous systems (Gomez et al., 2006a; Yang et al., 2010), being the BMIM-Cl only partially miscible (for  $x_{IL} < 0.5$ ). These systems have been also measured by other authors with very similar results (Gaillon et al., 2004; Zafarani et al., 2005; Gardas et al., 2008; Dong et al., 2009; Calvar et al., 2007). As observed density increases from the pure IL value when water is added for HMIM-Cl and OMIM-Cl, and then it decreases for more water content. This is a curious fact that we have

not found in any other aqueous system with IL. In Figure 3 we plot data for ILs with alkyl sulfate anion (Rodríguez et al., 2006; García-Miaja et al., 2009; Domanska et al., 2006). Again the lowest size of the cation and anion means higher  $\rho$  values, but curves are essentially the same than for the aqueous systems presented in Figure 1. Other published results for these same systems exist in literature (Calvar et al., 2007; Vicent et al., 2006; Yang et al., 2005). Finally, in Figure 4 we include data for ILs with anions containing cyanamide (Cy) (Stoppa et al., 2009; Carvalho et al., 2010) and trifluoromethanesulfonate (OTf) (Rodríguez et al., 2006; García-Miaja et al., 2009). Density of the ILs with OTf anion has a very high density value taking into account its size, while the ILs with Cy anion present a very small  $\rho$  value. The ILs with hexafluoro phosphate as anion is not miscible in water except for very diluted mixtures, and so data are not plotted (Ali et al., 2007; Fu et al., 2006; Jacquemin et al., 2006).

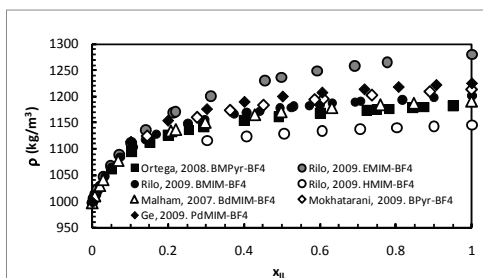


Fig. 1. Density vs. IL molar fraction for seven aqueous systems with  $\text{BF}_4$  as anion.

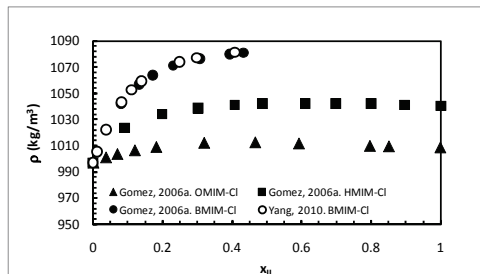


Fig. 2. Density vs. IL molar fraction for three aqueous systems with halogen anion.

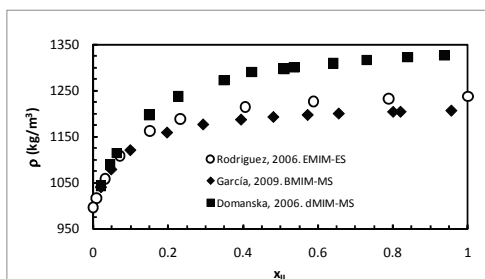


Fig. 3. Density vs. IL molar fraction for three aqueous systems with alkyl sulfate anion.

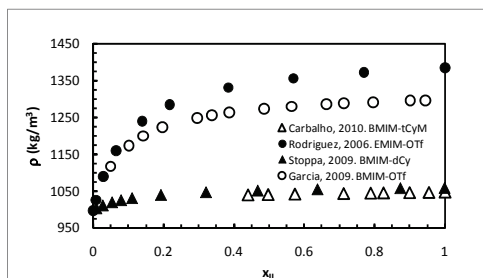


Fig. 4. Density vs. IL molar fraction for four aqueous systems with organic anion.

In Figures 5 to 9 we present the density data for the published IL + ethanol systems also at 298.15 K. Thus in Figure 5 we present systems with ILs containing the  $\text{BF}_4$  anion, four alkyl imidazoliums (Rilo et al., 2009) and one pyridinium (Ortega et al., 2008). Curves are similar that those with water, but the density value decreasing is more progressive than corresponding systems with water. In Figure 6 we plot data for three alkyl imidazoliums with  $\text{PF}_6$  as anion (Pereiro et al., 2007) with a same behaviour with  $x_{\text{IL}}$  than those of Figure 5. In Figure 7 we present data for three alkyl imidazolium (Arce et al., 2006b; Pereiro et al., 2007; Garcia-Miaja et al., 2008) and one pyridinium (Gonzalez et al., 2009) alkyl sulfates. Again the decrease of density is similar in shape than in the systems presented before. In Figure 8 we plot four alkyl imidazolium with Cl (Gomez et al., 2006; Gonzalez et al., 2006; Calvar et al., 2006) or pCl anion (Mokhtarani et al., 2008). Now the halogenated ILs decrease continuously with ethanol content, in contrast with the same aqueous systems plotted in

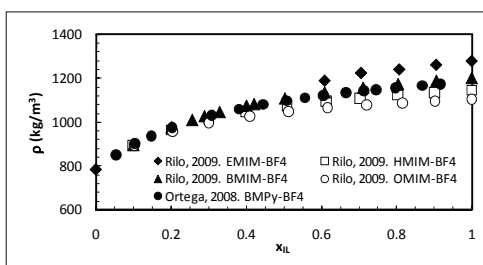


Fig. 5. Density vs. IL molar fraction for five systems with ethanol and  $\text{BF}_4$  anion.

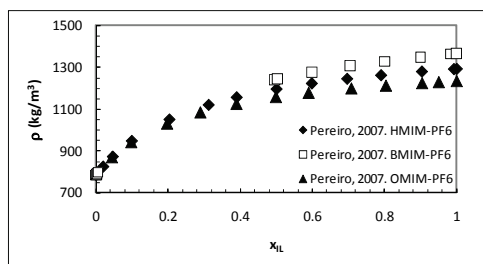


Fig. 6. Density vs. IL molar fraction for three systems with ethanol and  $\text{PF}_6$  anion.

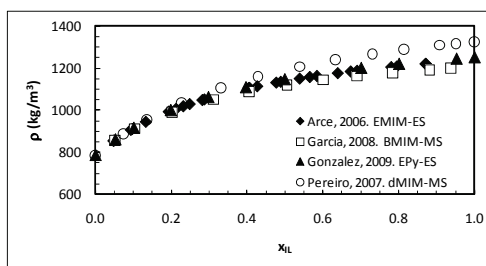


Fig. 7. Density vs. IL molar fraction for four systems with ethanol and alkyl sulfate anion.

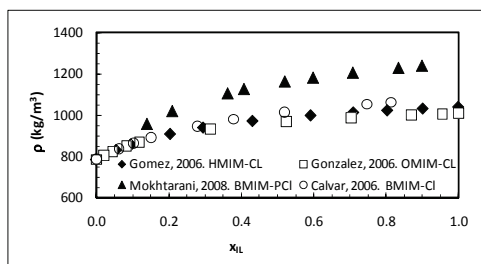


Fig. 8. Density vs. IL molar fraction for four systems with ethanol and chlorate anion.

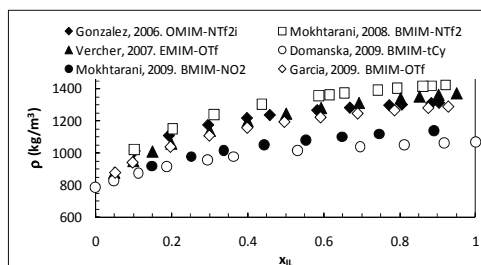


Fig. 9. Density vs. IL molar fraction for four systems with ethanol and organic anion.

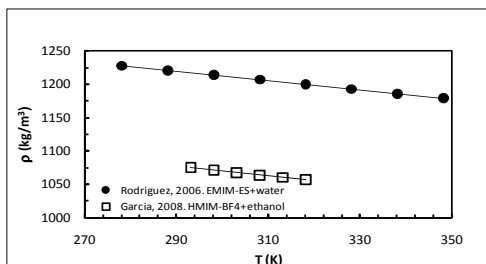


Fig. 10. Density vs. temperature for an aqueous mixture with  $x_{IL} = 0.59$  (solid dots) and with ethanol with  $x_{IL} = 0.49$ . The curves are the best fit of a straight line.

Figure 2. Also note that pCl anion increases considerably the density value, which seems to be opposite to the effect of increasing cation length, which decreases density value. Finally, in Figure 9 we show data for six systems with alkyl imidazolium based ILs, being cations NTf<sub>2</sub> (Gonzalez et al., 2006; Mokhtarani et al., 2009), OTf (Vercher et al., 2007; Garcia-Miaja et al., 2009), NO<sub>2</sub> (Mokhtarani et al., 2009) and tCy (Domanska et al., 2009). For these compounds a bigger size of the anion implies a bigger density value.

### 3.2 Temperature influence

The temperature dependence of a mixture about equimolar have been also taken from literature. As observed in Figure 10 (above) density decreases linearly with temperature for a aqueous mixture of EMIM-ES (Rodriguez et al., 2006) with  $x_{IL} = 0.59$ , and also for a mixture of HMIM-BF<sub>4</sub> with ethanol (Garcia-Miaja et al., 2008) having  $x_{IL} = 0.49$ . We guess that this linear behaviour of density with temperature is a common trend for all mixtures with water and ethanol. In fact, pure ILs also present the same linear trend with temperature (Lu et al., 2005; Zafarani et al., 2005).

## 4. Refractive index

The refractive index,  $n_D$ , of a compound is defined as the ratio of the speed of light in a vacuum to that in a medium. This phenomenon is described by the well known Snell's law, which expresses the relationship between the refractive index, the incident and the transmitted angles of the light. In general refractive indices of compounds increase with increasing atomic number of the constituent atoms (Roger & Seddon, 2005) and furthermore, the refractive index of a compound is a physical property that can potentially be used, like a melting point, to establish its identity very easily. In the case of mixtures with solvents, the refractive index values can be related with density of the same mixture using some phenomenological models that work fairly well, as we will observe later.

The refractive indices of liquids are generally measured using commercially available refractometers, which provide simple and rapid measurements. For pure ILs  $n_D$  decreases with the increase of temperature smoothly, following a second order polynom, similarly to the behaviour of density.

### 4.1 Discussion of results

In this section we will present refractive index measurements published up to now for ILs with water and ethanol, thus in Figures 11 to 13 we plot data for aqueous mixtures while in Figures 14 to 16 the IL + ethanol systems. Figure 11 present data for three systems with alkyl sulfate anion (Gomez et al., 2006b; Gomez et al., 2008; Gonzalez et al., 2008) while in Figure 12 we include two systems with BF<sub>4</sub> as anion (Malhan & Turmine, 2008) comparing the data for BMIM and BdmIM as cations. In Figure 13 we show  $n_D$  data of three systems with alkyl-MIM-Cl (Calvar et al., 2006, Gomez et al., 2006c; Gonzalez et al., 2006). A longer alkyl chain means a lower refractive index value, just as happens for density. All data presents a rounded decreasing of  $n_D$  with  $x_{IL}$ , similar to that presented by density, and this will be the norm for all systems.

In Figure 14 we include the only two systems formed by ethanol and a IL with BF<sub>4</sub> anion, being the cation OMIM (Arce et al., 2006a) and BMIM (Iglesias-Otero et al., 2008), and also we show data for the three published systems with Cl anion and alkyl imidazolium cation (Calvar et al., 2006, Gomez et al., 2006c; Gonzalez et al., 2006). The dependence of  $n_D$  with  $x_{IL}$

is similar to that presented by  $\rho$  for the corresponding systems with ethanol, and it is more rounded than that presented by the aqueous systems. In Figure 15 we plot the data for IL systems having  $\text{NTf}_2$  anion (Andreatta et al., 2009; Andreatta et al., 2010), while in Figure 16 systems with alkyl imidazolium with other kind of anions as OTf (Vercher & Rodriguez, 2010),  $\text{PF}_6$  and  $\text{MS}$  (Pereiro et al., 2007). The behaviour is very similar for all systems.

## 4.2 Temperature influence

There are very scarce published data about dependence of  $n_D$  with temperature for mixtures with water and ethanol. We have not found any measurement for any aqueous system, and in Figure 17 we plot the data for a equimolar mixture of  $\text{OMIM-BF}_4$  + ethanol (Mokhtarani et al., 2008). The curve is the best fit of a straight line.

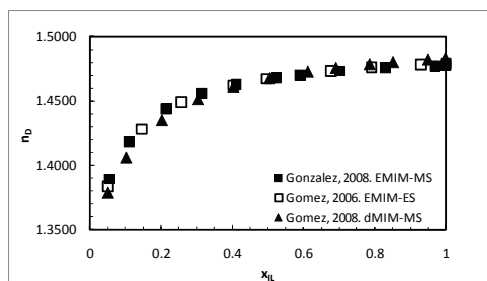


Fig. 11. Refractive index vs. IL molar fraction for three aqueous systems with alkyl sulfate anion.

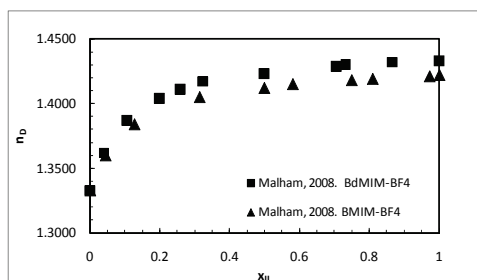


Fig. 12. Refractive index vs. IL molar fraction for two aqueous systems with tetrafluoroborate anion.

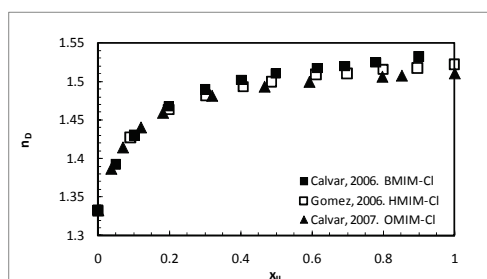


Fig. 13. Refractive index vs. IL molar fraction for three aqueous systems with halogen anion.

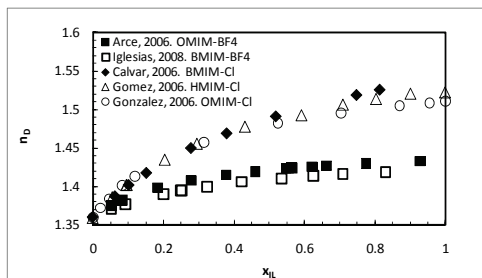


Fig. 14. Refractive index vs. IL molar fraction for systems with ethanol, three with halogen anion and two with tetrafluoro borate anion.

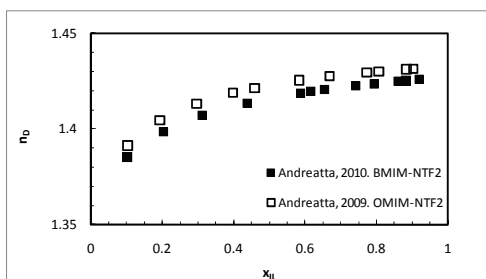


Fig. 15. Refractive index vs. IL molar fraction for two systems with ethanol and bis(trifluoromethylsulfonyl)imide anion.

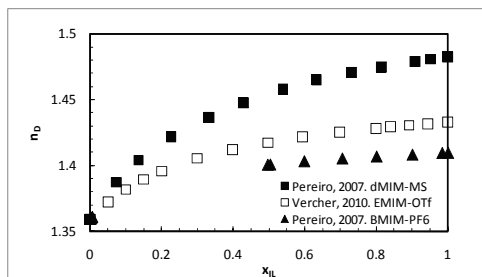


Fig. 16. Refractive index vs. IL molar fraction for three systems with ethanol and different anions.

### 4.3 Relationship with density

The refractive index  $n_D$  of any mixture can be correlated with the corresponding density of the same system using different expressions, as it happens with mixtures of non electrolyte organic compounds (Rilo et al., 2003). Among the different empirical expressions to do that, which gives the best results is that given by Newton, which reads

$$n_D = \left[ 1 + \phi_1 (n_{D1}^2 - 1) + \phi_2 (n_{D2}^2 - 1) \right]^{1/2}. \quad (3)$$

where  $n_{Di}$  is the refractive index of the pure compound. The parameter  $\phi_i$  represents the volume fraction of component  $i^{\text{th}}$  in the mixture, and can be defined as

$$\phi_i = \frac{x_i M_i}{x_1 M_1 + x_2 M_2} \frac{\rho}{\rho_i}, \quad (4)$$

where  $x_i$ ,  $M_i$  and  $\rho_i$  are, respectively, the mole fraction, the molecular mass and the density of compound  $i$ , and  $\rho$  is the density of the corresponding mixture. Let observe that there is not any fitting parameter, and  $n_D$  for each mixture only depends on its density. In Figure 18 the continuous line represents Newton's model given in equation (3) applied to data of BMIM-BF<sub>4</sub> + water, being the fit obtained very good. This is the first time that some of the data plotted in Figure 18, and the relationship between  $\rho$  and  $n_D$  in any IL system, is published. There exist in the literature many more empirical equations to estimate the refractive index of a binary mixture from their corresponding density (Rilo et al., 2003) but results are not so good as with Newton's model, at least for the systems investigated.

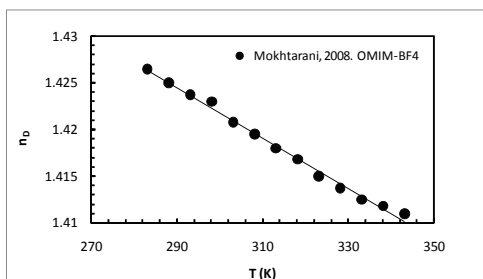


Fig. 17. Refractive index vs. temperature for a mixture with ethanol  $x_{IL} = 0.51$ . The curve is the best fit of a straight line.

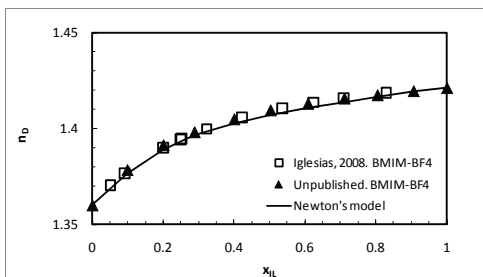


Fig. 18. Refractive index vs. IL molar fraction for the BMIM-BF<sub>4</sub> + ethanol system. The curve is the prediction from Newton's model.



## 5. Viscosity

Viscosity,  $\eta$ , characterizes the inner friction of liquids. Its value is necessary for all process where liquid flow exists, so its knowledge in chemical engineering is of great interest. The viscosity of ILs ranges from 0.1 to 20 Pa s, which results too high for many applications (Rogers et al., 2002). The mixture with a solvent such water or ethanol decreases its value exponentially for all ILs studied and for both solvents, but there are differences among the systems studied. Also, temperature reduces exponentially its value following in ILs a Vogel-Tamman-Fulcher (VTF) behaviour (Seddon et al., 2002).

$$\eta(T) = A \cdot \exp\left(\frac{B}{T - T_g}\right) \quad (5)$$

where  $T_g$  is roughly the glass transition temperature, at which the relaxation time of the melt equals infinity, i.e., the pseudo-lattice structure characteristic of the liquid and under-cooled liquid gets frozen in a crystal structure similar to the ordinary inorganic salts. The parameter  $B$  in Equation (5) is related with the activation energy needed by a particle in the pseudolattice to jump to the neighbour free site. In the case of ILs, where the organic cation size is usually much bigger than the inorganic anion size, it could be expected that the viscosity value would be given by the motion of the bigger, thus the more sluggish ion. In fact, as we will observe, it does not work like that exactly.

The experimental techniques to measure viscosity are falling ball, capillary tube or the two cylinder Stabinger method. We think this last is the ideal to measure IL mixtures, where the viscosity value changes some orders of magnitude with the concentration of solvent, because there is not necessary vary the measurement cell with the viscosity value, as it happens in the two first techniques.

### 5.1 Discussion of results

In Figures 19 to 23 we present viscosity for all mixtures of IL + water published, while in figures 24 to 27 all systems IL + ethanol. As observed, all ILs analyzed for both solvents decrease exponentially with the molar fraction of the IL, but that behaviour is not complete because for mixtures rich in the solvent the exponential behaviour disappears (linear relationship in the semi-logarithm representation shown), and the fall of  $\eta$  to the value of the pure solvent is increased. The excess viscosity ( $\Delta\eta = \eta - \eta_{id}$ ) is negative for all mixtures if we define the ideal viscosity as usual

$$\eta_{id} = x_S \eta_S + x_{IL} \eta_{IL} \quad (6)$$

where the suffix  $S$  means solvent. If we define  $\eta_{id}$  as,

$$\eta_{id} = \eta_S^{x_S} \cdot \eta_{IL}^{x_{IL}} \quad (7)$$

the excess is positive and it represents only a maximum about a 20% of the measured  $\eta$ .

We have found 17 different systems of any IL with water. In Figure 19 we present  $\eta$  data for BMIM-Cl and EMIM-Br (Liu et al., 2008), which concentration as molarity, m(mol/L). As observed the viscosity is bigger for the smallest ion (Cl), probably due to the fact that its electrical charge surface density is higher and so electrostatic interactions with the cation are also higher. In Fig. 20 we plot three systems with common Cl anion and cation of the same

alkyl-MIM family with the alkyl chain increasing (Gomez et al., 2006c). Except for OMIM-Cl at high solvent concentration (which could be wrong data), it seems that the three systems present a similar viscosity value. In Figure 21 we present six different systems with common  $\text{BF}_4$  anion and different cations: three alkyl-MIM (Rilo et al., 2010a), two alkyl-dMIM (Malhan& Turmine, 2008; Ge et al., 2009) and one alkyl pyridinium (Mokhtarani et al., 2009b). As expected the viscosity value increases with the size of the cation, being much higher for the dimethyl cation IL mixtures. We plot in Fig. 22 the only three aqueous mixtures of IL with a alkyl-sulphate anion (Gomez et al., 2006b; Gonzalez et al., 2008). As expected the length of the cation alkyl chain marks the value of viscosity. Finally, in Figure 23 we include the last three aqueous systems found, here all anions are organic ones (Rodriguez et al., 2006; Carbalho et al., 2010). In spite of the very different anions, viscosity is very similar for all of systems.

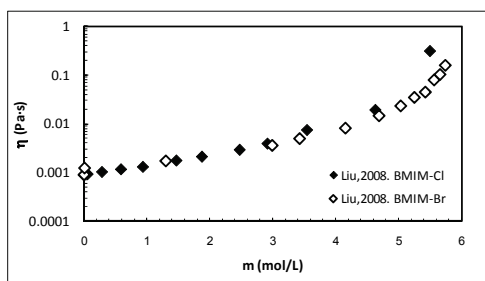


Fig. 19. Viscosity vs. molarity for two aqueous systems with halogen anion.

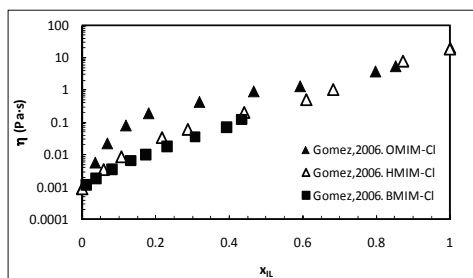


Fig. 20. Viscosity vs. IL molar fraction for three aqueous systems with halogen anion.

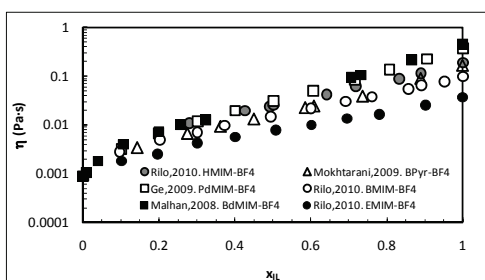


Fig. 21. Viscosity vs. IL molar fraction for six aqueous systems with tetrafluoroborate anion.

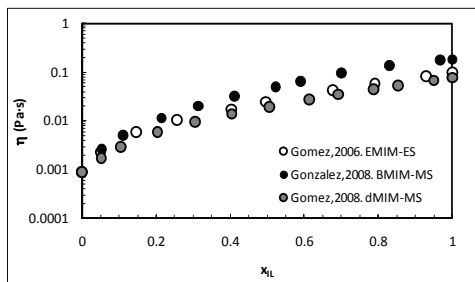


Fig. 22. Viscosity vs. IL molar fraction for three aqueous systems with alkyl sulfate anion.

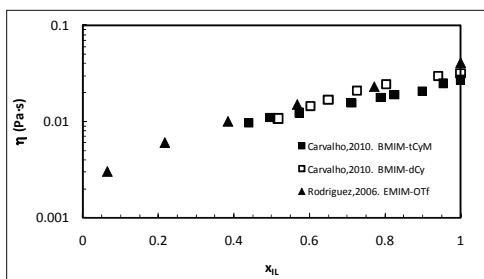


Fig. 23. Viscosity vs. IL molar fraction for three aqueous systems with organic anion.

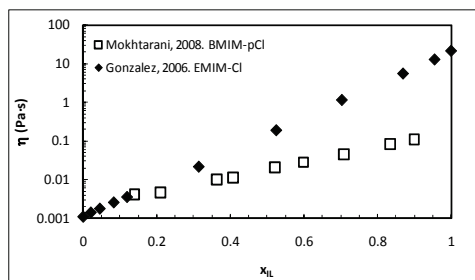


Fig. 24. Viscosity vs. IL molar fraction for two systems with ethanol and chlorate anion.

In figures 24 to 27 we plot the 14 systems IL + ethanol at 298.15 published. Thus, in Figure 24 (above) we plot the two published mixtures with a halogen anion (Mokhtarani et al., 2008; Gonzalez et al., 2006). In Figure 25 the systems with alkyl-MIM-BF<sub>4</sub> (Rilo et al., 2010b; Mokhtarani et al., 2008), where the dotted lines represent the ideal behaviour given in Eq. (7). In figure 26 we show the  $\eta$  data for systems with alkyl sulphate as anion (Gonzalez et al., 2009; Gomez et al., 2008). Finally in 27 we plot the published  $\eta$  data in systems with IL + ethanol with an organic anion (Andreatta et al., 2009; Domanska & Laskowska, 2009) or nitrate one (Mokhtarani et al., 2009a). All systems present an exponential dependence of  $\eta$  with  $x_{IL}$  for rich mixtures, being the curves very similar to the aqueous systems, except that the linearity between  $\log \eta$  and  $x_{IL}$  is lost for lower IL content, i.e. the exponential behaviour extends a smaller range of concentrations. Other experimental data for some of the systems presented have been also published, with similar results (Andreatta et al., 2009; Andreatta et al., 2010).

## 5.2 Temperature influence

The temperature dependence of viscosity for mixtures with water or ethanol also follows an exponential dependence, as observed for two selected equimolar IL mixtures with water (Ge et al., 2008) and ethanol (Rilo et al., 2010b), plotted in Figure 28. We have chosen two mixtures with the same cation and very different anions among those scarce data published.

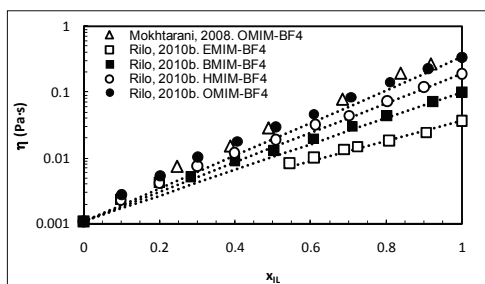


Fig. 25. Viscosity vs. IL molar fraction for four systems with ethanol and tetrafluoro borate anion. Lines represent the ideal behavior from Eq. (7).

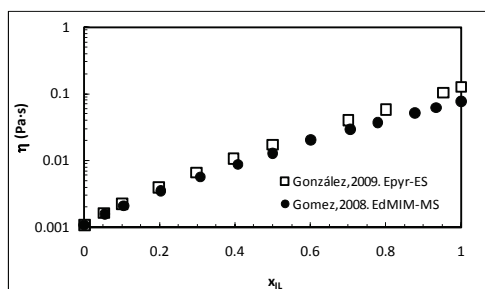


Fig. 26. Viscosity vs. IL molar fraction for two systems with ethanol and alkyl sulfate as anion.

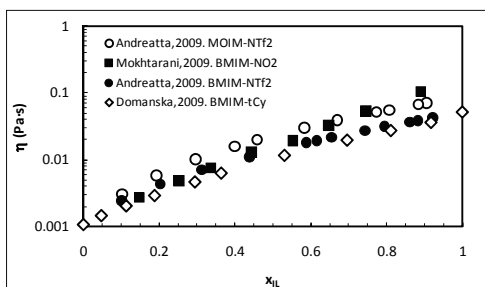


Fig. 27. Viscosity vs. IL molar fraction for four systems with ethanol and organic or nitrate anions.

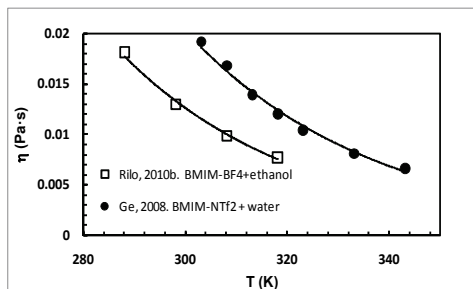


Fig. 28. Viscosity vs. temperature for two mixtures with  $x_{IL} = 0.50$ . The lines are the best fit of an exponential curve.

## 6. Electrical conductivity

Electrical conductivity,  $\kappa$ , of IL mixtures is of considerable interest both from practical as well as theoretical points of view. By means of conductivity data, conclusions on the structure and transport theories of ILs may be tested. Furthermore, the current and energy efficiencies of electrolytic processes are closely related to the electrical conductivity of the electrolyte. It has been observed that the electrical conductivity of the ILs increases more than 10 times when mixed with water, and about 5 times if mixed with ethanol. Electrical conductivity of pure ILs increases exponentially with temperature following a VTF type equation, as that given in Equation (5) (Vila et al., 2006b; Vila et al., 2007). The obtained value of the activation energy for  $\kappa$  does not agree with that taken from viscosity data because both have a different physical origin. Also  $T_g$  obtained with both magnitudes does not exactly match.

### 6.1 Discussion of results

We have found in literature only nine systems IL + water measured, and only four systems with ethanol as solvent. As in previous curves, all the data presented was measured at 298.15 K. In Figure 29 we plot the  $\kappa$  data published for mixtures of ILs with a halogen anion (Liu et al., 2008) with the concentration given in molarity (mol/L) as it was in the original paper. As observed the electrical conductivity decreases with the size of the cation but increases with the size of the anion (with a common cation). This last behaviour was found before in concentrated solutions of halogenated aluminium salts (Vila et al., 2005), and it is explained taking into account the fact that the electrostatic interactions are lower for bigger anions, and so its mobility is increased. In contrast, the increase of the alkyl chain length of the cation will decrease its mobility (now electrical charge is not located in the alkyl chain). In Figure 30 we include data for the only three aqueous miscible systems of the family alkyl-MIM-BF<sub>4</sub> (Vila et al., 2006; Rilo et al., 2010a; Stoppa et al., 2009). As in the previous case, the increase of the alkyl chain length decreases the electrical conductivity value. Data of the two sources agree fairly well among them for BMIM and HMIM, but for EMIM-BF<sub>4</sub> there are some differences in the published  $\kappa$  values, probably due to the presence of different impurity grades in both EMIM samples. In figure 31 we plot the three remain aqueous systems found in literature (Vila et al., 2006; Lin et al., 2009; Stoppa et al., 2009). Again the value of the electrical conductivity increases with the anion size. The values for the two system with EMIM-ES published do not agree between the two references, probably due again to the sample impurities.

The data published about electrical conductivity of systems with ethanol is really scarce, and we have only found a very recent paper from us reporting  $\kappa$  for three alkyl-MIM-BF<sub>4</sub> systems (Rilo et al., 2010b), which data are shown in Figure 32. If we compare with data for the same ILs but with water, shown in Figure 30, we observe that with ethanol the maximum value of  $\kappa$  is roughly half of that with water, it appears at higher molar fraction of the IL, and also the peak is more rounded. Let us note that while HMIM-BF<sub>4</sub> is only partially

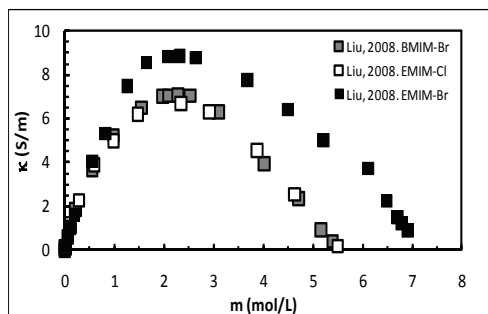


Fig. 29. Electrical conductivity vs. molarity for three aqueous systems with halogen anions.

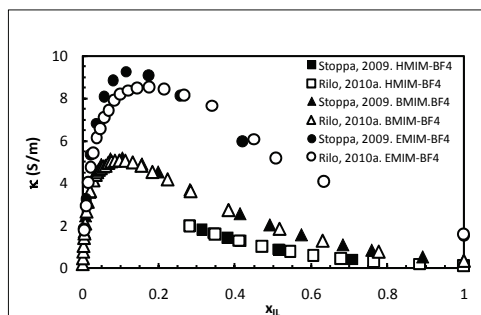


Fig. 30. Electrical conductivity vs. IL molar fraction for three aqueous systems with tetrafluoroborate anions.

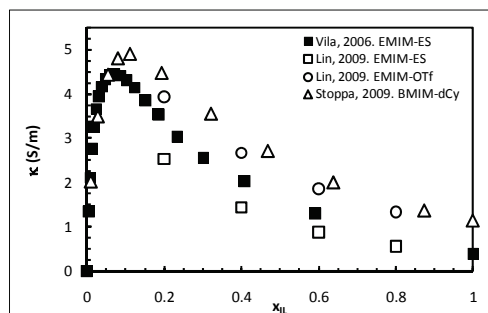


Fig. 31. Electrical conductivity vs. IL molar fraction for three aqueous systems with different anions.

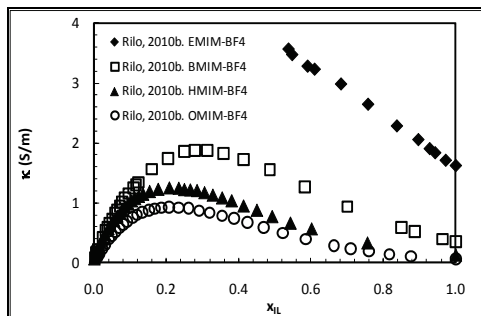


Fig. 32. Electrical conductivity vs. IL molar fraction for four systems with ethanol and tetrafluoro borate anion.

miscible with water and all the other members with shorter alkyl chain are completely miscible, for ethanol it happens opposite. EMIM is partially miscible and all the other members with longer alkyl chain are totally miscible with ethanol.

### 6.2 Temperature influence

As it is expected, electrical conductivity of the mixtures increases with temperature, because mobility of ions also increases. In contrast with viscosity, that increase is not exponential, but it follows a second order polynomial relationship, at least for the temperature range measured. This behaviour can be observed in Figure 33 where we plot two mixtures with  $x_{IL} = 0.60$  for two different IL systems (Lin et al., 2009).

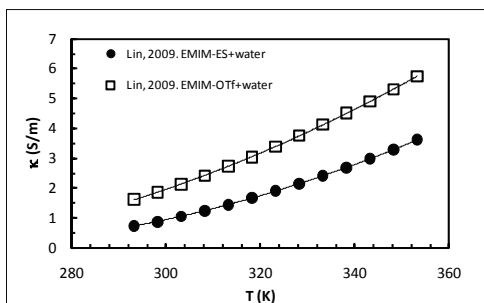


Fig. 33. Electrical conductivity vs. temperature for two mixtures with  $x_{IL} = 0.60$ . The lines are the best fit of a second order polynomial curve.

### 6.3 Relationship with viscosity. Walden's rule.

As it happens for molten salts (Danek, 2006) the original Walden's rule that relates viscosity with the specific conductivity ( $\Lambda = \kappa/m$ , where  $m$  is molarity in mol/L) does not work for IL mixtures. That rule affirms that

$$\Lambda \eta = K \quad (8)$$

where  $K$  is constant. This relationship does not happen for the IL + solvent, as published recently (Rilo et al., 2010a; Rilo et al., 2010b) and shown in Figure 34 for systems with

ethanol. Thus, in systems with an IL we must use the so called fractional Walden's rule, where viscosity is elevated to a given power  $\gamma$  (which value is between 0 and 1). So the modified Walden's rule will be

$$\Delta \eta^\gamma = K \quad (9)$$

which is most adequate when sizes of cation and anion are very different, and so the ionic motion is not coupled (Gaune-Escard & Seddon, 2010).

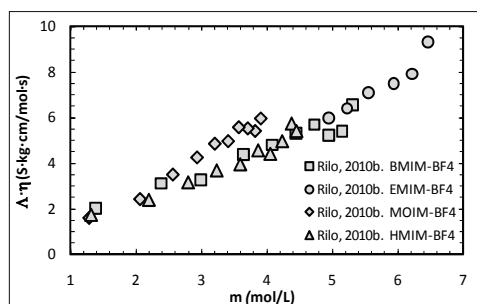


Fig. 34. Application of Walden's rule to four systems with ethanol and alkyl-MIM-BF<sub>4</sub>.

## 7. Surface tension

This is one of the most important technological parameters in ionic liquid chemistry, as the majority of reactions take place at the interface of electrolytes. The surface tension,  $\sigma$ , is related with the inter-ionic forces that take place in the surface of a liquid. Its unity is N/m, being the  $\sigma$  value the same than the surface energy or energy of the unit area, which unities are J/m<sup>2</sup>. The surface tension of pure ILs decreases linearly with temperature (Lin et al., 2009). When mixing two components the surface tension value depend on the surface composition, not in the bulk composition as all other magnitudes presented here do, so it will give information about the surfactant character of each IL with the different solvents. As we will observe,  $\sigma$  is the analyzed magnitude that changes more with the nature of the solvent. The best experimental technique to measure the surface tension is the falling drop volume, because others as suspended ring or plate techniques have a much bigger uncertainty.

### 7.1 Discussion of results

We have only found five papers presenting experimental measurements of the surface tension of aqueous mixtures of ILs, four of them for systems with alkyl-MIM (Yang et al., 2007; Liu et al., 2006; Liu et al., 2008; Rilo et al., 2009), one for EMIM-ES (Torrecilla et al., 2008) and another one for halogenated alkyl-MIM (Liu et al., 2008). One of the references cited is the only found that includes data for mixtures with ethanol (Rilo et al., 2009). Thus, in Figure 35 we show data for aqueous mixtures of alkyl-MIM-BF<sub>4</sub>, where we observe a sharp drop of  $\sigma$  from pure water value for very small IL concentrations. From that sharp drop surface tension is nearly constant equal to that of the pure IL, independently of the solvent concentration. The other authors that measure the same samples do not study the range of very diluted samples, and so they do not report the sharp drop, being the data in



the concentration range they present very similar to ours. In Figure 36 we plot the EMIM-Br, BMIM-Br and EMIM-Cl aqueous systems with the concentration expressed in molarity,  $m(\text{mol/L})$  (Liu et al., 2008). For these systems it is not observed the sharp drop. Another interesting fact is that the halogen anion has more influence in the  $\sigma$  value than the alkyl chain length and in an opposite form, bigger anion means higher  $\sigma$  value, but longer alkyl chain means lower  $\sigma$  value. We do not plot data for EMIM-ES because it is very noisy and do not covers the very diluted region, where the sharp drop of  $\sigma$  takes place.

As mentioned, only one very recent paper publish data for surface tension in any system IL + ethanol. In Figure 37 we plot those data for four systems with alkyl-MIM-BF<sub>4</sub> (with EMIM-BF<sub>4</sub> being only partially miscible with ethanol). We observe a complete different behavior than the corresponding aqueous systems shown in Figure 35. Now  $\sigma$  varies linearly with  $x_{IL}$  for the four systems, being the  $\sigma$  value of the equimolar mixture the same for the four systems, decreasing linearly with  $x_{IL}$  to the pure ethanol value, following the three miscible ILs the same straight line.

## 7.2 Temperature influence

If data of surface tension is scarce, data about the temperature dependence of surface tension is even scarcer. In fact we have only found one paper where  $\sigma$  vs.  $T$  appears (Yang et al., 2007). Those data are plotted in Figure 38 for the aqueous system with EMIM-BF<sub>4</sub>, which roughly follows a quadratic polynomial equation with temperature (line in the figure).

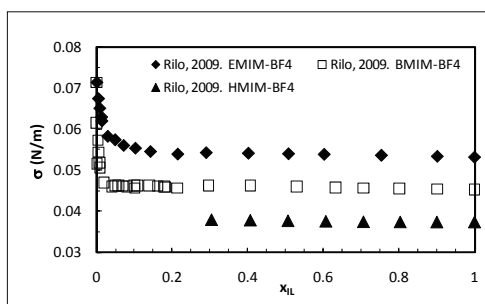


Fig. 35. Surface tension vs. IL molar fraction for three aqueous systems with 1-alkyl-3-methyl-imidazolium tetrafluoro borate.

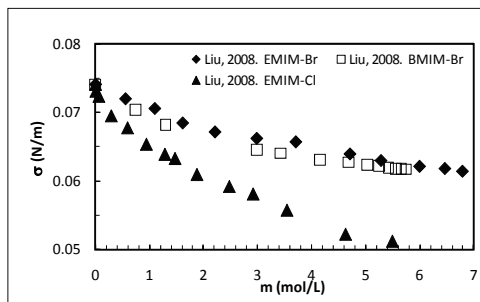


Fig. 36. Surface tension vs. IL molar fraction for three aqueous systems with 1-alkyl-3-methyl-imidazolium halogenated.

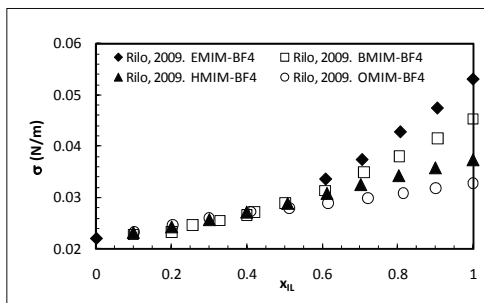


Fig. 37. Surface tension vs. IL molar fraction for four systems with ethanol and 1-alkyl-3-methyl-imidazolium tetrafluoro borate.

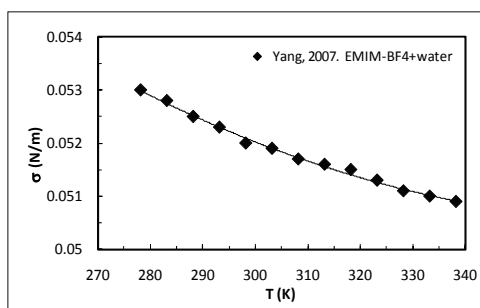


Fig. 38. Surface tension vs. temperature for a mixture with  $x_{IL} = 0.875$ . The line is the best fit of a second order polynomial curve.

## 8. Conclusion

We present in this work all published data on density, refractive index, viscosity, electrical conductivity and surface tension for all systems IL + water and + ethanol covering a broad range of concentrations. For density, refractive index and viscosity the data for mixtures with water or ethanol are very similar, and also their behaviour with concentration is not really dependent of the IL mixed with any solvent (except for its value). Density and refractive index can be deduced one from another using Newton's model, which demonstrates the close relationship between both magnitudes. For electrical conductivity and surface tension, the solvent nature determines the data behaviour obtained. Thus, the electrical conductivity value of the pure IL for aqueous systems increases up to 10 times, while that increase is halved for ethanol systems. In the case of surface tension the behaviour is completely different depending on the solvent and IL studied. For alkyl-methyl-imidazolium tetrafluoroborate the IL acts like a surfactant in water, and the surface tension value decreases sharply from that of water to that of the pure IL for small concentrations of this last, effect that does not appear for halogenated imidazolium ILs. If we change the water for ethanol, that surfactant like effect disappear, and the surface tension value of the only four ILs measured decreases linearly with the ethanol content down to a common value at about equimolar mixture, and then all data has the same value,

decreasing linearly again down to the pure ethanol value. As observed, the behaviour of water and ethanol in the surface of IL is completely different.

## 9. Acknowledgments

We thank financial support from Spanish “Ministerio de Educación y Ciencia” with references FIS2007-66823-C02-01 and FIS2007-66823-C02-02, which are partially supported by FEDER funds.

## 10. References

- Ali, M.; Sarkar, A.; Tariq, M.; Ali, A. & Pandey, S. (2007). Dilute aqueous 1-butyl-3-methylimidazolium hexafluorophosphate properties and solvatochromic probe behavior. *Green Chem.* 9, 11 (2007) 1252-1258.
- Andreatta, A.E.; Arce; A.; Rodil, E. & Soto, A. (2009). Physical Properties of Binary and Ternary Mixtures of Ethyl Acetate, Ethanol, and 1-Octyl-3-methyl-imidazolium bis(trifluoromethylsulfonyl)imide at 298.15 K. *J.Chem.Eng.Data* 54, 3 (March 2009) 1022-1028.
- Andreatta, A.E.; Arce; A.; Rodil, E. & Soto, A. (2010). Physico-chemical Properties of Binary and Ternary Mixtures of Ethyl Acetate + Ethanol + 1-Butyl-3-methyl-imidazolium bis(trifluoromethylsulfonyl)imide at 298.15 K and Atmospheric Pressure. *J.Sol.Chem.* 39, 3 (March 2010) 371-383.
- Arce, A.; Rodríguez, H. & Soto, A. (2006a). Effect of anion fluorination in 1-ethyl-3-methylimidazolium as solvent for the liquid extraction of ethanol from ethyl tert-butyl ether. *Fluid Phase Equilib.* 242, 2 (May 2006) 164-168.
- Arce, A.; Rodil, E. & Soto, A. (2006b). Volumetric and Viscosity Study for the Mixtures of 2-Ethoxy-2-ethylpropane, Ethanol, and 1-Ethyl-3-methylimidazolium Ethyl Sulfate Ionic Liquid. *J.Chem.Eng.Data* 51, 4 (July 2006) 1453-1457.
- Bahe, L.W. (1972) Structure in concentrated solutions of electrolytes. Field-dielectric-gradient forces and energies. *J. Phys. Chem.* 76, 7 (July 1972) 1062-1071.
- Brennecke, J.F.; Rogers, R.D. & Seddon, K.N. Ed. (2007). *Ionic Liquids IV: not just solvents anymore*, American Chemical Society, ISBN:978-0-8412-7445-7, Washington.
- Calvar, N.; González, B.; Gómez, E. & Domínguez, A. (2006). Vapor-Liquid Equilibria for the Ternary System Ethanol + water + 1-Butyl-3-methylimidazolium Chloride and the Corresponding Binary Systems at 101.3 kPa. *J.Chem.Eng.Data*, 51, 6 (Nov. 2006) 2178-2181.
- Calvar, N.; Gómez, E.; González, B. & Domínguez, A. (2007). Experimental Determination, Correlation, and Prediction of Physical Properties of the Ternary Mixtures Ethanol + Water with 1-Octyl-3-methylimidazolium Chloride and 1-Ethyl-3-methylimidazolium Ethylsulfate. *J.Chem.Eng.Data*, 52, 6 (Nov. 2007) 2529-2535.
- Carvalho, P.J.; Regueira, T.; Santos, L.M.N.B.F.; Fernandez, J. & Coutinho, J.A.P. (2010). Dicyanamide and 1-Butyl-3-methylimidazolium Tricyanomethane at Atmospheric Pressure. *J.Chem.Eng.Data*, 55, 2 (Feb. 2010) 645-652.
- Danek, V. (2006). *Physico-Chemical Analysis of Molten Electrolytes*, Elsevier, ISBN-10:0-444-52116-X, Netherlands.
- Domńska, U.; Pobudkowska, A. & Wisniewska, A. (2006). Solubility and Excess Molar Properties of 1,3-dimethylimidazolium Methylsulfate, or 1-Butyl-3-

- Methylimidazolium Methylsulfate, or 1-Butyl-3-Methylimidazolium Octylsulfate Ionic Liquids with *n*-Alkanes and Alcohols: Analysis in Terms of the PFP and FBT Models1. *J.Sol.Chem*, 35, 3 (March 2006) 311-334.
- Domńska, U. & Laskowska, M. (2009). Temperature and Composition Dependence of the Density and Viscosity of Binary Mixtures of {1-Butyl-3-methylimidazolium Thiocyanate + 1-Alcohols}. *J.Chem.Eng.Data*, 54, 7 (July 2009) 2113-2119.
- Dong, L.; Zheng D.X.; Wei, Z. & Wu, X.H. (2009). Synthesis of 1,3-Dimethylimidazolium Chloride and Volumetric Property Investigations of Its Aqueous Solution. *Int.J.Thermophys.* 30, 5 (2009) 1480-1490.
- Fu, D.; Sun, X.; Pu, J. & Zhao, S. (2006). Effect of Water Content on the Solubility of CO<sub>2</sub> in the Ionic Liquid [bmim][PF<sub>6</sub>]. *J.Chem.Eng.Data*, 51, 2 (March 2006) 371-375.
- Gaillon, L.; Sirieix-Plenet, J. & Letellier, P. (2004). Volumetric Study of Binary Solvent Mixtures Constituted by Amphiphilic Ionic Liquids at Room Temperature (1-Alkyl-3-Methylimidazolium Bromide) and Water. *J.Sol.Chem*, 33, 11 (Nov. 2004) 1333-1347.
- Galán, J.J.; Del Castillo, J.L.; González-Pérez, A.; Czapkiewicz, J. & Rodríguez, J.R. (2003). Density and Sound Velocity Studies of Aqueous Solutions of Tetradecyltrimethylammonium Nitrate at Different Temperatures. *J.Sol.Chem*, 32, 10 (Oct. 2003) 919-927.
- García-Miaja, G.; Troncoso, J. & Romani, L. (2008). Excess properties for binary systems ionic liquid + ethanol: Experimental results and theoretical description using the ERAS model. *Fluid Phase Equilib.* 274, 1-2 (Dec. 2008) 59-67.
- García-Miaja, G.; Troncoso, J. & Romani, L. (2009). Excess enthalpy, density, and heat capacity for binary systems of alkylimidazolium-based ionic liquids + water. *J.Chem.Thermodynamics* 41, 2 (March 2009) 161-166.
- Gardas, R. L.; Dagade, D.H.; Terdale, S.S.; Coutinho, J.A.P. & Patil, K.J. (2008). Acoustic and volumetric properties of aqueous solutions of imidazolium based ionic liquids at 298.15 K. *J.Chem.Thermodynamics* 40, 4 (April 2008) 695-701.
- Gardas, R.L.; Freire, M.G.; Carvalho, P.J.; Marrucho, I.M.; Fonseca, I.M.A.; Ferreira, A.G.M. & Coutinho, J.A.P. (2007). High-Pressure Densities and Derived Thermodynamic Properties of Imidazolium-Based Ionic Liquids. *J.Chem.Eng.Data*, 52, 1 (January 2007) 80-88.
- Gaune-Escard, M. & Seddon, K.N. Ed. (2010). Molten salts and ionic liquids, never the twain?, J. Wiley & Sons, ISBN: 978-0-471-77392-4, USA.
- Ge, M.-L.; Zhao, R.-S.; Yi, Y.-F.; Zhang, Q. & Wang, L.-S. (2008). Densities and Viscosities of 1-Butyl-3-methylimidazolium Trifluoromethanesulfonate + H<sub>2</sub>O Binary Mixtures at T) (303.15 to 343.15) K. *J.Chem.Eng.Data*, 53, 10 (Oct. 2008) 2408-2411.
- Ge, M.-L.; Ren, X.-G.; Song, Y.-J. & Wang, L.-S. (2009). Densities and Viscosities of 1-Propyl-2,3-dimethylimidazolium Tetrafluoroborate + H<sub>2</sub>O at T) (298.15 to 343.15) K. *J.Chem.Eng.Data*, 54, 4 (April 2009) 1400-1402.
- Gómez, E.; González, B.; Domínguez, A.; Tojo, E. & Tojo, J. (2006a). Dynamic Viscosities of a Series of 1-Alkyl-3-methylimidazolium Chloride Ionic Liquids and Their Binary Mixtures with Water at Several Temperatures. *J.Chem.Eng.Data*, 51, 2 (March 2006) 696-701.
- Gómez, E.; González, B.; Calvar, N.; Tojo, E. & Domínguez, A. (2006b). Physical Properties of Pure 1-Ethyl-3-methylimidazolium Ethylsulfate and Its Binary Mixtures with

- Ethanol and Water at Several Temperatures. *J.Chem.Eng.Data*, 51, 6 (Nov. 2006) 2096-2102.
- Gómez, E.; Calvar, N.; Domínguez, I. & Domínguez A. (2006c). Physical properties of the ternary mixture ethanol water 1-hexyl-3-methylimidazolium chloride at 298.15 K. *Phys.Chem.Liq.* 44, 4 (2006) 409-417.
- Gómez, E.; González, B.; Calvar, N. & Domínguez, A. (2008). Excess molar properties of ternary system (ethanol + water + 1,3-dimethylimidazolium methylsulphate) and its binary mixtures at several temperatures. *J.Chem.Thermodynamics* 40, 8 (August 2008) 1208-1216.
- González, E.J.; Alonso, L. & Domínguez, A. (2006). Physical Properties of Binary Mixtures of the Ionic Liquid 1-Methyl-3-octylimidazolium Chloride with Methanol, Ethanol, and 1-Propanol at  $T = (298.15, 313.15, \text{ and } 328.15) \text{ K}$  and at  $P = 0.1 \text{ MPa}$ . *J.Chem.Eng.Data*, 51, 4 (July 2006) 1446-1452.
- González, B.; Calvar, N.; Gómez, E. & Domínguez, A. (2008). Physical properties of the ternary system (ethanol + water + 1-butyl-3-methylimidazolium methylsulphate) and its binary mixtures at several temperatures. *J.Chem.Thermodynamics* 40, 8 (August 2008) 1274-1281.
- González, B.; Calvar, N.; Gómez, E.; Domínguez, I. & Domínguez, A. (2009). Synthesis and Physical Properties of 1-Ethylpyridinium Ethylsulfate and its Binary Mixtures with Ethanol and 1-Propanol at Several Temperatures. *J.Chem.Eng.Data*, 54, 4 (April 2009) 1353-1358.
- Huddleston, J.G.; Visser, A.E.; Reichert, W.M.; Willauer, H.D.; Broker, G.A. & Rogers, R.D. (2001). Characterization and comparison of hydrophilic and hydrophobic room temperature ionic liquids incorporating the imidazolium cation. *Green Chem.* 3 (2001) 156-164.
- Iglesias-Otero, M.A.; Troncoso, J.; Carballo, E. & Romani, L. (2008). Density and refractive index in mixtures of ionic liquids and organic solvents: Correlations and predictions. *J.Chem.Thermodynamics* 40, 6 (June 2008) 949-956.
- Jacquemin, J.; Husson, P.; Padua, A.A.H. & Majer, V. (2006). Density and viscosity of several pure and water-saturated ionic liquids. *Green Chem.* 8, 2 (2006) 172-180.
- Lin, P.-Y.; Soriano, A. N.; Caparanga A.R. & Li, M. -H. (2009). Electrolytic conductivity and molar heat capacity of the solvent system: 1-ethyl-3- methylimidazolium ethylsulfate + water and 1-ethyl-3-methylimidazolium trifluoromethanesulfonate + water. *Thermochim. Acta* 496, 1 (December 2009) 105-109.
- Liu, W.; Zhao, T.; Zhang, Y.; Wang, H. & Yu, M. (2006). The Physical Properties of Aqueous Solutions of the Ionic Liquid [BMIM][BF<sub>4</sub>]. *J.Sol.Chem.* 35, 10 (Oct. 2006) 1337-1346.
- Liu, W.; Cheng, L.; Zhang, Y.; Wang, H. & Yu, M. (2008). The physical properties of aqueous solution of room-temperature ionic liquids based on imidazolium: Database and evaluation. *Journal of Molecular Liquids*, 140, 1 (January 2008) 68-72.
- Lu, X.-M.; Xu, W.-G.; Gui, J.-S.; Li, H.-W. & Yang, J.Z. (2005). Volumetric properties of room temperature ionic liquid 1. The system of {1-methyl-3-ethylimidazolium ethyl sulfate + water} at temperature in the range (278.15 to 333.15) K. *J.Chem.Thermodynamics* 37, 1 (January 2005) 13-19.
- Malham, I.B.; Letellier, P.; Mayaffre, A. & Turmine, M. (2007). Part I: Thermodynamic analysis of volumetric properties of concentrated aqueous solutions of 1-butyl-3-methylimidazolium tetrafluoroborate, 1-butyl-2,3-dimethylimidazolium

- tetrafluoroborate, and ethylammonium nitrate based on pseudo-lattice theory. *J.Chem.Thermodynamics* 39, 8 (July 2007) 1132-1143.
- Malham, I.B. & Turmine, M. (2008). Viscosities and refractive indices of binary mixtures of 1-butyl-3-methylimidazolium tetrafluoroborate and 1-butyl-2,3-dimethylimidazolium tetrafluoroborate with water at 298 K. *J.Chem.Thermodynamics* 40, 4 (April 2008) 718-723.
- Marsh, K.N.; Boxall, J.A. & Lichtenthaler, R. (2004). Room temperature ionic liquids and their mixtures-a review. *Fluid Phase Equilib.* 219, 1 (May 2004) 93-98.
- Mokhtarani, B.; Mojtahedi, M.M.; Mortaheb, H.R.; Mafi, M.; Yazdani, F. & Sadeghian, F. (2008). Densities, Refractive Indices, and Viscosities of the Ionic Liquids 1-Methyl-3-octylimidazolium Tetrafluoroborate and 1-Methyl-3-butylimidazolium Perchlorate and Their Binary Mixtures with Ethanol at Several Temperatures. *J.Chem.Eng.Data*, 53, 3 (March 2008) 677-682.
- Mokhtarani, B.; Sharifi, A.; Mortaheb, H.R.; Mirzaei, M.; Mafi, M. & Sadeghian, F. (2009a). Density and viscosity of 1-butyl-3-methylimidazolium nitrate with ethanol, 1-propanol, or 1-butanol at several temperatures. *J.Chem.Thermodynamics* 41, 12 (Dec. 2009) 1432-1438.
- Mokhtarani, B.; Sharifi, A.; Mortaheb, H.R.; Mirzaei, M.; Mafi, M. & Sadeghian, F. (2009b). Density and viscosity of pyridinium-based ionic liquids and their binary mixtures with water at several temperatures. *J.Chem.Thermodynamics* 41, 3 (March 2009) 323-329.
- Ohno, H. Ed. (2005). *Electrochemical aspects of ionic liquids*, Wiley, ISBN: 0-471-64851-5, New Jersey.
- Ortega, J.; Vreekamp, R.; Penco, E. & Marrero, E. (2008). Mixing thermodynamic properties of 1-butyl-4-ethylpyridinium tetrafluoroborate [b4mpy][BF<sub>4</sub>] with water and with an alkan-1-ol (methanol to pentanol). *J.Chem.Thermodynamics* 40, 7 (July 2008) 1087-1094.
- Pereiro, A.B. & Rodríguez, A. (2007). Study on the phase behaviour and thermodynamic properties of ionic liquids containing imidazolium cation with ethanol at several temperatures. *J.Chem.Thermodynamics* 39, 6 (June 2007) 978-989.
- Rilo, E.; Freire, S.; Segade, L.; Cabeza, O.; Franjo, C. & Jiménez, E. (2003). Surface tensions, densities and refractive indexes of mixtures of dibutyl ether and 1-alkanol at T=298.15 K. *J.Chem.Thermodynamics* 35, 5 (May 2003) 839-850.
- Rilo, E.; Pico, J.; García-Garabal, S.; Varela, L.M. & Cabeza, O. (2009). Density and surface tension in binary mixtures of CnMIM-BF<sub>4</sub> ionic liquids with water and ethanol. *Fluid Phase Equilib.* 285, 1-2 (Nov. 2009) 83-89.
- Rilo, E.; Vila, J.; Pico, J.; García-Garabal, S.; Segade, L.; Varela, L.M. & Cabeza, O. (2010a). Electrical Conductivity and Viscosity of Aqueous Binary Mixtures of 1-Alkyl-3-methyl Imidazolium Tetrafluoroborate at Four Temperatures. *J.Chem.Eng.Data*, 55, 2 (February 2010) 639-644.
- Rilo, E.; Vila, J.; García, M.; Varela, L.M. & Cabeza, O. (2010b). Viscosity and electrical conductivity of binary mixtures of CnMIM-BF<sub>4</sub> with ethanol at 288 K, 298 K, 308 K and 318 K. Accepted for publication in *J.Chem.Eng.Data*.
- Rilo, E.; Ferreira, A.G.M.; Fonseca, I.M.A. & Cabeza, O. (2010c). Densities and derived thermodynamic properties of ternary mixtures 1-butyl-3-methyl-imidazolium

- tetrafluoroborate + ethanol + water at seven pressures and two temperatures. *Fluid Phase Equilib.* 296, 1 (September 2010) 53-59.
- Rodríguez, H.; Brennecke, J.F. (2006). Temperature and Composition Dependence of the Density and Viscosity of Binary Mixtures of Water + Ionic Liquid. *J.Chem.Eng.Data*, 51, 6 (Nov. 2006) 2145-2155.
- Rogers, R.D. & Seddon, K.N. Ed. (2002). *Ionic Liquids. Industrial applications to green chemistry*, ACS Symp. Series 818. ISBN: 0-8412-3789-1, USA.
- Rogers, R.D. & Seddon, K.N. Ed. (2005). *Ionic Liquids IIIA: Fundamentals, Progress, Challenges and Opportunities*, American Chemical Society, ISBN: 0-8412-3893-6, USA.
- Rogers, R.D.; Seddon, K.N. & Volkov, S. Ed. (2002). *Green Industrial Applications of Ionic liquids*, Nato Science Series, ISBN: 1-4020-1136-9, Netherlands.
- Seddon, K.R.; Stark, A. & Torres, M.J. (2000). Influence of chloride, water, and organic solvents on the physical properties of ionic liquids. *Pure Appl. Chem.*, 72, 12 (December 2000) 2275-2287.
- Stoppa, A.; Hunger, J. & Buchner, R. (2009). Conductivities of Binary Mixtures of Ionic Liquids with Polar Solvents. *J.Chem.Eng.Data*, 54, 2 (February 2009) 472-479.
- Torrecilla, J.S.; Rafione, T.; García, J. & Rodríguez, F. (2008). Effect of Relative Humidity of Air on Density, Apparent Molar Volume, Viscosity, Surface Tension, and Water Content of 1-Ethyl-3-methylimidazolium Ethylsulfate Ionic Liquid. *J.Chem.Eng.Data*, 53, 4 (April 2008) 923-928.
- Varela, L.M.; García, M.; Sarmiento, F.; Attwood, D. & Mosquera, V. (1997). Pseudolattice theory of strong electrolyte solutions. *J. Chem. Phys.* 107, 16 (October 1997) 6415-6419.
- Varela, L.M.; Carrete, J.; Turmine, M.; Rilo, E. & Cabeza, O. (2009). Pseudolattice theory of the surface tension in ionic liquid-water mixture. *J. Phys. Chem. B* 113, 37 (September 2009) 12500-12505.
- Vercher, E.; Vicent Orchillés, A.; Miguel, P.J. & Martínez-Andreu, A. (2007). Volumetric and Ultrasonic Studies of 1-Ethyl-3-ethylimidazolium Trifluoromethanesulfonate Ionic Liquid with Methanol, Ethanol, 1-Propanol, and Water at Several Temperatures. *J.Chem.Eng.Data*, 52, 4 (July 2007) 1468-1482.
- Vercher, E.; Llopis, F.J.; González-Alfaro, V. & Martínez-Andreu, A. (2010). Refractive Indices and Deviations in Refractive Indices for Binary Mixtures of 1-Ethyl-3-methylimidazolium Trifluoromethanesulfonate with Methanol, Ethanol, 1-Propanol, and 2-Propanol at Several Temperatures. *J.Chem.Eng.Data*, 55, 3 (March 2010) 1430-1433.
- Vicent-Orchillés, A.; González-Alfaro, V.; Miguel, P.J.; Vercher, E. & Martínez-Andreu, A. (2006). Volumetric properties of binary mixtures of ionic liquid 1-butyl-3-methylimidazolium octylsulfate with water or propanol in the temperature range of 278.15 K to 328.15 K. *J.Chem.Thermodynamics* 38, 9 (Sept. 2006) 1124-1129.
- Vila, J.; Rilo, E.; Segade, L.; Varela, L.M. & Cabeza, O. (2005). Electrical conductivity of aqueous solutions of aluminum salts. *Phys. Rev. E* 71, 3 (March 2005) 031201 1-8.
- Vila, J.; Ginés, P.; Rilo, E.; Cabeza, O. & Varela, L.M. (2006a). Great increase of the electrical conductivity of ionic liquids in aqueous solutions. *Fluid Phase Equilib.* 247, 1-2 (September 2006) 32-39.
- Vila, J.; Ginés, P.; Pico, J.M.; Franjo, C.; Jiménez, E.; Varela, L.M. & Cabeza, O. (2006b). Temperature dependence of the electrical conductivity in EMIM-based ionic

- liquids. Evidence of Vogel-Tamman-Fulcher behavior. *Fluid Phase Equilib.* 242, 2 (April 2006) 141-146
- Vila, J.; Varela, L.M. & Cabeza, O. (2007). Cation and anion sizes influence in the temperature dependence of the electrical conductivity in nine imidazolium based ionic liquids. *Electrochimica Acta* 52, 26 (June 2007) 7413-7417.
- Woodward, C.E. & Harris, K.R. (2010). A lattice-hole theory for conductivity in ionic liquid mixtures: application to ionic liquid + water mixtures. *Phys. Chem. Chem. Phys.* 12, 5 (February 2010) 1172-1176.
- Wu, B.; Zhang, Y.M. & Wang, H.P. (2009). Volumetric Properties and Conductivities of 1-Butyl-3-methylimidazolium Tetrafluoroborate + Sucrose + Water Mixtures. *J.Chem.Eng.Data*, 54, 5 (May 2009) 1430-1434.
- Yang, J.-Z.; Lu, X.-M.; Gui, J.-S.; Xu, W.-G. & Li, H.-W. (2005). Volumetric properties of room temperature ionic liquid 2.The concentrated aqueous solutions of {1-methyl-3-ethylimidazolium ethyl sulfate + water} in a temperature range of 278.2 K to 338.2 K. *J.Chem.Thermodynamics* 37,11 (Nov. 2005) 1250-1255.
- Yang J.-Z.; Li, J.; Tong, J. & Hong, M. (2007). Study on the Density and Surface Tension of Ionic Liquid EMIBF<sub>4</sub> in Terms of Standard Addition Method. *Acta Chimica Sinica* 65, 8 (April 2007) 655-659.
- Yang, Q.; Zhang, H.; Su, B.; Yang, Y.; Ren, Q. & Xing, H. (2010). Volumetric Properties of Binary Mixtures of 1-Butyl-3-methylimidazolium Chloride + Water or Hydrophilic Solvents at Different Temperatures. *J. Chem. Ing. Data* 55, 4 (April 2010) 1750-1754.
- Yu, Y.-H.; Soriano, A.N. & Li, M.-H. (2009). Heat capacities and electrical conductivities of 1-ethyl-3-methylimidazolium-based ionic liquids. *J.Chem.Thermodynamics* 41, 1 (January 2009) 103-108.
- Zafarani-Moattar, M.T. & Shekaari, H. (2005). Apparent molar volume and isentropic compressibility of ionic liquid 1-butyl-3-methylimidazolium bromide in water, methanol, and ethanol at T = (298.15 to 318.15) K. *J.Chem.Thermodynamics* 37, 10 (Oct. 2005) 1029-1035.
- Zafarani-Moattar, M.T.; Majdan-Cegincara, R. (2007). Viscosity, Density, Speed of Sound, and Refractive Index of Binary Mixtures of Organic Solvent + Ionic Liquid, 1-Butyl-3-methylimidazolium Hexafluorophosphate at 298.15 K. *J.Chem.Eng.Data*, 51, 6 (November 2007) 2359-2364.
- Zhang, Q.-G.; Xue, F.; Tong, J.; Guan, W. & Wang, B. (2006). Studies on Volumetric Properties of Concentrated Aqueous Solutions of the Ionic Liquid BMIBF<sub>4</sub>. *J.Sol.Chem*, 35, 3 (March 2006) 297-309.
- Zhou, Q.; Wang, L.-S. & Chen, H.-P. (2006). Densities and Viscosities of 1-Butyl-3-methylimidazolium Tetrafluoroborate + H<sub>2</sub>O Binary Mixtures from (303.15 to 353.15) K. *J.Chem.Eng.Data*, 51, 3 (May 2006) 905-908.



# Photochromism in Ionic Liquids. Theory and Applications

Fernando Pina and Luís C. Branco  
*REQUIMTE, Departamento de Química, Faculdade de Ciências e Tecnologia,  
Universidade Nova de Lisboa, 2829-516 Caparica,  
Portugal*

## 1. Introduction

Research on photochromic compounds by itself is an important issue with great industrial impact from ophthalmic lens fabrication to the achievement of intelligent windows and displays.[1,2] Furthermore, the possibility of having photochromism in ionic liquids is an appealing objective due to the unique properties exhibited by these compounds. The research on this field is very recent and can be divided in two main categories: i) photochromic compounds dissolved in ionic liquids, ii) and more recently the preparation and study of intrinsically photochromic ionic liquids.

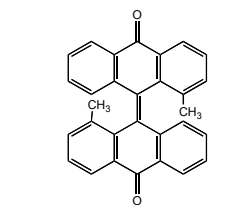
## 2. Photochromism in common solvents

The term photochromism was coined by Hirshberg in a series of papers appearing during the first years of the fifties of the last century.[3] Photochromism can be defined as a reversible photo-induced change of colour, the back reaction taking necessarily place through a thermal or a photochemical process.

The photochromism early reported by Hirshberg and co-workers was observed in bianthrone (dianthraquinones), Scheme 2.1, and spiropyrans, Scheme 2.2. Through the years, photochromism of (a few) other families of compounds have been reported, the most relevant are described above.[2]

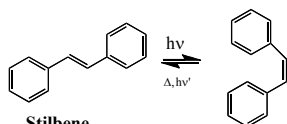
In order to achieve photochromism, a photo-induced reaction leading to a new species possessing different physical and chemical properties, in particular the absorption spectra, should occur. In the case of the spiropyrans, spirooxazines and chromenes, the initial photochemical step consists of the spirocarbon C-O bond cleavage followed by the rearrangement of the molecule, Scheme 2.2.

The other common photo-induced initial step is the *cis-trans* isomerisation as in the case of stilbenes and azobenzenes, Scheme 2.3. Other systems consist of two steps, a *cis-trans* isomerisation followed by cyclization, as in diarylethenes, Scheme 2.4, and fulgides, Scheme 2.5. In the case of diarylethenes the photoisomerisation step is avoided by “freezing” the compound in its *cis* configuration through an appropriate structural modification. This prevents the initial isomerisation process and the photochromism is only controlled by the cyclization reaction, Scheme 2.4, bottom.[4]

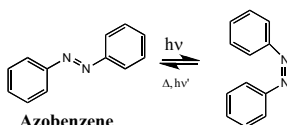


Hirshberg's bianthrone

Scheme 2.1

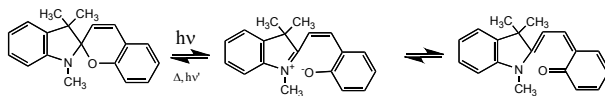


Stilbene

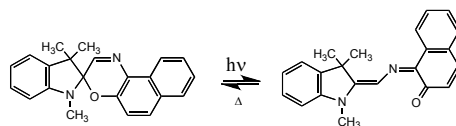


Azobenzene

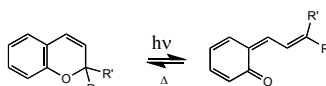
Scheme 2.3



Spiropyrans

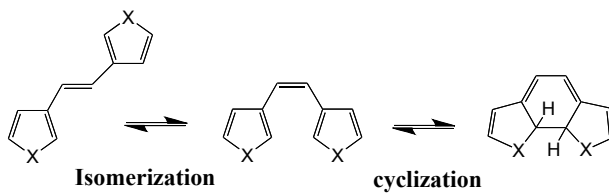


Spirooxazines



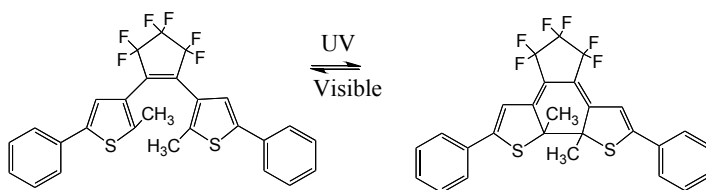
Chromenes

Scheme 2.2



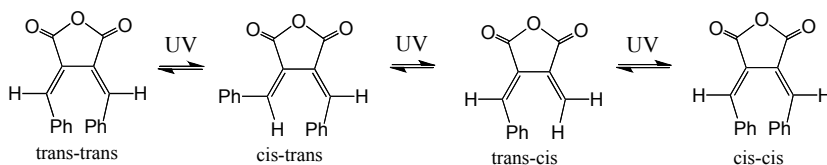
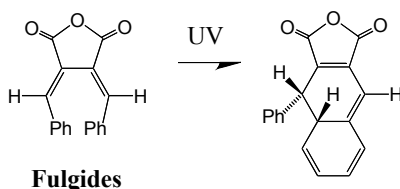
Isomerization

cyclization



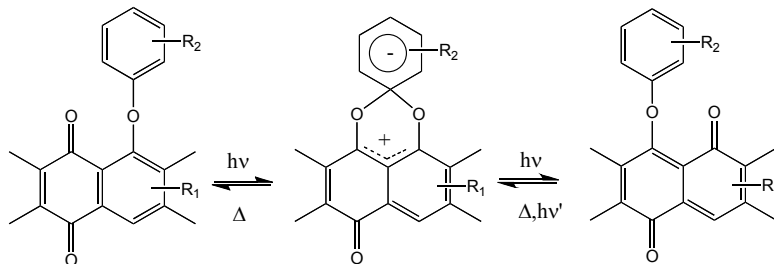
Diarylethenes

Scheme 2.4

**Fulgides**

Scheme 2.5

Quinones can also exhibit photochromism, which is caused by a reversible photoinduced migration of hydrogen, aryl or acyl groups. The following mechanism considering the formation of a  $\delta$  complex was claimed, Scheme 2.6.[2]

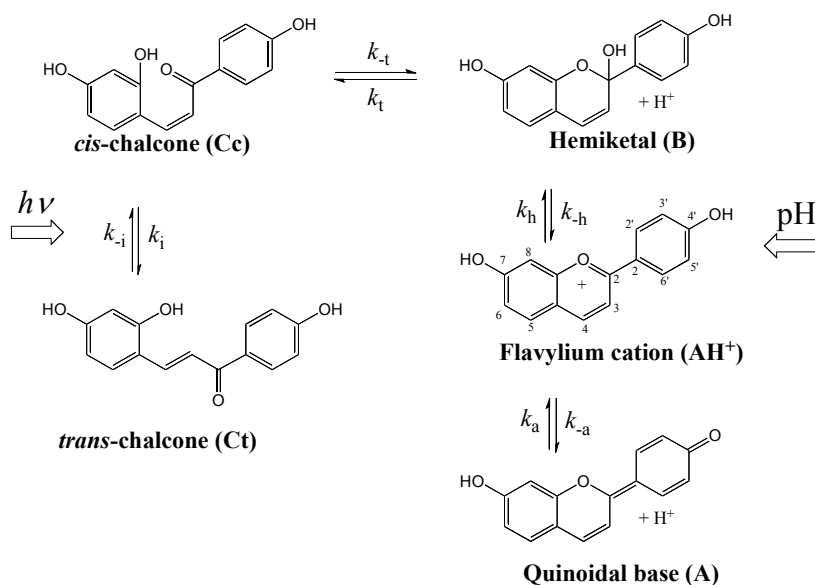


Scheme 2.6

### 2.1 The Flavylium network of chemical reactions. A new photochromic system.

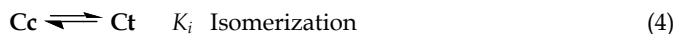
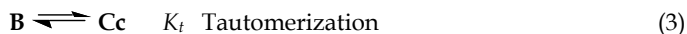
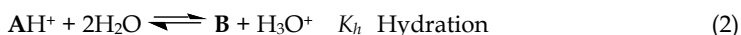
During the last decade the photochromism of flavylium derivatives has been the object of some attention.[5] This family of compounds comprises anthocyanins, the ubiquitous colorants of flowers and fruits. In spite of the fact that anthocyanins by themselves do not show significant photochromism, many synthetic[5] and also natural[6] flavylium derivatives exhibit a versatile photochemistry.

The photochromic behaviour of synthetic flavylium compounds, more properly the one of the *trans*-chalcone species, only recently was perceived as a new photochromic system with many potentialities.[7] In spite of its apparent complexity is a simple sequence of three well known elementary steps: i) photo induced isomerisation ii) cyclization and iii) dehydration to give the coloured product, the flavylium cation, (or the very coloured quinoidal base, depending on pH), Scheme 2.7.

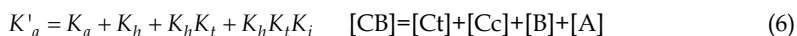
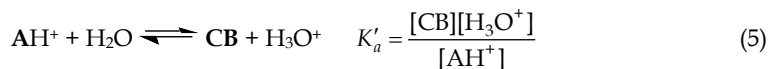


Scheme 2.7

The network of flavylum compounds in water (acid to moderately acid) is easily accounted for by eq.(1) to eq.(4)[8,9]



Equations (1) to (4) can be substituted by a single acid-base equilibrium



The mole fraction distribution of the different species is calculated as follows:

$$\chi_{\text{AH}^+} = \frac{[\text{H}^+]}{[\text{H}^+] + K'_a}; \chi_{\text{A}} = \frac{K_a}{[\text{H}^+] + K'_a}; \chi_{\text{B}} = \frac{K_h}{[\text{H}^+] + K'_a}; \chi_{\text{Cc}} = \frac{K_h K_t}{[\text{H}^+] + K'_a}; \chi_{\text{Ct}} = \frac{K_h K_t K_i}{[\text{H}^+] + K'_a} \quad (7)$$

In practical terms, it is now well established a routine procedure based on pH dependent UV-visible spectroscopy, NMR spectroscopy and stopped flow measurements that permits the calculation of the kinetic and equilibrium constants of the flavylum network.[9,10] Using these constants, the mole fraction distribution of the several species at the equilibrium

can be calculated, see Figure 2.1 a) for 7,4'-dihydroxyflavylium: flavylium is the dominant species at very low pH values and the respective "bases" CB, at moderately acid to neutral, their relative amounts being dependent on the nature and position of the substituents. A convenient way to represent the flavylium network is the use of an energy level diagram where the Gibbs free energy,  $\Delta G^\circ$ , of the different equilibria is represented at different pH values, Figure 2.1 b).[11]

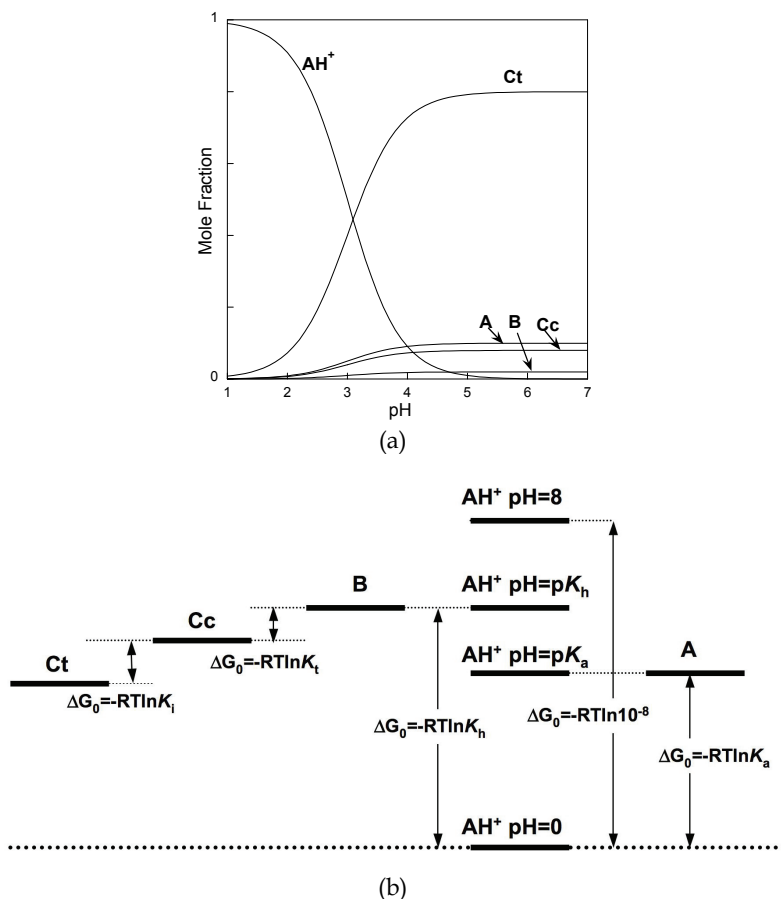
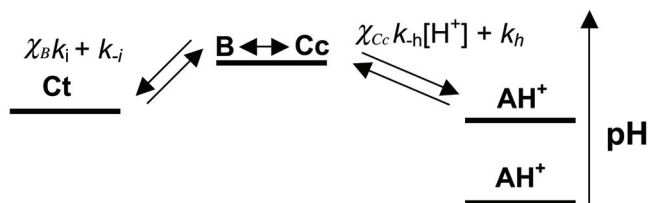


Fig. 2.1. a) Mole fraction distribution of the compound 7,4'-dihydroxyflavylium: b) Energy level diagram of the species involved in a flavylium network.

The photochemical performance and in particular the presence or absence of a thermal *cis-trans* isomerisation barrier as well as the flavylium (and base) colour, is dramatically dependent on the nature and position of the substituents, making the system particularly versatile. For example, hydroxyl substituents at position 4' of the flavylium backbone lead to a network exhibiting the barrier, while at position 7 its absence is favoured.[12] In the case of the flavylium network lacking of the *cis-trans* isomerisation barrier, the appearance of the colour upon irradiation of the Ct, is a balance between the back reaction that restores Ct

from **Cc**, and the sequence of reactions, cyclization and dehydration, leading to **AH<sup>+</sup>**. Due to the fact that usually the isomerisation (timescale of seconds to hours) and the dehydration (timescale of seconds to minutes) are slower than cyclization (subseconds) the network of reactions can be approximately described as in Scheme 2.8, the meaning of the symbols being reported above.



Scheme 2.8

The system is equivalent to two competitive parallel reactions with the particularity that one of them is dependent on pH. The best pH value to observe the colour contrast is thus the result of two opposite effects that follow immediately the irradiation: by one hand higher proton concentration favours the appearance of the flavylum cation, by the other hand the proton concentration should not be excessive otherwise flavylum cation is the most stable specie (colour exists prior to the irradiation). Once the coloured species are formed, flavylum or quinoidal base, the system reverts completely back to the equilibrium according to eq.(8).[7] In other words, the bleaching of **Ct** due to the irradiation is recovered in two steps: i) faster one from **Cc** in competition with the hydration that leads to the coloured species, ii) slower one from the coloured species via hydration followed by ring opening and isomerisation, eq.(8).

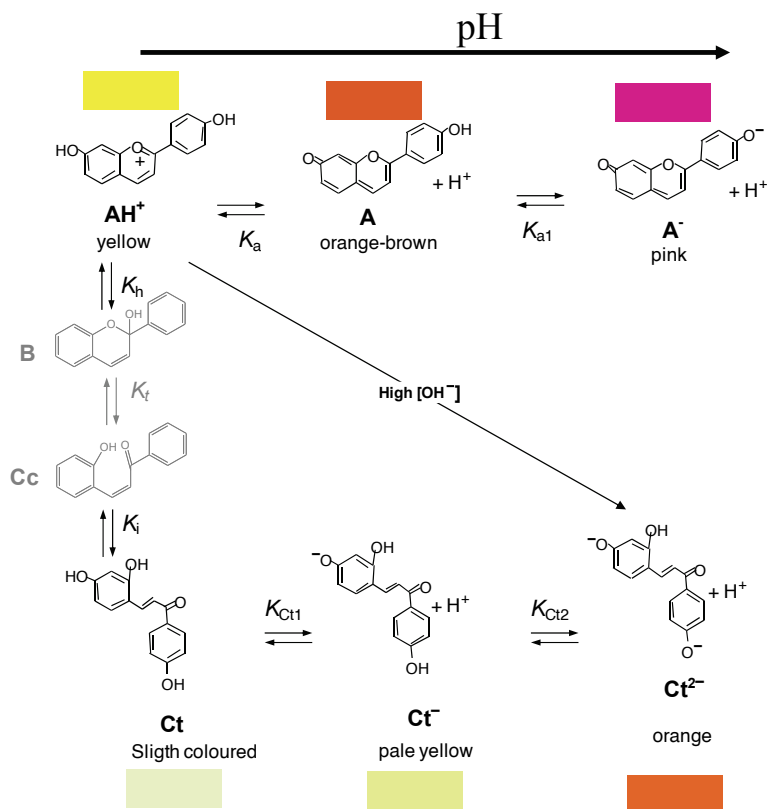
$$k_{obs} = \left( \frac{\frac{[H^+]}{[H^+] + K_a} K_i K_t K_i + [H^+]}{\frac{K_i K_i}{k_{-h}} + \frac{[H^+]}{k_{-i}}} \right) \quad (8)$$

A limiting situation occurs at sufficiently high pH values: **Cc** (in equilibrium with **B**) is formed upon irradiation, but reverts completely back to **Ct** in a few seconds and no coloured species are formed.

The network of chemical reactions can be extended to the basic medium. One example of a complete flavylum network (in water) lacking of the thermal barrier is the compound 7,4'-dihydroxyflavylum, presented in Scheme 2.9 and used above as a probe for biphasic systems water/IL.[13]

At pH=1 the yellow flavylum, **AH<sup>+</sup>**, is the dominant species and the solution is yellow. When the pH is raised, (direct pH jump) the orange quinoidal base, **A**, is immediately formed around pH=4-6 and the pink ionized base, **A<sup>-</sup>**, at higher pH values. However these are transient species: when **A** is formed disappears in several minutes (depends on pH) to give the most stable species and only slightly coloured *trans*-chalcone, **Ct**; when **A<sup>-</sup>** is formed reverts to the ionized chalcones **Ct<sup>-</sup>** or **Ct<sup>2-</sup>**, depending on pH with a rate which is also dependent on pH. At pH>12 the **A<sup>-</sup>** is transformed in **Ct<sup>2-</sup>** in a few minutes. If now the stable **Ct<sup>2-</sup>** at pH=12 suffers a pH jump to acidic (reverse pH jump), the protonated chalcones are

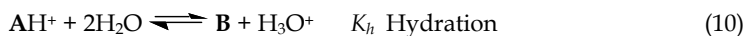
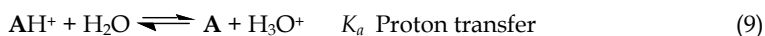
immediately formed, because proton transfer is the fastest reaction occurring in the network. The chalcones are the equilibrium species up to pH *circa* 4.[14] If the final pH of the reverse pH jump is lower than 4 (pH= 1 for example), Ct is immediately formed but after some minutes gives the yellow flavylum,  $AH^+$ , the stable species at this pH value.

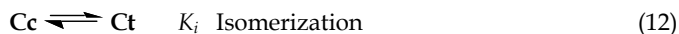
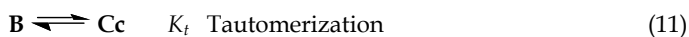


Scheme 2.9

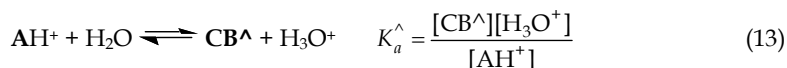
Irradiation of **Ct** (pH=4 for example) photo-induces the isomerisation as shown in Scheme 2.8. In spite of the competition between the direct recovery of **Ct** from **Cc**, part of **Cc** leads the photoproducts  $AH^+$  (**A**) which are thus accumulate under irradiation. The photostationary state is reached when the thermal rate of  $AH^+$  (**A**) disappearance equals the rate of its photochemical production.

In the case of flavylum networks possessing a high *cis-trans* isomerisation barrier, as 4'-methoxyflavylum[9] no significant back reaction takes place immediately after the irradiation (**Ct** recovered from **Cc**) and a pseudo-equilibrium can be assumed. The pseudo-equilibrium is mathematically treated by means of the following expressions:





Equations (9) to (12) can be substituted by a single acid-base equilibrium



$$K_a^{\wedge} = K_a + K_h + K_h K_t \quad [CB^+] = [Cc] + [B] + [A] \quad (14)$$

The mole fraction distribution of the different species can be written as follows:

$$\chi_{AH^+}^{\wedge} = \frac{[H^+]}{[H^+] + K_a^{\wedge}}; \chi_A^{\wedge} = \frac{K_a}{[H^+] + K_a^{\wedge}}; \chi_B^{\wedge} = \frac{K_h}{[H^+] + K_a^{\wedge}}; \chi_{Cc}^{\wedge} = \frac{K_h K_t}{[H^+] + K_a^{\wedge}} \quad (15)$$

In order to select the best pH value to obtain the great colour contrast, it is very convenient to represent the mole fraction distribution of the equilibrium together with the one of the pseudo-equilibrium, the distribution reached if complete photo-conversion of Ct takes place, Figure 2.2.

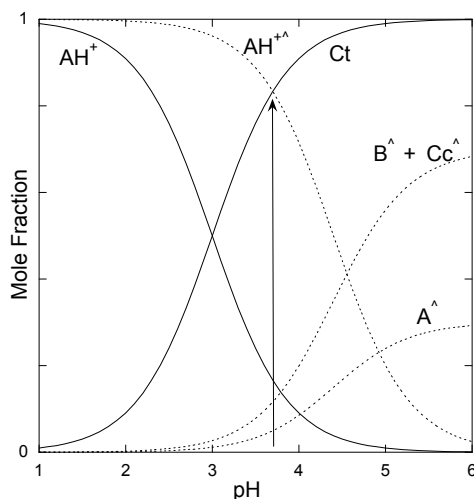
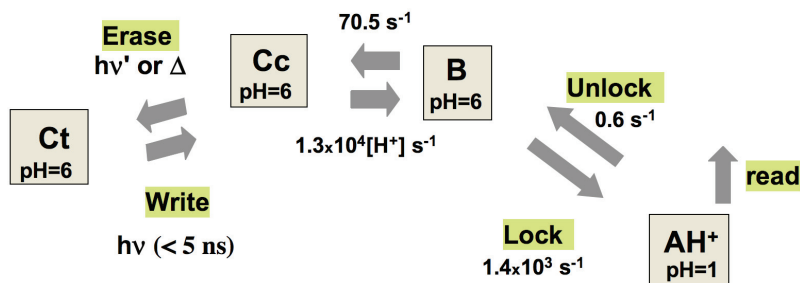


Fig. 2.2 Mole fraction distribution of the equilibrium (full line) and pseudo-equilibrium (traced line) of a flavylum network.

In this case the pH should not be too high because the fraction of flavylum cation after the irradiation (that corresponds to the one of the pseudo-equilibrium) becomes lower. Conversely, it can not be too low otherwise the flavylum is the dominant species before irradiation. In some cases the mole fraction of the base at the pseudo-equilibrium is high enough to see colour, and profit can be taken from irradiation at higher pH values.

In the case of flavylum systems possessing the *cis-trans* isomerization barrier, they are special useful to illustrate the concept of optical memory, Scheme 2.10.[15]





Scheme 2.10

The write step consists on the formation of Cc in equilibrium with B. This photochemical reaction is not interesting for the scope of an optical model memory by two essential motives: i) the colour contrast is small, ii) using an optical detection of the signal, irradiation of Cc produces Ct, a common effect in *cis-trans* systems. The present system allows the introduction of a lock step, by acidifying the solution. When this is done, B (and Cc through B) is spontaneously converted into AH<sup>+</sup>, see also the thermodynamic Scheme in Figure 2.1. AH<sup>+</sup> is stable at low pH and the information (its colour) can be read without being erased. To erase the system, it is necessary to add base that converts the flavylum cation into Cc and B and heat the solution or use light. One drawback of this system is the need of adding acid and base. Some attempts to use light to change the pH of the solution without adding mass have been undertaken.[16]

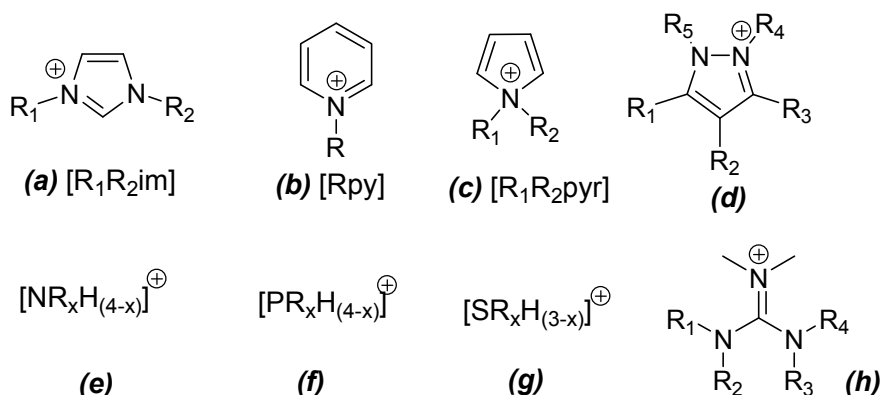
### 3. Properties of ionic liquids

Ionic Liquids (ILs) can be defined as organic salts with a melting point below than 100°C.[17]

This class of compounds have received much attention mainly due their peculiar physico-chemical properties[18] such as high chemical and thermal stability, negligible vapour pressure, high ionic conductivity and a large electrochemical window.

Generally, ILs mainly comprise bulk organic cations with low symmetry based on (a) 1,3-dialkylimidazolium[19], (b) N-alkylpyridinium[20], (c) N,N-dialkylpyrrolidinium[21], (d) N,N-dialkylpyrazolium[22], N,N-dialkyltriazolium[23], (e) tetra-alkylammonium[24], (f) tetra-alkylphosphonium[25], (g) trialkylsulphonium[26] and (h) tetra-alkyldimethylguanidinium[27] structures, among others. All of these organic cations have been combined with several inorganic or organic anions such as halides (e.g. chloride, bromide, iodide), hexafluorophosphate, tetrafluoroborate, hexafluoroantimonate, dicyanamide, triflate, bistrifluoromethanesulfonylimide, tiocyanate, trifluoroacetate, among others.

Some of the cations that have been used in order to prepare ILs are described in scheme 3.1. All organic salts that have a melting point lower than ambient temperature are called as room temperature ionic liquids (RTILs). Wilkes et al.[28] firstly reported a RTIL based on the 1-alkyl-3-methylimidazolium cation in 1982. Then, many other ILs containing a variety of cations and anions of different sizes have been synthesized to provide specific characteristics.



Scheme 3.1.

Depending on the anion and type of organic cation, the ILs can solubilise organic compounds (e.g. carbonyl compounds, alcohols, alkyl halides) as well as inorganic or organometallic complexes and polymeric materials.[29] Furthermore, they can have low miscibility with dialkyl ethers, alkanes, water and can be insoluble in supercritical  $CO_2$  ( $scCO_2$ ). Particularly relevant the behaviour of ILs in the presence of  $scCO_2$  which is soluble into ILs, but the different types of ILs are insoluble in  $scCO_2$ . This peculiar solubility property can be useful for specific applications related with separation and extraction processes.

In this context the ILs can be called as “designer solvents”[30] because their physical properties (such as melting point, viscosity, density and hydrophobicity) can be modified according to the nature of the desired application by modification of their cations and anions. The range of available anion and cation combinations could provide up to  $10^{18}$  different ILs.

Applications of ILs include their use as solvents or co-catalysts in many catalytic and non-catalytic synthetic methodologies and separations, polymerizations processes such as extraction with organic solvent and  $scCO_2$ , pervaporation, and as supporting membranes. More recent, ILs have found useful application in solar cells, batteries, sensors, lubricants, and dissolution of bio- and nanomaterials. Novel ILs based on a specific organic cation and/or anion for several potential applications have been also described. Particularly relevant are the examples of chiral ionic liquids (using natural or synthesized chiral units) for asymmetric catalytic transformations, enantioselective resolution or separation processes; pharmaceutical ionic liquids (called API-ILs incorporating an active principle ingredient as cation or anion); magnetic ionic liquids (based on  $FeCl_4$  anions) for efficient separation processes and others ionic liquids as intrinsically functional materials (for example luminescent, photochemical or electrochemical ILs).

Attending the recent applications of ILs, one of the most relevant parameters is related with the purity of ILs. Several studies have been reported about the significant impact of impurities such as halogen or water content, in some values of density, viscosity and conductivity of ILs. For similar ILs is possible to find discrepancies in terms of these physico-chemical properties. Also, the electrochemical and thermal stability and solubility parameters can be completely changed according with the final purity of ILs.

Nowadays, the possibility to develop alternative synthetic and purification methodologies in order to improve the final purity of ILs is one of the most important issues for further technological and industrial applications.

## 4. Photochromic compounds dissolved in ionic liquids

Ionic liquids due to their peculiar properties are very appealing as solvent to study photochromic molecules. Two main objectives can be achieved in these studies: the influence of ionic liquids in the performance of the photochromic compounds and the information about the properties of the ILs themselves. The ionic liquid can influence the photo-induced step that gives the photoproduct or the thermal back reaction.

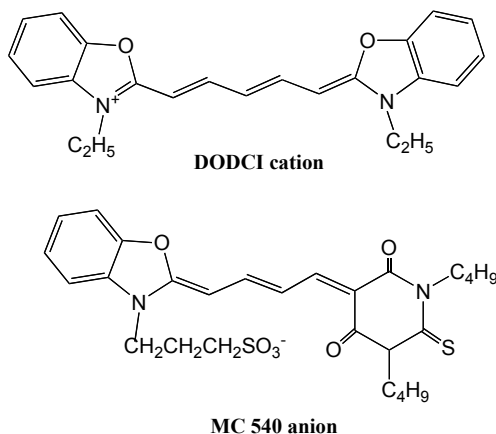
### 4.1 Monophasic systems

#### 4.1.1 Photoinduced process

The photoisomerization of *trans*-stilbene, Scheme 2.3, was investigated in the ionic liquid 1-butyl-3-methylimidazolium hexafluorophosphate, [BMIM][PF<sub>6</sub>].[31] Steady state irradiation followed by UV absorption confirms that formation of the *cis*-isomer takes place in the ionic liquid, in spite of its very high viscosity. Moreover, from the lifetime of the fluorescence decay of *trans*-stilbene in [BMIM][PF<sub>6</sub>], 138 ps, the isomerisation rate constant,  $k_{\text{iso}} = 6.6 \times 10^9 \text{ s}^{-1}$ , was calculated. This value lays in the same order of magnitude of the isomerisation rate constants found for stilbene in alcohols and is more or less in agreement with the expected polarity of [BMIM][PF<sub>6</sub>], obtained through the  $E_{\text{T}}(30)$  value (which is also close to those of the alcohols). However, when the isomerisation rate constant in alcohols is extrapolated to the viscosity of [BMIM][PF<sub>6</sub>], 312 cP at 303 K,[32] a much lower value,  $k_{\text{iso}} = 9.7 \times 10^8 \text{ s}^{-1}$ , is predicted. Viscosity cannot be the controlling parameter for the isomerisation of this molecule at least in [BMIM][PF<sub>6</sub>]. This was interpreted as an evidence of the intriguing nature of ionic liquids and the problems that arise in the conventional framework of polarity and viscosity parameters.[31]

An opposite behaviour regarding the effect of the viscosity was reported by Sarkar and co-workers[33] on the study of the photoisomerization of 3,3'-diethyloxadicarbocyanine iodide (DODCI) in [BMIM][PF<sub>6</sub>], Scheme 4.1. They found that photoisomerization of DODCI in the ionic liquid is 36 times slower when compared with the isopolar conventional solvent (methanol) and also slower than in water. The results were interpreted as a consequence of the high viscosity of the ionic liquid that inhibits the twisting motion about the conjugated double bonds of DODCI.

The photoisomerization of DODCI and another cyanine derivative, MC 540, Scheme 4.1, was investigated in the IL [BMIM][PF<sub>6</sub>] and aqueous glycerol (90% wt glycerol:3% wt water).[34] In the case of DODCI, it was observed that the non-radiative rate constant, which represents the rates of photoisomerization, are almost identical in the ionic liquid and aqueous glycerol at a given temperature, confirming that the viscosity governs the photoisomerization of this compound. In contrast, the photoisomerization rate constant of MC 540 is higher by a factor of 2 in aqueous glycerol when compared to the IL. The stabilization of the twisted state (due to the zwitterionic character of MC 540) by the solute-solvent hydrogen bonding interactions in aqueous glycerol explains the lowering of the isomerisation barrier and the consequent increasing of the isomerisation rate.



Scheme 4.1

### 4.1.2 The thermal back reaction

#### 4.1.2.1 Spiropyran

Nitrobenzospiropyran and its derivatives are up to now the photochromic system most studied in ILs, see Table 1. These compounds have been widely reported in molecular solvents and it is well established that the back thermal reaction decreases with increasing the polarity of the solvent. This is due to the zwitterionic character of merocyanine, stabilized in polar solvents, differently from the closed form, stabilized in non-polar solvents.

The photo and solvatochromic properties of nitrobenzopyran was studied in ILs: i) containing the same bistrifluoromethanesulfonylimide  $[\text{NTf}_2]^-$  anion and several cations, entries 10 to 15 in Table 1, set A in Scheme 4.2,[35] ii) possessing the same phosphonium  $[\text{P}_{6,6,6,14}]$  and  $[\text{P}_{1,4,4,4}]$  cations and different anions, entries 16 to 20 in Table 1, set B in Scheme 4.2[36] and iii) having the same anion  $[\text{NTf}_2]^-$  and 1-alkyl-3-methylimidazolium  $[\text{C}_n\text{MIM}]$  cation, with different chains,[37] entries 21 to 26, Table 1, set C in Scheme 4.2. Similarly to the behaviour in molecular solvents, irradiation of BSP- $\text{NO}_2$  in these ILs leads to the merocyanine (MC). In a few cases the merocyanine is more stable and negative photochromism is observed, *i.e.*, formation of the spiropyran from the merocyanine. The rates of the thermal recovery are dependent on the IL cation and anion. No linear relation seems to occur between the logarithm of the rate constants and the polarity parameter  $E_T(30)$ , as observed in molecular solvents,[38] see Figure 4.1. In general, the rate constant in ILs is lower than the one in molecular solvents of the same  $E_T(30)$  polarity: from  $2.1 \times 10^{-4} \text{ s}^{-1}$  for  $[\text{EMIM}][\text{NTf}_2]$ [35] to  $2.5 \times 10^{-3} \text{ s}^{-1}$  for  $[\text{P}_{6,6,6,14}][\text{DCA}]$ ,[36] that compare with polar solvents like ethanol and acetonitrile, but not with non-polar solvents like *n*-hexane  $47.4 \times 10^{-3} \text{ s}^{-1}$ . [39]

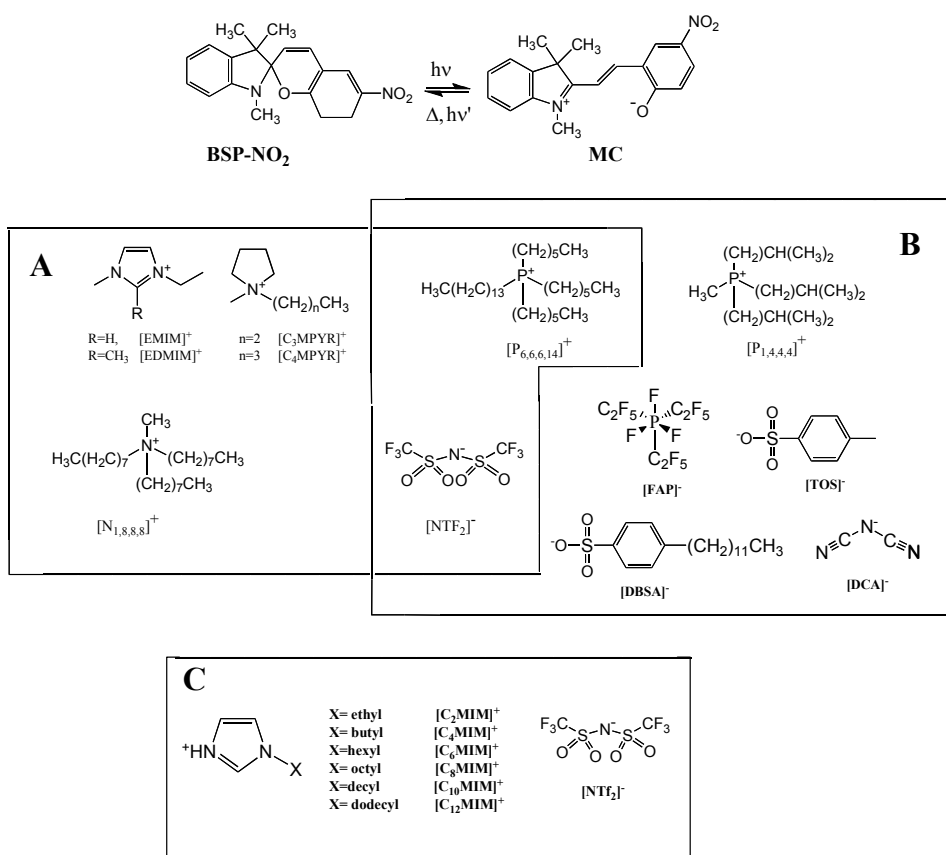
	Solvent	$K_e$ ( $\times 10^2$ )	$K_{\text{recovery}}(\text{s}^{-1})$	$E_T(30)$ (Kcal mol <sup>-1</sup> )	$E_a$ (kJmol <sup>-1</sup> )	$\Pi^*$	$\alpha$	$\beta$
1	Acetonitrile	3.85	8.4 $\times 10^{-4}$ a) 8.8 $\times 10^{-4}$ b)* 2.92 $\times 10^{-3}$ d) 4.61 $\times 10^{-3}$ p) (31°C)	45.5 <sup>a)</sup> 45.6 <sup>i)</sup> 46.4 <sup>e)</sup>	102.4 <sup>d)</sup>	0.79 <sup>e)</sup>	0.42 <sup>e)</sup> 0.35 <sup>g)</sup>	0.37 <sup>e)</sup>
2	Ethanol	4.57 <sup>a)</sup>	1.91 $\times 10^{-4}$ a) 0.612 $\times 10^{-3}$ d) 0.5 $\times 10^{-3}$ k) 1.59 $\times 10^{-3}$ p) (31°C)	51.8 <sup>a)</sup> 51.9 <sup>f)</sup> 52.1 <sup>e)</sup>	102.2 <sup>d)</sup> 102.01 <sup>k)</sup>	0.63 <sup>e)</sup> 0.54 <sup>h)</sup>	0.90 <sup>e)</sup> 0.83 <sup>h)</sup>	0.72 <sup>e)</sup> 0.77 <sup>h)</sup>
3	Methanol			55.4 <sup>e)f)</sup>		0.71 <sup>e)</sup> 0.73 <sup>h)</sup>	1.06 <sup>e)</sup> 1.05 <sup>h)</sup>	0.62 <sup>e)</sup> 0.61 <sup>h)</sup>
4	Dichloromethane	0.51 <sup>a)</sup>	7.0 $\times 10^{-3}$ a)	40.6 <sup>a)</sup> 40.7 <sup>i)</sup>				
5	Hexane		47.7 $\times 10^{-3}$ m)		76.4 <sup>d)</sup>			
6	Benzene		66.2 $\times 10^{-3}$ m)		70.6 <sup>d)</sup>			
7	1,4-Dioxane		56.6 $\times 10^{-3}$ m)		77.4 <sup>d)</sup>			
8	Acetone		7.28 $\times 10^{-3}$ d) 5.3 $\times 10^{-3}$ k) 1.07 $\times 10^{-3}$ p) (31°C)	42.5 <sup>e)</sup>	101 <sup>d)</sup> 104.5 <sup>k)</sup>	0.67 <sup>e)</sup> 0.70 <sup>h)</sup>	0.25 <sup>e)</sup> 0.20 <sup>h)</sup>	0.57 <sup>e)</sup> 0.54 <sup>h)</sup>
9	DMF		1.55 $\times 10^{-3}$ m)		96.2 <sup>d)</sup>			
10	[C <sub>3</sub> MPYR][NTf <sub>2</sub> ] <sup>b)</sup>	4.16 <sup>b)</sup>	6.90 $\times 10^{-4}$ b)*	48.9 <sup>b)</sup>				
11	[C <sub>4</sub> MPYR][NTf <sub>2</sub> ] <sup>b)</sup>	3.85 <sup>b)</sup>	7.80 $\times 10^{-4}$ b)*	48.1 <sup>b)</sup> 48.3 <sup>l)</sup>				
12	[P <sub>6,6,6,14</sub> ][NTf <sub>2</sub> ] <sup>b), e)</sup>	1.15 <sup>b)</sup>	8.50 $\times 10^{-4}$ b)*	47.97 <sup>b)</sup> 46.1 <sup>e)</sup>		0.83 <sup>e)</sup>	0.37 <sup>e)</sup>	0.27 <sup>e)</sup>
13	[EMIM][NTf <sub>2</sub> ] <sup>b)</sup>	4.57 <sup>b)</sup>	2.10 $\times 10^{-4}$ b)*	53.3 <sup>b)</sup> 53.1 <sup>i)</sup>				
14	[EDMIM][NTf <sub>2</sub> ] <sup>b)</sup>	3.24 <sup>b)</sup>	3.90 $\times 10^{-4}$ b)*	51.79 <sup>b)</sup>				
15	[N <sub>1,8,8,8</sub> ][NTf <sub>2</sub> ] <sup>b), e)</sup>	4.16 <sup>b)</sup>	4.00 $\times 10^{-4}$ b)*	49.13 <sup>b)</sup> 45.9 <sup>e)</sup>		0.87 <sup>e)</sup>	0.33 <sup>e)</sup>	0.23 <sup>e)</sup>
16	[P <sub>6,6,6,14</sub> ][DSBA] <sup>a)</sup>	1.45 <sup>a)</sup>	8.12 $\times 10^{-4}$ a)	46.6 <sup>a)</sup>	88 <sup>a)</sup>			
17	[P <sub>6,6,6,14</sub> ][DCA] <sup>a)</sup>	0.57 <sup>a)</sup>	25.03 $\times 10^{-4}$ a)	46.1 <sup>a)</sup>	75 <sup>a)</sup>			
18	[P <sub>6,6,6,14</sub> ][NTf <sub>2</sub> ] <sup>a)</sup>	1.16 <sup>a)</sup>	6.5 $\times 10^{-4}$ a)	47.9 <sup>a)</sup> (47.97)	90 <sup>a)</sup>			
19	[P <sub>1,4,4,4</sub> ][TOS] <sup>a)</sup>	1.74 <sup>a)</sup>	5.19 $\times 10^{-4}$ a)	48.2 <sup>a)</sup>	71 <sup>a)</sup>			
20	[P <sub>6,6,6,14</sub> ][FAP] <sup>a)</sup>	1.16 <sup>a)</sup>	7.31 $\times 10^{-4}$ a)	48 <sup>a)</sup>	76 <sup>a)</sup>			

	Solvent	$K_e$ ( $\times 10^2$ )	$K_{\text{recovery}}(\text{s}^{-1})$	$E_T(30)$ (Kcal mol <sup>-1</sup> )	$E_a$ (kJmol <sup>-1</sup> )	$\Pi^*$	$\alpha$	$\beta$
21	[C <sub>2</sub> MIM] [NTf <sub>2</sub> ] <sup>j,k</sup>	0.866 <sup>k</sup>	1.2 $\times 10^{-3}$ <sup>k</sup>	52.6 <sup>k,i</sup>	106.69 <sup>k</sup>			
22	[C <sub>4</sub> MIM] [NTf <sub>2</sub> ] <sup>j</sup>	0.702 <sup>k</sup>	1.0 $\times 10^{-3}$ <sup>j</sup>	52.4 <sup>j</sup> 51.6 <sup>i</sup>	96.93 <sup>j,k</sup>			
23	[C <sub>6</sub> MIM] [NTf <sub>2</sub> ] <sup>j</sup>	0.116 <sup>k</sup>	1.0 $\times 10^{-3}$ <sup>j</sup>	53.3 <sup>j</sup> 51.9 <sup>i</sup>	98.84 <sup>j,k</sup>			
24	[C <sub>8</sub> MIM] [NTf <sub>2</sub> ] <sup>j</sup>	0.53 <sup>k</sup>	1.7 $\times 10^{-3}$ <sup>j</sup>	51.2 <sup>j</sup> 51.1 <sup>i</sup>	103.34 <sub>j,k</sub>			
25	[C <sub>10</sub> MIM] [NTf <sub>2</sub> ] <sup>j</sup>	0.794 <sup>k</sup>	1.8 $\times 10^{-3}$ <sup>j</sup>	51.6 <sup>j</sup> 51.0 <sup>i</sup>	106.68 <sub>j,k</sub>			
26	[C <sub>12</sub> MIM] [NTf <sub>2</sub> ] <sup>j</sup>	0.763 <sup>k</sup>	2.0 $\times 10^{-3}$ <sup>j</sup>	51.2 <sup>j</sup>	105.27 <sub>j,k</sub>			
27	[BMIM][BF <sub>4</sub> ] <sup>c,d</sup>	4.62 <sup>d</sup>	0.396 $\times 10^{-3}$ <sup>d</sup>	52.4 <sup>l</sup>	73.8 <sup>d</sup>	1.05 <sup>c</sup>	0.63 <sup>c</sup>	0.38 <sup>c</sup>
28	[BMIM][PF <sub>6</sub> ] <sup>c,d</sup>	1.88 <sup>d</sup>	0.792 $\times 10^{-3}$ <sup>d</sup>	51.1 <sup>l</sup>	70.6 <sup>d</sup>	1.03 <sup>c</sup>	0.63 <sup>c</sup>	0.21 <sup>c</sup>
29	[BMIM][TfO] <sup>c</sup>			51.1 <sup>l</sup>		1.00 <sup>c</sup>	0.62 <sup>c</sup>	0.46 <sup>c</sup>
30	[BMMIM][BF <sub>4</sub> ] <sup>d</sup>	1.48 <sup>d</sup>	0.107 $\times 10^{-3}$ <sup>d</sup>	49.4 <sup>d</sup>	90.9 <sup>d</sup>			
31	[EMIM][BF <sub>4</sub> ] <sup>d</sup>	3.76 <sup>d</sup>	0.232 $\times 10^{-3}$ <sup>d</sup>		70.9 <sup>d</sup>			
32	[EMIM][DCA] <sup>d</sup>	6.78 <sup>d</sup>	0.382 $\times 10^{-3}$ <sup>d</sup>		96.1 <sup>d</sup>			
33	[HOEMIM][PF <sub>6</sub> ] <sup>d</sup>	15.24 <sup>d</sup> <sup>#</sup>	0.0237 $\times 10^{-3}$ <sup>d</sup>		97.0 <sup>d</sup>			
34	[HOEMIM][NO <sub>3</sub> ] <sup>d</sup>	4.69 <sup>d</sup>	0.407 $\times 10^{-3}$ <sup>d</sup>	61.7 <sup>d</sup>	-			
35	[BMMIM][DCA] <sup>d</sup>	4.23 <sup>d</sup>	0.404 $\times 10^{-3}$ <sup>d</sup>		81.5 <sup>d</sup>			
36	[EMIM][CH <sub>3</sub> SO <sub>3</sub> ] <sup>d</sup>	3.64 <sup>d</sup>	0.336 $\times 10^{-3}$ <sup>d</sup>		75.9 <sup>d</sup>			
37	[BMIM][NO <sub>3</sub> ] <sup>d</sup>	2.64 <sup>d</sup>	0.498 $\times 10^{-3}$ <sup>d</sup>		88.5 <sup>d</sup>			

\*In the original paper these values are 100 times greater, but this should be an error in their table. See values for the solvents. # negative photochromism

References indicated on Table 1: a) R. Byrne, S. Coleman, K. J. Fraser, A. Raduta, D. R. McFarlane, D. Diamond, *Phys. Chem. Chem. Phys.*, **2009**, 11, 7286-7291. b) R. Byrne, K. J. Fraser, E. Izgorodina, D. R. MacFarlane, M. Forsyth D. Diamond, *Phys. Chem. Chem. Phys.*, **2008**, 10, 5919-5924. c) Y. Wu, T. Sakaki, K. Kazusi, T. Seo, K. Sakurai, *J. Phys. Chem. B*, **2008**, 112, 7530-7536. d) S. Zhang, Q. Zhang, B. Ye, X. Li, X. Zhang, Y. Deng, *J. Phys. Chem. B*, **2009**, 113, 6012-6019. e) S. Coleman, R. Byrne, S. Minkovska, D. Diamond, *Phys. Chem. Chem. Phys.*, **2009**, 11, 5608-5614. f) K. Iwata, M. Kabita, H. Hamaguchi, *J. Chem. Phys. B*, 2007, 111, 4914-4919. g) Book "Photochromism: Molecules and systems", Ed. by H. Dürr, H. Bouas-Laurent, Elsevier B. V., 2003. h) A. K. Burrell, R. E. D. Sesto, S. N. Backer, T. M. McCleskey, G. A. Backer, *Green Chemistry*, **2007**, 9, 449-454. i) C. Reichardt, *Green Chemistry*, **2005**, 7, 339-351; *Chem. Rev.* **1994**, 94, 2319-2358. j) S. Coleman, R. Byrne, N. Alhshimy, K. J. Fraser, D. R. MacFarlane, D. Diamond, *Phys. Chem. Chem. Phys.*, **2010**, 12, 7009-7017. k) S. Coleman, R. Byrne, S. Minkovska, D. Diamond, *J. Phys. Chem. B*, **2009**, 113, 15589-15596. l) L. Crowhurst, P. R. Mawdsley, J. M. Perez-Arlandis, P. A. Salter, T. Welton, *Phys. Chem. Chem. Phys.*, **2003**, 5, 2790-2794. m) Y. Sueishi, M. Ohcho, N. Nishimura, *Bull. Chem. Soc. Jpn.* **1985**, 58, 2608-2613. n) J. Figueras, *J. Am. Chem. Soc.*, **1971**, 93, 3255-3263. o) R. Byrne, S. Coleman, S. Gallagher, D. diamond, *Phys. Chem. Chem. Phys.*, **2010**, 12, 1895-1904. p) X. Song, J. Zhou, Y. Li, Y. Tang, *J. Photochem. Photobiology A*, **1955**, 92, 99-103.

Table 1. Photochromism and polarity parameters for nitrospiropyran



Scheme 4.2

A similar system regarding the photochromism of nitrospiropyran derivatives in a series of ionic liquids was independently reported, Scheme 4.3.[40] The overall solvent polarity was characterized by the Reichardt's dye E<sub>T</sub>(30), as well as by 4-nitroaniline and *N,N'*-diethyl-4-nitroaniline for the Kamlet-Taft parameters ( $\alpha$ - hydrogen bond donor,  $\beta$ - hydrogen bond acceptor, and  $\pi^*$ -dipolarity/polarizability). The ionic liquids were divided into 3 categories: **A** (strong hydrogen bond basicity),  $\alpha < 0.9 < \beta$ ; **B** (moderate hydrogen bond acidity and basicity),  $\alpha$  and  $\beta < 0.9$ ; **C** (strong hydrogen bond acidity),  $\beta < 0.9 < \alpha$ . In group **A** only the spiropyran forms are observed at the (dark) equilibrium and no evident change of colour takes place upon irradiation (no *trans* merocyanine was detected) possibly due to the stabilization of the *cis*-isomers of the merocyanine by the ionic liquid.[41] Solutions of the spiropyran in ionic liquids of group **B** show a small fraction of merocyanine at the (dark) equilibrium, which is increased upon irradiation at 365 nm (positive photochromism). In solvents of group **C**, the *trans*-merocyanine is formed at the (dark) equilibrium and irradiation leads to the formation of the spiropyran form at the expenses of the *trans*-merocyanine. The system reverts back to the equilibrium in the dark (negative photochromism).

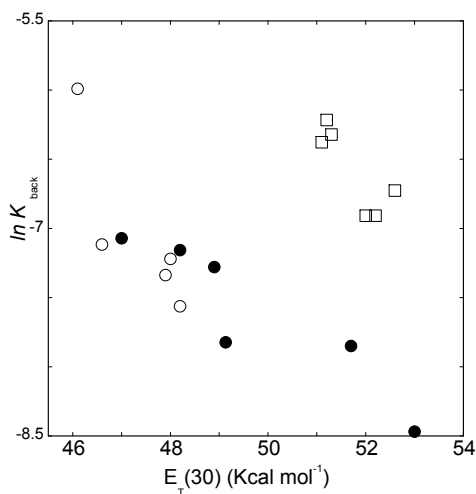
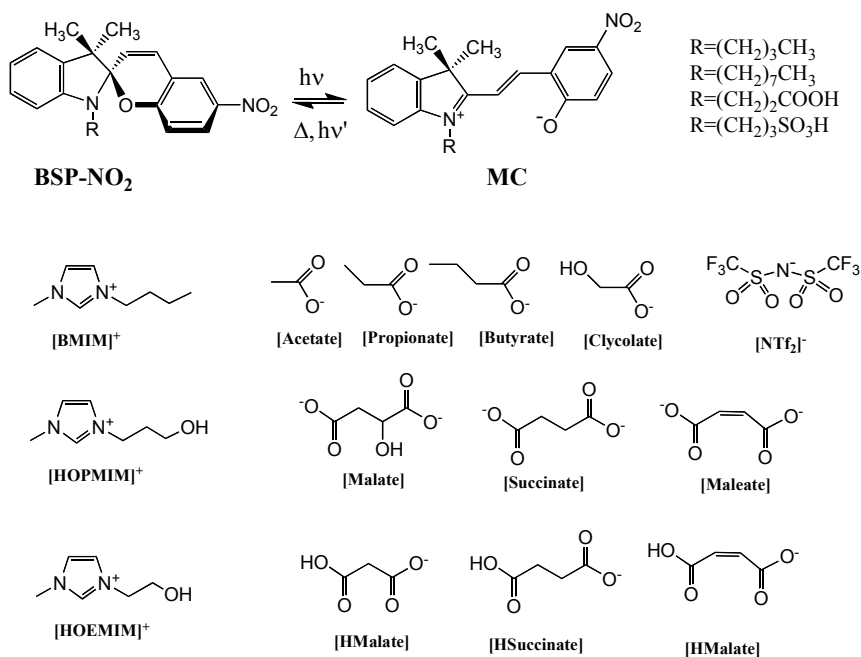


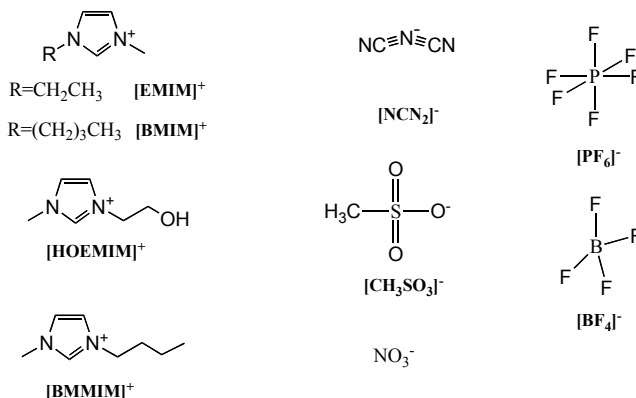
Fig. 4.1. Comparison of the logarithm of the rate constants of the back thermal reaction of the nitrobenzospirropyran: in the ionic liquids based on the  $[\text{NTf}_2]$  anion (black circles), set A in Scheme 4.2; [35] in ionic liquids based on  $[\text{P}_{6,6,6,14}]$ ,  $[\text{P}_{1,4,4,4}]$  [36] cations (open circles) set B in Scheme 4.2, and same anion  $[\text{NTf}_2]$  together with 1-alkyl-3-methylimidazolium  $[\text{C}_n\text{MIM}]$  cation, with different chains [37] (open squares) set C in Scheme 4.2.



Scheme 4.3

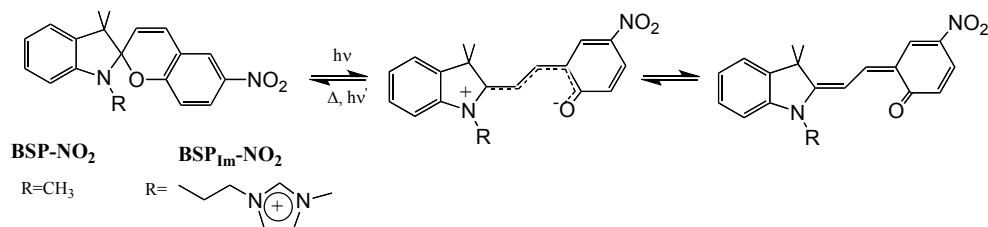


The BSP-NO<sub>2</sub> was studied in some ILs reported in Scheme 4.4, entries 27 to 37 in Table 1.[42] The authors obtained an excellent linear correlation between the logarithm of the thermal reversion as a function of the parameter  $E_{sp}$  defined as  $28591/\lambda_{max}(nm)$  where  $\lambda_{max}$  represents the maximum absorption of the merocyanin form. Moreover, a direct proportionality between the activation energy for the thermal reversion as a function of the activation entropy ( $\Delta S^*$ ) was observed.



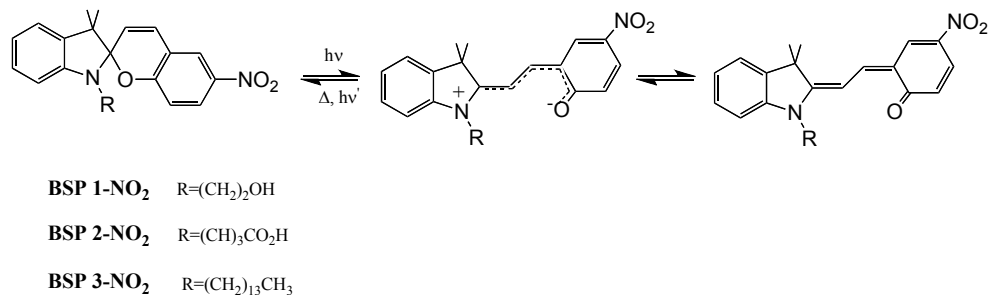
Scheme 4.4

Diamond and co-workers extended their previous work by attaching an imidazolium cation to the spiropyran, Scheme 4.5.[43] The new compound BSP<sub>im</sub>-NO<sub>2</sub> was studied in several ILs based on derivatives of the benzimidazolium cation and [NTf<sub>2</sub>]<sup>-</sup> anion, set C in Scheme 4.2. The rate of thermal recovery of BSP<sub>im</sub>-NO<sub>2</sub> was found to be 14 times faster than the reference compound BSP-NO<sub>2</sub> in [C<sub>6</sub>MIM][NTf<sub>2</sub>]. In addition, the BSP<sub>im</sub>-NO<sub>2</sub> equilibrium is shifted towards the closed form. The authors considered that the IL forms nano-structured domains of polar and non-polar nature. The side group of BSP<sub>im</sub>-NO<sub>2</sub> would interact with the polar domain, while the photoswitchable part of the molecule would be accommodate in the non-polar domain. The compound would be unable to move to more polar regions capable of stabilizing the open form. In contrast, unbound BSP is relatively free to migrate from one domain to the other.



Scheme 4.5

The same system was further investigated using three nitrobenzopyrans BSP 1-NO<sub>2</sub>, R=(CH<sub>2</sub>)<sub>2</sub>OH; BSP 2-NO<sub>2</sub>, R=(CH<sub>2</sub>)<sub>3</sub>CO<sub>2</sub>H and BSP 3-NO<sub>2</sub>, R=(CH<sub>2</sub>)<sub>13</sub>CH<sub>3</sub>, Scheme 4.6, based on the ILs from set B, Scheme 4.2.[44]



Scheme 4.6

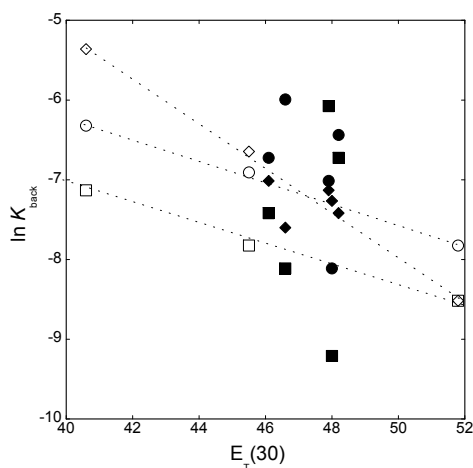
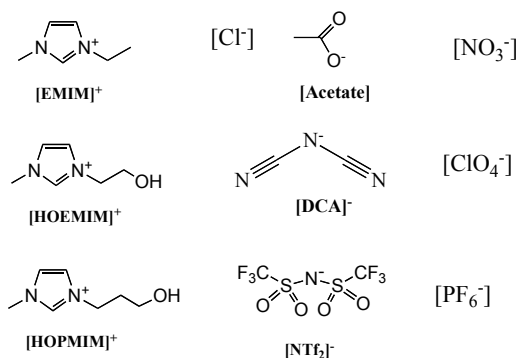


Fig. 4.2. Representation of the logarithm of the rate constants for BSP 1-NO<sub>2</sub> (●), BSP 1-NO<sub>2</sub> (■), BSP 1-NO<sub>2</sub> (◆) in the ILs from set B, Scheme 4.2. The same for the solvents ethanol, acetonitrile and dichloromethane (equivalent open symbols)[44]

Clearly the  $E_T(30)$  still gives a linear relation with the logarithm of the rate constant in molecular solvents, but fails of significance in ILs.

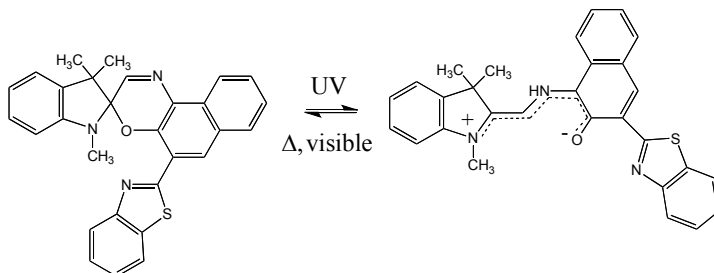
Hydroxyl ILs were compared with non-hydroxyl analogs, Scheme 4.7.[45] The  $E_T(30)$  parameter is lower (51.6-52.4) Kcal.mol<sup>-1</sup> for non-hydroxyl than for hydroxyl ILs (55.5-62.0) Kcal mol<sup>-1</sup>. Positive photochromism takes place only for the lower  $E_T(30)$  values (< 56.2), while negative photochromism occurs for higher  $E_T(30)$  values (>60.1); ILs based on [HOEMIM]<sup>+</sup> and the anions [PF<sub>6</sub>]<sup>-</sup>, [NTf<sub>2</sub>]<sup>-</sup> and [ClO<sub>4</sub>]<sup>-</sup>. This is in accordance with a stabilization of the merocyanine form in polar solvents. No linear correlation was obtained for the back thermal reaction with the  $E_T(30)$  value.



Scheme 4.7

## 4.1.2.2-Spirooxazines

Spirooxazine Scheme 4.8 was also studied in the presence of the ILs, Set C, Scheme 4.2.[37] The effect of the increasing of the side chain length of ILs based on imidazolium cations of different lengths and  $[\text{NTf}_2]^-$  was found to have only minor effects on the rate of the thermal recovery of the merocyanine form in spirooxazines as well as in nitrobenzospiropyran.



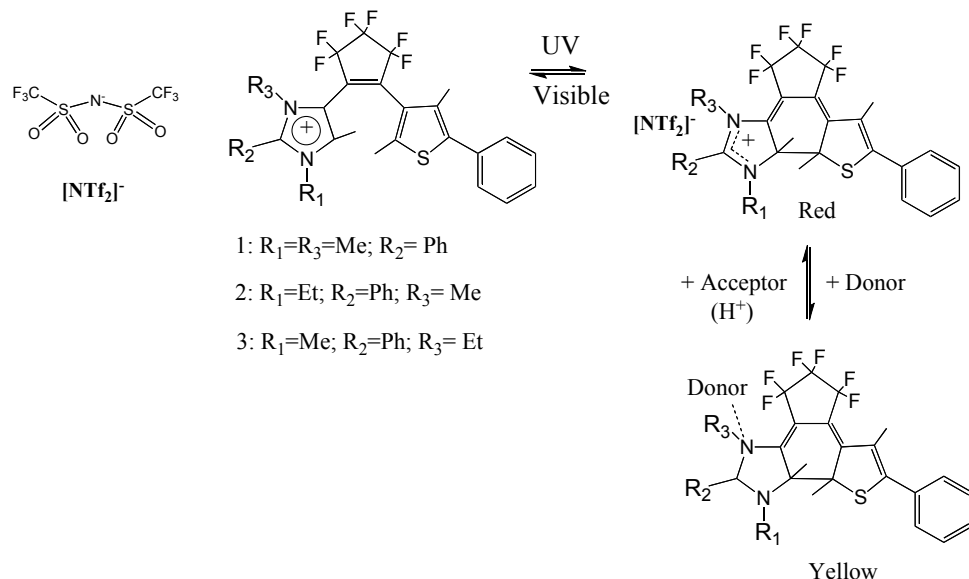
Scheme 4.8

The thermal reversion of spirooxazine, Scheme 4.7 was also studied in the ILs of set A in Scheme 4.2.[46] The recovery is slower in ionic liquids than in molecular solvents with similar polarity, indicating a greater degree of interaction between ILs and  $\text{MC}_{(\text{SO})}$ , lifetime of 90.9 s in  $[\text{P}_{6,6,6,1}][\text{NTf}_2]$  that compares with 19.6 s in acetonitrile. The thermal back reaction  $\text{MC}_{(\text{SO})}$  to BSP is more dependent on the temperature in polar protic ILs like  $[\text{BMIM}]^+$  than in aprotic ILs as  $[\text{P}_{6,6,6,14}]^+$ .

## 4.1.2.3-Diarylethenes

Cationic diarylethenes were synthesized by appending an imidazolium directly connected to the central ethane unit as an aryl group in order to participate in the photochromic hexatriene-cyclohexadiene reaction, Scheme 4.9.[47] At least one of these compounds (1-open form) is described in the experimental part as being an oil, and probably is an intrinsically photochromic ionic liquid, see below.[48] The solvatochromic behaviour of 1 was studied in two ionic liquids,  $[\text{EMIM}][\text{NTf}_2]$  and  $[\text{EMIM}][\text{EtSO}_4]$ , as well as in some common solvents. The closed ring form shows different absorption spectra depending on the anion of the IL. The red form is stabilized in  $[\text{EMIM}][\text{EtSO}_4]$  while the yellow form in

[EMIM][NTf<sub>2</sub>]. The changes in colour were attributed to the different donor-acceptor properties of the solvents.



Scheme 4.9

#### 4.1.3 Photochromism in magnetic ionic liquids.

The photochromism of azobenzene, Scheme 2.3, was investigated in a greenish paste of equimolar quantities of the magnetic IL constituted by [BMIM][Fe<sup>III</sup>Cl<sub>4</sub>] and the photochromic compound.[49] Before irradiation, the mixture showed a paramagnetic linear response similar to the pure IL. Irradiation of the system gives rise to an increase of the magnetic moment tending asymptotically to a limit. The photochromic system is reversible, but the magnetic transformation is irreversible. This irreversibility was explained by the formation of aggregates of the iron chloride complex.

#### 4.2 Biphasic systems

Some ILs are not miscible with water giving rise to biphasic systems, as for example [BMIM][PF<sub>6</sub>] and water. The question is how the existence of these two phases can influence the photochromism. The flavylum photochromic system is very adequate to carry out these kind of studies due to the existence of a network of species exhibiting different properties, in particular colour, and reversibly reached through pH, light and thermal inputs and the possibility of switching from one phase to another.

##### 4.2.1 Flavylium compound with cis-trans isomerisation thermal barrier

A simple example of this behaviour is the biphasic system involving 4'-hydroxyflavylium in water/[BMIM][PF<sub>6</sub>],[50] Figure 4.3. Similarly to Scheme 2.9, in acidic water solutions of 4'-hydroxyflavylium, it is possible to distinguish the usual species, flavylium cation (AH<sup>+</sup>),

quinoidal neutral base (**A**), hemiketal (**B**), *cis*-chalcone (**Cc**), and *trans*-chalcone (**Ct**). In basic water, ionised *cis* and *trans*-chalcones (**Cc<sup>2-</sup>**, **Ct<sup>2-</sup>** and **Ct<sup>2-</sup>**), obtained by deprotonation of phenolic hydroxyl groups, can be observed in the equilibrium or as transient species. The thermal barrier between the *cis*-chalcone and *trans*-chalcone in water was calculated, 129 kJ mol<sup>-1</sup>. One interesting feature of this system in water is the transformation of the flavylum cation, **AH<sup>+</sup>** (pH=1) into **Cc<sup>2-</sup>** upon a pH jump to pH=12, for example. The ionized *cis*-chalcone takes more or less 1 day to be transformed into the thermodynamic product, **Ct<sup>2-</sup>**. In other words, the *cis-trans* isomerisation thermal barrier is also observed for the di-ionized chalcones. A faster conversion takes place if the solution is irradiated. This is in contrast with the analogous 7'4'-dihydroxyflavylium behaviour where the appearance of **Ct<sup>2-</sup>** from **AH<sup>+</sup>** at the same pH takes only a few minutes. The practical result is the possibility of isolating in the aqueous solution the species **Cc<sup>2-</sup>**, see Figure 4.3.

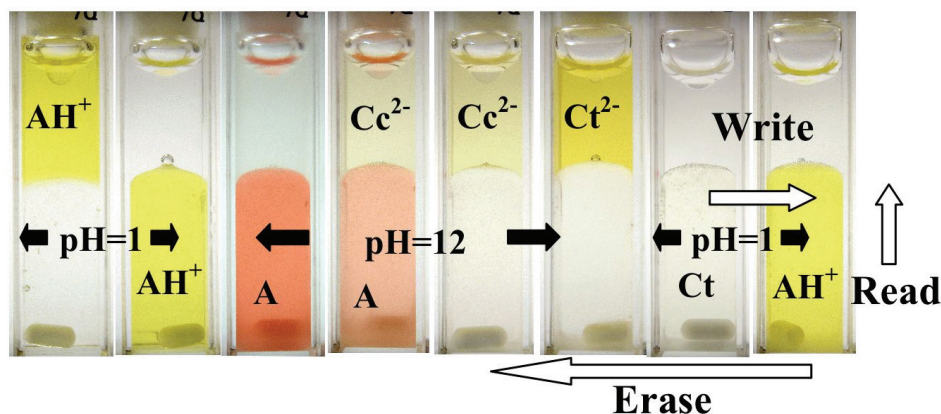


Fig. 4.3 - See from left side: a - [BMIM][PF<sub>6</sub>] (bottom phase) and 4'-hydroxyflavylium perchlorate in 0.01 M HCl (upper phase); b - after strong shaking of both solutions; c - after alkalisation of the aqueous phase (pH≈12) with minimum shaking; d - after medium shaking; e - after strong shaking; f - after several minutes at room temperature or upon irradiation of the aqueous phase; g - after reacidification of the aqueous phase (pH≈1) and strong shaking; h - after irradiation of the ionic liquid phase.

When an aqueous solution of the compound 4'-hydroxyflavylium perchlorate, at pH=1.0, is added to a similar volume of the ionic liquid, the diffusion to the IL is slow and the photo in Fig. 4.3a can be obtained. However, after *ca.* 1 minute of vigorous shaking, the bottom IL solution becomes yellow, indicating that the **AH<sup>+</sup>** species was transferred to the IL phase Fig. 4.3b. Figs. 4.3c – 4.3f show four stages obtained upon a pH jump from 1 to 12 carried out in the aqueous phase. A few seconds shaking makes basic the IL phase and by consequence the orange base, **A**, is formed. The base, **A**, is transformed in to the ionized **Cc<sup>2-</sup>**, that is more stable in the water phase and goes up. In Figure 4.3e this species is already almost completely transferred into the water phase. As mentioned, **Cc<sup>2-</sup>** gives **Ct<sup>2-</sup>** slowly, but the respective conversion can be accelerated by light or heating. The final equilibrium in this step is obtained with the **Ct<sup>2-</sup>** species completely dissolved into the aqueous phase, Fig. 4.3f. A further step of the cycle consists into a pH jump in the aqueous phase, back to pH=1.0,

followed by vigorous shaking of the two phases. This procedure allows the **Ct** species formed in the aqueous phase to be completely transferred into the IL, Fig. 4.3g. At this pH value, **AH**<sup>+</sup> is the thermodynamic species at the equilibrium (in water and in IL), but due to the isomerisation barrier the **Ct** species in the IL is relatively stable, with a lifetime of 9.7 days at room temperature, in the dark. This value compares with the shorter lifetime of 0.3 days in aqueous solutions obtained under similar conditions.[51] The much lower back reaction to reach the equilibrium in ILs is in agreement with behaviour observed in section 3.3.2. The flash photolysis of the compound in the IL is similar to water, with two processes taking place after the light pulse: the first one corresponds to the bleaching of the solution at 340 nm occurring during the lifetime of the flash, Fig. 4.4b, assigned to the *trans-cis* isomerisation that is faster than *circa* 5 ns (the limit of flash photolysis apparatus); the second one is the formation of **AH**<sup>+</sup> from **Cc**, with  $k_{\text{obs}}=0.2 \text{ s}^{-1}$ , clearly shown by the increasing absorption at 440 nm, Fig. 4.4a. In aqueous solution, at pH 1 flavylum is formed from the meta-stable state in  $7.6 \text{ s}^{-1}$ . In the ionic liquid, the equivalent process occurs with a rate constant of  $0.2 \text{ s}^{-1}$ , Fig. 4.4a. The lowering of the rate constant in the IL could be due to its peculiar structure or reflect the expected lower proton concentration in the ionic liquid phase.

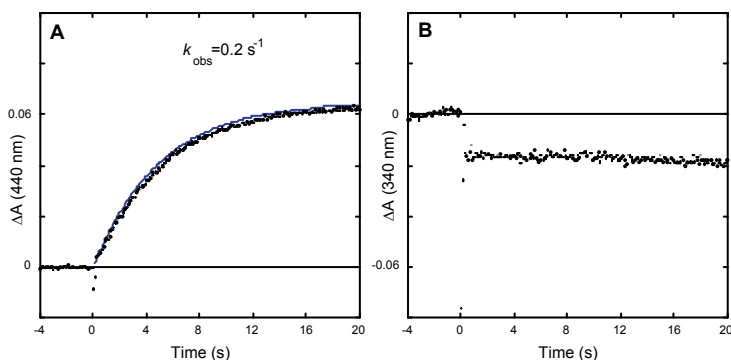


Fig. 4.4 - Flash photolysis of the **Ct** species in [BMIM][PF<sub>6</sub>], in contact with an aqueous solution at pH=1: A) kinetics of **AH**<sup>+</sup> formation; B) kinetics of **Ct** disappearance.

The system allows to concept a write-read-erase cycle as shown in Figure 4.3: i) the *write* step consists on the irradiation of the **Ct** species dissolved in the ionic liquid, with formation of flavylum cation, **AH**<sup>+</sup>, ii) the information thus obtained can be *read* at a wavelength where the **AH**<sup>+</sup> (or **A**) absorbs but the **Ct** species does not, *e. g.* 440 nm, iii) to *erase* the system and prepare it for a new cycle, a sequence of operations should be carried out: pH jump to 12 and vigorous shaking in order to extract the compound from the ionic liquid to water in its **Ct**<sup>2-</sup> form, followed by a second pH jump back to 1.0 and vigorous shaking in order to dissolve the **Ct** species in the ionic liquid, see Scheme 3.

#### 4.2.2 Flavylum compound lacking of the *cis-trans* isomerisation thermal barrier

In the case of the compound 7'4'-dihydroxyflavylum in the same biphasic system water/[BMIM][PF<sub>6</sub>] the situation is similar but due to the existence of one more hydroxyl substituent an ionized quinoidal base, **A**<sup>-</sup>, can be formed, and in water no *cis-trans* isomerisation barrier exists.[13]

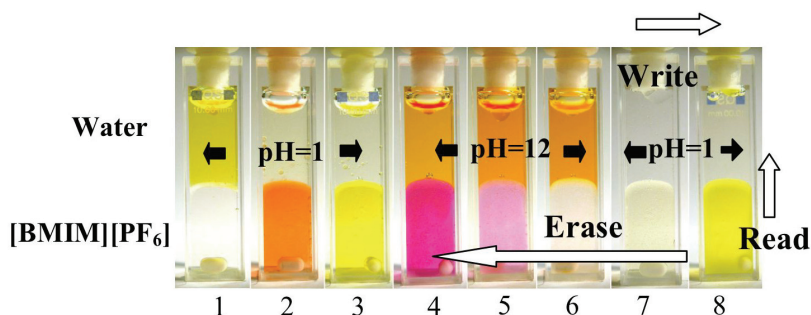
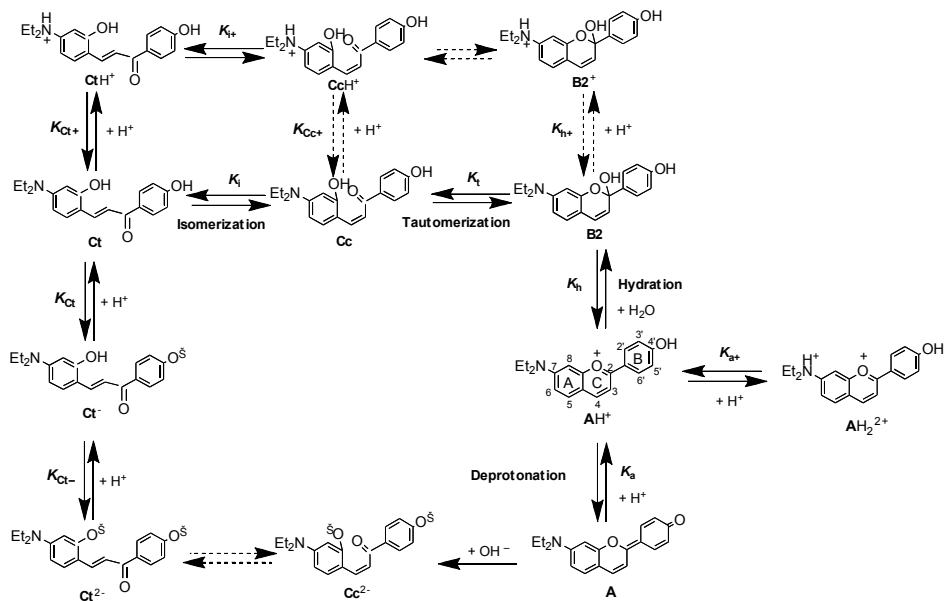


Fig. 4.5. A cycle involving the compound 7'-dihydroxyflavylium<sup>[13]</sup>

The solution of the flavylium compound was dissolved in water at pH=1.0 (flavylium cation) and poured in a cell previously filled with the ionic liquid (1). The diffusion of the flavylium compound from the water to the ionic liquid is very slow and shows two bands (like a chromatographic separation) the front band being orange (quinoidal base) and the back band yellow flavylium cation (not shown). This effect can also be observed if the mixture is shaken only a few seconds (2) or vigorously shaken for 1-2 minutes (3) before allow separation of the two phases. Assuming the polar and non-polar nano-domains of the ionic liquid, these results seem to indicate that diffusion to the non-polar domain is faster than diffusion to the polar domain, probably because in this last there is a competition with water. Apart the existence of the A<sup>-</sup> species, this system is similar to the previous one and a cycle to write-read-erase can also be performed. This is possible because contrary to water the Ct form is metastable in the IL phase (after 1 hour at 40 °C less than 2% of flavylium cation was formed).



Scheme 4.10

A beautiful palette of colours is achieved when amine substituents are introduced in the flavylium backbone. In the case of the compound *trans*-4-(*N,N*-diethylamino)-2,4'-dihydroxychalcone, the network is once more similar to the previous compounds, Scheme 4.10.[52]

The presence of the amine not only permits to achieve red and blue colours but also introduces some peculiarities to the system, due to the possibility of the amine protonation. It is worth noting the formation of the species  $CtH^+$  that is spontaneously transformed into  $AH^+$ , in a time scale of minutes, depending on pH. For this compound, as for those bearing amines substituents in general, there is no significant *cis-trans* isomerization barrier and no photochromic activity was detected in water[53]

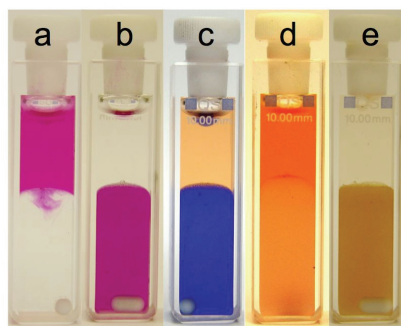


Fig. 4.6 Behaviour of 7-(*N,N*-diethylamino)-4'-hydroxyflavylium tetrafluoroborate in biphasic systems constituted by aqueous solution (upper phase) and 1-*n*-butyl-3-methylimidazolium hexafluorophosphate, [bmim][PF<sub>6</sub>] (lower phase), upon pH jumps in the aqueous phase. a) pH=1.0 in the aqueous phase,  $AH^+$  species, before shaking; b) after shaking,  $AH^+$  completely transfers to the ionic liquid; c) upon addition of base and shaking for two minutes; d) upon 10 minutes (shaking); e) upon addition of acid and shaking.

Fig. 4.6 presents a sequence of photos showing how 7-(*N,N*-diethylamino)-4'-hydroxyflavylium is partitioned in the biphasic system constituted by water and [BMIM][PF<sub>6</sub>]. Aqueous solutions of 7-(*N,N*-diethylamino)-4'-hydroxyflavylium at pH=1.0 contain exclusively the flavylium cation,  $AH^+$ , that only very slowly diffuses to the ionic liquid phase, remaining at the upper aqueous phase, Fig. 4.6a. When the system is vigorously shaken and the two phases allowed to separate, the flavylium cation completely dissolves into the ionic liquid phase, Fig. 4.6b. The upper aqueous phase can be made basic by addition of NaOH (or by substitution of the acidic phase by a basic solution), followed by vigorous shaking of the mixture. When the two phases are separated, it is possible to see a blue colour in the ionic liquid phase due to the base, **A**, Fig. 4.6c. The blue colour is not stable and leads to chalcones or ionized chalcones with a rate and protonation stage that are pH dependent. An interesting feature is that at moderately basic pH values of the aqueous solution, it is possible to have the yellow chalcone completely dissolved in the ionic liquid phase (not shown in Fig. 4.6). On the other hand, high hydroxyl concentrations favour the formation of orange  $Ct^{2-}$  that is transferred to the aqueous phase, Fig. 4.6d. Acidification of this last solution followed by immediate shaking of the two phases, leads to dissolution of  $Ct/CtH^+$  into the ionic liquid, Fig. 4.6e. The thermal stability of this species in the ionic liquid



depends on the amount of proton added. High proton concentrations lead to spontaneous formation of  $AH^+$ , (because  $Ct^+$  is formed) while at lower proton concentrations the  $Ct$  species is the thermodynamic product. In conclusion, as in the previous examples neutral and mono-charged species will reside preferentially into ionic liquid, while double charged species prefer water. The most interesting feature of this system is however its photochemistry in the IL phase, in contrast with its absence in water. When the ionic liquid phase containing  $Ct$  at pH=6.8 (measured in the upper aqueous phase) is irradiated, the photochemical product  $AH^+$  appears. The system reverts back to  $Ct$  after ca. 11 hours in the dark, at 22 °C, Fig. 4.7.

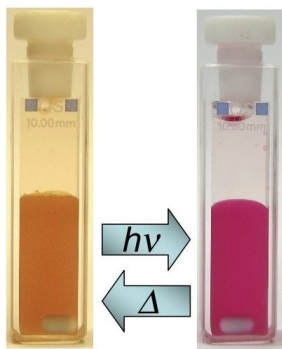


Fig. 4.7 Photochromic system of 7-(*N,N*-diethylamino)-4'-hydroxyflavylium in the IL phase of water/ionic liquid [BMIM][PF<sub>6</sub>] biphasic systems.

Flash photolysis was carried out in the  $Ct$  species on the bottom phase and the transient absorptions at 450 nm (where  $Ct$  absorbs) and at 510 nm (where  $AH^+$  absorption spectrum peaks) were monitored. A depletion of  $Ct$  is immediately observed, while  $AH^+$  appears in a concomitant way. Both flash photolysis traces follow a first order kinetics at pH values between 5 and 8.5, the range where  $Ct$  is found on the ionic liquid phase (see Fig. 4.8). The recovery is very extensive but not complete, and in fact a small but significant offset is observed, which increases with decreasing pH. The rate constant is pH independent within the pH range of  $Ct$ , and is equal to 0.58 s<sup>-1</sup>.

The appearance of an offset explains why net photochemistry is observed in the IL, in spite of an efficient back reaction, Fig. 4.7. The chalcone should be preferentially solvated by the [BMIM] organic cation rather than water. As  $Cc$  is formed by photoisomerization of  $Ct$ , it is either readily converted back to  $Ct$  (the back isomerization reaction) or to  $B2$  and  $AH^+$ . Afterwards,  $AH^+$  in the ionic liquid can be preferentially solvated by the anion and probably by the water molecules present on the water-saturated ionic liquid phase. Therefore, the photochemical production of net  $AH^+$  in water/ionic liquids biphasic systems for this chalcone could be explained by the existence of a microheterogeneous structure, where a small fraction of the flavylium cations would be stabilized by hydrogen bonding and electrostatic interactions with the anions into the polar domains that contain water.[54]

In conclusion, the IL phase permits the existence of photochromism in chalcones that are not photochromic in water. Moreover, ILs can be used to increase the kinetic barrier for *trans-cis* isomerization of chalcones, allowing the use their respective network as models for optical memories.

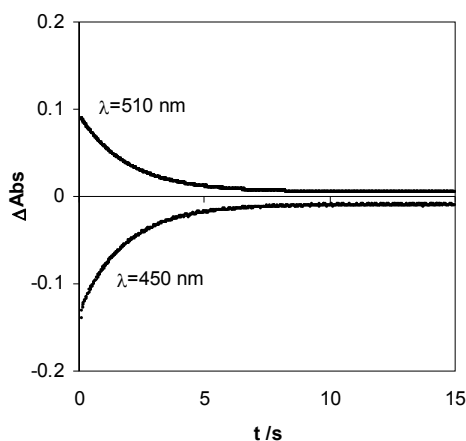
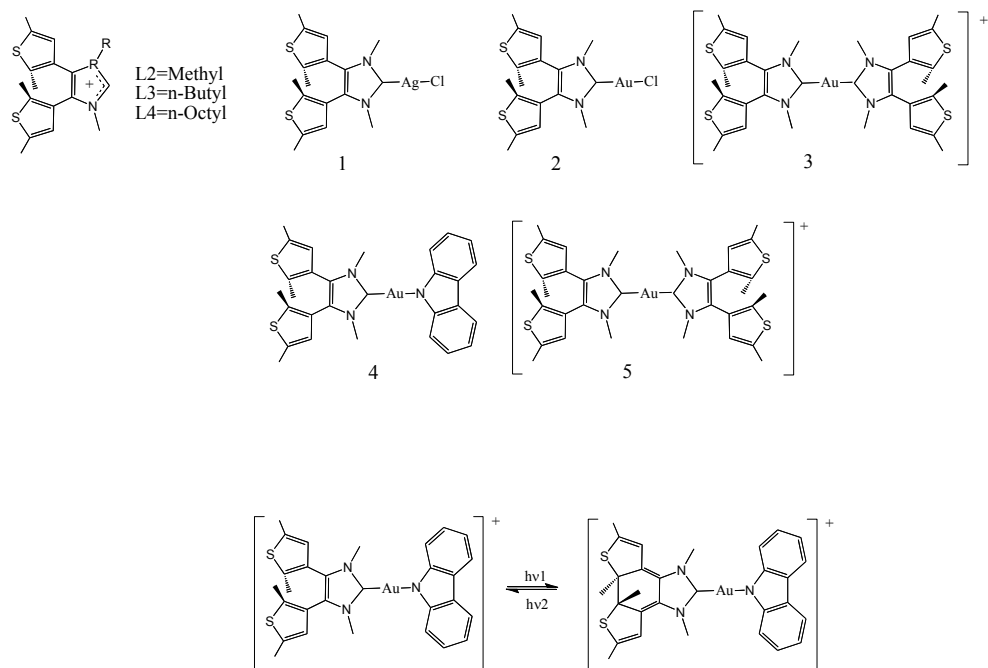


Fig. 4.8 Flash photolysis traces taken in the ionic liquid phase, after shaking with the aqueous phase at pH 6, and waiting *ca.* 30 minutes to obtain a good transparency of the ionic liquid solution.

## 5. Intrinsically photochromic ionic liquids.

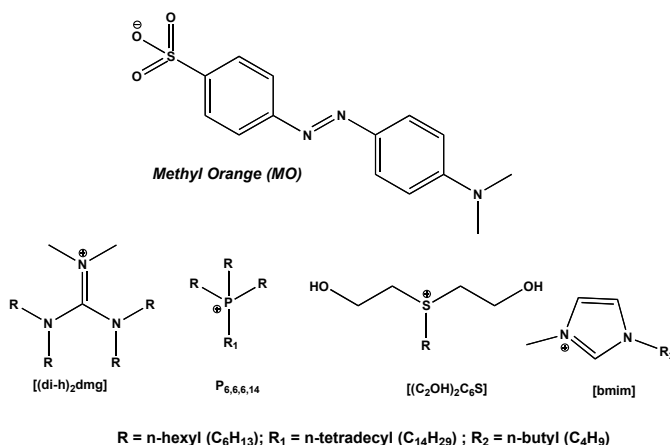
A series of diarylethene containing N-heterocyclic carbenes was reported.[55]



Scheme 5.1.

The quantum yields of photocyclization and cycloreversion as well as the half life of the closed forms of L2-PF<sub>6</sub>, L3-PF<sub>6</sub>, L4-PF<sub>6</sub> 1, 2, 3, 4, Scheme 5.1, were presented in the supplementary material of ref.[55]. The compound [L3][NTf<sub>2</sub>] is the only one presenting the melting point below 100 °C (<20 °C) and thus the only behaving as a RTIL. The authors claim that the RTIL [L3][NTf<sub>2</sub>] is also photochromic but no further experimental data is available in the communication or in the supplementary material.

The first claim of the term intrinsically photochromic IL regards the use of methyl orange and the appropriate organic cations in order to render the assemble liquid, Scheme 5.2.[56] In particular the guanidinium has a low melting point (48 °C) and the sulfonium, phosphonium are RTILs, Table 2.



Scheme 5.2.

The photochromism of these ILs was studied in ethanol, in matrixes of a Polaroid B72 polymer or in tin films obtained by pressing the ionic liquid between two lamellas of quartz. This last experiment allows the study of the ionic liquids without any additional solvent or polymeric matrix. The *trans* form of the methyl orange ILs (the stable one in the dark) was irradiated with a light flash and the kinetics of the back *cis-trans* isomerisation monitored. The results are summarized in Table 2.

Photochromic Salt	Mp (T <sub>g</sub> ) <sup>a)</sup> / °C	<i>k</i> <sub>back</sub> (s <sup>-1</sup> ) 25 °C
Na MO	> 300	0.2 (Ethanol)
[BMIM][MO]	85 (-42)	1.2(Ethanol)/ <sup>b)</sup> / <sup>b)</sup>
[(di-H) <sub>2</sub> DMG][MO]	48(-41)	0.3 (Ethanol)/ <sup>c)</sup> /0.003(PB72)
[(C <sub>2</sub> OH) <sub>2</sub> C <sub>6</sub> S][MO]	RTIL	2 (Ethanol)/0.3 (film)/ 0.1(PB72)
[P <sub>6,6,6,14</sub> ][MO]	RTIL	42.6 (Ethanol) / 2.1 (film)/ <sup>d)</sup>

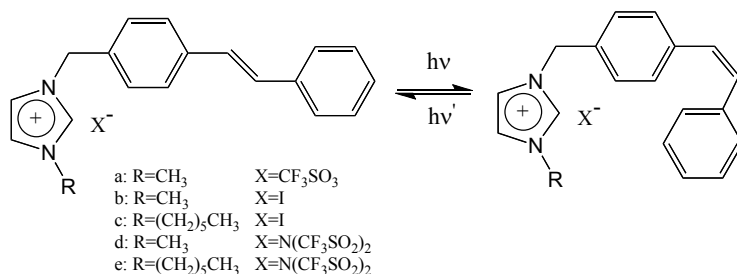
a) Melting point (glass transition); b) Solid at room temperature; c) Films not stable (very hygroscopic);

d) no mixing

Table 2. Ionic liquids form methyl orange[56]

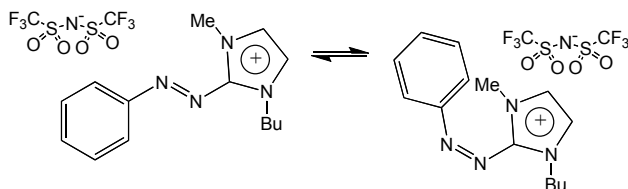
The thermal back reaction in ethanol depends strongly on the cation. Regarding the two RTILs, the slower process corresponds to the sulfonium cation, which is highly viscous and the only one able to form hydrogen bonds with methyl orange. Dissolution of the ILs in the polymer or in the films decreases the absolute rate of isomerisation, but the trend observed in ethanol is the same. The more rigid structure of the polymer is expected to introduce some constraints in the isomerisation process. In the case of the ILs films, the structural organization of the ILs, in particular its higher viscosity also renders the isomerisation slower.

A strategy to obtain photochromic ionic liquids was reported by Arai and co-workers and consists on appending an imidazolium substituent to a stilbene, Scheme 5.3.[57] The *cis* isomers are RTILs except for b) and the *trans* analogs are solids except for d) and e) which while being IL are not RTILs. Moreover, while the *trans* isomers are moderately emissive with quantum yields around 0.02, the *cis* analogs practically do not show fluorescence. This permits the authors to claim the possibility of switching photochemically from solid to liquid as well as from emissive to non-emissive systems.



Scheme 5.3

Another strategy to obtain photochromic ILs is represented in Scheme 5.4,[58] (melting point 50 °C). The photochromism of this compound was studied in organic solvents and ILs. *Trans-cis* isomerisation takes place by irradiation and the system is thermally reversible. The quantum yield of isomerisation decrease only slightly with the increasing viscosity of the solvent, from 0.12 in [BMIM][PF<sub>6</sub>], ( $\eta=241$  cP), to 0.19 in toluene ( $\eta<1$  cP). No solvent dependence was observed for Arrhenius parameters of the thermal back reaction. No information is given about its behaviour as pure solvent.



Scheme 5.4

## 6. References

- [1] C. Bechinger, S. Ferrer, A. Zaban, A. J. Sprague, B. A. Gregg, *Nature*, 1996, 383, 608-610.
- [2] a) J. C. Crano, R. J. Guglielmetti, ed. "Organic Photochromic and Thermochromic Compounds", Plenum, New York, 1999.

- b) H.I Bouas-Laurent, H. Dürr, *Pure Appl. Chem.*, 2001, 73, 639–665.
- [3] a) Y. Hirshberg, *Compt. Rend. Acad. Sci.* 1950, 231, 903; b) E. Fischer, Y. Hirshberg, *J. Chem. Soc.* 1952, 4522-4524; c) Y. Hirshberg, E. Fischer, *J. Chem. Soc.* 1953, 629-636; d) Y. Hirshberg, *J. Am. Chem. Soc.* 1956, 78, 2304-2312.
- [4] K. Uchido, M. Irie; in *"Handbook of Organic Photochemistry and Photobiology"*, Chapter "Photochromism of diarylethene derivatives", Ed. by W.M.Horspool, F. Lenci, CRC Press, Taylor and Francis group, 2003.
- [5] P. Figueiredo, J. C. Lima, H. Santos, M. C. Wigand, R. Brouillard, A. L. Maçanita, F. Pina, *J. Am. Chem. Soc.* 1994, 116, 1249-1254.
- [6] M. J. Melo, M. Sousa, A. J. Parola, J. S de Melo, F. Catarino, J. Marçalo, F. Pina, *Chem. Eur. J.* 2007, 13, 1417-1422.
- [7] M. Maestri, F. Pina, V. Balzani; in *Molecular Switches*, Ed. by B. Feringa, Wiley-VCH, Weinheim, Germany, 2001, Chapter 10, 309-334.
- [8] McClelland, R.A.; McGall, G.H. *J. Org. Chem.* 1982, 47, 3730-3736.
- [9] Pina, F.; Maestri, M.; Balzani, V.; in *Handbook of Photochemistry and Photobiology*, ed. Nalwa, H. S.; ASP, 2003, Vol. 3, Chapter 9, 411- 449.
- [10] A. Roque, C. Lodeiro, F. Pina, M. Maestri, S. Dumas, P. Passaniti, V. Balzani, *J. Am. Chem. Soc.* 2003, 125, 987-994.
- [11] F. Pina, M. J. Melo, R. Ballardini, L. Flamigni, M. Maestri, *New. J. Chem.* 1997, 21, 969-976.
- [12] F. Pina, M. J. Melo, A. J. Parola, M. Maestri, V. Balzani *Chem. Eur. J.* 1998, 4, 2001-2007.
- [13] F. Pina, J. C. Lima, A. J. Parola, C. A. M. Afonso, *Angew. Chem. Int. Ed.* 2004, 43, 1525-1527.
- [14] In some cases as in 7,4'-dihydroxyflavylium Ct (90%) is in equilibrium with A (10%), and the solution is slightly coloured
- [15] F. Pina, M. J. Melo, M. Maestri, R. Ballardini, V. Balzani, *J. Am. Chem. Soc.* 1997, 119, 5556-5561.
- [16] F. Pina, M. J. Melo, M. Maestri, P. Passaniti, V. Balzani, *J. Am. Chem. Soc.* 2000, 122, 4496-4498.
- [17] a) P. Wasserscheid, W. Keim, *Angew. Chem. Int. Ed.* 2000, 39, 3772-3789. b) T. Welton, *Chem. Rev.* 1999, 99, 2071-2084.
- [18] a) M. Freemantle, *Chem. Eng. News* 2001, 79, 21. b) L. A Blanchard, D. Hancu, E. J. Beckman, J. F. Brennecke, *Nature* 1999, 399, 28-29.
- [19] P. Bonhote, A. P. Dias, N. Papageorgiou, K. Kalyanasundaram, M. Gratzel, *Inorg. Chem.* 1996, 35, 1168-1178.
- [20] S. Tait, R. A. Osteryoung, *Inorg. Chem.* 1984, 23, 4352-4360.
- [21] D. R. MacFarlane, P. Meakin, J. Sun, N. Amini, M. Forsyth, *J. Phys. Chem. B* 1999, 103, 4164-4170.
- [22] G. Mamantov, J. Caja, T. D. Dunstan, *J. Electrochemical Systems Inc.*, 1996, Patent US5552241,.
- [23] B. Vestergaard, N. J. Bjerrum, I. Petrushina, H. A. Hjuler, R. W. Berg, M. Begtrup, *J. Electrochem. Soc.* 1993, 140, 3108-3113.
- [24] J. Sun, M. Forsyth, D. R. MacFarlane, *J. Phys. Chem. B* 1998, 102, 8858-8864.
- [25] H. S. Kim, Y. J. Kim, J. Y. Bae, S. J. Kim, M. S. Lah, C. S. Chin, *Organometallics* 2003, 22, 2498-2504.
- [26] K. Miyatake, K. Yamamoto, K. Endo, E. Tsuchida, *J. Org. Chem.* 1998, 63, 7522-7524.
- [27] N. M. M. Mateus, L. C. Branco, N. M. T. Lourenço, C. A. M. Afonso, *Green Chem.* 2003, 5, 347 - 352.
- [28] J. S. Wilkes, J. A. Levisky, R. A. Wilson, C. L. Hussey, *Inorg. Chem.* 1982, 21, 1263-1264

- [29] A. S. Larsen, J. D. Holbrey, F. S. Tham, C. A. Reed, *J. Am. Chem. Soc.* 2000, 122, 7264-7272.
- [30] M. Freemantle, *Chem. Eng. News* 1998, 76, 32.
- [31] R. Ozawa, H. Hamaguchi, *Chem. Lett.* 2001, 736-737.
- [32] P. A. Z. Auarez, S. Einloft, J. E. L. Dullius, R. F. de Souza, J. Dupont, *J. Chim. Phys.* 1998, 5, 651-667.
- [33] D. Chakrabarty, A. Chakraborty, P. Hazra, D. Seth, N. Sarkar, *Chem. Phys. Lett.* 2004, 397, 216-221.
- [34] K. S. Mali, G. B. Dutt, T. Mukherjee, *J. Chem. Phys.* 2008, 128, 124515-124523.
- [35] R. Byrne, K. J. Fraser, E. Izgorodina, D. R. MacFarlane, M. Forsyth D. Diamond, *Phys. Chem. Chem. Phys.* 2008, 10, 5919-5924.
- [36] R. Byrne, S. Coleman, K. J. Fraser, A. Raduta, D. R. McFarlane, D. Diamond, *Phys. Chem. Chem. Phys.* 2009, 11, 7286-7291.
- [37] S. Coleman, R. Byrne, S. Minkovska, D. Diamond, *J. Phys. Chem. B* 2009, 113, 15589-15596.
- [38] X. Song, J. Zhou, Y. Li, Y. Tang, *J. Photochem. Photobiology A* 1955, 92, 99-103.
- [39] Y. Sueishi, M. Ohcho, N. Nishimura, *Bull. Chem. Soc. Jpn.* 1985, 58, 2608-2613.
- [40] Y. Wu, T. Sakaki, K. Kazusi, T. Seo, K. Sakurai, *J. Phys. Chem. B* 2008, 112, 7530-7536.
- [41] *cis*-merocyanins are generally blue shifted and relatively unstable in comparison with the *trans* isomer.
- [42] S. Zhang, Q. Zhang, B. Ye, X. Li, X. Zhang, Y. Deng, *J. Phys. Chem. B* 2009, 113, 6012-6019.
- [43] S. Coleman, R. Byrne, N. Alhshimy, K. J. Fraser, D. R. MacFarlane, D. Diamond, *Phys. Chem. Chem. Phys.* 2010, 12, 7009-7017.
- [44] R. Byrne, S. Coleman, S. Gallagher, D. Diamond, *Phys. Chem. Chem. Phys.* 2010, 12, 1895-1904.
- [45] S. Shang, X. Qi, X. Ma, L. Lu, Y. Deng, *J. Phys. Chem. B* 2010, 114, 3912-3920.
- [46] S. Coleman, R. Byrne, S. Minkovska, D. Diamond, *Phys. Chem. Chem. Phys.* 2009, 11, 5608-5614.
- [47] T. Nakashima, K. Miyamura, T. Sakai, T. Kawai, *Chem. Eur. J.* 2009, 15, 1977-1984.
- [48] No remarks about this possibility appear in the paper.
- [49] T. Akitsu, Y. Einaga, *Inorg. Chem. Commun.* 2006, 9, 1108-1110.
- [50] D. Fernandez, F. Pina, A. J. Parola, C. A. M. Afonso, L. C. Branco, *J. Photochem Photobiology Chemistry A* 2004, 168, 185-189.
- [51] McClelland, G. H. McGall, *J. Org. Chem.* 1982, 47, 3730-3736.
- [52] M. C. Moncada, D. Fernández, J. C. Lima, A. J. Parola, C. Lodeiro, F. Folgosa, M. J. Melo, F. Pina, *Org. Biomol. Chem.* 2004, 2, 2802-2808.
- [53] No reaction of the amine in water.
- [54] a) L. Cammarata, S.G. Kazarian, P.A. Salter, T. Welton, *Phys. Chem. Chem. Phys.* 2001, 3, 5192-5200; b) C.G. Hanke, R.M. Lynden-Bell, *J. Phys. Chem.* 2003, 107, 10873-10878. An alternative is that the observed photochemistry would be due to less vibrational de-excitation of the Ct excited state in the ionic liquid leading to the formation of Cc; in water, such vibrational de-excitation would be promoted by the O-H vibration, preventing the isomerization.
- [55] V. W.-W. Yam, J. K.-W. Lee, C.-C. Ko, N. Zhu, *J. Am. Chem. Soc.* 2009, 131, 912-913.
- [56] L. C. Branco, F. Pina, *Chem. Commun.* 2009, 6204-6206.
- [57] H. Tamura, Y. Shinohara T. Arai, *Chem. Lett.* 2010, 39, 240-241.
- [58] T. Asaka, N. Akai, A. Kawai, K. Shibuya, *J. Photochem. Photobiology A* 2010, 209, 12-18.

# Dynamic Heterogeneity in Room-Temperature Ionic Liquids

Daun Jeong,<sup>1</sup> Daekeon Kim,<sup>2</sup> M. Y. Choi,<sup>3</sup> Hyung J. Kim,<sup>4</sup>  
and YounJoon Jung<sup>5\*</sup>

<sup>1</sup>*Department of Chemistry, University of California, Irvine, CA 92697*

<sup>2,5</sup>*Department of Chemistry, Seoul National University, Seoul 151-747*

<sup>3</sup>*Department of Physics and Astronomy, Seoul National University, Seoul 151-747*

<sup>4</sup>*Department of Chemistry, Carnegie Mellon University, Pittsburgh, PA 15213*

<sup>1,4</sup>*USA*

<sup>2,3,5</sup>*Korea*

## 1. Introduction

Room temperature ionic liquids (RTILs) are comprised of bulky organic cations and anions (Holbrey & Seddon, 1999; Weingärtner, 2008). Because of the intricate interplay of various inter- and intramolecular interactions, RTILs have rich dynamical properties and have found diverse applications. In particular, negligible vapor pressure of RTILs makes them a green alternative of conventional organic solvent. For understanding of RTIL's dynamical behavior at the molecular level, solvation and rotational dynamics have been studied experimentally (Arzhantsev et al., 2007; 2006; Cang et al., 2003; Funston et al., 2007; Ingram et al., 2003; Jin et al., 2007; Karmakar & Samanta, 2002a;b; Lang et al., 2006) and theoretically (Jeong et al., 2007; Kobrak, 2006; 2007; Kobrak & Znamenskiy, 2004; Shim et al., 2006; 2007; Shim & Kim, 2009). It is found that the ultrafast relaxation in a subpicosecond time regime contributes substantially to solvation dynamics, disproving the diffusion-controlled solvation in RTILs. On the other hand, in the long time regime, solvation and rotational dynamics of RTILs show slow nonexponential relaxations, which is a characteristic of glassy liquids (Jeong et al., 2008; Shim et al., 2005b).

In this chapter, we particularly focus on the dynamical properties of RTILs as a viscous liquid (Rodriguez & Brennecke, 2006). High viscosity of RTILs has two different aspects in nanoscale applications such as solar cells (Noda et al., 2003; Wang et al., 2003) and capacitors (Tsuda & Hussey, 2007): it is advantageous to preventing the leakage of electrolyte, but disadvantageous to enhancing transport properties. In order to realize the potential applications of RTILs, it is necessary to scrutinize the transport process and relaxation dynamics in RTILs microscopically via molecular dynamics (MD) simulations (Bhargava & Balasubramanian, 2005; Klähn et al., 2008; Popolo & Voth, 2004; Zhao et al., 2009). One notable feature observed in simulation studies of RTILs is so called dynamic heterogeneity (Habasaki

---

\*Corresponding author. E-mail: yjjung@snu.ac.kr

& Ngai, 2008; Hu & Margulis, 2006), which refers to spatially inhomogeneous relaxation behavior (Ediger, 2000; Richert, 2002) in glassy or supercooled liquids (Debenedetti & Stillinger, 2001). Dynamic heterogeneity in RTILs has been observed in the fluorescence spectroscopy experiments (Hu & Margulis, 2006; Samanta, 2006).

In this chapter, we present an overview on our recent MD studies of dynamic heterogeneity of RTILs employing a coarse-grained model of 1-ethyl-3-methylimidazolium hexafluorophosphate ( $\text{EMI}^+\text{PF}_6^-$ ) (Jeong et al., 2010; Jeong & Jung, 2010; Kim et al., 2010). Dynamic heterogeneity has been investigated numerically in various models of supercooled liquids and glass (Chakrabarti & Bagchi, 2006; Chaudhuri et al., 2007; 2008; Kob et al., 1997; Lačević et al., 2003; Leonard & Berthier, 2005). Regardless of detailed description in modelling, observed in common are the nonexponential relaxation, breakdown of Stokes-Einstein (SE) or Debye-Stokes-Einstein relation, and decoupling of the exchange and persistence times (Hedges et al., 2007; Jung et al., 2004; 2005). Our model of RTILs has molecular interactions which are strikingly different from those in supercooled liquids due to the Coulomb interactions. The dynamical properties mentioned above are also observed similarly in our model and suggested to be essential features of dynamic heterogeneity in RTILs.

The heterogeneity in RTILs may imply structural heterogeneity in mesoscale such as the assembled structure of long alkyl chains (Wang et al., 2007; Wang & Voth, 2005). We point out that the cation in our model employs a united atom description for short alkyl chain. Thus, locally ordered structures and hydrogen bond networks are not expected to appear in our simulation results. However, structural influence on inhomogeneous dynamics is still an intriguing and open question in this simplified model.

This chapter is organized as follows: In Sec. 2, a coarse-grained model of a RTIL is introduced. In Sec. 3, we present the MD results for glassy dynamics. Various dynamic properties manifesting dynamic heterogeneity are demonstrated in Sec. 4, while Sec. 5 is devoted to analyzing the dynamic propensity and Coulomb potential energy. Finally, we conclude in Sec. 6.

## 2. A coarse-grained model of ionic liquids

We introduce a coarse-grained models to study the dynamics of RTILs via MD simulations covering many orders of magnitude in time scale (Jeong et al., 2010). Fast degrees of freedom which engage the hydrogen atom as well as the vibration of bonds are excluded by employing the united atom representation. Our coarse-grained model is based on the model studied by Kim and coworkers (Shim et al., 2005a). To be specific, the methyl group (M1) and the moieties of the ethyl group (E1, M3) in the cation,  $\text{EMI}^+$ , were represented by united atoms, using the AMBER force field (Cornell et al., 1995) and the partial charge assignments proposed by Lynden-Bell and coworkers. (Hanke et al., 2001) The anion  $\text{PF}_6^-$  was also described as a united atom. One further simplification employed in our model is that five atoms in the imidazole ring and three attached H atoms are represented by a united atom T1 positioned at the center of mass of 8 atoms. The Lennard-Jones (LJ) parameters of T1 were adjusted, so that our model reproduces the liquid structure of the model studied by Kim and coworkers. MD simulations of the coarse-grained model for  $\text{EMI}^+\text{PF}_6^-$  are performed using the DL\_POLY program. (Forster & Smith, 2001). Atoms  $i$  and  $j$  at positions  $\mathbf{r}_i$  and  $\mathbf{r}_j$  interact with each other through the LJ and Coulomb potentials:

$$U_{ij} = 4\epsilon_{ij} \left[ \left( \frac{\sigma_{ij}}{r_{ij}} \right)^{12} - \left( \frac{\sigma_{ij}}{r_{ij}} \right)^6 \right] + \frac{q_i q_j}{r_{ij}}, \quad (1)$$



atom	$\sigma_{ii}$ (Å)	$\epsilon_{ii}$ (kJ/mol)	$q_i$ (e)	mass (amu)
M1	3.905	0.7330	0.316	15.04092
T1	4.800	1.5000	0.368	67.08860
E1	3.800	0.4943	0.240	14.03298
M3	3.800	0.7540	0.076	15.04092
PF6	5.600	1.6680	-1.000	144.97440

Table 1. The LJ parameters, partial charges, and masses of coarse-grained atoms (Jeong et al., 2010)

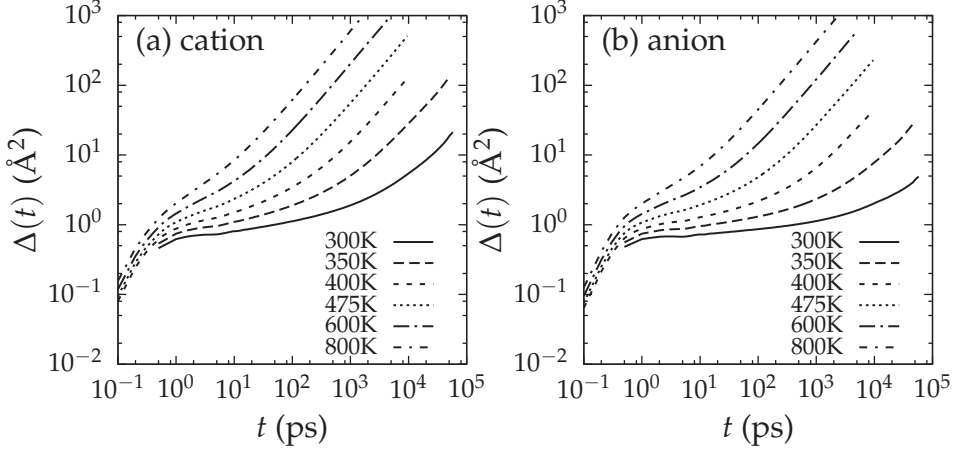


Fig. 1. Mean square displacement of (a) cations and (b) anions at various temperatures.

where  $r_{ij} \equiv |\mathbf{r}_i - \mathbf{r}_j|$  is the distance between the two atoms. The parameters of our coarse-grained model are compiled in Table 1.

The model system comprises 512 pairs of rigid cations and anions. We performed simulations in the canonical ensemble using the Nosé-Hoover thermostat and at density  $\rho = 1.31 \text{ g/cm}^3$  at six different temperatures. Periodic and cubic boundary conditions were employed and long-range electrostatic interactions were computed via the Ewald method.

### 3. Glassy dynamics

Glassy dynamics of the coarse-grained RTIL is studied using MD simulation results. We analyze ion diffusion and structural relaxation with the mean square displacement,

$$\Delta(t) = \left\langle \frac{1}{N} \sum_{i=1}^N |\mathbf{r}_i(t) - \mathbf{r}_i(0)|^2 \right\rangle, \quad (2)$$

and self-intermediate scattering function,

$$F_s(q_0, t) \equiv \left\langle \frac{1}{N} \sum_{i=1}^N e^{i\mathbf{q}_0 \cdot [\mathbf{r}_i(t) - \mathbf{r}_i(0)]} \right\rangle, \quad (3)$$

where  $\langle \dots \rangle$  denotes the equilibrium ensemble average,  $N$  the number of ions, and  $\mathbf{q}_0$  the wave vector which corresponds to the position of the first peak in the static structure factor

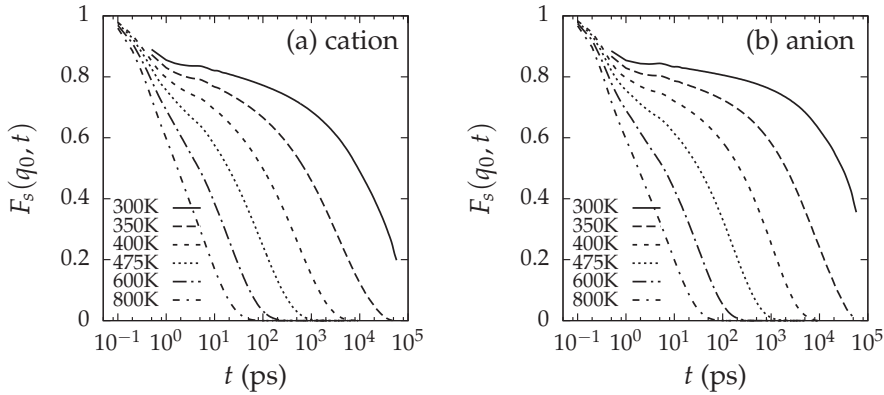


Fig. 2. Self-intermediate scattering function  $F_s(q_0, t)$  for (a) cations and (b) anions. The wave vector  $q_0$  is set to  $1.24 \text{ \AA}^{-1}$  in (a) and (b), which corresponds to the position of the first peak in the static structure factor for all ions.

for all ions. In this model,  $q_0$  is found to be  $1.24 \text{ \AA}^{-1}$  regardless of the temperature. It is attributed to the constant density employed in our model, while the density increases slightly in real RTILs and so does  $q_0$ , as the temperature is lowered.

In Figs. 1 and 2, the ionic liquid exhibits subdiffusive behavior and nonexponential relaxation more apparently, as the temperature is lowered.  $\Delta(t)$  shows sublinear dependence in the intermediate time scale, which is followed by a crossover to Fickian behavior eventually. In the time scale of non-Fickian behavior, we observe the plateau regime ( $\beta$  relaxation) in  $F_s(q_0, t)$ , while the slow  $\alpha$  relaxation follows in the long time regime. The latter is well described by a stretched exponential function,  $c \exp[-(t/\tau_0)^\beta]$ . At 300 K, the exponent  $\beta$  is found to be 0.64 and 0.59 for cations and anions, respectively, while 0.89 and 0.92 at 800 K. The exponent  $\beta$  being less than unity as well as the subdiffusion and  $\beta$  relaxation is known to be a good indicator of the glassy dynamics. The origin of the stretched exponential relaxation has been discussed to be either the superposition of different exponential relaxations which arise from heterogeneous dynamics or intrinsically nonexponential relaxation (Colmenero et al., 1999). The structural relaxation time  $\tau_\alpha$  is determined by the relation  $F_s(q_0, \tau_\alpha) = e^{-1}$  using the results in Fig 2. The temperature dependence of  $\tau_\alpha$  is presented in Fig. 3. We observe that  $\tau_\alpha$  does not follow the Arrhenius law  $\tau_\alpha \propto \exp(d_2/T)$ , but rather a super-Arrhenius behavior given by  $\tau_\alpha \propto \exp(d_1/T^2)$ . This indicates that our model of RTILs belongs to a fragile glass former. A super-Arrhenius behavior in a similar RTIL has been also observed in a recent experiment (Xu et al., 2003) For clarity, we note that we have assumed constant density at all temperatures in our model. If the variation of density were employed, the structural relaxation would be accelerated at high temperatures and decelerated at low temperatures. This would not change the fragile behavior of our model qualitatively.

#### 4. Dynamic heterogeneity

Dynamic heterogeneity of our ionic liquid system is investigated by verifying dynamic correlations between local excitations. We first provide our working definition of local excitations, and present various statistical analyses of them to prove and characterize dynamic heterogeneity.

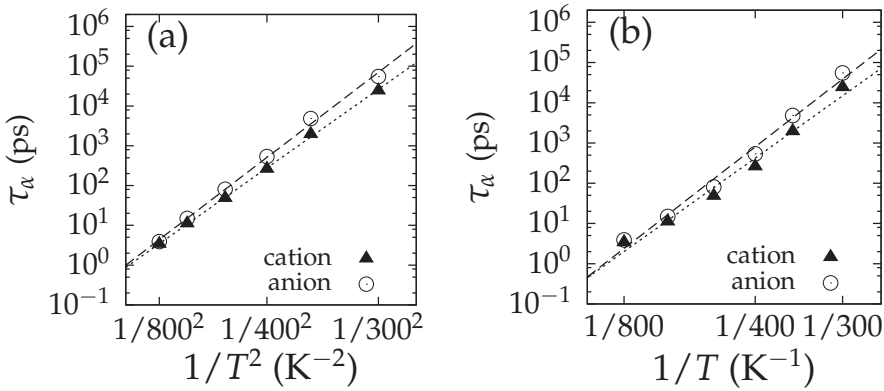


Fig. 3. Temperature dependence of structural relaxation time  $\tau_\alpha$  (Jeong et al., 2010). Lines are the fitted results using (a)  $\tau_\alpha = c_1 \exp(d_1/T^2)$  and (b)  $\tau_\alpha = c_2 \exp(d_2/T)$ . A super-Arrhenius behavior shown in (a) and (b) suggest that our model of RTILs resembles a fragile glass former.

#### 4.1 Correlated local excitations

A general feature in the diffusive dynamics of supercooled or viscous liquids is that particles are trapped in a cage for a long time because the thermal motions are not activated enough. This is also the case of our model of ionic liquids at low temperatures; an ion exhibits merely oscillatory motions, occasionally interrupted by significant movements. We monitor such large motions of each ion and thereby quantify local dynamics in the ionic liquid. In this study, local excitation events refer to the instances  $t_1, t_2, t_3, \dots$ , where the displacement of an ion  $i$  exceeds a threshold distance, i.e.,  $|\mathbf{r}_i(t_1) - \mathbf{r}_i(0)| > d$ ,  $|\mathbf{r}_i(t_2) - \mathbf{r}_i(t_1)| > d$ ,  $|\mathbf{r}_i(t_3) - \mathbf{r}_i(t_2)| > d$ ,  $\dots$ , etc (Hedges et al., 2007). The more local excitation occurs frequently, the more the ion is mobile. The cut off distance  $d$  should be chosen appropriately in order to probe the local dynamics. We display the results for  $d = 3.0 \text{ \AA}$ , for example, and note that other choices of  $d$  on the order of the inter-ion distances do not alter our results qualitatively.

An initial excitation of an ion may perturb the local environment and thereby lead to another excitation to the ion or neighboring ions. In the system where the excitations are sparse, the first excitation and subsequent ones indicate different physical circumstances (Jung et al., 2005). The molecular environment providing dynamic constraints persists until the first excitation occurs during fluctuations. Then, the excitation is followed by exchange events due to the dynamic correlations. To verify this, we define the persistence and exchange times to be the waiting times for the first excitation and following ones, and they are denoted by  $\tau_p$  and  $\tau_x$ , respectively. The facilitated dynamics would result in the decoupling of the exchange and persistence times. The distributions of persistence and exchange times at various temperature for cations and anions are displayed in Fig. 4. At 800 K, the two distributions almost coincide with each other, while they become separated as  $T$  is lowered. The correlated excitations bring about the decoupled distributions. This implies that the excitation events should not belong to the Poisson process.

We remark that the above idea has been originally proposed in the kinetically-constrained model (KCM) (Garrahan & Chandler, 2002), which describes the dynamics of supercooled liquids successfully employing a two-state variable with kinetic constraint. Prior to our study

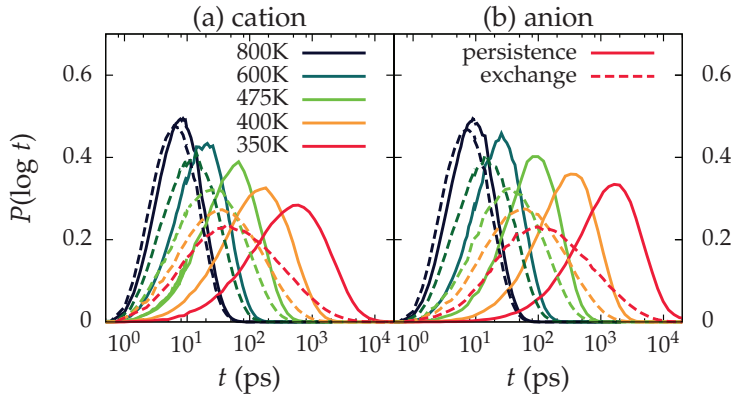


Fig. 4. Decoupling of persistence and exchange times for (a) cations and (b) anions in a coarse-grained model of  $\text{EMI}^+\text{PF}_6^-$  (Jeong et al., 2010).

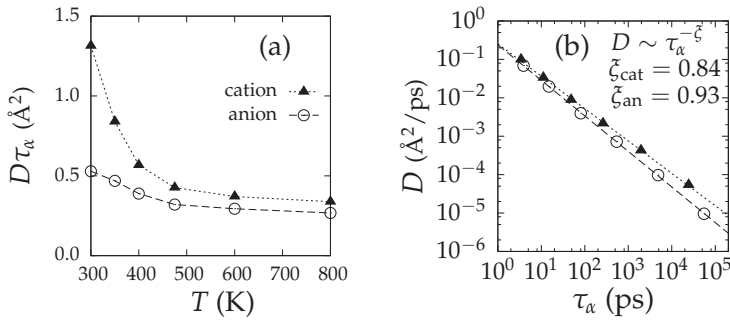


Fig. 5. Violation of the Stokes-Einstein relation in a coarse-grained model of  $\text{EMI}^+\text{PF}_6^-$  (Jeong et al., 2010). (a) As the temperature is lowered,  $D\tau_\alpha$  increases. The deviation from a constant is more substantial in case of cations. Lines are guides for the eyes. (b) The exponents in the scaling relation  $D \sim \tau_\alpha^{-\zeta}$  are found to be 0.84 and 0.93 for cations and anions, respectively, while  $\zeta = 1$  corresponds to the Stokes-Einstein relation. Lines are the fitted results.

of the ionic liquid, the decoupling of the exchange and persistence times has been shown in not only the KCM but also the WCA model (Hedges et al., 2007), which is an atomistic model for supercooled liquids.

#### 4.2 Violation of Stokes-Einstein relation

The Stokes-Einstein(SE) relation is one of hydrodynamic relations for transport properties. In normal liquids, the relation

$$D \propto \frac{T}{\eta} \quad (4)$$

is usually accurate. In this study, we use another equivalent relation,

$$D \propto \frac{1}{\tau_\alpha}, \quad (5)$$

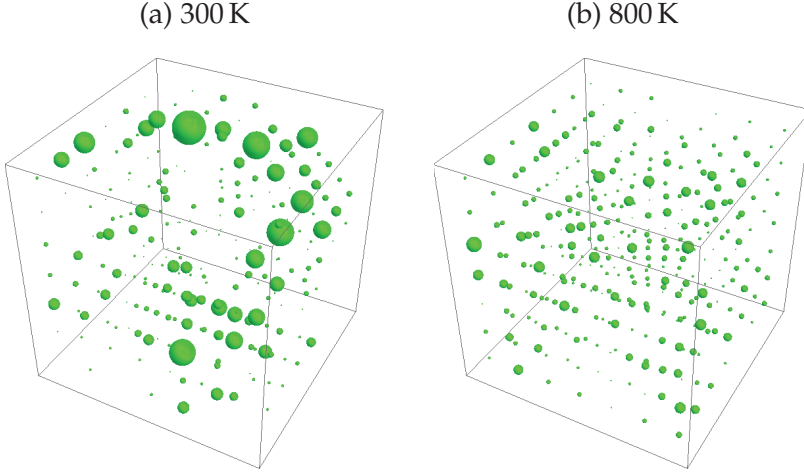


Fig. 6. Spatial heterogeneity of the mobility in a coarse-grained model of  $\text{EMI}^+\text{PF}_6^-$  at (a) 300 K and (b) 800 K. For each cell, the sphere depicts the mobility  $m_k$  such that its radius is proportional to  $m_k$ .

where  $\tau_\alpha$  is the structural relaxation time assuming that  $\tau_\alpha$  is proportional to  $\eta/T$ . We obtain the diffusion constant  $D$  from the mean square displacement  $\Delta[t - t_0] = \langle N^{-1} \sum_{i=1}^N |\mathbf{r}_i(t) - \mathbf{r}_i(t_0)|^2 \rangle$ , using the relation  $\lim_{t \rightarrow \infty} \Delta[t - t_0] = 6D(t - t_0)$ . At low temperatures, sub-diffusive behavior is pronounced in the intermediate time scale. Thus, we find the time  $t_0$  when the Fickian behavior appears in  $\Delta[t - t_0]$  to specify the diffusion regime correctly (Szamel & Flenner, 2006). The structural relaxation time  $\tau_\alpha$  has been obtained in Sec. 3.

If Equation 5 holds,  $D\tau_\alpha$  would be a constant for all temperatures. We display the deviation of  $D\tau_\alpha$  for cations and anions in Fig. 5 (a), which means the structural relaxation decouples from diffusive dynamics as  $T$  is lowered. To characterize the decoupling behavior in comparison with supercooled liquids, we employ the scaling relation,

$$D \sim \tau_\alpha^{-\xi}, \quad (6)$$

where  $\xi = 1$  corresponds to the SE relation. The results  $\xi = 0.84$  for cations and  $0.93$  for anions reveal a relatively weak SE violation in our model (Fig. 5 (b)), compared with supercooled liquids. In the KCM,  $\tau_\alpha$  corresponds to the average persistence time  $\langle \tau_p \rangle$  (Berthier et al., 2005), while the mechanism of self-diffusion is related to the dynamic exchange events. Therefore, the violation of SE relation has a deep connection with the decoupling of the exchange and persistence times. In this sense, the violation of the SE relation is another manifestation of dynamic heterogeneity. It is also noteworthy that the exponent for the cation is less than that for the anion. This indicates that cations should contribute more significantly to the dynamic heterogeneity, which we turn to later.

#### 4.3 Heterogeneity relaxation

We use the excitations defined in Sec. 4.1 to characterize the dynamic heterogeneity by quantifying the local dynamics. We count excitations during a time interval to specify mobile

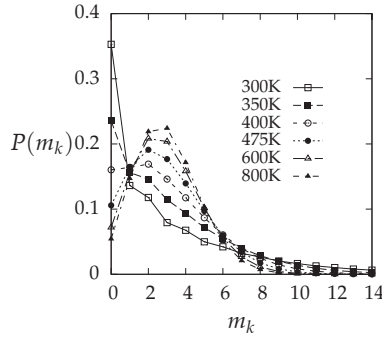


Fig. 7. Probability distributions of  $m_k$  at various temperatures.

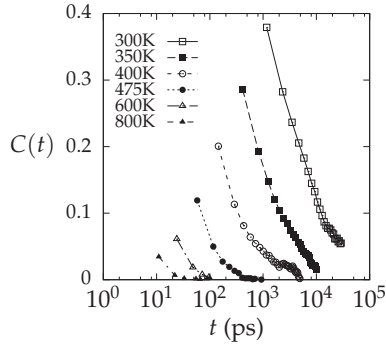


Fig. 8. Time correlation functions of  $m_k(t)$  given by Eq. 7.

and immobile regions. The simulation box is divided into  $7 \times 7 \times 7$  cells. The mobility  $m_k(t)$  is defined to be the number of excitations which occur at time between  $t - \tau_{cg}/2$  and  $t + \tau_{cg}/2$  in the  $k$ -th cell. We hereby obtain the mobility as a function of the position and time which are both coarse-grained. The time interval  $\tau_{cg}$  is determined to accommodate three excitations on average and depends on the temperature accordingly.

Figure 6 (a) describe the spatial heterogeneity of the mobility at 300 K, where the radius of the spheres centered at the  $k$ -th cell is proportional to  $m_k$ . We observe the clustering of mobile and immobile regions. In contrast, the mobility appears relatively more homogeneous at 800 K, in Fig. 6 (b). We confirm this by observing the distributions of the mobility in Fig. 7. At 800 K,  $P(m_k)$  exhibits a Gaussian distribution. As the temperature is lowered,  $P(m_k)$  becomes asymmetric and develops a tail at large  $m_k$  demonstrating a clustering of excitations. Note that the the average of  $m_k$  over all cells is set to be 3.0 by adjusting  $\tau_{cg}$ .

The heterogeneity of the mobility is expected to relax with a long time scale. We obtain the time scale of the heterogeneity relaxation by computing the normalized time correlation function given by

$$C(t) \equiv \frac{\overline{\langle m_k(t)m_k(0) \rangle} - \overline{\langle m_k(0) \rangle}^2}{\overline{\langle m_k(0)^2 \rangle} - \overline{\langle m_k(0) \rangle}^2}, \quad (7)$$

where the overline and  $\langle \dots \rangle$  denote the averages over  $k$  and the equilibrium ensemble, respectively. The results for  $C(t)$  at  $T = 300 \sim 800$  K are displayed in Fig. 8.  $C(t)$  shows rapid decay for  $t \lesssim \tau_{cg}$  followed by nonexponential decay thereafter. The characteristic time

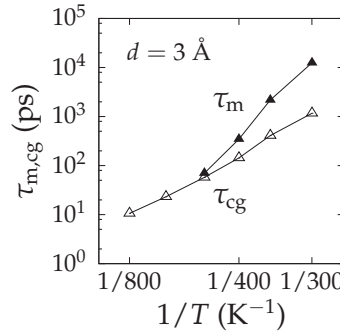


Fig. 9. Temperature dependences of  $\tau_{cg}$  and  $\tau_m$ .  $\tau_{cg}$  increases exponentially with the inverse temperature. The time scale  $\tau_m$  for the mobility relaxation is determined from  $C(\tau_m) = 0.1$  displayed in Fig. 8. The increase of  $\tau_m$  is faster than that of  $\tau_{cg}$ .

scale  $\tau_m$  of the heterogeneity is determined by the relation  $C(\tau_m) = 0.1$ . Figure 9 shows the temperature dependences of  $\tau_m$  and  $\tau_{cg}$ . The increase in  $\tau_{cg}$  with a decrease in the temperature indicates the slowing down of the dynamics. In particular,  $\tau_m$  increases faster than that of  $\tau_{cg}$  as the temperature is lowered. At low temperatures, the correlation of the mobility maintains for a significantly long time, e.g., about ten nanoseconds at 300 K which is about a hundred times longer than the time interval for measuring the mobility.

## 5. Structural heterogeneity

Dynamic properties presented in Sec. 4 demonstrate that local dynamic constraint in fluctuation-dominated dynamics is responsible for the dynamic heterogeneity in our coarse-grained ionic liquid. To consider the structural origin producing the dynamic constraint in RTILs, we examine dynamic propensity to probe the role of initial structure in Sec. 5.1. Then, we analyze the Coulomb potential energy which represent the heterogeneous structures of RTILs in Sec. 5.2.

### 5.1 Dynamic propensity

Dynamic propensity has been introduced to study structural influences on the heterogeneous dynamics of supercooled liquids (Rodriguez Fris et al., 2009; Widmer-Cooper & Harrowell, 2007; Widmer-Cooper et al., 2004). Dynamic propensity of the ion  $i$ , denoted by  $p_i$ , is defined as the mean squared displacement of the ion  $i$  for  $t^*$ , which is averaged over the trajectories starting from a given initial configuration with different initial momenta, i.e., the isoconfigurational (IC) ensemble,

$$p_i \equiv \langle |\mathbf{r}_i(t^*) - \mathbf{r}_i(0)|^2 \rangle_{IC}. \quad (8)$$

The initial configuration is taken from the equilibrium ensemble and the initial momenta are chosen to follow the Maxwell-Boltzmann distribution corresponding to the temperature. In this study, we repeat simulations 200 times for each initial structure. The time interval  $t^*$  is chosen to be  $1.5\tau_\alpha$  at each temperature, where  $\tau_\alpha$ 's have been determined in Sec. 3. The averages over the IC ensemble exclude the influence of the direction and magnitude of initial momenta on the resultant dynamics. Thus,  $p_i$  would reveal how the ion  $i$  tends to be mobile, resulted by, if any, the initial configuration. Previous studies of supercooled liquids

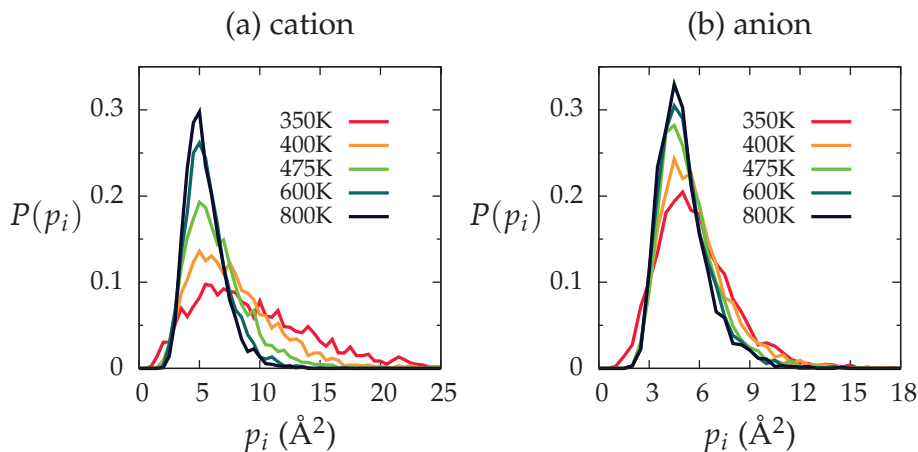


Fig. 10. Probability distributions of dynamic propensity in a coarse-grained model of  $\text{EMI}^+\text{PF}_6^-$  for (a) cations and (b) anions.

have found that several local structural quantities and the potential energy do not have any direct correlations with the propensity of individual particle, but a general overlap of spatial distributions in a large length scale (Berthier & Jack, 2007; Widmer-Cooper & Harrowell, 2006; Widmer-Cooper et al., 2004; 2008).

Figure 10 shows the probability distributions  $P(p_i)$  of dynamic propensities for cations and anions at five temperatures. The distributions are obtained by performing averages over the results from five uncorrelated initial configurations at each temperature. At 800 K, the highest temperature we studied,  $P(p_i)$  follow a narrow Gaussian distribution for both cations and anions. As the temperature is lowered,  $P(p_i)$  becomes more broad and asymmetric. The Gaussian shape of  $P(p_i)$  implies that each ion has an identical environment statistically for  $t^*$  according to the central limit theorem. Thus, a substantial deviation from the Gaussian distribution means that each ion is located in heterogeneous environments. Though not specified yet, there might be relatively more restrictive structures resulting in small propensity, while less restrictive structures facilitate large propensity. Thus, the change of the distributions with the decrease of the temperature indicates the development of the dynamic heterogeneity.

One interesting feature in Fig. 10 is that the tails of  $P(p_i)$  at large propensity become more distinct in case of the cations, as the temperature is lowered. It implies that cations make more dominant contributions to the heterogeneous dynamics in our model. In Sec. 3, we have observed that  $\tau_a$  for anions is much longer than that of cations, especially at low temperatures, and so is  $t^*$ . Therefore, most of surrounding cations for an anion undergo complete structural relaxation, resulting in relatively homogeneous environment for the anion. It is consistent with the result in Sec. 4.2, where the breakdown of SE relation is prominent in case of cations.

## 5.2 Coulomb potential energy

To examine a heterogeneous environment which may affects motions of individual ion, we calculate the Coulomb potential energy  $U_i$  at the position of the ion  $i$  using the Ewald



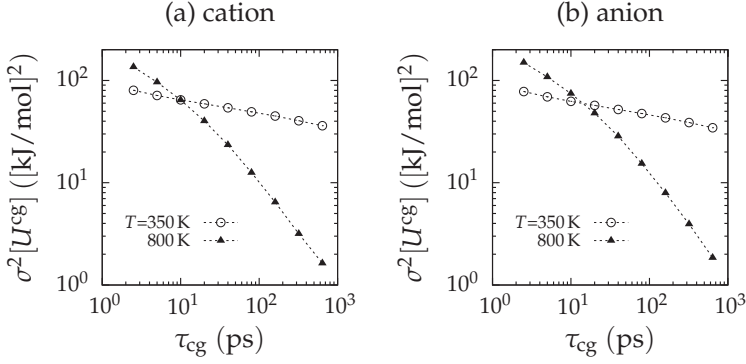


Fig. 11. The variance of  $U_i^{\text{cg}}$  for (a) cations and (b) anions versus  $\tau_{\text{cg}}$ , where  $U_i^{\text{cg}}$  is obtained using Eq. 10 for each  $\tau_{\text{cg}}$ .

method (Forster & Smith, 2001),

$$U_i = \sum_{\mathbf{k} \neq 0} \sum_{j=1}^N \frac{4\pi q_i q_j}{k^2} \exp[i\mathbf{k} \cdot (\mathbf{r}_i - \mathbf{r}_j)] \exp(-k^2/4\alpha) + \sum_{j(\neq i)} \frac{q_i q_j}{|\mathbf{r}_i - \mathbf{r}_j|} \text{erfc}(\sqrt{\alpha}|\mathbf{r}_i - \mathbf{r}_j|), \quad (9)$$

where  $q_i$  is the charge of the ion  $i$  and  $\alpha$  is a parameter which determines a Gaussian distribution for screening and compensating charges in the Ewald method.

Due to the inertial dynamics of ions,  $U_i$  fluctuates with large amplitude. We take average of  $U_i$  during a coarse-graining time interval  $\tau_{\text{cg}}$  to probe only the structural aspect. The coarse-grained Coulomb potential energy for the ion  $i$  is given by

$$U_i^{\text{cg}}(t) \equiv \frac{1}{\tau_{\text{cg}}} \int_{t-\tau_{\text{cg}}/2}^{t+\tau_{\text{cg}}/2} U_i(t') dt'. \quad (10)$$

We study how the distribution of  $U_i^{\text{cg}}$  depends on  $\tau_{\text{cg}}$  here. With the increase of  $\tau_{\text{cg}}$ , the variance of  $U_i^{\text{cg}}$  over ions,  $\sigma^2[U^{\text{cg}}]$ , should decrease in general. However, Figure 11 shows that  $\sigma^2[U^{\text{cg}}]$  does not decrease substantially as  $\tau_{\text{cg}}$  increases at a low temperature 350 K. It is because the values of  $\tau_{\text{cg}}$  employed in Fig. 11 are shorter than the structural relaxation time  $\tau_{\alpha}$ , which are found to be 1960 ps and 4840 ps for cations and anions, respectively, in Sec. 3. On the other hand,  $\sigma^2[U^{\text{cg}}]$  decreases faster at  $T = 800$  K, where  $\tau_{\alpha}$  are 3.4 ps for cations and 3.9 ps for anions. Specifically, the variance scales as  $\sigma[U^{\text{cg}}] \sim \tau_{\text{cg}}^{-1}$  at 800 K, as it should be when  $U_i^{\text{cg}}$  follows an identical distribution for all  $i$ , according to the central limit theorem. We thus consider the weak decreasing of  $\sigma^2[U^{\text{cg}}]$  with  $\tau_{\text{cg}}$  at 350 K as a result of heterogeneous structures. If we further increase  $\tau_{\text{cg}}$  to the time much longer than  $\tau_{\alpha}$ ,  $\sigma^2[U^{\text{cg}}]$  would start to decrease substantially, and the heterogeneity would be averaged out, eventually. On this account, we consider  $U_i^{\text{cg}}$  as a quantity which has structural information for individual ion at a low temperature.

To verify the environment which facilitates ions to be mobile or immobile, we consider  $U_i^{\text{cg}}$  and the mobility  $m_i$ , which is defined as the number of excitations of the ion  $i$  during  $\tau_{\text{cg}}$ . We obtain conditional probability distributions of  $U_i^{\text{cg}}$  on the conditions that the ion  $i$  has the mobility  $m_i$  larger and smaller than  $m_c$ . At 300 K,  $\tau_{\text{cg}}$  are set to be 1 ns and 2.5 ns for cations and anions, respectively, while 15 ps and 18 ps at 800 K. We choose  $m_c = 2$  for cations

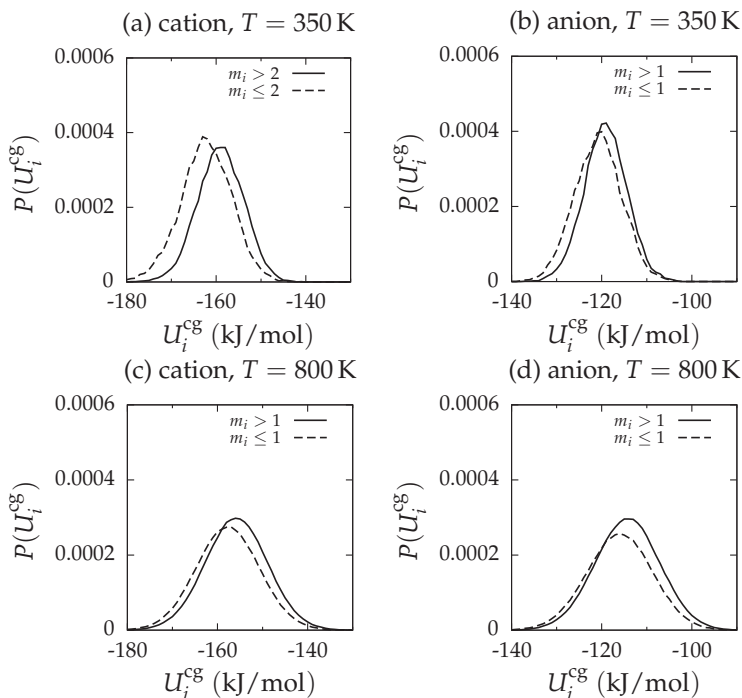


Fig. 12. Conditional probability distributions for  $U_i^{cg}$  corresponding to the cases of  $m_i > m_c$  and  $m_i \leq m_c$  for (a) cations at 350 K, (b) anions at 350 K, (c) cations at 800 K, and (d) anions at 800 K. The coarse-graining time intervals  $\tau_{cg}$  to obtain  $U_i^{cg}$  and  $m_i$  are chosen to be 1 ns and 2.5 ns for cations and anions at 350 K, respectively, while  $\tau_{cg}$  is determined to be 15 ps for cations and 18 ps for anions at 800 K.  $m_c = 1$  in (b),(c), and (d), while  $m_c = 2$  in (a).

at 350 K, otherwise,  $m_c = 1$ . In Fig. 12, the conditional probability distributions for  $m_i > m_c$  are observed to shift to higher energies for all cases. We first point out that mobile ions have higher  $U_i^{cg}$  on average at 800 K as well as 350 K. At 800 K, we have not observed the heterogeneity of  $m_i$  or  $U_i^{cg}$  which persists significantly. Therefore, higher mobility would not be facilitated by higher  $U_i^{cg}$ . It is conjectured that the shift of  $P(U_i^{cg})$  should be mainly attributed to the perturbed structures caused by local excitations. Moreover, two distributions exhibit considerable overlaps. Ions can have relatively lower  $U_i^{cg}$  even though the ions are mobile in a variety of situations made by complicated dynamics in liquids. In this sense, larger values of  $U_i^{cg}$  cannot be a decisive factor to make the ion mobile. However, we also observe more distinct discrepancy between two distributions for cations at 350 K in Fig. 12 (a), compared to other cases. This might be a contribution from heterogeneous structures, which will be specified further in detail as a future study. It is also necessary to examine if these structures act as mobile or immobile environments.

## 6. Conclusions

To summarize the chapter, we have shown various dynamic properties manifesting the dynamic heterogeneity in a coarse-grained model of  $\text{EMI}^+\text{PF}_6^-$ . As the temperature is

lowered, our model system exhibits nonexponential relaxation, subdiffusive behavior, the breakdown of the Stokes-Einstein relation, and the decoupling of persistence and exchange times. We point out that all the properties have been observed in models of supercooled liquids before. The dynamical similarity regardless of strikingly different molecular details is of particular interest. We essentially attribute the universality to the dynamic correlations existed in glassy liquids. Furthermore, the dynamic heterogeneity of our model have been verified by introducing the mobility, which we claim a convenient quantity to describe local dynamic states. We have also studied how the dynamic correlations are developed, specifically whether they are structurally originated, by computing the dynamic propensity and Coulomb potential energy. In conclusion, the dynamic propensity and Coulomb potential energy demonstrate the dynamic heterogeneity well. However, they do not seem to affect the dynamics decisively. The dynamics of RTILs resolve itself into the fluctuation-dominated dynamics. Nevertheless, it is still necessary to improve microscopic understanding of the diffusion mechanism in terms of the Coulomb interactions. More detailed analyses on the Coulomb potential energy are in progress.

## 7. Acknowledgements

This work was supported by the National Research Foundation of Korea (Grant Nos. 2010-0001631, 2010-0015243, and 2010-0014525), the KISTI Supercomputing Center (KSC-2009-502-0003), and the BK21 Program.

## 8. References

- Arzhantsev, S., Jin, H., Baker, G. A. & Maroncelli, M. (2007). Measurements of the complete solvation response in ionic liquids, *J. Phys. Chem. B* 111(18): 4978–4989.
- Arzhantsev, S., Jin, H., Ito, N. & Maroncelli, M. (2006). Observing the complete solvation response of DCS in imidazolium ionic liquids, from the femtosecond to nanosecond regimes, *Chem. Phys. Lett.* 417(4-6): 524–529.
- Berthier, L., Chandler, D. & Garrahan, J. (2005). Length scale for the onset of Fickian diffusion in supercooled liquids, *Europhys. Lett.* 69(3): 320–326.
- Berthier, L. & Jack, R. L. (2007). Structure and dynamics of glass formers: Predictability at large length scales, *Phys. Rev. E* 76(4): 041509.
- Bhargava, B. & Balasubramanian, S. (2005). Dynamics in a room-temperature ionic liquid: A computer simulation study of 1,3-dimethylimidazolium chloride, *J. Chem. Phys.* 123(14): 144505.
- Cang, H., Li, J. & Fayer, M. (2003). Orientational dynamics of the ionic organic liquid 1-ethyl-3-methylimidazolium nitrate, *J. Chem. Phys.* 119(24): 13017–13023.
- Chakrabarti, D. & Bagchi, B. (2006). Decoupling phenomena in supercooled liquids: Signatures in the energy landscape, *Phys. Rev. Lett.* 96(18): 187801.
- Chaudhuri, P., Berthier, L. & Kob, W. (2007). Universal nature of particle displacements close to glass and jamming transitions, *Phys. Rev. Lett.* 99(6): 060604.
- Chaudhuri, P., Karmakar, S. & Dasgupta, C. (2008). Signatures of dynamical heterogeneity in the structure of glassy free-energy minima, *Phys. Rev. Lett.* 100(12): 125701.
- Colmenero, J., Arbe, A., Alegría, A., Monkenbusch, M. & Richter, D. (1999). On the origin of the non-exponential behaviour of the relaxation in glass-forming polymers: Incoherent neutron scattering and dielectric relaxation results, *J. Phys.:Condens. Matter* 11: A363–A370.

- Cornell, W., Cieplak, P., Bayly, C., Gould, I., Merz, K., Ferguson, D., Spellmeyer, D., Fox, T., Caldwell, J. & Kollman, P. (1995). A second generation force field for the simulation of proteins, nucleic acids, and organic molecules, *J. Am. Chem. Soc.* 117(19): 5179–5197.
- Debenedetti, P. & Stillinger, F. (2001). Supercooled liquids and the glass transition, *Nature* 410(6825): 259–267.
- Ediger, M. (2000). Spatially heterogeneous dynamics in supercooled liquids, *Annu. Rev. Phys. Chem.* 51: 99–128.
- Forster, T. R. & Smith, W. (2001). *The DL\_POLY-2.13 Reference Manual*, Daresbury Laboratory, Warrington, CCLRC.
- Funston, A. M., Fadeeva, T. A., Wishart, J. F. & Castner, E. W. (2007). Fluorescence probing of temperature-dependent dynamics and friction in ionic liquid local environments, *J. Phys. Chem. B* 111(18): 4963–4977.
- Garrahan, J. & Chandler, D. (2002). Geometrical explanation and scaling of dynamical heterogeneities in glass forming systems, *Phys. Rev. Lett.* 89(3): 035704.
- Habasaki, J. & Ngai, K. (2008). Heterogeneous dynamics of ionic liquids from molecular dynamics simulations, *J. Chem. Phys.* 129(19): 194501.
- Hanke, C., Price, S. & Lynden-Bell, R. (2001). Intermolecular potentials for simulations of liquid imidazolium salts, *Mol. Phys.* 99(10): 801–809.
- Hedges, L. O., Maibaum, L., Chandler, D. & Garrahan, J. P. (2007). Decoupling of exchange and persistence times in atomistic models of glass formers, *J. Chem. Phys.* 127(21): 211101.
- Holbrey, J. & Seddon, K. (1999). Ionic liquids, *Clean Products and Processes* 1: 223–236.
- Hu, Z. & Margulis, C. (2006). Heterogeneity in a room-temperature ionic liquid: Persistent local environments and the red-edge effect, *Proc. Natl. Acad. Sci. USA* 103(4): 831–836.
- Ingram, J., Moog, R., Ito, N., Biswas, R. & Maroncelli, M. (2003). Solute rotation and solvation dynamics in a room-temperature ionic liquid, *J. Phys. Chem. B* 107(24): 5926–5932.
- Jeong, D., Choi, M., Jung, Y. & Kim, H. (2008). 1/f spectrum and memory function analysis of solvation dynamics in a room-temperature ionic liquid, *J. Chem. Phys.* 128(17): 174504.
- Jeong, D., Choi, M., Kim, H. & Jung, Y. (2010). Fragility, Stokes–Einstein violation, and correlated local excitations in a coarse-grained model of an ionic liquid, *Phys. Chem. Chem. Phys.* 12: 2001–2010.
- Jeong, D. & Jung, Y. (2010). Role of the Coulomb interaction in the heterogeneous dynamics of an ionic liquid, *in preparation*.
- Jeong, D., Shim, Y., Choi, M. & Kim, H. (2007). Effects of solute electronic polarizability on solvation in a room-temperature ionic liquid, *J. Phys. Chem. B* 111(18): 4920–4925.
- Jin, H., Baker, G. A., Arzhantsev, S., Dong, J. & Maroncelli, M. (2007). Solvation and rotational dynamics of coumarin 153 in ionic liquids: Comparisons to conventional solvents, *J. Phys. Chem. B* 111(25): 7291–7302.
- Jung, Y., Garrahan, J. & Chandler, D. (2004). Excitation lines and the breakdown of Stokes–Einstein relations in supercooled liquids, *Phys. Rev. E* 69(6): 061205.
- Jung, Y., Garrahan, J. & Chandler, D. (2005). Dynamical exchanges in facilitated models of supercooled liquids, *J. Chem. Phys.* 123(8): 084509.
- Karmakar, R. & Samanta, A. (2002a). Solvation dynamics of coumarin-153 in a room-temperature ionic liquid, *J. Phys. Chem. A* 106(18): 4447–4452.
- Karmakar, R. & Samanta, A. (2002b). Steady-state and time-resolved fluorescence behavior of C153 and PRODAN in room-temperature ionic liquids, *J. Phys. Chem. A* 106(28): 6670–6675.

- Kim, D., Jeong, D. & Jung, Y. (2010). Dynamic propensity as an indicator of heterogeneity in room-temperature ionic liquids, *in preparation*.
- Klähn, M., Seduraman, A. & Wu, P. (2008). A model for self-diffusion of guanidinium-based ionic liquids: A molecular simulation study, *J. Phys. Chem. B* 112(44): 13849–13861.
- Kob, W., Donati, C., Plimpton, S., Poole, P. & Glotzer, S. (1997). Dynamical heterogeneities in a supercooled Lennard-Jones liquid, *Phys. Rev. Lett.* 79(15): 2827–2830.
- Kobrak, M. N. (2006). Characterization of the solvation dynamics of an ionic liquid via molecular dynamics simulation, *J. Chem. Phys.* 125(6): 064502.
- Kobrak, M. N. (2007). A comparative study of solvation dynamics in room-temperature ionic liquids, *J. Chem. Phys.* 127(18): 184507.
- Kobrak, M. & Znamenskiy, V. (2004). Solvation dynamics of room-temperature ionic liquids: Evidence for collective solvent motion on sub-picosecond timescales, *Chem. Phys. Lett.* 395(1-3): 127–132.
- Lačević, N., Starr, F., Schröder, T. & Glotzer, S. (2003). Spatially heterogeneous dynamics investigated via a time-dependent four-point density correlation function, *J. Chem. Phys.* 119(14): 7372.
- Lang, B., Angulo, G. & Vauthey, E. (2006). Ultrafast solvation dynamics of coumarin 153 in imidazolium-based ionic liquids, *J. Phys. Chem. A* 110(22): 7028–7034.
- Leonard, S. & Berthier, L. (2005). Lifetime of dynamic heterogeneity in strong and fragile kinetically constrained spin models, *J. Phys.:Condens. Matter* 17(45): S3571–S3577.
- Noda, A., Susan, M. A. B. H., Kudo, K., Mitsushima, S., Hayamizu, K. & Watanabe, M. (2003). Brønsted acid-base ionic liquids as proton-conducting nonaqueous electrolytes, *J. Phys. Chem. B* 107(17): 4024–4033.
- Popolo, M. D. & Voth, G. (2004). On the structure and dynamics of ionic liquids, *J. Phys. Chem. B* 108(5): 1744–1752.
- Richert, R. (2002). Heterogeneous dynamics in liquids: Fluctuations in space and time, *J. Phys.:Condens. Matter* 14(23): R703–R738.
- Rodriguez, H. & Brennecke, J. (2006). Temperature and composition dependence of the density and viscosity of binary mixtures of water + ionic liquid, *J. Chem. Eng. Data* 51(6): 2145–2155.
- Rodriguez Fris, J. A., Alarcon, L. M. & Appignanesi, G. A. (2009). Time evolution of dynamic propensity in a model glass former: The interplay between structure and dynamics, *J. Chem. Phys.* 130(2): 024108.
- Samanta, A. (2006). Dynamic Stokes shift and excitation wavelength dependent fluorescence of dipolar molecules in room temperature ionic liquids, *J. Phys. Chem. B* 110(28): 13704–13716.
- Shim, Y., Choi, M. & Kim, H. (2005a). A molecular dynamics computer simulation study of room-temperature ionic liquids. I. Equilibrium solvation structure and free energetics, *J. Chem. Phys.* 122(4): 044510.
- Shim, Y., Choi, M. & Kim, H. (2005b). A molecular dynamics computer simulation study of room-temperature ionic liquids. II. Equilibrium and nonequilibrium solvation dynamics, *J. Chem. Phys.* 122(4): 044511.
- Shim, Y., Jeong, D., Choi, M. & Kim, H. (2006). Rotational dynamics of a diatomic solute in the room-temperature ionic liquid 1-ethyl-3-methylimidazolium hexafluorophosphate, *J. Chem. Phys.* 125(6): 061102.

- Shim, Y., Jeong, D., Manjari, S., Choi, M. Y. & Kim, H. J. (2007). Solvation, solute rotation and vibration relaxation, and electron-transfer reactions in room-temperature ionic liquids, *Acc. Chem. Res.* 40(11): 1130–1137.
- Shim, Y. & Kim, H. (2009). Adiabatic electron transfer in a room-temperature ionic liquid: Reaction dynamics and kinetics, *J. Phys. Chem. B* 113(39): 12964–12972.
- Szamel, G. & Flenner, E. (2006). Time scale for the onset of Fickian diffusion in supercooled liquids, *Phys. Rev. E* 73(1): 11504.
- Tsuda, T. & Hussey, C. L. (2007). Electrochemical applications of room-temperature ionic liquids, *Interface* 16: 42–49.
- Wang, P., Zakeeruddin, S., Moser, J. & Gratzel, M. (2003). A new ionic liquid electrolyte enhances the conversion efficiency of dye-sensitized solar cells, *J. Phys. Chem. B* 107(48): 13280–13285.
- Wang, Y., Jiang, W., Yan, T. & Voth, G. A. (2007). Understanding ionic liquids through atomistic and coarse-grained molecular dynamics simulations, *Acc. Chem. Res.* 40(11): 1193–1199.
- Wang, Y. & Voth, G. (2005). Unique spatial heterogeneity in ionic liquids, *J. Am. Chem. Soc.* 127(35): 12192–12193.
- Weingärtner, H. (2008). Understanding ionic liquids at the molecular level: Facts, problems, and controversies, *Angew. Chem. Int. Ed.* 47(4): 654–670.
- Widmer-Cooper, A. & Harrowell, P. (2006). Predicting the long-time dynamic heterogeneity in a supercooled liquid on the basis of short-time heterogeneities, *Phys. Rev. Lett.* 96(18): 185701.
- Widmer-Cooper, A. & Harrowell, P. (2007). On the study of collective dynamics in supercooled liquids through the statistics of the isoconfigurational ensemble, *J. Chem. Phys.* 126(15): 154503.
- Widmer-Cooper, A., Harrowell, P. & Fynewever, H. (2004). How reproducible are dynamic heterogeneities in a supercooled liquid?, *Phys. Rev. Lett.* 93(13): 135701.
- Widmer-Cooper, A., Perry, H., Harrowell, P. & Reichman, D. R. (2008). Irreversible reorganization in a supercooled liquid originates from localized soft modes, *Nature Physics* 4(9): 711–715.
- Xu, W., Cooper, E. & Angell, C. (2003). Ionic liquids: Ion mobilities, glass temperatures, and fragilities, *J. Phys. Chem. B* 107(25): 6170–6178.
- Zhao, W., Leroy, F., Heggen, B., Zahn, S., Kirchner, B., Balasubramanian, S. & Müller-Plathe, F. (2009). Are there stable ion-pairs in room-temperature ionic liquids? molecular dynamics simulations of 1-n-butyl-3-methylimidazolium hexafluorophosphate, *J. Am. Chem. Soc.* 131(43): 15825–15833.

# Peculiarities of Intramolecular Motions in Ionic Liquids

Alexander I. Kokorin

*N.Semenov Institute of Chemical Physics RAS, Moscow  
Russian Federation*

## 1. Introduction

Room temperature ionic liquids (RTILs) have been studied intensely during last two decades, because they can often be used as green and efficient solvents for many chemical reactions in organic chemistry, for electrochemical applications, and for industrial catalytic and extraction processes (Mamantov & Popov, 1994; Wasserscheid & Welton, 2002, 2008; Rogers & Seddon, 2003; Dyson & Geldbach, 2005; Anastas et al., 2010). RTILs have been investigated with various physical-chemical methods because they can easily interact with different surfaces and chemical environments, that is sure important for practice. For better practical applications, characterization of the transport and solvating properties, of the molecular mobility in RTILs as in a new class of reaction media. Recent studies with the use of different spectroscopic methods form now a new research area, although to date there are rather few reports on fundamental investigations of such systems.

Among various unique properties distinguish ionic liquids from common molecular solvents, such as: high viscosity, a broad liquid temperature range, high thermal stability, negligible vapor pressure, a wide electrochemical window, recyclability, and high solvation ability, the mechanism of molecular motions in RTILs media is of great importance. There are two, from the first view independent, types of reorientation movements: mobility of the whole particle (any molecule or ion, including both ionic parts of RTIL itself and dissolved molecules) and the intramolecular reorganization. Also, historically, all movements are usually divided on rotational and translational with different physical formalism for describing them. Relatively recently it was experimentally shown by Wasserman & Kovarski, 1986; Kovarski, 1997 that there is a certain quantitative correlation between rotational,  $D_{\text{rot}}$ , and translational,  $D_{\text{tr}}$ , diffusion coefficients. Easy to see, that knowledge of such dynamic characteristics for various ionic liquids is very valuable for applications, i.e., in catalysis, organic synthesis, absorption and separation, for electro-chemical processes in RTILs.

Traditional physical and physico-chemical methods present information about various macroscopic (bulk) parameters such as viscosity,  $\eta$ , dielectric constants  $\epsilon$ , dipole moments  $\mu$ , refractive indices  $n_D$ , and some others at different temperatures. Several experimental methods are used for recording molecular dynamic properties in liquid solutions: nuclear magnetic resonance spectroscopy (NMR), fluorescence, ionic conductivity, electron paramagnetic resonance (EPR) spectroscopy, and some others. However, such processes as solvation, chemical interaction between reagents, electron and energy transfer, etc., take

place on a microscopic (molecular) level with non-directed interaction forces (dipole/dipole, ion/dipole forces) and directed interactions (hydrogen bonding, electron pair acceptor-donor interactions) between solute and solvent molecules (Israelachvili, 1991; Reichardt, 2005; Akdogan et al., 2010).

All these processes are much more complex in ionic liquids than in molecular solvents since they consist of cations and anions, which both have their own distinct space interactions. Besides the electrostatic interactions, the RTIL ions can act as hydrogen-bond donors (or acceptors) and also can have hydrophobic interactions, i.e. interact by associating hydrophobic hydrocarbon moieties to avoid an unfavorable polar environment (Israelachvili, 1991). Molecular modeling and computer simulations have been used to describe structures and interactions in some ionic liquids (Pádua et al., 2007). The structural features of several RTILs were described as selforganized phases with some segregation of the charged zones from the non-polar side chain zones, which depend on the length of side chains. Longer side chains form larger non-polar domains, which "diluted" the electrostatic interactions between the charged groups (zones), similar to micellar arrangements of surfactants in water (Tokuda et al., 2005). Evidently, the existence of two kinds of domains in ionic liquids determines different solvation of various solutes by RTILs according to their polarity, charges and also the hydrophobic aliphatic chains.

The 1-alkyl-3-methylimidazolium ionic liquids can be depicted in general as it is shown in Fig. 1, where  $A^-$  is an anion, and  $C_n^+$  means a cation alkyl group  $C_nH_{2n+1}$ . All RTILs of this line have common abbreviations: Mmim $^+A^-$ , or simply MmimA ( $n = 1$ , M is methyl), EmimA ( $n = 2$ , E is ethyl), PmimA ( $n = 3$ , P is propyl), BmimA ( $n = 4$ , B is butyl), HmimA ( $n = 6$ , H is hexyl), OmimA ( $n = 8$ , O is octyl), DmimA ( $n = 10$ , D is decyl), etc.

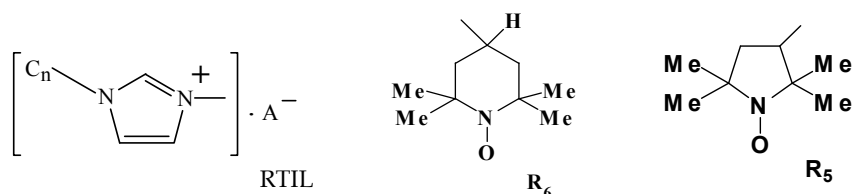


Fig. 1. The imidazoline ionic liquid structure and a paramagnetic fragments  $-R_6$  and  $-R_5$

One of the most powerful methods for investigation the structure, spatial organization and physical-chemical properties of complex and supramolecular systems on the microscopic, molecular level is EPR spectroscopy in its spin label/probe technique variant (Berliner, 1976; Buchachenko & Wasserman, 1976; Likhtenstein, 1976). Usually, nitroxide radicals of different structure were used for studying of structural peculiarities of ionic liquids and the mobility of spin probes in them. We will discuss shortly the most important results obtained by different authors below.

Seems, the first paper on the EPR study of RTIL Emim $^+I^-$ , was published by Noël et al., 1992. EPR spectra of 2,2,6,6-tetramethylpiperidin-1-yl ( $R_6H$ , see Fig. 1) and of 4-amino-2,2,6,6-tetramethylpiperidin-1-yl ( $R_6NH_2$ ) were obtained at several temperatures, and the rotational correlation time values,  $\tau_c$ , were plotted vs. Stokes coordinates  $T/\eta$ , where  $T$  is the absolute temperature, and  $\eta$  is a macroscopic viscosity. In the molecular solution, mineral oil, the rotational correlation time of  $R_6NH_2$  was ca. 30 times longer than for  $R_6H$ .



This was explained as the result of a specific interaction of the RTIL ions with the  $\text{NH}_2$  moiety of  $\text{R}_6\text{NH}_2$  contrary to  $\text{R}_6\text{H}$ .

Polarity of several ionic liquids was examined by  $^{14}\text{N}$  hyperfine coupling constant of nitroxide radical measured by EPR method. Polarity parameters measured from EPR data agreed well with those by solvatochromic dyes, and it was judged that EPR spectroscopy is another valuable technique for the determination polarity of ionic liquids (Kawai et al., 2004).

A combined electrochemical and EPR spectroscopic study has been applied to investigate the translational and rotational diffusion of probe molecule  $\text{R}_6\text{H}$  in five RTILs (Evans et al., 2005). It was revealed that two types of motion, rotation and translational diffusion, were followed an Arrhenius dependence on the temperature. In the isotropic RTILs, the activation energies calculated from Arrhenius plots for the translational diffusion coefficient  $D_{\text{tr}}$ , obtained by electrochemical measurements, correlation time  $\tau_c$  and solvent viscosity  $\eta$  were essentially equivalent in a given ionic liquid. In two ionic liquids containing the tris(*n*-hexyl)tetradecylphosphonium cation, however, the rotational activation energies,  $E_{\text{rot}}$ , were determined to be 5–10 kJ/mol lower than those estimated from simple hydrodynamic model and translational diffusion. The authors explained this due to the adoption of a more ordered bilayer structure in these systems consisting of alternating ionic and lipophilic regions: the discrepancy in the activation energies reflected the more significant proportion of time, which spin probes spend rotating in the non-polar areas (Evans, et al., 2005).

The rotational and translational movements of several different spin probes ( $\text{R}_6\text{H}$ ,  $\text{R}_6\text{OH}$ ,  $\text{R}_6\{\text{N}(\text{CH}_3)_3\}^+\text{I}^-$ ) in various RTILs ( $[\text{C}_n\text{H}_{2n+1}]\text{mim}^+\text{A}^-$  at  $n = 2, 4-10$  and  $\text{A}^- = \text{BF}_4^-, \text{PF}_6^-$ ) at 293 K were carried out in (Stoesser et al., 2006; Strehmel et al., 2006). Analysis of EPR spectra showed that the mentioned spin probes as well as  $^{15}\text{N}$ - $\text{R}_6\text{H}$  and completely deuterated  $^{15}\text{N}$ - $\text{R}_6\text{O-D}_{17}$  allowed obtain qualitative information about microviscosity and micropolarity of ionic liquids. Rotational correlation times  $\tau_c$  and hyperfine coupling constant  $a$  of the probes were obtained by computer simulation of the EPR spectra. The idea of “microviscosity effects” allowed the authors explain the spin probe behavior in RTILs. Investigation of spin exchange of  $\text{R}_6\text{H}$ ,  $\text{R}_6\text{OH}$ , and  $\text{R}_6\{\text{N}(\text{CH}_3)_3\}^+\text{I}^-$  dissolved in ionic liquids showed a tendency of probes aggregation in the case of the nonpolar  $\text{R}_6\text{H}$ . It was surprising that authors did not calculate the spin exchange rate constants  $k_e$  at least in some cases: this could put the work to the quantitative level. Two different kinds of species (isolated and aggregated ones) were observed in the case of polar spin probes  $\text{R}_6\text{OH}$  and  $\text{R}_6\{\text{N}(\text{CH}_3)_3\}^+\text{I}^-$ . EPR tomography investigations of lateral diffusion of spin probes in RTILs corresponded to the results obtained in rotational diffusion experiments (Stoesser et al., 2006).

Dynamic line broadening effects caused by electron-self exchange reactions within the methylviologene redox couple  $\text{MV}^{++} \leftrightarrow \text{MV}^{\bullet+}$  have been studied by EPR spectroscopy in ionic liquids  $\text{BmimBF}_4$ ,  $\text{BmimPF}_6$ , and  $\text{Emim}^+[\text{SO}_4(\text{C}_2\text{H}_5)]^-$  (Grampp et al., 2006). In this case, methylviologene radicals,  $\text{MV}^{\bullet+}$ , acted as specific spin probes with well-resolved EPR spectra. The temperature dependences of the EPR coupling constants were similar to those measured in usual organic solvents, and allowed estimate the activation energy values in the range of 27.4 kJ/mol in  $\text{Emim}^+[\text{SO}_4(\text{C}_2\text{H}_5)]^-$  to 42.1 kJ/mol in  $\text{BmimPF}_6$ , respectively. Such large values of thermodynamic constants,  $E_a$ , are also reported in (Chumakova et al., 2010).

Structural and dynamic microheterogeneity of  $\text{OmimBF}_4$  were observed by EPR spectroscopy using  $\text{R}_6\text{OH}$  spin probe at low ( $c_1 = 4.6 \cdot 10^{-3}$  M) and high ( $c_2 = 5.3 \cdot 10^{-2}$  M) concentrations (Pergushov et al., 2009). In the experiments with increasing temperature over

77 K, the authors observed that practically all spin probes (within the accuracy of EPR spectra recording) were concentrated in the areas with very high concentration ( $c_3 \approx 1.0$  M) in a narrow temperature range at  $210 \pm 10$  K. The mechanism of this effect was discussed in the paper but was not proved by independent other experimental methods. It is interesting that microstructuring of this RTIL occurs at temperatures which are at 10–50 K higher than  $T_g$  - the glass transition temperature of OmimBF<sub>4</sub>.

Results of the EPR study of rotational diffusion ( $\tau_c$ ) in viscous ionic liquids: BmimBF<sub>4</sub> and BmimPF<sub>6</sub> with proxyl radical (R<sub>5</sub>COOH) in a molecular and anionic forms were analysed in (Miyake et al., 2009). The experimental average  $\tau_c$  values and activation energies for rotational diffusion disagreed with those calculated from fractional Stokes-Einstein-Debye equations.

The effects of halides, carbon dioxide and water on the physical properties of Emim<sup>+</sup>[(CF<sub>3</sub>SO<sub>3</sub>)<sub>2</sub>N]<sup>−</sup> have been extensively studied by Barrosse-Antle et al., 2009. The system was studied using cyclic voltammetry, chronoamperometry, and EPR spectroscopy. Diffusion coefficients in the pure and CO<sub>2</sub>-saturated ionic liquid revealed a decrease in activation energy  $E_{a_{tr}}$  of translational diffusion from 29.0 to 14.7 kJ/mol, suggesting a reduction in the viscosity of the RTIL with addition of CO<sub>2</sub>. EPR spectroscopy was used to calculate  $\tau_c$  coefficients of a spin probe R<sub>6</sub>H. Arrhenius plots of  $\tau_c$  in the pure and CO<sub>2</sub>-saturated RTIL resulted in a similar drop in  $E_{a_{rot}}$  from 28.7 to 18.2 kJ/mol. It was concluded that the voltammetric response of the electroactive species in RTILs is not independent of other solutes.

The influence of the alkyl chain length in 1-alkyl-mim [(CF<sub>3</sub>SO<sub>3</sub>)<sub>2</sub>N]<sup>−</sup>, alkyls are: C<sub>n</sub>H<sub>2n+1</sub>, n = 1, 2, 3, 4, 6, 8, 10, on the rotation of piperidine-1-yloxy (R<sub>6</sub>−) derivatives substituted in the fourth position has been reported in (Strehmel et al., 2010). The substitution was done with either hydrogen bonding OH- group (R<sub>6</sub>OH) or with ionic fragments, such as the cationic (R<sub>6</sub>{N(CH<sub>3</sub>)<sub>3</sub>}<sup>+</sup>I<sup>−</sup>, R<sub>6</sub>{N(CH<sub>3</sub>)<sub>3</sub>}<sup>+</sup>(CF<sub>3</sub>SO<sub>2</sub>)<sub>2</sub>N<sup>−</sup>) or the anionic sulfate group (R<sub>6</sub>SO<sub>4</sub><sup>−</sup>K<sup>+</sup>). Structural variation of the ionic liquids resulted in differences of their viscosity influenced the rotation  $\tau_c$  values of the spin probes. The average rotational correlation times  $\tau_c^{aver}$  of the spin probes dissolved in RTILs depended strongly on the substituent in 4<sup>th</sup> position in the piperidine ring.  $\tau_c$  values depended linearly on the ionic liquid viscosity in the case of the R<sub>6</sub>OH probe forming hydrogen bonding with the RTILs, while in contrast to this, a deviation from the Stokes–Einstein behavior was found in the case of rotation of the charged spin probes in the ionic liquid with an alkyl chain longer hexyl, i.e., with  $n \geq 6$ . This effect was explained by phase separation on a molecular level between the charged part of the RTIL and the long alkyl chains bound to the imidazolium ion. The anionic spin probes strongly interacted with the imidazolium ion (Strehmel et al., 2010).

The solvation of nitroxide radicals in ionic liquids studied by high-field EPR spectroscopy was investigated in (Akdogan et al., 2010). Better to understand of RTILs solvating spin probes of different chemical structure, a pulsed high-field EPR spectroscopy at W-band ( $\approx 94$  GHz) and continuous wave EPR at X-band ( $\approx 9.4$  GHz) were used. Three spin probes with various substitutes at the 4-position of the nitroxide ring: R<sub>6</sub>OH, R<sub>6</sub>{N(CH<sub>3</sub>)<sub>3</sub>}<sup>+</sup>I<sup>−</sup>, and R<sub>6</sub>COO<sup>−</sup>Na<sup>+</sup> were dissolved in imidazolium RTILs: EmimBF<sub>4</sub>, BmimBF<sub>4</sub>, BmimPF<sub>6</sub>, HmimBF<sub>4</sub>, as well as in molecular solvents (methanol, water-glycerol). The rotational motion of the charged spin probes in RTILs was about fivefold slower than that of R<sub>6</sub>OH. The anion variation from BF<sub>4</sub><sup>−</sup> to PF<sub>6</sub><sup>−</sup> in RTILs decreased the rotational mobility measured by  $\tau_c$ . The use of high-field EPR gave very important, especially for the EPR spectra

simulation, spin-Hamiltonian parameters of the Zeeman,  $\hat{g}$ , and hyperfine,  $\hat{A}$ , tensors of several radicals dissolved in ionic liquids. Possible environment of spin probes was proposed. The  $R_6\text{COO}^-$  probe was sensitive to the length of alkyl group, i.e., this probe should be close to the nonpolar region of RTILs. These results showed that spin probes used could report about their localization in different RTIL domains with different dielectric properties. These results are in good agreement with a nanophase separation model discussed in literature.

Unfortunately, all measurements in two last perfect works were done at room temperature, and the energetic parameters could not be determined. Also, the authors did not try to simulate EPR spectra, therefore, they could operate only with average rotational correlation time constants  $\tau_c^{\text{aver}}$ , while it was recently proved that  $\tau_c$  values differ noticeably for the rotation around x-, y- and z-axes in the case of imidazolium ionic liquids (Chumakova et al., 2010). Indeed,  $\tau_c^{\text{aver}} = (\tau_c^x \cdot \tau_c^y \cdot \tau_c^z)^{1/3}$  or  $\tau_c^{\text{aver}} = [\tau_c^{\parallel} \cdot (\tau_c^{\perp})^2]^{1/3}$ , where  $\tau_c^x$ ,  $\tau_c^y$ ,  $\tau_c^z$  correspond to the appropriate axes, and  $\tau_c^{\parallel}$  and  $\tau_c^{\perp}$  are  $\tau_c$  values in the case of the axial rotation; the same relations are correct for the rotational diffusion coefficients  $D_{\text{rot}}^{\text{aver}}$  (Schneider & Freed, 1989; Akdogan et al., 2010). Therefore, the results obtained in (Strehmel et al., 2010; Akdogan et al., 2010) are qualitative but not quantitative.

We would like to stress that in all these publications the authors investigated peculiarities of the rotational and translational diffusion of spin-probe molecules in various room temperature ionic liquids, compared them with molecular dynamics in common organic solvents. Correlations with Stokes-Debye-Einstein or Stokes-Einstein laws were found. Areas in RTILs (polar, non-polar), in which spin probes (hydrophilic, charged, hydrophobic) are localized were determined. Just recently, attention of the scientists was attracted to another type of molecular motions in the ionic liquids (Tran et al., 2007a, 2009). Such processes as well as solvent effects on them can be examined in detail by EPR spectroscopy with the use of stable nitroxide biradicals (Parmon et al., 1977a, 1980).

Solvent effects on intramolecular electron spin exchange in biradicals have been investigated in various solvents, including Bmim<sup>+</sup>PF<sub>6</sub><sup>-</sup>, by electron spin resonance (ESR) spectroscopy at room temperature (Tran et al., 2007a). Using biradicals contained different radical fragments and bridges of various length and composition, it was demonstrated that interactions among solvent molecules and biradicals took place at the radical fragment and also at the functional group in the connecting bridge. The experimentally measured parameters: the exchange integral  $|J|$  and characteristic time of an intramolecular movements,  $\tau_{\text{eff}}$ , have been compared with solvent viscosity and polarity parameters (macroscopic level) and longitudinal solvent relaxation time (microscopic level). The strong evidence of hydrogen bonding between solvent and different sites of the biradicals was found, in some cases even surpassing the other effects.

Intramolecular electron spin exchange has been studied in detail in Bmim<sup>+</sup>PF<sub>6</sub><sup>-</sup> for four nitroxide biradicals,  $(\text{CH}_2)_5[\text{CONHR}_6]_2$ ,  $R_6\text{--C}\equiv\text{C--C}\equiv\text{C--R}_6$ ,  $(\text{H}_3\text{C}_6)\text{O=P}(\text{OR}_6)_2$ , and  $\text{O=S}(\text{OR}_6)_2$ , as a function of temperature and the nature of the connecting bridge between two  $>\text{NO}^\bullet$  centers (Tran et al., 2009). Temperature variations of the isotropic nitrogen hyperfine splitting (hfs) constant  $a$ , and exchange integral values  $|J/a|$  were measured from EPR spectra. Thermodynamic parameters of the conformational rearrangements were obtained for rigid and flexible biradicals dissolved in Bmim<sup>+</sup>PF<sub>6</sub><sup>-</sup>, and were compared with that in toluene solutions. The analysis of spin exchange in biradicals dissolved in BmimPF<sub>6</sub> showed, and the data were explained as a result of the specific intramolecular conformational

transitions in a biradical molecule. It was revealed that some biradical molecules, which are rather rigid in common molecular solvents, became flexible under the influence of the ionic liquid. Such strange behaviour of these "semi-rigid" molecules needed special investigation and explanation.

Therefore, the main goal of this work is the investigation and analysis of regularities and peculiarities of the intramolecular movements in nitroxide biradicals dissolved in various RTILs, their correlation with macroscopic parameters, first of all, viscosity, and determining their energetic characteristics. To aid in this effort, we have explored the temperature dependence of the dynamic changes in probe molecules of different structure in several RTIL solvents using traditional CW X-band EPR technique. Theoretical aspects, experimental details, obtained results and conclusions will be reported in the following sections.

## 2. Dynamic aspects of the intramolecular electron spin exchange

All biradicals can be conditionally divided by their structural peculiarities of the bridge connecting radical centers, and dynamic properties at three groups: rigid, long-chain flexible, and short chain flexible molecules (Parmon et al., 1980; Kokorin, 2004). Rigid biradicals, in which nitroxide rings bound via acetylene or p-phenylene fragments, can not be useful for studying the intramolecular mobility and transformations (Kokorin, 2004; Kokorin et al., 2006). The short-chain biradicals can reflect only rotational mobility because the only mechanism of intramolecular spin exchange in them is the indirect one, i.e. via a chain of atoms and bonds connecting the radical rings (Parmon et al., 1980; Grampp et al., 2004; Tran et al., 2009). Structural features of such biradicals do not allow realize a straight collision between radical centers of the same molecule, therefore, the direct mechanism of spin exchange is impossible for them. The electron spin exchange in flexible biradicals of the third group, the long-chain biradicals, occurs via direct collisions of the radical centers and the overlapping of the electron orbitals of two unpaired electrons (Parmon et al., 1975; Tran et al., 2007b, 2009). In these conformational transitions take place both translational and rotational motions. This difference in mechanisms of spin exchange is reflected in a formal procedure of determination the dynamic characteristics and thermodynamic parameters for flexible biradicals of different length.

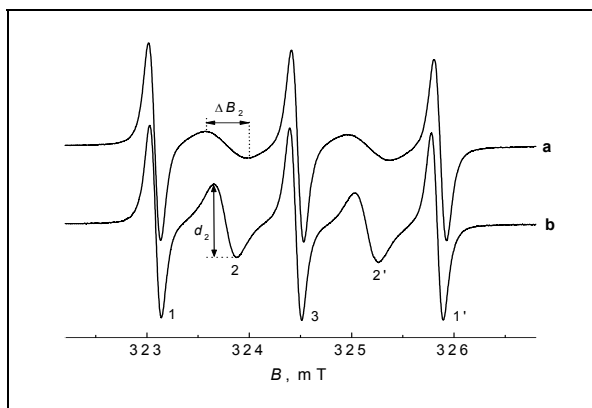


Fig. 2. EPR spectra of biradical I in toluene at 295 (a) and 344 K (b).

Fig. 2 shows typical changes in EPR spectra of long-chain nitroxide biradicals in a molecular solvent. For such flexible rather long-chain molecules, the dynamic properties of the chain can be described as the "cage effect", and they are modeled well by a three-conformational model (Parmon et al., 1975; Tran et al., 2007b). If one attach two nitroxide radicals to the opposite ends of any molecule, it may be possible to characterize the intramolecular movements of the chain and the influence of temperature and solvents on them, measuring parameters of the spin-spin interaction between the unpaired electrons. In the dynamic system, temperature changes of the quintet EPR spectra of flexible biradicals are typical for the case of strong ( $|J| \gg a$ ) exchange among three conformations: an "elongated" conformation A with  $J_A = 0$  (and lifetime  $\tau_A$ ), and two conformations B and C (with total lifetime  $\tau_{BC}$ ), in which the radical fragments are nearby each other in the "cage" of the solvent molecules, but with  $J_B = 0$ , and ( $|J_C| \gg a$ ) (Parmon et al., 1975). The movement of the radical fragments inside the cage is fast, and transitions from outside to inside the cage are slow, i.e.,  $a \cdot \max(\tau_A, \tau_{BC}) > 1$  (Parmon et al., 1975, 1977a). This model allows one to obtain the thermodynamic parameters for the intramolecular transitions in the long-chain biradical. The ratio  $\tau_{BC}/\tau_A$  can be calculated from the experimental EPR spectra by comparison with the integral intensities  $I_2$  and  $I_1$  of the lines 2, 2' and 1, 1' respectively, according to (Parmon et al., 1975):

$$I_2/I_1 \approx d_2(\Delta B_2)^2/d_1(\Delta B_1)^2, \quad (1)$$

where  $d_1$  and  $d_2$  are the amplitudes and  $\Delta B_1$  and  $\Delta B_2$  the widths of lines 1 and 2 (averaged over the lines 1 and 1' or 2 and 2'). It has been obtained that (Parmon et al., 1975).

$$\tau_{BC}/\tau_A = 3(I_2/I_1)/[2 - (I_2/I_1)]. \quad (2)$$

The analysis of the lines 2 and 2' narrowing with temperature allows one to make conclusions about the motion of the radical fragments inside the cage. In the case of the fast modulation of the exchange interaction, the exchange broadening  $1/T_2$  of these lines is described by the expression (Parmon et al., 1980):

$$1/T_2 = a^2\tau_{\text{eff}}/4, \quad (3)$$

where  $\tau_{\text{eff}}$  is a complex combination of the modulation parameters and its value is close to the longest of characteristic times of the intramolecular motions. For the Lorentzian lines (Buchachenko & Wasserman, 1976):

$$a\tau_{\text{eff}} = 2\sqrt{3} |\gamma_e| (\Delta B_2 - \Delta B_1)/a \quad (4)$$

where  $a$  is taken in frequency units and  $\gamma_e$  is the magnetogyric ratio of the free electron. Supposing the Arrhenius dependence between  $\tau_{BC}/\tau_A$ ,  $\tau_{\text{eff}}$  and the temperature  $T$ , we obtain:

$$\tau_{BC}/\tau_A = \exp(\Delta S/R - \Delta H/RT), \quad (5)$$

$$\tau_{\text{eff}} = \tau_0 \exp(\varepsilon/RT), \quad (6)$$

one can calculate the values of the enthalpy  $\Delta H$  and of the entropy  $\Delta S$  of the cage, as well as the parameters  $\varepsilon$  and  $\tau_0$ , which characterize movements inside the cage. Here  $\tau_0$  is the characteristic time of the motions by which a transition between the effective conformation with  $J_B = 0$  and  $|J_C| \gg a$ , would take place at the absence of the activation energy barrier  $\varepsilon$  between them.

For the flexible short-chain biradicals, the temperature changes of the EPR spectra are analogous to those shown in Fig. 2. In this case, changes could be described in terms of the two-conformational model with fast transitions taking place between conformations (Parmon et al., 1980; Grampp et al., 2004). In this model, one conformation is with  $J_1 = 0$  (and lifetime  $\tau_1$ ), and another conformation (with lifetime  $\tau_2$ ) is with  $|J_2| \gg a$ . This model allows one to obtain the thermodynamic parameters for the intramolecular transitions. The analysis of the narrowing of the “exchange” lines (2 and 2' shown in Fig. 2) with temperature results in calculation parameters:  $a\tau_{\text{eff}}$ ,  $\tau_0$  and  $\varepsilon$  using Eqs. (4) and (6) in the case of fast modulation of the exchange interaction, and for the Lorentzian lines (Grampp et al., 2004). Parameters  $\varepsilon$  and  $\tau_0$ , again, characterize the movements inside the biradical molecule.

### 3. Experimental details

Five ionic liquids: OmimPF<sub>6</sub>, OmimBF<sub>4</sub>, BmimBF<sub>4</sub>, BmimPF<sub>6</sub>, and EmimBF<sub>4</sub> (purity  $\geq 98.5\%$  for all of them), were purchased from Fluka for our investigation. The problem of RTILs purity is very important, therefore, in order to remove remaining water, before using, all RTILs were dried at high vacuum ( $< 5 \cdot 10^{-5}$  Torr) at elevated temperatures (50-60°C) during at least 24 h. This set of RTILs should allowed us compare the intramolecular mobility in flexible biradicals in solutions with different viscosity, and also to study influence of the alkyl length, i.e., of the cation nature, as well as of the anion nature. The volume of the RTIL was estimated by measuring the exact mass of the solvent and literature data for the corresponding densities at room temperature. The sample solutions were transferred under argon atmosphere into capillaries of 0.8 mm inner diameter and, after freeze were sealed off in vacuum. This procedure was used to remove molecular oxygen and to prevent the influence of spin exchange between the triplet form, <sup>3</sup>O<sub>2</sub>, and nitroxide radicals.

Three biradicals, (CH<sub>2</sub>)<sub>5</sub>[CONHR<sub>6</sub>]<sub>2</sub> (**I**), O=S(OR<sub>6</sub>)<sub>2</sub> (**II**), and (H<sub>5</sub>C<sub>6</sub>)O=P(OR<sub>6</sub>)<sub>2</sub> (**III**), where R<sub>6</sub> is shown in Fig. 1, were used in this work. Biradical concentrations were kept sufficiently low ( $\leq 2 \cdot 10^{-4}$  M) to eliminate intermolecular exchange broadening (Molin, et al., 1980). EPR spectra were recorded on a Bruker ELEXSYS 560 series spectrometer equipped with an ER 4131VT temperature control system (accuracy  $\pm 0.5$  K) and a field-frequency controlled unit. The sample temperature was varied in the region from 290 to 390 K. In addition, EPR spectra of each sample were recorded at 120 K before and after measuring each temperature series. At least for 10 minutes were allowed for the sample to reach thermal equilibrium with the heat bath before the measurements have been initiated. For each experimental spectrum, the hfs constant  $a$  as well as the line positions, widths and intensities were measured. The modulation amplitude never exceeded 0.2 G to avoid overmodulation of EPR lines.

Parameters of the intramolecular motions at different temperatures  $T$  were compared with the appropriate viscosity value,  $\eta$ . Fig. 1 presents the dependence of  $\eta$  as a function of temperature in Arrhenius co-ordinates for biradical **I** dissolved in OmimBF<sub>4</sub>, OmimPF<sub>6</sub> (Harris et al., 2006), BmimBF<sub>4</sub> (Harris et al., 2007), BmimPF<sub>6</sub> (Harris et al., 2005), and EmimBF<sub>4</sub> (Noda et al., 2001). It is seen from Fig. 1 that the Arrhenius plots are not linear in a wide temperature range, but they are practically linear at temperatures  $320 < T < 390$  K, at which we have studied the exchange behaviour and mobility in biradicals; linearity of  $\ln \eta$  vs.  $T^{-1}$  is typical for usual molecular solvents (Grampp et al., 2004).

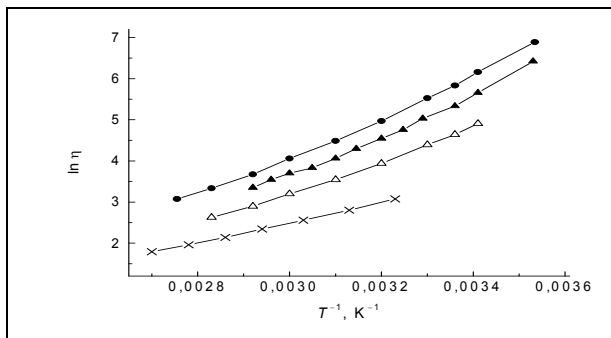


Fig. 3. Viscosity of RTILs  $\eta$  as a function of temperature: EmimBF<sub>4</sub> (x), BmimBF<sub>4</sub> ( $\Delta$ ), OmimBF<sub>4</sub> ( $\bullet$ ), BmimPF<sub>6</sub> ( $\blacktriangle$ )

#### 4. Motions in long flexible molecules

Flexible rather long-chain biradicals with 10 or more bonds in a chain binding two nitroxide radical rings allow modeling both translational and rotational intramolecular motions. Biradical **I** is soluble in various polar and non-polar solvents, therefore, it was chosen for temperatures are given in Fig. 4. Similar spectra have been recorded in many classical solvents earlier (Tran et al., 2007b), as it is seen in Fig. 2, and the temperature behaviours of the spectra is similar in all the solvents, but an interval of these changes sufficiently depends on the solvent nature. EPR spectra presented in Fig. 4 are analogous to that recorded in viscose solvents such as cyclohexanol and 1-octanol (Tran et al., 2007b).

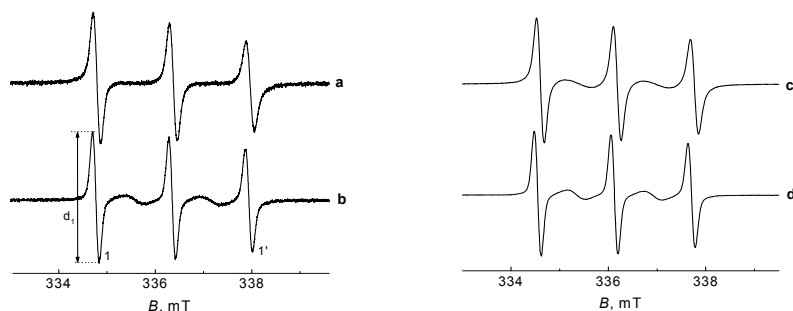


Fig. 4. EPR spectra of biradical **I** in OmimBF<sub>4</sub> at 370 (a), 410 (b), and in BmimPF<sub>6</sub> at 410 (c), 430°K (d).

The hyperfine splitting constant  $a$ , as a function of temperature, for biradicals **I-III**, dissolved in different ionic liquids, is given in Fig 5. One can see that changes of  $a$  with temperature for all biradicals in RTILs are smaller to those in various molecular solvents in the case of piperidine-1-oxyl ring radicals and biradicals (Kokorin, 2004; Kokorin et al., 2006; Tran et al., 2009). It means that the electrostatic interaction between cations and anions of the ionic liquids and paramagnetic  $>\text{N}-\text{O}^\bullet$  groups do not reveal any specific peculiarities in comparison with molecular organic solvents.

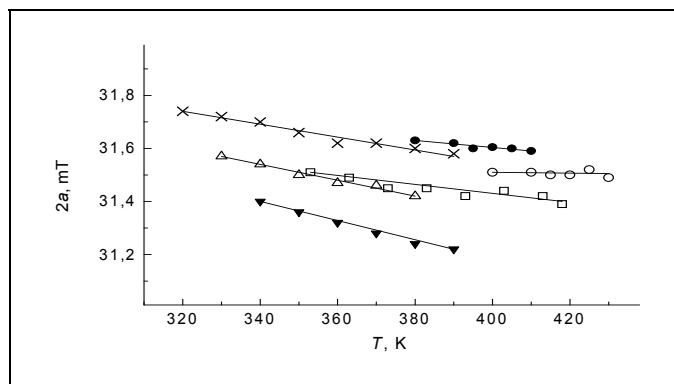


Fig. 5. Hyperfine splitting constant  $a$  as a function of temperature for biradicals **I** in OmimBF<sub>4</sub> (●), BmimPF<sub>6</sub> (○), **II** in OmimPF<sub>6</sub> (▼), BmimBF<sub>4</sub> (Δ), EmimBF<sub>4</sub> (×), and **III** in BmimPF<sub>6</sub> (□).

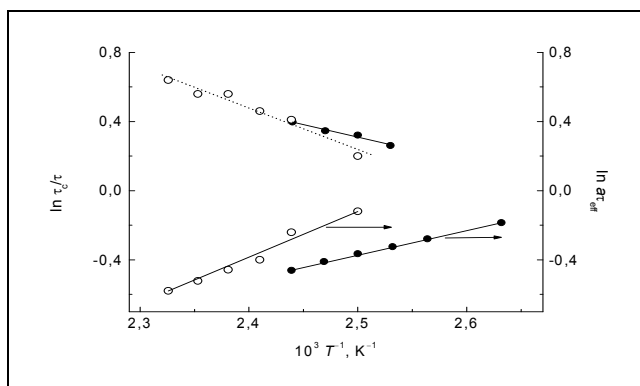


Fig. 6.  $\tau_c/\tau$  and  $a\tau_{\text{eff}}$  as a function of temperature for biradical **I** in OmimBF<sub>4</sub> (●) and BmimPF<sub>6</sub> (○).

Linear temperature dependences of the ratio  $\tau_{\text{BC}}/\tau_{\text{A}}$  and  $a\tau_{\text{eff}}$  on temperature in Arrhenius coordinates (Eqs. 5 and 6) for **I** dissolved in BmimPF<sub>6</sub> and OmimBF<sub>4</sub> are shown in Fig. 6, and thermodynamic parameters  $\Delta H$ ,  $\Delta S$ ,  $\varepsilon$  and  $\tau_0$ , calculated by these equations are given in Table 1. The parameter  $\tau_{\text{BC}}/\tau_{\text{A}}$  increases with temperature, while  $a\tau_{\text{eff}}$  decreases. Temperature changes of  $\tau_{\text{BC}}/\tau_{\text{A}}$  in BmimPF<sub>6</sub> and OmimBF<sub>4</sub> are reasonably larger than in toluene, which themselves are slight since for the long-chain biradicals, the entrance into the cage is mainly connected with steric, i.e. entropic, rather than energetic factors (Parmon et al., 1975; Grampp et al., 2004). One can see that the values of the enthalpy and entropy of the solvent cage formed around the biradical **I** are noticeably larger in the case of RTILs compared with those obtained in toluene (Parmon et al., 1975; Tran et al., 2007b), but also differ for BmimPF<sub>6</sub> and OmimBF<sub>4</sub>. This means that structural rearrangements in ionic liquids, necessary for the conformational changes of **I**, need additional energy for their realization. Only further experiments with variation RTILs and new long-chain biradicals will allow real understanding of the role of RTILs cations and anions in this effect.



Solvent	Temperature range, K	$\Delta H$ , kJ/mol	$\Delta S$ , J/mol K	$\varepsilon$ , kJ/mol	$-\log \tau_0 \pm 0.3$
BmimPF <sub>6</sub>	400-430	$20.0 \pm 2$	$52 \pm 5.4$	$22.0 \pm 0.8$	11.4
OmimBF <sub>4</sub>	380-410	$11.9 \pm 1.2$	$32.4 \pm 3.1$	$11.7 \pm 0.2$	10.2
Toluene <sup>a</sup>	295-344	$3.6 \pm 0.3$	$16.7 \pm 1.8$	$10.6 \pm 0.3$	10.8
Cyclohexanol <sup>a</sup>	354-385	-	-	$28.6 \pm 0.5$	12.4
1-octanol <sup>a</sup>	324-384	-	-	$23.0 \pm 0.3$	11.9
Water <sup>a</sup>	293-364	-	-	$18.9 \pm 0.4$	12.0

<sup>a</sup> Tran et al., 2007b

Table 1. Thermodynamic parameters  $\varepsilon$ ,  $\tau_0$ ,  $\Delta H$ , and  $\Delta S$  for biradical **I** in different solvents

The  $\varepsilon$  value, which characterizes movements inside the cage, is twice larger in BmimPF<sub>6</sub> compared to toluene but similar to the value in aqueous solutions and in viscous alcohols such as 1-octanol or cyclohexanol (Table 1). It is surprising that  $\varepsilon$  in OmimBF<sub>4</sub> is also twice less compared to BmimPF<sub>6</sub>, and very close to a toluene value. Clarifying of these effects will become possible after collecting new results obtained for the same spin probe dissolved in different ionic liquids. Values of  $\log \tau_0$  are still similar to each other as it has been predicted by the theory (Parmon et al., 1973, 1980) and confirmed experimentally for many solvents (Grampp et al., 2004; Tran et al., 2007b).

## 5. Motions in short molecules

Another type of nitroxide biradicals with short and rather rigid bridges between the radical fragments is represented by **II** and **III**. Their EPR spectra at 370 K in different ionic liquids are shown in Fig. 7. During many years, such biradicals were known as rigid molecules, they were investigated and described in several papers and reports (Nakajima et al., 1972; Buchachenko & Wasserman, 1976; Parmon et al., 1980; Kokorin, 2004; Kokorin et al., 1974, 2006), and it was assumed that these molecule are rigid and exist in only one conformation in all solvents used, up to glassy solutions at 77°K (Parmon et al., 1977b, 1980). Weak  $|J/a|$

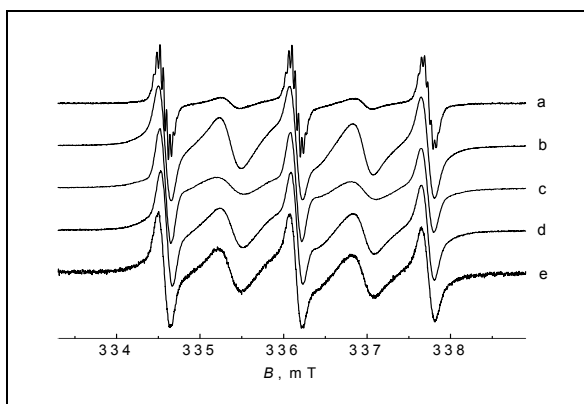


Fig. 7. EPR spectra of biradical **II** in EmimBF<sub>4</sub> (a), BmimBF<sub>4</sub> (b), OmimBF<sub>4</sub> (c), OmimPF<sub>6</sub> (d), and **III** in OmimBF<sub>4</sub> (e) at 370 K.

variations with temperature were explained as specific interactions of solvent molecules with  $>\text{N}-\text{O}^\bullet$  groups or with heteroatoms in the bridge (Kokorin et al., 2006). It should be mentioned that in the case of really rigid molecules with the indirect mechanism of spin exchange, the exchange integral value remains constant at all temperatures and varies slightly only with the solvent polarity or specific solvation (Kokorin et al., 2006).

It should be noted that in  $\text{BmimPF}_6$  at temperatures above 410–420°K, partial destruction of the biradicals takes place, with the appearance of the superimposed three-line EPR spectrum, for all the systems **I–III**. This was revealed by the noticeable increase of the main “nitroxide” lines amplitude in EPR spectra (lines 1, 3 and 1' in Fig. 2). It seems, that thermal decomposition of  $\text{BmimPF}_6$  started at 415–420°K (Huddleston et al., 2001) and the generated products react with biradical paramagnetic centers of **I–III** with formation of the appropriate radicals. The temperature at which such biradical “decay” starts depends on the ionic liquid.

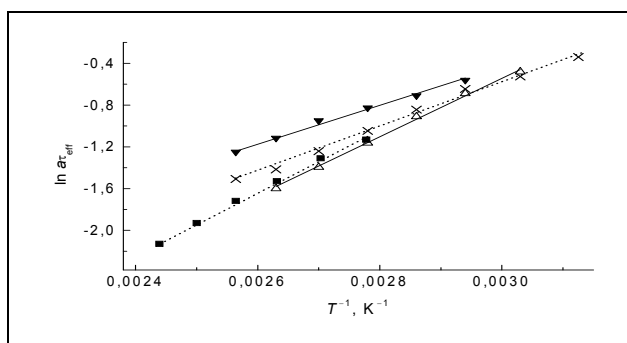


Fig. 8.  $a\tau_{\text{eff}}$  as a function of temperature for biradical **II** in  $\text{OmimPF}_6$  ( $\blacktriangledown$ ),  $\text{BmimBF}_4$  ( $\Delta$ ),  $\text{EmimBF}_4$  ( $\times$ ), and **III** in  $\text{OmimBF}_4$  ( $\blacksquare$ ).

Great difference in the behaviour of the spin exchange in all RTILs studied respectively to common molecular solvents was revealed in the case of the short-chain rather rigid biradicals **II** and **III**. Typical temperature changes in EPR spectra of these biradicals in RTILs (Fig. 7) allowed us calculate the energetic parameters  $\varepsilon$  and  $\tau_0$  of the rotational diffusion from the line width narrowing with the increase of temperature (Fig. 8) using Eq. (6). Such spectral changes can be explained by the model of two conformations with  $J_1 = 0$  and  $|J_2/a| \gg 1$ , and fast transitions between them. Conformation “2” with a large value of the exchange integral is realized at high temperatures. Experimentally measured values of  $\varepsilon$  and  $\tau_0$  are listed in Table 2.

One can see from Table 2 that elongation of the alkyl chain in the RTIL cation from ethyl to octyl at the same anion ( $\text{BF}_4^-$ ) causes the increase of the activation energy  $\varepsilon$  at 10 kJ/mol, while changing the anion,  $\text{BF}_4^-$  to  $\text{PF}_6^-$ , at the same  $\text{Bmim}^+$  seems, does not effect on the  $\varepsilon$  value. From this results, we suppose that these biradical probes are probably localized in hydrophobic areas of RTILs.

We should stress that such behaviour of **II** and **III** in room temperature ionic liquids indicates that the process of spin exchange within these biradicals has changed compared to molecular solvents (Kokorin et al., 2006, 2010): their structure became non-rigid, and intramolecular motions in **II** and **III** could be realized only at high temperatures, although the mechanism of indirect exchange was not changed in RTILs. The spectral changes due to

Biradical	Solvent	Temperature range, K	$\epsilon$ , kJ/mol	$-\log \tau_0$	$E_\eta$ , kJ/mol
<b>II</b>	OmimBF <sub>4</sub>	340-390	$27.8 \pm 1.3$	$13.0 \pm 0.3$	$36.6^d$
	BmimBF <sub>4</sub>	330-380	$23.3 \pm 0.9$	$12.3 \pm 0.2$	$32.7^g$
	EmimBF <sub>4</sub>	320-390	$18.0 \pm 0.6$	$11.6 \pm 0.2$	$20.1^f$
	BmimPF <sub>6</sub> <sup>a</sup>	345-418	$24.0 \pm 2.2$	$12.3 \pm 0.3$	$37.6^{c,e}$
	BmimPF <sub>6</sub> <sup>b</sup>	345-420	$24.5 \pm 2.3$	$12.3 \pm 0.3$	$37.6^{c,e}$
	OmimBF <sub>4</sub> <sup>a</sup>	360-410	$20.8 \pm 2.1$	$12.1 \pm 0.2$	$37.6^{c,e}$
<b>III</b>	OmimBF <sub>4</sub> <sup>a</sup>	360-410	$24.0 \pm 2.2$	$12.5 \pm 0.4$	

<sup>a</sup> Kokorin et al., 2010; <sup>b</sup> Tran et al., 2009; <sup>c</sup> Chiappe & Pieraccini, 2004; <sup>d</sup> Harris et al., 2006; <sup>e</sup> McLean et al., 2002; <sup>f</sup> Noda et al., 2001; <sup>g</sup> Harris et al., 2007

Table 2. Thermodynamic parameters  $\epsilon$  and  $\tau_0$  for biradicals **II** and **III** in different RTILs

modulation of the exchange integral  $|J|$  value with the temperature variations are similar to those observed for analogous short-chain and flexible biradicals: R<sub>6</sub>-NHCH<sub>2</sub>CH<sub>2</sub>-R<sub>6</sub> or R<sub>6</sub>O-S-OR<sub>6</sub> (Parmon et al., 1973, 1980). Seems, this is the first example when the influence of the solvent becomes so strong that rather rigid biradical molecules (**II** and **III**) became significantly more flexible. One may assume that the solvent polarity and other electrostatic parameters of the ionic liquids strongly influence the dynamic and relaxation properties of the dissolved biradicals, causing changes in the intramolecular spin exchange mechanism.

## 6. Comparison with macroscopic parameters

We assume that the experimental  $\Delta H$  and  $\epsilon$  values for **I** in different liquids including ionic liquids qualitatively should correlate, first of all, with the viscosity of the solvent, though the viscosity of BmimPF<sub>6</sub>, for example, is reported as  $\eta = 257.1$  cP at 298 K (Chiappe & Pieraccini, 2004). Indeed, the  $E_\eta$  values, which characterize temperature dependence of  $\eta$ :

$$\ln \eta(T) = \ln \eta_0 + E_\eta/RT, \quad (7)$$

are equal to 37.6, 36.6, 9.1, 15.3 and 41.7 kJ/mol for BmimPF<sub>6</sub>, OmimBF<sub>4</sub>, toluene, water and cyclohexanol, respectively. One can see that they correlate rather well with  $\epsilon$  listed in Table 2 and for  $\epsilon = 28.6$  kJ/mol in cyclohexanol (Tran et al., 2007b). This linear correlation between  $\ln(a\tau_{\text{eff}})$  and  $\ln \eta$  (Kokorin et al., 2010) is valid for different RTILs at rather high temperatures ( $T > 330$  K), when RTIL structure becomes homogeneous enough for spin probes, and structural heterogeneities are already lost (Triolo et al., 2007; Xiao et al., 2007). Which factors of ionic liquids influence the intramolecular spin exchange in biradicals will be clarified after further detail investigations.

One of the most important classical properties of the translational and rotational diffusion is their correlation with Stokes-Einstein and Debye-Stokes-Einstein laws correspondingly. A lot of articles have been published on this topic, and in some cases of ionic liquids and ionic-liquid mixtures their validity was not fulfilled. Therefore, we have analyzed this question in our systems. Dependences of  $\tau_c/\tau$  and  $a\tau_{\text{eff}}$  as a function of Stokes parameter  $T/\eta$  for biradicals **I-III** dissolved in OmimBF<sub>4</sub>, BmimBF<sub>4</sub>, EmimBF<sub>4</sub>, and BmimPF<sub>6</sub> are shown in Figs. 9 and 10. It is seen that linearity of all plots is good enough in all RTILs. The identical dependence for  $\tau_{\text{BC}}/\tau_{\text{A}}$  on  $T/\eta$  is not surprising because viscosities of OmimBF<sub>4</sub> and BmimBF<sub>4</sub> are rather close in this temperature range, and this dynamic process: movements of two radical groups for their collision, relates to translational diffusion. Rather unexpected

was validity of the Debye-Stokes-Einstein correlation for small rotational movements inside the “cage” – this process is really microscopic and its correlation with a macroscopic parameter was not obvious.

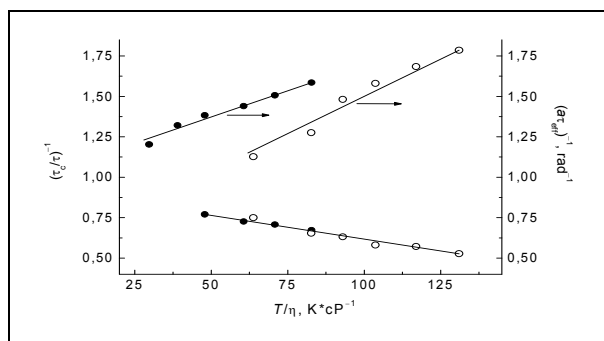


Fig. 9.  $\tau_c/\tau$  and  $a\tau_{\text{eff}}$  as a function of Stokes parameter  $T/\eta$  for biradical **I** in OmimBF<sub>4</sub> (●) and BmimPF<sub>6</sub> (○)

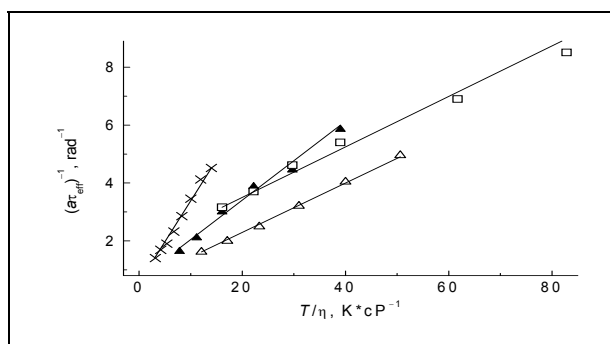


Fig. 10.  $a\tau_{\text{eff}}$  as a function of Stokes parameter  $T/\eta$  for biradical **II** in OmimBF<sub>4</sub> (▲), BmimBF<sub>4</sub> (Δ), EmimBF<sub>4</sub> (×), and **III** in BmimPF<sub>6</sub> (□)

## 7. Conclusion

The behaviour of three stable nitroxide biradicals dissolved in five imidazolium ionic liquids has been studied by EPR spectroscopy. All systems studied revealed relatively good correlation with Stokes-Einstein and Debye-Stokes-Einstein laws. Quantitative differences in thermodynamic parameters and temperature ranges of conformational changes of the biradical molecule are most likely connected to the high viscosity  $\eta$  and the high value of characteristic activation energy  $E_\eta$  of RTILs. Ionic liquids revealed new qualitative features as solvents in the case of short-chain, rather rigid nitroxide biradicals. RTILs performed specific influence on structural rearrangements and features of the intramolecular spin exchange in such biradicals dissolved in RTILs, in comparison with molecular solvents. This specificity was observed in realization of a new type of conformational transitions in such biradicals, which were explained by electrostatic interaction between polar groups of the

biradical and ions forming RTILs. Dynamics of these transitions correlates with viscosity of the ionic liquid at high temperatures and with Stokes parameter.

## 8. Acknowledgement

The author thanks the Russian Foundation for Basic Research (grant 08-03-00478) for financial support of the work. I also thank Drs. N. A. Chumakova, V. I. Pergushov, A. Kh. Vorobiev, G. A. Vorobieva (Moscow, Russia), V. A. Tran, B. Mladenova, K. Rasmussen and Prof. G. Grampp (Graz, Austria) for help in some experiments and useful discussions.

## 9. References

- Akdogan, Y.; Heller, J.; Zimmermann, H. & Hinderberger, D. (2010). The solvation of nitroxide radicals in ionic liquids studied by high-field EPR spectroscopy. *Phys. Chem. Chem. Phys.*, Vol. 12, No. 28, 7874-7882, ISSN 1463-9076
- Anastas, P. T.; Leitner, W.; Jessop, P. G.; Li, C.-J.; Wasserscheid, P. & Stark, A. (2010). *Handbook of Green Chemistry - Green Solvents*, Wiley-VCH, SBN 3-527-31574-8, Weinheim
- Barrosse-Antle, L. E.; Hardacre, C. & Compton, R. G. (2009). Voltammetric currents in room temperature ionic liquids can reflect solutes other than the electroactive species and are influenced by carbon dioxide. *J. Phys. Chem. B*, Vol. 113, No. 9, 2805-2809, ISSN 1089-5647
- Berliner, L. J. (1976). *Spin Labeling. Theory and Applications*, Academic Press, ISBN 0120923505, New York
- Buchachenko, A. L. & Wasserman, A. M. (1976). *Stable Radicals*. Wiley, ISBN 9067642592, London
- Chiappe C. & Pieraccini D. (2004). Kinetic study of the addition of trihalides to unsaturated compounds in ionic liquids. Evidence of a remarkable solvent effect in the reaction of  $\text{ICl}_2$ . *J. Org. Chem.*, Vol. 69, No. 18, 6059-6064, ISSN 0022-3263
- Chumakova, N. A.; Pergushov, V. I.; Vorobiev, A. Kh. & Kokorin, A. I. (2010). Rotational and translational mobility of nitroxide spin probes in ionic liquids and molecular solvents. *Appl. Magn. Reson.*, ISSN 0937-9347 (in press)
- Dyson, P. J. & Geldbach, T. J. (2005). *Metal Catalysed Reactions in Ionic Liquids*, Series: Catalysis by Metal Complexes, Springer, ISBN 978-1-4020-3914-0, Dordrecht
- Evans, R. G.; Wain, A. J.; Hardacre, Ch. & Compton, R. G. (2005). An electrochemical and ESR spectroscopic study on the molecular dynamics of TEMPO in room temperature ionic liquid solvents. *ChemPhysChem*, Vol. 6, No. 6, 1035-1039, ISSN 1439-4235
- Grampp, G.; Kattinig, D. & Mladenova, B. (2006). ESR-spectroscopy in ionic liquids: Dynamic line broadening effects caused by electron-self exchange reactions within the methylviologene redox couple. *Spectrochimica Acta, A*, Vol. 63, No. 4, 821-825, ISSN 1386-1425
- Grampp, G.; Rasmussen, K. & Kokorin, A. I. (2004). Intramolecular spin exchange in short-chain biradicals in solutions with various viscosity. *Appl. Magn. Reson.*, Vol. 26, No. 1-2, 245-252, ISSN 0937-9347
- Harris, K. R.; Kanakubo, M. & Woolf, L. A. (2006). Temperature and pressure dependence of the viscosity of the ionic liquids 1-methyl-3-octylimidazolium hexafluorophosphate

- and 1-methyl-3-octylimidazolium tetrafluoroborate. *J. Chem. Eng. Data*, Vol. 51, No. 3, 1161-1167, ISSN 0021-9568
- Harris, K. R.; Kanakubo, M. & Woolf, L. A. (2007). Temperature and pressure dependence of the viscosity of the ionic liquid 1-butyl-3-methylimidazolium tetrafluoroborate: viscosity and density relationships in ionic liquids. *J. Chem. Eng. Data*, Vol. 52, No. 6, 2425-2430, ISSN 0021-9568
- Harris, K. R.; Woolf, L. A. & Kanakubo, M. (2005). Temperature and pressure dependence of the viscosity of the ionic liquid 1-butyl-3-methylimidazolium hexafluorophosphate. *J. Chem. Eng. Data*, Vol. 50, No. 5, 1777-1782, ISSN 0021-9568
- Huddleston J. G.; Visser A. E.; Reichert W. M.; Willauer H. D.; Broker G. A. & Rogers R. D. (2001). Characterization and comparison of hydrophilic and hydrophobic room temperature ionic liquids incorporating the imidazolium cation. *Green Chem.*, Vol. 3, No. 2, 156-164, ISSN 1463-9270
- Israelachvili, J. N. (1991). *Intermolecular and Surface Forces*, 2nd edn, Academic Press, ISBN 0-12-375181-0, London
- Kawai, A.; Hidemori, T. & Shibuya, K. (2004). Polarity of ionic liquid as examined by EPR spectroscopy. *Chem. Lett.*, Vol. 33, No. , 1464-1465, ISSN 0366-7022
- Kokorin, A. I. (2004). Regularities of the spin-exchange coupling through a bridge in nitroxide biradicals. *Appl. Magn. Reson.*, Vol. 26, No. 1-2, 253-274, ISSN 0937-9347
- Kokorin, A. I.; Tran, V. A. & Vorobieva, G. A. (2010). Features of spin exchange in short-chain nitroxide biradicals in ionic liquids. *Appl. Magn. Reson.*, Vol. 30, No. 1-4, 473-481, ISSN 0937-9347
- Kokorin, A. I.; Parmon, V. N.; Suskina, V. I.; Rozantsev, E. G. & Zamaraev, K. I. (1974). Intramolecular exchange and dipole-dipole interactions in solutions of some iminoxyl biradicals. *Russ. J. Phys. Chem.*, Vol. 48, No. 4, 548-551, ISSN 0036-0244
- Kokorin, A. I.; Tran, V. A.; Rasmussen, K. & Grampp, G. (2006). Effect of solvent nature on spin exchange in rigid nitroxide biradicals. *Appl. Magn. Reson.*, Vol. 30, No. 1, 35-42, ISSN 0937-9347
- Kovarski, A. L. (1997). *Molecular Dynamics of Additives in Polymers*, Brill Academic Pub, ISBN 90-67-64259-2, Utrecht
- Likhtenstein, G. I. (1976). *Spin Labeling Methods in Molecular Biology*, Wiley-Interscience, ISBN 0471534153, New York
- Mamantov, G. & Popov A. I. (1994). *Chemistry of Nonaqueous Solutions, Current Progress*, VCH, ISBN 1560815469, New York
- McLean, A. J.; Muldoon, M. J.; Gordon, C. M. & Dunkin, I. R. (2002). Bimolecular rate constants for diffusion in ionic liquids. *Chem. Comm.*, No. 17, 1880-1881, ISSN 1359-7345
- Miyake, Y.; Hidemori, T.; Akai, N.; Kawai, A.; Shibuya, K.; Koguchi, S. & Kitazume, T. (2009). EPR study of rotational diffusion in viscous ionic liquids: Analysis by a fractional Stokes-Einstein-Debye law. *Chem. Lett.*, Vol. 38, No. 2, 124-125, ISSN 0366-7022
- Molin, Yu. N.; Salikov, K. M. & Zamaraev, K. I. (1980). *Spin Exchange*, Springer-Verlag, ISBN 3-540-10095-4, Berlin, New York
- Nakajima, A.; Ohya-Nishiguchi, H. & Deguchi Y. (1972). Magnetic properties of some iminoxyl polyradicals. III. Exchange interaction in iminoxyl biradicals. *Bull. Chem. Soc. Japan*, Vol. 45, No. 3, 713-716, ISSN 0009-2673

- Noda, A.; Hayamizu, K. & Watanabe, M. (2001). Pulsed-gradient spin-echo  $^1\text{H}$  and  $^{19}\text{F}$  NMR ionic diffusion coefficient, viscosity, and ionic conductivity of non-chloroaluminate room-temperature ionic liquids. *J. Phys. Chem. B*, Vol. 105, No. 20, 4603-4610, ISSN 1089-5647
- Noël, M. A. M.; Allendoerfer, R. D. & Osteryoung, R. A. (1992). Solvation in ionic liquids: An EPR study. *J. Phys. Chem.*, Vol. 96, No. 5, 2391-2394 ISSN 0022-3654
- Pádua, A. A. H.; Gomes, M. F. C. & Lopes, J. N. A. C. (2007). Molecular solutes in ionic liquids: A structural perspective. *Acc. Chem. Res.*, Vol. 40, No. 11, 1087-1096, ISSN 1520-4898
- Parmon, V. N.; Kokorin, A. I. & Zhidomirov, G. M. (1977a). Conformational structure of nitroxide biradicals. Use of biradicals as spin probes. *Russ. J. Struct. Chem.*, Vol. 18, No. 1, 104-147, ISSN 0022-4766
- Parmon, V. N.; Kokorin, A. I. & Zhidomirov, G. M. (1977b). The interpretation of the polycrystalline ESR spectra of nitroxide biradicals. *J. Magn. Res.*, Vol. 28, No. 2, 339-349, ISSN 1090-7807
- Parmon, V. N.; Kokorin, A. I. & Zhidomirov, G. M. (1980). *Stable Biradicals*, Nauka, Moscow
- Parmon, V. N.; Kokorin, A. I., Zhidomirov, G. M. & Zamaraev, K. I. (1973). Evidence of slow exchange in the EPR spectra of nitroxide biradicals. *Molec. Phys.*, Vol. 26, No. 6, 1565-1569, ISSN 0026-8976
- Parmon, V. N.; Kokorin, A. I., Zhidomirov, G. M. & Zamaraev, K. I. (1975). On the mechanism of spin exchange in long-chain nitroxide biradicals. *Molec. Phys.*, Vol. 30, No. 3, 695-701, ISSN 0026-8976
- Pergushov, V. I.; Chumakova, N. A.; Mel'nikov, M. Ya.; Grampp, G. & Kokorin, A. I. (2009). Structural and dynamic microheterogeneity of ionic liquid. *Doklady Physical Chemistry*, Vol. 425, No. 2, 69-72, ISSN 0012-5016
- Reichardt, C. (2005). Polarity of ionic liquids determined empirically by means of solvatochromic pyridinium N-phenolate betaine dyes. *Green Chem.*, Vol. 7, No. 2, 339-351, ISSN 1463-9270
- Rogers, R. D. & Seddon, K. R. (2003). *Ionic Liquids As Green Solvents: Progress and Prospects*, ACS Symposium Series, ISBN 0-8412-3856-1, Washington, DC
- Schneider, D.J. & Freed, J. (1989). *Calculation slow motion magnetic resonance spectra: a user's guide*. In: *Biological Magnetic Resonance*, Berliner, L. J. & Reuben, J. (Eds.), 1-76, Plenum Press, ISBN 0306485060, New York
- Stoesser, R.; Herrmann, W.; Zehl, A.; Laschewsky, A. & Strehmel, V. (2006). Microviscosity and micropolarity effects of imidazolium based ionic liquids investigated by spin probes. Their diffusion and spin exchange. *Z. Phys. Chem.*, Vol. 220, No. 10, 1309-1342, ISSN 0942-9352
- Stoesser, R.; Herrmann, W.; Zehl, A.; Strehmel, V. & Laschewsky, A. (2006). ESR spin probes in ionic liquids. *ChemPhysChem*, Vol. 7, No. 7, 1106-1111, ISSN 1439-4235
- Strehmel, V.; Laschewsky, A.; Stoesser, R.; Zehl, A. & Herrmann, W. (2006). Mobility of spin probes in ionic liquids. *J. Phys. Org. Chem.*, Vol. 19, No. 5, 318-325, ISSN 1099-1395
- Strehmel, V.; Rexhausen, H. & Strauch, P. (2010). Influence of imidazolium bis(trifluoromethylsulfonylimide)s on the rotation of spin probes comprising ionic and hydrogen bonding groups. *Phys. Chem. Chem. Phys.*, Vol. 12, No. 11, 1933-1940, ISSN 1463-9076.

- Tokuda, H.; Hayamizu, K.; Ishii, K.; Sudan, M. A. B. H. & Watanabe, M. (2005). Physicochemical properties and structures of room temperature ionic liquids. 2. Variation of alkyl chain length in imidazolium cation. *J. Phys. Chem. B*, Vol. 109, No. 13, 6103-6110, ISSN 1089-5647
- Tran, V. A.; Rasmussen, K.; Grampp, G. & Kokorin, A. I. (2007a). Solvent effects on the intramolecular spin exchange in biradicals at room temperature. *Molec. Phys.*, Vol. 105, No. 15-16, 2119-2125, ISSN 0026-8976
- Tran, V. A.; Rasmussen, K.; Grampp, G. & Kokorin, A. I. (2007b). The solvent effect on spin exchange in long-chain nitroxide biradicals. *Appl. Magn. Reson.*, Vol. 32, No. 3, 395-406, ISSN 0937-9347
- Tran, V. A.; Kokorin, A. I.; Grampp, G. & Rasmussen, K. (2009). Peculiarities of spin exchange in nitroxide biradicals in the ionic liquid bmimPF<sub>6</sub>. *Appl. Magn. Reson.*, Vol. 35, No. 3, 389-398, ISSN 0937-9347
- Triolo, A.; Russina, O.; Bleif, H.-J. & Di Cola, E. (2007). Nanoscale segregation in room temperature ionic liquids. *J. Phys. Chem. B*, Vol. 111, No. 18, 4641-4644, ISSN 1089-5647
- Wasserman, A. M. & Kovarsky, A. L. (1986). *Spin Labels and Probes in Physical Chemistry of Polymers*. Nauka, Moscow (in Russian)
- Wasserscheid, P. & Welton, T. (2002). *Ionic Liquids in Synthesis*, Wiley-VCH, ISBN 3-527-30515-7, Weinheim
- Wasserscheid, P. & Welton, T. (2008). *Ionic Liquids in Synthesis (Green Chemistry)*, Wiley-VCH, ISBN 978-3-527-31239-9, Weinheim
- Weil, J. A. & Bolton, J. R. (2007). *Electron Paramagnetic Resonance: Elementary Theory and Practical Applications*, Wiley-Interscience, ISBN 978-0-471-75496-1, Hoboken
- Xiao, D.; Rajian, J. R.; Cady, A.; Li, S.; Bartsch, R. A. & Quitevis, E. L. (2007). Nanostructural organization and anion effects on the temperature dependence of the optical Kerr effect spectra of ionic liquids. *J. Phys. Chem. B*, Vol. 111, No. 18, 4669-4677, ISSN 1089-5647



# Atom Substitution Effects in Ionic Liquids: A Microscopic View by Femtosecond Raman- Induced Kerr Effect Spectroscopy

Hideaki Shirota and Hiroki Fukazawa

*Department of Nanomaterial Science & Department of Chemistry  
Chiba University  
Japan*

## 1. Introduction

It is well known that the physical and chemical properties of ionic liquids (ILs) vary when the combination of cations and anions changes. It is thus possible to tune the properties of ILs on demand by choosing a suitable cation and anion combination. Consequently, ILs are commonly referred to as designer fluids. Many studies have demonstrated the usefulness of this strategy for controlling the properties of ILs (Wasserscheid & Welton, 2008; Ohno, 2005). It is possible to systematically examine the physical and chemical properties of ILs by changing an ionic species, while leaving a counter ion unchanged, in order to understand the relationships between an IL's chemical and physical properties and its constituent ion species. Extensive efforts along this line of study have clarified the relationships between the physical and chemical properties and the ionic species.

On the other hand, the effects of replacing an atomic element in an ionic species on the physical and chemical properties of ILs have not been very well understood. It is obvious that one of the main themes in chemistry is to develop an understanding of how chemical and physical properties depend on the atomic elements in molecular liquids as well as in ILs. In 2005, C and Si in a side group of an imidazolium cation (1-methyl-3-neopentylimidazolium: [C-MIm]<sup>+</sup> and 1-methyl-3-trimethylsilylmethylimidazolium: [Si-MIm]<sup>+</sup>) were compared (Shirota & Castner, 2005). The shear viscosities of the silicon substituted ILs are substantially reduced in comparison with those of the respective carbon ILs, when ILs with the same anions are compared. Actually, this feature of ILs is the opposite of that observed in conventional neutral molecular liquids. For example, the shear viscosity of bromobenzene at a standard ambient condition is approximately 1.4 times larger than that of chlorobenzene, and the ambient shear viscosity of diethyl sulfide is approximately 1.9 times larger than that of diethyl ether (Lide, 2008). Heavier atom substitution in the hexafluoropnictogenate anion ([XF<sub>6</sub>]<sup>-</sup>; X: P, As, and Sb) for 1-butyl-3-methylimidazolium ILs also gives a lower shear viscosity (Shirota et al., 2009). In addition to aromatic cation-based ILs, reductions in the shear viscosities of ILs with heavier atoms in the same position were also confirmed in nonaromatic cation-based ILs (Tsunashima & Sugiyama, 2007; Seki et al., 2009; Shirota et al., 2010).

Interionic interaction is a key parameter for determining the physical and chemical properties of ILs. Because the interionic interactions in ILs are delicately balanced between

the attractive and repulsive forces, the salts fit to be a liquid at room temperature. The physical properties of ILs depend on the interionic interaction. Therefore, it is important to gain an in-depth understanding of the molecular-level aspects of the interionic interaction in ILs. Intermolecular vibration in condensed phases is a measure of the microscopic intermolecular interaction. Most intermolecular vibrations in condensed phases are in the frequency range of approximately 1–150  $\text{cm}^{-1}$ . Several groups have studied the interionic vibrations in this low frequency region to reveal the microscopic structure and interaction in ILs using sophisticated time-resolved spectroscopic techniques such as femtosecond Raman-induced Kerr effect spectroscopy (RIKES) (Castner et al., 2007) and terahertz time-domain spectroscopy (THz-TDS) (Asaki et al., 2002; Yamamoto et al., 2007; Koeberga et al., 2007) as well as steady-state low-frequency Raman and far-infrared spectroscopies (Dominguez-Vidal et al., 2007; Iwata et al., 2007; Fumino et al., 2008; Buffeteau et al., 2010). Among these spectroscopic techniques, femtosecond RIKES can cover the frequency range of the intermolecular (interionic) vibrational band in molecular liquids including ILs.

Quitevis and co-workers reported the first RIKES-based study of ILs in 2002 (Hyun et al., 2002). The Quitevis group extensively studied the detailed aspects for the microstructures of neat ILs (Xiao et al., 2009; Russina et al., 2010), as well as binary IL mixtures (Xiao et al., 2006; Xiao et al., 2007; Xiao et al., 2008). They also reported a temperature dependent experiment (Rajian et al., 2004). Wynne and co-workers examined the interionic vibrational dynamics in some imidazolium cation-based ILs with different cation and anion combinations and found that an anion substitution produced a significant difference in the interionic vibrations of the ILs (Giraud et al., 2003). A similar feature was also observed in nonaromatic cation-based ILs (Shirota et al., 2005). Wynne's group also compared the low-frequency Kerr spectra of a few ILs with the spectra measured by THz-TDS and dielectric spectroscopy (Turton et al., 2009). We demonstrated some comparative studies such as IL vs. neutral binary solution (Shirota & Castner) and ILs vs. concentrated electrolyte solutions (Fujisawa et al., 2009) using femtosecond RIKES to bring out the unique natures of the ILs. Several novel silyl- and siloxy-group-substituted imidazolium-based ILs were also compared (Shirota et al., 2007). Fayer and co-workers focused on the slower dynamical processes, which included  $\alpha$ - and  $\beta$ -relaxations and the crossover process between intermolecular vibrations and  $\alpha$ -relaxation, and examined the adequacy of the mode coupling theory for several imidazolium-based ILs (Cang, 2003; Li, 2006). Some theoretical studies based on molecular dynamics (MD) simulations further explored deeper molecular aspects of the intermolecular dynamics of ILs reported in the experimental studies. Urahata and Ribeiro performed MD simulations for some imidazolium-based ILs and compared their results with the experimental data reported by Wynne and co-workers (Urahata & Ribeiro, 2005). Their study showed that the density of states profile for the cation was similar to the experimental Kerr spectrum shape. Hu et al. also computed the Kerr spectrum of 1-methoxyethylpyridinium dicyanamide and compared it with the experimental Kerr spectrum (Hu et al., 2008). They showed the importance of the interaction-induced motion on nanosecond timescale, which is not dominant for neutral molecular liquids. Although these studies reveal detailed molecular aspects of the ultrafast dynamics in ILs and help to provide a better and deeper understanding of ILs, we will focus on the heavy atom substitution effects in ILs rather than the studies in this chapter. We will provide an overview of the heavy atom substitution effects in ILs on some static physical properties and will discuss the features using the microscopic interionic interaction investigated by measuring the interionic vibrations with femtosecond RIKES.

## 2. Femtosecond Raman-induced Kerr effect spectroscopy: principle and data analysis

Femtosecond RIKES is a third-order nonlinear spectroscopic technique (McMorrow et al., 1988; Lotshaw et al., 1995; Righini, 1993). This spectroscopic technique can be used to observe the molecular motions such as the reorientation and inter- and intramolecular vibrations in time domain within a range of approximately  $10^{-14}$  to  $10^{-9}$  s. Fig. 1 shows a schematic diagram of the basic principle of femtosecond RIKES. The first (pump) pulse produces a vibrational coherence between  $\omega_1$  and  $\omega_2$  (impulsive Raman process). Then, the second (probe) pulse, which arrives at time  $\tau$  from the first pulse, induces the Raman scattering,  $\omega_s$ . It should be noted that a femtosecond laser pulse is sufficiently short in time domain to obtain a wide spectrum in frequency domain, which shows the intermolecular vibrations and some intramolecular vibrational modes with the frequencies smaller than  $\omega_1 - \omega_2 (\leq \nu_n)$ . Typical femtosecond RIKES can be used to detect the signal by mixing it with a local oscillator. This method is referred to as the optical heterodyne detection and is used to enhance the signal and obtain a linear response to the signal polarization/electric field (Mukamel, 1995). This pump-probe spectroscopic technique is also referred to as optical Kerr effect (OKE) spectroscopy. The difference between the two spectroscopic techniques is attributed to the number of light sources (different colors) used. However, if the light source is a spectrally broad pulse such as a femtosecond pulse, the two spectroscopic techniques are interchangeable. We use the acronym RIKES for the spectroscopic technique in this chapter.

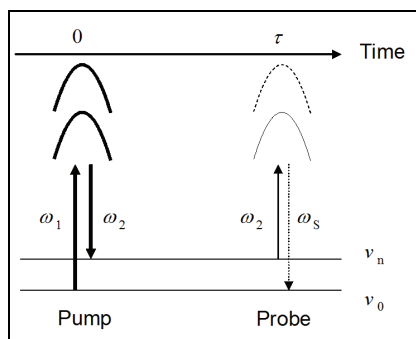


Fig. 1. Schematic diagram of Raman-induced Kerr effect signal.

Femtosecond RIKES can provide a high-quality low-frequency spectrum with the frequency range of approximately  $0.2\text{--}750\text{ cm}^{-1}$  via Fourier-transform deconvolution analysis (McMorrow & Lotshaw, 1990; McMorrow & Lotshaw, 1991). As an example, Fig. 2 shows the Kerr transient and the Fourier-transform Kerr spectra of ethylbenzene. The femtosecond RIKES directly captures a Kerr transient in time domain, as shown in Fig. 2a. In time-domain data, the diffusive orientational relaxation with a timescale greater than a few picoseconds is often characterized by a multi-exponential function (a biexponential function in the case of ethylbenzene, as shown in Fig. 2a). The Kerr transient is then analyzed by carrying out a Fourier-transform deconvolution procedure using the instrument's response, which is characterized by the cross correlation of the pump and probe pulses in a RIKES system. A Fourier-transform Kerr spectrum with the frequency range of  $0\text{--}750\text{ cm}^{-1}$  is shown

in Fig. 2b. Clear intramolecular vibrational modes are observed at 156, 486, 556, and 621  $\text{cm}^{-1}$ . The broad band located in below 150  $\text{cm}^{-1}$  is caused by the intermolecular vibrations. In order to discuss the intermolecular vibrational band, the contribution of the diffusive orientational relaxation ( $\tau_2$ ) is subtracted from the entire Kerr spectrum. An enlarged view of the low frequency region is shown in Fig. 2c. It should be noted that the depolarization condition is used for the RIKES setups discussed here (the polarization angles are  $0^\circ$  for the pump,  $+45^\circ$  for the probe, and  $-45^\circ$  for the analyzer). Accordingly, the diffusive orientational relaxation for a spherical molecule is forbidden, and the isotropic vibrational modes are silent for this spectroscopic condition. It is also possible to detect the isotropic vibrational modes by changing the polarization angles for the spectroscopic setup (Khalil et al., 2000; Wiewior et al., 2002; Heisler & Meech, 2010).

Line-shape analysis is also carried out to characterize the Kerr spectra. A common model used to fit a low-frequency Kerr spectrum is the sum of the Bucaro-Litovitz ( $I_{\text{BL}}(\omega)$ ) (Bucaro & Litovitz, 1971) and antisymmetrized Gaussian functions ( $I_{\text{G}}(\omega)$ ) (Chang & Castner, 1993).

$$I_{\text{BL}}(\omega) = A_{\text{BL}} \omega^\alpha \exp(-\omega/\omega_{\text{BL}}) \quad (1)$$

$$I_{\text{G}}(\omega) = A_{\text{G}} \{ \exp[-2(\omega - \omega_{\text{G}})^2/\Delta\omega_{\text{G}}^2] - \exp[-2(\omega + \omega_{\text{G}})^2/\Delta\omega_{\text{G}}^2] \} \quad (2)$$

where  $A_n$  is the amplitude parameter,  $\omega_n$  is the characteristic frequency parameter, and  $\Delta\omega_n$  is the width parameter for the model functions. When the index  $\alpha$  in Eq. 1 is unity, the function is an Ohmic function. We used an Ohmic function rather than a Bucaro-Litovitz function to fit the Kerr spectra for simplicity. The Bucaro-Litovitz function was developed to express the depolarized light scattering in atomic and molecular liquids (Bucaro & Litovitz, 1971). The antisymmetrized Gaussian function is assumed to be an inhomogeneously broadened vibrational mode (often regarded as a librational mode) and has been empirically used to fit the low-frequency Kerr spectrum in molecular liquids (Chang & Castner, 1993). In reality, the model functions do not express the shape of a motion in spectrum, but this analysis is useful to qualitatively discuss the spectral feature. Although the multi-mode Brownian oscillator model (Tanimura & Mukamel, 1993; Nagata & Tanimura, 2006) is also commonly used to characterize the low-frequency spectra (Giraud et al., 2003; Shirota et al., 2005), the former analytical model is used throughout this chapter.

Most of the earlier femtosecond RIKES studies were conducted to clarify the intermolecular vibrational and orientational dynamics in pure molecular liquids and binary mixtures (Kinoshita et al., 1996; Castner & Maroncelli, 1998; Smith & Meech, 2002; Zhong & Fourkas, 2008; Shirota et al., 2009). Nowadays, femtosecond RIKES is also used to study the intermolecular vibrational dynamics, reorientation, and microscopic intermolecular interactions of complex condensed phases (Hunt et al., 2007; Farrer & Fourkas, 2003) such as polymer liquids and solutions, microemulsions, aqueous protein films and solutions, and solvents in nanoporous glasses. As mentioned above, femtosecond RIKES has also been used to investigate ILs (Castner et al., 2007).

The details of the femtosecond RIKES setups used for the studies described in this chapter have been reported elsewhere (Wiewior et al., 2002; Shirota, 2005; Shirota et al., 2009). In short, the light sources for the setups were titanium:sapphire lasers pumped by approximately 3.5 W of 532-nm light from a neodymium:vanadate laser (Spectra Physics). The center wavelength of the titanium:sapphire lasers was 800–810 nm, with a full width at half maximum value of ca. 60 or 75 nm and a repetition frequency of ca. 85 MHz. The output

power was 300–350 mW. The temporal response for the femtosecond RIKES setups was approximately 30–40 fs.

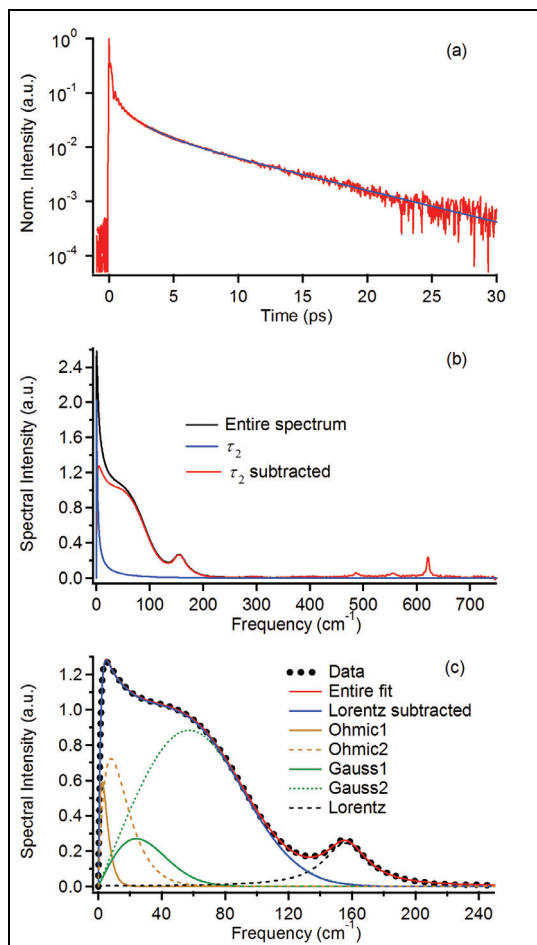


Fig. 2. (a) Kerr transient of liquid ethylbenzene (red) and its biexponential fit (blue). The fit starts from 3 ps. (b) Fourier-transform Kerr spectrum (black), contribution of the slowest relaxation time  $\tau_2$  (blue), and  $\tau_2$ -subtracted Kerr spectrum (red). (c) Magnification of the  $\tau_2$ -subtracted Kerr spectrum. The black dotted line, red line, brown lines, green lines, black broken line, and blue line denote the Fourier-transform Kerr spectrum, its entire fit, Ohmic functions, antisymmetrized Gaussian functions, Lorentzian function, and Lorentzian function subtracted spectrum, respectively.

### 3. Target ionic liquids, electronic structures, and static properties

The sample ILs discussed in this chapter were synthesized according to the standard procedure (Wasserscheid & Welton, 2008; Saurez et al., 1998; Holbrey & Seddon, 1999;

Dzyuba & Bartsch, 2002; Tsunashima & Sugiya, 2007), except for 1-butyl-3-methylimidazolium hexafluorophosphate ([BMIm][PF<sub>6</sub>], Wako Pure Chemical) and 1-butyl-3-methylimidazolium hexafluoroantimonate ([BMIm][SbF<sub>6</sub>], Fluka), which were used as received. Before the measurements, the ILs were dried in vacuo, typically at approximately 315 K for 36 h. The details of these sample ILs have been described elsewhere (Shirota & Castner, 2005; Shirota et al., 2009; Shirota et al., 2010). The ILs and their abbreviations are as follows.

1-Methyl-3-neopentylimidazolium bis(trifluoromethylsulfonyl)amide: [C-MIm][NTf<sub>2</sub>]; 1-methyl-3-trimethylsilylmethylimidazolium bis(trifluoromethylsulfonyl)amide: [Si-MIm][NTf<sub>2</sub>]; 1-methyl-3-neopentylimidazolium tetrafluoroborate: [C-MIm][BF<sub>4</sub>]; 1-methyl-3-trimethylsilylmethylimidazolium tetrafluoroborate: [Si-MIm][BF<sub>4</sub>]; 1-butyl-3-methylimidazolium hexafluoroarsenate: [BMIm][AsF<sub>6</sub>]; triethyloctylammonium bis(trifluoromethylsulfonyl)amide: [N<sub>228</sub>][NTf<sub>2</sub>]; triethyloctylphosphonium bis(trifluoromethylsulfonyl)amide: [P<sub>228</sub>][NTf<sub>2</sub>]; (2-ethoxyethoxy)ethyltriethylammonium bis(trifluoromethylsulfonyl)amide: [N<sub>222(2O2O2)</sub>][NTf<sub>2</sub>]; (2-ethoxyethoxy)ethyltriethylphosphonium bis(trifluoromethylsulfonyl)amide: [P<sub>222(2O2O2)</sub>][NTf<sub>2</sub>]; (2-ethoxyethoxy)ethyltriethylammonium hexafluorophosphate: [N<sub>222(2O2O2)</sub>][PF<sub>6</sub>]; (2-ethoxyethoxy)ethyltriethylphosphonium hexafluorophosphate: [P<sub>222(2O2O2)</sub>][PF<sub>6</sub>]; (2-ethoxyethoxy)ethyltriethylammonium hexafluoroarsenate: [N<sub>222(2O2O2)</sub>][AsF<sub>6</sub>]; (2-ethoxyethoxy)ethyltriethylphosphonium hexafluoroarsenate: [P<sub>222(2O2O2)</sub>][AsF<sub>6</sub>]. The chemical structures of the target cations and anions for the heavy atom substitution studies are shown in Fig. 3.

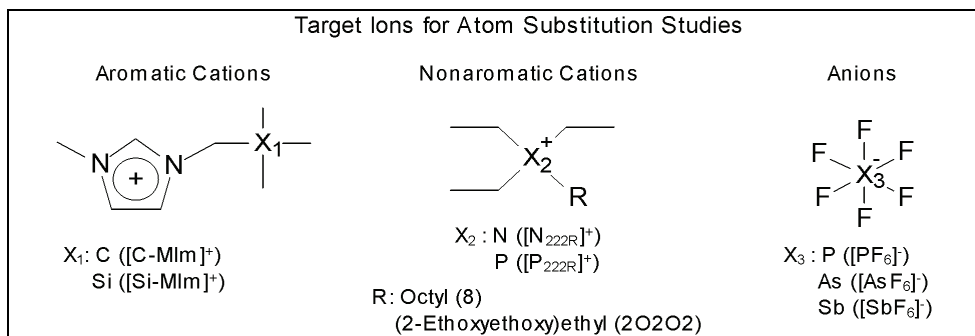


Fig. 3. Chemical structures of target ions for atom substitution studies.

Because ions have charges in nature, it is important to understand the charge magnitudes of the atoms in the ions. Fig. 4 shows the optimized geometries and atom charges of the target ions. The geometry optimization calculations were performed based on the density functional theory of the B3LYP/6-311++G(d,p) level for the [X-MIm]<sup>+</sup> and [X<sub>228</sub>]<sup>+</sup> cations and the B3LYP/aug-cc-pVDZ or aug-cc-pVDZ-PP level for the [XF<sub>6</sub>]<sup>-</sup> anions. The charges were estimated using the CHelpG algorithm.

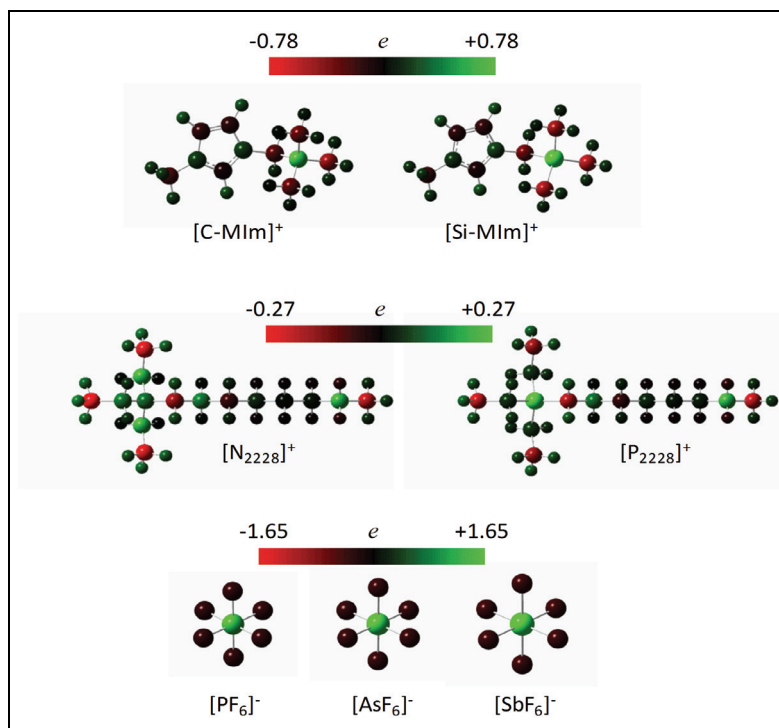


Fig. 4. Atom charges of target ions for atom substitution studies.

Overall, the features of the heavy atom substitutions in the three categories ( $[X\text{-MIm}]^+$ ,  $[X_{2228}]^+$ , and  $[XF_6]^-$ ) were similar. That is, the charge magnitude of the heavier atom in the ions was larger than that of the corresponding lighter atom of the respective ions in most cases: Si in  $[\text{Si-MIm}]^+$  (+0.773) vs. C in  $[\text{C-MIm}]^+$  (+0.602); P in  $[\text{P}_{2228}]^+$  (+0.250) vs. N in  $[\text{N}_{2228}]^+$  (+0.102); Sb in  $[\text{SbF}_6]^-$  (+1.650) vs. As in  $[\text{AsF}_6]^-$  (+1.393) vs. P in  $[\text{PF}_6]^-$  (+1.414). In addition, the bond length of the target atoms became longer with the heavy atom substitution: Si-CH<sub>3</sub> in  $[\text{Si-MIm}]^+$  (1.880 Å) vs. C-CH<sub>3</sub> in  $[\text{C-MIm}]^+$  (1.539 Å); P-CH<sub>2</sub>CH<sub>3</sub> in  $[\text{P}_{2228}]^+$  (1.832 Å) vs. N-CH<sub>2</sub>CH<sub>3</sub> in  $[\text{N}_{2228}]^+$  (1.531 Å); Sb-F in  $[\text{SbF}_6]^-$  (1.937 Å) vs. As-F in  $[\text{AsF}_6]^-$  (1.775 Å) vs. P-F in  $[\text{PF}_6]^-$  (1.660 Å). The ab initio quantum chemistry calculation results thus suggest that the heavy atom substitution in ions produces two opposing features in relation to the interionic interaction. A bigger charge magnitude in an atom produces a stronger interionic interaction at the local site (attractive Coulomb or dipole-dipole interaction), but a larger ionic volume brings a weaker interionic interaction (steric repulsive force).

Table 1 summarizes the data for the liquid density, shear viscosity, and surface tension at 297 K for the sample ILs, as well as their formula weights and molar volumes. The molar volumes were estimated from the formula weights and liquid densities at 297 K. In the data for the liquid densities, the result of the heavy atom substitutions is slightly confusing: C →

Si and N  $\rightarrow$  P in the cations ( $[\text{C-MIm}]^+ \rightarrow [\text{Si-MIm}]^+$  and  $[\text{N}_{222\text{R}}]^+ \rightarrow [\text{P}_{222\text{R}}]^+$ ) decrease the liquid density, whereas P  $\rightarrow$  As  $\rightarrow$  Sb in the anions ( $[\text{PF}_6]^- \rightarrow [\text{AsF}_6]^- \rightarrow [\text{SbF}_6]^-$ ) increase the liquid density. A larger atom definitely has a heavier mass and a larger volume. These effects on the liquid density arising from the heavy atom substitution are thus counterintuitive. If we look at the periodic table, the gap in the atomic masses between the periods 2 and 3 is much smaller than that between the periods 3 and 4 and between the periods 4 and 5 (Lide, 2008). Conversely, the difference in the atomic volumes between the periods 2 and 3 is larger than that between the periods 3 and 4 and between the periods 4 and 5 (Bondi, 1964). As a result, the heavy atom substitutions, C  $\rightarrow$  Si and N  $\rightarrow$  P, in the cations give a lower liquid density as a dominant factor for the volume effect, whereas the heavy atom substitutions, P  $\rightarrow$  As  $\rightarrow$  Sb, in the anions give a higher liquid density as the dominant parameter of the mass effect.

ILs	FW	$d$ (g/mL)	$\eta$ (cP)	$\gamma$ (mN/m)	$V$ (mL/mol)
$[\text{C-MIm}][\text{NTf}_2]$	433.4	1.413	161.4	31.6	306.7
$[\text{Si-MIm}][\text{NTf}_2]$	449.5	1.398	90.7	30.1	321.5
$[\text{C-MIm}][\text{BF}_4]$	240.1	1.207	3337	40.0	198.9
$[\text{Si-MIm}][\text{BF}_4]$	256.1	1.188	546.2	36.8	215.6
$[\text{BMIm}][\text{PF}_6]^{\text{a}}$	248.2	1.368	289.6	43.7	181.4
$[\text{BMIm}][\text{AsF}_6]^{\text{a}}$	328.1	1.540	228.0	44.8	213.1
$[\text{BMIm}][\text{SbF}_6]^{\text{a}}$	375.0	1.690	133.7	45.2	221.9
$[\text{N}_{2228}][\text{NTf}_2]^{\text{b}}$	494.6	1.249	227.0	32.8	396.0
$[\text{P}_{2228}][\text{NTf}_2]^{\text{b}}$	511.5	1.244	123.3	32.7	411.2
$[\text{N}_{222(2\text{O}_2\text{O}_2)}][\text{NTf}_2]^{\text{b}}$	498.5	1.328	70.4	35.3	375.4
$[\text{P}_{222(2\text{O}_2\text{O}_2)}][\text{NTf}_2]^{\text{b}}$	515.5	1.319	43.7	35.0	390.8
$[\text{N}_{222(2\text{O}_2\text{O}_2)}][\text{PF}_6]^{\text{b}}$	363.3	1.255	699.0	45.0	289.5
$[\text{P}_{222(2\text{O}_2\text{O}_2)}][\text{PF}_6]^{\text{b}}$	380.3	1.250	232.8	44.3	304.2
$[\text{N}_{222(2\text{O}_2\text{O}_2)}][\text{AsF}_6]^{\text{b}}$	407.3	1.381	607.4	45.3	294.9
$[\text{P}_{222(2\text{O}_2\text{O}_2)}][\text{AsF}_6]^{\text{b}}$	424.2	1.368	216.1	44.5	310.1

Table 1. Formula weights FW, liquid densities  $d$ , shear viscosities  $\eta$ , surface tensions  $\gamma$  and molar volume  $V$  at 297 K for ILs. The data are from <sup>a</sup> Shirota et al., 2009, and <sup>b</sup> Shirota et al., 2010. Data at 297 K for the upper four ILs are newly published data.

In the data for the shear viscosity, the heavy atom substitution effect is clearly observed with the same trend for any ILs: the heavier atom substitution gives a lower shear viscosity. As mentioned previously, this effect is the opposite of that for common neutral molecular liquids (e.g.,  $\eta(\text{fluorobenzene})$ : 0.550 cP <  $\eta(\text{chlorobenzene})$ : 0.753 cP <  $\eta(\text{bromobenzene})$ : 1.074 cP and  $\eta(\text{diethyl ether})$ : 0.224 cP <  $\eta(\text{diethyl sulfide})$ : 0.442 cP at 298 K (Lide, 2008)). In



general, this effect in conventional molecular liquids arises from the heavier mass and larger molar volume (dispersion force).

In ILs, the ion volume is critical for the interionic interaction strength because the distance between a cation and an anion affects the interionic interaction strength. In the simplest case, e.g., in a spherical ion pair, the Coulombic energy,  $E_{\text{Coulomb}}(r)$ , is inversely proportional to the distance between a cation and an anion:  $E_{\text{Coulomb}}(r) \propto 1/r$  (Israelacvili, 1992). Moreover, the total interaction energy in ionic crystals is proportional to the inverse of the distance between a cation and anion (the Madelung constant) (Israelacvili, 1992). As seen in Table 1, we can confirm that the molar volume in the ILs becomes larger as the cation and anion become heavier. Although the self-diffusion, interionic interaction, and ion-pair formation do not always correlate to the ionic volume (Tsuzuki et al., 2005; Katsuta et al., 2008), it is suggested that discussing the interionic interaction with the effect of the ion volume is appropriate when comparing the present ions because the structures of the ions are relatively less influenced by a heavy atom substitution compared to the case in which a whole ion is exchanged.

Polarizability is another factor responsible for the intermolecular (or interionic) interaction. The polarizability increases with a longer bond length (and thus a larger molecule), according to the charge response kernel model (Iuchi et al., 2002). Because the increased polarizability could soften the force between the charges, the polarizability effect can reasonably explain the tendency for the shear viscosities of the three ILs to decrease, as well as the volume effect. Indeed, the increased polarizability also provides the stronger interionic interaction because of the larger dispersion and inductive forces. However, the trend of the shear viscosities for the ILs is inconsistent with the effects of the dispersion and inductive forces. With regard to the charge population, the study of the atom charges of the ions indicates that the negative charge magnitude of F for  $[\text{XF}_6]^-$  and the positive charge magnitude of the target element for the cations are larger for a heavier ion. The charge localization in the ions should have a stronger interaction with a counter ion than the ions with the delocalized charge distribution, and the stronger interaction between the cation and anion provides the larger shear viscosity in fluids. Accordingly, the calculation results for the charge magnitude of the anion cannot be used to explain the observed heavy atom substitution effect on the shear viscosity in the ILs. Therefore, the present result of the shear viscosity trend of the three types of ILs can be reasonably explained in the context of the interionic interaction arising from the ionic volume effect.

On the other hand, the trend in the surface tension by the heavy atom substitutions is somewhat complicated in comparison with that in the shear viscosity. As listed in Table 1, the surface tension becomes slightly smaller with the heavier element substitution in the aromatic and nonaromatic “cations” but becomes larger with the heavier element substitution in the “anions”. There is an inverse correlation between surface tension and molar volume in molten salts, including ILs (Jin et al., 2008). The change in surface tension for the ILs by the heavy atom replacement in the cation is well explained by the empirical scheme. However, the feature in the anions is evidently the opposite of the predicted heavy atom substitution effect on the surface tension.

In addition to the shear viscosity, the surface tension in conventional neutral molecular liquids increases with a heavier atom substitution (e.g.,  $\gamma$ (fluorobenzene): 26.66 mN/m <

$\gamma$ (chlorobenzene): 32.99 mN/m <  $\gamma$ (bromobenzene): 35.24 mN/m and  $\gamma$ (diethyl ether): 16.65 mN/m <  $\gamma$ (diethyl sulfide): 24.57 mN/m at 298 K (Lide, 2008)). Therefore, the characteristics of the atom substitutions in the anions of ILs are fairly normal for liquids, but the heavy atom substitutions in the aromatic and nonaromatic cations show an unusual feature. It seems that the mass effect is greater than the volume effect for the surface tension as well as the liquid density.

#### 4. Interionic vibrational band

As shown in Fig. 2, the intermolecular vibrational band in molecular liquids is broad and located in the low frequency region below ca. 150  $\text{cm}^{-1}$ , in contrast to most of the intramolecular vibrational modes. The same is also true for ILs. Actually, a detailed molecular-level understanding of the intermolecular vibrations in molecular liquids, including ILs, is not simple at all. This is because the molecules or ions in liquids are fluctuating, these molecular or ionic fluctuations give different intermolecular or interionic vibrational modes, and such intermolecular or interionic vibrational modes are often coupled to each other and are fairly anharmonic. In addition, the spectral shape is more complicated than simple Gaussian and Lorentzian line shapes which are usually used to express the line shapes of intramolecular or intraionic vibrational modes. However, this spectrum contains a large quantity of microscopic or molecular-level information. Because heavy atom substitutions in ILs do not have a very great effect on the constituent ionic shape in comparison with a whole ion exchange, a specific comparison between ILs with lighter and heavier atom-substituted ions is possible. The details of such a comparison are given below.

##### 4.1 Cation in aromatic ionic liquids

The first example of an atom substitution study of the interionic vibrational dynamics in ILs is C vs. Si for a side group of an imidazolium cation:  $[\text{C-MIm}]^+$  vs.  $[\text{Si-MIm}]^+$  (Shirota & Castner, 2005). Fig. 5 shows the low-frequency Kerr spectra and fits for the ILs with  $[\text{NTf}_2]^-$  and  $[\text{BF}_4]^-$ . It should be noted that the contributions of the picosecond orientational relaxations were removed from the full Kerr spectra to focus on the vibrational motions in the ILs.

The low-frequency spectral region from ca. 1 to 150  $\text{cm}^{-1}$  is usually dominated by the intermolecular vibrational components in most neutral molecular liquids. The same is true for ILs, but the spectrum is somewhat shifted to a higher frequency (Shirota & Castner, 2005). The substantial flexibility of the IL cations and anions often leads to low frequency modes, which are found at the same low-frequency region of the spectrum. Fig. 5 shows how sharper Lorentzian features arising from the cation and anion intraionic vibrational modes are superposed on the broad spectra in the 0 to 150  $\text{cm}^{-1}$  spectral range. For strongly dipolar liquids such as acetonitrile, the dominant contributions to the intermolecular vibrational dynamics arise from librational and density fluctuation (translational) dynamics, with the former dominating the spectral density (Ryu & Stratt, 2004; Madden & Cox, 1981; Madden, 1983; Geiger & Ladanyi, 1988; Geiger & Ladanyi, 1989). Because these motions have a strong overlap on timescale and are in fact likely coupled for such strongly interacting ions as those in the ILs reported here, it is difficult to distinguish between them.

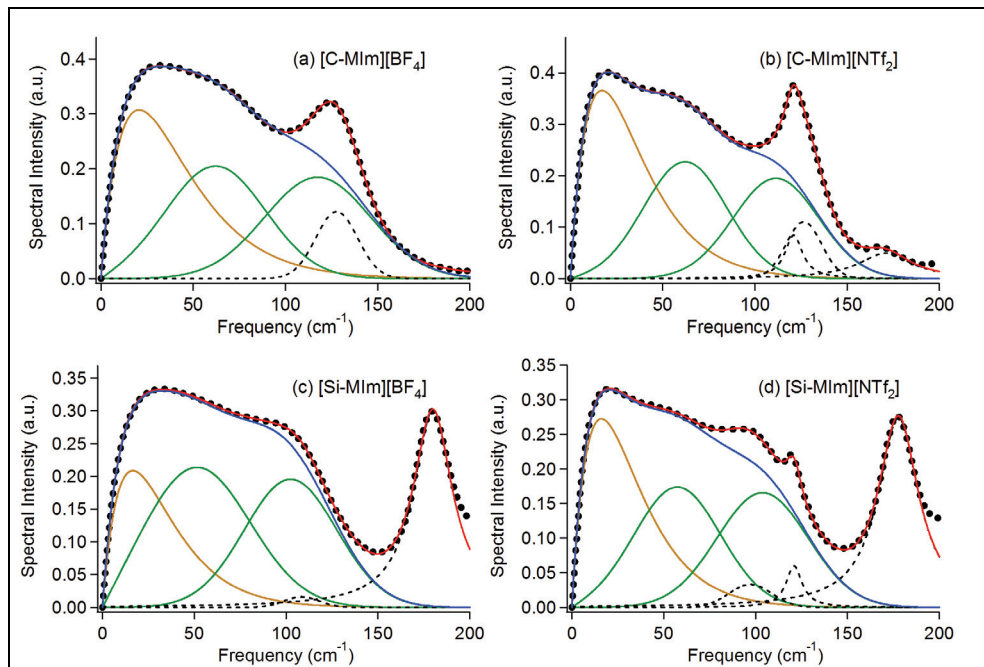


Fig. 5. Low-frequency Kerr spectra of ILs (a) [C-MIm][BF<sub>4</sub>], (b) [C-MIm][NTf<sub>2</sub>], (c) [Si-MIm][BF<sub>4</sub>], and (d) [Si-MIm][NTf<sub>2</sub>]. The black dotted lines, red solid lines, brown solid lines, green solid lines, and black broken lines denote the Fourier-transform Kerr spectra, entire fits, Ohmic components (Eq. 1), antisymmetrized Gaussian components (Eq. 2), and Lorentzian components (intraionic vibrations), respectively. The blue solid lines denote the spectra with the Lorentzian components subtracted.

It is quite likely that the features that fit to Eqs. 1 and 2 cannot be correlated directly with any simple decomposition of the line shape into orientational and translational motions.

From the line-shape features in the interionic vibrational spectra and the line-shape analysis shown in Fig. 5, it becomes clear that (1) the first moments,  $M_1$ , (and the peak frequencies of all model functions) for the [Si-MIm]<sup>+</sup> ILs are lower than those for the [C-MIm]<sup>+</sup> ILs (71.1 cm<sup>-1</sup> for the [C-MIm][BF<sub>4</sub>], 65.8 cm<sup>-1</sup> for the [Si-MIm][BF<sub>4</sub>], 64.3 cm<sup>-1</sup> for the [C-MIm][NTf<sub>2</sub>], and 63.1 cm<sup>-1</sup> for the [Si-MIm][NTf<sub>2</sub>]) and (2) the magnitudes of the differences for the spectral first moments are larger for the [BF<sub>4</sub>]<sup>-</sup> ILs than for the [NTf<sub>2</sub>]<sup>-</sup> ILs.

Considering a harmonic oscillator,  $\omega = (k/\mu)^{1/2}$ , where  $k$  is the force constant and  $\mu$  is the reduced mass, we might expect that the frequencies for such an intermolecular mode would be reduced for the [Si-MIm]<sup>+</sup> ILs relative to the [C-MIm]<sup>+</sup> ILs for at least two reasons: (i) The effective mass for the [Si-MIm]<sup>+</sup> cation is larger than that for the [C-MIm]<sup>+</sup> cation and (ii) the intermolecular interactions for the [Si-MIm]<sup>+</sup> ILs are weaker than those for the [C-MIm]<sup>+</sup> ILs.

In a neutral aprotic molecular liquid, there is a single correlation between the spectral first moment and the square root of the value of surface tension divided by density,  $(\gamma/d)^{1/2}$  (Shirota et al., 2009). The ratios of the surface tensions,  $\gamma([\text{Si-MIm}]^+ \text{ IL})/\gamma([\text{C-MIm}]^+ \text{ IL})$ , are 0.89 for ILs with the  $[\text{BF}_4]^-$  anion and 0.95 for the ILs with the  $[\text{NTf}_2]^-$  anion. Because of the reduction in  $M_1$  by the heavy atom substitution in the cation, the trends are the same, since the difference in liquid density is tiny. We also recall that the ratios of the shear viscosities  $\eta([\text{Si-MIm}]^+ \text{ IL})/\eta([\text{C-MIm}]^+ \text{ IL})$  are 0.135 for ILs with the  $[\text{BF}_4]^-$  anion and 0.625 for the ILs with the  $[\text{NTf}_2]^-$  anion. The interionic vibrational spectrum can be seen to be lower in frequency for the  $[\text{Si-MIm}]^+$  ILs than for the corresponding  $[\text{C-MIm}]^+$  ILs by the first spectral moment. The magnitude of the difference in frequencies resulting from the silicon substitution on the cation does not correlate with the difference in effective mass for either the  $[\text{NTf}_2]^-$  or  $[\text{BF}_4]^-$  ILs. Therefore, the difference in effective mass or liquid density between silicon-substituted and normal IL cations is not the only factor in determining the interionic vibrational frequencies in these four ILs. We think that liquids with lower shear viscosities and surface tensions should have weaker interionic interactions, and thus overall lower frequency interionic vibrational modes, relative to the liquids having higher shear viscosities and surface tensions.

#### 4.2 Anion in aromatic ionic liquids

Next, we compare 1-butyl-3-methylimidazolium  $[\text{BMIm}]^+$  based ILs with a series of hexafluoropnictogenate anions ( $[\text{XF}_6]^-$ : X is P, As, or Sb) (Shirota et al., 2009). As discussed above, the substitution of C by Si in the cation shifts the first moment of the low-frequency spectrum of an IL to a lower value. However, a change in the dipole moment of an ion caused by atom substitution gives a difference in the spectra. Because the hexafluoropnictogenate anion is octahedral, the substitution of a center atom affects the mass and volume (mean polarizability) of the ion, but does not affect the shape (dipole moment and polarizability anisotropy). Thus, it is more ideal to simply examine the atom substitution effects caused by the mass and volume on the interionic vibration in the ILs.

Fig. 6 focuses on the low-frequency Kerr spectra in the frequency range of 0–200  $\text{cm}^{-1}$ . To clearly see the heavy atom substitution effect, the spectral intensities were normalized to make them uniform. To find the regional frequency differences of the low-frequency Kerr spectra for the three ILs, the fit components (Eqs. 1 and 2) are also compared. As shown in the figure, the spectral differences between the three ILs are not very large. However, if we look closely at the low frequency Kerr spectra of the  $[\text{XF}_6]^-$  ILs, there are two meaningful differences. In the higher-frequency region (100–150  $\text{cm}^{-1}$ ), a small spectral difference can be observed: the spectral band shifts to a higher frequency or becomes broader with the smaller  $[\text{XF}_6]^-$  anion of the IL. A clearer heavy atom substitution effect on the interionic vibrational spectrum is seen in the lower frequency region ( $<50 \text{ cm}^{-1}$ ). In addition, the order of the first spectrum moments for the three ILs is  $[\text{BMIm}][\text{PF}_6] > [\text{BMIm}][\text{AsF}_6] > [\text{BMIm}][\text{SbF}_6]$  (69.6  $\text{cm}^{-1}$  for  $[\text{BMIm}][\text{PF}_6]$ , 69.3  $\text{cm}^{-1}$  for  $[\text{BMIm}][\text{AsF}_6]$ , and 68.2  $\text{cm}^{-1}$  for  $[\text{BMIm}][\text{SbF}_6]$ ). The effect of the heavy atom substitution on the interionic vibration (first moment) is similar to the tendency for the shear viscosity, rather than that for the surface tension. However, it is obvious that the tendency for the first spectrum moment in the three ILs is the same as that for the square root of the value of the surface tension divided by the liquid density, which is derived from a simple consideration of a harmonic oscillator, as well as the case for the  $[\text{X-}$

MIm]<sup>+</sup> ILs. That is, the mass effect is significant compared to the interionic interaction effect coming from the ionic volume for the [XF<sub>6</sub>]<sup>-</sup> ILs.

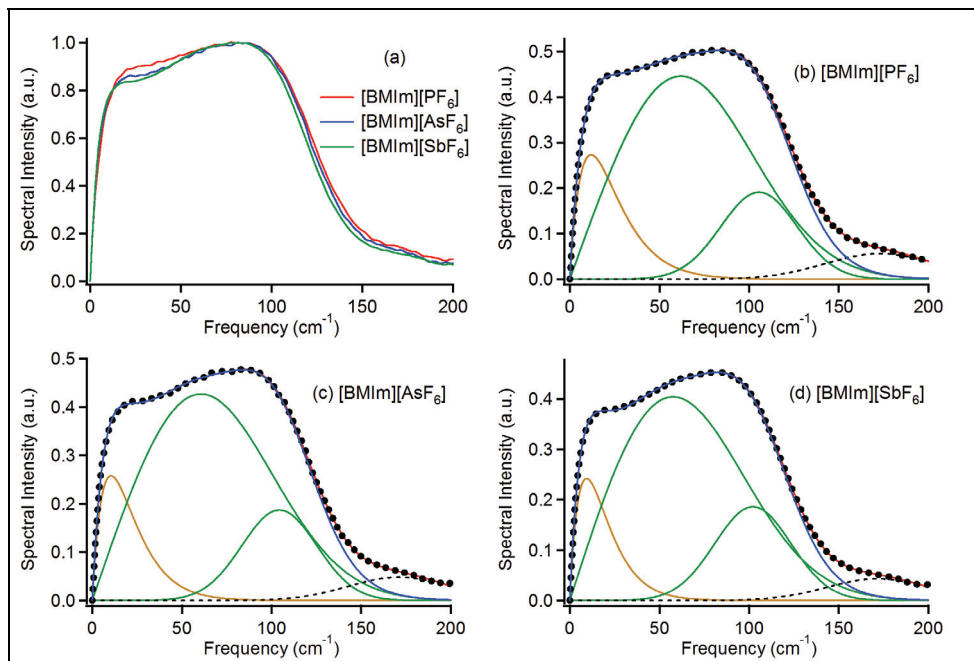


Fig. 6. (a) Normalized low-frequency Kerr spectra of [BMIm][PF<sub>6</sub>] (red), [BMIm][AsF<sub>6</sub>] (blue), and [BMIm][SbF<sub>6</sub>] (green). Low-frequency Kerr spectra and fits for (b) [BMIm][PF<sub>6</sub>], (c) [BMIm][AsF<sub>6</sub>], and (d) [BMIm][SbF<sub>6</sub>]. The black dotted lines, red solid lines, brown solid lines, green solid lines, and black broken lines denote the Fourier-transform Kerr spectra, entire fits, Ohmic components (Eq. 1), antisymmetrized Gaussian components (Eq. 2), and Lorentzian components (intraionic vibrations), respectively. The blue solid lines denote the spectra with the Lorentzian components subtracted.

For further insights, we compare the experimental result with the MD simulation result (Ishida et al., 2009). The decomposition analysis of the computed Kerr spectra based on the MD simulations of the three ILs shows that the composition of the spectrum for the [BMIm][PF<sub>6</sub>] is dominated by the cation-anion cross correlation, while the dominant contribution for the other two ILs is the cation's motion. This indicates that the interionic interaction between the cation and anion becomes weaker with an increase in the volume of the anion, which is in good agreement with the experimental results. The MD simulation work further reveals that the contribution of the reorientation of the cations and anions mainly dominates the Kerr spectrum profile in the three ILs, but the collision-induced and cross (coupling motion) terms do not show large contributions to the Kerr spectrum profile. A comparison between the heavy atom substitution effects of the [XF<sub>6</sub>]<sup>-</sup> anion and [X-MIm]<sup>+</sup> cation on the low-frequency Kerr spectrum provides further detailed aspects for the heavy atom substitution effect on the interionic vibrational dynamics in the aromatic ILs. Let us

recall the key points for the silicon substitution effect of an imidazolium cation ( $[\text{C-MIm}]^+ \rightarrow [\text{Si-MIm}]^+$ ) on the interionic vibrational dynamics discussed above. First, the characteristic frequency such as the first moment of the low-frequency broad spectrum shifts to a lower value with the silicon substitution of the side group from the neopentyl group  $((\text{CH}_3)_3\text{CCH}_2-)$  to the trimethylsilylmethyl group  $((\text{CH}_3)_3\text{SiCH}_2-)$  of the imidazolium cation. Second, the silicon substitution effect is larger for the  $[\text{BF}_4]^-$  IL than for the  $[\text{NTf}_2]^-$  IL, because the  $[\text{BF}_4]^-$  IL has a larger shear viscosity and surface tension. Third, the silicon substitution effect on the Kerr spectra is clear in the higher frequency region ( $100\text{--}150\text{ cm}^{-1}$ ) than in the lower frequency region ( $<50\text{ cm}^{-1}$ ). From a comparison of the present results for the  $[\text{XF}_6]^-$  ILs with the results for the silicon substitution effect, we find a remarkable point, besides the lower frequency shift in the vibrational band by the heavy atom substitution. The frequency region of the spectral difference caused by the heavy atom substitution for the  $[\text{XF}_6]^-$  ILs is clearly different from that for the  $[\text{X-MIm}]^+$  ILs. It is a lower frequency region for the  $[\text{XF}_6]^-$  ILs and a higher frequency region for the  $[\text{X-MIm}]^+$  ILs.

In the case of aromatic molecular liquids, the intermolecular vibrational dynamics in the lower frequency region, which is typically less than  $50\text{ cm}^{-1}$ , includes the interaction-induced motion, which is translation-like, coupled with the librational motion, which is rotation-like, whereas that in the higher frequency region is predominantly due to the librational motion (Ryu & Stratt, 2004; Elola & Ladanyi, 2006). If the molecular motions and timescale of the interionic vibrational dynamics in the ILs are similar to those of simple aromatic molecular liquids, it would be permissible to consider the origins of the heavy atom substitution effects on the interionic vibrational dynamics in the ILs by taking into account the analogy of simple aromatic liquid dynamics.

The spectral difference for the  $[\text{XF}_6]^-$  ILs is evident in the lower frequency region, and that for the  $[\text{X-MIm}]^+$  ILs is dominant in the higher frequency region. Thus, the interaction-induced (translation-like) motion is sensitive to the heavy atom substitution effect of the  $[\text{XF}_6]^-$  anion, and the substitution for the  $[\text{X-MIm}]^+$  cation is critical for the librational (rotation-like) motion. Why do the heavy atom substitution effects of the  $[\text{X-MIm}]^+$  cation and the  $[\text{XF}_6]^-$  anion on the interionic vibrational spectra appear in the different frequency regions?

It is worthwhile to think of the shapes of the constituent ions of the ILs. Because the  $[\text{XF}_6]^-$  anion has an octahedral symmetry, the effective dipole, which is defined as the vector from the center of mass to the center of charge by Kobrak and co-workers (they called it the "charge arm") (Kobrak & Sandalow, 2006; Li et al., 2008), never changes with the heavy atom substitution of the  $[\text{XF}_6]^-$ . On the other hand, the (static) effective dipole of the  $[\text{X-MIm}]^+$  varies with the heavy atom substitution: the effective dipole of the  $[\text{Si-MIm}]^+$  is approximately 20% larger than that of the  $[\text{C-MIm}]^+$  (Shirota & Castner, 2005).

The nonzero effective dipole of the ion (and the molecule) contributes to both orientational and translational motions, but the zero effective dipole of the ion (and the molecule) never contributes to rotational motion. Accordingly, a comparison between the present and previous studies indicates that the change in the effective dipole (or asymmetric molecular shape) by the heavy atom substitution of the ion provides the dominant heavy atom substitution effect on higher-frequency interionic vibrational dynamics. On the other hand, the change in the pure mass and spherical volume by the heavy atom substitution of the ion gives the large substitution effect on the lower-frequency interionic vibrational dynamics.

Qualitatively, the MD simulation showed the same picture as the experiment (Ishida et al., 2009). The larger masses of As and Sb, compared to P, in the  $[XF_6]^-$  anion inactivate the translational motion (and its coupling motion with librational motion).

### 4.3 Nonaromatic ionic liquids

Now, let us move to nonaromatic ILs. The unique characteristics of nonaromatic ILs include their flexibility and charge distribution. The comparisons are the ammonium and phosphonium cations, as well as the  $[PF_6]^-$  and  $[AsF_6]^-$  anions (Shirota et al., 2010). Fig. 7 shows the low-frequency Kerr spectra of  $[N_{2228}][NTf_2]$ ,  $[P_{2228}][NTf_2]$ ,  $[N_{222(2O2O2)}][NTf_2]$ , and  $[P_{222(2O2O2)}][NTf_2]$ , and Fig. 8 compares the low-frequency Kerr spectra of  $[N_{222(2O2O2)}][PF_6]$ ,  $[P_{222(2O2O2)}][PF_6]$ ,  $[N_{222(2O2O2)}][AsF_6]$ , and  $[P_{222(2O2O2)}][AsF_6]$ . The results of the line-shape analysis are also shown in the figures. It is clear from these figures that the intensity in the high frequency region ( $>50\text{ cm}^{-1}$ ) is low for the nonaromatic ILs, in comparison with the aromatic ILs (Figs. 5 and 6). A similar feature was also confirmed in conventional molecular liquids (Shirota et al., 2009). Some MD simulations have indicated that the rotation-like motions, such as libration, of aromatic molecules are dominant in the high frequency region, as mentioned before (Ryu & Stratt, 2004; Elola & Ladanyi, 2006). Thus, it seems that the spectral difference in the high frequency region between the aromatic and nonaromatic ILs is caused by the presence or absence of a flat aromatic ring.

The first moments of the low-frequency spectra for the phosphonium-based ILs are slightly lower overall or are similar to those for the ammonium-based ILs, and that the first moment in ILs with the  $[XF_6]^-$  anion becomes lower through the heavy atom substitution of As for P in the  $[XF_6]^-$  anion ( $50.6\text{ cm}^{-1}$  for  $[N_{2228}][NTf_2]$ ,  $50.0\text{ cm}^{-1}$  for  $[P_{2228}][NTf_2]$ ,  $52.3\text{ cm}^{-1}$  for  $[N_{222(2O2O2)}][NTf_2]$ ,  $52.3\text{ cm}^{-1}$  for  $[P_{222(2O2O2)}][NTf_2]$ ,  $66.6\text{ cm}^{-1}$  for  $[N_{222(2O2O2)}][PF_6]$ ,  $64.0\text{ cm}^{-1}$  for  $[P_{222(2O2O2)}][PF_6]$ ,  $64.5\text{ cm}^{-1}$  for  $[N_{222(2O2O2)}][AsF_6]$ , and  $63.5\text{ cm}^{-1}$  for  $[P_{222(2O2O2)}][AsF_6]$ ). A similar feature was observed in aromatic ILs, as seen above (Shirota & Castner, 2005; Shirota et al., 2009). Thus far, we have discussed the change in the interionic vibrational spectra of the ILs caused by the heavy atom substitution in terms of the microscopic interionic interaction. The interionic vibrational frequency decreases with heavy atom substitution. If we consider a harmonic oscillator as a simple model for an interionic vibration, it is clear that the vibrational frequency becomes lower with the weaker interionic interaction because of the heavy atom substitution. The experimental results and ab initio quantum chemistry calculations have shown the nearly neutral charges of the central heteroatoms of the ammonium and phosphonium cations, the large difference in the N-C and P-C bond lengths, and the larger volume of the ion pair for the heavy-atom-substituted ILs. Therefore, it is plausible that the interionic interactions become weaker because of the larger ionic volumes.

On the other hand, the reduced mass is another parameter for the peak frequency of the harmonic oscillator model. The liquid density is substantially increased by the heavy atom substitution of As for P in  $[XF_6]^-$ , but becomes slightly lower by the substitution of P for N in a cation (Table 1). By an analogy of the better correlation between the first moment of the intermolecular vibrational spectrum and the square root of the value of surface tension divided by liquid density than by formula weight in aprotic molecular liquids (Shirota et al., 2009), we find that the relatively large substitution effect on the low-frequency spectrum in the  $[XF_6]^-$  ILs could be attributed to the difference in liquid density.

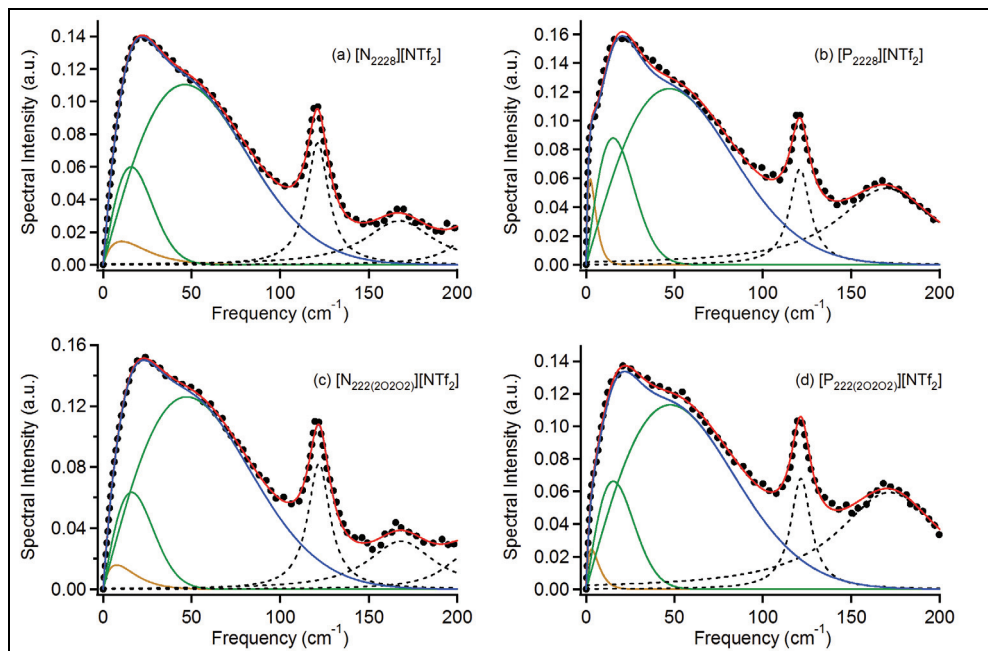


Fig. 7. Low-frequency Kerr spectra and fits for (a)  $[N_{2228}][NTf_2]$ , (b)  $[P_{2228}][NTf_2]$ , (c)  $[N_{222(2O2O2)}][NTf_2]$ , and (d)  $[P_{222(2O2O2)}][NTf_2]$ . The black dotted lines, red solid lines, brown solid lines, green solid lines, and black broken lines denote the Fourier-transform Kerr spectra, entire fits, Ohmic components (Eq. 1), antisymmetrized Gaussian components (Eq. 2), and Lorentzian components (intraionic vibrations), respectively. The blue solid lines denote the spectra with the Lorentzian components subtracted.

We will further discuss this correlation in the eight ILs later. In any event, the liquid density affects the interionic vibrational spectrum in ILs, as well as the interionic interaction.

We also found that the dual heavy atom substitution effect on the interionic vibrational spectrum of both the cation and anion ( $[N_{222(2O2O2)}][PF_6] \rightarrow [P_{222(2O2O2)}][AsF_6]$ ) is almost the sum of the respective effects of the cation and anion. In summary, the heavy atom substitution effects on the interionic vibration are rather general for any ion constituents: cation, anion, aromatic, or nonaromatic species.

In addition to the heavy atom substitution effects, we found clear changes caused by the (2-ethoxyethoxy)ethyl group substitution for the octyl group in the cations. The first moment of the low-frequency Kerr spectrum becomes higher with the ether group substitution in both the ammonium and phosphonium cations. The shear viscosity of  $[N_{222(2O2O2)}][NTf_2]$  is lower than that of  $[N_{2228}][NTf_2]$  (Table 1). As well as the ammonium-based ILs, phosphonium-based ILs show a similar substitution effect on the shear viscosity. However, the surface tension becomes larger with the substitution of the (2-ethoxyethoxy)ethyl group for the octyl group in the cations. That is, the substitution effect of the ether group



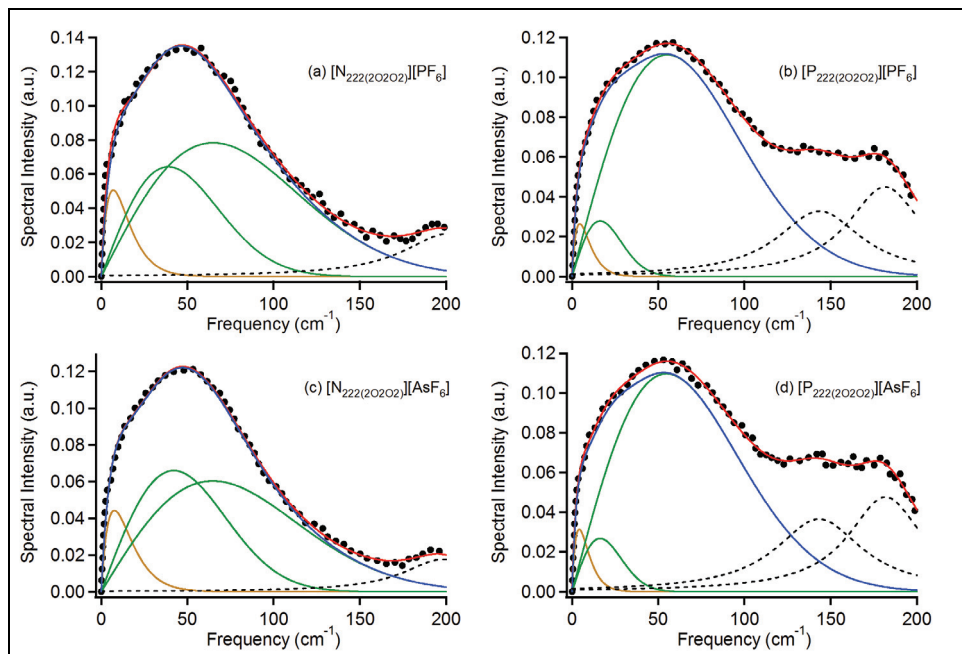


Fig. 8. Low-frequency Kerr spectra and fits for (a)  $[N_{222(20202)}][PF_6]$ , (b)  $[P_{222(20202)}][PF_6]$ , (c)  $[N_{222(20202)}][AsF_6]$ , and (d)  $[P_{222(20202)}][AsF_6]$ . The black dotted lines, red solid lines, brown solid lines, green solid lines, and black broken lines denote the Fourier-transform Kerr spectra, entire fits, Ohmic components (Eq. 2), antisymmetrized Gaussian components (Eq. 2), and Lorentzian components (intraionic vibrations), respectively. The blue solid lines denote the spectra with the Lorentzian components subtracted.

on the first moment of the low-frequency Kerr spectrum is similar to that on the surface tension, but not the shear viscosity.

Finally, it might be worth mentioning a comparison between the low-frequency spectrum (microscopic aspect) and bulk property (macroscopic feature) for a broad range of ILs. Unlike conventional molecular liquids (Shirota et al., 2009), the correlations for the ILs are not great. In particular, the correlations of the aromatic and nonaromatic ILs seem to be different (Fujisawa et al., 2009; Shirota et al., 2010). Obviously, ILs are much more complicated than conventional molecular liquids. Because ILs are mixtures of cations and anions in nature and most ILs, particularly ILs containing an ion with a long alkyl group, consist of ionic and hydrophobic parts, the inhomogeneity could give bulk and microscopic interionic/intermolecular interactions that are different from those of neat liquids. Traces of inhomogeneity in ILs were reported in experiments (Triolo et al., 2007; Xiao et al., 2009; Shigeto & Hamaguchi, 2006), as well as MD simulations (Lopes et al., 2006; Wang & Voth, 2006). These natures of ILs surely provide more complicated microscopic features. However, the heavy atom substitution effect on the interionic vibrational band in the ILs is reasonably accounted for by the harmonic oscillator scheme.

## 5. Conclusions

In this chapter, we provided an overview of the heavy atom substitution effects of the constituent ions in some ILs on the static properties such as liquid density, shear viscosity, and surface tension, along with the effects on the interionic vibrational dynamics. With respect to the static properties, we can summarize the heavy atom substitution effects in the ILs as follows.

- The liquid density slightly decreases because of the heavy element substitution from the period 2 element to the period 3 element, but the substitution from the period 3 element to the period 4 element and the period 4 element to the period 5 element substantially increases the liquid density. This complicated feature arises from the counter parameters: volume and mass.
- The shear viscosity is reduced by the heavy atom substitution in any cationic, anionic, aromatic, or nonaromatic species. In addition, the reduction in shear viscosity by a dual cation and anion substitution is simply the sum of the respective effects of the cation and anion substitutions (no synergistic or compensative effect).
- The heavy atom substitution effect on the surface tension shows the same trend as that on the liquid density.

With regard to the interionic vibrational spectrum, the heavy atom substitutions provide a lower frequency shift of the characteristic frequency, the first spectrum moment,  $M_1$ . This feature is observed for both the cation and anion. Comparing the interionic vibrational spectra with the bulk properties, the heavy atom substitution effect on the interionic vibration in the ILs is the same as that on the shear viscosity. The shifts in the interionic vibrational band by heavy atom substitution in both the aromatic and nonaromatic cations are also reasonably accounted for by the feature of the surface tension. However, the substitution in an anion cannot be simply explained by the surface tension. Considering a harmonic oscillator as a simple model, the heavy atom substitution effect on the interionic vibration in the ILs arises from the differences in both the interionic interactions (or volumes) and masses (or liquid densities). The spectral shift in the interionic vibrational band by the heavy atom substitution in the cations is mainly caused by the interionic interaction, whereas the mass effect is large for the substitution in the anions. Although, within the same group, the heavy atom substitution effects on the interionic vibration in the ILs are reasonably taken into account by the harmonic oscillator scheme, the whole picture of the interionic vibrations in ILs still remains unclear. Additional and broader studies will provide a further understanding of the general and deeper aspects of ILs.

## 6. Acknowledgements

We would like to greatly thank the co-workers, Prof. Edward W. Castner, Jr. (Rutgers University), Dr. Tomotsumi Fujisawa (Chiba University), Prof. Tateki Ishida (Institute for Molecular Science), Prof. Keiko Nishikawa (Chiba University), Mr. Kazuya Sugimoto (Chiba University), and Dr. James F. Wishart (Brookhaven National Laboratory). These works were financially supported by the Ministry of Education, Culture, Sports, Science and Technology (MEXT) of Japan (Grant-in-Aids for Special Purposes/Scientific Research (C): 19559001 and Young Scientists (A): 21685001), the Izumi Science and Technology Foundation, and the Futaba Electronics Memorial Foundation.

## 7. References

- Asaki, M. L. T.; Redondo, A.; Zawodzinski, T. A. & Taylor, A. J. (2002). Dielectric relaxation and underlying dynamics of acetonitrile and 1-ethyl-3-methylimidazolium triflate mixtures using THz transmission spectroscopy, *Journal of Chemical Physics*, 116, 10377-10385
- Bondi, A. (1964). van der Waals volumes and radii, *Journal of Physical Chemistry*, 68, 441-451
- Bucaro, J. A. & Litovitz, T. A. (1971). Rayleigh scattering: collisional motions in liquids, *Journal of Chemical Physics*, 54, 3846-3853
- Buffeteau, T.; Grondin, J.; Danten, Y. & Lassegues, J.-C. (2010). Imidazolium-based ionic liquids: quantitative aspects in the far-infrared region, *Journal of Physical Chemistry B*, 114, 7587-7579
- Cang, H.; Li, J. & Fayer, M. D. (2003). Orientational dynamics of the ionic organic liquid 1-ethyl-3-methylimidazolium nitrate, *Journal of Chemical Physics*, 119, 13017-13023
- Castner, E. W., Jr. & Maroncelli, M. (1998). Solvent dynamics derived from optical Kerr effect, dielectric dispersion, and time-resolved Stokes shift measurements: an empirical comparison, *Journal of Molecular Liquids*, 77, 1-36
- Castner, E. W., Jr.; Wishart, J. F. & Shirota, H. (2007). Intermolecular dynamics, interactions, and solvation in ionic liquids, *Accounts of Chemical Research*, 40, 1217-1227
- Chang, Y. J. & Castner, E. W., Jr. (1993). Fast responses from "slowly relaxing" liquids: a comparative study of the femtosecond dynamics of triacetin, ethylene glycol, and water, *Journal of Chemical Physics*, 99, 7289-7299
- Dominguez-Vidal, A.; Kaun, N.; Ayora-Canada, M. J. & Lendl, B. (2007). Probing intermolecular interactions in water/ionic liquid mixtures by far-infrared spectroscopy, *Journal of Physical Chemistry B*, 111, 4446-4452
- Dzyuba, S. V. & Bartsch, R. A. (2002). Influence of structural variations in 1-alkyl(aralkyl)-3-methylimidazolium hexafluorophosphates and bis(trifluoronethylsulfonyl)imides on physical properties of the ionic liquids, *CHEMPHYSICHEM*, 3, 161-166
- Elola, M. D. & Ladanyi, B. M. (2006). Molecular dynamics study of polarizability anisotropy relaxation in aromatic liquids and its connection with local structure, *Journal of Physical Chemistry B*, 110, 15525-15541
- Farrer, R. A. & Fourkas, J. T. (2003). Orientational dynamics of liquids confined in nanoporous sol-gel glass studied by optical Kerr effect spectroscopy, *Accounts of Chemical Research*, 36, 605-612
- Fujisawa, T.; Nishikawa, K. & Shirota, H. (2009). Comparison of interionic/intermolecular vibrational dynamics between ionic liquids and concentrated electrolyte solutions, *Journal of Chemical Physics*, 131, 244519/1-14
- Fumino, K.; Wulf, A. & Ludwig, R. (2008). The cation-anion interaction in ionic liquids probed by far-infrared spectroscopy, *Angewandte Chemie – International Edition*, 47, 3830-3834
- Geiger, L. C. & Ladanyi, B. M., (1988). Higher-order interaction-induced effects on the allowed Raman spectra of liquid CS<sub>2</sub>, *Journal of Chemical Physics*, 89, 6588-6599
- Geiger, L. C. & Ladanyi, B. M., (1989). Molecular dynamics simulation study of nonlinear optical response of fluids, *Chemical Physics Letters*, 159, 413-420

- Giraud, G.; Gordon, C. M.; Dunkin, I. R. & Wyyne, K. (2003). The effects of anion and cation substitution on the ultrafast solvent dynamics of ionic liquids: a time-resolved optical Kerr-effect spectroscopic study, *Journal of Chemical Physics*, 119, 464-477
- Hansen, J.-P. & McDonald, I. R. (2006). *Theory of Simple Liquids*, 3rd ed., Academic Press, ISBN 978-0-12-370535-8, London
- Heisler, I. A. & Meech, S. R. (2010). Low-frequency modes of aqueous alkali halides solutions: glimpsing the hydrogen bonding vibration, *Science*, 327, 857-860
- Holbrey, J. D. & Seddon, K. R. (1999). The phase behaviour of 1-alkyl-3-methylimidazolium tetrafluoroborates; ionic liquids and ionic liquid crystals, *Journal of Chemical Society, Dalton Transaction*, 2133-2139
- Hu, Z.; Huang, X.; Annappureddy, H. V. R. & Margulis, C. J. (2008). Molecular dynamics study of the temperature-dependent optical Kerr effect spectra and intermolecular dynamics of room temperature ionic liquid 1-methoxyethylpyridinium dicyanoamide, *Journal of Physical Chemistry B*, 112, 7837-7849
- Hunt, N. T.; Jaye, A. A. & Meech, S. R. (2007). Ultrafast dynamics in complex fluids observed through the ultrafast optically-heterodyne-detected optical-Kerr-effect (OHD-OKE), *Physical Chemistry Chemical Physics*, 9, 2167-2180
- Hyun, B.-R.; Dzyuba, S. V.; Bartsch, R. A. & Quitevis, E. L. (2002). Intermolecular dynamics of room-temperature ionic liquids: femtosecond optical Kerr effect measurements on 1-alkyl-3-ethylimidazolium bis((trifluoromethyl)sulfonyl)imides, *Journal of Physical Chemistry A*, 106, 7579-7585.
- Ishida, T.; Nishikawa, K. & Shirota, H. (2009). Atom substitution effects of  $[\text{XF}_6]^-$  in ionic liquids. 2. Theoretical study, *Journal of Physical Chemistry B*, 113, 9840-9851
- Israelachvili, J. N. (1992). *Intermolecular and Surface Forces*, 2nd Ed., Academic Press, ISBN 0-12-375181-0, London
- Iuchi, S.; Morita, A. & Kato, S. (2002). Molecular dynamics simulation with the charge response kernel: vibrational spectra of liquid water and *N*-methylacetamide in aqueous solution, *Journal of Physical Chemistry B*, 106, 3466-3476
- Iwata, K.; Okajima, H.; Saha, S. & Hamaguchi, H. (2007). Local structure formation in alkyl-imidazolium-based ionic liquids as revealed by linear and nonlinear Raman spectroscopy, *Accounts of Chemical Research*, 40, 1174-1181
- Jin, H.; O'Hare, B.; Dong, J.; Arzhantsev, S.; Baker, G. A.; Wishart, J. F.; Benesi, A. J. & Maroncelli, M. (2008). Physical properties of ionic liquids consisting of the 1-butyl-3-methylimidazolium cation with various anions and the bis(trifluoromethylsulfonyl)imide anion with various cations, *Journal of Physical Chemistry B*, 112, 81-92
- Katsuta, S.; Imai, K.; Kudo, Y.; Takeda, Y.; Seki, H. & Nakakoshi, M. (2008). Ion pair formation of alkylimidazolium ionic liquids in dichloromethane, *Journal of Chemical Engineering Data*, 53, 1528-1532
- Khalil, M.; Golonzka, O.; Demirdoven, N.; Fecko, C. J. & Tokmakoff, A. (2000). Polarization-selective femtosecond Raman spectroscopy of isotropic and anisotropic vibrational dynamics in liquids, *Chemical Physics Letters*, 321, 231-237

- Kinoshita, S.; Kai, Y.; Ariyoshi, T. & Shimada, Y. (1996). Low frequency modes probed by time-domain optical Kerr effect spectroscopy, *International Journal of Modern Physics B*, 10, 1229–1272
- Koeberg, M.; Wu, C.-C.; Kim, D. & Bonn, M. (2007). THz dielectric relaxation of ionic liquid:water mixtures, *Chemical Physics Letters*, 439, 60-64
- Kobrak, M. N. & Sandalow, N. (2006). An electrostatic interaction of structure-property relationships in ionic liquids, In: *Molten Salts XIV*, Mantz, R. A., Ed., 417-425, Electrochemical Society, ISBN 978-156677514-4, Pennington
- Li, H.; Ibrahim, M.; Agberemi, I. & Kobrak, M. N. (2008). The relationship between ionic structure and viscosity in room-temperature ionic liquids, *Journal of Chemical Physics*, 129, 124507/1-12
- Li, J.; Wang, I.; Fruchey, K. & Fayer, M. D. (2006). Dynamics in supercooled ionic organic liquids and mode coupling theory analysis, *Journal of Physical Chemistry A*, 110, 10384-10391
- Lide, D. R., Editor-in-Chief (2008). *CRC Handbook of Chemistry and Physics*, 89th Ed., CRC Press, ISBN 978-1-4200-6679-1, Boca Raton
- Lopes, J. N. C.; Gomes, M. F. C. & Padua, A. A. H. (2006). Nonpolar, polar, and associating solutes in ionic liquids, *Journal of Physical Chemistry B*, 110, 16816-16818
- Lotshaw, W. T.; McMorro, D.; Thant, N.; Melinger, J. S. & Kitchenham, R. (1995). Intermolecular vibrational coherence in molecular liquids, *Journal of Raman Spectroscopy*, 26, 571-583
- Madden, P. A. & Cox, T. I. (1981). A comparative study of the interaction-induced spectra of liquid CS<sub>2</sub>. II. Lineshapes. *Molecular Physics*, 43, 287-305
- Madden, P. A. (1984). Interaction-induced phenomena, In: *Molecular Liquids – Dynamics and Interactions*, Barnes, A. J.; Orville-Thomsa, W. J. & Yarwood, J., Eds., 431-451, D. Reidel Publishing Company, ISBN 90-277-1817-2, Dordrecht
- McMorro, D.; Lotshaw, W. T. & Kenney-Wallace, G. A. (1988). Femtosecond optical Kerr effect studies on the origin of the nonlinear responses in simple liquids, *IEEE Journal of Quantum Electronics*, 24, 443-454
- McMorro, D. & Lotshaw, W. T. (1990). The frequency response of condensed-phase media to femtosecond optical pulses: spectral-filter effects, *Chemical Physics Letters*, 174, 85-94
- McMorro, D. & Lotshaw, W. T. (1991). Intermolecular dynamics in acetonitrile probed with femtosecond Fourier transform Raman spectroscopy, *Journal of Physical Chemistry*, 95, 10395-10406
- McQuarrie, D. A. (2000). *Statistical Mechanics*, University Science Books, ISBN 1-891389-15-7, Sausalito
- Mukamel, S. (1995). *Principles of Nonlinear Spectroscopy*, Oxford University Press, ISBN 0-19-509278-3, New York
- Nagata, Y. & Tanimura, Y. (2006). Two-dimensional Raman spectra of atomic solids and liquids, *Journal of Chemical Physics*, 124, 024508/1-9
- Ohno, H., Ed. (2005). *Electrochemical Aspects of Ionic Liquids*, ISBN 978-0-471-64851-2, Wiley-Interscience, Hoboken

- Rajian, J. R.; Li, S.; Bartsch, R. A.; Quitevis, E. L. (2004). Temperature-dependence of the low-frequency spectrum of 1-pentyl-3-methylimidazolium bis(trifluoromethanesulfonyl)imide studied by optical Kerr effect spectroscopy, *Chemical Physics Letters*, 393, 372-377
- Righini, R. (1993). Ultrafast optical Kerr effect in liquids and solids, *Science*, 262, 1386-1390
- Russina, O.; Triolo, A.; Gontrani, L.; Caminiti, R.; Xiao, D.; Hines, L. G., Jr.; Bartsch, R. A.; Quitevis, E. L.; Plechkova, N. & Seddon, K. R. (2010). Morphology and intermolecular dynamics of 1-alkyl-3-methylimidazolium bis[(trifluoromethane)sulfonyl]amide ionic liquids: structural and dynamic evidence of nanoscale segregation, *Journal of Physics: Condensed Matter*, 21, 424121/1-9
- Ryu, S. & Stratt, R. M. (2004). A case study in the molecular interpretation of optical Kerr effect spectra: Instantaneous-normal-mode analysis of the OKE spectrum of liquid benzene, *Journal of Physical Chemistry B*, 108, 6782-6795
- Seki, S.; Hayamizu, K.; Tsuzuki, S.; Fujii, K.; Umebayashi, Y.; Mitsugi, T.; Kobayashi, T.; Ohno, Y.; Kobayashi, Y.; Mita, Y.; Miyashiro, H. & Ishiguro, S. (2009). Relationships between center atom species (N, P) and ionic conductivity, viscosity, density, self-diffusion coefficient of quaternary cation room-temperature ionic liquids, *Physical Chemistry Chemical Physics*, 11, 3509-3514
- Shigeto, S. & Hamaguchi, H. (2006). Evidence for mesoscopic local structures in ionic liquids: CARS signal spatial distribution of  $C_n\text{mim}[\text{PF}_6]$  ( $n = 4,6,8$ ), *Chemical Physics Letters*, 427, 329-332
- Shirota, H. (2005). Ultrafast molecular dynamics of liquid aromatic molecules and the mixtures with  $\text{CCl}_4$ , *Journal of Chemical Physics*, 122, 044514/1-12
- Shirota, H. & Castner, E. W., Jr. (2005). Physical properties and intermolecular dynamics of an ionic liquid compared with its isoelectronic neutral binary solution, *Journal of Physical Chemistry A*, 109, 9388-9392
- Shirota, H. & Castner, E. W., Jr. (2005). Why are viscosities lower for ionic liquids with  $-\text{CH}_2\text{Si}(\text{CH}_3)_3$  vs  $-\text{CH}_2\text{Si}(\text{CH}_3)_3$  substitutions on the imidazolium cations?, *Journal of Physical Chemistry B*, 109, 21576-21585
- Shirota, H.; Funston, A. M.; Wishart, J. F. & Castner, E. W., Jr., (2005). Ultrafast dynamics of pyrrolidinium cation ionic liquids, *Journal of Chemical Physics*, 122, 184512/1-12
- Shirota, H.; Wishart, J. F. & Castner, E. W., Jr. (2007). Intermolecular interactions and dynamics of room temperature ionic liquids that have silyl and siloxy-substituted imidazolium cations, *Journal of Physical Chemistry B*, 111, 4819-4829
- Shirota, H.; Nishikawa, K. & Ishida, T. (2009). Atom substitution effects of  $[\text{XF}_6]^-$  in ionic liquids. 1. Experimental study, *Journal of Physical Chemistry B*, 113, 9831-9839
- Shirota, H.; Fujisawa, T.; Fukazawa, H. & Nishikawa, K. (2009). Ultrafast dynamics in aprotic molecular liquids: a femtosecond Raman-induced Kerr effect spectroscopic study, *Bulletin of the Chemical Society of Japan*, 82, 1347-1366
- Shirota, H.; Fukazawa, H.; Fujisawa, T. & Wishart, J. F. (2010). Heavy atom substitution effects in non-aromatic ionic liquids: Ultrafast dynamics and physical properties, *Journal of Physical Chemistry B*, 114, 9400-9412

- Smith, N. A. & Meech, S. R. (2002). Optically-heterodyne-detected optical Kerr effect (OHD-OKE): applications in condensed phase dynamics, *International Reviews in Physical Chemistry*, 21, 75-100
- Suarez, P. A. Z.; Einloft, S.; Duflius, J. E. L.; de Souza, R. F. & Dupont, J. (1998). Synthesis and physical-chemical properties of ionic liquids based on 1-n-butyl-3-methylimidazolium cation, *Journal de Chimie Physique et de Physico-Chimie Biologique*, 95, 1626-1639
- Tanimura, Y. & Mukamel, S. (1993). Two-dimensional femtosecond vibrational spectroscopy of liquids, *Journal of Chemical Physics*, 99, 9496-9511
- Triolo, A.; Russina, O.; Bleif, H.-J. & Di Cola, E. (2007). Nanoscale segregation in room temperature ionic liquids, *Journal of Physical Chemistry B*, 111, 4641-4644
- Tsunashima, K. & Sugiya, M. (2007). Physical and electrochemical properties of low-viscosity phosphonium ionic liquids as potential electrolytes, *Electrochemistry Communications*, 9, 2353-2358
- Tsuzuki, S.; Tokuda, H.; Hayamizu, K. & Watanabe, M. (2005). Magnitude and directionality of interaction in ion pairs of ionic liquids: relationship with ionic conductivity, *Journal of Physical Chemistry B*, 109, 16474-16481
- Turton, D. A.; Hunger, J.; Stoppa, A.; Hefter, G.; Thoman, A.; Walther, M.; Buchner, R. & Wynne, K. (2009). Dynamics of imidazolium ionic liquids from a combined dielectric relaxation and optical Kerr effects study: evidence for mesoscopic aggregation, *Journal of the American Chemical Society*, 131, 11140-11146
- Urahata, S. M. & Ribeiro, M. C. C. (2005). Single particle dynamics in ionic liquids of 1-alkyl-3-methylimidazolium cations, *Journal of Chemical Physics*, 122, 024511/1-9
- Wang, Y. & Voth, G. A. (2006). Tail aggregation and domain diffusion in ionic liquids, *Journal of Physical Chemistry B*, 110, 18601-18608
- Wasserscheid, P. & Welton, T., Eds. (2008). *Ionic Liquids in Synthesis*, 2nd Ed., WILEY-VCH, ISBN 978-3-527-31239-9, Weinheim
- Wiewior, P. P.; Shirota, H. & Castner, E. W., Jr. (2002). Aqueous dimethyl sulfoxide solutions: Inter- and intra-molecular dynamics, *Journal of Chemical Physics*, 116, 4643-4654
- Xiao, D.; Rajian, J. R.; Hines, L. G., Jr.; Li, S.; Bartsch, R. A. & Quitevis, E. L. (2006). Additivity in the optical Kerr effect spectra of binary ionic liquid mixtures: implications for nanostructural organization, *Journal of Physical Chemistry B*, 110, 16174-16178
- Xiao, D.; Rajian, J. R.; Cady, A.; Li, S.; Bartsch, R. A. & Quitevis, E. L. (2007). Nanostructural organization and anion effects on the temperature dependence of the optical Kerr effect spectra of ionic liquids, *Journal of Physical Chemistry B*, 111, 4669-4677
- Xiao, D.; Rajian, J. R.; Hines, L. G., Jr.; Li, S.; Bartsch, R. A. & Quitevis, E. L. (2008). Nanostructural Organization and anion effects in the optical Kerr effect spectra of binary ionic liquids mixtures, *Journal of Physical Chemistry B*, 112, 13316-13325
- Xiao, D.; Hines, L. G., Jr.; Li, S.; Bartsch, R. A.; Quitevis, E. L.; Russina, O. & Triolo, A. (2009). Effect of cation symmetry and alkyl chain length on the structure and intermolecular dynamics of 1,3-dialkylimidazolium bis(trifluoromethanesulfonyl)amide, *Journal of Physical Chemistry B*, 113, 6426-6433

- Yamamoto, K.; Tani, M. & Hangyo, M. (2007). Terahertz time-domain spectroscopy of imidazolium ionic liquids, *Journal of Physical Chemistry B*, 111, 4854-4859
- Zhong, Q. & Fourkas, J. T. (2008). Optical Kerr effect spectroscopy of simple liquids, *Journal of Physical Chemistry*



# Interactions between Organic Compounds and Ionic Liquids. Selectivity and Capacity Characteristics of Ionic Liquids

Fabrice Mutelet and Jean-Noël Jaubert

*Ecole Nationale Supérieure des Industries Chimiques, Nancy-Université  
France*

## 1. Introduction

Nowadays, environmental protection is one of the most important matter of concerns. In the last century, chemical engineering industry developed processes involving unit operation using volatile organic components (VOC). Solvents comprise 2/3 of all industrial emissions and 1/3 of all VOC emissions nationwide. Many factories also produce long-lasting gases that do not occur naturally, yet contribute significantly to the enhanced greenhouse effect and global warming that is currently under way. The new constraints facing chemical engineers are to continue to provide society with the products necessary for sustaining a high standard of living, while, at the same time, significantly reduce the environmental impact of the processes we use to do this. Therefore, the reduction of the use of VOCs is a significant research topic in recent years.

In the last ten years, a new class of compounds has emerged and may become a key ally in helping us meet the twin challenges of efficient and environmentally benign chemical processing. These compounds known as Ionic liquids (ILs) or room temperature ionic liquids (RTILs) have received increased attention from both industrial and academic communities because they have the potential to revolutionize the way we think of and use solvents. Because of the lack of measurable vapor pressure, easy recyclability, and no flammability, ionic liquid solvents are viewed by many as "green" solvents. They are organic salts, whose cations, substituents and anions can be varied at will to change their chemical and physical properties. They can be used to redesign processes in order to reduce or eliminate loss of solvents particularly volatile organic compounds (VOCs) (Letcher, 2007). The growth in development in ionic liquids is not only being driven by their potential as green solvents but also by potential improvement in process economics, chemical reactivity, selectivity, and yield. Nowadays, ILs are emerging as alternative green solvents, in other words, as alternative reaction media for synthesis, catalysis and biocatalysis, but also as electrolytes, lubricants or modifiers of mobile and stationary phases in the separation sciences (Letcher, 2007; Rodgers & Seddon, 2002; Rodgers & Seddon, 2003; Alonso et al., 2008; Cadena et al, 2004).

Ionic liquids have been used in industrial processes for more than a decade and their applications continue to expand. For instance, extractive distillation and liquid-liquid extraction with ionic liquids as separating agent is a novel method for separation of ethanol-

water mixture (Arlt et al, 2001), of thiophene from aliphatic hydrocarbons (Alonso et al, 2008). It is clear that ionic liquids may play an important role since regulations regarding liquid hydrocarbon fuels are continuously requiring sulfur content to be reduced to lower levels. The current specification in Europe and in the USA has defined the maximum sulphur content as less as 50 parts per million in gasoline starting from 2005. This level will be reduced to 10 ppm by the year 2010. Their attractiveness has led to the development of several new commercial processes. For example, BASF's BASIL process uses ionic liquids to remove acids from reaction mixtures. The French Petroleum Institute's process called Difasol also uses ionic liquids as reaction solvents for dimerizing butene to octenes. Many new areas of application in the petroleum, chemical and allied industries are emerging for ionic liquids.

The knowledge of the physico-chemical properties of ionic liquids is of great importance. Indeed, a large thermodynamic databank will give a better understanding of the behaviour of ILs in mixtures depending on the ionic structures and the intermolecular interactions. Furthermore, measurement of physical properties for these substances is essential to evaluate the actual potential of an IL as solvent for a particular application. While data on activity coefficients, vapor-liquid equilibria and liquid-liquid equilibria are now available for a number of binary and a few ternary systems, the situation is still not satisfying with respect to a systematic knowledge of these properties and further research work have to fill the remaining gaps. In the beginning of 2000, the majority of research works were focussed on organic synthesis of ILs and on the study of chemical reactions in ILs. Systematic investigations of thermodynamic properties of pure ILs and their mixtures with organic compounds or gases are not always performed. Nevertheless, data for these properties are of considerable importance for selecting appropriate ILs in different applications of chemical engineering.

In this article, we present a general behaviour of organic compounds with ionic liquids using thermodynamic properties such as partition coefficients or activity coefficients at infinite dilution determined using inverse gas chromatography. Infinite dilution activity coefficients ( $\gamma^\infty$ ) are very useful for process synthesis and design. For example, activity coefficients at infinite dilution can be directly used for the selection of solvents for azeotropic/extractive distillation, liquid extraction, solvent-aided crystallization, and even chemical reaction. Activity coefficients at infinite dilution  $\gamma^\infty$  give a direct measure of interactions between unlike molecules in the absence of solute-solute interactions. With others respects, numerous approaches may be used to characterize the interactions between the solute and the ionic liquids. Using chromatographic data, we propose to characterize solute-ionic liquids interactions using a solvation model. Then, the last part will be devoted to a brief presentation of the influence of structure of ionic liquid on selectivity and capacity for four separation problems.

## 2. Solvation models used in gas chromatography

### 2.1 Linear solvation energy relationship

In numerous solvation models, the partition of a solute between the gas phase and a solvent (or stationary phase) may be described by a cavity theory of solution (Vitha & Carr, 2006; Abraham et al., 1999) in which the solvation process is divided into three steps. In the step 1, a cavity of suitable size to accommodate the solute is created in the solvent (Figure 1). This process is endoergic because work is required to disrupt solvent-solvent interactions. In the

second step, the solvent molecules around the cavity are reorganized from their original positions to the positions they will adopt when the solute is in equilibrium with the solvent. Of course, these positions are not fixed but are averages of solvent positions. The Gibbs energy change for such reorganization is assumed to be negligible, by analogy with the melting of a solid. However, enthalpy and entropy changes in reorganizations may be large, again by analogy with the melting of a solid. In the last step, the solute is introduced into the reorganized cavity, and various solute-solvent interactions are set up, all of which are exoergic.

Several thermodynamic properties are related to partitioning between water and other phases, for example octanol ( $K_{ow}$ ) or the pure compound itself (water solubility). These partitioning processes can be understood from thermodynamic concepts—like free energy, chemical potential and fugacity. The equilibrium partition constant between two phases, on a mole fraction basis, can be expressed as:

$$K_{i12} = \exp(-\Delta_{12}G_i/RT) \quad (1)$$

where  $\Delta_{12}G_i$  is the Gibbs energy (or free energy) of transfer between the two phases,  $R$  is the general gas constant and  $T$  is the absolute temperature. The Gibbs energy sums up both the enthalpic ( $\Delta_{12}H$ ) and entropic ( $\Delta_{12}S$ ) effects resulting from changes in intermolecular interactions:

$$\Delta_{12}G_i = \Delta_{12}H_i - T \Delta_{12}S_i \quad (2)$$

The calculation of partitioning from structural or other descriptors therefore requires the modelling of these effects. The Gibbs energy change can also be separated into the contributions of van der Waals and polar interactions, assuming that these are additive:

$$\Delta_{12}G_i = \Delta_{12}G_{i,vdW} + \Delta_{12}G_{i,polar} \quad (3)$$

In the early 1980's, (Taft & Kamlet, 1976; Kamlet et al., 1977; Kamlet et al., 1983; Kamlet & Taft, 1985; Kamlet et al., 1988) have developed the basic concept of linear solvation energy relationships (LSERs). They have demonstrated for thousands of chemical systems that some property which is linearly related to either a free energy of reaction, a free energy of transfer, or an activation energy can be correlated with various fundamental molecular properties of the solvents or solutes involved. Chromatographic retention and in particular logarithmic retention factors ( $\log k'$ ), logarithmic partition coefficients ( $\log K_L$ ) are linear free energy parameters and as such one can linearly correlate these data with the molecular properties of the solutes using the LSER model (Abraham & Whiting, 1992; Abraham et al., 1993a; Park & Carr, 1989; Weckwerth & Carr, 1998).

The most recent representation of the LSER model proposed by (Abraham et al., 1987; Abraham et al., 1990, Abraham et al., 1991, Abraham et al., 1993b) is given by equation (4)

$$\log SP = c + eE + sS + aA + bB + IL \quad (4)$$

Where  $SP$  is a solvation parameter related with the free energy change such as gas-liquid partition coefficient, specific retention volume or adjusted retention time at a given temperature. The capital letters represent the solutes properties and the lower case letters the complementary properties of the ionic liquids. The solute descriptors are the excess molar refraction  $E$ , dipolarity/ polarizability  $S$ , hydrogen bond acidity/basicity,  $A$  and  $B$ , respectively, and the gas-liquid partition coefficient on *n*-hexadecane at 298 K,  $L$ . The solute

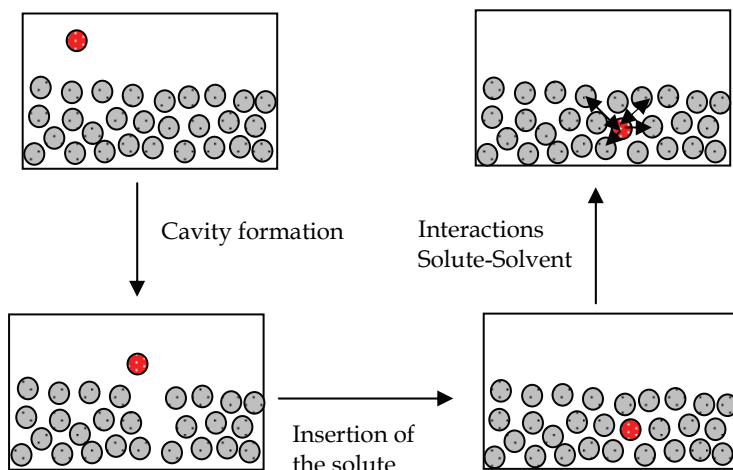


Fig. 1. Model of the solvation process.

descriptors may be determined using inverse gas chromatography or estimated using a group contribution method. A databank of descriptors for about 3000 compounds may be found in the literature (Platts et al., 1999, Abraham & Platts, 2001, Mutelet & Rogalski, 2001). The coefficients  $c$ ,  $e$ ,  $s$ ,  $a$ ,  $b$  and  $l$  are not simply fitting coefficients, but they reflect complementary properties of the solvent phase. These coefficients are determined by multiple linear regression of equation (4). This model was strongly applied to characterize chemicals products, petroleum fluids.

### 3.2 Application of linear solvation energy relationship on ionic liquids

In the literature, there is a large amount of data of partition coefficients or activity coefficients measured by gas-liquid chromatography or by dilutor technique. Some system constants for various ionic liquids and classical solvents at 25 °C are summarized in Table 1. The data for the 1-ethanol-3-methylimidazolium tetrafluoroborate, 1-ethanol-3-methylimidazolium hexafluorophosphate, 1,3-dimethylimidazolium dimethylphosphate and 1-ethyl-3-methylimidazolium diethylphosphate (Revelli et al., 2009a), 1-Butyl-3-methylimidazolium tetrafluoroborate (Revelli et al., 2009b), n-Acryloyloxypropyl-N-methylimidazolium bromide and n-Methacryloyloxyhexyl-N-methylimidazolium bromide (Mutelet et al., 2008), 1-Propenyl-3-alkyl-imidazolium bromide (Mutelet et al., 2006), 1-butyl-3-methylimidazolium octyl sulfate and 1-ethyl-3-methylimidazolium tosylate (Mutelet & Jaubert, 2006), Triethylsulphonium bis(trifluoromethylsulfonyl)imide (Domańska & Marciniak, 2009a), 1-Methyl-3-ethylimidazolium bis(trifluorosulfonyl)-amide and 1,2-Dimethyl-3-ethylimidazolium bis(trifluorosulfonyl)-amide (Krummen et al., 2002) were taken from the sources indicated. (Poole & Poole, 2010) found that the system constants of LSER model for the room temperature ionic liquids fall into the range  $e = -0.62$  to  $0.86$ ,  $s = 1.7$ – $2.8$ ,  $a = 2.1$ – $7.3$ ,  $b = 0$ – $1.07$ , and  $l = 0.35$ – $0.96$ . Compared with the scale of the polar organic solvents  $e = -0.60$  to  $0.82$ ,  $s = 0.54$ – $2.8$ ,  $a = 0.28$ – $5.50$ ,  $b = 0$ – $4.8$ , and  $l = -0.21$  to  $0.98$ , we can see that both scales are similar indicating that the solvation properties for the room temperature ionic liquids are classical and fit quite well into the scales developed for polar molecular solvents.

Ionic liquids	System constants					
	e	s	a	b	l	c
1-ethanol-3-methylimidazolium hexafluorophosphate	0	3.03	2.89	1.13	0.47	-1.14
1-ethanol-3-methylimidazolium tetrafluoroborate	0	3.03	3.64	0.763	0.5	-1.35
1,3-dimethylimidazolium dimethylphosphate	0.86	2.59	7.27	0	0.35	-0.61
1-ethyl-3-methylimidazolium diethylphosphate	0.26	1.97	6.9	0	0.54	-0.09
1-Butyl-3-methylimidazolium tetrafluoroborate	0.56	2.82	3.27	0.48	0.5	-0.77
n-Acryloyloxypropyl-N-methylimidazolium bromide	0	2.88	5.5	0	0.48	-1.03
n-Methacryloyloxyhexyl-N-methylimidazolium bromide	0	2.46	5.36	0	0.57	-0.87
1-Propenyl-3-methyl-imidazolium bromide	0	2.16	5.19	0	0.53	-1.86
1-Propenyl-3-octyl-imidazolium bromide	0	1.72	4.96	0	0.57	-1.6
1-Propenyl-3-decyl-imidazolium bromide	0	1.73	4.89	0	0.66	-1.58
1-Propenyl-3-dodecyl-imidazolium bromide	0	1.44	4.87	0	0.72	-1.51
1-Butyl-3-methylimidazolium octyl sulfate	0	1.47	4.05	0	0.68	-0.237
1-Ethyl-3-methylimidazolium tosylate	0.54	2.4	4.81	0.17	0.48	-0.84
n-Butylammonium thiocyanate	0.14	1.65	2.76	1.32	0.45	-0.75
1-Methyl-3-ethylimidazolium bis(trifluorosulfonyl)-amide	0.148	2.277	2.172	1.041	0.629	-0.439
1,2-Dimethyl-3-ethylimidazolium bis(trifluorosulfonyl)-amide	0.214	2.347	2.075	0.896	0.655	-0.565
Triethylsulphonium bis(trifluoromethylsulfonyl)imide	0.114	2.37	2.34	0.696	0.642	-0.803
1-Ethyl-3-methylimidazolium Trifluoroacetate	0.608	1.63	4.21	1.81	0.584	-0.918
1-Butyl-3-methylimidazolium Trifluoromethanesulfonate	0.399	2.03	3.49	0.681	0.647	-0.784
Organic solvents						
Trifluoroethanol	-0.547	1.339	2.213	3.807	0.645	-0.092
Methanol	-0.22	1.17	3.7	1.43	0.769	-1.27
Water	0.82	2.74	3.9	4.81	-0.213	0
1,2 Dichloroethane	-0.47	1.676	0.92	0.486	0.927	0.025
Dry methyl acetate	-0.447	1.675	2.625	0.213	0.874	0.129
Dry ethyl acetate	-0.352	1.316	2.891	0	0.916	0.182
Ethylene glycol	0.217	1.427	4.474	2.687	0.568	-0.898
Benzene	-0.313	1.053	0.457	0.169	1.02	0.107
2-(Cyclohexylamino)ethanesulfonate	0.07	1.57	3.67	0	0.51	-0.83

Table 1. LSER descriptors of ionic liquids and classical solvents determined at 313.15 K.

The ( $c + IL$ ) term gives information on the effect of cohesion of the ionic liquids on solute transfer from the gas phase. In general, the ionic liquids are cohesive solvents; they interact weakly via nonbonding and  $\pi$ -electrons ( $r$  system constant is zero) and are not much different to other polar non-ionic liquids. The ionic liquids are roughly as dipolar/polarizable as classical solvents. The hydrogen-bond basicity of the ionic liquid ( $a$  system constants) are considerably larger than values obtained for non ionic phases (0-2.1) (Poole, 2004). The hydrogen-bond basicity of ILs depends on the anion grafted on the cation. ILs can be slightly more hydrogen-bond basic than dimethyl sulfoxide and *N*-methylpyrrolidinone, and are weak to moderate hydrogen-bond acids, similar to the aliphatic alcohols. From Table 1 and data collected by (Poole & Poole, 2010), we can see that the hydrogen-bond acidity of the ionic liquids depends largely on the cation and is lower for the 1,3-dialkylimidazolium salts with an alkyl group at C-2 position than 1,3-dialkylimidazolium salts.

### 3.1 Predictive models based on LSER model coupled to a group contribution method

In order to quantify intermolecular solute-IL interactions, (Abraham et al., 2003; Acree & Abraham, 2006) reported mathematical correlations based on the general Abraham solvation parameter model for the gas-to-solvent,  $K_L$ , and water-to-solvent,  $P$ , partition coefficients. Recently, (Sprunger et al., 2007; Sprunger et al., 2008; Sprunger et al., 2009a; Sprunger et al., 2009b) modified the Abraham solvation parameter model:

$$\begin{aligned} \text{Log } K_L = & c_{\text{cation}} + c_{\text{anion}} + (e_{\text{cation}} + e_{\text{anion}}) \cdot E + (s_{\text{cation}} + s_{\text{anion}}) \cdot S + (a_{\text{cation}} + a_{\text{anion}}) \cdot A \\ & + (b_{\text{cation}} + b_{\text{anion}}) \cdot B + (l_{\text{cation}} + l_{\text{anion}}) \cdot L \end{aligned} \quad (5)$$

$$\begin{aligned} \text{Log } P = & c'_{\text{cation}} + c'_{\text{anion}} + (e'_{\text{cation}} + e'_{\text{anion}}) \cdot E + (s'_{\text{cation}} + s'_{\text{anion}}) \cdot S + (a'_{\text{cation}} + a'_{\text{anion}}) \cdot A \\ & + (b'_{\text{cation}} + b'_{\text{anion}}) \cdot B + (v_{\text{cation}} + v_{\text{anion}}) \cdot V \end{aligned} \quad (6)$$

by rewriting each of the six solvent equation coefficients as a summation of their respective cation and anion contribution. The dependent variables in eqs 5 and 6 are solutes descriptors as follows: **E** and **S** refer to the excess molar refraction in units of (cm<sup>3</sup>.mol<sup>-1</sup>)/10 and dipolarity/polarizability descriptors of the solute, respectively, **A** and **B** are measures of the solute hydrogen-bond acidity and basicity, **V** is the McGowan volume in units of (cm<sup>3</sup>.mol<sup>-1</sup>)/100 and **L** is the logarithm of the gas-to-hexadecane partition coefficient at 298 K. Sprunger et al. calculated equation coefficients for 8 cations and 4 anions using a database that contained 584 experimental log  $K_L$  and 571 experimental log  $P$  values. No loss in predictive accuracy was observed by separating the equation coefficients into individual cation-specific and anion-specific values. The major advantage of splitting the equation coefficients into individual cation-specific and anion-specific contributions is that one can make predictions for more ILs. In Sprunger's approach, the major advantage of splitting the equation coefficients into individual cation-specific and anion-specific contributions is that one can make predictions for more ILs. Most of the cations are alkylimidazolium. The use of this model is somewhat limited since it can not be extrapolated to alkylimidazolium ionic liquids not initially defined by the method (e.g. with long alkyl chains).

In the development of (Revelli et al, 2010a), the cation with its alkyl chains is splitted in different contributions: (CH<sub>3</sub>, CH<sub>2</sub>, N, CH<sub>cyclic</sub>...). The approach allows to have a predictive model. The aim of this work was to develop a group contribution method allowing to estimate the log  $K_L$  and Log  $P$  of organic compounds in ionic liquids at 298 K. Using the LSER model proposed by Abraham, the group contribution method expresses LSER coefficients  $c_i$ ,  $e_i$ ,  $s_i$ ,  $a_i$ ,  $b_i$  and  $l_i$  of equation (7) or  $c'_i$ ,  $e'_i$ ,  $s'_i$ ,  $a'_i$ ,  $b'_i$  and  $v_i$  of equation (8) by:

$$\text{Log} K_L = \sum_i^{21} n_i \times c_i + \sum_i^{21} n_i \times e_i \cdot \mathbf{E} + \sum_i^{21} n_i \times s_i \cdot \mathbf{S} + \sum_i^{21} n_i \times a_i \cdot \mathbf{A} + \sum_i^{21} n_i \times b_i \cdot \mathbf{B} + \sum_i^{21} n_i \times l_i \cdot \mathbf{L} \quad (7)$$

$$\text{Log} P = \sum_i^{21} n_i \times c'_i + \sum_i^{21} n_i \times e'_i \cdot \mathbf{E} + \sum_i^{21} n_i \times s'_i \cdot \mathbf{S} + \sum_i^{21} n_i \times a'_i \cdot \mathbf{A} + \sum_i^{21} n_i \times b'_i \cdot \mathbf{B} + \sum_i^{21} n_i \times v_i \cdot \mathbf{V} \quad (8)$$

Where  $n_i$  is the number of group  $i$  present in the ionic liquid.

The experimental data used to calculate Abraham's model ion-specific equation coefficients were taken from the collection of (Sprunger et al., 2007; Sprunger et al., 2008; Sprunger et al., 2009a; Sprunger et al., 2009b) and were updated with recent data (Revelli et al., 2010a). A total of 1450 gas-liquid partition coefficients and 1410 water-to-liquid partition coefficients were used for the calculation. Solutes were mainly n-alkanes, cycloalkanes, alkenes, alkynes, aromatics, alcohols, ethers, aldehydes, ketones, chloroalkanes. The  $E$ -scale varies from 0 to 1.5, the  $S$ -scale from 0 to 1.72, the  $A$ -scale from 0 to 1.04, the  $B$ -scale from 0 to 1.28, the  $L$ -scale from -1.200 to 7.833 and the  $V$ -scale from 0.109 to 1.799. The dataset is composed of 27 imidazolium based ionic liquids, 3 ammonium, 3 pyridinium and 4 pyrrolidinium based ionic liquids. The authors also add sulphonium and phosphonium ionic liquids although only one set of  $K_L$  (or  $P$ ) data may be found for these families. The twenty one groups which are defined in this method are listed in Table 2. The decomposition into groups of the ionic liquids is very easy, that is as simple as possible. No substitution effects are considered. No exceptions are defined. In Figure 2 are represented all ionic liquids studied in this work. Five groups are defined to describe the chains  $R_1$ ,  $R_2$ ,  $R_3$  and  $R_4$  grafted on the cation: CH<sub>3</sub>, CH<sub>2</sub>, -O-, -O-N<sub>cycl</sub> and -OH. These groups allow the calculation of partition coefficients of alkyl based ionic liquids but also functionalized ionic liquids such as ether, alcohols. The remaining seven groups are: CH<sub>2cyclic</sub>, CH<sub>cyclic</sub>, C<sub>cyclic</sub>, N<sub>cyclic</sub>, N<sup>+</sup> (ammonium cation), P<sup>+</sup> (phosphonium cation) and S<sup>+</sup> (sulphonium cation).

More precisely, N<sub>cyclic</sub> represents two structures:  $-N^+$  and  $-N-$ . Nine groups are used

for anions: bis(trifluoromethylsulfonyl)imide:  $(TF)_2N^-$ , hexafluorophosphate:  $PF_6^-$ , tetrafluoroborate:  $BF_4^-$ , ethylsulfate:  $EtSO_4^-$ , octylsulfate:  $OcSO_4^-$ , thiocyanate:  $SCN^-$ , trifluoromethylsulfonate:  $CF_3SO_3^-$ , trifluoroacetate:  $ACF_3^-$  and dicyanamide:  $(CN)_2N^-$ . As an example, let's have a look at the decomposition of 1-butyl-3-methylimidazolium hexafluorophosphate. In this case, the decomposition of the molecule into elementary groups is: 2 groups 1 (-CH<sub>3</sub>) + 3 groups 2 (-CH<sub>2</sub>) + 3 groups 7 (C<sub>cyclic</sub>) + 2 groups 9 (N<sub>cyclic</sub>) + 1 group 14 (PF<sub>6</sub><sup>-</sup>).

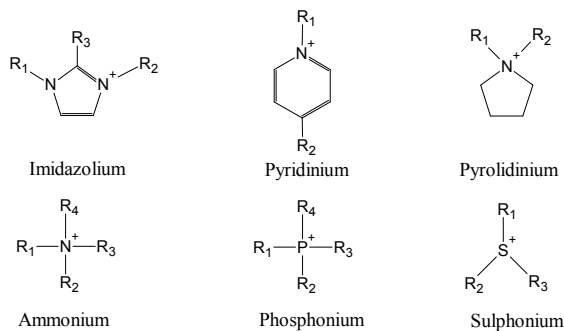


Fig. 2. Cation of six families of ionic liquids.

Cation's group	Definition	Anion's group	Definition
Group 1	CH <sub>3</sub> - CH <sub>3</sub> from alkyl chain R <sub>1</sub> , R <sub>2</sub> , R <sub>3</sub> or R <sub>4</sub>	Group 13	(TF) <sub>2</sub> N <sup>-</sup> bis(trifluoromethyl sulfonyl)imide
Group 2	-CH <sub>2</sub> - CH <sub>2</sub> from alkyl chain R <sub>1</sub> , R <sub>2</sub> , R <sub>3</sub> or R <sub>4</sub>	Group 14	PF <sub>6</sub> <sup>-</sup> hexafluorophosphate
Group 3	-O- -O- in alkyl chain R <sub>1</sub> , R <sub>2</sub> , R <sub>3</sub> or R <sub>4</sub>	Group 15	BF <sub>4</sub> <sup>-</sup> tetrafluoroborate
Group 4	-O-N <sub>cyclic</sub> - Oxygenated atom connected directly to N <sub>cyclic</sub>	Group 16	EtSO <sub>4</sub> <sup>-</sup> Ethylsulfate
Group 5	-OH -OH from alkyl chain R <sub>1</sub> , R <sub>2</sub> , R <sub>3</sub> or R <sub>4</sub>	Group 17	OcSO <sub>4</sub> <sup>-</sup> Octylsulfate
Group 6	CH <sub>2</sub> <sub>cyclic</sub> CH <sub>2</sub> cyclic in pyrrolidinium's cation	Group 18	SCN <sup>-</sup> Thiocyanate
Group 7	CH <sub>cyclic</sub> CH cyclic in imidazolium or pyridinium's cation	Group 19	CF <sub>3</sub> SO <sub>3</sub> <sup>-</sup> trifluoromethylsulfonate
Group 8	C <sub>cyclic</sub> C cyclic in imidazolium or pyridinium's cation	Group 20	ACF <sub>3</sub> <sup>-</sup> trifluoroacetate
Group 9	N <sub>cyclic</sub> Cyclic nitrogen (imidazolium, pyridinium and pyrrolidinium)	Group 21	(CN) <sub>2</sub> N <sup>-</sup> dicyanamide
Group 10			
Group 11			
Group 12			

Table 2. Description of the 21 groups used for the estimation of LogK<sub>L</sub> and LogP



Group contribution model coupled to LSER (GC-LSER) for estimating the gas-to-ionic liquids partition coefficients and water-to-ionic liquids partition coefficients allows to predict with good accuracy  $\text{Log } K_L$  and  $\text{Log } P$  at 298 K of not only alkyl based ionic liquids but also functionalized ionic liquids. The parameters of the group contribution methods were determined for imidazolium, pyridinium, pyrrolidinium, phosphonium, ammonium and sulphonium based ionic liquids containing several different anions. A comparison between the experimental and calculated values showed that the proposed models describe the experimental data available with a mean absolute error of about 0.15 log unit. The predictive power of the model was appreciated with three ionic liquids not taken into account in the database, 1-ethyl-3-methylimidazolium trifluoromethylsulfonate (Olivier et al., 2010), 1-hexadecyl-3-methylimidazolium tetrafluoroborate (Mutelet & Jaubert, 2007) and 1-ethanol-3-methylimidazolium hexafluorophosphate (Revelli et al., 2009a). This training set composed of 130  $\text{log } K_L$  and 126  $\text{log } P$  is estimated with a mean absolute error on  $\text{Log } K_L$  and  $\text{Log } P$  of about respectively, 0.15 and 0.19. A study of results indicated that light hydrocarbons showed larger deviations. In the case of data coming from inverse gas chromatography, it is well known that light hydrocarbons are prime to adsorption. If retention data are not corrected from this adsorption, partition coefficient may be over or underestimated. Plots of calculated values of  $\text{Log } K_L$  of solutes in 1-butyl-4-methylpyridinium thiocyanate and in 1-butyl-1-methylpyrrolidinium thiocyanate based on equation 7 against the measured values by (Domańska and Krolikowska, 2010) are presented in Figure 3. While the model is probably somewhat limited in prediction for pyridinium and pyrrolidinium based ionic liquids because of the poor dataset for these cations, results obtained are satisfactory.

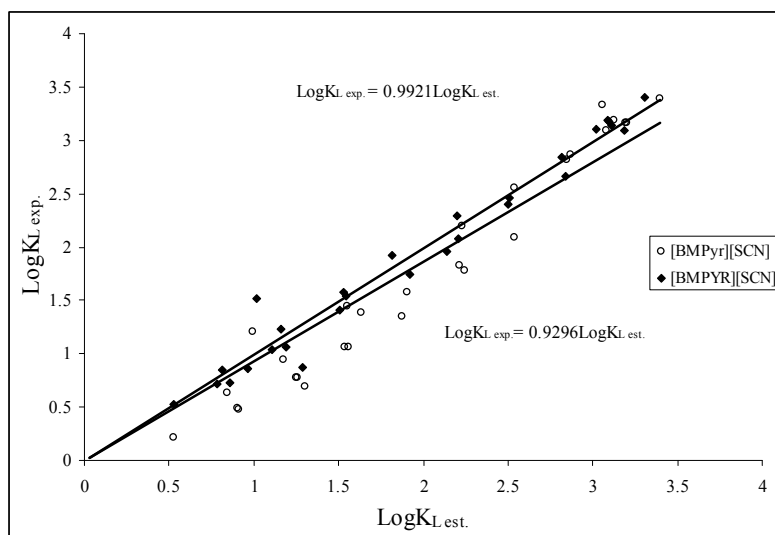


Fig. 3. Prediction of  $\text{Log } K_L$  at 298.15 K of organic compounds in two ionic liquids using the GC-LSER. 1-butyl-4-methylpyridinium thiocyanate [BMPyr][SCN] and 1-butyl-1-methylpyrrolidinium thiocyanate [BMPYR][SCN].

### 3. General behaviour of ionic liquids with organic compounds.

The large dataset of partition coefficients (or activity coefficients at infinite dilution) published in the literature may be used to present a general behaviour of solutes in ionic liquids. The values of activity coefficients at infinite dilution ( $\gamma^\infty$ ) for the *n*-alkanes increase with an increase in carbon number. In most ionic liquids, the high  $\gamma^\infty$  values observed with *n*-alkanes indicate their low solubility in ionic liquids. The  $\gamma^\infty$  values of *n*-alkanes are higher than the values obtained with cyclohexane, alkenes, alkynes and aromatics. Introduction of a double or triple bond in the *n*-alkanes decreases the  $\gamma^\infty$  values.

Cyclization of the alkane skeleton reduces the value of  $\gamma^\infty$  in comparison to that of the corresponding linear alkanes (e.g., hexane). Aromatics with their  $\pi$ -delocalized electrons have smaller  $\gamma^\infty$  values, presumably because of the interaction with the cation species. Using computer simulation, (Lynden-Bell et al., 2007) showed that the cations are found to interact predominantly with the ring of the benzene while the anions interact with the ring hydrogens to a first approximation.

In the series of chloromethanes, it is usually observed that  $\gamma^\infty$  values strongly increase from dichloromethane to tetrachloromethane. This behavior observed with all types of ionic liquids indicates that polar compounds have better solubility in the ILs when attractive interaction between polar molecules and the charged ions of the solvent is possible. The  $\gamma^\infty$  values for the alcohols are relatively small (ranging between 1.2 and 4.6). The lone pair of electrons on the oxygen atom could interact with the ionic liquid cation, and the acidic proton is attracted by oxygen atoms in the cation.  $\gamma^\infty$  values of branched alkanol skeleton are smaller than  $\gamma^\infty$  values of the corresponding linear alcohol.  $\gamma^\infty$  values of *n*-alkanols increase with increasing chain length.  $\gamma^\infty$  values of ethers and amine are higher in comparison with those of the alcohols. For most solutes, their solubility increases when the alkyl chain length grafted on the ionic liquid increases. The behavior of solutes with ionic liquids is also strongly affected by the nature of the chain grafted on the ionic liquids. For example, grafting a polar chain on the cation of dicyanamide based ionic liquid increases strongly the interactions. Replacing the 1-ethyl-3-methylimidazolium cation by 1-(3-cyanopropyl)-3-methylimidazolium in dicyanamide based ionic liquids, the activity coefficients values of *n*-hexane are divided by two (241 to 111).

The alkoxymethyl-group grafted on the imidazolium cation makes the ionic liquid more polar and with the possible anti-microbial activities (Pernak et al., 2001). (Domańska, A. Marciniak, 2009b) studied the interaction between organic compounds and 1-hexyloxymethyl-3-methylimidazolium bis(trifluoromethylsulfonyl)-imide and 1,3-dihexyloxymethyl-imidazolium bis(trifluoromethylsulfonyl)-imide. The authors found that ILs with two alkoxymethyl groups in the cation reveals stronger interactions with solutes, e.g. additional interaction of the IL with *n*-alkanes, alkenes and alkynes (i.e. Van der Waals interaction between alkane chains of the solute and the cation), and also stronger interaction with aromatic hydrocarbons, thiophene and alcohols (hydrogen bonding,  $n-\pi$ , or  $\pi-\pi$  interactions).

(Revelli et al, 2009c) measured activity coefficients at infinite dilution of organic compounds in the ionic liquid trihexyl(tetradecyl) phosphonium bis(trifluoromethylsulfonyl)imide. As observed with imidazolium-based ionic liquids, cations with a long alkyl chain tend to increase the solubility of most organic compounds in IL. The activity coefficients of 39 organic compounds in this IL are below unity apart from the alkanes and alcohols indicating a strong affinity of the solutes for the ionic liquid. The introduction of a cyanoalkyl chain dramatically decreases the solubility of apolar compounds in ILs. Aromatics, alkenes and

alkynes have lower interactions with cyanoalkylimidazolium based ILs than dialkylimidazolium. There is a lack of information concerning piperidinium based ionic liquids. In their recent study, (Domańska & Paduszyński, 2010a) demonstrate that 1-propyl-1-methylpiperidinium bis[(trifluoromethyl)sulfonyl]imide behaves like the other measured ionic liquids based on different cations.

#### 4. Selectivity and capacity of ionic liquids

From the data of activity coefficients at infinite dilution, selectivities  $S_{12}^{\infty}$  and capacities  $k_1^{\infty}$  at infinite dilution may be estimated using the classical equations (9) and (10):

$$S_{12}^{\infty} = \frac{\gamma_{1/RTL}^{\infty}}{\gamma_{2/RTL}^{\infty}} \quad (9)$$

$$k_1^{\infty} = \frac{1}{\gamma_{1/RTL}^{\infty}} \quad (10)$$

In figure 4, the influence of the anion on the selectivity is presented for the separation of {benzene/hexane} using 1-ethyl-3-methylimidazolium based ionic liquids. The highest selectivity is obtained with the thiocyanate anion followed by tetrafluoroborate and tosylate anions. The increasing of the fluor atoms number on fluorinated anions decreases the selectivity of ionic liquids. In the family of fluorinated anions, hydrocarbons have a better affinity with anions containing the lowest fluor atoms number. The solubility of nonpolar compounds increases with an increasing of the alkyl chain length grafted on the cation. This means that the selectivity of separation of organic compounds in binary systems {organic compounds + aliphatics} decreases when the alkyl chain length of the IL increases (Figure 5). The influence of the anion for 1-ethyl-3-methylimidazolium based ionic liquids on the

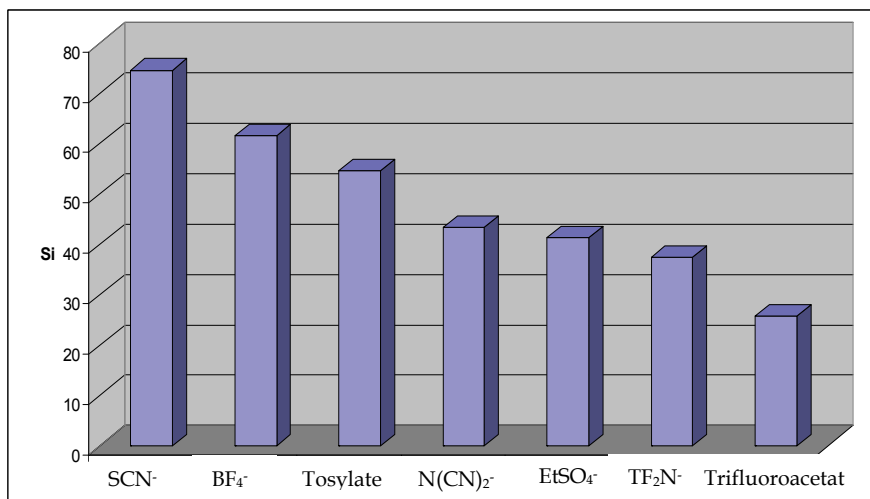


Fig. 4. Influence of the anion on the separation of {benzene-hexane} using 1-ethyl-3-methylimidazolium based ionic liquids at 323.15K.

capacity  $k_1^\infty$  is represented in figure 6. The best capacity is obtained for  $[\text{TF}_2\text{N}]$  anion and is close to classical solvents used in the industry. Changing  $[\text{TF}_2\text{N}]$  anion by dicyanamide or tosylate or trifluoromethanesulfonate anions divides by two the capacity of the corresponding ionic liquid. (Marciniak, 2010) analysed the influence of the cation and anion structures of the ionic liquid but also the effect of the temperature on the selectivity and the capacity for aliphatics/aromatics and n-hexane/hex-1-ene separation problems. The author showed that the highest values of selectivity is observed with ionic liquids containing small alkyl chains, e.g. based on the following cations  $[\text{mmim}]^+$ ,  $[\text{emim}]^+$ ,  $[\text{ePY}]^+$ ,  $[\text{Et}_3\text{S}]^+$  coupled to a thiocyanate group in the structure. Unfortunately, when the ionic liquid reveals high values of the selectivity, the capacity always takes low values.

Selectivities  $S_{12}^\infty$  and capacities  $k_1^\infty$  are listed in Table 3 for four separation problems: hexane/benzene, hexane/methanol, hexane/thiophene, cyclohexane/thiophene for ILs at  $T = 323.15$  K. The selectivities and capacities were calculated using experimental activity coefficient at infinite dilution in 1-ethanol-3-methylimidazolium bis((trifluoromethyl)-imide, 1,3-dimethoxyimidazolium bis((trifluoromethyl)sulfonyl)imide, 1-(methylethylether)-3-methylimidazolium bis((trifluoromethyl)sulfonyl)sulfonylimide and 1-(3-cyanopropyl)-3-methylimidazolium dicyanamide, (Revelli et al., 2010b), 1-ethyl-3-methyl-imidazolium bis(trifluoromethylsulfonyl)imidate (Deenadayalu et al., 2005), 1-hexyloxymethyl-3-methylimidazolium bis(trifluoromethylsulfonyl)-imide and 1,3-di-hexyloxymethyl-imidazolium bis(trifluoromethylsulfonyl)-imide (Domańska & Marciniak, 2009b), 4-methyl-N-butyl-pyridinium bis(trifluoromethylsulfonyl)-imide (Domańska & Marciniak, 2009c), triethylsulphonium bis(trifluoromethylsulfonyl)imide (Domańska & Marciniak, 2009a), 1-hexyl-3-methylimidazolium bis(trifluoromethylsulfonyl)imide (Heintz et al., 2006), trihexyl(tetradecyl)phosphonium bis(trifluoromethylsulfonyl)imide (Revelli et al., 2009c), 1-butyl-3-methylimidazolium bis(trifluoromethylsulfonyl)imide (Krummen et al., 2002), 1-ethyl-3-methylimidazolium dicyanamide and trimethylhexylammonium bis((trifluoromethyl)sulfonyl)amide (Mutelet et al., 2010), 1-ethanol-3-methylimidazolium tetrafluoroborate, 1-ethanol-3-methylimidazolium hexafluorophosphate (Revelli et al., 2009a). Selectivities obtained with  $[\text{TF}_2\text{N}]$  based ionic liquids and classical solvent used in industry such as sulfolane (30.5), dimethylsulfide (22.7) and n-methylpyrrolidinone (12.5) are of the same order of magnitude. The selectivity of such ionic liquids does not increase by replacing the alkyl chain by an ether chain. Concerning dicyanamide ionic liquids, 1-cyanopropyl-3-methylimidazolium dicyanamide has a relatively high selectivity. The  $S_{12}^\infty$  values obtained with dicyanamide based ILs show the possibility of using these ILs as an extractive medium for different separation processes. The selectivity of dicyanamide based ILs for {hexane + methanol} mixture is particularly large compared to the value for classical solvents. Then,  $[\text{C}_2\text{OHmim}]$  cation coupled to the  $[\text{TF}_2\text{N}]$  anion has a small selectivity.

The temperature is an important parameter on selectivity and capacity. For most problems of separation, the selectivity decreases with an increase of the temperature for all imidazolium based ionic liquids. (Marciniak, 2010) found that the influence of the temperature is more important with cations with short aliphatic chains. Because most of the activity coefficients of solutes in ILs decrease with an increase of temperature, the corresponding capacities increase. The selectivities for the extraction of thiophene from benzene follow a similar trend than the selectivities for the system {hexane/ benzene}. For ionic liquids based on phosphonium and ammonium cations with long alkyl chains, the influence of the temperature is weak.

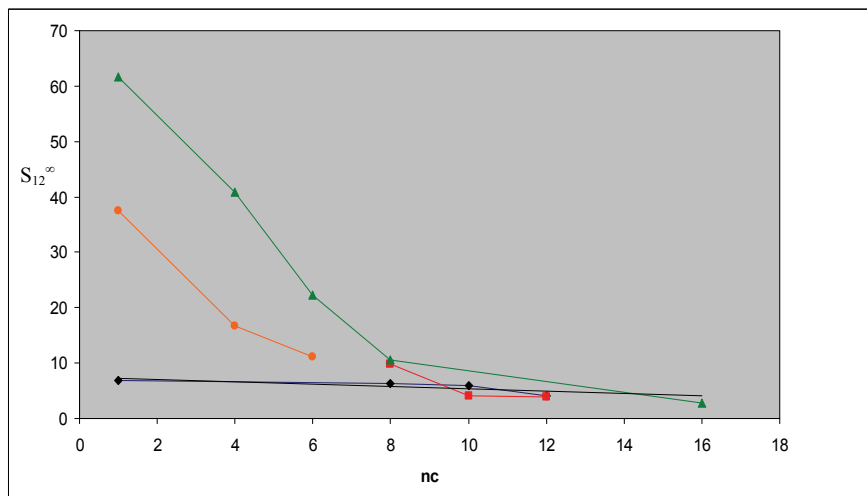


Fig. 5. Influence of the alkyl chain length grafted on the cation on the separation of {benzene-hexane} using : ▲ n-alkyl-3-methylimidazolium tétrafluoroborate, ● 1-alkyl-3-methylimidazolium bis(trifluoromethylsulfonyl)imide, ■ 1-propyl boronic acid-3-alkyl-imidazolium bromide et ◆ 1-propenyl-3-alkyl-imidazolium bromide.

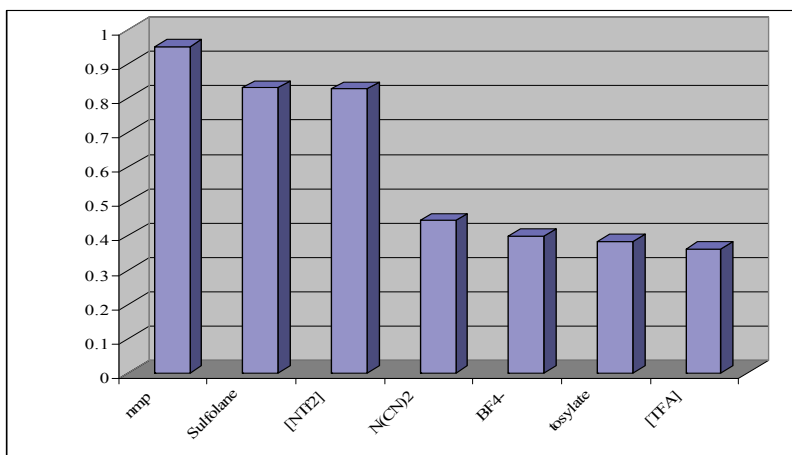


Fig. 6. Influence of the anion on the capacity of {benzene-hexane} using 1-ethyl-3-methylimidazolium based ionic liquids at 323.15 K.

Ionic liquids		$S_{12}^{\infty} / k_1^{\infty}$			
Anion	Cation	Hexane/ Benzene	Hexane/ Methanol	Hexane/ Thiophene	Cyclohexane/ Thiophene
[Tf <sub>2</sub> N]	1,3-dimethoxyimidazolium	21.3 / 0.47	42.05 / 0.94	24.8 / 0.94	12.6 / 0.94
	1-(methylethylether)-3-methylimidazolium	15.5 / 0.85	17.4 / 0.93	18.1 / 1.0	10.9
	1-ethanol-3-methylimidazolium	20.6 / 0.47	49.1 / 1.12	24.7 / 0.56	14.2 / 0.56
	1-ethyl-3-methylimidazolium	37.5 / 1.43	19.5 / 1.20	-	-
	1-(hexylmethylether)-3-methylimidazolium	9.1 / 1.23	6.8 / 0.91	10.0 / 1.35	6.4 / 1.35
	1,3-di(hexylmethylether)imidazolium	4.9 / 1.67	3.2 / 1.06	5.3 / 1.75	3.7 / 1.75
	1-butyl-3-methylimidazolium	16.7 / 1.11	-	-	-
	1-hexyl-3-methylimidazolium	9.5 / 1.29	6.1 / 0.82	-	-
	trimethylhexylammonium	9.9 / 1.01	8.5 / 0.86	10.7 / 1.09	7.2 / 1.09
	4-methyl-N-butyl-pyridinium	18.8 / 1.43	21.2 / 0.83	10.6 / 1.56	6.1 / 1.56
	triethylsulphonium	21.6 / 0.91	17.8 / 0.77	25.5 / 1.05	14.3 / 1.05
	trihexyl(tetradecyl)phosphonium	2.7 / 2.56	1.1 / 1.02	2.6 / 2.5	1.95 / 2.5
[DCA]	1-cyanopropyl-3-methylimidazolium	56.0 / 0.22	432 / 1.69	105 / 0.41	41.3 / 0.41
	1-ethyl-3-methylimidazolium	43.4 / 0.39	255 / 2.27	69.6 / 0.63	28.8 / 0.63
[BF <sub>4</sub> ]	1-ethanol-3-methylimidazolium	- / 0.10	- / 0.98	- / 0.17	136.1 / 0.17
[PF <sub>6</sub> ]	1-ethanol-3-methylimidazolium	- / 0.17	- / 0.77	- / 0.23	59.7 / 0.23

Table 3. Selectivity  $S_{12}^{\infty}$  and capacity  $k_1^{\infty}$  values for different separation problems at 323.15 K.

The selectivities for the trihexyl(tetradecyl) phosphonium bis(trifluoromethylsulfonyl)imide are very low compared to the value obtained with imidazolium-based ionic liquids, indicating the limited potential of this phosphonium IL for separation. For instance, the selectivity for hexane/ benzene is 2.2, while it is 60.1 with 1-butyl-3-methylimidazolium tetrafluoroborate or 30.5 with sulfolane used commercially for separating aliphatic/ aromatic hydrocarbons. As observed with imidazolium-based ionic liquids, phosphonium ILs with a long alkyl chain on the cation have a low selectivity. Selectivities obtained with phosphonium or ammonium based ILs are generally of the same magnitude as with classical solvents used in industry. The triethylsulphonium bis(trifluoromethylsulfonyl)imide presents an average values of selectivity and capacity for the aliphatic/aromatic separation problems. (Domańska & Paduszyński, 2010a) found that 1-propyl-1-methylpiperidinium bis((trifluoromethyl)sulfonyl)imide has higher selectivity in the separation of aliphatic from aromatic hydrocarbons than commonly used entrainers. The selectivity is also higher for 1-propyl-1-methylpiperidinium bis((trifluoromethyl)sulfonyl)imide than for 4-methyl-*N*-butylpyridinium bis((trifluoromethyl)sulfonyl)imide, triethylsulphonium bis((trifluoromethyl)sulfonyl)imide [Et<sub>3</sub>S][NTf<sub>2</sub>], 1-ethyl-3-methylimidazolium bis((trifluoromethyl)sulfonyl)imide [EMIM][NTf<sub>2</sub>] and many other ionic liquids with the bis((trifluoromethyl)sulfonyl)imide anion. In the case of bis((trifluoromethyl)sulfonyl)imide anion, the authors found that changing the cation from imidazolium [EMIM]<sup>+</sup>, or sulphonium to piperidinium increases slightly the selectivity and also increases the capacity. Changing the anion from [TF<sub>2</sub>N]<sup>-</sup> to [SCN]<sup>-</sup> increases the selectivity more than three times, but unfortunately decreases the capacity. Selectivities obtained with ammonium based ionic liquid are generally of the same magnitude as with classical solvent used in industry.

## 7. Conclusion

The increasing interest in ionic liquids leads to more research activities concerning thermodynamic properties of mixtures containing ionic liquids. While data on activity coefficients, VLE and LLE are now available for a number of binary and a few ternary systems, the situation is still not satisfying with respect of a systematic knowledge of these properties and further research work has to fill the remaining gaps. The values of selectivities and capacities obtained for numerous ionic liquids indicate that majority of ionic liquids may replace conventional entrainers applied for the separation processes. These last ten years, few teams around the world demonstrated that the choice of the anion, of the cation but also of the chain influence the efficiency of the ionic liquids to extract a volatile organic compounds. To have a good knowledge on the interactions of ionic liquids with organic compounds, the future work should be focussed on sulphonium, pyrrolidinium, piperidinium based ionic liquids since there is still a lack of data.

## 8. References

Abraham, M. H.; Grellier, P. L. & Mc Gill R.A. (1987). Determination of Olive Oil-Gas and Hexadecane-Gas Partition Coefficients, and calculation of the corresponding Olive

- Oil-Water and Hexadecane-Water Partition Coefficients. *J. Chem. Soc. PERKIN TRANS II*, 797-803.
- Abraham, M. H.; Whiting, G. S. & Doherty R. M. (1990). Hydrogen Bonding. Part 13. A New Method for the Characterization of GLC Stationary Phases-The Lafford Data Set. *J. Chem. Soc. PERKIN TRANS II*, 1451-1460.
- Abraham, M. H.; Whiting, G. S.; Doherty, R. M. & Shuely, W. J. (1991). Hydrogen bonding XVI. A new solute solvation parameter,  $\pi_2^H$ , from gas chromatographic data. *J. Chromatogr.*, 587, 213-228.
- Abraham, M. H. & Whiting, G.S. (1992). Hydrogen-bonding. Part 22. Characterization of soybean oil and prediction of activity coefficients in soybean oil from inverse gas chromatographic data. *J. Am. Oil Chem. Soc.*, 69, 1236-1238.
- Abraham, M.H.; Andonian-Hanftvan, J. ; Osei-Owusu, J.P.; Sakellariou, P.; Urieta, J.S.; López, M.C. & Fuchs, R. (1993a). Hydrogen bonding. Part 25. The solvation properties of methylene iodide. *J. Chem. Soc., PERKIN TRANS. II*, 3,299-304.
- Abraham, M. H. (1993b). Scales of Solute Hydrogen-bonding: Their construction and Application to Physicochemical and Biochemical Processes. *Chem. Soc. Rev.*, 22,73-83.
- Abraham, M.H., Poole, C.F. & Poole, S.K. (1999). Classification of stationary phases and other materials by gas chromatography *J. Chromatogr. A*, 842, 1-2, 79-114.
- Abraham, M.H. & Platts, J.A. (2001). Hydrogen bond structural group constants. *J. Org. Chem.*, 66, 3484-3491.
- Abraham, M.H.; Zissimos, A.M.; Huddleston, J.G.; Willauer, H.D.; Rogers, R.D. & Acree, W.E., Jr. (2003). Some novel liquid partitioning systems: Water-ionic liquids and aqueous biphasic systems. *Ind. Eng. Chem. Res.*, 42, 413-418.
- Acree, W.E., Jr. & Abraham, M.H. (2006). The analysis of solvation in ionic liquids and organic solvents using the Abraham model linear free energy relationship. *J. Chem. Technol. Biotechnol.*, 81, 1441-1446.
- Alonso, L.; Arce, A.; Francisco, M. & Soto, A. (2008). Solvent extraction of thiophene from n-alkanes (C7, C12, and C16) using the ionic liquid [C8mim][BF4]. *J. Chem. Thermodyn.*, 40, 966-972.
- Arlt, M.; Seiler, M.; Jork, C. & Schneider, T. *DE Patent No. 10114734*, 2001.
- Cadena, C.; Anthony, J.L.; Shah, J.K.; Morrow, T.I.; Brennecke, J.F. & Maginn, E.J. (2004). Why is CO<sub>2</sub> soluble in imidazolium-based ionic liquids?. *J. Am. Chem. Soc.*, 126, 5300-5308.
- Deenadayalu, N.; Letcher, T. M. & Reddy, P. (2005). Determination of Activity Coefficients at Infinite Dilution of Polar and Nonpolar Solutes in the Ionic Liquid 1-Ethyl-3-methylimidazolium Bis(trifluoromethylsulfonyl) Imidate Using Gas-Liquid Chromatography at the Temperature 303.15 K or 318.15 K. *J. Chem. Eng. Data*, 50, 105-108.
- Domańska, U. & Marciniak, A. (2009a). Activity coefficients at infinite dilution measurements for organic solutes and water in the ionic liquid triethylsulphonium bis(trifluoromethylsulfonyl)imide. *J. Chem. Thermodyn.*, 6, 41, 754-758.



- Domańska, U. & Marciniak, A. (2009b). Activity coefficients at infinite dilution measurements for organic solutes and water in the 1-hexyloxymethyl-3-methylimidazolium and 1,3-dihexyloxymethyl-imidazolium bis(trifluoromethylsulfonyl)-imide ionic liquids—The cation influence. *Fluid Phase Equilib.*, 2, 286, 154-161.
- Domańska, U. & Marciniak, A. (2009c). Activity coefficients at infinite dilution measurements for organic solutes and water in the ionic liquid 4-methyl-N-butylpyridinium bis(trifluoromethylsulfonyl)-imide. *J. Chem. Thermodyn.*, 12, 41, 1350-1355.
- Domańska, U. & Paduszyński, K. (2010a). Measurements of activity coefficients at infinite dilution of organic solutes and water in 1-propyl-1-methylpiperidinium bis{(trifluoromethyl) sulfonyl}imide ionic liquid using g.l.c.. *J. Chem. Thermodyn.*, 11, 42, 1361-1366.
- Domańska, U. & Paduszyński, K. (2010). Gas-liquid chromatography measurements of activity coefficients at infinite dilution of various organic solutes and water in tri-iso-butylmethylphosphonium tosylate ionic liquid. *J. Chem. Thermodyn.*, 6, 42, 707-711.
- Domańska, U. & Królikowska, M. (2010a). Measurements of activity coefficients at infinite dilution in solvent mixtures with thiocyanate-based ionic liquids using glc technique. *J. Phys. Chem. B*, 25, 114, 8460-8466.
- Heintz, A.; Verevkin, S.P. & Ondo, D. (2006). Thermodynamic properties of mixtures containing ionic liquids. 8. Activity coefficients at infinite dilution of hydrocarbons, alcohols, esters, and aldehydes in 1-hexyl-3-methylimidazolium bis(trifluoromethylsulfonyl) imide using gas-liquid chromatography. *J. Chem. Eng. Data*, 2, 51, 434-437.
- Kamlet, M.J.; Abboud, J.L. & Taft, R.W. (1977). The solvatochromic comparison method. 6. The  $\pi$  scale of solvent polarities. *J. Am. Chem. Soc.*, 18, 99, 6027-6038.
- Kamlet, M.J.; Abboud, J.-L.M.; Abraham, M.H. & Taft, R.W. (1983). Linear solvation energy relationships. 23. A comprehensive collection of the solvatochromic parameters,  $\pi^*$ ,  $\alpha$ , and  $\beta$ , and some methods for simplifying the generalized solvatochromic equation. *J. Org. Chem.*, 17, 48, 2877-2887.
- Kamlet, M.J. & Taft, R.W. (1985). Linear Solvation Energy Relationships. Local Empirical Rules -- or Fundamental Laws of Chemistry? A Reply to the Chemometricians., *Acta Chem. Scand.*, B 39, 611-628.
- Kamlet, M.J.; Doherty, R.M.; Abraham, M.H.; Marcus, Y. & Taft, R.W. (1988). Linear solvation energy relationships. 46. An improved equation for correlation and prediction of octanol/water partition coefficients of organic nonelectrolytes (Including strong hydrogen bond donor solutes). *J. Phys. Chem. B*, 18, 92, 5244-5255.
- Krummen, M.; Wasserscheid, P. & Gmehling, J. (2002). Measurement of activity coefficients at infinite dilution in ionic liquids using the dilutor technique. *J. Chem. Eng. Data*, 6, 47, 1411-1417.
- Letcher, T. (2007) *Thermodynamics, solubility and environmental issues*, Elsevier Science, Amsterdam, The Netherlands.

- Lynden-Bell, R.M.; Del Pópolo, M.G.; Youngs, T.G.A.; Kohanoff, J.; Hanke, C.G.; Harper, J.B. & Pinilla, C.C. (2007). Simulations of ionic liquids, solutions, and surfaces. *Accounts of Chemical Research*, 11, 40, 1138-1145.
- Marciniak, A. (2010). Influence of cation and anion structure of the ionic liquid on extraction processes based on activity coefficients at infinite dilution. A review. *Fluid Phase Equilib.*, 1-2, 294, 213-233.
- Mutelet, F. & Rogalski, M. (2001). Experimental determination and prediction of the gas-liquid n-hexadecane partition coefficients. *J. Chromatogr. A*, 923, 153-163.
- Mutelet, F.; Jaubert, J.-N.; Rogalski, M.; Boukherissa, M. & Dicko, A. (2006). Thermodynamic properties of mixtures containing ionic liquids: Activity coefficients at infinite dilution of organic compounds in 1-propyl boronic acid-3-alkylimidazolium bromide and 1-propenyl-3-alkylimidazolium bromide using inverse gas chromatography. *J. Chem. Eng. Data*, 4, 51, 1274-1279.
- Mutelet, F. & Jaubert, J.-N. (2006). Accurate measurements of thermodynamic properties of solutes in ionic liquids using inverse gas chromatography. *J. Chromatogr. A*, 1-2, 1102, 256-267.
- Mutelet, F. & Jaubert, J.-N. (2007). Measurement of activity coefficients at infinite dilution in 1-hexadecyl-3-methylimidazolium tetrafluoroborate ionic liquid. *J. Chem. Thermodyn.*, 8, 39, 1144-1150.
- Mutelet, F., Jaubert, J.-N.; Rogalski, M.; Harmand, J.; Sindt, M. & Mieloszynski, J.-L. (2008). Activity coefficients at infinite dilution of organic compounds in 1-(meth)acryloyloxyalkyl-3-methylimidazolium bromide using inverse gas chromatography. *J. Phys. Chem. B*, 12, 112, 3773-3785.
- Mutelet, F.; Revelli, A.-L.; Jaubert, J.-N.; Sprunger, L.M.; Acree Jr., W.E. & Baker, G.A. (2010). Partition coefficients of organic compounds in new imidazolium and tetralkylammonium based ionic liquids using inverse gas chromatography. *J. Chem. Eng. Data*, 1, 55, 234-242.
- Olivier, E.; Letcher, T. M.; Naidoo, P. & Ramjugernath, D. (2010). Activity coefficients at infinite dilution of organic solutes in the ionic liquid 1-ethyl-3-methylimidazolium trifluoromethanesulfonate using gas-liquid chromatography at  $T = (313.15, 323.15, \text{ and } 333.15)$  K. *J. Chem. Thermodyn.*, 42, 78-83.
- Park, J.H. & Carr, P.W. (1989). Interpretation of normal-phase solvent strength scales based on linear solvation energy relationships using the solvatochromic parameters  $\pi^*$ ,  $\alpha$  and  $\beta$ . *J. Chromatogr.*, 3, 465, 123-136.
- Pernak, J.; Czepukowicz, A.; Pozniak, R. (2001). New ionic liquids and their antielectrostatic properties. *Ind. Eng. Chem. Res.*, 11, 40 (2001) 2379-2383.
- Platts, J.A.; Butina, D.; Abraham, M.H. & Hersey, A. (1999). Estimation of molecular linear free energy relation descriptors using a group contribution approach. *J. Chem. Inf. Comp. Sci.*, 39, 835-845.
- Poole, C.F. (2004). Chromatographic and spectroscopic methods for the determination of solvent properties of room temperature ionic liquids. *J. Chromatogr. A*, 1-2, 1037, 49-82.
- Poole, C.F. & Poole, S.K. (2010). Extraction of organic compounds with room temperature ionic liquids. *J. Chromatogr. A*, 16, 1217, 2268-2286.

- Revelli, A.-L.; Mutelet, F. & Jaubert, J.-N. (2009a). Partition coefficients of organic compounds in new imidazolium based ionic liquids using inverse gas chromatography. *J. Chromatogr. A*, 23, 1216, 4775-4786.
- Revelli, A.-L.; Mutelet, F.; Turmine, M.; Solimando, R. & Jaubert, J.-N. (2009b). Activity coefficients at infinite dilution of organic compounds in 1-butyl-3-methylimidazolium tetrafluoroborate using inverse gas chromatography. *J. Chem. Eng. Data*, 1, 54, 90-101.
- Revelli, A.-L.; Sprunger, L.M.; Gibbs, J.; Acree Jr. W.E.; Baker, G.A. & Mutelet, F. (2009c). Activity coefficients at infinite dilution of organic compounds in trihexyl(tetradecyl)phosphonium Bis(trifluoromethylsulfonyl)imide using inverse gas chromatography. *J. Chem. Eng. Data*, 3, 54, 977-985.
- Revelli, A.-L.; Mutelet, F. & Jaubert, J.-N. (2010a). Prediction of partition coefficients of organic compounds in ionic liquids: Use of a linear solvation energy relationship with parameters calculated through a group contribution method. *Ind. Eng. Chem. Res.*, 8, 49, 3883-3892.
- Revelli, A.-L.; Mutelet, F.; Jaubert, J.-N.; Garcia-Martinez, M.; Sprunger, L.M.; Acree Jr., W.E. & Baker, G.A. (2010b). Study of ether-, alcohol-, or cyano-functionalized ionic liquids using inverse gas chromatography. *J. Chem. Eng. Data*, 7, 55, 2434-2443.
- Rogers, R.D. & Seddon, K.R. (2002). Ionic liquids: Industrial applications for green chemistry, ACS symposium series.
- Rogers, R.D. & Seddon, K.R. (2003). Ionic liquids as green solvents: Progress and Prospects, ACS symposium series.
- Sprunger, L.; Clark, M.; Acree, W.E., Jr. & Abraham, M.H. (2007) Characterization of room-temperature ionic liquids by the Abraham model with cation-specific and anion-specific equation coefficients. *J. Chem. Inf. Model.*, 47, 1123-1129.
- Sprunger, L.M.; Proctor, A.; Acree, W.E., Jr. & Abraham, M.H. (2008) LFER correlations for room temperature ionic liquids: Separation of equation coefficients into individual cation-specific and anion-specific contributions. *Fluid Phase Equilib.*, 265, 104-111.
- Sprunger, L.M.; Achi, S.S.; Acree Jr. W.E.; Abraham, M.H.; Leo, A.J. & Hoekman, D. (2009a) Correlation and prediction of solute transfer to chloroalkanes from both water and the gas phase. *Fluid Phase Equilib.*, 281, 144-162.
- Sprunger, L.M.; Gibbs, J.; Proctor, A.; Acree Jr., W.E.; Abraham, M.H.; Meng, Y.; Yao, C. & Anderson, J.L. (2009b). Linear free energy relationship correlations for room temperature ionic liquids: revised cation-specific and anion-specific equation coefficients for predictive applications covering a much larger area of chemical space. *Ind. Eng. Chem. Res.*, 48, 4145-4154.
- Taft, R.W. & Kamlet, M.J. (1976). The solvatochromic comparison method. 2. The  $\alpha$ -scale of solvent hydrogen-bond donor (HBD) acidities. *J. Am. Chem. Soc.*, 10, 98, 2886-2894.
- Vitha, M. & Carr, P.W. (2006). The chemical interpretation and practice of linear solvation energy relationships in chromatography. *J. Chromatogr. A*, 1-2, 1126, 143-194.

Weckwerth, J.D. & Carr, P.W. (1998). Study of Interactions in Supercritical Fluids and Supercritical Fluid Chromatography by Solvatochromic Linear Solvation Energy Relationships. *Anal. Chem.*, 70, 1404-1410.

# Nonaqueous Microemulsions Containing Ionic Liquids – Properties and Applications

Oliver Zech,<sup>1,2</sup> Agnes Harrar,<sup>1</sup> and Werner Kunz<sup>1</sup>

<sup>1</sup>*Institute of Physical and Theoretical Chemistry,  
University of Regensburg, 93040 Regensburg,*

<sup>2</sup>*Current address: Max-Planck Institute of Colloids and Interfaces,  
14424 Potsdam,  
Germany*

## 1. Introduction

There is a still growing interest in ionic liquids (ILs) in general and room temperature ionic liquids (RTILs) in particular resulting from their fascinating and outstanding properties and wide range of potential applications. The research field of ILs was almost entirely related to imidazolium, pyridinium and pyrrolidinium based substances in the last decade (Welton 1999; Earle & Seddon 2000; Wasserscheid & Keim 2000). Beside these classical aprotic ionic liquids, attention has been paid to protic (Greaves & Drummond 2007; Greaves et al., 2008 b) and to the development of less toxic ILs (Tao et al., 2006; Fukaya et al., 2007; Pernak et al., 2007; Zech et al., 2009 a). ILs are often considered as future solvents for catalysis (Welton 1999; Wasserscheid & Keim 2000; Pârvulescu & Hardacre 2007; van Rantwijk & Sheldon 2007), chemical reactions (Haumann & Riisager 2008; Martins et al., 2008), extractions (Blanchard et al., 1999), and electrochemical purposes (Hapiot & Lagrost 2008).

Apart from these applications, ILs also stimulated research in classical colloid and surface chemistry. The formation of amphiphilic association structures in and with ionic liquids, such as micelles, vesicles, microemulsions and liquid crystalline phases has been reviewed three times between 2007 (Hao & Zemb 2007) and 2008 (Qiu & Texter 2008; Greaves & Drummond 2008 a), reflecting the growing interest and progress in this field. In this review we focus on ILs in nonaqueous microemulsions, because significant new work has been reported in this field since these earlier reviews have been published.

Microemulsions are thermodynamically stable, isotropic transparent mixtures of at least a hydrophilic, a hydrophobic and an amphiphilic component. The first microemulsion structures termed at that time “oleophatic hydro-micelle” were discovered in 1943 by Hoar and Schulman (Hoar & Schulman 1943). The term microemulsion was introduced by Schulman and coworkers in 1959 describing optically isotropic transparent solutions consisting of water, oil, surfactant and alcohol (Schulman et al., 1959). A more recent definition was given by Danielsson and Lindman: “A microemulsion is a system of water, oil and an amphiphile which is a single optically isotropic and thermodynamically stable liquid solution” (Danielsson & Lindman 1981). Herein, “water” corresponds to a polar phase that is classically an aqueous solution that can contain electrolytes and other

additives. The word “amphiphile” from *amphi* (both sides) and *philos* (liking) was coined by Winsor (Winsor 1954) to describe substances with an affinity towards both non-polar and polar phases. In this context, surfactants are the most important amphiphiles, since their amphiphilic character is strong to drive them to the interface where the polar part is located in the polar phase and vice versa. The term “oil” refers to an organic phase that is immiscible or at least to a certain extent immiscible with the polar phase. Consequently, non-polar substances such as hydrocarbons, partially or totally chlorinated or fluorinated hydrocarbons, unbranched alkanes, cyclic or aromatic hydrocarbons, but also triglyceride natural oils can be used (Salager & Antón 1999). A great variety in structure of these single phase microemulsions is known in literature ranging from water-in-oil (w/o) over bicontinuous to oil-in-water (o/w) structures. In the case of a w/o microemulsion, oil is the continuous phase with water droplets stabilized by surfactant molecules and vice versa for o/w structures. The microemulsion structure depends on the volume fraction of oil, water and amphiphile as well as on the nature of the interfacial film. o/w microemulsion structures preferentially form when the oil volume fraction is low and vice versa for w/o microemulsions. Bicontinuous structures, which are networks of oil and water nanodomains separated and stabilized by a surfactant interfacial film with a net curvature close to zero, can be found at almost equal amounts of water and oil. When using non-ionic surfactants and ionic double-chain surfactants, such as sodium bis (2-ethylhexyl) sulfosuccinate (AOT) no cosurfactant is necessary for the formation of microemulsions (Angel et al., 1983). This results from the ability of these amphiphiles to reduce the interfacial tension between oil and water to a very low value, a requirement to form stable microemulsions. Many other surfactants like single-chain ionic surfactants do not exhibit this characteristic and hence cosurfactants, i.e. *n*-alcohols or *n*-amines, are indispensable to obtain the required low interfacial tension for the formation of stable microemulsions (Bellocq et al., 1984; Rakshit & Moulik 2009).

Another important phase classification that can often be found in literature has been introduced by Winsor (Winsor 1948), who found four general types of phase equilibria. A Winsor type IV phase corresponds to classical single phase microemulsions consistent with Hoar's & Schulman's definition (Hoar & Schulman 1943). A Winsor type I system denotes two phases in equilibrium, an o/w structure and an almost pure oil upper phase. On the contrary, in a Winsor type II system an aqueous phase containing surfactant is in equilibrium with an w/o microemulsion in the upper phase. Finally, Winsor type III structures equal a three-phase system consisting of a surfactant poor water phase, a bicontinuous middle phase, and an upper almost pure oil phase.

Apart from these classical microemulsions composed of water, oil, and surfactant (and cosurfactant, where appropriate), it has been demonstrated that the polar phase is not necessarily water and the non-polar phase not compulsorily oil. The idea of nonaqueous microemulsions is not new (Friberg & Podzimek 1984; Rico & Lattes 1984; Friberg & Liang 1987; Rico & Lattes 1987), for example water can be replaced by glycerol (Saidi et al., 1990), glycol or formamide (Ray & Moulik 1994). Efforts have further been made to replace water by a mixture of molten salts (nitrate mixtures of ethylenediamine / ammonia / potassium) in a system composed of sodium dodecyl sulfate (SDS), 1- pentanol and decane (Chang 1990).

These pioneer studies stimulated research on the formulation of nonaqueous microemulsions containing ionic liquids. This review focuses on nonaqueous microemulsions with ionic liquids with a subdivision of microemulsions containing aprotic and protic ionic liquids,

since they exhibit substantial differences with respect to phase behavior and microstructures. A strong emphasis has been placed on highlighting the differences of aqueous and ionic liquid microemulsions in general and regarding the effect of temperature in particular. Finally, an outlook concerning applications of these IL- microemulsions and future challenges and prospects is presented.

## 2. Ionic liquids in nonaqueous microemulsions

The definition of ionic liquids allows distinguishing them from a classical molten salt. A molten salt is mostly a high-melting, highly viscous and very corrosive substance while ionic liquids are already liquid at lower temperatures ( $< 100^{\circ}\text{C}$ ) and exhibit in most cases relatively low viscosities. Conventional ILs typically contain bulky organic cations with a low degree of symmetry such as imidazolium, pyrrolidinium, tetraalkylphosphonium, trialkylsulfonium or quaternary ammonium. These cations hinder the regular packing in a crystal lattice. Consequently, the solid crystalline state becomes energetically less favorable, leading to low melting points (Krossing et al., 2006). This effect can be enhanced further by the implementation of an anion with a delocalized charge, resulting in decreased interionic interactions (Xue et al., 2006).

Depending on the combination of the cation and the anion, ILs can have either hydrophilic or hydrophobic character. The most frequently investigated ILs are based on imidazolium cations. Anions such as halides, acetate, nitrate and ethylsulfate form hydrophilic ILs while anions such as bis(trifluoromethylsulfonyl)imide and hexafluorophosphate lead to hydrophobic ILs. Apart from these aprotic imidazolium or pyridinium based ionic liquids there was recently a growing interest in protic ionic liquids (PILs). A comprehensive overview about types and physicochemical properties of PILs was currently given in a review of Greaves & Drummond (Greaves & Drummond 2007). Ethylammonium nitrate (EAN), which represents the first room temperature ionic liquid described in literature, has already been reported in 1914 (Walden 1914) and is nowadays probably the most frequently studied PIL.

Prior to going into detail with ternary and quaternary systems, self-assembled structures in binary IL/surfactant mixtures remain to be discussed. As a matter of principle, solvents that promote the ability of amphiphiles to form micelles should exhibit a high dielectric constant, a high solvating power and should be highly structured (Lattes & Rico 1989). Micelle formation of alkyltrimethylammonium bromides, alkylpyridinium bromides and octylphenol ethoxylate (TX-100) in EAN was first reported almost 30 years ago (Evans et al., 1982; Evans et al., 1983 a). In addition to micellar structures in binary IL/EAN mixtures, liquid crystals of lipids in EAN have been found (Evans et al., 1983 b). There has been a renewed strong research interest in this field mainly in the past few years. ILs as solvents to promote self-assembly have been reviewed in 2005, where only few studies were available in literature (Baker & Pandey 2005) and more recently in 2007 (Hao & Zemb 2007) and 2008 (Greaves & Drummond 2008 a). Although a detailed discussion of the phase behavior of binary IL/surfactant mixtures is beyond the scope of this review, some general conclusions can be drawn. The critical micelle concentration (cmc) is significantly higher in ILs compared to water. For example Evans et al. found that the cmc of conventional surfactants in EAN is between 5 and 10 times higher compared to water (Evans et al., 1982). Greaves et al. studied the self-assembly behavior of amphiphiles in 22 different protic ILs (Greaves et al., 2008 b), fourteen of those were found to promote self-assembly of amphiphiles. The

concept of the Gordon parameter, which represents a measure of the cohesive energy density of a solvent and hence the driving force of a solvent as promoter for self-assembly was applied to these systems. Whilom it was generally accepted that no amphiphilic aggregation exists for solvents with a Gordon parameter below  $1.3 \text{ J m}^{-3}$  (Evans & Wennerström 1998). Nowadays, ethylammonium butyrate with a value of  $0.576 \text{ J m}^{-3}$  is the solvent with the lowest Gordon parameter known to promote self-assembly of amphiphiles (Greaves et al., 2007). The self-assembly is not restricted to protic ILs, it has been documented for several aprotic ILs as well (Anderson et al., 2003; Hao et al., 2005; Patrascu et al., 2006). In addition to the extensive amount of research conducted into binary IL/surfactant mixtures progress has been made in the formulation and characterization of nonaqueous microemulsions, the actual topic of this review.

## 2.1 Aprotic ionic liquids

Studies concerning the use of aprotic ILs in microemulsions are almost entirely related to imidazolium based substances. Herein, the most extensively studied microemulsions comprise the RTIL 1-butyl-3-methylimidazolium tetrafluoroborate ([bmim][BF<sub>4</sub>]) as water substitute, the non-ionic surfactant TX-100 and oil as apolar phase.

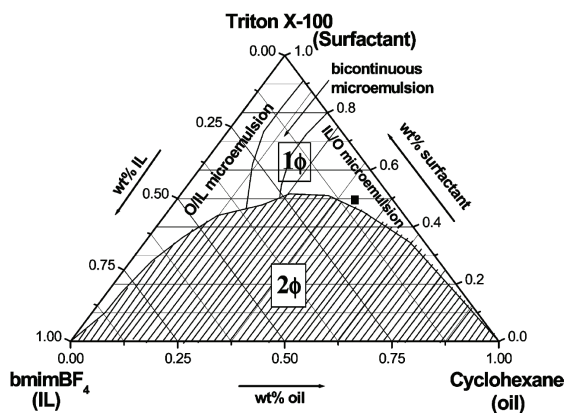


Fig. 1. Ternary phase diagram of [bmim][BF<sub>4</sub>]/TX-100/cyclohexane at 23 °C. (Reproduced from (Gao et al., 2008) with permission, copyright American Chemical Society, 2008).

The first microemulsion, where water has been replaced by an RTIL has been reported by Gao et al. (Gao et al., 2004). They replaced water by [bmim][BF<sub>4</sub>], while cyclohexane has been used as apolar phase and TX-100 as surfactant. The corresponding ternary phase diagram at 35°C has been recorded, while the phase diagram for the identical system has been reported by Li et al. at 25 °C (Li et al., 2008) and by Gao et al. at 23°C (Gao et al., 2008). Since the phase diagrams do not differ significantly between 23°C and 35°C, the phase diagram at 23 °C is exemplarily illustrated in Figure 1.

In the following, the state of research on [bmim][BF<sub>4</sub>]/TX-100/cyclohexane microemulsions is discussed in detail. Different microemulsion subregions have been identified by means of conductivity measurements (Gao et al., 2004). Typical cuts in the phase diagram have been made, where the weight fraction of [bmim][BF<sub>4</sub>]/TX-100 was kept constant while the amount of cyclohexane increases. Consistent with microstructures known for aqueous



microemulsions, oil-in-IL (o/IL) microregions at low amounts of cyclohexane, followed by bicontinuous and IL-in-oil (IL/o) structures with increasing oil content have been identified via conductivity measurements. Further, freeze fracture transmission electron micrographs (FF-TEM) in the IL/o microregion indicated droplet structures with increasing size when  $R$  value, defined as the molar ratio of [bmim][BF<sub>4</sub>]/surfactant, was risen. The results are consistent with apparent hydrodynamic radii extracted from dynamic light scattering (DLS) measurements. Nonetheless, the droplet sizes inferred from DLS measurements of the order of 0.1  $\mu\text{m}$  at  $R = 1.5$  appear to be extraordinary large and are outside the range of conventional microemulsions. These outstandingly large droplet dimensions may be related to collective scattering effects that have not been taken into account (Qiu & Texter 2008).

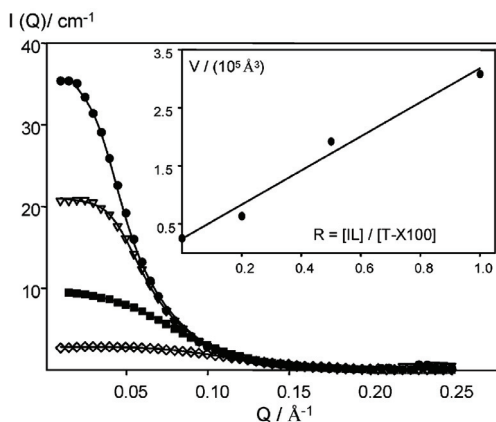
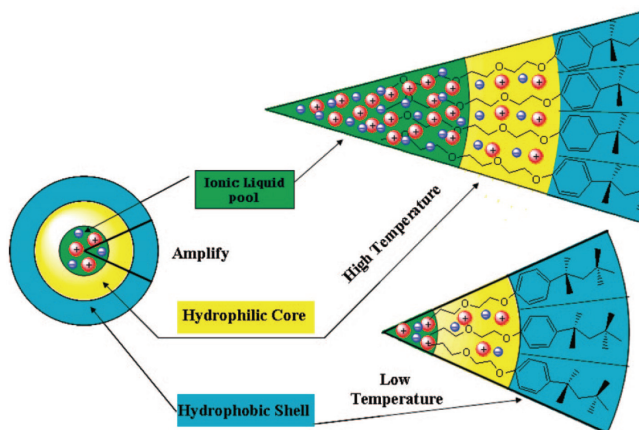


Fig. 2. SANS from single-phase  $[h\text{-bmim}][\text{BF}_4]$  in cyclohexane- $d_{12}$  microemulsions at 55°C.  $R = 0$  ( $\diamond$ ), 0.2 ( $\blacksquare$ ), 0.5 ( $\triangle$ ), and 1.0 ( $\bullet$ );  $\phi_{\text{TX-100}} = 0.41$ . The fits shown as lines are to a form factor for homogeneous ellipsoids. Inset shows the micelle swelling behavior in terms of the ellipsoid volume  $V$  as a function of added IL. (Reproduced from (Eastoe et al., 2005), with permission, copyright American Chemical Society, 2008).

Eastoe et al. performed small angle neutron scattering (SANS) experiments on the same systems at 55°C, except that cyclohexane- $d_{12}$  was used to improve the scattering contrast (Eastoe et al., 2005). The scattering curves for different  $R$  values, comparable to the  $R$  values investigated by Gao et al. (Gao et al., 2004) could well be described by a model of homogeneous diluted ellipsoidal particles, which was in agreement with IL/o structures. A swelling behavior of the IL nanodomains with increasing  $R$  value was observed consistent with the observations of Gao et al. The SANS curves with the corresponding fits for ellipsoidal structures are illustrated in Figure 2. By contrast, the extracted sizes were in the typical range of aqueous microemulsions arguing strongly against the DLS radii reported by Gao et al.

The solvation dynamics and rotational relaxation of Coumarin 153, a rigid molecule having a single low-lying excited state and simple solvatochromic behavior (Maroncelli & Fleming 1987) has been investigated for the same system by Chakrabarty et al. (Chakrabarty et al., 2005). With steady state and time resolved fluorescence spectroscopy measurements at different  $R$  values they observed a red shift in the emission spectra with increasing [bmim][BF<sub>4</sub>] content indicating the formation of RTIL pools. The solvation times in the RTIL pools were found to be nearly independent of [bmim][BF<sub>4</sub>] content and size of the

microemulsion droplets. By contrast, a decrease in solvation time in aqueous reverse microemulsions with increasing  $R$  values has been documented in literature (Sarkar et al., 1996; Riter et al., 1998). Using isothermal titration microcalorimetry Li et al. determined the heat of dilution and extracted the second virial coefficient,  $b_2$  of these microemulsions (Li et al., 2008). Both heat of dilution and  $b_2$  are significantly larger compared to conventional aqueous microemulsions (Chen et al., 2000). From these studies Li et al. deduced substantial stronger interactions of the IL nanodroplets compared to aqueous systems. Further, the data suggested weakened interdroplet interactions with increasing temperature. With respect to the influence of temperature important results have been obtained studying temperature induced microstructural changes with DLS, freeze-fracture transmission electron microscopy (FF-TEM) and two-dimensional nuclear Overhauser effect (ROESY) experiments (Gao et al., 2009 a). By visual inspection a single phase microemulsions has been observed up to 74°C, which corresponds to the boiling point of cyclohexane. DLS measurements indicate an increase in droplet size with rising temperature within (24 - 44)°C with diameters between 54 nm (24°C) and 153 nm (44°C). Gao et. al proposed that the formation of microemulsions in a system consisting of [bmim][BF<sub>4</sub>] and TX-100 is driven by the electrostatic attraction between the positively charged [bmim]<sup>+</sup> cation and the ethylene oxide (EO) units in TX-100 (Gao et al., 2006 b). Hence, the effective interaction area of EO units is higher than in water resulting in an increased size of the reverse microemulsion droplets (Gao et al., 2009 a). FF-TEM images confirmed the existence of a droplet structure within (25 - 55)°C and are in agreement with increasing droplet size with rising temperature. 2D ROESY spectra indicated structures with [bmim][BF<sub>4</sub>] domains, stabilized by a surfactant interfacial film in a continuous oil phase. Further, it was proposed that EO moieties penetrate into the RTIL interior with the hydrophobic chain pointing towards the continuous oil phase. Moreover, an increase in droplet size with rising temperature is related to a decrease in interfacial curvature of the surfactant film. Gao et al. supposed that the electrostatic interaction between the [bmim]<sup>+</sup> cation and the EO units is relatively temperature independent while the solubility of the hydrophobic surfactant chain is temperature sensitive and thus causes the change in interfacial curvature (Gao et al., 2009 a). A schematic picture of the proposed microemulsion structure in dependence of temperature including the change in interfacial curvature is illustrated in Scheme 1. However, these microemulsions are relatively temperature insensitive compared to common nonionic surfactant based aqueous microemulsions (Wormuth et al., 2002) highlighting fundamental differences between IL and water based microemulsions. The temperature sensitivity of aqueous microemulsions with nonionic surfactants is related to the interaction of water molecules with the EO moieties of the nonionic surfactant. Hence, a temperature change can provoke transitions from w/o to bicontinuous and o/w structures (Wormuth et al., 2002). For [bmim][BF<sub>4</sub>]/TX-100/oil microemulsions the influence of replacing the oil phase has been extensively studied as well. Beside cyclohexane as described in the previous paragraph, phase diagrams with toluene (Gao et al., 2006 a; Li et al., 2007), p-xylene (Gao et al., 2006 b) and even benzene (Gao et al., 2007 a; Gao et al., 2007 b) have been reported. The resulting phase diagrams are comparable to the phase diagram shown in Figure 1 indicating that there is no major influence of the type of the oil with respect to the single phase region and type of occurring microstructures. Similar to the systems described for cyclohexane transition from o/IL over bicontinuous to IL/o structures with increasing toluene (Gao et al., 2006 a), p-xylene (Gao et al., 2006 b) and benzene content (Gao et al., 2009 b), respectively have been detected with conductivity measurements. Further, a swelling of the IL



Scheme 1. Schematic illustration of the  $[\text{bmim}][\text{BF}_4]/\text{o}$  microemulsion structure, accompanied by the curvature change of TX-100 interfacial film at  $[\text{bmim}][\text{BF}_4]/\text{o}$  two phases with changing temperature. (Reproduced from (Gao et al., 2009 a) with permission, copyright American Chemical Society, 2009).

nanodomains with increasing amount of  $[\text{bmim}][\text{BF}_4]$  has been verified by DLS measurements for the  $[\text{bmim}][\text{BF}_4]/\text{p}$ -xylene microemulsions (Gao et al., 2006 b). The micropolarity of  $[\text{bmim}][\text{BF}_4]/\text{TX-100}/\text{toluene}$  has been studied via UV-vis spectroscopy and methyl orange (MO) as probe. With increasing amount of  $[\text{bmim}][\text{BF}_4]$  the absorption spectra were red shifted indicating an increase in micropolarity until a plateau was reached when the RTIL pool was formed. Similar results have been reported by Han and coworkers for  $[\text{bmim}][\text{BF}_4]/\text{TX-100}/\text{cyclohexane}$  systems (Gao et al., 2004). Fu et al. studied the electrochemical properties with toluene as oil phase using cyclic voltammetry (CV) and electrochemical impedance with potassium ferricyanide as electroactive probe (Fu et al., 2008). Their measurements indicated that the reversibility of  $[\text{Fe}(\text{CN})_6]^{3-}/[\text{Fe}(\text{CN})_6]^{4-}$  electrode reaction in the o/IL microemulsion was enhanced compared to IL/o structures and the neat IL, respectively. Concerning the effect of temperature an increase in droplet size with increasing temperature was reported with toluene as continuous phase similar to the systems with cyclohexane (Gao et al., 2009 a). Recently, FF-TEM was used to detect the swelling process of o/IL microemulsions. Herein, bicontinuous IL containing microemulsions have been visualized for the first time with FF-TEM (Gao et al., 2009 b). The structural evolution monitored by FF-TEM is illustrated exemplarily for the  $[\text{bmim}][\text{BF}_4]/\text{TX-100}/\text{toluene}$  system in Figure 3.

Therein, the  $R$  value was kept constant at  $R = 0.5$ , while the organic solvent weight fraction  $F$  successively increases. For  $F \leq 0.25$  a nearly spherical droplet structure could be detected, while the o/IL diameter increased with  $F$  confirming the swelling behavior. Moreover, the aggregates changed from spherical structures ( $F \leq 0.25$ ) to droplet clusters and larger aggregates. At a toluene weight fraction of  $F = 0.30$ , a bicontinuous structure could be detected. A comparable structural evolution has been observed for the  $[\text{bmim}][\text{BF}_4]/\text{TX-100}/\text{p}$ -xylene microemulsions ranging from droplet structures over droplet clusters to bicontinuous systems. By contrast, bicontinuous structures could not be identified for  $[\text{bmim}][\text{BF}_4]/\text{TX-100}/\text{cyclohexane}$  systems since phase separation occurred at higher cyclohexane weight fractions.

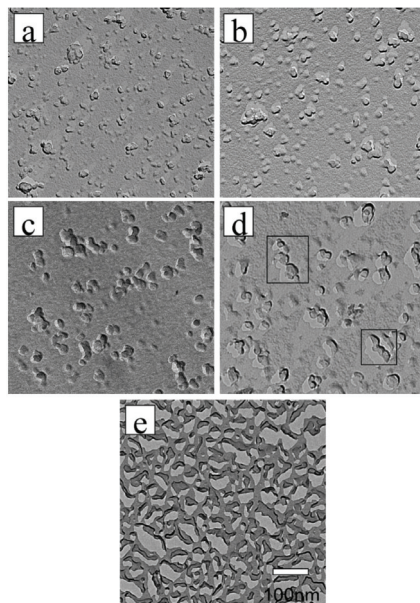


Fig. 3. FF-TEM images of the toluene/[bmim][BF<sub>4</sub>] microemulsion aggregates with  $R = 0.5$  and  $F = 0.10$  (a), 0.15 (b), 0.20 (c), 0.25 (d), and 0.30 (e). Scale bar is 100 nm for all samples in the figure. (Reproduced from (Gao et al., 2009 b) with permission, copyright American Chemical Society, 2009).

Adhikari et al. investigated microemulsions comprising 1-pentyl-3-methylimidazolium tetrafluoroborate ([pmim][BF<sub>4</sub>])/TX-100/benzene (Adhikari et al., 2007; Adhikari et al., 2009). Surprisingly, the ternary phase diagram has not yet been documented in literature. However, interesting results have been obtained studying the solvation dynamics in different subregions of these microemulsions with Coumarin 480 (C480) as probe. The probe can be distributed in both polar and apolar regions of the microemulsions. Since the solute absorption and emission spectra are dependent on the polarity of the solvent, the probe can be excited selectively by a variation of the excitation wavelength  $\lambda_{\text{ex}}$ . A so-called red edge excitation shift (REEs) denotes the shift in the wavelength of maximum fluorescence emission towards higher wavelengths, caused by a shift in the excitation wavelength towards the red edge of the absorption band (Demchenko 1982; Mukherjee & Chattopadhyay 2005). For the RTIL microemulsion faster solvation dynamics and a slower anisotropy decay with increasing  $\lambda_{\text{ex}}$  has been reported (Adhikari et al., 2007). The authors explained these observations by a higher viscosity and polarity of the core of the reverse microemulsion compared to that at the interface. Therefore, a long  $\lambda_{\text{ex}}$  accompanied with slow anisotropy decay probes a highly viscous core. Moreover, fluorescence resonance energy transfer (FRET) from C480 and rhodamine 6G (R6G) has been studied in the same microemulsion by picosecond and femtosecond emission spectroscopy (Adhikari et al., 2009). Three different time scales of FRET of (1, 250 and 3000) ps have been found. It was proposed that in the highly polar IL pool FRET is very fast based on the close proximity of the donor and the acceptor species. The 250 ps component could be allocated to FRET from

a donor inside the surfactant chains and the long component was assigned to FRET from a donor in the continuous phase and an acceptor in the RTIL core. Further, Mojumdar et al. studied the proton transfer of pyranine via femtosecond up-conversion (Mojumdar et al., 2010) in the same microemulsions.

In the previous paragraphs the state of research concerning microemulsions with [bmim][BF<sub>4</sub>] and [pmim][BF<sub>4</sub>] as polar phase has been summarized. Li et al. varied the ionic liquid representing the polar phase in nonaqueous microemulsions (Li et al., 2005). They replaced water by 1-butyl-3-methylimidazolium hexafluorophosphate ([bmim][PF<sub>6</sub>]). The idea of using [bmim][PF<sub>6</sub>] as polar phase represents an unconventional idea and important progress, since [bmim][PF<sub>6</sub>] is considered as apolar and not miscible with water. The single-phase region of the ternary phase diagram toluene/TX-100/[bmim][PF<sub>6</sub>] covered an area about 75% of the phase diagram. Different subregions could be detected via conductivity measurements. With increasing weight fraction of TX-100 + [bmim][PF<sub>6</sub>] a transition from a [bmim][PF<sub>6</sub>]/o microstructure via a bicontinuous region to an o/[bmim][PF<sub>6</sub>] microstructure has been reported. Small angle X-ray scattering (SAXS) experiments that have been performed in the [bmim][PF<sub>6</sub>]/o sub-region indicated a swelling of the droplet structure with increasing amount of RTIL. The apparent gyration radii ( $R_g$ ) extracted from Guinier analyses lay in a typical size range for microemulsions between (4.4 and 6.2) nm at different  $R$  values ( $0.3 \leq R \leq 0.98$ ). Zheng et al. investigated microemulsions consisting of toluene/Tween 80/ [bmim][PF<sub>6</sub>] (Zheng & Eli 2009; Zheng et al., 2009). These systems have been characterized via conductivity and FTIR spectroscopy (Zheng et al., 2009), the micropolarity has been monitored via UV- VIS spectroscopy (Zheng & Eli 2009). Conductivity measurements indicated a transition from o/[bmim][PF<sub>6</sub>] via bicontinuous to [bmim][PF<sub>6</sub>]/o microregions with increasing toluene weight fraction at a fixed  $R$  value. The transitions monitored by conductivity measurements, exemplarily shown for these systems, are illustrated in Figure 4. Since Figure 4 represents a typical example for phase transitions in microemulsions that can be detected with conductivity measurements, the characteristics of the curve will be discussed in the following. The increase in conductivity along the curve from point A to B can be allocated to an o/RTIL microstructure. With increasing amount of

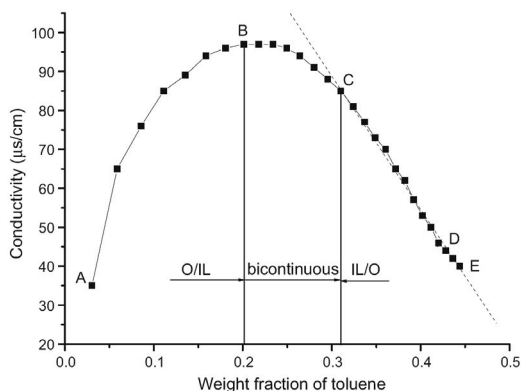


Fig. 4. Electrical conductivity of the microemulsions toluene/Tween80/[bmim][PF<sub>6</sub>] as a function of toluene content, [bmim][PF<sub>6</sub>]/Tween 80 = 1.9. (Reproduced from (Zheng et al., 2009) with permission copyright Springer-Verlag, 2009).

oil (toluene) the conductivity increases, which correlates with an increase in the mobility of charge carriers. The addition of a cosolvent, in the present case toluene, increases the mobility of charge carriers, because less of ion pairs are then present in the solution. With increasing toluene content the volume of the microdroplets rises correlating with an improved ionic mobility due to the dissociation of ion pairs in the solution. From point B to C the conductivity decreases slightly indicating a change in microemulsion structure. This subregion can be assigned to a bicontinuous structure. When the oil content is further increased a significant decrease in conductivity can be observed between point C and E representing a typical IL/o structure. The authors attributed the change in conductivity from point D to E to a percolation phenomenon that might be present in this system, but to our opinion this can not clearly be confirmed from these data.

FTIR spectra indicated the presence of hydrogen-bonds between [bmim][PF<sub>6</sub>] and Tween 80. Zheng et al. reported hydrogen-bond interactions between the C2-H of the [bmim]<sup>+</sup> cation and the EO units in Tween 80 and an interaction of the [PF<sub>6</sub>]<sup>-</sup> anion with the terminal hydroxyl group of Tween 80 (Zheng et al., 2009). The authors suggested that these hydrogen-bonded interactions between [bmim][PF<sub>6</sub>] and Tween 80 might be the driving force for the solubilization of the RTIL into the core of the Tween 80 aggregates.

Cheng et al. investigated promising systems consisting of ethylene glycol (EG) as polar phase, [bmim][PF<sub>6</sub>] as oil substituent and TX-100 as surfactant (Cheng et al., 2007 a). Since the vapor pressure of both EG and [bmim][PF<sub>6</sub>] are very low at ambient temperature, these microemulsions represent an important step towards systems consisting entirely of non-volatile components. The microemulsions have been studied by means of conductivity, DLS, UV-Vis and FF-TEM measurements. With conductivity measurements [bmim][PF<sub>6</sub>]/EG, bicontinuous and EG/[bmim][PF<sub>6</sub>] subregions could be identified. The [bmim][PF<sub>6</sub>]/EG subregion has further been characterized by DLS measurements, for different R values ( $0 \leq R \leq 0.28$ ) apparent hydrodynamic radii between (5 – 19) nm have been extracted confirming a swelling behavior with increasing amount of RTIL. Further, the radii extracted from CONTIN analysis (Provencher 1982 a; Provencher 1982 b) are consistent with a swelling law for spherical microemulsions, where the size of the droplets should be a linear function of R (Zhu et al., 1992). The swelling law can be expressed as  $R_{H}^{app} = 3 V_{disp} R A_h^{-1}$ , where  $R_{H}^{app}$  is the apparent droplet radius,  $V_{disp}$  the molecular volume of the dispersed phase and  $A_h$  the effective area per headgroup at the interface (Cheng et al., 2007 a). The [bmim][PF<sub>6</sub>]/EG microemulsions obeyed this swelling law confirming a spherical droplet structure. FF-TEM images further confirmed the existence of spherical [bmim][PF<sub>6</sub>]/EG microregions, while the sizes agreed reasonably well with the droplet dimensions extracted from DLS measurements. Using MO as probe, UV-Vis measurements indicated an increasing micropolarity of the EG domains with rising amount of EG in the EG/[bmim][PF<sub>6</sub>] subregion.

Most studies concerning aprotic ionic liquids in microemulsions are attendant on the use of nonionic surfactants. In contrast, we reported microemulsions consisting of the ionic surfactant 1-hexadecyl-3-methylimidazolium chloride ([C<sub>16</sub>mim][Cl]), which is at the same time an ionic liquid (Zech et al., 2009 b). Further, [bmim][BF<sub>4</sub>] has been used as polar phase, dodecane as apolar phase and decanol as cosurfactant. Along an experimental path in the corresponding phase diagram, these systems have been characterized by means of conductivity, viscosity and SAXS measurements. Moreover, we have directly compared microemulsions with the aprotic ionic liquid [bmim][BF<sub>4</sub>] and the protic ionic liquid ethylammonium nitrate (EAN). The major advantage of using ionic surfactants is that the

microemulsions become even less sensitive towards temperature. A detailed comparison of the [bmim][BF<sub>4</sub>] systems with the protic RTIL EAN is given in section 2.2.

Rabe & Koetz investigated phase diagrams of 1-ethyl-3-methylimidazolium ethylsulfate ([emim][etSO<sub>4</sub>])/cetyltrimethylammonium bromide (CTAB)/toluene+pentanol and 1-ethyl-3-methylimidazolium hexylsulfate ([emim][hexSO<sub>4</sub>])/CTAB/toluene+pentanol, respectively (Rabe & Koetz 2010). They studied the phase behavior of these systems in dependence of oil/cosurfactant ratio and temperature. Interesting results have been obtained although these systems are on the boarderline of nonaqueous microemulsions, since the authors reported water contents in the IL up to 5wt%. To our opinion terming an IL with 5wt% water “nearby water-free” (Rabe & Koetz 2010) is questionable, since 5wt% of water correspond for example for [emim][hexSO<sub>4</sub>] to a water molar ratio of  $x_{\text{H}_2\text{O}} = 46\%$ ! For the system [emim][etSO<sub>4</sub>]/CTAB/toluene+pentanol different toluene/pentanol ratios have been investigated ranging from 1:1 to 20:1 at ambient temperature. In the absence of cosurfactant two separated isotropic phase channels could be found, where one was attributed to an IL/o structure and the second to an o/IL microstructure. With increasing amount of cosurfactant the area of these single phase regions increased until they became connected at a toluene:pentanol ratio of 1:1. Further, the effect of temperature on the pseudo-ternary phase diagrams was studied. For a ratio toluene:pentanol of 5:1 the two separated phase channels present at ambient temperature were connected at 50°C, with increasing temperature (80°C) the area of the one phase region further augmented. These temperature dependent phase diagrams are illustrated in Figure 5. With conductivity measurements a typical percolation phenomenon with increasing amount of IL in the IL/o region was observed, the threshold was found to be relatively independent of the IL anion chain length. The percolation behavior was further confirmed with viscosity measurements. From DLS measurements two separate peaks were extracted in the intensity plot with sizes in the typical range for microemulsions. Cryo scanning electron microscopy (cryo-SEM) images below the percolation threshold indicate separated spherical structures which were attributed to IL/o microstructures. An increase in droplet size with increasing amount of IL was further confirmed by cryo-SEM.

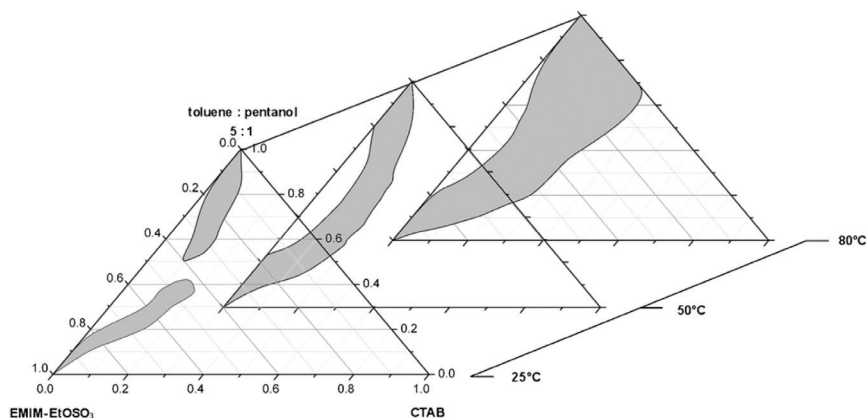


Fig. 5. Pseudo ternary phase diagrams of CTAB/toluene+pentanol/[emim][etSO<sub>4</sub>] between (25 – 80)°C. (Reproduced from (Rabe & Koetz 2010), with permission, copyright Elsevier, 2010).



Gayet et al. characterized microemulsions composed of benzylpyridinium bis-(trifluoromethanesulfonyl)imide ([bnpyr][NTf<sub>2</sub>])/TX-100/toluene (Gayet et al., 2009). The microstructure has been investigated with DLS, SANS, viscosity and pulse field gradient spin-echo (PGSE) NMR measurements. A transition of o/IL over bicontinuous to IL/o microstructures with increasing toluene content has been identified by means of conductivity measurements. Relative self-diffusion coefficients determined via PGSE NMR measurements were in line with the existence of IL/o structures. Hydrodynamic radii in the IL/o regime were in the typical order of magnitude for microemulsion structures, while radii from DLS measurements ( $2.2 \leq R_h \leq 3.4$ ) nm were slightly larger compared to the PGSE NMR measurements ( $1.8 \leq R_h \leq 1.9$ ) nm. SANS and SANS contrast variation data in the IL/o regime could be described using a polydisperse homogeneous ellipsoid model, while for the bicontinuous regime the domain size  $D^*$  was evaluated via the Bragg relation  $D^* = 2 \pi q_{\max}^{-1}$  where  $q_{\max}$  corresponds to the position of the correlation peak.

Cheng et al. highlighted a major contribution towards the formulation of nonaqueous microemulsions with two types of ionic liquids (Cheng et al., 2007 b). For the first time they reported ionic liquid in ionic liquid (IL/IL) structures. For this purpose, the hydrophobic ionic liquid [bmim][PF<sub>6</sub>] and the hydrophilic protic ionic liquid propylammonium formate (PAF) were used as apolar and polar phase, respectively. Moreover, these microemulsions contained the anionic surfactant sodium bis (2-ethylhexyl) sulfosuccinate (AOT). One

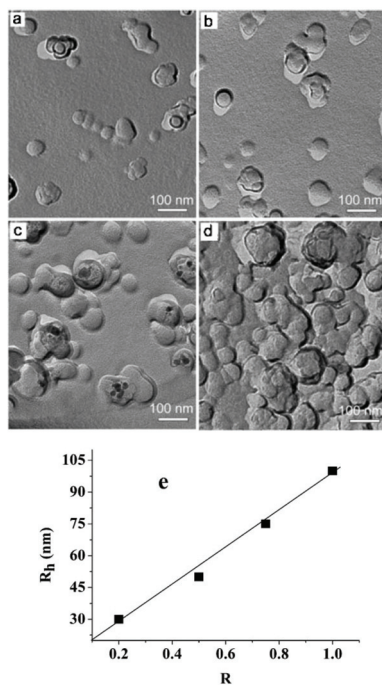


Fig. 6. TEM images of FFEM replicas of [bmim][PF<sub>6</sub>]-AOT-PAF microemulsions. (a)  $R = 0.2$ , (b)  $R = 0.5$ , (c)  $R = 0.75$ , (d)  $R = 1.0$  (weight fraction of AOT is 0.16); (e) dependence of the droplet diameter ( $R_h$ ) on [bmim][PF<sub>6</sub>]-to-AOT molar ratio ( $R$ ). (Reproduced from (Cheng et al., 2007 b), with permission, copyright Royal Society of Chemistry, 2007).



important precondition for the formation of stable microemulsions is that the polar and the apolar phase do not mix. By the tricky combination of PAF and [bmim][PF<sub>6</sub>], whose solubility in PAF was less than 0.1 wt% under ambient conditions (Cheng et al., 2007 b) this requirement could be fulfilled. However, the single phase region in the ternary phase diagram was exceptionally small. FF-TEM images at different R values and a constant amount of surfactant indicated droplet like structures with droplet radii ranging from (15 – 50) nm as illustrated in Figure 6. The authors proposed [bmim][PF<sub>6</sub>]/PAF structures, the extracted radii increased linearly with R.

For a better overview, the different microemulsion systems with aprotic ionic liquids, the methods used to characterize them and the corresponding references are summarized in Table 1.

microemulsion system	methods	references
[bmim][BF <sub>4</sub> ] TX-100 cyclohexane	conductivity, FF-TEM, DLS, UV-Vis SANS DLS, FTIR, <sup>1</sup> H-NMR, ITC, conductivity ITC steady-state and picosecond time resolved emission spectroscopy IT-microcalorimetry, conductivity DLS, FF-TEM, ROESY conductivity, ROESY, FF-TEM	(Gao et al., 2004) (Eastoe et al., 2005) (Gao et al., 2008) (Li et al., 2008) (Chakrabarty et al., 2005) (Chen et al., 2000) (Gao et al., 2009 a) (Gao et al., 2009 b)
[bmim][BF <sub>4</sub> ] TX-100 p-xylene	conductivity, DLS, <sup>1</sup> H-NMR, FTIR, UV-Vis conductivity, ROESY, FF-TEM	(Gao et al., 2006 b) (Gao et al., 2009 b)
[bmim][BF <sub>4</sub> ] TX-100 toluene	conductivity, CV conductivity, DLS, UV-Vis conductivity, CV, impedance spectroscopy DLS, FF-TEM, ROESY conductivity, ROESY, FF-TEM	(Gao et al., 2006 a) (Li et al., 2007) (Fu et al., 2008) (Gao et al., 2009 a) (Gao et al., 2009 b)
[bmim][BF <sub>4</sub> ] TX-100 benzene	FTIR, <sup>1</sup> H-NMR, <sup>19</sup> F-NMR, DLS conductivity, ROESY, FF-TEM	(Gao et al., 2007 a) (Gao et al., 2009 b)
[pmim][BF <sub>4</sub> ] TX-100 benzene	femtosecond up-conversion, DLS FRET femtosecond up-conversion	(Adhikari et al., 2007) (Adhikari et al., 2009) (Mojumdar et al., 2010)
[bmim][PF <sub>6</sub> ] TX-100 toluene	conductivity, SAXS	(Li et al., 2005)
[bmim][PF <sub>6</sub> ] Tween 80 toluene	UV-Vis, conductivity conductivity, FTIR	(Zheng & Eli 2009) (Zheng et al., 2009)
ethylene glycol	conductivity, DLS, FF-TEM, UV-Vis	(Cheng et al., 2007 a)

TX-100 [bmim][PF <sub>6</sub> ]		
[bmim][BF <sub>4</sub> ] [C <sub>16</sub> mim][Cl]+1-decanol dodecane	conductivity, viscosity, SAXS	(Zech et al., 2009 b)
[emim][etSO <sub>4</sub> ] or [emim][hexSO <sub>4</sub> ] CTAB toluene+pentanol	conductivity, viscosity, oscillation measurements, DLS, cryo-SEM	(Rabe & Koetz 2010)
[bnpyr][NTf <sub>2</sub> ] TX-100 toluene	conductivity, PGSE NMR, DLS, SANS	(Gayet et al., 2009)
PAF AOT [bmim][PF <sub>6</sub> ]	surface tension, FF-TEM	(Cheng et al., 2007 b)

Table 1. Summary of the different microemulsions systems with aprotic ionic liquids together with the references and methods used.

## 2.2 Protic ionic liquids

Atkin & Warr reported microemulsions composed of nonionic alkyl oligoethyleneoxide surfactants (C<sub>i</sub>E<sub>j</sub>), alkanes and EAN as polar phase (Atkin & Warr 2007). They studied the phase behavior of the ternary mixtures by applying typical slices through the phase prism at a 1:1 oil to water ratio while the amount of surfactant was varied. Since phase prisms of microemulsions with nonionic surfactants, where the dependence of temperature is taken into account are relatively complicated and difficult to interpret, greater understanding comes from going back to two-dimensional space by taking slices through the phase prisms. The phase diagram, where the mass fraction of surfactant is shown as a function of temperature, takes the shape of a fish. These so-called fish cuts are the most often used two-dimensional phase diagrams concerning microemulsions with non-ionic surfactants and have been studied systematically for aqueous microemulsions by Kahlweit et al. (Kahlweit et al., 1988; Kahlweit et al., 1989). Atkin and Warr presented fish-cuts obtained for an equal ratio of water to oil for surfactants with increasing amphiphilicity (C<sub>8</sub>E<sub>2</sub>, C<sub>12</sub>E<sub>3</sub>, C<sub>14</sub>E<sub>4</sub>). With dodecane as oil the phase diagrams were very similar to the corresponding aqueous systems (Kahlweit et al., 1993). A tricritical point (Kahlweit et al., 1985; Kahlweit et al., 1986), where the formation of a three phase body occurred was found for the EAN/C<sub>i</sub>E<sub>j</sub>/dodecane systems at amphiphilicities between C<sub>8</sub>E<sub>2</sub> and C<sub>12</sub>E<sub>3</sub>. Compared to water (Kahlweit et al., 1986) and formamide (Schubert et al., 1993) the tricritical point was shifted for EAN to higher amphiphilicities i.e. longer alkyl chain lengths. Additionally, Atkin & Warr studied the microemulsions phase behavior as a function of the oil alkyl length (octane, decane, dodecane, tetradecane and hexadecane) and headgroup size. Exemplarily fish-cuts for EAN microemulsions with dodecane and tetradecane are illustrated in Figure 7.

The phase behavior response to these changes was found to be broadly consistent with aqueous systems, while the effective area of interaction for each EO unit was found to be significantly higher in EAN compared to aqueous systems.  $\bar{X}$  defines the point of the

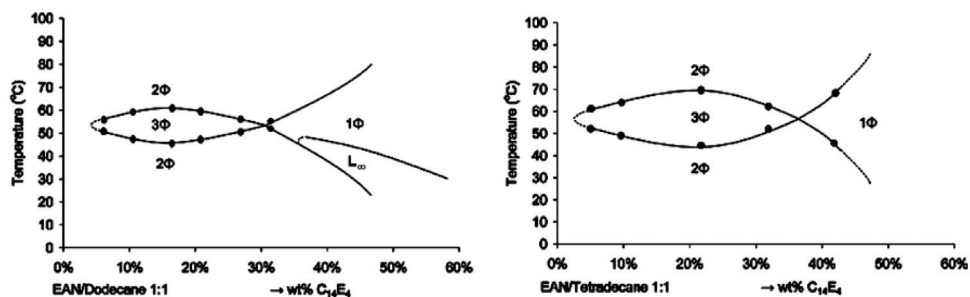


Fig. 7. Vertical section through the phase prisms for  $C_{14}E_4$ /EAN/alkane systems with equal masses of EAN and alkane. (Reproduced from (Atkin & Warr 2007), with permission, copyright American Chemical Society, 2007).

maximum surfactant efficiency i.e. the minimum amount of surfactant required to solubilize two immiscible solvents. SAXS curves near  $\bar{X}$  exhibit a single broad scattering peak followed by a  $q^{-4}$  decay at large  $q$  values. The curves could well be described with the Teubner-Strey model (Teubner & Strey 1987). The oil and water regimes are coupled via the surfactant film resulting in a broad scattering peak. Both, the scattering peak and the  $q^{-4}$  dependence at large  $q$  can be described with the TS formula and two characteristic length scales, the domain size  $d$  and the correlation length  $\xi$  can be extracted. From the SAXS experiments the authors concluded that the changes in  $d$  and  $\xi$  with amphiphilicity and oil alkyl chain length are consistent with observations made for aqueous systems. Nevertheless, the SAXS data suggested that the structuring in EAN microemulsions is higher compared to their aqueous counterparts. Zemb interpreted the SAXS data of Atkin and Warr on the  $C_iE_j$ /EAN/alkane systems in terms of a dimensionless dilution plot (Zemb 2009). Data have been compared to predictions of the models of de Gennes and Taupin (De Gennes & Taupin 1982), disordered open connected (DOC) cylinders and DOC lamellar structures (Zemb et al., 1990; Zemb 1997). None of the existing models was compatible with the experimental results. Nevertheless, a simple random microstructure without local order could be excluded, the data suggested that a connected microstructure is more likely to exist. Recently, Atkin et al. studied microemulsions composed of propylammonium nitrate (PAN),  $C_iE_j$  and different alkanes (Atkin et al., 2009). Although no cloud points of nonionic surfactants could be found in PAN, the phase behavior of ternary systems equals that of EAN and water based systems. Conductivity measurements and phase behavior of PAN/ $C_iE_j$ /oil microemulsions indicated that the microemulsions are weakly structured up to surfactant chain length of  $C_{18}$ . SANS data could well be described by the TS formula. Further, SANS contrast variation revealed a cosurfactant like role of the propylammonium cation in these ternary microemulsions.

Beside the implementation of protic ILs in microemulsions with nonionic surfactants, pseudo-ternary systems with ionic surfactants have been reported as well. We compared microemulsions composed of  $[C_{16}mim][Cl]$ +decanol/ RTIL/dodecane with EAN and  $[bmim][BF_4]$  as polar phase, respectively at ambient temperature (Zech et al., 2009 b). A significant difference with respect to phase behavior and microemulsions structure has been found. The area of the one phase region was considerably larger in the case of EAN than for microemulsions with  $[bmim][BF_4]$ . For the microemulsions with EAN a typical percolation behavior for the EAN/o region with increasing EAN content has been found. DLS

measurements indicated a swelling with increasing EAN content, which was further confirmed by SAXS measurements. At low EAN content a droplet EAN/o structures followed by the formation of larger connected EAN/o aggregates were supposed, while in the case of [bmim][BF<sub>4</sub>] a bicontinuous structure is more likely to exist. Since all ingredients show an excellent thermal stability combined with high boiling points and decomposition temperatures, respectively, we have recently investigated the thermal stability of the [C<sub>16</sub>mim][Cl]+decanol/ EAN/dodecane microemulsions. It could be demonstrated that these microemulsions were stable within a temperature range between (30 – 150)°C. Therefore, these microemulsions represent the first high temperature microemulsions with ILs, exhibiting a thermal stability that cannot be achieved with their aqueous counterparts (Zech et al., 2010 a). The percolation behavior in the EAN/o region could be observed over the whole investigated temperature range, as illustrated in Figure 8, where the specific conductivity is shown as a function of the volume fraction  $\phi$ . From the inset of the plot in Figure 8 it is obvious that the threshold, where the conductivity increases remarkably and percolation appears, is shifted with increasing temperature to the left hand side i.e. to lower volume fractions. The corresponding percolation threshold volume fraction  $\phi_p$  was shifted continuously with increasing temperature to lower volume fractions. This effect can be explained by the increased motion of the formed IL nanodomains when the temperature is risen. Hence, the probability that two RTIL pools meet each other is higher and the threshold is shifted to smaller  $\phi$ . DLS measurements at 30°C indicated a swelling of the EAN/o nanodroplets with increasing amount of EAN, until a bimodal decay was observed in the intensity normalized autocorrelation functions. The threshold, where a bimodal decay occurred was consistent with the percolation threshold extracted from conductivity measurements (Zech et al., 2010 b). The high thermal stability was further confirmed by temperature dependent SANS experiments (Zech et al., 2010 b). Below the percolation threshold, the data treated by generalized indirect Fourier transformation (Brunner-Popela & Glatter 1997; Weyerich et al., 1999) (GIFT) analysis suggest a droplet like EAN/o microemulsion structure. The resulting pair distance distribution functions  $p(r)$  were interpreted in a classical way as histogram of distances inside the particle. The maxima of

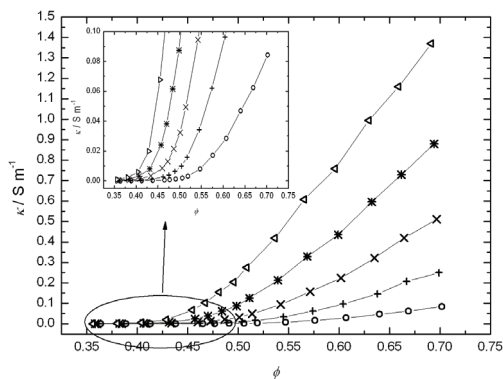


Fig. 8. Specific conductivity as a function of the volume fraction  $\phi$  demonstrating the percolative behavior at different temperatures (30°C (○), 60°C (+), 90°C (×), 120°C (□) and 150°C (Δ)) (Reproduced from (Zech et al., 2010 a) with permission, copyright Wiley-VCH Verlag, 2010).

these bell shaped functions are related to half of the diameter. Within (30 - 150)°C bell shaped  $p(r)$  functions were obtained, consistent with a swelling of the EAN/o nanodomains with increasing amount of IL. Further, the size of the EAN nanodroplets stabilized by surfactant remained constant at a given EAN content within (30 - 90)°C and increased slightly for 150°C. For a concentration series the shape of the  $p(r)$  functions did not change significantly. The same was valid for the shape at 30°C and 150°C. Consequently, the SANS data demonstrated that there is no essential structural variation within the measured concentration (below  $\phi_p$ ) and within the measured temperature range. However, the conductivity and SANS studies clearly demonstrated that one major benefit of the formulation of nonaqueous microemulsions with ILs is the extraordinary thermal stability that can be achieved. These systems represented the first high temperature microemulsions with ionic liquids with thermal stabilities far above the boiling point of water at ambient pressure.

Moreover, we could demonstrate that biodiesel can act as oil phase in high temperature microemulsions highlighting a way towards the formulation of biocompatible microemulsions (Zech et al., 2010 c). These model systems can be extended to other ILs, with [bmim][BF<sub>4</sub>] instead of EAN as polar phase, where a remarkable thermal stability can be achieved as well (Zech 2010). The different microemulsions containing protic ionic liquids, the methods used to characterize them and the corresponding references are summarized in Table 2.

microemulsion system	methods	references
EAN C <sub>i</sub> E <sub>j</sub> <i>n</i> -alkane	fish cuts, SAXS	(Atkin & Warr 2007)
PAN C <sub>i</sub> E <sub>j</sub> <i>n</i> -alkane	fish cuts, conductivity, SANS	(Atkin et al., 2009)
EAN [C <sub>16</sub> mim][Cl]+1-decanol dodecane	conductivity, viscosity, DLS, SAXS conductivity, SANS DLS, SANS	(Zech et al., 2009 b) (Zech et al., 2010 a) (Zech et al., 2010 b)
EAN [C <sub>16</sub> mim][Cl]+1-decanol biodiesel	conductivity, viscosity, SAXS	(Zech et al., 2010 c)

Table 2. Summary of the different microemulsions systems with protic ionic liquids together with the references and methods used.

### 2.3 Applications

Applications in the field of nonaqueous microemulsions containing ionic liquids are still scarce up to date. Nevertheless, the few studies available in the open literature demonstrate the great potential of these microemulsions in a diversity of different fields.

The synthesis of nanoparticles is one of the most promising potential applications of these new systems. Zhao et al. used benzene/TX-100/[bmim][BF<sub>4</sub>] microemulsions as template for the synthesis of silica nanoparticles under both basic and acidic conditions (Zhao et al., 2009). Herein, ellipsoidal nanoparticles have been obtained under acidic conditions, while hollow silica spheres were formed under alkaline conditions.

Moniruzzaman et al. reported a strategy for transdermal drug delivery by nonaqueous microemulsions with ILs (Moniruzzaman et al., 2010). A large number of drugs are sparingly soluble in both water and most organic solvents. Since the solubility of several drugs is remarkably higher in ILs, IL microemulsions can provide an effective carrier for transdermal drug delivery. In particular they studied the topical (into the skin) and transdermal (across the skin) delivery of acyclovir (ACV), which is an effective antiviral drug. Figure 9 shows the topological and transdermal delivery of ACV for various formulations. Figure 9 demonstrates that by using IL/o microemulsions as drug carrier the skin permeability of Yucatan hairless micropig skin to ACV was increased by several orders of magnitude. Moreover, IL/o microemulsions as drug carrier induced significant transdermal permeation of ACV. However, there is still necessity of improvement with respect to the cytotoxicity of several ILs.

Gayet et al. studied the efficiency of Matsuda-Heck coupling in reverse microemulsions by replacing the ionic liquid [bnpyr][NTf<sub>2</sub>] by a chiral structural analogue, 1-phenylethylpyridinium bis(trifluoromethanesulfonyl)imide ([pyr\*][NTf<sub>2</sub>]) in the system [bnpyr][NTf<sub>2</sub>]/TX-100/toluene described in section 2.1. (Gayet et al., 2009). The efficiency of the Matsuda-Heck reaction between p-methoxyphenyldiazonium salt and 2,3-dihydrofuran and a palladium catalyst in neat IL, the bicontinuous and the IL/o regime was evaluated. The reaction was regioselective regardless of the nature of the media, while the yields were increased when the amount of IL was rised. However, no enantiomeric excess of one of the products could be detected although “chiral” microemulsions with [R-(+)-pyr\*][NTf<sub>2</sub>] and [S-(-)-pyr\*][NTf<sub>2</sub>] were used.

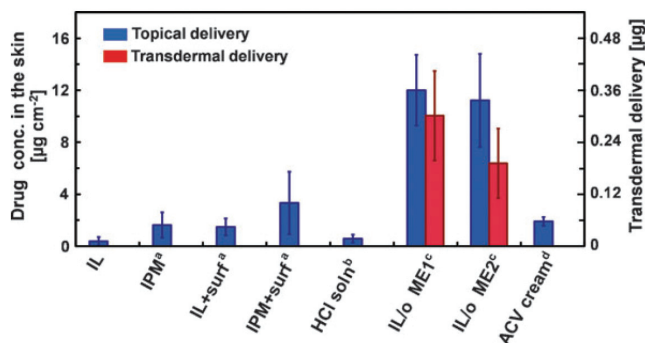


Fig. 9. Penetration of ACV from drug carriers into Yucatan hairless micropig skin under in vitro conditions. [ACV] = 5 mg mL<sup>-1</sup>, weight fraction of surfactant was 0.2 (Tween-80:Span-20 = 3:1 (w/w)). <sup>a</sup> Almost all ACV remained as suspended powders in formulations. <sup>b</sup> HCl concentration was 0.1 M. <sup>c</sup> R = 0.7 and surfactant fractions were 0.2 and 0.3 for ME1 and ME2, respectively. <sup>d</sup> ACV herpetic topical cream (equivalent to 5 mg ACV) used for penetration study. The data represent the average of three experiments and the errors bars indicate the standard deviation. (Reproduced from (Moniruzzaman et al., 2010) with permission, copyright Royal Chemical Society, 2010).

IL microemulsions have also been used for the fabrication of polymer electrolyte membranes (Yan et al., 2009). These nonaqueous proton conducting membranes have been prepared via the polymerization of microemulsions comprising PILs, surfactant and a

polymerizable oil, which was a mixture of styrene and acetonitrile. Although the resulting vinyl polymers were insoluble in the IL, nanodomains were found to be uniform, transparent and flexible. A conductivity of these membranes up to  $0.1 \text{ S m}^{-1}$  was found due to connected PIL nanochannels preserved in the membrane. Further, these proton conducting membranes offered good mechanical properties, thermal and chemical stability. On the other side, there exists a progressive release of the PIL that may affect the long-term stability of these new promising materials.

Chen et al. used microemulsions composed of methyl methacrylate (MMA)/1-dodecyl-3-methylimidazolium bromide/[bmim][BF<sub>4</sub>] microemulsions for free radical and atom transfer radical polymerizations (Chen et al., 2010). Polymers with reproducible size, well controlled molecular weight and low polydispersity could be produced. After the polymerization process, the remaining components could be recycled and reused.

### 3. Conclusions and outlook

In this review we have focused on nonaqueous microemulsions containing ionic liquids. A large diversity in phase diagrams and microstructures can be obtained in dependence of the ingredients and their proportions. Ionic liquids can act as polar phase to replace water, as oil substitute, as surfactant and they may even act as cosurfactant. It was further highlighted that the choice of the ionic liquid influences the phase behavior in general and the microstructure in particular. Many similarities compared to aqueous microemulsions have been found, but also some differences that underline the great potential of these systems with respect to applications. One obvious drawback is that the area of the single phase regions of ternary phase diagrams is smaller for ionic liquid microemulsions compared to their aqueous counterparts. Moreover, to reach the point of optimum formulation the amount of surfactant required is generally higher. Generally spoken ILs are less polar compared to water and hence the amount of surfactant (or its amphiphilicity, respectively) necessary to form micelles and microemulsions increases. Note that several studies can be found in literature, where the IL represents the apolar phase in aqueous microemulsions. Moreover, miscellaneous investigations report a remarkable effect when small amounts of water are added into the polar IL phase. However, this review has been focused on nonaqueous microemulsions and thence systems containing water were not implemented. One major point is that the stiffness of the interfacial film and the phase behavior can be tuned by the choice of the IL. For nonaqueous microemulsions containing ionic liquids it can be generalized that the temperature sensitivity is reduced. We believe that mainly the effect of temperature demonstrates one of the eminent benefits of these new colloidal systems. Since the vapor pressure of ILs is very low, systems can be designed that are stable far above the temperature range of conventional microemulsions, which may represent extraordinary reaction media. Further, it is obvious that by the choice of the components the stability range could also be extended towards low temperature microemulsions. One future challenge in this field will surely be the formulation and characterization of microemulsions that solely consist of ionic liquids. Moreover, more detailed investigations concerning the curvature, the rigidity of the interfacial and bending energies will be useful to provide a deeper understanding of these new promising systems. Although applications in this field are still scarce so far, it is evident that nonaqueous microemulsions will attract considerable interest in manifold fields. A strong future growth area might probably be their application as template materials or in nanoparticle synthesis. Furthermore, these systems are promising

candidates for chemical reactions in water-free organic or inorganic reactions. Moreover, they might find applications on separation science, encapsulation or nanocontainers, as well as in catalysis and biocatalysis.

#### 4. References

- Adhikari, A.; Sahu, K.; Dey, S.; Ghosh, S.; Mandal, U. & Bhattacharyya, K. (2007). Femtosecond solvation dynamics in a neat ionic liquid and ionic liquid microemulsion: excitation wavelength dependence. *Journal of Physical Chemistry B*, 111(44), 12809-12816.
- Adhikari, A.; Das, D. K.; Sasmal, D. K. & Bhattacharyya, K. (2009). Ultrafast FRET in a room temperature ionic liquid microemulsion: a femtosecond excitation wavelength dependence study. *Journal of Physical Chemistry A*, 113(16), 3737-3743.
- Anderson, J. L.; Pino, V.; Hagberg, E. C.; Sheares, V. V. & Armstrong, D. W. (2003). Surfactant solvation effects and micelle formation in ionic liquids. *Chemical Communications*, (19), 2444-2445.
- Angel, L. R.; Evans, D. F. & Ninham, B. W. (1983). Three-component ionic microemulsions. *Journal of Physical Chemistry*, 87(4), 538-40.
- Atkin, R. & Warr, G. G. (2007). Phase behavior and microstructure of microemulsions with a room-temperature ionic liquid as the polar phase. *Journal of Physical Chemistry B*, 111(31), 9309-9316.
- Atkin, R.; Bobillier, S. M. C. & Warr, G. G. (2009). Propylammonium nitrate as a solvent for amphiphile self-assembly into micelles, lyotropic liquid crystals, and microemulsions. *Journal of Physical Chemistry B*, 114(3), 1350-1360.
- Baker, G. A. & Pandey, S. (2005). Amphiphilic self organization in ionic liquids. *ACS Symposium Series*. Rogers, R. D. and Seddon, K. R. 901, 234-243.
- Belloq, A. M.; Biais, J.; Bothorel, P.; Clin, B.; Fourche, G.; Lalanne, P.; Lemaire, B.; Lemanceau, B. & Roux, D. (1984). Microemulsions. *Advances in Colloid and Interface Science*, 20(3-4), 167-272.
- Blanchard, L. A.; Hancu, D.; Beckman, E. J. & Brennecke, J. F. (1999). Green processing using ionic liquids and CO<sub>2</sub>. *Nature*, 399(6731), 28-29.
- Brunner-Popela, J. & Glatter, O. (1997). Small-angle scattering of interacting particles. I. Basic principles of a global evaluation technique. *Journal of Applied Crystallography*, 30(4), 431-442.
- Chakrabarty, D.; Seth, D.; Chakraborty, A. & Sarkar, N. (2005). Dynamics of solvation and rotational relaxation of coumarin 153 in ionic liquid confined nanometer-sized microemulsions. *Journal of Physical Chemistry B*, 109(12), 5753-5758.
- Chang, D. R. (1990). Conductivity of molten salts in the presence of oil and surfactant. *Langmuir*, 6(6), 1132-1135.
- Chen, W.-Y.; Kuo, C.-S. & Liu, D.-Z. (2000). Determination of the second virial coefficient of the interaction between microemulsion droplets by microcalorimetry. *Langmuir*, 16(2), 300-302.
- Chen, Z.; Yan, F.; Qiu, L.; Lu, J.; Zhou, Y.; Chen, J.; Tang, Y. & Texter, J. (2010). Sustainable polymerizations in recoverable microemulsions. *Langmuir* 26(6), 3803-3806.
- Cheng, S.; Fu, X.; Liu, J.; Zhang, J.; Zhang, Z.; Wei, Y. & Han, B. (2007 a). Study of ethylene glycol/TX-100/ionic liquid microemulsions. *Colloids and Surfaces A: Physicochemical and Engineering Aspects*, 302(1-3), 211-215.



- Cheng, S.; Zhang, J.; Zhang, Z. & Han, B. (2007 b). Novel microemulsions: ionic liquid-in-ionic liquid. *Chemical Communications*, (24), 2497-2499.
- Danielsson, I. & Lindman, B. (1981). The definition of microemulsion. *Colloids and Surfaces*, 3(4), 391-392.
- De Gennes, P. G. & Taupin, C. (1982). Microemulsions and the flexibility of oil/water interfaces. *Journal of Physical Chemistry*, 86(13), 2294-304.
- Demchenko, A. P. (1982). On the nanosecond mobility in proteins : edge excitation fluorescence red shift of protein-bound 2-(p-toluidinylnaphthalene)-6-sulfonate. *Biophysical Chemistry*, 15(2), 101-109.
- Earle, M. J. & Seddon, K. R. (2000). Ionic liquids. Green solvents for the future. *Pure and Applied Chemistry*, 72, 1391-1398.
- Eastoe, J.; Gold, S.; Rogers, S. E.; Paul, A.; Welton, T.; Heenan, R. K. & Grillo, I. (2005). Ionic liquid-in-oil microemulsions. *Journal of the American Chemical Society*, 127(20), 7302-7303.
- Evans, D. F.; Yamauchi, A.; Roman, R. & Casassa, E. Z. (1982). Micelle formation in ethylammonium nitrate, a low-melting fused salt. *Journal of Colloid and Interface Science*, 88(1), 89-96.
- Evans, D. F.; Yamauchi, A.; Wei, G. J. & Bloomfield, V. A. (1983 a). Micelle size in ethylammonium nitrate as determined by classical and quasi-elastic light scattering. *Journal of Physical Chemistry*, 87(18), 3537-41.
- Evans, D. F.; Kaler, E. W. & Benton, W. J. (1983 b). Liquid crystals in a fused salt: beta ,gamma -distearoylphosphatidylcholine in N-ethylammonium nitrate. *Journal of Physical Chemistry*, 87(4), 533-5.
- Evans, D. F. & Wennerström, H. (1998). *The colloidal domain: where physics, chemistry, biology, and technology meet*, 2<sup>nd</sup> edition, Wiley-VCH, pp. 37-42.
- Friberg, E. & Podzimek, M. (1984). A non-aqueous microemulsion. *Colloid and Polymer Science*, 262(3), 252-253.
- Friberg, S. E. & Liang, Y.-C. (1987). Phase equilibria in the glycerol-aerosol OT system with decanol or hydrocarbon. *Surfactant Science Series*, 24(Microemulsion Systems), 103-113.
- Fu, C.; Zhou, H.; Wu, H.; Chen, J. & Kuang, Y. (2008). Research on electrochemical properties of nonaqueous ionic liquid microemulsions. *Colloid & Polymer Science*, 286(13), 1499-1504.
- Fukaya, Y.; Iizuka, Y.; Sekikawa, K. & Ohno, H. (2007). Bio ionic liquids: room temperature ionic liquids composed wholly of biomaterials. *Green Chemistry*, 9(11), 1155-1157.
- Gao, H.; Li, J.; Han, B.; Chen, W.; Zhang, J.; Zhang, R. & Yan, D. (2004). Microemulsions with ionic liquid polar domains. *Physical Chemistry Chemical Physics*, 6(11), 2914-2916.
- Gao, Y.; Wang, S.; Zheng, L.; Han, S.; Zhang, X.; Lu, D.; Yu, L.; Ji, Y. & Zhang, G. (2006 a). Microregion detection of ionic liquid microemulsions. *Journal of Colloid and Interface Science*, 301(2), 612-616.
- Gao, Y.; Zhang, J.; Xu, H.; Zhao, X.; Zheng, L.; Li, X. & Yu, L. (2006 b). Structural studies of 1-butyl-3-methylimidazolium tetrafluoroborate/TX-100/p-xylene ionic liquid microemulsions. *ChemPhysChem*, 7(7), 1554-1561.
- Gao, Y.; Li, N.; Zheng, L.; Bai, X.; Yu, L.; Zhao, X.; Zhang, J.; Zhao, M. & Li, Z. (2007 a). Role of solubilized water in the reverse ionic liquid microemulsion of 1-butyl-3-

- methyylimidazolium tetrafluoroborate/TX-100/benzene. *Journal of Physical Chemistry B*, 111(10), 2506-2513.
- Gao, Y.; Li, N.; Zheng, L.; Zhao, X.; Zhang, J.; Cao, Q.; Zhao, M.; Li, Z. & Zhang, G. (2007 b). The effect of water on the microstructure of 1-butyl-3-methyylimidazolium tetrafluoroborate/TX-100/benzene ionic liquid microemulsions. *Chemistry - A European Journal* 13(9), 2661-2670.
- Gao, Y.; Hilfert, L.; Voigt, A. & Sundmacher, K. (2008). Decrease of droplet size of the reverse microemulsion 1-butyl-3-methyylimidazolium tetrafluoroborate/triton X-100/cyclohexane by addition of water. *Journal of Physical Chemistry B*, 112(12), 3711-3719.
- Gao, Y.; Li, N.; Hilfert, L.; Zhang, S.; Zheng, L. & Yu, L. (2009 a). Temperature-induced microstructural changes in ionic liquid-based microemulsions. *Langmuir*, 25(3), 1360-1365.
- Gao, Y.; Li, N.; Zhang, S.; Zheng, L.; Li, X.; Dong, B. & Yu, L. (2009 b). Organic solvents induce the formation of oil-in-ionic liquid microemulsion aggregations. *Journal of Physical Chemistry B*, 113(5), 1389-1395.
- Gayet, F.; El Kalamouni, C.; Lavedan, P.; Marty, J.-D.; Brûlet, A. & Lauth-de Viguier, N. (2009). Ionic liquid/oil microemulsions as chemical nanoreactors. *Langmuir*, 25(17), 9741-9750.
- Greaves, T. L. & Drummond, C. J. (2007). Protic ionic liquids: properties and applications. *Chemical Reviews*, 108(1), 206-237.
- Greaves, T. L.; Weerawardena, A.; Fong, C. & Drummond, C. J. (2007). Many protic ionic liquids mediate hydrocarbon-solvent interactions and promote amphiphile self-assembly. *Langmuir*, 23(2), 402-404.
- Greaves, T. L. & Drummond, C. J. (2008 a). Ionic liquids as amphiphile self-assembly media. *Chemical Society Reviews*, 37(8), 1709-1726.
- Greaves, T. L.; Weerawardena, A.; Krodkiewska, I. & Drummond, C. J. (2008 b). Protic ionic liquids: physicochemical properties and behavior as amphiphile self-assembly solvents. *Journal of Physical Chemistry B*, 112(3), 896-905.
- Hao, J.; Song, A.; Wang, J.; Chen, X.; Zhuang, W.; Shi, F.; Zhou, F. & Liu, W. (2005). Self-assembled structure in room-temperature ionic liquids. *Chemistry - A European Journal*, 11(13), 3936-3940.
- Hao, J. & Zemb, T. (2007). Self-assembled structures and chemical reactions in room-temperature ionic liquids. *Current Opinion in Colloid & Interface Science*, 12(3), 129-137.
- Hapiot, P. & Lagrost, C. (2008). Electrochemical reactivity in room-temperature ionic liquids. *Chemical Reviews*, 108(7), 2238-2264.
- Haumann, M. & Riisager, A. (2008). hydroformylation in room temperature ionic liquids (RTILs): catalyst and process developments. *Chemical Reviews*, 108(4), 1474-1497.
- Hoar, T. P. & Schulman, J. H. (1943). Transparent water-in-oil dispersions: the oleopathic hydro-micelle. *Nature* 152, 102-103.
- Kahlweit, M.; Strey, R.; Firman, P. & Haase, D. (1985). Phase behavior of ternary systems: water-oil-nonionic surfactant as a near-tricritical phenomenon. *Langmuir*, 1(3), 281-8.
- Kahlweit, M.; Strey, R. & Firman, P. (1986). Search for tricritical points in ternary systems: water-oil-nonionic amphiphile. *Journal of Physical Chemistry*, 90(4), 671-7.

- Kahlweit, M.; Strey, R.; Haase, D. & Firman, P. (1988). Properties of the three-phase bodies in water-oil-nonionic amphiphile mixtures. *Langmuir* 4(4), 785-90.
- Kahlweit, M.; Strey, R.; Schomaecker, R. & Haase, D. (1989). General patterns of the phase behavior of mixtures of water, nonpolar solvents, amphiphiles, and electrolytes. 2. *Langmuir* 5(2), 305-15.
- Kahlweit, M.; Strey, R. & Busse, G. (1993). Weakly to strongly structured mixtures. *Physical Review E*, 47(6), 4197-209.
- Krossing, I.; Slattery, J. M.; Daguene, C.; Dyson, P. J.; Oleinikova, A. & Weingaertner, H. (2006). Why are ionic liquids liquid? A simple explanation based on lattice and solvation energies. *Journal of the American Chemical Society*, 128(41), 13427-13434.
- Lattes, A. & Rico, I. (1989). Aggregation in formamide solution: reactivity and structure of non-aqueous microemulsions. *Colloids and Surfaces*, 35(2-4), 221-35.
- Li, J.; Zhang, J.; Gao, H.; Han, B. & Gao, L. (2005). Nonaqueous microemulsion-containing ionic liquid [bmim][PF<sub>6</sub>] as polar microenvironment. *Colloid & Polymer Science*, 283(12), 1371-1375.
- Li, N.; Gao, Y. a.; Zheng, L.; Zhang, J.; Yu, L. & Li, X. (2007). Studies on the micropolarities of bmimBF<sub>4</sub>/TX-100/toluene ionic liquid microemulsions and their behaviors characterized by UV visible spectroscopy. *Langmuir*, 23(3), 1091-1097.
- Li, N.; Zhang, S.; Zheng, L.; Gao, Y. a. & Yu, L. (2008). Second virial coefficient of bmimBF<sub>4</sub>/Triton X-100/ cyclohexane ionic liquid microemulsion as investigated by microcalorimetry. *Langmuir*, 24(7), 2973-2976.
- Maroncelli, M. & Fleming, G. R. (1987). Picosecond solvation dynamics of coumarin 153: the importance of molecular aspects of solvation. *Journal of Chemical Physics* 86(11), 6221-39.
- Martins, M. A. P.; Frizzo, C. P.; Moreira, D. N.; Zanatta, N. & Bonacorso, H. G. (2008). Ionic liquids in heterocyclic synthesis. *Chemical Reviews*, 108(6), 2015-2050.
- Mojumdar, S. S.; Mondal, T.; Kumar Das, A.; Dey, S. & Bhattacharyya, K. (2010). Ultrafast and ultraslow proton transfer of pyranine in an ionic liquid microemulsion. *Journal of Chemical Physics*, 132(19), 194505-8.
- Moniruzzaman, M.; Tahara, Y.; Tamura, M.; Kamiya, N. & Goto, M. (2010). Ionic liquid-assisted transdermal delivery of sparingly soluble drugs. *Chemical Communications*, 46(9), 1452-1454.
- Mukherjee, S. & Chattopadhyay, A. (2005). Influence of ester and ether linkage in phospholipids on the environment and dynamics of the membrane interface: a wavelength-selective fluorescence approach. *Langmuir*, 21(1), 287-293.
- Părvulescu, V. I. & Hardacre, C. (2007). catalysis in ionic liquids. *Chemical Reviews*, 107(6), 2615-2665.
- Patrascu, C.; Gauffre, F.; Nallet, F.; Bordes, R.; Oberdisse, J.; de Lauth-Viguerie, N. & Mingotaud, C. (2006). Micelles in ionic liquids: aggregation behavior of alkyl poly(ethyleneglycol)-ethers in 1-butyl-3-methyl-imidazolium type ionic liquids. *ChemPhysChem*, 7(1), 99-101.
- Pernak, J.; Syguda, A.; Mirska, I.; Pernak, A.; Nawrot, J.; Pradzynska, A.; Griffin, S. T. & Rogers, R. D. (2007). Choline derivative-based ionic liquids. *Chemistry - A European Journal*, 13(24), 6817-6827.

- Provencher, S. W. (1982 a). A constrained regularization method for inverting data represented by linear algebraic or integral equations. *Computer Physics Communications*, 27(3), 213-227.
- Provencher, S. W. (1982 b). CONTIN: A general purpose constrained regularization program for inverting noisy linear algebraic and integral equations. *Computer Physics Communications*, 27(3), 229-242.
- Qiu, Z. & Texter, J. (2008). Ionic liquids in microemulsions. *Current Opinion in Colloid & Interface Science*, 13(4), 252-262.
- Rabe, C. & Koetz, J. (2010). CTAB-based microemulsions with ionic liquids. *Colloids and Surfaces A: Physicochemical and Engineering Aspects*, 354(1-3), 261-267.
- Rakshit, A. K. & Moulik, S. P. (2009). Physicochemistry of W/O microemulsions. Formation, stability, and droplet clustering. *Surfactant Science Series*, 144(Microemulsions), 17-57.
- Ray, S. & Moulik, S. P. (1994). Dynamics and thermodynamics of Aerosol OT-aided nonaqueous microemulsions. *Langmuir*, 10(8), 2511-2515.
- Rico, I. & Lattes, A. (1984). Waterless microemulsions. *Nouveau Journal de Chimie*, 8(7), 429-431.
- Rico, I. & Lattes, A. (1987). Formamide as a water substitute. IX. Waterless microemulsions. 6. A new type of water-insoluble surfactants and nonaqueous microemulsions. *Surfactant Science Series*, 24(Microemulsion Systems), 357-375.
- Riter, R. E.; Undiks, E. P. & Levinger, N. E. (1998). Impact of counterion on water motion in Aerosol OT reverse micelles. *Journal of the American Chemical Society*, 120(24), 6062-6067.
- Saidi, Z.; Mathew, C.; Peyrelasse, J. & Boned, C. (1990). Percolation and critical exponents for the viscosity of microemulsions. *Physical Review A*, 42(2), 872-876.
- Salager, J.-L. & Antón, R. E. (1999). Ionic microemulsions. *Handbook of Microemulsions Science and Technology*. Kumar, P. and Mittal, K. L. New York, Dekker. chap. 8, 247-280.
- Sarkar, N.; Das, K.; Datta, A.; Das, S. & Bhattacharyya, K. (1996). Solvation dynamics of coumarin 480 in reverse micelles. Slow relaxation of water molecules. *Journal of Physical Chemistry*, 100(25), 10523-10527.
- Schubert, K. V.; Busse, G.; Strey, R. & Kahlweit, M. (1993). Microemulsions with formamide as polar solvent. *Journal of Physical Chemistry*, 97(1), 248-54.
- Schulman, J. H.; Stoeckenius, W. & Price, L. M. (1959). Mechanism of formation and structure of micro emulsions by electron microscopy. *Journal of Physical Chemistry*, 63, 1677-1680.
- Tao, G.-h.; He, L.; Liu, W.-s.; Xu, L.; Xiong, W.; Wang, T. & Kou, Y. (2006). Preparation, characterization and application of amino acid-based green ionic liquids. *Green Chemistry*, 8(7), 639-646.
- Teubner, M. & Strey, R. (1987). Origin of the scattering peak in microemulsions. *Journal of Chemical Physics*, 87(5), 3195-200.
- van Rantwijk, F. & Sheldon, R. A. (2007). Biocatalysis in ionic liquids. *Chemical Reviews*, 107(6), 2757-2785.
- Walden, P. (1914). Molecular weights and electrical conductivity of several fused salts. *Bulletin de l'Academie Imperiale des Sciences de St.-Petersbourg*, 8, 405-422.
- Wasserscheid, P. & Keim, W. (2000). Ionic liquids - new "solutions" for transition metal catalysis. *Angewandte Chemie, International Edition*, 39(21), 3772-3789.

- Welton, T. (1999). Room-temperature ionic liquids. Solvents for synthesis and catalysis. *Chemical Reviews*, 99(8), 2071-2084.
- Weyerich, B.; Brunner-Popela, J. & Glatter, O. (1999). Small-angle scattering of interacting particles. II. Generalized indirect Fourier transformation under consideration of the effective structure factor for polydisperse systems. *Journal of Applied Crystallography*, 32(2), 197-209.
- Winsor, P. A. (1948). Hydrotrophy, solubilization, and related emulsification processes. I. *Transactions of the Faraday Society*, 44, 376-382.
- Winsor, P. A. (1954). *Solvent properties of amphiphilic compounds*. London, Butterworth.
- Wormuth, K.; Lade, O.; Lade, M. & Schomacker, R. (2002). Microemulsions. *Handbook of Applied Surface and Colloid Chemistry* 2, 55-77.
- Xue, H.; Verma, R. & Shreeve, J. n. M. (2006). Review of ionic liquids with fluorine-containing anions. *Journal of Fluorine Chemistry*, 127(2), 159-176.
- Yan, F.; Yu, S.; Zhang, X.; Qiu, L.; Chu, F.; You, J. & Lu, J. (2009). Enhanced proton conduction in polymer electrolyte membranes as synthesized by polymerization of protic ionic liquid-based microemulsions. *Chemistry of Materials*, 21(8), 1480-1484.
- Zech, O.; Kellermeier, M.; Thomaier, S.; Maurer, E.; Klein, R.; Schreiner, C. & Kunz, W. (2009 a). Alkali metal oligoether carboxylates - a new class of ionic liquids. *Chemistry - A European Journal*, 15(6), 1341-1345.
- Zech, O.; Thomaier, S.; Bauduin, P.; Rück, T.; Touraud, D. & Kunz, W. (2009 b). Microemulsions with an ionic liquid surfactant and room temperature ionic liquids as polar pseudo-phase. *Journal of Physical Chemistry B*, 113(2), 465-473.
- Zech, O. (2010). Ionic liquids in microemulsions - a concept to extend the conventional thermal stability range of microemulsions. *Dissertation, Regensburg*.
- Zech, O.; Thomaier, S.; Kolodziejski, A.; Touraud, D.; Grillo, I. & Kunz, W. (2010 a). Ionic liquids in microemulsions-a concept to extend the conventional thermal stability range of microemulsions. *Chemistry - A European Journal* 16(3), 783-786.
- Zech, O.; Thomaier, S.; Kolodziejski, A.; Touraud, D.; Grillo, I. & Kunz, W. (2010 b). Ethylammonium nitrate in high temperature stable microemulsions. *Journal of Colloid and Interface Science* 347(2), 227-232.
- Zech, O.; Bauduin, P.; Palatzky, P.; Touraud, D. & Kunz, W. (2010 c). Biodiesel, a sustainable oil, in high temperature stable microemulsions containing a room temperature ionic liquid as polar phase. *Energy & Environmental Science*, 3(6), 846-851.
- Zemb, T. N.; Barnes, I. S.; Derian, P. J. & Ninham, B. W. (1990). Scattering as a critical test of microemulsion structural models. *Progress in Colloid & Polymer Science*, 81(Trends Colloid Interface Sci. 4), 20-9.
- Zemb, T. N. (1997). The DOC model of microemulsions: microstructure, scattering, conductivity and phase limits imposed by sterical constraints. *Colloids and Surfaces, A: Physicochemical and Engineering Aspects*, 129,130, 435-454.
- Zemb, T. N. (2009). Flexibility, persistence length and bicontinuous microstructures in microemulsions. *Comptes Rendus Chimie*, 12(1-2), 218-224.
- Zhao, M.; Zheng, L.; Bai, X.; Li, N. & Yu, L. (2009). Fabrication of silica nanoparticles and hollow spheres using ionic liquid microemulsion droplets as templates. *Colloids and Surfaces A: Physicochemical and Engineering Aspects* 346(1-3), 229-236.

- Zheng, Y. & Eli, W. (2009). Study on the polarity of bmimPF<sub>6</sub>/Tween80/toluene microemulsion characterized by UV-visible spectroscopy. *Journal of Dispersion Science and Technology* 30(5), 698-703.
- Zheng, Y.; Eli, W. & Li, G. (2009). FTIR study of Tween80/1-butyl-3-methylimidazolium hexafluorophosphate/toluene microemulsions. *Colloid & Polymer Science*, 287(7), 871-876.
- Zhu, D. M.; Wu, X. & Schelly, Z. A. (1992). Reverse micelles and water in oil microemulsions of Triton X 100 in mixed solvents of benzene and n-hexane. Dynamic light scattering and turbidity studies. *Langmuir*, 8(6), 1538-40.

# H/D Effects of Water in Room Temperature Ionic Liquids

Hiroshi Abe<sup>1</sup> and Yukihiro Yoshimura<sup>2</sup>

<sup>1</sup>*Department of Materials Science and Engineering,  
National Defense Academy, Yokosuka 239-8686,*

<sup>2</sup>*Department of Applied Chemistry, National Defense Academy, Yokosuka 239-8686,  
Japan*

## 1. Introduction

In life science, the 3D structure, sequence and hyperstructure of biomolecules are summarized from the viewpoint of hydrogen bonding (Marechal, 2007). The bonding nature gives rise to network-forming, flexible, mobile and adjustable properties. As dynamic properties, 'function and structure' are affected directly or indirectly by hydrogen bonding. At different times and in different places, hydrogen bonding is variant, fluctuating and cooperative. In particular, a simulation study suggested that, in an inhomogeneous local circumstance, the dynamics of biomolecules are influenced by the hydration water (Kumar et al., 2006).

As we know, a variety of crystal structures of pure water can be induced by changing the bonding angle and the distance between water molecules under high pressure (Salzmann et al., 2009). The complicated phase diagram of water contains metastable phases. The simple molecular structure but complicated nature of water leads us to a significant finding: there exist at least two glassy states in water, the low-density amorphous ice (LDA) and the high-density amorphous ice (HDA), called polyamorphisms (Mishima & Stanley, 1998). This behavior is one of the entirely 'mysterious' properties of water. Moreover, the possibility of a liquid-liquid phase transition is noted, with hypothesized 'second' critical points. This phase transition may occur, for example, from a low-density liquid (LDL) phase at low pressure to a high-density liquid (HDL) at high pressure, and vice versa.

In this study, we focus on the 'hidden' behavior of water in room temperature ionic liquids (RTILs). RTILs consist only of a cation and an anion. Near-zero vapor pressure and nano-heterogeneity are representative features of RTILs. Both in previous experiments (Triolo et al., 2007) and molecular dynamics (MD) simulations (Jiang et al., 2007), the nano-heterogeneity was well explained by introducing polar and non-polar regions. In RTIL-H<sub>2</sub>O systems, it was found experimentally that density fluctuations decrease with increasing H<sub>2</sub>O concentration (Aono et al., 2011). In MD simulations of RTIL-H<sub>2</sub>O mixtures (Jiang et al., 2007), as the water network develops with increasing H<sub>2</sub>O concentration, the interrupted process of nano-heterogeneity is visualized in the simulation box. RTILs provide an appropriate electrostatic field such as the protein-water system in cells or membranes. In simple RTIL-water systems, ambiguous factors in the complicated protein-water system are

substantially decreased. Therefore, we can discover the role of water from the water-assisted functions in simple RTIL-water systems.

A the non-imidazolium RTIL, *N, N*-diethyl-*N*-methyl-*N*-(2-methoxyethyl) ammonium tetrafluoroborate, [DEME][BF<sub>4</sub>], was selected for this study. In [DEME][BF<sub>4</sub>]-water systems, an unusual geometrical effect is seen both in the liquid and solid states. In the liquid state, a 'hierarchy structure' (Aono et al., 2011) is formed at a specific water concentration. In the solid state, two kinds of superstructures, an anomalous domain structure and volume contraction, are observed only in 1 mol% H<sub>2</sub>O mixtures. This anomaly is weakened by substitution of heavy water (D<sub>2</sub>O) at the fixed 1 mol% concentration of water. Moreover, three different kinds of glassy states are obtained by slow cooling and rapid quenching. 'Nearly-free hydrogen bonded' (NFHB) water in the liquid state still exists in the rapidly quenched glassy state.

## 2. Hydrogen bonding: geometrical effects and proton dynamics

Generally, the hyperstructures of biomolecules are derived from multifunctional hydrogen bonding, which is mainly induced by water molecules. In such biomolecule-water systems, the bonding nature depends on the competition between geometrical effects and proton dynamics. In some circumstances, the competition between molecules is enhanced by the local charge balance, since charge imbalance is compensated for by geometrical effect or proton dynamics. Not only the local balance but also the stabilization of the system is realized by hydrogen bonding. The bonding network is optimized energetically through hydrogen bonding. Analogous with networks in synapses, the water-assisted system inherently possesses (i) information, (ii) information transfer (including feedback mechanisms), (iii) information selectivity (or switching mechanisms) and (iv) information memory.

Many studies associated with proton dynamics have been carried out in the crystal state, since degrees of freedom are reduced in crystal systems. For instance, the 'bonding structure' of carboxylic acid-based crystals is summarized in a previous study (Foces-Foces et al., 2001). The bonding length of hydrogen bonding is responsible for degenerate double proton transfers between O-H...N and O...H-N. In addition, a proton order-disorder transition is observed directly by NMR measurements. Generally, the hydrogen bonding network consists of dimers, trimers, tetramers and higher molecular sequences. An amorphous solid is formed by curved or *zigzag* molecular sequences as a disordered state, while a linear molecular sequence contributes to the crystal structure. Consequently, a scenario describing the formation of crystals or amorphous solids is provided by the 'hierarchy structure' (Fig. 1): (i) on the atomic scale, proton dynamics are derived from the local environment, (ii) on the mesoscopic scale, a variety of molecular sequences are induced by hydrogen bonding. Here, we have a big question: why can proton dynamics govern the molecular network to determine whether the crystal or amorphous solid is stabilized? To answer this question, the hydrogen/deuteron (H/D) effect was investigated as another approach. For instance, proton dynamics are drastically changed by deuteron replacement. It should be noted that the H/D effect is not simply a mass effect. In solid state NMR methods, intermolecular multiple proton-transfer processes were explained by H/D isotope effects (Klein et al., 2004). The kinetic behaviors of the double proton and deuteron transfer in the solid state are well described by the Bell-Limbach tunneling model.



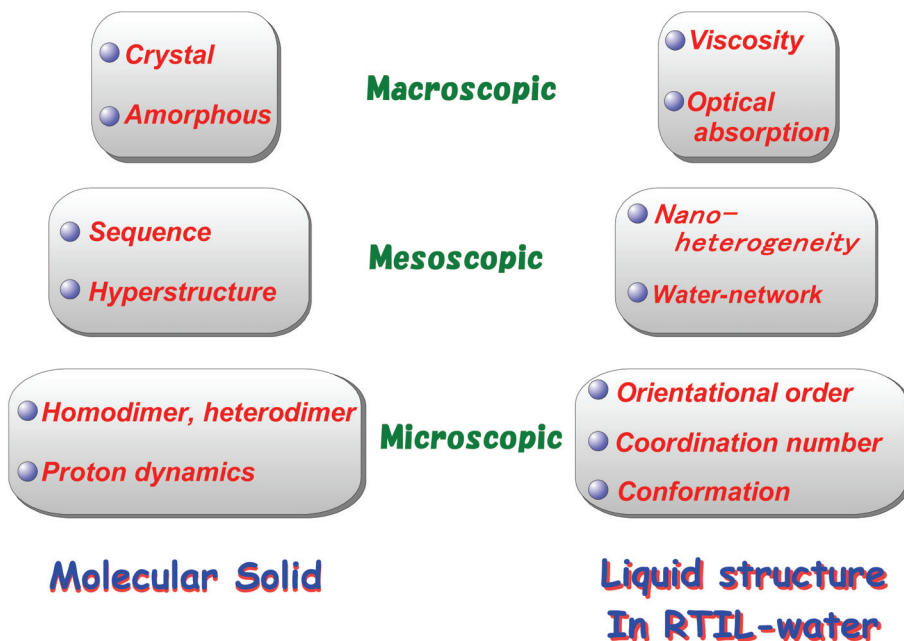


Fig. 1. Hierarchy structure in a molecular solid and RTIL-water system in the liquid state.

A part of the universal aspect of biochemistry is also seen in ferroelectric materials. Well-ordered molecular ferroelectric materials, whose charge is highly balanced in the lattice, can minimize their positional, orientational and conformational ambiguity, apart from protons. Therefore, proton dynamics are enhanced in the 3D network. The 'giant isotope effect' on hydrogen bonds is one example describing spatially restricted protons or deuterons. For instance, potassium dihydrogen phosphate ( $\text{KH}_2\text{PO}_4$ ) and its deuterated compound ( $\text{KD}_2\text{PO}_4$ ) have quite different phase transition temperatures,  $T_c$ . The  $T_c$  of  $\text{KH}_2\text{PO}_4$  is around 122 K, while that of  $\text{KD}_2\text{PO}_4$  is 229 K. DFT (density functional theory) calculations indicate the atomic positions of hydrogen: the on-centering of H (O-H-O) and the off-centering of D ( $\text{O} \cdots \text{D} - \text{O}$ ) (Koval et al., 2002). This centering can determine the bonding length, which is regarded as a 'geometrical effect'. The distances between oxygens,  $d_{\text{OO}}$ , are estimated to be 0.242 nm (H) and 0.251 nm (D), respectively. The quantum delocalization of the proton contributes to the attractive interaction, that is, the 'proton-mediated covalent bonding' (PMCB). As a geometrical effect, below  $T_c$ , the off-centering of proton induces positional shifts of the P and K ions to stabilize the total energy. In further *ab initio* calculations of  $\text{KH}_2\text{PO}_4$  and  $\text{KD}_2\text{PO}_4$  (Koval et al., 2005), it was pointed out that proton motions are strongly correlated with the heavier ions within clusters in addition to the geometrical effect. The feedback effect of the geometrical modifications can explain not only the isotope effect but also the phase transitions under pressure. Further *ab initio* calculations introducing two different kinds of cluster models (Lasave et al., 2005) suggest that rotational defects of  $\text{PO}_4$  cause a lattice contraction in  $\text{KH}_2\text{PO}_4$ . Domain wall motion around the domain freezing temperature,  $T_F$  ( $=T_c-60^\circ\text{C}$ ), is connected with a polarization flip. Both the domain wall and polarization dynamics are controlled extensively by the proton motion.

### 3. Experimental and calculation methodology

#### 3.1 Materials

As the sample RTIL in this study, we used *N,N*-diethyl-*N*-methyl-*N*-(2-methoxyethyl) ammonium tetrafluoroborate, [DEME][BF<sub>4</sub>] (Fig. 2) (Kanto Chemical Co., Tokyo, Japan), which is a hydrophilic RTIL (Sato et al., 2004). The as-received sample contains a small amount of water (126 ppm). Generally, RTILs are easily contaminated by vacuum drying to reduce H<sub>2</sub>O, so we used the sample without further purification. Mixtures were prepared by dissolving RTILs in a dry box, under a flow of He gas to exclude atmospheric H<sub>2</sub>O. The amount of water was estimated on the basis of the Karl-Fischer titration method. Special care was taken not to contaminate chemicals further with atmosphere. For H<sub>2</sub>O mixtures, distilled water (Wako Pure Chemical Co. Japan), was used, while D<sub>2</sub>O (99.9%) (Cambridge Isotope Laboratories, Inc.) was used for D<sub>2</sub>O mixtures. H<sub>2</sub>O concentrations,  $x$ , ranged from 0.0 to 98.5 mol% H<sub>2</sub>O. H<sub>2</sub>O-D<sub>2</sub>O mixtures are represented as (1- $y$ )H<sub>2</sub>O  $y$ D<sub>2</sub>O. Sample solutions were prepared simply by dissolving the required amounts of water in [DEME][BF<sub>4</sub>] in the dry box filled with He gas.

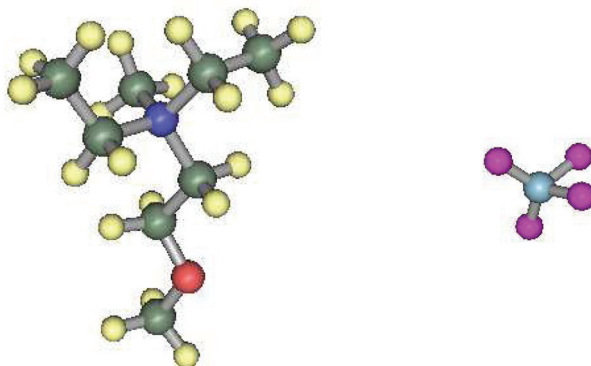


Fig. 2. Molecular structures of the cation [DEME] and the anion [BF<sub>4</sub>].

#### 3.2 Simultaneous wide angle X-ray scattering and differential scanning calorimetry measurements

In-situ observations were performed using a simultaneous wide angle X-ray scattering (WAXS) and differential scanning calorimetry (DSC) (RINT-Ultima III; Rigaku Co., Tokyo, Japan), where the DSC is attached on a vertical goniometer. For in-situ observations of the liquids, the sample stage is fixed horizontally. The sample is put on an Al sample holder inside the DSC. A sealed X-ray tube (2 kW) and a scintillation counter move simultaneously. A parallel beam is obtained by a parabolic multilayer mirror. A long Soller slit is placed in front of the scintillation counter. Cu K $\alpha$  radiation ( $\lambda=0.1542$  nm) was selected for the simultaneous measurements. Beam divergence with the beam optics is estimated to be  $0.1^\circ$  by measuring a standard Si polycrystal. DSC windows for X-ray are metal coated Mylar films. During the simultaneous measurements, dry N<sub>2</sub> gas was flowing at 20 cc/min in order to reduce moisture.

In this study, two kinds of scan modes,  $\theta$ - $2\theta$  and  $\theta$  scans, were carried out. For conventional WAXS, a  $\theta$ - $2\theta$  scan was used. The  $\theta$ - $2\theta$  scan mode is the radial scan in reciprocal space. Peak

shifts and widths along the radial scan contain information of lattice distortions. The direction of the  $\theta$  scan (rocking curve) is transverse to the radial direction in reciprocal space. The  $\theta$  scan can detect the preferred orientation on the Debye ring of polycrystalline structures and mosaicity of a single crystal. Peak widths along the transverse direction contain information of crystal domain formation. The  $\theta$  scans are performed by asymmetric movement of the X-ray tube and counter, while the sample stage is held horizontal. Crystal structures and precise lattice constants are determined by JADE application software (Rigaku Co.).

### 3.3 Conventional WAXS and small angle X-ray scattering

At room temperature, WAXS and small angle X-ray scattering (SAXS) of the liquid state were measured using an 18 kW X-ray generator (RINT2500; Rigaku Co., Tokyo, Japan). Cu K $\alpha$  radiation was selected for both WAXS and SAXS. Scattered intensity was monochromated for WAXS by curved highly oriented pyrolytic graphite (002). Transmission geometry of the sample was set for both measurements. Windows for the sample holder were made of 7.5  $\mu\text{m}$  thick polyimide thin films (Kapton; Nilaco Co., Tokyo, Japan). Using step scan mode at a fixed intervals, a few thousand counts were collected even at high scattering angles for both the sample and the background. Instead of the monochromator, Ni filter was set to decrease K $\beta$  in the SAXS. The beam divergence in SAXS was 0.052°. DATA were collected above 0.2° in 2 $\theta$ . A vacuum path was placed between the sample and the scintillation counter in order to reduce air scattering.

To analyze the WAXS patterns quantitatively (electron units per molecule), we measured several integrated intensities of a standard powdered sample of Ni (Abe et al., 2007a). The calculated Compton scattering was subtracted from the corrected WAXS patterns. Here, the scattering vector,  $Q$ , is defined to be  $4\pi(\sin\theta)/\lambda$  (nm<sup>-1</sup>). The radial distribution function (RDF) is given by (Nishikawa & Iijima, 1984; Katayanagi et al., 2004),

$$4\pi r^2(\rho - \rho_0) = \frac{2r}{\pi z^2} \int_0^\infty Qi(Q)\sin(Qr)dQ. \quad (1)$$

$z^2$  is provided by  $z^2 = \sum_n z_n^2$ , where  $z_n$  is the atomic number of the  $n$ th component atom.

In SAXS analysis, the Ornstein-Zernicke (OZ) correlation function (Stanley, 1971),  $\chi(r)$  is introduced by analyzing critical scattering. The correlation function is given by,

$$\chi(r) = \frac{1}{r} e^{-r/\xi}, \quad (2)$$

where  $\xi$  is the correlation length. By Fourier transform of Eq. (2), the SAXS intensity using the OZ correlation function is obtained as  $I_0/(1+\xi^2 Q^2)$ . By modifying the equation,  $\xi$  is calculated from a plot of  $Q^2$  vs.  $1/I(Q)$ .

### 3.4 Conventional DSC and differential thermal analysis measurements

Conventional DSC experiments were also carried out using DSC2910 (TA Instruments Japan Co., Tokyo, Japan) to ensure the complete phase behavior, cooling or heating rate dependence of the phase transitions was examined at 2, 4, 8, 9 and 10 °C/min, respectively. Thermal cycle experiments without replacing the sample were also performed repeatedly from 20 to -150 °C.

A simple differential thermal analysis (DTA) system designed for rapid quenching experiments was employed. As a reference material for the measurements, benzene (Wako Pure Chemical Co., Japan) was used. A sample cell (about 35 mm long and 2 mm i.d. glass tube with one side sealed) was filled with a mixture, and then a thermocouple junction was placed 25–30 mm from the mouth of the sample cell. As a precooling procedure, a vitrification was done by putting the whole sample solution directly into liquid nitrogen (500 °C/min). After removing the sample from the liquid nitrogen, the DTA traces were recorded.

### 3.5 Raman spectroscopy and optical absorption measurements

Raman spectra were measured by a NR-1800 Raman spectrophotometer (JASCO Co., Tokyo, Japan) equipped with a single monochromator and a CCD detector. The 514.5 nm/line from a Lexel Ar<sup>+</sup> ion laser was used as an excitation source with a power of 250 mW. The Raman spectra were measured in the OH-stretching vibrational region for water along with the CH-stretching band of [DEME] cation. Using a THMS-600 (Linkam Co., UK) temperature controller, the sample temperature was controlled between room temperature and -100 °C. Both the cooling and heating rate was 5 °C/min.

The optical absorption spectra were measured using a ultraviolet and visible (UV-vis) spectrometer (V-570; JASCO Co., Tokyo, Japan) with a 1 cm path length quartz cell. All the measurements were performed at room temperature.

### 3.6 DFT calculation

DFT calculations were used as the investigation methodology for the interactions between the RTIL and water molecules (Zhang et al., 2008; Danten et al., 2010). Here, we performed DFT calculations on the optimized arrangement of the BF<sub>4</sub><sup>-</sup>⋯*n*(H<sub>2</sub>O) complexes (*n*=1–4, where *n* is the number of H<sub>2</sub>O) to investigate the interaction between the BF<sub>4</sub><sup>-</sup> anions and water molecules. All DFT calculations were carried out using the Gaussian03 program (Frisch et al., 2003). For calculations on the BF<sub>4</sub><sup>-</sup>⋯*n*(H<sub>2</sub>O) complexes, we used Becke's three-parameter (B3) exchange function (Becke, 1988). The B3 exchange function was combined with the Lee-Yang-Pear correlation function (B3LYP) (Lee, 1988). All calculations by this method were performed using the 6-311++G(d,p) basis set.

## 4. Experimental results and discussion

### 4.1 Phase stability of solid

Examples of simultaneous WAXS-DSC measurements are shown in Figs. 3(a) and 3(b). WAXS on cooling reveal broad diffraction patterns due to the amorphous solid of [DEME][BF<sub>4</sub>] at 60.5 mol% H<sub>2</sub>O (Fig. 3(a)). Crystallization of [DEME][BF<sub>4</sub>] is completely suppressed even upon slow cooling (8 °C/min), although quite weak but sharp Bragg reflections from ice crystals of H<sub>2</sub>O were detected in the broad diffraction pattern. The green triangles in Figs. 3(a) and 3(b) are calculated 2θ values of the ice crystal. The red circle is an ideal peak position of the Bragg reflection, which is identified as an Al sample holder. At the same time, corresponding phase changes at 60.5 mol% H<sub>2</sub>O were obtained from the DSC thermograph as shown in Figs. 3(a) and 3(b). On cooling, small exothermal peaks, which are derived from the ice crystallization temperature (*T*<sub>i</sub>) and glass transition temperature of [DEME][BF<sub>4</sub>] (*T*<sub>g</sub>), were observed. The *T*<sub>i</sub> and *T*<sub>g</sub> lie very close together. By systematic

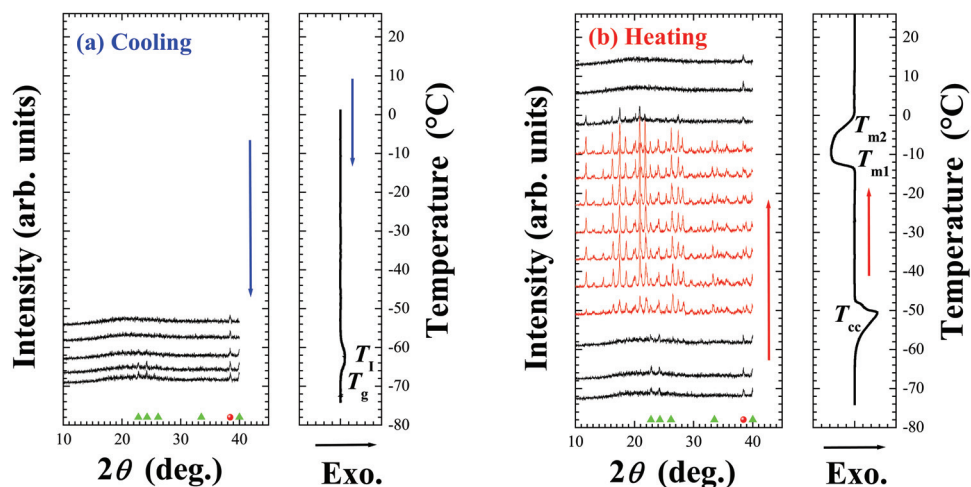


Fig. 3. Wide angle X-ray scattering (WAXS) of [DEME][BF<sub>4</sub>]-H<sub>2</sub>O mixture at 60.5 mol % H<sub>2</sub>O both on (a) cooling and (b) heating. On cooling, an amorphous solid of [DEME][BF<sub>4</sub>] is formed at low temperature and a small amount of H<sub>2</sub>O ice crystals appears below -60 °C. Closed green triangles and red circles indicate the calculated  $2\theta$  values of Bragg reflections of H<sub>2</sub>O ice crystals and the Al sample holder, respectively. DSC thermograms of the [DEME][BF<sub>4</sub>]-H<sub>2</sub>O mixture at 60.5 mol % H<sub>2</sub>O are plotted along with the WAXS. A weak exothermal peak is observed on cooling. The glass transition of [DEME][BF<sub>4</sub>] ( $T_g$ ) and crystallization of a small amount of H<sub>2</sub>O ice crystal ( $T_l$ ) occur simultaneously. On heating, 'cold crystallization' of [DEME][BF<sub>4</sub>] is observed at  $T_{cc}$  accompanying the exotherm. Additionally, two kinds of melting points,  $T_{m1}$  and  $T_{m2}$ , are observed.

measurements, we found that ice crystals of H<sub>2</sub>O (I-phase) exist above 60 mol % ( $x_1$ ). Upon heating, the distinct exothermal peak at -60 °C ( $T_{cc}$ ), which is due to 'cold crystallization', appears on the thermograph. This is in accordance with the appearance of Bragg reflections in WAXS on heating as shown in Fig. 3(b). By further heating, the crystal melts with two endotherms characterized by two stages of melting, at  $T_{m1}$  and  $T_{m2}$ , which are caused by two kinds of crystal structures in the system (Imai et al., 2008a). By simultaneous WAXS-DSC measurements, we can successfully determine the  $T_c$ ,  $T_l$ ,  $T_g$ ,  $T_{cc}$ ,  $T_{m1}$  and  $T_{m2}$  experimentally. Here, we define the normal crystallization temperature of [DEME][BF<sub>4</sub>],  $T_c$ . A variety of phase behaviors both on cooling and heating is shown in Figs. 4(a) and 4(b), respectively (Abe et al., 2009). Since the diagrams obtained in this study may depend on the cooling and heating rates, here we tentatively call these 'kinetic phase diagrams'. Closed circles in the 'kinetic phase diagrams' indicate the phase transitions observed by the simultaneous WAXS-DSC measurements. L indicates the liquid phase. First, we explain the results of the downstroke direction on cooling (Fig. 4(a)). From the experimental facts, we find that the crystal phase of [DEME][BF<sub>4</sub>] (C-phase) exists only for a small range of water content ( $0 < x < 4$  mol %). The crystallization temperature of [DEME][BF<sub>4</sub>],  $T_c$ , decreases with increasing water concentration. At 4-10 mol %, pure amorphous phase (A-phase) appears. The slow-cooled glass is described in detail in the next section. A two-phase coexistence, the (A+C)-phase, is

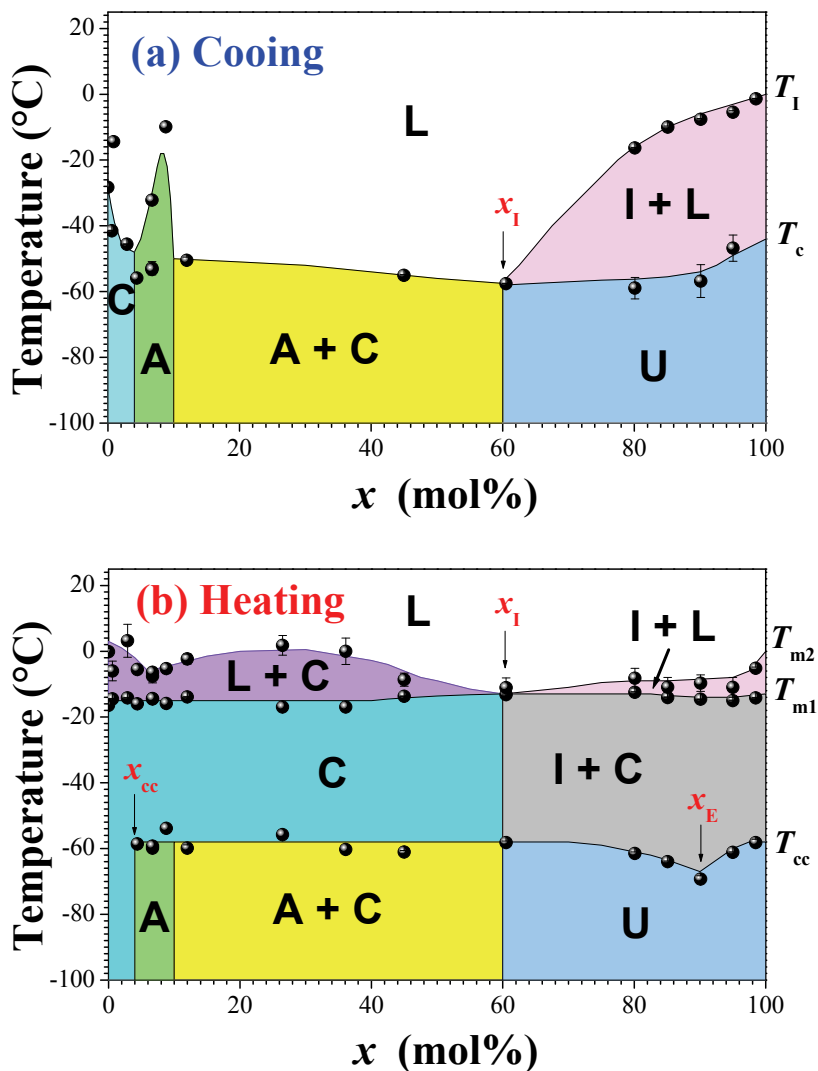


Fig. 4. 'Kinetic phase diagrams' of [DEME][BF<sub>4</sub>]-H<sub>2</sub>O mixtures on (a) cooling and (b) heating. Closed circles represent observed data, which are determined by simultaneous WAXS-DSC measurements.  $x_{cc}$  and  $x_I$  are defined to be a critical concentration of the 'cold crystallization' and the formation of H<sub>2</sub>O ice crystal, respectively.  $T_{cc}$  is the 'cold crystallization' temperature with an exothermal peak on heating.  $T_{m1}$  and  $T_{m2}$  are the melting temperatures, respectively. L, C, A, I and U represent the liquid, [DEME][BF<sub>4</sub>] crystal, amorphous, H<sub>2</sub>O ice and undefined phases. U is classified further into (I+A)-, (I+C)- and (I+A+C)-phases.

realized from 10 to 60 mol%, whereas a coexistence of the A-phase of [DEME][BF<sub>4</sub>] and H<sub>2</sub>O ice crystals (I-phase) is formed at  $x_1$  (=60 mol%). Here, we define the temperature  $T_1$  as the crystallization temperature of H<sub>2</sub>O ice. In contrast to  $T_c$ , the  $T_1$  of the ice increases gradually with increasing water concentration. At  $x > x_1$ , another interesting feature is found. The solid phase of the mixture of [DEME][BF<sub>4</sub>]-H<sub>2</sub>O is hardly uniquely defined in this region. U represents undefined phases. That is, despite using the same sample and cooling rate, the same solid phase did not appear in a reproducible manner. Here, three kinds of phases, classified as (i) (I+A)-, (ii) (I+C)- and (iii) (I+A+C)-phases, appear randomly.

## 4.2 Comparison of the slow-cooled and quenched glasses

Despite a normal cooling rate (1-10 °C/min), A-phases appeared in specific regions ( $4 < x < 10$  mol% and  $x = 60$  mol%) as shown in Fig. 4(a). The  $T_g$  of the A-phase at 6.7 mol% depends on cooling rate systematically, though  $T_c$  of the pure [DEME][BF<sub>4</sub>] is almost constant (Imai et al., 2008a). The slow-cooled glass at 6.7 mol% is characterized by 'two dynamic components' in its Raman spectra. These spectra were measured at -80 °C ( $T < T_c$ ), apart from the spectra of the liquid states at 6.7 and 60.1 mol% H<sub>2</sub>O, which were obtained at 25 °C in order to compare with the Raman spectra in the slow-cooled glasses. The Raman spectra in the region of 2700-3200 cm<sup>-1</sup> (Fig. 5(a)) concern the CH stretching vibrational mode of the cation. The signal at 680 cm<sup>-1</sup> (shown in Fig. 5(b)) is assigned to the C<sub>4</sub>N symmetric modes of the cation (Imai et al., 2008a) and the signal at 740 cm<sup>-1</sup> is in the BF<sub>4</sub> stretching region. The Raman spectrum of the slow-cooled glass ( $x = 6.7$  mol%) is similar to that of the crystal (Fig. 5(b)). In contrast, the Raman spectrum at around 3000 cm<sup>-1</sup> (CH-stretching vibrational region of the cation) is almost the same as that of the liquid phase. The crystal-like and liquid-like spectra are emphasized as 'two dynamic components', although no difference between the liquid and the slow-cooled glass ( $x = 6.7$  mol%) was observed in WAXS.

Apart from the slow cooled glass ( $4 < x < 10$ ), at around 60 mol%, a 'competitive glass' is generated as a crossover point from [DEME][BF<sub>4</sub>]-based to H<sub>2</sub>O-based properties. Basically, the competitive glass is similar to a spin glass, described as a locally frustrated system. In some cases, the frustration is caused by a competition between ferro-like and antiferro-like interactions (Satoh et al., 1978). In fact, crystallization of the mixture is completely suppressed at 60.1 mol%, apart from a small amount of ice crystallization as shown in Fig. 3(a). In the Raman spectra both at low and high bands, the profile of the 60 mol% glass is similar to that of the liquid at 60.1 mol% (Figs. 5(a) and 5(b)).

This implies that the 'two dynamic components' seen in the 6.7 mol% glass were not seen at 60.1 mol%. On the other hand, a similarity between them is that 'nearly-free hydrogen bonded' (NFHB) water disappeared upon solidification in both cases. NFHB water is described in the following section.

Although glassy states are realized even by slow cooling processes, we performed rapid quenching experiments. By DTA measurements,  $T_g$  varied extensively with the water concentration (Fig. 6) (Imai et al., 2010). On heating, pure [DEME][BF<sub>4</sub>] shows a glass transition at -100 °C. Rapid quenching prevents the pure [DEME][BF<sub>4</sub>] from crystallizing below  $T_c$ . Above  $T_g$ , the melted liquid from metastable glass was crystallized by further heating ( $T_{cc} = -74$  °C). Since pure [DEME][BF<sub>4</sub>] has no 'cold crystallization' on slow cooling, the quenched glass of pure [DEME][BF<sub>4</sub>] is regarded as a highly non-equilibrium state. A significant finding in the quenched mixtures is that a double glass transition occurs at  $16 < x < 30$  mol% (Imai et al., 2010). For instance, at  $x = 18.1$  mol%, a first glass transition was

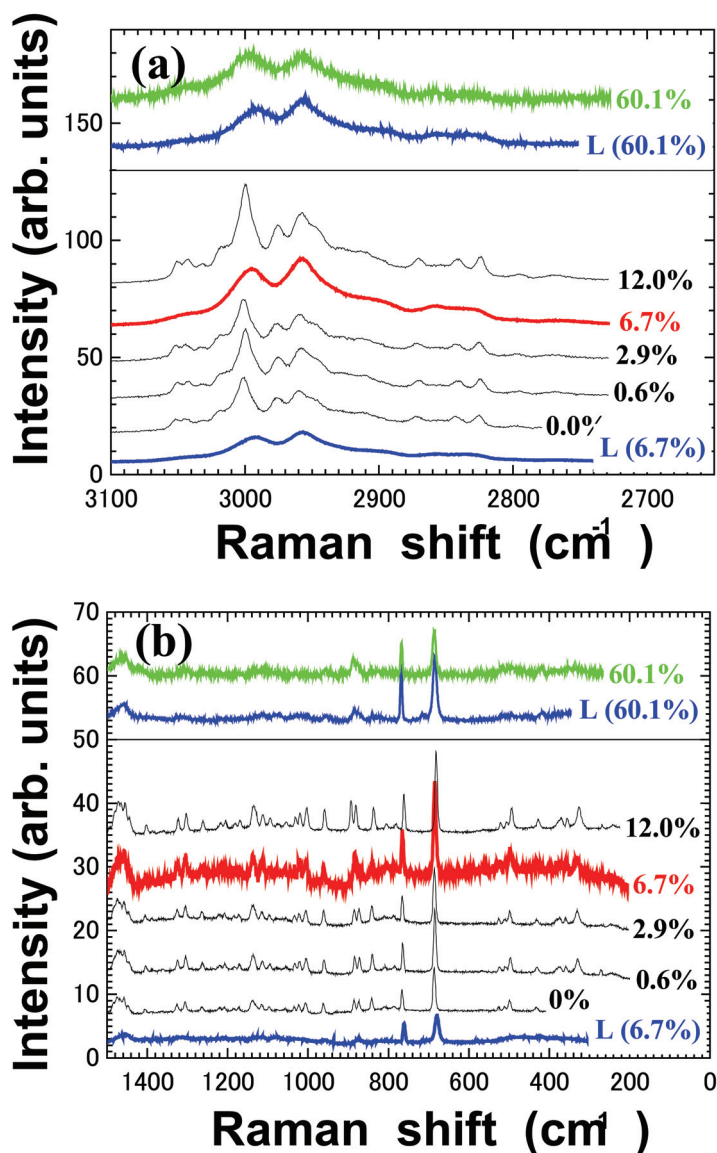


Fig. 5. H<sub>2</sub>O concentration dependence of Raman spectra for [DEME][BF<sub>4</sub>]-H<sub>2</sub>O mixtures in the regions of (a) 2700-3200 cm<sup>-1</sup> and (b) 200-1500 cm<sup>-1</sup>. Raman spectra of the liquid state (6.7 and 60.1 mol%) were measured at 25 °C for a comparison with the slow-cooled glasses. Other Raman spectra were observed at -80 °C. The slow-cooled glass at 6.7 mol% H<sub>2</sub>O provides two kinds of dynamic properties: liquid-like behavior around 3000 cm<sup>-1</sup> and crystal-like behavior around 1000 cm<sup>-1</sup>. In contrast, the other slow-cooled glass at 60.1 mol% has no crystal-like spectrum.



detected at around  $-100\text{ }^{\circ}\text{C}$  ( $=T_{g1}$ ) by an exothermic peak on the DTA trace. A second glass transition was carefully checked by re-quenching the sample (Imai et al., 2010). The second glass transition temperature,  $T_{g2}$ , is found to be around  $-95\text{ }^{\circ}\text{C}$ . Finally, the metastable mixture is stabilized at  $-100\text{ }^{\circ}\text{C}$  by ‘cold crystallization’ in the same manner as other water-rich regions with a single glass transition. Here, we predict that a new heterogeneous region, which is different from polar and non-polar heterogeneity (Triolo et al., 2007; Jiang et al., 2007), is formed by rapid quenching. One reason for this is that, in the liquid state, SAXS intensity in  $[\text{DEME}][\text{BF}_4]\text{-H}_2\text{O}$  decreased at  $16 < x < 30\text{ mol\%}$  (Aono et al., 2011). Simply, we consider that the new heterogeneity is explained by the difference in hardness, since the melting point is roughly proportional to the interaction between molecules. The soft part melts at  $T_{g1}$  and the relatively hard part melts at  $T_{g2}$ . As shown in Fig. 6, the  $T_{g1}$  of  $[\text{DEME}][\text{BF}_4]\text{-H}_2\text{O}$  mixtures look likely to be connected with the  $T_g$  of the water-poor region, while the  $T_{g2}$  curve is linked continuously with the  $T_g$  of the water-rich region. Therefore, in  $[\text{DEME}][\text{BF}_4]\text{-H}_2\text{O}$ , we suppose that the coexisting water-rich and water-poor regions are permitted from  $16 < x < 30\text{ mol\%}$  to change continuously from water-poor to water-rich regions. The water-poor region corresponds to the soft region and the relatively hard region is generated by the water-rich region. Very recently, in other RTILs, we found multiple glass transitions in  $[\text{DEME}][\text{I}]\text{-H}_2\text{O}$  (Imai et al., 2011) and  $[\text{C}_4\text{mim}][\text{BF}_4]\text{-H}_2\text{O}$  (Yoshimura et al., 2011). Here,  $[\text{C}_4\text{mim}][\text{BF}_4]$  is 1-butyl-3-methylimidazolium tetrafluoroborate. Generally, a series of cations such as 1-alkyl-3-methyl imidazolium is expressed by  $[\text{C}_n\text{mim}]$  where  $n$  is the alkyl chain length.

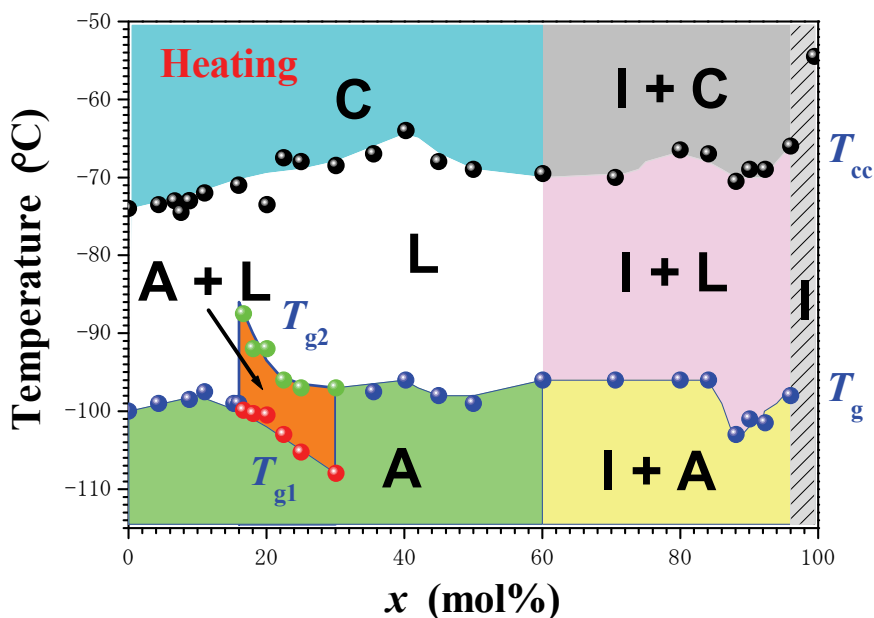


Fig. 6.  $T_g$  variations with  $\text{H}_2\text{O}$  concentration,  $x$ , in a quenched glass on heating.

In other systems, double glass transitions have already been reported. For instance, the double glass transition phenomenon in aqueous tetraalkylammonium halide solutions is

derived from a metastable liquid-liquid immiscibility (Kanno et al., 1983). It is interpreted that the homogeneous solution at room temperature is separated into a water-rich phase and a salt-rich phase by lowering its temperature. In comparison with the previous instances of double glass transitions, the following differences in glass transition behavior appeared in the [DEME][BF<sub>4</sub>]-H<sub>2</sub>O mixed solutions. For one thing, the glass-forming composition region of [DEME][BF<sub>4</sub>]-H<sub>2</sub>O mixtures is much wider than those of aqueous solutions of tetraalkylammonium halides (91-94 mol% H<sub>2</sub>O). Also, the difference between the two glass transitions,  $\Delta T_g (=T_{g2}-T_{g1})$ , is at most 15 °C, and this is much smaller than that of glycerol-H<sub>2</sub>O mixtures ( $\Delta T_g=90$  °C) (Inaba & Andersson, 2007). In general, domain dynamics in multiple phase transitions are described by density and the domain boundary, size and elasticity, which are related to differences of enthalpy and phase transition temperature,  $\Delta T$ . Therefore, we deduce that the small  $\Delta T_g$  in [DEME][BF<sub>4</sub>]-H<sub>2</sub>O reflects the small difference in density (between the water-rich and water-poor regions) and its fluctuation size.

Another significant point in the quenched mixture is that ice crystals were observed in the Raman spectra above 60 mol%, in the region denoted by I in Fig. 6. Figure 7 shows the Raman spectra of the quenched mixtures at -196 °C. The OH stretching mode of the ice crystal is indicated by the arrows in Fig. 7. The appearance of ice in the quenched mixtures coincides with the water concentration in the slow-cooled solid (Fig. 4(b)). This means that excess water molecules tend to form conventional hydrogen bonds as in bulk water above 60 mol% at any cooling rate, though the extent strongly depends on the cooling rate.

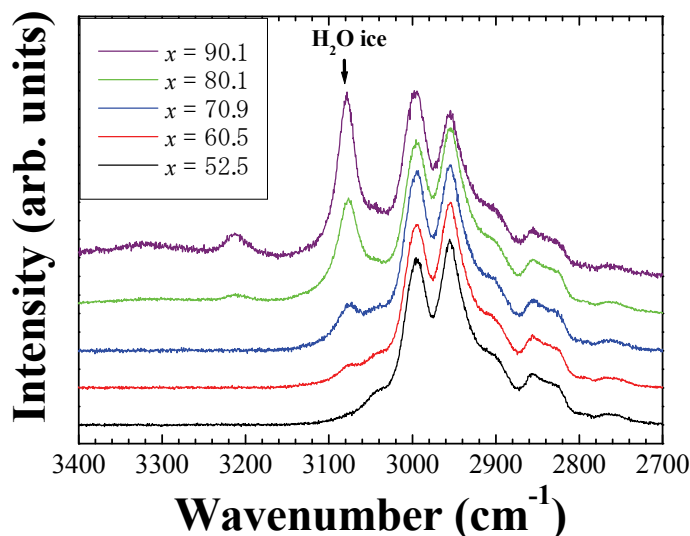


Fig. 7. Raman spectra in a quenched glass. Above 60 mol% H<sub>2</sub>O, ice crystals appeared.

#### 4.3 Nearly-free hydrogen bonding in liquid and quenched glass

Now, we have a big question: excess water molecules with bulk water properties cannot exist below 60 mol% in the solid state. The idea of a confined water molecule may be the key to resolving this problem. It should be noted that the Raman signal at around 3650 cm<sup>-1</sup>,

which is assigned to 'nearly-free hydrogen bonded' (NFHB) water molecules, exists below 80 mol% in the liquid state (Yoshimura et al., 2009). NFHB water means single molecules that do not form a hydrogen bonding network. In the quenched glass, NFHB water was observed at -196 °C in quenched mixtures below 80 mol% (Yoshimura et al., 2009). The entirely opposite tendency is seen in the slow-cooled glasses. Typically, the NFHB bands at 6.7 and 60.1 mol% (A-phase) seem to disappear at around -80 °C on slow cooling, as shown in Figs. 8(a) and 8(b). Theoretically, a picture of NFHB water can be simply visualized by DFT calculations (Abe et al., 2010a). Since  $\text{H} \cdots \text{F}$  bonding between  $\text{BF}_4^-$  and  $\text{H}_2\text{O}$  is relatively strong, a  $\text{BF}_4^- \cdots n(\text{H}_2\text{O})$  ( $n=1-4$ ) cluster is preferred (Figs. 9(a), 9(b), 9(c) and 9(d)). Certainly, Raman bands calculated by DFT are in good agreement with the observed spectra. If we take into account fully connected F ( $\text{BF}_4^-:\text{H}_2\text{O}=1:4$ ), it is natural that bulk water tends not to appear at  $x < 80$  mol %. The picture in the liquid state does not contradict the existence of NFHB water below 80 mol%. However, the population of the NFHB water in 60-80 mol% is estimated to be relatively small in the liquid state (Abe et al., 2009). Thus, on solidification both of slow cooling and rapid quenching processes, quite a small amount of ice crystals appears above 60 mol%.

We summarize three different glassy states as shown in Fig. 10. It is found that the three glasses are formed at specific water concentrations by slow cooling (SC) and rapid quenching (RQ) in the  $[\text{DEME}][\text{BF}_4]-\text{H}_2\text{O}$  system. The three types are classified as (i) 'two dynamic components' (SC), (ii) a crossover from RTIL to water (SC) and (iii) NFHB assisted-glasses (RQ). In the liquid state, nano-heterogeneity, which is separated into polar and non-

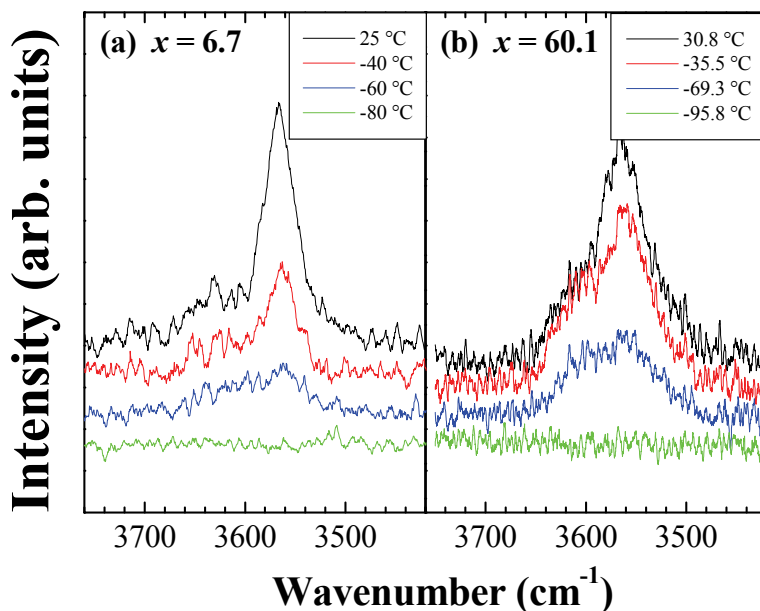


Fig. 8. Spectral changes in the nearly-free hydrogen bonded band of  $[\text{DEME}][\text{BF}_4]-\text{H}_2\text{O}$  at (a)  $x=6.7$  mol% and (b)  $x=60.1$  mol% by slow cooling.

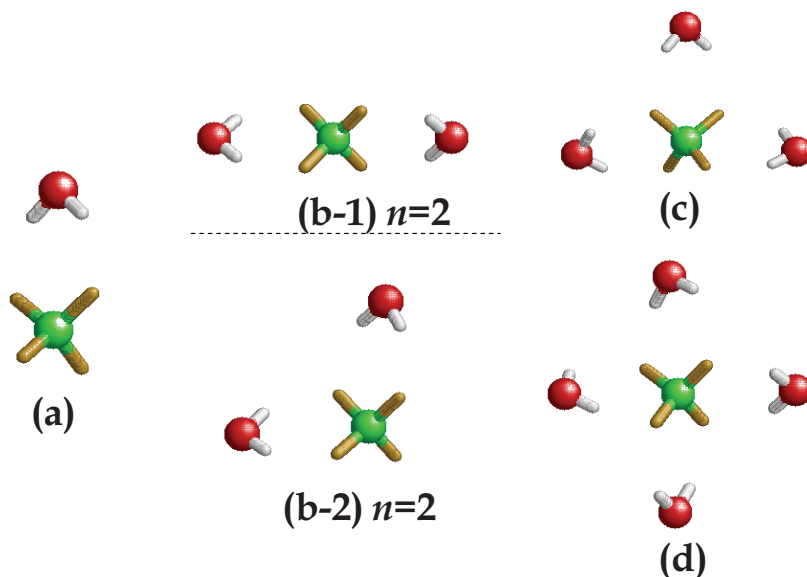


Fig. 9. Optimized structures of the  $\text{BF}_4^- \cdots n(\text{H}_2\text{O})$  ( $n=1-4$ ) complex using the B3LYP/6-311++G(d,p) basis set. In the case of the  $\text{BF}_4^- \cdots 2(\text{H}_2\text{O})$  complex, the  $\text{BF}_4^-$  anion takes two arrangement patterns with two water molecules: one is a linear arrangement (b-1) and another is a perpendicular arrangement (b-2). The former is energetically more stable than the latter ( $\Delta E=1.6$  kJ/mol).

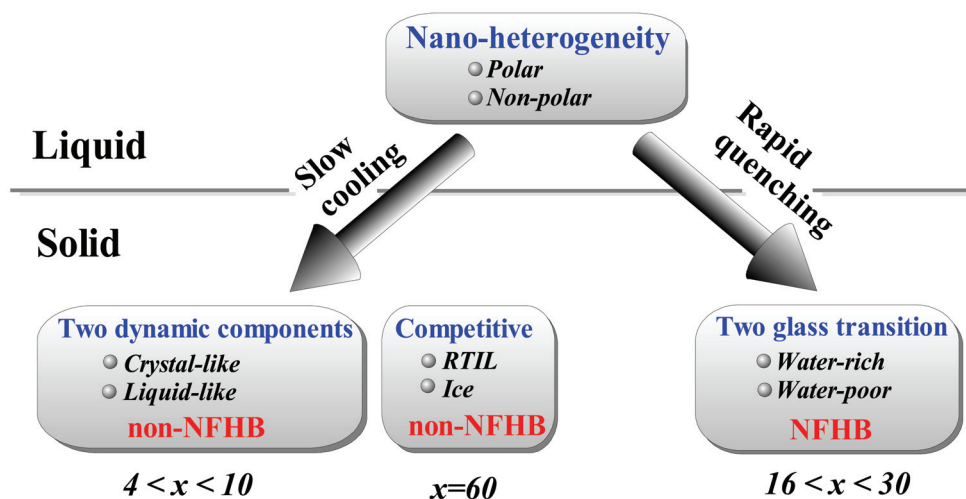


Fig. 10. Three glassy states in the  $[\text{DEME}][\text{BF}_4]\text{-H}_2\text{O}$  system. The existence of a nearly-free hydrogen bonded (NFHB) band of water implies that glass-forming mechanisms are different to each other.

polar parts, is stable in satisfying a charge balance. In the quenched glass, the double glass transition at 16–30 mol% suggests water compositional modulation (water-rich and water-poor). Supposedly, the  $T_{g1}$  and  $T_{g2}$  splitting corresponds to soft and hard glasses. NFHB water still exists even if some local diffusion to the modulation is permitted in rapid solidification. In contrast to this, the slow-cooled glass at 6.7 mol% is formed under a competition between liquid and crystal. The experimentally obtained ‘two dynamic components’ suggest that the local environment is decomposed into soft (liquid-like) and hard (crystal-like) parts. At the crossover point (60 mol%), the absence of the ‘two dynamic components’ suggests that the crossover-type glass appears simply as an intermediate state. Finally, we emphasize that the glass-forming mechanism is entirely different in the three glasses.

#### 4.4 H/D effects at 1 mol% water mixture

As mentioned earlier, intensity modulation on the Debye ring connects with the crystal domain structure, which reflects on nucleation and growth processes. In crystallization, a highly preferred orientation on the Debye ring was observed in [DEME][BF<sub>4</sub>]-0.9 mol% H<sub>2</sub>O (Fig. 11(a)) (Imai et al., 2008b). Rocking curves ( $\theta$  scan mode) in the [DEME][BF<sub>4</sub>]-water mixtures are obtained at a fixed  $2\theta$  value (17.4°). The full width at half maximum (FWHM) of the peaks is estimated to be around 0.2°, where the mosaicity is equivalent to that of a single crystal. Moreover, each peak has a specific orientational relation of twin-crystal structure, such as can be observed in a shape memory alloys (Abe et al., 1994). A twinlike structure is represented by a pair of peak splittings. At 0.6 mol% and just below 1 mol%, the distinct sharp peaks vanished but broad modulations of intensity remained on the Debye ring. This is typical or preferred orientations as seen in conventional microdomains, which have weak orientational relationships. However, the preferred orientation disappears completely above 2.9 mol%. The ideal Debye ring show fairly fine domains or particles are randomly located with little orientational correlation to each other. Considering the conventional domain size,  $\eta_0$ , domain formations in the present system are classified into three types; (I) weakly orientated microdomains ( $x < 0.7$  mol%;  $\eta \approx \eta_0$ ), (II) composite domain structure of weakly orientated microdomains and large twin-related domains ( $x = 0.9$  mol%;  $\eta_0 < \eta$ ), and (III) ideal randomly orientated microdomains ( $2.0 < x < 4.4$  mol%;  $\eta < \eta_0$ ). Domain sizes are drastically changed by a small amount of water. In addition to the domain formations, we mention the strain in the crystal. It is found that no strain occurs in the crystal lattice at 0–4.4 mol%, since no peak broadening of Bragg reflections along the radial direction ( $\theta$ - $2\theta$  scan mode) was observed in this water concentration range. It is curious that this complicated domain is formed without any intrinsic strain. We wonder whether, in other additives, anomalous type II domains occur. The rocking curves of [DEME][BF<sub>4</sub>]-D<sub>2</sub>O, -CH<sub>3</sub>OH, -C<sub>2</sub>H<sub>5</sub>OH and -C<sub>6</sub>H<sub>6</sub> are shown in Fig. 11(b). The preferred orientations are similar to those at 0.6 (type I) or 2.9 (type III) mol% H<sub>2</sub>O. Consequently, we note that the type II domain is limited to the 0.9 mol% H<sub>2</sub>O mixture. Therefore, H<sub>2</sub>O-mediated hydrogen bonding is peculiar to the crystallization process. It is considered that the Type II domain at 0.9 mol% H<sub>2</sub>O mixture is caused by a macroscopic elastic anomaly such as a shape memory effect (Abe et al., 1994).

Not only the domain structure, but also the crystal structure of 0.9 mol% H<sub>2</sub>O are obviously different from pure, 0.6 and 2.9 mol% H<sub>2</sub>O mixtures (Imai et al., 2009). The orthorhombic lattice of pure [DEME][BF<sub>4</sub>] is determined to be  $a_0 = 1.012$ ,  $b_0 = 1.347$ ,  $c_0 = 0.893$  nm ( $Z = 4$ ).

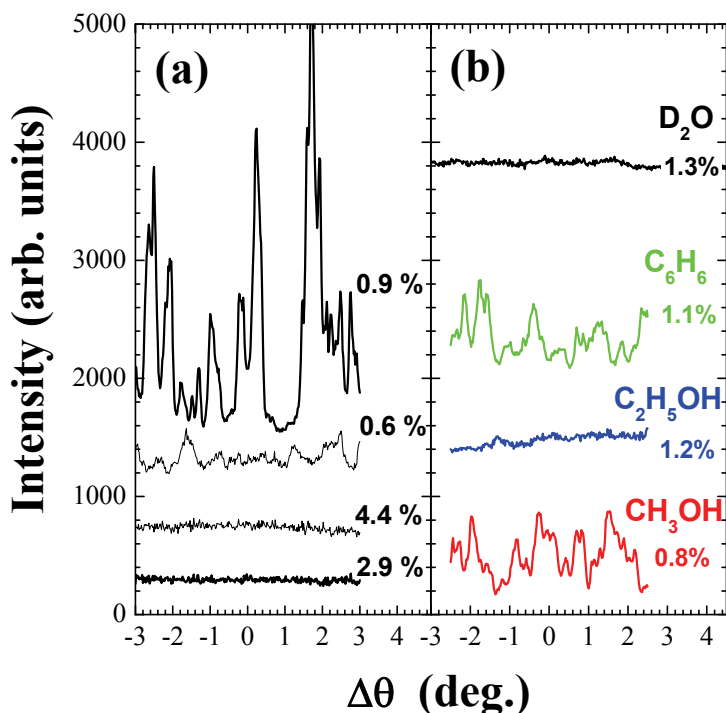


Fig. 11. Rocking curves of (a) H<sub>2</sub>O and (b) other additives at -70 °C. Extensive preferred orientation occurs at a specific region of water concentration in [DEME][BF<sub>4</sub>]-water mixtures.

WAXS patterns at 0.6, 0.9 and 2.9 mol% H<sub>2</sub>O are shown in Fig. 12. If we assume a smaller unit cell and two different kinds of modulated structures (superstructures), the observed  $2\theta$  values are almost the same as the calculated ones. The smaller orthorhombic unit cell is expressed by  $a_O'$ ,  $b_O'$  and  $c_O'$ . Blue circles represent the supercell of  $a_O' \times b_O' \times 2c_O'$  ( $Z=8$ ), while red circles indicate another supercell of  $2a_O' \times b_O' \times 2c_O'$  ( $Z=16$ ) (Fig. 12). Unit cells and the volume per four [DEME][BF<sub>4</sub>] units,  $V_4$ , of [DEME][BF<sub>4</sub>]-H<sub>2</sub>O are listed in Table 1. A significant finding is that  $V_4$  at 0.9 mol % is distinctly small. It should be noticed that the twin-related domain at 0.9 mol% H<sub>2</sub>O ( $\eta_0 < \eta$ ) is formed with two accompanying kinds of superstructures ( $Z=4m$ ;  $m=2$  and 4) and a volume contraction (small  $V_4$ ).

In order to interpret the elastic and structural anomaly at 0.9 mol% H<sub>2</sub>O, we introduce a sublattice, which has the equivalent length (2.7 nm) of a sublattice constant,  $a_{\text{sub}}$ . The sublattice has a peculiar geometric relationship with the orthorhombic lattice (Fig. 13). The lattice relationship is given by,

$$a_{\text{sub}} = 2b_O = 3c_O = 2\sqrt{a_O'^2 + c_O'^2} . \quad (3)$$

The sublattice contains 48 molecules of [DEME][BF<sub>4</sub>]. If we assume that one water molecule exists in two sets of sublattices, the elastic anomaly is explained by a water network over the

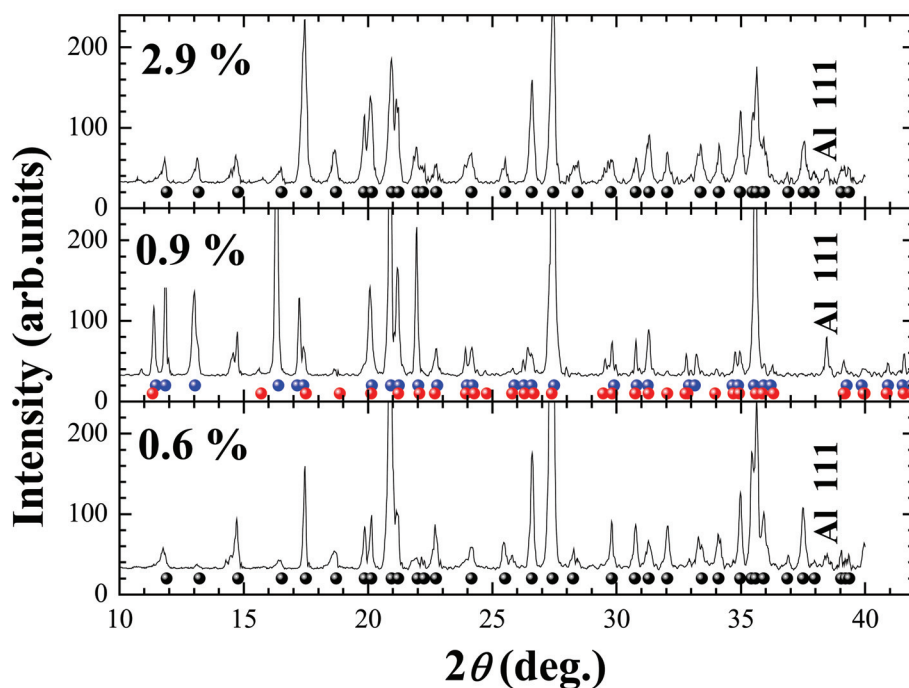


Fig. 12. WAXS patterns of [DEME][BF<sub>4</sub>]-H<sub>2</sub>O mixtures. Crystal structures of 0.6, 0.9 and 2.9 mol% H<sub>2</sub>O are calculated. Only the crystal structure of 0.9 mol % H<sub>2</sub>O is not calculated by unit cells of pure [DEME][BF<sub>4</sub>]. Blue circles indicate the  $a_{O'} \times b_{O'} \times 2c_{O'}$  modulated lattice and red circles indicate the  $2a_{O'} \times b_{O'} \times 2c_{O'}$  modulated lattice.

$x$	Structure	$V_4$ (nm <sup>3</sup> )	$T_c$
0.6 %	$a_O \times b_O \times c_O$	1.210	-41.5
0.9 %	$a_{O'} \times b_{O'} \times 2c_{O'}$	1.145	-14.4
	$2a_{O'} \times b_{O'} \times 2c_{O'}$	1.101	
2.9 %	$a_O \times b_O \times c_O$	1.210	-45.6
4.4 %	$a_O \times b_O \times c_O$	1.214	-32.8
	$a_O \times b_O \times 2c_O$	1.209	
8.8 %	$a_O \times b_O \times c_O$	1.216	-41.2
12.0 %	$a_O \times b_O \times c_O$	1.219	-50.5

Table 1. Each unit cell in the [DEME][BF<sub>4</sub>]-H<sub>2</sub>O mixtures is expressed in terms of the lattice constants of pure [DEME][BF<sub>4</sub>], where  $a_O$ ,  $b_O$  and  $c_O$  indicate those of the orthorhombus.  $a_{O'}$ ,  $b_{O'}$  and  $c_{O'}$  are smaller lattice constants.  $V_4$  is volume per four molecules ( $Z=4$ ).

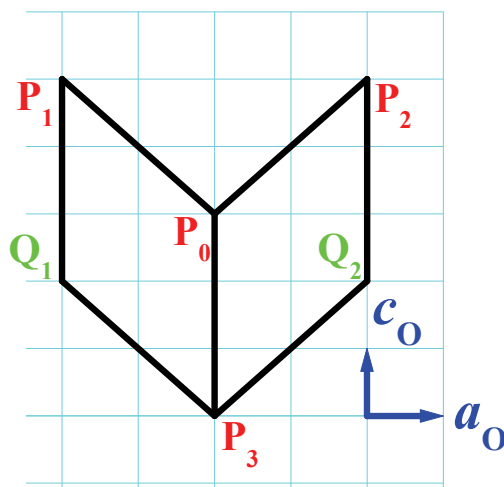


Fig. 13. The geometrical relationship between the orthorhombic lattice and its sublattice is drawn on the  $a_O$ - $c_O$  plane. The sublattice is rhombic and the edge length of the rhombus is equal to  $2b_O$ .

medium-range (Imai et al., 2009). Since the above assumption is defined to be one  $H_2O$  molecule and 96 molecules of  $[DEME][BF_4]$ ,  $1/(1+96)$  provides 1.03 mol%. This means that an average distance of 1 mol% additives is equal to the sublattice parameters. The single  $H_2O$  molecule in two sets of sublattices is based on the following idea: one molecule can occupy sites at  $P_1$ - $P_2$ - $Q_1$ - $Q_2$ ,  $P_0$ - $P_3$  and  $Q_1$ - $Q_2$ - $P_3$  on the sublattice points (Fig. 13). Since the lengths of  $P_0Q_1$  and  $P_0Q_2$  are too short,  $H_2O$  molecules probably cannot be located at the sublattice points simultaneously. Thus, we consider that the perfect order of  $H_2O$  can be realized only at 1 mol%. Also, a medium-range order (MRO) (Abe, 2007b) of  $H_2O$  can contribute to the elastic anomaly, supercell and volume contractions at 0.9 mol%  $H_2O$ . The geometric effect is enhanced by additions of  $H_2O$ , which may be derived from strong hydrogen bonding of  $H_2O$ . Recently, water network simulations are carried out by developing this idea (Abe et al., 2010b). The MRO of  $H_2O$  is developing in the simulation box.

Our next step is to clarify the anomalous behaviors at 0.9 mol%  $H_2O$  by another approach. Since we consider that the anomalies are induced by particular hydrogen bonding of  $H_2O$ , we examine the H/D effects at 0.9 mol%  $H_2O$  in the same manner as the 'giant isotope effect' of ferroelectrics. In fact, the deuterated effect in RTILs has not been discussed much so far, though various kinds of RTIL-water mixtures have been investigated experimentally and theoretically. By fixing the water concentration at 1 mol%, we prepared  $[DEME][BF_4]$ - $H_2O$ ,  $-0.75H_2O$   $0.25D_2O$ ,  $-0.5H_2O$   $0.5D_2O$  and  $-D_2O$  mixtures, where  $(1-y)H_2O$   $yD_2O$  mixtures are provided by the  $y$  parameter. We have determined the crystal structures and crystallization temperatures,  $T_c$ , of  $[DEME][BF_4]$ - $H_2O$ ,  $-0.75H_2O$   $0.25D_2O$ ,  $-0.5H_2O$   $0.5D_2O$  and  $-D_2O$  mixtures by simultaneous WAXS and DSC measurements (Abe et al., 2010a). The  $T_c$ , unit cell ( $Z=4m$ ) and  $V_4$  of the mixtures are revealed in Table 2. It is obvious that  $T_c$  decreases with increasing D substitution. Also, superstructures vanish and  $V_4$  increases



	H <sub>2</sub> O		0.75H <sub>2</sub> O•0.25D <sub>2</sub> O	0.5H <sub>2</sub> O•0.5D <sub>2</sub> O	D <sub>2</sub> O
$x$ (mol%)	0.9		1.0	0.9	1.3
$T_c$ (°C)	-14.4		-21.4	-34.8	-39.7
unit cell	$a_O' \times b_O' \times 2c_O'$	$2a_O' \times b_O' \times 2c_O'$	$a_O' \times b_O' \times c_O'$	$a_O \times b_O \times c_O$	$a_O \times b_O \times c_O$
$V_4$ (nm <sup>3</sup> )	1.145	1.101	1.181	1.212	1.209

Table 2. Crystallization temperatures,  $T_c$ , unit cells of crystal structures and volume per four molecules ( $Z=4$ ),  $V_4$ , of [DEME][BF<sub>4</sub>]-0.9 mol% H<sub>2</sub>O, -1.0 mol% 0.75H<sub>2</sub>O 0.25D<sub>2</sub>O, -0.9 mol% 0.5H<sub>2</sub>O 0.5D<sub>2</sub>O and -1.3 mol% D<sub>2</sub>O.

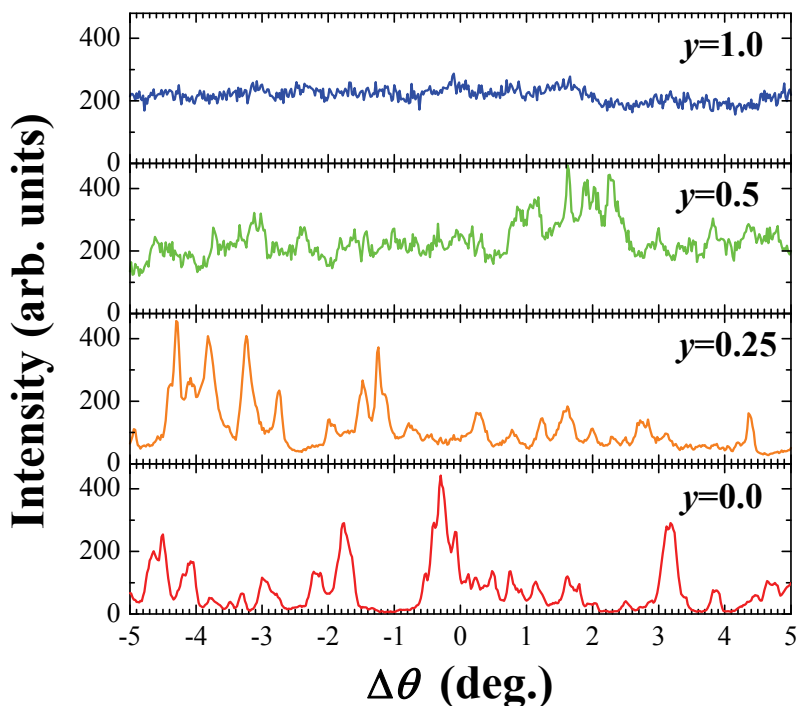


Fig. 14. Rocking curves at -80 °C of [DEME][BF<sub>4</sub>]-0.9 mol % H<sub>2</sub>O ( $y=0.0$ ), -1.0 mol % 0.75H<sub>2</sub>O 0.25D<sub>2</sub>O ( $y=0.25$ ), -0.9 mol % 0.5H<sub>2</sub>O 0.5D<sub>2</sub>O ( $y=0.5$ ) and -1.3 mol % D<sub>2</sub>O ( $y=1.0$ ).

gradually with increasing  $y$ . In addition to the  $\theta$ - $2\theta$  scan mode, crystal domain structures of (1- $y$ )H<sub>2</sub>O  $y$ D<sub>2</sub>O mixtures were examined by  $\theta$  scan mode. Figure 14 reveals the rocking curves on the Debye rings of the [DEME][BF<sub>4</sub>]-0.9 mol% H<sub>2</sub>O, -1.0 mol% 0.75H<sub>2</sub>O 0.25D<sub>2</sub>O, -0.9 mol% 0.5H<sub>2</sub>O 0.5D<sub>2</sub>O and -1.3 mol% D<sub>2</sub>O mixtures, respectively. The rocking curves were obtained at a fixed  $2\theta$  value (27.4°). In the case of [DEME][BF<sub>4</sub>]-0.9 mol% H<sub>2</sub>O and -1.0 mol% 0.75H<sub>2</sub>O 0.25D<sub>2</sub>O, an extraordinary highly preferred orientation appears on the Debye ring. Judging from the asymmetric peak profiles or two peak tops, a twin-related domain (Type II;  $\eta_0 < \eta$ ) occurs at  $y=0.0$  and  $y=0.25$ . Whereas for the 0.9 mol% 0.5H<sub>2</sub>O 0.5D<sub>2</sub>O

( $y=0.5$ ), a conventional preferred orientation is observed. Weak intensity modulations on the Debye ring are expressed by much broader and weaker peaks (Type I;  $\eta \approx \eta_0$ ). Interestingly, the preferred orientation disappears completely in 1.3 mol%  $D_2O$  ( $y=1.0$ ). The domain ( $y=1.0$ ) that gives an ideal Debye ring corresponds to Type III ( $\eta < \eta_0$ ). Systematically, a very strong H/D effect is obtained in the [DEME][BF<sub>4</sub>]-1 mol% water system. The D substitution parameter,  $y$ , effects continuous changes of crystallization temperature ( $T_c$ ), domain structures ( $\eta$ ), superstructures ( $Z=4m$ ) and volume ( $V_4$ ).

Based on the idea of the protonated effect in  $KH_2PO_4$  (Koval et al., 2002; Koval et al., 2005; Lasave et al., 2005), we assume the hydrogen bonding in the solid, from a microscopic perspective, is as follows: (i) NFHB water in the liquid state might be bound to the F of the anion and also the O of the large cation as shown in Fig. 15(a), once the mixture is

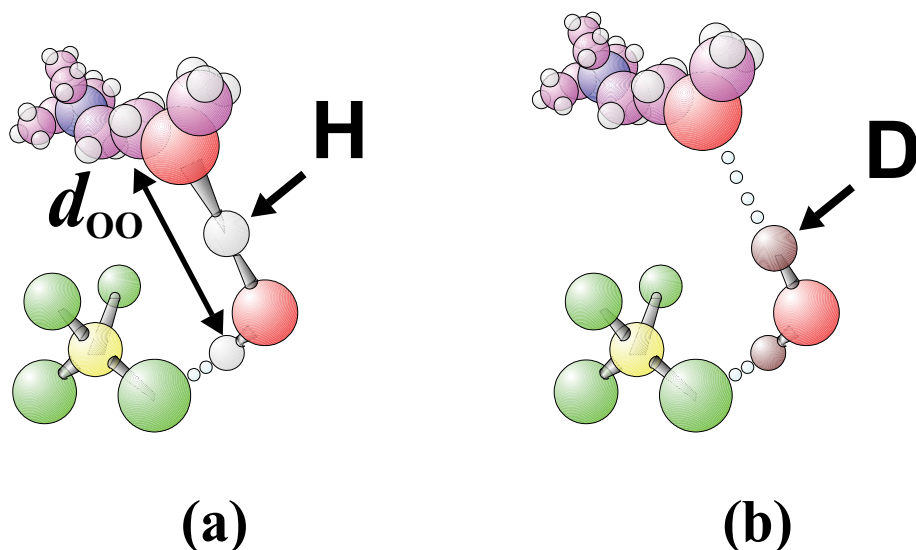


Fig. 15. The bonding scheme of (a)  $H_2O$  and (b)  $D_2O$  in crystal. In protonated water, 'on-centering' is preferred, whereas 'off-centering' occurs in deuterated water. The atomic distance between oxygens,  $d_{oo}$ , varies depending on the interaction.

crystallized by slow cooling. Due to the highly packed solid structure, PMCB (H-O-H) is employed. (ii) D in the solid stays in its off-centered position ( $O \cdots D-O$ ), as shown in Fig. 15(b). Where there is PMCB (hydrogen delocalization) in the crystal, the atomic distance between O and O,  $d_{oo}$ , becomes shorter (Fig. 15(a)), but this attractive interaction does not occur in deuterated water, since the deuteron is stabilized in the off-center position as with  $KD_2PO_4$ . From assumption (ii), it follows that associating with deuterated water leads to a larger  $d_{oo}$ . We infer that the PMCB in the [DEME][BF<sub>4</sub>]-0.9 mol%  $H_2O$  crystal causes an extraordinary volume contraction, partly seen in the results in Table 2. A large contribution from PMCB in the 1.0 mol %  $0.75H_2O \cdot 0.25D_2O$  also provides a small volume contraction. Next, we focus on the influence of D on the domain structure related to PMCB. Domain morphology changes successively with the  $y$  parameter as shown in Fig. 14. Using the above PMCB mechanism, the discrepancy of the difference in scale might be resolved. From the

strong H/D effect, we consider that the previously introduced sublattice network is treated as a PMCB perturbation. The geometrical network is a bridge between local atomic shifts (PMCB) and the macroscopic twin-related domain. Similarly, the  $T_c$ , which depends on the nucleation process, is connected to the H/D effect. However, the dynamic process connecting the microscopic to the macroscopic still remains unclear. Certainly, it is not sufficient to describe the dynamic motion of the domain wall by WAXS alone. Dynamic properties relating to its local structure could be interpreted from the Raman data, but there is further difficulty of detection with such a small content of water. In fact, we could not detect the differences due to the H/D effects in the Raman spectra at 1 mol % water.

#### 4.5 Hierarchy structure and its relationship to the nearly-free hydrogen bonding in the liquid state

H/D effects on the crystal can lead us to the distinct ‘hierarchy’ structure based on hydrogen bonding. Considering our experimental results in the liquid state as a whole, the ‘hierarchy’ of the liquid structure seems to be deeply connected to NFHB water. Figure 16 shows WAXS patterns of [DEME][BF<sub>4</sub>]-H<sub>2</sub>O mixtures at room temperature. At around 85 mol%, the patterns are modulated differently, and the  $Q$  position at the maximum intensity of the principal peak  $Q_{\max}$  shifts to higher  $Q$  (Aono et al., 2011). The same tendency of  $Q_{\max}$  is seen in [DEME][BF<sub>4</sub>]-D<sub>2</sub>O mixtures.  $Q_{\max}$  as a function of H<sub>2</sub>O and D<sub>2</sub>O concentrations is plotted in Fig. 17. From the viewpoint of H/D effects in the liquid state, the local structure as a function of water concentration does not depend on H<sub>2</sub>O or D<sub>2</sub>O. Compared with the dense crystal, [DEME][BF<sub>4</sub>] and water are loosely bound to each other. The PMCB seen in crystals is not activated in the liquid. The sudden shift of  $Q_{\max}$  can be regarded as a crossover point,  $x_c$  (=85 mol%), to a different liquid structure. In a radial distribution function (RDF) at around 90 mol%, we found that the liquid structure is not represented by a simple superposition of pure [DEME][BF<sub>4</sub>] and H<sub>2</sub>O (Abe et al., 2010a). This implies that hydrogen bonding is coupled with other factors. In the WAXS, another significant finding was the appearance of a low- $Q$  component such as a ‘prepeak’ (Allen et al., 1992; Salanne et al., 2008). The intensity of the low- $Q$  component ( $Q \sim 2 \text{ nm}^{-1}$ ) increased only between 85 and 95 mol% (Fig. 18). The low- $Q$  component is related to MRO in network-forming ionic liquids, like ZnCl<sub>2</sub> or SiO<sub>2</sub>. In ZnCl<sub>2</sub>, voids in the simulated liquid are analyzed using Voronoi polyhedra (Wilson & Madden, 1998). The weak ordering of the voids provides spatial contrast, that is, cation density fluctuations. Generally, the low- $Q$  component is extremely sensitive to the density (Barker et al., 2000). Consequently, the liquid structure in the [DEME][BF<sub>4</sub>]-H<sub>2</sub>O mixtures has anomalies in coordination number, orientational order and density in the vicinity of 85 mol%.

The liquid structures are roughly divided into three regimes: (i) an RTIL-based structure ( $x < 80 \text{ mol\%}$ ), (ii) an intermediate state ( $80 < x < 95 \text{ mol\%}$ ) and (iii) bulk water ( $95 \text{ mol\%} < x$ ). The intermediate state is not a simple mixing state, but an intrinsically complicated one. For instance, the low- $Q$  component suddenly increases in this region, and RDF analysis indicates that the liquid structure is modified extensively by additional factors. From the viewpoint of molecular configurations, we can discuss the liquid structures in the anomalous mixing state. A simple aggregation of  $\text{BF}_4 \cdots n(\text{H}_2\text{O})$  as shown in Figs. 9(a), 9(b), 9(c) and 9(d) is preferred below 80 mol%. The optimized arrangements can explain the observed Raman modes in the liquid state well (Takekiyo et al., in preparation.). Since water

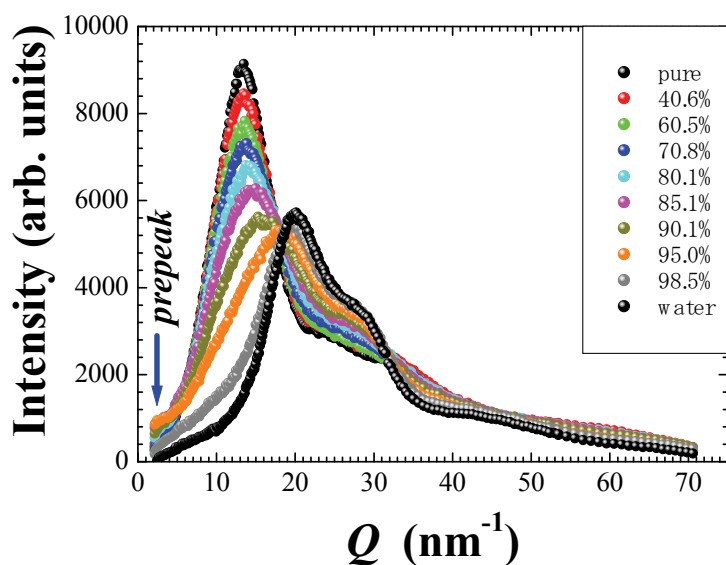


Fig. 16. WAXS intensity changes in [DEME][BF<sub>4</sub>]-H<sub>2</sub>O mixtures at room temperature. Above 80 mol% H<sub>2</sub>O, the maximum position of the normal principal peak in WAXS gradually shifts to that of pure water.

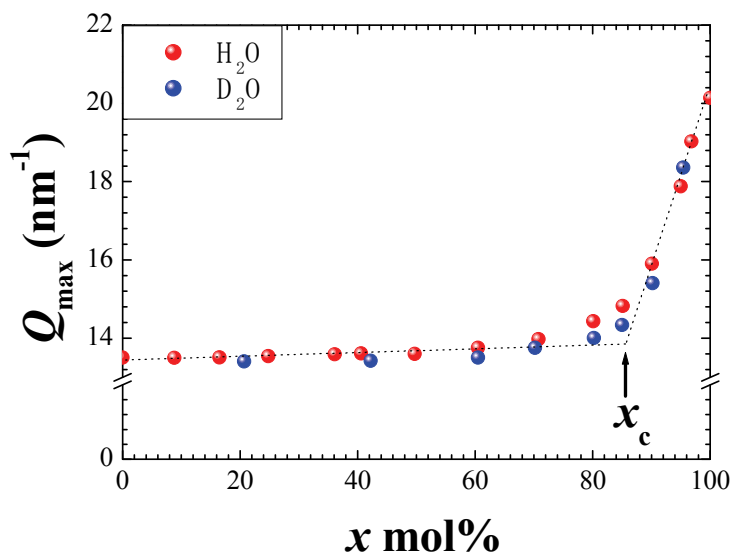


Fig. 17. H<sub>2</sub>O and D<sub>2</sub>O concentration dependences of  $Q$  position at the maximum intensity,  $Q_{\max}$ , of WAXS patterns (Fig. 16).  $Q_{\max}$  values increase drastically above 90 mol% H<sub>2</sub>O and D<sub>2</sub>O.

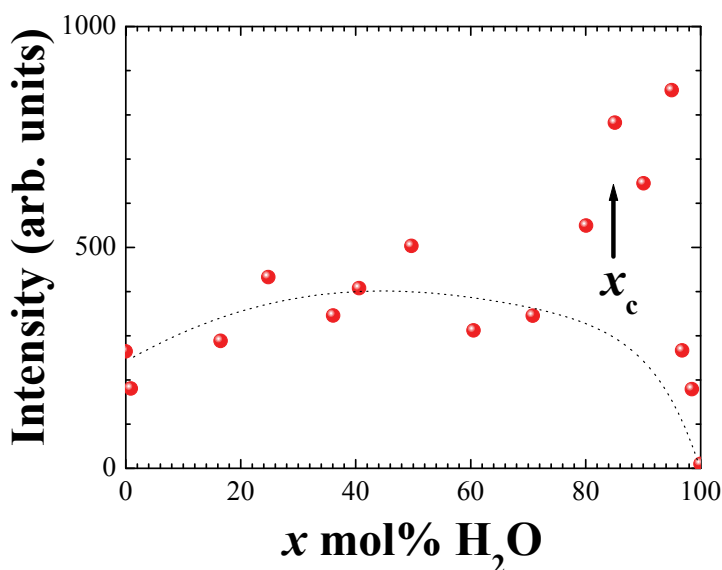


Fig. 18. H<sub>2</sub>O concentration dependence of intensity of the low-Q component in WAXS. Q position is 2.1 nm<sup>-1</sup>, which is provided by the allowances in Fig. 16.

is loosely bound to a BF<sub>4</sub><sup>-</sup> anion, bulk water is not formed. This corresponds to the RTIL-based liquid structure below 80 mol%. In contrast, the intermediate scheme with a hierarchy structure requires a new concept, where the idea of BF<sub>4</sub><sup>-</sup>⋯*n*(H<sub>2</sub>O) complexes is developed to interpret the anomalous mixing state at 80-95 mol%.

In order to gather clues about this new concept, SAXS experiments of [DEME][BF<sub>4</sub>]-H<sub>2</sub>O mixtures were carried out. The SAXS intensity of pure [DEME][BF<sub>4</sub>] is relatively strong. The SAXS data do not fit well with representative models such as fractal morphology, lamellar structure, and spinodal decomposition. Therefore, we used the Ornstein-Zernicke (OZ) correlation function in Eq. (2) (Stanley, 1971). The correlation length,  $\xi$ , as a function of H<sub>2</sub>O concentration was estimated by the OZ correlation function, as shown in Fig. 19. The correlation length of pure [DEME][BF<sub>4</sub>] amounts to 1.7 nm in which the large cation size is 0.8 nm. The nanoscale heterogeneity becomes smaller with increasing water content up to 50 mol%. Around 50 mol%, the nanoscale fluctuation almost disappears because the correlation length is almost equal to the cation size. At 65-85 mol%, the correlation length, however, increases again. Finally, the correlation length is suppressed at greater than 90 mol%. The increment of SAXS at 65-85 mol% does not originate from polar and non-polar regions, since the formation of nano-heterogeneity is interrupted by the water network with increasing water concentrations. We confirm that density fluctuations at 65-85 mol% are induced as a precursor phenomenon of the above anomalous mixing state at 80-95 mol%.

In addition to the density fluctuations, the anomalous mixing state of [DEME][BF<sub>4</sub>]-H<sub>2</sub>O is seen in optical absorption (Aono et al., 2011; Aono et al., submitted). The optical absorption spectra in the UV-vis region are shown in Fig. 20. The absorption spectrum of pure water is provided in the inset of Fig. 20. Pure water has an absorption at 4.7 eV (Laasonen et al., 1993). With an increase in the water content, the optical absorption gradually decreases.

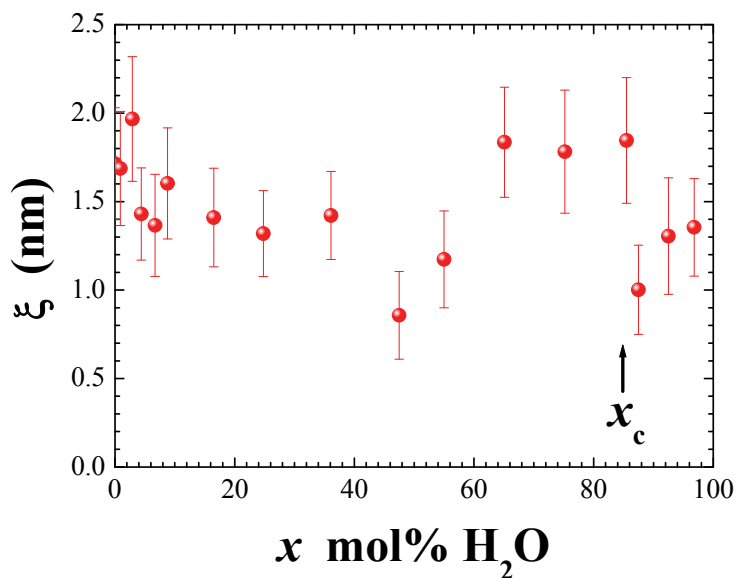


Fig. 19.  $\text{H}_2\text{O}$  concentration dependence of correlation length,  $\xi$ , which is obtained with the Ornstein-Zernike correlation function

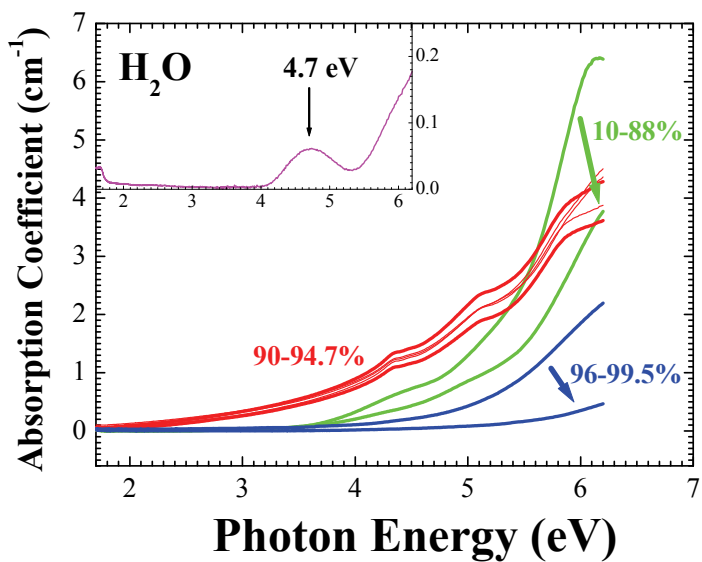


Fig. 20. Optical absorption spectra as a function of water concentration. The inset shows the absorption spectrum of pure water.

However, an unusual increase is seen between 90 and 95 mol%. To see this anomaly, we plot the optical absorption as a function of water concentration in Fig. 21, where the photon energy is fixed at 4.7 eV. Apart from the rapidly increasing region described subsequently, a crossover point in the absorption coefficient,  $x_c$ , is observed at 85 mol%. On the simple optical absorption curve, very high absorption appears between 90 and 95 mol%. In a previous study on  $[\text{C}_4\text{mim}][\text{PF}_6]$  (Paul et al., 2005), the optical absorption in the UV-vis spectra was explained well. The electronic absorption around 4.4 eV in  $[\text{C}_4\text{mim}][\text{PF}_6]$  provides information on the polarity of the RTIL and the dynamics of the diffusion. Here, the possible excited species are induced by the donor-acceptor charge transfer, proton transfer, molecular conformational change, hydrogen bonding ability, and polarity (Mahanta et al., 2008). For the  $[\text{DEME}][\text{BF}_4]\text{-H}_2\text{O}$  mixture, we focus on the anomalous optical absorption at 90-95 mol%. We introduce the cluster model (Aono et al., submitted), which consists of an inner core and outer shell in an analogy with a micelle structure. The core corresponds to a  $\text{BF}_4 \cdots 4(\text{H}_2\text{O})$  cluster, based on DFT calculations (Fig.9 (d)). In the outer shell, water molecules are loosely bonded to the inner core. A large cation is excluded from the cluster. The model is not contradicted by the experimentally obtained non-NFHB water above 90 mol%. In the model, four  $\text{H}_2\text{O}$  molecules of the inner core should be hydrogen bonded with outer  $\text{H}_2\text{O}$  molecules.

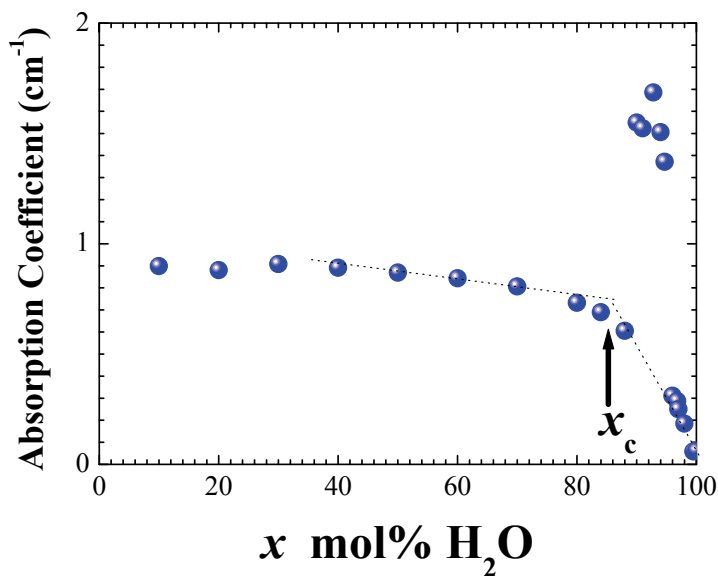


Fig. 21. Water concentration dependence of the optical absorption coefficient at 4.7 eV.

## 5. Summary

In this study, we explore a variety of water-mediated molecular interactions. Both in the liquid and solid states, the  $[\text{DEME}][\text{BF}_4]\text{-H}_2\text{O}$  system, a non-imidazolium RTIL, has a lot of phases and states, including a non-equilibrium state. Moreover, some of them are

characterized by self-assembly or hyperstructure. Here, it is crucial that well-organized structure on the mesoscopic scale contributes to the hierarchy. In the case of [DEME][BF<sub>4</sub>]-H<sub>2</sub>O, hydrogen bonding plays an important role in structural formation at each scale. The hierarchy structure in the liquid state is summarized in Fig. 22. As an intermediate state between RTIL and bulk water, the hierarchy appears at 80-95 mol%. In order to explain the extraordinary mixing state, we introduce a hybrid cluster (core + shell), which is self-assembled. A core part, described by BF<sub>4</sub>···*n*(H<sub>2</sub>O), is aggregated by H··F bonding. Non H··F bonding water above 80 mol% surrounds the core part. It is predicted that a (core + shell) cluster has a size distribution and its own relaxation time. Possibly, self-assembled clusters can make a striking contrast in density over the medium-range. If the size of density fluctuations is distributed widely, optical absorption over the whole UV-vis range is recognized by light scattering. We emphasize that the hierarchy of the liquid structure is regarded as one of self-organization based on hydrogen bonding, although there is no H/D effect.

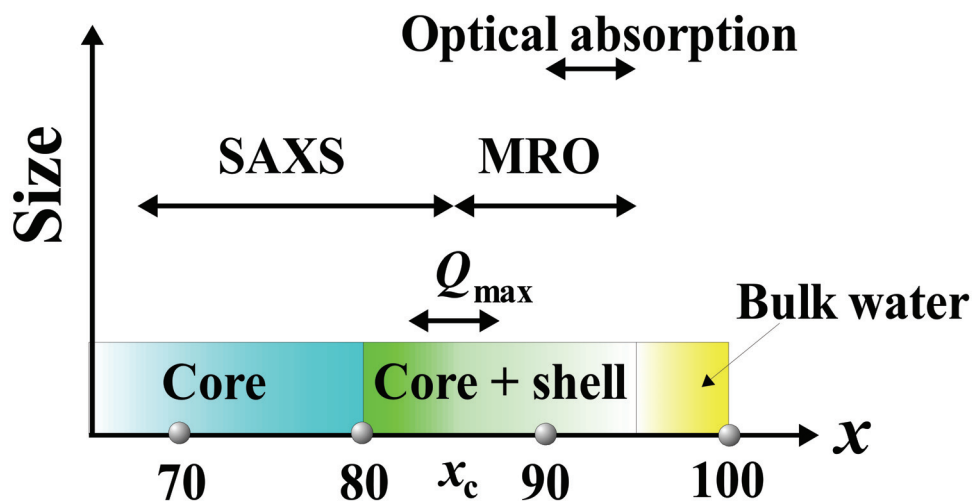


Fig. 22. Hierarchy structure in a liquid state at 80-95 mol% H<sub>2</sub>O. MRO (medium-range order) and SAXS (small angle X-ray scattering) reveal density fluctuations at each scale.

In the three different glassy states illustrated in Fig. 10, thermal treatments, heterogeneity and NFHB can distinguish the glass forming mechanism. In the denser solid state, hydrogen bonding effectively acts on the glasses instead of forming a non-equilibrium state. The big difference in hydrogen bonding is described by the non-NFHB of slow-cooled glasses and NFHB of quenched ones. Furthermore, a double glass transition is observed in the quenched glass, which is formed extremely far from an equilibrium state. Freezing separately into water-poor and water-rich regions proves that there are two kinds of water roles. In the water-rich region,  $T_{g2}$  becomes higher alongside a change to hard glass, where water molecules act as binding between other molecules. On the other hand, water-poor glass is unstable, with lower  $T_{g1}$ . In the soft glass of the water-poor region, water molecules tend conversely to break the glassy state. Hence, heterogeneity (water-rich + water-poor) formed



by the two different roles of water is distinguished from the nano-heterogeneity (polar + non-polar) of pure RTILs. Since  $\Delta T_g$  in the double glass transition is quite small, each region of water-rich and water-poor is estimated to be relatively small. Therefore, coexistence of hard and soft glasses in the double glass transition is regarded as a kind of hierarchic anomaly related to macroscopic glass transition temperatures.

In the crystal state, at 1 mol%  $\text{H}_2\text{O}$  only, macroscopic anomalies are observed. The anomalies are as follows; (i) high crystallization temperature ( $T_c$ ), (ii) twin-related domain ( $\eta \gg \eta_0$ ), (iii) superstructures ( $Z=4m$ ) and (iv) volume contraction (small  $V_4$ ). In proportion to D substitution, these anomalies gradually disappear. The H/D effect reveals that H is extensively involved in hydrogen bonding despite the small amount of water. The inherent bonding nature of H is explained by introducing attractive PMCB on the microscopic scale (Abe et al., 2010a) and repulsive water in the sublattice network (Abe et al., 2010b) (Fig. 23). If just 1 mol% of water is fully ordered on the sublattice with an equivalent sublattice constant, the geometrical order provides an elastic influence on the whole lattice. The mutual effects of the virtual PMCB and sublattice network become more realistic with strong H/D effects.

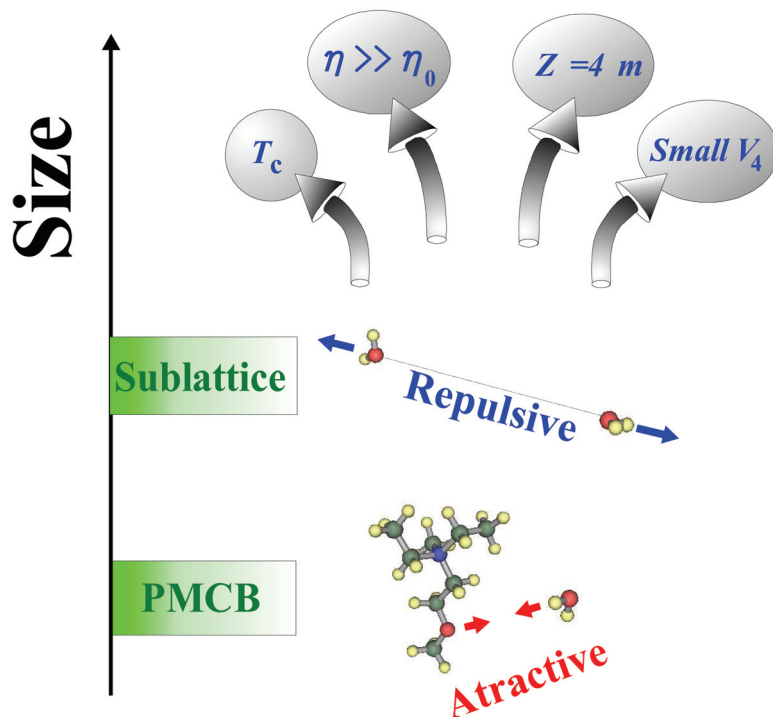


Fig. 23. Hierarchy structure of crystals at 1 mol%  $\text{H}_2\text{O}$ . Proton-mediated covalent bonding (PMCB) controls macroscopic properties such as crystallization temperature,  $T_c$ , twin-related domain ( $\eta \gg \eta_0$ ), superstructures ( $Z=4m$ ) and volume contraction ( $V_4$ ). The H/D effect is dominant only at 1 mol%  $\text{H}_2\text{O}$ .

A water molecule can bring out hidden properties of other molecules. For instance, proteins fully utilize the effects of water molecules. To understand the hydrogen bonding of water geometrically is significant for clarifying its 'function and structure'. The grouping of hydrogen bonding has just begun in simple molecular systems such as [DEME][BF<sub>4</sub>]-H<sub>2</sub>O.

## 6. Acknowledgements

We appreciate Ms. M. Yasaka and Mr. A. Kishi of Rigaku Co. for experimental support and helpful discussions. Also, the authors sincerely thank Mr. Y. Imai, Mr. T. Goto of National Defense Academy for experimental support. Dr. M. Aono and Dr. T. Takekiyo are our collaborators and some experimental results were obtained by them. Also, we provide special thanks to Prof. N. Hamaya of Ochanomizu University, Prof. A. Shimizu of Soka University, Professor H. Matsumoto and Professor T. Arai of National Defense Academy for helpful discussions.

## 7. References

- Abe, H., Ishibashi, M., Ohshima, K., Suzuki, T., Wuttig, M. & Kakurai, K. (1994) Kinetics of martensitic transition in In-Tl alloys, *Phys. Rev. B* Vol. 50: 9020-9024.
- Abe, H., Yamamoto, K., Matsuoka, S. & Matsuo, Y. (2007a) Atomic short-range order in an Al<sub>72</sub>Ni<sub>18</sub>Fe<sub>10</sub> decagonal quasicrystal studied by anomalous x-ray scattering, *J. Phys.: Condens. Matter* Vol. 19: 466201-14.
- Abe, H. (2007b) Reverse Monte Carlo Modeling of Local Structure Using Short-Range and Medium-Range Order Parameters, *J. Phys. Soc. Jpn.* Vol. 76: 094601-6.
- Abe, H., Yoshimura, Y., Imai, Y., Goto, T. & Matsumoto, H. (2009) Phase behavior of room temperature ionic liquid-H<sub>2</sub>O mixtures: *N, N*-diethyl-*N*-methyl-*N*-2-methoxyethyl ammonium tetrafluoroborate, *J. Mol. Liq.* Vol. 150: 16-21.
- Abe, H., Imai, Y., Takekiyo, T. & Yoshimura, Y. (2010a) Deuterated Water Effect in a Room Temperature Ionic Liquid: *N,N*-Diethyl-*N*-methyl-*N*-2-methoxyethyl Ammonium Tetrafluoroborate, *J. Phys. Chem. B* Vol. 114 : 2834-2839.
- Abe, H., Imai, Y., Goto, T., Yoshimura, Y., Aono, M., Takekiyo, T., Matsumoto, H. & Arai, T. (2010b) Water Network in Room-Temperature Ionic Liquid: *N, N*-Diethyl-*N*-Methyl-*N*-2-Methoxyethyl Ammonium Tetrafluoroborate, *Metal. Mater. Trans. A* Vol. 41: 1137-1143.
- Allen, D. A., Howe, R. A., Wood, N. D. & Howells, W. S. (1992) The structure of molten zinc chloride and potassium chloride mixtures, *J. Phys.: Condens. Matter* Vol. 4: 1407-1418.
- Aono, M., Imai, Y., Ogata, Y., Abe, H., Goto, T., Yoshimura, Y., Takekiyo, T., Matsumoto, H. and Arai, T. (2011) Anomalous Mixing State in Room-Temperature Ionic Liquid-Water Mixtures: *N, N*-diethyl-*N*-methyl-*N*-(2-methoxyethyl) Ammonium Tetrafluoroborate, *Metal. Mater. Trans.*, Vol. 42A: 37-40.
- Aono, M., Imai, Y., Abe, H., Matsumoto, H. & Yoshimura, Y., Optical Interaction of Room Temperature Ionic Liquid- Water Mixtures : *N, N*-diethyl-*N*-methyl-*N*- (2-methoxyethyl) Ammonium Tetrafluoroborate, submitted to *Thermochim. Acta*.
- Barker, D. R., Wilson, M., Madden, P. A., Medvedev, N. N. & Geiger, A. (2000) Voids in the H-bonded network of water and their manifestation in the structure factor, *Phys. Rev. E* Vol. 62: 1427-1430.
- Becke, A. D. (1988) Density-functional exchange-energy approximation with correct asymptotic behavior, *Phys. Rev. A* Vol. 38: 3098-3100.

- Danten, Y., Cabaço, M. I. & Besnard, M. (2010) Interaction of water diluted in 1-butyl-3-methyl imidazolium ionic liquids by vibrational spectroscopy modeling, *J. Mol. Liq.* Vol. 153: 57-66.
- Foces-Foces, C., Echevarria, A., Jagerovic, N., Alkorta, I., Elguero, J., Langer, U., Klein, O., Minguet-Bonvehi, M. & Limbach, H-. (2001) A Solid-State NMR, X-ray Diffraction, and ab Initio Computational Study of Hydrogen-Bond Structure and Dynamics of Pyrazole-4-Carboxylic Acid Chains, *J. Am. Chem. Soc.* Vol. 123: 7898-7906.
- Frish, M. J.; Trucks, G. W.; H.B. Schlegel, G. E.; Scuseria, M. A.; Robb, J. R.; Cheeseman, V. G.; Zakrzewski, J. A.; Montgomery, A. D.; Daniels, K. N.; Kudin, M. C.; Strain, O.; Farkas, J.; Tomasi, V.; Barone, M.; Cossi, R.; Cammi, B.; Mennucci, C.; Pomelli, C.; Adamo, S.; Clifford, J.; Ochterski, G. A.; Petersson, P. Y.; Ayala, Q. Cui, Morokuma, K.; Malick, D. K.; Rabuck, A. D.; Raghavachari, K.; Foresman, J. B.; Cioslowski, J.; Ortiz, J. V.; Baboul, A. G.; Stefanov, B. B.; Liu, G.; Liashenko, A.; Piskorz, P.; Komaromi, I.; Gomperts, R.; Martin, R. L.; Fox, D. J.; Kieth, T.; Al-Laham, M. A.; Peng, C. Y.; Nanayakkara, A.; Gonzalez, C.; Challacombe, M. P.; Gill, M.W.; Johnson, B.; Chen, W.; Wong M. W.; Andres, J. L.; Gonzalez, C.; Head-Gordon, M.; Replogle, E.S.; Pople, J. A. (2003) *GAUSSIAN 03*, Gaussian, Inc., Pittsburgh, PA.
- Imai, Y., Abe, H., Goto, T., Yoshimura, Y., Michishita, Y. & Matsumoto, H. (2008a) Structure and thermal property of *N*, *N*-diethyl-*N*-methyl-*N*-2-methoxyethyl ammonium tetrafluoroborate-H<sub>2</sub>O mixtures, *Chem. Phys.* Vol. 352: 224-230.
- Imai, Y., Abe, H., Goto, T., Yoshimura, Y., Kushiya, S. & Matsumoto, H. (2008b) Orientational Ordering of Crystal Domains in Ionic Liquid Based Mixtures, *J. Phys. Chem. B* Vol. 112: 9841-9846.
- Imai, Y., Abe, H. & Yoshimura, Y. (2009) X-ray Diffraction Study of Ionic Liquid Based Mixtures, *J. Phys. Chem. B* Vol. 113: 2013-2018.
- Imai, Y., Abe, H., Miyashita, T., Goto, T. Matsumoto, H. & Yoshimura, Y. (2010) Two glass transitions in *N*, *N*-diethyl-*N*-methyl-*N*-(2-methoxyethyl) ammonium tetrafluoroborate-H<sub>2</sub>O mixed solutions, *Chem. Phys. Lett.* Vol. 486: 37-39.
- Imai, Y., Abe, H., Matsumoto, H., Shimada, O., Hanasaki, T. & Yoshimura, Y. (2011) Glass Transition Behavior of the Quaternary Ammonium Type Ionic Liquid, [DEME][I]-H<sub>2</sub>O Mixtures, *J. Chem. Thermodynamics*, in press.
- Inaba, A. & Andersson, O. (2007) Multiple glass transitions and two step crystallization for the binary system of water and glycerol, *Thermochim. Acta* Vol. 461: 44-49.
- Jiang, W., Wang, Y. & Voth, G. A. (2007) Molecular Dynamics Simulation of Nanostructural Organization in Ionic Liquid/Water Mixtures, *J. Phys. Chem. B* Vol. 111: 4812-4818.
- Kanno, H., Shimada, K. & Katoh, K. (1983) Two glass transitions in the tetraethylammonium chloride – water system: Evidence for a metastable liquid – liquid immiscibility at low temperatures, *Chem. Phys. Lett.* Vol. 103: 219-221.
- Katayanagi, H., Hayashi, S., Hamaguchi, H. & Nishikawa, K. (2004) Structure of an ionic liquid, 1-*n*-butyl-3-methylimidazolium iodide, studied by wide-angle X-ray scattering and Raman spectroscopy, *Chem. Phys. Lett.* Vol. 392: 460-464.
- Klein, O., Aguilar-Parrilla, F., Lopez, J., Jagerovic, N., Elguero, J. & Limbach, H-H. (2004) Dynamic NMR Study of the Mechanisms of Double, Triple, and Quadruple Proton and Deuteron Transfer in Cyclic Hydrogen Bonded Solids of Pyrazole Derivatives, *J. Am. Chem. Soc.* Vol. 126: 11718-11732.
- Koval, S., Kohanoff, J., Migoni, R. L. & Tosatti, E. (2002) Ferroelectricity and Isotope Effects in Hydrogen-Bonded KDP Crystals, *Phys. Rev. Lett.* Vol. 89: 187602-4.

- Koval, S., Kohanoff, J., Lasave, J., Colizzi, G. & Migoni, R. L. (2005) First-principles study of ferroelectricity and isotope effects in H-bonded  $\text{KH}_2\text{PO}_4$  crystals, *Phys. Rev. B* Vol. 71: 184102-15.
- Kumar, P., Yan, Z., Xu, L., Mazza, M. G., Buldyrev, S.V., Chen, S.-H., Sastry S. & Stanley, H. E. (2006) Glass Transition in Biomolecules and the Liquid-Liquid Critical Point of Water, *Phys. Rev. Lett.* Vol. 97: 177802-4.
- Laasonen, K., Sprik, M., Parrinello, M. & Car, R. (1993) 'Ab initio' liquid water, *J. Chem. Phys.* Vol. 99: 9080-9089.
- Lasave, J., Koval, S., Dalal N. S. & Migoni R. L. (2005) Slater and Takagi defects in  $\text{KH}_2\text{PO}_4$  from first principles, *Phys. Rev. Lett. B* Vol. 72: 104104-8.
- Lee, C., Yang, W. & Parr, R. G. (1988) Development of the Colle-Salvetti correlation-energy formula into a functional of the electron density, *Rhys. Rev. B* Vol. 37: 785-789.
- Mahanta, S., Singh, R. B., Kar, S. & Guchhait, N. (2008) Evidence of coupled photoinduced proton transfer and intramolecular charge transfer reaction in para-N,N-dimethylamino orthohydroxy benzaldehyde: Spectroscopic and theoretical studies, *Chemical Physics* Vol. 354: 118-129.
- Marechal, Y. (2007). *The Hydrogen Bond and the Water Molecule*, Elsevier, Amsterdam.
- Mishima, O. & Stanley, H. E. (1998) The relationship between liquid, supercooled and glassy water, *nature* Vol. 396: 329-335.
- Nishikawa, K. & Iijima, T. (1984) Corrections for Intensity Data in Energy-dispersive X-Ray Diffractometry of Liquids. Application to Carbon Tetrachloride, *Bull. Chem. Soc. Jpn.* Vol. 57: 1750-1759.
- Paul, A., Mandal, P.K. & Samanta A. (2005) How transparent are the imidazolium ionic liquids? A case study with 1-methyl-3-butylimidazolium hexafluorophosphate, [bmim][PF<sub>6</sub>], *Chem. Phys. Lett.* Vol. 402: 375-379.
- Salanne, M., Simon, C., Turq, P. & Madden, P. A. (2008) Intermediate range chemical ordering of cations in simple molten alkali halides, *J. Phys.: Condens. Matter* Vol. 20: 2101-5.
- Salzmann, C. G., Radaelli, P. G., Mayer, E. & Finney, J. L. (2009) Ice XV: A New Thermodynamically Stable Phase of Ice, *Phys. Rev. Lett.* Vol. 103: 105701-4.
- Sato, T., Masuda, G. & Takagi, K. (2004) Electrochemical properties of novel ionic liquids for electric double layer capacitor applications, *Electrochim. Acta* Vol. 49: 3603-3611.
- Satoh, T., Goldfarb, R. B. & Patton, C. E. (1978) Exchange-anisotropy field in disordered nickel-manganese alloys, *J. Appl. Phys.* Vol. 49: 3439-3453.
- Stanley H. E. (1971) *Introduction to phase Transition and Critical Phenomena*, Oxford University Press.
- Takekiyo, T., Yoshimura, Y., Imai, Y. & H. Abe, in preparation.
- Triolo, A., Russina, O., Bleif, H-J. & Cola, E. D. (2007) Nanoscale Segregation in Room Temperature Ionic Liquids, *J. Phys. Chem. B* Vol. 111: 4641-4644.
- Yoshimura, Y., Goto, T., Abe, H. & Imai, Y. (2009) Existence of Nearly-Free Hydrogen Bonds in an Ionic Liquid, N, N-Diethyl-N-methyl-N-(2-methoxyethyl) Ammonium Tetrafluoroborate-Water at 77 K, *J. Phys. Chem. B* Vol. 113: 8091-8095.
- Yoshimura, Y., Kimura, H., Okamoto, C., Miyashita, T., Imai, Y. and H. Abe, (2011) Glass transition behavior of ionic liquid, 1-butyl-3-methylimidazolium tetrabluoroborate- $\text{H}_2\text{O}$  mixed solutions, *J. Chem. Thermodynamics*, in press.
- Wilson, M. & Madden, P. A. (1998) Voids, Layers, and the First Sharp Diffraction Peak in  $\text{ZnCl}_2$ , *Phys. Rev. Lett.* Vol. 80: 532-535, in press.
- Zhang, L., Xu, Z., Wang, Y. & Li, H. (2008) Prediction of the Solvation and Structural Properties of Ionic Liquids in Water by Two-Dimensional Correlation Spectroscopy, *J. Phys. Chem. B* Vol. 112: 6411-6419.

## **Part 2**

### **Physical Simulations (Theory and Modelling)**



# Using Molecular Modelling Tools to Understand the Thermodynamic Behaviour of Ionic Liquids

Lourdes F. Vega<sup>\*1,2</sup>, Oriol Vilaseca<sup>1,2</sup>, Edoardo Valente<sup>1</sup>, Jordi S. Andreu<sup>1,2</sup>,  
Fèlix Llorell<sup>1,2</sup>, and Rosa M. Marcos<sup>3</sup>

<sup>1</sup>*MATGAS Research Center (Carburros Metálicos/Air Products Group, CSIC, UAB),  
Campus de la UAB, 08193 Bellaterra, Barcelona*

<sup>2</sup>*Institut de Ciència de Materials de Barcelona. Consejo Superior de Investigaciones Científicas. ICMA-B-CSIC. Campus de la UAB. 08193 Bellaterra, Barcelona.*

<sup>3</sup>*Departament d'Enginyeria Mecànica. Escola Tècnica Superior d'Enginyeria. Universitat  
Rovira i Virgili. Campus Sescelades. 43007 Tarragona.  
Spain*

## 1. Introduction

Ionic liquids, also known as liquid electrolytes, ionic melts, ionic fluids, liquid salts, or ionic glasses, is a term generally used to refer to salts that form stable liquids. Nowadays it is considered that any organic salt that is liquid below 100°C falls into this category. They are usually formed by a large organic cation combined with an anion of smaller size and more symmetrical shape, although some symmetric cations are also combined with asymmetric anions to form ionic liquids. In spite of their strong charges, their asymmetry frustrates them from being solid below 100°C and this is why they remain liquid at these low temperatures.

These compounds are receiving great attention in recent years due to the fact that their properties can be tuned with a well-judged selection of the cation-anion pair, giving the opportunity to choose among a vast range of different ionic liquids. In addition, these compounds can also be tuned by the modification of the cation and/or the anion molecular structure adding appropriate functional groups in order to obtain ionic liquids with a set of desired physico-chemical properties, which are known as Task Specific Ionic Liquids (TSIL). At present time, hundreds of ionic liquids have been synthesized and there is virtually no limit in the number of possible counterion pairs and mixtures of them that can be obtained. Their tunable and unique properties make them a good alternative to conventional volatile organic compounds (VOCs) used in reaction and separation processes, solvents for cleaning and purification operations, as electrolytes in fuel cells, lubricants, heat transfer fluids and storage media (Brennecke and Maginn, 2001; Yokozeki and Shiflett, 2007; Tempel et al, 2008, Welton, 1999). For instance, understanding carbon dioxide solubility in ionic liquids has become an important issue for supercritical fluid extraction (Blanchard and Brennecke, 2001), gas separations in a supported ionic liquids membranes, alternative to the conventional amine scrubbing operation (Baltus et al., 2005) and in catalytic reactions (Wasserscheid and Keim, 2000). A summary of capabilities and limitations of ionic liquids in

CO<sub>2</sub> based separations respect to a variety of materials is provided in a recent and detailed contribution by Bara and co-authors (Bara et al., 2009).

These ionic liquids should be fully characterized before put into use for a specific application. Given the great amount of possible ionic liquids, and the need for accurate characterization, a good understanding about the dependence of their physico-chemical properties on their microscopic structure is desired in order to enhance the design of new ionic liquids for promising chemical and industrial processes in a systematic and efficient manner.

In spite of their prospective applications in several fields, there is an important gap between the synthesis and characterization of ionic liquids for potential different uses and the small amount of ionic liquids available in the market for industrial applications. This fact was already addressed in a recent report entitled "Accelerating ionic liquid commercialization" (BSC Incorporated Report 2004). Among the barriers identified to be circumvented for the commercialization of ionic liquids, one of them deals with fundamental understanding of compositional structure versus performance: ionic liquid commercialization requires discovery researchers to not only develop fundamental understanding of ionic liquid synthesis and properties, but to impart these liquids with the chemical processing features needed for important industrial applications and markets. Developing an understanding of the reactions that form ionic liquids, ionic liquid chemical and physical properties, mechanisms/functions in catalysis and separation systems, and interactions with other materials (e.g., container vessels) is essential to their usefulness in industrial applications. Since the combinations of ions for potential ionic liquids are virtually infinite, this is a needed but expensive and time-consuming task.

In this sense, modelling tools are excellent candidates to advance in this field, as they are cheap and fast. However, ionic liquids are extremely non-ideal systems, with charged and asymmetric ions and, hence, most classical equations will fail in capturing their physico-chemical properties, unless the specific interactions are taken into account since the inception of the model. It is in this area where molecular modelling tools such as molecular simulations or molecular-based equations of state can play a key role, accelerating the characterization of these systems.

In recent years, some attempts trying to model the solubility of gases in ionic liquids in the framework of equations of state (EoS) and other modelling approaches have been done at different thermodynamic conditions and by different authors. A recent review summarizes most of them, together with their success and remaining challenges (Vega et al., 2010). In this review, the methods were classified according to the "molecular model" used to describe the ionic liquid in the different approaches: classical cubic equations, activity coefficient and group contribution methods, quantum methods and statistical mechanics-based molecular approaches. One of the main advantages of using classical equations of state is that they are straightforward to use and they are present in any process simulator. However, several parameters, temperature and composition dependent, are needed, in most of the cases, to make them readily accessible for ionic liquids calculations. This is due to the fact that, in general, classical equations are missing an important part of the physical nature of ionic liquids. Even if the anion and cation are considered as a neutral pair, they exhibit polarity and hydrogen bonding ability, two facts not taken into account in an explicit manner in cubic EoSs. In addition, a major drawback in the use of cubic EoS is the fact that they require the critical parameters of the ionic liquids, which can only be obtained indirectly and with large uncertainties. This fact limits the predictive ability of these equations, and they are used for correlation purposes.



A step forward in modelling is provided by the use of activity coefficient models and group contribution methods. One of the most valuable features of these methods is their applicability to multi-component systems under the assumption that local compositions can be described in this case by a relationship similar to that obtained for binary systems. However, one of the main disadvantages of these methods is that they depend on an extremely large amount of experimental data. Furthermore, the absence of the volume and surface parameters poses a hindrance in the calculation of the binary interaction parameters for UNIQUAC and UNIFAC models. These limitations can be overcome by the use of quantum-based models, such as COSMO-RS (see, for instance, the works of Shah et al., (2002) and of Guo et al. (2007)). In this method no experimental data is needed as an input to model the ionic liquids, being the main constraint the extensive computational time and also that, in some cases, the comparison with experimental data is only qualitative.

Some molecular-based equations of state such as lattice models, chain fluid theories and SAFT-type approaches have also been used to model ionic liquids and their behaviour in mixtures. The advantage of building a model for the molecule describing the physics of the system is related to a major predictive ability, hence enhancing the possibility of extending the range of application of the equation. In the next sections of this chapter, some examples of successful applications and current limitations of the use of one of these tools, the soft-SAFT equation, will be presented and discussed.

In addition to density-temperature and solubility data, transport properties such as viscosity, self diffusion and electric conductivity are particularly important parameters that must be accounted for in the selection of a given ionic liquid for its applications as alternative solvent or conductor. Ionic liquids present relatively high viscosities, normally of the same order of magnitude as oils. This poses a limitation to some of their possible applications. For instance, a low viscosity would be desirable in order to enhance mass transfer in two-phase separation processes with ionic liquids; the relatively long equilibration times in the absorption of gases by ionic liquids are a consequence of the low diffusivity of the solutes on a highly viscous medium (Anthony et al., 2002). The transport properties are also crucial when considering the reaction kinetics in a synthetic process or ion transport in an electrochemical device. Regarding the important role of ionic liquids as reaction media, the significance of transport properties is manifested, among other things, in the fact that chemical reactions can be diffusion limited even for highly soluble molecules (Wasserscheid & Welton, 2003). In fact, most of the current research for the development of new and more useful ionic liquids is focused on the synthesis of products with improved transport properties (low viscosity, high electrical and heat conductivities, etc).

Great advance in the understanding of transport properties of ionic liquids, and the relationship between their structure and the properties, has been done thanks to molecular simulations. The work of several researchers, including Maginn and co-authors (Morrow & Maginn, 2002; Maginn 2009 and references therein), Padua and Canongia-Lopes with co-workers (Lopes et al., 2004; Lopes & Padua 2004; Padua et al., 2007) and Rey-Castro et al. (Rey-Castro & Vega, 2006; Rey-Castro et al., 2007), among others, show good examples of these applications. In addition to these works, see also Bhargava et al. (2008) for an extensive bibliography on molecular simulation studies done in the field. These simulation results have greatly helped in understanding the local structure of ionic liquids, the solubility of some given compounds in them, and their transport properties. Although very useful from this perspective, the vast amount of computational time required to obtain these properties precludes the use of molecular simulations as standard tools to characterize these systems

for screening purposes before selecting an optimum one for a given application. Hence, a combination of molecular simulations for transport properties together with equations of state or models for phase and solubility data remains an excellent alternative for a quick description of the selected ionic liquids.

As an illustration of the capabilities of modelling tools for understanding ionic liquids we present in the next sections some examples concerning their characterization within two different and complementary approaches: (1) the soft-SAFT equation of state (Blas & Vega, 1997), used to predict the solubility of several compounds in different families of alkyl-imidazolium ionic liquids, as well as interfacial properties, and (2) classical molecular dynamic simulations, used to study transport properties like self-diffusion, viscosity and electrical conductivity of ionic liquids. These tools help in getting additional insights into the underlying mechanisms governing the behaviour of these systems, which is the basic knowledge needed for a rational design previous to their use.

## 2. soft-SAFT as a tool to model the thermodynamic properties of ionic liquids

### 2.1 The soft-SAFT equation

Several different theoretical approaches, correlations and equations of state (EoS) have been used to model ionic liquids and their behaviour in mixtures. We will highlight here the implementation of one of the most successful approaches for that purpose, the soft-SAFT equation of state. Soft-SAFT belongs to a family of SAFT-based equations in which the chain and association term in the equation come from Wertheim's first order thermodynamic perturbation theory (TPT1) for associating fluids (Wertheim, 1984a; 1984b; 1986a; 1986b).

SAFT provides a framework in which the effects of molecular structure on the thermodynamic properties can be separated and quantified. Hence, non-ideal contributions such as chain length and/or molecular shape, molecular association and polar interactions can be introduced in the development of the equation. An additional advantage of SAFT is that the underlying theory of the equation allows systematic extensions in a well-sounded manner. In this sense, different versions of the equation have been recently extended into several directions:

1. the calculation of second order thermodynamic derivative properties (Colina et al., 2002; Llovel & Vega 2006b; 2007; Llovel et al., 2006; Laffite et al., 2006) and tricritical points (Vega & Blas, 2000)
2. the precise characterization of the critical region of pure fluids and mixtures (Llovel et al., 2004; Llovel & Vega 2006a; 2007) through a crossover treatment based on White's work (White, 2002; Salvino & White, 1992) from the renormalization group theory or through other approaches (Kiselev & Ely, 2000); and
3. the calculation of interfacial vapor-liquid and liquid-liquid properties by coupling the van der Waals density gradient theory to the soft-SAFT equation (Duque et al., 2004; Mejia et al., 2005; Mejia & Vega, 2006; Vilaseca & Vega, 2010) or a density functional theory to the SAFT-VR version (Blas et al., 2001; Gloor et al., 2004; Llovel et al., 2010a).

As other SAFT-type equations, soft-SAFT is written in terms of the total Helmholtz energy of the system. When applied to ionic liquids, the residual Helmholtz energy is written as:

$$a^{res} = a^{ref} + a^{chain} + a^{assoc} + a^{polar} \quad (1)$$

where  $a^{res}$  is the residual Helmholtz free energy density of the system ( $a^{res} = a^{total} - a^{ideal}$ ). The superscripts *ref*, *chain*, *assoc* and *polar* refer to the contributions from the reference term,

the formation of the chain, the association, and the polar interactions, respectively, depending on the system under study.

In soft-SAFT (Blas & Vega, 1997; Blas & Vega, 1998a; 1998b; Pàmies & Vega, 2001) the reference term is a Lennard-Jones (LJ) spherical fluid (a “soft” reference fluid), which accounts for both, the repulsive and attractive interactions of the monomers forming the chain. For the case of mixtures, the same equation is used by applying the van der Waals one-fluid theory, with generalized Lorentz-Berthelot mixing rules:

$$\sigma_{ij} = \eta_{ij} \left( \frac{\sigma_{ii} + \sigma_{jj}}{2} \right) \quad \text{and} \quad \varepsilon_{ij} = \xi_{ij} \left( \varepsilon_{ii} \varepsilon_{jj} \right)^{1/2},$$

where  $\eta_{ij}$  and  $\xi_{ij}$  are the size and energy binary adjustable parameters, respectively. The equation is used in a purely predictive manner from the pure component parameters when  $\eta_{ij}$  and  $\xi_{ij}$  are equal to unity, while values different from unity mean the use of one or two binary parameters, taking into account the differences in size and/or energy of the segments forming the two compounds in the mixture. The parameter  $\xi_{ij}$  is equivalent to  $(1-k_{ij})$  in most EoSs.

The chain and association terms come from Wertheim’s theory (Wertheim 1984a; 1984b; 1986a; 1986b), and they are formally identical in the different versions of SAFT:

$$a^{chain} = \rho k_B T \sum_i x_i (1 - m_i) \ln g_{LJ} \quad (2)$$

$$a^{assoc} = \rho k_B T \sum_i x_i \sum_{\alpha} \left( \ln X_i^{\alpha} - \frac{X_i^{\alpha}}{2} \right) + \frac{M_i}{2} \quad (3)$$

where  $\rho$  is the molecular density,  $T$  is the temperature,  $m$  is the chain length,  $x_i$  is the molar fraction of component  $i$ ,  $k_B$  is the Boltzmann constant and  $g_{LJ}$  is the radial distribution function of a fluid of LJ spheres at density  $\rho_m = m\rho$ , evaluated at the bond length  $\sigma$ .  $M_i$  is the number of associating sites of component  $i$ , and  $X_i^{\alpha}$  the mole fraction of molecules of component  $i$  non bonded at site  $\alpha$ , which accounts for the contributions of all the associating sites in each species (see, for instance, Blas & Vega 1997).

The leading multipolar term for fluids of linear symmetrical molecules, like carbon dioxide, nitrogen, acetylene, etc., is the quadrupole-quadrupole potential (Gubbins & Twu, 1978). An expansion of the Helmholtz free energy density in terms of the perturbed quadrupole-quadrupole potential with the Padé approximation was proposed by Stell et al. (1974):

$$a^{qq} = a_2^{qq} \left( \frac{1}{1 - \frac{a_3^{qq}}{a_2^{qq}}} \right) \quad (4)$$

Expressions for  $a_2^{qq}$  and  $a_3^{qq}$ , the second and third-order perturbation terms, were derived for an arbitrary intermolecular reference potential (Twu et al., 1975). A detailed derivation of these expressions is given elsewhere (Gubbins & Two, 1978). This term in the soft-SAFT EoS involves an additional molecular parameter,  $Q$ , the quadrupolar moment.

In order to calculate interfacial properties, the soft-SAFT equation is extended by coupling it with the Density Gradient Theory (DGT) of van der Waals (van der Waals, 1894; translated by Rowlinson, 1976). Within the context of this theory, the Helmholtz energy density  $a$  of the inhomogeneous fluid is expressed as a function of the mole density and its derivatives with respect to the space coordinates. It is also assumed that the density gradient is small compared to the reciprocal value of the intermolecular distance, thus allowing treating the density and its derivatives as independent variables. Then the function  $a$  is expanded in a Taylor series about  $a_0$ , the Helmholtz free energy density of the homogeneous fluid at the local density  $\rho$  and truncated after the second order term. This series may not converge but, because of the short range of the intermolecular potential, it is assumed to have at least an asymptotic validity (Bongiorno & Davis, 1975). In the absence of an external potential, the expression for the Helmholtz energy of the system  $A$  reads:

$$A = \int \left[ a_0(\rho) + \sum_i \sum_j \frac{1}{2} c_{ij} \nabla \rho_i \nabla \rho_j \right] d^3r \quad (5)$$

where the integration is performed in the entire system volume and  $\rho_i$  is the molar density of component  $i$ . The parameter  $c_{ij}$  for the components  $i$  and  $j$  is known as the influence parameter (Bongiorno & Davis, 1975). In this work we have assumed a constant value for  $c$ , obtained by fitting to experimental data, as previously done in other works (Kahl & Enders 2000; 2002; Vilaseca & Vega, 2010).

DGT also allows obtaining density profiles by the minimization of the total free energy of the system. Considering that the chemical potential of a species remains constant across the interface (Davis & Scriven, 1982), the following Euler-Lagrange equations result from equation (5):

$$\sum_j \nabla \cdot (c_{ij} \nabla \rho_j) - \frac{1}{2} \sum_k \sum_j \frac{\partial c_{kj}}{\partial \rho_i} \nabla \rho_k \cdot \nabla \rho_j = - \frac{\partial \left( a_0(\rho_0) - \sum_i \rho_i \mu_{0i} \right)}{\partial \rho_i} \quad i, j, k = 1, \dots, N \quad (6)$$

where all symbols were previously defined. Equation (6) is mathematically a nonlinear boundary value problem. Details of the various numerical approaches to solve this equation are provided in the work by McCoy & Davis (1979).

The interfacial tension is a macroscopical consequence of the density profile. Considering a planar interface and assuming that the density dependence of the influence parameter can be neglected, an expression that relates the interfacial tension to the square of the density gradient can be derived from equation (6) (Davis & Scriven, 1982):

$$\gamma = \sum_i \sum_j \int_{-\infty}^{\infty} c_{ij} \frac{d\rho_i}{dz} \frac{d\rho_j}{dz} dz = 2 \int_{-\infty}^{\infty} \left[ a_0(\rho) - \sum_i \rho_i \mu_{0i} - p_0 \right] dz \quad (7)$$

where  $\mu_0$  and  $p_0$  are the equilibrium chemical potential and pressure, respectively, and  $z$  is the direction perpendicular to the interface. The approximation  $\partial c_{ij} / \partial \rho = 0$  is supported by the works of McCoy and Davis (1979) and those of Carey et al. (1978a; 1978b; 1980). Further

details on how to obtain the density profiles and interfacial tensions from these expressions can be obtained in the original references and in (Vilaseca & Vega, 2010).

## 2.2 The molecular models of the compounds

In order to use the soft-SAFT EoS for a particular system a molecular model of each compound should be chosen. Based on results obtained from molecular dynamics simulations showing the ion pairing of these systems, Andreu and Vega (2007) modelled the  $[\text{C}_n\text{-mim}][\text{BF}_4]$  and  $[\text{C}_n\text{-mim}][\text{PF}_6]$  families as LJ chains with one associating site in each molecule (see Fig. 1). This model mimics the neutral pairs (anion plus cation) as a single chain molecule with this association site describing the specific interactions because of the charges and the asymmetry. The model has been used to accurately describe the solubility of  $\text{CO}_2$  in ionic liquids (Andreu & Vega, 2007), as well as the absorption of  $\text{BF}_3$  in  $[\text{C}_4\text{-mim}][\text{BF}_4]$  (Vega et al., 2010).

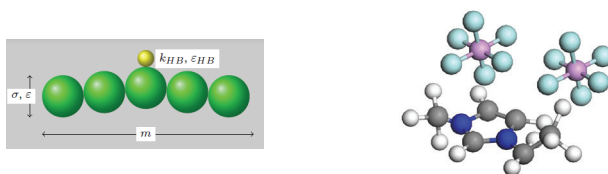


Fig. 1. Schematic representations of the  $[\text{C}_n\text{-mim}][\text{PF}_6]$  ionic liquid. Left: the soft-SAFT simplified model; right: all atom model.

As the delocalization of the anion electric charge due the oxygen groups enhances the possibility of interaction with the surrounding cations, the members of the alkyl-imidazolium- $[\text{Tf}_2\text{N}]$  family are modelled as LJ chains with three associating sites in each molecule instead of one (let's say one "A" site, represented in yellow in Fig. 2, and 2 "B" sites, represented in red in Fig. 2). According to these interactions, we use a site "A" representing the nitrogen atom interactions with the cation and a "B" site representing the delocalized charge due to the oxygen molecules on the anion (Andreu & Vega, 2008). Each type of associating site is identically defined, but only AB interactions between different ionic liquids molecules are allowed in the model, according to the modelled specific interactions on such systems.

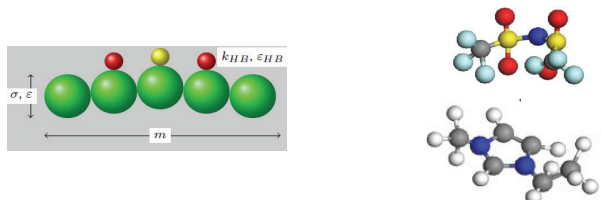


Fig. 2. Schematic representations of the  $[\text{C}_n\text{-mim}][\text{Tf}_2\text{N}]$  ionic liquid. Left: the soft-SAFT simplified model; right: all atom model.

To sum up, in all cases ionic liquids are modelled using five molecular parameters:  $m$ , the chain length,  $\sigma$ , the diameter of the spheres forming the chain,  $\epsilon$ , the energy of interaction between them,  $k_{HB}$ , the volume of association and  $\epsilon_{HB}$ , the association energy. The chain

length, size and energy parameters can be obtained by fitting to available density-temperature data, while the association parameters were transferred from the alkanols (Pàmies, 2003), thus avoiding further fitting.

The carbon dioxide molecule is modelled (Dias et al., 2006; Belkadi et al., 2010) as a LJ chain in which explicit quadrupolar interactions are taken into account. In this case, the molecule is represented by  $m$ ,  $\sigma$ , and  $\epsilon$ , plus two additional parameters: the quadrupolar moment  $Q$  and  $x_p$ , defined as the fraction of segments in the chain that contain the quadrupole. This model has already been used with success to describe the behaviour of  $\text{CO}_2$  on different systems; see for instance the recent work of Belkadi et al. (2010) and references therein.

Alkanol molecules are represented as sites: each site is assigned parameter values to represent a group of atoms in the molecule of interest, such as  $\text{CH}_3$ ,  $\text{CH}_2$  or  $\text{CH}$  groups. In the soft-SAFT approach these molecules are modelled as  $m$  LJ segments of equal diameter,  $\sigma$ , and the same dispersive energy,  $\epsilon$ , bonded to form the chain. The hydroxyl group is mimicked by two square-well sites embedded off-centre in one of the LJ segments, with volume and energy of association  $\kappa_{\text{HB}}$  and  $\epsilon_{\text{HB}}$ , respectively. These two sites are represented by "A" and "B" and only AB association is allowed (Pàmies 2003; Llovel & Vega 2006a).

The water molecules are modelled as a single spherical LJ core with four embedded off-centre square well bonding sites. These four associating sites account for the two electron lone pairs and the two hydrogen sites of the water molecule. They are represented by two "A" sites and two "B" sites, and only AB association is allowed between different molecules. This model has proven to give excellent results for pure water, including interfacial properties (Vilaseca and Vega, 2010) and also for water-hydrocarbon mixtures (Vega et al, 2009).

### 2.3 Results for pure ionic liquids

As an illustration we present here the application of this approach to characterize the  $[\text{C}_n\text{-mim}][\text{Tr}_2\text{N}]$  family. The parameterization was done following the same assumptions as in previous works (Andreu & Vega, 2007; 2008): the molecular parameters  $m$ ,  $\sigma$  and  $\epsilon$  were obtained by fitting to selected experimental density data from literature, while the association parameters were transferred from those of  $[\text{BF}_4]$  and  $[\text{PF}_6]$  imidazolium ionic liquids families. One of the greatest issues when modelling ionic liquids is the scattering in the experimental data found in the literature. Hence, after a detailed comparison with available data, we have used data from Tariq et al. (2010), which includes experimental data for a wide variety of members of the  $[\text{Tr}_2\text{N}]$  family in the whole liquid temperature range at atmospheric pressure. The choice was based on the extended temperature range investigated (from 293 till 473K) and also because of their agreement with other published data. Results for the temperature density diagram are shown in Fig. 3. Note that association parameters are kept constant for the whole family, with values  $\epsilon_{\text{HB}}/k_B = 3450\text{K}$  and  $\kappa_{\text{HB}} = 2250 \text{ \AA}^3$ , respectively. See Llovel et al., (2010b), for more details on the procedure. As it can be observed, excellent agreement is achieved between the theory and the experimental data.  $m$ ,  $\sigma$  and  $\epsilon$  for the  $[\text{C}_n\text{-mim}][\text{Tr}_2\text{N}]$  family correlate with the molecular weight in the following way:

$$m = 0.0056M_w + 3.8337 \quad (8)$$

$$m\sigma^3 = 1.9733M_w + 366.33 (\text{\AA}^3) \quad (9)$$

$$m\epsilon/k_B = 3.3986 M_w + 1043.3 (\text{K}) \quad (10)$$

The correlations were done using the molecular parameters from  $n=2$  till  $n=8$ , both included. The density AAD% for this series of ionic liquids is 0.09%. Using these correlations and keeping constant the volume and energy of association soft-SAFT can be used to predict the behaviour of heavier members of the series (see Fig. 3).

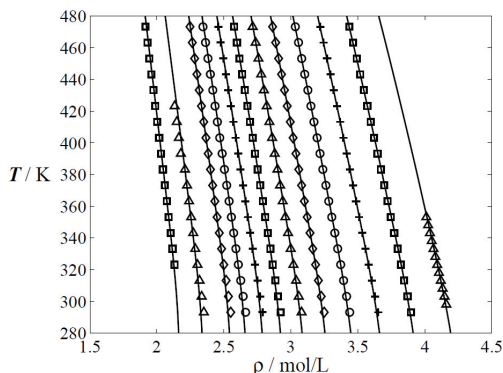


Fig. 3. Temperature-density diagram for the  $[C_n\text{-mim}][\text{Tf}_2\text{N}]$  family, from  $n=1$  (right) to  $n=14$  (left), excepting  $n=11$  and  $n=13$ .  $[C_2\text{-mim}][\text{Tf}_2\text{N}]$  to  $[C_8\text{-mim}][\text{Tf}_2\text{N}]$  compounds were used in the molecular parameters fitting procedure, while the rest of the family is predicted with the molecular parameters correlations (equations (8)-(10)).

The accuracy of the parameters for predicting other properties not included in the fitting procedure has been checked by comparing calculations from the equation with available experimental data on pressure-density. Fig. 4 depicts the diagram for  $[C_2\text{-mim}][\text{Tf}_2\text{N}]$ ,  $[C_4\text{-mim}][\text{Tf}_2\text{N}]$ ,  $[C_6\text{-mim}][\text{Tf}_2\text{N}]$  and  $[C_8\text{-mim}][\text{Tf}_2\text{N}]$  as obtained with soft-SAFT with the parameters previously optimized up to a pressure of 60 MPa. Several isotherms at 293 and 313 K have been plotted and compared to experimental data (Gomes de Azevedo et al., 2005; Gardas et al., 2007). The agreement between the data and the prediction with soft-SAFT is very good, with no loss of accuracy with increasing pressures.

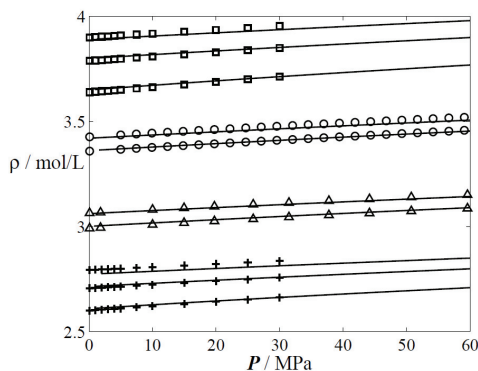


Fig. 4. Pressure-density diagram for  $[C_2\text{-mim}][\text{Tf}_2\text{N}]$  (squares),  $[C_4\text{-mim}][\text{Tf}_2\text{N}]$  (circles),  $[C_6\text{-mim}][\text{Tf}_2\text{N}]$  (triangle up) and  $[C_8\text{-mim}][\text{Tf}_2\text{N}]$  (crosses). Symbols: experimental data (Gomes de Azevedo et al., 2005; Gardas et al., 2007); solid lines: soft-SAFT calculations.

The molecular parameters fitted to single-phase equilibrium data were used in a transferable manner to calculate interfacial properties. The only additional parameter within the soft-SAFT+DGT approach is the influence parameter. In this work we have optimized this parameter for each pure compound using interfacial tension experimental data from the triple to the critical point (Carvalho et al., 2008). The resulting values are given in Table 1.

Compounds	$10^{19}c$ (J m <sup>5</sup> mol <sup>-2</sup> )
[C <sub>2</sub> -mim]-[Tf <sub>2</sub> N]	15.932
[C <sub>3</sub> -mim]-[Tf <sub>2</sub> N]	16.540
[C <sub>4</sub> -mim]-[Tf <sub>2</sub> N]	17.952
[C <sub>5</sub> -mim]-[Tf <sub>2</sub> N]	20.100
[C <sub>6</sub> -mim]-[Tf <sub>2</sub> N]	22.278
[C <sub>7</sub> -mim]-[Tf <sub>2</sub> N]	24.857
[C <sub>8</sub> -mim]-[Tf <sub>2</sub> N]	28.037

Table 1. Optimized influence parameters of the [C<sub>n</sub>-mim][Tf<sub>2</sub>N] ionic liquid family.

Soft-SAFT+DGT results compared to experimental data (Carvalho et al., 2008) are presented in Fig. 5. As in the experimental case a decreasing interfacial tension value with the alkyl chain length is obtained. This behaviour is very surprising as it is contrary to the other chemical families where the interfacial tension increases as the chain length increases.

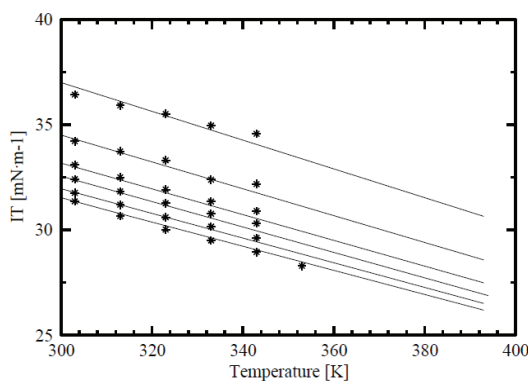


Fig. 5. Vapour-liquid interfacial tensions of the [C<sub>n</sub>-mim][Tf<sub>2</sub>N] ionic liquid family, as a function of temperature, from top to bottom: [C<sub>2</sub>-mim][Tf<sub>2</sub>N], [C<sub>3</sub>-mim][Tf<sub>2</sub>N], [C<sub>4</sub>-mim][Tf<sub>2</sub>N], [C<sub>5</sub>-mim][Tf<sub>2</sub>N], [C<sub>6</sub>-mim][Tf<sub>2</sub>N] and [C<sub>7</sub>-mim][Tf<sub>2</sub>N]. Symbols: experimental data (Carvalho et al., 2008); lines: soft-SAFT+DGT calculations.

## 2.4 Results for mixtures

The solubility of CO<sub>2</sub> in the ionic liquids [C<sub>2</sub>-mim][Tf<sub>2</sub>N], [C<sub>4</sub>-mim][Tf<sub>2</sub>N] and [C<sub>6</sub>-mim][Tf<sub>2</sub>N] over a wide temperature range (313K-453K) was calculated with soft-SAFT and results compared to available experimental data. These calculations were performed from pure component parameters (no mixture parameters adjusted), i.e., the soft-SAFT was used in a predictive manner. As depicted in Fig. 6 the agreement between the theoretical predictions and the experimental data is excellent in all cases, showing the robustness of the



parameters obtained from pure fluid data and of the method of calculation. No specific interactions between  $\text{CO}_2$  and the ionic liquids were considered to obtain these results.

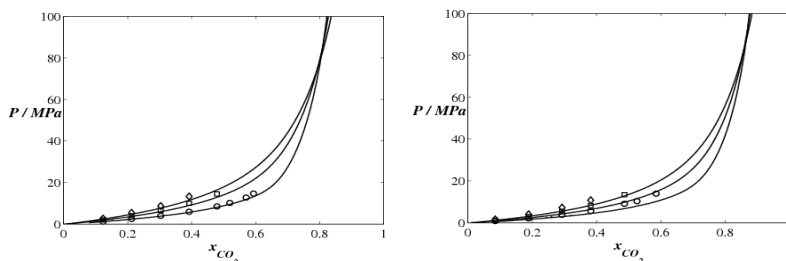


Fig. 6. Prediction of the solubility of  $[\text{C}_2\text{-mim}][\text{Tf}_2\text{N}]$  (left) and  $[\text{C}_4\text{-mim}][\text{Tf}_2\text{N}]$  (right) in  $\text{CO}_2$  at three different temperatures. Symbols experimental data (Raessi & Peters, 2009), lines: soft-SAFT calculations.

The solubility results of methanol and ethanol in  $[\text{C}_4\text{-mim}][\text{Tf}_2\text{N}]$  were also modelled with soft-SAFT. These mixtures are challenging as alcohols are associating molecules with a hydroxyl group that will interact with the ionic liquid with interactions stronger than just van der Waals forces, being also localized in space. Results for these calculations are presented in Fig. 7. Good agreement is found between the soft-SAFT predictions and the measured experimental data (Verevkin, et al., 2005) in the whole range of compositions. It is important to remark that these are pure predictions from the equation. The agreement can be improved by using an adjustable binary parameter, hence losing the predictive power.

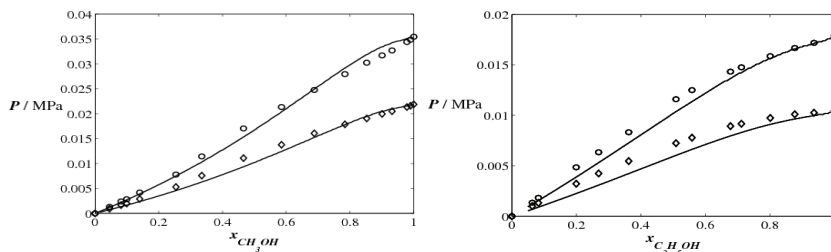


Fig. 7. Solubility of alkanols in  $[\text{C}_4\text{-mim}][\text{Tf}_2\text{N}]$ . Left: Pressure-composition diagram of a methanol +  $[\text{C}_4\text{-mim}][\text{Tf}_2\text{N}]$  mixture at 303K (diamonds) and 313K (squares). Right: Pressure-composition diagram of an ethanol +  $[\text{C}_4\text{-mim}][\text{Tf}_2\text{N}]$  mixture at 303K (diamonds) and 313K (squares). Symbols: experimental data (Verevkin, et al., 2005); lines: soft-SAFT predictions. Cross-associating values are calculated using the Lorentz-Berthelot rules.

The solubility of water in  $[\text{C}_2\text{-mim}][\text{Tf}_2\text{N}]$  at several temperatures is shown in Fig. 8. Vapour-liquid equilibrium diagrams at 292.75K, 303.15K, 323.2K and 353.15K were predicted using the soft-SAFT equation and compared to experimental data (Husson et al., 2010). An excellent agreement is found in the whole range of compositions. A liquid-liquid region has been detected over the constant pressure three-phase-line. Similar results can be seen in the pressure-composition diagram of a water +  $[\text{C}_4\text{-mim}][\text{Tf}_2\text{N}]$  mixture at 353.15K, also shown in Fig. 8, again in very good agreement with the experimental measurements.

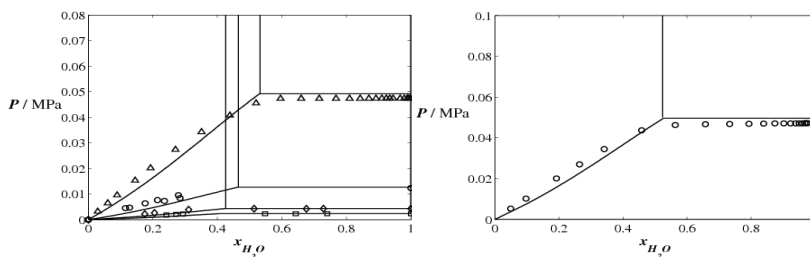


Fig. 8. Solubility of water in [C<sub>n</sub>-mim][Tf<sub>2</sub>N]. Left: Pressure-composition diagram of a water + [C<sub>2</sub>-mim][Tf<sub>2</sub>N] mixture at 292.75K (squares), 303.15K (diamonds), 323.2K (circles) and 353.15K (triangles). Experimental data was taken from reference (Husson et al., 2010). Right: Pressure-composition diagram of a water + [C<sub>4</sub>-mim][Tf<sub>2</sub>N] mixture at 353.15K. Symbols: experimental data (Nebig et al., 2007); lines: soft-SAFT predictions.

### 3. Transport properties of ionic liquids by molecular simulations

#### 3.1 Calculation of the transport coefficients through the Green-Kubo formalism

As stated in the introduction, molecular simulations can be used as complementary tools to characterize ionic liquids from a modelling approach. The transport coefficients can be calculated through the corresponding Green-Kubo relations (Allen & Tildesley, 1987; Frenkel & Smit, 2002). Within this formalism, the self-diffusion coefficient ( $D$ ) of each ion is calculated from its velocity autocorrelation function (vacf) through the following expression:

$$D = \frac{1}{3N} \int \sum_{i=1}^N \langle \vec{v}_i(t_0 + t) \cdot \vec{v}_i(t_0) \rangle dt \quad (11)$$

Here the brackets  $\langle \dots \rangle$  represent the average over all time origins  $t_0$  within the trajectory,  $\vec{v}_i$  represents the velocity of the centre of mass of particle  $i$  at any specific time, and  $t$  is the delay time of the correlation function. The velocity autocorrelation function is a single particle function, and therefore the sum over all molecules in the system as well as the inclusion of the three velocity coordinates improves the statistics in the calculated coefficients (Rey-Castro & Vega, 2006). In practical terms, the upper limit of the integral in equation (11) means that the integral must be calculated up to a point where the autocorrelation function decays to zero. In this work, an empirical exponential decay function has been fitted to the asymptotic part of the running integral in equation (11) in order to extrapolate the diffusion coefficients:

$$D(t) = D + a \cdot \exp(-b \cdot t) \quad (12)$$

where  $D(t)$  is the running integral in equation (11), and  $a$ ,  $b$  are empirical fitting parameters. The shear viscosity ( $\eta$ ) at zero shear rate is calculated from the integral over time of the pressure tensor autocorrelation function following the Green-Kubo relation:

$$\eta = \frac{V}{k_B T} \int_0^\infty \langle P_{\alpha\beta}(t_0 + t) \cdot P_{\alpha\beta}(t_0) \rangle dt \quad (13)$$

The brackets indicate that average must be taken over all time origins  $t_0$ ,  $V$  is the volume of the system,  $T$  is the temperature and  $k_B$  is the Boltzmann constant.  $P_{a\beta}$  denotes the element  $a\beta$  of the pressure tensor. Unlike self-diffusion, the shear viscosity is a collective function; hence, it cannot be statistically improved by averaging over the number of particles in the system. The elements of the pressure tensor are calculated during the simulation using the following expression:

$$P_{a\beta} = \frac{1}{V} \left[ \sum_j m_j v_{aj} v_{\beta j} + \frac{1}{2} \sum_{i \neq j} r_{a ij} f_{\beta ij} \right] \quad (14)$$

where,  $m_j$  is the mass of particle  $j$ ,  $v_j$  is its velocity, while  $r_{ij}$  and  $f_{ij}$  represent the distance and the force between particles  $i$  and  $j$ , respectively. The subscripts  $a$  and  $\beta$  refer to the corresponding components of the vectors.

The electrical conductivity,  $\sigma$ , is calculated as the time integral of the electrical current autocorrelation function:

$$\sigma = \frac{1}{3k_B T V} \int_0^\infty \langle \vec{J}(t_0 + t) \cdot \vec{J}(t_0) \rangle dt \quad (15)$$

where the electrical current  $\vec{J}(t)$  is given by:

$$\vec{J} = \sum_{i=1}^N q_i \vec{v}_i \quad (16)$$

and  $q_i$  represents the charge of ion  $i$ .

Like the shear viscosity, the electrical conductivity is a collective dynamical property, and for this reason suffers from relatively high statistical uncertainty. Again, an exponential decay function was fitted to the long-time behaviour of the integral of the autocorrelation function in order to obtain an extrapolated value of  $\sigma$ .

### 3.2 The molecular models used in the MD simulations

In order to investigate the influence of the molecular structure and temperature in the transport properties of ionic liquids, equilibrium molecular dynamics simulations were performed with two different models for the  $[\text{C}_2\text{-mim}][\text{Cl}]$  ionic liquid, the rigid model of Shim et al. (2005) and the flexible model proposed by Urahata and Ribeiro (2005).

In the rigid model of Shim et al., the united atom representation for the  $\text{CH}_2$  and  $\text{CH}_3$  groups is used. Hence, the cation is represented by a rigid body and its geometry (bond lengths, angles) was taken from experimental x-ray diffraction data obtained from crystals of  $[\text{C}_2\text{-mim}][\text{Br}]$  (Elaiwi et al., 1995). The electrostatic description of the cation consists of fixed partial charges centred on the atoms (Hanke et al., 2001). The interaction potential in the system is represented by a sum of pairwise additive interatomic LJ and Coulombic potentials:

$$U = \sum_{i=1}^{N-1} \sum_{j>1}^N \left\{ U^{\text{LJ}}(r_{ij}) + U^{\text{Coul}}(r_{ij}) \right\} \quad (17)$$

The model of Shim et al., sketched in Fig. 9, is based on the Amber force field for the Lennard-Jones (LJ) parameters of the individual atoms and makes use of the conventional Lorentz-Berthelot combining rules. The chloride atom is represented by a LJ sphere with  $\sigma = 4.4 \text{ \AA}$  and  $\epsilon/k_B = 50.4 \text{ K}$  carrying a unit negative charge. It must be mentioned that there is a relatively large uncertainty in the parameterization of the force field of most of the common anions in ionic liquids, and of chloride ion in particular (Lopes et al., 2004). As far as the cation is concerned, the force field employed here is one of the simplest models found in bibliography (de Andrade et al., 2005), since it does not account for any intramolecular degree of freedom, nor the electronic polarizability of the molecule. Despite this, the model still incorporates basic molecular features of  $[\text{C}_2\text{-mim}][\text{Cl}]$ , such as size, cation asymmetry and charge distribution.

The united atom representation for the  $\text{CH}_2$  and  $\text{CH}_3$  groups is also adopted in the flexible model (Urahata and Ribeiro, 2005), as well as for C-H moieties i.e. hydrogen atoms are not explicitly considered. The cation is therefore described by an 8-site body. The model is sketched in Fig. 9. The interaction potential in the system is represented by two different contributions: the intermolecular and the intramolecular interactions. The intermolecular interactions are represented by two different pairwise additive contributions; a set of interatomic Lennard-Jones potentials between individual united atoms and a Coulombic potential term according to the different partial charges used in the model, also used in the rigid model. In addition to aforementioned intermolecular contributions, the different intramolecular interactions are also taken into account, including bond stretching ( $r$ ), angle bending ( $\theta$ ) and torsion of dihedral angles ( $\psi$ ):

$$U_{\text{intra}} = \sum_{\text{bonds}} k_b (r - r_{eq})^2 + \sum_{\text{angles}} k_\theta (\theta - \theta_{eq})^2 + \sum_{\text{dihedrals}} k_\psi [1 + \cos(m\psi - \delta)] \quad (18)$$

Parameters of the intramolecular interactions were based on the all-atom model of Morrow and Maginn (2002). The LJ parameters were taken from the united model of Shah et al. (2002) and are based on the OPLS force field and makes use of the conventional Lorentz-Berthelot combining rules. The set of partial charges was proposed by Urahata and Ribeiro (2005). This model also assigns negative partial charges to nitrogen atoms, in line with the model of Hanke et al. (2001). The dispersive and electrostatic interactions between atoms belonging to the same dihedral angles were corrected by 0.5 in both cases. The chlorine anion is represented by a sphere carrying a unit negative charge, with LJ parameters from (Rey-Castro et al., 2007).



Fig. 9. Schematic representation of the 1-ethyl-3-methylimidazolium chloride ionic liquid,  $[\text{C}_2\text{-mim}][\text{Cl}]$ , with the rigid model (Shim et al., 2005) (left) and the flexible model (Urahata and Ribeiro, 2005) (right).

### 3.3 Simulation details

The simulated systems with the rigid and the flexible model consisted of cubic boxes with periodic boundary conditions and 125 ion pairs (1500 atoms). The starting configurations were simple cubic regular lattices.

For the rigid model the initial MD simulations were performed in the NPT ensemble (using the Melchionna modification of the Hoover algorithm (Melchionna et al., 1993), first at 1000K, then at 600K, and finally at the desired temperature, at least for 200 ps each stage, keeping an external pressure of 1 bar (Rey-Castro & Vega, 2006). The systems were further equilibrated by velocity rescaling at constant volume and temperature for at least an additional 200 ps interval. Finally, the production runs were obtained in the NVE ensemble. Shear viscosities were obtained from trajectories of 8 ns, for which the components of the stress tensor were recorded in intervals of 20 fs. For the calculation of self-diffusion and conductivity shorter runs (800 ps) were employed, with position and velocity of all particles being recorded every 40 fs. The equations of motion were integrated through the Verlet and Fincham's implicit quaternion algorithms as implemented in the DL\_POLY package (version 2.13) with a constant timestep of 0.002 ps. This timestep provided a good energy conservation with small fluctuations, the relative drift in the total energy being less than  $2 \cdot 10^{-5}$  in 4 ns. The Coulombic interactions were evaluated through the Ewald method using the convergence parameter ( $\alpha$ ) and largest reciprocal space vector ( $k_{max}$ ) that yielded a relative accuracy of  $1 \cdot 10^{-5}$  in the electrostatic energy. The accuracy of the Ewald sum was checked by comparison of the estimated Coulombic energy and the coulombic virial in absolute value.

Some simulation details were different in the case of the flexible model (Andreu & Vega, 2010), given the different nature of the model. The initial configuration was equilibrated at 1000K for 500ps in the NpT ensemble, using the Nose-Hoover algorithm as implemented in DL\_POLY 2.19 package, keeping an external pressure of 1 bar. A set of sequential simulations of 500ps were used in order to obtain the desired starting configurations by decreasing the temperature by 200K at each stage. Previous to the production runs, a 200ps velocity rescaling simulations were performed for each temperature at constant volume. With this procedure, we set up the starting configurations at 6 different temperatures: 323, 350, 400, 450, 500, and 550 K.

The simulation scheme applied for the production runs in the flexible model simulations was the following: for each temperature, we performed a 4ns run in the NpT ensemble. The thermostat and the barostat constants were set to 0.5ps. The equilibrium properties for these simulations were calculated by averaging over the last 3ns. Then, two different sets of production runs in the NVE ensemble were done. The first set was 4ns long and it was used to collect the statistical information for the calculation of the diffusion and conductivity coefficients. A second set of runs with a total of 15ns was used to calculate the viscosity coefficients. The equations of motion were integrated through the Verlet Leapfrog algorithm as implemented in the DL\_POLY 2.19 package. The timestep was set up to 0.002ps for all simulations, providing good energy conservation with small fluctuations, with a relative drift in the total energy being less than  $3 \cdot 10^{-5}$ . The Coulombic interactions were evaluated by the Single Particle Mesh Ewald (SPME) with an accuracy of  $10^{-5}$  in the electrostatic energy. We selected the Ewald SPME method versus the standard Ewald sum due to its better performance when applied to the flexible model, as observed in several test simulations.

For both sets of simulations the real space cut-off for both the Lennard-Jones and the Coulombic interactions were set to 15Å and standard long range corrections to the potential energy and the virial of the system were applied.

For the flexible model simulations two different approaches were used when calculating those properties: the first one was performing the simulations in the NVT ensemble, as has been done in several previous works, even they do not used the Green-Kubo relations the calculation but other statistical equivalent methods, and the second one was by simulating the system in the NVE ensemble, as previously done by some authors (Rey-Castro & Vega, 2006; Rey-Castro et al., 2007).

### 3.4 Flexibility and temperature effect on the transport properties of [C<sub>2</sub>-mim][Cl]

In order to illustrate the use of MD simulations to calculate transport properties of ionic liquids we present results for self-diffusion, electrical conductivity and shear viscosity for the ionic liquid [C<sub>2</sub>-mim][Cl] using a rigid model and a flexible model. This study provides additional insights into important aspects of the physical chemistry of ionic liquids, such as the relevance of cation-anion correlations, or the link between local structure and dynamic behaviour. The comparison with available experimental data provides a reference for the suggestion and validation of molecular force fields of ionic liquids. In addition, as one of the attractive features of the ionic liquids is the extended temperature range of liquid-state behaviour they offer, it is also important to understand the effect of temperature on the various transport properties.

The self-diffusion coefficients at temperatures  $T = 380, 404, 450$  and  $486$  K were calculated from the Green-Kubo relations for the rigid model. The diffusion coefficients of the ions were calculated from the time integrals of the vacf, as explained in the previous subsection. As observed in Fig. 10 this coefficient is larger for the cation than for the anion at all the temperatures studied, in apparent contradiction with its larger size and mass compared with the Cl<sup>-</sup> ion. The fact that the lighter anions have smaller diffusion coefficients has also been observed experimentally, and it has been attributed to the smaller hindrance of the cation motion along the direction perpendicular to the nitrogen atoms on the ring plane.

The diffusion coefficients for the [C<sub>2</sub>-mim][Cl] with the flexible model were obtained from NVT and NVE simulations, at different temperatures within the 323-500K temperature range, just below its decomposition temperature (558K) (Huddleston et al., 2001). The diffusion coefficients were calculated following the same procedure as for the rigid model. The values obtained for the cation diffusion as well as for the anion, are almost one order of magnitude larger than the ones obtained with the rigid model, as shown in Fig. 10.

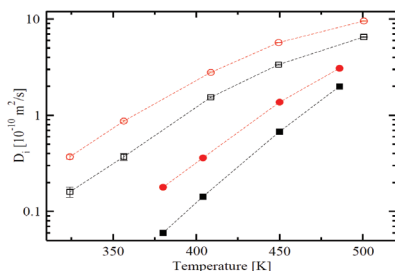


Fig. 10. Diffusion coefficient for the [C<sub>2</sub>-mim]<sup>+</sup> (circles) and Cl<sup>-</sup> (squares) ions calculated by the Green-Kubo relations using the rigid model (full symbols) and the flexible model from the NVE ensemble (open symbols). Results obtained for the flexible model in the NVT ensemble were very similar to the NVE ensemble and are not presented here. The symbols represent MD simulation results while the lines are just guides to the eyes.

Fig. 11 depicts a comparison between simulated and experimental values of the shear viscosity at different temperatures. It is clearly observed that MD simulations performed with the rigid model overestimate this property by ca. one order of magnitude while the flexible model reproduces quite well the experimental data, indicating that flexibility is a key property in a molecular model regarding the viscosity of these ionic liquids.

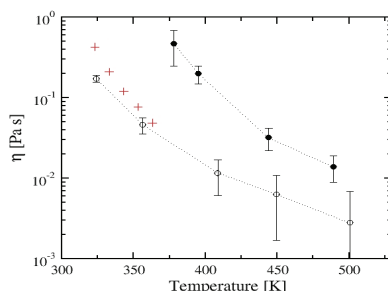


Fig. 11. Shear viscosity for the [C<sub>2</sub>-mim][Cl] ionic liquid at different temperatures. Solid symbols are results obtained by the rigid model, while open symbols are the values from the flexible model, using the Green-Kubo formalism in the NVE simulations. Crosses represent experimental (Earle & Seddon, 2002). The lines are just a guide to the eyes.

The ionic conductivity was also evaluated by the GK approach. However, as the mechanism of charge transport in these systems is related with the process of self-diffusion of the ions it is also possible to relate electric conductivity with the diffusion coefficients of the cation and the anion, known as the Nernst-Einstein relation (NE) (Hansen & McDonald, 1986):

$$\sigma = \frac{e^2}{k_B T} \sum_i \rho_i q_i D_i \quad (19)$$

where  $e$  is the electric charge unit,  $\rho$  and  $q$  are the molar density and charge of the ions, respectively, and  $i$  denotes cation or anion. Deviations from equation (19) are interpreted in terms of cross-correlations among ions. Thus, if the ratio between the experimental value of  $\sigma$  and the conductivity calculated from NE is smaller than unity, then a significant fraction of oppositely charged ions are moving together in the time scale of diffusive motion. The motion of these neutral, short-lived ion clusters contributes therefore to self-diffusion, but not to the net charge transport. The values of the conductivity estimated using the GK relations and the NE relations with the diffusion coefficients obtained from the MD simulations are depicted in Fig. 12. Results obtained with the rigid model show that the molecular model does not lead to a significant overall cross-correlation among ions and, therefore, cation and anion behave as independent ions regarding diffusion and charge transport; however, this is not the case for the flexible model. Results from the NE relation show higher values with deviation becoming more important as the temperature increases, indicating some kind of correlation between ions.

In general, in electrolyte solutions, the conductivity is often found to be inversely proportional to viscosity (Xu et al., 2003), a behaviour that is usually called Walden's rule:

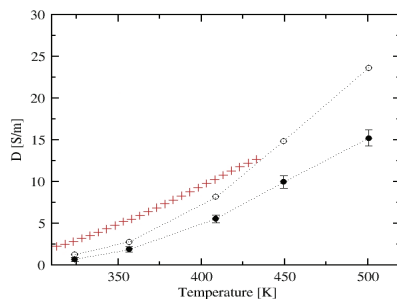


Fig. 12. The ionic conductivity evaluated by the Green-Kubo approach (solid symbols) and by the Nernst-Einstein relation (open symbols). The model used in both cases was the flexible model. Experimental data (crosses) was taken from (Vila et al., 2007).

$$\Lambda \eta = \text{constant} \quad (20)$$

where  $\Lambda$  is the molar conductivity:

$$\Lambda = \frac{\sigma M}{\rho} \quad (21)$$

and  $\sigma$ ,  $M$ ,  $\rho$  are the electrical conductivity ( $\text{S} \cdot \text{m}^{-1}$ ), molecular weight and density, respectively. Ideally, the Walden product is independent of the temperature for a given ionic liquid. It has been found that most ionic liquids fit this linear relationship. Furthermore, the values of the Walden product have been found to be fairly independent of the presence of traces of water (Widegren et al., 2005). However, relatively small to significant variations in the Walden products with temperature have been described in ionic liquids based on alkyl/arenyltrifluoroborate anions (Zhou et al., 2005). The experimental fulfillment of equation (21) indicates that the density of mobile charge carriers in an ionic liquid is strongly correlated with its viscosity.

The application of Walden's rule in the MD simulation results is represented in Fig. 13. A good linear relationship  $\log \Lambda$  vs.  $\log \eta^{-1}$  is obtained, with a slope of 0.9, close to the

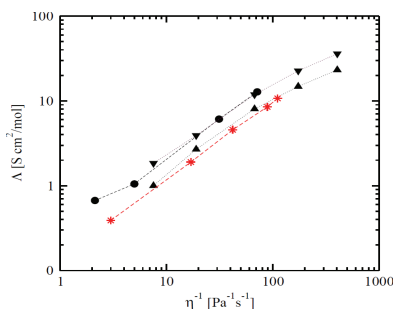


Fig. 13. Walden plot of the molar conductivity and shear viscosity calculated from MD simulations of  $[\text{C}_2\text{-mim}][\text{Cl}]$  at different temperatures. Circles: the rigid model (Rey-Castro & Vega, 2006), triangles up: the flexible model using the GK relations and triangles down: the flexible model and the NE relations (Andreu & Vega, 2010). The red asterisks were calculated from the experimental conductivities (Fannin et al., 1984) and viscosities (Seddon et al. 2002), respectively.



theoretical value of 1, and in excellent agreement with experimental results. Deviations are observed for very low viscosities. The behaviour of the flexible model with properties obtained from the NE relations overlaps with those obtained with the rigid model, while results from the flexible model with transport properties calculated from GK equations are lower and in almost quantitative agreement with the experimental data.

#### 4. Conclusions and future directions

We have presented here an overview and some selected results on the application of two refined and complementary tools for obtaining thermodynamic and transport properties of ionic liquids from a molecular perspective: a molecular-based equation of state (named soft-SAFT) for obtaining PVT data, as well as solubility of gases and mixtures behaviour, and a molecular dynamic procedure to calculate transport properties. In both cases the methods were used in a predictive manner and compared to experimental data in order to assess the validity of the model and to empower them with predictive capabilities for other properties. Concerning the application of soft-SAFT to these systems, it has been shown that a simple model and the appropriate selection of experimental data to obtain the pure component parameters give excellent predictive results for different mixtures. In particular, the procedure was applied to the  $[C_n\text{-mim}][\text{Tf}_2\text{N}]$  family and mixtures of these with other compounds. The molecular parameters obtained from density-temperature data of the pure fluids were tested for pressure-density and interfacial property data, providing quantitative agreement with experimental results. Pure component parameters were also used to predict the solubility of  $\text{CO}_2$  in selected ionic liquids from this family, as well as  $\text{alkanol}+[C_n\text{-mim}][\text{Tf}_2\text{N}]$  and  $\text{water}+[C_n\text{-mim}][\text{Tf}_2\text{N}]$  mixtures, obtaining excellent agreement with experimental data in all cases. Although the results obtained from soft-SAFT are also very encouraging, given the relative simplicity of the model, its predictive power and the agreement obtained with experimental data, the main limitation of the approach is that it considers the anion and cation as a unique molecule. Considering the cation and anion as two independent species will empower the equation with more predictive power.

Regarding transport properties, the aim of this study was to analyze the ability of a simple molecular model of an ionic liquid to describe the behavior of some transport properties as a function of the temperature as well as their mutual relationships, through MD simulations. In addition, the effect of the flexibility on the transport properties was also examined by using two models of the same ionic liquid, a rigid and a flexible one.

The diffusion coefficients, the ionic conductivity and the zero-shear viscosity coefficients of  $[C_2\text{-mim}][\text{Cl}]$  were computed in a wide range of temperatures by using the Green-Kubo formalism and results compared to experimental data. We showed that this approach is suitable when analyzing the properties of this light ionic liquid. The inclusion of the internal degrees of freedom on the cation description is an essential ingredient when the short time scale behaviour of the anion/cation dynamics was analyzed. The model was able to reproduce the experimental measurement of those transport properties in a wide range of temperatures, in closer agreement to experimental data than the rigid model. The simulations reproduce remarkably well the slope of the Walden plots obtained from experimental data of  $[C_2\text{-mim}][\text{Cl}]$ , confirming that temperature does not alter appreciably the extent of ion pairing. However, further studies on the dynamics of relaxation of the solvation shells are suggested in order to corroborate these conclusions. All our results reinforce the importance of including internal degrees of freedom, such as flexibility, for

calculating transport properties. It would also be interesting to explore whether other more refined force fields than the non-polarizable, united atom model used in this work will lead to a different description of the collective dynamics of cations and anions in the melt.

## 5. Acknowledgements

We are very grateful to Carlos Rey-Castro for his contribution to this work. Discussions with Joao A.P. Coutinho and John Prausnitz are also acknowledged. F. Llovel acknowledges a JAE-Doctor fellowship from the Spanish Government. This work has been partially financed by the Spanish government, Ministerio de Ciencia e Innovación, under projects CTQ2008-05370/PPQ, NANOSELECT and CENIT SOST-CO2 CEN2008-01027. Additional support from Carburros Metálicos, Air Products group, and from the Catalan government, under projects SGR2005-00288 and 2009SGR-666, is also acknowledged.

## 6. References

- Allen, M. P. & Tildesley, D. J. (1987). *Computer Simulation of Liquids*; Oxford University Press: New York.
- Andreu, J.S. & Vega, L. F. (2007). Capturing the Solubility Behavior of CO<sub>2</sub> in Ionic Liquids by a Simple Model. *J. Phys. Chem. C* 111, 16028-16034.
- Andreu, J.S. & Vega, L. F. (2008). Modeling the Solubility Behavior of CO<sub>2</sub>, H<sub>2</sub>, and Xe in [Cn-mim][Tf<sub>2</sub>N] Ionic Liquids. *J. Phys. Chem. B* 112, 15398-15406.
- Andreu, J.S. & Vega, L.F. (2010). On the Transport properties of [emim]Cl through the Green Kubo formalism. *Submitted*.
- Anthony, J. L.; Maginn, E. J. & Brennecke, J. F. (2002). Solubilities and Thermodynamic Properties of Gases in the Ionic Liquid 1-n-Butyl-3-methylimidazolium Hexafluorophosphate. *J. Phys. Chem. B*, 106, 7315-7320.
- Baltus, R.E.; Counce, R.M.; Culbertson, B.H. ; Luo, H.; DePaoli, D. W.; Dai, S. & Duckworth, D.C. (2005). Examination of the potential of ionic liquids for gas separations. *Sep. Sci. Technol.* 40, 525.
- Bara, J. E. ; Carlisle, T. K. ; Gabriel, C. J.; Camper, D.; Finotello, A.; Gin, D. L. & Noble, R. (2009). Effects of temperature and anion species on CO<sub>2</sub> permeability and CO<sub>2</sub>/N<sub>2</sub> separation coefficient through ionic liquid membranes. *Ind. Eng. Chem. Res.* 48, 2739-2751.
- Belkadi, A.; HadjKali, M.K.; Llovel, F.; Gerbaud, V. & Vega, L.F. (2010). Soft-SAFT modeling of vapor-liquid equilibria of nitriles and their mixtures. *Fluid Phase Equilib.* 289, 191-200.
- Bhargava B.L.; Balasubramanian, S. & Klein M.L. (2008). Modelling room temperature ionic liquids. *Chem Commun (Camb)*, 29, 3339-3351.
- Blanchard, L.A. & Brennecke, J.F. (2001). Recovery of Organic Products from Ionic Liquids Using Supercritical Carbon Dioxide. *Ind. Eng. Chem. Res.* 40, 287-292.
- Blas, F.J.; del Rio, E.M.; de Miguel, E. & Jackson, G. (2001). An examination of the vapour-liquid interface of associating fluids using a SAFT-DFT approach. *Mol. Phys.* 99, 1851-1865.
- Blas, F.J. & Vega, L.F. (1997). Thermodynamic behaviour of homonuclear and heteronuclear Lennard-Jones chains with association sites from simulation and theory. *Mol. Phys.*, 92, 135-150.

- Blas, F. J.; Vega, L. F. (1998a). Critical behavior and partial miscibility phenomena in binary mixtures of hydrocarbons by the statistical associating fluid theory. *J. Chem. Phys.* 109, 7405-7413.
- Blas, F. J.; Vega, L. F. (1998b). Prediction of Binary and Ternary Diagrams Using the Statistical Associating Fluid Theory (SAFT) Equation of State. *Ind. Eng. Chem. Res.* 1998, 37, 660-674.
- Bongiorno, V. & Davis, H.T. (1975). Modified van der Waals theory of fluids interfaces. *Physical Review A* 12, 2213-2224.
- Brennecke, J.F. & Maginn, E.J. (2001). Ionic Liquids: Innovative Fluids for Chemical Processing. *AIChE J.* 47, 2384-2389.
- BCS Incorporated Report "Accelerating Ionic Liquid Commercialization. Research Needs to Advance New Technology" June 2004, report supported by the Chemical Industry VISION2020 Technology Partnership, the Department of Energy of USA and the American Chemical Society.
- Cadena, C.; Zhao, Q.; Snurr, R. Q. & Maginn, E. J. (2006). Molecular modeling and experimental studies of the thermodynamic and transport properties of pyridinium-based ionic liquids. *J. Phys. Chem. B* 110, 2821-2832.
- Canongia Lopes, J. N. & Padua, A. A. H. (2006). Nanostructural Organization in Ionic Liquids. *J. Phys. Chem. B* 110, 3330-3335.
- Carey, B.S. ; Scriven, L.E. & Davis, H.T. (1978a). Semiempirical theory of surface tensions of pure normal alkanes and alcohols. *AIChE J.* 24, 1076-1080.
- Carey, B.S. ; Scriven, L.E. & Davis, H.T. (1978b). On gradient theories of fluid interfacial stress and structure. *Journal of Chemical Physics* 69, 5040-5049.
- Carey, B.S. ; Scriven, L.E. & Davis, H.T. (1980). Semiempirical theory of surface tensions of binary systems. *AIChE J.* 26, 705-711.
- Carvalho, P. J. ; Freire, M. G.; Marrucho, I. M.; Queimada, A. J. & Coutinho, J. A. P. (2008). Surface Tensions for the 1-Alkyl-3-methylimidazolium Bis(trifluoromethylsulfonyl)imide Ionic Liquids *J. Chem. Eng. Data* 53, 1346-1350.
- Colina, C.M.; Turens, L.F.; Olivera-Fuentes, C.; Gubbins, K.E. & Vega, L.F. (2002). Predictions of the Joule-Thomson Inversion Curve for the n-Alkane Series and Carbon Dioxide from the Soft-SAFT Equation of State. *Ind. Eng. Chem. Res.* 41, 1069-1075.
- de Andrade, J.; Boes, E. S. & Stassen, H. (2005). In *Ionic Liquids IIIA: Fundamentals, Progress, Challenges, and Opportunities, Properties and Structure*; Rogers, R. D., Seddon, K. R., Eds.; American Chemical Society: Washington DC, Vol. 901; pp 118.
- Davis, H.T. & Scriven, L. E. (1982). Stress and structure in fluid phase interfaces. *Advances in Chemical Physics* 49, 357-454.
- Dias, A.M.A.; Carrier, H.; Daridon, J.L.; Pàmies, J.C.; Vega, L.F.; Coutinho, J.A.P. & Marrucho, I.M. (2006). Vapor-Liquid Equilibrium of Carbon Dioxide-Perfluoroalkane Mixtures: Experimental Data and SAFT Modeling. *Ind. Eng. Chem. Res.* 45, 2341-2350.
- Duque, D.; Pàmies, J.C. & Vega, L.F. (2004). Interfacial properties of Lennard-Jones chains by direct simulation and density gradient theory. *J. Chem. Phys.* 121, 11395-11401.
- Earle M. J. & Seddon K. R. (2002). In *Clean Solvents*; American Chemical Society: Washington, DC, p 10-25.

- Elaiwi, A.; Hitchcock, P. B.; Seddon, K. R.; Srinivasan, N.; Tan, Y. M.; Welton, T. & Zora, J. A. (1995). Hydrogen bonding in imidazolium salts and its implications for ambient-temperature halogenoaluminate(III) ionic liquids. *J. Chem. Soc., Dalton Trans.* 3467-3472.
- Fannin, A. A.; Floreani, D. A.; King, L. A.; Landers, J. S.; Piersma, B. J.; Stech, D. J.; Vaughn, R. L.; Wilkes, J. S. & Williams, J. L. (1984). Properties of 1,3-dialkylimidazolium chloride-aluminum chloride ionic liquids. 2. Phase transitions, densities, electrical conductivities, and viscosities. *J. Phys. Chem.* 88, 2614-2621.
- Frenkel, D. & Smit, B. (2002). *Understanding Molecular Simulation. From algorithms to applications*, 2nd ed.; Academic Press.
- Gardas, R. L.; Freire, M. G.; Carvalho, P. J.; Marrucho, I. M.; Fonseca, I. M. A.; Ferreira A. G. M. & Coutinho, J. A. P. (2007). PGT Measurements of Imidazolium-Based Ionic Liquids. *J. Chem. Eng. Data* 52, 1881-1888.
- Gloor, G.J.; Jackson, G.; Blas, F.J.; del Rio, E.M. & de Miguel, E. (2004). An accurate density functional theory for the vapor-liquid interface of associating chain molecules based on the statistical associating fluid theory for potentials of variable range. *J. Chem. Phys.* 121, 12740-12759.
- Gomes de Azevedo R., Esperança J.M.S.S., Szydłowska J., Visak Z.P., Pires P.F., Guedes H.J.R., Rebelo L.P.N., Thermophysical and thermodynamic properties of ionic liquids over an extended pressure range: [bmim][NTf<sub>2</sub>] and [hmim][NTf<sub>2</sub>]. *J. Chem. Thermod.* (2005), 37, 888-899.
- Gubbins, K. E.; Twu, C. H. (1978). Thermodynamics of polyatomic fluid mixtures. I. Theory. *Chem. Eng. Sci.* 33, 863-868
- Guo, Z.; Lue, B.-M.; Thomsen, K.; Meyer, A.S. & Xu, X. (2007). Predictions of flavonoid solubility in ionic liquids by COSMO-RS: experimental verification, structural elucidation, and salvation characterization. *Green Chem.* 9, 1362-1373.
- Hanke, C. G.; Price, S. L. & Lynden-Bell, R. M. (2001). Intermolecular potentials for simulations of liquid imidazolium salts. *Mol. Phys.* 99, 801-809.
- Hansen, J. P. & McDonald, I. R. (1986). *Theory of Simple Liquids*; Academic Press.
- Huddleston, J. G.; Visser, A. E.; Reichert, W. M.; Willauer, H. D.; Broker, G. A. & Rogers, R. D. (2001). Characterization and comparison of hydrophilic and hydrophobic room temperature IL incorporating the imidazolium cation. *Green Chem.* 3, 156-164.
- Husson, P; Pison, L; Jacquemin, J & Gomes, M.F.C. (2010). Influence of water on the carbon dioxide absorption by 1-ethyl-3-methylimidazolium bis(trifluoromethylsulfonyl)amide. *Fluid Phase Equilib.* 294, 98-104.
- Kahl, H. & Enders, S. (2000). Calculation of surface properties of pure fluids using density gradient theory and SAFT-EOS. *Fluid Phase Equilib.* 172, 27-42.
- Kahl, H. & Enders, S. (2002), Interfacial properties of binary mixtures. *Physical Chemistry Chemical Physics* 4, 931-936.
- Kiselev, S.B. & Ely, J.F. (2000). Simplified crossover SAFT equation of state for pure fluids and fluid mixtures. *Fluid Phase Equilib.* 174, 93-113.
- Krummen, M.; Wasserscheid, P.; Gmehling, J. (2002). Measurement of Activity Coefficients at Infinite Dilution in Ionic Liquids Using the Dilutor Technique. *J. Chem. Eng. Data* 47, 1411-1417.

- Lafitte, T.; Bessi eres, D.; Pi eiro, M. M. & Daridon, J.L. (2006). Simultaneous estimation of phase behavior and second-derivative properties using the statistical associating fluid theory with variable range approach. *J. Chem. Phys.* 124, 024509: 1-16.
- Llorell, F.; P amies, J.C. & Vega, L.F. (2004). Thermodynamic properties of Lennard-Jones chain molecules: Renormalization-group corrections to a modified statistical associating fluid theory. *J. Chem. Phys.* 121, 10715-10724.
- Llorell, F. & Vega, L.F. (2006a). Global Fluid Phase Equilibria and Critical Phenomena of Selected Mixtures Using the Crossover Soft-SAFT Equation. *J. Phys. Chem. B* 110, 1350-1362.
- Llorell, F. & Vega, L.F. (2006b). Prediction of Thermodynamic Derivative Properties of Pure Fluids through the Soft-SAFT Equation of State. *J. Phys. Chem. B*, 110, 11427-11437.
- Llorell, F.; Peters, C.J. & Vega, L.F. (2006). Second-order thermodynamic derivative properties of selected mixtures by the soft-SAFT equation of state. *Fluid Phase Equilib.* 248, 115-122.
- Llorell, F. & Vega, L.F. (2007). Phase equilibria, critical behavior and derivative properties of selected n-alkane/n-alkane and n-alkane/1-alkanol mixtures by the crossover soft-SAFT equation of state. *J. Supercrit. Fluids* 41, 204-216.
- Llorell, F.; Galindo, A.; Blas, F.J.; Jackson, G. (2010a). Classical density functional theory for the prediction of the surface tension and interfacial properties of fluids mixtures of chain molecules based on the statistical associating fluid theory for potentials of variable range. *J. Chem. Phys.* 133, 024704: 1-19.
- Llorell, F.; Valente, E.; Vilaseca, O. & Vega, L.F. (2010b). Modelling complex associating mixtures with [Cn-mim][Tf<sub>2</sub>N] Ionic Liquids with the soft-SAFT equation. *Submitted*.
- Lopes, J.N.C.; Deschamps, J. & Padua, A.A.H. (2004). Modeling ionic liquids using a systematic all-atom force field. *J. Phys. Chem. B* 108, 2038-2047.
- Lopes, J. N.C. & Padua, A.A. H. (2004). Molecular force field for ionic liquids composed of triflate or bistriflylimide anions. *J. Phys. Chem. B* 108, 16893-16898.
- Lopes, J.N.C. ; Shimizu, K.; Padua, A.A.H. ; Umebayashi, Y. ; Fukuda, S.; Fujii, K. & Ishiguro, S.I. (2008). A tale of two ions: The conformational landscapes of bis(trifluoromethanesulfonyl)amide and N,N-dialkylpyrrolidinium. *J. Phys. Chem. B* 112, 1465-1472.
- Lopes, J.N.C.; Padua, A.A.H. & Shimizu, K. (2008). Molecular force field for ionic liquids IV: Trialkylimidazolium and alkoxycarbonyl-imidazolium cations; alkylsulfonate and alkylsulfate anions. *J. Phys. Chem. B* 112, 5039-5046.
- Maginn, E.J. (2009). *Atomistic simulation of ionic liquids Reviews in Computational Chemistry* vol 26 Ed. K B Lipkowitz, R Larter and T Cundari 2009 (Hoboken, NJ: Wiley).
- Maginn, E.J. (2009). E. J. Maginn, Molecular simulation of ionic liquids: current status and future opportunities. *J. Phys. Cond. Matter* 21, 373101:1-17.
- McCoy, B.F. & Davis, H.T. (1979). Free-energy theory of inhomogeneous fluids. *Physical Review A* 20, 1201-1207.
- Mej a, A.; P amies, J.C.; Duque, D.; Segura, H. & Vega, L.F. (2005). Phase and interface behaviors in type-I and type-V Lennard-Jones mixtures: Theory and simulations. *J. Chem. Phys.* 123, 034505: 1-10.
- Mej a, A. & Vega, L.F. (2006). Perfect wetting along a three-phase line: Theory and molecular dynamics simulations. *J. Chem. Phys.* 124, 244505: 1-7.

- Melchionna, S.; Ciccotti, G. & Holian, B. L. (1993). Hoover NPT dynamics for systems varying in shape and size. *Mol. Phys.* 78, 533-535.
- Morrow, T. & Maginn, E. J. (2002). Molecular dynamics study of the ionic liquid 1-n-butyl-3-methylimidazolium hexafluorophosphate. *J. Phys. Chem. B* 106, 12807-12813.
- Nebig, S.; Bolts, R. & Gmehling, J. (2007). Measurement of vapor-liquid equilibria (VLE) and excess enthalpies (HE) of binary systems with 1-alkyl-3-methylimidazolium bis(trifluoromethylsulfonyl)imide and prediction of these properties and  $\gamma^\infty$  using modified UNIFAC (Dortmund). *Fluid Phase Equilib.* 258, 168-178.
- Pàmies, J. C. & Vega, L. F. (2001). Vapor-liquid equilibria and critical behavior of heavy n-alkanes using transferable parameters from the soft-SAFT equation of state. *Ind. Eng. Chem. Res.* 40, 2532-2543.
- Pàmies, J.C. (2003). *Bulk and interfacial properties of chain fluids*. Ph.D. Thesis, Universitat Rovira i Virgili, Tarragona, Spain.
- Raeissi, S. & Peters, C. J. (2009). Carbon Dioxide Solubility in the Homologous 1-Alkyl-3-methylimidazolium Bis(trifluoromethylsulfonyl)imide Family. *J. Chem. Eng. Data* 54, 382-386.
- Rey-Castro, C. & Vega, L. F. (2006). Transport properties of the ionic liquid 1-ethyl-3-methylimidazolium chloride from equilibrium molecular dynamics simulation. The effect of temperature. *J. Phys. Chem. B* 110, 14426-14435.
- Rey-Castro, C.; Tormo, A. L. & Vega, L. F. (2007). Effect of the flexibility and the anion in the structural and transport properties of ethyl-methyl-imidazolium ionic liquids. *Fluid Phase Equilib.* 256, 62-69.
- Seddon, K. R.; Stark, A. & Torres, M. J. (2002). In *Clean Solvents: alternative media for chemical reactions and processing*; Abraham, M. A., Moens, L., Eds.; American Chemical Society: Washington DC Vol. 819; pp 34.
- Shah, J.; Brennecke, J. & Maginn, E. J. (2002). Thermodynamic properties of the ionic liquid 1-n-butyl-3-methylimidazolium hexafluorophosphate from Monte Carlo simulations. *Green Chem.* 4, 112-118.
- Shah, J. K. & Maginn, E. J. (2004). A Monte Carlo simulation study of the ionic liquid 1-n-butyl-3-methylimidazolium hexafluorophosphate: liquid structure, volumetric properties and infinite dilution solution thermodynamics of CO<sub>2</sub>. *Fluid Phase Equilib.* 222, 195-203.
- Shah, J. & Maginn, E. J. (2005). Monte Carlo simulations of gas solubility in the ionic liquid 1-n-butyl-3-methylimidazolium hexafluorophosphate. *J. Phys. Chem. B* 109, 10395-10405.
- Shim, Y.; Choi, M. Y. & Kim, H. J. (2005). A molecular dynamics computer simulation study of room-temperature ionic liquids. I. Equilibrium solvation structure and free energetic. *J. Chem. Phys.* 122, 044510 (12 pages).
- Stell, G.; Rasaiah, J. C.; Narang, H. (1974). Thermodynamic perturbation-theory for simple polar fluids. 2. *Mol. Phys.* 27, 1393-1414.
- Tariq, M.; Serro, A. P.; Mata, J. L.; Saramago, B.; Esperança, J. M. S. S.; Canongia Lopes, J. N. & Rebelo, L. P. N. (2010). High-temperature surface tension and density measurements of 1-alkyl-3-methylimidazolium bistriflamide ionic liquids. *Fluid Phase Equilib.* 294, 131-138.

- Temple, D.J. ; Henderson, P.B. ; Brzozowski, J.R. ; Pearlstein, R.M. & Cheng, H. (2008). High Gas Storage Capacities for Ionic Liquids through Chemical Complexation. *J. Am. Chem. Soc.*, 130, 400-401.
- Twu, C.H.; Gubbins, K.E. and Gray, C.G. (1975). Excess Thermodynamic Properties for Liquid Mixtures of Non-Spherical Molecules. *Molecular Physics*, 29, 713-729.
- Urahata, S. M. & Ribeiro, M. C. C. (2005). Single particle dynamics in ionic liquids of 1-alkyl-3-methylimidazolium cations. *J. Chem. Phys.* 122, 024511.
- van der Waals, J. D. (1894). Thermodynamische Theorie der Kapillarität unter voraussetzung stetiger Dichteänderung. *Zeitschrift für Physikalische Chemie*-Leipzig 13, 657-725.
- van der Waals, J. D. (1976). The thermodynamic theory of capillarity under the hypothesis of a continuous density variation. Translated by J.S. Rowlinson. *Journal of Statistical Physics* 20, 197-244.
- Vega, L. F. & Blas, F. J. (2000). Tricritical phenomena in chainlike mixtures from a molecular-based equation of state. *Fluid Phase Equilib.* 171, 91-104.
- Vega, L.F.; Llovel, F. & Blas, F. J. (2009). Capturing the Solubility Minima of n-Alkanes in Water by Soft-SAFT. *J. Phys. Chem. B* 113, 7621-7630.
- Vega, L.F.; Vilaseca, O.; Llovel, F. & Andreu, J.S. (2010). Modeling ionic liquids and the solubility of gases in them: Recent advances and perspectives. *Fluid Phase Equilib.* 294, 15-30.
- Verevkin, S. P.; Safarov, J; Bich, E.; Hassel, E. & Heintz, A. (2005). Thermodynamic properties of mixtures containing ionic liquids: Vapor pressures and activity coefficients of n-alcohols and benzene in binary mixtures with 1-methyl-3-butyl-imidazolium bis(trifluoromethyl-sulfonyl) imide. *Fluid Phase Equilib.* 236, 222-228.
- Vila, J.; Varela, L. M. & Cabeza, O. (2007). Cation and anion sizes influence in the temperature dependence of the electrical conductivity in nine imidazolium based ionic liquids. *Electrochim Acta* 52, 7413-7417.
- Vilaseca, O. & Vega, L.F. (2010). Direct calculation of interfacial properties of fluids close to the critical region by a molecular-based equation of state. *Fluid Phase Equilib.* doi:10.1016/j.fluid.2010.09.018.
- Wasserscheid, P. & Keim, W. (2000). Ionic liquids-new "solution" for transition metal catalysis. *Angew. Chem. Int. Ed. Engl.* 39, 3772-3789.
- Wasserscheid, P. & Welton, T. (eds) (2003) *Front Matter and Index, in Ionic Liquids in Synthesis*, Wiley-VCH Verlag GmbH & Co. KGaA, Weinheim, FRG. ISBN: 9783527305155.
- Welton, T. (1999). Room-Temperature Ionic Liquids. Solvents for Synthesis and Catalysis. *Chem. Rev.* 99, 2071-2084.
- Wertheim, M. S. (1984a) Fluids with Highly Directional Attractive Forces. 1. Statistical Thermodynamics. *J. Stat. Phys.* 35, 19-34.
- Wertheim, M. S. (1984b). Fluids with Highly Directional Attractive Forces. 2. Thermodynamic Perturbation Theory and Integral Equations. *J. Stat. Phys.* 35, 35-47.
- Wertheim, M. S. (1986a). Fluids with Highly Directional Attractive Forces. 3. Multiple Attraction Sites. *J. Stat. Phys.* 42, 459-476.
- Wertheim, M. S. (1986b). Fluids with Highly Directional Attractive Forces. 4. Equilibrium Polymerization. *J. Stat. Phys.* 42, 477-492.

- Widegren, J. A.; Saurer, E. M.; Marsh, K. N. & Magee, J. W. (2005). Electrolytic conductivity of four imidazolium-based room-temperature ionic liquids and the effect of a water impurity. *J. Chem. Thermodyn.* 37, 569-575.
- Xiaoyan J. & Adidharma H. (2009). Thermodynamic modeling of ionic liquid density with heterosegmented statistical associating fluid theory. *Chem. Eng. Science* 64, 1985-1992.
- Xu, W.; Cooper, E. I. & Angell, C. A. (2003). Ionic Liquids: Ion Mobilities, Glass Temperatures, and Fragilities. *J. Phys. Chem. B* 107, 6170-6178.
- Yokozeki, A. & Shiflett, M.B. (2007). Hydrogen purification using room-temperature ionic liquids. *Apply. Energ.* 84, 351-361.
- Zhou, Z. B.; Matsumoto, H. & Tatsumi, K. (2005). Structure and Properties of New Ionic Liquids Based on Alkyl- and Alkenyltrifluoroborates. *ChemPhysChem* 6, 1324-1332.



# Self-Consistent Mean-Field Theory for Room-Temperature Ionic Liquids

Yansen Lauw<sup>1</sup> and Frans Leermakers<sup>2</sup>

<sup>1</sup>*CSIRO Process Science and Engineering, Bayview Avenue, Clayton South, Victoria 3169*

*Bragg Institute, ANSTO, PMB 1, Menai, NSW 2234*

<sup>2</sup>*Laboratory of Physical Chemistry and Colloid Science, Wageningen University,  
Dreijenplein 6, Wageningen 6700 EK*

<sup>1</sup>*Australia*

<sup>2</sup>*The Netherlands*

## 1. Introduction

Research in room-temperature ionic liquids (RTILs) has exploded in the last two decades, which are marked by an exponential increase in the number of theoretical and experimental publications in this field. The typically good thermal stability, ionic conductivity, and solvability of RTILs make them superior electrolytes in many electrochemical applications, such as metal electrodeposition and energy storage.(Armand et al., 2009; Endres et al., 2008; Ohno, 2005; Simon & Gogotsi, 2008) The efficiency of RTILs in such applications is determined by a number of factors, one of which is the relationship between the interfacial structure of RTILs and their electrochemical properties. The use of RTILs as solvents in supercapacitors is of particular interest since they can generate significant electrical double-layer (EDL) capacitance due to the formation of thin layer of ions on an Angstrom-scale at RTIL-electrode interfaces.(Atkin & Warr, 2007; Baldelli, 2008; Horn et al., 1988; Mezger et al., 2008; 2009; Rivera-Rubero & Baldelli, 2004; Santos et al., 2006; Yuan et al., 2010) The formation of ultra thin EDL is mainly caused by the absence of any solvation shells around RTILs, which also enhances the accessibility of ions to penetrate nanoporous electrodes, thus increasing their useability in electrochemical applications.(Chmiola et al., 2008; Largeot et al., 2008)

The precise form of EDL structure in RTILs has been a point of argument recently. Experimental results from the sum frequency generation spectroscopy suggest a monolayer of ion formed at the interface.(Baldelli, 2008; Rivera-Rubero & Baldelli, 2004) However, a similar study using the surface force apparatus,(Horn et al., 1988) atomic force microscopy,(Atkin & Warr, 2007; Atkin et al., 2009) and x-ray reflectometry (Mezger et al., 2009) indicate that an alternating layer of ions is instead present. Analytical and numerical models also predict the formation of alternating layer of counterions and coions on polar surfaces due to strong steric and electrostatic correlations in RTILs.(Fedorov & Kornyshev, 2008; Feng et al., 2009; Kornyshev, 2007; Lauw et al., 2009; 2010; Oldham, 2008; Reed et al., 2008) Such an alternating layer typically occurs through the so-called charge overcompensation/overscreening mechanism when the electrostatic screening length is practically less than the size of the ion.(Outhwaite et al., 1980; Parsons, 1990; Stillinger & Kirkwood, 1960) In the highly charged system like RTILs, the charge overcompensation

understandably occurs since the ions are rather bulky. At the RTIL-electrode interface, the surface charge would be overscreened by counterions in the Helmholtz layer and the resulting net charge would be further overcompensated by coions in the subsequent layer, and so on.

The formation of the EDL in RTILs at charged interfaces can induce a large electrostatic potential field ( $\sim 10^9$  V/m), which would greatly influence the rate of electrochemical reactions at the interface and the overall EDL capacitance values. In general, the EDL capacitance reflects the extent to which the electrostatic potential at the interface is screened by the ions that accumulate there. A better screening is reflected by a higher capacitance value. This parameter contains a valuable information on the thickness of the EDL and the composition and polarization of ions at the interface. A correct analysis of the shape of the EDL capacitance curve in RTILs requires an *a priori* knowledge on the EDL structure as a function of the electrostatic potential field. Analytical model to study the relationship between the EDL structure and capacitance in RTILs has been carried out (Kornyshev, 2007; Oldham, 2008) using Poisson-Fermi equation to model spherical ions with certain excluded volume.(Bazant et al., 2009; Bikerman, 1942; Freise, 1952; Kilic et al., 2007) A similar study has been done using numerical model, such as molecular dynamic simulations,(Fedorov & Kornyshev, 2008; Feng et al., 2009) Monte Carlo simulations,(Trulsson et al., 2010) and the self-consistent mean-field theory (SCMFT).(Lauw et al., 2009; 2010) Numerical modelling techniques are generally more realistic to model RTILs than existing analytical approaches due to their ability to accommodate internal degree of freedoms in RTILs and complicated (non-spherosymmetrical) structures of RTILs. These aspects are typically not accessible in analytical models.

This chapter describes the use of SCMFT to predict the structure of RTILs at electrified interfaces and the corresponding EDL capacitance. Special attention is paid to study the effect of ion-size and specific (non-electrostatic) adsorption of ions on the shape of the EDL capacitance curve. Results from this study is used to shed light on the unusual shape of the differential capacitance curve in RTILs observed in experiments. In general, the capacitance curve in RTILs has a shape of inverse parabola or a camel-like with two maxima around the point of zero charge (pzc),(Alam et al., 2007; 2008; Lockett et al., 2008) which are in contrast to the parabola-shaped capacitance curve typically found in aqueous electrolytes.

In SCMFT, the EDL capacitance is studied based on a detailed molecular model of RTILs and the use of local (effective) dielectric constant. Each ion is modelled as a freely-jointed chain of segments. The local polarization is implemented by assigning a higher relative permittivity to polar (more conductive) components in RTILs and a lower value to less polar (less conductive) components. The effective relative permittivity, which depends on the local distribution of the polar and apolar components, is thus higher at the surface than in the bulk since the polar components of the counterion are accumulated on the electrode's surface. This is the opposite trend to the one typically found in aqueous electrolytes,(James & Healy, 1972; Teschke & de Souza, 1999) in which the ion polarizability is known to decrease in high electrostatic fields. Details of the SCMFT used to model RTILs at electrified interface are given in the following section.

## 2. Self-consistent mean-field theory

The SCMFT is a molecular modelling technique used to study physical and thermodynamic properties of systems at equilibrium.(Fleer et al., 1993; Leermakers et al., 2005) It has been successfully implemented in the past to predict the equilibrium structure in polymeric systems.(Claessens et al., 2004; Lauw et al., 2008; Lauw, 2009; Leermakers et al., 2003; Matsen,

1995; Thompson et al., 2001) Here, it is used to study RTILs by considering a grand canonical ensemble of small systems, in which each system consists of cations and anions adjacent to an electrified solid surface. A periodic boundary condition is applied to all sides perpendicular to the surface and a Neumann boundary condition on the side opposite to the surface to reflect bulk properties. Each ion is modelled as a chain of charged and uncharged segments which formed a tetramer, as shown in Fig. 1. This implies that the charged group is situated at the center and the uncharged segments are located at the arms of the tetramer. For the cation, the positively charged segment  $P$  is surrounded by four arms, where each arm is composed of  $n_A$  neutral segments  $A$ . For the anion, the negatively charged segment  $N$  is also surrounded by four arms, comprising  $n_B$  neutral segments  $B$  per arm. Each segment is identified by its ranking number  $s$ , which marks the position of the segment in the tetramer. The density of each segment at any points  $\mathbf{r}$  in the system is quantified by its local volume fraction  $\varphi(\mathbf{r})$ . This relatively simple molecular model is a representation of typical RTILs with a similar ion-size and a well-hidden charged group.

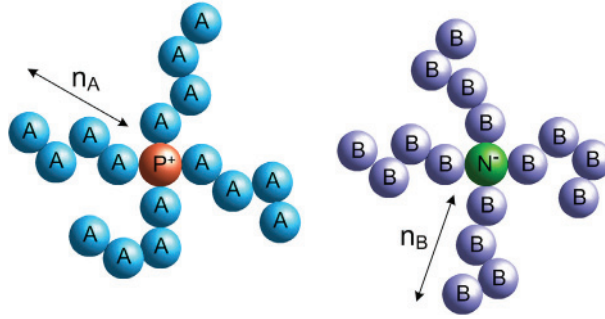


Fig. 1. Schematic of the tetrameric cation (left) and anion (right) used in the SCMFT.

In SCMFT, the total free energy ( $F_{total}$ ) of a small system is expressed as a sum of its enthalpic, entropic, and electrostatic components,

$$F_{total} = F_{enthalpy} + F_{entropy} + F_{electrostatic} \quad (1)$$

The enthalpic part of the free energy reads,

$$\frac{F_{enthalpy}}{k_B T} = \int \left[ \frac{1}{2} \sum_{i,j} \chi_{ij} \varphi_i(\mathbf{r}) \varphi_j(\mathbf{r}) + \delta(\mathbf{r} - \mathbf{r}_S) \sum_i \chi_{iS} \varphi_i(\mathbf{r}) \right] d\mathbf{r} \quad (2)$$

where the first term is the mixing enthalpy based on the Flory-Huggins formulation, (Flory, 1953) and the second term is originated from the specific adsorption. The indices  $i$  and  $j$  refer to the segment type in the cation and anion, i.e.,  $\{i, j\} \in \{A, P, B, N\}$ ; the index  $S$  represents the electrode's surface;  $\chi_{ij}$  is the Flory-Huggins interaction parameter between segment- $i$  and  $-j$ ;  $\varphi_i(\mathbf{r})$  and  $\varphi_j(\mathbf{r})$  are the volume fraction of segment- $i$  and  $-j$  at point  $\mathbf{r}$  in the system;  $\delta(\mathbf{r} - \mathbf{r}_S)$  is the Dirac delta function at  $\mathbf{r} = \mathbf{r}_S$ , where  $\mathbf{r}_S$  is the position of the electrode's surface;  $\chi_{iS}$  is the interaction parameter between segment- $i$  and the surface. A more positive  $\chi_{iS}$  indicates a more repulsion between segment- $i$  and the electrode's surface, and alternatively, a more negative  $\chi_{iS}$  means segment- $i$  has a stronger affinity towards the surface.

The entropic contribution to the total free energy is expressed as a sum of the translational entropy of the cation and anion, local mean-field interactions, and the additional term due to the incompressibility constraint of the system,

$$\begin{aligned} \frac{F_{entropy}}{k_B T} = & \frac{Vf_+}{N_+} \ln \left( \frac{Vf_+}{N_+ Q_+} \right) + \frac{Vf_-}{N_-} \ln \left( \frac{Vf_-}{N_- Q_-} \right) \\ & - \int \left[ \sum_i w_i(\mathbf{r}) \varphi_i(\mathbf{r}) + \lambda(\mathbf{r}) \left( 1 - \sum_i \varphi_i(\mathbf{r}) \right) \right] d\mathbf{r} \end{aligned} \quad (3)$$

In Equation 3, the volume of the system is denoted by  $V$ ; the indices  $+$  and  $-$  represent the cation and anion, respectively;  $f_+$  and  $f_-$  are the total (volume) fraction of the cation and anion;  $N_+$  and  $N_-$  are the total number of segments in the cation and anion;  $Q_+$  and  $Q_-$  are the so-called partition function of the cation and anion;  $w_i(\mathbf{r})$  is the potential of mean-force of segment- $i$  at  $\mathbf{r}$  and  $\lambda(\mathbf{r})$  is the Lagrange multiplier at  $\mathbf{r}$ .

The electrostatic contribution to the free energy is expressed as a sum of all Coulombic interactions in the system as follows,

$$\frac{F_{electrostatic}}{k_B T} = -\frac{1}{2} \int \sum_i e v_i \varphi_i(\mathbf{r}) \psi(\mathbf{r}) d\mathbf{r} \quad (4)$$

where  $v_i$  is the valence of segment- $i$  and  $\psi(\mathbf{r})$  is the electrostatic potential at  $\mathbf{r}$ .

The total free energy  $F_{total}$  is extremized with respect to the order parameters ( $w_i(\mathbf{r})$  and  $\varphi_i(\mathbf{r})$ ), subject to the incompressibility constraint  $\sum_i \varphi_i(\mathbf{r}) = 1$  at all  $\mathbf{r}$ . The results is a set of governing equations described in details below.

For the cation, the volume fraction of each segment is determined by the corresponding segment-weighting factor  $q_+(\mathbf{r}, s)$  and its complementary factor  $q'_+(\mathbf{r}, s)$ . They quantify the probability to find a given segment in the cation with a ranking number  $s$  at point  $\mathbf{r}$  in the system. The segment-weighting factor  $q_+(\mathbf{r}, s)$  is calculated from the open-end of the arm towards the center of the tetramer, whereas the complementary segment-weighting factor  $q'_+(\mathbf{r}, s)$  is calculated from the center of the tetramer towards the open-end of the arm. The overall connectivity of segments is governed by the Edwards diffusion equation, (Edwards, 1965)

$$\frac{\partial q(\mathbf{r}, s)}{\partial s} = \frac{a^2}{6} \nabla^2 q(\mathbf{r}, s) - \delta_{i_+, s} w_{i_+}(\mathbf{r}) q(\mathbf{r}, s) \quad (5)$$

where  $q(\mathbf{r}, s)$  refers to either  $q_+(\mathbf{r}, s)$  or  $q'_+(\mathbf{r}, s)$ ,  $a$  is the size of the segment,  $\delta_{i_+, s}$  is a Kronecker delta that equals to one if the segment-ranking number  $s$  of the cation is of type  $i_+ \in \{A, P\}$  and zero otherwise. Equation 5 is solved numerically subject to the initial and boundary conditions of the system. Since the open-end of the arm is occupied by an uncharged segment  $A$  and the center of the tetramer by the charged segment  $P$ , the initial condition at the open-end is  $q_+(\mathbf{r}, s_0) = \exp(-w_A(\mathbf{r}))$ , whereas the initial condition at the center is  $q'_+(\mathbf{r}, s_0) = [q_+(\mathbf{r}, s_{n_A})]^3$ . The volume fraction  $\varphi_{i_+}(\mathbf{r})$  of segment- $i_+$  in the cation is calculated from the convolution of  $q_+(\mathbf{r}, s)$  and its complementary value  $q'_+(\mathbf{r}, s)$ ,

$$\varphi_{i_+}(\mathbf{r}) = \frac{Vf_+}{N_+ Q_+} \int_0^{N_+} \delta_{i_+, s} q_+(\mathbf{r}, s) q'_+(\mathbf{r}, s) ds \quad (6)$$

in which  $Q_+ = \int q_+(\mathbf{r}, s) q'_+(\mathbf{r}, s) d\mathbf{r}$  is the partition function of the cation, which is independent to the segment-ranking number.

For the anion, the volume fraction of segment- $i_-$ , where  $i_- \in \{B, N\}$ , is calculated in a similar manner as its cation counterpart. The corresponding diffusion equation for the chain connectivity of segments in the anion is,

$$\frac{\partial q(\mathbf{r}, s)}{\partial s} = \frac{a^2}{6} \nabla^2 q(\mathbf{r}, s) - \delta_{i_-, s} w_{i_-}(\mathbf{r}) q(\mathbf{r}, s) \quad (7)$$

where  $q(\mathbf{r}, s)$  now refers to either  $q_-(\mathbf{r}, s)$  or  $q'_-(\mathbf{r}, s)$ , and  $\delta_{i_-, s}$  equals to one if the segment-ranking number  $s$  of the anion is of type  $i_-$  and zero otherwise. The initial condition at the open-end becomes  $q_-(\mathbf{r}, s_0) = \exp(-w_B(\mathbf{r}))$ , whereas the initial condition at the center is  $q'_-(\mathbf{r}, s_0) = [q_-(\mathbf{r}, s_{n_B})]^3$ . The segment volume fraction in anion  $\varphi_{i_-}(\mathbf{r})$  now reads,

$$\varphi_{i_-}(\mathbf{r}) = \frac{V f_-}{N_- Q_-} \int_0^{N_-} \delta_{i_-, s} q_-(\mathbf{r}, s) q'_-(\mathbf{r}, s) ds \quad (8)$$

where the partition function of the anion is  $Q_- = \int q_-(\mathbf{r}, s) q'_-(\mathbf{r}, s) d\mathbf{r}$ .

The free energy formulation in Equations 1-4 implies that the local volume fraction  $\varphi(\mathbf{r})$  and the local mean-field potential  $w(\mathbf{r})$  are not independent towards one another. However, in a thermodynamical equilibrium the relationship between these two order parameters can be written based on a so-called saddle-point approximation, i.e.,

$$\begin{aligned} w_i(\mathbf{r}) = & \sum_{j \in \{A, P, B, N\}, j \neq i} \chi_{ij} (\varphi_j(\mathbf{r}) - \varphi_j^b) + \chi_{is} \int \delta(\mathbf{r} - \mathbf{r}_s) d\mathbf{r} \\ & + \lambda(\mathbf{r}) + e v_i \psi(\mathbf{r}) - \frac{1}{2} \epsilon_0 (\epsilon_{r,i}(\mathbf{r}) - 1) |\nabla \psi(\mathbf{r})|^2 \end{aligned} \quad (9)$$

where the Flory-Huggins parameter  $\chi_{ij}$  in the first term represents the magnitude of the mean-field interaction between segment- $i$  and - $j$ . A more positive  $\chi_{ij}$  indicates a more repulsive interaction. The parameter  $\varphi_j^b$  is the volume fraction of segment- $j$  in the bulk. The local electrostatic potential  $\psi(\mathbf{r})$  in the fourth term is obtained from the Poisson law,  $\epsilon_0 \nabla \cdot (\epsilon_r(\mathbf{r}) \nabla \psi(\mathbf{r})) = -\sum_i e v_i \varphi_i(\mathbf{r})$ . The last term of Equation 9 is a contribution from the polarization charges. (Feynman et al., 1964) Here, the permittivity of RTIL is considered a function of the collective permittivity of its constituent segments. (Bohmer et al., 1990; Reis et al., 2009) The local relative permittivity of the system is thus calculated from a linear combination of the local composition of its components, i.e.,  $\epsilon_r(\mathbf{r}) = \sum_i \epsilon_{r,i} \varphi_i(\mathbf{r})$ , where  $i \in \{A, P, B, N, S\}$ . This involves a heuristic approach to assign a specific value of the relative permittivity  $\epsilon_{r,i}$  to each segment- $i$  in the system under a constraint that the overall (bulk) relative permittivity of the RTIL still mimics experimental values. (Koeberg et al., 2007; Krossing et al., 2006)

A complete self-consistent mean-field (SCMF) calculation consists of the following four steps: (i) a set of initial potential of segments is randomly generated; (ii) the corresponding volume fraction of all segments are obtained from Equations (6) and (8) after solving the chain propagators in Equations (5) and (7) by using the Scheutjens-Fleer scheme; (Scheutjens & Fleer, 1979; 1980) (iii) the Poisson equation is used to calculate the value of local electrostatic potential; (iv) a new set of segment potentials is calculated from Equation 9. Steps (i)-(iv) are then repeated until the difference between the volume fraction from the previous two iterations at any point  $\mathbf{r}$  is less than  $10^{-7}$ , which indicates that the free energy is extremized and the order parameters are self-consistent. Multiple independent calculations were performed with random initial segment potentials to ensure the results satisfy the ergodicity condition.

### 3. EDL structure and capacitance in RTILs

To study the shape of EDL capacitance curve for RTIL with the same ion size and without non-electrostatic (specific) affinity towards the electrode's surface, a series of SCMF calculation is performed using a tetrameric model of cation and anion (cf. Fig. 1) with  $n_A = n_B = 4$ .<sup>1</sup> For simplicity, the volume fraction of ions is assumed to vary only in the direction perpendicular to the electrode's surface. This means that the volume fraction of ions are homogeneous throughout each plane parallel to the surface. The size of all segments are set equal to 3 Å, which is of a similar order of magnitude to an ethyl chain or a heterocyclic polar group in typical RTILs, such as pyrrolidinium and imidazolium rings. The system size is chosen large enough such that the bulk properties are reached within the boundaries of the modelled system. The relative permittivity of segments and electrode's surface used in the calculation are  $\epsilon_{r,A} = \epsilon_{r,B} = 10$ ,  $\epsilon_{r,P} = \epsilon_{r,N} = 30$ , and  $\epsilon_{r,S} = 10$ . These values are chosen such that the relative permittivity of the modelled RTIL in the bulk is similar to the real value, which is  $\sim 11$ -12. (Koeberg et al., 2007; Krossing et al., 2006) The interaction parameter  $\chi_{AB} = 1$  is used to represent an adequate repulsion between uncharged segment-A of cation and -B of anion.

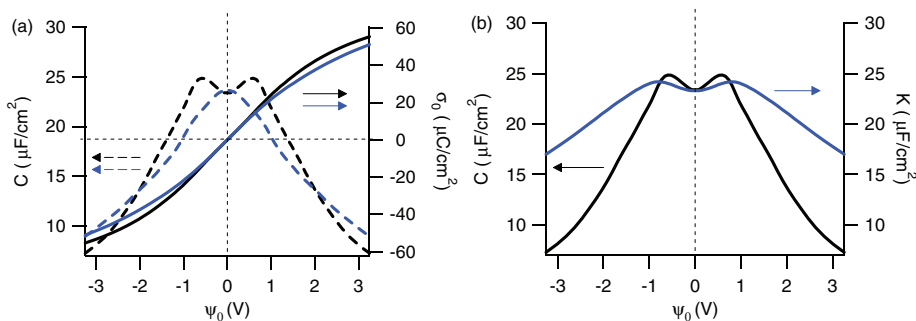


Fig. 2. (a) Full line: plot of the surface charge ( $\sigma_0$ ) as a function of the surface potential ( $\psi_0$ ). Dashed line: plot of the corresponding differential capacitance curve ( $C$ ). The black and the blue curves are generated with and without the use of an effective dielectric constant, respectively. (b) Plot of the differential capacitance curve (black) compared to the integral capacitance curve (blue).

The surface charge ( $\sigma_0$ ) and the differential capacitance ( $C$ ) are plotted as functions of the surface potential ( $\psi_0$ ) in Fig. 2a. For comparison, the differential and integral capacitance curves are depicted together in Fig. 2b. The differential capacitance is calculated from the first derivative of the surface charge ( $\sigma_0$ ) with respect to  $\psi_0$ , i.e.,  $C = \frac{\partial \sigma_0}{\partial \psi_0}$ . The integral capacitance is obtained by dividing the surface charge with the surface potential, i.e.,  $K = \frac{\sigma_0}{\psi_0}$ . Note that the value of differential capacitance based on an equilibrium model like SCMF can only be related to that obtained from impedance spectroscopy at very low frequencies. Figure 2a shows that the bell-shaped differential capacitance curve is obtained when a uniform dielectric constant of segments is used. In this case, the value used is  $\epsilon_{r,A} = \epsilon_{r,P} = \epsilon_{r,B} = \epsilon_{r,N} = 11$ . When the effective dielectric constant is taken into account, the differential capacitance curve has a camel-like shape with two maxima. This is also the case for the integral capacitance (cf.

<sup>1</sup> The detailed version of this part can be found in (Lauw et al., 2009).

Fig. 2b) although compared to the differential capacitance the maxima are reached at slightly larger potential values and the decrease in capacitance at both potential wings is less steep. The curve of surface charge in Fig. 2a comprises two regimes, namely a quasi-linear regime at low electrostatic potentials ( $-0.63 \text{ V} < \psi_0 < 0.63 \text{ V}$ ) and a non-linear regime at high potentials ( $|\psi_0| > 0.63 \text{ V}$ ). The term quasi-linear is used here since within this region the relationship between the surface charge and the surface potential appears to be linear, yet from the capacitance curve it is clear that the surface charge has a point of inflection at the pzc, which in this case is located at  $\psi_0 = 0$ . In the quasi-linear regime, the electrode's surface is still not yet fully saturated by counterions, whereas the counterions saturate the electrode's surface and accumulate further away towards the bulk in the non-linear regime, as illustrated by the set of volume fraction profile of cation and anion in Fig. 3. Note that the fluctuation of electrostatic potential at the interface at various applied potentials (cf. Fig. 4a) indicates that the charge overscreening takes place in both quasi-linear and non-linear regimes.

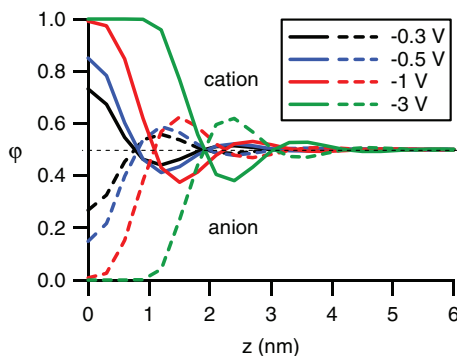


Fig. 3. Profile of the volume fraction of cation and anion at the interface at different surface potential values. The abscissa  $z$  indicates the distance from the electrode's surface.

Figure 2 shows that the capacitance curve has a camel-like shape, which is symmetric with respect to the pzc and reaches maxima at  $|\psi_0| = 0.63 \text{ V}$ . It is worth noting that the camel-shaped capacitance curve is not unique to RTILs. It was first observed decades ago in the study of aqueous solutions of NaI, NaF,  $\text{KPF}_6$ , and  $\text{KBF}_4$  on Au or Ag electrodes, where specific adsorptions occur (Clavilier & Huong, 1977; Grahame, 1947; Hamelin & Stoicoviciu, 1987; Valette, 1981). In aqueous electrolytes, the hump on the capacitance curves is typically a direct consequence of non-homogeneous polarization in the EDL (MacDonald, 1954; MacDonald & Barlow Jr., 1962; Parsons, 1961). Arguably, the primary cause for such a capacitance curve in RTILs may be different. The camel-shaped capacitance curves can be obtained using theoretical models, in which ions are considered to have finite sizes. This approach goes beyond typical Poisson-Boltzmann approximation which assumes ions as point charges. In SCMFT, the excluded volume effect is incorporated by modelling ions as segmented dendrimers with a sufficient repulsion between uncharged segments A and B in the branches of each cation and anion. It is apparent from Figure 2a that the excluded volume is not the only effect causing the camel-shaped capacitance curve. By considering the effective dielectric constant of RTILs as a function of the local segment density, it is shown that the polarizability of ions at the interface turns out to be another key factor. The camel-shaped capacitance curve can be analysed based on the potential-dependence of the structure of RTILs at the interface. This structure-property relationship is elaborated further as follows:



a) Within the quasi-linear regime ( $|\psi_0| < 0.63$  V), the capacitance increases with the surface potential. Following the trend of the volume fraction profiles of ions shown in Fig. 3, one can conclude that at the points where the capacitance reaches its maximum values ( $|\psi_0| = 0.63$  V), the electrode's surface is saturated with counterions. Between these two points, some coions can still be found at the surface. The alternating layer of ions can be considered as a series of capacitors with the corresponding capacitance value is obtained from  $1/C = \sum_l 1/C_l$ , where  $C_l$  is the capacitance of layer- $l$ . Based on this representative formula, the capacitance of the EDL in RTILs is determined by a non-trivial balance between the thinning/thickening of each layer and the decreasing/increasing polarization. A higher capacitance value can be a result of thinner layers and/or a larger interfacial polarization. Results from SCMFT indicate that the thickness and periodicity of each alternate layer throughout the quasi-linear regime is relatively the same, whereas the local dielectric constants  $\epsilon_r$  differ following the local distribution of molecular segments (cf. Fig. 4b for the case of  $\psi_0 = -0.3$  V and  $-0.5$  V). Therefore, an increasing capacitance in the quasi-linear regime is likely to be driven by an increasing polarization of RTILs at the interface.

b) Within the non-linear regime ( $|\psi_0| > 0.63$  V), the surface charge is less than a linear function of the surface potential and the capacitance decreases with increasing surface potential. The physical interpretation is that the energy needed to bring one counterion from the bulk to the surface increases more than linearly with an increasing surface charge. In this regime, the interface is already saturated with counterions such that the EDL thickness grows with an increasing surface potential, as shown in Fig. 3 for  $\psi_0 = -1$  V and  $-3$  V. Moreover, the charged segment of the counterions is primarily located at the electrode's surface, causing a higher dielectric constant value there (cf. Fig. 4b). A thicker EDL overcomes the effect of an increasing polarization at the interface to lower the capacitance. The scaling of the capacitance in the non-linear regime is  $C \propto |\psi_0|^{-0.82}$ . As a comparison, the scaling for the bell-shaped capacitance curve is  $C \propto |\psi_0|^{-0.60}$ , which indicates that the effective dielectric constant plays an important role in determining the scale of the capacitance at the electrostatic potential wings.

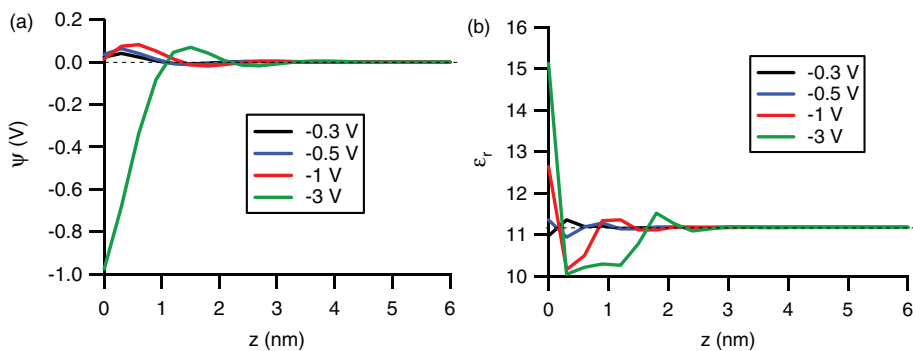


Fig. 4. (a) Profile of the diffuse electrostatic potential at the interface at different surface potentials. (b) Profile of the corresponding local dielectric constant ( $\epsilon_r$ ).

In aqueous electrolyte solutions, an increasingly charged electrode leads to a more effective screening of the electrostatic potential. The screening effect intensifies as the interface is more densely populated by counterions which replace electroneutral water molecules. As a result, the curvature of  $\sigma_0(\psi_0)$  goes beyond linear. At a first glance, the overall capacitance



curve of the EDL in aqueous electrolytes seems to differ from that in RTILs. The capacitance curve in aqueous electrolytes usually reaches a minimum at pzc and increases monotonically with surface potential, whereas the capacitance curve in RTILs has a camel-like shape. Nevertheless, under similar premises both curves would have the same camel-like shape if similar potential limits could be attained. This means that the maxima of the capacitance curve in aqueous electrolytes occur at potentials beyond the electrochemical window of water, such that one never observed this camel-shaped capacitance curve in reality.

The effects of different ion-size and specific adsorption of ions to the EDL capacitance in RTILs are discussed in the following two sections. The complete version of these sections can be found in (Lauw et al., 2010).

### 3.1 Effect of different ion-size

Results from the SCMFT described above were based on a uniform dendrimeric model of cation and anion, without taking into account ions of different size. In most RTILs, the anions are relatively smaller than the cations. Here, three size ratios of cation and anion are used to study the effect of ion-size on capacitance. This is achieved by varying the length of each arm in the anion while keeping the cation size the same. Three ratios of the arm's length used in this study are  $n_A : n_B = 4:4$ ,  $4:3$ , and  $4:2$ . The differential capacitance curve for the three size ratios of cation and anion are plotted in Fig. 5a. Each differential capacitance curve has a camel-shaped feature, which is symmetric for RTIL with the same ion-size ( $n_A:n_B = 4:4$ ) and asymmetric for ions with unequal size ( $n_A:n_B = 4:3$  and  $4:2$ ). The asymmetry is caused by the deviation in the corresponding  $\sigma_0(\psi_0)$  curves at positive applied potentials, as shown in Fig. 5a. The comparison between the differential and integral capacitance curves for unequal ion-size is shown in Fig. 5b. Although in principle the shape of both curves are similar, the integral capacitance curve is non-continuous at  $\psi_0 = 0$ .

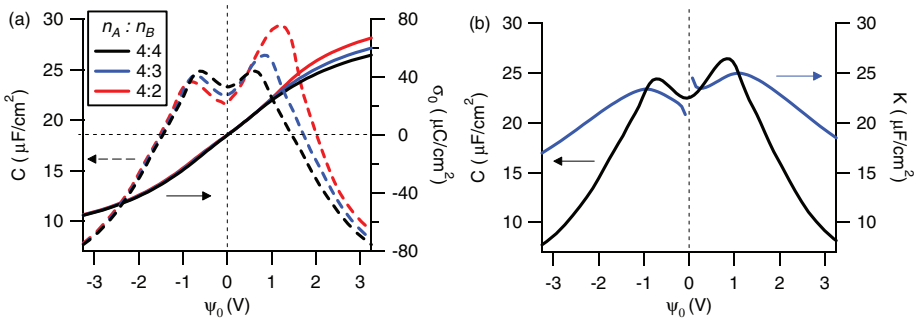


Fig. 5. (a) Plot of the differential capacitance (left) and the corresponding surface charge (right) as functions of the surface potential of the modelled RTIL with different ratios of  $n_A:n_B$ , as indicated. (b) Plot of the differential capacitance curve (black) and the integral capacitance curve (blue) for the case of  $n_A:n_B = 4:3$ .

It is known that the minimum differential capacitance is typically reached at the pzc, where the electrode's surface charge is practically zero. As described in the previous section, the quasi-linear regime is located around the pzc. For the modelled RTIL with  $n_A:n_B = 4:4$ , this regime is located within  $-0.63 \text{ V} < \psi_0 < 0.63 \text{ V}$ . It expands further for RTILs with unequal ion-size, i.e.,  $-0.73 \text{ V} < \psi_0 < 0.83 \text{ V}$  for  $n_A:n_B = 4:3$ , and  $-0.83 \text{ V} < \psi_0 < 1.19 \text{ V}$  for  $n_A:n_B = 4:2$ . The complete list of the pzc, location of both maximum potential values ( $\psi_0^{\text{max-}}$

and  $\psi_0^{\max+}$ ), and the extrema of the capacitance curves ( $C_{pzc}$ ,  $C_{\max-}$ , and  $C_{\max+}$ ) are shown in Table 1. Here, the indices  $\max-$  and  $\max+$  indicate values at the maximum capacitance on the left-hand and right-hand sides of pzc, respectively. Parameters  $\alpha-$  and  $\alpha+$  are the exponents from the scaling of the capacitance with respect to each surface potential wing in the non-linear regime, i.e.,  $C \propto |\psi_0|^{\alpha-}$  for  $\psi_0 < \psi_0^{\max-}$  and  $C \propto |\psi_0|^{\alpha+}$  for  $\psi_0 > \psi_0^{\max+}$ .

$n_A:n_B$	pzc (mV)	$\psi_0^{\max-}$ (V)	$\psi_0^{\max+}$ (V)	$C_{pzc}$ ( $\mu\text{F}/\text{cm}^2$ )	$C_{\max-}$ ( $\mu\text{F}/\text{cm}^2$ )	$C_{\max+}$ ( $\mu\text{F}/\text{cm}^2$ )	$\alpha-$	$\alpha+$
4:4	0	-0.63	0.63	23.30	24.85	24.85	-0.82	-0.82
4:3	-6	-0.73	0.83	22.46	24.40	26.42	-0.82	-1.04
4:2	-12	-0.83	1.19	21.60	23.80	29.39	-0.82	-1.32

Table 1. List of critical values and scaling parameters for differential capacitance curves in Fig. 5a.

Figure 5 indicates that the impact of smaller anions on capacitance becomes more significant with an increasingly positive potential, as also shown by a more prominent deviation of  $\sigma_0(\psi_0)$  there. It is also apparent that the shape of capacitance curve is strongly influenced by the size of counterion, whereas the effect of coion size seems to be limited. In general, smaller ions have a larger packing density and screen electrostatic potential more effectively. For smaller anions, these two factors cause a positive shift in  $\psi_0^{\max+}$  and, to a lesser extent, a negative shift in  $\psi_0^{\max-}$ . The positive shift is needed to accommodate the increasing number of anions required to saturate the Helmholtz layer, whereas the negative shift would counter the increase in screening effect of anions at the interface. A slightly negative pzc found for smaller anions is a result of the size mismatch between anion and cation, which leads to a population imbalance of ions near the surface. At zero surface charge (pzc), this imbalance results in a slightly non-zero (negative) excess charge in the Helmholtz layer, which is then overcompensated by opposite charges in subsequent layers. Besides causing the shift in critical potentials, less bulky anions raise the capacitance value at  $\psi_0 > 0.63$  V and lower it in  $-0.83$  V  $< \psi_0 < 0.63$  V. The former occurs due to the formation of more compact alternate layers by smaller anions, as illustrated in Fig. 6a; the latter is a result of less polarized alternate layers, as the screening effect of smaller anions dampens the potential field more effectively. To illustrate the last point, the mole fraction profile of ions at this region ( $\psi_0 = -0.6$  V) is shown in Fig. 6b. The changes in capacitance described here are in a good agreement with those from spectroscopic study of RTILs composed of imidazolium-based cations and Cl or BF<sub>4</sub> anions on glassy carbon, gold, or mercury electrodes.(Alam et al., 2007; 2008; Lockett et al., 2008)

The scaling of differential capacitance in RTILs with applied potential at both potential wings is a good indication of the extent of the compression of ions due to a high electrostatic field (electrostriction) in the EDL. For the case of  $n_A : n_B = 4:4$ , the scale is identical in the first non-linear regime ( $\psi_0 < \psi_0^{\max-}$ ) and the second non-linear regime ( $\psi_0 > \psi_0^{\max+}$ ), which is  $C \propto |\psi_0|^{-0.82}$ . For asymmetric capacitance curves, this scale persists in the first non-linear regime and becoming more pronounced in the second regime, in which the scaling is  $C \propto |\psi_0|^{-1.04}$  for  $n_A : n_B = 4:3$ , and  $C \propto |\psi_0|^{-1.32}$  for  $n_A : n_B = 4:2$ . Each scaling exponent corresponds to the change in thickness of alternate layers with electrostatic potential since the capacitance in the non-linear regime is mainly determined by the size of these layers. In principle, less bulky anions are geometrically more susceptible to variation in potential field by forming thicker (thinner) alternate layers at a more (less) positive applied potential. This

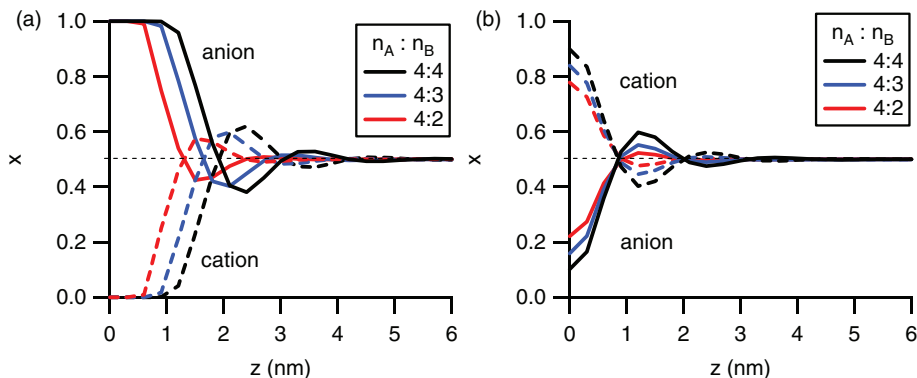


Fig. 6. Profile of the mole fraction ( $x$ ) of cation and anion at the interface with different ratios of  $n_A:n_B$  at  $\psi_0 = 3$  V (a), and  $\psi_0 = -0.6$  V (b).

explains a more rapid decay of the capacitance in the second non-linear regime for smaller anions. It is interesting to note that all scaling exponents obtained here are considerably less than  $-0.5$ , which is the value predicted analytically based on the Poisson-Fermi distribution of spherical ions at a charged interface. (Kornyshev, 2007) This discrepancy is originated from different underlying assumptions in the analytical and SCMFT model. The analytical model incorporated the excluded volume by introducing a fixed lattice saturation parameter into the Boltzmann distribution of ions. In SCMFT, the lattice saturation parameter would not be homogeneous throughout the system since the ions are modelled as flexible chain molecules and their compression or relaxation within the EDL would depend on the local electrostatic potential field. This makes the EDL structure more responsive to the applied potential, which results in a more rapid decay of  $C(\psi_0)$  than analytically predicted.

### 3.2 Effect of specific adsorption

Asymmetric capacitance curves in RTILs do not only occur when the corresponding ions have different size. They also occur for same-size ions with different specific affinity towards the electrode's surface. In aqueous electrolytes, specific adsorption is strongly related to the solvation shell of ions. A steric hindrance provided by a thick solvation shell prevents the ions from forming chemical bonds with the surface. For ions with thin-enough solvation shells, the solvent molecules would be removed from the surface to accommodate adsorption of more ions. This eventually leads to a redistribution of local charges on the surface, changes the surface dipole, and induces a partial charge transfer. (Lipowski et al., 1998; Lorenz & Salie, 1977; Magnussen, 2002) In the absence of any solvation shells surrounding RTILs, the specific adsorption of ions would arguably occur more strongly than in aqueous electrolytes. (Aliaga & Baldelli, 2006; Gale & Osteryoung, 1980) An example of specific adsorption in pure RTILs has been reported for 1-butyl-3-methylimidazolium dicyanamide RTIL on Pt-electrode. (Aliaga & Baldelli, 2006)

To study the effect of specific adsorption to the capacitance in RTILs, the affinity of anion towards the electrode's surface is systematically varied, while the size of the cation and anion is kept the same at  $n_A:n_B = 4:4$ . Three different sets of interaction parameters used here are  $\chi_{BS} = \chi_{NS} = 0, -1$ , and  $-2$ . The more negative interaction parameter indicates a stronger specific affinity of anion towards the surface. The values of interaction parameter used here are within the typical limit of adsorption energy due to specific interactions, which

is in the order of few  $k_B T$  for each adsorbed ion. (Lamperski, 1997; Lyklema, 1995; Nikitas, 1994; Parsons, 1955)

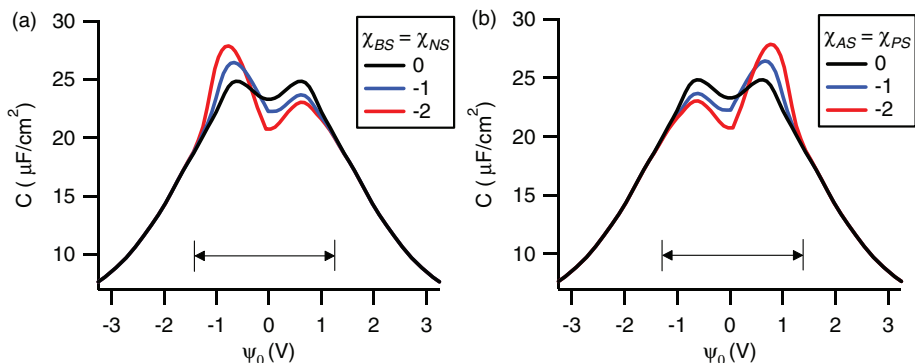


Fig. 7. (a) The differential capacitance curves of the modelled RTIL with  $n_A:n_B = 4:4$  and  $\chi_{BS} = \chi_{NS} = 0, -1$ , and  $-2$ . (b) Similar curves with  $\chi_{AS} = \chi_{PS} = 0, -1$ , and  $-2$ . In both cases, the impact of specific adsorption is limited in the  $\psi_0$ -zone marked by the arrow. It is apparent that the curve is asymmetric with respect to the pzc when the specific adsorption is present.

The differential capacitance curves of the aforementioned system are plotted in Fig. 7a. For comparison, a series of differential capacitance curves for the case of specific adsorption of cation is shown in Fig. 7b. These curves are understandably the mirror image of those obtained when the specific adsorption of anion is present. The critical values for the capacitance curves in Fig. 7a are listed in Table 2. It appears that a stronger specific adsorption of anion increases the capacitance value at  $-1.2 \text{ V} < \psi_0 < -0.3 \text{ V}$  and decreases it at  $-0.3 \text{ V} < \psi_0 < 1.2 \text{ V}$ . The trend is reversed when the specific adsorption of cation is stronger (cf. Fig. 7b). The physical interpretation of these trends is that the amount of energy to bring one counterion from the bulk to the surface would be either reduced by the presence of specifically adsorbed coion, or increased when some counterion is already specifically adsorbed on the surface.

$\chi_{BS} = \chi_{NS}$	pzc (mV)	$\psi_0^{\text{max-}}$ (V)	$\psi_0^{\text{max+}}$ (V)	$C_{\text{pzc}}$ ( $\mu\text{F}/\text{cm}^2$ )	$C_{\text{max-}}$ ( $\mu\text{F}/\text{cm}^2$ )	$C_{\text{max+}}$ ( $\mu\text{F}/\text{cm}^2$ )
0	0	-0.63	0.63	23.30	24.85	24.85
-1	-52	-0.66	0.61	22.27	26.45	23.67
-2	-95	-0.77	0.60	20.76	27.86	23.03

Table 2. List of critical values for differential capacitance curves in Fig. 7a.

The impact of specific adsorption is typically confined within a limited range of applied potential from the pzc. (Graves, 1970) This  $\psi_0$ -zone is located in  $-1.2 \text{ V} < \psi_0 < 1.2 \text{ V}$  for capacitance curves depicted in Fig. 7. As discussed above, specifically adsorbed ions tend to increase the gradient of  $C(\psi_0)$  in the  $\psi_0$ -zone. Such a steep capacitance curve is typically caused by partial charge transfers at a non-ideally polarized surface, which can be induced by specifically adsorbed ions. (Lipowski et al., 1998; Lorenz & Salie, 1977; Magnussen, 2002; Parsons, 1981) Beyond the  $\psi_0$ -zone, the long-range electrostatic interaction overcomes the short-range effect of specific adsorption to diminish the amount of adsorbed anion on the

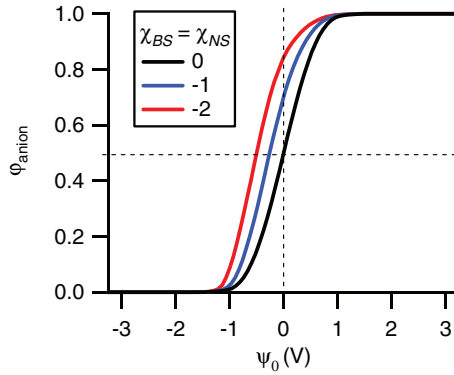


Fig. 8. Plot of the volume fraction of anion on the electrode's surface ( $\phi_{anion}$ ) as a function of applied potential. There is a significant amount of anion on the electrode's surface even at negative potentials due to the specific adsorption.

surface ( $\phi_{anion}$ ) at negative potential, as shown in Fig. 8. There are two additional trends observed by increasing the specific affinity of anion. Firstly, the  $\phi_{anion}$  curve shifts to the left, indicating an increasing presence of anion on a negatively charged surface. Secondly, the pzc and both saturation limits ( $\psi_0^{\max-}$  and  $\psi_0^{\max+}$ ) shift to more negative values since, in principle, a more negative surface is needed to counter the increasing amount of specifically adsorbed anion.

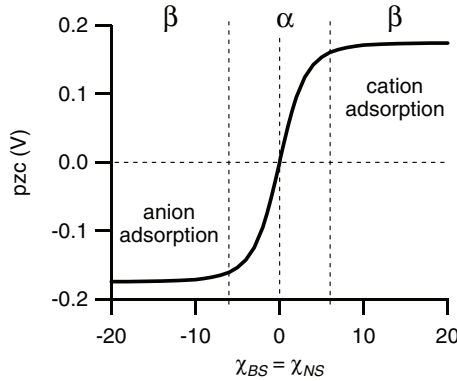


Fig. 9. Plot of the pzc as a function of the strength of specific adsorption of ion. For  $\chi_{BS} = \chi_{NS} < 0$ , the anion is adsorbed specifically to the surface, whereas for  $\chi_{BS} = \chi_{NS} > 0$ , the cation is specifically adsorbed.

The pzc is a robust parameter to detect the existence of specific adsorption in RTILs. The shift of pzc due to specific adsorption is relatively larger than that for unequal ion-size (cf. Tables 1 and 2). The relationship between the pzc and the strength of specific adsorption is shown in Fig. 9. The pzc varies steadily in the  $\alpha$ -zone ( $|\chi_{BS}| = |\chi_{NS}| < 6$ ) and goes to asymptotic values at the limit of extreme adsorption in the  $\beta$ -zone ( $|\chi_{BS}| = |\chi_{NS}| > 6$ ). The gradient of the pzc curve in the  $\alpha$ -zone is  $\sim 2k_B T$  per ion for each unit of interaction parameter ( $\chi_{BS} = \chi_{NS}$ ). In the  $\beta$ -zone, the gradient is close to zero, indicating the saturation of Helmholtz layer by specifically adsorbed ions.

#### 4. Concluding remarks

The interfacial structure and capacitance in RTILs are studied by the SCMFT. Each ion is modelled as a tetramer composed of polar and apolar segments. The results show that the alternating layer of ions is formed at charged interfaces and the corresponding capacitance curve has a camel-shaped feature. The latter is caused by a combination of the excluded volume and ion polarizability effects in the EDL. The introduction of unequal ion-size leads to asymmetric capacitance curves. The shape of these curves is strongly determined by the size of counterion and only weakly influenced by coion size. In general, smaller ions have a higher packing density and screen the electrostatic potential more effectively. These two factors cause a shift in critical values of the capacitance curves. The presence of a specific affinity of ions towards the electrode's surface also leads to asymmetric capacitance curves. The impact occurs only within a limited range of applied potential from the pzc. Besides changing the capacitance values, specifically adsorbed ions shift the pzc and both saturation limits of the capacitance curves to one direction, depending on the type of their charge and the strength of specific adsorption.

The change in the pzc can be used as a qualitative tool to predict, e.g., the type of RTIL-metal species specifically adsorbed on the electrode's surface during metal electrodeposition, provided that each species has a distinct size but similar affinity towards the surface. The trends in capacitance curve and pzc presented in this study are generally useful to assist in the choice of RTILs for specific electrochemical applications, and in the design of new RTILs with tailored electrochemical properties.

#### 5. Acknowledgement

The authors would like to thank Bart Follink, Theo Rodopoulos, Mike Horne (CSIRO), and Andy Nelson (ANSTO) for helpful discussion in this work.

#### 6. References

- Alam, M.T.; Islam, M.M.; Okajima, T. & Ohsaka, T. (2007). Measurements of differential capacitance at mercury/room-temperature ionic liquids interfaces. *Journal of Physical Chemistry C*, Vol. 111, 18326-18333.
- Alam, M. T.; Islam, M.M.; Okajima, T. & Ohsaka, T. (2008). Capacitance measurements in a series of room-temperature ionic liquids at glassy carbon and gold electrode interfaces. *Journal of Physical Chemistry C*, Vol. 112, 16600-16608.
- Aliaga, C. & Baldelli, S. (2006). Sum frequency generation spectroscopy and double-layer capacitance studies of the 1-butyl-3-methylimidazolium dicyanamide-platinum interface. *Journal of Physical Chemistry B*, Vol. 110, 18481-18491.
- Armand, M.; Endres, F.; MacFarlane, D.R.; Ohno, H. & Scrosati, B. (2009). Ionic-liquid materials for the electrochemical challenges of the future. *Nature Materials*, Vol. 8, 621-629.
- Atkin, R. & Warr, G.G. (2007). Structure in confined room-temperature ionic liquids. *Journal of Physical Chemistry C*, Vol. 111, 5162-5168.
- Atkin, R.; El Abedin, S.Z.; Hayes, R.; Gasparotto, L.H.S.; Borisenko, N. & Endres, F. (2009). AFM and STM studies on the surface interaction of [BMP]TFSA and [EMIm]TFSA ionic liquids with Au(111). *Journal of Physical Chemistry C*, Vol. 113, 13266-13272.
- Baldelli, S. (2008). Surface structure at the ionic liquid-electrified metal interface. *Accounts of Chemical Research*, Vol. 41, 421-431.

- Bazant, M.Z.; Kilic, M.S.; Storey, B.D. & Ajdari, A. (2009). Nonlinear electrokinetics at large voltages. *New Journal of Physics*, Vol. 11, 075016.
- Bikerman, J.J. (1942). Structure and capacity of electrical double layer. *Philosophical Magazine*, Vol. 33, 384-397.
- Bohmer, M.R.; Evers, O.A. & Scheutjens, J.M.H.M. (1990). Weak polyelectrolytes between two surfaces: Adsorption and stabilization. *Macromolecules*, Vol. 23, 2288-2301.
- Chmiola, J.; Largeot, C.; Taberna, P.L.; Simon, P. & Gogotsi, Y. (2008). Desolvation of ions in subnanometer pores and its effect on capacitance and double-layer theory. *Angewandte Chemie International Edition*, Vol. 47, 3392-3395.
- Claessens, M.M.A.E.; van Oort, B.F.; Leermakers, F.A.M.; Hoekstra, F.A. & Cohen Stuart, M.A. (2004). Charged lipid vesicles: Effects of salts on bending rigidity, stability, and size. *Biophysical Journal*, Vol. 87, 3882-3893.
- Clavilier, J. & Huong, C.N.V. (1977). Etude de l'interface de l'or polycristallin au contact de solutions aqueuses de perchlorate de potassium et d'acide perchlorique. *Journal of Electroanalytical Chemistry*, Vol. 80, 101-114.
- Edwards, S.F. (1965). The statistical mechanics of polymers with excluded volume. *Proceedings of the Physical Society of London*, Vol. 85, 613-624.
- Endres, F.; MacFarlane, D. & Abbott, A. (2008). *Electrodeposition from ionic liquids*, Wiley-VCH, Weinheim, Germany.
- Fedorov, M.V. & Kornyshev, A.A. (2008). Towards understanding the structure and capacitance of electrical double layer in ionic liquids. *Electrochimica Acta*, Vol. 53, 6835-6840.
- Feng, G.; Zhang, J.S. & Qiao, R. (2009). Microstructure and capacitance of the electrical double layers at the interface of ionic liquids and planar electrodes. *Journal of Physical Chemistry C*, Vol. 113, 4549-4559.
- Feynman, R.P.; Leighton, R.B. & Sands, M. (1964). *Lectures on Physics II*, Addison-Wesley Publishing Company, Reading, MA.
- Fleer, G.J.; Cohen Stuart, M.A.; Scheutjens, J.M.H.M.; Cosgrove, T. & Vincent, B. (1993). *Polymers at interface*, Chapman and Hall, London, UK.
- Flory, P.J. (1953). *Principles of Polymer Chemistry*, Cornell University Press, New York.
- Freise V. (1952). Zur Theorie der diffusen Doppelschicht. *Zeitschrift fur Elektrochemie*, Vol. 56, 822-827.
- Gale, R.J. & Osteryoung, R.A. (1980). The electrical double layer at mercury in room temperature aluminum chloride: 1-butylpyridinium chloride ionic liquids. *Electrochimica Acta*, Vol. 25, 1527-1529.
- Grahame, D.C. (1947). The electrical double layer and the theory of electrocapillarity. *Chemical Reviews*, Vol. 41, 441-501.
- Graves, A.D. (1970). The electrical double layer in molten salts. Part 1. The potential of zero charge. *Journal of Electroanalytical Chemistry* Vol. 25, 349-356.
- Hamelin, A. & Stoicoviciu, L. (1987). Study of gold low index faces in KPF<sub>6</sub> solutions. Part I. Experimental behaviour and determination of the points of zero charge. *Journal of Electroanalytical Chemistry*, Vol. 234, 93-105.
- Horn, R.G.; Evans, D.F. & Ninham, B.W. (1988). Double-layer and solvation forces measured in a molten salt and its mixtures with water. *Journal of Physical Chemistry*, Vol. 92, 3531-3537.



- James, R.O. & Healy, T.W. (1972). Adsorption of hydrolyzable metal ions at the oxide-water interface. III. A thermodynamic model of adsorption. *Journal of Colloid and Interface Science*, Vol. 40, 65-81.
- Kilic M.S.; Bazant, M.Z. & Ajdari, A. (2007). Steric effects in the dynamics of electrolytes at large applied voltages. I. Double-layer charging. *Physical Review E*, Vol. 75, 021502.
- Koeberg, M.; Wu, C.C.; Kim, D. & Bonn, M. (2007). THz dielectric relaxation of ionic liquid:water mixtures. *Chemical Physics Letters*, Vol. 439, 60-64.
- Kornyshev, A.A. (2007). Double-layer in ionic liquids: Paradigm change? *Journal of Physical Chemistry B*, Vol. 111, 5545-5557.
- Krossing, I.; Slattery, J.M.; Daguenet, C.; Dyson, P.J.; Oleinikova, A. & Weingartner, H. (2006). Why are ionic liquids liquid? A simple explanation based on lattice and solvation energies. *Journal of American Chemical Society*, Vol. 128, 13427-13434.
- Lamperski, S. (1997). Molecular model for anion adsorption from electrolyte of constant ionic strength. *Journal of Electroanalytical Chemistry*, Vol. 437, 225-231.
- Largeot, C.; Portet, C.; Chmiola, J.; Taberna, P.L.; Gogotsi, Y. & Simon, P. (2008). Relation between the ion size and pore size for an electric double-layer capacitor. *Journal of American Chemical Society*, Vol. 130, 2730-2731.
- Lauw, Y.; Kovalenko, A. & Stepanova, M. (2008). Phase behavior of amphiphilic lipid molecules at air-water interfaces: An off-lattice self-consistent-field modeling. *Journal of Physical Chemistry B*, Vol. 112, 2119-2127.
- Lauw, Y. (2009). Equilibrium morphologies of nonionic lipid-nanoparticle mixtures in water: A self-consistent mean-field prediction. *Journal of Colloid and Interface Science*, Vol. 332, 491-496.
- Lauw, Y.; Horne, M.D.; Rodopoulos, T. & Leermakers, F.A.M. (2009). Room-temperature ionic liquids: Excluded volume and ion polarizability effects in the electrical double-layer structure and capacitance. *Physical Review Letters*, Vol. 103, 117801.
- Lauw, Y.; Horne, M.D.; Rodopoulos, T.; Nelson, A. & Leermakers, F.A.M. (2010). Electrical double-layer capacitance in room temperature ionic liquids: ion-size and specific adsorption effects. *Journal of Physical Chemistry B*, Vol. 114, 11149-11154.
- Leermakers, F.A.M.; Rabinovich, A.L. & Balabaev, N.K. (2003). Self-consistent-field modeling of hydrated unsaturated lipid bilayers in the liquid-crystal phase and comparison to molecular dynamics simulations. *Physical Review E*, Vol. 67, 011910.
- Leermakers, F.A.M.; Eriksson, J.C. & Lyklema, J. (2005). *Fundamentals of Interface and Colloid Science V, Chapter 4*, Elsevier, Amsterdam, The Netherlands.
- Lipowski, J.; Shi, Z.; Chen, A.; Pettinger, B. & Bilger, C. (1998). Ionic adsorption at the Au(111) electrode. *Electrochimica Acta*, Vol. 43, 2875-2888.
- Lockett, V.; Sedev, R.; Ralston, J.; Horne, M.D. & Rodopoulos, T. (2008). Differential capacitance of the electrical double layer in imidazolium-based ionic liquids: Influence of potential, cation size, and temperature. *Journal of Physical Chemistry C*, Vol. 112, 7486-7495.
- Lorenz, W. & Salie, G.G. (1977). Partial charge transfer reactions in electrochemical kinetics. Review on the theory of measuring methods for electrode processes with adsorbed intermediates. *Journal of Electroanalytical Chemistry*, Vol. 80, 1-56.
- Lyklema, J. (1995). *Fundamentals of Interface and Colloid Science II, Chapter 3*, Elsevier, Amsterdam, The Netherlands.
- MacDonald, J.R. (1954). Theory of the differential capacitance of the double layer in unadsorbed electrolytes. *Journal of Chemical Physics*, Vol. 22, 1857-1866.



- MacDonald, J.R. & Barlow Jr., C.A. (1962). Theory of double-layer differential capacitance in electrolytes. *Journal of Chemical Physics*, Vol. 36, 3062-3080.
- Magnussen, O.M. (2002). Ordered anion adlayers on metal electrode surfaces. *Chemical Reviews*, Vol. 102, 679-725.
- Matsen, M.W. (1995). Phase behavior of block copolymer/homopolymer blends. *Macromolecules*, Vol. 28, 5765-5773.
- Mezger, M.; Schroder, H.; Reichert, H.; Schramm, S.; Okasinski, J.S.; Schoder, S.; Honkimaki, V.; Deutsch, M.; Ocko, B.M.; Ralston, J.; Rohwerder, M.; Stratmann, M. & Dosch, H. (2008). Molecular layering of fluorinated ionic liquids at a charged sapphire (0001) surface. *Science*, Vol. 322, 424-428.
- Mezger, M.; Schramm, S.; Schroder, H.; Reichert, H.; Deutsch, M.; De Souza, E.J.; Okasinski, J.S.; Ocko, B.M.; Honkimaki, V. & Dosch, H. (2009). Layering of [BMIM]<sup>+</sup>-based ionic liquids at a charged sapphire interface. *Journal of Chemical Physics*, Vol. 131, 094701.
- Nikitas, P. (1994). A new approach to development of ionic isotherms of specific adsorption in the electrical double layer. *Journal of Physical Chemistry B*, Vol. 98, 6577-6585.
- Ohno, H. (2005). *Electrochemical aspects of ionic liquids*, John Wiley & Sons, Inc., Hoboken, NJ.
- Oldham, K.B. (2008). A Gouy-Chapman-Stern model of the double layer at a (metal)/(ionic liquid) interface. *Journal of Electroanalytical Chemistry*, Vol. 613, 131-138.
- Outhwaite, C.W.; Bhuiyan, L.B. & Levine, S. (1980). Theory of the electric double layer using a modified Poisson-Boltzmann equation. *Journal of Chemical Society - Faraday Transactions*, Vol. 76, 1388-1408.
- Parsons, R. (1955). The specific adsorption of ions at the metal-electrolyte interphase. *Transactions of the Faraday Society*, Vol. 51, 1518-1529.
- Parsons, R. (1961). *Advances in Electrochemistry and Electrochemical Engineering Volume I, Chapter 1*, Interscience Publishers, NY.
- Parsons, R. (1981). The contribution to the capacity of an electrode from a species adsorbed with partial charge transfer. *Canadian Journal of Chemistry*, Vol. 59, 1898-1902.
- Parsons, R. (1990). Electrical double layer: Recent experimental and theoretical developments. *Chemical Reviews*, Vol. 90, 813-826.
- Reed, S.K.; Madden, P.A. & Papadopoulos A. (2008). Electrochemical charge transfer at a metallic electrode: A simulation study. *Journal of Chemical Physics*, Vol. 128, 124701.
- Reis, J.C.R.; Iglesias, T.P.; Douheret, G. & Davis, M.I. (2009). The permittivity of thermodynamically ideal liquid mixtures and the excess relative permittivity of binary dielectrics. *Physical Chemistry Chemical Physics*, Vol. 11, 3977-3986.
- Rivera-Rubero, S. & Baldelli, S. (2004). Surface spectroscopy of room-temperature ionic liquids on a platinum electrode: A sum frequency generation study. *Journal of Physical Chemistry B*, Vol. 108, 15133-15140.
- Santos, V.O., Jr.; Alves, M.B.; Carvalho, M.S.; Suarez, P.A.Z. & Rubim, J.C. (2006). Surface-enhanced Raman scattering at the silver electrode/ionic liquid (BMIPF6) interface. *Journal of Physical Chemistry B*, Vol. 110, 20379-20385.
- Scheutjens, J.M.H.M. & Fleer, G.J. (1979). Statistical theory of the adsorption of interacting chain molecules. 1. Partition function, segment density distribution, and adsorption isotherms. *Journal of Physical Chemistry*, Vol. 83, 1619-1635.
- Scheutjens, J.M.H.M. & Fleer, G.J. (1980). Statistical theory of the adsorption of interacting chain molecules. 2. Train, loop, and tail size distribution. *Journal of Physical Chemistry*, Vol. 84, 178-190.

- Simon, P. & Gogotsi, Y. (2008). Materials for electrochemical capacitors. *Nature Materials*, Vol. 7, 845-854.
- Stillinger, F.H. & Kirkwood, J.G. (1960). Theory of the diffuse double layer. *Journal of Chemical Physics*, Vol. 33, 1282-1290.
- Teschke, O. & de Souza, E.F. (1999). Dielectric exchange: The key repulsive or attractive transient forces between atomic force microscope tips and charged surfaces. *Applied Physics Letters*, Vol. 74, 1755-1757.
- Thompson, R.B.; Ginzburg, V.V.; Matsen, M.W. & Balazs, A.C. (2001). Predicting the mesophases of copolymer-nanoparticle composites. *Science*, Vol. 292, 2469-2472.
- Trulsson, M.; Algotsson, J.; Forsman, J.; Woodward, C.E. (2010). Differential capacitance of room temperature ionic liquids: the role of dispersion forces. *Journal of Physical Chemistry Letters*, Vol. 1, 1191-1195.
- Valette, G. (1981). Double layer on silver single-crystal electrodes in contact with electrolytes having anions which present a slight specific adsorption. *Journal of Electroanalytical Chemistry*, Vol. 122, 285-297.
- Yuan, Y.X.; Niu, T.C.; Xu, M.M.; Yao, J.L. & Gu, R.A. (2010). Probing the adsorption of methylimidazole at ionic liquids/Cu electrode interface by surface-enhanced Raman scattering spectroscopy. *Journal of Raman Spectroscopy*, Vol. 41, 516-523.

# Pseudolattice Theory of Ionic Liquids

L. M. Varela<sup>1,1</sup>, J. Carrete<sup>1</sup>, M. García<sup>1</sup>, J. R. Rodríguez<sup>1</sup>,  
L.J. Gallego<sup>1</sup>, M. Turmine<sup>2</sup> and O. Cabeza<sup>3</sup>

<sup>1</sup>*Grupo de Nanomateriales y Materia Blanda. Departamento de Física de la Materia Condensada, Universidade de Santiago de Compostela, E-15782. Santiago de Compostela,*

<sup>2</sup>*Université Pierre et Marie Curie-PARIS6; Laboratoire Interfaces et Systèmes Electrochimiques, CNRS, UPR15-LISE, Paris, F-75005*

<sup>3</sup>*Facultad de Ciencias. Universidade de A Coruña. Campus A Zapateira s/n. E-15072. A Coruña,*

<sup>1,3</sup>*Spain*

<sup>2</sup>*France*

## 1. Introduction

In this chapter we summarize the main features of the pseudolattice theory of ionic fluids, starting with the experimental evidence of the existence of this kind of structural arrangement in these systems. The so-called Bahe-Varela formalism of concentrated electrolyte solutions is reviewed, and its generalization to transport phenomena introduced. On the other hand, the pseudolattice approach to equilibrium and transport properties of pure room temperature molten salts (ILs) and their mixtures with molecular fluids is analyzed. Particularly, pseudolattice theory is seen to provide an adequate understanding of both volumetric and surface properties of ionic liquid mixtures, as well as of electrical and thermal transport in these systems.

Charged complex fluids play a leading role among the systems which comprise the whole category of complex fluids, a category that essentially covers the whole spectrum of liquid matter. The presence of charges –and consequently of central, long-ranged interaction potentials– tends to make objects soluble in water, and so structures and processes involving electrostatic interactions are ubiquitous in soft matter and play an important role in colloidal, polymeric, and biological systems (Boroudjerdi et al., 2005). The Coulomb interaction, the main contribution to the intermolecular potential, is responsible for most part of the properties of these systems, including homogeneization of molecular structures and the existence of concentration gradients and mesoscopic structures among others. Thus, the importance of this system in many theoretical and applied fields is beyond any doubt, and therefore, it is not surprising that very few topics in the field of physical chemistry have attracted so much attention as that of equilibrium and transport properties of ionic fluids. The paradigm of charged complex fluid is the ionic liquid, a category which comprises liquid metals, high-temperature and room-temperature molten salts, and ionic solutions.

---

<sup>1</sup> Corresponding author: E-mail: luismiguel.varela@usc.es

Among these, in this chapter we shall focus our attention essentially in the latter and in room-temperature molten salts (or simply referred to as ionic liquids, ILs).

Ionic solutions are neutral systems formed by a solute of positive and negative ions immersed in a neutral polar solvent. This category includes systems of very different complexity degree, ranging from electrolyte solutions with cations and anions of comparable size and charge, to highly asymmetric macromolecular ionic liquids in which macroions (polymers, micelles, proteins...) coexist with microscopic counterions. Undoubtedly, electrolyte solutions represent the model system for the whole category, and they were the first to concentrate research attention in the final part of the XIX<sup>th</sup> century and the beginning of XX<sup>th</sup> century. Due to the works of Kohlrausch, Lewis and other pioneers, it soon became clear that these systems have equilibrium and transport properties that greatly differ from those of conventional non-electrolyte systems.

Gouy and Chapman (GC) for inhomogeneous solutions (electric double layer) (Gouy, 1910; Chapman, 1913), and Debye and Hückel for homogeneous ones (Debye & Hückel, 1923), reported the theoretical framework for an adequate understanding of the behavior of ionic solutions. Particularly, the latter provided an essentially correct theoretical understanding of the thermodynamics of electrolyte solutions. Introducing the concept of the ionic atmosphere, they were able to show that the electrostatic potential created by an ion in the bulk solution is screened by the charges in its surroundings, the screening length being controlled by the ionic concentration of the solution. This screened potential is on the basis of the well-known universal law that the activity coefficients of electrolyte solutions obey at extremely low concentrations (Debye-Hückel limiting law), which states the proportionality of the logarithm of the average activity coefficient to the squared-root of concentration. This law for binary ionic solutions reads

$$\ln \gamma_{\pm} = -\frac{k_D}{2} \frac{|q_+ q_-|}{\epsilon k_B T} \quad (1)$$

where  $k_D$  is Debye's parameter or Debye's screening constant,  $q_{+(-)}$  is the cation (anion) charge,  $\epsilon$  is the dielectric constant of the solvent (since Debye-Hückel mean-field theory is formulated in the framework of the primitive model of solutions, the solvent is assumed to provide only a uniform, structureless background), and  $k_B T$  is the thermal energy. The Debye parameter is proportional to the square root of the ionic concentration

$$k_D^2 = \frac{1}{\epsilon k_B T} \sum_{i=1}^s n_i q_i^2 \quad (2)$$

where  $n_i$  stands for the number density of ions of the  $i$ -th species, and the sum extends to all the species present in the bulk solution. This parameter controls the spatial range of the electrostatic interactions in the solution, since the electrostatic potential created by an ion immersed in a statistically distributed ensemble of ions is

$$\psi_i(r) = \frac{q_i}{4\pi\epsilon} \frac{e^{-k_D r}}{r} \quad (3)$$

The inverse of the screening constant is called the Debye length, and it determines the range of the electrostatic interactions and, consequently, the size of the ionic atmosphere.

Debye-Hückel universal limiting law supposed a revolution in the understanding of the physics of ionic systems, and undoubtedly constitutes a major achievement of XX<sup>th</sup> century physics. It has been shown to be exact on statistical mechanical grounds by Kirkwood and Poirier (Kirkwood & Poirier, 1954) and the limit of validity of the Debye-Hückel model (in distinction to that of their mathematical approximations) has been set by Frank and Thompson (Frank & Thompson, 1959) at about 0.001 M (mole l<sup>-1</sup>) for aqueous solutions of 1:1 electrolytes at 25 °C, the concentration limit at which the thickness of the ionic cloud equals the average interionic distance. On the basis of this structural model of ionic solutions, the thermodynamic properties of extremely dilute ionic solutions have been successfully understood including surface properties (see, for example, the classic books of Harned and Owen (Harned & Owen, 1958) and of Robinson and Stokes (Robinson & Stokes, 1959) for a detailed overview of classical theory of electrolyte solutions). Nowadays, mean-field, Poisson Boltzmann (PB) equation-based theories which provide simple, elegant expression that can be applied in practical situations continue to be the most frequently used to describe ionic fluids, despite the huge amount of contributions to the field of ionic solutions reported during the last century, that include different extensions of the Debye-Hückel formalism, integral equation techniques, field theory studies and computer simulation results (for a review, see (Varela et al., 2003) and references therein). Indeed, the mean-field approach is very successful in describing qualitatively (and usually also quantitatively) experiments and simulation in Coulomb systems because every ion interacts with many other ions simultaneously. This is the reason why mean-field approximations, despite ignoring ion-ion correlations, continue to be the basis of the theoretical understanding of many phenomena like ionic and colloidal stability, electrolyte solutions thermodynamics and phase transitions in ionic fluids.

On the other hand, almost all our theoretical understanding of charge transport in ionic fluids is almost completely constrained to dilute ionic solutions, for which the so called Debye-Hückel-Onsager or Onsager-Fuoss theory was originally developed (for the series of results which constitute this theory see (Fuoss et al, 1965) and references therein). This framework is built on the structural basis of the Debye-Hückel model of ionic solutions, and therefore the basic structural feature continues to be the ionic atmosphere. According to the Debye-Hückel-Onsager theory, the perturbation of this structure by the external electric field provokes that the field actually experienced by an ion in the bulk differs from the external one due to the existence of an internal or relaxation field associated to the loss of spherical symmetry of the ionic cloud. Moreover, the ion-solvent interactions cause the solvent to be dragged during the motion of an ion together with its ionic cloud, so the motion does not take place in a medium at rest. This effect is known as electrophoretic effect, and together with the relaxation field, is responsible for the concentration-dependent decrease of the ionic mobilities with respect to their limiting values. Once again, both effects are proportional to the Debye parameter  $k_D \sim c^{1/2}$  and therefore to the square-root of the ionic concentration,  $c$ , and this behavior is extrapolated to the ionic mobilities in solution. This leads to the so-called Onsager limiting law of ionic conductance

$$\Lambda = \Lambda^0 - S_\Lambda c^{1/2} \quad (4)$$

where  $\Lambda^0$  is the limiting conductance, and  $S_\Lambda$  is a concentration-independent coefficient peculiar to each electrolyte type. This universal law allowed an adequate understanding of the detailed conductivity measurements performed by Kohlrausch in the late nineties of the

XIX<sup>th</sup> century (Harned & Owen, 1958), and has been repeatedly verified for highly dilute ionic solutions.

As stated above, the central concepts in the Debye-Hückel theory of homogeneous electrolyte solutions, and in Gouy-Chapman theory of inhomogeneous ionic solutions are the ionic atmosphere (Debye-Hückel, homogeneous case) or the electrical double layer (Gouy-Chapman, inhomogeneous case). These inhomogeneities in the distribution of charge in the bulk solution are associated to local electroneutrality and they provide the structural tools for the understanding of these systems in the dilute concentration regime. Moreover, it is now well-stated that the mean-field Poisson-Boltzmann formalism can be extended to regions where it should not be qualitatively valid (Varela et al. 2003; Kjellander & Mitchell, 1992; Kjellander & Mitchell, 1994; Attard, 1993; McBride et al, 1998; Varela et al. 1998; Varela et al. 1999,a,b). Indeed, an effective, formally exact mean-field theory can be defined where the screening length and charges are renormalized from their bare values (Varela et al., 2003). Using these extensions, the Poisson-Boltzmann formalism can be extended in order to treat solutions of very high ionic concentrations for which the interionic correlations must be considered.

However, it has long been known that the preservation of the continuous ionic atmosphere underlying the Poisson-Boltzmann formalism at concentrations beyond 0.01 M is doubtful since, as pointed out by Bockris (Bockris, 2000), at this concentration *"only one ion produces the 50% of the effect of the ionic atmosphere on the central ion"* and it is to be smeared out over a sphere of about 25 Å. In order to interpret the X-ray diffraction patterns of concentrated electrolyte solutions, Prins suggested long ago (Prins, 1935) the existence of medium range correlations in the positions of heavy ions in solution. Frank and Thompson (Frank & Thompson, 1959a,b) suggested that the structure of the ionic solution must vary with concentration: a continuous ionic cloud model is correct for very dilute solutions, but a disordered lattice model would be more satisfactory at intermediate and high concentrations and lead to a cube-root law in salt concentration for the logarithm of the activity coefficient. Robinson and Stokes (Robinson & Stokes, 1959) included experimental evidence of the existence of a lattice arrangement in concentrated NaCl solutions and a short description of a pseudolattice model in their classical book in electrolytes. Beck (Bahe, 1972a) reported X-ray data for concentrated solutions of LiBr (up to 12.3 M) and LiCl (up to 13.3 M). The curves of LiBr and LiCl showed distinct peaks at about  $2\theta = 21^\circ$  and  $2\theta = 19^\circ$  with unit cell lengths of face-centered-cubic structures at maximum concentrations of 8.14 and 7.94 Å respectively. Moreover, Hyman and Vaughn (Hyman and Vaughn, 1967) reported the dispersion curves for aqueous solutions of chloroplatinic acid, and they showed that the X-ray diffracting anions can be examined as an fcc lattice with a unit cell length of the corresponding fluorite cell, a fact this compound shares with all the other 1:2 and 2:1 electrolytes (Bahe, 1972a,b; Bahe & Parker, 1975). Desnoyers and Conway (Desnoyers & Conway, 1964) experimentally demonstrated the validity of the cube-root law both for 1:1 electrolyte solutions and for 1:2 electrolyte solutions, although in this latter case they suggested that corrections for finite size of the ions must be taken into account because the distance of closest approach is important for highly hydrated ions and multivalent ions. To end this list of experimental evidence of the existence of loose-lattice structure in ionic solutions, we must mention a series of papers which started in the beginnings of the 60's and still continues nowadays (see for example (Alves Marques et al., 2007) and references therein). In this series, Alves Marques and collaborators demonstrated the existence of *"well-*

*defined positional correlations of the ions of the larger valence in concentrated aqueous solutions*" by means of Raman spectroscopy, neutron scattering and X-ray scattering.

The result which constitutes the basis of the contemporary pseudolattice theory of ionic solutions is due to Lowell W. Bahe (Bahe, 1972a). In this paper the author reports a qualitatively and quantitatively correct interpretation of the thermodynamic properties of concentrated electrolyte solutions in terms of the existence of a statistical arrangement of the ions in the bulk –in agreement with X-ray data- induced by long-range Coulomb interactions and dielectric constant gradients. He provided an essentially correct deduction of the cube-root law which was known to fit activity coefficient data down to concentrations as low as 0.01 M and even lower, taking into account Coulomb forces and the interactions between the electric fields of the ions and the gradient of dielectric constant near the surface of ions in solution induced by their electric fields.

In 1997 Varela et al. (Varela et al., 1997) generalized Bahe's theory introducing short-range ion-ion interactions in the pseudolattice formalism modeling them by a hard-core potential with an attractive tail representing van der Waals interactions. The resulting theory is capable of describing the thermodynamic and transport properties of highly concentrated solutions in a satisfactory manner. Indeed, as we shall see later, the validity of this theoretical framework extends almost to the whole concentration range of electrolyte solutions and IL mixtures (excluding extremely diluted solutions, where the previously revisited Debye-Hückel limiting law applies).

After 1997, other pseudolattice approaches to equilibrium properties of electrolyte solutions deserve some comment. Moggia and Bianco (Moggia & Bianco, 2007; Moggia, 2008) provided expressions for the activity and osmotic coefficients following a pseudolattice approach. The authors assumed that the solute ions evolve from a disordered lattice model within a continuous solvent at extremely dilute solutions to a disordered lattice of local arrangements of both solute ions and solvent dipoles at higher concentrations, and they were able to satisfactorily explain the thermodynamic properties of these systems.

On the other hand, in what transport theory is concerned, very limited activity has been registered. Indeed, up to our knowledge, until this year 2010, the only reported results are those due to the group of D. Lemordant and coworkers in Tours (Chagnes et al., 2001; Chagnes et al., 2002; Chagnes et al., 2003), who showed that if the Debye constant corresponding to an ionic cloud model is replaced by the average distance between ions,

$$k_D \rightarrow R = \left(\frac{V}{N}\right)^{\frac{1}{3}} = M'' \left(\frac{2N_A c}{1000}\right)^{-\frac{1}{3}} \quad (5)$$

where  $M''$  is a Madelung-like constant for the pseudolattice,  $N_A$  is Avogadro's number and  $c$  the molar concentration of the solution, then the Debye-Hückel-Onsager result in Eq. (4) leads to an expression for the electrical conductance

$$\Lambda = \Lambda^{0'} - S'_\Lambda c^{1/3} \quad (6)$$

Indeed, at concentrations higher than 0.2 M, the authors proved that the molar conductivity of aqueous (Chagnes et al, 2001) and non-aqueous (Chagnes et al., 2002) solutions of  $\text{LiClO}_4$  follows a  $c^{1/3}$  law, reflecting the underlying lattice-like arrangement of the ions of this strong binary electrolyte. Moreover, the experimental value found by these authors for the slope of the conductance vs.  $c^{1/3}$  plot was in good agreement with the calculated one.

As it is perfectly known, room temperature molten salts or ionic liquids (ILs) are charged complex fluids formed exclusively by ions. They can be seen as an infinitely concentrated electrolyte solution, and one can think about these systems as the opposite limit to that of the applicability of the DH theory of ions solutions. It is well-known that a polar network exists in these systems, as can be seen for example in (Wei Jiang et al., 2007), so, from the theoretical perspective, one expects that a pseudolattice model is particularly well adapted to the peculiarities of ILs. Indeed, Turmine and coworkers (Bou Malham et al., 2007; Bouguerra et al. 2008) proved that the so called Bahe-Varela (BV) pseudolattice theory of electrolyte solutions is capable of accounting for the thermodynamic properties of binary and ternary mixtures of ILs up to the limit of pure IL.

The structure of this chapter is as follows. The next section is devoted to the presentation of the main features of the BV theory, and in section 3 we present some experimental results concerning equilibrium and transport properties of ionic solutions and ILs analyzed in this theoretical framework. Finally, in section 4 we summarize the main conclusions of the chapter.

## 2. Theoretical section

Let us consider an aqueous binary electrolyte solution of type  $z_+ : z_-$ , charge density  $\rho$ , and mass density  $\rho_m$ . We shall adopt a primitive model description of the bulk solution, assuming a continuous model for the solvent and that the only relevant property with which it contributes to the problem is its dielectric constant,  $\epsilon$ . Moreover, the ions are assumed to be incompressible spheres with charge located at the center. The volume force vector acting on a region of space in a dielectric is given by (Panofsky & Phillips, 1977)

$$\vec{F} = \rho \vec{E} - \frac{1}{2} E^2 \vec{\nabla} \epsilon + \frac{1}{2} \vec{\nabla} \left( E^2 \frac{d\epsilon}{d\rho_m} \rho_m \right) \quad (7)$$

The first term on the right hand side of the above equation is the standard Coulomb term and the second one stands for the coupling of the electric field in the bulk solution with the gradient of dielectric field in the region. On the other hand, the third term is the electrostriction term which can be ignored –as we shall do in the rest of the chapter– for incompressible fluids. Considering the region of the ionic solution between an anion and a cation whose centers are separated by a distance  $R^*$ , we can obtain the force acting on the anion integrating Eq. (7) in the relevant volume. For what the first term on the right hand side of that equation is concerned,, the integration region corresponds to that where the charge generating the field (the cation in our case) is placed, and the integration region for the second term on the right is that containing a gradient in the dielectric constant. In this region, of approximately 3 Å deep as shown by Padova (Padova, 1963), and known as the dielectric sea, the transition between the dielectric constant of bulk water to that of the ions takes place. The integral of the first term immediately leads to the conventional Coulomb force between the ions,

$$\int_V \rho E dV = \frac{q_+ q_-}{4\pi \epsilon} \frac{1}{R^{*2}}. \quad (8)$$



On the other hand, as shown by Bahe in the Appendix to the first of his 1972 papers, to a first approximation the integral in the volume of the dielectric sea of the second term in the right hand side of Eq. (7) leads to the following form for the field-dielectric-gradient force between the two ions along the line of centers:

$$-\int_V E^2 \vec{\nabla} \varepsilon dV = \frac{3q_+^2}{32\pi^2 \varepsilon_0^2} \left| \frac{d\varepsilon}{dR^*} \right| V_{sea} \frac{1}{R^{*4}}. \quad (9)$$

The total force acting on the anion in an incompressible fluid is obtained from the addition of Eqs. (8) and (9), and the Helmholtz free energy of interaction of the two ions can be straightforwardly proved to be

$$F(T, V) = \frac{q_+ q_-}{4\pi \varepsilon R^*} + \frac{q_+^2}{32\pi^2 \varepsilon_0^2} \left| \frac{d\varepsilon}{dR^*} \right| V_{sea} \frac{1}{R^{*3}}. \quad (10)$$

As pointed out by Bahe (Bahe, 1972a), this Helmholtz free energy is essentially identical to the Gibbs free energy for ionic solutions.

Taking now into account the previously mentioned experimental facts about the existence of loose lattice structures in electrolyte solutions, the electrical contribution to the free energy of the ions can be calculated from Eq. (10) just by inserting a Madelung constant,  $A''$ , in the Coulomb term and a Madelung-like constant,  $B''$ , in the second term on the right hand side to give

$$\frac{G_{el}}{N} = A'' \frac{q_+ q_-}{4\pi \varepsilon R^*} + B'' \frac{q_+^2}{32\pi^2 \varepsilon_0^2} \left| \frac{d\varepsilon}{dR^*} \right| V_{sea} \frac{1}{R^{*3}} \quad (11)$$

One must recall that  $R^*$  represents the minimum distance between cations and anions in the loose lattice fcc structure, so for a binary electrolyte solution it can be replaced by

$$R^* = \left( \frac{V}{N} \right)^{\frac{1}{3}} = \left( \frac{2N_A c}{1000} \right)^{-\frac{1}{3}}, \quad (12)$$

Thus, it is straightforward to obtain the expression for the rational activity coefficient of the electrolyte solution

$$\ln f_{\pm} = \frac{G_{el}}{2RT} = -Ac^{1/3} + Bc \quad 2RT \ln f_{\pm} = G_{el} = -Ac^{1/3} + Bc, \quad (13)$$

being  $R$  the gas constant, and the constants  $A$  and  $B$  given by

$$A = A'' \frac{q_+ q_-}{8\pi \varepsilon RT} \left( \frac{2N_A}{1000} \right)^{\frac{1}{3}} \quad (14)$$

$$B = B'' \frac{q_+^2}{64\pi RT \varepsilon_0^2} \left| \frac{d\varepsilon}{dR} \right| V_{sea} \frac{2N_A}{1000}$$

As noted by Bahe,  $A=0.28894$  at 298,15 K in  $H_2O$ , and  $B$  could be estimated but is normally used as a fitting parameter. Simple as it is, Eq. (13) contains the whole thermodynamic

properties of the solutions<sup>2</sup>, and it somehow culminated five decades of efforts devoted to get a clear understanding of the microscopic origin of the cube-root law for thermodynamic properties of electrolyte solutions. This result allowed Bahe to give an adequate interpretation to the huge number of observations of activity coefficients of electrolyte solutions reported during precedent decades, and also of other magnitudes of aqueous solutions of 1:1 electrolytes such as the relative partial molar enthalpies and heats of dilution (Bahe, 1972b). 1:2 and 2:1 electrolytes were also considered by Bahe in collaboration with D. Parker (Bahe & Parker, 1975), who proved that the activity coefficients of these asymmetric electrolytes can be accurately fitted by Eq. (13) considering now that the ions form a loose fluorite-like structure.

Successful as it proved to be, the original formalism of Bahe could not give account of the thermodynamic properties of highly concentrated electrolyte solutions. Indeed, the theory is not able to fit the experimental data of 1:1 electrolytes beyond 4 M, and of 1:2 electrolytes beyond 3 M. For more concentrated solutions, deviations of the activity coefficients experimental results from the prediction of Eq. (13) are registered due to the influence of short-ranged, non-coulombic interactions, essentially hard sphere repulsions and van der Waals attraction forces. As the concentration of the electrolyte solution increases, the average distance between ions decreases, so the short-range interactions between them become progressively more important with respect to their Coulomb counterparts. In 1997, Varela et al. (Varela et al., 1997) introduced short-range ion-ion interactions in the pseudolattice formalism modeling them by a hard-core potential with an attractive tail. Indeed, the authors considered an interaction potential  $U^{SR}(r_{ij})$  modeling short-range ion-ion forces in solutions by a hard-core potential and an attractive tail representing van der Waals interactions. Assuming a restricted primitive model (RPM) description, all the ions were treated in this article as having the same hard-core radius,  $r_m = (r_+ + r_-)/2$ , where  $r_+$  and  $r_-$  are the radii of cations and anions, respectively. The energy of interaction between ions  $i$  and  $j$  separated by a distance  $r_{ij}$  is

$$U^{SR}(r_{ij}) = \begin{cases} -\frac{\Lambda}{r_{ij}^6} & r_{ij} > r_m \\ \infty & r_{ij} \leq r_m \end{cases} \quad (15)$$

The attractive tail of the potential defined in the above result includes attractive dispersive London forces together with permanent dipole–permanent dipole (Keesom) and permanent dipole-induced dipole (Debye) forces, if any of the ions in the bulk has a permanent dipole. Thus, the constant  $\Lambda$  in Eq. (15) is formed by the contribution of three terms,  $\Lambda = \Lambda_{\text{Keesom}} + \Lambda_{\text{Debye}} + \Lambda_{\text{London}}$ . London dispersion interaction takes place between dipoles instantaneously induced in the ions, arising from fluctuations in the electronic charge cloud of an ion caused by the electric field created by another one in its neighbourhood. Recalling the quantum mechanical theory of dispersion forces, the dispersive interaction energy between two dipoles is given by (Cohen-Tannoudji et al., 2006)

<sup>2</sup> However, it is interesting to note that the activity coefficient (equivalently, the Gibbs free energy) is not expressed in terms of its natural variables  $T, P, N$ , but it instead contains the volume as a variable, so this result cannot be considered to be a proper expression of a thermodynamic potential.

$$U^{disp}(r_{ij}) = -\frac{3\alpha_i\alpha_j I_i I_j}{4\pi\epsilon(I_i + I_j)} \frac{1}{r_{ij}^6} \quad (16)$$

so the constant  $\Lambda$  in Eq. (15) can be straightforwardly deduced from the above result. Recalling that in the pseudolattice formalism,  $r_{ij} = a_{ij}R$ , then  $U^{disp}(r_{ij}) \sim c^2$ . The same applies to Keesom and Debye forces in the case of ions with permanent dipoles, since both them show the same dependence on the interionic distance as that of the London interaction (Israelachvili, 1992).

In their original 1997 paper, Varela et al. proved that the contributions of both hard sphere repulsive part of the interionic potential, and that of the van der Waals forces to the activity coefficient are given by

$$\ln f_{\pm}^{att} = -\frac{\Lambda D'' v N_A^3}{2 \cdot 10^6 RT a_A^6} c^2 \quad (17)$$

$$\ln f_{\pm}^{HS} = 2.2063 \times 10^{-3} r_m^3 c + 2.6269 \times 10^{-6} r_m^6 c^2,$$

where  $D'' = \sum_{ij} a_{ij}^{-6}$  is a Madelung-like constant. Consequently, combining the above expression with that in Eq. (13) we get

$$\ln f_{\pm} = \frac{G_{el}}{2RT} = -Ac^{1/3} + Bc + Dc^2 \quad (18)$$

The above result states that at high concentrations the rational activity coefficient exhibits quadratic concentration dependence rather than the linear one predicted by Bahe's purely electrostatic pseudolattice treatment. As can be seen in Table I, this dependence can be proved to be valid for several electrolytes (Varela et al., 1997), where  $\ln f_{\pm} + Ac^{1/3} - Bc$  is fitted to  $Dc^x$ . As can be seen in the table, Varela et al. obtained that, for several 1:1 and 1:2 electrolytes, the calculated exponent is  $x=2$ , within the limits of experimental uncertainty for all the analyzed data.

Electrolyte	x
HClO <sub>4</sub>	2.05 ± 0.03
HNO <sub>3</sub>	1.93 ± 0.05
LiBr	1.93 ± 0.05
LiNO <sub>3</sub>	1.90 ± 0.10
NaOH	2.00 ± 0.20
KCl	1.80 ± 0.20
NaBr	2.04 ± 0.04
MgCl <sub>2</sub>	2.01 ± 0.02
MnCl <sub>2</sub>	2.04 ± 0.04

Table 1. Results of fitting  $\ln f_{\pm} + Ac^{1/3} - Bc$  to  $Dc^x$  for several 1:1 and 1:2 electrolytes (Varela et al., 1997).

Considering short range forces, Varela et al. were able to fit reported activity coefficient for symmetric 1:1 and asymmetric 1:2 and 2:1 electrolytes up to concentrations of 14 M (LiBr,

HNO<sub>3</sub>, HClO<sub>4</sub>) and 6 M respectively. Moreover, they were able to give quantitative account of the relative partial molar enthalpies of these strong electrolyte solutions in terms of expressions quadratic in the molar concentration.

Fig. 1 shows previously reported data of the molar dependence of the relative partial molar enthalpy of KF (Lobo, 1990), together with the predictions of the above equation and those of Bahe original formalism. As one can see, the relative partial molar enthalpies of concentrated KF solutions are completely impossible to be reproduced by a linear equation such as that predicted in Bahe original formalism. However, the quadratic term associated to short-range interactions in the bulk solution allows the theoretical prediction of the experimental results up to high concentrations. In this way, the role of short-range interactions in highly concentrated electrolyte solutions is completely clarified.

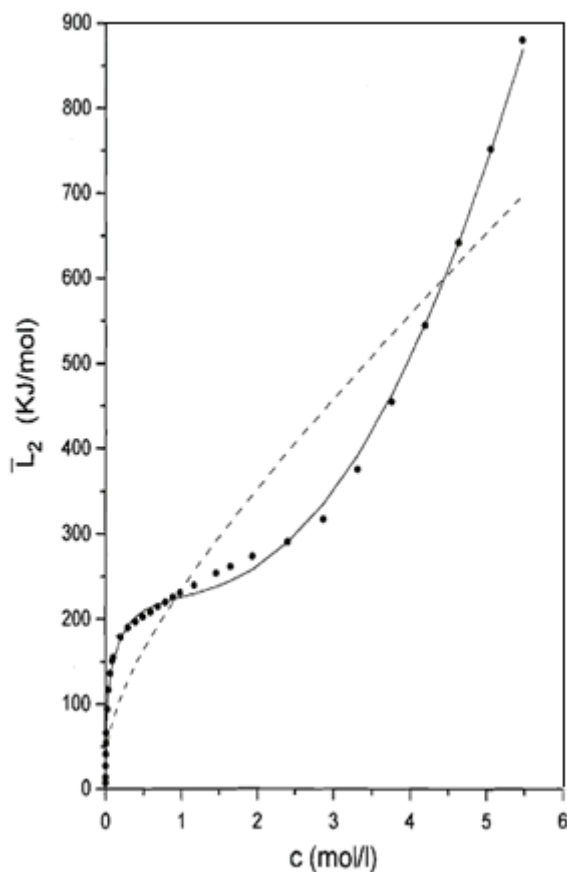


Fig. 1. Relative partial molar enthalpy of an aqueous solution of KF. (---) Bahe predictions (—) BV predictions. Data taken from (Lobo, 1990).

In what the transport properties of concentrated aqueous solution is concerned, they are expected to be determined by the structural features of the system. The predictions of the

Debye-Hückel-Onsager theory mentioned in the Introduction to this chapter are expected to break down as soon as the totally random structure found in highly dilute solutions gives way to the statistical lattice. Indeed, as can be seen in Fig. 2, the electrical conductance of electrolyte solutions is fitted by a relation linear in  $c^{1/3}$  over a large range of concentrations, while the validity of the predictions of the Debye-Hückel-Onsager theory based on the existence of inhomogeneous charge clouds in the bulk is restricted to extremely dilute systems. As we have seen in the Introduction, Lemordant and coworkers introduced a purely heuristic derivation of a pseudolattice expression for the electrical conductance of electrolyte solutions linear in the cube root of the molar concentration. Up to our knowledge, a detailed derivation of this relation has not been reported yet in literature, and a tentative demonstration is included in the following.

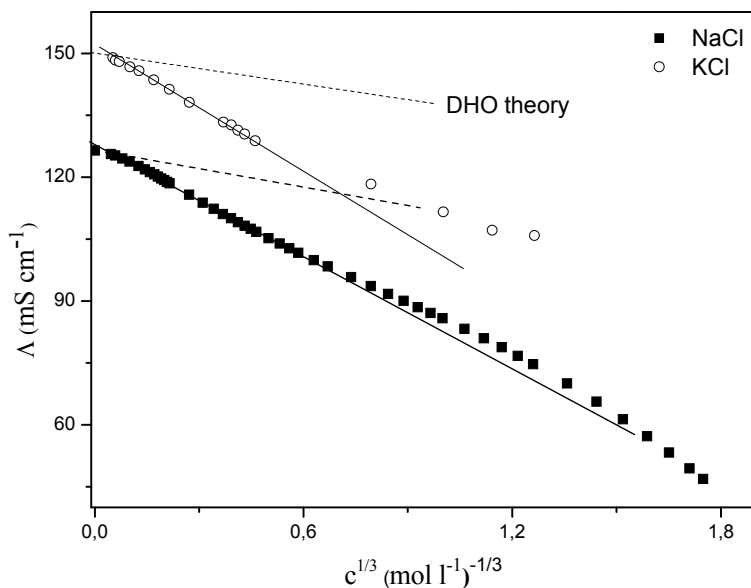
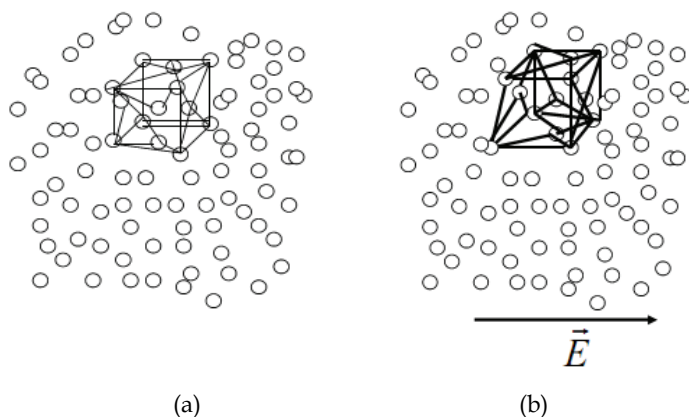


Fig. 2. Electrical conductance of 1:1 electrolyte solutions at 298.15 K (data taken from Lobo, 1990). The solid lines and the dashed lines represent, respectively, the predictions of a cube-root linear law (pseudolattice theory) and a square-root linear law in concentration (Debye-Hückel-Onsager theory).

Let us assume that point ions move in a concentrated electrolyte solution under the influence of an external electric field weak enough so as to preserve the underlying pseudolattice structure throughout the ionic motion. However, the external electric field perturbs the pseudolattice cell structure in the way that is shown in Scheme 1.

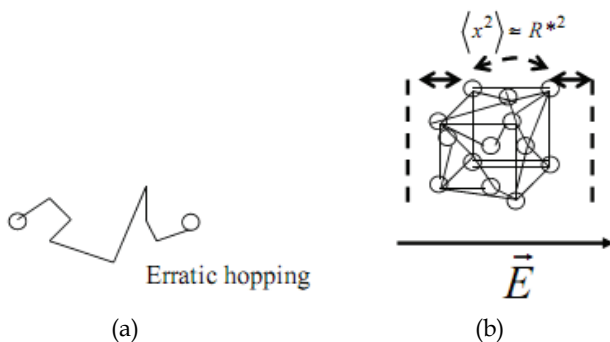
As with the perturbed ionic cloud, the perturbed pseudolattice cell reduces the mobility of the ions with respect to the infinitely dilute system, so  $\mu_j = \mu_j^0 - |\delta\mu_j|$ . The ions wander under the action of the electric field from one position to another of the pseudolattice in a



Scheme 1. Action of the electric field on the structure of a bulk electrolyte solution. (a) Unperturbed situation, b) perturbed situation.

kind of “erratic hopping” due to the collisions with the solvent molecules. As shown in Scheme 2, the average of the squared displacement is approximately equal to the lattice distance between ions (cell size), so the relaxation time associated to this diffusion mechanism is

$$\tau = \frac{\langle x^2 \rangle}{2D} = \frac{R^2}{2D} \quad (19)$$



Scheme 2. Average of the squared displacement of an ion under the action of an external electric field. The lateral arrows in (b) represent the limits of the distorted cell.

The amount by which the pseudolattice cell is distorted during the motion of the ion under the effect of the external electric field is equal to the distance travelled by the ion during its relaxation time

$$d \approx v^0 \tau = v^0 \frac{R^2}{2D} \quad (20)$$

Inside the distorted pseudolattice cell, a force exists associated to the internal electric field associated to the breaking of the symmetry of the equilibrium structure. In the case of the distorted ionic cloud, this field is called the relaxation field and is one of the components responsible for the reduction of the mobility of the ions with respect to the ideal, non-interacting situation (Harned & Owen, 1958; Robinson & Stokes, 1959). This relaxation force can be proved to be

$$\begin{aligned}\bar{F}_R &= -\frac{q^2}{4\pi\epsilon R^{*2}}\left(\frac{\bar{d}}{R^*}\right) \approx -\frac{q^2}{4\pi\epsilon R^*}\left(\frac{\bar{v}^0}{2D}\right) \\ &= -\frac{q^2}{4\pi\epsilon R^*}\left(\frac{\bar{v}^0}{2\mu^0 k_B T}\right) = -\frac{q^3}{8\pi\epsilon k_B T} \frac{1}{R^*} \bar{F}_{ext}\end{aligned}\quad (21)$$

The dependence in  $1/R^*$  of the above force clearly suggests that the dependence of the associated mobility reduction will show a  $c^{1/3}$  dependence, in line with the experimental results and the previously reported theoretical results of Lemordant and coworkers previously cited.

The other physical phenomenon responsible for the reduction of the ionic mobility in the bulk electrolyte solution is the electrophoretic effect, which arises from the motion of an ion in a medium (solvent) not at rest. This electrophoretic correction to the mobility of the ions in the bulk concentrated electrolyte solutions can be calculated by the following arguments. In the steady state of the ionic transport the electrophoretic velocity is the result of the equilibrium between the electric force driving the ionic cloud and the viscous force

$$q\bar{E} = 6\pi\eta R^* \bar{v}, \quad (22)$$

where we have used the conventional Stokes-Einstein relation for the viscous force acting on a spherical particle of radius  $R^*$  in a fluid of viscosity  $\eta$ . Obviously, this implies that we are ignoring the effects of the distortion of the ionic clouds, which is a good approximation for low electric fields). Taking now into account that the radius of our moving entity is approximately that of the distorted pseudolattice cell,  $R^*$ , in the above equation acquires the meaning of the distance between ions in the statistical arrangement in the bulk, so

$$v = \frac{qE}{6\pi\eta R^*} \approx c^{1/3} \quad (23)$$

As follows from Eqs. (21) and (23), both the electrophoretic correction and the relaxation field correction to the mobility are directly dependent functions of  $c^{1/3}$ . Consequently, the mobility of the ions submitted to the relaxation force and the electrophoretic correction is reduced by

$$\begin{aligned}\bar{v} &= \mu^0 \bar{F}_{eff} = \mu^0 \left[1 - g(q, T) c^{1/3}\right] \bar{F}_{ext} \\ \mu_{eff} &= \mu^0 \left[1 - g(q, T) c^{1/3}\right]\end{aligned}\quad (24)$$

where  $\bar{F}_{eff}$  is the total force acting on the central ion due to the external electric field, the internal relaxation field and the electrophoretic effect. Therefore, it is straightforward to see

that the ionic conductance follows a linear law in the cube root of the concentration in accordance with the experimental observations.

### 3. Pseudolattice theory models of room temperature molten salts

After the work of Varela et al. in 1997, very limited activity was registered in the field of pseudolattice theory of concentrated electrolyte solutions, besides the previously cited works of Moggia and Moggia & Bianco reported in this decade. However, in 2006 the group of Prof. Turmine in Paris described the acid-base properties of aqueous solutions of ILs up to the highest concentrations (pure IL) using Bahe's approach completed by Varela et al. concerning structured electrolyte solutions with large short-range interactions (Bou Malham et al., 2007). As we have previously mentioned, this group successfully applied the Bahe-Varela formalism to the understanding of volumetric properties (apparent molar volumes and partial molar volumes) of several aqueous and non-aqueous mixtures of ILs. Consequently, the pseudolattice theory was for the first time proved to be valid for mixtures of conventional molecular solvent and room-temperature molten salts, for which it can be applied throughout the whole concentration range, without the limitations of precipitation phenomena. In this fashion, the pseudolattice proved to be a unifying structural framework for the understanding of IL-solvent mixtures, and consequently of pure ILs themselves.

Recently, some of us have completed the pseudolattice Bahe-Varela theory analyzing the implications of the existence of a statistical lattice arrangement of ions in the bulk ionic fluid on the surface and transport phenomena of ionic solutions and IL-solvent mixtures (Varela et al, 2009; Varela et al. 2010). In what the surface properties are concerned, up to our knowledge, until 2009 the only reported theory of the surface tension of electrolyte solutions was the so called Onsager-Samaras theory (Onsager and Samaras, 1934), based on the continuous model underlying Debye-Hückel theory of ionic solutions and valid for infinitely diluted solutions. In 2009 some of us reported a pseudolattice theory of the surface tension of electrolyte solutions and IL-solvent mixtures. Despite in the original version of the pseudolattice theory a hard-core potential was used to model the short-range interionic repulsions (Varela et al. 1997), the importance of these interactions in the pure IL regime and in extremely concentrated solutions lead the authors to assume that the short-range non-Coulomb interactions are well described by a Lennard-Jones (LJ) potential with a  $r^{-12}$  attractive tail

$$u_{ij}^{LJ}(r_{ij}) = \frac{A}{r_{ij}^{12}} - \frac{\Lambda}{r_{ij}^6}. \quad (25)$$

On the basis of this potential, and using similar arguments to those which lead to Eq. (10) it is rather easy to prove that the free energy of the system is

$$F = A'' \frac{q_+ q_-}{4\pi\epsilon} \frac{1}{R^*} + B'' \frac{q_+^2}{(4\pi\epsilon_0)^2} \left| \frac{d\epsilon}{dR^*} \right| V_{sea} \frac{1}{R^{*3}} - D'' \frac{\Lambda}{R^{*6}} + E'' \frac{A}{R^{*12}} \quad (26)$$

Given their structural characteristics, the surface tension of the pseudolattice ionic systems can be calculated as that of solids. As shown by Shuttleworth (Shuttleworth, 1950) the surface tension of a crystal face is related to the surface free energy by the relation



$\gamma = F + S(dF/dS)$ , where  $S$  stands for the area of the surface. This surface area can be related to the pseudolattice cell size since it scales as  $S \sim R^{*2}$ , so

$$\gamma = A'' \frac{q_+ q_-}{8\pi\epsilon} \frac{1}{R^*} - B'' \frac{q_+^2}{2(4\pi\epsilon_0)^2} \left| \frac{d\epsilon}{dR^*} \right| V_{\text{cell}} \frac{1}{R^{*3}} + 2D'' \frac{\Lambda}{a_A^6} \frac{1}{R^{*6}} - 5E'' \frac{1}{R^{*12}} \quad (27)$$

Considering that in pure ILs ion-solvent interactions are absent, and that the short-range repulsive term is expected to be dominant due to the great number of ionic contacts, the main contribution to the surface tension of pure ILs is expected to scale like  $R^{*-12} \sim \rho^4$ , where  $\rho$  is the IL density

$$P = CF_W = \frac{F_W \gamma^{1/4}}{\rho - \rho_v} \cong \frac{F_W \gamma^{1/4}}{\rho} \quad (28)$$

$F_W$  being the formula weight,  $C$  a constant characteristic of the liquid, and  $\rho_v$  the density of air. The above equation agrees with the predictions for the parachor of liquids, which establishes the proportionality between the surface tension and the density of the liquid,  $\gamma \propto \rho^4$ , a result recently verified for ILs by Deetlefs et al. (Deetlefs, 2006). Eq. (28) stands exclusively on the basis of a pseudolattice model for the bulk liquid, in contrast with what happens in the hole and interstice models, where surface tension is treated as a purely experimental input necessary for the determination of the hole or interstice average radius respectively.

Moreover, in the same paper (Varela et al., 2009) the reduced surface pressure of IL-water mixtures was calculated assuming a pseudolattice structure in the bulk, and a localized adsorption scheme on the surface of the liquid employing the Langmuir isotherm. Thus, cations are assumed to migrate through the mixture and to be adsorbed on localized adsorption sites on the surface of the mixture. The interactions of cations with other molecules present in the system are treated in the Bragg-Williams approximation. Under these assumptions the calculated reduced surface pressure of the system was

$$\pi^* = \frac{\gamma - \gamma_B}{\gamma_A - \gamma_B} = \frac{x_A \exp\left(e^{-\frac{\beta z \omega_{AA}}{2}}\right) e^{-\frac{\beta z \omega(1-x_A)^2}{2}}}{1 + x_A \exp\left(e^{-\frac{\beta z \omega_{AA}}{2}}\right) e^{-\frac{\beta z \omega(1-x_A)^2}{2}}} \quad (29)$$

where  $z$  stands here for the number of neighbors in the pseudolattice,  $\omega_{AA}$  ( $\omega_{BB}$ ) represents the interaction between molecules of the  $A$  ( $B$ ) species in the pseudolattice and  $\omega = \omega_{AA} + \omega_{BB} - 2\omega_{AB}$  and  $x_A$  the molar fraction of the cation species. The predictions of Eq. (29) for IL-water mixtures are shown in Fig. 3 for EMIM-BF<sub>4</sub> and BMIM-BF<sub>4</sub>.

On the other hand, transport theory has been the last update (up to now) of the pseudolattice theory of concentrated electrolyte solutions and IL mixtures (Varela et al., 2010). In this latter reference a statistical mechanical pseudolattice model of charge transport in ionic fluid-solvent mixtures was introduced, and the predictions were compared with data of the electric conductivity of aqueous electrolyte solutions, IL-water and IL-ethanol

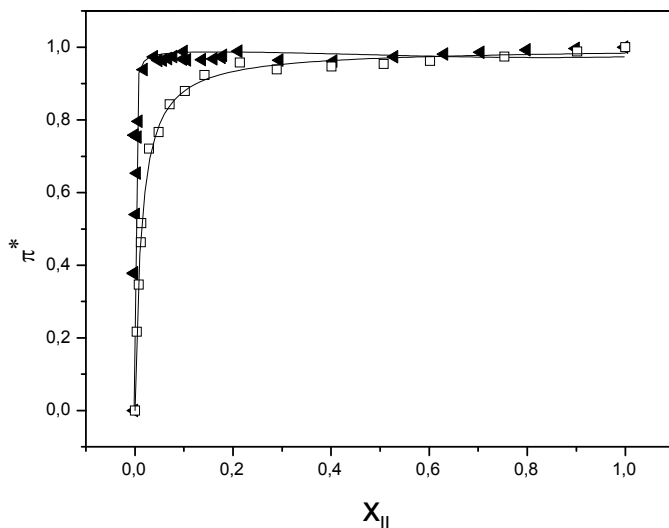


Fig. 3. Reduced surface pressure of aqueous mixtures of EMIM-BF<sub>4</sub> (□) BMIM-BF<sub>4</sub> mixtures (◼). The solid lines correspond to the predictions of Eq. (29) and the fitting parameters can be found in (Varela et al., 2009). Data taken from (Rilo et al., 2009).

mixtures. The ions were assumed to move randomly between the cells in a statistical lattice representing the cooperatively rearranging regions in the liquid, defined by Adam and Gibbs as “the smallest region that can undergo a transition to a new configuration without a requisite simultaneous configurational change on and outside its boundary” (Adams & Gibbs, 1965). Classical hopping over energy barriers is between adjacent cells are the main mechanism by which the charge transport takes place. On average, only two different types of ionic environments of an ion were supposed to occur: i)  $\beta$ -cells with no ions in nearest neighbour cells, on which an ion experiences an energy barrier  $\varepsilon_\beta$ , and ii)  $\alpha$ -cells associated to ions in its neighbourhood, with a well depth  $\varepsilon_\alpha$ . The first ones are mainly associated to solvent molecules in the lattice or even to low density regions in the bulk (hole-like regions), and the latter to other ions.

In the presence of an external electric field the weighted average excess probability of jumping in the direction of the field can be written as (Varela et al., 2010)

$$\begin{aligned} \bar{v}_p &= \sum_{i=\alpha,\beta} \phi_i \bar{v}_{pi} = \frac{1}{3} \frac{(k_B T)^3}{h^3} \left( \phi_\alpha \frac{e^{-\varepsilon_\alpha/k_B T}}{v_{s\alpha}^2} + \phi_\beta \frac{e^{-\varepsilon_\beta/k_B T}}{v_{s\beta}^2} \right) \frac{aqE}{k_B T}, \\ &= \frac{qa}{k_B T} (\phi_\alpha \bar{v}_\alpha + \phi_\beta \bar{v}_\beta) E \end{aligned} \quad (30)$$

where  $k_B T$  is the thermal energy,  $h$  is Planck's constant and  $v_{si}$  is the vibration frequency of an ion in the two directions of the saddle point perpendicular to the direction of flow in a cell of the  $i$  type ( $i=\alpha,\beta$ ). On the other hand,  $\varepsilon_i$  represents the energy barrier height of cells

of the  $i$ -th type and  $\bar{v}_i$  is the probability per unit time of an ion jumping a barrier of the  $i$ -th type. The electric polarization associated to each ion jump is  $qa$  (with  $a$  the lattice constant and  $q$  the ionic charge), so, if we represent by  $n_\alpha$  the number density of mobile ions in the pseudolattice, and considering that for low excess volumes of ILs it can be assumed that  $n_\alpha \approx \phi_\alpha / V_\alpha$ , where  $V_\alpha$  is the ionic volume, then the current density is given by  $j_\alpha = n_\alpha qa \bar{v}_\alpha$ . So, the electrical conductivity of the pseudolattice mixture reads

$$\kappa = \frac{q^2 a^2}{V_\alpha k_B T} \left[ \phi_\alpha^2 \bar{v}_\alpha + (1 - \phi_\alpha) \phi_\alpha \bar{v}_\beta \right]. \quad (31)$$

One can easily notice that the coefficients  $\bar{v}_i$  in the right hand side of the above result comprise all the relevant features of ion-ion and ion-solvent interactions, so they are expected to be functions of the concentration (Varela et al., 2010). For non-correlated ion transport, conductivity maxima are predicted in terms of the probability of jumping between different types of cells, and the behaviour of the conductivity normalized to its maximum value with the scaled ionic concentration is seen to approximately fit to a universal corresponding states law given by

$$\frac{\kappa}{\kappa_{\max}} = 2 \xi_\alpha \left( 1 - \frac{\xi_\alpha}{2} \right) \quad (32)$$

$\xi_\alpha = \phi_\alpha / \phi_{\max}$  being the scaled ionic concentration.  $\kappa_{\max}$  and  $\phi_{\max}$  are the maximum electrical conductivity of the mixture and the volume fraction at which it is reached, respectively. As can be seen in (Varela et al., 2010), the above equation accurately predicts the electrical conductivity of electrolyte solutions and IL mixtures throughout the whole range of concentration. Deviations from this law registered at high volume fractions are attributable to ion-ion and ion-solvent interactions, and they were analyzed in the same paper in the Bragg-Williams (BW) mean-field approximation.

Finally, we must mention that the thermal conductivity of pure ILs is known to exhibit a very weak dependence on temperature (van Valkenburg et al., 2005). These constancy clearly suggests that the mechanism that phonon scattering at the grain boundaries of the nanostructured IL prevails over phonon interactions. The pseudolattice theory -with its microscopic picture of an IL as a disordered ensemble of nanostructured lattice rearranging regions- is expected to provide the structural framework which, combined with a mechanism of phonon hopping through the boundaries of these regions (Bragisnky et al., 2002), gives a satisfactory explanation of this magnitude.

#### 4. Conclusions

In the present chapter we have reviewed the origins and historical evolution of the pseudolattice theory of ionic solutions, from the seminal work of Gosh in the second decade of the XX<sup>th</sup> century, to the contemporary Bahe-Varela theory, which includes interionic Coulomb interactions, the coupling of the electric field in the bulk solution with the gradient of dielectric field in the region, and short-range ion-ion interactions in a statistical lattice environment. The main features of the equilibrium formalism were revisited, and a heuristic derivation of a pseudolattice equation of the electric conductance introduced. Moreover, the

main applications of the theory to concentrated electrolyte solutions and IL-solvent mixtures (predictions of volumetric properties, surface properties and charge transport) were reviewed. From all the exposed material, pseudolattice theory emerges as the unifying theoretical framework which accounts for the properties of ionic fluids irrespective of their ionic concentrations. In future works, the extension of the transport theory to give account for the deviations of the electrical conductivity from the ideal behavior represented by Eq. (32) is to be done, together with the systematic application of the theory to new experimental data of IL mixtures. Finally, it is worth mentioning that a pseudolattice theoretical framework for the thermal conductivity of ILs is under current investigation.

## 5. Acknowledgements

This work was supported by the Spanish Ministry of Science and Innovation in conjunction with the European Regional Development Fund (Grants No. FIS2007-66823-C02-01, No. FIS2007-66823-C02-02, and No. FIS2008-04894/FIS), and by the Directorate General for R+D+i of the Xunta de Galicia (Grant N° INCITE09E2R206033ES). J. Carrete thanks the Spanish Ministry of Education for an FPU grant.

## 6. References

- Adam, G. & Gibbs, J. H. (1965) On the temperature dependence of cooperative relaxation properties of glass-forming liquids. *J. Chem. Phys.* 43, 1, 139-146, ISSN 0021-9606
- Alves Marques, M.; de Barros Marques, M. I.; Cabaço, M. I.; Gaspar, A. M.; Marques, M. P. M.; Amado, A. M. & Amorim da Costa A. M. (2007) Evidence of a local order in concentrated aqueous solutions of salts constituted by ions of different valences: X-ray diffraction and Raman spectroscopy experiments. *J. Mol. Liquids* 134, 1-3, 142-150, ISSN 0167-7322
- Attard, P. (1993) Asymptotic analysis of primitive model electrolytes and the electrical double layer. *Phys. Rev. E* 48, 5, 3604-3621, ISSN 1063-651X
- Bahe, L. W., (1972a) Structure in concentrated electrolyte solutions. Field-dielectric-gradient forces and energies. *J. Phys. Chem.*, 76, 7, 1062-1071, ISSN 0022-3654
- Bahe, L. W., (1972b) Relative partial molar enthalpies and heats of dilution of electrolytes in water. *J. Phys. Chem.*, 76, 11, 1608-1611, ISSN 0022-3654
- Bahe, L. W. & Parker, D. (1975) Activity coefficients of 2:1 electrolytes in structured electrolyte solutions. *J. Am. Chem. Soc.*, 92, 20, 5664-5670, ISSN 0002-7863
- Bockris, J. O'M. & Reddy, A. K. N (2000) *Modern Electrochemistry. Vol. 1 Ionics. 2<sup>nd</sup> edition.* Plenum Press, ISBN 9783527323906, New York
- Boroudjerdi, H.; Kim, Y.-W.; Naji A.; Netz, R. R.; Schlagberger, X. & Serr, A. (2005) Statics and dynamics of strongly charged soft matter. *Phys. Rep.* 416, 3-4, 129-199 ISSN 0370-1573
- Bou Malham, I.; Letellier, P. & Turmine, M. (2007a) Application of the Bahe's pseudolattice-theory to water-1-butyl-3-methylimidazolium tetrafluoroborate (bmimBF<sub>4</sub>) mixtures at 298.15 K: Part I. Autoprotolysis constants. *Talanta*, 72,1, 155-164, ISSN: 0039-9140
- Bou Malham, I.; Letellier, P.; Mayaffre, A. & Turmine, M. (2007b) Part I: Thermodynamic analysis of volumetric properties of concentrated aqueous solutions of 1-butyl-3-methylimidazolium tetrafluoroborate, 1-butyl-2,3-dimethylimidazolium

- tetrafluoroborate, and ethylammonium nitrate based on pseudo-lattice theory. *J. Chem. Thermodyn.*, 39, 8, 1132-1143, ISSN 0021-9614
- Bouguerra, S.; Bou Malham, I.; Letellier, P.; Mayaffre, A. & Turmine, M. (2008) Part 2: Limiting apparent molar volume of organic and inorganic 1:1 electrolytes in (water + ethylammonium nitrate) mixtures at 298 K – Thermodynamic approach using Bahe-Varela pseudo-lattice theory. *J. Chem. Thermodyn.*, 40, 2, 146-154, ISSN 0021-9614
- Braginsky, L; Lukzen, N.; Shklover, V. & Hofmann, H. (2002) High-temperature phonon thermal conductivity of nanostructures. *Phys. Rev. B* 66, 13, 134203, 1-7, ISSN 1098-0121
- Chagnes, A.; Carre, B.; Willmann, P. & Lemordant, D. (2001) Ion transport theory of nonaqueous electrolytes.  $\text{LiClO}_4$  in  $\gamma$ -butyrolactone: the quasi lattice approach *Electrochimica Acta* 46, 12, 1783-1791, ISSN 0013-4686.
- Chagnes, A.; Carre, B.; Willmann, P. & Lemordant, D. (2002) Modeling viscosity and conductivity of lithium salts in  $\gamma$ -butyrolactone, *J. Power Sources* 109, 1, 203-213, ISSN 0378-7753
- Chagnes, A.; Nicolis, S.; Carre, B.; Willmann, P. & Lemordant, D. (2003) Ion -dipole interactions in concentrated organic Electrolytes. *Chem. Phys. Chem.* 4, 6, 559 -566 ISSN 1439-4235
- Chapman, D.L.(1913) A contribution to the theory of electrocapillarity. *Phil. Mag.* 25, 475-481
- Cohen-Tannoudji, C., Diu, B. & Laloe, F. (2006) *Quantum Mechanics*. Wiley-Interscience, ISBN 0471569526, New York.
- Debye, P.; Hückel, E. (1923) On the Theory of Electrolytes. I. Freezing Point Depression and Related Phenomena. *Phys. Z.* 24 , 185-206
- Deetlefs, M.; Seddon, K. R. & Sharab, M. (2006) Predicting physical properties of ionic liquids. *Phys. Chem. Chem. Phys.*, 8, 642-649, ISSN 1463-9076
- Desnoyers, J. E. & Conway, B. E., (1964) Activity Coefficients of Electrolytes at Intermediate Concentrations and the “Cube-Root” Law. *J. Phys. Chem.* 68, 8, 2305-11, ISSN 0022-3654
- Frank H. S. & Thompson, P. T. (1959a) Fluctuations and the Limit of Validity of the Debye-Hückel Theory *J. Chem. Phys.* 31, 4, 1086-1095, ISSN 0021-9606
- Frank H. S. & Thompson P. T. (1959b) *The Structure of Electrolyte Solutions*. W. J. Hamer, Ed., John Wiley and Sons, Inc., New York.
- Fuoss, R. M.; Onsager, L. & Skinner, J. F. (1965) The conductance of symmetrical electrolytes V. The conductance equation. *J. Phys. Chem.*, 69, 8, 2581-2594, ISSN 0022-3654
- Ghosh, G. C. (1918) The abnormality of strong electrolytes. Part I. Electrical conductivity of aqueous salt solutions., *J. Chem. Soc.* 113, 449-458
- Gouy, G. (1910) Sur la constitution de la charge électrique à la surface d'un électrolyte, *J. Phys.* 9, 1, 457-468
- Harned, H.S. & B.B. Owen (1958), *The Physical Chemistry of Electrolyte Solutions*, 3<sup>rd</sup> edition, Reinhold, New York.
- Hyman, A. & Vaughn, V. (1967) *Small-Angle Scattering*, Proceedings of the Conference Held at Syracuse University, June, 1966, Gordon and Breach, ISBN , New York.
- Israelachvili, J. (1992) *Intermolecular and Surface Forces*, 2<sup>nd</sup> Ed., Academic Press, ISBN 0123751810, London
- Jiang, W.; Wang, T. & Voth, G. A. (2007) Molecular Dynamics Simulation of Nanostructural Organization in Ionic Liquid/Water Mixtures *J. Phys. Chem. B* 111, 18, 4812-4818, ISSN 1089-5647

- Kirkwood, J. G. & Poirier, J. C. (1954) The Statistical Mechanical Basis of the Debye-Hückel Theory of Strong Electrolytes. *J. Phys. Chem.* 58, 8, 591-596, ISSN 0022-3654
- Kjellander, R. & Mitchell, D.J. (1992) An exact but linear and Poisson-Boltzmann-like theory for electrolytes and colloid dispersions in the primitive model. *Chem. Phys. Lett.* 200, 1-2, 76-82, ISSN 0009-2614
- Kjellander, R. & Mitchell, D.J. (1994) Dressed-ion theory for electrolyte solutions: A Debye-Hückel-like reformulation of the exact theory for the primitive model. *J. Chem. Phys.* 101, 1, 603-626, ISSN 0021-9606
- Lobo, V.M.M. (1990) *Handbook of electrolyte solutions*, Elsevier, ISBN 0444988475, Amsterdam
- McBride, A.; Kohonen, M. & Attard, P. (1998) The screening length of charge-asymmetric electrolytes: A hypernetted chain calculation. *J. Chem. Phys.* 109, 6, 2423-2428, ISSN 0021-9606
- Moggia, E. & Bianco, B. (2007) Mean activity coefficients of electrolyte solutions. *J. Phys. Chem. B* 111, 12, 3183-3191, ISSN 1089-5647
- Moggia, E. (2008) Osmotic coefficients of electrolyte solutions. *J. Phys. Chem. B*, 112, 4, 1212-1217, ISSN 1089-5647
- Onsager, L. & Samaras, N.N.T. (1934) The surface tension of Debye-Hückel electrolytes. *J. Chem. Phys.* 2, 8, 528-536, ISSN 0021-9606
- Padova, J. (1963) Ion-Solvent Interaction. II. Partial Molar Volume and Electrostriction: a Thermodynamic Approach. *J. Chem. Phys.* 39, 6, 1552-1557, ISSN 0021-9606
- Panofsky, W. and Phillips, M. (1977). *Classical electricity and magnetism*. Addison-Wesley, Reading, Massachusetts.
- Prins, J. A. & Fonteyne, R. (1935) Molecular Arrangement and X-Ray Diffraction in Ionic Solutions, *J. Chem. Phys.* 3, 2, 72-80, ISSN 0021-9606
- Rilo, E.; Pico, J.; García-Garabal, S.; Varela, L.M. & Cabeza, O. (2009) *Fluid Phase Equilibria*, 285, 1-2, 83-89, ISSN 0378-3812
- Robinson, R.A. & Stokes R.H. (1959), *Electrolyte Solutions*, Butterworths, London.
- van Valkenburg, M. E. Vaughn, R. L.; Williams, M. & Wilkes, J. S. (2005) Thermochemistry of ionic liquids heat-transfer fluids. *Thermochimica Acta* 425, 1-2, 181-188, ISSN 0040-6031
- Varela, L.M.; García, M.; Sarmiento, F.; Attwood, D. & Mosquera, V. (1997) Pseudolattice theory of strong electrolyte solutions. *J. Chem. Phys.* 107, 16, 6415- 6419, ISSN 0021-9606
- Varela, L.M.; Pérez-Rodríguez, M.; García, M.; Sarmiento, F. & Mosquera, V. (1998) Static structure of electrolyte systems and the linear response function on the basis of a dressed-ion theory. *J. Chem. Phys.* 109, 5, 1930- 1938, ISSN 0021-9606
- Varela, L.M.; Ruso, J.M.; García, M. & Mosquera, V. & Sarmiento, F. (1999a) Relaxation of the ionic cloud on the basis of a dressed-ion theory *J. Chem. Phys.* 110, 9, 4483-4492, ISSN 0021-9606
- Varela, L.M.; Pérez-Rodríguez, M.; García, M.; Sarmiento, F. & Mosquera, V. (1999b) Conductance of symmetric electrolyte solutions: Formulation of the dressed-ion transport theory (DITT). *J. Chem. Phys.* 111, 24, 10986-10997, ISSN 0021-9606
- Varela, L. M.; García, M. & Mosquera, V. (2003) Exact mean field theory of ionic solutions: Non-Debye screening *Phys. Rep.* 382, 1-2, 1-111, ISSN: 0370-1573.
- Varela, L.M.; Carrete, J.; Turmine, M.; Rilo, E. & Cabeza, O. (2009) Pseudolattice Theory of the Surface Tension of Ionic Liquid-Water Mixtures. *J. Phys. Chem. B*, 113, 37, 12500-12505, ISSN 1089-5647
- Varela, L.M.; Carrete, J.; García, M.; Gallego, L. J.; Turmine, M.; Rilo, E. & Cabeza, O. (2010) *Fluid Phase Equilibria*, 298, 2, 280-286, ISSN 0378-3812

# Ionic Liquids as Designer Solvents for the Synthesis of Metal Nanoparticles

Vipul Bansal and Suresh K. Bhargava  
*RMIT University  
Australia*

## 1. Introduction

Size and shape-controlled synthesis of metal nanostructures has received significant interest in materials research, as metal nanoparticles are likely to have a considerable impact upon the fields of catalysis, sensing, photonics, optoelectronics and biology, due to their unique size- and shape-tunable physico-chemical properties (Hao et al., 2004; Burda et al., 2005; Shukla et al., 2005; Lu et al., 2009; Sardar et al., 2009). With significant developments in this field, the current focus is predominantly on synthesis of ultra-fine (sub-10 nm) metal nanoparticles with narrow size distribution that remain stable in reaction media, tuning the shape of metal nanostructures, to understand the metal nanoparticles shape-guiding mechanisms, and to understand their structure-property correlation (Lu et al., 2009). To prepare metal nanoparticles (colloids), the most commonly employed approach is the bottom-up wet-chemistry approach. In this approach, typically in the presence of a capping/stabilizing agent, metal ions are controllably reduced, wherein individual metal atoms combine to form metal nanoparticles stabilized by capping agents. Although in few instances reducing agents themselves act as stabilizers, capping agents are generally considered essential to minimize the surface free energy of metal nanoparticles, which would otherwise aggregate in the absence of these capping agents. In most of the well established wet-chemistry routes of metal nanoparticles synthesis, aqueous or organic solvents are generally employed, while the use of ionic liquids (ILs) for synthesis of metal nanoparticles is a relatively recent phenomenon.

As an aqueous solvent, water is although a naturally-available, environmentally-benign, non-toxic and non-inflammable media for nanomaterials synthesis, it remains liquid only in a narrow temperature range (0-100 °C), and have low solubility for organic molecules. Conversely, organic solvents might although offer diverse physico-chemical properties (e.g. density, polarity and solubility), most of them are highly toxic, flammable, have low boiling points and low solubility of inorganic reactants. These drawbacks associated respectively with water and organic solvents may therefore limit their applicability as versatile solvents for nanomaterials synthesis conducted at relatively higher or lower temperatures. Similarly, although few traditional molten salts have been tested as alternative reaction media, their high melting points (usually above 100 °C) limit the practical applicability of such solvents for nanomaterials synthesis.

Ionic liquids (ILs), conventionally refereed as 'room temperature ionic liquids' (RTILs) or 'room-temperature molten salt' have recently become attractive reaction media for the

“green” synthesis of inorganic nanomaterials due to their interesting physico-chemical properties. For instance, ILs are typically liquid over a range of temperatures (RTILs are liquid at room temperatures, with some showing melting point down to  $-80\text{ }^{\circ}\text{C}$ ), possess negligible vapour pressures, high thermal and chemical stability, high ionic conductivity, broad electrochemical potential window, and high ionic density (Dobbs et al, 2006; Dupont and Scholten, 2009; Ma et al., 2010; Neouze, 2010). These interesting properties of ILs offer distinct advantages over conventional aqueous and organic solvents to explore a range of organic and inorganic materials synthesis.

The history of ILs goes as early as 1914, when Walden reported the first ionic liquid  $[\text{C}_2\text{H}_5\text{NH}_3][\text{NO}_3]$  with melting point  $13\text{--}14\text{ }^{\circ}\text{C}$ . This was termed as a protic ionic liquid (PIL), since it involved a proton-transfer reaction during synthesis (Walden, 1914). In 1951, Hurtley and Weir synthesized aprotic ionic liquids (APILs) by mixing alkylpridinium chlorides with  $\text{AlCl}_3$  (Hurtley & Weir, 1951). However these ILs were found to be sensitive to moisture and air and are not in active use nowadays. Thereafter in 1992, Wilkes and Zaworotko developed a new series of water-stable ILs containing tetrafluoroborate  $[\text{BF}_4]$ , hexafluorophosphate  $[\text{PF}_6]$ , nitrate  $[\text{NO}_3]$ , sulphate  $[\text{SO}_4]$  and acetate  $[\text{CH}_3\text{COO}]$  anions (Wilkes and Zaworotko, 1992). Since then, a range of ILs containing organic cations and organic or inorganic anions has been developed (Gordon and Muldone, 2008).

In the recent development of ILs, imidazolium (Im)-based ILs have attracted particular attention because Im-based compounds are very versatile with generally high solubilisation ability and high thermal and electrochemical stability. Moreover, varying the counter-anion in Im-based ILs can drastically influence the physicochemical properties of these systems. For instance, considering a butylmethylimidazolium  $[\text{BMIm}]$  cation, a strongly coordinating anion like chloride will render the  $[\text{BMIm}][\text{Cl}]$  IL as hydrophilic, while a low coordinating anion like hexafluorophosphate will create a hydrophobic  $[\text{BMIm}][\text{PF}_6]$  IL (Mehdi et al., 2010; Soni et al., 2010). The current chapter aims to predominantly focus on use of Im-based ILs for synthesis of metal nanoparticles, mainly because imidazolium moieties have been the most investigated until now with a significant potential for further development. It is also noteworthy that in context of nanomaterials synthesis, Im-based ILs not only play a role of versatile solvent, but they also stabilize nanoparticles, which is particularly important for use of nanoparticles towards various applications including catalysis. Therefore, when combining Im salts and nanoparticles, the need to understand the interactions occurring between Im species and nanoparticles begins to be pressing that will also be touched upon in this chapter. In addition, the chapter will also discuss some of the interesting applications that IL-mediated synthesis of metal nanoparticles may offer.

## 2. ILs as solvents for stabilization of metal nanoparticles

ILs, in general, differ from the classical ammonium salts, at least in one very important aspect: ILs possess pre-organized structures, mainly through hydrogen bonds (Hardacre et al., 2003; Tsuzuki et al., 2005; Dupont & Suarez, 2006), which induce 3-D structure dimensionality in these systems (*IL effect*). Conversely, aggregates of classical salts display charge-ordered structures. Since ILs can form extended hydrogen-bond networks at the liquid state, therefore they demonstrate this very unique property of high self-organization on the nanomolecular scale, and can be classified as ‘supramolecular’ fluids. This nanoscale structural organization of ILs can be used to drive the spontaneous extended ordering of nanomaterials (Pearson et al., 2010; Soni et al., 2010). Some of the classical examples that



have illustrated this concept include IL-mediated synthesis of ordered mesoporous materials and microporous aluminophosphates, wherein ILs served both as the solvent and structure-directing agents (Endres, 2002; Antonietti et al., 2004; Zhou, 2005). One another example in this category includes synthesis of protein and silica nanocapsules in [BMIm][BF<sub>4</sub>] IL via self-organization process, as was demonstrated recently by our group (Soni et al., 2010). It has also been established that the properties of Im-based ILs are dependent on their organized nano-aggregates, rather than merely on their isolated cations and anions (Suarez et al., 1998; Neto et al., 2006). The 3-D arrangement of the Im-based ILs is generally formed through chains of the cationic imidazolium rings, which generates supramolecular channels in which anions are typically accommodated as chains (Lopes & Padua, 2006) (Figure 1). The formation of this 3-D ionic network entails high directional polarizability, which provides an opportunity to adapt a range of external species in either hydrophilic or hydrophobic regions of ILs (Dupont & Suarez, 2006). Therefore, size and shape of the metal nanoparticles synthesized in ILs is typically modulated by the volume of these 3-dimensionally arranged regions within IL environment. It would probably not be an overstatement to classify ILs as nanostructured solvents, with a potential to direct the tailored synthesis of nanoscale materials.

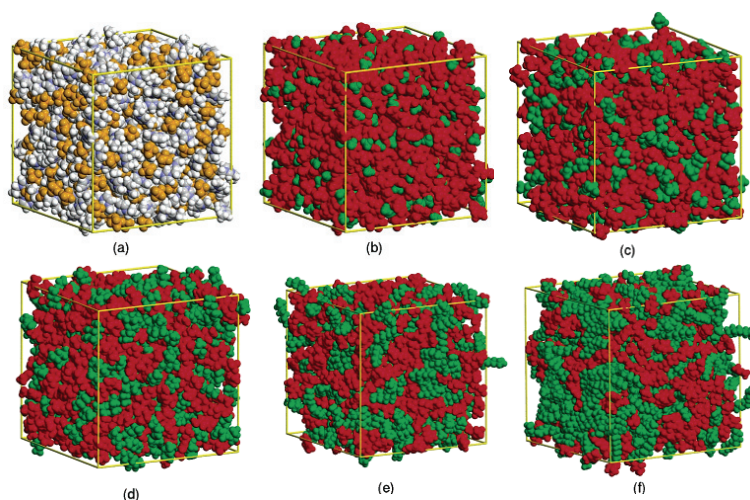


Fig. 1. Snapshots of simulation study of  $[C_n\text{MIm}][\text{PF}_6]$  ILs (boxes contain 700 ions) showing the polar (red) and non-polar (green) domains of ILs. In panels (a)-(f),  $n$  corresponds to 2, 2, 4, 6, 8 and 12 respectively (adapted from Lopes & Padua, 2006 with permission from the American Chemical Society).

A series of studies in the literature suggests that ILs interact relatively strongly with the surface of metal nanoparticles, which have been summarized in a recent report (Neouze, 2010). In fact, transition metal nanoclusters and nanoparticles stabilization by Im-based ILs is now considered as a classical stabilization method (Ott & Finke, 2007). Although capping agents are generally considered essential during metal nanoparticles synthesis in conventional solvents to stabilize them (Neouze & Schubert, 2008), they are typically not required for nanomaterials synthesis in Im-based ILs. However, it is notable that ligand-free

synthesis of metal nanoparticles in ILs, as reported in few reports, is probably a misleading assumption because in these synthesis protocols, although no external ligand is added to stabilize nanoparticles, the Im moiety itself plays the role of both as a solvent, and a stabilizer (Campbell et al., 2010; de Caro et al., 2010; Neouze, 2010; von Prondzinski et al., 2010). Considering the importance of nanoparticles stabilization feature of ILs, we will elaborate on this concept later in this chapter.

### 3. ILs as solvents for synthesis of metal nanoparticles

#### 3.1 Serendipitous discovery of metal nanoparticles formation in ILs

The discovery that ILs can act as novel media for the preparation and stabilization of metal nanoparticles is rather serendipitous. It began with the isolation of metal nanoparticles during catalytic hydrogenation and C-C coupling reactions using organometallic or metal salt catalysts in ILs. For instance, when Deshmukh and co-workers carried out the Heck reaction using  $\text{Pd}(\text{OAc})_2$  and  $\text{PdCl}_2$  catalysts in 1,3-dibutylimidazolium bromide  $\{[\text{BBIm}][\text{Br}]\}$  IL under ultrasonic irradiation conditions, they observed formation of 20 nm Pd nanoparticles composed of 1 nm nanoclusters formed via reduction of  $\text{Pd}^{2+}$  ions during catalytic reaction (Deshmukh et al., 2001). Similarly Hamill and co-workers observed formation of 0.8-1.6 nm Pd clusters during the Heck reaction in several ILs (Hamill et al., 2002). Following these, among the first publications in this field, Dupont and co-workers made a deliberate attempt towards synthesis of uniform-sized Ir nanoparticles in  $[\text{BMIm}][\text{PF}_6]$  IL and used them as catalysts for the hydrogenation of olefins (Dupont et al., 2002). This pioneering work stimulated many subsequent studies, leading to synthesis of Ir (Fonseca et al., 2003; 2006; Singh et al., 2008a), Rh (Fonseca et al., 2003; Bruss et al., 2006), Pt (Scheeren et al., 2003; 2006), Ru (Silveira et al., 2004; Gutel et al., 2007), Pd (Umpierre et al., 2005; Durand et al., 2008), Ni (Migowski et al., 2007), Cu (Singh et al., 2008b; 2008c; 2009) and Ag (An et al., 2009) nanoparticles by reducing the corresponding transition metal salts or by decomposing organometallic compounds in different ILs (Dupont & de Oliveira Silva, 2008). Similarly, uniform Ru nanoparticles were obtained by reducing  $\text{RuO}_2$  hydrate by  $\text{H}_2$  in a range of Im-based ILs with  $[\text{BMIm}]$  as a cation and  $[\text{BF}_4]$ ,  $[\text{PF}_6]$  or  $[\text{SO}_3\text{CF}_3]$  as anions (Rossi et al., 2004; 2009). These Ru nanoparticles synthesized in ILs demonstrated excellent performance towards the hydrogenation of olefins. In another study, importance of external parameters such as temperature and stirring during synthesis of Ru nanoparticles was highlighted to control nanoparticle size by utilizing the self-organization feature of  $[\text{BMIm}][\text{N}(\text{SO}_2\text{CF}_3)_2]$  IL (Gutel et al., 2007). Additionally, in a series of reports,  $[\text{BMIm}][\text{BF}_4]$  IL was utilized towards the synthesis of Cr, Mo, W, Fe, Ru, Os, Co, Rh and Ir nanoparticles (Redel et al., 2008a; 2009; Kramer et al., 2008). It is notable that in most of these studies, ILs themselves acted as stabilizing agents without requiring any external capping agent during synthesis of uniform, ultrasmall metal nanoparticles. This is significantly different from metal nanoparticles synthesis in conventional aqueous and organic solvent, wherein an external stabilizing/ capping agent is typically required during synthesis.

#### 3.2 Metal nanoparticles synthesis in ILs using “task-specific” ILs

In addition to the aforementioned reports on use of non-functionalized ILs towards synthesis of metal nanoparticles, a recent noteworthy trend is towards synthesis of functionalized ILs, e.g. metal ion-containing ILs, which can be directly reduced, leading to metal nanoparticles synthesis in ILs without requiring any additional metal salts. One of the

examples of these include synthesis of Ag nanoparticles via reducing Ag-containing ILs such as bis(*N*-2-ethylhexylethylenediamine)silver nitrate {[Ag(eth-hex-en)<sub>2</sub>][NO<sub>3</sub>]} and bis(*N*-hexylethylenediamine)silver hexafluorophosphate {[Ag(hex-en)<sub>2</sub>][PF<sub>6</sub>]} by NaBH<sub>4</sub> (Iida et al., 2008).

Another category of functionalized ILs includes those which contain certain functional groups that may bond onto metal surfaces, and thus stabilize the formed metal nanoparticles more effectively. This has led to development of a range of new functionalized ILs, which are also often termed as "task-specific ILs" (Davis, 2004; Fei et al., 2006; Lee, 2006; Li et al., 2006; Davis & Wasserschmidt, 2008). To this end, thiol-containing ILs are particularly notable towards stabilization of metal nanoparticles, as thiols are well-known to interact strongly with metal surfaces. For instance, IL 3,3'-[disulfanylbis(hexane-1,6-diyl)]-bis(1-methyl-1*H*-imidazol-3-ium)dichloride was utilized for the synthesis of 5 nm, water-soluble Au nanoparticles via reducing HAuCl<sub>4</sub> with NaBH<sub>4</sub> (Itoh et al., 2004). Lee and co-workers developed a range of thiol-functionalized ILs to prepare Au, Pt, and Pd nanoparticles, wherein the sizes of nanoparticles was found to be reduced with an increase in the number of thiol groups in ILs (Kim et al., 2004; Kim et al., 2005). Additionally, Au nanoparticles were stabilized by using a zwitterionic imidazolium sulfonate-terminated thiol (Tatumi & Fujihara, 2005), and Au nanoparticles and Pd nanowires could be prepared by using a thiol functionalized IL, 1-methyl-3-(2'-mercaptoacetoxyethyl) imidazolium chloride (Gao et al., 2005). Similarly, nitrile-functionalized (Zhao et al., 2004; Chiappe et al., 2006; Fei et al., 2007) and amine-functionalized (Wang et al., 2008) ILs were also used towards metal nanoparticles stabilization, and superior ability of nitrile-functionalized ILs over non-functionalized ILs was demonstrated in this particular context (Zhao et al., 2004; Chiappe et al., 2006; Fei et al., 2007). Since synthesis of thiol- and nitrile-functionalized ILs usually involves hazardous and odorous raw materials and multiple synthesis steps, other functionalized ILs such as *N*-(2-hydroxyethyl)-*N*-methylmorpholinium tetrafluoroborate {[HEM<sup>+</sup> Mor][BF<sub>4</sub>]} were prepared using more environmentally-benign synthesis and utilized for the synthesis of 4.3 nm Au nanoparticles (Kim et al., 2006). By using longer chain ILs such as [C<sub>12</sub>HEM<sup>+</sup> Im][Cl] and [C<sub>14</sub>HEM<sup>+</sup> Im][Cl], the same authors could also prepare 3.1 and 2.8 nm Au nanoparticles respectively. In another interesting study, Choi and co-workers could prepare 4.1 and 2.1 nm Ag nanoparticles by reducing AgNO<sub>3</sub> in 1-(2-hydroxyethyl)-3-methylimidazolium tetrafluoroborate {[HEM<sup>+</sup> Im][BF<sub>4</sub>]} IL (Choi et al., 2007). More recently, Dinda and co-workers utilized several ascorbic acid-based ILs to prepare Au nanostructures, wherein ascorbate present in the anionic part of IL acts a reducing agent during nanoparticles synthesis (Dinda et al., 2008). Some of the metal nanostructures formed in ILs have been illustrated in Figure 2.

The examples discussed above demonstrate the potential of using task-specific ILs in the stabilization and preparation of metal nanoparticles. As is evident from the above discussed examples, one of the major advantages of using ILs for synthesis of metal nanoparticles is that the metal nanoparticles prepared in ILs are generally monodispersed and very small in size, predominantly due to the IL stabilization effect and low interface tensions of ionic liquids (Antonietti et al., 2004; Migowski & Dupont, 2007; Dupont & de Oliveira Silva, 2008). However it should also be noted that in certain cases ILs by themselves cannot effectively stabilize metal nanoparticles and additional stabilizing/capping agents may still be needed to assist with their stabilization in ILs. This indicates that more research is warranted to correlate the influence of type of ILs with metal nanoparticles stabilization and their size profile. Particularly interesting is the observation that ILs can themselves be functionalized

to either incorporate metal ions (Iida et al., 2008) or reducing agent (Dinda et al., 2008) within the IL structure. This provides a great deal of flexibility towards facile synthesis and stabilization of metal nanoparticles towards narrow and small size range with a potential ability to control their shape anisotropy (Davis, 2004; Fei et al., 2006; Lee, 2006; Li et al., 2006; Davis & Wassercheid, 2008). However, in our opinion, it is not truly remarkable if one seeks to use functionalized ILs just for the sake of making nanoparticles. The true potential of functionalized ILs towards metal nanoparticles synthesis will require extensive exploration of additional advantages associated with IL-based synthesis of nanomaterials. This may include phase transfer ability of such nanomaterials or their improved catalytic and sensing properties, some of which will be discussed later in this chapter.

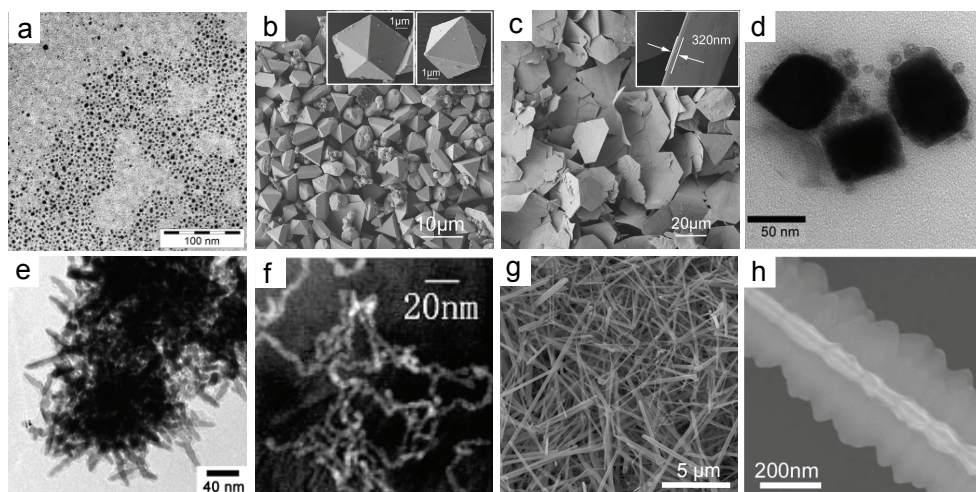


Fig. 2. Transmission and scanning electron micrographs exemplifying different morphologies of metal nanoparticles formed in ILs. (a) Ag nanospheres formed in [BMIm][BF<sub>4</sub>] with *n*-butylimidazole as a scavenger; (b & c) Au nanostructures synthesized via microwave heating of 150 (b) and 100 mg (c) of HAuCl<sub>4</sub>·4H<sub>2</sub>O in [BMIm][BF<sub>4</sub>] at 200 °C for 5 min; (d) Co nanocubes prepared in {DMI}[NTf<sub>2</sub>]; (e) Co-Pt nanorods obtained in [BMIm][NTf<sub>2</sub>]; (f) Pd nanowires synthesized in a thiol-functionalized IL; (g) Ag nanowires formed in [BMIm][MeSO<sub>4</sub>]; (h) Au nanodendrites formed in [BMIm][PF<sub>6</sub>]. (adapted from (a) Redel et al., 2008b; (b & c) Ren et al., 2008; (d) Scariot et al., 2008; (e) Wang & Yang, 2005; (f) Gao et al., 2005; (g) Kim et al., 2009; (h) Qin et al., 2008 with permissions).

### 3.3 Metal nanoparticles synthesis in ILs using additional stabilizers or scavengers

In sections 3.2 and 3.3, we discussed some of the cases wherein ILs used during metal nanoparticles synthesis acted as a stabilizer, which predominantly resulted in small sized nanoparticles. However, sometimes additional stabilizing agents are required for metal nanoparticles stabilization in IL, which provide additional flexibility for the phase transfer of metal nanoparticles to different solvent media. Stabilizing agents such as citrate (Wei et al., 2004), oleic acid (Wang & Yang, 2006), dendrimers (Ou et al., 2008), phenanthroline (Huang et al., 2003), bipyridine (Leger et al., 2008), poly(vinylpyrrolidone) (Yang et al., 2008), and IL-like polymers (Zhao et al., 2007) have been used during metal nanoparticles

synthesis in ILs. Despite these studies, it is still not encouragingly clear how ILs and additional stabilizing agents interact with metal nanoparticles surface.

An interesting alternative to using additional stabilizing agents in IL during metal nanoparticles synthesis is the use of scavenging agents to remove the acidic products typically formed as by-products during nanoparticles synthesis. For instance, reduction of a metal salt by  $H_2$  may lead to formation of acidic molecules, which might promote unwanted aggregation of metal nanoparticles during their synthesis. To address this issue, Redel and co-workers reduced  $AgBF_4$  in the presence of both  $[BMIm][BF_4]$  and *n*-butylimidazole (Redel et al., 2008b). In this particular case,  $HBF_4$  formed as a reaction by-product spontaneously reacted with *n*-butylimidazole and got neutralized that resulted in 2.8 nm Ag nanoparticles. Conversely, 66 nm Ag particles were formed in the absence of *n*-butylimidazole. Although interesting and with significant potential for further development, such scavengers have not been explored in great details for metal nanoparticles synthesis in ILs. We believe that the future studies in this area will focus upon use of such scavenging molecules, stabilizers, shape-directing agents, etc to achieve highly functional metal nanostructures in IL solvents for various applications.

### 3.4 Shape-controlled synthesis of metal nanoparticles in ILs

Shape-controlled synthesis of metal nanostructures is as important as size-control, because different morphologies of metal nanoparticles may lead to distinctly different physico-chemical properties (Lu et al., 2009). Considering the importance of metal nanoparticles shape control, significant efforts have been directed towards shape-controlled synthesis of metal nanostructures in ILs. For instance, Co-Pt nanorods were synthesized in  $[BMIm][NTf_2]$  IL while using cetyltrimethylammonium bromide (CTAB) as a shape-directing agent (Wang & Yang, 2005). The ionic nature and thermal stability of imidazolium-based ILs also make them good absorbers of microwaves. The microwave absorbing ability of ILs was utilized for the formation of Au nanosheets of 50 nm thickness and size larger than 30  $\mu m$  by microwave heating of  $HAuCl_4$  in  $[BMIm][BF_4]$  IL, wherein role of both the IL and the microwave heating in shape control was claimed (Li et al., 2005). In another microwave-mediated synthesis of Au nanoparticles in ILs, miscellaneous Au nanostructures were obtained in  $[BMIm][BF_4]$ ,  $[BMIm][NTf_2]$ ,  $[BMIm][PF_6]$ ,  $[BMIm][Br]$ ,  $[BMIm][Cl]$  and  $[BMIm][Tos]$  ILs (Ren et al., 2008). Zhu and co-workers synthesized 60 nm thick hexagonal- and triangular-shaped Au nanosheets by a photochemical reduction method in  $[BMIm][BF_4]$  (Zhu et al., 2007). Other metal nanostructures reported in ILs include anisotropic Au nanoparticles (Firestone et al., 2005), Au nanorods (Kumar et al., 2007), Pd nanowires (Kumar et al., 2007), Co nanocubes (Scariot et al., 2008) and Ag nanorods (Kim et al., 2009).

Similarly electrochemical syntheses of metal nanostructures in the presence of ILs have also been reported, and readers are encouraged to look at associated references for a detailed understanding of these systems (Endres, 2002; Huang & Sun, 2004; Huang & Sun, 2005; Abbott & McKenzie, 2006; Dobbs et al., 2006; El Abedin & Endres, 2006; Yeh et al., 2006; Endres & El Abedin, 2008). It is however noteworthy that the use of ILs, particularly Im-based ILs as solvents for electrochemical reactions is predominantly dominated due to their electrochemical stability, excellent oxidative and reductive stability, and a large electrochemical potential window, which is typically notably larger than the electrochemical window of conventional molecular solvents (MacFarlane & Pringle, 2006; Endres et al., 2008).

### 3.5 Galvanic replacement-mediated shape-controlled synthesis of metal nanoparticles in ILs

Another interesting aspect of metal nanostructure synthesis that is becoming interesting popular, and thus deserves particular focus is galvanic replacement reactions, which are also termed as transmetallation reactions. Galvanic replacement reactions are single-step reactions that utilize the differences in the standard electrode potentials of various elements, leading to deposition of the more noble element and dissolution of the less noble component without any applied external potentials. A classical example of this includes dipping an iron nail in aqueous  $\text{CuSO}_4$  solution, which will result in spontaneous deposition of Cu onto Fe nail, while Fe will be leached out in the surrounding aqueous environment in the form of  $\text{Fe}^{2+}$  ions. Notably, since these reactions involve atom-by-atom replacement of metal template with a more noble metal ion, these reactions have the potential to develop high surface area nanostructures materials. Although these types of reactions are well known, it has been only recently that such facile electroless chemistry has been used for nanomaterials development. For instance, galvanic replacement reactions involving sacrificial metal nanoparticles and suitable metal ions have been employed by various groups (Sun et al., 2002; Sun & Xia, 2004; Liang et al., 2004; 2005; Shukla et al., 2005; Selvakannan & Sastry, 2005) for the synthesis of hollow/porous metal (Sun et al., 2002; Sun & Xia, 2004) and metal alloy (Liang et al., 2004; 2005) nanostructures in aqueous (Sun & Xia, 2004; Liang et al., 2004; 2005; Shukla et al., 2005) and organic environments (Selvakannan & Sastry, 2005). The electroless nature of galvanic replacement reactions also provides them the unique and significant advantage of simplicity. It is noteworthy that galvanic replacement reactions have hitherto mostly been confined to aqueous and organic solvents, wherein predominantly formation of hollow nanoarchitectures, without significant solvent effect has been observed (Figure 3).

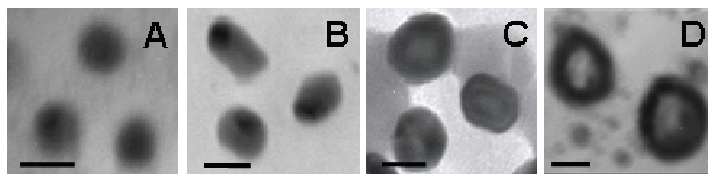


Fig. 3. Transmission electron micrographs of Ag nanoparticles in water before (A), and after galvanic replacement with (B) 0.1 %, (C) 1 %, and (D) 10 M % of  $[\text{AuBr}_4]^-$  ions for 48 h. Scale bars correspond to 20 nm (adapted from Pearson et al., 2010 with permission from the Royal Society of Chemistry).

To this end, our group has also previously demonstrated that highly active bimetallic nanocatalysts can be developed in aqueous media by using galvanic replacement approach (Bansal et al., 2008; Bansal et al., 2009). In an interesting work, Qin and co-workers could synthesize threefold symmetrical dendritic Au nanostructures by galvanic replacement reaction between a Zn plate and a solution of  $\text{HAuCl}_4$  in  $[\text{BMIm}][\text{PF}_6]$  IL (Qin et al., 2008). In this study, the choice of the Zn plate and the IL  $[\text{BMIm}][\text{PF}_6]$  were both claimed to be important for the formation of Au dendrites. Similarly Cu substrates have been used as templates for the growth of anisotropic Ag nanostructures in IL (Abbott et al., 2008). More recently, we performed a systematic study to explore galvanic replacement reaction in the IL  $[\text{BMIm}][\text{BF}_4]$ , wherein when spherical Ag nanoparticles were reacted with  $\text{KAuBr}_4$ , this led to the shape transformation of Ag nanospheres into hierarchical Au-Ag dendritic



nanostructures (Figure 4; Pearson et al., 2010), which showed high electrocatalytic activity and good surface enhanced Raman scattering (SERS) sensing ability (unpublished findings).

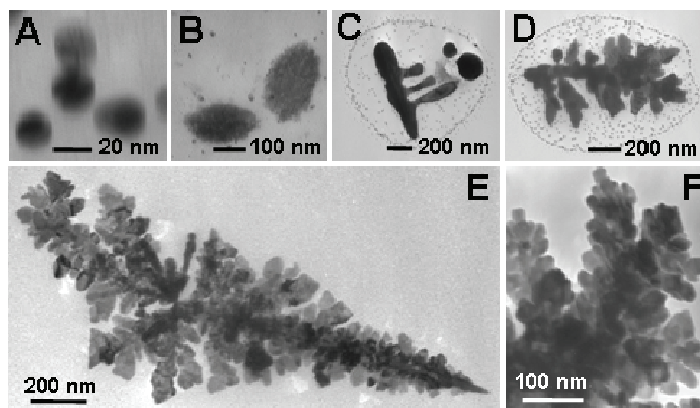


Fig. 4. Transmission electron micrographs of Ag nanoparticles in ionic liquid [BMIm][BF<sub>4</sub>] before (A), and after galvanic replacement with (B) 0.1 M%, (C and D) 1 M%, and (E and F) 10 M % of [AuBr<sub>4</sub>]<sup>-</sup> ions for 48 h (adapted from Pearson et al., 2010 with permission from the Royal Society of Chemistry).

The detailed investigation of the reaction mechanism of nanodendrites formation in [BMIm][BF<sub>4</sub>] revealed the stabilization of Au<sup>+1</sup> species in the highly viscous IL followed by a diffusion-limited-aggregation (DLA) mediated self-organization process, that led to such dendritic forms (Figure 5). Stabilization of Au<sup>+1</sup> species in IL [BMIm][BF<sub>4</sub>] is rather

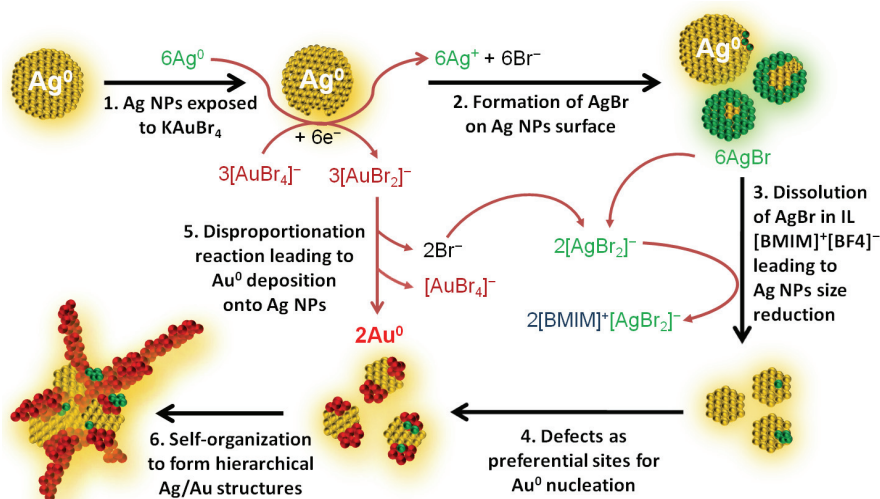


Fig. 5. Reaction scheme explaining the mechanism for synthesis of Au-Ag hierarchical dendritic structures in the IL [BMIm][BF<sub>4</sub>] (adapted from Pearson et al., 2010 with permission from the Royal Society of Chemistry).

interesting, because it is extremely difficult to stabilize such metastable metal species in aqueous environments. This report also suggests that if regularly employed aqueous and organic solvents are replaced with non-conventional (e.g. viscous) solvents such as ILs during replacement reactions, the reaction kinetics may change significantly either due to restricted movement of ions and/or stabilization of intermediate reaction species in such solvents. Hence, this may lead to markedly different reaction nanoproducts in ILs and the ability to control shape anisotropy, thus posing ILs as true designer solvents for the shape-controlled synthesis of anisotropic nanomaterials. This is only one of the very few examples wherein a detailed reaction mechanism of anisotropic metal nanoparticles formation has been undertaken in an IL. However, systematic knowledge regarding the metal nanoparticles formation mechanisms and control of shape anisotropy is yet to be generalized, which will also most possibly also require understanding of these systems through computational modelling studies.

#### 4. Applications of metal nanoparticles synthesized in ILs

It has been well established that physico-chemical properties of metal nanoparticles for various applications strongly depend on their surface properties, in addition to the more commonly known size and shape effects. These surface properties of metal nanoparticles may vary significantly from one synthesis protocol to another, predominantly because concentration and type of stabilizing agents used in these synthesis methods can be quite different. Since ILs generally act as *in situ* stabilizing agents during synthesis of metal nanoparticles, the nanomaterials synthesized in ILs may offer significantly new properties for a myriad of applications. For this reason, among others, when combining ILs and metal nanoparticles, the need to understand the interactions between ILs and metal nanoparticles surface is becoming increasingly important. To this end, in order to understand the interactions between an Im-based IL and Au nanoparticles, Schrekker and co-workers used an ether-modified imidazolium species, which could absorb the near-infrared radiation, and thus made SERS study of the surface of Au nanoparticle feasible (Schrekker et al., 2007). The SERS study clearly showed an interaction of imidazolium cation with Au nanoparticles surface by means of a parallel coordination, however almost no interaction between the methanesulfonate anion and Au nanoparticle surface was observed (Figure 6). A series of other reports also strongly suggested interaction between metal nanoparticles and Im-based ILs. However it was found that this interaction with metal surface can take place either via cationic imidazolium ring or the anion or both, which may vary from one IL system to another (Neouze, 2010).

In a pioneering work, Dupont and co-workers demonstrated that metal nanoparticles synthesized in Im-based ILs possess outstanding catalytic properties for biphasic hydrogenation reactions, with almost 100% yield (Dupont et al., 2002). From this work, the high catalytic performance of the metal nanoparticles could be linked to the presence of imidazolium medium, which allowed the synthesis of monodispersed, 2 nm sized small nanoparticles. In another study, 3 nm sized, monodispersed Rh nanoparticles synthesized in [BMIm][BF<sub>4</sub>] IL in the presence of a copolymer, were used for benzene hydrogenation reaction (Mu et al., 2005). These Rh nanoparticles showed unprecedented activity and recyclability, thus performing the catalytic reaction in five complete recycles of 4000 total turnover each. In another interesting report, Rh and Ir nanoparticles dispersed in an Im-based IL were employed as reusable active catalysts in the biphasic hydrogenation of cyclohexane (Redel et



al., 2009). In a more recent study, to understand the high catalytic performance of metal nanoparticles synthesized in Im-based ILs, Au nanorods were synthesized using an ionic capping agent dodecyltrimethylammonium bromide (CTAB), and its imidazolium equivalent, 1-dodecyl-3-methylimidazolium bromide (Bai et al., 2009). Following this, the interaction energies of these molecules with Au (111) plane were calculated using COMPASS force fields which yield smaller interaction energies for imidazolium ( $174.1 \text{ kcal mol}^{-1}$ ) than that for CTAB ( $216.5 \text{ kcal mol}^{-1}$ ). The authors claimed that due to the smaller interaction between Au and imidazolium group, more active sites of Au were accessible during catalytic reactions, which led to higher catalytic activity in IL-based systems.

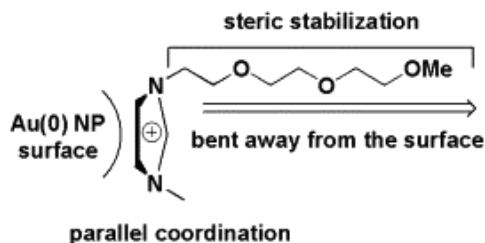


Fig. 6. Imidazolium cation coordination and stabilization mode demonstrating the parallel coordination of the imidazolium cation onto the Au nanoparticle surface (adapted from Schrekker et al., 2007 with permission from the Elsevier Inc.).

Metal nanoparticles formed in other solvents when incorporated in Im-based ILs, also demonstrated interesting catalytic properties (Cassol et al., 2005). Notably, in a large number of Im-based systems, different groups detected the presence of an *N*-heterocyclic carbene (NHC) species associated with metal nanoparticles (Ott et al., 2005; Zhao et al., 2009). The NHC radical species can on one hand significantly enhance the catalytic performance of these materials in ILs, while on another, it might promote nanoparticles aggregation. The promising catalytic activity of NHC species associated with various metal nanoparticles such as Ir, Au and Rh in Im-based ILs was outlined by various groups (Cavell, 2008; CAi & Liu, 2009; Aldeco-Perez et al., 2009). Conversely, Ott and co-workers suggested that presence of these NHC species associated with Ir nanoparticles can act as potent inhibitor of Heck reactions (Ott et al., 2005).

In addition to the above highlighted few cases, several other studies have investigated the catalytic performance of metal nanoparticles in ILs. All these studies point to the fact that careful choice of the IL is the key to obtain desired catalytic performance. If chosen appropriately, ILs can not only enhance the catalytic activity, but can also provide much desired substrate and product stability. As is clear from these illustrations, the presence of NHC species in Im-based systems cannot be omitted, and therefore metal nanoparticles associated with ILs can even be considered as one material, a single catalytic system. In fact, in one of the studies, it was demonstrated that during Suzuki C-C coupling reactions, Pd nanoparticles were catalytically active only when they were formed *in situ* in an Im-based IL (Fernandez et al., 2007).

## 5. Conclusion

Through this chapter, our aim was to discuss some of the most important developments in the field of ionic liquid-assisted synthesis of metal nanoparticles and their promising

applications in the area of catalysis. It was not an intention of this chapter to provide an exhaustive review of the developments in this field; however the aim was to familiarize the readers with this developing field by discussing few of the leading case studies. Although most of the illustrations discussed in this chapter are from imidazolium-based IL systems, the scope of this chapter can also be equally extended to other ILs. From the illustrations provided in this chapter, some major outcomes can be drawn: (i) ILs can act as new designer solvents for the size- and shape-controlled synthesis of metal nanoparticles, wherein synthesis of ultra-small size, monodispersed metal nanoparticles of different compositions is achievable in ILs. (ii) The interactions between metal nanoparticle surface and IL can be a bit complex: while ILs can assist in *in situ* stabilization of metal nanoparticles, nanoparticles can themselves influence the nanostructural organization of ILs in which they form. (iii) ILs play multiple roles towards metal nanoparticles synthesis which include their solvent, template, and stabilizing capabilities. (iv) In case of imidazolium-based ILs, formation of NHC radical species is particularly notable for catalysis reactions, because this can either positively or negatively influence the catalytic performance of metal nanoparticles. Therefore choice of an appropriate IL and metal nanoparticles for a particular catalysis reaction can be considerably important. (v) Moreover, in future, potentially numerous ILs can be synthesized by a combination of appropriate cations and anions. This creates a huge potential for use of ILs as preferred solvent system for nanomaterials synthesis in general, and metal nanoparticles in particular. The large scale commercial implications of IL-mediated synthesis of metal nanoparticles cannot be overemphasized.

## 6. References

- Abbott, A. P.; Griffith, J.; Nandhra, S.; O'Connor, C.; Postlethwaite, S.; Ryder, K. S. & Smith, E. L. (2008) *Surface and Coatings Technology*, 202, 2033-2039.
- Abbott, A. P. & McKenzie, K. J. (2006) *Physical Chemistry Chemical Physics*, 8, 4265-4279.
- Aldeco-Perez, E.; Rosenthal, A. J.; Donnadieu, B.; Parameswaran, P.; Frenking, G. & Bertrand, G. (2009) *Science*, 326, 556-559.
- An, J.; Wang, D. S.; Luo, Q. Z. & Yuan, X. Y. (2009) *Materials Science and Engineering: C*, 29, 1984-1989.
- Antonietti, M.; Kuang, D. B.; Smarsly, B. & Yong, Z. (2004) *Angewandte Chemie International Edition*, 43, 4988-4992.
- Bai, X.; Gao, Y.; Liu, H. G. & Zheng, L. (2009) *Journal of Physical Chemistry C*, 113, 17730-17736.
- Bansal, V.; Jani, H.; du Plessis, J.; Coloe, P. J. & Bhargava, S. K. (2008) *Advanced Materials*, 20, 717-723.
- Bansal, V.; O'Mullane, A. P. & Bhargava, S. K. (2009) *Electrochemical Communications*, 11, 1639-1642.
- Bruss, A. J.; Gelesky, M. A.; Machado, G. & Dupont, J. (2006) *Journal of Molecular Catalysis A: Chemical*, 252, 212-218.
- Burda, C.; Chen, X.; Narayanan, R. & El-Sayed, M. A. (2005) *Chemical Reviews*, 105, 1025.
- Cai, Y. & Liu, Y. (2009) *Catalysis Communications*, 10, 1390-1393.
- Campbell, P. S.; Santini, C. C.; Bouchu, D.; Fenet, B.; Philippot, K.; Chaudret, B.; Padua, A. A. H. & Chauvin, Y. (2010) *Physical Chemistry Chemical Physics*, 12, 4217-4223.
- Cassol, C. C.; Umpierre, A. P.; Machado, G.; Wolke, S. I. & Dupont, J. (2005) *Journal of the American Chemical Society*, 127, 3298-3299.

- Cavell, K. (2008) *Dalton Transactions*, 6676-6685.
- Chiappe, C.; Pieraccini, D.; Zhao, D. B.; Fei, Z. F. & Dyson, P. J. (2006) *Advanced Synthesis & Catalysis*, 348, 68.
- Choi, S.; Kim, K. S.; Yeon, S. H.; Cha, J.H.; Lee, H.; Kim, C. J. & Yoo, I. D. (2007) *Korean Journal of Chemical Engineering*, 24, 856-859.
- Davis, J. H. & Wassercheid, P. (2008) *Ionic Liquids in Synthesis*, (Eds: Wassercheid, P. & Welton, T.), Wiley-VCH, Weinheim, p. 45.
- Davis, J. H. (2004) *Chemistry Letters*, 33, 1072-1077.
- de Caro, D.; Jacob, K.; Faulmann, C.; Legros, J.-P.; Senocq, F.; Fraxedas, J. & Valade, L. (2010) *Synthetic Metals*, 160, 1223-1227.
- Deshmukh, R. R.; Rajagopal, R. & Srinivasan, K. V. (2001) *Chemical Communications*, 1544-1545.
- Dinda, E.; Si, S.; Kotal, A. & Mandal, T. K. (2008) *Chemistry - A European Journal*, 14, 5528-5537.
- Dobbs, W.; Suisse, J.-M.; Douce, L. & Welter, R. (2006) *Angewandte Chemie International Edition*, 45, 4179-4182.
- Dupont, J. & de Oliveira Silva, D. (2008) *Nanoparticles and Catalysis*, (Ed: Astruc, D.), Wiley-VCH, Weinheim, p. 195.
- Dupont, J. & Scholten, J. D. (2010). *Chemical Society Reviews*, 39, 1780-1804.
- Dupont, J. & Suarez, P. A. Z. (2006) *Physical Chemistry Chemical Physics*, 8, 2441-2452.
- Dupont, J.; Fonseca, G. S.; Umpierre, A. P.; Fichtner, P. F. P. & Teixeira, S. R. (2002) *Journal of the American Chemical Society*, 124, 4228-4229.
- Durand, J.; Teuma, E.; Malbosc, F.; Kihn, Y. & Gomez, M. (2008) *Catalysis Communications*, 9, 273-275.
- El Abedin, S. Z. & Endres, F. (2006) *ChemPhysChem*, 7, 58-61.
- Endres, F. (2002) *ChemPhysChem*, 3, 144-154.
- Endres, F.; Abbot, A. P. & MacFarlane, D. R. (2008), *Electrodeposition from Ionic Liquids*, Wiley-VCH, Weinheim.
- Fei, Z. F.; Geldbach, T. J.; Zhao, D. B. & Dyson, P. J. (2006) *Chemistry - A European Journal*, 12, 2122-2130.
- Fei, Z. F.; Zhao, D. B.; Pieraccini, D.; Ang, W. H.; Geldbach, T. J.; Scopelliti, R.; Chiappe, C. & Dyson, P. J. (2007) *Organometallics*, 26, 1588-1598.
- Fernandez, F.; Cordero, B.; Durand, J.; Muller, G.; Malbosc, F.; Kihn, Y.; Teuma, E. & Gomez, M. (2007) *Dalton Transactions*, 5572-5581.
- Firestone, M. A.; Dietz, M. L.; Seifert, S.; Trasobares, S.; Miller, D. J. & Zaluzec, N. J. (2005) *Small*, 1, 754-760.
- Fonseca, G. S.; Domingos, J. B.; Nome, F. & Dupont, J. (2006) *Journal of Molecular Catalysis A: Chemical*, 248, 10-16.
- Fonseca, G. S.; Umpierre, A. P.; Fichtner, P. F. P.; Teixeira, S. R. & Dupont, J. (2003) *Chemistry - A European Journal*, 9, 3263-3269.
- Gao, S. Y.; Zhang, H. J.; Wang, X. M.; Mai, W. P.; Peng, C. Y. & Ge, L. H. (2005) *Nanotechnology*, 16, 1234-1237.
- Gordon, C. M. & Muldoon, M. J. (2008) *Ionic Liquids in Synthesis*, 2nd ed. (Eds: Wassercheid, P. & Welton, T.), Wiley-VCH, Weinheim p. 7.
- Gutel, T.; Garcia-Anton, J.; Pelzer, K.; Philippot, K.; Santini, C. C.; Chauvin, Y.; Chaudret, B. & Basset, J. M. (2007) *Journal of Materials Chemistry*, 17, 3290-3292.

- Hamill, N. A.; Hardacre, C. & McMath, S. E. J. (2002) *Green Chemistry*, 4, 139-142.
- Hao, E.; Schatz, G. C. & Hupp, J. (2004) *Journal of Fluorescence*, 14, 331-341.
- Hardacre, C.; Holbrey, J. D.; McMath, S. E. J.; Bowron, D. T. & Soper, A. K. (2003) *Journal of Chemical Physics*, 118, 273-278.
- Huang, J. F. & Sun, I. W. (2004) *Chemistry of Materials*, 16, 1829-1831.
- Huang, J. F. & Sun, I. W. (2005) *Advanced Functional Materials*, 15, 989-994.
- Huang, J.; Jiang, T.; Han, B. X.; Gao, H. X.; Chang, Y. H.; Zhao, G. Y. & Wu, W. Z. (2003) *Chemical Communications*, 1654-1655.
- Hurtley, F. H. & Wier, T. P. (1951). *Journal of Electrochemical Society*, 98, 203-206.
- Iida, M.; Baba, C.; Inoue, M.; Yoshida, H.; Taguchi, E. & Furusho, H. (2008) *Chemistry - A European Journal*, 14, 5047-5056.
- Itoh, H.; Naka, K. & Chujo, Y. (2004) *Journal of the American Chemical Society*, 126, 3026-3027.
- Kim, K. S.; Choi, S.; Cha, J. H.; Yeon, S. H. & Lee, H. (2006) *Journal of Materials Chemistry*, 16, 1315-1317.
- Kim, K. S.; Demberelnyamba, D. & Lee, H. (2004) *Langmuir*, 20, 556-560.
- Kim, K. S.; Demberelnyamba, D.; Yeon, S. W.; Choi, S.; Cha, J. H. & Lee, H. (2005) *Korean Journal of Chemical Engineering*, 22, 717-720.
- Kim, T. Y.; Kim, W. J.; Hong, S. H.; Kim, J. E. & Suh, K. S. (2009) *Angewandte Chemie International Edition*, 48, 3806-3809.
- Kramer, J.; Redel, E.; Thomann, R. & Janiak, C. (2008) *Organometallics*, 27, 1976-1978.
- Kumar, A.; Murugesan, S.; Pushparaj, V.; Xie, J.; Soldano, C.; John, G.; Nalamasu, O.; Ajayan, P. M. & Linhardt, R. J. (2007) *Small*, 3, 429-433.
- Lee, S. G. (2006) *Chemical Communications*, 1049-1063.
- Leger, B.; Denicourt-Nowicki, A.; Roucoux, A. & Olivier-Bourbigou, H. (2008) *Advanced Synthesis & Catalysis*, 350, 153-159.
- Li, X. H.; Zhao, D. B.; Fei, Z. F. & Wang, L. F. (2006) *Science in China, Series B: Chemistry*, 49, 385-401.
- Li, Z. H.; Liu, Z. M.; Zhang, J. L.; Han, B. X.; Du, J. M.; Gao, Y. N. & Jiang, T. (2005) *Journal of Physical Chemistry B*, 109, 14445-14448.
- Liang, H. P.; Wan, L. J.; Bai, C. L. & Jiang, L. (2005) *Journal of Physical Chemistry B*, 109, 7795-7800.
- Liang, H.; Guo, Y.; Zhang, H.; Hu, J.; Wan, J. & Bai, C. L. (2004) *Chemical Communications*, 1496-1497.
- Lopes, J. N. A. C. & Padua, A. A. H. (2006) *Journal of Physical Chemistry B*, 110, 3330-3335.
- Lu, X.; Rycenga, M.; Skrabalak, S. E.; Wiley, B. & Xia, Y. (2009) *Annual Reviews of Physical Chemistry*, 60, 167-179.
- Ma, Z.; Yu, J. & Dai, S. (2010). *Advanced Materials*, 22, 261-285.
- MacFarlane D. R. & Pringle, J. M. (2006) *Chemistry in Australia*, 73, 11-14.
- Mehdi, H.; Binnemans, K.; Hecke, K. V.; Meervelt, L. V. & Nockemann, P. (2010) *Chemical Communications*, 46, 234-236.
- Migowski, P. & Dupont, J. (2007) *Chemistry - A European Journal*, 13, 32-39.
- Migowski, P.; Machado, G.; Texeira, S. R.; Alves, M. C. M.; Morais, J.; Traverse, A. & Dupont, J. (2007) *Physical Chemistry Chemical Physics*, 9, 4814-4821.
- Mu, X. -D.; Meng, J. -Q.; Li, Z. -C. & Kou, Y. (2005) *Journal of the American Chemical Society*, 127, 9694-9695.
- Neouze, M.-A. & Schubert, U. (2008) *Monatshefte fur Chemie*, 139, 183-195.

- Neouze, M.-A. (2010). *Journal of Materials Chemistry*, DOI: 10.1039/c0jm00616e.
- Neto, B. A. D.; Santos, L. S.; Nachtigall, F. M.; Eberlin, M. N. & Dupont, J. (2006) *Angewandte Chemie International Edition*, 45, 7251-7254.
- Ott L. S. & Finke, R. G. (2007) *Coordination Chemistry Review*, 251, 1075-1100.
- Ott, L. S.; Cline, M. L.; Deetlefs, M.; Seddon, K. R. & Finke, R. G. (2005) *Journal of the American Chemical Society*, 127, 5758-5759.
- Ou, G. N.; Xu, L.; He, B. Y. & Yuan, Y. Z. (2008) *Chemical Communications*, 4210-4212.
- Pearson, A.; O'Mullane, A. P.; Bansal, V. & Bhargava, S. K. (2010) *Chemical Communications*, 46, 731-733.
- Qin, Y.; Song, Y.; Sun, N.; Zhao, N.; Li, M. & Qi, L. (2008) *Chemistry of Materials*, 20, 3965-3972.
- Redel, E.; J. Kramer, J.; Thomann, R. & Janiak, C. (2009) *Journal of Organometallic Chemistry*, 694, 1069-1075.
- Redel, E.; Thomann, R. & Janiak, C. (2008a) *Chemical Communications*, 1789-1791.
- Redel, E.; Thomann, R. & Janiak, C. (2008b) *Inorganic Chemistry*, 47, 14-16.
- Ren, L. Z.; Meng, L. J.; Lu, Q. H.; Fei, Z. F. & Dyson, P. J. (2008) *Journal of Colloid and Interface Science*, 323, 260-266.
- Rossi, L. M. & Machado, G. (2009) *Journal of Molecular Catalysis A: Chemical*, 298, 69-73.
- Rossi, L. M.; Machado, G.; Fichtner, P. F. P.; Teixeira, S. R. & Dupont, J. (2004) *Catalysis Letters*, 92, 149-155.
- Sardar, R.; Funston, A. M.; Mulvaney, P. & Murray, R. W. (2009) *Langmuir*, 25, 13840-13851.
- Scariot, M.; Silva, D. O.; Scholten, J. D.; Machado, G.; Teixeira, S. R.; Novak, M. A.; Ebeling, G. & Dupont, J. (2008) *Angewandte Chemie International Edition*, 47, 9075-9078.
- Scheeren, C. W.; Machado, G.; Dupont, J.; Fichtner, P. F. P. & Texeira, S. R. (2003) *Inorganic Chemistry*, 42, 4738-4742.
- Scheeren, C. W.; Machado, G.; Teixeira, S. R.; Morais, J.; Bomingos, J. B. & Dupont, J. (2006) *Journal of Physical Chemistry B*, 110, 13011-13020.
- Schrekker, H. S.; Gelesky, M. A.; Stracke, M. P.; Schrekker, C. M. L.; Machado, G.; Teixeira, S. R.; Rubim, J. C. & Dupont, J. (2007) *Journal of Colloid and Interface Science*, 316, 189-195.
- Selvakannan, P. R. & Sastry, M. (2005) *Chemical Communications*, 1684-1686.
- Shukla, R.; Bansal, V.; Chaudhary, M.; Basu, A.; Bhonde, R. R. & Sastry, M. (2005) *Langmuir*, 21, 10644-10654.
- Shukla, S.; Priscilla, A.; Banerjee, M.; Bhonde, R. R.; Ghatak, J.; Satyam, P. V. & Sastry, M. (2005) *Chemistry of Materials*, 17, 5000-5005.
- Silveira, E. T.; Umpierre, A. P.; Rossi, L. M.; Machado, G.; Morais, J.; Soares, G. V.; Baumvol, I. L. R.; Teixeira, S. R.; Fichtner, P. F. P. & Dupont, J. (2004) *Chemistry - A European Journal*, 10, 3734-3740.
- Singh, P.; Kumar, S.; Katyal, A.; Kalra, R. & Chandra, R. (2008a) *Materials Letters*, 62, 4164-4166.
- Singh, P.; Katyal, A.; Kalra, R. & Chandra, R. (2008b) *Tetrahedron Letters*, 49, 727-730.
- Singh, P.; Katyal, A.; Kalra, R. & Chandra, R. (2008c) *Catalysis Communications*, 9, 1618-1623.
- Singh, P.; Kumar, K.; Katyal, A.; Kalra, R. & Chandra, R. (2009) *Catalysis Letters*, 127, 119-124.
- Soni, S. K.; Ramanathan, R.; Coloe, P. J.; Bansal, V. & Bhargava, S. K. (2010) *Langmuir*, Doi: 10.1021/la101965j.

- Suarez, P. A. Z.; Einloft, S.; Dullius, J. E. L.; de Souza, R. F. & Dupont, J. (1998) *Journal de Chimie Physique et de Physico-Chimie Biologique*, 95, 1626–1639.
- Sun, Y. & Xia, Y. (2004) *Journal of the American Chemical Society*, 126, 3892–3901.
- Sun, Y.; Mayers, B. T. & Xia, Y. (2002) *Nano Letters*, 2, 481–485.
- Tatumi, R. & Fujihara, H. (2005) *Chemical Communications*, 83.
- Tsuzuki, S.; Tokuda, H.; Hayamizu, K. & Watanabe, M. (2005) *Journal of Physical Chemistry B*, 109, 16474–16481.
- Umpierre, A. P.; Machado, G.; Fecher, G. H.; Morais, J. & Dupont, J. (2005) *Advanced Synthesis & Catalysis*, 347, 1404–1412.
- von Prondzinski, N.; Cybinska, J. & Mudring, A.-V. (2010) *Chemical Communications*, 46, 4393–4395.
- Walden, P. (1914). *Bulletin de l'Académie Impériale des Sciences*, 8, 405.
- Wang, Y. & Yang, H. (2005) *Journal of the American Chemical Society*, 127, 5316–5317.
- Wang, Y. & Yang, H. (2006) *Chemical Communications*, 2545–2547.
- Wang, Z. J.; Zhang, Q. X.; Kuehner, D.; Ivaska, A. & Niu, L. (2008) *Green Chemistry*, 10, 907–909.
- Wei, G. T.; Yang, Z. S.; Lee, C. Y.; Yang, H. Y. & Wang, C. R. C. (2004) *Journal of the American Chemical Society*, 126, 5036–5037.
- Wilkes, J. S. & Zaworotko, M. J. (1992). *Chemical Communications*, 965–967.
- Yang, X.; Yan, N.; Fei, Z. F.; Crespo-Quesada, R. M.; Laurenczy, G.; Kiwi-Minsker, L.; Kou, Y.; Li, Y. D. & Dyson, P. J. (2008) *Inorganic Chemistry*, 47, 7444–7446.
- Yeh, F. H.; Tai, C. C.; Huang, J. F. & Sun, I. W. (2006) *Journal of Physical Chemistry B*, 110, 5215–5222.
- Zhao, C.; Wang, H. Z.; Yan, N.; Xiao, C. X.; Mu, X. D.; Dyson, P. J. & Kou, Y. (2007) *Journal of Catalysis*, 250, 33–40.
- Zhao, D. B.; Fei, Z. F.; Geldbach, T. J.; Scopelliti, R. & Dyson, P. J. (2004) *Journal of the American Chemical Society*, 126, 15876–15882.
- Zhao, J.; Yan, F.; Chen, Z.; Diao, H.; Chu, F.; Yu, S. & Lu, J. (2009) *Journal of Polymer Science, Part A: Polymer Chemistry*, 47, 746–753.
- Zhou, Y. (2005) *Current Nanoscience*, 1, 35–42.
- Zhu, J. M.; Shen, Y. H.; Xie, A. J.; Qiu, L. G.; Zhang, Q. & Zhang, S. Y. (2007) *Journal of Physical Chemistry C*, 111, 7629–7633.

# Evaluation of Mobility, Diffusion Coefficient and Density of Charge Carriers in Ionic Liquids and Novel Electrolytes Based on a New Model for Dielectric Response

T.M.W.J. Bandara<sup>1,2</sup> and B.-E. Mellander<sup>1</sup>

<sup>1</sup>*Department of Applied Physics, Chalmers University of Technology, Göteborg,*

<sup>2</sup>*Department of Physical Sciences, Rajarata University of Sri Lanka, Mihintale,*

<sup>1</sup>*Sweden*

<sup>2</sup>*Sri Lanka*

## 1. Introduction

Ionic conductors are key components for many electrochemical applications, mainly in the field of energy conversion, for example, in photo-electrochemical (PEC) solar cells and fuel cells, in energy storage devices like batteries and in other technological applications like electro-chromic devices, super-capacitors, electrochemical sensors [1,2], separation membranes [3], new types of memory and computer architecture as well as in biomedical applications [4,5]. In the last few decades ionic conductors have gained a revolutionary development owing to intense research inspired by their potential use in many electrochemical device applications. However, improved electrolytes are necessary in order to optimize the performance of the device applications. Hence, the need for new electrolytes with improved property regarding conductivity, stability, durability and operating temperature range has called for solutions involving ionic liquids in solid or gel polymer electrolytes.

The enormous number of research articles published in this field proves the broadening of a worldwide research interest on these materials. However, despite the present outstanding development of electrolyte materials, most of the theoretical advancement in this field goes far back, nearly half a century. Hence, to develop theories applicable for these newly developed electrolytes as well as for traditional electrolytes is vitally important for the advancement of the field.

The most important property of an electrolyte is the ionic conductivity,  $\sigma_{dc}$ , and that of an ionic conductor containing many ionic species can be described by,

$$\sigma_{dc} = \sum n_i e |Z_i| \mu_i \quad (1)$$

where  $n_i$  is the number of charge carriers per unit volume,  $\mu_i$  the mobility,  $Z_i$  the valance for the ionic species  $i$  in the electrolyte and  $e$  is the electronic charge. For a system containing one type of cation and one type of anion equation (1) can be modified as,

$$\sigma = n_- e |Z^-| \mu_- + n_+ e |Z^+| \mu_+ \quad (2)$$

where  $n_+, n_-$  are the number of positive and negative charge carriers per unit volume respectively,  $e$  is the electronic charge,  $\mu_+, \mu_-$  are the mobility of the cation and anion and  $Z^+, Z^-$  are the valance of the positive and negative charge carriers. The mean mobility ( $\mu$ ) of two ionic species is defined as,

$$\mu = (n_- \mu_- + n_+ \mu_+) / n \quad (3)$$

where  $n$  is the total charge carrier density ( $n = n_+ + n_-$ ). If we consider the case where the valance of both the cation and the anion are one, then equation (3) can be simplified to,

$$\sigma_{dc} = ne\mu \quad (4)$$

Hence, in order to obtain a high ionic conductivity the charge carrier density,  $n$ , and the mobility,  $\mu$ , should thus be as high as possible. However, to determine  $n$  and  $\mu$  values is not an easy task although desirable in order to optimize such parameters in electrolytes. On the other hand, the study of  $n$  and  $\mu$  is not only important for the characterization and development of good quality electrolytes for electrochemical device applications but also for other applications, for example it can be employed to quantify the density of viable biological cells in suspensions [6]. A number of approaches have been made to determine ion mobility under an applied electric field, including impedance spectroscopic methods. Transient ionic direct current measurements have also been used to determine the ion mobility [7,8]. This method employs a *dc* voltage until a steady state is reached after which the voltage is reversed and the current is measured as a function of time in order to determine the mobility. Nuclear Magnetic Resonance, NMR, spectroscopy has also been used to obtain this type of information, for instance, NMR has been applied for ionic liquids and polymer electrolytes however there are limitations. For example, the NMR method cannot be employed for all types of ionic species. [9]. However, despite a number of efforts, the mechanisms of ion conduction are still not well understood in many systems [10,11] and in particular there is still some controversy about the values of ion mobility in some solid-state electrolyte systems [11]. Therefore, a reliable and convenient method to determine the mobility and density of charge carriers is required.

Impedance analysis has advantages compared to potentiometric and amperometric electrochemical analysis in that a small perturbation potential is applied across the cell or electrolyte minimizing possible charge carrier concentration changes during the measurements. In impedance analysis, the voltage applied is very small and the time average of the changes, due to the applied sinusoidal potential, is zero. Some committed approaches to determine the mobility and charge carrier concentration based on impedance spectroscopic methods have been reported in the literature [6,11,12]. However none of the methods have been stated to be applicable for liquid electrolytes where simple tests can be used to assess the accuracy. The method used by Schütt *et al* [13] for ion conducting glasses is interesting; in that method the frequency that is selected for the calculations is the one where the real part of the dielectric constant is ten times that of the high frequency plateau ( $\epsilon'_{HF}$ ) value. Another recently developed model by Runt *et al* uses the frequency dependence of complex dielectric loss,  $\epsilon''$ , and loss tangent,  $\tan(\phi)$ , data in order to extract both the ion mobility and the mobile ion concentration [11]. This method is based on an analysis of



electrode polarization at low frequency electric fields. However, the values obtained for the mobile charge carrier concentrations are very low, nearly four orders of magnitude lower than that of the total number of ions available in the salt. As a consequence of this the analysis leads to very high mobility values for such solid electrolytes.

This chapter is basically aimed at developing a method to calculate the mobile charge carrier concentration and the mobility using impedance spectroscopic data which should be applicable for a wide range of electrolytes including ionic liquids. This new approach to determine  $n$  and  $\mu$  values is basically based on the studies by Coelho [14], Schütt and Gerdes [15,16] and by Jönsson *et al* [6]. In this work, new equations were derived to determine the charge carrier concentration and the mobility by modeling the space charge relaxation, and the required parameters can be obtained using boundary values of the dielectric function or using curve fitting to the dielectric function. The method is tested with known liquid electrolytes and then applied for various ionic liquids and polymer electrolytes containing an ionic liquid.

## 2. Theory

### 2.1 Impedance and impedance analysis

The standard widely used method to determine the bulk ionic conductivity of an electrolyte is complex impedance analysis. The electrical behaviour under an applied electric signal of an electrolyte sandwiched between two blocking electrodes can in the simplest case be described by the equivalent circuit and schematic diagram of a sample cell in Figure 1. When an electrical signal with angular frequency  $\omega$  is applied to the sample cell negative and positive ions are accumulated at the relevant interfaces of the electrodes as shown in the Figure 1, forming the well known Helmholtz double layer. These two double layers, result in electrode polarization and they behave as two capacitors with capacitance  $C_e$ . The geometrical capacitance,  $C$ , of the capacitor is formed by the electrolyte and two electrodes (without considering double layer capacitance) and  $R$  represents the bulk resistance of the electrolyte. In a real cell a more intricate equivalent circuit is needed to fully describe the electric behaviour but this simple model is sufficient for the moment.

The impedance of a capacitance is purely imaginary and its reactance is given by  $1/j\omega C$  where,  $j = \sqrt{-1}$ . Thus, the total impedance for an electrolyte with blocking electrodes can be represented by,

$$Z^*_{(\omega)} = \frac{R}{1 + j\omega RC} + \frac{2}{j\omega C_e} \quad (5)$$

Therefore, by means of equivalent circuits the real and imaginary parts of the impedance of an electrolyte in blocking electrodes can be represented by,

$$Z' = \frac{R}{1 + \omega^2 R^2 C^2} \quad (6)$$

and

$$Z'' = - \left( \frac{\omega R^2 C}{1 + \omega^2 R^2 C^2} + \frac{2}{\omega C_e} \right) \quad (7)$$

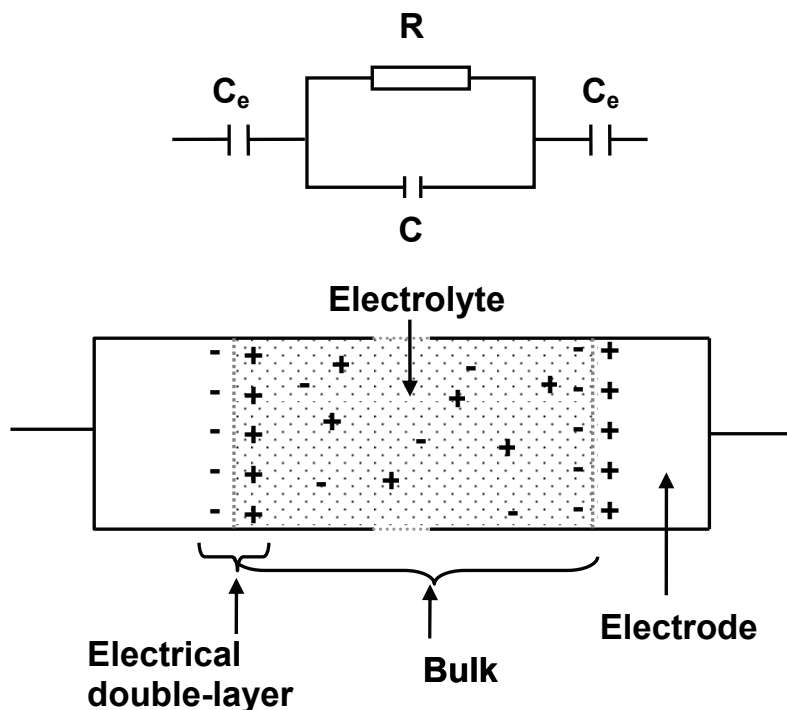


Fig. 1. Schematic diagram showing polarization in sample cell and simplified equivalent circuit for an electrolyte sandwiched between two blocking electrodes.

Using equations (6) and (7) the following equation can be obtained,

$$Z'' = - \left( \omega R C Z' + \frac{2}{\omega C_e} \right) \quad (8)$$

Actually, the Argand diagram of the complex impedance shows a semicircle with diameter  $R$  and a spike (straight line  $Z' = R$ ) as seen in the schematic diagram in Figure 2 based on the assumption that  $C$  is very small compared to  $C_e$  since the thickness of the electrical double layer is of the order of the Debye length ( $\lambda$ ), (that is, very small compared to the thickness of the electrolyte approximately 1 mm). The corresponding representation of equations (6) and (7) in the complex impedance plane is shown in Figure 3 and the real and the imaginary parts of the impedance versus frequency are shown in Figure 4 for a hypothetical case where  $R = 1000 \, \Omega$ ,  $C = 10 \, \text{pF}$  and  $C_e = 400 \, \text{nF}$ . The angular frequency corresponding to the maximum and the minimum of the imaginary part of the impedance is denoted by  $\omega_1$  and  $\omega_2$ . Expressions for the frequencies corresponding to the maximum and minimum of  $Z''$  can be derived under the assumption that  $C$  is very small compared to  $C_e$ . The angular frequency  $\omega_1$  corresponding to the maximum in  $Z''$  shown in Fig. 3 can be obtained simply by substituting ( $Z' = Z'' = R/2$ ) in equations (6) or (7). Thus

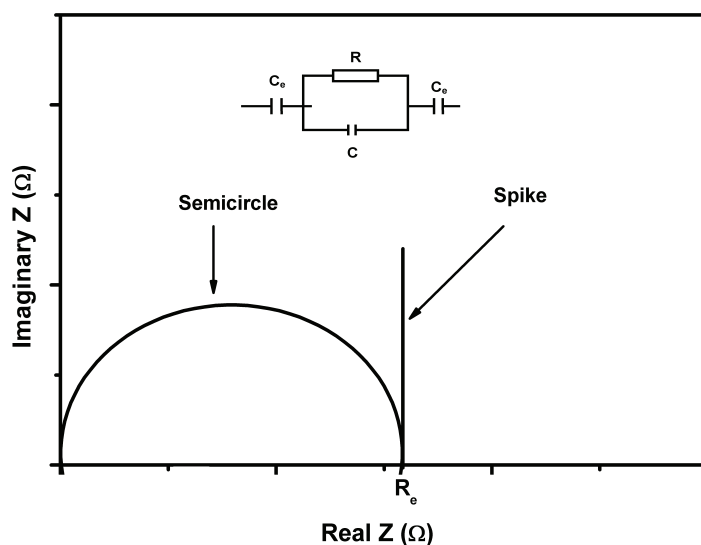


Fig. 2. Schematic diagram of equivalent circuit and the representation of real and imaginary parts of the impedance in a complex impedance plane based on the assumption that  $C$  is very small compared to  $C_e$ .

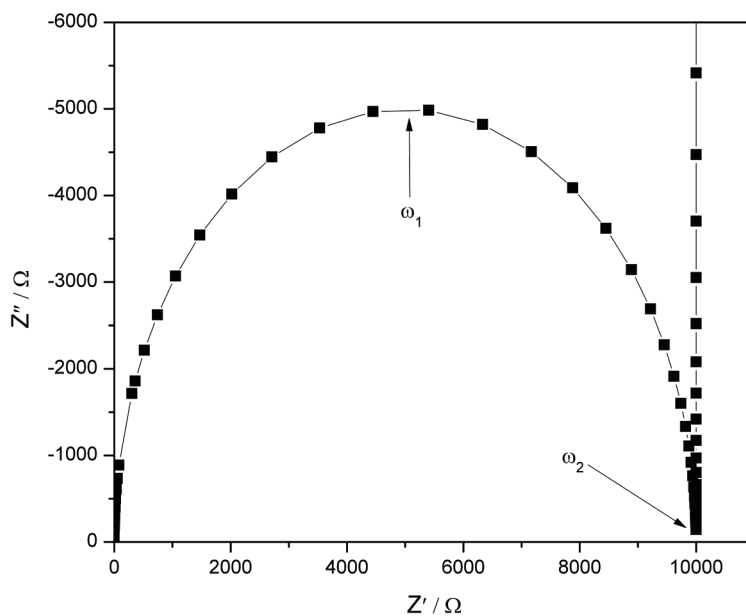


Fig. 3. The corresponding representation of equations (6) and (7) in the complex impedance plane for  $R=1000 \Omega$ ,  $C=10 \text{ pF}$  and  $C_e = 400 \text{ nF}$ .

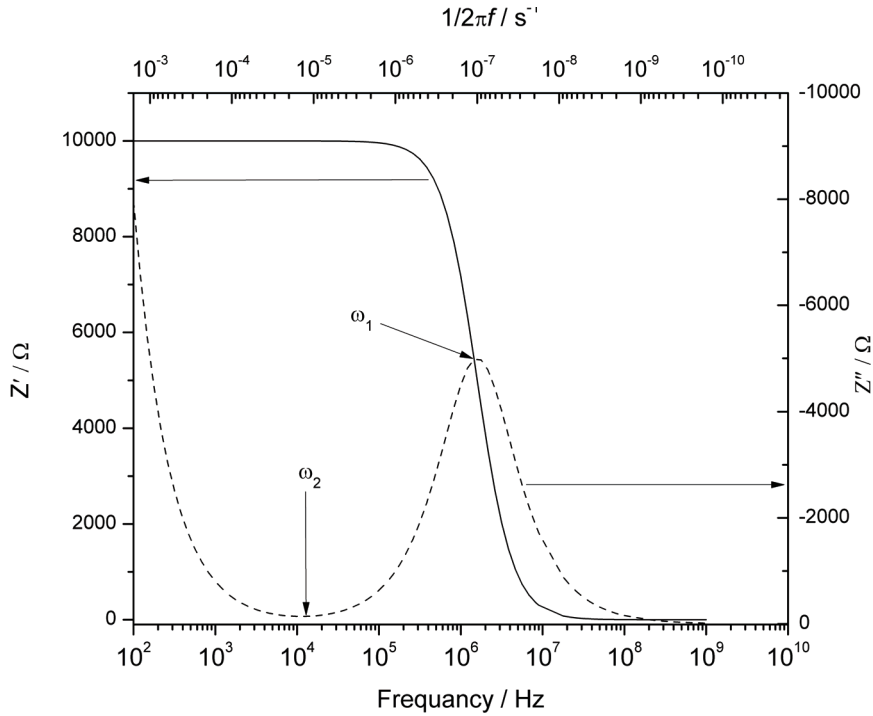


Fig. 4. The corresponding representation of equations (6) and (7), real and the imaginary parts of the impedance, as a function of frequency for  $R=1000 \Omega$ ,  $C=10 \text{ pF}$  and  $C_e = 400 \text{ nF}$ .

$$\omega_1 = \frac{1}{\tau_1} = \frac{1}{RC} \quad (9)$$

where  $\tau_1$  is characteristic time constant corresponding to the maximum in  $Z''$ . The angular frequency  $\omega_2$  corresponding to minimum in  $Z''$  shown in Fig 3 can be obtained simply substituting ( $Z'=R$ ,  $Z''=0$ ) in equation (8). Then,

$$\omega_2 = \frac{1}{\tau_2} = \frac{1}{RC} \sqrt{\frac{2C}{C_e}} \quad (10)$$

where,  $\tau_2$  is the characteristic time constant corresponding to the minimum in  $Z''$ . For a cylindrical electrolyte sample of cross section area  $A$ , sample thickness  $2d$  and mean thickness of the electrical double layer  $\lambda$  (equal to the Debye length) the  $R$ ,  $C$  and  $C_e$  can be represented by;

$$R = \frac{2d}{\sigma_{dc} A} \quad (11)$$

$$C = \epsilon_r \epsilon_0 \frac{A}{2d} \quad (12)$$

$$C_e = \varepsilon_r \varepsilon_o \frac{A}{\lambda} \quad (13)$$

where  $\sigma_{dc}$  is dc conductivity of the electrolyte,  $\varepsilon_r$  the dielectric constant of the electrolyte and  $\varepsilon_o$  the vacuum permittivity. The  $R$ ,  $C$  and  $C_e$  in equations (9) and (10) can be substituted using equations (11), (12) and (13) to obtain;

$$\omega_1 = \frac{1}{\tau_1} = \frac{\sigma_{dc}}{\varepsilon_o \varepsilon_r} = \frac{n\mu e}{\varepsilon_o \varepsilon_r} \quad (14)$$

$$\omega_2 = \frac{1}{\tau_2} = \frac{\sigma_{dc}}{\varepsilon_o \varepsilon_r \sqrt{\delta}} = \frac{n\mu e}{\varepsilon_o \varepsilon_r \sqrt{\delta}} \quad (15)$$

where  $\delta = d/\lambda = C_e/2C$

Using equations (14) and (15) the relationship between  $\tau_1$  and  $\tau_2$  can be obtained,

$$\tau_2 = \tau_1 \sqrt{\delta} \quad (16)$$

According to Coelho [14], by modelling the macroscopic space-charge polarization, the effective permittivity  $\tilde{\varepsilon}^*$  of an ionic conductor sandwiched between two blocking electrodes can be described by,

$$\tilde{\varepsilon}^* = \varepsilon_o \varepsilon_r \left\{ \left( \frac{1 + i\omega\tau_1}{i\omega\tau_1 + (\tanh Y)/Y} \right) \right\} \quad (17)$$

where  $Y$  is given by,

$$Y = (1 + i\omega\tau_1)^{1/2} \frac{d}{\lambda} \quad (18)$$

Using the approximation  $\tanh(Y)/Y = (1 - i\omega\tau_1/2)/\delta$  valid for  $\delta \gg 1$ , and recalling that  $\delta$  is given by,

$$\delta = \frac{d}{\lambda} \quad (19)$$

equation (17) can be simplified to,

$$\tilde{\varepsilon}^* = \varepsilon'_\infty \left\{ \left( 1 + \frac{\delta}{1 + (\omega\tau_1\delta)^2} \right) - i \left( \frac{\omega\tau_1\delta^2}{1 + (\omega\tau_1\delta)^2} \right) \right\} \quad (20)$$

where,  $\varepsilon_\infty = \varepsilon'_\infty$  is high frequency permittivity,

The real ( $\varepsilon'$ ) and imaginary ( $\varepsilon''$ ) parts of the dielectric constant as well as the dielectric loss tangent ( $\tan\phi$ ) can be extracted from equation (20),

$$\varepsilon' = \varepsilon'_\infty \left( 1 + \frac{\delta}{1 + (\omega\tau_1\delta)^2} \right) \quad (21)$$

$$\varepsilon'' = \varepsilon'_\infty \left( \frac{\omega \tau_1 \delta^2}{1 + (\omega \tau_1 \delta)^2} \right) \quad (22)$$

$$\tan(\phi) = \frac{\varepsilon''}{\varepsilon'} = \frac{\omega \tau_1 \delta^2}{1 + \delta + (\omega \tau_1 \delta)^2} \approx \frac{\omega \tau_1 \delta}{1 + \omega^2 \tau_1^2 \delta} \quad (23)$$

As illustrated in Appendix 1 it can be proved that the relaxation time  $\tau_2$  corresponds to the frequency of the maximum in dielectric loss tangent ( $\tan \phi$ ). In this method the characteristic time constant  $\tau_2$  was chosen from the frequency at the maximum in  $\tan(\phi)$ . Hence, by using the relation  $\tau_2 = \tau_1 \sqrt{\delta}$  equation (20) can be modified to

$$\tilde{\varepsilon}^* = \varepsilon'_\infty \left\{ \left( 1 + \frac{\delta}{1 + (\omega \tau_2)^2 \delta} \right) - i \left( \frac{\omega \tau_2 \delta^{3/2}}{1 + (\omega \tau_2)^2 \delta} \right) \right\} \quad (24)$$

to take this characteristic time constant,  $\tau_2$ , into account. It is noteworthy that the relaxation time  $\tau_2$  correspond to the frequency where the *dc* resistance is obtained from complex impedance plots and thus the real part of the impedance and the frequency dependence of the conductivity remains relatively unchanged close to this frequency, for an example, see Fig. 5 that shows the frequency dependence of the conductivity for KI solution electrolytes. Hence, graphical representations of the dielectric function can be used to extract  $\tau_2$ . Fig. 6 shows the frequency dependence of the imaginary part of the dielectric constant ( $\varepsilon''$ ) and dielectric loss tangent ( $\tan \phi$ ) if  $\delta = 2 \times 10^4$  and  $\tau_2 = 1.4 \times 10^{-7}$  s according to equation (24). On the other hand, when  $\omega = 1/\tau_2$  the conductivity is in the *dc* limit and  $\tau_2 \gg \tau_1$ . The net ionic diffusion coefficient (*D*) due to the conduction and diffusion in the electrolyte at the *dc* limit is given by;

$$\lambda = (D \tau_2)^{1/2} \quad (25)$$

For a single ion conductor,  $D = D_{ion}$  can be used and in case both cations and anions are mobile, an effective *D* value may be used [17,18]. Anyhow, by using equation (18) one can obtain;

$$\delta = \frac{d}{(D \tau_2)^{1/2}} \quad (26)$$

Hence;

$$D = \frac{d^2}{\tau_2 \delta^2} \quad (27)$$

As the diffusion coefficient, *D*, can be obtained using equation (27), by means of dielectric data that gives  $\tau_2$  and  $\delta$ , the well known Nernst-Einstein relation,

$$\mu = \frac{eD}{kT} \quad (28)$$

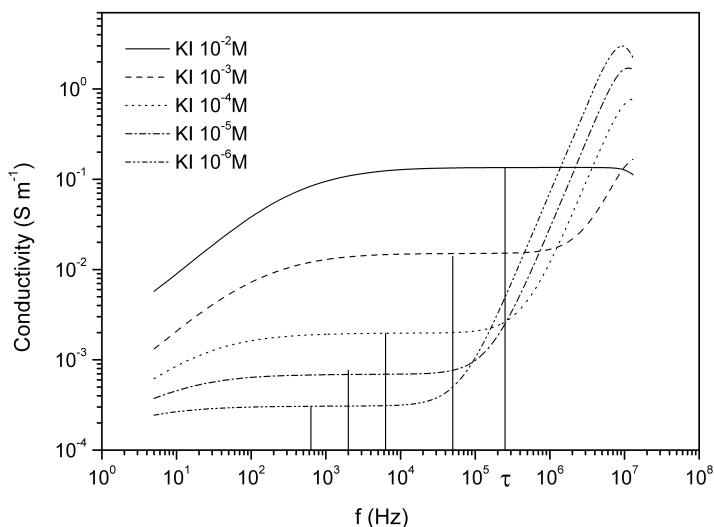


Fig. 5. The real part of the *ac* conductivity vs. frequency for  $10^{-2}$ ,  $10^{-3}$ ,  $10^{-4}$ ,  $10^{-5}$ ,  $10^{-6}$  M KI solutions. The corresponding characteristic time constant,  $\tau_2$ , is also shown using a vertical line.

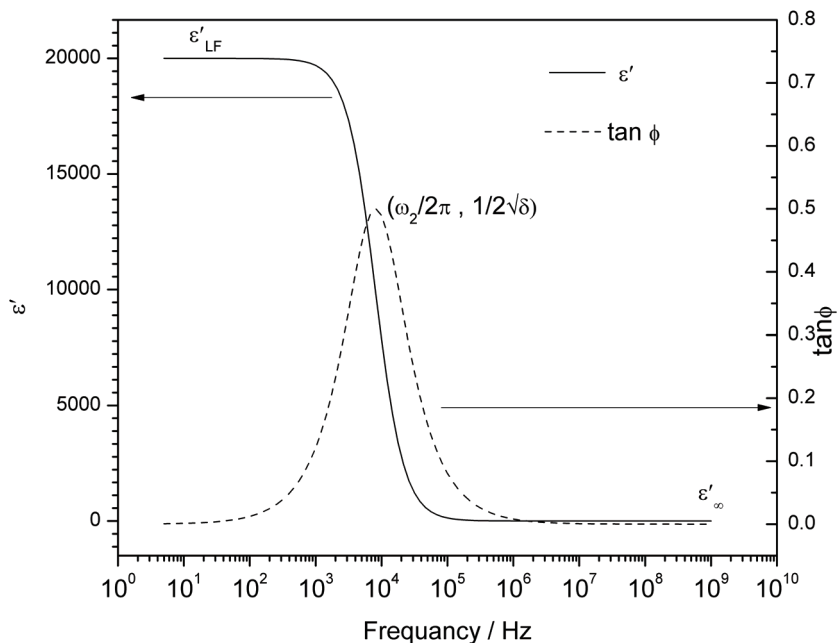


Fig. 6. The frequency dependent of imaginary part of the dielectric constant ( $\epsilon''$ ) and dielectric loss tangent ( $\tan \phi = \epsilon''/\epsilon'$ ) according to equation (24) for  $\delta = 2 \times 10^4$  and  $\tau_2 = 1.4 \times 10^{-7}$  s.

where  $k$  is the Boltzmann constant and  $T$  the absolute temperature, can be used to deduce an equation for the mobility. Thus,  $\mu$  can be obtained using equations (27) and (28).

$$\mu = \frac{ed^2}{kT\tau_2\delta^2} \quad (29)$$

In order to obtain the  $n$  value,  $\mu$  in equation (4) is substituted into equation (29), thus

$$n = \frac{\sigma_{dc}kT\tau_2\delta^2}{e^2d^2} \quad (30)$$

If  $\tau_2$  and  $\delta$  can be evaluated from dielectric measurement, equations (27) (29) and (30) can be used to determine  $D$ ,  $\mu$  and  $n$  values.

## 2.2 Determination of density and mobility of charge carriers

In order to calculate diffusion coefficient, mobility and mobile charge carrier density of an electrolyte values of  $\tau_2$  and  $\delta$  should thus be obtained. There are actually many ways to estimate  $\tau_2$  and  $\delta$  using electrical and dielectric measurements.

### a. Using Complex Impedance data

Complex impedance data can be used to estimate  $\tau_2$  and  $\delta$ . Using the frequencies corresponding to the maximum and minimum in  $Z''$  values,  $\omega_1$  and  $\omega_2$  can be obtained, see Fig. 3. Hence, equations (14) – (16) can be used to calculate  $\tau_2$  and  $\delta$  in order to determine diffusion coefficient, mobility and mobile charge carrier concentration.

### b. Using measured real part of the dielectric constant

The frequency dependence of the measured real part of the dielectric constant can also be used to calculate  $\tau_2$  and  $\delta$ . A schematic graph of the real part of the dielectric constant as a function of frequency is shown in Fig. 6. Curve fitting to the equation,

$$\epsilon'_r = \epsilon'_\infty \left( 1 + \frac{\delta}{1 + (\omega\tau_2)^2 \delta} \right) \quad (31)$$

obtained using equation (24), can be used to estimate values for  $\tau_2$  and  $\delta$  using measured data. In addition, as the Debye length is very small compared to sample thickness and thus the  $\delta$  value is very large ( $\delta \gg 1$ ). Therefore, the low frequency limit in equation (31) can be used to derive an equation for  $\delta$ ,

$$\epsilon'_{LF} = \epsilon'_\infty (1 + \delta) \quad (32)$$

Since  $\delta \gg 1$ ,  $\delta$  is given by the equation

$$\delta = \frac{\epsilon'_{LF}}{\epsilon'_\infty} \quad (33)$$

Hence, the low and high frequency limits of the measured dielectric constant can be used in order to calculate  $\delta$  using equation (33) see Fig 6. Equations (29) and (30) can also be modified to use the low and high frequency limits of  $\epsilon'$ .



$$\mu = \frac{ed^2}{kT\tau_2} \left( \frac{\epsilon'_{\infty}}{\epsilon'_{LF}} \right)^2 \quad (34)$$

$$n = \frac{kT\sigma\tau_2}{e^2d^2} \left( \frac{\epsilon'_{LF}}{\epsilon'_{\infty}} \right)^2 \quad (35)$$

c. *Using measured real part of the dielectric loss tangent*

According to this model, an equation for the dielectric loss tangent,  $\tan\phi$ , can be obtained using equation (24);

$$\tan\phi = \left( \frac{\omega\tau_2\sqrt{\delta}}{1 + (\omega\tau_2)^2} \right) \quad (36)$$

Fig. 6 shows a typical example for dielectric loss tangent,  $\tan\phi$ , curve according to equation (36). The measured data for dielectric loss tangent can be fitted to equation (36) in order to estimate values for  $\delta$  and  $\tau_2$ . In addition, to estimate  $\delta$  and  $\tau_2$  the coordinates at the peak value (maximum) in  $\tan\phi$  can also be used (see Fig 6). The  $\tau_2$  can be calculated using the frequency corresponding to the maximum in  $\tan\phi$  and  $\delta$  can be estimated using the peak value of  $\tan\phi$  as described in Appendix 1.

### 2.3 Real systems with blocking electrodes

The equations described above are valid for Debye type relaxations. In general, real systems do not follow exactly the behaviour described by these equivalent circuits and model equations. For example, the spike shown in Fig 2 is inclined and deformed due to electrode effects etc. Thus to broaden the applicability of the method to Cole-Cole type relaxations [19] the real and imaginary parts of the dielectric constant and dielectric loss tangent shown in equation can be modified to,

$$\epsilon' = \epsilon'_{\infty} \left( 1 + \frac{\delta}{1 + (\omega\tau_m)^{2(1-\alpha)}} \right) \quad (37)$$

$$\epsilon'' = \epsilon'_{\infty} \left( \frac{\omega\tau_2\delta^{3/2}}{1 + (\omega\tau_2)^{2(1-\alpha)}} \right) \quad (38)$$

$$\tan\phi = \left( \frac{\omega\tau_2\sqrt{\delta}}{1 + (\omega\tau_2)^{2(1-\alpha)}} \right) \quad (39)$$

where,  $\alpha$  is a constant ( $\alpha < 1$ ) [19]. Dielectric measurements of real electrolyte systems with blocking electrodes can successfully be fit to equations (37) or (38) or (39) and values of  $\delta$  and  $\tau_2$  can be estimated in order to calculate diffusion coefficient, charge carrier density and mobility.

### 3. Diffusion coefficient ( $D$ ), charge carrier density ( $n$ ) and mobility ( $\mu$ )

#### 3.1 $D$ , $n$ and $\mu$ in KI Solutions.

To test the applicability of the model  $10^{-2}$  M KI and  $10^{-3}$  M KI solutions were investigated, the graphs of  $\epsilon'$  vs. frequency are shown in Fig. 7. For KI solutions with lower concentrations (less than  $10^{-4}$  M KI) the low frequency plateau appears outside the measured frequency window. The KI solutions with concentrations  $10^{-2}$  M and  $10^{-3}$  M KI showed more or less sigmoidal curves within the measured frequency range. The curves in Fig. 7 were fitted to equation (37) and the obtained parameters were used for the calculations. An appropriate  $\epsilon'_\infty$  value was determined using the plots in Fig. 7 prior to the curve fitting. During the fitting an appropriate  $\alpha$  value was also selected. The  $\alpha$  value was in the range 0.15 to 0.25 for both KI solutions. The fitted curves are also shown in Fig. 7 and the obtained parameters  $\tau_2$  and  $\delta$  are given in Table 1. The low frequency plateaus of the experimental curves have an incline probably due to contributions from other low frequency relaxations apart from the space charge relaxation possibly due to electrode effects. To take such other relaxations into account the model will require modifications but the major concern of this chapter is the determination of the charge carrier density and the mobility in electrolytes by modelling the space charge relaxation. The selection of the appropriate frequency region for curve fitting (dominated by the space charge relaxation) can improve the accuracy of the results. Accordingly, the low frequency region in Fig. 7 was omitted from fitting in order to reduce the errors due to other relaxation effects.

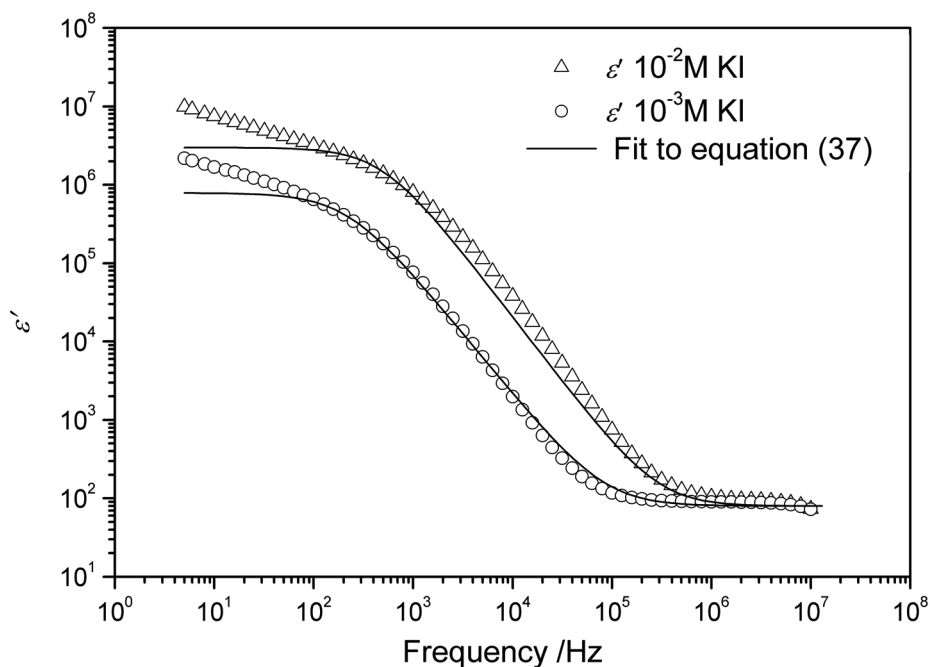


Fig. 7. The  $\epsilon'$  versus frequency for  $10^{-2}$  M and  $10^{-3}$  M KI solutions at temperatures 25 °C. The solid lines represent curves fitted to equation (37).

The parameters  $\tau_2$  and  $\delta$  extracted from curve fitting were used in equations (27), (29) and (30) to determine the  $D$ ,  $n$ , and  $\mu$  values shown in Table 1. The standard deviation of  $\tau_2$  and  $\delta$  values obtained from the curve fitting remained less than 10% and the error in  $\sigma$  and  $T$  was maintained less than 5%. Based on this, the error limit of the  $n$  and  $\mu$  values obtained in this method is estimated to be within  $\pm 20\%$ .

KI Concentration	$\sigma_{dc} / \text{mS cm}^{-1}$	$\tau_2 / \text{s}$	$\delta$	$D / \text{m}^2 \text{s}^{-1}$	$n / \text{m}^{-3}$	$\mu / \text{m}^2 \text{V}^{-1} \text{s}^{-1}$
$10^{-2} \text{ M}$	1.34	$5.09 \times 10^{-7}$	46341.33	$2.0 \times 10^{-9}$	$1.09 \times 10^{25}$	$7.7 \times 10^{-8}$
$10^{-3} \text{ M}$	0.15	$27.0 \times 10^{-7}$	9014.65	$2.2 \times 10^{-9}$	$1.11 \times 10^{24}$	$8.6 \times 10^{-8}$

Table 1. The conductivity ( $\sigma_{dc}$ ), fitting parameters ( $\tau_2$ ,  $\delta$ ), diffusion coefficient ( $D$ ), charge carrier density ( $n$ ) and mobility ( $\mu$ ) determined for  $10^{-2} \text{ M}$  and  $10^{-3} \text{ M}$  KI solutions at  $25^\circ \text{C}$ .

Fig. 8 shows the dielectric loss tangent,  $\tan \phi$ , as a function of frequency for KI solutions with concentrations  $10^{-2}$ ,  $10^{-3}$ ,  $10^{-4}$ ,  $10^{-5}$ ,  $10^{-6} \text{ M}$ . In order estimate  $\tau_2$  and  $\delta$ ,  $\tan \phi$  plots can also be used. For instance, curve fitting to equation (39) or the coordinates  $(\tau_2, \frac{\sqrt{\delta}}{2})$  of the maximum in  $\tan \phi$  can be used to determine  $\tau_2$  and  $\delta$  and then equations (29) and (30) can be used to calculate the mobility and charge carrier density.

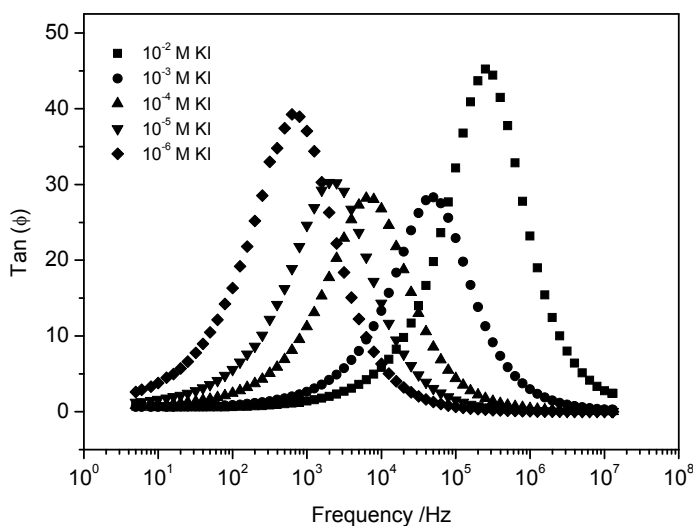


Fig. 8. Dielectric loss tangent,  $\tan \phi$  vs. frequency for  $10^{-2}$ ,  $10^{-3}$ ,  $10^{-4}$ ,  $10^{-5}$ ,  $10^{-6} \text{ M}$  KI solutions at  $25^\circ \text{C}$ .

### 3.2 $D$ , $n$ and $\mu$ in the Ionic Liquid, 1-methyl-3 propyl imidazolium iodide

This method of calculating mobility and charge carrier density was applied to estimate the  $n$ ,  $\mu$  and  $D$  values for the ionic liquid 1-methyl-3 propyl imidazolium iodide which is a useful electrolyte material for solar cell applications. Some of the fitted curves and measured data are shown in Figure 9 in the temperature range 8 to 60 °C. The reliability of the model equations for this ionic liquid was established by the excellent fitting of the measured data to equation (37) as shown in Figure 9. In fact, the data fitted well and the standard deviations of  $\delta$  and  $\tau$  values were less than 2 %. The values of  $n$ ,  $\mu$  and  $D$  calculated using this method are shown in Fig. 10 and 11. The conductivity values obtained directly from impedance measurements are also shown in Fig. 10. It can be immediately seen that in this system, the increase in conductivity with increasing temperature is dominated by the increase in the charge carrier concentration rather than by the increase in the mobility.

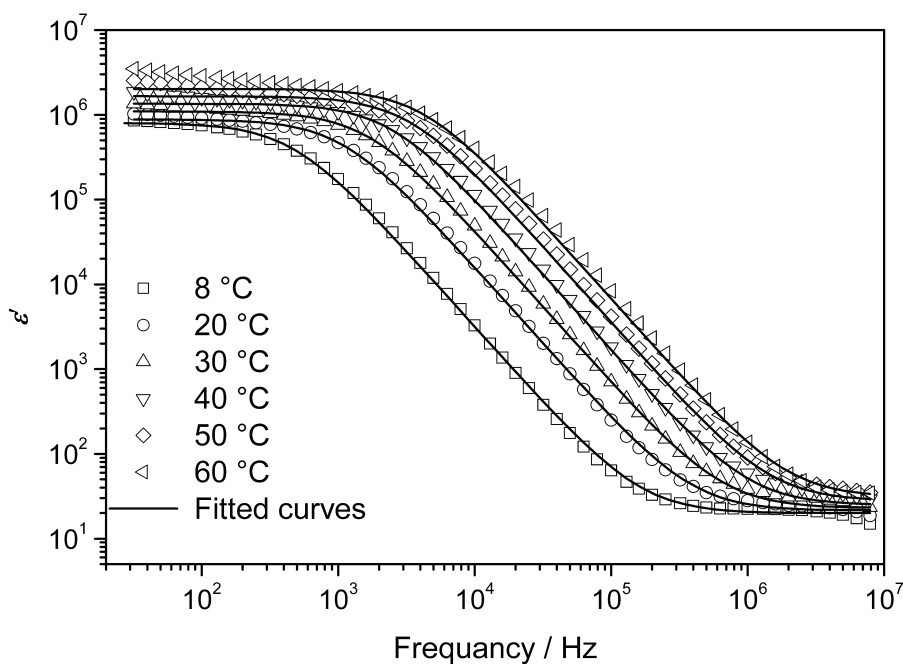


Fig. 9. The measured real part of the dielectric constant ( $\epsilon'$ ) and the fitted curves to model equation (37) for ionic liquid, 1-methyl-3-propyl imidazolium iodide, at different temperatures.

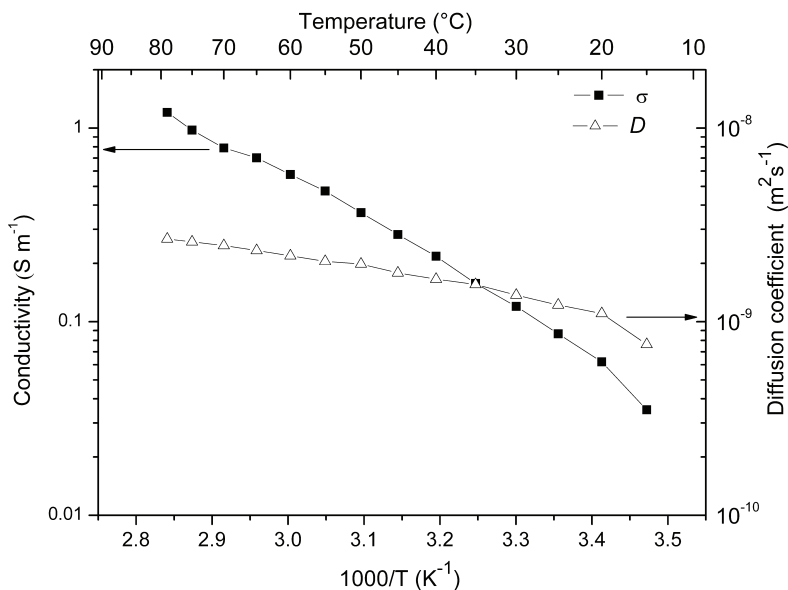


Fig. 10. The conductivity,  $\sigma$ , and diffusion coefficient,  $D$ , versus  $1000/T$  for the ionic liquid, 1-methyl-3-propyl imidazolium iodide.

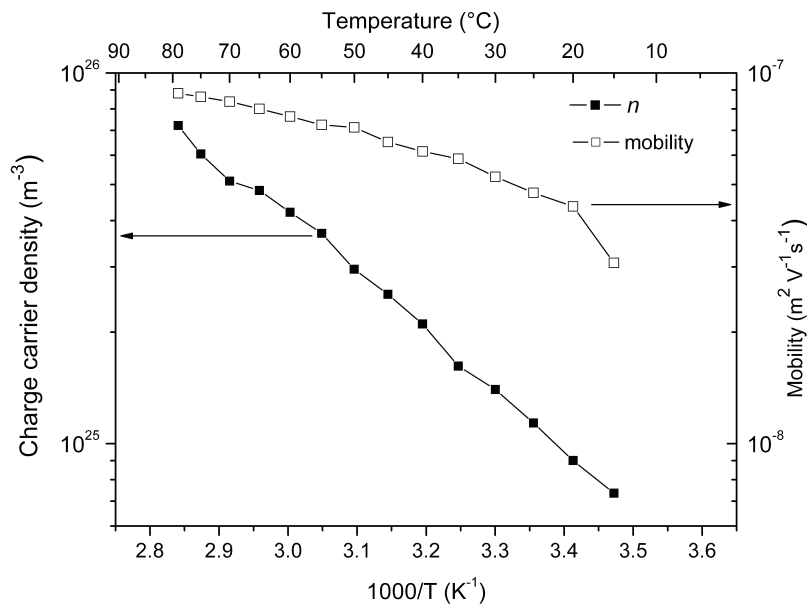


Fig. 11. The charge carrier density,  $n$ , and the mobility,  $\mu$ , calculated using the new method, as a function of  $1000/T$  for the ionic liquid, 1-methyl-3-propyl imidazolium iodide, at different temperatures.

Fig. 11 shows the dielectric loss tangent,  $\tan\phi$ , as a function of frequency for 1-methyl-3-propyl imidazolium iodide, at different temperatures. In order to estimate  $\tau_2$  and  $\delta$  this  $\tan\phi$  plots can also be employed.

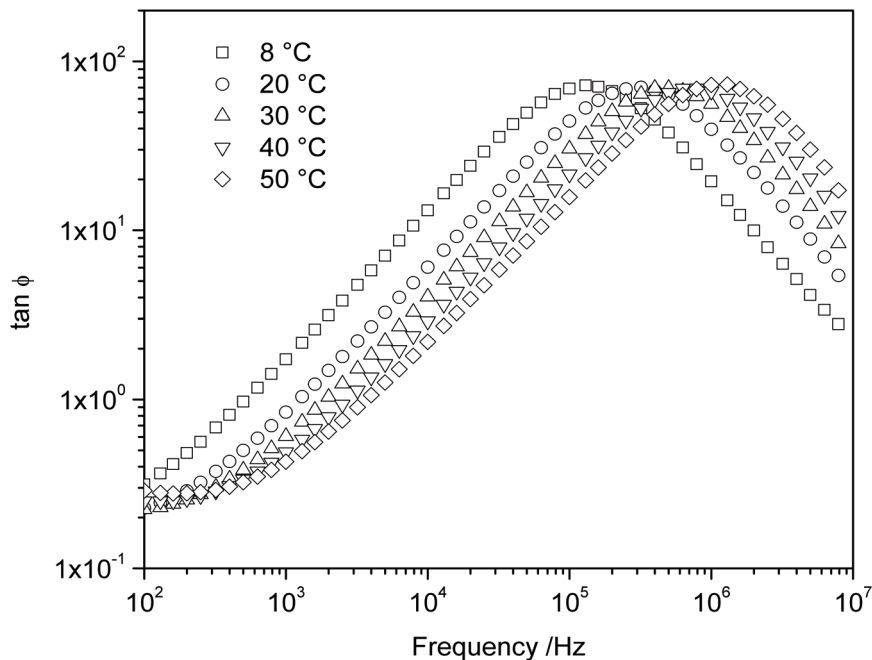


Fig. 12. The measured dielectric loss tangent as a function of frequency for the ionic liquid, 1-methyl-3-propyl imidazolium iodide, at different temperatures.

### 3.3 $D$ , $n$ and $\mu$ in 1-Butyl-1-methylpyrrolidinium bis(trifluoromethanesulfonyl) imide

The method was employed to estimate the  $n$ ,  $\mu$  and  $D$  values in the ionic liquid 1-Butyl-1-methylpyrrolidinium bis(trifluoromethanesulfonyl) imide (PYR<sub>14</sub>TSFI). Some of the fitted curves and measured data in the temperature range 0 to 50 °C for this ionic liquid are shown in Figure 13. The measured data for this ionic liquid also showed a good fit to equation (37) as shown in Figure 13, demonstrating the applicability of the method to this ionic liquid. The values obtained for the standard deviation of  $\delta$  and  $\tau$  was less than 5 %. The values of  $n$ ,  $\mu$  and  $D$  calculated using this method are shown in Fig. 14 and 15. The conductivity values obtained directly from impedance measurements are also shown in Fig. 14 for PYR<sub>14</sub>TSFI. It can be inferred that the increase in conductivity with increasing temperature is dominated by the increase in the mobility rather than by the increase in the charge carrier concentration in this system.

Fig. 16 shows the dielectric loss tangent,  $\tan\phi$ , as a function of frequency for PYR<sub>14</sub>TSFI, at different temperatures. In order to estimate  $\tau_2$  and  $\delta$  these  $\tan\phi$  plots can also be used. Curve fitting to equation (39) or coordinates of the maximum in  $\tan\phi$  can be used to determine  $\tau_2$  and  $\delta$ .

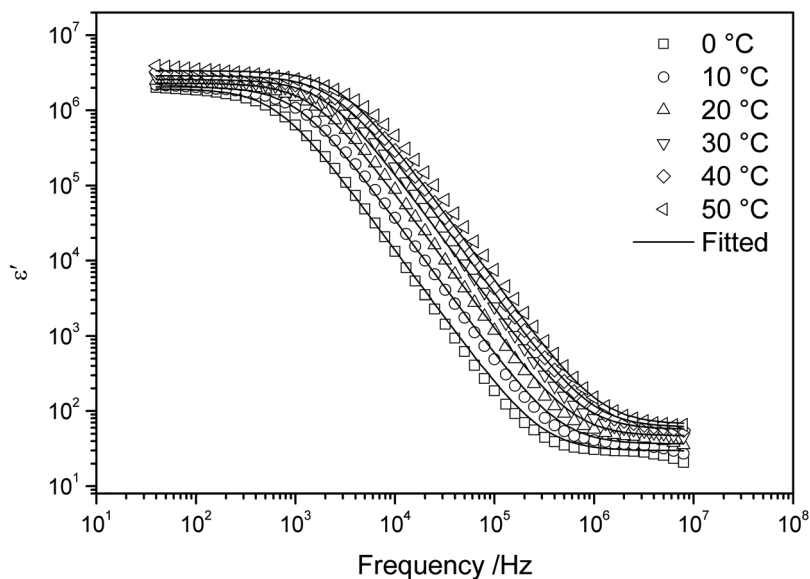


Fig. 13. The measured real part of the dielectric constant ( $\epsilon'$ ) and the fitted curves to model equation (37) for the ionic liquid, PYR<sub>14</sub>TSFI, at different temperatures.

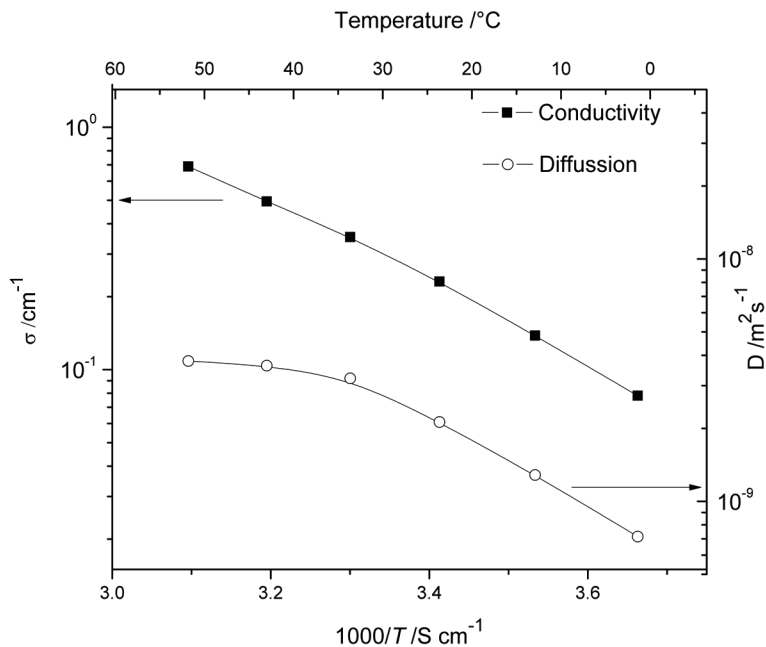


Fig. 14. The conductivity,  $\sigma$ , and diffusion coefficient,  $D$ , obtained using impedance measurements, versus  $1000/T$  for the ionic liquid, PYR<sub>14</sub>TSFI.

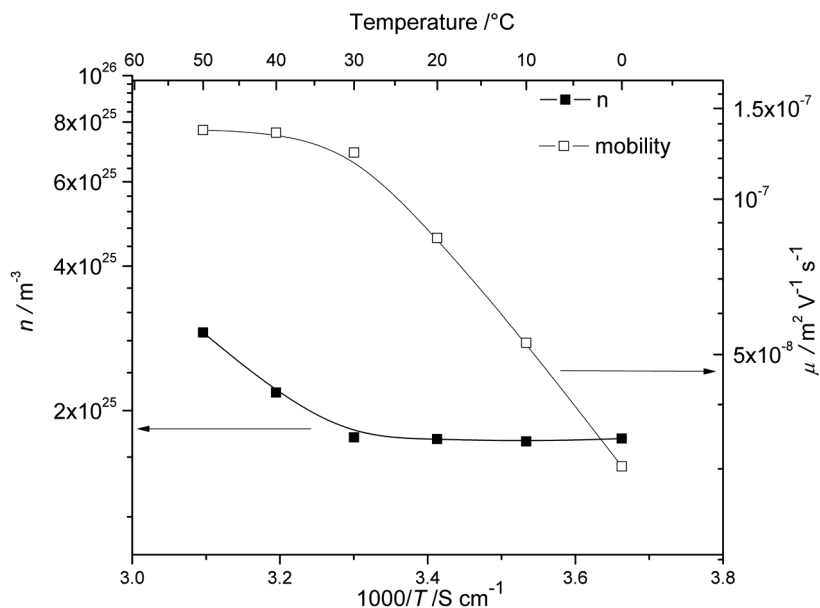


Fig. 15. The charge carrier density,  $n$ , and the mobility,  $\mu$ , calculated using the new method, as a function of  $1000/T$  for the ionic liquid, PYR<sub>14</sub>TSFI, at different temperatures.

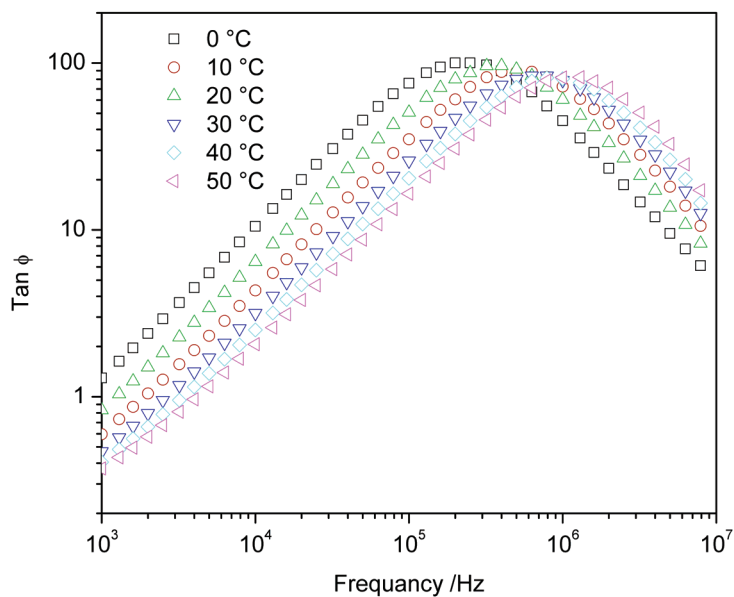


Fig. 16. The measured the dielectric loss tangent as a function of frequency for ionic liquid, PYR<sub>14</sub>TSFI, at different temperatures.



### 3.4 $D$ , $n$ and $\mu$ in a polymer electrolyte containing an ionic liquid.

An iodide ion ( $\text{I}^-$ ) conducting polymer electrolyte, based on polyethylene oxide (PEO) and tetrahexylammonium iodide ( $\text{Hex}_4\text{N}^+\text{I}^-$ ) salt was selected for application of the method [20]. The electrolyte contained ethylene carbonate (EC) 100% mass fraction and  $\text{Hex}_4\text{N}^+\text{I}^-$  60% mass fraction with respect to the weight of PEO in the electrolyte. The measured real part of the dielectric constant and the fitted curves for the PEO/ $\text{Hex}_4\text{N}^+\text{I}^-$ /EC electrolyte for different temperatures are shown in Fig. 17. The obtained conductivities from impedance measurements for the PEO/ $\text{Hex}_4\text{N}^+\text{I}^-$ /EC electrolyte samples are shown in Fig. 18 and the diffusion coefficient,  $D$ , calculated using curve fitted parameters is also shown in Fig. 18. The charge carrier density,  $n$ , and the mobility  $\mu$  calculated using this method are shown in Fig. 19. The model equation (37) fitted rather well giving less than 5% standard deviation, thus exhibiting the reliability of the model equations. This type of electrolytes show two melting peaks that relates to the PEO rich phase and the EC rich phase at about 60 °C and 30 °C [20]. Before melting these phases in the PEO/ $\text{Hex}_4\text{N}^+\text{I}^-$ /EC electrolyte shows high mobility values and low charge carrier density. In general, for temperatures higher than 30 °C both the mobility and density of charge carriers increases with increasing temperature.

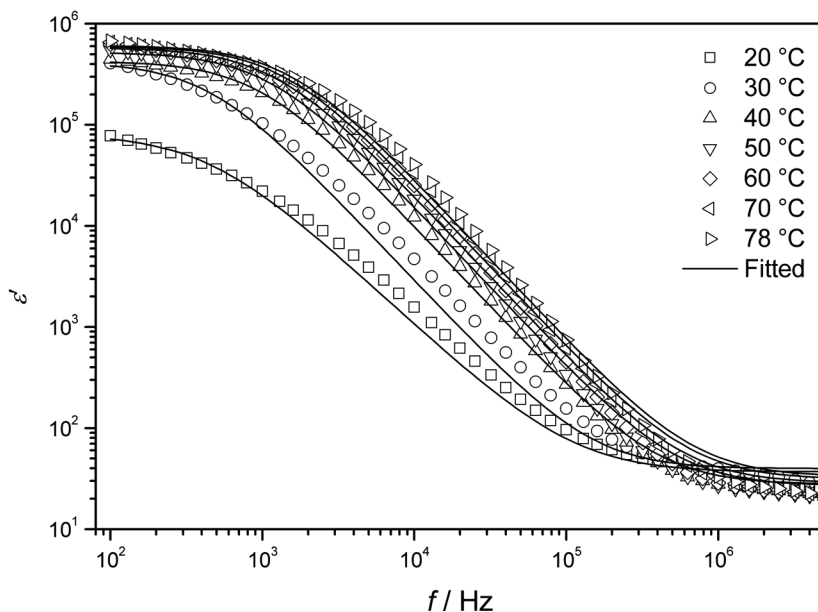


Fig. 17. The measured real part of the dielectric constant ( $\epsilon'$ ) and the fitted curves to model equation (37) for PEO/ $\text{Hex}_4\text{N}^+\text{I}^-$ /EC electrolyte at different temperatures

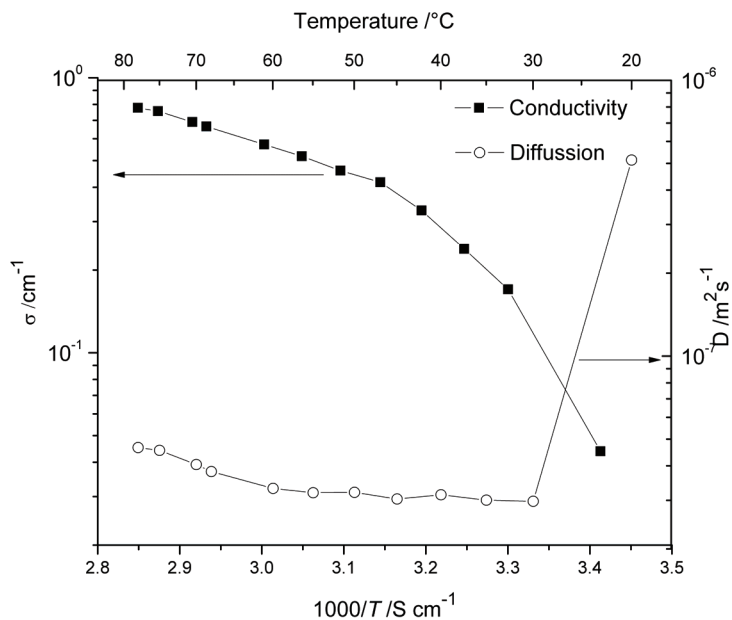


Fig. 18. The conductivity, obtained using impedance measurements, versus  $1000/T$  for PEO/Hex<sub>4</sub>N<sup>+</sup>I<sup>-</sup>/EC electrolyte.

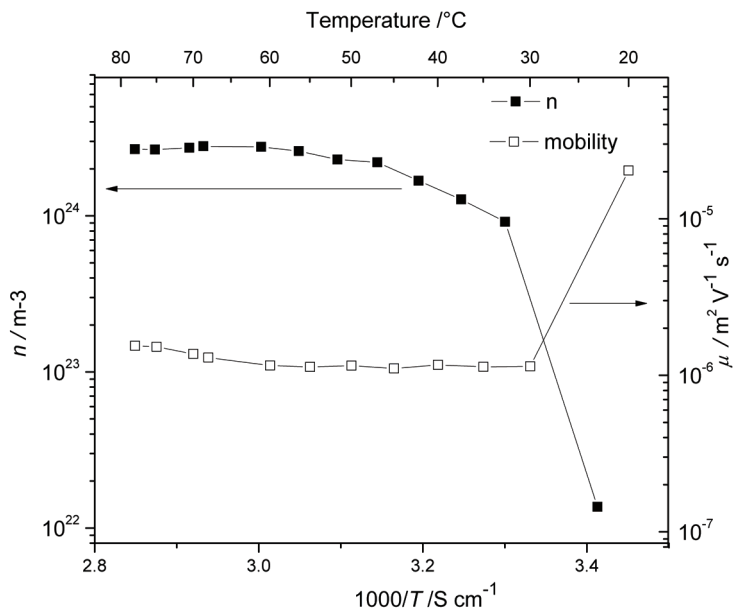


Fig. 19. The charge carrier density,  $n$ , and mobility,  $\mu$ , calculated using the new method, as a function of  $1000/T$  for PEO/Hex<sub>4</sub>N<sup>+</sup>I<sup>-</sup>/EC.

### 3.5 The $n$ and $\mu$ in a KI solution without curve fitting

The complex impedance measurements are the basis for the evaluation of  $\mu$  and  $n$  and the complex impedance measurements can actually be directly employed to determine  $\tau_2$  and  $\delta$ . As another test measurements on aqueous solutions were made using KI. Figure 20 shows the graph of imaginary part of the complex impedance  $Z''$  against the real part  $Z'$  for  $3 \times 10^{-4}$  M solution at different temperatures. The relaxation time,  $\tau_2$ , was obtained from the frequency corresponding to the minimum in  $Z''$  shown in Figure 20. This  $\tau_2$  value coincides with the frequency of the maximum in  $\tan\phi$  as described in the theory section.

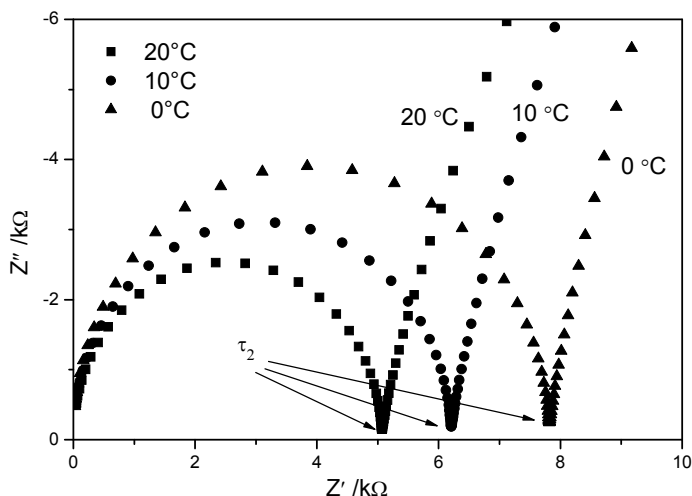


Fig. 20. Complex part of the impedance ( $Z''$ ) versus real part of the impedance ( $Z'$ ) for the  $3 \times 10^{-4}$  M KI solution at 0, 10 and 20 °C respectively.

The graphs given in Fig. 21 show the real part of  $ac$  conductivity as a function of frequency for  $10^{-2}$  M and  $10^{-3}$  M KI concentration at temperatures between 0 and 20 °C. The curves have the expected appearance and  $\sigma$  can be extracted from either the value of  $Z'$  at the minimum  $Z''$  in Fig. 20 or from the plateau values of the graphs in Fig. 21.

The  $\epsilon'$  vs frequency curves have the expected appearance, however, for lower concentrations ( $10^{-4}$  M KI) the  $\epsilon'_{LF}$  is difficult to estimate as it is shifting outside the measurement window.  $10^{-3}$  M and  $10^{-2}$  M KI solutions gave relatively sigmoidal curves within the measurement window.

The  $\sigma_{dc}$ ,  $\tau_2$  and  $\delta$  ( $\epsilon'_{LF}/\epsilon'_{\infty}$ ) values were determined using the plots shown in Figures 20, 21 and 22. However, the determination of  $\epsilon'_{LF}$  was difficult due to the inclination of the low frequency plateau of  $\epsilon'$ , which, in turn, is due to the existence of other relaxations apart from the space charge relaxation. In order to improve accuracy, a method to properly determine  $\epsilon'_{LF}$  is needed when curve fitting is not used. The  $n$  and  $\mu$  values were in this case determined using equations (34) and (35) and the calculated values are shown in Tables 2 and 3. The obtained values differ somewhat compared to those obtained using curve fitting.

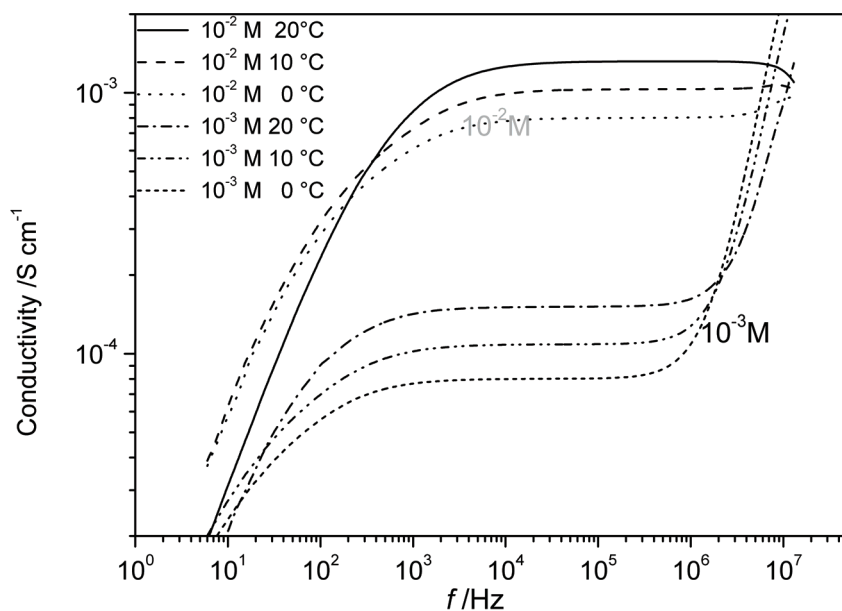


Fig. 21. Conductivity isotherms for  $10^{-2}$  M and  $10^{-3}$  M KI solutions as a function of frequency for temperatures 0, 10 and 20 °C.

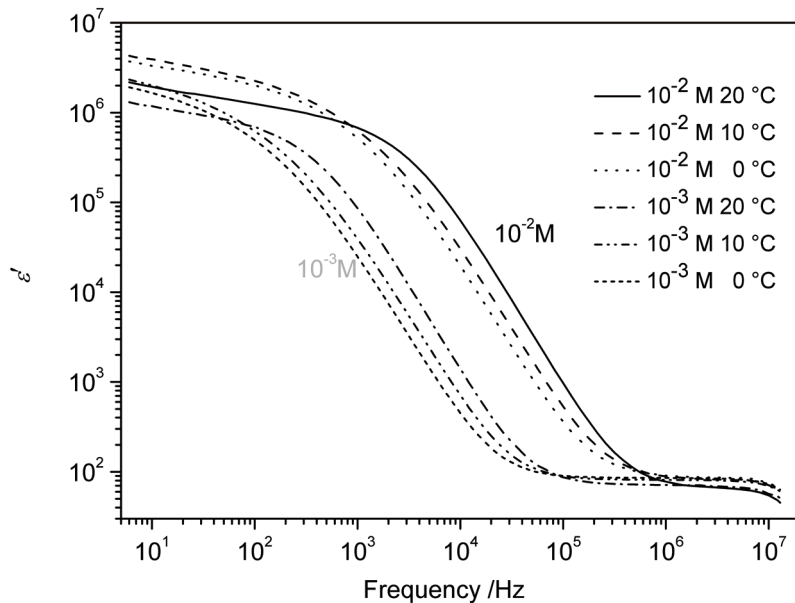


Fig. 22. The  $\epsilon'$  versus frequency for  $10^{-2}$  M and  $10^{-3}$  M KI solutions at temperatures 0, 10 and 20 °C.

The evaluation done without curve fitting is generally regarded as less reliable as long as the determination of  $\varepsilon'_{LF}$  is uncertain. However, this method is simple and convenient in cases where reliable data are available.

Temperature (°C)	$\sigma$ (mS m <sup>-1</sup> )	$\tau_m \times 10^{-6}$ (s)	$\varepsilon'_{LF} / \varepsilon'_{\infty}$ $\times 10^4$	$D \times 10^{-9}$ (m <sup>2</sup> s <sup>-1</sup> )	$n \times 10^{24}$ (m <sup>-3</sup> )	$n\%$	$\mu \times 10^{-7}$ (m <sup>2</sup> V <sup>-1</sup> s <sup>-1</sup> )
20	1.3	4.154	1.291	1.36	1.52	127	5.42
10	1.1	6.097	1.152	1.16	1.42	118	4.44
0	0.8	7.387	1.101	1.05	1.12	93	4.38

Table 2. Calculated  $n$ , and  $\mu$  values for 10<sup>-3</sup> M KI, with parameters  $\sigma_{dc}$ ,  $\tau_2$  and  $\delta$  ( $=\varepsilon'_{LF}/\varepsilon'_{\infty}$ )

Temperature (°C)	$\sigma$ (mS m <sup>-1</sup> )	$\tau_m \times 10^{-7}$ (s)	$\varepsilon'_{LF} / \varepsilon'_{\infty}$ $\times 10^4$	$D \times 10^{-9}$ (m <sup>2</sup> s <sup>-1</sup> )	$n \times 10^{25}$ (m <sup>-3</sup> )	$n\%$	$\mu \times 10^{-8}$ (m <sup>2</sup> V <sup>-1</sup> s <sup>-1</sup> )
20	12	5.03	4.995	1.34	1.4	117	5.3
10	10	7.38	4.778	1.40	1.3	114	4.7
0	08	10.76	3.988	0.98	1.2	100	4.2

Table 3. Calculated values for 10<sup>-2</sup> M KI the values are shown in the order they were performed

## 4. Conclusions

Finally, it can be concluded that the mobile charge carrier density of electrolytes can be obtained from the expression  $\frac{\sigma k T \tau_m \delta^2}{e^2 d^2}$  and mobility can be obtained from  $\frac{e d^2}{k T \tau_m \delta^2}$ . It is applicable for aqueous electrolytes, ionic liquids and plasticized polymer electrolyte containing ionic liquids. Use of curve fitting is a reliable and convenient method for the proper estimation of the parameters. However the mobility and density of mobile ions can be calculated even without using curve fitting.

## Appendix 1

At frequencies close to the maximum in  $\tan \phi$  both the  $Z''$  and  $\varepsilon''$  values are close to minimum and the electric displacement remains constant. Furthermore, the conductivity is in its  $dc$  limit and effects of ionic and dipole polarizations are negligible since they take place at lower frequencies.

$\tau_m$  is the relaxation time corresponding to the frequency where  $\tan \phi$  shows a maximum. According to equation (23) the dielectric loss tangent is given by;

$$\tan(\phi) = \frac{\varepsilon''}{\varepsilon'} = \frac{\omega \tau \delta^2}{1 + \delta + (\omega \tau \delta)^2} \approx \frac{\omega \tau \delta}{1 + \omega^2 \tau^2 \delta} \quad (40)$$

When  $\tan \phi$  is maximum

$$\frac{d}{d\omega} \tan(\phi) = 0 = \frac{\tau\delta((1 + \omega^2\tau^2\delta) - 2\omega^2\tau^3\delta^2)}{(1 + \omega^2\tau^2\delta)} \quad (41)$$

$$\text{thus } \omega_m^2\tau^2\delta = 1 \quad (42)$$

$$\text{Therefore } \tau_m = \tau\sqrt{\delta} = \tau_2 \quad (43)$$

$$\text{thus } \tan(\phi)_{Max} = \frac{\sqrt{\delta}}{2} \quad (44)$$

## 5. References

- [1] A. Radu, A.J. Meir, E. Bakker, *Anal. Chem.*, 74 (2004) 6402-6409.
- [2] S. Sodaye, G. Suresh, A.K. Pandey, A. Goswami, *J. Membrane Science*, 295 (2007) 108-113.
- [3] Y.M. Scindia, A.K. Pandey, A.V.R. Reddy, S.B. Manohar, *Anal. Chem.*, 74 (2004) 4204-4212.
- [4] F. M. Gray, *Solid Polymer electrolytes fundamentals and technological applications* Vol. (1991 )VCH Publishers, New York, 1-4.
- [5] A.K. Shukla, A.S. Arico, V. Antonucci, *Renewable and Sustainable Energy Reviews* 5 (2001) 137-155.
- [6] M. Jönsson, K. Welch, S. Hamp, M Stromme, *J. Phys. Chem. B*, 110 (2006) 10165 -10169.
- [7] M. Watanabe, S. Nagano, K. Sanui, and N. Ogata, *Solid State Ionics*, 911 (1988) 28.
- [8] M. Watanabe, S. Nagano, K. Sanui, and N. Ogata, *Solid State Ionics*, 338 (1986) 18-19.
- [9] K. Hayamizu, E. Akiba, T. Bando, Y. Aihara, *J. Chem. Phys.* (2002) 117-12, 5929-5939
- [10] R.C. Agrawal, R. Kumar. R. K. Gupta, *Materials Science and Engineering B* 57 (1998) 46-51.
- [11] R.J. Klein, S. Zhang, S. Dou, B. H. Jones, R. H. Colby, J. Runt, *J. Chemical Physics* 124, (2006) 144903-8.
- [12] Niklasson, G. A.; Jonsson, A. K.; Stromme, M. *Impedance Response of Electrochromic Materials and Devices*. In *Impedance Spectroscopy*, 2nd ed.; Barsoukov, Y., Macdonald, J. R., Eds.; Wiley: New York, 2005 (302-326).
- [13] H.J Schütt, *Solid State Ionics*, 505 (1994) 70-71.
- [14] R. Coelho, *Physics of Dielectrics*, Elsevier Scientific Publishing Company, New York 1979 pp 97-102.
- [15] H.J. Schütt and E. Gerdes, *Journal of Non-Crystalline Solids*, 144 (1992) 1-13.
- [16] H.J. Schütt and E. Gerdes, *Journal of Non-Crystalline Solids*, 144 (1992) 14-20.
- [17] S. Bhattacharja, S. W. Smoot, D. H. Whitmore, *Solid State Ionics*, 18-19, (1986) 306-314.
- [18] P.G. Bruce, C. A. Vincent, *Faraday Discuss. Chem. Soc.*, 88, (1989) 43-54.
- [19] K.S. Cole, R.H. Cole, *J. Chem. Phys.* 9 (1941) 341-51.
- [20] T. M. W. J. Bandara, P. Ekanayake, M. A. K. L. Dissanayake, I. Albinsson, B.-E. Mellander, *J. Solid State Electrochem.* DOI 10.1007/s10008-009-0951-x

## **Part 3**

### **Nanomaterials**





# Aggregates in Ionic Liquids and Applications Thereof

J. D. Marty and N. Lauth de Viguerie  
*University of Toulouse*  
*France*

## 1. Introduction

Due to the increasing consciousness of environmental problems, chemical processes were developed with their environmental burden in mind. This results in the past decade, to the definition of Green chemistry encouraging the design of products and processes that reduce or eliminate the use and generation of hazardous substances. Moreover regulation (EC) No 1907/2006 of the European Parliament and of the Council of 18 December 2006 concerning the Registration, Evaluation, Authorisation and Restriction of Chemicals (REACH), gives greater responsibility to industry to manage the risks from chemicals and to provide safety information on the substances. REACH Regulation also calls for the progressive substitution of the most dangerous chemicals when suitable alternatives have been identified. Hence, from both societal and legislative point of views, there is a great need to find viable replacements for volatile organic compounds (VOC) used in usual chemical process. Of special interest is the case of solvents. They are used in most areas including synthetic chemistry, analytical chemistry, pharmaceutical production and processing, product purification, extraction and separation technologies, and also in the modification of materials. Due to the hazards of many conventional solvents (e.g. toxicity and flammability), knowledge of alternative, greener solvents is compulsory. The most useful alternatives to traditional solvents are supercritical CO<sub>2</sub> (where the gas is compressed until it is nearly as dense as a liquid), ionic liquids and water.

Room temperature ionic liquids (RTILs) are of special interest with unique applications as tunable and environmentally benign solvents with negligible vapor pressures, high chemical and thermal stability, high fire resistance and wide liquid temperature range and electrochemical windows. Moreover, owing to their molecular structure associating a cation and an anion, their physicochemical properties can be easily modulated by changing one of the ions. Hence, ionic liquids are now widely used in organic synthesis and chemical separations due to their high solvation ability and their tunable nature. (Dupont et al., 2002; Ranke et al., 2007) Lastly, corresponding to structured polar medium, RTILs can be also exploited to investigate molecular aggregation. Some authors have described in the past few years the ability of ILs to form various aggregates such as micelles, (Patrascu et al., 2006; Gayet et al., 2010b) vesicles, (Kimizuka and Nakashima, 2001; Nakashima and Kimizuka, 2002; Hao et al., 2005; Gayet et al., 2010a) non aqueous microemulsions (Gao et al., 2004; Eastoe et al., 2005; Gayet et al., 2009) or lyotropic phases (Evans et al., 1983; Wang et al., 2004; Araos and Warr, 2005). This gives access to new applications in green chemistry and

opens new research directions towards micellar catalysis in IL media, solvation enhancement for apolar entities, biocatalysis, nanomaterials synthesis, etc. (Hao and Zemb, 2007; Greaves and Drummond, 2008) The organized phases in ionic liquids make it possible to consider a new control of the reactivity including the properties of ILs and of organized media. Thus, the replacement of water by ILs for which the physicochemical structure and properties can be customised, should make it possible to widen the choice of the reactions considerably. Here we will describe some examples of each class of materials and will try to compare the results obtained to those given in water or structured solvents.

## 2. Methodology.

In this section, the main physical-chemistry methods involved in the characterization of aggregates in ILs were described.

### 2.1 Materials

Alkyl poly-(oxyethyleneglycol) ethers (purity  $\geq 98\%$ ), 1,2-dipalmitoyl-*sn*-glycero-3-phosphocholine (DPPC) and anhydrous toluene were purchased from Sigma-Aldrich and were used as received. Triton® X-100 (TX-100) from Sigma-Aldrich was dried at  $60^\circ\text{C}$  under vacuum for 3 hours and filtered under nitrogen through PTFE ( $0.45\ \mu\text{m}$ ) prior to use. Ionic liquids, 1-butyl-3-methylimidazolium tetrafluoroborate ( $\text{bmimBF}_4$ ), 1-butyl-3-methylimidazolium hexafluorophosphate ( $\text{bmimPF}_6$ ), 1-butyl-3-methylimidazolium bis(trifluoromethylsulfonyl)imide ( $\text{BmimNTf}_2$ ), 1-ethyl-3-methylimidazolium bis(trifluoromethylsulfonyl)imide ( $\text{emimNTf}_2$ ) were purchased from Solvionic ([www.solvionic.com](http://www.solvionic.com); purity  $\geq 98\%$ ) and were dried under low pressure around  $70^\circ\text{C}$  before use. N-benzylpyridinium bis(trifluoromethylsulfonyl)imide ( $\text{bnPyNTf}_2$ ) was synthesized as previously described (Patrascu et al., 2004).

### 2.2 Micelles in ILs

The viscosity of the ionic liquids was measured with an AR 1000 rheometer (from TA) equipped with a temperature controller and a cone/plate geometry (diameter =  $40\ \text{mm}$ , angle =  $2^\circ$ ). Zero-shear viscosities were extrapolated from the steady state shear viscosities curves obtained at  $25^\circ\text{C}$ . Surface tension experiments were performed using the pending-drop technique (KRÜSS instrument, model DSA10-Mk2). The  $\text{C}_{n\text{E}_{\text{m}}}/\text{bmimX}$  solutions were prepared by dissolving a precise weight of surfactant [using a Sartorius microbalance Genius model ( $\pm 0.05\ \text{mg}$ )] in a defined volume of ionic liquid [measured by a Finnpiptette PDP from Labsystem ( $\pm 0.1\ \mu\text{l}$ ) and a Repeater Plus Pipette, model 4980 from Eppendorf ( $\pm 2\ \mu\text{l}$ )]. The solutions were stirred and held at  $60^\circ\text{C}$  for 2 h and then cooled to  $25^\circ\text{C}$  before use.

Light scattering measurements of micelles were performed on a homemade instrument based on a  $647.1\ \text{nm}$  ionized krypton laser source (Innova 90 model from Coherent, vertically polarized beam), focalized on the sample by a lens corrected for spherical aberrations (focal length  $100\ \text{mm}$ ). A EMI 9863 photomultiplier with a  $200\ \mu\text{m}$  slit detector mounted on a BI200-SM goniometric arm from Brookhaven Instruments was used as detector. The amplified signal was treated by a BI9 K digital correlator from Brookhaven Instruments. The samples were filtered ( $0.45\ \mu\text{m}$  hydrophobic Teflon filters for the  $\text{BmimPF}_6$  solutions and on  $0.45\ \mu\text{m}$  hydrophilic cellulose acetate Sartorius filters for the  $\text{BmimBF}_4$  solutions). The scattering cells were previously rinsed with filtered ionic liquids. The following viscosity values were used:  $78\ \text{cP}$  for  $\text{bmimBF}_4$  and  $250\ \text{cP}$  for  $\text{bmimPF}_6$ .

### 2.3 Vesicles in ILs

*Preparation of lipid vesicles.* A stock solution of DPPC ( $2.10^{-2}$  mol.L $^{-1}$ ) in chloroform/methanol (9:1, v/v) was prepared and stored at 4°C. 400  $\mu$ L of these lipid solutions were placed in a vial and solvent were evaporated under a nitrogen stream. Residues were desiccated under vacuum for 2 h (1 Torr). The dried lipid samples were hydrated in 200  $\mu$ L of pure IL or IL/water mixtures and heated to 80°C for 20 min (this temperature is higher than the gel-to-liquid transition temperature ( $T_m$ )). The sample was immediately vortexed for 4 min. The vesicle solutions ([DPPC] =  $4.10^{-2}$  mol.L $^{-1}$  i.e. 2.93% w/v) so prepared were then stored at 4°C overnight.

*Differential Scanning Calorimetry (DSC).* Thermal transitions in vesicles were measured on a Perkin-Elmer PYRIS1 calorimeter, using heating and cooling rates from 2 to 20°C/min. A 25  $\mu$ L quantity of each vesicular solution was loaded in pans and allowed to equilibrate at initial temperature for 20 minutes. Data were collected at different rates from 1 to 20°C between 0 and 120°C. Main transition temperature was determined as the peak maximum of an endothermic transition extrapolated to 0°C/min. Lipid concentration in ionic liquids was fixed at  $4.2.10^{-2}$  mol.L $^{-1}$ .

*Transmission electronic microscopy (TEM).* TEM measurements were made on a Jeol JEM - 2100 Transmission Electron Microscope operated at an accelerating voltage of 100 kV in the Institut Fédératif d'Exploration Fonctionnelle des Génomes (Toulouse, France). Samples were negatively stained by a solution of sodium phosphotungstate.

*Small Angle Neutron Scattering (SANS).* SANS experiments were performed with the PACE spectrometer at the Orphée reactor (LLB, Saclay). DPPC-IL and DPPC-IL-water mixture were put inside quartz cells of 1 or 2 mm gap and measured at 20° ([DPPC] = 1 %w/v). Three spectrometer configurations were used: a neutron wavelength ( $\lambda$ ) of 7 Å with a sample to detector distance of 3 m, then another distance of 1 m and a wavelength of 17 Å with a distance of 4.8 m. The scattering vector range thus reached was  $0.0025 < q \text{ (Å}^{-1}\text{)} < 0.35$ . Scattering intensities have also been normalized by the incoherent signal delivered by a 1 mm gap water sample in order to account for efficiency of detector cells. Absolute values of the scattering intensity,  $I(q)$  in cm $^{-1}$ , were obtained from the direct determination of the number of neutrons in the incident beam and the detector cell solid angle. No background has been subtracted to the copolymer sample scattering, thus a flat incoherent signal has been observed at high  $q$  values.

### 2.4 Non-aqueous microemulsions

*Phase diagram determination.* Each component (anhydrous toluene, Triton® X-100 and bnPyrNTf $_2$ ) was added by weight under inert atmosphere on a Sartorius balance with a precision of  $\pm 0.01$  mg. The mixtures were stirred until clear and homogeneous at 27°C. The phase diagram was built by titration with TX-100 as follows: required weight of toluene and bnPyrNTf $_2$  were initially mixed, then TX-100 was added until transition from turbidity to transparency.

*Electrical conductivity experiments.* Conductivity measurements were performed on a Mettler Toledo SevenMulti conductimeter using an InLab730 probe with a platinum electrode of cell constant of 0.563 cm $^{-1}$ . In the experiments, the sample and the electrode were sealed in a glass cell, which was placed in a water bath at  $27.0 \pm 0.1^\circ\text{C}$ . Fractionated volumes of toluene (100  $\mu$ L) were successively added to the microemulsion using a Hamilton syringe.

*Dynamic Light Scattering measurements (DLS).* DLS Measurements were carried out at  $27.0^\circ\text{C} \pm 0.1^\circ\text{C}$  with a Malvern Instrument Nano-ZS equipped with a He-Ne laser ( $\lambda = 633$  nm). Samples were introduced into Helma cells (111-OS 10 mm) through 0.45  $\mu$ m PTFE micro-

filters prior to measurements. The correlation function was analyzed via the general purpose method to obtain the distribution of diffusion coefficients ( $D$ ) of the solutes, and then the apparent equivalent hydrodynamic radius ( $R_h$ ) was determined using the Stokes-Einstein equation.

**Small Angle Neutron Scattering.** SANS experiments were performed with the PAXY spectrometer at the Orphée reactor (Laboratoire Léon Brillouin, Saclay). Microemulsion solutions were put inside Hellma quartz cells of 1 or 2 mm gap. Temperature was maintained constant at  $27 \pm 0.2^\circ\text{C}$ . Two spectrometer configurations were used: a neutron wavelength ( $\lambda$ ) of 4 Å with a sample to detector distance of 1.435 m and a wavelength of 10 Å with a distance of 2.035 m. The neutron wavelength distribution  $\Delta\lambda/\lambda$  is 0.11 (FWHM). The incident collimation was obtained from two circular holes 2.5 m apart, one with a diameter of 22 mm and the second, close to the sample, with a diameter of 7.6 mm. The scattering vector range thus reached was  $0.01 < q \text{ (Å}^{-1}\text{)} < 0.4$ . The efficiency of the detector cells was normalized by the incoherent signal delivered by 1 mm gap water cell. Absolute values of the scattering intensity,  $I(q)$  in  $\text{cm}^{-1}$ , were obtained from the direct determination of the number of neutrons in the incident beam and the detector cell solid angle. Several series of blank samples (mixtures of H and D toluene) were also measured to plot precise calibration curves to subtract from each IL solution.

### 3. Micelles in room temperature ionic liquids

The micellar aggregation behavior of surfactants in ILs has been investigated in recent years. Evans and co-workers first reported the aggregation behavior of alkyltrimethylammonium bromides, alkylpyridiniums bromides and Triton X-100 in ethyl ammonium nitrate (Evans et al., 1982; Evans et al., 1983). More recently, premicellar aggregation in 1-butyl-3-methylimidazolium chloride and hexafluorophosphate was detected using inverse gas chromatography (Anderson et al., 2003). Merrigan et al. have demonstrated that imidazolium cations with long fluorinated tails act as surfactants and appear to self-aggregate within imidazolium-based ILs (Merrigan et al., 2000). The possible aggregate formation by nonionic surfactants Brij-35, Brij-700, Tween-20, and Triton X-100 in emimNTf<sub>2</sub> was observed on the basis of the response of solvatochromic probes (Fletcher and Pandey, 2004). Tran and Yu have reported that nonionic surfactants N-dodecylsultaine and caprylyl sulfobetaine formed micelles in bmimPF<sub>6</sub> and emimNTf<sub>2</sub> (Tran and Yu, 2005). Moreover, nonionic surfactant self-assembly into micelles in ethylammonium nitrate was examined (Araos and Warr, 2008).

The ability of a series of pure alkyl poly-(oxyethyleneglycol) ethers in 1-butyl-3-methylimidazolium (bmim) ILs with various counter ions [BF<sub>4</sub><sup>-</sup>, PF<sub>6</sub><sup>-</sup> and Tf<sub>2</sub>N<sup>-</sup>, that is, bis(trifluoromethylsulfonyl)amide; Figure 1] to form micellar systems was investigated.

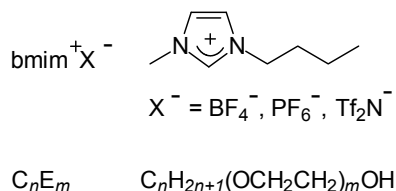


Fig. 1. Molecular structures of the ILs and surfactants used herein ( $n=12-16$ ;  $m=4-8$ ).

Nonionic surfactants, denoted  $C_nE_m$  ( $n=12-16$ ;  $m=4-8$ ), were chosen to avoid the exchange of counter ions with the solvent. The formation of micelles was clearly evidenced using surface tension, multi-angle dynamic light scattering (DLS) and small-angle neutron scattering (SANS) measurements (Patrascu et al., 2006).

### 3.1 Surface tension measurements.

Surface tension measurements were performed to probe the aggregation behavior of the surfactants in  $\text{bmimBF}_4$ . For all the selected surfactants, the surface tension of the  $C_nE_m/\text{bmimBF}_4$  solutions decreased when the surfactant concentration increased (Figure 2a and 2b). This indicated their adsorption at the air/solution interface. The Szyszkowski-Langmuir adsorption equation (Fainerman et al., 1998) fitted well this decrease, leading to an estimation of the area per surfactant molecule at the air/ $\text{bmimBF}_4$  interface, comparable or lower than the one found at the air/water interface (Table 1). The differences between  $\text{bmimBF}_4$  and water may be related to a change in the organization and/or solvation state of the adsorbed surfactants. In  $\text{bmimBF}_4$ , like in water, the molecular area of the surfactant decreased with increasing alkyl chain length or decreasing number of oxyethylene groups. This reflects the equilibrium conditions of the self-assembly process.

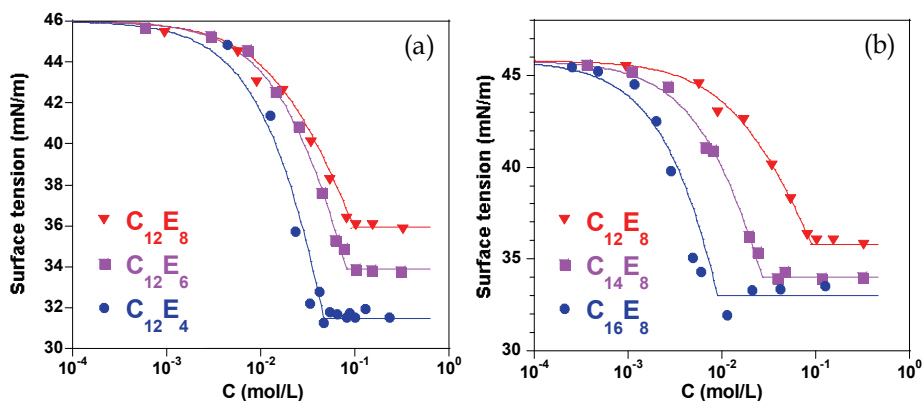


Fig. 2. Surface tension of solutions of  $C_nE_m$  ( $n=12-16$ ;  $m=4-8$ ) in  $\text{bmimBF}_4$ . a) Effect of hydrophilic ethyleneoxide part ; b) Effect of hydrophobic alkyl chain length

This initial decrease of the surface tension is followed by an abrupt change in the slope of the surface tension versus  $C$  (Figures 2a and 2b). After this breaking point, the surface tension of the solutions remains more or less constant. Such behavior suggested the formation of micelles within the ILs, where the break point corresponds to a critical micelle concentration (cmc). The cmc values in ILs were two to four orders of magnitude higher than those in aqueous systems but are equivalent to or slightly higher than those in formamide (Table 1).

The influence of the hydrophilic and hydrophobic moieties on the cmc in each solvent (water, formamide and  $\text{bmimBF}_4$ ) was shown in Figures 3a and 3b respectively. The values of the slope are related to the contribution of hydrophilic and hydrophobic groups on the cmc. In formamide, these contributions are significantly lower than in water and IL.

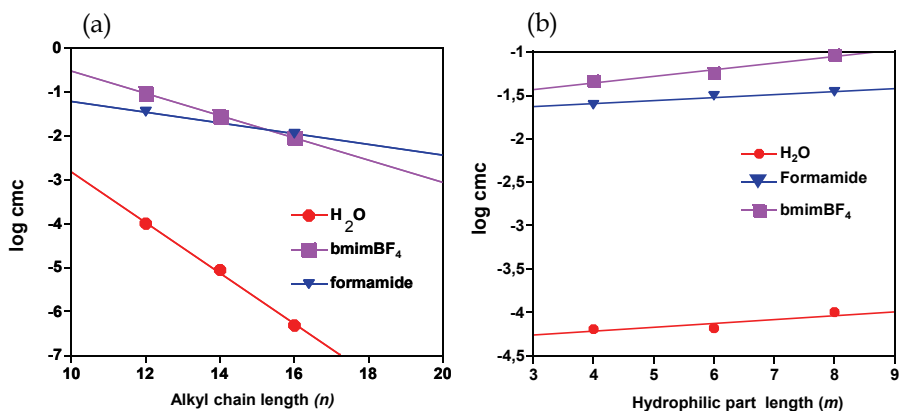


Fig. 3. log cmc versus a) hydrophobic alkyl chain length ( $n=12, 14, 16$ ) ; b) number of ethyleneoxide groups ( $m=4, 6, 8$ ).

$C_nE_m$	$S [\text{\AA}^2]^{[a]}$	bmimBF <sub>4</sub> cmc [mmol L <sup>-1</sup> ] <sup>[b]</sup>	$S [\text{\AA}^2]^{[c]}$	H <sub>2</sub> O cmc [mmol L <sup>-1</sup> ] <sup>[d]</sup>	$S [\text{\AA}^2]^{[e]}$	Formamide cmc [mmol L <sup>-1</sup> ] <sup>[f]</sup>
C <sub>16</sub> E <sub>8</sub>	22±2	9±1		0.0005		11
C <sub>14</sub> E <sub>8</sub>	38±3	27±1	49	0.009		
C <sub>12</sub> E <sub>8</sub>	65±2	93±2	66	0.1		35
C <sub>12</sub> E <sub>6</sub>	30±2	57±2	61	0.067	63	31
C <sub>12</sub> E <sub>4</sub>	26±2	46±1	46	0.065		25

Table 1. Cmc and molecular area ( $S$ ) of  $C_nE_m$  in bmimBF<sub>4</sub>, water and formamide at 25 °C. [a] Estimated through a fit to the Szyszkowski-Langmuir adsorption equation. [b] Deduced from surface tension measurements. [c] From (Rosen et al., 1982; van Os et al., 1993). [d] From (Berthod et al., 2001). [e] From (Couper et al., 1975). [f] From (McDonald, 1967; Jonstrome et al., 1990), some cmc measurements were performed at 21 °C.

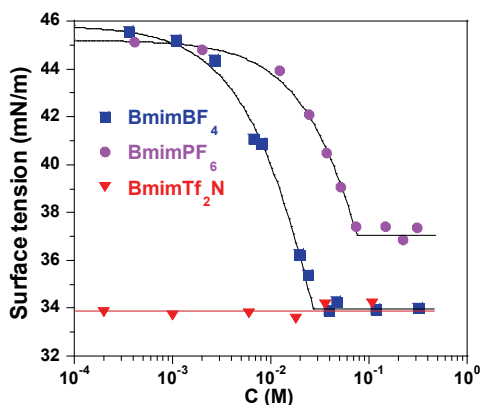


Fig. 4. Surface tension of C<sub>14</sub>E<sub>8</sub> in bmimBF<sub>4</sub> (■), bmimPF<sub>6</sub> (●) and bmimNTf<sub>2</sub> (▲) at 25 °C.

### 3.2 Multi-angle dynamic light scattering and small-angle neutron scattering experiments.

To verify the shape and size of aggregates in ILs, multi-angle DLS and SANS measurements were performed and results were summarized in Table 2.

$C_nE_m$	bmimBF <sub>4</sub>		bmimPF <sub>6</sub>		H <sub>2</sub> O		formamide	
	$r_H$ [nm] [a]	$N_{agg}$ [b]	$r_H$ [nm] [a]	$N_{agg}$ [b]	$r_H$ [nm] [d]	$N_{agg}$ [e]	$r_H$ [nm] [f]	$N_{agg}$ [g]
C <sub>16</sub> E <sub>8</sub>	3.2±0.4	≈145	1.4±0.1	≈15	≈3.7	10±15	≈4	
C <sub>14</sub> E <sub>8</sub>	2.5±0.3	≈75						
C <sub>12</sub> E <sub>8</sub>	1.6±0.1	≈20			≈3.1	95±5		
C <sub>12</sub> E <sub>6</sub>	2.3±0.1	≈75			≈3.2	140±15	≈2	≈30
C <sub>12</sub> E <sub>4</sub>	- [c]	- [c]				165±62	≈2	

Table 2. Hydrodynamic radius ( $r_H$ ) and aggregation number ( $N_{agg}$ ) of  $C_nE_m$  micelles in bmimBF<sub>4</sub>, water and formamide at 25 °C. [a] Deduced from DLS measurements at 4 cmc and 8 cmc concentrations. [b] See text. [c] At 25 °C and 4 cmc concentration cloud point is already reached. [d] From (Zulauf et al., 1985) [e] From (Herrington and Sahi, 1988); (Zulauf et al., 1985), the data corresponding to the C<sub>12</sub>E<sub>4</sub> surfactant was obtained near 0 °C. [f] From (Couper et al., 1975; Jonstromer et al., 1990), the data corresponding to the C<sub>16</sub>E<sub>8</sub> surfactant was obtained at 40 °C. [g] From (Couper et al., 1975).

DLS experiments realized on the  $C_nE_m$ /bmimBF<sub>4</sub> solutions showed the presence of spherical objects with sizes between 1.6 and 3.2 nm (Table 2). The hydrodynamic radii in ILs were smaller than those in water and close to those found in formamide. The use of bmimBF<sub>4</sub> did not allow us to achieve SANS due to the neutron absorption by boron atoms. Thus, SANS experiments were performed on bmimBF<sub>6</sub> solutions. For concentrations higher than the cmc, the scattered neutron intensity versus the scattering vector was well-fitted by a general Guinier model. The presence of globular aggregates with a radius of approximately 1.3±0.2 nm was identified for C<sub>14</sub>E<sub>8</sub>/bmimBF<sub>6</sub> system. This value was comparable with the one obtained from DLS measurements.

Using an approximation of the surfactant volumes occupied in the micelle (Zulauf et al., 1985; van Os et al., 1993), we estimated the aggregation number in the micelles. Either increasing the alkyl chain length or decreasing the poly(oxyene) chain length contributes to both an enhanced hydrophobicity and an increase in aggregation number. Aggregation numbers in RTILs are smaller than those in water. As in water (Herrington and Sahi, 1988; van Os et al., 1993) micelle size and aggregation number increased with the alkyl chain length or the number of oxyethylene groups.

All these results proved that surfactant aggregation can occur in ILs and that the formed aggregates were micelle-like. The size and aggregation number of the micelles can be tuned by changing the exact nature of the IL.

## 4. Vesicles

Only few examples of vesicles have been observed in pure ILs. Their formation was first evidenced with a glycolipid L-glutamate derivative in two ether-containing ILs (N,N'-dialkylimidazolium bromides Me-Im-C<sub>2</sub>OC<sub>1</sub> and Me-Im-C<sub>1</sub>OC<sub>1</sub>) by means of differential scanning calorimetry (DSC) and dark-field optical microscopy (Kimizuka and Nakashima,

2001). DSC measurements showed an endothermic peak ( $T_c$ ) at 40°C and at 51°C in Me-Im- $C_2OC_1$  and in Me-Im- $C_4OC_1$  respectively. This indicates that the phase transition characteristics of the glycolayers are affected by the chemical structure of the IL. In addition, a similar behavior was observed for dialkyldimethylammonium bromides in the same ILs (Nakashima and Kimizuka, 2002). In both studies, bilayer vesicles were observed by dark-field optical micrographs only above the transition temperature. Moreover, no aggregate was formed with these surfactants in a conventional IL BmimPF<sub>6</sub>.

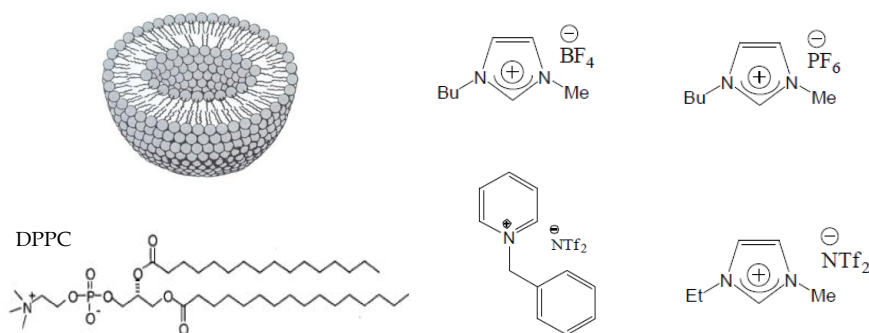


Fig. 5. Chemical structures of ILs and DPPC used to study the formation of vesicles in ILs.

In a more recent study, vesicle structures were obtained with a  $Zn^{2+}$ -fluorous surfactant ( $[Zn(OOC-CH_2C_6F_{13})_2]$ ) and a  $Zn^{2+}$ -fluorous surfactant/zwitterionic surfactant mixture ( $[Zn(OOC-CH_2C_6F_{13})_2]/C_{14}DMAO$ ) in bmimBF<sub>4</sub> and bmimPF<sub>6</sub> (Hao et al., 2005). The authors determined the size and interlamellar spacing between the bilayers in the vesicles through FF-TEM and SAXS observations. Diameters were about 30 to 90 nm and about 20 to 150 nm in bmimPF<sub>6</sub> for  $[Zn(OOC-CH_2C_6F_{13})_2]$  and  $[Zn(OOC-CH_2C_6F_{13})_2]/C_{14}DMAO$  respectively. The membrane thickness was about 51.9 Å.

The formation of vesicles from glycerophospholipids (DPPC) was investigated in bmimBF<sub>4</sub>, bmimPF<sub>6</sub>, emimNTf<sub>2</sub> and bnPyNTf<sub>2</sub> (Figure 5) (Gayet et al., 2010a). Multilamellar vesicles (MLV) were formed using the method of dehydration-rehydration usually employed in water (see section 2.2) (Lasic, 1988). Aggregates formed from DPPC in ILs are first visualized by negative-staining transmission electronic microscopy. As shown in Figure 6a, they are distinctly spherical with diameters of about 200 nm to 1000 nm.

In order to assess vesicle formation, the morphological characteristics of those aggregates in ILs in particular membrane thickness was further investigated by SANS (Figure 6b). Better results were obtained with hydrogenated DPPC in a deuterated IL (bnPyNTf<sub>2</sub>D). At low  $q$ , the curve is flattening as expected for the typical  $q^{-2}$  dependence characteristic of the flat membrane of large vesicles (Chen et al., 1980). Whereas a Bragg peak at  $q \sim 0.098 \text{ \AA}^{-1}$  ( $d \sim 64 \text{ \AA}$ ) was observed with water, only a small bump is observed at large  $q$  in the case of bnPyNTf<sub>2</sub>D. From the latter, we deduced a mean bilayer thickness of  $d \sim 63 \pm 1 \text{ \AA}$ . Moreover self-assembly of the solutions of DPPC in bnPyNTf<sub>2</sub>D could be a mixture of vesicles and small amount of lamellar phase.

The phase physical properties of MLV were further investigated by DSC. As in water, an endothermic pre-transition that corresponds to the transition from the lamellar gel phase ( $L_{\beta'}$ ) to the ripple-gel phase ( $P_{\beta'}$ ), followed by the main transition that corresponds to the



transition to a liquid crystalline phase ( $L_\alpha$ ) were detected in ILs. As shown in Table 3, the values were slightly higher in ILs.

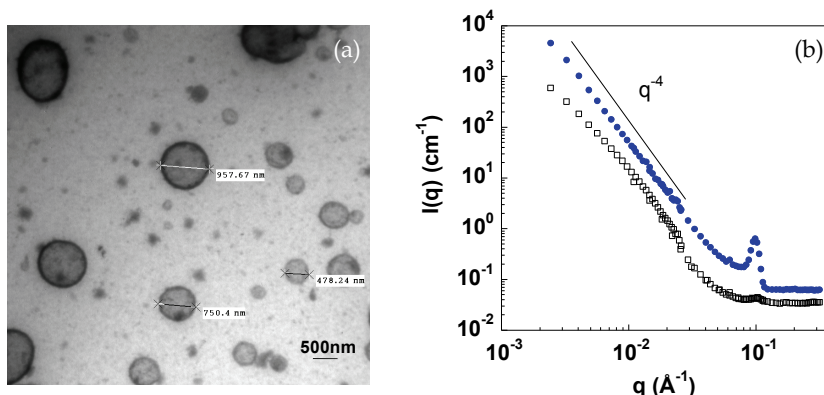


Fig. 6. (a) Negative staining-TEM of vesicles of DPPC in  $\text{bmimBF}_4$ . Sodium phosphotungstate was used as the negatively charged dye. (The smallest spots correspond to the IL) ; (b) SANS curves of DPPC solutions in  $\text{D}_2\text{O}$  (●) and in  $\text{bnPyNTf}_2$  (□) ;  $[\text{DPPC}] = 1 \text{ \% w/v}$  (Gayet et al, 2010).

Solvent	$L_{\beta'} \rightarrow P_{\beta'}$		$P_{\beta'} \rightarrow L_\alpha$	
	T (°C)	$\Delta H$ (kJ/mol)	T (°C)	$\Delta H$ (kJ/mol)
$\text{bmimBF}_4$	55.9	$0.5 \pm 0.1$	61.7	$85 \pm 2$
$\text{bmimPF}_6$	48.5	$0.4 \pm 0.1$	57.5	$85 \pm 2$
$\text{emimNTf}_2$	50.5	$7.1 \pm 1.8$	56.5	$92 \pm 6$
$\text{bnPyNTf}_2$	52.0	$0.3 \pm 0.2$	56.3	$89 \pm 2$
$\text{H}_2\text{O}$	36.9	$1.6 \pm 0.7$	44.4	$42 \pm 2$

Table 3. Thermodynamic parameters of the phase transitions of DPPC MLV in  $\text{bmimBF}_4$ ,  $\text{bmimPF}_6$ ,  $\text{bmimNTf}_2$ ,  $\text{bnPyNTf}_2$  and in water determined by DSC measurements.

## 5. Microemulsions

Microemulsions are thermodynamically stable, isotropic and optically transparent dispersions of two immiscible liquids stabilized by a surfactant or by a surfactant/co-surfactant mixture (Zana, 1995). Water-containing microemulsions have been extensively used in separation, drug delivery, nanomaterial synthesis and biocatalysis (Engberts et al., 2006; Holmberg, 2007). As water-in-oil or oil-in-water microemulsions are good solvents for both polar and non-polar substrates, they are also useful for carrying out chemical reactions and usually enhance reactivity and regio/stereoselectivity (Holmberg, 2007).

In the past decade, non aqueous microemulsions, in which water is replaced by polar solvents such as formamide, glycerol, glycol or dimethylformamide, have attracted great interest from both theoretical and practical points of view (Ray and Moulik, 1994). Furthermore, it has been reported that these systems have a number of distinct advantages

over aqueous ones, especially when used as media for organic reactions which need to avoid contact with water (Das et al., 1987). Of special interest is the use in of ionic liquid (IL) microemulsions (Qiu and Texter, 2008). In recent years, ILs have been used as each of the three components required to formulate a microemulsion – the “water like” solvent, the hydrophobic solvent, and/or the surfactant. Recently great attention has been focused on non-aqueous ionic liquid/oil microemulsions. It has been shown that common ILs including 1-butyl-3-imidazolium tetrafluoroborate (bmimBF<sub>4</sub>) can be dispersed in certain non-polar organic solvents (cyclohexane, *p*-xylene, benzene and toluene) to form reverse IL-in-oil microemulsions stabilized by non-ionic surfactants. Electron microscopy, light scattering, and small-angle neutron scattering results have provided evidence for the existence of nanodomains of the type IL-in-oil in microemulsions (Gao et al., 2004; Eastoe et al., 2005). They have furthermore shown a regular increase in droplet volume with added IL (Eastoe et al., 2005). BmimPF<sub>6</sub> was also used as a polar solvent in non-aqueous microemulsions and were studied by small-angle X-ray scattering (Li et al., 2005). In spite of the broad spectrum of structural research undertaken in IL microemulsions, their effect on reactivity poses many intriguing questions, the answers to which could open the way to enhancing their potential applications. Reverse IL-in-oil microemulsions may have potential applications owing to the unique features of ILs and of microemulsions: they offer a wide choice of structures (e.g. cation/anion), such as chiral structures, and allow the use of a lower quantity of ionic liquid compared to bulk-phase IL reactions. Moreover these nanostructured surfactant assemblies provide hydrophobic or hydrophilic nanodomains, thereby expanding the potential uses of ILs in reactions. Lastly, changing the microemulsion size could allow one to tune the ratio of unbounded to bounded IL (due to interactions with the polar heads of the surfactants) and hence its solvation properties. This confinement can enable reactivity to be controlled. The formation of non-aqueous microemulsions from a ternary system composed of an ionic liquid (benzylpyridinium bis(trifluoromethanesulfonyl)imide), an nonionic surfactant (TX-100) and toluene was studied (Figure 7) (Gayet et al., 2008).

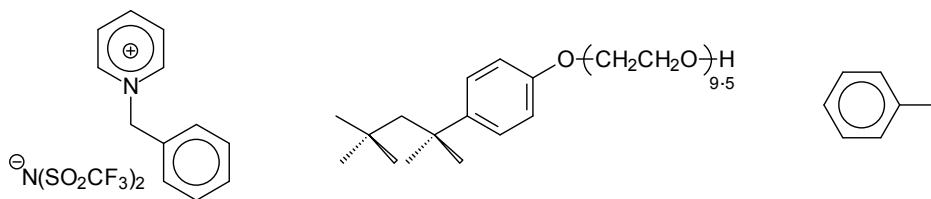


Fig. 7. Chemical structures of IL (benzylpyridinium bis(trifluoromethanesulfonyl) imide, bnPyrNTf<sub>2</sub>), surfactant (polyethylene glycol *p*-(1,1,3,3-tetramethylbutyl)-phenyl ether, TX-100) and oil (toluene) used to study the formation of microemulsions.

### 5.1 Ternary phase diagram

The phase diagram of this ternary system was built by direct observation of the phase behaviour and by conductrimetry at 27°C (Figure 8). Three micro-regions were identified by conductivity measurements according to the percolation theory (Clausse et al., 1981).

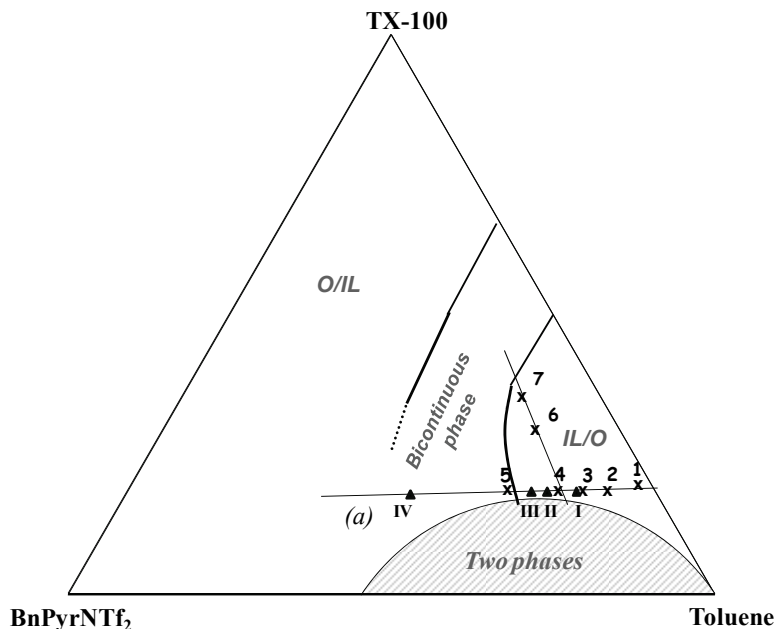


Fig. 8. Phase diagram of BnPyrNTf<sub>2</sub>/TX-100/toluene three-component system at 27°C. O/IL, bicontinuous and IL/O are toluene-in-bnPyrNTf<sub>2</sub>, bicontinuous phase and bnPyrNTf<sub>2</sub>-in-toluene regions respectively (Gayet et al, 2009).

## 5.2. Structural studies in the microemulsion IL/O region.

*PGSE NMR Self-Diffusion and DLS Measurements.* The sizes of IL-in-oil microemulsions with various IL fractions were then determined by pulse field gradient spin-echo NMR and by dynamic light scattering measurements. Translational displacements over macroscopic distances were monitored using molecular self-diffusion coefficients ( $D$ ). Its values are sensitive to friction, obstruction and solvation phenomena, but in particular to confinement in closed domains. They can therefore be used to obtain information on solution microstructure (Fedotov et al., 1996; Yaghmur et al., 2003). Figure 9 shows the values of self-diffusion of bnPyrNTf<sub>2</sub>, TX-100 and toluene as a function of the total volume fraction of TX-100 and IL along dilution line (a) for samples 2, 3 and 4 in Figure 8. The self-diffusion coefficients of TX-100 and IL are equal and are one order of magnitude less than that of toluene. As the three components have roughly the same size, this implies that the IL and surfactant diffuse together as one entity in toluene.

The hydrodynamic radius  $R_h$  of the IL micelles in this toluene phase rich region can be roughly estimated using the Stokes-Einstein equation:

$$R_h = k_B T / (6\pi\eta D) \text{ with } D = D_\infty(1 - k\Phi)$$

where  $D_\infty$  is the micelle diffusion coefficient at infinite dilution,  $k$  is a constant and  $\Phi$  is the volume fraction of both TX-100 and IL (Fedotov et al., 1996; Nyden, 2001).  $R_h$  values obtained are summarized in Table 4 for both PGSE NMR and DLS measurements. Average sizes thus obtained are compatible with a microemulsion structure.

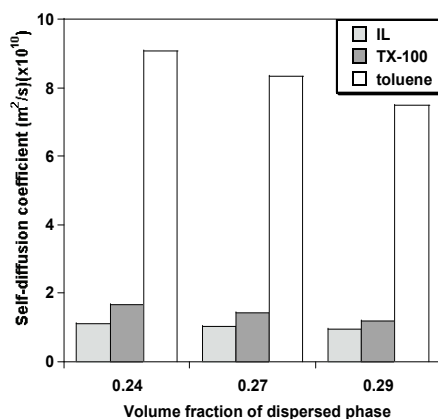


Fig. 9. Self Diffusion coefficients of TX-100, toluene and IL (bnPyrNTf<sub>2</sub>) obtained by PGSE NMR plotted as the volume fraction of the droplets i.e. volume fraction of TX-100+IL (standard deviation was below  $0.2 \cdot 10^{-10} \text{ m}^2 \cdot \text{s}^{-1}$ ).

*SANS measurements.* SANS measurements were employed to determine the structural features of microemulsions and the respective arrangement of IL and TX-100, by using three different contrasts. The first set of SANS data, named “full contrast”, was obtained with microemulsions in deuterated toluene and allowed the determination of the global form of objects. Data obtained with deuterated ionic liquid in hydrogenated toluene and Triton X100 show the objects formed by IL: it is “core contrast” since IL is assumed to be in the core of the micelles. Third, data obtained in toluene mixture, which matches the deuterated ionic liquid, give the scattering from the TX-100 object: it is named “shell contrast”.

Number μE	$\phi_{\text{IL}}$	$\phi_{\text{TX-100}}$	$R_g$ (nm)	$R_g$ (nm)	$R_g$ (nm)	$R_h$ (nm)	$R_h$ (nm)
			Full contrast (SANS)	Core contrast (SANS)	Shell contrast (SANS)	(PGSE NMR)	(DLS)
1	0.02	0.18	$2.00 \pm 0.05$	$2.08 \pm 0.05$	$2.00 \pm 0.05$	n.d.	n.d.
2	0.06	0.18	$2.9 \pm 0.1$	$3.3 \pm 0.1$	$3.1 \pm 0.1$	$1.8 \pm 0.2$	$3.4 \pm 0.8$
3	0.08	0.19	$2.9 \pm 0.1$	n.d.	$2.8 \pm 0.1$	$1.8 \pm 0.2$	$2.4 \pm 0.7$
4	0.1	0.19	$2.8 \pm 0.1$	$2.8 \pm 0.1$	$2.6 \pm 0.1$	$1.9 \pm 0.2$	$2.2 \pm 0.8$
5	0.15	0.19	$1.6 \pm 0.1$	$2.4 \pm 0.1$	$1.5 \pm 0.2$	n.d.	n.d.
6	0.1	0.27	$1.10 \pm 0.05$	$1.13 \pm 0.05$	$0.90 \pm 0.05$	n.d.	n.d.
7	0.1	0.36	$0.72 \pm 0.05$	$0.86 \pm 0.05$	$0.64 \pm 0.05$	n.d.	n.d.

Table 4. Apparent radii of gyration of bnPyrNTf<sub>2</sub>/TX-100/toluene microemulsions deduced from SANS in different contrast conditions<sup>a</sup>. <sup>a</sup>Hydrodynamic radii deduced from PGSE NMR and DLS measurements.  $\phi_{\text{IL}}$  and  $\phi_{\text{TX-100}}$  are the volume fractions of bnPyrNTf<sub>2</sub> (the IL) and TX-100 (the surfactant). In μE 1 to 5,  $\phi_{\text{TX-100}}$  was kept constant ( $\sim 0.18$ - $0.19$ ) and  $\phi_{\text{IL}}$  increased. In μE 6 and 7,  $\phi_{\text{IL}}$  was fixed at 0.1 and  $\phi_{\text{TX-100}}$  increased. n.d.: not determined

Typical curves for bnPyNTf<sub>2</sub>/TX-100/Toluene mixtures in the microemulsion IL/O region of the phase diagram are shown in Figure 10 for three different contrasts (full contrast, core contrast and shell contrast). Both intensities and shapes look similar: the scattering signals, which are not very strong, decrease with increasing  $q$ , while they level off at low  $q$  values. Such similar curves indicate that whole objects, the objects formed by IL and those formed by surfactant are not very different.

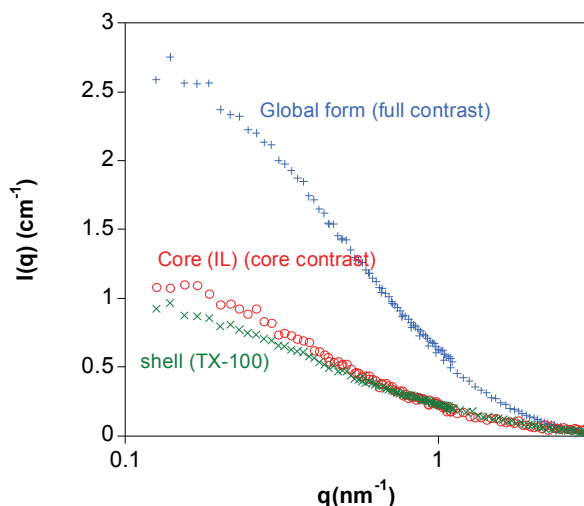


Fig. 10. SANS of bnPyNTf<sub>2</sub>/TX-100/Toluene  $\mu$ E 2 ( $\phi_{IL}=0.06$ ) measured at 27°C in three contrast conditions (+ full contrast, o core contrast, x shell contrast).

These observations were confirmed by the values of the radius of gyration determined from the Guinier plot (around 3 nm, see Table 4). SANS experiments on IL/oil microemulsions clearly demonstrate the formation of surfactant-stabilized dispersed nanodroplets with IL cores.

### 5.3 Reverse microemulsions as nanoreactors for the Matsuda-Heck reaction

The reverse IL-in-oil microemulsions were used as nanoreactors to perform a Matsuda-Heck reaction between two reactants of opposite polarity, *p*-methoxyphenyl diazonium salt and 2,3-dihydrofuran, in the presence of a palladium catalyst (Figure 11). Two palladium catalysts were used Pd<sub>2</sub>(dba)<sub>3</sub>·CHCl<sub>3</sub> and a chiral compound bis [(*R*)-1-phenylethylpyridinium)] tetrachloropalladate (noted [Pyr]<sub>2</sub>[PdCl<sub>4</sub>]). This reaction occurred at room temperature and allowed the formation of two regioisomers A and B.

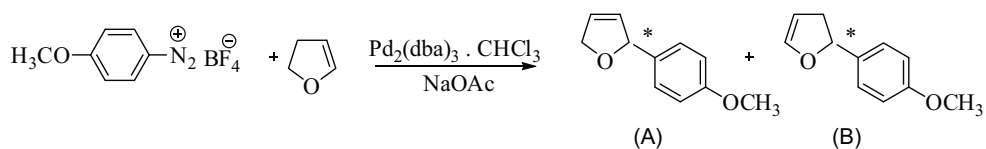


Fig. 11. Matsuda Heck reaction between *p*-methoxyphenyl diazonium salt and 2,3-dihydrofuran using a palladium catalyst.

This reaction was performed at 27°C in pure IL (bnPyrNTf<sub>2</sub>), in three IL/O microemulsions (points I, II, and III on line (a) in Figure 8) and in one bicontinuous phase (point IV on line (a) in Figure 8). Only regioisomer A was formed. Yields calculated from GC analysis were up to twice as high in microemulsions (33 to 56%) as those obtained in bulk phase (around 30%) as reported in Table 5. Geometrical constraints and reactant partitioning between the different phases in microemulsions could result in specific orientation of the reactants and catalyst, which have been shown to strongly influence the yield of reaction (Pasc-Banu et al., 2004). Moreover yields became higher on increasing the amount of IL (bicontinuous phase). The use of microemulsions as media for organic reactions suffers from one inherent drawback: the need of large amounts of surfactant to form microemulsions which then have to be separated from the products. However, it is possible, by using a non-ionic surfactant such as here TX-100 to break the single-phase ternary oil-IL-surfactant systems used as reaction media into a 2-phase system by increasing the temperature (called Winsor systems). In the system studied here, an increase in temperature of 27°C to 36°C reversibly changed a Winsor I system (reaction media) into a Winsor II system involving separation of the IL phase and the toluene phase. The products were extracted from the organic phase and the IL phase containing NPs of Pd was successfully reused for another run.

Yields (%) in bnPyrNTf <sub>2</sub>	Yields (%) in microemulsions	
28 <sup>i</sup> (33) <sup>ii</sup>	<b>I</b>	33 <sup>i</sup> (37) <sup>ii</sup>
	<b>II</b>	35 (45)
	<b>III</b>	47 (54)
	<b>IV</b>	51 (56)

Table 5. Yields obtained for Matsuda Heck coupling between the *p*-methoxyphenyl diazonium salt and 2, 3-dihydrofuran using Pd<sub>2</sub>(dba)<sub>3</sub>.CHCl<sub>3</sub><sup>i</sup> or [Pyr]<sub>2</sub>[PdCl<sub>4</sub>]<sup>ii</sup> as catalyst (1% mol) in microemulsions I, II, III and IV formed with bnPyrNTf<sub>2</sub> (on line (a) of Figure 8) at 27°C. Standard deviation on yields was around 2%.

The reaction yields obtained greater in microemulsions than in pure IL highlight a strong effect of confinement. Moreover, a direct correlation between the quantity of IL and the reaction yield was observed. IL in oil microemulsions confined the reaction and offered the advantage of using a smaller quantity of ionic liquid compared to bulk phase.

## 6. Conclusion

In this article, we have discussed the use of ionic liquids as solvent for the self-assembly of surfactants. In ionic liquids, the formation of the same types of amphiphile self-assembly phases as aqueous systems (micelles, vesicles and microemulsions) was evidenced. These aggregates were characterized by surface tension measurements, differential scanning calorimetry, scattering experiments (DLS and SANS), pulse field gradient spin-echo NMR, electrical conductivity measurements, electron microscopy.

Our experiments demonstrated that micelle formation is possible in ILs and that size and aggregation number of the micelles can be tuned by changing the exact nature of the IL. Moreover, as observed in water the formation of lamellar structures of DPPC in different ILs was demonstrated. Lastly three micro-regions of the microemulsion – ionic liquid in oil, bicontinuous and oil in ionic liquid – were identified in the ternary system

bnPyrNTf<sub>2</sub>/TX-100/toluene. The reverse IL-in-oil microemulsions have an average gyration radius of approximately 2-3 nm. The reverse IL-in-oil microemulsions were used for the first time as nanoreactors to perform an organic reaction. In addition to the well-known benefits induced by the use of RTILs as solvents, the confinement of IL improved the reactivity of Matsuda-Heck coupling and displayed the advantage of using less ionic liquid than a reaction in the bulk phase. These positive effects can be used in various domains such as biocatalysis or nanomaterials synthesis.

Surfactant self-assembly should open unique opportunities to design nanoscale architectures in green solvents. Such nanostructures are interesting not only from the standpoint of the assembly of advanced materials and environmental concerns, but also may be useful in applications in nanoscience such as nanoreactors for organic and inorganic synthesis, templates for the synthesis of nanostructured materials and in formulation.

## 7. References

- Anderson, J. L.; Pino, V.; Hagberg, E. C.; Sheares, V. V. and Armstrong, D. W. (2003). Surfactant solvation effects and micelle formation in ionic liquids. *Chemical Communications*, 2444-2445.
- Araos, M. U. and Warr, G. G. (2005). Self-assembly of nonionic surfactants into lyotropic liquid crystals in ethylammonium nitrate, a room-temperature ionic liquid. *Journal of Physical Chemistry B*, 109, 30, 14275-14277.
- Araos, M. U. and Warr, G. G. (2008). Structure of nonionic surfactant micelles in the ionic liquid ethylammonium nitrate. *Langmuir*, 24, 17, 9354-9360.
- Berthod, A.; Tomer, S. and Dorsey, J. G. (2001). Polyoxyethylene alkyl ether nonionic surfactants: physicochemical properties and use for cholesterol determination in food. *Talanta*, 55, 1, 69-83.
- Chen, S. C.; Sturtevant, J. M. and Gaffney, B. J. (1980). Scanning calorimetric evidence for a 3rd phase-transition in phosphatidylcholine bilayers. *Proceedings of the National Academy of Sciences of the United States of America-Biological Sciences*, 77, 9, 5060-5063.
- Clausse, M.; Peyrelasse, J.; Heil, J.; Boned, C. and Lagourette, B. (1981). Bicontinuous structure zones in microemulsions. *Nature*, 293, 5834, 636-638.
- Couper, A.; Gladden, G. P. and Ingram, B. T. (1975). Adsorption of Surface-Active Agents in a Non-Aqueous Solvent. *Faraday Discussions*, 59, 59, 63-75.
- Das, K. P.; Ceglie, A. and Lindman, B. (1987). Microstructure of formamide microemulsions from NMR self-diffusion measurements. *Journal of Physical Chemistry*, 91, 11, 2938-2946.
- Dupont, J.; de Souza, R. F. and Suarez, P. A. Z. (2002). Ionic liquid (molten salt) phase organometallic catalysis. *Chemical Reviews*, 102, 10, 3667-3691.
- Eastoe, J.; Gold, S.; Rogers, S. E.; Paul, A.; Welton, T.; Heenan, R. K. and Grillo, I. (2005). Ionic liquid-in-oil microemulsions. *Journal of the American Chemical Society*, 127, 20, 7302-7303.
- Engberts, J.; Fernandez, E.; Garcia-Rio, L. and Leis, J. R. (2006). Water in oil microemulsions as reaction media for a Diels-Alder reaction between N-ethylmaleimide and cyclopentadiene. *Journal of Organic Chemistry*, 71, 11, 4111-4117.
- Evans, D. F.; Kaler, E. W. and Benton, W. J. (1983). Liquid-crystals in a fused salt-beta, alpha-distearoylphosphatidylcholine in N-ethylammonium nitrate. *Journal of Physical Chemistry*, 87, 4, 533-535.

- Evans, D. F.; Yamauchi, A.; Roman, R. and Casassa, E. Z. (1982). Micelle formation in ethylammonium nitrate, a low-melting fused salt. *Journal of Colloid and Interface Science*, 88, 89-96.
- Fainerman, V. B.; Lucassen-Reynders, E. and Miller, R. (1998). Adsorption of surfactants and proteins at fluid interfaces. *Colloids and Surfaces a-Physicochemical and Engineering Aspects*, 143, 2-3, 141-165.
- Fedotov, V. D.; Zuev, Y. F.; Archipov, V. P.; Idiyatullin, Z. S. and Garti, N. (1996). A Fourier transform pulsed-gradient spin echo nuclear magnetic resonance self-diffusion study of microemulsions and the droplet size determination. 11th International Symposium on Surfactants in Solution, Jerusalem, Israel.
- Fletcher, K. A. and Pandey, S. (2004). Surfactant aggregation within room-temperature ionic liquid 1-ethyl-3-methylimidazolium bis(trifluoromethylsulfonyl)imide. *Langmuir*, 20, 1, 33-36.
- Gao, H. X.; Li, J. C.; Han, B. X.; Chen, W. N.; Zhang, J. L.; Zhang, R. and Yan, D. D. (2004). Microemulsions with ionic liquid polar domains. *Physical Chemistry Chemical Physics*, 6, 11, 2914-2916.
- Gayet, F.; El Kalamouni, C.; Lavedan, P.; Marty, J. D.; Brulet, A. and Lauth-de Viguerie, N. (2009). Ionic Liquid/Oil Microemulsions as Chemical Nanoreactors. *Langmuir*, 25, 17, 9741-9750.
- Gayet, F.; Marty, J.-D. and Lauth-de Viguerie, N. (2008). Palladate Salts from Ionic Liquids as Catalysts in the Heck Reaction. *Arkivoc*, 17, 61-76.
- Gayet, F.; Marty, J. D.; Brulet, A. and Lauth-de Viguerie, N. (2010). Liposomes in ionic liquids. *submitted*.
- Gayet, F.; Marty, J.-D.; Brûlet, A. And Lauth-de Viguerie, N. (2011). Vesicles in ionic liquids. *Under press*.
- Gayet, F.; Patrascu, C.; Marty, J. D. and Lauth-de Viguerie, N. (2010). Surfactant Aggregates in Ionic Liquids and Reactivity in Media. *International Journal of Chemical Reactor Engineering*, 8.
- Greaves, T. L. and Drummond, C. J. (2008). Ionic liquids as amphiphile self-assembly media. *Chemical Society Reviews*, 37, 8, 1709-1726.
- Hao, J. and Zemb, T. (2007). Self-assembled structures and chemical reactions in room-temperature ionic liquids. *Current Opinion in Colloid & Interface Science*, 12, 129-137.
- Hao, J. C.; Song, A. X.; Wang, J. Z.; Chen, X.; Zhuang, W. C.; Shi, F.; Zhou, F. and Liu, W. M. (2005). Self-assembled structure in room-temperature ionic liquids. *Chemistry-a European Journal*, 11, 13, 3936-3940.
- Herrington, T. M. and Sahi, S. S. (1988). Temperature-Dependence of the Micellar Aggregation Number of N-Dodecylpolyethyleneoxide Surfactants. *Journal of Colloid and Interface Science*, 121, 1, 107-120.
- Holmberg, K. (2007). Organic reactions in microemulsions. *European Journal of Organic Chemistry*, 5, 731-742.
- Jonstromer, M.; Sjöberg, M. and Warnheim, T. (1990). Aggregation and Solvent Interaction in Nonionic Surfactant Systems with Formamide. *Journal of Physical Chemistry*, 94, 19, 7549-7555.
- Kimizuka, N. and Nakashima, T. (2001). Spontaneous self-assembly of glycolipid bilayer membranes in sugar-philic ionic liquids and formation of ionogels. *Langmuir*, 17, 22, 6759-6761.



- Lasic, D. D. (1988). The mechanism of vesicle formation. *Biochemical Journal*, 256, 1, 1-11.
- Li, J. C.; Zhang, J. L.; Gao, H. X.; Han, B. X. and Gao, L. (2005). Nonaqueous microemulsion-containing ionic liquid [bmim][PF<sub>6</sub>] as polar microenvironment. *Colloid and Polymer Science*, 283, 12, 1371-1375.
- McDonald, C. (1967). Micellar Properties of Some Non-Ionic Surface-Active Agents in Polar Solvents. *Journal of Pharmacy and Pharmacology*, 19, 6, 411-&.
- Merrigan, T. L.; Bates, E. D.; Dorman, S. C. and Davis, J. H. (2000). New fluoruous ionic liquids function as surfactants in conventional room-temperature ionic liquids. *Chemical Communications*, 20, 2051-2052.
- Nakashima, T. and Kimizuka, N. (2002). Vesicles in salt: Formation of bilayer membranes from dialkyltrimethylammonium bromides in ether-containing ionic liquids. *Chemistry Letters*, 10, 1018-1019.
- Nyden, M. (2001). Handbook of Applied Surface and Colloid Chemistry, John Wiley and sons, Ltd.
- Pasc-Banu, A.; Sugisaki, C.; Gharsa, T.; Marty, J. D.; Gascon, I.; Pozzi, G.; Quici, S.; Rico-Lattes, I. and Mingotaud, C. (2004). A catalytic Langmuir film as a model for heterogeneous and homogeneous catalytic processes. *Angewandte Chemie-International Edition*, 43, 45, 6174-6177.
- Patrascu, C.; Gauffre, F.; Nallet, F.; Bordes, R.; Oberdisse, J.; de Lauth-Viguerie, N. and Mingotaud, C. (2006). Micelles in ionic liquids: Aggregation behavior of alkyl poly(ethyleneglycol)-ethers in 1-butyl-3-methyl-imidazolium type ionic liquids. *Chemphyschem*, 7, 1, 99-101.
- Patrascu, C.; Sugisaki, C.; Mingotaud, C.; Marty, J. D.; Genisson, Y. and Lauth-de Viguerie, N. (2004). New pyridinium chiral ionic liquids. *Heterocycles*, 63, 9, 2033-2041.
- Qiu, Z. and Texter, J. (2008). Ionic liquids in microemulsion. *Current Opinion in Colloid & Interface Science*, 13, 252-262.
- Ranke, J.; Stolte, S.; Stormann, R.; Arning, J. and Jastorff, B. (2007). Design of sustainable chemical products - The example of ionic liquids. *Chemical Reviews*, 107, 6, 2183-2206.
- Ray, S. and Moulik, S. P. (1994). Dynamics and thermodynamics of aerosol-OT-aided nonaqueous microemulsions. *Langmuir*, 10, 8, 2511-2515.
- Rosen, M. J.; Cohen, A. W.; Dahanayake, M. and Hua, X. Y. (1982). Relationship of Structure to Properties in Surfactants .10. Surface and Thermodynamic Properties of "2-Dodecyloxypoly(Ethenoxyethanol)S, C<sub>12</sub>H<sub>25</sub>(OC<sub>2</sub>H<sub>4</sub>)Xoh, in Aqueous-Solution. *Journal of Physical Chemistry*, 86, 4, 541-545.
- Tran, C. D. and Yu, S. F. (2005). Near-infrared spectroscopic method for the sensitive and direct determination of aggregations of surfactants in various media. *Journal of Colloid and Interface Science*, 283, 2, 613-618.
- van Os, N. M.; Haas, S. S. and Rupert, L. A. M. (1993). Physico-Chemical properties of selected anionic, cationic and nonionic surfactants. New-York.
- Wang, L. Y.; Chen, X.; Chai, Y. C.; Hao, J. C.; Sui, Z. M.; Zhuang, W. C. and Sun, Z. W. (2004). Lyotropic liquid crystalline phases formed in an ionic liquid. *Chemical Communications*, 24, 2840-2841.
- Yaghmur, A.; Aserin, A.; Antalek, B. and Garti, N. (2003). Microstructure considerations of new five-component Winsor IV food-grade microemulsions studied by pulsed gradient spin-echo NMR, conductivity, and viscosity. *Langmuir*, 19, 4, 1063-1068.

- Zana, R. (1995). Aqueous surfactant-alcohol systems: a review. *Advances in Colloid and Interface Science*, 57, 1-64.
- Zulauf, M.; Weckstrom, K.; Hayter, J. B.; Degiorgio, V. and Corti, M. (1985). Neutron-scattering study of micelle structure in isotropic aqueous-solutions of poly(oxyethylene) amphiphiles. *Journal of Physical Chemistry*, 89, 15, 3411-3417.

# Supramolecular Structures in the Presence of Ionic Liquids

Xinghai Shen, Qingde Chen, Jingjing Zhang and Pei Fu  
College of Chemistry and Molecular Engineering, Peking University, Beijing 100871,  
P. R. China

## 1. Introduction

Supramolecular chemistry is defined as “chemistry beyond the molecule”, bearing on the organized entities of higher complexity that result from the association of two or more chemical species held together by intermolecular forces (Lehn, 1988, 1995). Supramolecular chemistry may be divided into two broad and partially overlapping areas concerning: (1) *supermolecules*, well-defined and discrete oligomolecular species that result from the intermolecular association of a few components (a receptor and its substrate(s)) following a built-in scheme based on the principles of molecular recognition; (2) *supramolecular assemblies*, polymolecular entities that result from the spontaneous association of a large undefined number of components into a specific phase having more or less well-defined microscopic organization and macroscopic characteristics depending on its nature (such as micelles, microemulsions, vesicles, films, layers, membranes, mesomorphic phase and so on) (Lehn, 1995). Investigation on supramolecular systems is receiving more and more attention (Beletskaya et al., 2009; Constable, 2008; Descalzo et al., 2006; He et al., 2008b; Metrangolo et al., 2008; Oshovsky et al., 2007).

Different from simple inorganic salts (such as NaCl) who often melt at very high temperature, ionic liquids (ILs) are a kind of organic salts that are liquid at or near room temperature, always taking 100 °C as an upper limit. Figure 1 shows the structures of some typical cations and anions of ILs. The imidazolium, especially 1-alkyl-3-methylimidazolium ( $C_n\text{mim}^+$ ), is one of the most popular cations. So far, ILs have attracted much attention and been widely used as an attractive class of green solvents in the fields of chemical reactions, organic and material syntheses, solvent extraction, and electrochemistry because of their negligible vapor pressure, nonflammability, high thermal and chemical stability, high polarity, wide electrochemical window and tunable physicochemical properties (Chiappe & Pieraccini, 2005; Dupont, 2004; Leclercq & Schmitzer, 2009a; Weingartner, 2008; Welton, 1999; Zhao et al., 2002).

In the field of supramolecular chemistry, ILs could either participate directly in the assembly of supramolecular organizations, or influence the assembly of various supramolecular structures in a certain way, leading to the appearance of many novel and interesting phenomena. In addition, there exist three-dimensional supramolecular networks with polar and non-polar regions in imidazolium ILs, which can be used as powerful supramolecular receptors (Dupont, 2004; Leclercq & Schmitzer, 2009a). Therefore, this review will summarize the work in the literature, concerning the above novel and

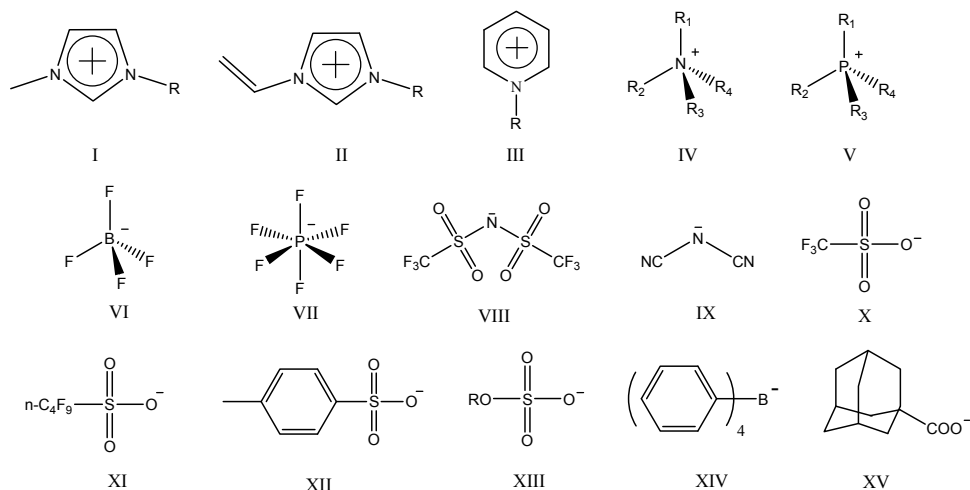


Fig. 1. Structures of some typical cations and anions of ionic liquids: I: 1-alkyl-3-methylimidazolium ( $C_n\text{mim}^+$ ); II: 1-alkyl-3-vinylimidazolium ( $C_n\text{vim}^+$ ); III: 1-alkylpyridinium ( $C_n\text{Py}^+$ ); IV: tetraalkylammonium; V: tetraalkylphosphonium; VI: tetrafluoroborate ( $\text{BF}_4^-$ ); VII: hexafluorophosphate ( $\text{PF}_6^-$ ); VIII: bis(trifluoromethylsulfonyl)imide ( $\text{Tf}_2\text{N}^-$ ); IX: dicyanamide ( $(\text{CN})_2\text{N}^-$ ); X: trifluoromethanesulfonate ( $\text{TfO}^-$ ); XI: nonafluorobutanesulfonate ( $\text{NfO}^-$ ); XII: tosylate ( $\text{OTos}^-$ ); XIII: alkylsulfate ( $C_n\text{OSO}_3^-$ ); XIV: tetraphenylborate ( $\text{TPhB}^-$ ); XV: adamantylcarboxylate ( $\text{AdCO}_2^-$ ).

interesting phenomena. The IL-relevant supramolecular systems include not only inclusion complexes with cyclodextrins (CDs), cucurbit[n]urils, calixarenes as host molecules, but also micelles, microemulsions, liquid crystals (LCs), gels. Supramolecular structures based on the host network of ILs themselves will also be presented. Furthermore, the effects of ILs on the assembly of supramolecular systems (such as rotaxanes and polyrotaxanes, etc.) will be discussed.

## 2. Supramolecules systems formed by ionic liquids with different host molecules

### 2.1 Ionic liquids as guests for native and modified cyclodextrins

#### 2.1.1 New structures and properties

Supramolecular systems formed by ILs with CDs demonstrate new structures and properties. ILs can affect the lower critical solution temperature (LCST) of polymers consisted of CDs (Amajjahe et al., 2008; Amajjahe & Ritter, 2008a). Amajjahe et al. (Amajjahe et al., 2008) investigated the influence of three different 1-butyl-3-vinylimidazolium ILs [ $C_4\text{vim}$ ][ $\text{Tf}_2\text{N}$ ], [ $C_4\text{vim}$ ][ $\text{NfO}$ ] and [ $C_4\text{vim}$ ][ $\text{AdCO}_2$ ] as guests on the LCST values of poly(NIPAAM-co- $\beta$ -CD Methacrylate) (PNCM). The copolymer PNCM can form supramolecular polyelectrolyte-type structures, so-called pseudopolyanions through host-guest interactions with suitable ionic guests. This increased hydrophilicity of pseudopolyanions results from the free carboxylate ( $\text{AdCO}_2^-$ ) and sulfonate ( $\text{NfO}^-$ ) groups, which are preferentially located in the aqueous phase and therefore responsible for the

increased LCST values. However, the complexation of  $\text{Tf}_2\text{N}^-$  leads to a decreased LCST value because the hydrophobic  $\text{Tf}_2\text{N}^-$  is preferentially located in the centre of the CD-cavity. With the increasing hydrophobicity of ILs, the cloud point of PNCM is reduced. Besides, the shrinkage and expansion behavior of pseudopolyanions could be controlled by supramolecular interaction of the CD components with three different ILs.

ILs can influence the properties of CDs and vice versa. The poly( $[\text{C}_4\text{vim}][\text{Tf}_2\text{N}]$ ) showed a pseudo-LCST effect in the presence of CD (Amajjahe & Ritter, 2008a). It was found that the CD ring complexes only the polymer anion and slips off at higher temperature when the poly(IL) becomes insoluble in water. The polymerization of ILs can be controlled by CDs (Amajjahe & Ritter, 2008b). The monomer  $[\text{C}_4\text{vim}][\text{Tf}_2\text{N}]$  cannot polymerize in water in the presence of  $\beta$ -CD by radical mechanism, which is the result of the complex formation and the spatial ion pair separation leading to quasi “naked vinylimidazolium cations” (Figure 2). This effect should be compensated with the addition of a foreign salt because of cation-cation repulsion and then polymerization occurs. As a result, the controllable polymerization is realized.

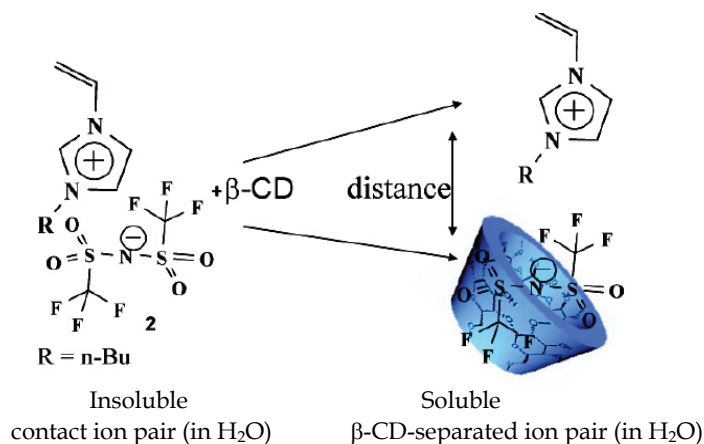


Fig. 2. Host-guest complex formation of  $[\text{C}_4\text{vim}][\text{Tf}_2\text{N}]$  with  $\beta$ -CD at 298K in water. Reprinted from Amajjahe & Ritter (2008b).

Besides, imidazolium salts can also be employed as carbene precursor for organometallic catalysis, where hydrogen/deuterium exchange reaction of the C(2)-proton occurs. Formation of the inclusion complexes (ICs) of imidazolium salts with the native  $\beta$ -CD and the heptakis-(2,6-di-O-methyl)- $\beta$ -CD (DM- $\beta$ -CD) is a simple and efficient method to modify the acidity of the imidazolium H(2) and its environment (Leclercq & Schmitzer, 2009b). Encapsulation of 1, 3-disubstituted imidazolium chloride by  $\beta$ -CDs results in the inhibition of the H(2)/D exchange in the complex.

Recently, Leclercq et al. (Leclercq et al., 2009a) discovered that the imidazolium surfactants  $[\text{C}_{12}\text{mim}]$  and  $[\text{C}_{16}\text{mim}]$  can be used as “micellar promoters” in catalyzing hydroformylation reactions. Because of the inclusion of surfactants in the CDs, the addition of  $\alpha$ -CD can modulate the aggregation properties of the surfactants. At high temperature, the supramolecular interactions of the imidazolium surfactants favor the micellization process. And by decreasing the temperature, CDs complex the surfactant monomers and destabilize the micelles.

### 2.1.2 Interaction between ionic liquids and cyclodextrins

The new properties of ILs on the addition of CDs originate from the interaction between ILs and CDs, mostly the inclusion complexation between them. Thus, the study on this topic is important. Various methods have been applied to investigate the interaction between ILs and CDs, such as the solubility (Gao et al., 2005a), infrared spectroscopy (Li et al., 2007c), ultra-violet spectroscopy, XRD (Gao et al., 2006c; Gao et al., 2005a; Li et al., 2007c), conductivity (Amajjahe & Ritter, 2008b; He et al., 2009), TGA (Gao et al., 2006c; Gao et al., 2005a; Li et al., 2007c), affinity CE (ACE) (Francois et al., 2007), NMR (Amajjahe & Ritter, 2008b; Gao et al., 2006c; He et al., 2009; Li et al., 2007c), fluorescence competition (He & Shen, 2008; He et al., 2009), microcalorimetry (Amajjahe et al., 2008; Amajjahe & Ritter, 2008b; Li et al.), surface tension measurements (Gao et al., 2006c) and so on. By these methods, the formation constants of ICs, the stoichiometry for ILs and CDs can be obtained. Gao et al. (Gao et al., 2005a) investigated the system of  $[C_4mim][PF_6]$  and  $\beta$ -CD using NMR and suggested that the whole imidazolium cation ( $C_4mim^+$ ) was probably included into the cavity of  $\beta$ -CD, while the  $PF_6^-$  ion dissociated near the  $\beta$ -CD. They also studied ICs formation of  $\beta$ -CD with three kinds of IL surfactants,  $[C_{12}mim][PF_6]$ ,  $[C_{14}mim][PF_6]$ , and  $[C_{16}mim][PF_6]$  (Gao et al., 2006c). There were two kinds of inclusion complexations, *i.e.*, 1:1 and 1:2 ( $\beta$ -CD/IL) stoichiometries for  $\beta$ -CD- $[C_{12}mim][PF_6]$  and  $\beta$ -CD- $[C_{14}mim][PF_6]$  ICs, and only 1:1 stoichiometry for  $\beta$ -CD- $[C_{16}mim][PF_6]$  ICs due to the strong steric inhibition of  $[C_{16}mim][PF_6]$ . Unlike the possible structure suggested for the  $[C_4mim][PF_6]/\beta$ -CD inclusion complex, only the alkyl side chain on the imidazolium ring of these three ILs entered into the cavity of  $\beta$ -CD. The similar result was obtained by Li et al. (Li et al., 2007c), which indicated that only the alkyl side chain of the  $[C_{12}mim][PF_6]$  was included into the cavity of  $\beta$ -CD. Francois et al. (Francois et al., 2007) developed ACE method to characterize the complex formation between seven cations of various imidazolium-based ILs ( $[C_2mim][Tf_2N]$ ,  $[C_4mim][Tf_2N]$ ,  $[C_4mim][BF_4]$ , 1-butyl-2,3-dimethylimidazolium tetrafluoroborate ( $[C_4dmim][BF_4]$ ),  $[C_8mim]Br$ ,  $[C_{10}mim][BF_4]$  and  $[C_{12}mim][BF_4]$ ) and eight neutral CDs ( $\alpha$ -CD,  $\beta$ -CD,  $\gamma$ -CD, hydroxypropyl- $\alpha$ -CD (HP- $\alpha$ -CD), hydroxypropyl- $\beta$ -CD (HP- $\beta$ -CD), hydroxypropyl- $\gamma$ -CD (HP- $\gamma$ -CD), heptakis-(2,6-di-O-methyl)- $\beta$ -CD (DM- $\beta$ -CD) and heptakis-(2,3,6-tri-O-methyl)- $\beta$ -CD (TM- $\beta$ -CD)). According to classical nonlinear and linear treatments, they obtained the complex stoichiometry and formation constant K. The majority of systems followed a 1:1 complexation stoichiometry model but in four cases ( $[C_{10}mim][BF_4]$ ,  $[C_{12}mim][BF_4]$  and  $\alpha$ -CD, DM- $\beta$ -CD) a 1:2 stoichiometry was better satisfied. It was established that the main factor influencing the strength of the inclusion complexation was the length of alkyl side chain on the imidazolium ring. The presence of a methyl group at the C(2) position and the nature of anion associated to the imidazolium cation in the IL did not show significant influence on the complexation constant obtained. Also, the size of the CD cavity noticeably impacts the stability of the 1:1 complexes, with stronger complexes being given by  $\beta$ -CD. Furthermore, it was shown that two CD molecules can likely be threaded along  $C_{10}$  and  $C_{12}$  alkyl side chains and there was no inclusion of the imidazolium ring into the cavity of  $\beta$ -CD. Mostly, the interaction of CDs and ILs are studied in aqueous solution. Recently, it was investigated that the dissolution of  $\beta$ -CD could be enhanced in some hydrophilic ILs and 1:1 inclusion complexes were formed between  $\beta$ -CD and imidazolium cations of the ILs (Zheng et al.).

Differently, several inclusion complexes of  $\beta$ -CD with anion of ILs were also reported. As mentioned in Section 2.1.1, the anion  $Tf_2N^-$  of  $[C_4vim][Tf_2N]$  formed exclusively host-guest

complex with  $\beta$ -CD (Amajjahe et al., 2008; Amajjahe & Ritter, 2008b). Similarly, the anion  $\text{PF}_6^-$  but not the cation  $\text{C}_4\text{vim}^+$  was found to be accommodated by  $\beta$ -CD. We reported that  $[\text{C}_4\text{mim}][\text{PF}_6]$ ,  $[\text{C}_4\text{mim}][\text{BF}_4]$ , and  $[\text{C}_4\text{mim}]\text{Cl}$  formed 1:1 inclusion complexes with  $\beta$ -CD, respectively (He & Shen, 2008). Through  $^{19}\text{F}$  NMR, we also found that  $\text{PF}_6^-$  and  $\text{BF}_4^-$  could interact with  $\beta$ -CD but the latter interaction was relatively weak.

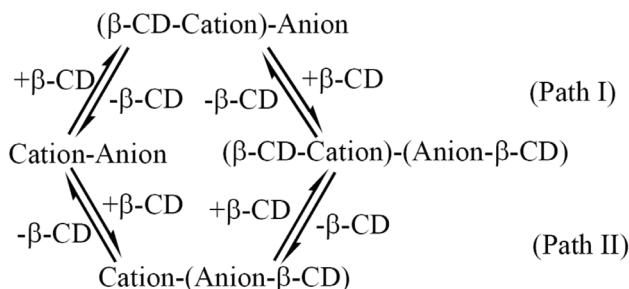


Fig. 3. Two-Step Equilibrium in an IL/ $\beta$ -CD System (Path I: the cation interacts with  $\beta$ -CD more strongly than the anion does, Path II: the anion interacts with  $\beta$ -CD more strongly than the cation does). Reprinted from He et al. (2009).

Considering the above studies, a general pattern in the IL/ $\beta$ -CD system and a two-step equilibrium was brought forward as shown in Figure 3. It was confirmed that the alkyl side chain on the imidazolium ring but not the imidazolium ring itself entered into the cavity of  $\beta$ -CD. As for the IL  $[\text{C}_{12}\text{mim}][\text{Tf}_2\text{N}]$ , the cation and the anion both exhibited strong interactions with  $\beta$ -CD simultaneously (He et al., 2009). It was suggested that the strength of the interaction of various cations and anions in ILs with  $\beta$ -CD follows the following order:  $\text{NfO}^- > \text{C}_{12}\text{mim}^+ > \text{Tf}_2\text{N}^- \sim \text{AdCO}_2^- \sim \text{C}_{10}\text{mim}^+ > \text{C}_8\text{mim}^+ > 1\text{-hexyl-2,3-dimethyl-imidazolium cation (C}_6\text{dmim}^+) \sim \text{PF}_6^- > \text{BF}_4^- > 1\text{-butyl-2,3-dimethylimidazolium cation (C}_4\text{dmim}^+) \sim \text{C}_4\text{vim}^+ \sim \text{C}_4\text{mim}^+ > \text{Cl}^-$ .

Leclercq et al. (Leclercq & Schmitzer, 2008) discovered multiple equilibria in the complexation of dibenzylimidazolium bromide by CDs. In aqueous solution, dibenzylimidazolium bromide forms dimeric assemblies by T-stacking between an acidic proton of the imidazolium and the benzyl aromatic ring of another cation (Figure 4). This dimeric association can be disturbed by the addition of native CDs. The control of the majority species in solution can be made by the judicious choice of CD concentration and its

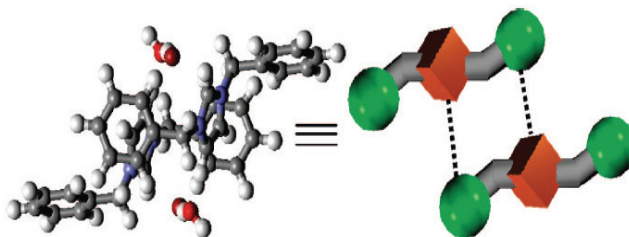


Fig. 4. Structure of the dibenzylimidazolium bromide water dimer obtained by PM3 in accordance with the crystalline structure and the conventional representation adopted in this study. Reprinted from Leclercq & Schmitzer (2008).

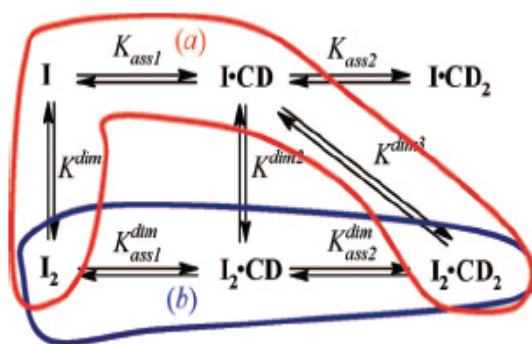


Fig. 5. Equilibrium distributions for the formation of  $I_2 \cdot CD_2$  from  $I_2$  in the presence of (a)  $\alpha$ -CD and (b)  $\beta$ -CD.  $I$  and  $I_2$  represent the dibenzylimidazolium bromide salt and the dimer, respectively. Reprinted from Leclercq & Schmitzer (2008).

macrocycle size. The dimer is complexed directly by  $\beta$ -CD, whereas in the presence of  $\alpha$ -CD, the dimer is dissociated to form a 1:1 IC; at higher concentration, this 1:1 complex can dimerize (Figure 5).

## 2.2 Ionic liquids as guests for Cucurbit[n]uril system

Cucurbit[n]uril (CBn) is another important host molecule in supramolecular chemistry. The complex formation of ILs and CBns is not all the same with CDs because of the different structure between them (Montes-Navajas et al., 2008).  $C_{1mim}^+$  forms a fairly stable complex with Cucurbit[7]uril (CB7), similarly, as the numbers of carbon atoms in the aliphatic chain grows, from  $C_{1mim}^+$  to  $C_{6mim}^+$ , the binding constant between ILs and CB7 increases (Miskolczy et al., 2009). However, further lengthening of the alkyl group destabilizes the complex, because a growing segment of the carbon chain cannot be confined in CB7. When inclusion complexes between 1,1'-dialkyl-3,3'-(1,4-phenylene)bisimidazolium dibromide salts and CB7 were studied, the stoichiometry of the complexes not only depends on the alkyl chains, but also lies on the relative concentration of the imidazolium salt and CB7 (Noujeim et al., 2009). Unlike  $\beta$ -CD, the fact that the anion barely influences the binding constant of IL-CB7 complexes is probably due to the significant negative charge density of the carbonyl-lined portals of CB7, which hinders the interaction with anions. Moreover, CB7 has a less polar cavity than  $\beta$ -CD, which disfavors the ion pairing. St-Jacques et al. (St-Jacques et al., 2008) studied the position of charge-diffuse peralkylated onium cations,  $NR_4^+$ ,  $PR_4^+$  and  $SR_3^+$  ( $R=Me$ ,  $Et$ ,  $nPr$ ,  $nBu$ ), which could be the cations of ILs, in the cavity of CB7. With cationic guests, the stability constants of the CB are larger than those of the corresponding CDs and can be several orders of magnitude larger when the guest is a dication. Different cations prefer to locate in different positions of CB. With simple hydrophilic cations, such as protons, alkali metal and alkali earth cations and transition metal ions, the preferred binding location(s) on CB are the carbonyl-lined portals, to take advantage of the ion-dipole interactions. With cationic organic or organometallic guests, very strong binding is achieved when the cationic portion(s) of the guest can be positioned near the portals. However, as these charge-diffuse peralkylated onium cations, when considering size selectivity, with the smaller guests inside its cavity, rather than at the carbonyl-lined portals by the study of NMR. At the same time, they discovered that the stability constants are dependent on the size and coordination number of the central atom and



the size and hydrophobicity of the alkyl group. The CB7 has a preference for Et over Me for  $\text{NR}_4^+$  and  $\text{SR}_3^+$  and the opposite for  $\text{PR}_4^+$ , with trends of  $\text{PMe}_4^+ > \text{NMe}_4^+ > \text{SMe}_3^+$  and  $\text{SEt}_3^+ > \text{NEt}_4^+ > \text{PEt}_4^+$  in binding constants with CB7.

Cucurbit[6]uril (CB6) is poorly soluble in water and insoluble in organic solvents. The interaction of CB6 and  $[\text{C}_n\text{mim}]\text{Br}$  was found to significantly increase the solubility of CB6 in neutral water (Zhao et al., 2010). CB6 was pulled into neutral water through encapsulation of an imidazolium-based IL (Liu et al., 2008). According to  $^1\text{H}$  NMR titration experiments,  $\text{C}_2\text{mim}^+$  and  $\text{C}_4\text{mim}^+$  demonstrated different binding modes with CB6. The small changes in alkyl chain length can dramatically increase the solubility of CB6. Besides, 2:1 stoichiometry between  $\text{C}_2\text{mim}^+$  and CB6 provides opportunities for a new type of self-assembly with CB6. However, the formation of 1:1 complex between  $\text{C}_2\text{mim}^+$  and CB6 was found recently (Kolman et al., 2009). The supramolecular interaction between series of 1-alkyl-3-methylimidazolium guests with variable alkyl substituent lengths and CB6 in the solution and the solid state was studied. All imidazolium guests form 1:1 complexes with CB6. However, the mode of inclusion binding depends on the length of the alkyl substituent (Figure 6). The imidazolium aromatic ring is polarized upon complexation with CB6 and the electron density shifts from the nitrogen located in the proximity of the carbonyl portal of CB6 toward the opposite nitrogen atom.

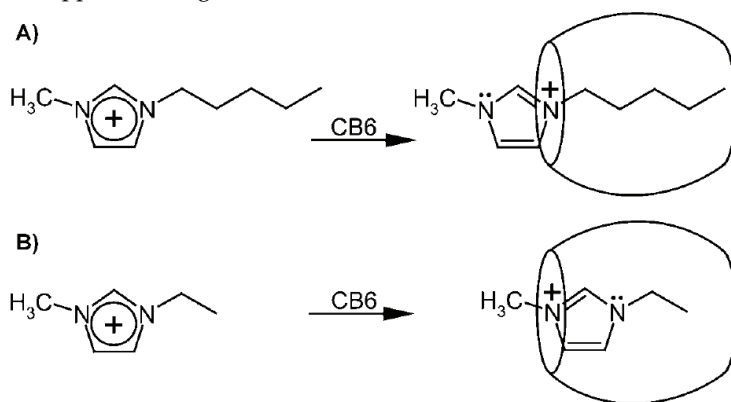


Fig. 6. Two different modes of inclusion binding between 1-alkyl-3-methylimidazolium guests and CB6. Reprinted from Kolman et al. (2009).

Commonly, inclusion complex formation with CB7 can be applied to enhance the fluorescence response of guest (Megyesi et al., 2008), for example berberine, a clinically important natural alkaloid. When using CB7 as macrocyclic host compound, a very stable 1:1 inclusion complex formed and led to about 500-fold fluorescence intensity enhancement, which can facilitate the detection of berberine even below nanomolar concentration. The change of association constant and the fluorescence quantum yield of the complex can be accomplished by the addition of NaCl. Interestingly, 1-alkyl-3-methylimidazolium type ILs can modify the fluorescent properties of the complex much more efficiently than NaCl. It is the result that the formation of ternary complex by time-resolved fluorescence studies. The results can be applied in enzyme assays, because berberine fluorescence is insensitive to the environment, such as pH and the other compounds. On the other hand, inclusion complex formation can be used to separation processes. Because  $[\text{C}_n\text{mim}]\text{Br}$  is only capable of

binding with CB7 in a CB5/CB7 mixture, CB7- $[\text{C}_n\text{mim}][\text{Br}]$  can be removed from the mixture and realize the isolation of CB7 (Jiao et al., 2010). Besides, it is also a green process since imidazolium ILs can be reused.

### 2.3 Ionic liquids as guests for Calixarene system

Inazumi et al. (Inazumi et al., 2007) studied the inclusion complexation of *p*-sulfonatocalix[6]arene (Calix-S6) with three kinds of phenothiazine dyes in a mixture of  $[\text{C}_4\text{mim}][\text{BF}_4]$  and ethanol. It was found that a competing complexation happened between the included dye and the IL molecules and that the 1:1 inclusion complex was formed by  $\text{C}_4\text{mim}^+$  and Calix-S6. Very recently, the inclusion complex formation of  $\text{C}_n\text{mim}^+$  type ILs with Calix-S6 and *p*-sulfonatocalix[4]arene (Calix-S4) was verified by the fluorescence competition method with berberine alkaloid as fluorescent probe (Miskolczy & Biczok, 2009). The stability of  $\text{C}_n\text{mim}^+$ -Calix-S4 complex was significantly larger than that of  $\text{C}_n\text{mim}^+$ -Calix-S6 supramolecules due to better size match in the former case. The influence of the length of the aliphatic side chain was opposite for Calix-S4 and Calix-S6. The lengthening of the aliphatic side chain of the imidazolium moiety diminished the equilibrium constant of the complexation with Calix-S4, but enhanced the stability of Calix-S6 complexes. The larger conformational mobility of Calix-S6 compared to that of Calix-S4 rendered the larger macrocycle more adaptable to the geometrical features of  $\text{C}_n\text{mim}^+$  permitting stronger host-guest interaction when the aliphatic chain of  $\text{C}_n\text{mim}^+$  is longer. They demonstrated that the electrostatic attraction between  $\text{C}_n\text{mim}^+$  ion and the sulfonato groups at the upper rim of calixarene macrocycle was not the dominant driving force of complexation. As for the anions, the strength of  $\text{C}_n\text{mim}^+$  inclusion in Calix-S6 was anion independent. It was different from the characteristics of ILs in  $\beta$ -CD because of ion pair formation within the  $\beta$ -CD cavity. In the case of  $\text{C}_n\text{mim}^+$ -Calix-S6 complex, such an interaction is not feasible because the negative charge of the macrocycle prevents anion ingress into the cavity of the host. Ling et al. reported the multicomponent materials containing Calix-S4, imidazolium or bis-imidazolium cations, phosphonium cations and different lanthanide ions (Ling et al., 2009, 2010a, b). It was investigated that the imidazolium head group resided in the calixarene cavity and the terminus of alkyl chain penetrated the adjacent hydrophobic bi-layer, comprising of the calixarenes and phosphonium ions.

## 3. Supramolecular assemblies based on ionic liquids

Generally, amphiphilic molecules self-assemble to form micelle, microemulsion, lyotropic liquid crystal and vesicle. Moreover, long-chain ILs can act as ionic surfactants and form similar self-assembly in water or oil. Qiu et al. summarized the studies of IL based microemulsions from the perspective of the role of ILs (Qiu & Texter, 2008). ILs participated in the formation of the microemulsions, in which ILs replaced oil, water or surfactants. Hao et al. reviewed the self-assembled structures (such as micelles, microemulsions, liquid crystals and vesicle) in ILs, which acted as the solvent (Hao & Zemb, 2007). In this part, we summarized the IL based organized assemblies, in which IL participated in the formation of micelles, microemulsions, vesicles and liquid crystals rather than acted as solvents.

### 3.1 IL based micelles (ionic liquid as surfactant)

Micelles generally form in water and the hydrophobic effect is the main driving force. Recently, micelles formed in nonaqueous polar solvents (including ILs) have been reported.

Because of the existence of electrostatic repulsion among the hydrophilic groups, surfactant molecules are kept apart and loosely arranged, which may result in the larger size of the aggregates in ILs than that in aqueous systems (Figure 7) (Li et al., 2008a). In addition, the aggregation of amphiphilic copolymers and surfactant-like ILs in ILs was reported.

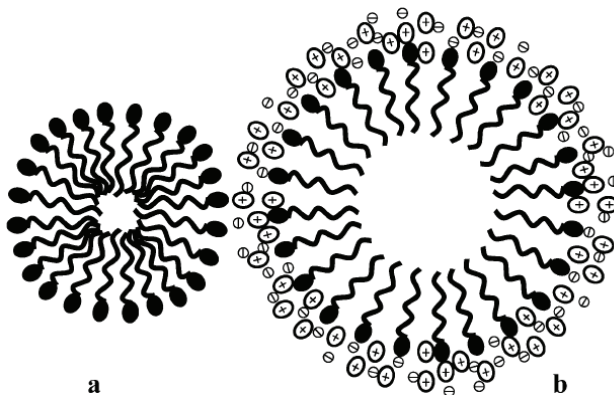


Fig. 7. Schematic representation of long-chain IL aggregates in water (a) and in  $[\text{C}_4\text{mim}][\text{BF}_4]$  (b). Hollow ellipses and hollow circles represent the cations and anions in ILs, respectively. Reprinted from Li et al. (2008a).

ILs based on the 1-alkyl-3-methylimidazolium cation ( $\text{C}_n\text{mim}^+$ ) possess an inherent amphiphilicity. In recent years, surfactant behaviors of such ILs received much attention. Miskolczy and his coworkers (Miskolczy et al., 2004) investigated the association of ILs possessing *n*-octyl moiety either in the cation or in the anion in aqueous solution. It was found that 1-butyl-3-methylimidazolium octyl sulfate acted as a surfactant above cmc (0.031 M). Whereas, 1-methyl-3-octylimidazolium chloride produced inhomogeneous solution of larger aggregates, which were dissolved on the addition of more than 2:1 molar excess of sodium dodecylsulfate (SDS) due to the formation of mixed micelle. The aggregation behavior of 1-alkyl-3-methylimidazolium ILs in aqueous solutions has been investigated (Bowers et al., 2004). It was proposed that the short-chain  $[\text{C}_4\text{mim}][\text{BF}_4]$  formed polydisperse spherical aggregates, whereas the  $[\text{C}_8\text{mim}]\text{I}$  formed regularly sized micelles above the cmc. The micelle formation of surface active  $[\text{C}_{2n}\text{mim}]^+$  ( $n = 4\sim 8$ ) in aqueous solution was investigated by several methods, such as surface tension, electrical conductivity measurements and fluorescence techniques et al. (Blesic et al., 2007; Blesic et al., 2008; Dong et al., 2007; Dong et al., 2008a; Dong et al., 2008b; El Seoud et al., 2007; Inoue et al., 2007; Jungnickel et al., 2008; Luczak et al., 2008; Luczak et al., 2009; Modaressi et al., 2007b; Singh & Kumar, 2007, 2008; Vanyur et al., 2007; Wang et al., 2008; Wang et al., 2007; Zhang et al., 2008b; Zhao et al., 2008a). Results showed that the long chain imidazolium ILs acted as ionic surfactants and stronger aggregation tendency of the ILs might be attributed to characteristic nature of imidazolium head group such as potency of H-bond formation, which is lacking in common ionic surfactants. The aggregation number of the ILs was found to increase with the increasing length of the alkyl chain and a possible microscopic aggregation structure such as stairs has been proposed (Zhao et al., 2008a). Aggregation-induced conformational changes in different ILs were shown to depend on the aromatic ring, alkyl chain, counterions, and their interactions with water. Fluorescence quenching

method in which pyridinium ILs acted as quenchers was firstly used to detect the aggregation behavior of surfactant ILs (Blesic et al., 2008).

The influence of the anions on the aggregation of ILs was first reported by Wang et al., and explained by the hydrated radius or Gibbs energy of hydration of the anions (Wang et al., 2008). The ring type of the cations also had significant effect on the aggregation behavior of the ILs, which was controlled mainly by the balance among the factors of hydrophobicity of the cations, binding strength of the cations with a given anion, and the steric repulsion between the head groups of the cations. The former two factors promote but the latter factor weakens the aggregates formation. Zheng and his coworkers (Dong et al., 2008a) studied the aggregation of surface active  $[\text{C}_{16}\text{mim}]\text{Br}$  and reported the formation of wormlike micelles in the presence of salts, similar to the situation of some traditional ionic surfactants in aqueous solution. Also,  $[\text{C}_{16}\text{mim}]\text{Br}$  was used as a new cationic surfactant for separation of phenolic compounds by MEKC (Niu et al., 2009).

ILs based on imidazolium and ammonium salts with longer-substituent cations self-assemble on negatively charged polyimide substrates via electrostatic force. Whereas for shorter-substituent cations, no aggregates formed due to the less hydrophobic interaction than the electrostatic repulsive interaction between the cations and the counter anions (Zhao et al., 2008b). Dorbritz et al. (Dorbritz et al., 2005) found that the formation of aggregates of  $[\text{C}_4\text{mim}][\text{BF}_4]$  and  $[\text{C}_4\text{mim}][\text{Tf}_2\text{N}]$  in aqueous solution depended on the solvent, the IL concentration and the anion structure of the ILs. They also mentioned that ILs can be used to improve the solubility of hydrophobic compounds.

Anderson's group (Pino et al., 2009) studied the micellar properties of aqueous solutions of two ILs, 1-hexadecyl-3-butylimidazolium bromide and 1,3-didodecylimidazolium bromide, in the presence of several organic solvents (methanol, 1-propanol, 1-butanol, 1-pentanol, and acetonitrile) by surface tensiometry. For both ILs, increases in the cmc values and minimum surface area per surfactant molecule, decreases in the maximum surface excess concentration, adsorption efficiency and effectiveness of surface tension reduction were obtained when increasing the organic solvent content.

The aggregation behavior and thermodynamic properties of micellization for the IL-type Gemini imidazolium surfactants with different spacer length ( $[\text{C}_{12-s}\text{-C}_{12}\text{im}]\text{Br}_2$ ,  $s = 2, 4, 6$ ) have been investigated. Results showed that the surface activity of  $[\text{C}_{12-s}\text{-C}_{12}\text{im}]\text{Br}_2$  decreased with increasing spacer length, and the micellization was entropy-driven when  $s=2$  and 4, whereas aggregation of  $[\text{C}_{12-6}\text{-C}_{12}\text{im}]\text{Br}_2$  is enthalpy-driven at lower temperature but entropy-driven at higher temperature (Ao et al., 2009).

	Compound	$n$	$m$	$n+m$
	<b>1</b>	8	1	9
	<b>2</b>	10	1	11
	<b>3</b>	12	1	13
	<b>4</b>	4	4	8
	<b>5</b>	4	8	12
	<b>6</b>	8	4	12
	<b>7</b>	8	8	16

Fig. 8. General structure of 1-alkyl-3-methylimidazolium alkylsulfonate ILs ( $[\text{C}_n\text{H}_{2n+1}\text{mim}][\text{C}_m\text{H}_{2m+1}\text{SO}_3]$ );  $m+n$  is the sum of the number of carbon atoms in the two alkyl-substituents. Reprinted from Blesic et al. (2009b).

Anionic and cationic alkyl-chain effects on the self-aggregation of both neat and aqueous solutions of 1-alkyl-3-methylimidazolium alkylsulfonate salts,  $[\text{C}_n\text{H}_{2n+1}\text{mim}][\text{C}_m\text{H}_{2m+1}\text{SO}_3]$  (Figure 8), have been investigated for the first time by Blesic et al. (Blesic et al., 2009b). They compared the effects of the alkyl-substitution patterns in both the cation and anion on the surfactant properties of these salts. It was found that the ILs with methylsulfonate anions ( $n = 8, 10$ , and  $12$ ) behaved as conventional cationic surfactants, showing a decrease of the cmc with the increase of the alkyl chain length in the cation. When the amphiphilic character is present in both the cation and anion ( $n = 4$  and  $8$ ,  $m = 4$  and  $8$ ), a synergistic packing effect appears to lead to the formation of novel catanionic surfactants with both cmc values lower than anticipated, and enhanced surface activity. Bhargava and his coworkers (Bhargava & Klein, 2009) applied molecular dynamics (MD) to study the cation aggregation of  $[\text{C}_{10}\text{mim}]\text{Br}$  in aqueous solution and found that the chains were buried inside the micelle to avoid unfavorable interactions with water, leaving the polar headgroups exposed to water. Recently, Kunz et al. (Thomaier & Kunz, 2007) have reported the aggregation behavior of surfactant-like ILs,  $[\text{C}_{16}\text{mim}]\text{Cl}$  and  $[\text{C}_{16}\text{mim}][\text{BF}_4]$ , in another IL ethylammonium nitrate (EAN), where the structures due to electrostatic interactions can persist at such high temperatures. The aggregation behavior of a series of long-chain ILs,  $[\text{C}_{2n}\text{mim}]\text{Br}$  ( $n = 5\sim 8$ ), in  $[\text{C}_4\text{mim}][\text{BF}_4]$  was studied by Li et al. (Li et al., 2008a) for the first time. The results indicated that the cmc for the long-chain ILs in  $[\text{C}_4\text{mim}][\text{BF}_4]$  are much larger than that in water and diameters of the spherical aggregates obtained by freeze-fracturing electron microscopy (FFEM) and dynamic light scattering (DLS) measurements were  $70\sim 100$  nm. Davis and his coworkers (Merrigan et al., 2000) synthesized four new surfactant fluorinated ILs (Figure 9) and reported the formation and stabilization of dispersions of perfluorocarbons in  $[\text{C}_6\text{mim}][\text{PF}_6]$  for the first time.

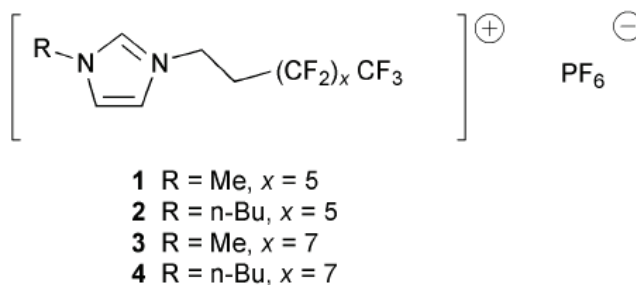


Fig. 9. General structures of the new fluoruous ILs. Reprinted from Merrigan et al. (2000).

### 3.2 Ionic liquid based microemulsions

IL based microemulsions, which utilize ILs to replace one or more components of classical microemulsions, are so attractive that lots of papers have been published to characterize these kinds of IL based microemulsions.

First of all, IL based microemulsions, in which ILs replaced water of traditional microemulsions, have been extensively characterized by a number of techniques. Microregion of phase diagram of IL based microemulsions was detected by cyclic voltammetric technique (Gao et al., 2006a), electrical conductivity (Gao et al., 2004; Gao et al., 2006b; Gao et al., 2007b; Gao et al., 2006d; Li et al., 2007b), and direct observation, where the phase boundaries were determined by observing the transition from transparency to

turbidity (Cheng et al., 2007a; Cheng et al., 2007b; Cheng et al., 2008; Gao et al., 2005b; Li et al., 2005a). Based on the phase diagram, DLS (Cheng et al., 2007a; Gao et al., 2004; Gao et al., 2006b; Gao et al., 2008b; Gao et al., 2005b; Li et al., 2007b), FFEM (Cheng et al., 2007a; Gao et al., 2004; Gao et al., 2008b), small-angle X-ray scattering (SAXS) (Li et al., 2005a) and small-angle neutron scattering (SANS) (Eastoe et al., 2005) have been applied to characterize the microemulsions with polar IL cores. These techniques proved the swollen of reversed micelle with the addition of IL, which indicated the formation of reversed microemulsion. More detailed information was gained through FTIR (Gao et al., 2006b),  $^1\text{H}$  NMR (Gao et al., 2006b; Gao et al., 2008b), UV-vis spectroscopy (Gao et al., 2006b; Gao et al., 2008b; Gao et al., 2005b; Li et al., 2007b) and conductivity measurements (Gao et al., 2006b; Gao et al., 2008b; Li et al., 2005a). Sarkar and his coworkers (Adhikari et al., 2007; Chakrabarty et al., 2005; Seth et al., 2006, 2007a; Seth et al., 2007b) initiated the work of applying steady-state and time-resolved fluorescence spectroscopy to investigate IL based microemulsions. Coumarin 151, 153 and 490 were adopted as the probes. The results showed the solvation time inside the polar cores of the microemulsions was retarded compared to that in neat IL because of restrictions in the ionic motions imposed by the microemulsions. Li et al. (Li et al., 2007b) studied the reversed microemulsion of TX-100 in toluene with  $[\text{C}_4\text{mim}][\text{BF}_4]$  cores, using methyl orange and methylene blue as probes. With the addition of  $[\text{C}_4\text{mim}][\text{BF}_4]$  into TX-100/toluene micelle, the polarity of the microemulsion increased firstly, and then became constant, indicating the formation of "IL pool".  $[\text{C}_4\text{mim}][\text{BF}_4]$ /TX-100/*p*-xylene reversed microemulsion was investigated and a plausible structure with "IL pool" was presented (Gao et al., 2006b). It was proposed that the electropositive imidazolium ring of IL destroyed the hydrogen-bonding between TX-100 molecules. Successive addition of  $[\text{C}_4\text{mim}][\text{BF}_4]$  led to the appearance of large-sized microemulsion droplet clusters (Gao et al., 2008b).

Additionally, ILs may also replace the other components of traditional microemulsions. In this field, Cheng et al. (Cheng et al., 2007b) reported the first microemulsion formed by two ILs, i.e., hydrophobic  $[\text{C}_4\text{mim}][\text{PF}_6]$  and hydrophilic propylammonium formate (PAF). The formation of IL based microemulsion in supercritical carbon dioxide with N-ethyl perfluorooctylsulfonamide was reported (Liu et al., 2007). The first microemulsion comprising an IL ( $[\text{C}_{16}\text{mim}]\text{Cl}$ ) as surfactant and another IL (EAN and  $[\text{C}_4\text{mim}][\text{BF}_4]$ , respectively) as polar pseudo-phase was presented (Zech et al., 2009). Zheng and his coworkers (Li et al., 2009c) reported the phase diagram of *p*-xylene- $[\text{C}_{14}\text{mim}]\text{Br}$ -water ternary system, where hexagonal, lamellar lyotropic liquid crystals or microemulsions formed depending on the composition. They confirmed the formation of oil-in-water (O/W) microemulsion through the linear increasing volume of the droplets with added *p*-xylene. Gao et al. (Gao et al., 2009a) considered the hydrophobic interaction between the added organic solvents and hydrophobic groups of surfactant molecules to be the driving force in the formation of oil-in-IL (O/IL) microemulsions (Figure 10). They observed a bicontinuous microstructure by FFEM for the first time with successive addition of organic solvents.

The effect of additional water on the microstructure and properties of IL based microemulsions has been studied. In the  $[\text{C}_4\text{mim}][\text{BF}_4]$ /TX-100/thriethylamine microemulsion, water located in the palisade layers and made a base environment which might be used to prepare metal hydroxides and metal oxides (Li et al., 2007a). For the  $[\text{C}_4\text{mim}][\text{BF}_4]$ /TX-100/benzene microemulsion, water molecules interacted with oxyethylene (OE) units of TX-100 through hydrogen-bonding and attracted electropositive imidazolium ring of IL with electronegative oxygen (Gao et al., 2007a; Gao et al., 2007b). Hence, the amount of solubilized  $[\text{C}_4\text{mim}][\text{BF}_4]$  enhanced with the increase of water content

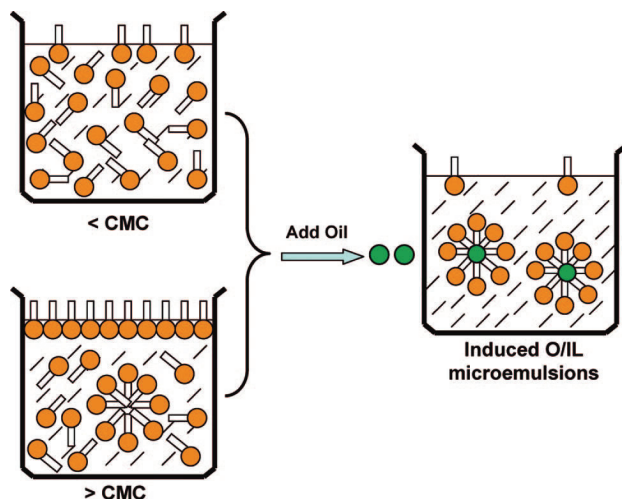


Fig. 10. Schematic diagrams of solution environments before (left) and after (right) adding organic solvents to the mixture of TX-100 and  $[\text{C}_4\text{mim}][\text{BF}_4]$ . Reprinted from Gao et al. (2009a).

because the water molecules were like “glue” that stuck the IL and OE units more tightly together. However, an increase in the amount of water in  $[\text{C}_4\text{mim}][\text{BF}_4]/\text{TX-100}/\text{cyclohexane}$  microemulsions led to the phase separation and a remarkable decrease in the size of droplets (Gao et al., 2008a). Therefore, the number of droplets increased, which was further confirmed by conductivity measurements. The opposite effects caused by the water added on IL based microemulsions with same composition except continuous oil attracted us to study the role of the water.

### 3.3 Ionic liquid based lyotropic liquid crystal systems

Liquid crystals are liquid anisotropic compounds, whose properties are intermediate between that of the crystalline solid state and that of the liquid state. The refractive index, the electric permittivity, the magnetic susceptibility, and the mechanical properties of a liquid crystal depend on the direction in which these quantities are measured (Binnemans, 2005). The investigations of the lyotropic liquid crystalline phase formation containing ILs are also of great interest.

Davis and his coworkers (Davis et al., 1998) obtained a novel IL by anion metathesis with  $\text{NaPF}_6$  after the imidazole-ring miconazole reacting with alkyl iodides to form imidazolium cations, which exhibited lyotropic liquid crystalline behavior while inducing the gelation of benzene. Firestone's group reported that lyotropic liquid crystalline formed in  $[\text{C}_{10}\text{mim}]\text{Br}$ -water (5–40% wt%) system (Firestone et al., 2002). They also obtained anisotropic gold nanoparticles with a variety of sizes and morphologies in the nanostructured  $[\text{C}_{10}\text{mim}]\text{Cl}$ -water ionogel template by photochemical reduction of  $\text{HAuCl}_4$  (Firestone et al., 2005).

Chen and his coworkers (Zhang et al., 2007) reported the formation of two lyotropic liquid crystals formed in a ternary system of  $[\text{C}_{16}\text{mim}]\text{Cl}$ , 1-decanol, and water at 298 K, where one was the hexagonal phase connected to the  $[\text{C}_{16}\text{mim}]\text{Cl}$ -water axis and the other was the lamellar phase in the center in the phase diagram (Figure 11). The formation of liquid



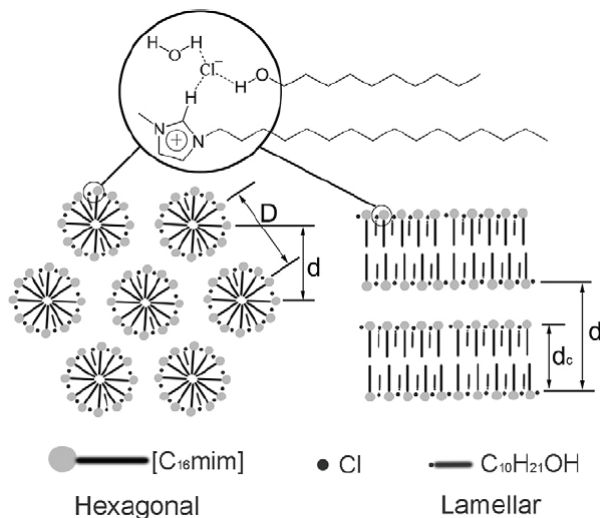


Fig. 11. Sectional schematic graph of possible structures formed in the hexagonal and lamellar phases. H-bonded network comprising  $H_2O$ ,  $Cl^-$ , the imidazolium cation, and  $C_{10}H_{21}OH$  (top). Reprinted from Zhang et al. (2007).

crystalline phases is believed to arise from a hydrogen-bonded network comprised of an imidazolium ring, anion, 1-decanol, and water. Two types of lyotropic liquid crystalline phases, hexagonal and lamellar, formed in the ternary mixtures of  $[C_{16}mim]Br/p$ -xylene/water, where the lattice parameters depended on the content of surfactant and water (Zhang et al., 2007). Phase behaviors of three long-chained imidazolium ILs, i.e.,  $[C_{12}mim]Br$ ,  $[C_{14}mim]Br$  and  $[C_{16}mim]Br$ , with  $p$ -xylene and water were studied by Li et al. For the first time, the formation of a lyotropic bicontinuous cubic phase in imidazolium-type IL system was reported (Li et al., 2009b). The hexagonal lyotropic liquid crystalline phase formed in the ternary system of the  $[C_{12}mim]Br$  in aqueous solution of  $[C_4mim][BF_4]$  (Wu et al., 2009b). In addition, it was found that the cylindrical units compacted much denser for the hexagonal phases formed by  $[C_{12}mim]Br$  in comparison with that formed by dodecyltrimethylammonium bromide (DTAB).

It was reported that a lamellar phase could be formed in aqueous solutions of Brij-97 by solubilizing  $[C_4mim][PF_6]$  and  $[C_4mim][BF_4]$  (Wang & Zhou, 2009).  $[C_4mim][PF_6]$  was dominantly penetrated between the OE chains of surfactant molecules, whereas  $[C_4mim][BF_4]$  was mainly located in the water layer of hexagonal phases and therefore, the strength of the network of hexagonal phase formed in the Brij-97/water/ $[C_4mim][BF_4]$  system was stronger than that of the Brij-97/water/ $[C_4mim][PF_6]$  system.

However, the reports on the molecular aggregations using IL as co-surfactants are still scarce in the literature. As a kind of co-surfactant, ILs are superior to alcohol because of its negligible vapor pressure, high stability and viscosity. Friberg et al. (Friberg et al., 2000) studied the solubilization of  $[C_4mim][PF_6]$  in the lamellar phase of Brij-30/water system, and the results showed that IL can be solubilized into the lamellar phase without changing the dimensions of the amphiphilic layer. Wang et al. (Wang et al., 2005) determined the phase diagram of ternary system of Brij-97/IL ( $[C_4mim][PF_6]$  or  $[C_4mim][BF_4]$ )/water and investigated the location of IL in the hexagonal liquid crystal. Ge et al. (Ge et al., 2007)



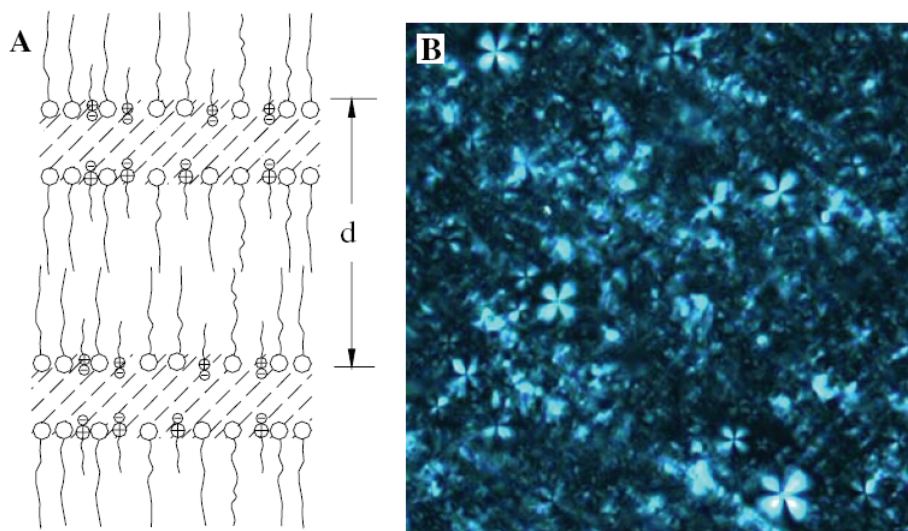


Fig. 12. Structure illustration (A) and typical micrograph (B) of lamellar phase in Brij-30/[C<sub>4</sub>mim][PF<sub>6</sub>]/H<sub>2</sub>O system. The weight ratio of B is Brij-30: [C<sub>4</sub>mim][PF<sub>6</sub>]: H<sub>2</sub>O = 54:6:40. Reprinted from Ge et al. (2007).

reported the microstructure of lamellar liquid crystal composed of Brij-30, [C<sub>4</sub>mim][PF<sub>6</sub>] and water (Figure 12), where the structure strength was enhanced by increasing the amount of Brij-30 and [C<sub>4</sub>mim][PF<sub>6</sub>] and impaired with the increase of water content. The lubrication properties of the ternary system were investigated and the effect of IL on the lubrication properties of traditional lamellar phase was confirmed.

Su et al. (Xiao et al., 2008) fabricated a new type of thermotropic liquid-crystalline photosensitive supramolecular ionic self-assembly of polyelectrolyte and functional unit azobenzene IL crystal (azo-ILC), where the thermal and phase behaviors can be modulated by changing the spacer length (methylene units in azo). Ma et al. (Ma et al., 2008) found that the addition of very small amounts of an alcohol or water into tri-*n*-decylmethylphosphonium chloride and bromide salts (1P10X) induced the formation of liquid crystalline, where strong association between the hydroxyl groups of alcohol or water and the head groups of 1P10X is indicated.

However, little attention has been given to the protein crystallization system where IL is added. Li et al. found that the addition of [C<sub>4</sub>mim][BF<sub>4</sub>] could promote the crystallization of lysozyme, which was probably resulted from the influence of the ionic polarization and kinetics in the lysozyme crystallization (Li et al., 2008c).

### 3.4 Ionic liquid based Vesicles and gels

Vesicles represent one class of self-assembly formed by phospholipids and synthetic surfactants. Generation of vesicles from single surfactants or from mixtures of anionic and cationic surfactants has been reported over the last several years.

Diakyl dimethylammonium bromide formed bilayer membranes in the designed IL systems and ionophilic ether groups of ILs were found to be indispensable for the stable solvation of ammonium bilayers (Nakashima & Kimizuka, 2002). This is the first report which supported

that IL is in favor of the formation of surfactant vesicle phase. Kimizuka and his coworkers (Kimizuka & Nakashima, 2001) reported that stable bilayer membranes formed when glycolipids were dispersed in sugar-philic ether-containing ILs, which displayed reversible thermal transformation from fibrous assemblies to vesicles. Marangoni and his coworkers (Singh et al., 2009) reported the formation of spontaneous vesicle in the binary mixture of SDS and an IL amphiphile, hexylpyridinium tetrafluoroborate. Strong electrostatic interactions between bulky organic ions are the main force of the formation of vesicle aggregates.

Tang et al. (Tang et al., 2006) reported that Brij-76 were temperature dependant on the self-assembly processes in  $[\text{C}_4\text{mim}][\text{BF}_4]$ , where passed gel, clear solution, vesicles and emulsion transformations at 30, 85, 90 and 110 °C, respectively. Zhao et al. (Zhao et al., 2009a) investigated the phase behavior of ternary system which was composed of  $[\text{C}_{16}\text{mim}]\text{Cl}$ , SDS and water. It was found that a novel gel phase with quite high water content could be fabricated and the lamellar structure was obtained in SDS-rich region. Both the hydrophobic interaction of alkyl chains and interactions between oppositely charged head groups played important roles for the gel formation.

The self-assembled surfactant vesicles formed by the fluorosurfactant  $\text{Zn}(\text{OOCCH}_2\text{C}_6\text{F}_{13})_2$  or by mixtures of tetradecyldimethylamine oxide ( $\text{C}_{14}\text{DMAO}$ ) and  $\text{Zn}(\text{OOCCH}_2\text{C}_6\text{F}_{13})_2$  were reported by Hao's group (Hao et al., 2005). Tan et al. (Tan et al., 2009) reported that the gelation of  $[\text{C}_4\text{mim}][\text{PF}_6]$  were induced by the self-assembly of gelators, where the mean minimum concentrations were found to be less than 2 wt% (Figure 13). The similar ion conductivities of  $[\text{C}_4\text{mim}][\text{PF}_6]$  gels to those of the pure  $[\text{C}_4\text{mim}][\text{PF}_6]$  indicated that the supramolecular structures in the  $[\text{C}_4\text{mim}][\text{PF}_6]$  gels had apparently no effect on the mobility of the ions. Thus, the  $[\text{C}_4\text{mim}][\text{PF}_6]$  gels formed by the gelators may be used as electrolytes in electrochemical devices.

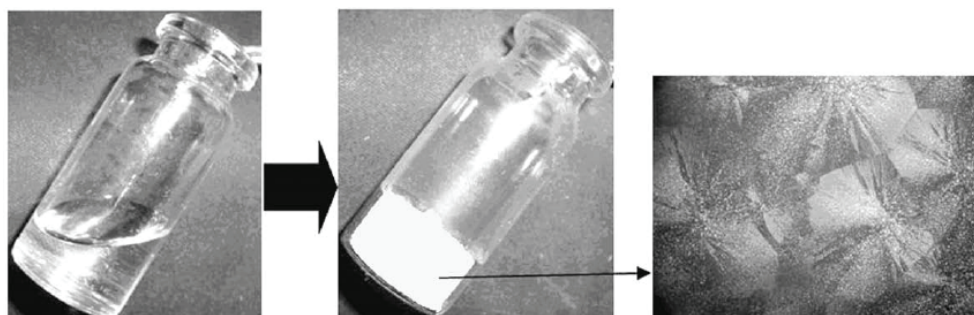


Fig. 13. Schematic illustration of gelation of  $[\text{C}_4\text{mim}][\text{PF}_6]$  and the POM image of a  $[\text{C}_4\text{mim}][\text{PF}_6]$  gel formed in the presence of 2 wt% of BODM (magnification: 1000). Reprinted from Tan et al. (2009).

#### 4. Supramolecular structures based on the host networks in ionic liquids

Generally, ILs are considered as homogeneous solvents, similar to the normal molecular solvents. However, it has been found that supramolecular networks exist in pure ILs, especially in imidazolium ILs, which have already been extensively reviewed in the literature (Dupont, 2004; Leclercq & Schmitzer, 2009a). Here, we illustrate the self-

organisation of ILs and some of the organisations observed in pure ILs in order to raise the interesting in exploring how the supramolecular structure of ILs affect the formation of supermolecules and supramolecular assemblies.

#### 4.1 Supramolecular networks in ionic liquids

##### 4.1.1 Supramolecular structures in solid state

A typical supramolecular model for imidazolium ILs in solid state (Dupont, 2004; Leclercq & Schmitzer, 2009a), suitable to small and spherical anions with symmetric cations, came from an overview of X-ray analyses results (Choudhury et al., 2005, 2006; Dupont et al., 2000; Fuller et al., 1994; Golovanov et al., 2005; Gordon et al., 1998; Holbrey et al., 2004; Saha et al., 2003), which indicates the existence of an extended network of cations and anions connected together by hydrogen bonding (Figure 14A) (Dupont, 2004; Leclercq & Schmitzer, 2009a). The unimeric unit is always constituted by one imidazolium cation surrounded by at least three anions and each anion is surrounded by at least three imidazolium cations. With respect to the specific number of anions/cations that surround the cation/anion, it depends on the geometry of anion and the nature of the imidazolium residues. The strongest hydrogen bond always involves the most acidic H(2) of imidazolium ring, followed by H(4) and H(5) of the imidazolium cation and sometimes by the proton of the  $\alpha$ -carbon on nitrogen. These hydrogen bonds, which are mostly electrostatic in nature, are weak to moderate ( $H \cdots X$  bond lengths  $> 2.2$  angstrom,  $C-H \cdots X$  bond angles between  $100^\circ$  and  $180^\circ$ ). Besides hydrogen bonding, other interactions (such as electrostatic interactions,  $\pi$ - $\pi$  stacking,  $C-H \cdots \pi$  interactions and combination of these interactions) between the cations and the anions can also lead to the formation of the supramolecular network. For example, anions with phenyl residues (such as  $TPhB^-$ ) can interact with imidazolium cations via  $C-H \cdots \pi$  interactions and form a supramolecular framework (Dupont et al., 2000). Recently, Leclercq et al. (Leclercq et al., 2009b) synthesized  $N,N'$ -diaromatic diimidazolium cations, which include electron-rich (aromatic) and electron-poor (imidazolium) rings, and found that a perfect alternation of electron-rich and electron-poor ring can maximize the  $\pi$ - $\pi$  stacking.

Furthermore, the above two-dimensional organization may evolve to three-dimensional structures through the chains of imidazolium rings (Figure 14B). In some cases,  $\pi$ - $\pi$  stacking interactions among imidazolium rings, and a relatively weak  $C-H \cdots \pi$  interactions through the methyl group and the  $\pi$  system of the imidazolium ring can also be found in 1-alkyl-3-

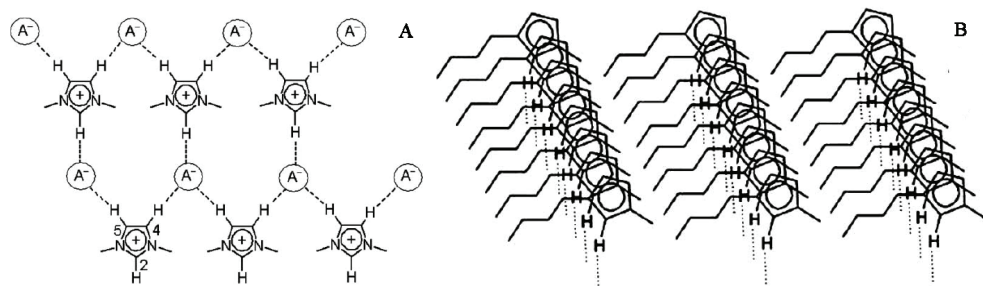


Fig. 14. Simplified two- (A) and three-dimensional (B) supramolecular structures of imidazolium ILs. Reprinted from Leclercq & Schmitzer (2009a).

methylimidazolium salts. Particularly, in some special confined circumstances, such as the hollow interiors in multi-walled carbon nanotubes and the nanospace between graphite walls, these weak interactions may be strengthened, resulting in high-melting-point crystals of imidazolium ILs (Chen et al., 2007; Sha et al., 2009). This molecular arrangement can form channels, where the spherical anions are accommodated as one-dimensional chains. This structural pattern also rests with the geometry of anion and the nature of the imidazolium residues.

Therefore, Dupont (Dupont, 2004) proposed that the best description for the imidazolium salts in the solid state is  $[I_xX_{x-n}]^{n+}[I_{x-n}X_x]^{n-}$ , where I represents the imidazolium cation and X represents anion.

As for other ILs, such as tetrabutylammonium trifluoromethanesulfonate, who is short of hydrogen band,  $\pi$ - $\pi$  stacking interactions and C-H  $\cdots \pi$  interactions, electrostatic interactions are important in the construction of the extended networks (Leclercq et al., 2008). Recently,

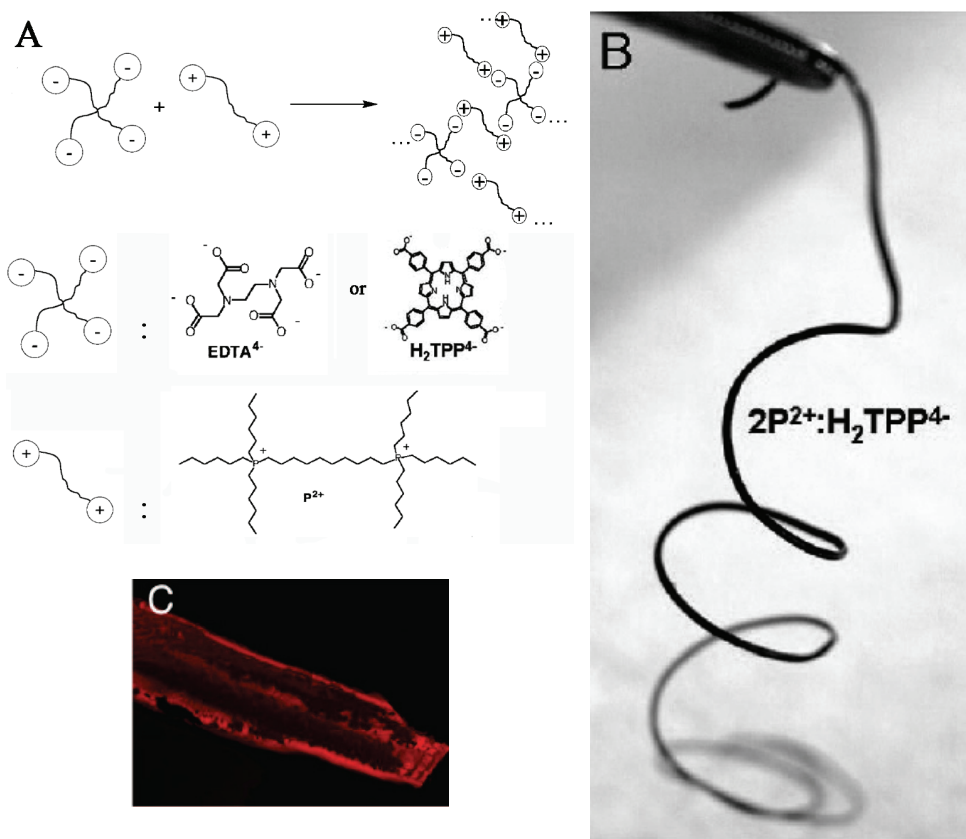


Fig. 15. (A) Schematic diagram of the formation of a supramolecular ionic network and the molecular structures of the corresponding units. (B) Photograph and (C) fluorescent micrograph ( $\lambda_{\text{ex}} = 514 \text{ nm}$ ) of an ionic network fiber prepared from  $2\text{P}^{2+}:\text{H}_2\text{TPP}^{4-}$ . Reprinted from Wathier & Grinstaff (2008) and Craig (2009).

Wathier and Grinstaff (Wathier & Grinstaff, 2008) prepared an IL with ionic networks using a phosphonium dication ( $P^{2+}$ ) and a tetraanion, ethylenediaminetetraacetate ( $EDTA^{4-}$ ) (Figure 15A), which has a viscosity of about  $1.2 \times 10^4$  Pa s. When  $EDTA^{4-}$  was replaced by *para*-tetracarboxy-5,10,15,20-tetraphenyl-21H,23H-porphine,  $H_2TPP^{4-}$  (Figure 15A), an IL with a viscosity of ca.  $10^6$  Pa s at 25 °C was obtained. While the  $2P^{2+}:H_2TPP^{4-}$  IL was heated to 160 °C, a fiber could be hand-pulled from the liquid (Figure 15B). Within the fiber, the porphyrins retained their fluorescence properties (Figure 15C), thus suggesting the potential utility in sensors, etc. Furthermore, the above work suggests that ionic networks formed from effective noncoordinating ionic pairs, in particular those found in ILs, might provide an interesting, useful, and complementary strategy for the formation of supramolecular structures (Craig, 2009).

#### 4.1.2 Supramolecular structures in liquid phase

When ILs are transformed from crystal to liquid state, the long-range order is lost, but long-range Coulomb interactions between cations and anions in ILs are maintained (Dupont, 2004; Leclercq & Schmitzer, 2009a). This concept is supported by the results of IR (Dieter et al., 1988; Ozawa et al., 2003; Talaty et al., 2004), Raman (Katayanagi et al., 2004; Talaty et al., 2004), neutron diffraction analysis (Deetlefs et al., 2006; Hardacre et al., 2003), X-ray reflectivity experiment (Carmichael et al., 2001), small-angle X-ray diffraction analysis (Bradley et al., 2002) and large-angle X-ray scattering experiment (Kanzaki et al., 2009), indicating that 1,3-dialkylimidazolium ILs have analogous structural patterns in the solid and liquid phases. It is the long-range Coulomb interactions in ILs that can lead to longer spatial correlations than those in comparable classic van der Waals organic liquids (Cang et al., 2003). In other words, the supramolecular structures observed in crystal are reserved in liquid state (Dupont, 2004; Leclercq & Schmitzer, 2009a). Although Fujii et al. (Fujii et al., 2008b) found that the liquid structure of  $[C_2mim][Tf_2N]$  IL is significantly different from its layered crystal structure, the ordered structure still exists, where the charge-charge interaction rather than the hydrogen bonding plays an essential role. Besides imidazolium ILs, other ILs (such as N-alkyl-N-methylpyrrolidinium ILs (Fujii et al., 2008a; Fukuda et al., 2008)) have also order structures in liquid state.

Several MD simulations (Lopes & Padua, 2006; Urahata & Ribeiro, 2004; Wang & Voth, 2005), especially the work of Lopes and Padua (Lopes & Padua, 2006), suggested the presence of polar domains that are formed by the head groups of the cations and anions, and of nonpolar domains that are formed by the alkyl groups in 1-alkyl-3-methylimidazolium ILs ( $C_n \geq C_4$ ). As the length of the alkyl chain increases, the nonpolar domains become larger and more connected, and cause swelling of the ionic network, in a manner analogous to microphase separation (Lopes & Padua, 2006). Recently, the results of X-ray diffraction (XRD) experiment (Triolo et al., 2007), fluorescent spectra (Hu & Margulis, 2006), Raman spectra (Iwata et al., 2007; Shigeto & Hamaguchi, 2006), NMR (Mele et al., 2006), femtosecond solvation dynamics study (Adhikari et al., 2007) and optical Kerr Effect spectra (Xiao et al., 2007) of 1-alkyl-3-methylimidazolium ILs also suggested the presence of heterogeneous structures. Furthermore, the result of the XRD experiment also reflected that the size of the inhomogeneous structures is proportional to the length of the alkyl chain (Triolo et al., 2007). Thus, this suggests that the above-mentioned nanodomains are built up by the aggregation of neutral alkyl chains surrounded by charges, whose uniform spatial distribution is determined by the strong electrostatic interactions (Triolo et al., 2007). Thus,



there will be a competition between the interactions of a given solute with those two regions (Blesic et al., 2009a). Rebelo et al. (Rebelo et al., 2007) suggested that a nonpolar solute (e.g., n-hexane) will interact preferentially with the nonpolar domains, while a dipolar or associative solutes (e.g., water) will interact with the polar domains. Therefore, this kind of heterogeneous structure of ILs will make the solubility and reactivity of solutes in ILs obviously different from those in the normal molecular solvents.

#### 4.1.3 Thermotropic liquid crystal phase of ionic liquids

As for imidazolium ILs with long alkyl chains ( $C_n \geq C_{12}$ ), liquid crystal (LC) phase often appears in the course of increasing temperature (Bowlas et al., 1996; Bradley et al., 2002; De Roche et al., 2003; Getsis & Mudring, 2008; Holbrey & Seddon, 1999; Lee et al., 2000; Lee et al., 1997; Li et al., 2005b; Zhou & Antonietti, 2004). If an anion has a long alkyl chain, the long alkyl chains on the imidazolium ring are not necessary for the formation of LC (Mukai et al., 2004). In addition, some metal complex anion, such as  $PdCl_4^-$  and  $CuCl_4^-$ , can be applied (Bowlas et al., 1996; Hardacre et al., 2001; Lee et al., 2004; Lin & Vasam, 2005). Generally, the temperature range for LCs can be adjusted by altering counter anion and the length of alkyl chain.

Up to now, most of the found LC structures of imidazolium ILs are smectic A phase, consisting of interdigitated bilayers. This supramolecular structure can be considered as the result of the alternate assembling of ionic layers and van der Waals layers. In the former, the ionic head groups interact with the counterions through Coulomb force, while the latter build from (anti)parallel stacking of the alkyl chains through van der Waals force. Moreover, the

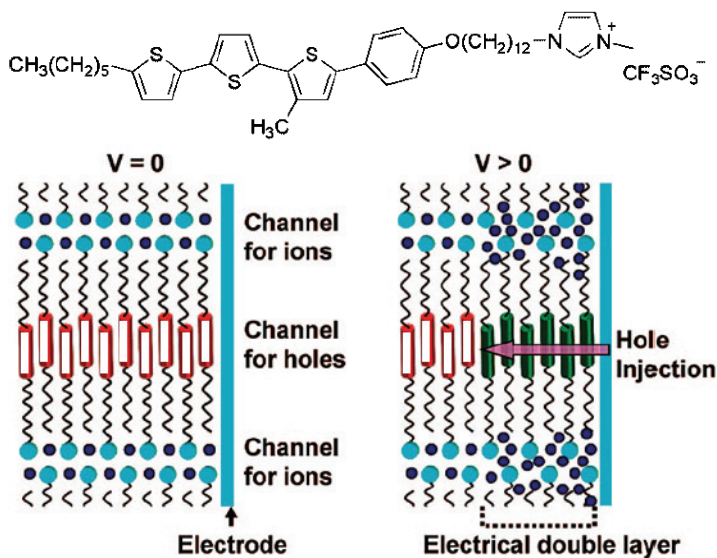


Fig. 16. Molecular structure of 1-methylimidazolium ILs containing phenylterthiophene moiety (up), and schematic image of a nanostructured liquid crystal consisting of ionic and  $\pi$ -conjugated moieties (bottom): blank cylinders are neutral phenylterthiophene moieties; dark cylinders are the oxidized ones; smaller spheres and larger plates are triflate anions and imidazolium moieties, respectively. Reprinted from Yazaki et al. (2008a).

hydrogen bonds between the H-atoms of imidazolium cations and anions are important in the formation and stabilization of ionic layers (Lee et al., 2000; Lee et al., 2004; Lee et al., 1997).

The functionalization of imidazolium is a useful method for the application of imidazolium ionic LCs. Recently, Kato and collaborators (Yazaki et al., 2008a) synthesized a new ILs with a 1-methylimidazolium group as an ion-conductive part and  $\pi$ -conjugated phenylterthiophene moiety related to the electronic charge transport (Figure 16). In its smectic A phase, the ionic and the  $\pi$ -conjugated moieties were nanosegregated, leading to the formation of two-dimensional ion-conductive channels between hole transport layers (Figure 16) (Yazaki et al., 2008a). Consequently, the holes were injected from the anode and transported into the hole transport layers consisting of phenylterthiophene moieties (Figure 16), resulting in the oxidation of the  $\pi$ -conjugated moieties (Yazaki et al., 2008a). In experiment, the IL exhibited electrochromism in the LC state without a liquid electrolyte layer, unlike conventional redox-active conjugated polymers and liquid crystals (Yazaki et al., 2008a). This LC would be applied to various electronic devices such as light-emitting electrochemical cells as well as the electrochromic devices.

The structure of imidazolium ionic LCs is much simple, which makes its application in many fields confined. In order to resolve this problem, much effective effort has been made (Goossens et al., 2008; Kumar & Pal, 2005; Pal & Kumar, 2006; Seo et al., 2007; Yasuda et al., 2010; Yazaki et al., 2008b; Yazaki et al., 2010; Yoshio et al., 2004; Yoshio et al., 2006; Yoshio et al., 2007; Yoshizawa et al., 2004; Zhang et al., 2008d), especially the work of Kato and collaborators (Yasuda et al., 2010; Yazaki et al., 2008b; Yazaki et al., 2010; Yoshio et al., 2004; Yoshio et al., 2006; Yoshio et al., 2007). They observed the appearance of a hexagonal columnar LC structure in 1-methylimidazolium ILs with tri-alkoxy substituted phenyl groups, a class of LC mesogens, attached to the nitrogen atom (Yoshio et al., 2004; Yoshio et al., 2006; Yoshio et al., 2007). Besides a wide temperature range of LC phase (Yoshio et al., 2004; Yoshio et al., 2006; Yoshio et al., 2007) and tunable feasible adjustment of LC properties by altering counter anions (Yoshio et al., 2007), the synthesized compounds in columnar LC state were highly anisotropic ion-conductive in one-dimension (Yoshio et al., 2004; Yoshio et al., 2006; Yoshio et al., 2007), which would be useful for transportation of ions, energy, and information at the nanometer level. Recently, Kato et al. (Yazaki et al., 2008b) prepared two new 1-methylimidazolium-based ionic LCs, containing an L-glutamic acid moiety and bis(alkyloxy)phenyl groups (Figure 17). The ionic conductivities and LC structures of the obtained 1-methylimidazolium ILs could be conveniently adjusted by anions, which would potentially be used as an on-off switch of ions (Figure 17) (Yazaki et al., 2008b).

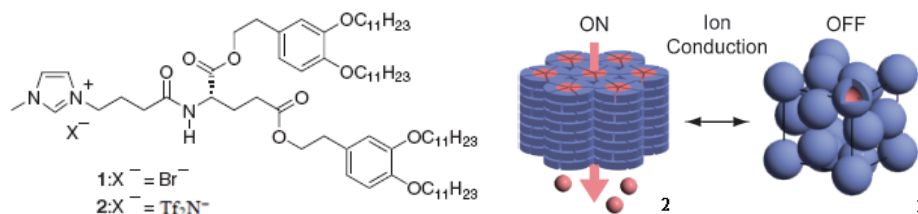


Fig. 17. Molecular structures of 1-methylimidazolium ILs containing an L-glutamic acid moiety and bis(alkyloxy)phenyl groups (left), and schematic illustration of an ideal on-off switch of ion conduction using the structural change from columnar to micellar cubic LC structures (right). Reprinted from Yazaki et al. (2008b).

Besides imidazolium ionic LCs, other thermotropic ionic LCs based on pyridinium (Bowlas et al., 1996; Cruz et al., 2000; Cui et al., 2002; Gordon et al., 1998; Neve et al., 2000; Neve et al., 2001; Taubert, 2004), quaternary ammonium (Alami et al., 1993; Arkas et al., 1999; Lu et al., 1997; Pott & Meleard, 2009; Tittarelli et al., 1997), quaternary phosphonium (Abdallah et al., 2000; Chen et al., 2002; Gowda et al., 2004), pyrrolidinium (Goossens et al., 2009), dithiolium (Artzner et al., 1997) and guanidinium ILs (Kim et al., 2005; Mathevet et al., 2005; Sauer et al., 2008) have also been explored. Two important phenomena should be especially noticed. Firstly, some of them have several kinds of liquid-crystalline structures. For example, with the change of alkyl chain length and counter anions, highly ordered smectic phases (the smectic E phase and the uncommon smectic T phase), smectic A phases, and hexagonal columnar phases were observed in the pyrrolidinium ILs (Goossens et al., 2009). Secondly, the behaviors of tri-alkyl-methyl-ammonium ionic LCs may be fine-tuned further to well defined hydrophobic thickness corresponding to uneven numbers of mean alkyl carbons, by the use of simple binary liquid mixtures (Pott & Meleard, 2009).

## 4.2 Inclusion phenomenon of guest compounds in the ionic liquid network

As the above description, neat imidazolium ILs have supramolecular framework. Furthermore, up to now, much evidence indicated that some of the supramolecular networks can be reserved when ILs are mixed with other materials and inclusion-type structures are formed.

### 4.2.1 Inclusion of water in ionic liquids

Because ILs can absorb significant amount of water from the atmosphere and trivial water is difficult to be removed, water becomes the most common impurity in ILs (Huddleston et al., 2001; Seddon et al., 2000; Takamuku et al., 2009). The existence of water in ILs may affect many of their physical and chemical properties, such as polarity, viscosity, conductivity, and reactivity as well as solvation and solubility properties (Brown et al., 2001; Cammarata et al., 2001; Najdanovic-Visak et al., 2003; Schroder et al., 2000; Widegren et al., 2005).

In order to explain the large differences in the effect of water on the diffusion coefficient for neutral and for ionic species in imidazolium IL media, Compton et al. (Schroder et al., 2000) postulated that "wet" ILs may not be regarded as homogeneous solvents, but have to be considered as "nano-structured" with polar and non-polar regions.

Through the research based on attenuated total reflectance IR spectroscopy, Cammarata et al. (Cammarata et al., 2001) considered that water molecules absorbed from the air by 1-alkyl-3-methylimidazolium ILs are mostly in the "free" (not self-associated) state, most of which act as bridge between anions ( $X^-$ ), such as  $BF_4^-$  and  $PF_6^-$ , via hydrogen bond of type  $X^- \cdots HOH \cdots X^-$ . Later, Mele et al. (Mele et al., 2003) found that the H(2), H(4) and H(5) within the imidazolium ring could interact with water molecules via hydrogen bond of type  $C-H \cdots O$  at very low water content by NMR spectroscopy through intermolecular nuclear Overhauser enhancements on  $[C_4mim][BF_4]$  IL. Based on the MD simulations and NMR experiment, Mele et al. (Moreno et al., 2008) further indicated that the ions of  $[C_4mim][BF_4]$  IL are selectively coordinated by individual water molecules, but the ionic network is largely unperturbed at low water content. Recently, Zhang et al. (Zhang et al., 2008c) found that water molecules tend to interact with the anion moiety of ILs first, via hydrogen bond, rather than with hydrogen atoms within the imidazolium, which is further confirmed by the most recent work of Takamuku et al. (Takamuku et al., 2009). It is also found that water is not homogeneously mixed with  $[C_2mim][BF_4]$  IL at low water content (Zhang et al., 2008c).



In addition, no direct hydrogen bonds between cations and anions were observed in the crystal structure of [1,3-dibenzylimidazolium]Br·H<sub>2</sub>O, but water molecules connected anions and cations in the supramolecular framework (Leclercq et al., 2009c). In other words, water molecules were included in the crystal lattice.

Thus, the existing states of water molecules in the liquid and crystal phases support the hypothesis of polar and non-polar regions of the supramolecular network. From another point of view, at low water content, the water could be regarded as guest included in the supramolecular framework of imidazolium ILs.

#### 4.2.2 Inclusion of aromatic compounds in ionic liquids

After mixing of some imidazolium ILs with excess of aromatic hydrocarbons, biphasic mixtures are obtained. The lower layer is IL-rich phase, which exhibits the characteristics of typical liquid clathrates, i.e., low viscosity (relative to the initial neat ILs), immiscibility with excess aromatic solvents, and non-stoichiometric (but reproducible) compositions, while the concentration of IL is too low to be detected in the upper layer. Recently, it was found that the immiscibility gap became smaller when the polarity of substituted benzenes increased and their molecular size decreased (Shiflett & Yokozeki, 2008; Shiflett et al., 2009; Shiflett & Niehaus, 2010). However, when both dipole and quadrupole moments are present in an aromatic compound, they have an antagonistic effect, reducing the solubility in the IL (Shimizu et al., 2009). Up to now, such liquid clathrates or IL-biphasic systems have been used in the fields of organic syntheses (Boxwell et al., 2002; Clavier et al., 2008; DeCastro et al., 2000; Surette et al., 1996), polymerization (Csihony et al., 2002), separations of aromatics from hydrocarbons (Arce et al., 2007; Selvan et al., 2000) and so on.

Holbrey et al. (Holbrey et al., 2003) obtained crystalline [C<sub>1</sub>mim][PF<sub>6</sub>]·0.5C<sub>6</sub>H<sub>6</sub> by cooling the lower phase of the [C<sub>1</sub>mim][PF<sub>6</sub>]-C<sub>6</sub>H<sub>6</sub> system to room temperature. The crystal structure of the clathrate (Figure 18A) shows that there is a three-dimensional array of hydrogen-bonded cations and anions, a typical supramolecular structure for imidazolium ILs in solid state. This three-dimensional framework results in the formation of “channels” along the (001) direction of the crystal lattice in which benzene molecules are included by a staggered  $\pi$ - $\pi$  “sandwich” between two imidazolium cations. Later, Lachwa et al. (Lachwa et al., 2006) draw the similar conclusion from the crystal structure of [C<sub>2</sub>mim][NTf<sub>2</sub>]-C<sub>6</sub>H<sub>6</sub> (Figure 18B). However, the formed structure has to allow for a higher proportion of benzene molecules, forming a tube-like structure with a rectangular cross-section around the cations of ILs. The formation of clathrate phases could be regarded as an example of the organization of guest molecules in the pre-organised host network.

Deetlefs et al. (Deetlefs et al., 2005) further indicated that the addition of benzene to [C<sub>1</sub>mim][PF<sub>6</sub>] leads to an expansion of the cation-cation contacts through the neutron diffraction study on the [C<sub>1</sub>mim][PF<sub>6</sub>]-C<sub>6</sub>H<sub>6</sub> mixtures. Moreover, around the benzene molecule, alternating cation-anion layers are observed with the first-shell anions interacting with the ring hydrogens while the cations interact with the ring electrons. The incorporation of benzene is found to displace the anions with approximate three benzenes replacing each anion, suggesting benzene intercalation into the structure as found in the solid. Benzene is also found to be homogeneously distributed throughout the IL with no evidence of micellar formation.

With respect to the inclusion crystal [C<sub>2</sub>mim][NTf<sub>2</sub>]-C<sub>6</sub>H<sub>6</sub>, through the MD study of its congruent melting, Alavi et al. (Kowsari et al., 2010) further found that the presence of a

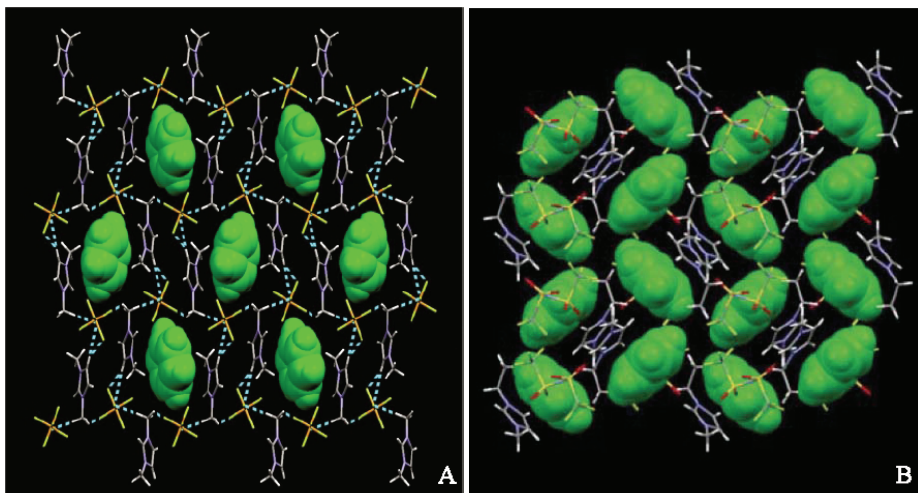


Fig. 18. Packing patterns in the crystal structures of  $[\text{C}_1\text{mim}][\text{PF}_6] \cdot 0.5\text{C}_6\text{H}_6$  (A) and  $[\text{C}_2\text{mim}][\text{NTf}_2] \cdot \text{C}_6\text{H}_6$  (B). Reprinted from Holbrey et al. (2003) and Lachwa et al. (2006).

stoichiometric number of benzene molecules does not affect the nearest neighbor ionic association between  $[\text{C}_2\text{mim}]^+$  and  $[\text{NTf}_2]^-$ , but increases the mean-square displacements of both cations and anions compared to pure liquid  $[\text{C}_2\text{mim}][\text{NTf}_2]$ , showing that second shell ionic associations are weakened.

Besides imidazolium ILs, other ILs based on quaternary ammonium (Coleman et al., 1990; Pickett, 1985), pyridinium (Christie et al., 1991) and so forth (Gaudet et al., 1988) can also form liquid/solid clathrates with aromatic molecules, in which suitable anions are important.

#### 4.2.3 Co-crystals of ionic liquids

It has been reported that imidazolium ILs are able to form co-crystals with quaternary ammonium ILs with same anions (Leclercq et al., 2007, 2008), *e. g.*,  $[\text{C}_2\text{mim}][\text{TfO}]$  with [tetrabutylammonium][TfO] ( $[\text{Bu}_4\text{N}][\text{TfO}]$ ) (Leclercq et al., 2008). The co-crystal structure of  $[\text{C}_2\text{mim}][\text{TfO}]$  and  $[\text{Bu}_4\text{N}][\text{TfO}]$  (Figure 19) could be described as a supramolecular framework formed by  $\text{C}_2\text{mim}^+$  and  $\text{TfO}^-$  through hydrogen bonding, in which all  $\text{Bu}_4\text{N}^+$  are trapped (Leclercq et al., 2008). This phenomenon may be considered to be another example of the inclusion of guest molecules in the supramolecular host network.

Besides the above three kinds of molecules, gas molecules (such as  $\text{CO}_2$ ) (Costantini et al., 2005; Dupont, 2004; Gutowski & Maginn, 2008; Huang et al., 2006; Weingartner, 2008) and (bio)macromolecules (Dupont, 2004; Feher et al., 2007; Leclercq & Schmitzer, 2009a), even nanoparticles (Dupont, 2004; Leclercq & Schmitzer, 2009a; Lee et al., 2009), may act as guests included in the supramolecular host framework of ILs.

### 5. Effects of ionic liquids on the formation of supramolecular structures

ILs can not only participate directly in the formation of supramolecular systems, but also influence the formation of various supramolecular structures.

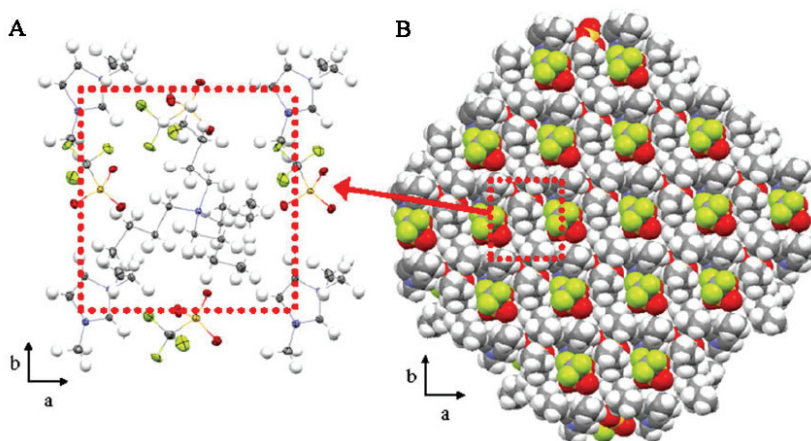


Fig. 19. (A) View of the local assembly around a tetrabutylammonium cation ( $\text{Bu}_4\text{N}^+$ ) and (B) space-filled view of the co-crystal of  $[\text{C}_2\text{mim}][\text{TfO}]$  and  $[\text{Bu}_4\text{N}][\text{TfO}]$ . Reprinted from Leclercq et al. (2008).

### 5.1 Effects of ionic liquids on the formation of polyrotaxanes and polypseudorotaxanes

Polyrotaxanes (PRs) and polypseudorotaxanes (PPRs) formed by CDs in the presence of ILs have been studied. Samitsu et al. (Samitsu et al., 2006) used ILs as new solvents for PR, consisting of  $\alpha$ -CD and poly (ethylene glycol). They found that halogen-containing ILs, such as chlorides or bromides, were good solvents for PRs, regardless of their cations. This discovery was applied in the preparation of IL-containing slide-ring gels (SR gels), which are supramolecular networks of PR swollen with ILs, using a devised “non-drying” technique accompanied by solvent exchange. A kind of PPRs were prepared by supramolecular self-assembly of  $\beta$ -CDs threaded onto the triblock copolymers (Pluronic F127) in  $[\text{C}_4\text{mim}][\text{PF}_6]$  with two different manners (Jing et al., 2007). It was found that not only the PO segments but also many EO segments are included by  $\beta$ -CD molecules in the PPRs. Interestingly, which one, F127 or  $[\text{C}_4\text{mim}][\text{PF}_6]$ , will finally be included inside  $\beta$ -CD, can be controlled by ethanol amount around the initially  $\beta$ -CD/ $[\text{C}_4\text{mim}][\text{PF}_6]$  ICs. At higher ethanol concentration, F127 may squeeze  $[\text{C}_4\text{mim}][\text{PF}_6]$  molecules out from  $\beta$ -CD and thread themselves instead into the cavity of  $\beta$ -CD and finally precipitate with more CDs being stacked (Figure 20).

### 5.2 Effects of ionic liquids on the formation of the supramolecular structures in the extraction systems based on crown ethers

No significant close contacts are observed between ILs and crown ethers based on the study of co-crystallisation of imidazolium based salts with 18-crown-6 (18C6), though coulomb interactions between the ionic (liquid) components and hydrogen bonding are important (Gjikaj et al., 2008). However, because of the influence of ILs to the system of crown ethers, they are being used in the extraction of metal ions, amino acid and so on.

For the first time, Dai et al. (Dai et al., 1999) used the system dicyclohexano-18-crown-6 (DCH18C6) - $[\text{R}_1\text{R}_2\text{mim}][\text{NTf}_2]/[\text{PF}_6]$  to extract  $\text{Sr}^{2+}$ , obtaining the distribution coefficient as

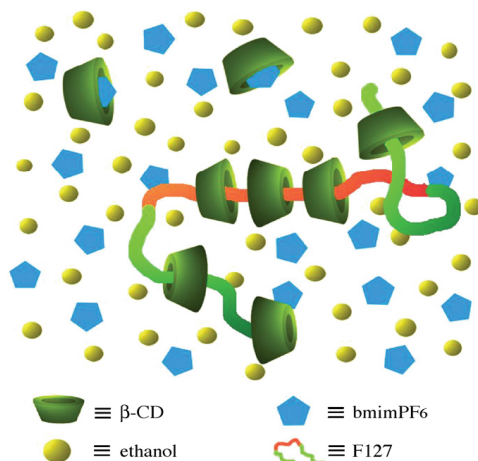


Fig. 20. Schematic representation of the inclusion choice between F127 and [C<sub>4</sub>mim][PF<sub>6</sub>]. Reprinted from Jing et al. (2007).

high as  $10^4$ . The extraction process can be easily tailored by varying the substituting groups in the imidazolium cation and the counter anions. In succession, more and more systems involved ILs and crown ethers were investigated (Chun et al., 2001; Langmaier et al., 2009; Nockemann et al., 2007; Okamura et al., 2010; Stepinski et al., 2010; Visser et al., 2000; Xu et al., 2009). These results discovered that as the alkyl group in the ILs was elongated, the extraction efficiency decreased, but the extraction selectivity increased. The distribution is not only related to the concentration and the hydrophobicity of crown ethers, but also to the composition of the aqueous phase. To increase the extraction efficiency of metal ions, the additives, such as TBP, were added into the system due to the formation of a synergistic adduct (Stepinski et al., 2005). The magnitude of the synergistic enhancement is shown to depend on the alkyl chain length of the ILs [C<sub>n</sub>mim][Tf<sub>2</sub>N] cation, with the effect diminishing as the cation hydrophobicity increases until for [C<sub>10</sub>mim][Tf<sub>2</sub>N].

The traditional crown ether, for example DCH18C6, can extract metal ions efficiently. However, metal ions are not easy to be stripped. In order to overcome this disadvantage, a series of *N*-alkyl aza-18-crown-6 ethers were synthesized (Luo et al., 2004a). These crown ethers in ILs were investigated as recyclable extractants for separation of Sr<sup>2+</sup> and Cs<sup>+</sup> from aqueous solutions. They discovered a strong dependence of selectivity on the type of ILs. Recently, Shimojo et al. (Shimojo et al., 2009) reported the first study on the “intramolecular” synergistic extraction of a metal ion in an IL-based system. Sr<sup>2+</sup> was extracted by a novel extractant  $\beta$ -diketone-substituted diaza-18-crown-6 (H2 $\beta$ DA18C6). By compared with 1-phenyl-3-methyl-4-benzoyl-5-pyrazolone (HPMBP) and *N,N'*-dibenzyl-4,13-diaza-18-crown-6 (DBzDA18C6), they found that H2 $\beta$ DA18C6 provides a remarkably high performance for Sr<sup>2+</sup> extraction into [C<sub>2</sub>mim][Tf<sub>2</sub>N] due to a cooperative “intramolecular” interaction when compared with the “intermolecular” synergy extraction system of the mixture of HPMBP and DBzDA18C6. The two protons from protonated H2 $\beta$ DA18C6 were released to extract Sr<sup>2+</sup>, the transfer of Sr<sup>2+</sup> into [C<sub>2</sub>mim][Tf<sub>2</sub>N] proceeds via the proton exchange reaction.

Because ILs are usually used in the separation of radioactive nuclides and the radiation effect on ILs for the extraction of metal ions is important. The influence of  $\gamma$ -radiation on the IL [C<sub>4</sub>mim][PF<sub>6</sub>] and [C<sub>4</sub>mim][Tf<sub>2</sub>N] during extraction of Sr<sup>2+</sup> by DCH18C6 was studied

(Yuan et al., 2008, 2009). The irradiation of IL influences greatly on this system. The  $\text{Sr}^{2+}$  partitioning in irradiated  $[\text{C}_4\text{mim}][\text{PF}_6]$  decreases as the absorption dose increases. This is the result of the formation of acid during the irradiation of  $[\text{C}_4\text{mim}][\text{PF}_6]$ . Due to the competition between  $\text{H}^+$  and  $\text{Sr}^{2+}$ , the extraction efficiency decreased and can be recovered by simple washing the irradiated  $[\text{C}_4\text{mim}][\text{PF}_6]$  with water.

Besides, stability constants of metal ion complexes with crown ethers in IL aqueous solutions were obtained (Popov et al., 2007) and the solubilization of the ILs  $[\text{C}_n\text{mim}][\text{Tf}_2\text{N}]$  by the presence of crown ether was studied (Rickert et al., 2007). It is also reported that the stability of cesium complexed with 18C6 in ILs is affected by the nature of both cation and anion of ILs (Vendilo et al., 2009; Vendilo et al., 2010b). Moreover, the complex stability is important for the extraction process (Vendilo et al., 2010a).

In the conventional organic solvents extractions, limited solubility of ionic species in nonionic organic solvents is the main problem and the toxicity of free crown ethers makes them unsuitable for industrial use. Task Specific ILs (Bates et al., 2002; Visser et al., 2001) (TSILs) contain specific functionality covalently incorporated within one of the ionic components of the IL, typically within the cation. Therefore, the "crowned" IL-crown ether as a functional group to functionalized IL was performed for a liquid/liquid extraction of metal ions (Park et al., 2006) and molecular-recognition ability (Ishida et al., 2004; Liu et al., 2005). The "crowned" ILs obtain their selectivity through their ability to fine-tune and reorganize their crown ether structure changing their number and type of donor atoms, appending ionizable groups, and modifying their lipophilicity. Ishida et al. (Ishida et al., 2004) designed and synthesized novel imidazolium-based ILs with a pseudo crown-ether moiety. The oxygen lone pairs had a potential as Lewis-basic and/or hydrogen-accepting functionality. Owing to the molecular-recognition ability, the enantiomeric imidazolium cations could differently sense the chirality of the europium complexes. A series of novel ILs comprising crown-ether functionalities in cations or anions (crowned ILs) were prepared and characterized (Liu et al., 2005). The physical properties of different functionalized ILs were different, for example the thermal decomposition temperatures ( $T_{\text{dec}}$ ) of the ILs containing crowned cations are generally 80-100 °C higher than those of the ILs having crowned anions. The ILs functionalized by the crown ether may display potential utility in catalytic application as well as in separation and electrochemical sensing. Luo et al. (Luo et al., 2006) synthesized a new class of TSILs based on the covalent attachment of imidazolium cations to a monoaza-crown ether fragment. These TSILs exhibited lower extraction efficiency than the IL extraction systems using DCH18C6 or N-octylaza-18-crown-6 as extractant. This can be attributed to the coulombic repulsion from the covalently attached imidazolium cation. The selectivity of these TSILs is dependent on the structure of substituents on the imidazolium ring.

The mechanism of ILs-crown ethers system for metal ions extraction has been studied extensively. There are several kinds of mechanisms: cation exchange (Dai et al., 1999; Dietz & Dzielawa, 2001; Dietz et al., 2003; Hirayama et al., 2008; Park et al., 2006; Popov et al., 2007), anion exchange (Jensen et al., 2003), mechanism of multiple distribution (Dietz & Stepinski, 2005). By changing the ILs, the hydrophobicity of the IL cation increase (from  $n=5$  to  $n=10$  in  $[\text{C}_n\text{mim}][\text{Tf}_2\text{N}]$ ), the predominant mode of partitioning changes from ion-exchange involving the cationic portion of the IL to conventional neutral nitrato complex extraction (Dietz et al., 2003). The stereochemistry of crown ethers can also affect the mechanism. Dietz et al. (Dietz et al., 2008) studied the DCH18C6 stereochemistry influence the mode of sodium ion transfer from acidic nitrate media into ILs. DCH18C6 have five

isomers, i.e., cis-syn-cis (csc), cis-anti-cis (cac), trans-syn-trans (tst), trans-anti-trans (tat) and cis-trans (ct) (Figure 21). For the cis isomers, rising nitric acid concentration is eventually accompanied by steeply falling values of the sodium distribution ratio. This was originated the crown ether-mediated exchange of a sodium ion for a hydronium ion in a DCH18C6- $\text{H}_3\text{O}^+$  adduct. In contrast, for the trans isomers, rising aqueous acidity is accompanied by increasing sodium extraction, consistent with partitioning of a neutral sodium nitrate-crown ether complex. A change from a cis to a trans isomer of DCH18C6 alters the predominant mode of sodium ion portioning into  $[\text{C}_{10}\text{mim}][\text{Trf}_2\text{N}]$  from ion-exchange to neutral complex extraction. As a result, the process of extracting can be controlled by the isomers of extractants.

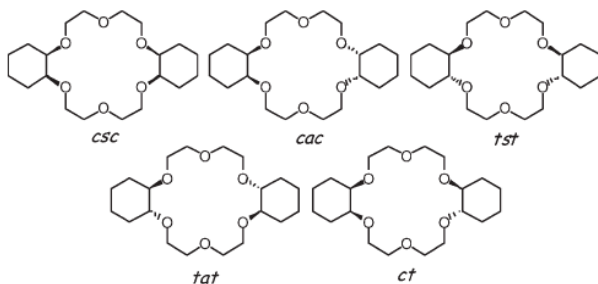


Fig. 21. Molecular structures of the cis-syn-cis (csc), cis-anti-cis (cac), trans-syn-trans (tst), trans-anti-trans (tat), and cis-trans (ct) isomers of DCH18C6. Reprinted from Dietz et al. (2008).

ILs and crown ethers used in biochemistry have also been a field of increasing interest and importance (Kragl et al., 2002; van Rantwijk et al., 2003). Amino acids are hydrophilic and therefore difficult compounds for conventional solvent extraction. Amino acids were not soluble in IL, however, by adding a crown ether to the IL phase, the positive form of amino acids is complexed by the crown ether and the complex is extracted in the IL phase (Carda-Broch et al., 2003). Amino acids Trp, Gly, Ala, Leu were efficiently extracted from aqueous solution as pH 1.5-4.0 (Lys and Arg at pH 1.5-5.5) into  $[\text{C}_4\text{mim}][\text{PF}_6]$  with DCH18C6 (Smirnova et al., 2004). The most hydrophilic amino acids such as Gly were extracted as efficiently as the less hydrophilic ones. Compared to the conventional organic solvents, ILs enabled quantitative recovery of amino acids and eliminated emulsion formation, which usually occurs when cationic or anionic extractants are used.

Shimojo et al. (Shimojo et al., 2006a; Shimojo et al., 2006b) investigated a hydroxyl-group-containing IL with DCH18C6 was capable of quantitative partitioning of heme protein cytochrome c (Cyt-c) via supramolecular complexation and that the resulting Cyt-c-DCH18C6 complex acts as a homogeneous biocatalyst in ILs. While using conventional organic solvents the protein transfer was negligibly small. The partitioning of a protein into ILs is controllable on the basis of hydrophobicity and type of the functional groups of ILs. This is the first report showing protein extraction into ILs.

Extractants comprised calixarene part in IL systems were also investigated (Shimojo & Goto, 2004a; Sieffert & Wipff, 2007). Shimojo et al. (Shimojo & Goto, 2004b) studied the extraction of metal ions by a calix[4]arene-bearing pyridine in a typical IL,  $[\text{C}_8\text{mim}][\text{PF}_6]$ . Pyridinocalix[4]arene showed a high extraction ability and selectivity for  $\text{Ag}^+$  in five different metal ions ( $\text{Ag}^+$ ,  $\text{Cu}^{2+}$ ,  $\text{Zn}^{2+}$ ,  $\text{Co}^{2+}$  and  $\text{Ni}^{2+}$ ). This compound transfers  $\text{Ag}^+$  into IL



phases via a cation-exchange mechanism and form a stable 1:1 complex with  $\text{Ag}^+$ . Recently, calixarene comprising crown ethers have been extensively studied in the IL-extraction system (Chen & Hussey, 2005; Chen, 2007; Luo et al., 2007; Rogers et al., 2004; Tsuda et al., 2006). Luo et al. (Luo et al., 2004b) extracted  $\text{Cs}^{2+}$  into  $[\text{C}_n\text{mim}][\text{Tf}_2\text{N}]$  using calix[4]arene-bis(tert-octylbenzo-crown-6) (BOBCalixC6) as an extractant by an ion-exchange mechanism. The shorter alkyl chain of the ILs, the less solubilities of BOBCalixC6 in the corresponding ILs and the higher distribution coefficients because the less hydrophobic imidazolium cations have higher ion-exchange capability. The addition of  $\text{NaBPh}_4$ , a sacrificial cation exchanger, can decrease the loss of ILs by 24%, as a result, ion exchange take a partial role. MD study of the interfacial behavior in the  $\text{Cs}^+$  and  $\text{Na}^+$  extraction by a calix[4]arene-crown-6 host (L) into ILs  $[\text{C}_4\text{mim}][\text{Tf}_2\text{N}]$  and  $[\text{C}_4\text{mim}][\text{PF}_6]$  demonstrated the IL forms a biphasic system with water (Sieffert & Wipff, 2006a, b). Compared with the classical molecular solvent (chloroform), much longer times are needed to “equilibrate” IL systems. There is more intersolvent mixing with the IL than with chloroform especially the water-in-oil content. In the aqueous phase, there is some excess of  $\text{C}_4\text{mim}^+$  over  $\text{Tf}_2\text{N}^-$ . The  $\text{LCs}^+$  complex and L ligand behave differently and they are better solvated by the IL than by chloroform. They are adsorbed at the chloroform interface and adopt well-defined amphiphilic orientations. At the IL interface, they are poorly attracted. The comparison of  $[\text{C}_4\text{mim}][\text{Tf}_2\text{N}]$  and  $[\text{C}_4\text{mim}][\text{PF}_6]$  of the dry versus humid form of the latter one. They discovered that the importance of humidity. In the  $[\text{C}_4\text{mim}][\text{PF}_6]$ -dry as in the  $[\text{C}_4\text{mim}][\text{Tf}_2\text{N}]$  liquid, the first solvation shell of the “naked”  $\text{M}^+$  ions is composed of solvent anions only, while in the  $[\text{C}_4\text{mim}][\text{PF}_6]$ -humid IL, it comprises from one to three solvent anions and about four  $\text{H}_2\text{O}$  molecules. In the  $\text{LM}^+$  complexes, the cation is shielded from solvent but still somewhat interacts with a solvent anion in the dry ILs and with water in the humid IL. These results provide a number of arguments explaining the specificity and efficiency of IL based extraction systems. Very recently, Xu et al. found that the bis(2-propyloxy)calix[4]crown-6 (BPC6)/ $[\text{C}_n\text{mim}][\text{Tf}_2\text{N}]$  system was highly efficient to remove  $\text{Cs}^+$  from aqueous solution. A dual extraction mechanism, exchange of BPC6- $\text{Cs}^+$  complex and  $\text{Cs}^+$  by  $\text{C}_n\text{mim}^+$  was mentioned (shown in Figure 22) (Xu et al., 2010).

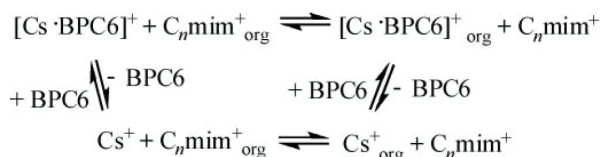


Fig. 22. A dual extraction mechanism for extraction  $\text{Cs}^+$  by the BPC6/ $[\text{C}_n\text{mim}][\text{Tf}_2\text{N}]$  system. Reprinted from Xu et al. (2010).

### 5.3 Effects of ionic liquids on other supermolecules

The primary role of IL is to maintain good solvent conditions over a very wide temperature range for supramolecular ion gel (Mohmeyer et al., 2006; Noro et al., 2008, 2009). Supramolecular gelation in IL could be used in many fields, such as actuators, polymer electrolytes, membranes, or gate dielectrics for organic transistors. The structures and characteristics of nanohybrids or nanocomposites or self-organized nanotubes can be changed by the assistant of ILs (Gopalan et al., 2009; Li et al., 2009a; Paramasivam et al., 2008; Park et al., 2009b; Wu et al., 2009a). There are two aspects about effects of ILs on these supermolecules,

which influence the system individually or jointly. One is that ILs affect the supermolecules because of the anions and cations of ILs and aromatic structures, which can result in electrostatic interactions, cation- $\pi$  and/or  $\pi$ - $\pi$  stacking interactions (Gopalan et al., 2009; Li et al., 2009a; Park et al., 2009a; Park et al., 2009b; Wu et al., 2009a; Zhang et al., 2009). The other is that self-assembly of ILs influence the supermolecules (Gutel et al., 2007; Ma et al., 2009; Xu et al., 2009). The sensitivity of molecularly imprinted polymers (MIPs) can be improved by IL-mediated method (Booker et al., 2006; He et al., 2008a; Wang et al., 2006; Wang et al., 2009). ILs are also used to synthesize other supramolecular host compounds (Scott et al., 2000) and can form different supramolecular networks from other solvents (Pediredi et al., 2005).

#### 5.4 Effects of ionic liquids on the formation of supramolecular assemblies

As mentioned above, ILs participated in the formation of micelles, microemulsions, liquid crystals and vesicles. In addition, IL also influenced the formation of the supramolecular assemblies as solvents and co-solvents.

The micelle formation of surfactants, such as SDS and Brij-35 in ILs ([C<sub>4</sub>mim]Cl and [C<sub>4</sub>mim][PF<sub>6</sub>]) was first studied by Armstrong and his coworkers (Anderson et al., 2003). The micelle formation is caused by the solvophobic interactions between the hydrocarbon chains of the surfactant molecules just like hydrophobic interactions in aqueous medium. Relative studies on the aggregation of nonionic surfactants in ILs have been reported (Evans et al., 1982; Evans et al., 1983b; Fletcher & Pandey, 2004; Gao et al., 2009b; Li et al., 2008b; Patrascu et al., 2006; Wu et al., 2008). Masahiro et al. (Moniruzzaman et al., 2008) reported the formation of reverse micelles in [C<sub>8</sub>mim][Tf<sub>2</sub>N] comprising sodium bis(2-ethyl-1-hexyl) sulfosuccinate (AOT) as surfactant with 1-hexanol as a cosurfactant. This formation of aqueous droplets in the IL is attributed to the hydrophobic effects between the AOT tails and the long hydrocarbon chain of IL and the strong tendency of the AOT head group to interact with water. In addition, amphiphilic Pluronic polymers were found to be able to form well defined micelles in IL, the micellization was found to be entropy driving (He et al., 2006; Inoue & Misono, 2008; Ueki et al., 2009; Zhang et al., 2008e).

ILs have also been found to influence the formation of micelles as co-surfactant. Behera et al. (Behera et al., 2007a; Behera et al., 2007b) reported that [C<sub>4</sub>mim][PF<sub>6</sub>] and [C<sub>4</sub>mim][BF<sub>4</sub>] participated in the TX-100 micellar phases. It was found that the addition of 30 wt % [C<sub>4</sub>mim][BF<sub>4</sub>] resulted in decreased micellar size, increased cmc, and decreased  $N_{agg}$ , all of which were unchanged in aqueous [C<sub>4</sub>mim][PF<sub>6</sub>]-TX-100 systems because of the low solubility of [C<sub>4</sub>mim][PF<sub>6</sub>]. These observations implied an overall unfavorable micellization process when the IL was present. Later, the concentration-dependent dual role of the ILs in altering physicochemical properties of ionic surfactant (SDS, CTAB) was demonstrated (Behera & Pandey, 2007a, b; Beyaz et al., 2004; Lei et al., 2007; Modaressi et al., 2007a; Sifaoui et al., 2007). It is found that ILs acted as a metal salt at low concentrations and participated in the micellar phase with increasing [C<sub>4</sub>mim][PF<sub>6</sub>] which led to a considerable decrease in the microfluidity of SDS micelles (Behera & Pandey, 2007a, b). ILs also influence the aggregation behavior of Pluronic polymers (Dey et al., 2009; Zheng et al., 2007). Zheng et al. (Zheng et al., 2007) studied the effect of [C<sub>4</sub>mim]Br on the aggregation behavior of PEO-PPO-PEO P104 aqueous solution. It suggested that when the concentration of [C<sub>4</sub>mim]Br was below 1.232 mol/L, there were P104 micelles in the aqueous solution with [C<sub>4</sub>mim]Br embedding to the micellar core, while above this concentration, P104 micelles and [C<sub>4</sub>mim]Br clusters coexisted in the system (Figure 23).



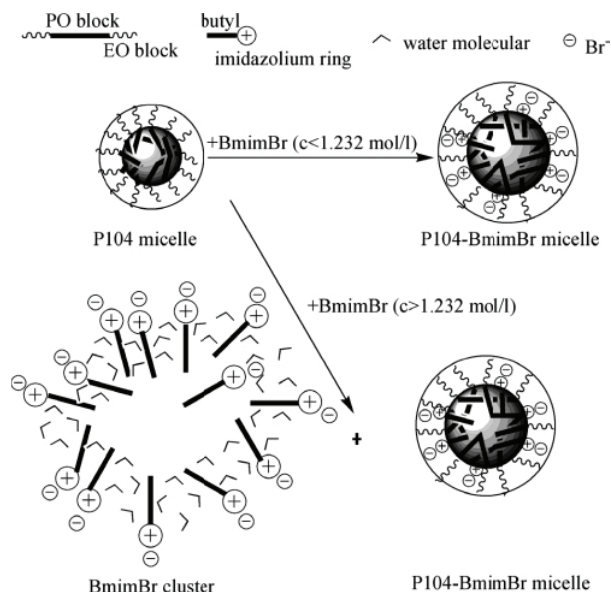


Fig. 23. Schematic illustration of the different types of complexes formed when  $[\text{C}_4\text{mim}]\text{Br}$  was added to 5% Pluronic P104 aqueous solution. Reprinted from Zheng et al. (2007).

The formation of liquid crystal in ILs was firstly reported by Evans and co-workers (Evans et al., 1983a) in 1983, which was formed by  $\beta,\gamma$ -distearoylphosphatidylcholine (DSPC) in EAN. Since then, many studies on the formation of liquid crystals in ILs are reported (Araos & Warr, 2005; Atkin & Warr, 2007; Greaves et al., 2007a, b; Tamuralis et al., 1987; Wang et al., 2004; Zhang et al., 2008a; Zhao et al., 2009b). Nonionic surfactants,  $\text{C}_{n}\text{E}_{m}$ , formed lyotropic liquid crystals in EAN and it was found that longer alkyl chains were necessary to drive the formation of liquid crystalline, suggesting that a rich pattern of "solvophobic" self-assembly (Araos & Warr, 2005; Atkin & Warr, 2007). The aggregation behavior of  $[\text{C}_{16}\text{mim}]\text{Cl}$  in EAN was also investigated and an additional  $\text{V}_2$  (reverse bicontinuous cubic) phase was identified when comparing such a phase behavior with that of the  $[\text{C}_{16}\text{mim}]\text{Cl}/\text{H}_2\text{O}$  binary system (Zhao et al., 2009b). Zhang et al. (Zhang et al., 2008a) reported the aggregation of Pluronic P123 in EAN, which was similar to those observed in  $\text{H}_2\text{O}$  or  $[\text{C}_4\text{mim}][\text{PF}_6]$  systems. They attributed the additional  $\text{V}_2$  phase in the P123-EAN system to the higher affinity for the hydrophobic PPO blocks to EAN than to water, which might reduce the effective area of the solvophilic headgroup and increase the volume of the solvophobic part.

## 6. Conclusions

In conclusion, ILs can act as guests to form supermolecules with several kinds of host molecules (i.e., cyclodextrins, cucurbit[n]urils and calixarenes), and can participate the constructing of supramolecular assemblies (i.e., micelles, microemulsions, lyotropic LCs, vesicles and gels). Besides, ILs can affect the formation of supramolecular structures, for example, the formation of polyrotaxanes and polypseudorotaxanes, the formation of the supramolecular structures in the extraction systems based on crown ethers, and so on. It is

also noticed that imidazolium ILs have a three-dimensional supramolecular network with polar and non-polar regions, which can be used as powerful supramolecular receptors. However, the host-guest interaction usually takes place in aqueous solution. In ILs, how do the host molecules interact with guest molecules, and how do ILs affect the interaction? These are two interesting and challenging subjects.

In addition, when ILs are used as solvents, how will the supramolecular structures of ILs themselves affect the formation of supramolecular assemblies. For example, when the surfactant is added into the IL/oil mixture, two cases would happen. If the hydrophobic interactions between oil and surfactant are stronger than the interactions between IL and oils, liquid clathrate can be destroyed and O/IL microemulsions form. Otherwise, a new state would exist instead of O/IL microemulsions. However, in the reference, this field has not been mentioned. Moreover, because trivial water is difficult to be removed and could be included in the supramolecular framework of imidazolium ILs, ILs are not pure, which makes the system more complicated. This supramolecular structure may also affect the formation of supramolecular assemblies. Recently, we noticed that water plays the key role in the formation of IL based microemulsions. A small quantity of water can lead to great change in the phase diagram of IL/TX-100/oil ternary systems. Therefore, the effect of the supramolecular structures of ILs on the formation of supramolecular assemblies is another valuable subject.

Now, these fields of ILs are just beginning to be noticed. With the development of the exploration in these fields, more and more interesting phenomena and important results will be obtained. Thus, the investigation of ILs will encounter a new chance and challenge.

## 7. Acknowledgements

This work was supported by the National Natural Science Foundation of China (Grant No. 90206020 and 20871009).

## 8. Abbreviations

18C6	18-crown-6
1P10X	tri-n-decylmethylphosphonium chloride and bromide
ACE	affinity capillary electrophoresis
AdCO <sub>2</sub> <sup>-</sup>	adamantylcarboxylate anion
AOT	sodium bis(2-ethyl-1-hexyl) sulfosuccinate
BF <sub>4</sub> <sup>-</sup>	tetrafluoroborate anion
BOBCalixC6	calix[4]arene-bis(tert-octylbenzo-crown-6)
BPC6	bis(2-propyloxy)calix[4]crown-6
Bu <sub>4</sub> N <sup>+</sup>	tetrabutylammonium cation
C <sub>3</sub> Br	propyl-(2-hydroxyethyl)-dimethyl-ammonium bromide
Calix-S4	4-sulfonatocalix[4]arene
Calix-S6	4-sulfonatocalix[6]arene
CBn	cucurbit[n]uril
CD(s)	cyclodextrin(s)
cmc	critical micelle concentration
C <sub>n</sub> dmim <sup>+</sup>	1-alkyl-2,3-dimethylimidazolium cation
C <sub>n</sub> E <sub>m</sub>	alkyl poly-(oxyethyleneglycol) ethers

$[C_nH_{2n+1}mim][C_mH_{2m+1}SO_3]$	1-alkyl-3-methylimidazolium alkylsulfonate
$C_nmim^+$	1-alkyl-3-methylimidazolium cation
$(CN)_2N^-$	dicyanimide anion
$C_nOSO_3^-$	alkylsulfate anion
$C_nPy^+$	1-alkylpyridinium cation
$C_nvim^+$	1-alkyl-3-vinylimidazolium cation
DBzDA18C6	N, N'-dibenzyl-4, 13-diaza-18-crown-6
DCH18C6	dicyclohexano-18-crown-6
[DDA][NO <sub>3</sub> ]	didecyl-dimethylammonium nitrate
DLS	dynamic light scattering
DM- $\beta$ -CD	heptakis-(2,6-di-O-methyl)- $\beta$ -CD
DPPC	L-dipalmitoylphosphatidylcholine
DSPC	$\beta$ , $\gamma$ -distearoylphosphotidylcholine
DTAB	dodecyltrimethylammonium bromide
EAN	ethylammonium nitrate
FFEM	freeze-fracturing electron microscopy
H2 $\beta$ DA18C6	$\beta$ -diketone-substituted diaza-18-crown-6
HP- $\beta$ -CD	hydroxypropyl- $\beta$ -CD
HPMBP	1-phenyl-3-methyl-4-benzoyl-5-pyrazolone
HP- $\alpha$ -CD	hydroxypropyl- $\alpha$ -CD
HP- $\gamma$ -CD	hydroxypropyl- $\gamma$ -CD
IC	inclusion complex
IL(s)	ionic liquid(s)
ITC	isothermal titration calorimetry
LC(s)	liquid crystal(s)
LCST	lower critical solution temperature
MD	molecular dynamics
$NfO^-$	nonafluorobutanesulfonate anion
O/IL	oil-in-IL
O/W	oil-in-water
OE	oxyethylene
OTos <sup>-</sup>	tosylate anion
PAF	propylammonium formate
$PF_6^-$	hexafluorophosphate anion
PNCM	poly(NIPAAM-co- $\beta$ -CD Methacrylate)
SANS	small-angle neutron scattering
SAXS	small-angle X-ray scattering
SDS	sodium dodecylsulfate
tat	trans-anti-trans
TBPFO	tetrabutylammonium perfluorooctanoate
Tdec	thermal decomposition temperatures
$Tf_2N^-$	bis(trifluoromethylsulfonyl)imide anion
$TfO^-$	trifluoromethanesulfonate anion
TM- $\beta$ -CD	heptakis-(2,3,6-tri-O-methyl)- $\beta$ -CD
TPhB <sup>-</sup>	tetraphenylborate anion
TSIL	task specific ionic liquid

tst	trans-syn-trans
V <sub>2</sub>	reverse bicontinuous cubic phase
XRD	X-ray diffraction

## 9. References

- Abdallah, D. J.; Robertson, A.; Hsu, H. F. & Weiss, R. G. (2000). Smectic liquid-crystalline phases of quaternary group VA (especially phosphonium) salts with three equivalent long n-alkyl chains. How do layered assemblies form in liquid-crystalline and crystalline phases? *J. Am. Chem. Soc.*, **122**, 3053-3062.
- Adhikari, A.; Sahu, K.; Dey, S.; Ghosh, S.; Mandal, U. & Bhattacharyya, K. (2007). Femtosecond solvation dynamics in a neat ionic liquid and ionic liquid microemulsion: Excitation wavelength dependence. *J. Phys. Chem. B*, **111**, 12809-12816.
- Alami, E.; Levy, H.; Zana, R.; Weber, P. & Skoulios, A. (1993). A new smectic mesophase with 2-dimensional tetragonal symmetry from dialkyldimethylammonium bromides-ST. *Liq. Cryst.*, **13**, 201-212.
- Amajjahe, S.; Choi, S.; Munteanu, M. & Ritter, H. (2008). Pseudopolyanions based on poly(NIPAAm-co- $\beta$ -cyclodextrin methacrylate) and ionic liquids. *Angew. Chem.-Int. Edit.*, **47**, 3435-3437.
- Amajjahe, S. & Ritter, H. (2008a). Supramolecular controlled pseudo-LCST effects of cyclodextrin-complexed poly(ionic liquids). *Macromolecules*, **41**, 3250-3253.
- Amajjahe, S. & Ritter, H. (2008b). Anion complexation of vinylimidazolium salts and its influence on polymerization. *Macromolecules*, **41**, 716-718.
- Anderson, J. L.; Pino, V.; Hagberg, E. C.; Sheares, V. V. & Armstrong, D. W. (2003). Surfactant solvation effects and micelle formation in ionic liquids. *Chem. Commun.*, 2444-2445.
- Ao, M. Q.; Huang, P. P.; Xu, G. Y.; Yang, X. D. & Wang, Y. J. (2009). Aggregation and thermodynamic properties of ionic liquid-type gemini imidazolium surfactants with different spacer length. *Colloid Polym. Sci.*, **287**, 395-402.
- Araos, M. U. & Warr, G. G. (2005). Self-assembly of nonionic surfactants into lyotropic liquid crystals in ethylammonium nitrate, a room-temperature ionic liquid. *J. Phys. Chem. B*, **109**, 14275-14277.
- Arce, A.; Earle, M. J.; Rodriguez, H. & Seddon, K. R. (2007). Separation of aromatic hydrocarbons from alkanes using the ionic liquid 1-ethyl-3-methylimidazolium bis[(trifluoromethyl) sulfonyl] amide. *Green Chem.*, **9**, 70-74.
- Arkas, M.; Tsiourvas, D.; Paleos, C. M. & Skoulios, A. (1999). Smectic mesophases from dihydroxy derivatives of quaternary alkylammonium salts. *Chem.-Eur. J.*, **5**, 3202-3207.
- Artzner, F.; Veber, M.; Clerc, M. & Levelut, A. M. (1997). Evidence of nematic, hexagonal and rectangular columnar phases in thermotropic ionic liquid crystals. *Liq. Cryst.*, **23**, 27-33.
- Atkin, R. & Warr, G. G. (2007). Phase behavior and microstructure of microemulsions with a room-temperature ionic liquid as the polar phase. *J. Phys. Chem. B*, **111**, 9309-9316.
- Bates, E. D.; Mayton, R. D.; Ntai, I. & Davis, J. H. (2002). CO<sub>2</sub> capture by a task-specific ionic liquid. *J. Am. Chem. Soc.*, **124**, 926-927.

- Behera, K.; Dahiya, P. & Pandey, S. (2007a). Effect of added ionic liquid on aqueous Triton X-100 micelles. *J. Colloid Interface Sci.*, 307, 235-245.
- Behera, K.; Pandey, M. D.; Porel, M. & Pandey, S. (2007b). Unique role of hydrophilic ionic liquid in modifying properties of aqueous Triton X-100. *J. Chem. Phys.*, 127, 184501.
- Behera, K. & Pandey, S. (2007a). Modulating properties of aqueous sodium dodecyl sulfate by adding hydrophobic ionic liquid. *J. Colloid Interface Sci.*, 316, 803-814.
- Behera, K. & Pandey, S. (2007b). Concentration-dependent dual behavior of hydrophilic ionic liquid in changing properties of aqueous sodium dodecyl sulfate. *J. Phys. Chem. B*, 111, 13307-13315.
- Beletskaya, I.; Tyurin, V. S.; Tsvivadze, A. Y.; Guillard, R. & Stern, C. (2009). Supramolecular chemistry of metalloporphyrins. *Chem. Rev.*, 109, 1659-1713.
- Beyaz, A.; Oh, W. S. & Reddy, V. P. (2004). Ionic liquids as modulators of the critical micelle concentration of sodium dodecyl sulfate. *Colloid Surf. B-Biointerfaces*, 35, 119-124.
- Bhargava, B. L. & Klein, M. L. (2009). Molecular dynamics studies of cation aggregation in the room temperature ionic liquid [C<sub>10</sub>mim]Br in aqueous solution. *J. Phys. Chem. A*, 113, 1898-1904.
- Binnemans, K. (2005). Ionic liquid crystals. *Chem. Rev.*, 105, 4148-4204.
- Blesic, M.; Marques, M. H.; Plechkova, N. V.; Seddon, K. R.; Rebelo, L. P. N. & Lopes, A. (2007). Self-aggregation of ionic liquids: micelle formation in aqueous solution. *Green Chem.*, 9, 481-490.
- Blesic, M.; Lopes, A.; Melo, E.; Petrovski, Z.; Plechkova, N. V.; Lopes, J. N. C.; Seddon, K. R. & Rebelo, L. P. N. (2008). On the self-aggregation and fluorescence quenching aptitude of surfactant ionic liquids. *J. Phys. Chem. B*, 112, 8645-8650.
- Blesic, M.; Lopes, J. N. C.; Padua, A. A. H.; Shimizu, K.; Gomes, M. F. C. & Rebelo, L. P. N. (2009a). Phase equilibria in ionic liquid-aromatic compound mixtures, including benzene fluorination effects. *J. Phys. Chem. B*, 113, 7631-7636.
- Blesic, M.; Swadzba-Kwasny, M.; Holbrey, J. D.; Lopes, J. N. C.; Seddon, K. R. & Rebelo, L. P. N. (2009b). New catanionic surfactants based on 1-alkyl-3-methylimidazolium alkylsulfonates, [C<sub>n</sub>H<sub>2n+1</sub>mim][C<sub>m</sub>H<sub>2m+1</sub>SO<sub>3</sub>]: mesomorphism and aggregation. *Phys. Chem. Chem. Phys.*, 11, 4260-4268.
- Booker, K.; Bowyer, M. C.; Holdsworth, C. I. & McCluskey, A. (2006). Efficient preparation and improved sensitivity of molecularly imprinted polymers using room temperature ionic liquids. *Chem. Commun.*, 1730-1732.
- Bowers, J.; Butts, C. P.; Martin, P. J.; Vergara-Gutierrez, M. C. & Heenan, R. K. (2004). Aggregation behavior of aqueous solutions of ionic liquids. *Langmuir*, 20, 2191-2198.
- Bowlas, C. J.; Bruce, D. W. & Seddon, K. R. (1996). Liquid-crystalline ionic liquids. *Chem. Commun.*, 1625-1626.
- Boxwell, C. J.; Dyson, P. J.; Ellis, D. J. & Welton, T. (2002). A highly selective arene hydrogenation catalyst that operates in ionic liquid. *J. Am. Chem. Soc.*, 124, 9334-9335.
- Bradley, A. E.; Hardacre, C.; Holbrey, J. D.; Johnston, S.; McMath, S. E. J. & Nieuwenhuyzen, M. (2002). Small-angle X-ray scattering studies of liquid crystalline 1-alkyl-3-methylimidazolium salts. *Chem. Mater.*, 14, 629-635.

- Brown, R. A.; Pollet, P.; McKoon, E.; Eckert, C. A.; Liotta, C. L. & Jessop, P. G. (2001). Asymmetric hydrogenation and catalyst recycling using ionic liquid and supercritical carbon dioxide. *J. Am. Chem. Soc.*, 123, 1254-1255.
- Cammarata, L.; Kazarian, S. G.; Salter, P. A. & Welton, T. (2001). Molecular states of water in room temperature ionic liquids. *Phys. Chem. Chem. Phys.*, 3, 5192-5200.
- Cang, H.; Li, J. & Fayer, M. D. (2003). Orientational dynamics of the ionic organic liquid 1-ethyl-3-methylimidazolium nitrate. *J. Chem. Phys.*, 119, 13017-13023.
- Carda-Broch, S.; Berthod, A. & Armstrong, D. W. (2003). Solvent properties of the 1-butyl-3-methylimidazolium hexafluorophosphate ionic liquid. *Anal. Bioanal. Chem.*, 375, 191-199.
- Carmichael, A. J.; Hardacre, C.; Holbrey, J. D.; Nieuwenhuyzen, M. & Seddon, K. R. (2001). Molecular layering and local order in thin films of 1-alkyl-3-methylimidazolium ionic liquids using X-ray reflectivity. *Mol. Phys.*, 99, 795-800.
- Chakrabarty, D.; Seth, D.; Chakraborty, A. & Sarkar, N. (2005). Dynamics of solvation and rotational relaxation of coumarin 153 in ionic liquid confined nanometer-sized microemulsions. *J. Phys. Chem. B*, 109, 5753-5758.
- Chen, H.; Kwait, D. C.; Gonen, Z. S.; Weslowski, B. T.; Abdallah, D. J. & Weiss, R. G. (2002). Phase characterization and properties of completely saturated quaternary phosphonium salts. Ordered, room-temperature ionic liquids. *Chem. Mater.*, 14, 4063-4072.
- Chen, P. Y. & Hussey, C. L. (2005). Electrochemistry of ionophore-coordinated Cs and Sr ions in the tri-1-butylmethylammonium bis((trifluoromethyl)sulfonyl)imide ionic liquid. *Electrochim. Acta*, 50, 2533-2540.
- Chen, P. Y. (2007). The assessment of removing strontium and cesium cations from aqueous solutions based on the combined methods of ionic liquid extraction and electrodeposition. *Electrochim. Acta*, 52, 5484-5492.
- Chen, S. M.; Wu, G. Z.; Sha, M. L. & Huang, S. R. (2007). Transition of ionic liquid [bmim][PF<sub>6</sub>] from liquid to high-melting-point crystal when confined in multiwalled carbon nanotubes. *J. Am. Chem. Soc.*, 129, 2416-2417.
- Cheng, S. Q.; Fu, X. G.; Liu, J. H.; Zhang, J. L.; Zhang, Z. F.; Wei, Y. L. & Han, B. X. (2007a). Study of ethylene glycol/TX-100/ionic liquid microemulsions. *Colloid Surf. A-Physicochem. Eng. Asp.*, 302, 211-215.
- Cheng, S. Q.; Zhang, J. L.; Zhang, Z. F. & Han, B. X. (2007b). Novel microemulsions: ionic liquid-in-ionic liquid. *Chem. Commun.*, 2497-2499.
- Cheng, S. Q.; Han, F.; Wang, Y. R. & Yan, H. F. (2008). Effect of cosurfactant on ionic liquid solubilization capacity in cyclohexane/TX-100/1-butyl-3-methylimidazolium tetrafluoroborate microemulsions. *Colloid Surf. A-Physicochem. Eng. Asp.*, 317, 457-461.
- Chiappe, C. & Pieraccini, D. (2005). Ionic liquids: solvent properties and organic reactivity. *J. Phys. Org. Chem.*, 18, 275-297.
- Choudhury, A. R.; Winterton, N.; Steiner, A.; Cooper, A. I. & Johnson, K. A. (2005). In situ crystallization of low-melting ionic liquids. *J. Am. Chem. Soc.*, 127, 16792-16793.
- Choudhury, A. R.; Winterton, N.; Steiner, A.; Cooper, A. I. & Johnson, K. A. (2006). In situ crystallization of ionic liquids with melting points below -25 °C. *Crystengcomm*, 8, 742-745.

- Christie, S.; Dubois, R. H.; Rogers, R. D.; White, P. S. & Zaworotko, M. J. (1991). Air stable liquid clathrates - solid-state structure and hydrocarbon solubility of organic cation triiodide salts. *J. Incl. Phenom. Mol. Recogn. Chem.*, 11, 103-114.
- Chun, S.; Dzyuba, S. V. & Bartsch, R. A. (2001). Influence of structural variation in room-temperature ionic liquids on the selectivity and efficiency of competitive alkali metal salt extraction by a crown ether. *Anal. Chem.*, 73, 3737-3741.
- Clavier, H.; Nolan, S. P. & Mauduit, M. (2008). Ionic liquid anchored "Boomerang" catalysts bearing saturated and unsaturated NHCs: Recyclability in biphasic media for cross-metathesis. *Organometallics*, 27, 2287-2292.
- Coleman, A. W.; Means, C. M.; Bott, S. G. & Atwood, J. L. (1990). Air-stable liquid clathrates. 1. crystal-structure of  $[\text{NBu}_4][\text{Br}_3]$  and reactivity of the  $[\text{NBu}_4][\text{Br}_3] \cdot 5\text{C}_6\text{H}_6$  liquid clathrate. *J. Cryst. Spectrosc. Res.*, 20, 199-201.
- Constable, E. C. (2008). Expanded ligands - An assembly principle for supramolecular chemistry. *Coord. Chem. Rev.*, 252, 842-855.
- Costantini, M.; Toussaint, V. A.; Shariati, A.; Peters, C. J. & Kikic, I. (2005). High-pressure phase Behavior of systems with ionic liquids: Part IV. Binary system carbon dioxide+1-hexyl-3-methylimidazolium tetrafluoroborate. *J. Chem. Eng. Data*, 50, 52-55.
- Craig, S. L. (2009). From ionic liquids to supramolecular polymers. *Angew. Chem.-Int. Edit.*, 48, 2645-2647.
- Cruz, C.; Heinrich, B.; Ribeiro, A. C.; Bruce, D. W. & Guillon, D. (2000). Structural study of smectic A phases in homologous series of N-alkylpyridinium alkylsulphates. *Liq. Cryst.*, 27, 1625-1631.
- Csihony, S.; Fischmeister, C.; Bruneau, C.; Horvath, I. T. & Dixneuf, P. H. (2002). First ring-opening metathesis polymerization in an ionic liquid. Efficient recycling of a catalyst generated from a cationic ruthenium allenylidene complex. *New J. Chem.*, 26, 1667-1670.
- Cui, L.; Sapagovas, V. & Lattermann, G. (2002). Synthesis and thermal behaviour of liquid crystalline pyridinium bromides containing a biphenyl core. *Liq. Cryst.*, 29, 1121-1132.
- Dai, S.; Ju, Y. H. & Barnes, C. E. (1999). Solvent extraction of strontium nitrate by a crown ether using room-temperature ionic liquids. *J. Chem. Soc. -Dalton Trans.*, 1201-1202.
- Davis, J. H.; Forrester, K. J. & Merrigan, T. (1998). Novel organic ionic liquids (OILs) incorporating cations derived from the antifungal drug miconazole. *Tetrahedron Lett.*, 39, 8955-8958.
- De Roche, J.; Gordon, C. M.; Imrie, C. T.; Ingram, M. D.; Kennedy, A. R.; Lo Celso, F. & Triolo, A. (2003). Application of complementary experimental techniques to characterization of the phase behavior of  $[\text{C}_{16}\text{mim}][\text{PF}_6]$  and  $[\text{C}_{14}\text{mim}][\text{PF}_6]$ . *Chem. Mater.*, 15, 3089-3097.
- DeCastro, C.; Sauvage, E.; Valkenberg, M. H. & Holderich, W. F. (2000). Immobilised ionic liquids as Lewis acid catalysts for the alkylation of aromatic compounds with dodecene. *J. Catal.*, 196, 86-94.
- Deetlefs, M.; Hardacre, C.; Nieuwenhuyzen, M.; Sheppard, O. & Soper, A. K. (2005). Structure of ionic liquid-benzene mixtures. *J. Phys. Chem. B*, 109, 1593-1598.

- Deetlefs, M.; Hardacre, C.; Nieuwenhuyzen, M.; Padua, A. A. H.; Sheppard, O. & Soper, A. K. (2006). Liquid structure of the ionic liquid 1,3-dimethylimidazolium bis{(trifluoromethyl)sulfonyl}amide. *J. Phys. Chem. B*, 110, 12055-12061.
- Descalzo, A. B.; Martinez-Manez, R.; Sancenon, R.; Hoffmann, K. & Rurack, K. (2006). The supramolecular chemistry of organic-inorganic hybrid materials. *Angew. Chem.-Int. Edit.*, 45, 5924-5948.
- Dey, S.; Adhikari, A.; Das, D. K.; Sasmal, D. K. & Bhattacharyya, K. (2009). Femtosecond solvation dynamics in a micron-sized aggregate of an ionic liquid and P123 triblock copolymer. *J. Phys. Chem. B*, 113, 959-965.
- Dieter, K. M.; Dymek, C. J.; Heimer, N. E.; Rovang, J. W. & Wilkes, J. S. (1988). Ionic structure and interactions in 1-methyl-3-ethylimidazolium chloride-AlCl<sub>3</sub> molten-salts. *J. Am. Chem. Soc.*, 110, 2722-2726.
- Dietz, M. L. & Dzielawa, J. A. (2001). Ion-exchange as a mode of cation transfer into room-temperature ionic liquids containing crown ethers: implications for the "greenness" of ionic liquids as diluents in liquid-liquid extraction. *Chem. Commun.*, 2124-2125.
- Dietz, M. L.; Dzielawa, J. A.; Laszak, I.; Young, B. A. & Jensen, M. P. (2003). Influence of solvent structural variations on the mechanism of facilitated ion transfer into room-temperature ionic liquids. *Green Chem.*, 5, 682-685.
- Dietz, M. L. & Stepinski, D. C. (2005). A ternary mechanism for the facilitated transfer of metal ions into room-temperature ionic liquids (RTILs): implications for the "greenness" of RTILs as extraction solvents. *Green Chem.*, 7, 747-750.
- Dietz, M. L.; Jakab, S.; Yamato, K. & Bartsch, R. A. (2008). Stereochemical effects on the mode of facilitated ion transfer into room-temperature ionic liquids. *Green Chem.*, 10, 174-176.
- Dong, B.; Li, N.; Zheng, L. Q.; Yu, L. & Inoue, T. (2007). Surface adsorption and micelle formation of surface active ionic liquids in aqueous solution. *Langmuir*, 23, 4178-4182.
- Dong, B.; Zhang, J.; Zheng, L. Q.; Wang, S. Q.; Li, X. W. & Inoue, T. R. (2008a). Salt-induced viscoelastic wormlike micelles formed in surface active ionic liquid aqueous solution. *J. Colloid Interface Sci.*, 319, 338-343.
- Dong, B.; Zhao, X. Y.; Zheng, L. Q.; Zhang, J.; Li, N. & Inoue, T. (2008b). Aggregation behavior of long-chain imidazolium ionic liquids in aqueous solution: Micellization and characterization of micelle microenvironment. *Colloid Surf. A-Physicochem. Eng. Asp.*, 317, 666-672.
- Dorbritz, S.; Ruth, W. & Kragl, U. (2005). Investigation on aggregate formation of ionic liquids. *Adv. Synth. Catal.*, 347, 1273-1279.
- Dupont, J.; Suarez, P. A. Z.; De Souza, R. F.; Burrow, R. A. & Kintzinger, J. P. (2000). C-H- $\pi$  interactions in 1-n-butyl-3-methylimidazolium tetraphenylborate molten salt: Solid and solution structures. *Chem.-Eur. J.*, 6, 2377-2381.
- Dupont, J. (2004). On the solid, liquid and solution structural organization of imidazolium ionic liquids. *J. Braz. Chem. Soc.*, 15, 341-350.
- Eastoe, J.; Gold, S.; Rogers, S. E.; Paul, A.; Welton, T.; Heenan, R. K. & Grillo, I. (2005). Ionic liquid-in-oil microemulsions. *J. Am. Chem. Soc.*, 127, 7302-7303.
- El Seoud, O. A.; Pires, P. A. R.; Abdel-Moghny, T. & Bastos, E. L. (2007). Synthesis and micellar properties of surface-active ionic liquids: 1-Alkyl-3-methylimidazolium chlorides. *J. Colloid Interface Sci.*, 313, 296-304.



- Evans, D. F.; Yamauchi, A.; Roman, R. & Casassa, E. Z. (1982). Micelle formation in ethylammonium nitrate, a low-melting fused salt. *J. Colloid Interface Sci.*, **88**, 89-96.
- Evans, D. F.; Kaler, E. W. & Benton, W. J. (1983a). Liquid-crystals in a fused salt -  $\beta,\alpha$ -distearoylphosphotidylcholine in n-ethylammonium nitrate. *J. Phys. Chem.*, **87**, 533-535.
- Evans, D. F.; Yamauchi, A.; Wei, G. J. & Bloomfield, V. A. (1983b). Micelle size in ethylammonium nitrate as determined by classical and quasi-elastic light-scattering. *J. Phys. Chem.*, **87**, 3537-3541.
- Feher, E.; Major, B.; Belafi-Bako, K. & Gubicza, L. (2007). On the background of enhanced stability and reusability of enzymes in ionic liquids. *Biochem. Soc. Trans.*, **35**, 1624-1627.
- Firestone, M. A.; Dzielawa, J. A.; Zapol, P.; Curtiss, L. A.; Seifert, S. & Dietz, M. L. (2002). Lyotropic liquid-crystalline gel formation in a room-temperature ionic liquid. *Langmuir*, **18**, 7258-7260.
- Firestone, M. A.; Dietz, M. L.; Seifert, S.; Trasobares, S.; Miller, D. J. & Zaluzec, N. J. (2005). Ionogel-templated synthesis and organization of anisotropic gold nanoparticles. *Small*, **1**, 754-760.
- Fletcher, K. A. & Pandey, S. (2004). Surfactant aggregation within room-temperature ionic liquid 1-ethyl-3-methylimidazolium bis(trifluoromethylsulfonyl)imide. *Langmuir*, **20**, 33-36.
- Francois, Y.; Varenne, A.; Sirieix-Plenet, J. & Gareil, P. (2007). Determination of aqueous inclusion complexation constants and stoichiometry of alkyl(methyl) - methylimidazolium-based ionic liquid cations and neutral cyclodextrins by affinity capillary electrophoresis. *J. Sep. Sci.*, **30**, 751-760.
- Friberg, S. E.; Yin, Q.; Pavel, F.; Mackay, R. A.; Holbrey, J. D.; Seddon, K. R. & Aikens, P. A. (2000). Solubilization of an ionic liquid, 1-butyl-3-methylimidazolium hexafluorophosphate, in a surfactant-water system. *J. Dispersion Sci. Technol.*, **21**, 185-197.
- Fujii, K.; Seki, S.; Fukuda, S.; Takamuku, T.; Kohara, S.; Kameda, Y.; Umebayashi, Y. & Ishiguro, S. (2008a). Liquid structure and conformation of a low-viscosity ionic liquid, N-methyl-N-propyl-pyrrolidinium bis(fluorosulfonyl) imide studied by high-energy X-ray scattering. *J. Mol. Liq.*, **143**, 64-69.
- Fujii, K.; Soejima, Y.; Kyoshoin, Y.; Fukuda, S.; Kanzaki, R.; Umebayashi, Y.; Yamaguchi, T.; Ishiguro, S. I. & Takamuku, T. (2008b). Liquid structure of room-temperature ionic liquid, 1-ethyl-3-methylimidazolium bis-(trifluoromethanesulfonyl) imide. *J. Phys. Chem. B*, **112**, 4329-4336.
- Fukuda, S.; Takeuchi, M.; Fujii, K.; Kanzaki, R.; Takamuku, T.; Chiba, K.; Yamamoto, H.; Umebayashi, Y. & Ishiguro, S. (2008). Liquid structure of N-butyl-N-methylpyrrolidinium bis-(trifluoromethanesulfonyl) amide ionic liquid studied by large angle X-ray scattering and molecular dynamics simulations. *J. Mol. Liq.*, **143**, 2-7.
- Fuller, J.; Carlin, R. T.; Delong, H. C. & Haworth, D. (1994). Structure of 1-ethyl-3-methylimidazolium hexafluorophosphate - model for room-temperature molten-salts. *J. Chem. Soc.-Chem. Commun.*, 299-300.

- Gao, H. X.; Li, J. C.; Han, B. X.; Chen, W. N.; Zhang, J. L.; Zhang, R. & Yan, D. D. (2004). Microemulsions with ionic liquid polar domains. *Phys. Chem. Chem. Phys.*, 6, 2914-2916.
- Gao, Y.; Li, N.; Zheng, L. Q.; Zhao, X. Y.; Zhang, S. H.; Han, B. X.; Hou, W. G. & Li, G. Z. (2006a). A cyclic voltammetric technique for the detection of micro-regions of bmimPF<sub>6</sub>/Tween 20/H<sub>2</sub>O microemulsions and their performance characterization by UV-Vis spectroscopy. *Green Chem.*, 8, 43-49.
- Gao, Y.; Zhang, J.; Xu, H. Y.; Zhao, X. Y.; Zheng, L. Q.; Li, X. W. & Yu, L. (2006b). Structural studies of 1-butyl-3-methylimidazolium tetrafluoroborate/TX-100/p-xylene ionic liquid microemulsions. *ChemPhysChem*, 7, 1554-1561.
- Gao, Y.; Zhao, X.; Dong, B.; Zheng, L.; Li, N. & Zhang, S. (2006c). Inclusion complexes of  $\beta$ -cyclodextrin with ionic liquid surfactants. *J. Phys. Chem. B*, 110, 8576-8581.
- Gao, Y.; Li, N.; Zheng, L. Q.; Bai, X. T.; Yu, L.; Zhao, X. Y.; Zhang, J.; Zhao, M. W. & Li, Z. (2007a). Role of solubilized water in the reverse ionic liquid microemulsion of 1-butyl-3-methylimidazolium tetrafluoroborate/TX-100/benzene. *J. Phys. Chem. B*, 111, 2506-2513.
- Gao, Y.; Li, N.; Zheng, L. Q.; Zhao, X. Y.; Zhang, J.; Cao, Q.; Zhao, M. W.; Li, Z. & Zhang, G. Y. (2007b). The effect of water on the microstructure of 1-butyl-3-methylimidazolium tetrafluoroborate/TX-100/benzene ionic liquid microemulsions. *Chem.-Eur. J.*, 13, 2661-2670.
- Gao, Y.; Hilfert, L.; Voigt, A. & Sundmachert, K. (2008a). Decrease of droplet size of the reverse microemulsion 1-butyl-3-methylimidazolium tetrafluoroborate/Triton X-100/cyclohexane by addition of water. *J. Phys. Chem. B*, 112, 3711-3719.
- Gao, Y. A.; Li, Z. H.; Du, J. M.; Han, B. X.; Li, G. Z.; Hou, W. G.; Shen, D.; Zheng, L. Q. & Zhang, G. Y. (2005a). Preparation and characterization of inclusion complexes of  $\beta$ -cyclodextrin with ionic liquid. *Chem.-Eur. J.*, 11, 5875-5880.
- Gao, Y. A.; Voigt, A.; Hilfert, L. & Sundmacher, K. (2008b). Nanodroplet cluster formation in ionic liquid microemulsions. *ChemPhysChem*, 9, 1603-1609.
- Gao, Y. A.; Li, N.; Zhang, S. H.; Zheng, L. Q.; Li, X. W.; Dong, B. & Yu, L. (2009a). Organic solvents induce the formation of oil-in-ionic liquid microemulsion aggregations. *J. Phys. Chem. B*, 113, 1389-1395.
- Gao, Y. N.; Han, S. B.; Han, B. X.; Li, G. Z.; Shen, D.; Li, Z. H.; Du, J. M.; Hou, W. G. & Zhang, G. Y. (2005b). TX-100/water/1-butyl-3-methylimidazolium hexafluorophosphate microemulsions. *Langmuir*, 21, 5681-5684.
- Gao, Y. N.; Wang, S. Q.; Zheng, L. Q.; Han, S. B.; Zhang, X.; Lu, D. M.; Yu, L.; Ji, Y. Q. & Zhang, G. Y. (2006d). Microregion detection of ionic liquid microemulsions. *J. Colloid Interface Sci.*, 301, 612-616.
- Gao, Y. N.; Li, N.; Li, X. W.; Zhang, S. H.; Zheng, L. Q.; Bai, X. T. & Yu, L. (2009b). Microstructures of micellar aggregations formed within 1-butyl-3-methylimidazolium type ionic liquids. *J. Phys. Chem. B*, 113, 123-130.
- Gaudet, M. V.; Peterson, D. C. & Zaworotko, M. J. (1988). Ternary hydrogen halide base benzene mixtures - a new generation of liquid clathrates. *J. Incl. Phenom.*, 6, 425-428.
- Ge, L. L.; Chen, L. P. & Guo, R. (2007). Microstructure and lubrication properties of lamellar liquid crystal in Brij 30/[Bmim][PF<sub>6</sub>]/H<sub>2</sub>O system. *Tribol. Lett.*, 28, 123-130.

- Getsis, A. & Mudring, A. V. (2008). Imidazolium based ionic liquid crystals: structure, photophysical and thermal behaviour of  $[C_n\text{mim}]\text{Br} \cdot x\text{H}_2\text{O}$  ( $n=12, 14$ ;  $x=0, 1$ ). *Cryst. Res. Technol.*, 43, 1187-1196.
- Gjikaj, M.; Brockner, W.; Namyslo, J. & Adam, A. (2008). Crown-ether enclosure generated by ionic liquid components - synthesis, crystal structure and Raman spectra of compounds of imidazolium based salts and 18-crown-6. *Crystengcomm*, 10, 103-110.
- Golovanov, D. G.; Lyssenko, K. A.; Antipin, M. Y.; Vygodskii, Y. S.; Lozinskaya, E. I. & Shaplov, A. S. (2005). Extremely short C-H $\cdots$ F contacts in the 1-methyl-3-propylimidazolium  $\text{SiF}_6^-$  - the reason for ionic "liquid" unexpected high melting point. *Crystengcomm*, 7, 53-56.
- Goossens, K.; Nockemann, P.; Driesen, K.; Goderis, B.; Gorller-Walrand, C.; Van Hecke, K.; Van Meervelt, L.; Pouzet, E.; Binnemans, K. & Cardinaels, T. (2008). Imidazolium ionic liquid crystals with pendant mesogenic groups. *Chem. Mater.*, 20, 157-168.
- Goossens, K.; Lava, K.; Nockemann, P.; Van Hecke, K.; Van Meervelt, L.; Driesen, K.; Gorller-Walrand, C.; Binnemans, K. & Cardinaels, T. (2009). Pyrrolidinium ionic liquid crystals. *Chem. Eur. J.*, 15, 656-674.
- Gopalan, A. I.; Lee, K. P. & Ragupathy, D. (2009). Development of a stable cholesterol biosensor based on multi-walled carbon nanotubes-gold nanoparticles composite covered with a layer of chitosan-room-temperature ionic liquid network. *Biosens. Bioelectron.*, 24, 2211-2217.
- Gordon, C. M.; Holbrey, J. D.; Kennedy, A. R. & Seddon, K. R. (1998). Ionic liquid crystals: hexafluorophosphate salts. *J. Mater. Chem.*, 8, 2627-2636.
- Gowda, G. A. N.; Chen, H.; Khetrapal, C. L. & Weiss, R. G. (2004). Amphotropic ionic liquid crystals with low order parameters. *Chem. Mater.*, 16, 2101-2106.
- Greaves, T. L.; Weerawardena, A.; Fong, C. & Drummond, C. J. (2007a). Formation of amphiphile self-assembly phases in protic ionic liquids. *J. Phys. Chem. B*, 111, 4082-4088.
- Greaves, T. L.; Weerawardena, A.; Fong, C. & Drummond, C. J. (2007b). Many protic ionic liquids mediate hydrocarbon-solvent interactions and promote amphiphile self-assembly. *Langmuir*, 23, 402-404.
- Gutel, T.; Garcia-Anton, J.; Pelzer, K.; Philippot, K.; Santini, C. C.; Chauvin, Y.; Chaudret, B. & Basset, J. M. (2007). Influence of the self-organization of ionic liquids on the size of ruthenium nanoparticles: effect of the temperature and stirring. *J. Mater. Chem.*, 17, 3290-3292.
- Gutowski, K. E. & Maginn, E. J. (2008). Amine-functionalized task-specific ionic liquids: a mechanistic explanation for the dramatic increase in viscosity upon complexation with  $\text{CO}_2$  from molecular simulation. *J. Am. Chem. Soc.*, 130, 14690-14704.
- Hao, J. C.; Song, A. X.; Wang, J. Z.; Chen, X.; Zhuang, W. C.; Shi, F.; Zhou, F. & Liu, W. M. (2005). Self-assembled structure in room-temperature ionic liquids. *Chem.-Eur. J.*, 11, 3936-3940.
- Hao, J. C. & Zemb, T. (2007). Self-assembled structures and chemical reactions in room-temperature ionic liquids. *Curr. Opin. Colloid Interface Sci.*, 12, 129-137.
- Hardacre, C.; Holbrey, J. D.; McCormac, P. B.; McMath, S. E. J.; Nieuwenhuyzen, M. & Seddon, K. R. (2001). Crystal and liquid crystalline polymorphism in 1-alkyl-3-methylimidazolium tetrachloropalladate(II) salts. *J. Mater. Chem.*, 11, 346-350.

- Hardacre, C.; Holbrey, J. D.; McMath, S. E. J.; Bowron, D. T. & Soper, A. K. (2003). Structure of molten 1,3-dimethylimidazolium chloride using neutron diffraction. *J. Chem. Phys.*, 118, 273-278.
- He, C. Y.; Long, Y. Y.; Pan, J. L.; Li, K. & Liu, F. (2008a). Molecularly imprinted silica prepared with immiscible ionic liquid as solvent and porogen for selective recognition of testosterone. *Talanta*, 74, 1126-1131.
- He, Y. F.; Fu, P.; Shen, X. H. & Gao, H. C. (2008b). Cyclodextrin-based aggregates and characterization by microscopy. *Micron*, 39, 495-516.
- He, Y. F. & Shen, X. H. (2008). Interaction between  $\beta$ -cyclodextrin and ionic liquids in aqueous solutions investigated by a competitive method using a substituted 3H-indole probe. *J. Photochem. Photobiol. A-Chem.*, 197, 253-259.
- He, Y. F.; Chen, Q. D.; Xu, C.; Zhang, J. J. & Shen, X. H. (2009). Interaction between ionic liquids and  $\beta$ -cyclodextrin: a discussion of association pattern. *J. Phys. Chem. B*, 113, 231-238.
- He, Y. Y.; Li, Z. B.; Simone, P. & Lodge, T. P. (2006). Self-assembly of block copolymer micelles in an ionic liquid. *J. Am. Chem. Soc.*, 128, 2745-2750.
- Hirayama, N.; Okamura, H.; Kidani, K. & Imura, H. (2008). Ionic liquid synergistic cation-exchange system for the selective extraction of lanthanum(III) using 2-thenoyltrifluoroacetone and 18-crown-6. *Anal. Sci.*, 24, 697-699.
- Holbrey, J. D. & Seddon, K. R. (1999). The phase behaviour of 1-alkyl-3-methylimidazolium tetrafluoroborates; ionic liquids and ionic liquid crystals. *J. Chem. Soc.-Dalton Trans.*, 2133-2139.
- Holbrey, J. D.; Reichert, W. M.; Nieuwenhuyzen, M.; Sheppard, O.; Hardacre, C. & Rogers, R. D. (2003). Liquid clathrate formation in ionic liquid-aromatic mixtures. *Chem. Commun.*, 476-477.
- Holbrey, J. D.; Reichert, W. M. & Rogers, R. D. (2004). Crystal structures of imidazolium bis(trifluoromethanesulfonyl)imide "ionic liquid" salts: the first organic salt with a cis-TFSI anion conformation. *Dalton Trans.*, 2267-2271.
- Hu, Z. H. & Margulis, C. J. (2006). Heterogeneity in a room-temperature ionic liquid: Persistent local environments and the red-edge effect. *Proc. Natl. Acad. Sci. U. S. A.*, 103, 831-836.
- Huang, J.; Riisager, A.; Wasserscheid, P. & Fehrmann, R. (2006). Reversible physical absorption of SO<sub>2</sub> by ionic liquids. *Chem. Commun.*, 4027-4029.
- Huddleston, J. G.; Visser, A. E.; Reichert, W. M.; Willauer, H. D.; Broker, G. A. & Rogers, R. D. (2001). Characterization and comparison of hydrophilic and hydrophobic room temperature ionic liquids incorporating the imidazolium cation. *Green Chem.*, 3, 156-164.
- Inazumi, N.; Yamamoto, S. & Sueishi, Y. (2007). A characteristic effect of pressure on inclusion complexation of phenothiazine dyes with p-sulfonatocalix[6]arene in a room-temperature ionic liquid. *J. Incl. Phenom. Macrocycl. Chem.*, 59, 33-39.
- Inoue, T.; Ebina, H.; Dong, B. & Zheng, L. Q. (2007). Electrical conductivity study on micelle formation of long-chain imidazolium ionic liquids in aqueous solution. *J. Colloid Interface Sci.*, 314, 236-241.
- Inoue, T. & Misono, T. (2008). Cloud point phenomena for POE-type nonionic surfactants in a model room temperature ionic liquid. *J. Colloid Interface Sci.*, 326, 483-489.

- Ishida, Y.; Sasaki, D.; Miyauchi, H. & Saigo, K. (2004). Design and synthesis of novel imidazolium-based ionic liquids with a pseudo crown-ether moiety: diastereomeric interaction of a racemic ionic liquid with enantiopure europium complexes. *Tetrahedron Lett.*, 45, 9455-9459.
- Iwata, K.; Okajima, H.; Saha, S. & Hamaguchi, H. O. (2007). Local structure formation in alkyl-imidazolium-based ionic liquids as revealed by linear and nonlinear Raman spectroscopy. *Accounts Chem. Res.*, 40, 1174-1181.
- Jensen, M. P.; Neufeind, J.; Beitz, J. V.; Skanthakumar, S. & Soderholm, L. (2003). Mechanisms of metal ion transfer into room-temperature ionic liquids: The role of anion exchange. *J. Am. Chem. Soc.*, 125, 15466-15473.
- Jiao, D. Z.; Zhao, N. & Scherman, O. A. (2010). A "green" method for isolation of cucurbit[7]uril via a solid state metathesis reaction. *Chem. Commun.*, 46, 2007-2009.
- Jing, B.; Chen, X.; Hao, J. C.; Qiu, H. Y.; Chai, Y. C. & Zhang, G. D. (2007). Supramolecular self-assembly of polypseudorotaxanes in ionic liquid. *Colloid Surf. A-Physicochem. Eng. Asp.*, 292, 51-55.
- Jungnickel, C.; Luczak, J.; Ranke, J.; Fernandez, J. F.; Muller, A. & Thoming, J. (2008). Micelle formation of imidazolium ionic liquids in aqueous solution. *Colloid Surf. A-Physicochem. Eng. Asp.*, 316, 278-284.
- Kanzaki, R.; Mitsugi, T.; Fukuda, S.; Fujii, K.; Takeuchi, M.; Soejima, Y.; Takamuku, T.; Yamaguchi, T.; Umebayashi, Y. & Ishiguro, S. I. (2009). Ion-ion interaction in room temperature ionic liquid 1-ethyl-3-methylimidazolium tetrafluoroborate studied by large angle X-ray scattering experiment and molecular dynamics simulations. *J. Mol. Liq.*, 147, 77-82.
- Katayanagi, H.; Hayashi, S.; Hamaguchi, H. O. & Nishikawa, K. (2004). Structure of an ionic liquid, 1-n-butyl-3-methylimidazolium iodide, studied by wide-angle X-ray scattering and Raman spectroscopy. *Chem. Phys. Lett.*, 392, 460-464.
- Kim, D.; Jon, S.; Lee, H. K.; Baek, K.; Oh, N. K.; Zin, W. C. & Kim, K. (2005). Anion-directed self-organization of thermotropic liquid crystalline materials containing a guanidinium moiety. *Chem. Commun.*, 5509-5511.
- Kimizuka, N. & Nakashima, T. (2001). Spontaneous self-assembly of glycolipid bilayer membranes in sugar-philic ionic liquids and formation of ionogels. *Langmuir*, 17, 6759-6761.
- Kolman, V.; Marek, R.; Strelcova, Z.; Kulhanek, P.; Necas, M.; Svec, J. & Sindelar, V. (2009). Electron density shift in imidazolium derivatives upon complexation with cucurbit[6]uril. *Chem.-Eur. J.*, 15, 6926-6931.
- Kowsari, M. H.; Alavi, S.; Ashrafizaadeh, M. & Najafi, B. (2010). Molecular dynamics study of congruent melting of the equimolar ionic liquid-benzene inclusion crystal [emim][NTf<sub>2</sub>] $\cdot$ C<sub>6</sub>H<sub>6</sub>. *J. Chem. Phys.*, 132, 044507.
- Kragl, U.; Eckstein, M. & Kaftzik, N. (2002). Enzyme catalysis in ionic liquids. *Curr. Opin. Biotechnol.*, 13, 565-571.
- Kumar, S. & Pal, S. K. (2005). Synthesis and characterization of novel imidazolium-based ionic discotic liquid crystals with a triphenylene moiety. *Tetrahedron Lett.*, 46, 2607-2610.
- Lachwa, J.; Bento, I.; Duarte, M. T.; Lopes, J. N. C. & Rebelo, L. P. N. (2006). Condensed phase behaviour of ionic liquid-benzene mixtures: congruent melting of a [emim][NTf<sub>2</sub>] $\cdot$ C<sub>6</sub>H<sub>6</sub> inclusion crystal. *Chem. Commun.*, 2445-2447.

- Langmaier, J.; Trojanek, A. & Samec, Z. (2009). Amperometric Ion-Selective Electrode for alkali metal cations based on a room-temperature ionic liquid membrane. *Electroanalysis*, 21, 1977-1983.
- Leclercq, L.; Suisse, I.; Nowogrocki, G. & Agbossou-Niedercorn, F. (2007). Halide-free highly-pure imidazolium triflate ionic liquids: Preparation and use in palladium-catalysed allylic alkylation. *Green Chem.*, 9, 1097-1103.
- Leclercq, L. & Schmitzer, A. R. (2008). Multiple equilibria in the complexation of dibenzylimidazolium bromide salts by cyclodextrins: Toward controlled self-assembly. *J. Phys. Chem. B*, 112, 11064-11070.
- Leclercq, L.; Suisse, I.; Nowogrocki, G. & Agbossou-Niedercorn, F. (2008). On the solid state inclusion of tetrabutylammonium cation in the imidazolium/trifluoromethanesulfonate H-bonds network observed in ionic co-crystals. *J. Mol. Struct.*, 892, 433-437.
- Leclercq, L.; Lacour, M.; Sanon, S. H. & Schmitzer, A. R. (2009a). Thermoregulated microemulsions by cyclodextrin sequestration: A new approach to efficient catalyst recovery. *Chem.-Eur. J.*, 15, 6327-6331.
- Leclercq, L.; Noujeim, N. & Schmitzer, A. R. (2009b). Development of N,N'-diaromatic diimidazolium cations: Arene interactions for highly organized crystalline materials. *Cryst. Growth Des.*, 9, 4784-4792.
- Leclercq, L. & Schmitzer, A. (2009a). Supramolecular effects involving the incorporation of guest substrates in imidazolium ionic liquid networks: Recent advances and future developments. *Supramol. Chem.*, 21, 245-263.
- Leclercq, L. & Schmitzer, A. R. (2009b). Supramolecular encapsulation of 1,3-bis(1-adamantyl)imidazolium chloride by  $\beta$ -cyclodextrins: towards inhibition of C(2)-H/D exchange. *J. Phys. Org. Chem.*, 22, 91-95.
- Leclercq, L.; Simard, M. & Schmitzer, A. R. (2009c). 1,3-Dibenzylimidazolium salts: A paradigm of water and anion effect on the supramolecular H-bonds network. *J. Mol. Struct.*, 918, 101-107.
- Lee, C. K.; Huang, H. W. & Lin, I. J. B. (2000). Simple amphiphilic liquid crystalline N-alkylimidazolium salts. A new solvent system providing a partially ordered environment. *Chem. Commun.*, 1911-1912.
- Lee, C. K.; Peng, H. H. & Lin, I. J. B. (2004). Liquid crystals of N,N'-dialkylimidazolium salts comprising  $\text{Pd}^{2+}$  and  $\text{Cu}^{2+}$  ions. *Chem. Mater.*, 16, 530-536.
- Lee, K. M.; Lee, C. K. & Lin, I. J. B. (1997). First example of interdigitated U-shape benzimidazolium ionic liquid crystals. *Chem. Commun.*, 899-900.
- Lee, U. H.; Kudo, T. & Honma, I. (2009). High-ion conducting solidified hybrid electrolytes by the self-assembly of ionic liquids and  $\text{TiO}_2$ . *Chem. Commun.*, 3068-3070.
- Lehn, J. M. (1988). Supramolecular chemistry - scope and perspectives molecules, supermolecules, and molecular devices. *Angew. Chem.-Int. Edit. Engl.*, 27, 89-112.
- Lehn, J. M. (1995). *Supramolecular Chemistry: Concepts and Perspectives*, VCH, 3527293116, Weinheim.
- Lei, S.; Zhang, J. & Huang, J. B. (2007). Promotion of the surface activity and aggregation ability of sodium dodecylsulfate in aqueous solution by ionic liquid 1-butyl-3-methyl-imidazolium tetrafluoroborate. *Acta Phys.-Chim. Sin.*, 23, 1657-1661.

- Li, F. H.; Wang, Z. H.; Shan, C. S.; Song, J. F.; Han, D. X. & Niu, L. (2009a). Preparation of gold nanoparticles/functionalized multiwalled carbon nanotube nanocomposites and its glucose biosensing application. *Biosens. Bioelectron.*, 24, 1765-1770.
- Li, H. G.; Zhang, Q. A.; Zhao, Q.; Liu, M.; Liu, J. & Sun, D. Z. Studies on interaction of ionic liquids with cyclodextrins in aqueous solution. *Indian J. Chem. Sect A-Inorg. Bio-Inorg. Phys. Theor. Anal. Chem.*, 49, 752-756.
- Li, J. C.; Zhang, J. L.; Gao, H. X.; Han, B. X. & Gao, L. (2005a). Nonaqueous microemulsion-containing ionic liquid [bmim][PF<sub>6</sub>] as polar microenvironment. *Colloid Polym. Sci.*, 283, 1371-1375.
- Li, L. B.; Groenewold, J. & Picken, S. J. (2005b). Transient phase-induced nucleation in ionic liquid crystals and size-frustrated thickening. *Chem. Mater.*, 17, 250-257.
- Li, N.; Cao, Q.; Gao, Y. A.; Zhang, J.; Zheng, L. Q.; Bai, X. T.; Dong, B.; Li, Z.; Zhao, M. W. & Yu, L. (2007a). States of water located in the continuous organic phase of 1-butyl-3-methylimidazolium tetrafluoroborate/Triton X-100/triethylamine reverse microemulsions. *ChemPhysChem*, 8, 2211-2217.
- Li, N.; Gao, Y. A.; Zheng, L. Q.; Zhang, J.; Yu, L. & Li, X. W. (2007b). Studies on the micropolarities of bmimBF<sub>4</sub>/TX-100/toluene ionic liquid microemulsions and their behaviors characterized by UV-visible spectroscopy. *Langmuir*, 23, 1091-1097.
- Li, N.; Liu, J.; Zhao, X. Y.; Gao, Y. A.; Zheng, L. Q.; Zhang, J. & Yu, L. (2007c). Complex formation of ionic liquid surfactant and  $\beta$ -cyclodextrin. *Colloid Surf. A-Physicochem. Eng. Asp.*, 292, 196-201.
- Li, N.; Zhang, S. H.; Zheng, L. Q.; Dong, B.; Li, X. W. & Yu, L. (2008a). Aggregation behavior of long-chain ionic liquids in an ionic liquid. *Phys. Chem. Chem. Phys.*, 10, 4375-4377.
- Li, N.; Zhang, S. H.; Zheng, L. Q.; Wu, J. P.; Li, X. W. & Yu, L. (2008b). Aggregation behavior of a fluorinated surfactant in 1-butyl-3-methylimidazolium ionic liquids. *J. Phys. Chem. B*, 112, 12453-12460.
- Li, X. W.; Zhang, J.; Dong, B.; Zheng, L. Q. & Tung, C. H. (2009b). Characterization of lyotropic liquid crystals formed in the mixtures of 1-alkyl-3-methylimidazolium bromide/p-xylene/water. *Colloid Surf. A-Physicochem. Eng. Asp.*, 335, 80-87.
- Li, X. W.; Zhang, J.; Zheng, L. Q.; Chen, B.; Wu, L. Z.; Lv, F. F.; Dong, B. & Tung, C. H. (2009c). Microemulsions of N-alkylimidazolium ionic liquid and their performance as microreactors for the photocycloaddition of 9-substituted anthracenes. *Langmuir*, 25, 5484-5490.
- Li, X. X.; Xu, X. D.; Dan, Y. Y.; Feng, J.; Ge, L. & Zhang, M. L. (2008c). The crystallization of lysozyme in the system of ionic liquid [BMIm][BF<sub>4</sub>]-water. *Cryst. Res. Technol.*, 43, 1062-1068.
- Lin, I. J. B. & Vasam, C. S. (2005). Metal-containing ionic liquids and ionic liquid crystals based on imidazolium moiety. *J. Organomet. Chem.*, 690, 3498-3512.
- Ling, I.; Alias, Y.; Sobolev, A. N. & Raston, C. L. (2009). Constructing multicomponent materials containing cavitands, and phosphonium and imidazolium cations. *Cryst. Growth Des.*, 9, 4497-4503.
- Ling, I.; Alias, Y.; Sobolev, A. N. & Raston, C. L. (2010a). Multi-component bi-layers featuring [1-octyl-2,3-dimethylimidazolium boolean and p-sulfonatocalix[4]arene] supermolecules. *New J. Chem.*, 34, 414-419.

- Ling, I.; Alias, Y.; Sobolev, A. N. & Raston, C. L. (2010b). Calixarene C-8-imidazolium interplay as a design strategy for penetrating organic bi-layers. *Crystengcomm*, 12, 573-578.
- Liu, H.; Wang, H. Z.; Tao, G. H. & Kou, Y. (2005). Novel imidazolium-based ionic liquids with a crown-ether moiety. *Chem. Lett.*, 34, 1184-1185.
- Liu, J. H.; Cheng, S. Q.; Zhang, J. L.; Feng, X. Y.; Fu, X. G. & Han, B. X. (2007). Reverse micelles in carbon dioxide with ionic-liquid domains. *Angew. Chem.-Int. Edit.*, 46, 3313-3315.
- Liu, L.; Zhao, N. & Scherman, O. A. (2008). Ionic liquids as novel guests for cucurbit[6]uril in neutral water. *Chem. Commun.*, 1070-1072.
- Lopes, J. & Padua, A. A. H. (2006). Nanostructural organization in ionic liquids. *J. Phys. Chem. B*, 110, 3330-3335.
- Lu, L.; Sharma, N.; Gowda, G. A. N.; Khetrapal, C. L. & Weiss, R. G. (1997). Enantiotropic nematic phases of quaternary ammonium halide salts based on trioctadecylamine. *Liq. Cryst.*, 22, 23-28.
- Luczak, J.; Hupka, J.; Thoming, J. & Jungnickel, C. (2008). Self-organization of imidazolium ionic liquids in aqueous solution. *Colloid Surf. A-Physicochem. Eng. Asp.*, 329, 125-133.
- Luczak, J.; Jungnickel, C.; Joskowska, M.; Thoming, J. & Hupka, J. (2009). Thermodynamics of micellization of imidazolium ionic liquids in aqueous solutions. *J. Colloid Interface Sci.*, 336, 111-116.
- Luo, H. M.; Dai, S. & Bonnesen, P. V. (2004a). Solvent extraction of  $\text{Sr}^{2+}$  and  $\text{Cs}^{+}$  based on room-temperature ionic liquids containing monoaza-substituted crown ethers. *Anal. Chem.*, 76, 2773-2779.
- Luo, H. M.; Dai, S.; Bonnesen, P. V.; Buchanan, A. C.; Holbrey, J. D.; Bridges, N. J. & Rogers, R. D. (2004b). Extraction of cesium ions from aqueous solutions using calix[4]arene-bis(tert-octylbenzo-crown-6) in ionic liquids. *Anal. Chem.*, 76, 3078-3083.
- Luo, H. M.; Dai, S.; Bonnesen, P. V. & Buchanan, A. C. (2006). Separation of fission products based on ionic liquids: Task-specific ionic liquids containing an aza-crown ether fragment. *J. Alloy. Compd.*, 418, 195-199.
- Luo, H. M.; Yu, M. & Dai, S. (2007). Solvent extraction of  $\text{Sr}^{2+}$  and  $\text{Cs}^{+}$  based on hydrophobic protic ionic liquids. *Z. Naturforsch. Sect. A-J. Phys. Sci.*, 62, 281-291.
- Ma, K.; Shahkhatuni, A. A.; Somashekhar, B. S.; Gowda, G. A. N.; Tong, Y.; Khetrapal, C. L. & Weiss, R. G. (2008). Room-temperature and low-ordered, amphotropic-lyotropic ionic liquid crystal phases induced by alcohols in phosphonium halides. *Langmuir*, 24, 9843-9854.
- Ma, L.; Chen, W. X.; Li, H. & Xu, Z. D. (2009). Synthesis and characterization of  $\text{MoS}_2$  nanostructures with different morphologies via an ionic liquid-assisted hydrothermal route. *Mater. Chem. Phys.*, 116, 400-405.
- Mathevet, F.; Masson, P.; Nicoud, J. F. & Skoulios, A. (2005). Smectic liquid crystals from supramolecular guanidinium alkanesulfonates. *J. Am. Chem. Soc.*, 127, 9053-9061.
- Megyesi, M.; Biczok, L. & Jablonkai, I. (2008). Highly sensitive fluorescence response to inclusion complex formation of berberine alkaloid with cucurbit[7]uril. *J. Phys. Chem. C*, 112, 3410-3416.
- Mele, A.; Tran, C. D. & Lacerda, S. H. D. (2003). The structure of a room-temperature ionic liquid with and without trace amounts of water: The role of  $\text{C-H}\cdots\text{O}$  and  $\text{C-H}\cdots\text{F}$



- interactions in 1-n-butyl-3-methylimidazolium tetrafluoroborate. *Angew. Chem.-Int. Edit.*, 42, 4364-4366.
- Mele, A.; Romano, G.; Giannone, M.; Ragg, E.; Fronza, G.; Raos, G. & Marcon, V. (2006). The local structure of ionic liquids: Cation-cation NOE interactions and internuclear distances in neat [BMIM][BF<sub>4</sub>] and [BDMIM][BF<sub>4</sub>]. *Angew. Chem.-Int. Edit.*, 45, 1123-1126.
- Merrigan, T. L.; Bates, E. D.; Dorman, S. C. & Davis, J. H. (2000). New fluororous ionic liquids function as surfactants in conventional room-temperature ionic liquids. *Chem. Commun.*, 2051-2052.
- Metrangolo, P.; Meyer, F.; Pilati, T.; Resnati, G. & Terraneo, G. (2008). Halogen bonding in supramolecular chemistry. *Angew. Chem.-Int. Edit.*, 47, 6114-6127.
- Miskolczy, Z.; Sebok-Nagy, K.; Biczok, L. & Gokturk, S. (2004). Aggregation and micelle formation of ionic liquids in aqueous solution. *Chem. Phys. Lett.*, 400, 296-300.
- Miskolczy, Z. & Biczok, L. (2009). Inclusion complex formation of ionic liquids with 4-sulfonatocalixarenes studied by competitive binding of berberine alkaloid fluorescent probe. *Chem. Phys. Lett.*, 477, 80-84.
- Miskolczy, Z.; Biczok, L.; Megyesi, M. & Jablonkai, I. (2009). Inclusion complex formation of ionic liquids and other cationic organic compounds with cucurbit[7]uril studied by 4',6'-diamidino-2-phenylindole fluorescent probe. *J. Phys. Chem. B*, 113, 1645-1651.
- Modaressi, A.; Sifaoui, H.; Grzesiak, B.; Solimando, R.; Domanska, U. & Rogalski, M. (2007a). CTAB aggregation in aqueous solutions of ammonium based ionic liquids; conductimetric studies. *Colloid Surf. A-Physicochem. Eng. Asp.*, 296, 104-108.
- Modaressi, A.; Sifaoui, H.; Mielcarz, M.; Domanska, U. & Rogalski, M. (2007b). Influence of the molecular structure on the aggregation of imidazolium ionic liquids in aqueous solutions. *Colloid Surf. A-Physicochem. Eng. Asp.*, 302, 181-185.
- Mohmeyer, N.; Kuang, D. B.; Wang, P.; Schmidt, H. W.; Zakeeruddin, S. M. & Gratzel, M. (2006). An efficient organogelator for ionic liquids to prepare stable quasi-solid-state dye-sensitized solar cells. *J. Mater. Chem.*, 16, 2978-2983.
- Moniruzzaman, M.; Noriho, K.; Nakashima, K. & Goto, M. (2008). Formation of reverse micelles in a room-temperature ionic liquid. *ChemPhysChem*, 9, 689-692.
- Montes-Navajas, P.; Corma, A. & Garcia, H. (2008). Supramolecular ionic liquids based on host-guest cucurbituril imidazolium complexes. *J. Mol. Catal. A-Chem.*, 279, 165-169.
- Moreno, M.; Castiglione, F.; Mele, A.; Pasqui, C. & Raos, G. (2008). Interaction of water with the model ionic liquid [bmim][BF<sub>4</sub>]: Molecular dynamics simulations and comparison with NMR data. *J. Phys. Chem. B*, 112, 7826-7836.
- Mukai, T.; Yoshio, M.; Kato, T. & Ohno, H. (2004). Effect of methyl groups onto imidazolium cation ring on liquid crystallinity and ionic conductivity of amphiphilic ionic liquids. *Chem. Lett.*, 33, 1630-1631.
- Najdanovic-Visak, V.; Esperanca, J.; Rebelo, L. P. N.; da Ponte, M. N.; Guedes, H. J. R.; Seddon, K. R.; de Sousa, H. C. & Szydłowski, J. (2003). Pressure, isotope, and water co-solvent effects in liquid-liquid equilibria of (ionic liquid plus alcohol) systems. *J. Phys. Chem. B*, 107, 12797-12807.
- Nakashima, T. & Kimizuka, N. (2002). Vesicles in salt: Formation of bilayer membranes from dialkyldimethylammonium bromides in ether-containing ionic liquids. *Chem. Lett.*, 1018-1019.

- Neve, F.; Crispini, A. & Francescangeli, O. (2000). Structural studies on layered alkylpyridinium iodopalladate networks. *Inorg. Chem.*, 39, 1187-1194.
- Neve, F.; Francescangeli, O.; Crispini, A. & Charmant, J. (2001). A<sub>2</sub>[MX<sub>4</sub>] copper(II) pyridinium salts. From ionic liquids to layered solids to liquid crystals. *Chem. Mater.*, 13, 2032-2041.
- Niu, J. G.; Qiu, H. D.; Li, J.; Liu, X. & Jiang, S. X. (2009). 1-Hexadecyl-3-methylimidazolium ionic liquid as a new cationic surfactant for separation of phenolic compounds by MEKC. *Chromatographia*, 69, 1093-1096.
- Nockemann, P.; Servaes, K.; Van Deun, R.; Van Hecke, K.; Van Meervelt, L.; Binnemans, K. & Gorller-Walrand, C. (2007). Speciation of uranyl complexes in ionic liquids by optical spectroscopy. *Inorg. Chem.*, 46, 11335-11344.
- Noro, A.; Matsushita, Y. & Lodge, T. P. (2008). Thermoreversible supramacromolecular ion gels via hydrogen bonding. *Macromolecules*, 41, 5839-5844.
- Noro, A.; Matsushita, Y. & Lodge, T. P. (2009). Gelation mechanism of thermoreversible supramacromolecular ion gels via hydrogen bonding. *Macromolecules*, 42, 5802-5810.
- Noujeim, N.; Jouvelet, B. & Schmitzer, A. R. (2009). Formation of inclusion complexes between 1,1'-dialkyl-3,3'-(1,4-phenylene)bisimidazolium dibromide salts and cucurbit[7]uril. *J. Phys. Chem. B*, 113, 16159-16168.
- Okamura, H.; Hirayama, N.; Morita, K.; Shimojo, K.; Naganawa, H. & Imura, H. (2010). Synergistic effect of 18-crown-6 derivatives on chelate extraction of lanthanoids(III) into an ionic liquid with 2-thenoyltrifluoroacetone. *Anal. Sci.*, 26, 607-611.
- Oshovsky, G. V.; Reinhoudt, D. N. & Verboom, W. (2007). Supramolecular chemistry in water. *Angew. Chem.-Int. Edit.*, 46, 2366-2393.
- Ozawa, R.; Hayashi, S.; Saha, S.; Kobayashi, A. & Hamaguchi, H. (2003). Rotational isomerism and structure of the 1-butyl-3-methylimidazolium cation in the ionic liquid state. *Chem. Lett.*, 32, 948-949.
- Pal, S. K. & Kumar, S. (2006). Microwave-assisted synthesis of novel imidazolium-based ionic liquid crystalline dimers. *Tetrahedron Lett.*, 47, 8993-8997.
- Paramasivam, I.; Macak, J. M.; Selvam, T. & Schmuki, P. (2008). Electrochemical synthesis of self-organized TiO<sub>2</sub> nanotubular structures using an ionic liquid [BMIM][BF<sub>4</sub>]. *Electrochim. Acta*, 54, 643-648.
- Park, C. L.; Jee, A. Y.; Lee, M. Y. & Lee, S. G. (2009a). Gelation, functionalization, and solution behaviors of nanodiamonds with ionic liquids. *Chem. Commun.*, 5576-5578.
- Park, H. S.; Choi, B. G.; Yang, S. H.; Shin, W. H.; Kang, J. K.; Jung, D. & Hong, W. H. (2009b). Ionic-liquid-assisted sonochemical synthesis of carbon-nanotube-based nanohybrids: Control in the structures and interfacial characteristics. *Small*, 5, 1754-1760.
- Park, S. H.; Demberelnyamba, D.; Jang, S. H. & Byun, M. W. (2006). Ionic liquid-type crown ether as a novel medium for a liquid/liquid extraction of radioactive metal ion <sup>85</sup>Sr<sup>2+</sup>. *Chem. Lett.*, 35, 1024-1025.
- Patrascu, C.; Gauffre, F.; Nallet, F.; Bordes, R.; Oberdisse, J.; de Lauth-Viguerie, N. & Mingotaud, C. (2006). Micelles in ionic liquids: Aggregation behavior of alkyl poly(ethyleneglycol)-ethers in 1-butyl-3-methyl-imidazolium type ionic liquids. *ChemPhysChem*, 7, 99-101.

- Pedireddi, V. R.; Shimpi, M. R. & Yakhmi, J. V. (2005). Room-temperature ionic liquids: For a difference in the supramolecular synthesis. *Indo-French Symposium on Fibrillar Networks as Advanced Materials*, pp. 83-87, Strasbourg, FRANCE, Sep 21-23, Wiley-VCH Verlag GmbH.
- Pickett, C. J. (1985). A simple hydrocarbon electrolyte - completing the electron-transfer series  $[\text{Fe}_4\text{S}_4(\text{SPh})_4]^{1-2-3-4}$ . *J. Chem. Soc.-Chem. Commun.*, 323-326.
- Pino, V.; Yao, C. & Anderson, J. L. (2009). Micellization and interfacial behavior of imidazolium-based ionic liquids in organic solvent-water mixtures. *J. Colloid Interface Sci.*, 333, 548-556.
- Popov, K.; Ronkkomaki, H.; Hannu-Kuure, M.; Kuokkanen, T.; Lajunen, M.; Vendilo, A.; Oksman, P. & Lajunen, L. H. J. (2007). Stability of crown-ether complexes with alkali-metal ions in ionic liquid-water mixed solvents. *J. Incl. Phenom. Macrocycl. Chem.*, 59, 377-381.
- Pott, T. & Meleard, P. (2009). New insight into the nanostructure of ionic liquids: a small angle X-ray scattering (SAXS) study on liquid tri-alkyl-methyl-ammonium bis(trifluoromethanesulfonyl)amides and their mixtures. *Phys. Chem. Chem. Phys.*, 11, 5469-5475.
- Qiu, Z. M. & Texter, J. (2008). Ionic liquids in microemulsions. *Curr. Opin. Colloid Interface Sci.*, 13, 252-262.
- Rebelo, L. P. N.; Lopes, J. N. C.; Esperanca, J.; Guedes, H. J. R.; Lachwa, J.; Najdanovic-Visak, V. & Visak, Z. P. (2007). Accounting for the unique, doubly dual nature of ionic liquids from a molecular thermodynamic, and modeling standpoint. *Accounts Chem. Res.*, 40, 1114-1121.
- Rickert, P. G.; Stepinski, D. C.; Rausch, D. J.; Bergeron, R. M.; Jakab, S. & Dietz, M. L. (2007). Solute-induced dissolution of hydrophobic ionic liquids in water. *Talanta*, 72, 315-320.
- Rogers, R. D.; Bridges, N. J.; Holbrey, J. D.; Luo, H.; Dai, S. & Bonnesen, P. V. (2004). The role of ion exchange vs solvent extraction processes in metal ion partitioning in ionic liquid/aqueous systems: Cesium extractions with calix[4]arene-bis(tert-octylbenzo-crown-6) in imidazolium bistriflylimide ionic liquids. *227th National Meeting of the American-Chemical Society*, pp. 227-IEC, Anaheim, CA, Mar 28-Apr 01, Amer Chemical Soc.
- Saha, S.; Hayashi, S.; Kobayashi, A. & Hamaguchi, H. (2003). Crystal structure of 1-butyl-3-methylimidazolium chloride. A clue to the elucidation of the ionic liquid structure. *Chem. Lett.*, 32, 740-741.
- Samitsu, S.; Araki, J.; Kataoka, T. & Ito, K. (2006). New solvent for polyrotaxane. II. Dissolution behavior of polyrotaxane in ionic liquids and preparation of ionic liquid-containing slide-ring gels. *J. Polym. Sci. Pt. B-Polym. Phys.*, 44, 1985-1994.
- Sauer, S.; Steinke, N.; Baro, A.; Laschat, S.; Giesselmann, F. & Kantlehner, W. (2008). Guanidinium chlorides with triphenylene moieties displaying columnar mesophases. *Chem. Mater.*, 20, 1909-1915.
- Schroder, U.; Wadhawan, J. D.; Compton, R. G.; Marken, F.; Suarez, P. A. Z.; Consorti, C. S.; de Souza, R. F. & Dupont, J. (2000). Water-induced accelerated ion diffusion: voltammetric studies in 1-methyl-3-[2,6-(S)-dimethylocten-2-yl]imidazolium tetrafluoroborate, 1-butyl-3-methylimidazolium tetrafluoroborate and hexafluorophosphate ionic liquids. *New J. Chem.*, 24, 1009-1015.

- Scott, J. L.; MacFarlane, D. R.; Raston, C. L. & Teoh, C. M. (2000). Clean, efficient syntheses of cyclotrimeratrylene (CTV) and tris-(O-allyl)CTV in an ionic liquid. *Green Chem.*, 2, 123-126.
- Seddon, K. R.; Stark, A. & Torres, M. J. (2000). Influence of chloride, water, and organic solvents on the physical properties of ionic liquids. *Pure Appl. Chem.*, 72, 2275-2287.
- Selvan, M. S.; McKinley, M. D.; Dubois, R. H. & Atwood, J. L. (2000). Liquid-liquid equilibria for toluene plus heptane+1-ethyl-3-methylimidazolium triiodide and toluene plus heptane+1-butyl-3-methylimidazolium triiodide. *J. Chem. Eng. Data*, 45, 841-845.
- Seo, S. H.; Park, J. H.; Tew, G. N. & Chang, J. Y. (2007). Thermotropic liquid crystals of 1H-imidazole amphiphiles showing hexagonal columnar and micellar cubic phases. *Tetrahedron Lett.*, 48, 6839-6844.
- Seth, D.; Chakraborty, A.; Setua, P. & Sarkar, N. (2006). Interaction of ionic liquid with water in ternary microemulsions (Triton X-100/water/1-butyl-3-methylimidazolium hexafluorophosphate) probed by solvent and rotational relaxation of coumarin 153 and coumarin 151. *Langmuir*, 22, 7768-7775.
- Seth, D.; Chakraborty, A.; Setua, P. & Sarkar, N. (2007a). Interaction of ionic liquid with water with variation of water content in 1-butyl-3-methylimidazolium hexafluorophosphate ([bmim][PF<sub>6</sub>])/TX-100/water ternary microemulsions monitored by solvent and rotational relaxation of coumarin 153 and coumarin 490. *J. Chem. Phys.*, 126, 224512.
- Seth, D.; Setua, P.; Chakraborty, A. & Sarkar, N. (2007b). Solvent relaxation of a room-temperature ionic liquid [bmim][PF<sub>6</sub>] confined in a ternary microemulsion. *J. Chem. Sci.*, 119, 105-111.
- Sha, M. L.; Wu, G. Z.; Liu, Y. S.; Tang, Z. F. & Fang, H. P. (2009). Drastic phase transition in ionic liquid [Dmim]Cl confined between graphite walls: New phase formation. *J. Phys. Chem. C*, 113, 4618-4622.
- Shiflett, M. B. & Yokozeki, A. (2008). Liquid-liquid equilibria in binary mixtures containing fluorinated benzenes and ionic liquid 1-ethyl-3-methylimidazolium bis-(trifluoromethylsulfonyl)imide. *J. Chem. Eng. Data*, 53, 2683-2691.
- Shiflett, M. B.; Niehaus, A. M. S. & Yokozeki, A. (2009). Liquid-liquid equilibria in binary mixtures containing chlorobenzene, bromobenzene, and iodobenzene with ionic liquid 1-ethyl-3-methylimidazolium bis(trifluoromethylsulfonyl)imide. *J. Chem. Eng. Data*, 54, 2090-2094.
- Shiflett, M. B. & Niehaus, A. M. S. (2010). Liquid-liquid equilibria in binary mixtures containing substituted benzenes with ionic liquid 1-ethyl-3-methylimidazolium bis(trifluoromethylsulfonyl)imide. *J. Chem. Eng. Data*, 55, 346-353.
- Shigeto, S. & Hamaguchi, H. (2006). Evidence for mesoscopic local structures in ionic liquids: CARS signal spatial distribution of [C<sub>n</sub>mim][PF<sub>6</sub>] (n=4,6,8). *Chem. Phys. Lett.*, 427, 329-332.
- Shimizu, K.; Gomes, M. F. C.; Padua, A. A. H.; Rebelo, L. P. N. & Lopes, J. N. C. (2009). On the role of the dipole and quadrupole moments of aromatic compounds in the solvation by ionic liquids. *J. Phys. Chem. B*, 113, 9894-9900.
- Shimojo, K. & Goto, M. (2004a). First application of calixarenes as extractants in room-temperature ionic liquids. *Chem. Lett.*, 33, 320-321.
- Shimojo, K. & Goto, M. (2004b). Solvent extraction and stripping of silver ions in room-temperature ionic liquids containing calixarenes. *Anal. Chem.*, 76, 5039-5044.

- Shimojo, K.; Kamiya, N.; Tani, F.; Naganawa, H.; Naruta, Y. & Goto, M. (2006a). Extractive solubilization, structural change, and functional conversion of cytochrome c in ionic liquids via crown ether complexation. *Anal. Chem.*, 78, 7735-7742.
- Shimojo, K.; Nakashima, K.; Kamiya, N. & Goto, M. (2006b). Crown ether-mediated extraction and functional conversion of cytochrome c in ionic liquids. *Biomacromolecules*, 7, 2-5.
- Shimojo, K.; Okamura, H.; Hirayama, N.; Umetani, S.; Imura, H. & Naganawa, H. (2009). Cooperative intramolecular interaction of diazacrown ether bearing  $\beta$ -diketone fragments on an ionic liquid extraction system. *Dalton Trans.*, 4850-4852.
- Sieffert, N. & Wipff, G. (2006a). Alkali cation extraction by calix[4]crown-6 to room-temperature ionic liquids. The effect of solvent anion and humidity investigated by molecular dynamics simulations. *J. Phys. Chem. A*, 110, 1106-1117.
- Sieffert, N. & Wipff, G. (2006b). Comparing an ionic liquid to a molecular solvent in the cesium cation extraction by a calixarene: A molecular dynamics study of the aqueous interfaces. *J. Phys. Chem. B*, 110, 19497-19506.
- Sieffert, N. & Wipff, G. (2007). The effect of a solvent modifier in the cesium extraction by a calix[4] arene: a molecular dynamics study of the oil phase and the oil-water interface. *Phys. Chem. Chem. Phys.*, 9, 3763-3775.
- Sifaoui, H.; Lugowska, K.; Domanska, U.; Modarelli, A. & Rogalski, M. (2007). Ammonium ionic liquid as modulator of the critical micelle concentration of ammonium surfactant at aqueous solution: Conductimetric and dynamic light scattering (DLS) studies. *J. Colloid Interface Sci.*, 314, 643-650.
- Singh, K.; Marangoni, D. G.; Quinn, J. G. & Singer, R. D. (2009). Spontaneous vesicle formation with an ionic liquid amphiphile. *J. Colloid Interface Sci.*, 335, 105-111.
- Singh, T. & Kumar, A. (2007). Aggregation behavior of ionic liquids in aqueous solutions: Effect of alkyl chain length, cations, and anions. *J. Phys. Chem. B*, 111, 7843-7851.
- Singh, T. & Kumar, A. (2008). Self-aggregation of ionic liquids in aqueous media: A thermodynamic study. *Colloid Surf. A-Physicochem. Eng. Asp.*, 318, 263-268.
- Smirnova, S. V.; Torocheshnikova, II; Formanovsky, A. A. & Pletnev, I. V. (2004). Solvent extraction of amino acids into a room temperature ionic liquid with dicyclohexano-18-crown-6. *Anal. Bioanal. Chem.*, 378, 1369-1375.
- St-Jacques, A. D.; Wyman, I. W. & Macartney, D. H. (2008). Encapsulation of charge-diffuse peralkylated onium cations in the cavity of cucurbit[7]uril. *Chem. Commun.*, 4936-4938.
- Stepinski, D. C.; Jensen, M. P.; Dzielawa, J. A. & Dietz, M. L. (2005). Synergistic effects in the facilitated transfer of metal ions into room-temperature ionic liquids. *Green Chem.*, 7, 151-158.
- Stepinski, D. C.; Vandegrift, G. F.; Shkrob, I. A.; Wishart, J. F.; Kerr, K.; Dietz, M. L.; Qadah, D. T. D. & Garvey, S. L. (2010). Extraction of tetra-oxo anions into a hydrophobic, ionic liquid-based solvent without concomitant ion exchange. *Ind. Eng. Chem. Res.*, 49, 5863-5868.
- Surette, J. K. D.; Green, L. & Singer, R. D. (1996). 1-ethyl-3-methylimidazolium halogenoaluminate melts as reaction media for the Friedel-Crafts acylation of ferrocene. *Chem. Commun.*, 2753-2754.

- Takamuku, T.; Kyoshoin, Y.; Shimomura, T.; Kittaka, S. & Yamaguchi, T. (2009). Effect of water on structure of hydrophilic imidazolium-based ionic liquid. *J. Phys. Chem. B*, 113, 10817-10824.
- Talaty, E. R.; Raja, S.; Storhaug, V. J.; Dolle, A. & Carper, W. R. (2004). Raman and infrared spectra and a initio calculations of C<sub>24</sub>MIM imidazolium hexafluorophosphate ionic liquids. *J. Phys. Chem. B*, 108, 13177-13184.
- Tamuralis, W.; Lis, L. J. & Quinn, P. J. (1987). Structures and mechanisms of lipid phase-transitions in nonaqueous media - dipalmitoylphosphatidylcholine in fused salt. *J. Phys. Chem.*, 91, 4625-4627.
- Tan, L.; Dong, X. L.; Wang, H. & Yang, Y. J. (2009). Gels of ionic liquid [C<sub>4</sub>mim][PF<sub>6</sub>] formed by self-assembly of gelators and their electrochemical properties. *Electrochem. Commun.*, 11, 933-936.
- Tang, J.; Li, D.; Sun, C. Y.; Zheng, L. Z. & Li, J. H. (2006). Temperature dependant self-assembly of surfactant Brij 76 in room temperature ionic liquid. *Colloid Surf. A-Physicochem. Eng. Asp.*, 273, 24-28.
- Taubert, A. (2004). CuCl nanoplatelets from an ionic liquid-crystal precursor. *Angew. Chem.-Int. Edit.*, 43, 5380-5382.
- Thomaier, S. & Kunz, W. (2007). Aggregates in mixtures of ionic liquids. *J. Mol. Liq.*, 130, 104-107.
- Tittarelli, F.; Masson, P. & Skoulios, A. (1997). Structural compatibility of smectic sublayers: Liquid crystals from oxynitrostilbene derivatives of dialkyldimethylammonium bromides. *Liq. Cryst.*, 22, 721-726.
- Triolo, A.; Russina, O.; Bleif, H. J. & Di Cola, E. (2007). Nanoscale segregation in room temperature ionic liquids. *J. Phys. Chem. B*, 111, 4641-4644.
- Tsuda, T.; Hussey, C. L.; Luo, H. M. & Dai, S. (2006). Recovery of cesium extracted from simulated tank waste with an ionic liquid: Water and oxygen effects. *J. Electrochem. Soc.*, 153, D171-D176.
- Ueki, T.; Watanabe, M. & Lodge, T. P. (2009). Doubly thermosensitive self-assembly of diblock copolymers in ionic liquids. *Macromolecules*, 42, 1315-1320.
- Urahata, S. M. & Ribeiro, M. C. C. (2004). Structure of ionic liquids of 1-alkyl-3-methylimidazolium cations: A systematic computer simulation study. *J. Chem. Phys.*, 120, 1855-1863.
- van Rantwijk, F.; Lau, R. M. & Sheldon, R. A. (2003). Biocatalytic transformations in ionic liquids. *Trends Biotechnol.*, 21, 131-138.
- Vanyur, R.; Biczok, L. & Miskolczy, Z. (2007). Micelle formation of 1-alkyl-3-methylimidazolium bromide ionic liquids in aqueous solution. *Colloid Surf. A-Physicochem. Eng. Asp.*, 299, 256-261.
- Vendilo, A. G.; Ronkkomaki, H.; Hannu-Kuure, M.; Lajunen, M.; Asikkala, J.; Chernikova, E. A.; Lajunen, L. H. J.; Tuomi, T. & Popo, K. I. (2009). Thermodynamics of complex formation in ionic liquids: cesium complexes with 18-crown-6. *Mendeleev Commun.*, 19, 196-197.
- Vendilo, A. G.; Djigailo, D. I.; Ronkkomaki, H.; Lajunen, M.; Chernikova, E. A.; Lajunen, L. H. J.; Pletnev, I. V. & Popov, K. I. (2010a). A correlation of caesium-18-crown-6 complex formation constants with the extraction capability for hydrophobic ionic liquids. *Mendeleev Commun.*, 20, 122-124.

- Vendilo, A. G.; Ronkkomaki, H.; Hannu-Kuure, M.; Lajunen, M.; Asikkala, J.; Krasovsky, V. G.; Chernikova, E. A.; Oksman, P.; Lajunen, L. H. J.; Tuomi, T. & Popov, K. I. (2010b). Thermodynamics of cesium complexes formation with 18-crown-6 in ionic liquids. *J. Incl. Phenom. Macrocycl. Chem.*, 66, 223-230.
- Visser, A. E.; Swatloski, R. P.; Reichert, W. M.; Griffin, S. T. & Rogers, R. D. (2000). Traditional extractants in nontraditional solvents: Groups 1 and 2 extraction by crown ethers in room-temperature ionic liquids. *Ind. Eng. Chem. Res.*, 39, 3596-3604.
- Visser, A. E.; Swatloski, R. P.; Reichert, W. M.; Mayton, R.; Sheff, S.; Wierzbicki, A.; Davis, J. H. & Rogers, R. D. (2001). Task-specific ionic liquids for the extraction of metal ions from aqueous solutions. *Chem. Commun.*, 135-136.
- Wang, H. F.; Zhu, Y. Z.; Yan, X. P.; Gao, R. Y. & Zheng, J. Y. (2006). A room temperature ionic liquid (RTIL)-mediated, non-hydrolytic sol-gel methodology to prepare molecularly imprinted, silica-based hybrid monoliths for chiral separation. *Adv. Mater.*, 18, 3266-3270.
- Wang, H. Y.; Wang, J. J.; Zhang, S. B. & Xuan, X. P. (2008). Structural effects of anions and cations on the aggregation behavior of ionic liquids in aqueous solutions. *J. Phys. Chem. B*, 112, 16682-16689.
- Wang, J. J.; Wang, H. Y.; Zhang, S. L.; Zhang, H. H. & Zhao, Y. (2007). Conductivities, volumes, fluorescence, and aggregation behavior of ionic liquids [C<sub>4</sub>mim][BF<sub>4</sub>] and [C<sub>n</sub>mim]Br (n = 4, 6, 8, 10, 12) in aqueous solutions. *J. Phys. Chem. B*, 111, 6181-6188.
- Wang, L. Y.; Chen, X.; Chai, Y. C.; Hao, J. C.; Sui, Z. M.; Zhuang, W. C. & Sun, Z. W. (2004). Lyotropic liquid crystalline phases formed in an ionic liquid. *Chem. Commun.*, 2840-2841.
- Wang, S. O.; Xu, Z. X.; Fang, G. Z.; Zhang, Y.; Liu, B. & Zhu, H. P. (2009). Development of a biomimetic enzyme-linked immunosorbent assay method for the determination of estrone in environmental water using novel molecularly imprinted films of controlled thickness as artificial antibodies. *J. Agric. Food Chem.*, 57, 4528-4534.
- Wang, Y. T. & Voth, G. A. (2005). Unique spatial heterogeneity in ionic liquids. *J. Am. Chem. Soc.*, 127, 12192-12193.
- Wang, Z. N.; Liu, F.; Gao, Y.; Zhuang, W. C.; Xu, L. M.; Han, B. X.; Li, G. Z. & Zhang, G. Y. (2005). Hexagonal liquid crystalline phases formed in ternary systems of Brij 97-water-ionic liquids. *Langmuir*, 21, 4931-4937.
- Wang, Z. N. & Zhou, W. (2009). Lamellar liquid crystals of Brij 97 aqueous solutions containing different additives. *J. Solut. Chem.*, 38, 659-668.
- Wathier, M. & Grinstaff, M. W. (2008). Synthesis and properties of supramolecular ionic networks. *J. Am. Chem. Soc.*, 130, 9648-9649.
- Weingartner, H. (2008). Understanding ionic liquids at the molecular level: Facts, problems, and controversies. *Angew. Chem.-Int. Edit.*, 47, 654-670.
- Welton, T. (1999). Room-temperature ionic liquids. Solvents for synthesis and catalysis. *Chem. Rev.*, 99, 2071-2083.
- Widegren, J. A.; Saurer, E. M.; Marsh, K. N. & Magee, J. W. (2005). Electrolytic conductivity of four imidazolium-based room-temperature ionic liquids and the effect of a water impurity. *J. Chem. Thermodyn.*, 37, 569-575.
- Wu, B. H.; Hu, D.; Kuang, Y. J.; Liu, B.; Zhang, X. H. & Chen, J. H. (2009a). Functionalization of carbon nanotubes by an ionic-liquid polymer: Dispersion of Pt and PtRu

- nanoparticles on carbon nanotubes and their electrocatalytic oxidation of methanol. *Angew. Chem.-Int. Edit.*, **48**, 4751-4754.
- Wu, J. P.; Li, N.; Zheng, L. Q.; Li, X. W.; Gao, Y. A. & Inoue, T. (2008). Aggregation behavior of polyoxyethylene (20) sorbitan monolaurate (Tween 20) in imidazolium based ionic liquids. *Langmuir*, **24**, 9314-9322.
- Wu, J. P.; Zhang, J.; Zheng, L. Q.; Zhao, X. Y.; Li, N. & Dong, B. (2009b). Characterization of lyotropic liquid crystalline phases formed in imidazolium based ionic liquids. *Colloid Surf. A-Physicochem. Eng. Asp.*, **336**, 18-22.
- Xiao, D.; Rajian, J. R.; Cady, A.; Li, S. F.; Bartsch, R. A. & Quitevis, E. L. (2007). Nanostructural organization and anion effects on the temperature dependence of the optical Kerr effect spectra of ionic liquids. *J. Phys. Chem. B*, **111**, 4669-4677.
- Xiao, S. F.; Lu, X. M.; Lu, Q. H. & Su, B. (2008). Photosensitive liquid-crystalline supramolecules self-assembled from ionic liquid crystal and polyelectrolyte for laser-induced optical anisotropy. *Macromolecules*, **41**, 3884-3892.
- Xu, C.; Shen, X. H.; Chen, Q. D. & Gao, H. C. (2009). Investigation on the extraction of strontium ions from aqueous phase using crown ether-ionic liquid systems. *Sci. China Ser. B-Chem.*, **52**, 1858-1864.
- Xu, C.; Yuan, L. Y.; Shen, X. H. & Zhai, M. L. (2010). Efficient removal of caesium ions from aqueous solution using a calix crown ether in ionic liquids: mechanism and radiation effect. *Dalton Trans.*, **39**, 3897-3902.
- Yasuda, T.; Tanabe, K.; Tsuji, T.; Coti, K. K.; Aprahamian, I.; Stoddart, J. F. & Kato, T. (2010). A redox-switchable 2 rotaxane in a liquid-crystalline state. *Chem. Commun.*, **46**, 1224-1226.
- Yazaki, S.; Funahashi, M. & Kato, T. (2008a). An electrochromic nanostructured liquid crystal consisting of  $\pi$ -conjugated and ionic moieties. *J. Am. Chem. Soc.*, **130**, 13206-13207.
- Yazaki, S.; Kamikawa, Y.; Yoshio, M.; Hamasaki, A.; Mukai, T.; Ohno, H. & Kato, T. (2008b). Ionic liquid crystals: Self-assembly of imidazolium salts containing an L-glutamic acid moiety. *Chem. Lett.*, **37**, 538-539.
- Yazaki, S.; Funahashi, M.; Kagimoto, J.; Ohno, H. & Kato, T. (2010). Nanostructured liquid crystals combining ionic and electronic functions. *J. Am. Chem. Soc.*, **132**, 7702-7708.
- Yoshio, M.; Mukai, T.; Ohno, H. & Kato, T. (2004). One-dimensional ion transport in self-organized columnar ionic liquids. *J. Am. Chem. Soc.*, **126**, 994-995.
- Yoshio, M.; Kagata, T.; Hoshino, K.; Mukai, T.; Ohno, H. & Kato, T. (2006). One-dimensional ion-conductive polymer films: Alignment and fixation of ionic channels formed by self-organization of polymerizable columnar liquid crystals. *J. Am. Chem. Soc.*, **128**, 5570-5577.
- Yoshio, M.; Ichikawa, T.; Shimura, H.; Kagata, T.; Hamasaki, A.; Mukai, T.; Ohno, H. & Kato, T. (2007). Columnar liquid-crystalline imidazolium salts. Effects of anions and cations on mesomorphic properties and ionic conductivity. *Bull. Chem. Soc. Jpn.*, **80**, 1836-1841.
- Yoshizawa, H.; Mihara, T. & Koide, N. (2004). Thermal properties and ionic conductivity of imidazolium salt derivatives having a calamitic mesogen. *Mol. Cryst. Liquid Cryst.*, **423**, 61-72.



- Yuan, L. Y.; Peng, J.; Xu, L.; Zhai, M. L.; Li, J. Q. & Wei, G. S. (2008). Influence of  $\gamma$ -radiation on the ionic liquid [C<sub>4</sub>mim][PF<sub>6</sub>] during extraction of strontium ions. *Dalton Trans.*, 6358-6360.
- Yuan, L. Y.; Peng, J.; Xu, L.; Zhai, M. L.; Li, J. Q. & Wei, G. S. (2009). Radiation effects on hydrophobic ionic liquid [C<sub>4</sub>mim][NTf<sub>2</sub>] during extraction of strontium ions. *J. Phys. Chem. B*, 113, 8948-8952.
- Zech, O.; Thomaier, S.; Bauduin, P.; Ruck, T.; Touraud, D. & Kunz, W. (2009). Microemulsions with an ionic liquid surfactant and room temperature ionic liquids as polar pseudo-phase. *J. Phys. Chem. B*, 113, 465-473.
- Zhang, G. D.; Chen, X. A.; Xie, Y. Z.; Zhao, Y. R. & Qiu, H. Y. (2007). Lyotropic liquid crystalline phases in a ternary system of 1-hexadecyl-3-methylimidazolium chloride/1-decanol/water. *J. Colloid Interface Sci.*, 315, 601-606.
- Zhang, G. D.; Chen, X.; Zhao, Y. R.; Ma, F. M.; Jing, B. & Qiu, H. Y. (2008a). Lyotropic liquid-crystalline phases formed by Pluronic P123 in ethylammonium nitrate. *J. Phys. Chem. B*, 112, 6578-6584.
- Zhang, H. C.; Li, K.; Liang, H. J. & Wang, J. J. (2008b). Spectroscopic studies of the aggregation of imidazolium-based ionic liquids. *Colloid Surf. A-Physicochem. Eng. Asp.*, 329, 75-81.
- Zhang, L. Q.; Xu, Z.; Wang, Y. & Li, H. R. (2008c). Prediction of the solvation and structural properties of ionic liquids in water by two-dimensional correlation spectroscopy. *J. Phys. Chem. B*, 112, 6411-6419.
- Zhang, Q. X.; Shan, C. S.; Wang, X. D.; Chen, L. L.; Niu, L. & Chen, B. (2008d). New ionic liquid crystals based on azobenzene moiety with two symmetric imidazolium ion group substituents. *Liq. Cryst.*, 35, 1299-1305.
- Zhang, S. H.; Li, N.; Zheng, L. Q.; Li, X. W.; Gao, Y. A. & Yu, L. (2008e). Aggregation behavior of pluronic triblock copolymer in 1-butyl-3-methylimidazolium type ionic liquids. *J. Phys. Chem. B*, 112, 10228-10233.
- Zhang, W.; Yang, T.; Zhuang, X. M.; Guo, Z. Y. & Jiao, K. (2009). An ionic liquid supported CeO<sub>2</sub> nanoshuttles-carbon nanotubes composite as a platform for impedance DNA hybridization sensing. *Biosens. Bioelectron.*, 24, 2417-2422.
- Zhao, D. B.; Wu, M.; Kou, Y. & Min, E. (2002). Ionic liquids: applications in catalysis. *Catal. Today*, 74, 157-189.
- Zhao, N.; Liu, L.; Biedermann, F. & Scherman, O. A. (2010). Binding studies on CB[6] with a series of 1-alkyl-3-methylimidazolium ionic liquids in an aqueous system. *Chem.-Asian J.*, 5, 530-537.
- Zhao, Y.; Gao, S. J.; Wang, J. J. & Tang, J. M. (2008a). Aggregation of ionic liquids [C<sub>n</sub>mim]Br (n=4, 6, 8, 10, 12) in D<sub>2</sub>O: A NMR study. *J. Phys. Chem. B*, 112, 2031-2039.
- Zhao, Y.; Li, M. & Lu, Q. H. (2008b). Tunable wettability of polyimide films based on electrostatic self-assembly of ionic liquids. *Langmuir*, 24, 3937-3943.
- Zhao, Y. R.; Chen, X.; Jing, B.; Wang, X. D. & Ma, F. M. (2009a). Novel gel phase formed by mixing a cationic surfactive ionic liquid [C<sub>16</sub>mim]Cl and an anionic surfactant SDS in aqueous solution. *J. Phys. Chem. B*, 113, 983-988.
- Zhao, Y. R.; Chen, X. & Wang, X. D. (2009b). Liquid crystalline phases self-organized from a surfactant-like ionic liquid [C<sub>16</sub>mim]Cl in ethylammonium nitrate. *J. Phys. Chem. B*, 113, 2024-2030.

- Zheng, L.; Guo, C.; Wang, J.; Liang, X. F.; Chen, S.; Ma, J. H.; Yang, B.; Jiang, Y. Y. & Liu, H. Z. (2007). Effect of ionic liquids on the aggregation behavior of PEO-PPO-PEO block copolymers in aqueous solution. *J. Phys. Chem. B*, *111*, 1327-1333.
- Zheng, Y.; Xuan, X. P.; Wang, J. J. & Fan, M. H. The enhanced dissolution  $\beta$ -cyclodextrin in some hydrophilic ionic liquids. *J. Phys. Chem. A*, *114*, 3926-3931.
- Zhou, Y. & Antonietti, M. (2004). A series of highly ordered, super-microporous, lamellar silicas prepared by nanocasting with ionic liquids. *Chem. Mater.*, *16*, 544-550.

# Formation of Complexes in RTIL and Ion Separations

Konstantin Popov<sup>1,2</sup>, Andrei Vendilo<sup>2</sup>, Igor Pletnev<sup>3</sup>, Marja Lajunen<sup>4</sup>,  
Hannu Rönkkömäki<sup>5</sup> and Lauri H.J. Lajunen<sup>4</sup>

<sup>1</sup>*Department of Physical and Colloid Chemistry, Moscow State University of Food  
Production, Moscow,*

<sup>2</sup>*Institute of Reagents and high purity Substances (IREA), Moscow,*

<sup>3</sup>*Department of Chemistry M.V.Lomonosov State University, Moscow,*

<sup>4</sup>*Department of Chemistry, Oulu University, Oulu,*

<sup>5</sup>*Finnish institute of Occupational Health, Oulu,*

<sup>1,2,3</sup>*Russia*

<sup>4,5</sup>*Finland*

## 1. Introduction

Room temperature ionic liquids (RTILs) are gaining an increasing interest as a unique medium for a complex formation and development of new inorganic materials (Cocalia et al, 2006; Billard et al, 2003; Yan et al, 2010; Vendilo et al, 2010; Nockemann et al, 2009; Nockemann et al, 2008; Murding & Tang, 2010; Billard & Gaillard, 2009; Taubert, 2004; Tang et al, 2008). Among the most promising fields the RTIL-based lithium batteries (Lewandowski & Swiderska-Mocek, 2009; Rosol et al, 2009) and recent applications of ionic liquids in the separation technology (Dundan & Kyung, 2010; Dietz, 2006) can be considered as a “hot” research topic. The present review is therefore focused on the role of cation complexes in RTIL-based metal ion separations, while the other important aspects of inorganic salt behaviour in RTILs are excellently summarised in another chapter of this book (Nockemann, 2011).

RTILs are intensively studied in solvent extraction processes due to such important advantages over conventional organic diluents as negligible vapor pressure, low flammability, moisture stability, relatively high radiation stability, different extraction properties and possibility to eliminate aqueous phase acidification (Cocalia et al, 2006a; Visser et al, 2000; Dai et al, 1999; Luo et al, 2006; Chen, 2007; Chun et al, 2001; Visser & Rogers, 2003). It is demonstrated that extraction efficacy of RTIL can be also modulated by a chelating agent administration. Dai *et al.* (Dai et al, 1999), for example, first discovered that highly efficient extraction of strontium ions can be achieved when dicyclohexane-18-crown-6 (DC18C6) is combined with RTILs. Visser *et al.* (Visser et al, 2000) reported the extraction of various alkali metal ions with crown ethers in RTILs. Visser and Rogers demonstrated that octyl(phenyl)-*N,N*-diisobutylcarbamoylmethylphosphine oxide dissolved in RTILs enhanced the extractability of lanthanides and actinides in comparison to conventional organic solvents (Visser & Rogers, 2003). The extraction of silver ions was found to be greatly enhanced by a combined application of RTIL and calyx[4]arene compared to that of

chloroform (Shimojo & Goto, 2004). In addition, the task-specific RTILs with coordination capacity built in the RTIL cation have been reported (Visser, et al, 2002; 2001a). Recently the efficiency of chelate extraction of 3d-cations with 8-sulfonamidoquinoline (Ajioka et al, 2008), Pu(IV) with carbamoylmethylphosphine oxide (Lohithakshan & Aggarwal, 2008) and uranyl ion with tributylphosphate (TBP) (Dietz & Stepinski, 2008) from aqueous phase into RTILs was reported. The higher selectivity of dibenzo-18-crown-6 (DB18C6) to  $K^+$  over  $Na^+$  in *N*-octadecylisoquinolinium tetrakis[3,5-bis(trifluoromethyl)phenyl]borate compared with that in molecular solvents suggests that RTIL provides a unique solvation environment for the complexation of crown ethers with the ions (Nishi et al, 2006). These research results provided numerous analytical applications of RTILs (Berton & Wuilloud, 2010; Ning et al, 2010; Manzoori, et al, 2009; Lertlapwasin et al, 2010). This Chapter is intended to present a review of data on complex formation of cations in hydrophilic and hydrophobic RTILs, (Table 1) in relevance to the extraction and separation processes.

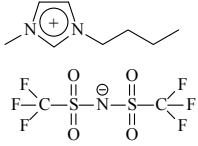
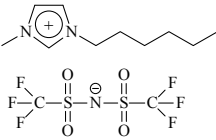
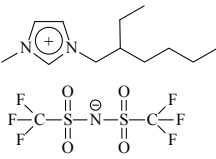
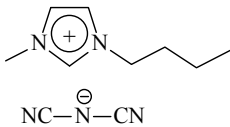
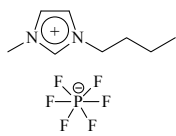
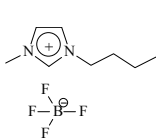
Chemical formula	Abbreviation	Name, Comment
	[BMIM][N(Tf) <sub>2</sub> ]	1-butyl-3-methylimidazolium bis[trifluoromethylsulphonyl]imide; hydrophobic RTIL
	[HMIM][N(Tf) <sub>2</sub> ]	1-hexyl-3-methylimidazolium bis[trifluoromethylsulphonyl]imide; hydrophobic RTIL
	[EtHMIM][N(Tf) <sub>2</sub> ]	1-(2-ethylhexyl)-3-methylimidazolium bis[trifluoromethylsulphonyl]imide; hydrophobic RTIL
	[BMIM][N(CN) <sub>2</sub> ]	1-butyl-3-methylimidazolium dicyanamide; hydrophilic RTIL
	[BMIM][PF <sub>6</sub> ]	1-butyl-3-methylimidazolium hexafluorophosphate; hydrophobic RTIL
	[BMIM][BF <sub>4</sub> ]	1-butyl-3-methylimidazolium tetrafluoroborate; hydrophilic RTIL

Table 1. Chemical formulae and abbreviations of RTILs commonly used in a present review

Chemical formula	Abbreviation	Name, Comment
	[TOMA][Sal]	trioctylmethylammonium salicylate; task-specific hydrophobic RTIL
	[THA][DHSS]	Tetrahexylammonium dihexylsulfosuccinate; task-specific hydrophobic RTIL
	[BMPy][BF <sub>4</sub> ]	N-butyl-4-methyl-pyridinium tetrafluoroborate; hydrophilic RTIL

Table 1. (Continued) Chemical formulae and abbreviations of RTILs commonly used in a present review

## 2. Thermodynamics of complex formation in RTIL

Inorganic salts usually have poor solubility in both hydrophobic and hydrophilic RTILs at a level of 0.05–0.005 mol/dm<sup>3</sup> (Yan et al, 2010; Seddon et al, 2000; Rosol et al, 2009; Djigailo, 2010), although in some cases (LiClO<sub>4</sub> in [BMIM][SCN]) it may exceed 4 mol/dm<sup>3</sup> at ambient temperature (Rosol et al, 2009). Thus for a successive extraction of cations from aqueous solution into a hydrophobic RTIL some complexing agents are required (Cocalia et al, 2006a; Visser et al, 2000) as well as in the case of conventional organic solvents. These agents are either added to RTIL or are synthetically included into the RTIL's anion or cation structure (task-specific RTILs). This in turn requires a knowledge of particular complexes participating the extraction equilibria and chemical speciations.

However, the number of reports on the complex composition, equilibrium constants and thermodynamics of complex formation is surprisingly small relative to that of conventional molecular solvents, Table 2. The data on  $\Delta H$  and  $\Delta S$  of complex formation are even less common (Vendilo et al, 2010a; 2010c; 2009a).

It should be noted that all the constants mentioned in Table 2 represent co-called "conditional" equilibrium constants defined as:

$$\beta_n = [\text{ML}_n][\text{M}]^{-1}[\text{L}]^{-n} \quad (1)$$

where [M], [L] and [ML<sub>n</sub>] represent the concentrations of cation M, ligand L and complex species ML<sub>n</sub> (electrostatic charges are omitted for simplicity).

In a same way:

$$K_n = [\text{ML}_n][\text{ML}_{n-1}]^{-1}[\text{L}]$$

Cation	Ligand	RTIL	Method	Ref.
UO <sub>2</sub> <sup>2+</sup>	NO <sub>3</sub> <sup>-</sup>	[BMIM][N(Tf) <sub>2</sub> ]	UV-Vis, 18.5 °C	Georg et al, 2010
Ag <sup>+</sup>	Cryptand 222	[EMIM][BF <sub>4</sub> ],[BMIM][BF <sub>4</sub> ] [EMIM][CF <sub>3</sub> SO <sub>3</sub> ] [EMIM][N(Tf) <sub>2</sub> ] [BMIM][N(Tf) <sub>2</sub> ] [BMIM][N(Tf) <sub>2</sub> ] [BMIM][N(Tf) <sub>2</sub> ] [MPPyr][N(Tf) <sub>2</sub> ] [BMPyr][N(Tf) <sub>2</sub> ] [TDMA][TFPB] <sup>a</sup>	Potentiom.; Ag-electrode 25 °C	Lewandowski et al, 2005;
H <sup>+</sup> ,Li <sup>+</sup> , Na <sup>+</sup> K <sup>+</sup> , Rb <sup>+</sup> , Cs <sup>+</sup> , NH <sub>4</sub> <sup>+</sup>	Valinomycin		Cyclic voltammetry; 25 °C	Langmaier & Samec, 2009
Li <sup>+</sup> , Na <sup>+</sup> K <sup>+</sup> , Rb <sup>+</sup>	DB-18-crown-6	[ODIQ][TFBP] <sup>b</sup>	Cyclic voltammetry; 56 °C	Nishi et al, 2006 ;
Li <sup>+</sup>	12-crown-4 15-crown-5 18-crown-6 Bz-15-crown-5	The binary molten salt mixture: 55/45 mol. % methyl-3-ethylimidazolium chloride and AlCl <sub>3</sub>	<sup>7</sup> Li <sup>+</sup> NMR, 1- 22 °C	Eyring et al, 1993
Li <sup>+</sup> Cs <sup>+</sup>	OH <sup>-</sup> 18-crown-6	[THA][DHSS] [BMIM][BF <sub>4</sub> ], [THA][DHSS] [BMIM][N(Tf) <sub>2</sub> ], [BMPy][BF <sub>4</sub> ] [BMIM][PF <sub>6</sub> ], [TOMA][Sal] [BMIM][N(CN) <sub>2</sub> ] [BMIM][CF <sub>3</sub> SO <sub>3</sub> ] [HMIM][N(Tf) <sub>2</sub> ] [EtHMIM][N(Tf) <sub>2</sub> ]	NMR,25 °C <sup>133</sup> Cs NMR, 25 - 50 °C in a water saturated RTIL	Djigailo, 2010 Popov et al, 2007; Vendilo, et al, 2010a,c; Vendilo et al, 2009, 2009a
Cs <sup>+</sup>	DB-18-crown-6	[BMIM][N(Tf) <sub>2</sub> ] [THA][DHSS],[TOMA][Sal]	NMR <sup>133</sup> Cs, 25 - 50 °C	Djigailo, 2010
Na <sup>+</sup> , Cs <sup>+</sup>	18-crown-6; DB-18-crown-6	[BMPy][BF <sub>4</sub> ]/water solvent	mixed NMR <sup>133</sup> Cs, <sup>23</sup> Na; 25 °C	Popov et al, 2007
Sr <sup>2+</sup>	Dichloromethylene- bis(phosphonic acid) triisopropyl ester	[BMIM][N(CN) <sub>2</sub> ]	NMR <sup>31</sup> P, 25 °C	Vendilo, 2010d
Ni <sup>2+</sup> , Pb <sup>2+</sup>	2-aminothiophenol	[BMIM][PF <sub>6</sub> ]	25 °C, extraction;	Lertlapwasin et al, 2010
Cu <sup>2+</sup>	ethylenediamine	[BPy][NO <sub>3</sub> ] <sup>c</sup>	UV-Vis; 25-45 °C	Song et al, 2005

<sup>a</sup> Tridodecylmethylammonium tetrakis[3,5-bis(trifluoromethyl)phenyl]borate; <sup>b</sup> N-octadecyl-isoquinolinium tetrakis[3,5-bis(trifluoromethyl)phenyl]borate; <sup>c</sup> N-butylpyridinium nitrate

Table 2. Complexes in RTIL, characterized by stability constants

Complex formation studies in aqueous solutions require the ionic strength control (Popov & Wanner, 2005), which is normally provided by an inert supporting electrolyte added in amounts that several orders of magnitude exceed the content of reagents participating in the equilibrium. Therefore the correct comparison of the equilibrium data is possible when they are referred to an equal ionic strength values.

In the case of RTILs the ionic strength is provided by the solvent itself. Thus the ionic strength  $I$  depends on a density and molar mass of a RTIL and varies in a rather wide range. For example,  $I = 5.35 \text{ mol} \cdot \text{dm}^{-3}$  for [BMIM][BF<sub>4</sub>], 4.83 for [BMIM][PF<sub>6</sub>], and 2.91 for [BMIM][N(Tf)<sub>2</sub>]. In our review we have used the “conditional” constants in the form they have been published, although these can be transformed into thermodynamic constants.

Unfortunately up to now there are no systems studied by at least two independent research groups. At the same time, the stability constants published evidently have different quality. For example, all constants presented in (Eyring et al, 1993) have too high SD to be treated by IUPAC even as provisional. Indeed,  $\log K_1$  values for Li<sup>+</sup> complexes with 12-crown-4, 15-crown-5, benzo-15-crown-5 (Bz-15-crown-5) and 18-crown-6 (18C6) in a mixture of RTILs are reported to be  $3.1 \pm 2.3$ ,  $4.1 \pm 3.5$ ,  $3.5 \pm 2.9$  and  $1.8 \pm 0.6$  respectively (Eyring et al, 1993).

The constants presented in (Lertlapwasin et al, 2010) are not actually the stability constants, but are some effective ones. Those published for valinomycin (Langmaier & Samec, 2009) seem to be overestimated, as far as they exceed any known constants for this ligand in any solvent by several orders of magnitude. However, the data that are reported for Ag<sup>+</sup> seem to be reliable, as the presented by this group value for DMSO fits in very well with the corresponding data of several independent research groups. Some of the  $\log K$  values for RTILs are presented in Tables 3-5 along with the stability of the same complexes in some molecular solvents (Ruas et al, 2006; Ikeda et al, 2008; Danil de Namor et al, 1995; Arnaud-Neu et al, 2003; Bessiere & Lejaille, 1979; Ernst & Jezowska-Trzebiatowska, Jezowska-Trzebiatowska & Chmielowska, 1961; Chmielowska, 1961; Kikuchi & Sakamoto, 2000).

As could be seen from Table 3 the stability of such different species as [UO<sub>2</sub>(NO<sub>3</sub>)<sub>3</sub>]<sub>i</sub>, [Ag(Cryptand 2.2.2)]<sup>+</sup> and [Cs(18C6)]<sup>+</sup> in a “classical” RTIL [BMIM][N(Tf)<sub>2</sub>], is generally higher than in water, but lower than in the less polar molecular solvents. The same result we recently got for complexes of Sr<sup>2+</sup> with dichloromethylene-bis(phosphonic acid) triisopropyl ester:  $\log K_1 = 3.5$  in [BMIM][N(CN)<sub>2</sub>], while in water  $\log K_1 = -0.37$  (Vendilo, 2010d). Only for Li<sup>+</sup> complex with OH<sup>-</sup> in [THA][DHSS],  $\log K_1 = -0.22$  is comparable within the error with the value obtained for water:  $-0.1$  (Djigailo, 2010).

This trend can be observed clearly for [Cs(18-crown-6)]<sup>+</sup> stability in a number of hydrophobic and hydrophilic RTILs, Table 4. The only one exception registered up to now is a case of task-specific RTIL [THA][DHSS], in which an anion of ionic liquid competes for Cs<sup>+</sup> with 18-crown-6 and therefore diminishes the  $\log K_1$  of [Cs(18-crown-6)]<sup>+</sup> complex. This conclusion is of importance for extraction of cations from aqueous solutions.

It was noted, that the  $\log K_1$  values for RTILs fall inside, but not outside the range of those for molecular solvents, with location between acetonitrile and water (Vendilo et al, 2010). At the same time, the  $\log K_1$  values for an alkali metal cation with crown ether in molecular solvents is correlated (Mei et al, 1977; Smetana & Popov, 1980) with donor number (DN) of the solvent (Reichardt, 2005), Table 5, although some exceptions for [Cs(18C6)]<sup>+</sup> are known (pyridine: DN 33.1;  $\log K_1 = 5.7$  (Mei et al, 1977)). In this sense, the  $\log K_1$  value presented in Table 5 suggest that hydrophobic RTILs [HMIM][N(Tf)<sub>2</sub>], [BMIM][N(Tf)<sub>2</sub>], [BMIM][PF<sub>6</sub>], [TOMA][Sal] as well as hydrophilic [BMIM][N(CN)<sub>2</sub>] [BMPy][BF<sub>4</sub>] [BPy][MeSO<sub>4</sub>] have DN between 33 (water) and 14 (acetonitrile), e.g. span the same range that polar molecular

solvents do, but are rather far from such nonpolar solvent as 1,2-dichloroethane (DN 0 (Kikuchi & Sakamoto, 2000)). This observation spreads out the data reported by Nishi *et al.* for  $\text{Li}^+$ ,  $\text{Na}^+$ ,  $\text{K}^+$  and  $\text{Rb}^+$  complexes with dibenzo-18-crown-6 in a hydrophobic RTIL *N*-octadecylisoquinolinium tetrakis[3,5-bis(trifluoromethyl)phenyl]borate, which is demonstrated to have DN between 4.4 (nitrobenzene) and 0 (1,2-dichloroethane).

Complex	$\log \beta_i$				
	[BMIM][N(Tf) <sub>2</sub> ]	H <sub>2</sub> O	Acetonitrile	DMSO	MeOH
[UO <sub>2</sub> NO <sub>3</sub> ] <sup>+</sup>	4.8 <sup>a</sup>	0.30 <sup>b</sup>	7.9 <sup>c</sup>		
[UO <sub>2</sub> (NO <sub>3</sub> ) <sub>2</sub> ]	8.3 <sup>a</sup>	0.31 <sup>b</sup>	15.0 <sup>c</sup>		<sup>d</sup>
[UO <sub>2</sub> (NO <sub>3</sub> ) <sub>3</sub> ] <sup>-</sup>	12.2 <sup>a</sup>		20.0 <sup>c</sup>		
[Ag(Cryptand 222)] <sup>+</sup>	10.0 <sup>e</sup>	9.6 <sup>f</sup>	9.01 <sup>j</sup>	8.4 <sup>e</sup>	12.3 <sup>f</sup>
[Cs(18-crown-6)] <sup>+</sup>	3.4 <sup>h</sup>	0.91 <sup>i</sup>	4.8 <sup>i</sup>	3.04 <sup>i</sup>	4.6 <sup>i</sup>
[Cs(18-crown-6)] <sub>2</sub> <sup>+</sup>	1.29 <sup>h</sup>		0.6 <sup>i</sup>		2.06 <sup>i</sup>

<sup>a</sup> (Georg *et al.*, 2010); <sup>b</sup> (Ruas *et al.*, 2006); <sup>c</sup> (Ikeda *et al.*, 2008); <sup>d</sup>  $\log K_2 = 3.67$  (Ernst & Jezowska-Trzebiatowska, 1966) and 3.4 (Jezowska-Trzebiatowska & Chmielowska, 1961); <sup>e</sup> (Lewandowski *et al.*, 2005); <sup>f</sup> (Bessiere & Lejaille, 1979); <sup>j</sup> (Danil de Namor *et al.*, 1995); <sup>h</sup> (Vendilo *et al.*, 2010); <sup>i</sup> (Arnaud-Neu *et al.*, 2003); all data for 23-30 °C.

Table 3. Stability constants of complexes in [BMIM][N(Tf)<sub>2</sub>] and in molecular solvents

M <sup>+</sup>	RTIL / L	$\log K_1$	RTIL / L	$\log K_1$
	(Nishi <i>et al.</i> , 2006)		(Langmaier & Samec, 2009)	
Li <sup>+</sup>	[TDMA][TFPB]/DB18C6	5.0	[TDMA][TFPB]/valinomycin	11.1
Na <sup>+</sup>	[TDMA][TFPB]/DB18C6	7.0	[TDMA][TFPB]/ valinomycin	12.8
K <sup>+</sup>	[TDMA][TFPB]/DB18C6	8.2	[TDMA][TFPB]/ valinomycin	17.2
Rb <sup>+</sup>	[TDMA][TFPB]/DB18C6	7.3	[TDMA][TFPB]/ valinomycin	15.7
Cs <sup>+</sup>	[BMIM] [N(Tf) <sub>2</sub> ]/ DB18C6	3.47 <sup>a</sup>	[TDMA][TFPB]/ valinomycin	15.1
NH <sub>4</sub> <sup>+</sup>			[TDMA][TFPB]/ valinomycin	14.7

<sup>a</sup> Ref. (Djigailo, 2010); for  $\text{Li}^+$ ,  $\text{Na}^+$ ,  $\text{K}^+$  and  $\text{Rb}^+$  complexes with DB18C6 in 1,2-dichloroethane  $\log K_1$ : 11.3; 11.2; 9.9; 8.3; in nitrobenzene: 4.8; 7.3; 7.2; 5.2; in DMFA: 3.0; 3.34; 3.54, 3.54; for  $\text{Na}^+$ ,  $\text{K}^+$  and  $\text{Rb}^+$  in water: 1.16; 1.67; 1.08 and in methanol: 4.40; 5.05 and 4.23 respectively (Nishi *et al.*, 2006); for  $\text{Cs}^+$  complex with valinomycin in methanol  $\log K_1=3.90$ , for  $\text{K}^+$  4.48-4.90; for  $\text{NH}_4^+$  1.67;  $\text{Na}^+$  0.67-1.1;  $\text{Rb}^+$  4.81 (IUPAC, 2007)

Table 4. Stability constants of alkali metal complexes with DB18C6 and valinomycin in RTIL at 25 °C

There is also some qualitative agreement of the  $\log K_1$  values and a solvent polarity derived from  $E_{\text{N}^{\text{T}}}$  scale (Reichardt, 2005) (empirical scale based on solvatochromic pyridinium *N*-phenolate betaine dye), Table 5. An examination of Table 5 reveals that the polarity of RTILs with a range of 0.60 – 0.65 fits well into the existing empirical solvent polarity scale for molecular solvents characterizing them not as “superpolar”, but as quite normal polar solvents (Reichardt, 2005). In this respect it is interesting to note, that the water content in RTIL strongly affects both stability constants (Popov *et al.*, 2007) and  $E_{\text{N}^{\text{T}}}$  values (Reichardt, 2005). As far as all  $\log K_1$  values in Table 5 correspond to a water saturated samples, this might be a reason of a far not ideal correlation between  $E_{\text{N}^{\text{T}}}$  and stability constants.



A tendency to form  $ML_2$  complexes decreases sybatic with DN, or antibatic with  $E_{N_T}$ .  $Cs^+$  forms therefore only ML complexes with 18-crown-6 in water ( $E_{N_T}$  10), DMSO ( $E_{N_T}$  0.45) and [BMIM][PF<sub>6</sub>], [TOMA][Sal], [BMIM][BF<sub>4</sub>] ( $E_{N_T}$  0.66-0.67), while in a weakly solvating solvents 1,2-dichloroethane ( $E_{N_T}$  0.3 for CH<sub>2</sub>Cl<sub>2</sub>), acetone ( $E_{N_T}$  0.35), DMFA ( $E_{N_T}$  0.4) and [HMIM][NTf<sub>2</sub>] ( $E_{N_T}$  0.654), [BMIM][NTf<sub>2</sub>] ( $E_{N_T}$  0.596) also  $ML_2$  species are registered. The  $\log K_2$  values for [EtHMIM][N(Tf)<sub>2</sub>], [HMIM][N(Tf)<sub>2</sub>] and [BMIM][N(Tf)<sub>2</sub>] appeared to be 2 to 3 log units lower then  $\log K_1$ , Table 5. These values correspond well to those found for molecular solvents, and for  $UO_2^{2+}$  complexes with  $NO_3^-$  in [BMIM][N(Tf)<sub>2</sub>], Table 3.

Solvent	DN <sup>b</sup>	$E_{N_T}$ <sup>c</sup>	$\log K_1$	$\log K_2$	Reference
1,2-Dichloroethane	0		7.98	2.58	Kikuchi & Sakamoto, 2000
Acetonitrile	14.1		4.8	0.6	Arnaud-Neu et al, 2003; Mei et al, 1977
Propylene carbonate	15.1		4.50	1.0	Arnaud-Neu et al, 2003; Mei et al, 1977
Acetone	17.0	0.35	4.51	1.5	Arnaud-Neu et al, 2003; Mei et al, 1977
[HMIM][N(Tf) <sub>2</sub> ]		0.654	4.4	1.13	Vendilo et al, 2010
DMFA	26.6	0.40	3.64	0.4	Arnaud-Neu et al, 2003; Mei et al, 1977 )
[EtHMIM][N(Tf) <sub>2</sub> ]			3.4	1.16	Vendilo et al, 2010
[BMIM][N(Tf) <sub>2</sub> ]		0.596	3.4	1.29	Vendilo et al, 2010
DMSO	29.8	0.45	3.04		Arnaud-Neu et al, 2003
[BMIM][N(CN) <sub>2</sub> ]			3.03		Popov, 2007a
[BMIM][BF <sub>4</sub> ]		0.673	2.8		Popov, 2007a
[BMPy][BF <sub>4</sub> ]		0.630	2.6		Popov, 2007a
[BMIM][PF <sub>6</sub> ]		0.667	2.4		Vendilo et al, 2010
[TOMA][Sal]			1.43		Vendilo et al, 2010
[BPy][MeSO <sub>4</sub> ]			1.20		Vendilo et al, 2008
Water	33	1.0	0.96	-	Arnaud-Neu et al, 2003
[THA][DHSS]			0.76		Vendilo et al, 2010

<sup>a</sup> For molecular solvents  $\log K_1$  values are given for  $I = 0 - 0.1 \text{ mol/dm}^3$ ; ref. (Arnaud-Neu et al, 2003) indicates IUPAC selection; <sup>b</sup> Ref. (Gutmann & Vichera, 1966); <sup>c</sup> Ref. (Reichardt, 2005)

Table 5. Stability constants of cesium complexes with 18C6 in RTILs and in molecular solvents at 25 °C.

Indeed N(Tf)<sub>2</sub>-anion has a very weak solvating ability, being easily substituted in coordination sphere of  $UO_2^{2+}$  even by nitrate ion, which in turn demonstrates a very high stability. For a long time it was believed that N(Tf)<sub>2</sub><sup>-</sup> does not form complexes, unless the crystal structures of [PMIM][Eu(N(Tf)<sub>2</sub>)<sub>4</sub>], [BMIM][Eu(N(Tf)<sub>2</sub>)<sub>4</sub>], [BMPy]<sub>2</sub>[Eu(N(Tf)<sub>2</sub>)<sub>5</sub>] (Tang et al, 2008) and [mppy]<sub>2</sub>[Yb(N(Tf)<sub>2</sub>)<sub>5</sub>], where PMIM indicates 1-propyl-3-methylimidazolium and mppy - 1-methyl-1-propylpyrrolidinium (Murdine, et al 2005), have demonstrated that it can coordinate as a bidentate ligand via oxygen atoms forming either 6-membered or 4-membered rings:



Similar structures have been found for alkaline earth metals: [mppy<sub>2</sub>][Ca(N(Tf)<sub>2</sub>)<sub>4</sub>], [mppy<sub>2</sub>][Sr(N(Tf)<sub>2</sub>)<sub>4</sub>] and [mppy<sub>2</sub>][Ba(N(Tf)<sub>2</sub>)<sub>3</sub>] (Babai & Murding, 2006). Even the alkali ions are found to form weak bonds with N(Tf)<sub>2</sub><sup>-</sup> (Yan et al, 2010). An X-Ray structure of [K(18C6)][N(Tf)<sub>2</sub>] revealed that bistriflimide anion forms an asymmetric bridge between two [K(18C6)]<sup>+</sup> units. One has a monodentate bond with an oxygen atom of one Tf fragment of N(Tf)<sub>2</sub><sup>-</sup> anion. Another Tf arm is coordinated via two oxygen atoms with a formation of a chelate ring with K<sup>+</sup> to the second [K(18C6)]<sup>+</sup> unit. The potassium ions have therefore the coordination numbers 7 and 8.

A saturation of RTILs with water leads generally to a decrease of stability constant value for alkali metal complexes with crown ethers. For [Cs(18C6)]<sup>+</sup> in [BMPy][BF<sub>4</sub>]/water mixed solvents a linear dependence of logK<sub>1</sub> on RTIL content was observed (Popov et al, 2007). This behavior is similar to that in water/ethanol mixtures (Arnaud-Neu et al, 2003).

An increase of temperature decreases the stability constants of CsL for [HMIM][N(Tf)<sub>2</sub>], [BMIM][N(Tf)<sub>2</sub>] and [BMIM][PF<sub>6</sub>], but increases them for [TOMA][Sal] and [THA][DHSS]. The thermodynamic quantities for the formation of [Cs18C6]<sup>+</sup> in RTIL are summarized in Table 6 together with those for molecular solvents.

With an exception of [THA][DHSS] and [TOMA][Sal], the cesium nitrate solubility in RTIL is much less than in water, the metal-solvent interaction is likely to be stronger in water, than in RTIL, *i.e.* less energy is needed for breaking the metal-(RTIL anion) bonds. Thus the

Solvent	$\Delta H_1$ , kJ/mol	$\Delta S_1$ , J/(mol K)	$\Delta H_2$ , kJ/mol	$\Delta S_2$ , J/(mol K)	Reference
Acetonitrile	-17 (1)	35			Arnaud-Neu et al, 2003
Propylene carbonate	-43.3	-17.6			Arnaud-Neu et al, 2003
Methanol	-47.2	-70.5	-13.9	-7.1	Arnaud-Neu et al, 2003
Acetone	-52.8 (0.4)	-27.2			Arnaud-Neu et al, 2003
DMFA	-49.2 (0.8)	-28.4			Arnaud-Neu et al, 2003
[EtHMIM][N(Tf) <sub>2</sub> ]	9 (18)	100 (60)	-17.5 (0.3)	-36.5 (1.0)	Vendilo et al, 2010
[HMIM][N(Tf) <sub>2</sub> ]	-9.5 (0.4)	53 (15)	-17.8 (0.3)	-38.3 (0.9)	Vendilo et al, 2010
[BMIM][N(Tf) <sub>2</sub> ]	-6.8 (1.9)	41.5 (6.1)	-41.3 (0.7) <sup>b</sup>	-114 (1) <sup>b</sup>	Vendilo et al, 2010
[BMIM][N(CN) <sub>2</sub> ]	-47 (2)	-30 (2)			Popov et al, 2007a
[BMIM][BF <sub>4</sub> ]	-80 (3)	-65 (3)			Popov et al, 2007a
[BMIM][PF <sub>6</sub> ]	-21.0 (1.4)	-25.4 (4.5)			Vendilo et al, 2010
[BMPy][BF <sub>4</sub> ]	-47 (1)	-32 (1)			Popov et al, 2007a
[TOMA][Sal]	3.85 (0.25)	40.3 (0.7)			Vendilo et al, 2010
Water	-17 (1)	-39			Arnaud-Neu et al, 2003
[THA][DHSS]	2.1 (0.3)	21.6 (1.1)			Vendilo et al, 2010

<sup>a</sup> Ref. (Arnaud-Neu et al, 2003), corresponds to 25 °C and *I* = 0 – 0.1 mol/dm<sup>3</sup>, IUPAC selection; <sup>b</sup> Ref. (Vendilo et al, 2008).

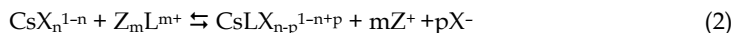
Table 6. Thermodynamic Quantities  $\Delta H_1$ ,  $\Delta S_1$ ,  $\Delta H_2$  and  $\Delta S_2$  of Cesium Complexes Formation with 18C6 in RTIL and in molecular solvents at 25 °C <sup>a</sup>.

differences in metal-solvent interactions are expected to make complex formation more exothermic in RTIL than in water. Indeed, for CsL formation  $\Delta H_1$  is negative for all hydrophilic RTILs, [HMIM][N(Tf)<sub>2</sub>], [BMIM][N(Tf)<sub>2</sub>], [BMIM][PF<sub>6</sub>] and almost for all polar molecular solvents.

Generally, it can be seen that enthalpy change promotes complex formation in hydrophilic RTIL, whereas the corresponding change of entropy is negative and provides the decomposition of [Cs(18C6)]<sup>+</sup>. However, this is not the case of hydrophobic RTILs [HMIM][N(Tf)<sub>2</sub>], [BMIM][N(Tf)<sub>2</sub>], [TOMA][Sal] and [THA][DHSS], that reveal a positive entropy change like acetonitrile. Moreover, the entropy change gives the dominating contribution to [Cs(18C6)]<sup>+</sup> stability in [BMIM][N(Tf)<sub>2</sub>], [TOMA][Sal] and [THA][DHSS]. Only one hydrophobic RTIL ([BMIM][PF<sub>6</sub>]) demonstrates the same behavior as hydrophilic RTILs and polar molecular solvents.

Thus, the thermodynamic quantities clearly indicate, that the contributions to the overall stability of CsL complex may differ rather significantly. The reaction enthalpies and entropies, show greater diversity, than  $\log K_1$  depending on RTIL composition. The complexation of Cs<sup>+</sup> is the most exothermic in [BMIM][BF<sub>4</sub>]. Moreover, the observed  $\Delta H_1$  value is the highest known for CsL in both molecular solvents and RTIL. At the same time the corresponding entropy change for this solvent is also the highest, diminishing the enthalpy contribution to the  $\log K_1$ . The data listed in Table 6 obviously indicate, that both cation and anion of RTIL affect the complex formation stability and thermodynamic functions change.

This is not simply explained in terms of the solvation of the cesium ion and 18C6. The tentative scheme of complex formation in RTIL (2) is more complicated than that in molecular solvents (Ohtsu & Ozutsumi, 2003; Ozutsumi et al, 1994). In general, both ions forming the ionic liquid (its cation Z<sup>+</sup> and anion X<sup>-</sup>) may react with cesium complex constituents. Z<sup>+</sup> is competing with cesium for the ligand, while X<sup>-</sup> solvates cesium, resisting complex formation:



In this respect <sup>133</sup>Cs NMR study can be considered as a very sensitive probe. The NMR chemical shift data, Table 7, indicate that crown ether does not substitute all RTIL anions X<sup>-</sup> in coordination sphere of cesium in [Cs18C6]<sup>+</sup> complexes, even in triflimide-based RTILs. This observation agrees well with X-ray structural data for cesium complexes with 18-crown-6 in solid state (Gjikaj & Adam, 2006; Ellerman et al, 1998) and in an aqueous solution (Ozutsumi et al, 1989), as well as with classical molecular dynamics simulations (Dang, 1995). In all these structures cesium is located above the mean oxygen plane of the crown ether ring since its size is larger than the cavity size of 18C6 (170 and 130 pm, respectively (Arnaud-Neu et al, 2003)). Thus the exposed part of Cs<sup>+</sup> may interact with RTIL anions making coordination number equal to 8 or 9 as it is observed crystallographically for molecular solvents. This supposition is also in a good agreement with the structural data for [K(18C6)][N(Tf)<sub>2</sub>] (Yan et al, 2010).

<sup>133</sup>Cs NMR chemical shifts of Cs<sup>+</sup> cation in RTILs span a very broad range from - 90 ppm ([BMIM][PF<sub>6</sub>]) to 90 ppm ([BMIM][N(CN)<sub>2</sub>]) clearly indicating their dependence on the RTIL's anion nature, but not of the cation's one. Indeed, for all three [N(Tf)<sub>2</sub>]-based RTILs the chemical shifts of Cs<sup>+</sup> are the same within the experimental error. At the same time the highly negative shift for [BMIM][PF<sub>6</sub>] is rather close to those observed for [BMPy][BF<sub>4</sub>] and [BMIM][BF<sub>4</sub>] (~ - 70 ppm).

Solvent	<sup>133</sup> Cs NMR chemical shift, ppm			Reference
	$\delta_{\text{Cs}}$	$\delta_{\text{CsL}}$	$\delta_{\text{CsL}_2}$	
Acetonitrile	24.1	14.8	-53 (7)	Mei et al, 1977
Propylene carbonate	-36.5	-8.1 (0.2)	-44.5 (0.3)	Mei et al, 1977
Acetone	-35.8	-6.4	-47 (9)	Mei et al, 1977
[HMIM][N(Tf) <sub>2</sub> ]	-30.7 (0.6)	-5 (1.0)	-50 (4)	Vendilo et al, 2010
DMFA	-0.8	3.37	-48 (1)	Mei et al, 1977
[EtHMIM][N(Tf) <sub>2</sub> ]	-30.6 (0.2)	-3.9 (0.2)	-51 (4)	Vendilo et al, 2010
[BMIM][N(Tf) <sub>2</sub> ]	-29.6 (0.5)	-5; -6.5	-47 (1)	Vendilo et al, 2010
DMSO	68.0	23.6	-49 (2)	Mei et al, 1977
[BMIM][N(CN) <sub>2</sub> ]	91 (1)	34 (1)	-	Popov et al, 2007a
[BMIM][BF <sub>4</sub> ]	-68 (4)	-22 (4)	-	Popov et al, 2007a
[BMPy][BF <sub>4</sub> ]	-70 (7)	-16 (5)	-	Popov et al, 2007a
[BMIM][PF <sub>6</sub> ]	-91 (2)	-7 (14)	-	Vendilo et al, 2010
[TOMA][Sal]	31 (0.7)	-29 (1)	-	Vendilo et al, 2010
[BPy][MeSO <sub>4</sub> ]	23.3 (0.5)	-7 (5)	-	Vendilo et al, 2008
[THA][DHSS]	22.5 (0.3)	-47 (2)	-	Vendilo et al, 2010

<sup>a</sup> All <sup>133</sup>Cs NMR chemical shifts are reported relative to external reference CsCl solution in D<sub>2</sub>O. Down field shifts are denoted as positive.

Table 7. <sup>133</sup>Cs NMR chemical shifts for [Cs(18C6)] and [Cs(18C6)<sub>2</sub>] complexes at 22-25 °C<sup>a</sup>

An increase of crown ether concentration in RTIL up to 1:1 cation/ligand molar ratio resulted in the corresponding monotonous increase of  $\delta_{\text{obs}}$  for [BMIM][N(Tf)<sub>2</sub>], [HMIM][N(Tf)<sub>2</sub>], [EtHMIM][N(Tf)<sub>2</sub>] and at a higher ligand excess for [BMIM][PF<sub>6</sub>] up to ~ -5 ppm, which corresponded to [Cs(18C6)]<sup>+</sup> species. By contrast, the chemical shifts of <sup>133</sup>Cs decreased as 18C6 was added to the [TOMA][Sal] and [THA][DHSS] solution. Thus, complex formation diminishes the differences in Cs<sup>+</sup> environment and makes chemical shifts  $\delta_{\text{CsL}}$  more close to each other for all RTIL, relative to  $\delta_{\text{Cs}}$ . This observation is consistent with the fact that in all solvents 18C6 occupies the major part of cesium coordination sphere in more or less similar way. However, the resonances of <sup>133</sup>Cs in [CsL]<sup>+</sup> still remain different in values and signs indicating different solvation and/or different ligand conformation of a complex, Table 7.

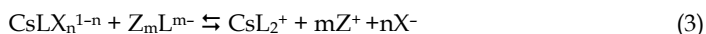
For [BMIM][N(Tf)<sub>2</sub>], [HMIM][N(Tf)<sub>2</sub>], [EtHMIM][N(Tf)<sub>2</sub>] an excess of 18C6 over [Cs][L] 1:1 molar ratio leads to decrease of a chemical shift indicating the CsL<sub>2</sub> complex formation. The upfield shift followed by a sharp break and a downfield shift which gradually approaches an almost the same limiting value for all three N(Tf)<sub>2</sub>-based RTILs can be explained by the formation of a strong CsL complex followed by addition of a second molecule of a ligand to form a "sandwich" CsL<sub>2</sub> complex. A similar break was also found for such molecular solvents as propylene carbonate, acetonitrile, and DMFA (Mei et al, 1977).

It is interesting to note that chemical shifts of [Cs(18C6)<sub>2</sub>]<sup>+</sup> are essentially independent of solvent's nature, Table 7, providing almost the same values for RTIL and for molecular solvents. This observation indicates that in a "sandwich"-type complex the two crown ether molecules effectively shield the cesium ion from interaction with solvent. By contrast, the chemical shifts of [Cs(18C6)]<sup>+</sup> are strongly solvent dependent both in RTIL and in molecular solvents.

Generally, chemical shift of  $^{133}\text{Cs}$  seems to depend rather on an anion's nature in RTIL, than on the cation's one. This can be expected reasonably, as the co-ordination sphere of  $\text{Cs}^+$  in RTIL is formed by anions. These anions are partly substituted by 18C6 due to complex formation, while the remaining ones provide the cause for differences in the chemical shifts of complexes. Indeed, the chemical shifts of  $\text{Cs}^+$  and  $[\text{Cs}18\text{C6}]^+$  are almost the same in  $[\text{BMIM}][\text{BF}_4]$  and  $[\text{BMPy}][\text{BF}_4]$  as well as in  $[\text{BMIM}][\text{N}(\text{Tf})_2]$ ,  $[\text{HMIM}][\text{N}(\text{Tf})_2]$  and  $[\text{EtHMIM}][\text{N}(\text{Tf})_2]$ . This is consistent with formation of similar species  $[\text{Cs} \cdot (\text{BF}_4)_n]^{1-n}$  and  $[\text{Cs}(18\text{C6}) \cdot (\text{BF}_4)_{n-x}]^{1-n+x}$  in both  $[\text{BF}_4]$ -based RTIL, as well as  $\{\text{Cs} \cdot [\text{N}(\text{Tf})_2]_m\}^{1-m}$  and  $\{\text{Cs}(18\text{C6}) \cdot [\text{N}(\text{Tf})_2]_{m-x}\}^{1-m+x}$  in those  $[\text{N}(\text{Tf})_2]$ -based. Meanwhile, for  $[\text{BMIM}][\text{N}(\text{CN})_2]$  and  $[\text{THA}][\text{DHSS}]$  the chemical shifts of  $\delta_{\text{Cs}}$  and  $\delta_{\text{CsL}}$  are definitely different, demonstrating a different environment of cesium in both species relative to those mentioned above.

On the other hand, a strong influence of the ionic liquid cation,  $Z^+$ , on  $\log K_1$ ,  $\Delta H_1$  and  $\Delta S_1$  values of complex formation is observed when  $[\text{BMIM}][\text{BF}_4]$  and  $[\text{BMPy}][\text{BF}_4]$  are compared, indicating  $Z^+$ -crown ether interactions of various intensity. Such interaction has also analogues among molecular solvents. For example, for AN, nitromethane (NM) and even for chloroform 18-crown-6 2AN, 18-crown-6 2NM and 18-crown-6 2 $\text{CH}_2\text{Cl}_2$  solvates have been isolated and their structures have been determined by X-ray crystallography (de Boer et al, 1982; Rogers et al, 1988; Garrell et al, 1988; Jones et al, 1994). Hence, both cation and anion of RTIL have an impact on the resultant stability constant and thermodynamic quantities of chelated compound.

For  $\text{ML}_2$  complexes in hydrophobic RTIL the situation is significantly different from that for ML complexes:  $\Delta H_2$  is more negative than  $\Delta H_1$ , at the same time  $\Delta S_2$  is negative, while  $\Delta S_1$  is positive. For the second crown ether molecule coordination in  $[\text{BMIM}][\text{N}(\text{Tf})_2]$ ,  $[\text{HMIM}][\text{N}(\text{Tf})_2]$  and  $[\text{EtHMIM}][\text{N}(\text{Tf})_2]$ , (3):



a possible explanation could be associated with a very weak  $X^-$  bonding in the  $\text{CsLX}_n^{1-n}$  species. An extreme case, when  $n = 0$ , is also possible. This is consistent with poor coordinating ability of the  $\text{N}(\text{Tf})_2^-$  anion towards alkali and alkaline earth cations (Jensen et al, 2002). Alternatively, in  $[\text{BMIM}][\text{PF}_6]$ ,  $[\text{BMIM}][\text{BF}_4]$ ,  $[\text{BMPy}][\text{BF}_4]$  and  $[\text{BMIM}][\text{N}(\text{CN})_2]$ , the solvent's anion  $X^-$  is bound to cesium more tightly and prevents  $\text{CsL}_2^+$  complex formation. Such interpretation is supported by a much better extraction of  $\text{CsNO}_3$  from water into RTIL for  $[\text{TOMA}][\text{Sal}]$ ,  $[\text{THA}][\text{DHSS}]$  and  $[\text{BMIM}][\text{PF}_6]$  relative to  $[\text{BMIM}][\text{N}(\text{Tf})_2]$ ,  $[\text{HMIM}][\text{N}(\text{Tf})_2]$  and  $[\text{EtHMIM}][\text{N}(\text{Tf})_2]$  in an absence of 18C6. Therefore a complex formation plays an important role in extraction processes.

### 3. Chelating agent assisted extraction of inorganic cations from water into RTIL

Solvent extraction represents a significant separation technique in both metal ion or organic compounds separations with numerous advantages over competing techniques. However, liquid-liquid extraction usually employs water-immiscible organic solvents, many of which are toxic, flammable and volatile (Dundan & Kyung, 2010; Dietz, 2006). Ionic liquids exhibit some properties that make them an attractive alternative to the conventional organic solvents: a good thermal stability, low vapor pressure, an ability to solubilize a wide range of solutes, low flammability, a wide liquid range and a very high tunability (Dietz, 2006).

Indeed, for the separations of gases, organic molecules and biomolecules (e.g. amino acids) the distribution coefficients have been found to exceed those of conventional solvents. At the same time, the situation with inorganic cation extraction is not so clear.

One of the first communications on  $\text{Sr}^{2+}$  extraction from water into a series of dialkylimidazolium-based RTILs in the presence of dicyclohexane-18-crown-6 reported  $\log D > 4$  (Dai et al, 1999), while most of molecular solvents revealed a very low extraction degree under same conditions. Moreover, this work has demonstrated that the extraction degree is tunable by varying either RTILs anion or a cation. Since this report an intensive research of RTILs extraction ability, selectivity and extraction mechanisms for inorganic cations separation was undertaken worldwide (Cocalia et al, 2006; Vendilo et al, 2010; Dundan & Kyung, 2010; Dietz, 2006; Visser et al, 2000; Chun et al, 2001; Visser & Rogers, 2003; Murding & Tang, 2010; Egorov et al, 2010; Davis, 2005; Djigailo, 2010; Manzoori, et al, 2009; Lertlapwasin et al, 2010). Within these the two distinct directions can be identified.

The first one is associated with attempts to vary the combination of a RTIL with an indifferent complexing ability and a complexing agent dissolved in a ionic liquid to enhance the target cation's solubility in order to obtain either a maximal  $D$  value or a higher extraction selectivity (Dietz, 2006; Cocalia et al, 2006a; Visser et al, 2000). This research area may be subdivided into two: the use of extractant systems employing neutral extractants (e.g., crown ethers, calixarenes, tri-*n*-butylphosphate) and acidic or anionic ones (e.g., organophosphorus acids, pseudohaloids, 2-thenoyltrifluoroacetone, etc.).

Another path assumes to gain the same objective by a modification of either a cation or an anion of RTIL's in such a way that they get an ability to form complexes with extracted substrates ("task-specific" RTILs) (Dietz, 2006; Egorov et al, 2010; Davis, 2005; Luo et al, 2006). In turn, the second area may also be subdivided into synthetic implementation of a complexing agent fragment in a RTIL's cation or in its anion. In some cases an anion itself can initially possess a sufficient complexing ability (e.g., [THA][DHSS], [TOMA][Sal]).

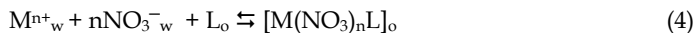
Recently the use of neutral extractants has received the most attention as they have played an important role in cation separations based on conventional solvents and therefore the direct comparison is possible (Dietz, 2006). Over a past decade some important peculiarities, advantages and drawbacks of RTILs relative to conventional solvents have been found.

An extraction efficiency of RTILs over conventional solvents was definitely observed for a series of cations in presence of neutral complexing agents (Dietz, 2006; Murding & Tang, 2010). At the same time, unlike for molecular solvents the  $D_M$  values for alkali and alkaline earth cations  $M$  in numerous RTIL/water systems in the presence of different crown ethers declined as  $\text{HNO}_3$  concentration in aqueous phase increased, then the  $D_M$  dependence passed a minimum at c.a.  $1 \text{ mol/dm}^3$  concentration and started to increase as nitric acid concentration increased up to  $3 \text{ mol/dm}^3$  (Dietz, 2006; Egorov et al, 2010). Our group has demonstrated that the pH-dependence of crown-ether assisted extraction from water into RTIL phase correlates well with the relative distribution of a crown (Vendilo, et al, 2009), Fig. 1, 2.

Such a behavior can be treated positively if an extraction from neutral aqueous solutions is considered. Then the elimination of the strong aqueous phase acidification usually needed for extraction enhancement by a molecular liquid is a definite advantage of RTILs. Meanwhile, the same effect becomes a disadvantage for some real liquid nuclear waste treatment, which is known to be initially highly acidic (Dietz, 2006; Djigailo, 2010).

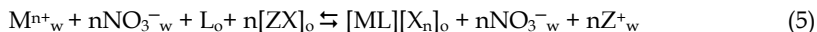
Another important peculiarity is a different extraction mechanism. For the conventional solvents an extraction of neutral species of a cation  $M^{n+}$  is required, e.g., if it is present in

aqueous solution in the form of nitrate, then its partitioning into the organic phase promoted by a neutral (nonionized) complexing agent L can be presented by a general equation (4):



where indexes "w" and "o" indicate aqueous and organic phase respectively.

Quite a different and a more complicated situation of ion exchange was observed for the extraction of metal ion nitrates from water into common RTILs, e.g., [BMIM][PF<sub>6</sub>] and [BMIM][N(Tf)<sub>2</sub>] (Dietz, 2006; Djigailo, 2010), equation (5):



where Z<sup>+</sup> and X<sup>-</sup> denote the cation and anion of a RTIL, respectively. A partitioning mechanism (5) in which metal ion transfer is accompanied by a loss of a RTIL's cation to an aqueous phase indicates a serious problem in potential applications of ionic liquids in liquid-liquid extraction. First of all, this mechanism questions the RTILs as "green" extractants. Indeed, solving the problem of air pollution by conventional solvents, RTILs give rise to an aqueous phase pollution by their cations. At the same time this process leads to the RTIL decomposition, shortens the number of extraction cycles and therefore makes the process more expensive.

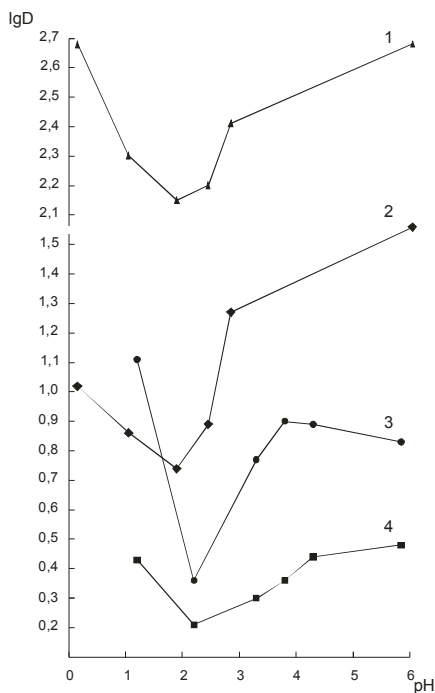


Fig. 1. pH profile of DB18C6 and 18C6 assisted cesium extraction (2) and (3) respectively, and of 18C6 (4) and DB18C6 (1) extraction from water into [TOMA][Sal] at 22 °C (Djigailo, 2010).

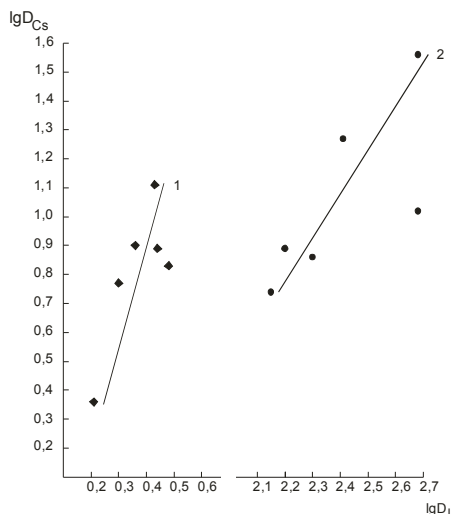
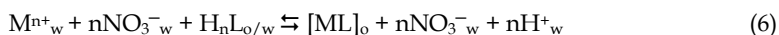


Fig. 2. Correlations between distribution coefficients of Cs<sup>+</sup> and crown ethers in [TOMA][Sal]: logD<sub>Cs</sub><sup>18C6</sup> and logD<sub>18C6</sub><sup>Cs</sup> (1); logD<sub>Cs</sub><sup>DB18C6</sup> and logD<sub>DB18C6</sub><sup>Cs</sup> (2)

The solution of this problem is possible if an ion exchange is somehow suppressed in favor of traditional extraction. Recently three approaches to diminish an ion exchange mechanism contribution have been described (Dietz, 2006): (i) an increase of alkyl chain length in 1-alkyl-3-methylimidazolium cation of RTIL; (ii) fluorination of this alkyl chain and (iii) use of a sacrificial cation exchanger.

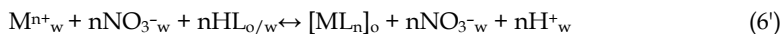
For the series of [RMIM][N(Tf)<sub>2</sub>] it was demonstrated that the partitioning mode of Sr<sup>2+</sup> into RTIL in presence of DC18C6 shifts from Scheme (5) to an equation (4) as R changes from pentyl to decyl, e.g. as the hydrophobicity of a RTIL cation increases (Dietz et al, 2003). Indeed, an increase of the alkyl chain length makes the transfer of [RMIM]<sup>+</sup> into aqueous phase more difficult and therefore shifts the balance of a relative contribution of ion exchange mechanism and of a neutral complex extraction in favor of the latter. However, the total extraction efficiency in this case decreases significantly. A similar result was obtained by fluorination of R (Dietz, 2006). Therefore both approaches (i) and (ii) seem to be the dead end. An alternative approach (iii) does not influence ion exchange mechanism, but simply aims to reduce the losses of imidazolium cations at the expense of specially added to a RTIL "sacrificial" cation. This cation partitions the aqueous phase instead of a RTIL's cation. For this purpose sodium tetraphenylborate was found to reduce [BMIM]<sup>+</sup> losses by 24% as Cs<sup>+</sup> was extracted into [BMIM][N(Tf)<sub>2</sub>] by "BOB-CalixC6" without any decrease of D<sub>Cs</sub> values (Luo et al, 2004). This approach looks better, but does not seem to become a universal and satisfactory solution. Anyhow, its further research is needed.

More advantageous looks the use of anionic complexing agents. Then the general extraction scheme may eliminate the ion exchange mechanism if a polydentate chelating agent H<sub>n</sub>L is properly selected in order to form zerocharged species [ML]<sub>0</sub>, equation (6):



or for a ligand HL of a lower denticity and basicity:





Here the index “o/w” indicates the presence of L in both organic and aqueous phases. For example, for  $Zr^{4+}$ ,  $U^{4+}$  and  $Pu^{4+}$  an ethylenediaminetetraacetic acid (EDTA,  $H_4\text{edta}$ ), which forms the neutral complexes  $[M(\text{IV})\text{edta}]^o$  might be a good choice, while for  $\text{Am}^{3+}$  and  $\text{Ln}^{3+}$  EDTA is undesirable, but the dialkyl ester of diethylenetriaminepentaacetic acid (DTPA,  $H_5\text{dtpa}$ ) -  $H_3R_2\text{dtpa}$  is expected to form the same zero charged species:  $[\text{Ln}(\text{R}_2\text{dtpa})]^o$ , where R indicated some alkyl.

Indeed it was demonstrated that for such d-metal ions as  $\text{Ni}^{2+}$ ,  $\text{Cu}^{2+}$  and  $\text{Pb}^{2+}$  an extraction by RTILs in the presence of  $\beta$ -diketonates (HL) proceeds in the same way as in chloroform, nitrobenzene or toluene as a neutral hydrated complex  $[\text{ML}_2(\text{H}_2\text{O})_n]^o$ , where  $n=1,2$  (Hirayama et al, 2005). A similar observation was reported for none chelating inorganic ligands:  $\text{CN}^-$ ,  $\text{OCN}^-$ ,  $\text{SCN}^-$  and halide ions (Visser et al, 2001).

At the same time an improper selection of an anionic ligand for a particular cation (Visser et al, 2001) can lead to an anionic complex formation, which has the same disadvantages of ion exchange mechanism as with neutral ligands. In fact it was demonstrated (Jensen et al, 2003) that  $\text{Eu}^{3+}$  with 2-thenoyltrifluoroacetone (Htta) forms besides the neutral species  $[\text{Eu}(\text{tta})_3]^o$  also  $[\text{Eu}(\text{tta})_4]^-$  and an undesirable anion exchange mechanism of  $[\text{Eu}(\text{tta})_4]^-$  for  $[\text{N}(\text{Tf})_2]^-$  prevails at a water/[BMIM][N(Tf)<sub>2</sub>] interface. This example indicates an importance of stability constant-based speciations of complexes formed by a ligand with a target cation both in aqueous and RTIL phases.

The data for aqueous solutions are generally available in the most comprehensive IUPAC Stability Constants Database (IUPAC, 2007), which embraces over 400 000 of stability constants measured for different solvents, including RTILs. Unfortunately, the number of published logK values for RTILs is still rather poor, Table 2.

Solvent	W, % <sup>e</sup>	$\log\beta_{2(1)}$	$\log D_{\text{Cs}}$	$\log D_{\text{Cs}^{18}\text{C6}}$	$\log D_{18\text{C6Cs}}$	$\log[D_{\text{Cs}^{18}\text{C6}}/(D_{\text{Cs}}D_{18\text{C6}})]$
[HMIM][N(Tf) <sub>2</sub> ]	1.3	5.57	-1.24	0.82	0.25	1.81
[EtHMIM][N(Tf) <sub>2</sub> ]	0.7	4.56	-0.81	0.56	-0.27	1.64
[BMIM][N(Tf) <sub>2</sub> ]	0.5	4.69	-0.67	1.56	0.77	1.46
[BMIM][PF <sub>6</sub> ]	1.9	2.4	-0.59	-0.20	0.13	0.26
[TOMA][Sal]	7.6	1.45	0.69	0.83	0.49	-0.38
[THA][DHSS]	4.4	0.77	1.21	0.25	-0.12	-0.84
1,2-dichloroethane		10.56 <sup>b</sup>	-7.7 <sup>f</sup>	0.8 <sup>c</sup>	0.03 <sup>d</sup>	6.93

<sup>a</sup> Extraction data for RTIL are taken from (Vendilo, et al, 2009) for 25 °C,  $\text{pH}_{\text{water}}=7$ ;  $[\text{Cs}]_o=0.0015$  mol/L,  $[\text{18C6}]_o=0.15$  and phases volume ratio  $V_{\text{water}}/V_{\text{RTIL}}=10$ ;  $D_{\text{Cs}}=[\text{Cs}]_{\text{RTIL}}/[\text{Cs}]_{\text{water}}$ ;  $D_{\text{Cs}^{18}\text{C6}}=[\text{Cs}]_{\text{RTIL}}/[\text{Cs}]_{\text{water}}$  in presence of 0.15 mol/L 18C6 in RTIL;  $D_{18\text{C6}}=[\text{18C6}]_{\text{RTIL}}/[\text{18C6}]_{\text{water}}$ ;  $\beta_{2(1)}=K_1$  if no  $\text{CsL}_2$  complexes are formed, and  $\beta_{2(1)}=K_1K_2$  if  $\text{CsL}_2$  complex exists in a particular RTIL; <sup>b</sup> Ref. (Kikuchi & Sakamoto, 2000), <sup>c</sup> Ref. (Abramov, 2000), picrate salt; <sup>d</sup> Ref. (Takeda et al, 1998), <sup>e</sup> W -equilibrium water content in RTIL phase after extraction in presence of 18C6, mass %; <sup>f</sup> Ref. (Levitskaia et al, 2007), picrate salt.

Table 8. Stability constants of cesium complex formation with 18C6 in RTIL and extraction efficacy from water at 25 °C<sup>a</sup>.

However, for  $\text{Cs}^+$  some comments are possible. Formation of crown ether complexes promotes cesium extraction (Vendilo, et al, 2009) into hydrophobic RTIL from water if the complex stability in RTIL is higher than in water, Table 8. Indeed for [BMIM][N(Tf)<sub>2</sub>], [HMIM][N(Tf)<sub>2</sub>], [EtHMIM][N(Tf)<sub>2</sub>], [BMIM][PF<sub>6</sub>] and [TOMA][Sal]  $\log K_{1\text{RTIL}} > \log K_{1\text{water}}$

and cesium content in RTIL increases due to 18C6 administration. For [THA][DHSS]  $\log K_{1\text{RTIL}} < \log K_{1\text{water}}$  and crown ether decreases cesium content in RTIL. The  $\log D_{\text{Cs}}^{18\text{C6}}$  values have the same order of magnitude for RTILs, 1,2-dichloroethane and other volatile organic diluents (Abramov, 2000; Takeda et al, 1998; Levitskaia et al, 2007), while the hazardous properties of the latter are much higher.

It should be noted that the complex stability in RTIL increases as the RTIL ability to extract cesium without 18C6 ( $D_{\text{Cs}}$ ) decreases, Fig.3. Meanwhile, there are no simple relationships between  $\log K_1$  ( $\log \beta_{1,2}$ ) and crown ether assisted extraction efficiency ( $D_{\text{Cs}}^{18\text{C6}}$ ), Table 8. This happens due to a superposition of at least two phenomena: the relative stability of complexes is superimposed on a relative solubility of the crown ether and its complexes in the RTIL/water systems. However, when the ligand's extraction ( $D_{\text{L}}$ ) and  $D_{\text{Cs}}$  are taken into account then a perfect linear relationship between  $[\log D_{\text{Cs}}^{18\text{C6}} - \log D_{\text{Cs}} - \log D_{\text{L}}]$  and  $\log \beta_{1,2}$  is observed, Fig 4.

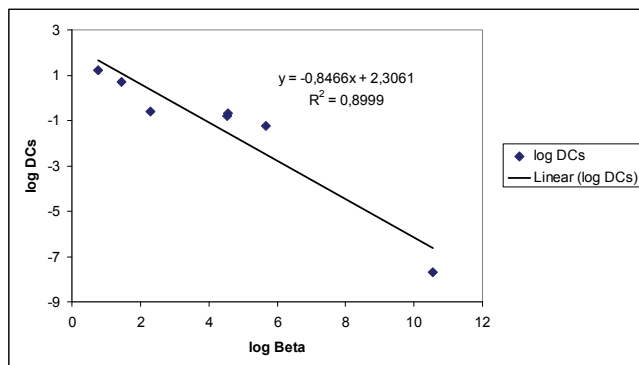


Fig. 3. Plot of  $\log D_{\text{Cs}}$  vs.  $\log \beta_{1,2}$  for [TOMA][Sal], [THA][DHSS], [BMIM][PF<sub>6</sub>], [BMIM][N(Tf)<sub>2</sub>], [HMIM][N(Tf)<sub>2</sub>], [EtHMIM][N(Tf)<sub>2</sub>] and 1,2-dichlorethane at 25 °C (Vendilo, et al, 2010a,c)

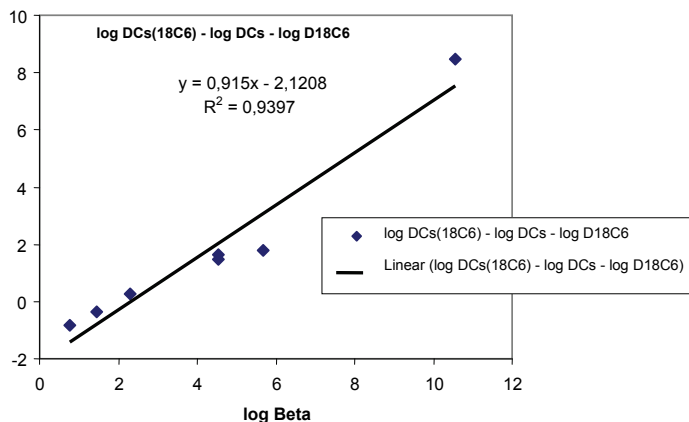


Fig. 4. Plot of  $[\log D_{\text{Cs}}^{18\text{C6}} - \log D_{\text{Cs}} - \log D_{18\text{C6}}]$  vs.  $\log \beta_{1,2}$  for [TOMA][Sal], [THA][DHSS], [BMIM][PF<sub>6</sub>], [BMIM][N(Tf)<sub>2</sub>], [HMIM][N(Tf)<sub>2</sub>], [EtHMIM][N(Tf)<sub>2</sub>] and 1,2-dichlorethane at 25 °C (Vendilo, et al, 2010a,c).

This linearity has a certain background. When an aqueous phase of cesium nitrate is in equilibrium with a RTIL organic phase containing crown ether L, the distribution ratio ( $D_{Cs^{18C6}}$ ) for such RTILs as [TOMA][Sal], [THA][DHSS] and [BMIM][PF<sub>6</sub>], where only CsL species are formed is represented by a simple equation (7):

$$D_{Cs^{18C6}} = ([Cs]^{RTIL} + [CsL]^{RTIL}) / ([Cs]^w + [CsL]^w) \quad (7)$$

where the superscripts "RTIL" and "w" denote organic and aqueous phase, respectively. When the total concentration  $[L]^t \gg [Cs]^t$  and the stabilities of complexes in both phases are high enough ( $\log K_1^{RTIL} \geq 2$ ;  $\log K_1^w \geq 2$ ), then  $[Cs]^{RTIL} \ll [CsL]^{RTIL}$  and  $[Cs]^w \ll [CsL]^w$ . In this case the equilibrium concentrations of  $[Cs]^{RTIL}$  and  $[Cs]^w$  in (7) can be neglected. The equation (7) is therefore transformed into (8):

$$D_{Cs^{18C6}} = [CsL]^{RTIL} / [CsL]^w \quad (8)$$

or

$$D_{Cs^{18C6}} = (K_1^{RTIL} [Cs]^{RTIL} [L]^{RTIL}) / (K_1^w [Cs]^w [L]^w) \quad (9)$$

as far as  $[Cs]^{RTIL} / [Cs]^w = D_{Cs}$  and  $[L]^{RTIL} / [L]^w = D_L$ , then

$$D_{Cs^{18C6}} = K_1^{RTIL} D_{Cs} D_L / K_1^w \quad (10)$$

or

$$\log D_{Cs^{18C6}} = \log K_1^{RTIL} + \log D_{Cs} + \log D_L - \log K_1^w \quad (11)$$

Thus the plot of  $(\log D_{Cs^{18C6}} - \log D_{Cs} - \log D_L)$  versus  $\log K_1^{RTIL}$  should be linear with a slope 1. For [BMIM][N(Tf)<sub>2</sub>], [HMIM][N(Tf)<sub>2</sub>], [EtHMIM][N(Tf)<sub>2</sub>] the equations (7), (9), (10) and (11) become more complicated due to formation of CsL<sub>2</sub> complexes and the lack of such complexes in water. For a molecular solvent 1,2-dichloroethane the equation (7) and its derivatives additionally have to involve the formation equilibrium for neutral complexes CsL(NO<sub>3</sub>) in both RTIL and aqueous phases. However, surprisingly all seven solvents fit equation (11) with a slope 0.92 and a correlation coefficient  $R^2=0.94$ .

This indicates clearly an importance of complex stability contribution for hydrophobic RTILs in extraction processes. At the same time this trend is strongly modulated by a relative solubility of the chelating agent, its complex with a target cation and a metal nitrate in water and in a RTIL phase. Our group has found that a more hydrophobic DB18C6 reveals better extraction of Cs<sup>+</sup> into [BMIM][NTf<sub>2</sub>], [TOMA][Sal] and [THA][DHSS] than 18C6, while the stability constants of complex formation are approximately the same (Djigailo, 2010).

Among other issues that make challenge for researchers in the field of RTIL extraction is the problem of an extracted cation regeneration from ionic liquid and therefore a RTIL regeneration. The low vapor pressure becomes here an evident disadvantage as far as RTIL can not be removed via evaporation like conventional solvents. However it was demonstrated that, for lanthanides the stripping from [BMIM][PF<sub>6</sub>] in the presence of *n*-octyl(phenyl)-*N,N*-diisobutylcarbamoylmethylphosphane oxide (CMPO) can be accomplished by using aqueous solutions of guanidine carbonate with either DTPA or EDTA (Levitskaia et al, 2007). For Am(III) complex with CMPO in [BMIM][N(Tf)<sub>2</sub>] more than 95% of americium was stripped by using 1.0 M oxalic acid (Nakashima et al, 2003).

Recovery of metal ion from ionic liquid could be also achieved by simply lowering pH (see (Murding & Tang, 2010) and references there), or by a back extraction by a supercritical CO<sub>2</sub> (Murding & Tang, 2010). It should be noted, that the extraction can be combined with an electrochemical recovery, as it was demonstrated for UO<sub>2</sub><sup>2+</sup> and Sm<sup>3+</sup> (Murding & Tang, 2010) or by electrodialysis (Vendilo et al, 2010), see below. At the same time it is reasonable to note, that for some RTIL's the distillation is possible (Earle et al, 2006).

It is also important that RTILs can generally withstand  $\alpha$ - and  $\gamma$ -radiation (Murding & Tang, 2010; Allen et al, 2002), although in some cases irradiation of RTIL and of a chelating agent can diminish the radioactive cation partitioning (Chao et al, 2010).

Recently a broad application of RTILs in extraction processes is limited by their relatively high cost, yet unclear toxicity and long-term stability. The first publications on the toxicity issues have appeared not long ago (Docherty et al, 2005; Jastorff et al, 2003) and a lot of work in this field is still ahead. The same situation refers to the RTILs solubility in water, which is critical for their recyclability and their time-of-life. The solubility data are available only for a small number of ionic liquids. At the same time, the cost of some recently developed RTILs, e.g. of [TOMA][Sal] is about an order of magnitude lower, then for those as [BMIM][N(Tf)<sub>2</sub>] and can be diminished if the production increases on the demand of the market.

#### 4. Cation separations by RTIL based liquid membranes and supported liquid membranes

The separations of inorganic cations can be provided by liquid-liquid extraction, the use of RTIL-based liquid membranes and supported membranes. It was observed, that the partitioning of lanthanides in [BMIM][PF<sub>6</sub>] in the presence of CMPO was higher and with better selectivity than that in dodecane (Levitskaia et al, 2007). The reversed extraction selectivity in RTILs relative to isooctane for a series of lanthanides in the presence of *N,N,N',N'*-tetra(*n*-octyl)diglycolamide was reported (Murding & Tang, 2010). The separation of Sc<sup>3+</sup> from a mixture of Sc<sup>3+</sup>, La<sup>3+</sup>, Y<sup>3+</sup> and Yb<sup>3+</sup> in an aqueous phase by Cyanex 925 into octylimidazolium hexafluorophosphate has been registered (Sun et al, 2007), while some task-specific RTILs provided almost quantitative uranyl ion extraction (Srnecik et al, 2009).

The use of RTILs-based liquid membranes for cation separations is less common. Our group has tested Cs<sup>+</sup> transfer from its nitrate salt aqueous solution from the anode chamber to a cathode chamber filled with water under voltage gradient through [BMIM][N(Tf)<sub>2</sub>] layer with 18C6 (Vendilo et al, 2010d), Fig. 5, 6. In the absence of crown ether c.a. 50 % of Cs<sup>+</sup> has been accumulated in a RTIL phase within 4 hours. The process seems to stop when 50% of a cation still remains in the initial solution. At the same time no any increase of cesium concentration at anode was observed, Fig.5. This clearly indicates the formation of either neutral or anionic species of cesium with RTIL's anions, e.g. [CsN(Tf)<sub>2</sub>]<sup>0</sup>, [Cs{N(Tf)<sub>2</sub>}]<sup>-</sup>, etc., and is in a good agreement with NMR data (Vendilo et al, 2010d). The neutral or negatively charged species do not strip into the anode compartment and partly stay in the RTIL's phase in equilibrium with anode compartment when the voltage gradient becomes compensated by the concentration gradient.

When 18C6 was added to the ionic liquid phase, then 90% of cesium placed initially in the anode chamber, move both to RTIL's phase (44 %) and to cathode compartment (46 %) within the same period of time, Fig.6. This is also consistent with the stability constants and NMR-based chemical speciation model which assumes the formation of cationic species in

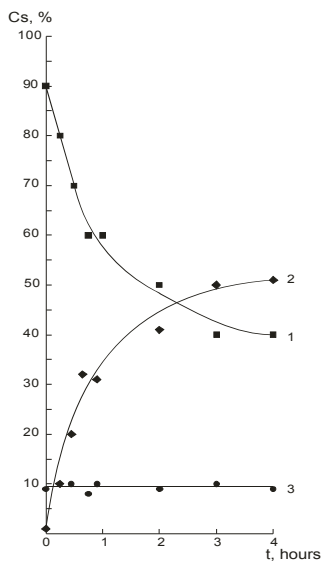


Fig. 5.  $\text{Cs}^+$  distribution in the electrokinetic cell: anode compartment (1),  $[\text{BMIM}][\text{N}(\text{Tf})_2]$  based liquid membrane (2) and cathode compartment (3). Initial cesium concentration: 0.005 mol/L in anode chamber; the solution equilibrated 24 hours at  $E=0$  V; then 1 V/cm gradient was applied

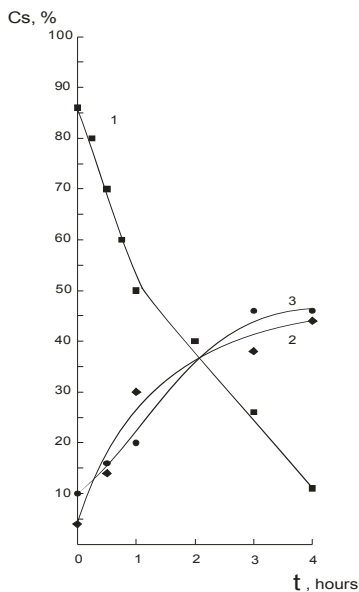


Fig. 6.  $\text{Cs}^+$  distribution in the electrokinetic cell: anode compartment (1),  $[\text{BMIM}][\text{N}(\text{Tf})_2]$  based liquid membrane with 0.15 mol/L 18C6 (2) and cathode compartment (3). Initial cesium concentration: 0.005 mol/L in anode chamber; the solution equilibrated 24 hours at  $E=0$  V; then 1 V/cm gradient was applied.

the presence of 18C6 excess:  $[\text{Cs}(\text{18C6})_2]^+$ . Therefore there are no obstacles for a cationic complex to strip into cathode compartment.

An application of chemical speciations makes the situation clearer, Fig. 7. Indeed, for the stability levels of 18C6 complexes with  $\text{Cs}^+$  in  $[\text{BMIM}][\text{N}(\text{Tf}_2)]$  the 1000-fold excess of 18C6 over  $\text{Cs}^+$  is needed to provide an absolute  $[\text{Cs}(\text{18C6})_2]^+$  species domination (93%). When only a 100-fold excess takes place as it happens after 4 hours of power supply, then almost 44% of cesium exist in either  $[\text{CsN}(\text{Tf}_2)_2]^0$  or  $[\text{Cs}\{\text{N}(\text{Tf}_2)_2\}^-$  forms ("free" Cs), which are not capable to move to the cathode compartment and the process intensity declines.

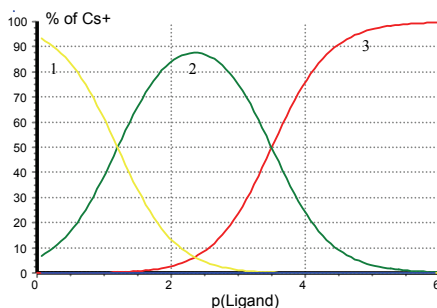


Fig. 7. Chemical speciations of 0.001 mol/L  $\text{Cs}^+$  in  $[\text{BMIM}][\text{N}(\text{Tf}_2)]$  as a function of 18C6 concentration,  $p[\text{18C6}]$ :  $[\text{Cs}(\text{18C6})]^+$  (1),  $[\text{Cs}(\text{18C6})_2]^+$  (2) and "free"  $\text{Cs}^+$  (3); Species, Academic Software (IUPAC, 2007).

It is worthwhile to note that the separation process can be significantly enhanced if different chelating agents are added at once into a RTIL phase and into anode compartment. We have recently got positive results when to a mixture of  $\text{Cu}^{2+}$  and  $\text{Cs}^+$  in anode chamber an aqueous solution of EDTA was added ( $\text{pH} \sim 5$ ), while 18C6 was dissolved in the RTIL's phase. The speciation scheme clearly demonstrates that under the experimental conditions copper forms negatively charged species  $[\text{Cu}(\text{edta})]^{2-}$ , while  $\text{Cs}^+$  ions do not interact with EDTA. Thus  $\text{Cs}^+$  strips into membrane and then into cathode compartment, while copper is retarded in the anode one.

The main problem in such process is a RTIL's decomposition due to its slow dissolution in water in both chambers. A possible solution could be associated with a fixation of a RTIL on some solid porous frame. Our preliminary experiments with porous  $\text{Al}_2\text{O}_3$  filled with  $[\text{BMIM}][\text{N}(\text{Tf}_2)]$  indicate this path to be a promising one. Various forms of RTIL's immobilization on solid phase are recently reported (Martinis et al, 2009; Gallardo et al, 2008; Vincent et al, 2008; Campos et al, 2008; Campos et al, 2008a; Guibal et al, 2008; Vincent et al, 2008a; Venkatesan et al, 2007).

The facts listed above indicate that ionic liquids are very promising solvents for liquid – liquid extraction of a variety of metal ions. At the same time a lot of physicochemical data on the properties of complexes formed in this medium has to be obtained before the practical application of RTILs in this field becomes real.

## 5. Acknowledgement

Present work was supported by the Russian Foundation for Fundamental Research (Project № 07-08-00246a), Russian Federal Programm (Contract 02.740.11.0640) and by the Academy of Finland. The authors thank Dr. Alexei Popov for the assistance in manuscript graphics preparation.

## 6. References

- Abramov, A.A. (2000) Extraction of cations with crown ethers, *Vestn. Mosk. Univ. (Moscow University Bull.) Ser.2*, 41: 3-15.
- Ajioka, T.; Oshima, S. & Hirayama, N. (2008) Use of 8-sulfonamidoquinoline derivatives as chelate extraction reagents in ionic liquid extraction system, *Talanta*, 74: 903-908.
- Allen, D.; Baston, G.; Bradley, A.E.; Gorman, T.; Haile, A.; Hamblett, I.; Hatter, J.E.; Healey, M.J.F.; Hodgson, B.; Lewin, R.; Lovell, K.V.; Newton, B.; Pitner, W.R.; Rooney, D.W.; Sanders, D.; Seddon, K. R. & Sims, E. (2002) An investigation of the radiochemical stability of ionic liquids, *Green Chem.*, 4: 152 - 148.
- Arnaud-Neu, F.; Delgado, R. & Chaves, S. (2003) Critical evaluation of stability constants and thermodynamic functions of metal complexes of crown ethers, *Pure Appl. Chem.*, 75: 71-102.
- Babai A. & Murding, A.-V. (2006) Homoleptic Alkaline Earth Metal Bis(trifluoromethanesulphyl)imide Complex Compounds Obtained from an Ionic Liquid, *Inorg. Chem.*, 45: 3249-3255.
- Bessiere, J. & Lejaille, M. (1979) Utilisation of Silver Cryptate [222] /Silver System as a Potential Reference for the Determination of the Solvation Transfer Coefficients of Ions. Stability of Cryptates in a Solvent Medium, *Anal. Lett.*, 12: 753 - 763.
- Berton, P. & Wuilloud, R.G. (2010) Highly selective liquid-based microextraction method for sensitive trace cobalt determination in environmental and biological samples, *Anal. Chim. Acta*, 662: 155-162.
- Billard, I.; Moutiers, G.; Labet, A.; El Azzi, A.; Gaillard, C.; Mariet, C. & Lutzenkirchen, K. (2003) Stability of divalent Europium in an Ionic Liquid: Spectroscopic investigations in 1-methyl-butylimidazolium Hexafluorophosphate, *Inorganic Chemistry* 42: 1726-1733.
- Billard, I. & Gaillard, C. (2009) Actinide and lanthanide speciation in imidazolium-based ionic liquids, *Radiochimica Acta*, 97: 355-359.
- de Boer, J.A.A.; Reinhoudt, D.N.; Harkema, S.; van Hummel, G.J. & de Jong, F. (1982) Thermodynamic Constants of Complexes of Crown Ethers and Uncharged Molecules and X-ray Structure of the 18-Crown-6  $(\text{CH}_3\text{NO}_2)_2$ , *J. Am. Chem. Soc.*, 104: 4073-4076.
- Campos K.; Vincent T.; Bunio P.; Trochimczuk A. & Guibal E. (2008) Gold Recovery from HCl Solutions using Cyphos IL-101 (a Quaternary Phosphonium Ionic Liquid) Immobilized in Biopolymer Capsules, *Solvent Extr. Ion Exch.*, 26 : 570 -601.
- Campos K.; Domingo R.; Vincent T.; Ruiz M.; Sastre A.M. & Guibal E. (2008a) Bismuth recovery from acidic solutions using Cyphos IL-101 immobilized in a composite biopolymer matrix, *Water Res.*, 42: 4019 - 4031.

- Chao X.; Liyong Y.; Xinghai S. & Maolin Z. (2010) Efficient removal of caesium ions from aqueous solutions using a calyx crown ether in ionic liquids: mechanism and radiation effect, *J. Chem. Soc. Dalton Trans.*, 39: 3897-3902.
- Chen P.-Y. (2007) The assessment of removing strontium and cesium cations from aqueous solutions based on the combined methods of ionic liquid extraction and electrodeposition, *Electrochim. Acta* 52: 5484-5492.
- Chun, S.; Dzyuba, S.V. & Bartsch R.A. (2001) Influence of Structural Variation in Room-Temperature Ionic Liquids on the Selectivity and Efficiency of Competitive Alkali Metal Salt Extraction by a Crown Ether, *Anal. Chem.*, 73: 3737-3741.
- Cocalia, V.A.; Gutowsky, K.E. & Rogers, R. (2006). The coordination chemistry of actinides in ionic liquids: A review of experiment and simulation, *Coord. Chem. Rev.*, 250: 755-764.
- Cocalia, V.A.; Holbrey, J.D.; Gutowski, K.E.; Bridges, N.J. & Rogers, R.D. (2006a) Separations of Metal Ions Using Ionic Liquids: The Challenges of Multiple Mechanisms, *Tsinghua Sci. Technol.*, 11: 188-193.
- Dai, S.; Ju, Y.H. & Barnes, C.E. (1999) Solvent extraction of strontium nitrate by a crown ether using room-temperature ionic liquids. *J. Chem. Soc., Dalton Trans.*, 1201-1202.
- Dang, L.X. (1995) Mechanism and Thermodynamics of Ion Selectivity in Aqueous Solutions of 18-crown-6 Ether: A molecular Dynamic Study, *J. Am. Chem. Soc.*, 117: 6954-6969.
- Danil de Namor, A.F.; Gil, E.; Tanko, M.A.L.; Tanaka, D.; Salazar, L.; Schulz, R. & Wang, J. (1995) Thermodynamics of Calix(4)arene Esters. 1. Complexation of Alkyl p-tert-Butylcalix(4)arenetetraethanoates and Alkali-Metal Cations in Acetonitrile and in Benzonitrile, *J. Phys. Chem.*, 99:16776-16780.
- Davis, J.H.Jr. (2005) Task-specific ionic liquids, *Chem. Lett.*, 33: 1072-1077.
- Djigailo, D. (2010) Extraction of cations from aqueous solutions into RTILs and task specific RTILs, PhD Theses, Lomonosov State University, Moscow, in Russian.
- Dietz, M.L.; Dzielawa, J.A.; Lazak, I.; Young, B.A., & Jensen, M.P. (2003) Influence of solvent structure variations on the mechanism of facilitated ion transfer into room-temperature ionic liquids, *Green Chem.*, 5: 682-685.
- Dietz, M.L. (2006) Ionic Liquids as Extraction Solvents: Where do we stand?, *Sep. Sci. Technol.*, 41: 2047-2063.
- Dietz, M.L. & Stepinski, D.C. (2008) Anion concentration-dependent partitioning mechanism in the extraction of uranium into room-temperature ionic liquids, *Talanta* 75:598-603.
- Docherty, K.M. & Kulpa C.F. (2005) Toxicity and antimicrobial activity of imidazolium and pyridinium ionic liquids, *Green Chem.*, 7: 185-189.
- Dundan Han & Kyung Ho Row (2010) Recent applications of ionic liquids in separation technology, *Molecules*, 15: 2405-2426.
- Earle M.J.; Esperança J.M.S.S.; Gilea M.A.; Lopes J.N.C.; Rebelo L.P.N.; Magee J.W.; Seddon K.R. & Widegren J.A. (2006) The distillation and volatility of ionic liquids, *Nature*, 439: 831 - 834.
- Egorov V.M.; Djigailo D.I.; Momotenko D.S.; Chernyshov D.V.; Torocheshnikova I.I.; Smirnova S.V. & Pletnev I.V. (2010) Task-specific ionic liquid



- trioctylmethylammonium salicylate as extraction solvent for transition metal ions, *Talanta*, 80: 1177 – 1182.
- Ellerman, J.; Bauer, W.; Schuetz, M.; Heinemann, F.W. & Moll M. (1998) Chemie Polyfunktioneller Moleculer 130 Mitt.[1]: Spaltprodukte, Kristallstrukturen und Festkoerper-NMR-Spektern, *Monatshefte fur Chemie*, 129: 547-566.
- Ernst, S. & Jezowska-Trzebiatowska, B. (1966) The behaviour and structure of uranyl nitrate in organic solvents – IV : Investigations of uranyl nitrate dihydrate in alcohols by conductivity, *J. Inorg. Nucl.Chem.*, 28: 2885 - 2887.
- Eyring, E. M.; Cobranchi, D. P.; Garland, B. A.; Gerhard, A.; Highley, A. M.; Huang, Y. H., Konya, G.; Petrucci, S. & Van Eldik, R. (1993) Lithium ion - crown ether complexes in a molten salt, *Pure Appl. Chem.*, 65: 451-454.
- Gallardo, V.; Navarro, R.; Saucedo, I.; Ávila, M., & Guibal, E. (2008) Zinc(II) Extraction from Hydrochloric Acid Solutions using Amberlite XAD-7 Impregnated with Cyphos IL 101 “(Tetradecyl(Trihexyl)Phosphonium Chloride), *Sep. Sci. Technol.*, 43: 2434 – 2459.
- Garrell, R.L.; Smyth, J.C.; Fronczek, F.R. & Gandour, R.D. (1988) Crystal Structure of the 2:1 Acetonitrile Complex of 18-Crown-6, *J. Inclusion Phenom.*, 6: 73-78.
- Georg, S.; Billard, I.; Quadi, A.; Gaillard, C.; Petitjean, L.; Picquet, M. & Solov'ev, V. (2010) Determination of Successive complexation constants in an ionic liquid: complexation of  $\text{UO}_2^{2+}$  with  $\text{NO}_3^-$  in  $\text{C}_4\text{-mimTf}_2\text{N}$  studied by UV-Vis Spectroscopy. *J.Phys.Chem. B* 114: 4276-4282.
- Gjikaj, M. & Adam, A. (2006) Complexation of Alkali Triflates by Crown Ethers: Synthesis and Crystal Structure of  $\text{Na(12-crown-4)}_2[\text{SO}_3\text{CF}_3]$ ,  $\text{Na(15-crown-5)}[\text{SO}_3\text{CF}_3]$ ,  $[\text{Rb(18-crown-6)}][\text{SO}_3\text{CF}_3]$  and  $[\text{Cs(18-crown-6)}][\text{SO}_3\text{CF}_3]$ , *Z. Anorg. Allg. Chem.*, 632: 2475-2480.
- Guibal, E.; Gavilan, K.C.; Bunio, P.; Vincent, T. & Trochimczuk, A. (2008) CYPHOS IL 101 (Tetradecyl(Trihexyl)Phosphonium Chloride) Immobilized in Biopolymer Capsules for Hg(II) Recovery from HCl Solutions, *Sep. Sci. Technol.* 43 : 2406 – 2433.
- Gutmann, V. & Vichera, E. (1966) Coordination reactions in non aqueous solutions - the role of the donor strength, *Inorg.Nucl.Chem.Lett.* 2: 257-260.
- Hirayama, N.; Deguchi, M.; Kawasumi, H. & Honjo, T. (2005) Use of 1-alkyl-3-methylimidazolium hexafluorophosphate room temperature ionic liquids as chelate extraction solvent with 4,4,4-trifluoro-1-(2-thienyl)-1,3-butanedione, *Talanta*, 65: 255-260.
- Ikeda, A.; Hennig, C.; Rossberg, A.; Tsushima, S.; Sceinost, C.A. & Bernhard, G. (2008) Structural Determination of Individual Chemical Species in a Mixed System by Iterative Transformation Factor Analysis-Based X-ray Absorption Spectroscopy Combined with UV-Visible Absorption and Quantum Chemical Calculation, *Anal. Chem.*, 80: 1102 - 1110.
- IUPAC Stability Constants Database. 2007, Academic Software, Timble, UK.
- Jastorff, B.; Störmann, R.; Ranke, J.; Mölter, K.; Stock, F.; Oberheitmann, B.; Hoffmann, W.; Nüchter, M.; Ondruschka, B., & Filser J. (2003) How hazardous are ionic liquids? Structure-activity relationships and biological testing as important elements for sustainability evaluation, *Green Chem.*, 5: 136-142.

- Jensen, M.P.; Dzielawa, J.A.; Ricket, P. & Dietz, M.L. (2002) EXAFS Investigations of the Mechanism of Facilitated Ion Transfer into a Room-Temperature Ionic Liquid, *J. Am. Chem. Soc.* 124: 10664-10665.
- Jensen, M.P.; Neuefind, J.; Beitz, J.V.; Skanthakumar, S., & Soderholm, L. (2003) Mechanisms of metal ion transfer into room-temperature ionic liquids: the role of anion exchange, *J. Am. Chem. Soc.*, 125: 15466-15473.
- Jezowska-Trzebiatowska, B. & Chmielowska, M. (1961) The behaviour and structure of uranyl nitrate in organic solvents— $\text{UO}_2^{2+}$ : The studies of uranyl nitrate hexahydrate organic solutions by conductivity method, *J. Inorg. Nucl. Chem.*, 20: 106 - 116.
- Jones, P.G.; Hiemisch, O. & Blaschette, A. (1994) Bildung und Kristallstruktur des Komplexes [(18-Krone-6)( $\text{CH}_2\text{Cl}_2$ )<sub>2</sub>], *Z. Naturforsch.* 49b: 852-854.
- Kikuchi, Y. & Sakamoto, Y. (2000) Complex formation of alkali metal ions with 18-crown-6 and its derivatives in 1,2-dichloroethane, *Anal. Chim. Acta*, 403: 325- 332.
- Langmaier, J. & Samec, Z. (2009) Voltametry of Ion Transfer across a polarized room-temperature ionic liquid membrane facilitated by valinomycin: theoretical aspects and application, *Anal. Chem.*, 81: 6382-6389.
- Lertlapwasin, R.; Bhawawet, N.; Imyim, A. & Fuangswasdi, S. (2010) Ionic liquid extraction of heavy metal ions by 2-aminothiophenol in 1-butyl-3-methylimidazolium hexafluorophosphate and their association constants. *Sep. Pur. Technol.*, 72: 70-76.
- Levitskaia, T.G.; Maya, L.; van Berkel, G.J. & Moyer, B. A. (2007) Anion Partitioning and Ion-Pairing Behavior of Anions in the Extraction of Cesium Salts by 4,5''-Bis(*tert*-octylbenzo)dibenzo-24-crown-8 in 1,2-Dichloroethane, *Inorg. Chem.*, 46: 261-272.
- Lewandowski, A.; Osinska, M. & Stepniak, I. (2005) Stability of  $\text{Ag}^+$  complexes with Cryptand 222 in ionic liquids. *J. Inclus. Phenom. Macrocyclic Chem.*, 52: 237-240.
- Lewandowski, A. & Swiderska-Mocek, A. (2009) Ionic liquids as electrolytes for Li-ion batteries – An overview of electrochemical Studies, *J. Power Sources* 194: 601-609.
- Lohithakshan, K.V. & Aggarwal, S.K. (2008) Solvent extraction studies of Pu(IV) with CMPO in 1-octyl-3-methylimidazolium hexafluorophosphate ( $\text{C}_8\text{mimPF}_6$ ) room temperature ionic liquid (RTIL). *Radiochim. Acta* 96: 93-97.
- Luo, H.; Dai, S. & Bonnesen, P.V. (2004) Solvent extraction of  $\text{Sr}^{2+}$  and  $\text{Cs}^+$  Based on Room-temperaure ionic liquids containing monoza-substituted crown ethers, *Anal. Chem.*, 76: 2773-2779.
- Luo, H.; Dai, S.; Bonnesen, P.V. & Buchanan, A.C. (2006) Separation of fission products based on ionic liquids: Task-specific ionic liquids containing an aza-crown ether fragment, *J. Alloys Compd.* 418: 195-199.
- Manzoori, J.L.; Amjadi, M. & Abulhassan, J. (2009) Ultra-trace determination of lead in water and food samples by using ionic liquid-based single drop microextraction-electrothermal atomic absorption spectrometry, *Anal. Chim. Acta*, 644: 48-52.
- Martinis, E.M.; Olsina, R.A.; Altamirano, J.C., & Wuilloud, R.G. (2009) On-line ionic liquid based preconcentration system coupled to flame atomic absorption spectrometry for trace cadmium determination in plastic food packaging materials, *Talanta*, 78 : 857 - 862.

- Mei, E.; Popov, A.I. & Dye, J.L. (1977) Complexation of the cesium cation by macrocyclic polyethers in various solvents. A cesium-133 Nuclear Magnetic Resonance study of the thermodynamics and kinetics of exchange, *J. Phys. Chem.*, 81, 1677-1681.
- Murding, A.-V.; Babai, A.; Arenz, S. & Giemoth, R. (2005) The "Noncoordinating" Anion  $\text{TF}_2\text{N}^-$  Coordinated to  $\text{Yb}^{3+}$ : A structurally Characterized  $\text{TF}_2\text{N}^-$  Complex from the ionic liquid [mppyrt][ $\text{TF}_2\text{N}$ ], *Angew. Chem. Int. Edit.*, 44: 5485-5488.
- Murding, A.-V. & Tang, S. (2010) Ionic Liquids for Lanthanide and Actinide Chemistry, *Eur. J. Inorg. Chem.*: 2569-2581.
- Nakashima, K.; Kubota, F.; Maruyama, T., & Goto, M. (2003) Ionic Liquids as a Novel Solvent for Lanthanide Extraction, *Anal. Sci.*, 19: 1097 - 1098.
- Ning Li; Guozhen Fang; Jia Zhang; Lijie Zhao & Shuo Wang (2010) A novel hydrophobic task specific ionic liquid for the extraction of Cd(II) from water and food samples as applied to AAS determination, *Anal. Sci.*, 26: 455-459.
- Nishi, N.; Murakami, H.; Imakura, S. & Kakiuchi, T. (2006) Facilitated Transfer of Alkali-Metal Cations by Dibenzo-18-crown-6 across the Electrochemically Polarized Interface between an Aqueous Solution and a Hydrophobic Room-Temperature Ionic Liquid, *Anal. Chem.* 78: 5805-5812.
- Nockemann, P, Thijs, B., Lunstroot, K., Van Hecke, K., Van Meervelt, L. & Binnemans, K. (2008) Polynuclear Metal Complexes obtained from the Task-Specific Ionic Liquid Betainium Bistriflimide, *Crystal Growth and Design*, 8: 1353-1363.
- Nockemann, P.; Thijs, B.; Lunstroot, K.; Parac-Vogt, T.N.; Görrler-Walrand, C.; Binnemans, K.; Van Hecke, K.; Van Meervelt, L.; Nikitenko, S.; Daniels, J.; Hennig, C. & Van Deun, R. (2009) Speciation of Rare-Earth Metal Complexes in Ionic Liquids: A Multiple-Technique Approach, *Chemistry - A European Journal* 15: 144-1461.
- Ohtsu, K. & Ozutsumi, K. (2003) Thermodynamics of Solvation of 18-crown-6 and its Alkali-Metal Complexes in Various Solvents, *J. Inclusion Phenom. Macrocycl. Chem.*, 45, 217-224.
- Ozutsumi, K.; Ohtsu, K. & Kawashima, T. (1994) Thermodynamics of Complexation of 18-Crown-6 with Sodium, Potassium, Rubidium, Caesium and Ammonium Ions in N,N-dimethylformamide, *J. Chem. Soc. Faraday Trans.*, 90: 127-131.
- Ozutsumi, K.; Natsuhara, M. & Ohtaki H. (1989) An X-ray Diffraction Study on the Structure of 18-crown-6 Ether Complexes with Alkali Metal Ions in Aqueous Solutions, *Bull. Chem. Soc. Jpn.*, 62: 2807-2818.
- Popov, K.I.; Rönkkömäki, H.; Hannu-Kuure, M.; Kuokkanen, T.; Lajunen, M.; Vendilo, A.; Glazkova, I.V. & Lajunen, L.H.J. (2007a) Stability Constant of the Sodium Complex with Dibenzo-18-Crown-6 in Mixed Water-Ionic Liquid Solvent, *Russ. J. Coord. Chem.*, 33: 393-395.
- Popov, K.; Rönkkömäki, H.; Hannu-Kuure, M.; Kuokkanen, T.; Lajunen, M.; Vendilo, A.; Oksmann, P. & Lajunen, L.H.J. (2007) Stability of Crown-Ether Complexes with Alkali-Metal Ions in Ionic Liquid-Water mixed Solvents, *J. Incl. Phenom. Macrocycl. Chem.*, 59: 377-381.
- Popov, K.I. & Wanner H. (2005) Stability constants data sources: critical evaluation and application for environmental speciation, p.p. 50-75; in *Biogeochemistry of Chelating*

- Agents* (B.Nowack, J. M. VanBriesen, Eds.) ACS Symposium Series, Vol. 910, Washington DS.
- Reichardt, C. (2005) Polarity of ionic liquids determined empirically by means of solvatochromic pyridinium N-phenolate betaine dyes, *Green Chem.*, 7: 339-351.
- Rogers, R.D.; Richards, P.F. & Voss, E.J. (1988) Neutral Solvent/Crown Ether Interactions, 4. Crystallization and Low Temperature (-150 °C) Structural Characterization of 18-Crown-6 2(CH<sub>3</sub>CN), *J. Inclusion Phenom.* 6: 65-71.
- Rosol, Z.P.; German, J. & Gross, S.M. (2009) Solubility, ionic conductivity and viscosity of lithium salts in room temperature ionic liquids, *Green Chem.*, 11: 1453-1457.
- Ruas, A.; Bernard, O.; Caniffi, B.; Simonin, P.J.; Turq, P. L. & Moisy, P. (2006) Uranyl(VI) Nitrate Salts: Modeling Thermodynamic Properties Using the Binding Mean Spherical Approximation Theory and Determination of "Fictive" Binary Data, *J.Phys.Chem. B.*, 110: 3435 – 3443.
- Seddon, K.R.; Stark, A. & Torres, M.-J. (2000) Influence of chloride, water and organic solvents on the physical properties of ionic liquids, *Pure Appl. Chem.*, 72: 2275-2287.
- Shimojo, K. & Goto, M. (2004) Solvent Extraction and Stripping of Silver Ions in Room-Temperature Ionic Liquids Containing Calixarenes, *Anal. Chem.* 76: 5039-5044.
- Smetana, A.J. & Popov, A.I. (1980) Lithium-7 Nuclear Magnetic Resonance and Calorimetric Study of Lithium Crown Complexes in Various Solvents, *J. Solut. Chem.*, 9: 183-196.
- Song, X.; Li, H.; Li, J.; Liu, J.; Li, Z.; Liu, S.; Li, C. & Wu, P. (2005) The study on the coordination equilibrium of Cu<sup>2+</sup> -ethylenediamine in ionic liquid, *Polymer Preprints*, 46: 842.
- Srncik, M.; Kogelnig, D.; Stojanovic, A.; Körner, W.; Krachler, R., & Wallner, G. (2009) Uranium Extraction from Aqueous Solution by Ionic Liquids, *Appl. Radiat. Isotopes*, 67: 2146-2149.
- Sun, X.; Wu, D.; Chen, J., & Li, D. (2007) Separation of scandium(III) from lanthanides(III) with room temperature ionic liquid based extraction containing Cyanex 925, *J. Chem. Technol. Biotechnol.*, 82: 267-272.
- Takeda, Y.; Kawarabayashi, A.; Endo, K.; Yahata, T.; Kudo, Y. & Katsuta, S. (1998) Solvent Extraction of Alkali Metal (Li-Cs) Picrates with 18-Crown-6 into Various Diluents. Elucidation of Fundamental Equilibria which Govern the Extraction-Ability and -Selectivity, *Anal. Sci.*, 14: 215-223.
- Tang, S., Babai, A. & Murding, A.-V. (2008) Europium-basierte ionische Flüssigkeiten als lumineszierende weiche Materialien, *Angew. Chem.*, 120: 7743-7746.
- Taubert, A. (2004) CuCl Nanoplatelets from an Ionic Liquid Crystal Precursor, *Angew. Chem. Int. Edit.*, 43: 5380-5382.
- Vendilo, A.G.; Rönkkömäki, H.; Hannu-Kuure, M.; Lajunen, M.; Asikkala, J.; Petrov, A.A.; Krasovsky, V.G.; Chernikova, E.A.; Oksman, P.; Lajunen, L.H.J. & Popov, K.I. (2008) Stability Constants of cesium complexes with 18-crown-6 in ionic liquids, *Koord Khim.* 34, 645-650; *Russ. J. Coord. Chem.*, 34: 635-640.
- Vendilo, A.G.; Djigailo, D.I.; Smirnova, S.V.; Torochesnikova, I.I.; Popov, K.I.; Krasovsky, V.G. & Pletnev, I.V. (2009) 18-Crown-6 and Dibenzo-18-crown-6 Assisted Extraction of Cesium from Water into Room Temperature Ionic Liquids and Its

- Correlation with Stability Constants for Cesium Complexes, *Molecules*, 14: 5001-5016.
- Vendilo, A.G.; Rönkkömäki, H.; Hannu-Kuure, M.; Lajunen, M.; Asikkala, J.; Chernikova, E.A.; Lajunen, L.H.J.; Tuomi, T., & Popov, K.I. (2009a) First Data on Thermodynamics of Complex Formation in Ionic Liquids: Cesium Complexes with 18-Crown-6, *Mendeleev Comm.*, 19: 196-197.
- Vendilo, A.G.; Djigailo, D.I.; Rönkkömäki, H.; Lajunen, M.; Chernikova, E.A.; Lajunen, L.H.J.; Pletnev, I.V. & Popov, K.I. (2010) Thermodynamics of cesium complexes formation with 18-crown-6 in hydrophobic ionic liquids. A correlation with extraction capability, in *Macrocyclic Chemistry: New Research Developments* (Ed.: D. W. Fitzpatrick and H. J. Ulrich) Nova Science Publishers, Inc., New York. p.p. 287-307.
- Vendilo, A.G.; Rönkkömäki, H.; Hannu-Kuure, M.; Lajunen, M.; Asikkala, J.; Krasovsky, V.G.; Chernikova, E.A.; Oksmann, P.; Lajunen, L.H.J. & Popov, K.I. (2010a) Thermodynamics of cesium complexes formation with 18-crown-6 in ionic liquids, *J.Incl. Phenom.Macrocycl. Chem.*, 66: 223-230.
- Vendilo, A.G.; Popov, K.I.; Artem'eva, A.A.; Kovaleva, N.E. (2010b) Hydrophobic ionic liquid and crown-ether based liquid membrane, *Kriticheskie tekhnologii. Membrany. (Critical Thechnologies. Membranes )*. 27-29 (in Russian).
- Vendilo, A.G.; Djigailo, D.I.; Rönkkömäki, H.; Lajunen, M.; Chernikova, E.A.; Lajunen, L.H.J.; Pletnev, I.V. & Popov, K.I. (2010c) A correlation of caesium-18-crown-6 complex formation constants with the extraction capability for hydrophobic ionic liquids, *Mendeleev. Comm.*, 20:122-124.
- Vendilo, A.G.; Rönkkömäki, H.; Kotova, N.N.; Hannu-Kuure, M.; Kovaleva, N.E. & Lajunen, M. (2010d) Complexes of Strontium with dichlormethylenebis(phosphonic acid triisopropyl ester, *Russ. J. Inorg. Chem.*, 55:1652-1655.
- Venkatesan, K.A.; Selvan, B.R.; Antony, M.P.; Srinivasan, T.G. & Rao, P.R.V. (2007) Extraction of palladium(II) from nitric acid medium by imidazolium nitrate immobilized resin, *Hydrometallurgy*, 86 : 221 - 229.
- Venkatesan, A.R.K.A.; Srivasan, T.G.& Rao, P.R.V. (2009) Extraction of americium(III) from nitric acid medium by CMPO-TBP extractants in ionic liquid diluent, *Radiochim. Acta*, 97, 719 - 725.
- Vincent, T.; Parodi, A. & Guibal, E. (2008) Immobilization of Cyphos IL-101 in biopolymer capsules for the synthesis of Pd sorbents, *React. Func. Polymers*, 68: 1159 - 1169.
- Vincent, T.; Parodi, A. & Guibal, E. (2008a) Pt recovery using Cyphos IL-101 immobilized in biopolymer capsules, *Sep. Purif. Technol.*, 62: 470 - 479.
- Visser, A.E.; Swatloski, R.P.; Reichert, W.M.; Griffin, S.T. & Rogers, R.D. (2000) Traditional Extractants in Nontraditional Solvents: Groups 1 and 2 Extraction by Crown Ethers in Room-Temperature Ionic Liquids, *Ind. Eng. Chem. Res.*, 39: 3596-3604.
- Visser, A.E.; Swatloski, R.P.; Griffin, S.T.; Hartman, D.H. & Rogers, R.D. (2001) Liquid-liquid extraction of metal ions in room-temperature ionic liquids, *Sep.Sci.Technol.*, 36: 785-804.

- Visser, A.E.; Swatloski, R.P.; Reichert, W.M.; Mayton, R.; Sheff, S.; Wierzbicki, A.; Davis, J.H., & Rogers, R.D. (2001a) Task-specific ionic liquids for the extraction of metal ions from aqueous solutions. *Chem. Commun.* , 135-136.
- Visser, A.E.; Swatloski, R.P.; Reichert, W.M.; Mayton, R.; Sheff, S.; Wierzbicki, A.; Davis, J.H. & Rogers, R.D. (2002) Task-Specific Ionic Liquids Incorporating Novel Cations for the Coordination and Extraction of  $\text{Hg}^{2+}$  and  $\text{Cd}^{2+}$ : Synthesis, Characterization, and Extraction Studies, *Environ. Sci. Technol.* 36: 2523-2529.
- Visser, A.E. & Rogers, R.D. (2003) Room-temperature ionic liquids: new solvents for f-element separations and associated solution chemistry. *J. Solid State Chem.*, 171 :109-113.
- Yan, N.; Fei, Z.; Scipelliti, R.; Laurenczy, G.; Kou, Y. & Dyson, P. J. (2010) Crystallisation of inorganic salts containing 18-crown-6 from ionic liquids, *Inorg. Chim. Acta* 363, 504-508.

# The Design of Nanoscale Inorganic Materials with Controlled Size and Morphology by Ionic Liquids

Elaheh Kowsari  
*Amirkabir University of Technology*  
*Islamic Republic of Iran*

## 1. Introduction

Recently, ionic liquids have successfully been employed in the preparation of inorganic materials (Antonietti et al., 2004, Taubert & Li, 2007). Ionic liquids often act as solvents, reactants or morphology templates, which enable the synthesis of inorganic materials with novel morphologies or improved properties. So far only a handful of studies have reported on the fabrications of nano- or micro-scaled materials including particles of metal oxide (Ding et al., 2007, Bühler & Fledmann, 2006) and sulfide (Jiang, et al., 2005, Jiang & Zhu, 2005). Many metal nanoparticles (NPs) such as Ir (Bühler & Fledmann, 2006), Rh (Wang & Zhu, 2005), Ru (Jiang, et al., 2005), Te (Jiang & Zhu, 2005), Al (Mu, et al., 2004), Ag (Zhu et al., 2004), Pt (Foneca et al., 2003), and Au (Dupont et al., 2002) have been prepared in the presence of ionic liquids.

Novel nanostructures can be produced by selecting suitable ionic liquid reaction systems:  $\text{TiO}_2$  (Nakashima & Kimizuka, 2003, Yoo et al., 2004, Zhou & Antonietti, 2003), Te nanorods (Zhu et al., 2004), Si (Abedin et al., 2004), CoPt nanorods (Wang & Yang, 2005), and porous silica (Zhou, et al., 2004, Zhou & Antonietti, 2004) have recently been synthesized, as reported. Žilková et al. have used 1-methyl-3-octylimidazolium chloride ( $\text{C}_8\text{mimCl}$ , an ionic liquid) as a template to prepare  $\gamma\text{-Al}_2\text{O}_3$  from the hydrolysis and condensation of  $\text{Al}_2\text{Cl}(\text{OH})_5$  (Žilková, et al., 2006). It was shown that the molar ratio of  $\text{Al}/\text{C}_8\text{mimCl}$  was important to define the porosity, i.e. the framework or textural type. Mumalo-Djokic and coworkers have put forward the concept of “all-in-one” solvent-reactant(-template)s, (Taubert & Li, 2007, Taubert 2004), that is ionic liquids or ionic liquid crystals (Binnemans, 2005) that are at the same time the solvent, the reactant, and the template for the fabrication of an inorganic. These special systems have been termed ionic liquid precursors and ionic liquid crystal precursors respectively (Taubert 2004, Zhu et al., 2006). Ionic liquid crystal precursors allow for the controlled mineralization of inorganics with complex structure and morphology. For example, they have made  $\text{CaF}_2$  tubes,  $\text{CuCl}$  platelets, and Au platelets from ionic liquid crystal precursors or their crystalline analogues (Taubert 2004, Taubert et al., 2007, Taubert et al., 2006, Taubert et al., 2005, Taubert 2005). Furthermore, other research groups have extended this concept of reactive ionic liquid crystals to other compounds (Zhu et al., 2006, Dobbs et al., 2006, Lee et al., 2006, Kem et al., 2006).

Although there are a few inspiring short accounts or perspectives focused on selected topics in materials synthesis using ionic liquids, a relatively comprehensive and updated review of this subject is still a gap, especially considering that the field is growing quite fast. Therefore, in the present contribution, the use of ionic liquids in the preparation of different categories of inorganic materials, including silicas, open framework structures, and ionic liquid-modified materials using ionic liquids by different methods, is systematically reviewed. Due to the abundance of research reported in the literature, the present chapter dealt only with some typical examples and key concepts proposed as highlights.

## 2. Methods

### 2.1 Sonochemical synthesis

Ionic liquids have favorable intrinsic properties that make them of interest as solvents for various chemical reactions. The same properties that make the liquids effective solvents also make them interesting liquids for studies involving sonochemistry, acoustic cavitation, and sonoluminescence (Suslick et al., 1991, Suslick, 1988). Recent interest in using ultrasound to accelerate chemical reactions conducted in ionic liquids necessitates an understanding of the effects of acoustic cavitation on these solvents (Flannigan et al., 2005).

The use of ultrasonic irradiation for producing nanomaterials has been a research topic of great interest (Dhasn et al., 1999). This is due to the simplicity of sonochemical method, the cheap price of the equipment and that in many cases the as-prepared material is obtained in the crystalline phase. The ultrasonic-assisted aqueous room temperature ionic liquid method was applied to prepare zinc sulfide and zinc oxide nanomaterials (Zheng et al. 2010; Jia et al. 2010), among many other nanomaterials. Selection of the room temperature ionic liquid was mainly based on the fact that it can be obtained at a relatively low price and the method for its synthesis is simple.

Nanosheet-based microspheres of ZnO with hierarchical structures were prepared by ultrasonic irradiation in acidic ionic liquids by Kowsari (Kowsari 2010). It is found that the ultrasonic irradiation time, ultrasonic frequency, and the acidic ionic liquids influence the growth mechanism and optical properties of ZnO nanostructures. By changing the type of acidic ionic liquids, ultrasonic irradiation time, ultrasonic frequency optical properties of ZnO nanostructure are manageable. The photocatalytic activity test results indicate that the hollow spheres-like ZnO nanophotocatalysts have good photocatalytic activities. Overall, the cited results indicate that the prepared ZnO nanophotocatalysts show good photocatalytic activity and can be considered as a promising photocatalyst for dyes wastewater treatment. Fig. 1. shows the precursor composed of plate-like nanostructures with edge thicknesses of about 40 nm and smooth surfaces. The structures synthesized in this experiment can indicate a new way to construct nanodevices by self-organization in one step.

In other report, flower like ZnO/MgO nanocomposites were prepared by ultrasonic irradiation and chiral ionic liquid, ditetrabutylammonium tartarate,  $[TBA]_2[L-Tar]$ . It is found that the ultrasonic frequency, the ultrasonic irradiation time and the chiral ionic liquid influence the growth mechanism and optical properties of ZnO/MgO nanocomposites. Enhancement of bandgap in the ZnO/MgO nanocomposites, due to morphology effect, was an interesting observation. The effect of the ultrasonic irradiation time on ZnO/MgO nanocomposites morphology (in the presence of chiral ionic liquid) is shown in Fig 2. As it can be observed in Fig 2, when the ultrasonic irradiation time increases, the thickness of the nanosheets making the flowerlike is reduced. Therefore, the morphology takes a more arranged shape.



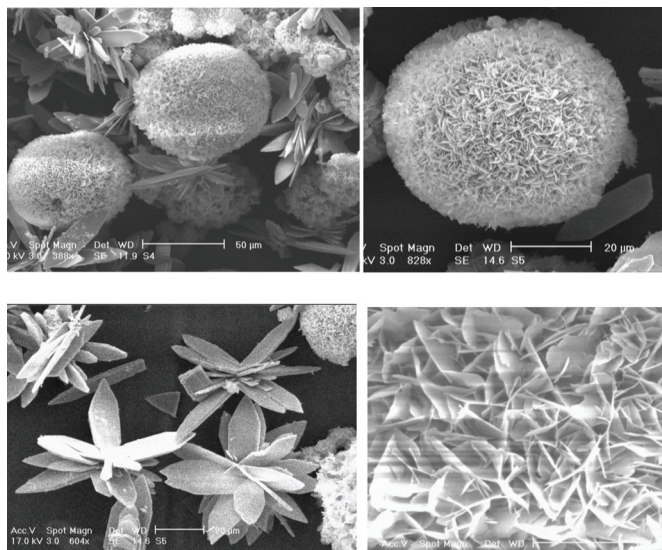


Fig. 1. Regular hollow spherical, composed of a number of nanosheets, with an average size of 50–70  $\mu\text{m}$ . and leaf-like ZnO nanostructure, synthesis by acidic ionic liquid, [(mim) hex(mim)][ $2\text{H}_2\text{PO}_4$ ] (kowsari (2010) , accepted for presentation 2<sup>nd</sup> Asia Pacific Conference on Ionic Liquids and Green Processes September 7-10, 2010 Dalian • China)

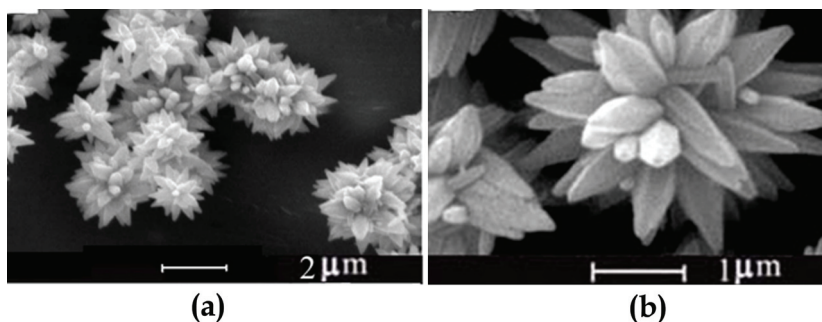


Fig. 2. The effect of ultrasonic irradiation time on the evolution of the morphologies of ZnO/MgO nanocomposite, (a) 2 h and (b) 2.5 h , (Ultrasonic frequencies = 40 kHz, The ultrasonic power was kept at 200 W) (kowsari (2010) , accepted for presentation 2<sup>nd</sup> Asia Pacific Conference on Ionic Liquids and Green Processes September 7-10, 2010 Dalian (China)

## 2.2 Sol-gel synthesis

A good number of works concerning the synthesis of inorganic nanomaterials are based on sol-gel route. The original use of ionic liquids as solvents for inorganic sol-gel reactions is the acid-catalyzed sol-gel synthesis of silica aerogels (Dai et al., 2003). It turned out that such aerogels can be dried without a supercritical drying procedure. Subsequently, 1-butyl-3-methylimidazolium hexafluorophosphate [BMIM][PF<sub>6</sub>] was used to synthesize hollow TiO<sub>2</sub> microspheres by interfacial sol-gel reaction (Nakashima & Kimizuka, 2003).

Zhou, et al. used  $\text{TiCl}_4$  as the precursor to synthesize very small  $\text{TiO}_2$  nanocrystals in  $[\text{BMIM}][\text{BF}_4]$  and obtained mesoporous spherical aggregates of  $\text{TiO}_2$  nanocrystals (Zhou & Antonietti, 2003). The synthesized titania aggregates exhibits structural mesoporosity with considerable high surface area and narrow pore size distribution, rendering the materials interesting for solar cell conversion, catalysis, and electronic devices. Smarsly, et al. synthesized rutile nanostructures at low temperature by sol-gel chemistry in 1-ethyl-3-methylimidazolium bis(trifluoromethylsulfonyl) imide (Kaper et al., 2003).

### 2.2.1 Synthesis $\text{Y}_2\text{O}_3$ nano-/microstructured phosphors without metal activators fabricated using functionalized ionic liquids

Flowerlike  $\text{Y}_2\text{O}_3$  nano-/microstructured phosphors without metal activators were fabricated by an ionic liquid assisted method (acid-catalyzed sol-gel synthesis) involving temperature ( $600^\circ\text{C}$ ) annealing by Kowsari and Faraghi (Kowsari & Faraghi, 2010). Also, the effect of ionic liquid concentration on the morphology of the product was investigated. The results revealed that the ionic liquids play a crucial role in the formation of various morphologies of  $\text{Y}_2\text{O}_3$ . The effect of the ionic liquid's cation and the counter anions on the  $\text{Y}_2\text{O}_3$  morphology of these nanostructures were studied experimentally. It was observed that  $\text{Y}_2\text{O}_3$  morphology and PL of these nanostructures was strongly influenced by the type of cation and anion. As the length of the subsidiary chain of cation section of ionic liquid (imidazole ion) reduces, the thickness of the nano-sheets increases. Since  $\text{Y}^{3+}$  itself is non-luminous, the observed luminescence from the  $\text{Y}_2\text{O}_3$  samples must be related to chemical-bond breakage with resultant carbon formation and/or non-stoichiometry (from ionic liquid) created by the oxygen deficiency in the system.

In this study, ionic liquid was used as a templating agent and produce different morphologies. The structures of ionic liquids show in Fig.3.

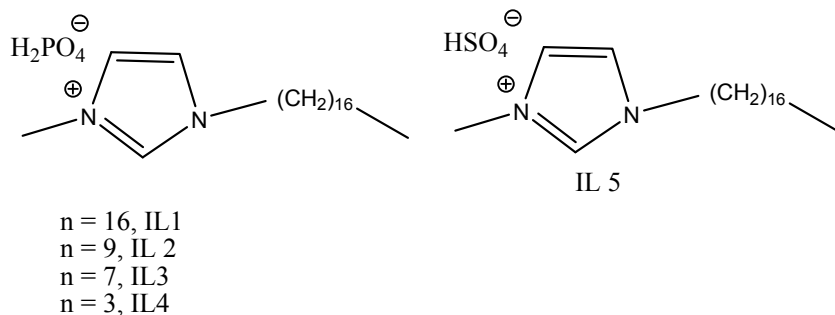


Fig. 3. Structures of ionic liquids (Reproduced from Kowsari & Faraghi, (2010) *Materials reserch Bull* 45, 8, 939-945, Copyright (2010), with permeation from Elsevier)

Here, the effect of ionic liquid concentration on the morphology of the product was investigated. Fig. 4 shows SEM photographs of products prepared with different ionic liquid concentrations. The results demonstrate that the concentration of ionic liquid is an important factor with regard to the formation of novel  $\text{Y}_2\text{O}_3$  microstructures. Since no surfactant or capping agent was employed in this synthesis, the ionic liquid used is believed to play an important role in the formation of the novel structure.

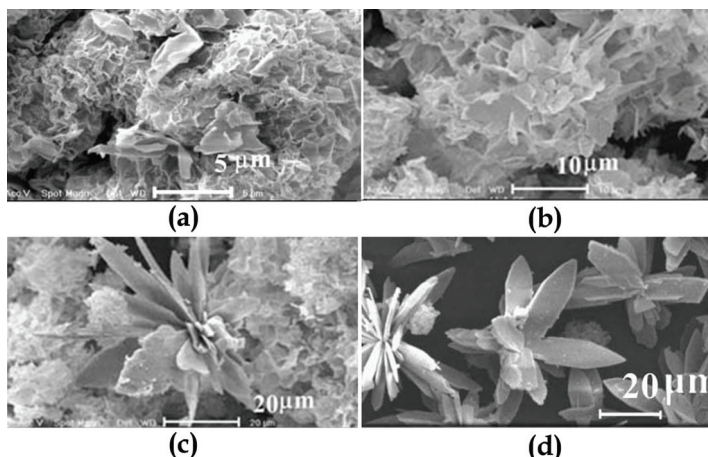


Fig. 4. SEM images showing the morphological evolution of  $\text{Y}_2\text{O}_3$  samples with different concentrations of IL1: (a) 0.036 M, (b) 0.027 M, (c) 0.018 M, and (d) 0.012 M, (Reproduced from Kowsari & Faraghi, (2010) *Materials research Bull* 45, 8, 939-945, Copyright (2010), with permission from Elsevier)

In high concentration of ionic liquid, (0.045 mmol) the  $\text{Y}_2\text{O}_3$  sample is irregular and crossed microsheets which overlap each other. When 0.012 mmol of ionic liquid is added in hydrothermal solution, the  $\text{Y}_2\text{O}_3$  sample is shaped as a uniform flowerlike architecture, as shown in Fig. 4c.

The formation mechanism of  $\text{Y}_2\text{O}_3$  flowers is obviously due to the templating effect in the present ionic liquid- water reaction system. The inset SEM images in Fig. 4e offer a clear view of the morphology from which it can be seen that the flowerlike  $\text{Y}_2\text{O}_3$  architecture is built up from  $\text{Y}_2\text{O}_3$  nanoflakes. The results suggested that the morphology of the  $\text{Y}_2\text{O}_3$  sample prepared by the solution-phase reactions is influenced by adding ionic liquid. The  $[\text{C}_{17}\text{mim}]^+$  cation of  $[\text{C}_{17}\text{mim}]^+[\text{H}_2\text{PO}_4]^-$  has a hydrophobic chain which, under proper experimental conditions  $[\text{C}_{17}\text{mim}]^+$ , could form micells with the positive ends stretch to the outside. After the  $\text{Y}(\text{NO}_3)_3$  is solved in water in the absence of  $[\text{H}_2\text{PO}_4]^-$ , which is an ionic liquid anion, there is the possibility of formation of  $[\text{Y}(\text{H}_2\text{O})_2(\text{NO}_3)_3 \cdot \text{H}_2\text{PO}_4]^-$ . Then,  $[\text{C}_{17}\text{mim}]^+$ , which is ionic liquid cation, can interact with precursor  $[\text{Y}(\text{H}_2\text{O})_2(\text{NO}_3)_3 \cdot \text{H}_2\text{PO}_4]^-$  ions through electrostatic attraction. Therefore, flowerlike  $\text{Y}_2\text{O}_3$  architecture can be obtained by hydrothermal route by adding a small amount of  $[\text{C}_{17}\text{mim}]^+[\text{H}_2\text{PO}_4]^-$ .

To further confirm the existence of the carbon impurity, the sample  $\text{Y}_2\text{O}_3$ -300, temperature (300 °C) annealing, was subjected to XPS analysis, which is a powerful tool for determining the surface composition of a material qualitatively. Fig. 5 shows the XPS analysis results of the sample. Signals of bonding energy from the Y (3d<sub>5/2</sub>, 158.4 eV), O (1s, 532.1 eV), C (1s, 285.0 eV), and N (1s, 399.0 eV) can be seen clearly in Fig. 10 (Wang & Ong, 2007, Ramí´rez et al., 2002) This provides additional evidence for the existence of the carbon impurity.

In this study, some  $\text{Y}_2\text{O}_3$  nanostructures were prepared in the presence of other ionic liquids with different cations, and anions each at a concentration of 0.027 M. The Effect of the ionic liquids cation and the counter anions on the  $\text{Y}_2\text{O}_3$  morphology of these nanostructures were studied experimentally. It was observed that  $\text{Y}_2\text{O}_3$  morphology and PL of these nanostructures was strongly influenced by the type of cation and anion. As the length of the

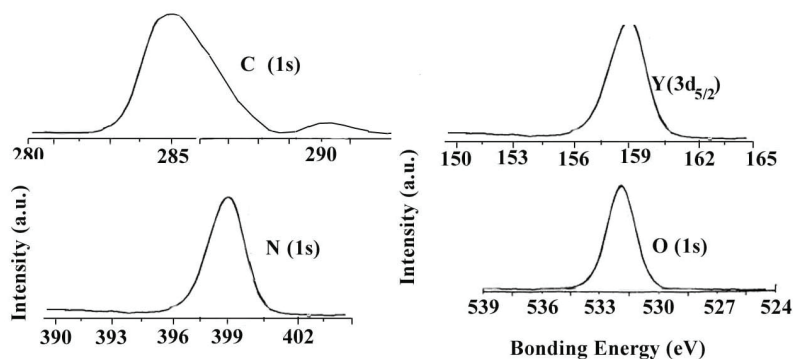


Fig. 5. XPS spectra of  $\text{Y}_2\text{O}_3$ -300 sample (Reproduced from Kowsari & Faraghi, (2010) *Materials research Bull* 45, 8, 939-945, Copyright (2010), with permeation from Elsevier)

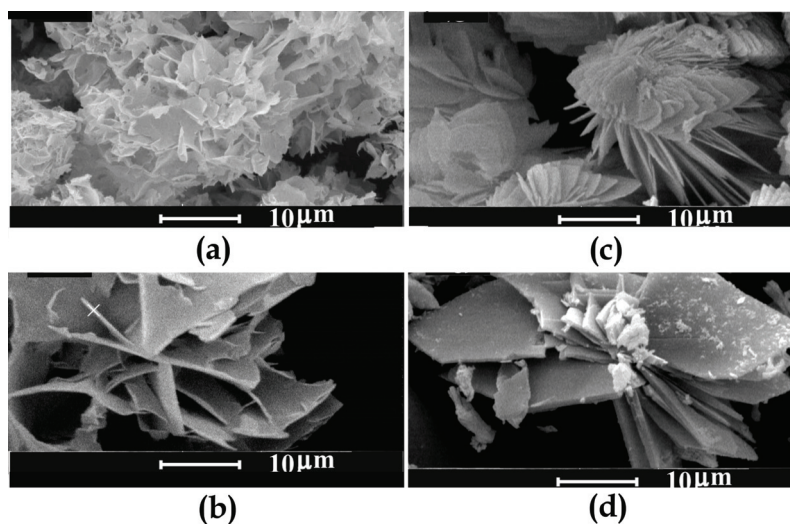


Fig. 6. SEM images showing the morphological evolution of  $\text{Y}_2\text{O}_3$  samples with different cation and anion of ionic liquids, [concentrations of IL = 0.027 M]: (a) IL1, (b) IL2, (c) IL3 and (d) IL4 [ IL1,  $([\text{C}_{17}\text{mim}]^+ [\text{H}_2\text{PO}_4]^-)$ , 1-heptadecyl-3-methylimidazolium dihydrogen phosphate), IL2,  $([\text{C}_{10}\text{mim}]^+ [\text{H}_2\text{PO}_4]^-)$ , 1-decyl-3-methylimidazolium dihydrogen phosphate), IL3,  $([\text{C}_8\text{mim}]^+ [\text{H}_2\text{PO}_4]^-)$ , 1-octyl-3-methylimidazolium dihydrogen phosphate), IL4,  $([\text{C}_4\text{mim}]^+ [\text{H}_2\text{PO}_4]^-)$ , 1-buthyl-3-methylimidazolium dihydrogen phosphate)]. (Reproduced from Kowsari & Faraghi, (2010) *Materials research Bull* 45, 8, 939-945, Copyright (2010), with permeation from Elsevier)

subsidiary chain of cation section of ionic liquid (imidazole ion) reduces, the thickness of the nano-sheets increase. And as anion section of ionic liquid changes ( $\text{H}_2\text{PO}_4^-$  to  $\text{HSO}_4^-$ ), as shown is Fig. 6, morphology changes from a nano-sheet-like structure to a coral-like one. Since  $\text{Y}^{3+}$  itself is non-luminous, the observed luminescence from the of  $\text{Y}_2\text{O}_3$  samples must be related to chemical-bond breakage with resultant carbon formation and/or non-

stoichiometry created by the oxygen deficiency in the system (Fujimaki et al., 1997, Green, 1997, Pifferi et al., 1997, Hayakawa et al., 2003). Here, we assume that the carbon-related impurities play a key role in the luminescence of  $\text{Y}_2\text{O}_3$ .

### 2.2.2 Morphogenesis and crystallization of $\text{Bi}_2\text{S}_3$ nanostructures by an ionic liquid-assisted templating route

An ionic liquid 1-butyl-3-methylimidazolium tetrafluoroborate ([BMIM][BF<sub>4</sub>]) solution system has been designed for the morphogenesis and crystallization of  $\text{Bi}_2\text{S}_3$  nanostructures at low temperature and ambient atmosphere by Jiang et al. (Jiang et al., 2005).

Uniform  $\text{Bi}_2\text{S}_3$  flowers with a size of 3–5  $\mu\text{m}$ , which are composed of nanowires with a diameter of 60–80 nm, can be prepared in large scale by the template effect of the ionic liquid solution, in which vesicles are formed as confirmed by laser light scattering analysis. With prolonged aging time, the flowerlike structures tend to become loose and fall off from the mother flowers, and finally the individual nanowires will form.

The results demonstrated that the shape evolution and phase transformation strongly depend on the reaction conditions, such as pH value, reaction temperature, and reaction time. The pH value of the reaction medium plays a key role in the present procedure for the synthesis of  $\text{Bi}_2\text{S}_3$  nanoflowers. First, a suitable pH value can effectively prevent  $\text{BiCl}_3$  hydrolysis to  $\text{BiOCl}$  in the initial reaction stage and kinetically control the growth rate of dendrite  $\text{Bi}_2\text{S}_3$  nanostructures. When the pH value is about 2, even within a short period, for example, about half an hour, large-scale and uniformly shaped  $\text{Bi}_2\text{S}_3$  nanoflowers with a size of 3.5  $\mu\text{m}$  can be prepared conveniently (Fig. 7).

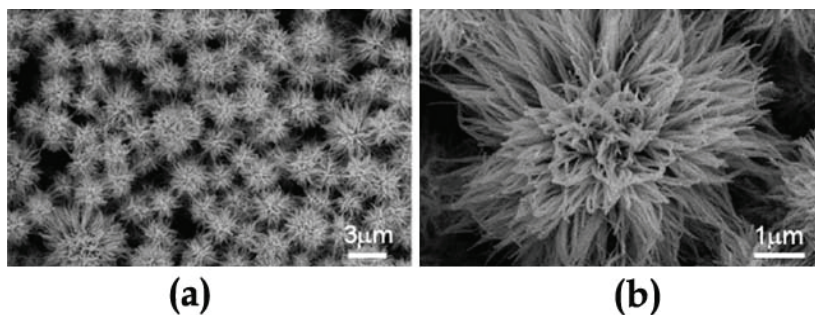


Fig. 7. SEM images of the product obtained in an ionic liquid system after reaction at 120 °C for 0.5 h. Starting pH = 2 (Reproduced from Jiang et al. *Chem. Mater.* 2005, 17, 6094–6100, Copyright (2009), with permission from American Chemical Society)

## 2.3 Thermal synthesis

### 2.3.1 Ionothermal synthesis

Ionic liquids are known for their nonvolatile, nonflammable, and thermally stable properties. These properties make the reactions in open reactor possible. The term “ionothermal” has been used to describe reactions that are conducted in ionic liquids at high temperature with ambient pressures. As a result, ionothermal reactions avoid high pressure of hydrothermal or solvothermal reactions and eliminate safety problems related to high pressure (Taubert & Li 2007). Cooper, et al. have demonstrated that imidazolium-based



ionic liquids can be utilized to synthesize several phosphate-based microporous zeolites by an ionothermal process (Cooper et al., 2004), Dai, et al. reported the use of a newly developed ionic liquid system containing zinc metal ions, which can serve as both solvents and metal-oxide precursors, for manufacturing nanostructured zinc oxide under the ionothermal condition (Zhu et al., 2006). The morphologies of ZnO are strongly dependent on the nature of the ionic liquid precursor (ligands), providing unique methodologies to control the growth conditions.

In ionothermal synthesis, the ionic liquid acts as the solvent, and in many cases also as a template provider playing a structure-directing role in the formation of zeolites and open-framework structures. The use of [EMim][Br] led to the formation of open-framework aluminophosphates SIZ-1, SIZ-3, SIZ-4, SIZ-5, and SIZ-6, (Cooper et al. 2004; Parnham et al. 2006) and the use of choline chloride/urea mixtures led to SIZ-2 and AlPO-CJ2 (Cooper et al. 2004). The ionic liquids acted as both solvent and template provider.

### 2.3.2 Hydrothermal synthesis

Several research groups have employed ionic liquids for the synthesis of nanostructures by hydrothermal method. Zhang and coworkers (Zhang et al. 2008) reported a hydrothermal method to synthesize sheaf-like CuO self-assembled by nanoplatelets in [BMIM]BF<sub>4</sub>. [BMIM]BF<sub>4</sub> was used as a cosolvent and modifiers in the formation of sheaflike CuO. Hollow molybdenum disulfide (MoS<sub>2</sub>) microspheres were synthesized in ionic liquids (1-butyl-3-methylimidazolium chloride, [BMIM]Cl)/water binary emulsions using the hydrothermal method at 180 °C by Luo and coworker (Lue et al. 2008). Liu and coworkers (Liu et al. 2009) have also reported a modified hydrothermal method for the synthesis of CdSe nanoparticles-assembled microspheres with macropores using 1-n-butyl-3-methylimidazolium bromide ([Bmim]Br) to assist the reaction. By changing the processing parameters, they fabricate wurtzite CdSe microspheres with an average diameter of about 3 μm. The possible growth mechanism of the CdSe microspheres is investigated.

Nanostructured ZnO was synthesized by a hydrothermal route using different ionic liquids as the morphology templates by Yavari et al. (Yavari et al. 2009). The morphology of ZnO changes from rod-like to star-like and flower-like in different ionic liquids. A 3D nano/micro structure ZnO with unique flower-like morphology has been synthesized (Fig. 9) via the assembly of dicationic ionic liquid and [Zn(OH)<sub>4</sub>]<sup>2-</sup>.

A typical SEM image of an individual ZnO hexagonal prism with hexagonal pyramid in tip is presented in Fig. 10. It is indicated that it can grow along the [0001] direction.

It has been known that the adsorption of growth units on crystal surfaces strongly affects the growth speed and orientation of crystals (Li et al., 1999). When a ZnO crystal grew, an ionic liquid (with pyridinium cation, for example) film could form at the interface between solution and the crystal. This landing process on the surface of ZnO [0 0 0 1] crystal face is shown graphically in Fig. 11. Since ionic liquid favors to form a film in which molecules tend to be perpendicular to the absorbed surface, the growth units would tend to face-land onto the growing interface as shown in Fig. 11. This kind of landing and dehydration will result in three Zn–O–Zn bonds, which make it predominant in competition with vertex- and edge-landing. Thus, the ZnO crystals should grow preferentially along the c-axis ([0 0 0 1] direction) as this kind of face-landing on [0 0 0 1] crystal face and the following dehydration steps are repeated (Li et al., 1999).

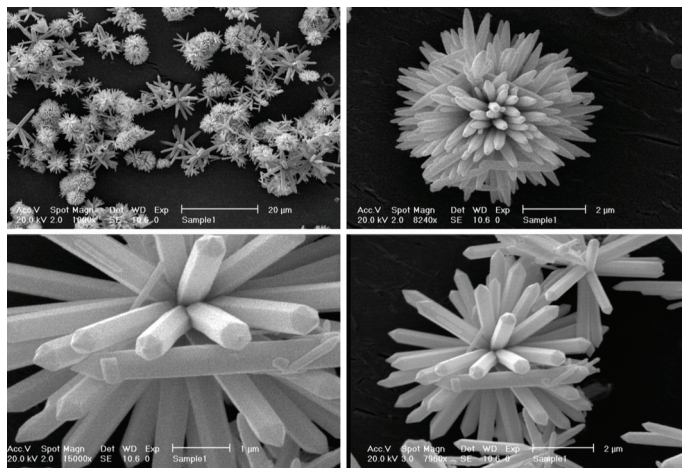


Fig. 9. SEM image of the flower-like ZnO in  $[(C_1)_2C_8(im)_2](Br)_2$ , mole ratio  $OH^-/Zn^{+2} = 30:1$  and  $[(C_1)_2C_8(im)_2](Br)_2 = 0.10$  g. (Reproduced from Yavari et al. (2009) *J. Nanopart. Res.*; 11, 861, Copyright (2009), with permeation from Springer)

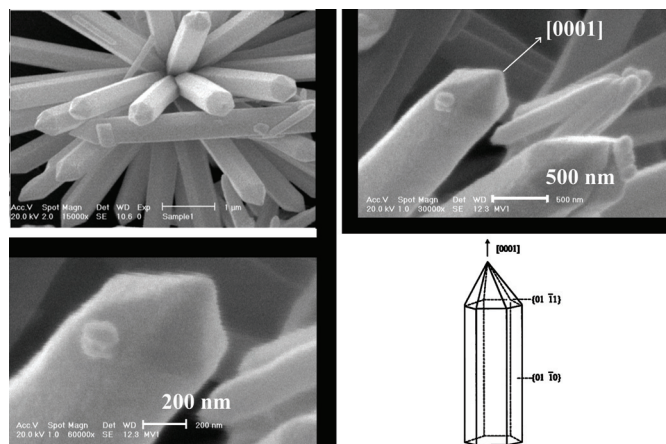


Fig. 10. A typical SEM image of an individual ZnO hexagonal prism with hexagonal pyramid in tip (Reproduced from Yavari et al. (2009) *J. Nano part. Res.*; 11, 861, Copyright (2009), with permeation from Springer)

According to the process described earlier, it is supposed that ionic liquid leads to the orientation growth of ZnO rods. Similarly, ZnO flower-like assemblies can be formed in the presence of ionic liquid which has two identical imidazolium cations.

The ZnO has been found to exhibit sensitivity to  $C_2H_5OH$ ,  $NH_3$  and other species. However, the ZnO based sensing devices possess several critical limitations, which are difficult to overcome, such as a limited maximum sensitivity and the operation at high temperature ( $400\text{--}500^\circ\text{C}$ ). Flower-like ZnO nanostructures improve performance such as sensitivity and working temperature (room temperature).

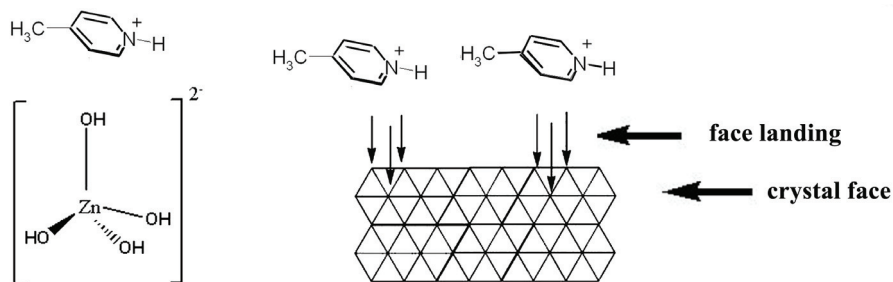


Fig. 11. (a) Schematic illustration of ion-pair formed between ionic liquid and  $[\text{Zn}(\text{OH})_4]^{2-}$ ; (b) landing process on the surface of ZnO [0001] crystal face by ionic liquid. (Reproduced from Yavari et al. (2009) *J. Nanopart. Res.*; 11, 861, Copyright (2009), with permission from Springer)

Flower-like ZnO morphology, with different shapes, have been synthesized via a novel and environment-friendly hydrothermal method using zinc acetate and a task specific dicationic dibasic ionic liquid,  $[\text{mmpim}]_2[\text{OH}]_2$ , which plays an important role in fabrication of ZnO structure (Movahedi et al., 2008). SEM images of ZnO nanostructure synthesized by task specific dicationic dibasic ionic liquid,  $[\text{mmpim}]_2[\text{OH}]_2$  is shown in fig. 12.

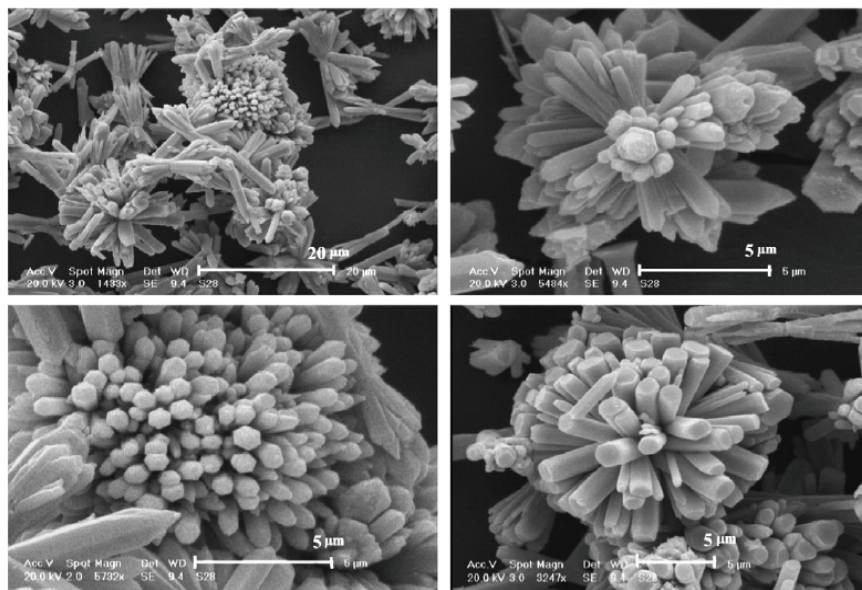


Fig. 12. SEM images of ZnO nanostructure synthesized by task specific dicationic dibasic ionic liquid,  $[\text{mmpim}]_2[\text{OH}]_2$ , (Reproduced from Movahedi et al. (2008) *Materials Letters* 62 3856–3858, Copyright (2008), with permission from Elsevier)

The  $\alpha\text{-Fe}_2\text{O}_3$  with various morphologies has been synthesized via an ionic liquid assisted hydrothermal synthetic method by Lian and coworkers (Lian et al. 2009) The results indicate that the as-prepared samples are  $\alpha\text{-Fe}_2\text{O}_3$  nanoparticles, mesoporous hollow microspheres,



microcubes, and porous nanorods. The UV-vis measurements suggest that the as-synthesized pure  $\alpha$ -Fe<sub>2</sub>O<sub>3</sub> with various morphologies possess different optical properties depending on the shape and size of the samples. The magnetic hysteresis measurements indicate the interesting magnetic property evolution in the as-prepared  $\alpha$ -Fe<sub>2</sub>O<sub>3</sub> samples, which is attributed to the superstructure or the shape anisotropy of the samples.

## 2.4 Microwave heating synthesis

The application of microwave heating in synthetic chemistry is a fast-growing research area due to its advantages such as rapid volumetric heating, higher reaction rate, and selectivity, reducing reaction time often by orders of magnitude and increasing yields of products compared with conventional heating methods. As a result, this has opened up the possibility of realizing fast synthesis of materials in a short time. From the perspective of microwave chemistry, one of the key important advantages of room temperature ionic liquids is the presence of large organic positive ions with a high polarizability. Therefore, room temperature ionic liquids are good media for absorbing microwaves, leading to a high heating rate. Lately, by combining the advantages of both room temperature ionic liquids and microwave heating, a new microwave-assisted ionic liquid method has developed for fast controlled synthesis of nanorods and nanowires of Te and ZnO (Jiang & Zhu, 2005). Zhu and coworkers (Zhu et al. 2004) synthesized single-crystal tellurium nanowires using microwave heating in *n*-butylpyridinium tetrafluoroborate ionic liquid in the presence of polymer surfactant of poly(vinylpyrrolidone) (PVP). Li and coworkers (Li et al. 2005) synthesized large-size single-crystal gold nanosheets by microwave heating of H<sub>2</sub>SO<sub>4</sub> in [BMIM][BF<sub>4</sub>], without any additional template agent. Subsequently, PbCrO<sub>4</sub> rods or bundle-like Pb<sub>2</sub>CrO<sub>5</sub>, Bi<sub>2</sub>Se<sub>3</sub> nanosheets, sulfide M<sub>2</sub>S<sub>3</sub> nanorods, single-crystalline cryptomelane-type manganese oxide octahedral molecular sieve (OMS-2) nanoneedles, and nanorods, metal fluorides such as FeF<sub>2</sub>, CoF<sub>2</sub>, ZnF<sub>2</sub>, LaF<sub>3</sub>, YF<sub>3</sub>, SrF<sub>2</sub>, metal-oxide like Fe<sub>2</sub>O<sub>3</sub>, carbon-coated core shell structured copper or nickel nanoparticles and CNTs/Pt or CNTs/Rh composites have successfully been fabricated by microwave-assisted synthesis method in ionic liquids (Wang & Zhu, 2005, Jiang et al., 2006, Singh et al., 2008, Liu et al., 2006).

Single-crystalline Bi<sub>2</sub>S<sub>3</sub> and Sb<sub>2</sub>S<sub>3</sub> nanorods have been synthesized using the microwave-assisted ionic liquid method by Jiang and Zhu (Jiang & Zhu, 2005). The starting reagents were Bi<sub>2</sub>O<sub>3</sub> or Sb<sub>2</sub>O<sub>3</sub>, HCl, Na<sub>2</sub>S<sub>2</sub>O<sub>3</sub>, and ethylene glycol (EG) or ethanolamine, and the ionic liquid used was 1-butyl-3-methylimidazolium tetrafluoroborate ([BMIM][BF<sub>4</sub>]). These experiments showed that the ionic liquid played an important role in the morphology of M<sub>2</sub>S<sub>3</sub> (M = Bi, Sb). Single-crystalline Bi<sub>2</sub>S<sub>3</sub> nanorods could be prepared in the presence of [BMIM][BF<sub>4</sub>]. However, urchinlike Bi<sub>2</sub>S<sub>3</sub> structures consisting of nanorods were formed without using [BMIM][BF<sub>4</sub>]. Single-crystalline Sb<sub>2</sub>S<sub>3</sub> nanorods were obtained in the presence of [BMIM][BF<sub>4</sub>]. However, single-crystalline Sb<sub>2</sub>S<sub>3</sub> nanosheets could be prepared in the absence of [BMIM][BF<sub>4</sub>].

The morphologies of the samples were investigated by transmission electron microscopy (TEM). Figure 13a,b shows TEM micrographs of sample 1 (Bi<sub>2</sub>S<sub>3</sub>) synthesized under microwave heating at 190 °C for 10 min without using the ionic liquid [BMIM][BF<sub>4</sub>], from which one can see the urchinlike morphology of Bi<sub>2</sub>S<sub>3</sub>.

## 2.5 Emulsions or microemulsions synthesis

Reverse microemulsions are mostly transparent, isotropic and thermodynamically stable liquid media with nanosized water droplets dispersing in a continuous oil phase and

stabilized by an adsorbed surfactant film at the liquid–liquid interface (Chokshi et al., 1989). One of the important applications of microemulsions involves the preparation of nanoparticles, nanowires, and nanorods (Qi et al., 1997). More recently, some investigations demonstrated that ionic liquids could substitute water or oil to form novel microemulsions in the presence of surfactant

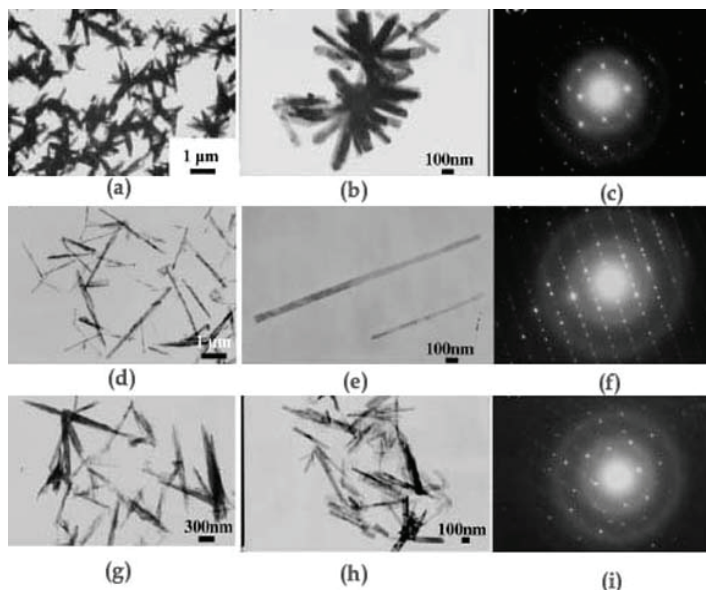


Fig. 13. TEM micrographs of three typical Bi<sub>2</sub>S<sub>3</sub> samples: (a and b) sample 1; (d and e) sample 2 synthesized via microwave-assisted ionic liquid method at 190 °C for 10 min; (g and h) sample 3 synthesized via microwave-assisted ionic liquid method at 190 °C for 30 s. (c, f, and i) Electron diffraction patterns of individual nanorods from samples 1, 2, and 3, respectively. (Reproduced from Jiang & Zhu (2005) *J. Phys. Chem. B*, 109, 4361-4364, Copyright (2005), with permission from American Chemical Society)

Ionic liquid microemulsions have both the advantages of ionic liquids and microemulsion, which can overcome the inability of ionic liquids to dissolve a number of chemicals including some hydrophilic substances and then broaden the utilization of ionic liquids. Some papers reported that ionic liquid could substitute water to form nonaqueous ionic liquid microemulsion and exist as nanosized polar domains dispersed in cyclohexane with the aid of surfactant (Li et al., 2007). Gao, et al. prepared and characterized TX-100/H<sub>2</sub>O/1-butyl-3-methylimidazolium hexafluorophosphate (bmimPF<sub>6</sub>) microemulsion using different techniques. Their research results showed that water domains existed in the water-in-bmimPF<sub>6</sub> microemulsion, which could dissolve salts (Gao et al., 2005).

## 2.6 Electrodeposition synthesis

Electrochemical deposition is an economical and convenient choice for preparing uniform and size controllable nano-materials. It is meaningful to combine the advantages of aqueous ionic liquid microemulsions and the electrodeposition method for preparing materials.

Aqueous ionic liquid microemulsions as electrolytes for electrochemical deposition are special and different from traditional aqueous solution and ionic liquids. Electrochemical approaches have been among the first to be used for the fabrication of inorganic nanoparticles and nanostructured films in ionic liquids. The properties of ionic liquids opened the door to the electrodeposition of metals and semiconductors at room temperature, which was previously only possible from high-temperature molten salts. For example, Al, Mg, Ti, Si, Ge and rare-earth-elements related materials can be obtained from ionic liquids.

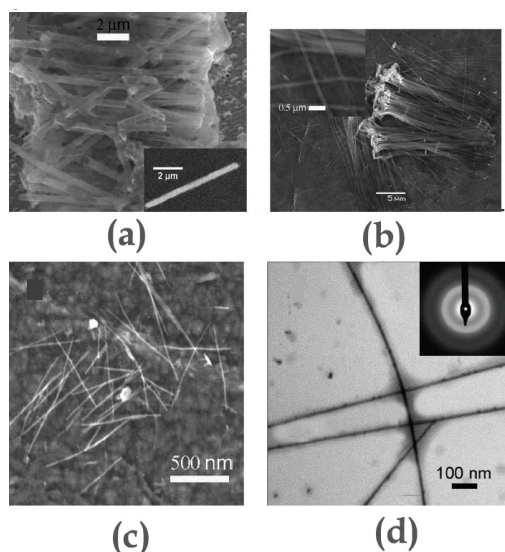


Fig. 14. SEM images of the Si NWs prepared with membranes with nominal pore diameter of 400 nm and a thickness of 12  $\mu\text{m}$  (a), 110 nm and 20  $\mu\text{m}$  (b), and 15 and 800 nm (c) after partial or total dissolution of the PC membranes. The inset of the image in panel a exhibits an isolated 400 nm NW after a supplementary washing procedure to show its smooth surface after total dissolution of the membrane. The inset of the image in panel b shows some isolated 110 nm NWs with a good uniformity for the diameters and regular and smooth edges. (d) A TEM picture of isolated 15 nm NWs with the corresponding electron diffraction pattern (Reproduced from Mallet et al (2008) *Nano Letter* 2008 8, 10, 3468-3474 Copyright (2008), with permeation from American Chemical Society)

Silicon nanowires were fabricated for the first time by electrochemical template synthesis at room temperature by J. Mallet and coworkers (Mallet et al. 2008). This innovative, cheap, and simple process consists of electroreduction of Si ions using a nonaqueous solvent and insulating nanoporous membranes with average pore diameters from 400 to 15 nm which fix the nanowires diameters

Characterization techniques such as scanning and transmission electron microscopies, infrared absorption measurements, X-ray diffraction experiments, energy dispersive X-ray, and Raman spectrometries show that the as-deposited silicon nanowires are amorphous, composed of pure Si and homogeneous in sizes with average diameters and lengths well matching with the nanopores' diameters and the thicknesses of the membranes. Thanks to

annealing treatments, it is possible to crystallize the Si nanowires, demonstrating the potentiality for this innovative electrochemical process to obtain a wide range of Si nanowires with well controlled diameters and lengths. Figure 14 panels a-c are SEM images of nanowires prepared in PC membrane with pore diameters of 400, 110, and 15 nm, respectively, and thicknesses of 12  $\mu\text{m}$ , 20  $\mu\text{m}$ , and 800 nm, respectively, after partial or total dissolution of the membranes and collection on a HOPG substrate. Figure 14d is a TEM image of 15 nm NWs deposited on a Ni grid.

Ultrafine monodisperse gold nanoparticles (AuNPs) were synthesized by an elegant sputtering of gold onto 1-*n*butyl-3-methylimidazolium hexafluorophosphate (BMI-PF<sub>6</sub>) ionic liquid by Khatri and coworkers (Khatri et al. 2008). It was found that the BMI-PF<sub>6</sub> supramolecular aggregates were loosely coordinated to the gold nanoparticles and were replaceable with thiol molecules. The selfassembly of BMI-PF<sub>6</sub>-stabilized AuNPs onto a (3-mercaptopropyl)trimethoxysilane (MPS)-functionalized silicon surface in 2D arrays, followed by dodecanethiol (DDT) treatment, have been demonstrated using X-ray photoelectron spectroscopy, field emission scanning electron microscopy, and contact angle measurements. DDT treatment of tethered

AuNPs revealed two types of interactions between AuNPs and the MPS-functionalized surface: (a) AuNPs anchor through Au-S chemisorption linkage resulting in strong immobilization and (b) some of the AuNPs are supported by physisorption, driven by BMI-PF<sub>6</sub>. The attachment of these particles remains unchanged with sonication. The replacement of BMI-PF<sub>6</sub> aggregates from physisorbed AuNPs with dodecanethiol molecules advances the dilution of their interaction with the MPS-functionalized surface, and they subsequently detach from the silicon surface. The present finding is promising for the immobilization of ionic liquid-stabilized nanoparticles, which is very desirable for electronic and catalytic device fabrication. Additionally, these environmentally friendly AuNPs are expected to replace conventional citrate-stabilized AuNPs.

## 2.7 Nanocasting technique and ionic liquid

A nanocasting technique (Attard et al., 1995, Polarz & Antonietti, 2002) was employed for the synthesis of several mesoporous SiO<sub>2</sub> materials. Zhou and Antonietti used [C<sub>16</sub>Mim][Cl] as the template to prepare monolithic super-microporous SiO<sub>2</sub> (pore diameter 1.3 nm, wall thickness 1.4 nm, surface area 1340 m<sup>2</sup> g<sup>-1</sup>) with lamellar order via a nanocasting technique. (Zhou & Antonietti, 2003) They further reported a systematic investigation employing [C<sub>10</sub>Mim][Cl] ([C<sub>10</sub>Mim]<sup>+</sup> = decyl-3-methylimidazolium), [C<sub>14</sub>Mim][Cl], [C<sub>16</sub>Mim][Cl], and [C<sub>18</sub>Mim][Cl] ([C<sub>18</sub>Mim]<sup>+</sup> = 1-octadecyl-3-methylimidazolium) as templates, and again obtained lamellar SiO<sub>2</sub> with pore diameters in the range of 1.2–1.5 nm. (Zhou & Antonietti, 2004) In addition, mesoporous SiO<sub>2</sub> with wormlike pores (pore diameter 2.5 nm, wall thickness 2.5–3.1 nm, surface area 801 m<sup>2</sup> g<sup>-1</sup>) was synthesized using [BMim][BF<sub>4</sub>] as the template. (Zhou & Schattka, 2004) The authors proposed a hydrogen bond-co- $\pi$ - $\pi$  stacking mechanism, in which the hydrogen bonds formed between [BF<sub>4</sub>]<sup>-</sup> and the SiO<sub>2</sub> matrix together with the  $\pi$ - $\pi$  stacking interaction of the neighboring imidazolium rings led to the mutual packing and formation of mesoporous SiO<sub>2</sub> (Fig. 16).

The synthesis of mesoporous SiO<sub>2</sub> using ionic liquids as new templates has furnished new examples in the synthesis of mesoporous materials. However, the efforts made in this regard are still minor, compared to the huge efforts made in the synthesis of mesoporous materials using other templates. The advantages of using ionic liquids instead of conventional solvents are not obvious, the synthesis mechanisms in different cases are not quite clear, and

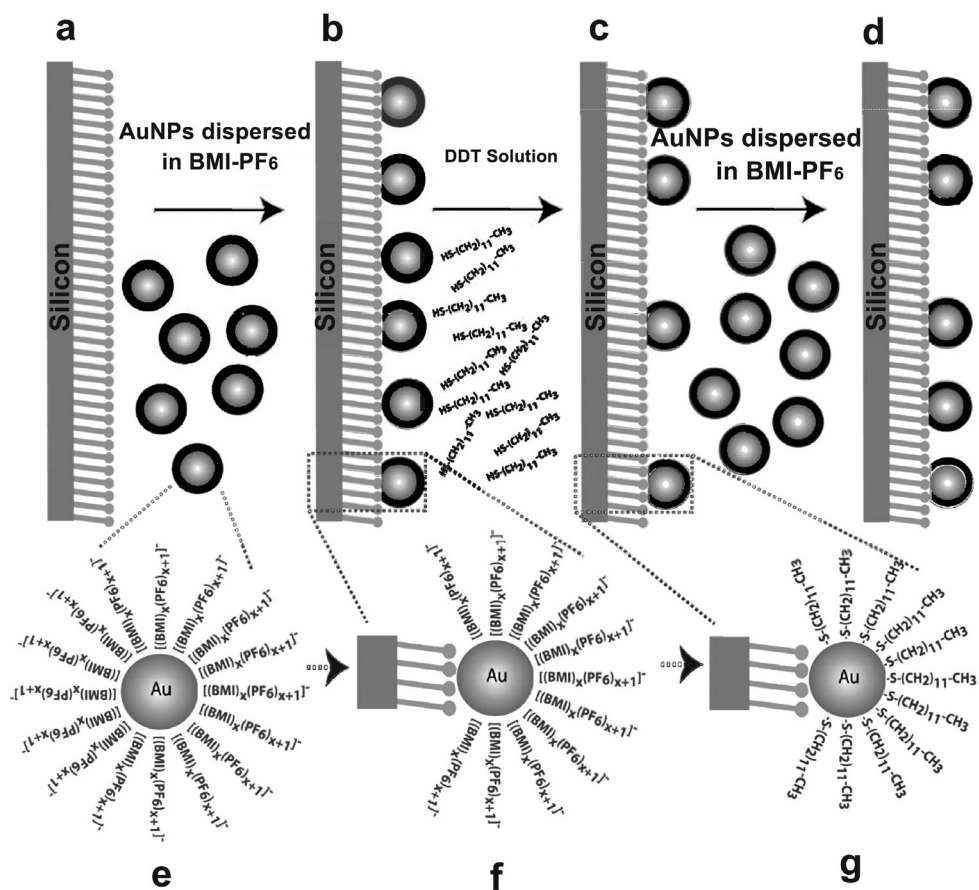


Fig. 15. Simple Model to Illustrate the Interaction of BMI-PF<sub>6</sub>-Stabilized AuNPs on the MPS-Functionalized Surface (Reproduced from Khatri et al. (2008) *Langmuir* 24, 7785-7792, Copyright (2008), with permission from American Chemical Society)

<sup>a</sup> Illustration of (a) an MPS monolayer on a silicon surface and (b) the immobilization of BMI-PF<sub>6</sub>-stabilized AuNPs on the mercapto-functionalized silicon surface followed by (c) dodecanethiol treatment, which replaces the protective coating of BMI-PF<sub>6</sub> supramolecular aggregates and detaches the physisorbed AuNPs from the silicon surface. (d) Immobilization of new AuNPs. These particles are probably tethered to vacant sites created by the detachment of physisorbed AuNPs. (e). BMI-PF<sub>6</sub>-stabilized ultrafine gold nanoparticles in the dispersed phase. (f). Interaction of BMI-PF<sub>6</sub>-stabilized AuNPs with a mercapto-functionalized surface. The strong affinity between gold and the mercapto group replaces the BMI-PF<sub>6</sub> aggregates from the localized area and results in Au-S chemisorption bonding. (g). Replacement of the BMI-PF<sub>6</sub> protective layer by dodecanethiol molecules.

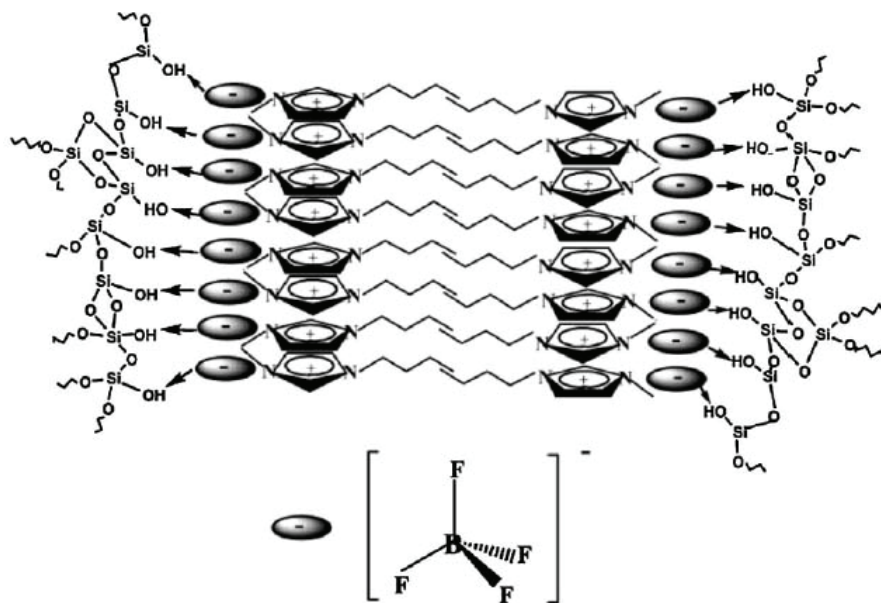


Fig. 16. A  $\pi$ - $\pi$  stacking model proposed to explain the formation of mesoporous  $\text{SiO}_2$  using  $[\text{BMim}][\text{BF}_4]$  as the template. In this model,  $[\text{BF}_4]^-$  anions interact with the silanol groups and arrange along the pore walls, and  $[\text{BMim}]^+$  cations are aligned accordingly, forming  $\pi$ - $\pi$  stacking interactions between the aromatic motifs. (Reproduced from Zhou et al. (2004) *Nano Lett.* 4, 477, Copyright 2004, with permission of the American Chemical Society)

the knowledge regarding the morphological control of mesoporous  $\text{SiO}_2$  is still limited. It is not clear how the use of different ionic liquids may lead to different morphologies and how synthesis conditions may influence the morphology. Regardless of these limitations, this idea has opened up new avenues for the synthesis of hierarchical porous materials and periodic mesoporous organosilicas.

### 3. Conclusion

The updated application of the ionic liquid in the synthesis of inorganic nanomaterials was briefly outlined. The main emphasis of the outline was a focus on the preorganized structure of the ionic liquid as template effect for inorganic nanomaterials. The particular strength of ionic liquids is their virtually unlimited flexibility of anions and cations combinations. As the cation or anion in the ionic liquid can be tailored by functional substitutes, the size and size distribution of the ionic liquid-stabilized metal nanoparticles can be easily controlled too. In case ionic liquid phase behavior, chemical composition, and reactivity are also considered, ionic liquids provide a flexible toolbox for the fabrication of inorganics with various (and variable) properties simply by designing the appropriate precursor. These precursors are entities which are defined molecularly, which can be well characterized and studied as the transformation to the inorganic proceeds.

Although the application of the ionic liquid in inorganic nanomaterials is still in its early days, many claim that the field of ionic liquid is becoming a promising area of research in the nanomaterials in the years to come.

#### 4. Acknowledgment

The author wishes to express her gratitude to National Elite Foundation for the financial support.

#### 5. References

- Abedin, S. Z. El.; Borissenko, N. & Endres, F. (2004). Electrodeposition of nanoscale silicon in a room temperature ionic liquid. *Electrochem. Commun.* 6, 5, 510-514. 1388-2481
- Antonietti, M.; Kuang, D. B.; Smarsly, B. & Zhou, Y. (2004). Ionic liquids for the convenient synthesis of functional nanoparticles and other inorganic nanostructures. *Angew. Chem. Int. Ed.* 43, 38, 4988-4992, 1521-3773
- Attard, G.S.; Glyde, J. C. & Goltner, C. G. (1995). Liquid-crystalline phases as templates for the synthesis of mesoporous silica. *Nature*, 378, 6555, 366-368, 0028-0836
- Binnemans, K. (2005). Ionic Liquid Crystals. *Chem. Rev.* 105, 11, 4148-4204, 0009-2665
- Bühler, G. & Feldmann, C. (2006). Microwave-assisted synthesis of luminescent LaPO<sub>4</sub>: Ce, Tb nanocrystals in ionic liquids. *Angew. Chem. Int. Ed.* 45, 29, 4864-4867, 1521-3773
- Chokshi, K.; Qutubuddin, S. & Hussam, A. (1989). Electrochemical investigation of microemulsions. *J. Colloid Interf. Sci.* 129, 2, 315-326, 0021-9797
- Cooper, E. R.; Andrews, C. D.; Wheatley, P. S.; Webb, P. B.; Wormald, P. & Morris, R. E. (2004). Ionic liquids and eutectic mixtures as solvent and template in synthesis of zeolite analogues. *Nature* 430, 7003, 1012-1016, 0028-0836
- Dai, S.; Ju, Y. H.; Gao, H. J.; Lin, J. S.; Pennycook, S. J. & Barnesc, C. E. (2000). Preparation of silica aerogel using ionic liquids as solvents. *Chem Commun*, 3, 243-244, 1359-7345
- Dhasn, N. A.; Zaban, A. & Gedanken, A. (1999). Article surface synthesis of Zinc Sulfide nanoparticles on silica microspheres: Sonochemical preparation, characterization, and optical properties. *Chem. Mater.* 11, 3, 806-813, 0897-4756
- Ding, K. L.; Miao, Z. J.; Liu, Z. J.; Zhang, Z. F., Han, B. X., An, G. M.; Miao, S. D. & Xie, Y. (2007) Facile synthesis of high quality TiO<sub>2</sub> nanocrystals in ionic liquid via a microwave-assisted process. *J. Am. Chem. Soc.* 129, 20, 6362-6363, 0002-7863
- Dobbs, W.; Suisse, J.-M.; Douce, L. & Welter, R. (2006). Electrodeposition of silver particles and gold nanoparticles from ionic liquid-crystal precursors. *Angew. Chem., Int. Ed.* 45, 25, 4179-4182, 1521-3773
- Dupont, J.; Fonseca, G. S.; Umpierre, A. P.; Fichtner, P. F. P. & Teixeira, S. R. (2002). Transition-metal nanoparticles in imidazolium ionic liquids: Recyclable catalysts for biphasic hydrogenation reactions. *J. Am. Chem. Soc.*, 124, 16, 4228-4229, 0002-7863
- Endres, F.; Bukowski, M.; Hempelmann, R. & Natter, H. (2003). Electrodeposition of nanocrystalline metals and alloys from ionic liquids, *Angew. Chem., Int. Ed.* 42, 29, 3428-3430, 1521-3773

- Flannigan, J. D.; Hopkins, D. S. D. & Suslick, K. S. (2005). Sonochemistry and sonoluminescence in ionic liquids, molten salts, and concentrated electrolyte solutions. *J Organomet Chem*, 690, 15, 3513–3517, 0022-328X
- Foneca, G. S.; Umpierre, A. P.; Fichtner, P. F.; Teixeira, S. R. & Dupont, J. (2003). The use of imidazolium ionic liquids for the formation and stabilization of Ir<sup>0</sup> and Rh<sup>0</sup> nanoparticles: efficient catalysts for the hydrogenation of arenes. *Chem. Eur. J.* 9, 14, 3263–3269, 1521-3765
- Fujimaki, M.; Ohki, Y. & Nishikawa, H. (1997) Energy states of Ge-doped SiO<sub>2</sub> glass estimated through absorption and photoluminescence. *J. Appl. Phys.*, 81, 3 1042-1046, 0021-8979
- Gao, Y. N.; Han, S. B.; Han, B. X.; Li, G. Z.; Shen, D. & Li, Z. G. (2005) TX-100/Water/1-Butyl-3-methylimidazolium hexafluorophosphate microemulsions. *Langmuir*, 21, 13, 5681-5684, 0743-7463
- Green, W. H.; Le, K. P.; Grey, J.; Au, T. T. & Sailor, M. J. (1997). White phosphors from a silicate-carboxylate sol-gel precursor that lack metal activator ions. *Science*, 276, 5320, 1826-1828, 0036-8075
- Hao, Y.; Meng, G.; Ye, C.; Zhang, X. & Zhang, L. (2005). Kinetics-Driven Growth of Orthogonally Branched Single-Crystalline Magnesium Oxide Nanostructures. *J. Phys. Chem. B.*, 109, 22, 11204-11208, 1520-6106
- Hayakawa, T.; Hiramitsu, A. & Nogami, M. (2003) White light emission from radical carbonyl-terminations in Al<sub>2</sub>O<sub>3</sub>-SiO<sub>2</sub> porous glasses with high luminescence quantum efficiencies. *Appl. Phys. Lett.*, 82, 18, 2975-2977, 0003-6951
- Huang, J.; Jiang, T.; Han, B. X.; Gao, H. X.; Chang, Y. H.; Zhao, G. Y. & Wu, W. Z. (2003). Hydrogenation of olefins using ligand-stabilized palladium nanoparticles in an ionic liquid. *Chem. Commun.* 14, 1654-1655, 1359-7345
- Jiang, J.; Yu, S. H.; Yao, W. T.; Ge, H. & Zhang, G. Z. (2005) Morphogenesis and crystallization of Bi<sub>2</sub>S<sub>3</sub> nanostructures by an ionic liquid-assisted templating route: synthesis, formation mechanism, and properties. *Chem. Mater.* 17, 24, 6094–6100, 0897-4756
- Jiang, Y. & Zhu, Y. J. (2005) Microwave-assisted synthesis of sulfide M<sub>2</sub>S<sub>3</sub> (M = Bi, Sb) nanorods using an ionic liquid *J. Phys. Chem. B* 109, 10, 4361–4364, 1520-6106
- Jiang, J.; Yu, S. H.; Yao, W. T.; Ge, H. & Zhang, G. H. (2005). Morphogenesis and crystallization of Bi<sub>2</sub>S<sub>3</sub> nanostructures by an ionic liquid-assisted templating route: synthesis, formation mechanism, and properties. *Chem. Mater.*, 17, 24, 6094–6100
- Jiang, Y.; Zhu, Y. J.; Cheng, G. F. (2006) Synthesis of Bi<sub>2</sub>Se<sub>3</sub> nanosheets by microwave heating using an ionic liquid. *Cryst Growth Des*, 6, 9, 2174–2176, 1528-7483
- Jia, X.; Fan, H.; Zhang, F. & Qin, L. (2010). Using sonochemistry for the fabrication of hollow ZnO microspheres. *Ultrasonics Sonochemistry*, 17, 2, 284–287, 1350-4177
- Kaper, H.; Endres, F.; Djerdj, I.; Antonietti, M.; Smarsly, B. M.; Maier, J. & Hu, Y. S. (2007) Direct low-temperature synthesis of rutile nanostructures in ionic liquids. *Small*, 3, 10, 1753-1763, 1613-6829
- Khatri, O. P.; Adachi, K.; Murase, K.; Okazaki, K.; Tsukasa Torimoto, T.; Tanaka, N.; Kuwabata, S. & Sugimura, H. (2008). Self-assembly of ionic liquid (BMI-PF<sub>6</sub>)-



- stabilized gold nanoparticles on a silicon surface: chemical and structural aspects. *Langmuir*, 24, 15, 7785-7792, 0743-7463
- Kim, K. S.; Choi, S.; Cha, J. H.; Yeon, S. H. & Lee, H. (2006). Facile one-pot synthesis of gold nanoparticles using alcohol ionic liquids. *J. Mater. Chem.* 16, 14, 1315-1317, 0959-9428
- Kowsari, E. & Faraghi, G. (2010) Ultrasound and ionic-liquid-assisted synthesis and characterization of polyaniline/Y<sub>2</sub>O<sub>3</sub> nanocomposite with controlled conductivity. *Ultrasonics Sonochemistry*, 17, 4, 718-725, 1350-4177
- Kowsari, E. & Faraghi, G. (2010). Synthesis by an ionic liquid-assisted method and optical properties of nanoflower Y<sub>2</sub>O<sub>3</sub>. *Materials reserch Bull*, 45, 8, 939-945, 0025-5408
- Lee, C. K.; Vasam, C. S.; Huang, T. W.; Wang, H. M. J.; Yang, R. Y.; Lee, C. S. & Lin, I. J. B. (2006). Silver(I) N-heterocyclic carbenes with long N-alkyl chains. *Organometallics* 25, 15, 3768-3775, 0276-7333
- Lyu, S. C.; Zhang, Y.; Ruh, H.; Lee, H. G.; Shim, H. W.; Suhc, E. K. & Lee, C. J. (2002) Low temperature growth and photoluminescence of well-aligned zinc oxide nanowires. *Chem. Phys. Lett.*, 363, 1-2, 134-138, 0009-2614
- Lee, Y. C.; Liu, Y. L.; Shen, J. L.; Hsu, I. J.; Cheng, P. W.; Cheng, C.F. & Ko, C. H. (2004). Blue-green luminescence from mesoporous MCM-48 molecular sieves. *J.Non-Cryst. Solids*, 341, 1-3, 16-20, 0022-3093
- Li, W. J.; Shi, E. W.; Zhong, W. Z. & Yin, Z. W. (1999) Growth mechanism and growth habit of oxide crystals. *J Cryst Growth*, 203, 1-2, 186-196, 0022-0248
- Li, Z.; Liu, Z.; Zhang, J.; Han, B.; Du, J.; Gao, Y., Jiang, T (2005). Synthesis of Single-Crystal Gold Nanosheets of Large Size in Ionic Liquids. *J Phys Chem B*, 109, 30, 14445-1448, 1520-6106
- Lian, J; Duan, X.; Ma, J; Peng, P.; Kim, T. & Zheng, W. (2009). Hematite ( $\alpha$ -Fe<sub>2</sub>O<sub>3</sub>) with various morphologies: ionic liquid-assisted synthesis, formation mechanism, and properties, *ACS Nano.*, 3, 11, 3749-3761, 1936-0851
- Liu, X.; Peng, P.; Ma, J.; Zheng, W. (2009) Preparation of novel CdSe microstructure by modified hydrothermal method, *Mater lett*, 63, 8, 673-675, 0167-577X
- Luo, H.; Xu, C; Zou, D.; Wang, L.; Ying, T. (2008). Hydrothermal synthesis of hollow MoS<sub>2</sub> microspheres in ionic liquids/water binary emulsions. *Mater lett*, 62, 20 3558-3560, 0167-577X
- Li, N; Gao, Y. A.; Zheng, L. Q.; Zhang, J.; Yu, L. & Li, X. W. (2007). Studies on the micropolarities of bmimBF<sub>4</sub>/TX-100/toluene ionic liquid microemulsions and their behaviors characterized by UV-Visible spectroscopy. *Langmuir* 23, 3, 1091-1097, 0743-7463
- Liu, Z.; Sun, Z.; Han, B., Zhang, J.; Huang, J.; Du, J. & Miao, S. (2006) Microwave-Assisted Synthesis of Pt Nanocrystals and Deposition on Carbon Nanotubes in Ionic Liquids. *J Nanosci Nanotech*, 2006, 6, 1, 175-179, 1550-7033
- Movahedi, M.; Kowsari, E.; Mahjoub, A. R.; Yavari, I. (2008) A task specific basic ionic liquid for synthesis of flower-like ZnO by hydrothermal method. *Mater lett*, 62, 23, 3856-3858, 0167-577X

- Mallet et al (2008) Growth of Silicon Nanowires of Controlled Diameters by Electrodeposition in Ionic Liquid at Room Temperature. *Nano Lett*, 8, 10, 3468-3474, 1530-6984
- Mu, X.; Evans, D. G. & Kou, Y. (2004) A general method for preparation of PVP-stabilized noble metal nanoparticles in room temperature ionic liquids. *Catal. Lett.* 97, 3-4, 151-154, 1011-372X
- Nakashima, T. & Kimizuka, N. (2003) Interfacial synthesis of hollow TiO<sub>2</sub> microspheres in ionic liquids. *J. Am. Chem. Soc.*, 125, 21 6386-6387, 0002-7863
- Parnham, E. R.; Wheatley, P. S.; Morris, R. E. (2006) The ionothermal synthesis of SIZ-6-a layered aluminophosphate, *Chem. Commun.*, 4, 380-382, 1359-7345
- Zhang, M.; Xu, X.; Zhang, M. (2008). Hydrothermal synthesis of sheaf-like CuO via ionic liquids. *Mater Lett*, 62, 3, 385-388, 0167-577X
- Pifferi, A.; Taroni, P.; Torricelli, A.; Valentini, G.; Mutti, P.; Ghislotti, G. & Zanghieri, L. (1997) Nanosecond time-resolved emission spectroscopy from silicon implanted and annealed SiO<sub>2</sub> layers. *Appl. Phys. Lett.*, 70, 3, 348-350, 0003-6951
- Polarz, S. & Antonietti, M. (2002). Porous materials via nanocasting procedures: innovative materials and learning about soft-matter organization. *Chem. Commun.* 22, 2593-2604, 1359-7345
- Qi, L.; Ma, J.; Cheng, H.; Zhao, Z. (1997) Reverse micelle based formation of BaCO<sub>3</sub> nanowires. *J. Phys. Chem. B* 101, 18, 3460-3463, 1520-6106
- Ramírez, E. B.; Huanosta, A.; Sebastian, J. P.; Huerta, L.; Ortiz, A.; Alonso, J. C. (2007). Structure, composition and electrical properties of YSZ films deposited by ultrasonic spray pyrolysis. *J. Mater. Sci.*, 42, 3, 901-907, 0022-2461
- Scheeren, C. W.; Machado, G.; Dupont, J.; Fichtner, P. F. P. & Texeira, S. R. (2003). Nanoscale Pt(0) particles prepared in imidazolium room temperature ionic liquids: Synthesis from an organometallic precursor, characterization, and catalytic properties in hydrogenation reactions. *Inorg. Chem.* 42, 15, 4738-4742, 0020-1669
- Singh, P.; Katyal, A.; Kalra, R.; Chandra, R. (2008). Copper nanoparticles in an ionic liquid: an efficient catalyst for the synthesis of bis-(4-hydroxy-2-oxothiazolyl)methanes. *Tetrahedron Lett*, 49, 4, 727-730, 0040-4039
- Suslick, K. S. (1988) Ultrasound; VCH, Weinheim, Germany.
- Suslick, K. S.; Choe, S. B.; Cichowlas, A. A. & Grinstaff, M. W. (1991). Sonochemical synthesis of amorphous iron. *Nature*, 353, 414-416, 0028-0836
- Taubert, A. & Li, Z. (2007). Inorganic materials from ionic liquids. *Dalton Trans.* 7, 723-727, 1477-9226
- Taubert, A. (2004) CuCl nanoplatelets from an ionic liquid-crystal precursor. *Angew. Chem., Int. Ed.* 43, 40, 5380-5382, 1433-7851
- Taubert, A.; Palivan, C.; Casse, O.; Gozzo, F. & Schmitt, B. (2007) Ionic liquid-crystal precursors (ILCPs) for CuCl platelets: The origin of the exothermic peak in the DSC curves. *J. Phys. Chem. C*, 111, 11, 4077-4082, 1932-7447
- Taubert, A.; Arbell, I.; Mecke, A. & Graf, P. (2006). Photoreduction of a crystalline Au(III) complex: a solid-state approach to metallic nanostructures. *Gold Bull.* 39, 4, 205-211, 0017-1557

- Taubert, A.; Steiner, P. & Manton, A. (2005). Ionic liquid crystal precursors for inorganic particles: phase diagram and thermal properties of a CuCl nanoplatelet precursor. *J. Phys. Chem. B* 109, 32, 15542-15547, 1520-6106
- Taubert, A. (2005) (Sub) Micron CaF<sub>2</sub> cubes and hollow rods from ionic liquid emulsions. *Acta Chim. Slov.* 52, 2, 168-170, 1318-0207
- Wang, S. L. & Ong, C. K. (2002). Epitaxial Y-stabilized ZrO<sub>2</sub> films on silicon: Dynamic growth process and interface structure. *Appl. Phys. Lett.*, 80, 14, 2541-2543, 0003-6951
- Wang, W. W. & Zhu, Y. J. (2005). Synthesis of PbCrO<sub>4</sub> and Pb<sub>2</sub>CrO<sub>5</sub> rods via a microwave-assisted ionic liquid method. *Cryst Growth Des.*, 5, 2, 505-507, 1528-7483
- Wang, Y. & Yang, H. (2005) Synthesis of CoPt nanorods in ionic liquids. *J. Am. Chem. Soc.* 127, 15, 5316-5317, 0002-7863
- Yavari, I.; Mahjoub, A. R.; Kowsari, E.; Movahedi, M. (2009). Synthesis of ZnO nanostructures with controlled morphology and size in ionic liquids. *J. Nanopart. Res.*, 11, 4, 861-868, 1388-0764
- Yoo, K.; Choi, H. & Dionysiou, D. D. (2004). Ionic liquid assisted preparation of nanostructured TiO<sub>2</sub> particles *Chem. Commun.* 17, 2000-2001, 1359-7345
- Zhu, H.; Huang, J.-F.; Pan, Z.; Dai, S. (2006). Ionothermal synthesis of hierarchical ZnO nanostructures from ionic-liquid precursors. *Chem. Mater.* 18, 18, 4473-4477, 0897-4756
- Zhu, Y.; Wang, W.; Qi, R. & Hu, X. (2004) Microwave-assisted synthesis of single-crystalline tellurium nanorods and nanowires in ionic liquids. *Angew. Chem., Int. Ed.* 43, 11, 1410-1414, 1521-3773
- Zhou, Y. & Antonietti, M. J. (2003). Synthesis of very small TiO<sub>2</sub> nanocrystals in a room-temperature ionic liquid and their self-assembly toward mesoporous spherical aggregates. *J. Am. Chem. Soc.* 125, 49 14960-14961, 0002-7863
- Zhu, Y. J.; Wang, W. W.; Qi, R. J. & Hu, X. L. (2004). Microwave-Assisted Synthesis of Single-Crystalline Tellurium Nanorods and Nanowires in Ionic Liquids. *Angew Chem Int Ed*, 43, 11, 1410-1414, 1521-3773
- Zhou, Y.; Schattka, J. H. & Antonietti, M. (2004). Room-temperature ionic liquids as template to monolithic mesoporous silica with wormlike pores via a sol-gel nanocasting technique. *Nano Lett.* 4, 3, 477-481, 1530-6984
- Zhou, Y. & Antonietti, M. (2004). A Series of highly ordered, super-microporous, lamellar silicas prepared by nanocasting with ionic liquids. *Chem. Mater.* 16, 3, 544-550, 0897-4756
- Zhou, Y. & Antonietti, M. (2003). Preparation of highly ordered monolithic super-microporous lamellar silica with a room-temperature ionic liquid as template via the nanocasting technique. *Adv. Mater.* 15, 17, 1452-1455, 1521-4095
- Žilková, N.; Zukal, Z. & Čejka, J. (2006). Synthesis of organized mesoporous alumina templated with ionic liquids. *Micropor. Mesopor. Mater.* 95, 1-3, 176-179. 1387-1811
- Zheng, Y.; Yu, X.; Xu, X.; Jin, D. & Yue, L. (2010). Preparation of ZnO particle with novel nut-like morphology by ultrasonic pretreatment and its luminescence property. *Ultrasonics Sonochemistry*, 17, 1, 7-10, 1350-4177

- Zhou, Y. & Antonietti, M. (2003). Synthesis of very small  $\text{TiO}_2$  nanocrystals in a room-temperature ionic liquid and their self-assembly toward mesoporous spherical aggregates. *J Am Chem Soc* 125, 49, 14960-14961, 0002-7863
- Zhu, H.; Huang, J.; Pan, Z. & Dai, S. (2006). Ionothermal Synthesis of Hierarchical ZnO Nanostructures from Ionic-Liquid Precursors. *Chem Mater*, 18,18, 4473-4477, 0897-4756

# Synthesis of Novel Nanoparticle - Nanocarbon Conjugates Using Plasma in Ionic Liquid

Toshiro Kaneko and Rikizo Hatakeyama  
*Tohoku University*  
*Japan*

## 1. Introduction

Since metal and semiconducting nanoparticles have high catalytic activity due to their size effects (Nishikawa et al., 2002), and carbon nanotubes functionalized by foreign atoms and molecules are very fascinating materials in nanoelectronics applications, the various kinds of nanoparticles conjugated with the carbon nanotubes (Georgakilas et al., 2007; Han et al., 2004) could constitute promising nanoelectronics devices such as gas sensors (Kong et al., 2000), field-effect transistors (Kim et al., 2007), and so on. Up to now, electrochemical decoration (Wildgoose et al., 2005), plasma-ion irradiation (Jeong et al., 2003), and supercritical fluid method (Ye et al., 2004) have been extensively utilized for the synthesis of the nanoparticles conjugated with the carbon nanotubes. However, the nanoparticles usually attach to the outside of the carbon nanotubes, and as a result, they easily agglutinate and change in quality by the heat or chemical reactions. Therefore, it has been claimed that the nanoparticles should be intercalated into the interlayer of the bundled carbon nanotubes. Based on these backgrounds, we attempt to develop a novel nanoparticles synthesis method using gas (plasma) / liquid (ionic liquids) interfacial fields under low gas pressures, where the various kinds of the nanoparticles can be generated and intercalated into the carbon nanotubes.

Recently, many works on the gas-liquid interfacial plasmas have been performed as fundamental and applied researches (Bruggeman & Leys, 2009). Among them, the nanoparticle synthesis using the plasma-liquid interfaces (Meiss et al., 2007; Torimoto et al., 2006; Xie & Liu, 2008; Hieda et al., 2008; Koo et al. 2005) is especially advantageous in that toxic stabilizers and reducing agents are unnecessary and the synthesis is continuous during the plasma irradiation. In these methods, although it has been reported that the metal salt is reduced by an electron or an active hydrogen, the optimal plasma conditions in terms of the synthesis rate, size control, and simplicity remain unclear because the inevitable high voltage discharge in the atmospheric pressure and the consequential dynamic behavior of the gas-liquid interface prevent us from analyzing the precise properties of the plasmas in the interfacial region. In this sense, we have claimed that the generation of the static gas-liquid interface under the low gas pressure condition is necessary to clarify the phenomena at the gas-liquid interface for application to the effective and controllable nanoparticle synthesis.

In this chapter, we present the development of a new plasma system to form the spatially and temporally stable plasma-liquid interfacial surface (Baba et al., 2007; Kaneko et al.,

2009a), i.e., a direct current (DC) discharge plasma is generated just above the liquid by applying the DC power to the electrodes immersed in the liquid and located in the gas phase region, and the precise potential structure between these electrodes through the gas-liquid interfacial region is measured. Furthermore, control of the plasma irradiation flux and energy to the liquid is revealed to be useful for the application such as creation of various kinds of nanoparticles (Baba et al., 2009; Kaneko et al., 2009b), and the nanoparticles conjugated with the carbon nanotubes (Baba et al., 2010).

## 2. Experimental apparatus

For the purpose of the generation of the static and stable plasma contacting with the liquid, we adopt ionic liquids (Seddon, 2003; Rogers & Seddon, 2003) which have recently gotten much attention in the electrochemistry field. The ionic liquids have the interesting characteristics such as their composition consisting of only positive and negative ions, i.e., no neutral solvent, extremely low vapor pressure, high heat capacity, and nonflammability. These characteristics enable us to introduce the ionic liquids to the vacuum system and the discharge plasma. Therefore, the ionic liquids are the most suitable liquid for the formation of nano-composite materials using the discharge plasmas in contact with the liquids.

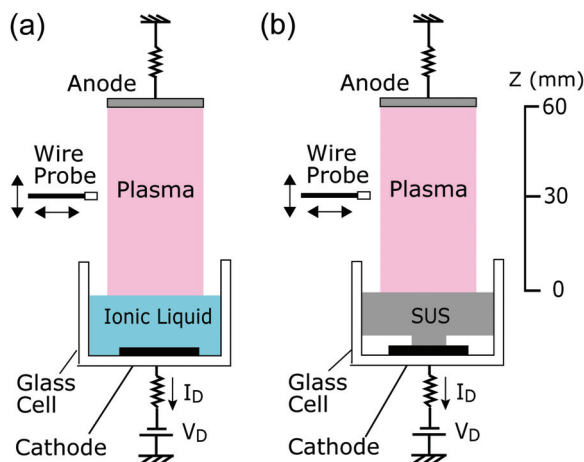


Fig. 1. Schematic diagrams of experimental setup for DC discharge plasmas, where the cathode is set in the glass cell, and is (a) the ionic liquid and (b) the SUS plate. The anode is located at the top of the gas plasma region. These configurations are defined as A-mode.

Figure 1 shows schematic diagrams of experimental setup which has a glass cell of 20 mm in diameter and 10 mm in depth in a cylindrical glass chamber of 15 cm in diameter and 50 cm in length. A cathode electrode which is made of a platinum (Pt) plate with 15 mm diameter is located inside the glass cell and the ionic liquid is introduced on the cathode electrode as shown in Fig. 1(a). Three types of ionic liquids, 1-Ethyl-3-methyl-imidazolium tetrafluoroborate ( $[\text{EMI}(\text{C}_6\text{H}_{11}\text{N}_2)^+][\text{BF}_4^-]$ ), 1-Butyl-3-methyl-imidazolium tetrafluoroborate ( $[\text{BMI}(\text{C}_8\text{H}_{15}\text{N}_2)^+][\text{BF}_4^-]$ ), and 1-Hexyl-3-methyl-imidazolium tetrafluoroborate ( $[\text{HMI}(\text{C}_{10}\text{H}_{19}\text{N}_2)^+][\text{BF}_4^-]$ ), which have different lengths of alkyl chain in the positive ions of them, are introduced into the glass cell, and the amount of the ionic liquid is 1.5 ml.

Removal of the water dissolved in the ionic liquid is performed under the vacuum condition for 2 hours after introducing the ionic liquid into the glass chamber. A DC power is supplied to the cathode electrode in the ionic liquid. On the other hand, a grounded anode electrode which is made of a stainless steel (SUS) plate is set in a gas phase (plasma) region at a distance of 60 mm from the surface of the ionic liquid.

For the purpose of investigating the effects of the ionic liquid on the discharge, the ionic liquid on the Pt plate is replaced by the SUS plate as shown in Fig. 1(b). Here, the surface position of the SUS plate is adjusted to that of the ionic liquid. These discharge configurations, in which the cathode electrode (the Pt plate with the ionic liquid or the SUS plate) is in the glass cell, are defined as "A-mode". Argon gas is adopted as a discharge medium, and the gas pressure  $P_{\text{gas}}$  is varied from 20 Pa to 80 Pa approximately.

In order to examine the effects of the DC power supplied to the electrode in the ionic liquid on discharge-related phenomena, the cathode electrode is switched to the SUS plate located at the top of the gas plasma region and the Pt plate in the ionic liquid is grounded instead, which is defined as "B-mode" as shown in Fig. 2(a). For the purpose of comparison, the configuration that the SUS plate in the glass cell is grounded, i.e., works as the anode electrode, is also introduced [Fig. 2(b)].

A high voltage probe is directly connected to the cathode electrode to measure the bias voltage of it. A Langmuir probe is inserted at the position of  $z = 0 - 60$  mm to measure parameters of the plasma in contact with the ionic liquid ( $z = 0$ : surface of the ionic liquid).

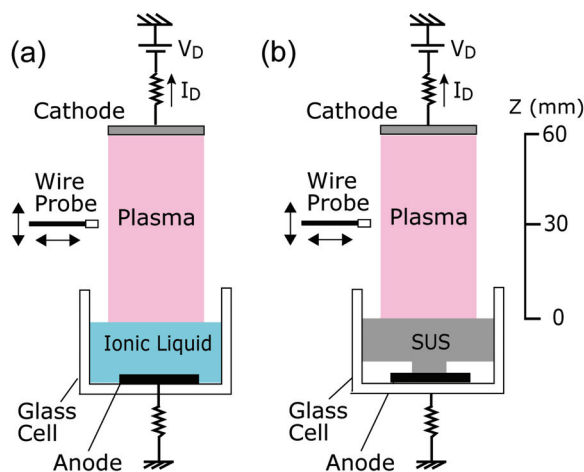


Fig. 2. Schematic diagrams of experimental setup for DC discharge plasmas, where the cathode is located at the top of the gas plasma region. The anode is set in the glass cell, and is (a) the ionic liquid and (b) the SUS plate. These configurations are defined as B-mode.

### 3. Experimental results and discussion

#### 3.1 Plasma properties

We successfully generate ionic liquid incorporated plasmas at low gas pressures with high stability, similar to normal glow discharge plasmas. Figure 3 shows the photos of the stable DC discharge plasma in A-mode in the regions below the anode electrode and above the

cathode electrodes consisting of the SUS and the ionic liquid (IL) as a function of gas pressure  $P_{\text{gas}}$ , where the discharge current  $I_D$  is fixed to 1 mA. It is found that the cathode glow is clearly observed and its volume becomes small with an increase in the gas pressures, while little emission is observed in the region below the anode electrode. There is little difference in the behavior of the cathode glow between the SUS and IL cathode electrodes.

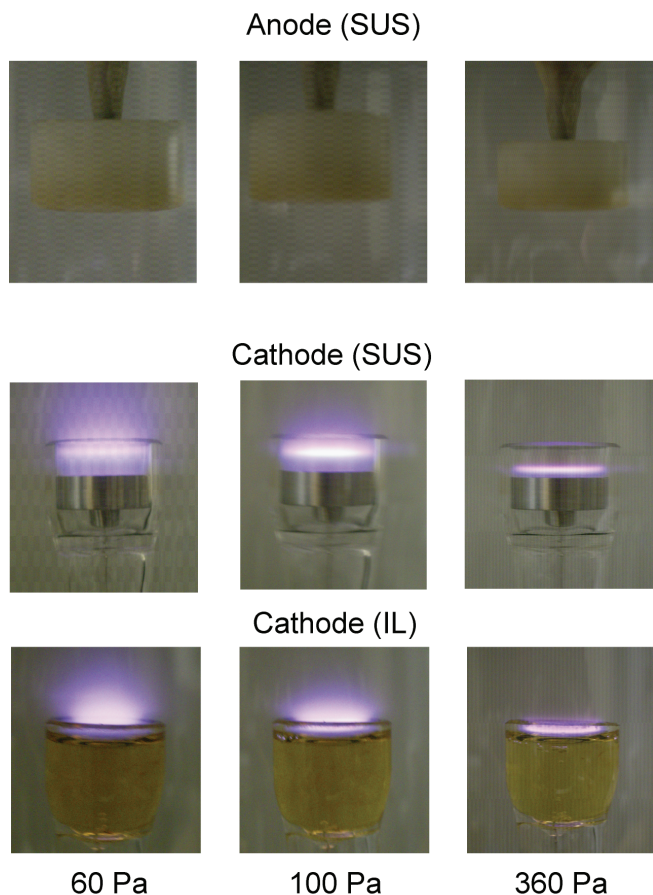


Fig. 3. Photos of the stable DC discharge plasma in A-mode in the regions below the anode electrode and above the cathode electrodes consisting of the SUS and the IL as a function of gas pressure  $P_{\text{gas}}$ .  $I_D = 1$  mA.

The photos of the discharge plasma in B-mode in the regions below the cathode and above the anodes as a function of gas pressure  $P_{\text{gas}}$  are given in Fig. 4. The cathode glow is observed below the cathode electrode and its volume becomes small with an increase in the gas pressure in the same way as the case of A-mode. Since the mean free path becomes short with an increase in the gas pressure, the electrons accelerated by the cathode sheath collide with the neutral gas closer to the cathode electrode, and then the glow region is considered to shrink.



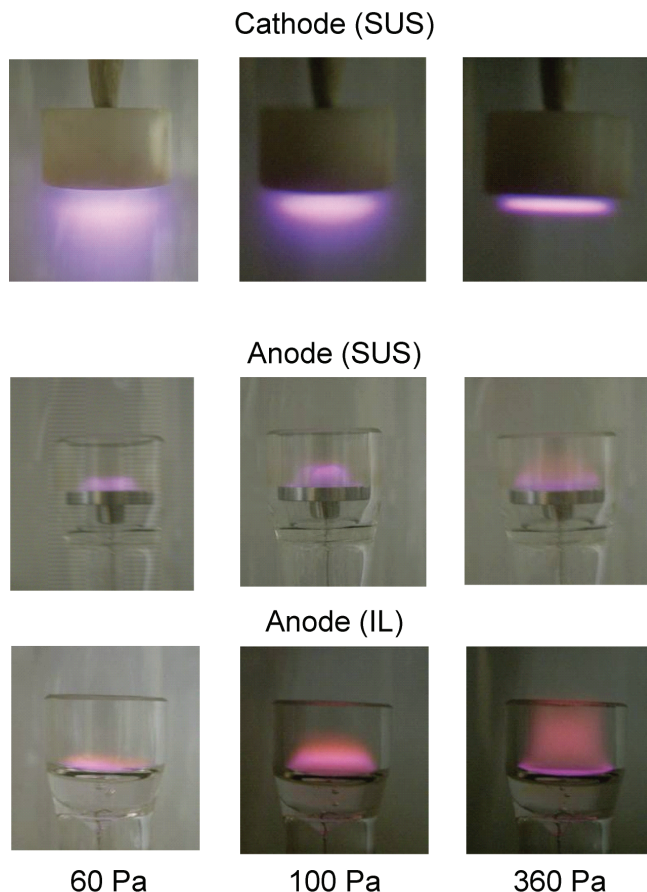


Fig. 4. Photos of the stable DC discharge plasma in B-mode in the regions below the cathode electrode and above the anode electrodes consisting of the SUS and the IL as a function of gas pressure  $P_{\text{gas}}$ .  $I_D = 1$  mA.

In addition, the anode glow is also observed above both the SUS and IL anode electrodes in the case of B-mode. The volume of the anode glow becomes larger with an increase in the gas pressure, because the recombination occurs more frequently at the high pressures and the anode glow extends to the plasma region. Furthermore, the volume of the anode glow in the IL electrode is larger than that in the SUS electrode. This phenomenon is explainable in terms of the high electron density due to the larger secondary electron emission coefficient of the IL electrode (Kaneko et al., 2009a).

Figure 5 presents axial profiles of the space potential  $\phi_s$  in (a) A-mode and (b) B-mode for  $P_{\text{gas}} = 60$  Pa and  $I_D = 1$  mA (discharge current), where the cathode electrodes are the IL (red circles) and the SUS plate (black diamonds). In A-mode, the discharge voltages  $V_D$ , i.e., the potentials of the cathode electrode are about  $-380$  V and  $-540$  V when the cathode materials are the IL and SUS, respectively. When the cathode electrode consists of the IL, a large number of secondary electrons are emitted from the IL cathode compared with the SUS

cathode, and therefore, the discharge voltage becomes small for fixed discharge current  $I_D=1$  mA. Furthermore, these many electrons emitted from the IL cathode make the space potential lower than that in the case of the SUS cathode. The space potential in the case of the IL cathode gradually increases around  $z=40$  mm toward the anode electrode. Since the potential difference between the plasma and the IL cathode is about 330 V, the sheath electric field is formed above the IL cathode, giving rise to the electrostatic acceleration of positive ions in the plasma toward the IL, namely ion irradiation on the IL.

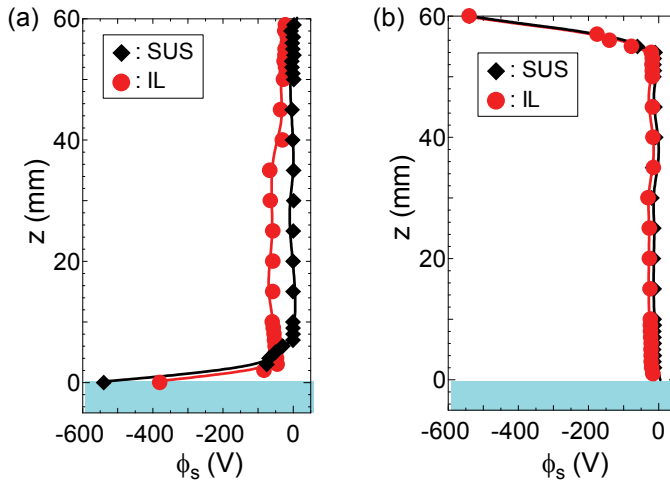


Fig. 5. Axial profiles of the space potential  $\phi_s$  in (a) A-mode and (b) B-mode.  $P_{Ar} = 40$  Pa,  $I_D=1$  mA.

In B-mode, on the other hand, the discharge voltages, i.e., the potentials of the upper SUS cathode electrodes are the same ( $V_D = -540$  V) and the axial profiles of the space potential are almost the same in both the cases with and without the IL. Since the potential in the plasma region is about  $-20$  V, the potential difference between the plasma and the IL anode electrode is relatively small ( $\sim 20$  V) and the electric field direction is opposite to that in A-mode. Therefore, the electrons in the plasma are injected into the IL with small energy instead of the positive ion irradiation with high energy. It is also found that the space potential in the case of the IL anode is slightly lower than that of the SUS anode. This result indicates that the secondary electrons are emitted from the IL anode more efficiently than the SUS anode by the injection of the electrons toward the IL, and then, the electron rich condition is realized in the case of the IL anode.

Figure 6 shows axial profiles of the electron density  $n_e$  in (a) A-mode and (b) B-mode for  $P_{gas} = 60$  Pa and  $I_D = 1$  mA, where the cathode is the IL (red circles) and the SUS plate (black diamonds). In both A-mode and B-mode, the electron density is large near the cathode electrode and gradually decreases toward the anode electrode. In the case of B-mode, the electron density in the region above the IL anode is much larger than that in the case of the SUS anode, while the electron densities in the region just below the cathode are almost the same independently of the presence of the IL. This increment of the electron density near the IL anode is considered to be attributed to the secondary electron emission from the IL by the collision of the electrons. In the case of A-mode, it is found that the electron density near the

IL cathode is smaller than that in the case of the SUS cathode. Since the discharge voltage in the case of the IL cathode is smaller than that in the SUS cathode case, the energy of electrons accelerated by the potential difference between the plasma and the cathode is small and the ionization rate also becomes low, resulting in the low density near the cathode region. On the other hand, the electron density near the anode electrode has opposite tendency, i.e., the density in the presence of the IL is larger than that in the absence of the IL. Judging from the result of the axial profiles of the space potential [Fig. 5(a)], the potential gradient is generated around  $z > 40$  mm in the presence of the IL, and therefore, it is considered that the electrons are accelerated by the electric field and cause the additional ionization near the anode.

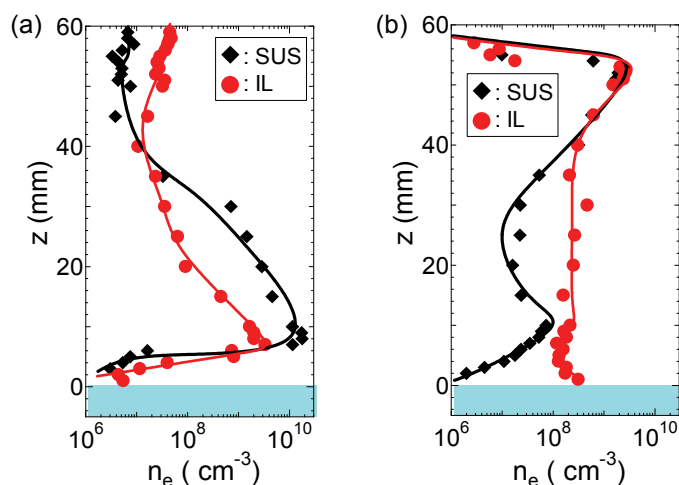


Fig. 6. Axial profiles of the electron density  $n_e$  in (a) A-mode and (b) B-mode.  $P_{Ar} = 40$  Pa,  $I_D = 1$  mA.

Based on these results, it is found that the secondary electrons are emitted from the IL more efficiently than the SUS electrode by the injection of the electrons to the anode electrode as well as the irradiation of the ions to the cathode electrode. Therefore, the IL electrodes are effective for the synthesis of nanomaterials at the interface between the plasma and the IL. These ion irradiation and electron injection to the ionic liquid in A- and B-modes, respectively, are expected to affect the discharge in the gas phase region. Therefore, the discharge voltage  $V_D$  - current  $I_D$  characteristics are measured in both the A- and B-modes, which are presented in Fig. 7, where we change materials of the electrodes in the glass cell, i.e., (a) the cathode electrode in A-mode and (b) the anode electrode in B-mode. When the materials of the cathode electrodes in A-mode are changed between SUS, nickel (Ni), and the ionic liquid ([BMI<sup>+</sup>][BF<sub>4</sub><sup>-</sup>]) [Fig. 7(a)], the discharge current in the case of the ionic liquid is found to be the largest in comparison with those in the cases of Ni and SUS. On the other hand, the change in materials of the anode electrodes in B-mode has no effect on the discharge characteristics as shown in Fig. 7(b). These results suggest that the ionic liquid works as the effective cathode electrode in A-mode and the secondary electrons are emitted from the ionic liquid more efficiently than the SUS and Ni electrodes, because the discharge voltage depends on the amount of the secondary electrons from the cathode electrode in the

case of the usual DC glow discharge. In B-mode, on the other hand, since the material of the cathode electrode is the same as in all cases of changing the anode materials, the discharge voltage-current characteristics do not change in spite of the various kinds of anode electrodes.

The increase in the discharge current in the case of the ionic liquid cathode in A-mode is considered to be attributed to the concentration of the cathode sheath electric field on the ionic liquid surface which is reported to have a string shaped alkyl chain aligned toward the gas-phase region (Sloutskin et al., 2005). The concentration of the electric field causes the efficient ion irradiation to the ionic liquid, resulting in the emission of a large amount of secondary electrons from the ionic liquid surface more than the conventional metal cathodes such as SUS and Ni.

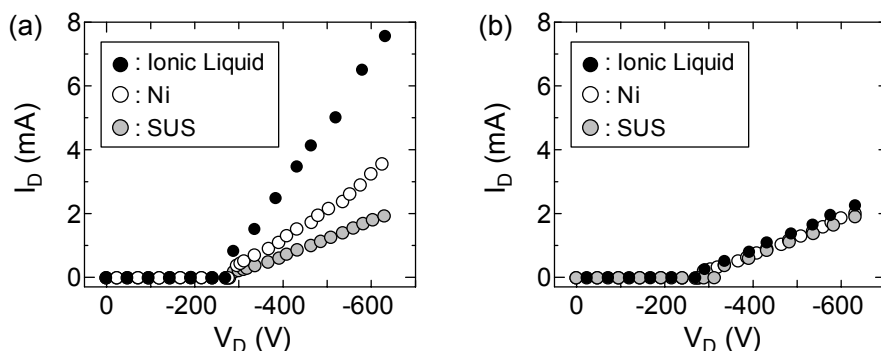


Fig. 7. Dependence of the discharge voltage  $V_D$  - current  $I_D$  characteristics on the materials of (a) the cathode electrode in A-mode and (b) the anode electrode in B-mode.  $P_{\text{gas}} = 40$  Pa. Ionic liquid is  $[\text{BMI}^+][\text{BF}_4^-]$ .

To confirm the effects of the alkyl chain length of the ionic liquid on the discharge, the discharge voltage  $V_D$  - current  $I_D$  characteristics are measured with the types of the ionic liquid changed as shown in Fig. 8. In A-mode, the discharge currents in the cases of  $[\text{HMI}^+][\text{BF}_4^-]$  and  $[\text{EMI}^+][\text{BF}_4^-]$  are the largest and the smallest, respectively. This result shows that the discharge current increases with increasing the length of the alkyl chain in the ionic liquid. These phenomena mean the long alkyl chain contributes to the concentration of the cathode sheath electric field on the ionic liquid surface. The concentration of the electric field causes the efficient ion irradiation to the ionic liquid, resulting in the emission of a larger amount of secondary electrons from the ionic liquid with longer alkyl chain. In B-mode, on the other hand, since the material of the cathode electrode is the same as in all cases of changing the ionic liquids, the discharge voltage- current characteristics do not change in spite of the various kinds of ionic liquids as the anode electrodes.

Figure 9 shows ultraviolet-visible (UV-vis) absorption spectra of the ionic liquid with the ion irradiation energy  $E_i$  as a parameter and the spectrum peak intensity at the wavelength of 297 nm as a function of  $E_i$  in A-mode, where  $I_D = 1$  mA and the plasma irradiation time  $t = 2$  min. The ion irradiation energy  $E_i$  is determined by the potential difference between the plasma and the ionic liquid cathode, which is almost equivalent to the discharge voltage, and control of  $E_i$  with the discharge current  $I_D$  kept constant is realized by changing the argon gas pressure.

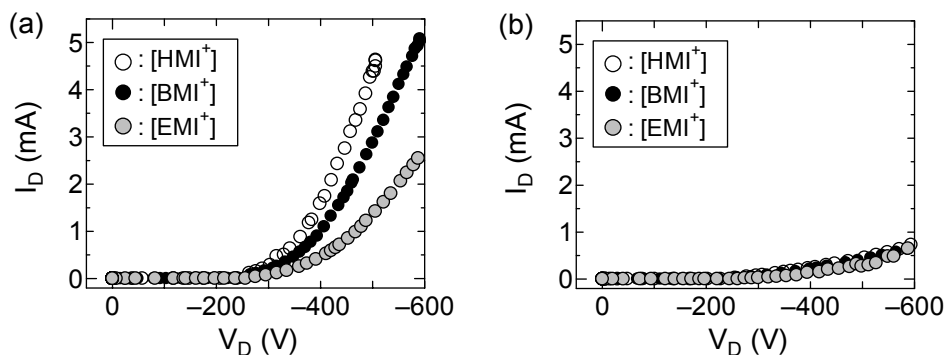


Fig. 8. Dependence of the discharge voltage  $V_D$  - current  $I_D$  characteristics on the types of the ionic liquids as (a) the cathode electrode in A-mode and (b) the anode electrode in B-mode.  $P_{\text{gas}} = 40$  Pa.

The spectrum peak intensity at 297 nm gradually increases with an increase in  $E_i$ , which corresponds to the phenomenon that the color of the ionic liquid gradually changes into thick yellow. Since these phenomena are not observed in B-mode, the increase in the absorption peak intensity is caused by the newly-generated bond due to the dissociation of the ionic liquid, which is enhanced by the increase in the ion irradiation energy. Therefore, the molecule structure of the ionic liquid can be varied by the ion irradiation with high energy in A-mode, in which the positive ions in the gas phase plasma are convincingly accelerated by the sheath electric field formed just above the ionic liquid cathode. We emphasize that this ion irradiation to the ionic liquid has the possibility to realize an effective reaction for the material synthesis at the gas-liquid interface.

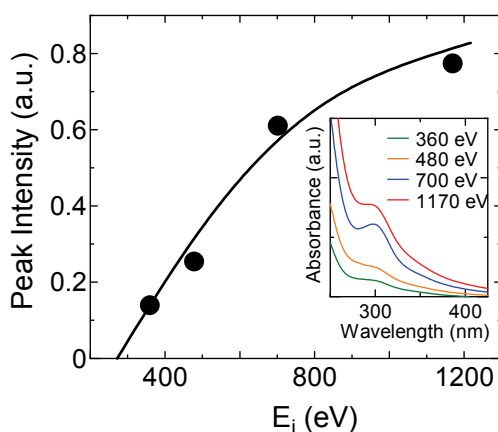


Fig. 9. Peak intensity of UV-Vis absorption spectra of the ionic liquid ( $[\text{BMI}^+][\text{BF}_4^-]$ ) at 297 nm as a function of the ion irradiation energy  $E_i$  in A-mode.  $I_D = 1$  mA,  $t = 2$  min. Inset is the absorption spectra with  $E_i$  as a parameter.

To investigate whether the species in the plasma is changed by the ion irradiation to the IL, optical emission spectra (OES) in the gas plasma region are measured as shown in Fig. 10, where the IL and SUS plate are used as (a) the cathode electrode in A-mode and (b) the anode electrode in B-mode. In A-mode, the spectrum peak at 390 nm, which corresponds to methylidyne radical (CH), is observed only in the presence of the IL [Fig. 10(a)]. In B-mode, on the other hand, the CH peak is not clear both in the presence and absence of the IL.

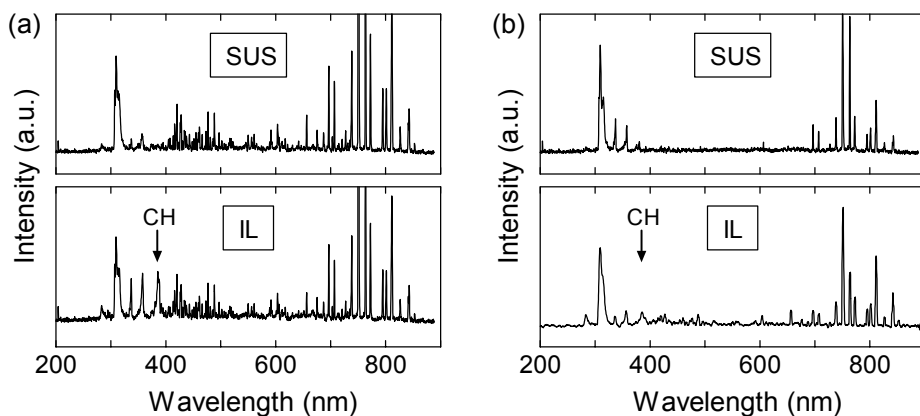


Fig. 10. Optical emission spectra in the gas plasma region in (a) A-mode and (b) B-mode, where the cathode electrode is the IL (bottom figures) and the SUS plate (upper figures).  $P_{\text{gas}} = 60 \text{ Pa}$ ,  $I_D = 2 \text{ mA}$ .

These phenomena can be explained by a process that the plasma ion irradiation with high energy causes the dissociation of the alkyl-chain of the IL and the dissociated CH is transported to the gas plasma region from the IL region. In these OES spectra, we can find the OH (308 nm) peak in both the cases of A-mode and B-mode. This peak comes from the tiny amount of water included in the IL as an impurity, which is evaporated and dissociated in the gas plasma region not only in A-mode but also in B-mode. This phenomenon is one of the evidence that the CH peak observed only in A-mode is caused by the high-energy ion irradiation to the IL.

### 3.2 Synthesis of nanoparticles

Using this ion irradiation, gold (Au) nanoparticles are synthesized in the ionic liquid by the reduction of Au chloride such as  $\text{HAuCl}_4 \cdot 3\text{H}_2\text{O}$ . Figure 11 gives transmission electron microscopy (TEM) images of the Au nanoparticles synthesized in (a) A-mode and (b) B-mode for  $P_{\text{Ar}} = 60 \text{ Pa}$ ,  $I_D = 1 \text{ mA}$ , and  $t = 40 \text{ min}$ . In both the cases, Au nanoparticles can be formed, however, it is found that, in A-mode, the diameter of the nanoparticle is averagely smaller and the particle number is larger than that in B-mode.

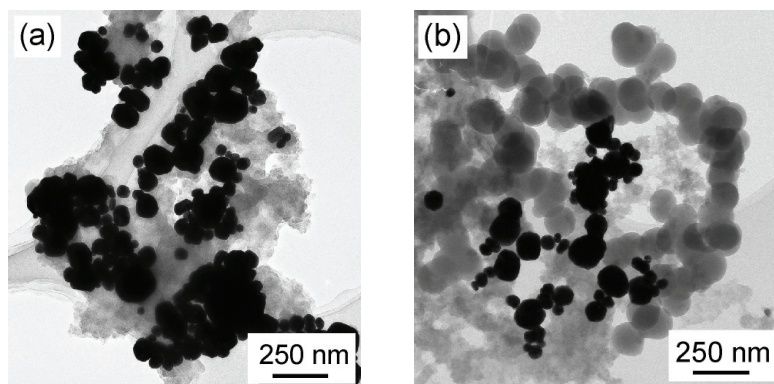


Fig. 11. TEM images of the Au nanoparticles synthesized in (a) A-mode and (b) B-mode.  $P_{Ar} = 60$  Pa,  $I_D = 1$  mA,  $t = 40$  min.

The reduction reaction of the Au ions is caused by the electrons injected from the plasma in B-mode, while the reduction is considered to be caused by hydrogen radical  $H^*$  in A-mode, which is generated by the dissociation of the ionic liquid. In our system, the Au nanoparticles are synthesized by firstly nucleation of the Au atoms after reduction of the Au chlorides and secondly growth of the nucleus due to attachment of the Au atoms. The density of the nucleus in A-mode is expected to be larger than that in B-mode, because the hydrogen radical effectively reduces the Au chlorides compared with the electron. Therefore, it is considered that the number of Au atoms attached to one nucleus in the growth phase in A-mode is smaller than that in B-mode, resulting in the averagely small diameter and large density of the Au nanoparticles in A-mode.

Since nanoparticles with diameter less than 100 nm are known to cause localized surface plasmon resonance, visible absorption spectra are obtained for a quantitative observation of the Au nanoparticle concentration. Figure 12(a) shows visible absorption spectra of the nanoparticles produced by the Ar plasmas in A-mode with  $E_i$  as a parameter. An absorption peak appears around 540 nm, corresponding to Au nanoparticle plasmon resonance and the absorption peak is obviously enhanced with an increase in  $E_i$ .

The spatially averaged number density  $N_p$  of the synthesized Au nanoparticles, which is counted from the TEM images is presented in Fig. 12(b) as a function of the ion irradiation energy  $E_i$ . It is found that  $N_p$  monotonically increases with an increase in  $E_i$ . The Ar ion can penetrate into the ionic liquid more deeply with an increase in the irradiation energy, resulting in enhancement of the generation of the hydrogen radicals. These increased hydrogen radicals affect the reduction of Au ions. The synthesis efficiency of the Au nanoparticles can be controlled by the irradiation energy of inert gas ions such as Ar.

Finally, we try to control the size of and distance between nanoparticles using the gas-liquid interfacial plasmas. In the beginning, the Au nanoparticles are synthesized using a deferent kind of ionic liquid (1-Butyl-3-methyl-imidazolium chloride,  $[BMI(C_8H_{15}N_2)^+][Cl^-]$ ), which has lager viscosity compared with conventional  $[BMI^+][BF_4^-]$ . Figure 13(a) shows a TEM image of the synthesized Au nanoparticles, the diameter distribution of which is measured

and plotted in Figs. 13(b) and 13(c). The Au nanoparticles with diameter in the range of 3-7 nm are observed to be formed, which are much smaller than those in the case of conventional ionic liquid  $[\text{BMI}^+][\text{BF}_4^-]$ . Since the viscosity of  $[\text{BMI}^+][\text{Cl}^-]$  is larger than that of  $[\text{BMI}^+][\text{BF}_4^-]$ , growth and aggregation of the Au nanoparticles are suppressed by the ionic liquid with high viscosity, resulting in the formation of the small and relatively mono-dispersed nanoparticles.

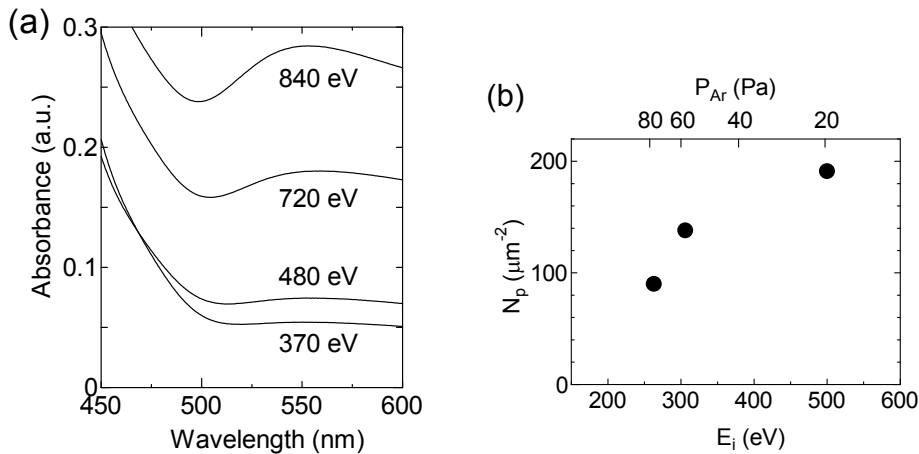


Fig. 12. (a) UV-vis absorption spectra of the Au nanoparticles produced by Ar plasmas as a function of ion irradiation energy  $E_i$  in A-mode.  $I_D = 1$  mA,  $t = 7$  min. (b) Spatially averaged number density  $N_p$  of the synthesized Au nanoparticles as a function of ion irradiation energy  $E_i$  in A-mode.  $I_D = 1$  mA,  $t = 40$  min.

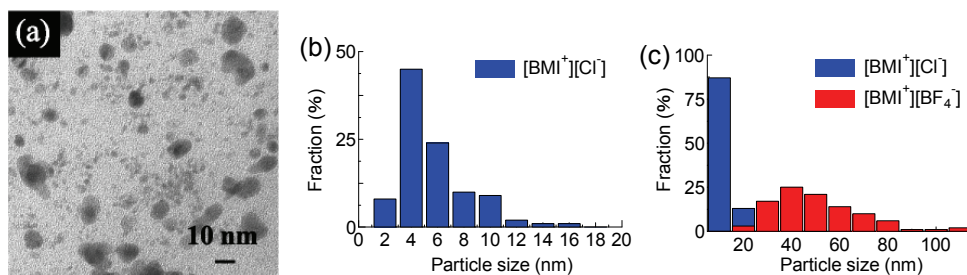


Fig. 13. (a) TEM images of the Au nanoparticles synthesized using the ionic liquid  $[\text{BMI}^+][\text{Cl}^-]$ .  $P_{\text{Ar}} = 60$  Pa,  $I_D = 1$  mA,  $t = 15$  min. (b) Particle size distribution of the Au nanoparticles synthesized in the ionic liquid  $[\text{BMI}^+][\text{Cl}^-]$  estimated by TEM image in Fig. 13(a). (c) Comparison of the particle size distributions between the cases of  $[\text{BMI}^+][\text{Cl}^-]$  and  $[\text{BMI}^+][\text{BF}_4^-]$ .



To control the size of nanoparticles, we attempt to make highly-ordered Au and palladium (Pd) nanoparticles using the single-walled carbon nanotubes (SWNTs) as a template. The bundled SWNTs are impregnated with the Au or Pd chloride dissolved in the ionic liquid, and are exposed to the plasma. As a result, the Au or Pd chloride is reduced inside the bundles of the SWNTs by the plasma irradiation and the Au or Pd nanoparticles are synthesized. Since the SWNTs inhibit the agglomeration of the nanoparticles due to their small inside space, the uniform nanoparticles are expected to be synthesized. Figure 14 presents the TEM image of (a) Au and (c) Pd nanoparticles synthesized between the SWNTs in the ionic liquid for  $P_{Ar} = 60$  Pa,  $I_D = 1$  mA, and  $t = 15$  min, and (b) particle size distribution of Au nanoparticles onto the SWNTs estimated by TEM image in Fig. 14(a). It is found that highly-ordered, high-density, mono-dispersed, and small-seized ( $\sim 2$  nm) metal nanoparticles are synthesized by controlling the gas-liquid interfacial plasmas.

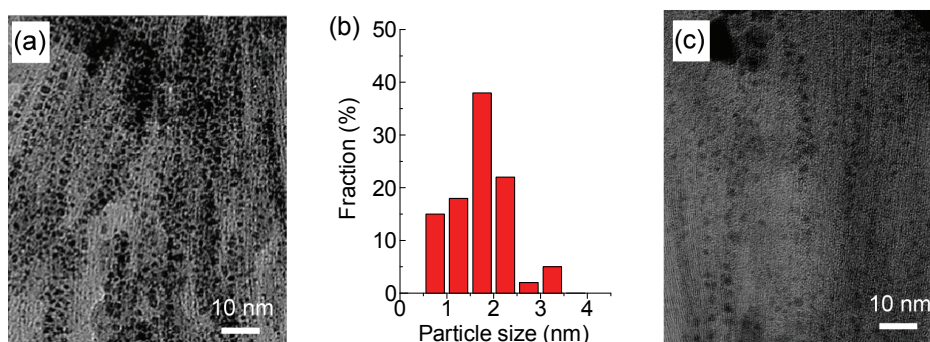


Fig. 14. TEM images of (a) Au and (c) Pd nanoparticles synthesized using the SWNTs as a template.  $P_{Ar} = 60$  Pa,  $I_D = 1$  mA,  $t = 15$  min. (b) Particle size distribution of Au nanoparticles onto the SWNTs estimated by TEM image in Fig. 14(a).

To synthesize distance-controlled nanoparticles, we attempt to make the Au nanoparticles using the functionalized single-walled carbon nanotubes (f-SWNTs) controlled by the irradiation of the gas-liquid interfacial discharge plasma. The SWNTs are dispersed in a new kind of ionic liquid (2-Hydroxyethylammonium formate) which consists of carboxyl groups, and the plasma is irradiated to the IL. The plasma ions or electrons can dissociate the IL and the dissociated carboxyl groups bond to the surface of the SWNTs. This functionalization of the SWNTs using the gas-liquid interfacial plasmas is very easy, fast, and controllable. When chlorauric acid trihydrate ( $\text{HAuCl}_4 \cdot 3\text{H}_2\text{O}$ ) is dissolved in the IL with the functionalized SWNTs, the Au chloride is reduced by the IL and the Au nanoparticles are selectively synthesized on the carboxyl groups bonding to the SWNTs. Since the density of the carboxyl groups on the SWNTs can be controlled by the plasma irradiation parameter, such as irradiation energy, flux, time, and so on, the density of the Au nanoparticles can also be controlled.

Figure 15 presents transmission electron microscope (TEM) images of the Au nanoparticles synthesized on the f-SWNTs, which have been treated in the IL for plasma irradiation time (b)  $t = 1$  min and (c)  $t = 10$  min,  $P_{Ar} = 60$  Pa, and  $I_D = 1$  mA. Here the TEM image of the f-SWNTs which are not previously treated by the plasma irradiation is also present as a reference in Fig. 15(a). It is found that the high density and mono-dispersed Au nanoparticles are synthesized on the f-SWNTs when the SWNTs are previously treated by the plasma irradiation, while only a few Au nanoparticles are observed on the f-SWNTs in the absence of the plasma irradiation. In addition, the distance between the Au nanoparticles becomes small with an increase in the plasma irradiation time. This result means that the distance between the Au nanoparticles can be controlled by functionalization of the SWNTs using the plasma irradiation in the ionic liquid.

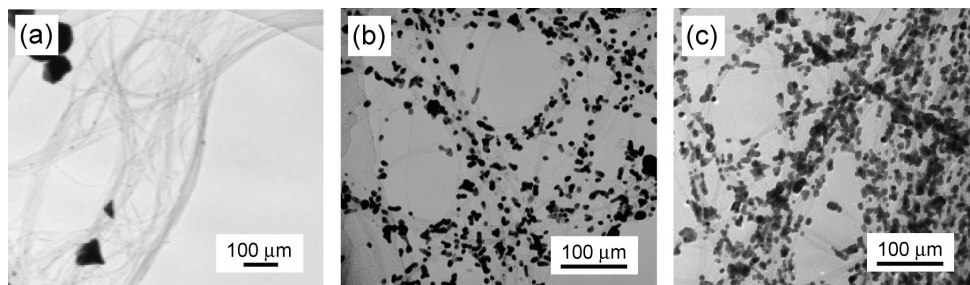


Fig. 15. TEM images of Au nanoparticles synthesized using the functionalized SWNTs, which are treated by the plasma irradiation in the ionic liquid for (a) 0 min, (b) 1 min, and (c) 10 min.  $P_{Ar} = 60$  Pa,  $I_D = 1$  mA.

#### 4. Conclusion

A direct current (DC) discharge plasma has been generated just above the ionic liquid by applying the DC voltage to the ionic liquid as the cathode electrode against a grounded anode electrode set in the gas phase region. On the other hand, the DC discharge plasma between the ionic liquid anode electrode and the negatively biased SUS cathode electrode in the gas phase region is also stably generated.

Using these gas-liquid interfacial plasmas, the precise potential and density structures and the resultant plasma ion and electron irradiations to the ionic liquid are revealed. In addition, it is found that the secondary electrons are efficiently emitted from the ionic liquid electrode by the irradiation of the electrons as well as the high energy ions, and the effects of the secondary electrons on the discharge are clarified. The alkyl chain of the ionic liquid is revealed to play an important role in the secondary electron emission in terms of the concentration of the sheath electric field on the ionic liquid surface.

This ion irradiation is found to be effective for the synthesis of metal nanoparticles in comparison with the conventional electron irradiation system, and has the possibility of application to the synthesis of the various kinds of size- and yield-controlled nanoparticles.

Furthermore, using the plasma irradiation method with single-walled carbon nanotubes as a template, the high density, mono-dispersed, and highly-ordered metal nanoparticles are synthesized by controlling the gas-liquid interfacial plasmas.

The results lead to creating innovative conjugates of carbon nanotubes and nanoparticles, which are expected to be applicable to nanoelectronics and biomedical nanotechnology.

The authors thank Prof. K. Tohji, K. Motomiya, T. Miyazaki, and H. Ishida for their technical assistance. We express our gratitude to Dr. K. Baba, Dr. Q. Chen, and T. Harada, for their collaboration.

## 5. References

- Baba, K.; Kaneko, T. & Hatakeyama, R. (2007). *Appl. Phys. Lett.*, Vol. 90, pp. 201501-1-3, 2007.
- Baba, K.; Kaneko, T. & Hatakeyama, R. (2009). *Appl. Phys. Express*, Vol. 2, pp. 035006-1-3, 2009.
- Baba K.; Kaneko T.; Hatakeyama R.; Motomiya K. & Tohji K. (2010). *Chem. Commun.* Vol. 46, pp. 255-257, 2010.
- Bruggeman P. & Leys, C. (2009). *J. Phys. D: Appl. Phys.*, Vol. 42, pp. 053001-1-28, 2009.
- Georgakilas V.; Gournis D.; Tzitzios V.; Pasquato L.; Guldie D. M. & Prato M. (2007). *J. Mater. Chem.* Vol. 17, pp. 2679-2694, 2007.
- Han L.; Wu W.; Kirk F. L.; Luo J.; Maye M. M.; Kariuki N. N.; Lin Y.; Wang C. & Zhong C.-J. (2004). *Langmuir* Vol. 20, pp. 6019-6025, 2004.
- Hieda, J.; Saito, N. & Takai, O. (2008). *J. Vac. Sci. Technol. A*, Vol. 26, pp. 854-856, 2008.
- Jeong, G-H.; Hatakeyama, R.; Hirata, T.; Tohji, K.; Motomiya, K.; Yaguchi, T. & Kawazoe, Y. (2003). *Chem. Commun.*, pp.152-153, 2003.
- Kaneko, T.; Baba, K. & Hatakeyama, R. (2009a). *J. Appl. Phys.*, Vol. 105, pp. 103306-1-5, 2009.
- Kaneko, T.; Baba, K.; Harada, T. & Hatakeyama, R. (2009b). *Plasma Proc. Polym.*, Vol. 6, pp. 713-718, 2009.
- Kim, H.; Kim, B.; Kim, J.; Lee, J. & Park, N. (2005). *Appl. Phys. Lett.*, Vol. 91, pp. 153113-1-3, 2007.
- Kong, J.; Franklin, N. R.; Zhou, C.; Chapline, M. G.; Peng, S.; Cho, K. & Dai, H. (2000). *Science*, Vol. 287, pp. 622-625, 2000.
- Koo I. G.; Lee M. S.; Shim J. H.; Ahn J. H. & Lee W. M. (2005). *J. Mater. Chem.* Vol. 15, pp. 4125-4128, 2005.
- Meiss, S. A.; Rohnke, M.; Kienle, L.; Zein El Abedin, S.; Endres, F. & Janek, J. (2007). *ChemPhysChem*, Vol. 8, pp. 50-53, 2007.
- Nishihata, Y.; Mizuki, J.; Akao, T.; Tanaka, H.; Uenishi, M.; Kimura, M.; Okamoto, T. & Hamada, N. (2002). *Nature*, Vol. 418, pp. 164-167, 2002.
- Rogers R. D. & Seddon K. R. (2003). *Science* Vol. 302, pp. 792-793, 2003.
- Seddon, K. R. (2003). *Nature Mater.*, Vol. 2, pp. 363-365, 2003.
- Sloutskin, E.; Ocko, B.M.; Tamam, L.; Kuzmenko, I.; Gog, T. & Deutsch, M. (2005). *J. Am. Chem. Soc.*, Vol. 127, pp. 7796-7804, 2005.
- Torimoto T.; Okazaki K.; Kiyama T.; Hirahara K.; Tanaka N. & Kuwabata S. (2006). *Appl. Phys. Lett.* Vol. 89, pp. 243117-1-3, 2006.
- Wildgoose, G. G.; Banks, C. E. & Compton, R. G. (2005). *Small*, Vol. 2, pp. 182-193, 2005.
- Xie Y. B. & Liu C. J. (2008). *Plasma Process. Polym.* Vol. 5, pp. 239-245, 2008.

Ye, X.; Lin, Y.; Wang, C.; Engelhard, M. H.; Wang, Y. & Wai, C. M. (2004). *J. Mater. Chem.*, Vol. 14, pp. 908-913, 2004.

# Nanoparticle Preparation in Room-Temperature Ionic Liquid under Vacuum Condition

Tetsuya Tsuda<sup>1,4</sup>, Akihito Imanishi<sup>2,5</sup>,  
Tsukasa Torimoto<sup>3,5</sup> and Susumu Kuwabata<sup>4,5</sup>

<sup>1</sup>*Frontier Research Base for Global Young Researchers, Graduate School of Engineering  
Osaka University*

*2-1 Yamada-oka, Suita, Osaka 565-0871,*

<sup>2</sup>*Department of Chemistry, Graduate School of Engineering Science, Osaka University  
1-3 Machikaneyama, Toyonaka, Osaka 560-8531,*

<sup>3</sup>*Department of Crystalline Materials Sciences, Graduate School of Engineering  
Nagoya University*

*Furo-cho, Nagoya, Aichi 464-8603,*

<sup>4</sup>*Department of Applied Chemistry, Graduate School of Engineering Osaka University  
2-1 Yamada-oka, Suita, Osaka 565-0871,*

<sup>5</sup>*CREST, Japan Science and Technology Agency  
Kawaguchi, Saitama 332-0012,  
Japan*

## 1. Introduction

Room-temperature ionic liquid (RTIL), which was formerly called room-temperature molten salt (RTMS) and ambient-temperature molten salt (ATMS), is just a salt but a liquid salt at room temperature. Once RTIL studies were limited because at that time the “classic” RTIL, which is composed of an anhydrous metal halide combined with a heterocyclic aromatic halide, e.g.,  $\text{AlCl}_3$ -1-ethyl-3-methylimidazolium chloride ( $[\text{EtMeIm}]\text{Cl}$ ) and  $\text{AlCl}_3$ -1-(1-butyl)pyridinium chloride ( $[\text{BuPy}]\text{Cl}$ ), was recognized as a highly moisture sensitive solvent, especially at higher Lewis acidity; that is, the RTIL must be handled in a glove box ( $\text{O}_2$ ,  $\text{H}_2\text{O}$  < 1 ppm) although it exhibits relatively low viscosity and high conductivity (Wilkes et al., 1982; Hussey & Stafford, 2001; Tsuda et al., 2007.). However, discovery of moisture-stable RTILs in 1992 took their science and technology to another level (Wilkes & Zaworotko, 1992; Cooper & O’Sullivan, 1992). Current RTIL studies in most cases use “modern” RTILs having fluoroanions such as  $[\text{BF}_4]^-$ ,  $[\text{PF}_6]^-$ ,  $[(\text{CF}_3\text{SO}_2)_2\text{N}]^-$  (=  $[\text{Tf}_2\text{N}]^-$ ),  $[\text{CF}_3\text{SO}_3]^-$  (=  $[\text{TfO}]^-$ ) and other water-stable anions including  $[\text{CH}_3\text{CO}_2]^-$ ,  $[\text{N}(\text{CN})_2]^-$  etc. Now RTIL’s anomalous physicochemical properties became known in all the scientific fields and a great number of applications have been proposed so far. Especially, the application to nanoparticle preparation is one of the hot topics in the RTIL studies, since RTIL can stabilize the nanoparticles yielded in the RTIL without any stabilizing agents. In fact, the number of articles on the nanoparticle synthesis in RTIL, which is often called ionic liquid (IL), has

been steadily growing since 2001. Today the nanoparticle-related article accounts for more than 10 % of all the RTIL-related articles (Figure 1). If you need general information on the nanoparticle synthesis in RTIL, we strongly recommend that you read recent review articles (Dupont & Scholten, 2010; Torimoto et al., 2010).

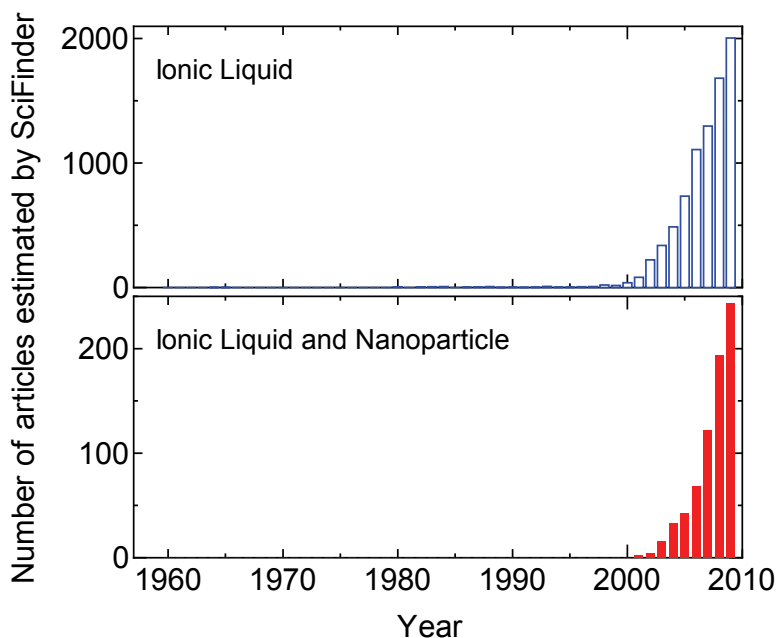


Fig. 1. Number of published articles as a function of year estimated from in-line searches using SciFinder. (top) "Ionic Liquid" and (bottom) "Ionic Liquid and Nanoparticle" were used as keywords.

The negligible vapor pressure of most RTILs at room-temperature invented a new technological concept. Only recently RTILs were beginning to be applied to vacuum technology. This must be a revolutionary incident in science history because people never would have imagined wet world in vacuum. There are many manufacturing machines and analytical instruments that require vacuum condition. Of course, they are designed under the premise that materials treated in them are dry and solid. Conventional procedures cannot be applied to a wet sample, although we occasionally get carried away with our desire to deal with it in these vacuum equipments. On the other hand, RTILs can be put in the vacuum equipments without particular care (Kuwabata et al., 2010). At this point, the numbers of researchers who exploit RTIL in vacuum equipment are quite limited. Several research groups including us have succeeded in metal nanoparticle preparation by using both RTIL and the vacuum technologies, e.g., physical vapor deposition (PVD) method (Richter et al., 2010; Prondzinski et al., 2010) and plasma deposition method (Meiss et al., 2007; Abedin et al., 2007; Baba et al., 2009; Kaneko et al., 2009; Brettholle et al., 2010).

In this chapter, we introduce our created nanoparticle preparation methods in RTIL under vacuum condition including electron beam (Imanishi et al., 2009; Tsuda et al., 2009a; Tsuda

et al., 2010a) and  $\gamma$ -ray radiation method (Tsuda et al., 2009a), magnetron sputtering onto IL (Hatakeyama et al., 2009; Hatakeyama et al., 2010; Kameyama et al., 2010; Khatri et al., 2008; Okazaki et al., 2008; Okazaki et al., 2009; Shishino et al., in press; Suzuki et al., 2009; Suzuki et al., in press; Torimoto et al., 2006; Tsuda et al., 2009; Tsuda et al., 2010b; Wender et al., 2010). The contents also include electrochemical applications of Pt nanoparticles produced by the methods established in our group.

## 2. Preparation of Room-Temperature Ionic Liquid

To prepare high-purity RTIL is quite important if RTIL is employed in the vacuum equipments because the impurities in RTIL often cause unexpected troubles and reactions (Tsuda & Hussey, 2009). Several procedures are proposed to prepare high-purity RTIL so far (Wasserscheid & Welton (eds.), 2003). For your information and guidance, here we indicate our RTIL preparation methods for nanoparticle synthesis experiments.

### 2.1 Hydrophobic RTIL

Liquid salts with bis((trifluoromethyl)sulfonyl)amide ([Tf<sub>2</sub>N]) anions, such as 1-ethyl-3-methylimidazolium bis((trifluoromethyl)sulfonyl)amide, [EtMeIm][Tf<sub>2</sub>N], and tri-*n*-butylmethylammonium bis((trifluoromethyl)sulfonyl)imide, [Bu<sub>3</sub>MeN][Tf<sub>2</sub>N], show very hydrophobic nature. This feature broadened the field of application in RTIL, e.g., lubricant (Torimoto et al., 2010) and chemical extraction (Koel (ed.), 2009). The hydrophobic RTIL is prepared by mixing exactly equal molar amounts of organic salt and Li[Tf<sub>2</sub>N] in ultrapure water. The former organic salt should be purified by an appropriate method before the preparation. This solution is agitated at room temperature for 24 hours, and the resulting hydrophobic RTIL is extracted with pure dichloromethane. This solution is washed with several portions of purified water until the wash water contains no chloride as determined by the addition of a drop or two of a dilute solution of silver nitrate. If necessary, the chloride content can also be evaluated with ion chromatography. Finally, the dichloromethane is removed by evacuating the solution at  $1 \times 10^{-3}$  Torr for 24 h while it is heated to 373 K. The resulting RTIL is usually colorless and very dry (H<sub>2</sub>O < 3 ppm) if the original organic salt is high purity. All hydrophobic RTILs can be prepared by using this same basic method. We know alumina and charcole columns work well for the purification but we do not use these columns since the usage would give very small nanoparticle contaminants. We recommend you do not use the column when you yield nanoparticles in the RTIL.

### 2.2 Hydrophilic RTIL

Although "classic" chloroaluminate RTIL that dangerously reacts with water especially at higher Lewis acidity is also one of hydrophilic RTILs, the preparation method is omitted here because we introduced the method in great detail in a previous literature (Tsuda et al., 2007). Common hydrophilic RTILs usually show low viscosity and high ionic conductivity compared to the hydrophobic one; that is, you should select hydrophilic RTIL for doing electrochemistry due to the electrochemical favorable properties if you do not have any reason that you use hydrophobic RTIL. The issue related to hydrophilic RTIL is the difficulty for preparation of high-purity hydrophilic RTIL more than hydrophobic one. We know there are many preparation methods for the hydrophilic RTIL. In our laboratory, the

hydrophilic RTIL synthesis is carried out as a suspension in dry dichloromethane (DCM) while the starting materials, e.g., [EtMeIm]Cl and LiBF<sub>4</sub>, are not fully soluble in the DCM. This solution is agitated at 300 K for 24 hours, and the halide byproducts, mainly metal halide, are removed by filtration. The resulting DCM solution containing the RTIL is washed with a little ultrapure water several times to reduce halide content in the final product. Of course, using a large volume of water in the washing process directly leads to low yield of the final product since hydrophilic RTIL easily dissolve in the water phase. Finally, the DCM is removed by evacuating the solution at  $1 \times 10^{-3}$  Torr for 24 h while it is heated to 373 K.

### 3. Nanoparticle preparation in RTILs under vacuum condition

We believe that nanoparticle preparation in RTIL will contribute to development of future technology because those nanoparticles are not covered with any covalently-adsorbed stabilizing agents that often adversely affect the physicochemical properties of the nanoparticles. The stabilization mechanism is not entirely clear but it would not be an exaggeration to say that RTIL has relatively-strong interaction with the surface of the metal nanoparticles. The nanoparticles have already been prepared in RTIL using various reaction modes. Those preparation methods and characteristics of the prepared nanoparticles were painstakingly reviewed by Dupont and Scholten (Dupont & Scholten, 2010). In cases of nanoparticle preparations by chemical reduction of metal ions or metal complexes, stabilizing agent is not required in RTIL but several kinds of byproducts must be dissolved in the resulting nanoparticle-suspended RTILs. Nanoparticle preparations in RTIL under vacuum condition, which are introduced here, are groundbreaking techniques that enable synthesis of target nanoparticles without significant amount of byproduct. In this section, we present our created nanoparticle preparation method called RTIL-magnetron sputtering method.

#### 3.1 Magnetron sputtering onto RTIL

This procedure called RTIL-magnetron sputtering method was established by our research group (Torimoto et al., 2006). Figure 2 depicts photographs of nonvolatile fluid materials after gold sputter deposition using a common magnetron sputtering equipment. Silicone-based materials (left and center) were completely covered with a gold thin film, like gold sputtering onto a solid substrate, but RTIL (right) is definitely not the case. The color of the RTIL altered from colorless to wine-colored solution after the treatment. In fact, this interesting phenomenon is caused by surface plasmon absorption of the gold nanoparticles that exist in the RTIL. In principle, all elements that can be ejected by Ar<sup>+</sup> and N<sub>2</sub><sup>+</sup> plasma bombardment are nanoparticulated by this method. Figure 3 shows a schematic illustration of this method that uses a common magnetron sputtering apparatus except for the use of RTIL as a substrate. This method has achieved the preparation of various pure metal nanoparticles, such as Au (Hatakeyama et al., 2009; Hatakeyama et al., 2010; Kameyama et al., 2010; Khatri, et al., 2008; Okazaki et al., 2009; Shishino et al., in press; Torimoto et al., 2006; Wender et al., 2010), Ag (Okazaki et al., 2008; Suzuki et al., 2009), Pt (Tsuda et al., 2009b; Tsuda et al., 2010b), In (Suzuki et al., in press) etc., possessing particle sizes less than 10 nm in diameter without any specific stabilizing agent. Small-angle X-ray scattering study revealed initial formation mechanism of the gold nanoparticles during the sputtering process onto several 1,3-dialkylimidazolium tetrafluoroborate (Hatakeyama et al., 2009). The proposed formation mechanism that is



divided into two phases, as shown in Figure 3, concluded that both surface tension and viscosity of the RTIL are important factors for the Au nanoparticle growth and its stabilization.

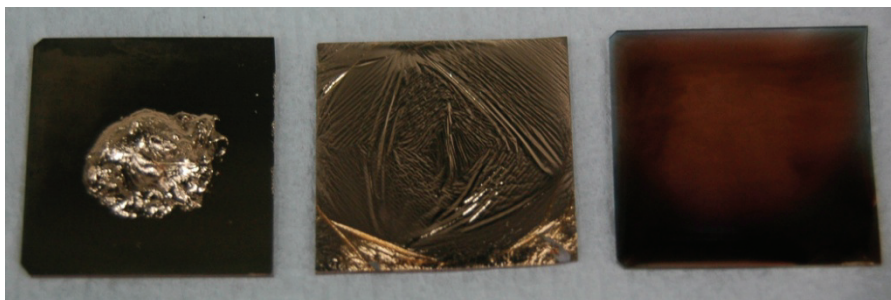


Fig. 2. Photographs of nonvolatile fluid materials placed on glass plates after gold sputter deposition using a common magnetron sputtering equipment. (left) silicone grease (center) silicone oil (right)  $[\text{Me}_3\text{PrN}][\text{Tf}_2\text{N}]$ . The sputtering time was 300 sec.

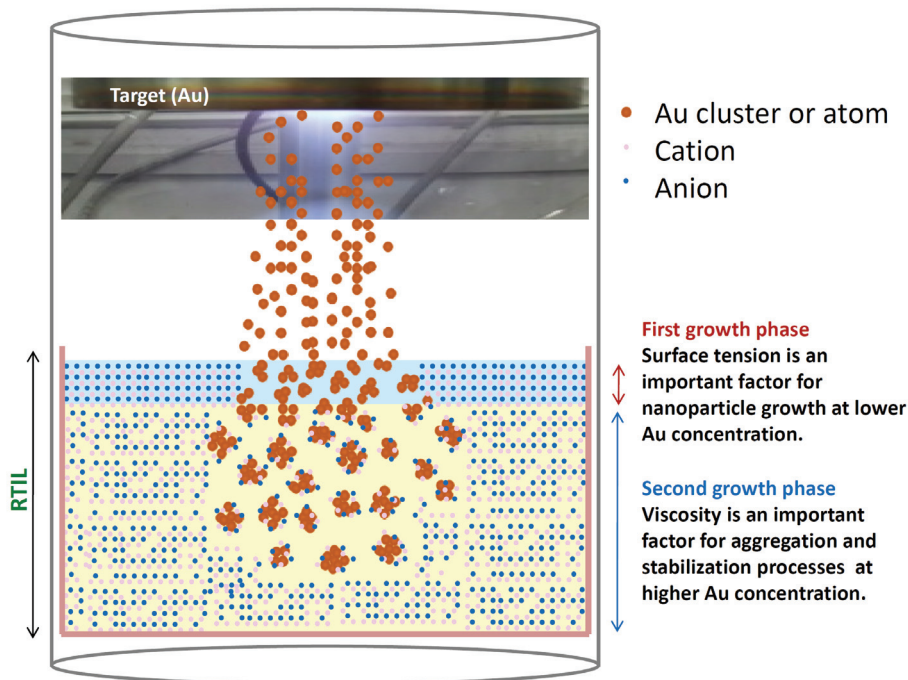


Fig. 3. Schematic illustration of Au nanoparticle formation mechanism during Au sputtering onto RTIL.

Figure 4 shows TEM images of Pt nanoparticles prepared by the RTIL-sputtering method under  $\text{N}_2$  or Ar atmosphere. In both cases, Pt nanoparticles dispersing in the  $[\text{Me}_3\text{PrN}][\text{Tf}_2\text{N}]$  were synthesized by the RTIL-sputtering method. Although any lattice fringe was not recognized in the particles, EDX, XRF, and ICP-OES analyses identified the observed

particles as Pt particles in the  $[\text{Me}_3\text{PrN}][\text{Tf}_2\text{N}]$ . The mean particle size strongly depended on gaseous species; the Pt particles prepared in Ar and  $\text{N}_2$  possessed the mean diameter of 2.2 nm (Standard Deviation (SD): 0.36) and 3.3 nm (SD: 0.60), respectively. It is likely that bombardment of  $\text{N}_2^+$  ions ejects larger Pt clusters than the case of  $\text{Ar}^+$  ions although the details are unknown at this moment. These Pt nanoparticles were stable without aggregation more than 6 weeks at room temperature while a stabilizing agent was never added to the RTIL. This simple process can reproducibly yield Pt nanoparticles. Figure 5 depicts TEM images of Pt nanoparticles obtained by the Pt sputtering onto  $[\text{Me}_3\text{PrN}][\text{Tf}_2\text{N}]$

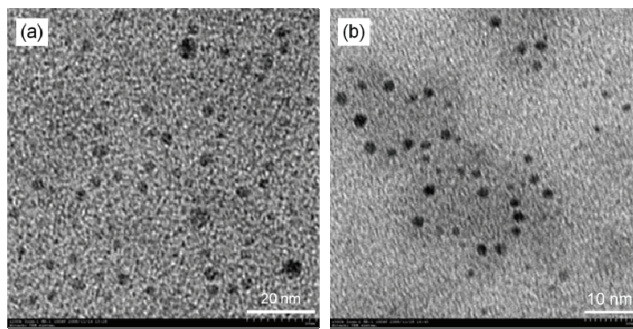


Fig. 4. TEM images of Pt nanoparticles synthesized by the RTIL-sputtering method under (a)  $\text{N}_2$  and (b) Ar atmosphere. The sputtering time and current were 300 sec and 40 mA, respectively. The RTIL was  $[\text{Me}_3\text{PrN}][\text{Tf}_2\text{N}]$ .

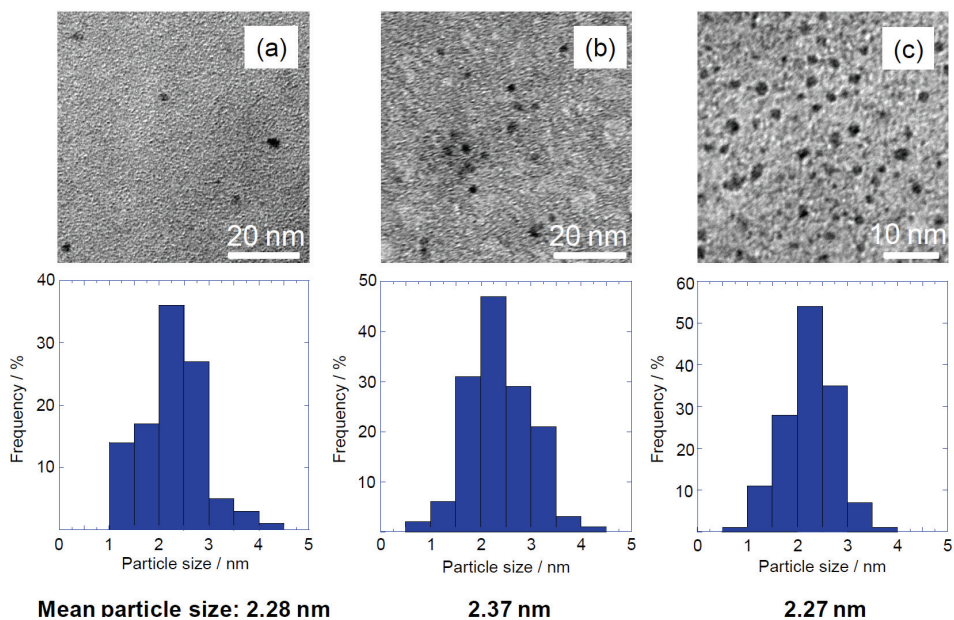


Fig. 5. TEM images and their size distribution diagrams at different sputtering time. (a) 300 sec; (b) 900 sec; (c) 1800 sec. The induced gas was Ar.

at different sputtering times and their size distribution diagrams constructed from the TEM images. The induced gas was Ar. All the Pt nanoparticles have mean particle size of ca. 2.3 ~ 2.4 nm, and the particle size was of little relevance to the sputtering time. But the Pt concentration in the sputtered RTILs linearly increased with increasing the sputtering time, suggesting that the number of Pt nanoparticles show a linear increase with the sputtering time. What is special about the Pt nanoparticles produced by the use of this method is that there is little change in the particle size even if the Pt-dispersed RTIL is heated to 373 K, but the size becomes slightly large after heat treatment exceeding 423 K. The mean particle size (ca.  $3.7 \pm 0.1$  nm) is substantially constant value independently of the heat temperature if the heat temperature is 423 ~ 573 K. 573 K was chosen as the maximum heat temperature to avoid pyrolysis of the RTIL.

Interestingly, this technique also enables to produce alloy nanoparticles by placing different elements as a target. Figure 6 shows the first attempt to prepare Au-Ag alloy nanoparticles

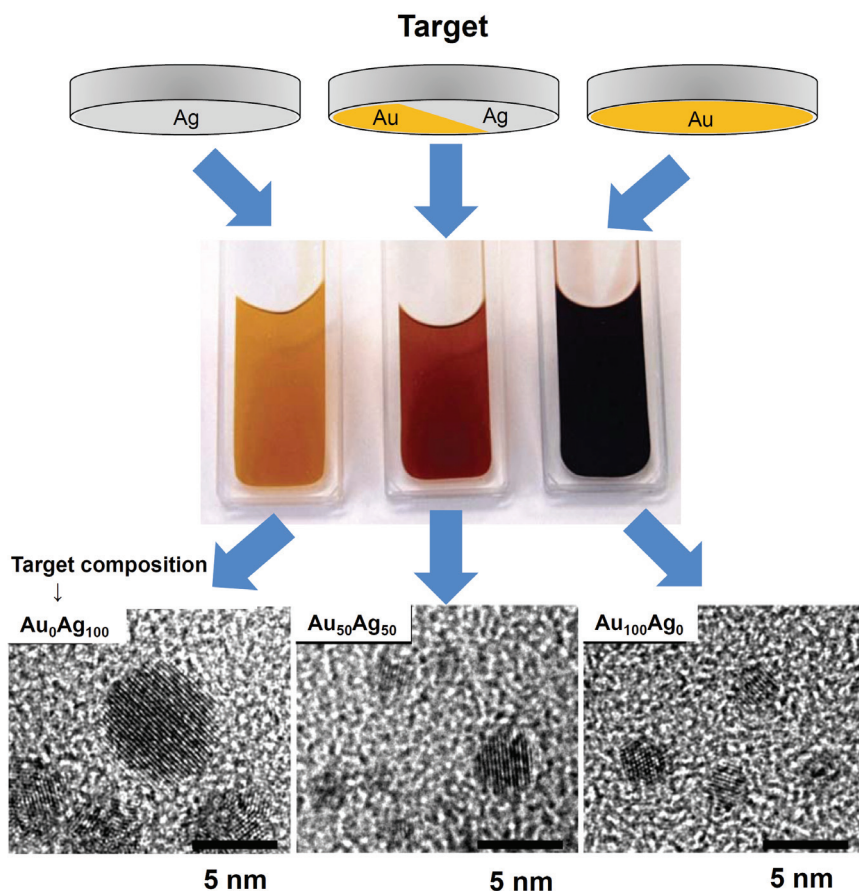


Fig. 6. Photographs of  $[\text{BuMeIm}][\text{PF}_6]$  after sputtering experiments at Au-Ag targets having different surface area ratio and TEM images of the resulting nanoparticles obtained at each Au-Ag targets.

by the sputtering method with a target having Au and Ag plates of the same area (Okazaki et al., 2008). Color of the  $[\text{BuMeIm}][\text{PF}_6]$  altered with the target composition. As recognized from TEM images, the mean particle size enlarges with an increase in the Ag area in the target. In addition to this, the chemical composition and the optical properties of the deposited alloy nanoparticles varied with the surface area ratio of Au to Ag, too. This approach will be a novel alloy nanoparticle fabrication method because of the simple process that can directly control the alloy composition by changing the ratio of the metal areas in the target.

### 3.2 Future difficulties about the RTIL- magnetron sputtering method

Due to the high physicochemical stability of RTILs, above-mentioned RTIL-vacuum techniques can produce even base-metal nanoparticles that cannot be produced in conventional aqueous or organic solvents. Future challenge in this field will be how we collect the metal nanoparticles suspended in RTILs and how we develop a metal nanoparticle mass production method. Regarding the former matter, we found a facile way that is adsorption of the suspended nanoparticles on a solid substance (Kameyama et al., 2010; Okazaki et al., 2009; Tsuda et al., 2009b; Tsuda et al., 2010b). Nanoparticles are stably suspended in RTIL by the interaction with ionic species existing around the nanoparticles. Heating of the suspension on a glassy carbon plate is likely to weaken the interaction, resulting in their adsorption on the plate. As described in next section, when the glassy carbon plate, on which Pt nanoparticles were adsorbed, is used as an electrode, it exhibits high catalytic activities against electrochemical  $\text{O}_2$  reduction due to the adsorbed Pt nanoparticles.

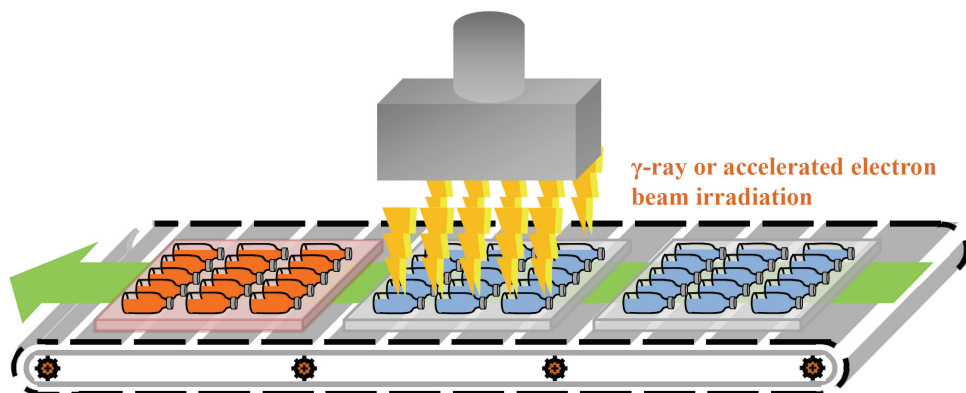


Fig. 7. Schematic illustration of an existing common  $\gamma$ -ray or accelerator electron beam irradiation industrial plant. The RTIL solution with metal salts is encapsulated in the glass ampoules under vacuum or Ar atmosphere condition.

A recent approach carried out at an existing common accelerator electron beam or  $\gamma$ -ray irradiation industrial plant for sterilizing medical kits may be a key in order to overcome the mass production issue (Tsuda et al., 2009a; Tsuda et al., 2010a). As illustrated in Fig. 7, if the glass ampoules, in which RTIL solution with metal salts are encapsulated under vacuum condition or inert gas condition, placed on the container are automatically transferred to irradiation position, metal salts should be reduced to metal state in the ampoules without



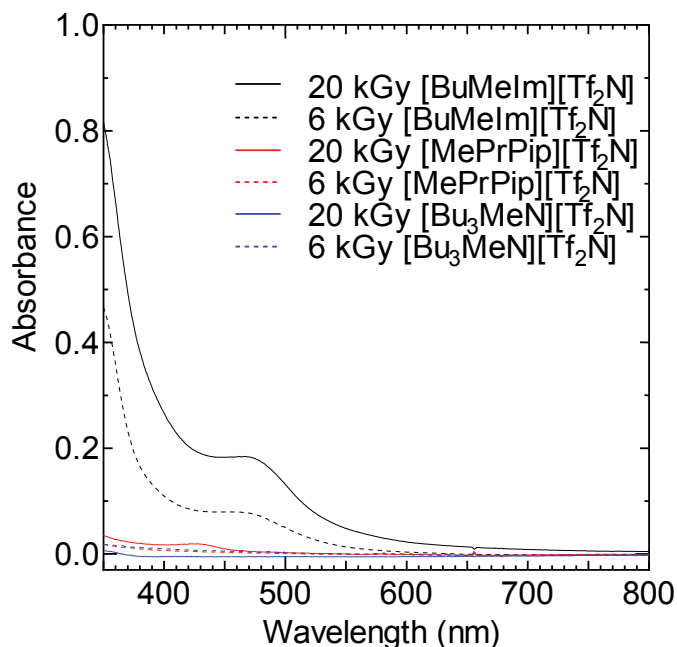


Fig. 8. UV-vis spectra of the RTILs with 0.5 mmol L<sup>-1</sup> NaAuCl<sub>4</sub>•2H<sub>2</sub>O after accelerator electron beam irradiation at 20 or 6 kGy.

contamination derived from air. This would be one way to churn out metal nanoparticles because the industrial plant can irradiate 200 glass ampoules × 100 mL at a time. The irradiation time of accelerated electron beam and  $\gamma$ -ray are 7 sec and 3 hrs, respectively, if the irradiation dose is 20 kGy. These electron beam (Imanishi et al., 2009; Tsuda et al., 2009a; Tsuda et al., 2010a) and  $\gamma$ -ray irradiation (Tsuda et al., 2009a) methods exploit solvated electrons and/or radicals yielded during the beam irradiation to the RTIL containing metal salts so as to synthesize metal nanoparticles. *Note that primary electron beam and  $\gamma$ -ray themselves cannot directly contribute to nanoparticle preparation because of their considerably strong energy!* In other words, no solvated electrons and no radicals would result in no nanoparticles. It has been already verified through the experiments using several [Tf<sub>2</sub>N]-based RTILs. As a typical example, variation in UV-vis spectra of the RTILs with 0.5 mmol L<sup>-1</sup> NaAuCl<sub>4</sub>•2H<sub>2</sub>O after accelerator electron beam irradiation is shown in Fig. 8 (Tsuda et al., 2009a). The accelerator electron beam irradiation of 20 kGy to [BuMeIm][Tf<sub>2</sub>N] and [MePrPip][Tf<sub>2</sub>N] resulted in appearance of broad absorption peak, which is attributable to plasmon absorption of Au nanoparticles, whereas irradiation to [Bu<sub>3</sub>MeN][Tf<sub>2</sub>N] caused almost no spectrum change. In case of electron beam irradiation at 6 kGy, only [BuMeIm][Tf<sub>2</sub>N] showed spectral change. These results indicate that Au nanoparticle generation in the RTILs become easier in the following order:



Our recent results on mass spectrometry measurements for the RTILs also support this order. Considering the fact that [Bu<sub>3</sub>MeN][Tf<sub>2</sub>N] is more radiochemically-stable than

[BuMeIm][Tf<sub>2</sub>N] (Bossé et al., 2008; Behar et al., 2001; Grodkowski et al., 2002; Shkrob et al., 2009), it is highly likely that radiochemically-unstable RTIL tends to generate Au nanoparticles. TEM observation revealed that the Au nanoparticles prepared in the experiments using the [BuMeIm][Tf<sub>2</sub>N] solution had mean particle size of 26.4 nm at 20 kGy irradiation and 7.6 nm at 6 kGy. We have succeeded in many types of nanoparticle preparation by using this method, e.g., Cu, Pt, etc. (Tsuda et al., 2010a).

#### 4. Application of metal nanoparticle prepared in RTILs under vacuum condition

In contrast to a simple one-electron oxygen reduction reaction (ORR) in RTIL (Tsuda & Hussey, 2009), it is well-known that the ORR occurs with several reaction paths in aqueous solution. However, Pt catalysts induce the ORR with the four electron reduction that is formulated as:



This reaction is the key to put almost all fuel cell systems to practical use. Very recently we have reported that a Pt-supported glassy carbon electrode (Pt-GCE), which was obtained by heat treatment of the RTIL with Pt nanoparticles that were prepared by the RTIL-magnetron sputtering method spreaded on a glassy carbon (GC), shows a favorable catalytic activity for oxygen reduction reaction (ORR) in 0.5 M H<sub>2</sub>SO<sub>4</sub> aqueous solution (Tsuda et al., 2009b). Also we revealed that important information on the surface condition of Pt nanoparticles on the Pt-GCE and on the catalytic ability of the Pt nanoparticles per unit area. The former was examined with infrared reflection absorption spectroscopy, and the latter was determined by a common electrochemical method. Figure 9a and b indicate infrared reflection spectra for pure [Me<sub>3</sub>PrN][Tf<sub>2</sub>N] and Pt-GCE rinsed with 1.67 M KOH *iso*-propanolic solution. After rinsing the Pt-GCE, there was no peak related to the RTIL, i.e., bare Pt surface appeared.

In order to determine active surface area of the Pt nanoparticles on the Pt-GCE, carbon monoxide, CO, stripping voltammetry was conducted. Steady state cyclic voltammograms recorded at CO-absorbed Pt-GCEs are shown in Fig. 10a-c. These Pt-GCEs were prepared by heat treatment temperature of 473, 523, and 573 K. At first cycle, in all figures, an obvious oxidation wave corresponding to CO stripping appears at 0.8 ~ 0.9 V, and the wave completely disappears at second cycle. The CO stripping wave becomes large with increasing the heat treatment temperature for the Pt-supported process. The Pt areas at the treatment temperature of 473, 523, and 573 K were 0.031, 0.100, and 0.200 cm<sup>2</sup>-Pt, respectively. Catalytic activity of these Pt-GCEs was examined by cyclic voltammetry in O<sub>2</sub>-saturated 0.5 mol L<sup>-1</sup> H<sub>2</sub>SO<sub>4</sub> aqueous solution. The observed current densities were based on the active surface area of the Pt nanoparticles. In each case, a distinct reduction wave for ORR appeared (Fig. 11). What is interesting is that the catalytic activity per unit area was enhanced at lower heat treatment temperature. In fact, we expected an opposite result; that is, the catalytic activity per unit area increases as the Pt-supported temperature increases because our previous result was that the reduction current for ORR increased at higher heat treatment temperature (Tsuda et al., 2009b). To understand this unexpected result precisely, surface morphology of these electrodes was observed by SEM. Figure 12 exhibits typical SEM images at various Pt-supported temperatures. Here, bright moiety should be Pt since

Pt nanoparticles can release more secondary electrons than the GC substrate. SEM images obviously whiten as the Pt-supported temperature increases, i.e., amount of deposited Pt

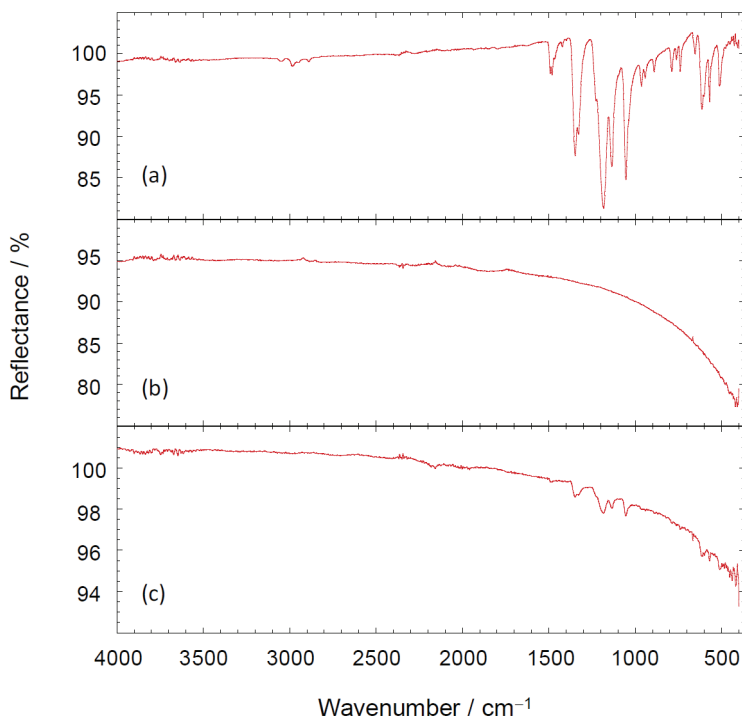


Fig. 9. Reflective FT-IR spectra of Pt-GCE prepared at 573 K. (a)  $[\text{MePrN}][\text{Tf}_2\text{N}]$  on GC without heat treatment; (b) Pt-GCE rinsed with KOH iso-propanolic solution and nitric acid; (c) Pt-GCE rinsed with acetonitrile. The Pt nanoparticles were prepared by RTIL-magnetron sputtering method.

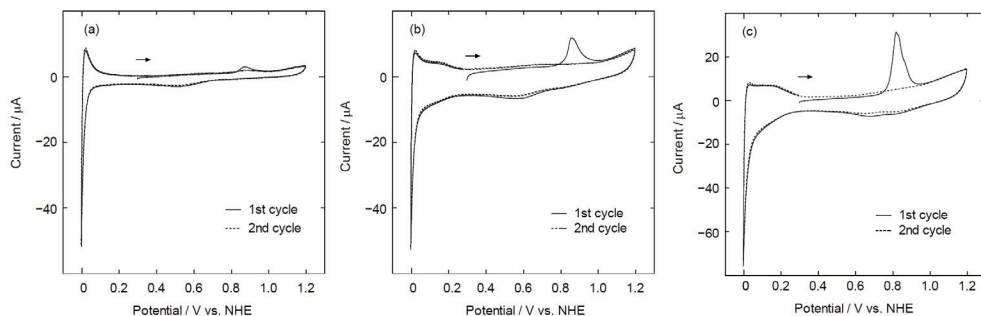


Fig. 10. Cyclic voltammograms recorded at Pt-GCEs, on which CO monolayer was absorbed. The heat temperatures for the Pt-GCE preparation were (a) 473 K, (b) 523 K, and (c) 573 K. The electrolyte was 0.5 M  $\text{H}_2\text{SO}_4$  aqueous solution at 298 K. The scan rate was 10  $\text{mV s}^{-1}$ . The Pt nanoparticles were prepared by RTIL-magnetron sputtering method.

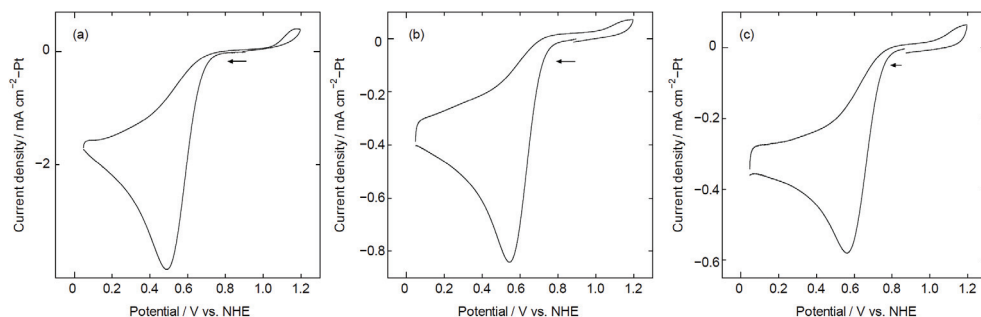


Fig. 11. Cyclic voltammograms recorded at Pt-GCEs in  $O_2$ -saturated 0.5 M  $H_2SO_4$  aqueous solution at 298 K. The heat temperatures for the Pt-GCE preparation were (a) 473 K, (b) 523 K, and (c) 573 K. The scan rate was  $10 \text{ mV s}^{-1}$ . The Pt nanoparticles were prepared by RTIL-magnetron sputtering method.

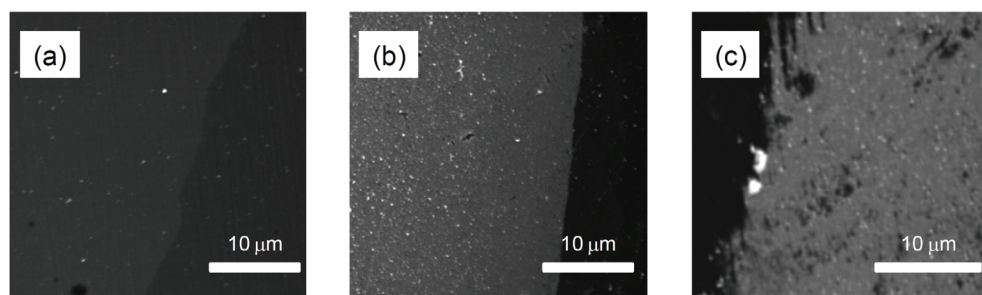


Fig. 12. SEM images of Pt-GCEs prepared at (a) 473 K, (b) 523 K, and (c) 573 K. The Pt-GCEs were rinsed with KOH iso-propanolic solution and nitric acid.

nanoparticles increases with the temperature. Therefore, increment in apparent reduction current for ORR should be caused by increase in Pt nanoparticles supported on the GC. However, as shown in Fig. 11, the catalytic activity per unit area for the ORR becomes small at higher Pt-embedded temperature. It is highly likely that effective Pt surface area decreases if the Pt-supported temperature increases because a dense Pt nanoparticle layer is formed on GC at higher temperature (Fig. 12).

Several research groups point out that RTIL improves a catalytic ability for ORR (Li et al., 2009; Wang et al., 2008; Wu et al., 2009; Yu et al., 2008; Zhao et al., 2006). We have investigated ORR using a RTIL-modified Pt-GCE. The RTIL-modified Pt-GCE was prepared by rinsing Pt-GCE with dry acetonitrile, not 1.67 M KOH iso-propanolic solution. The surface state of the Pt-GCE was examined with infrared reflection absorption spectroscopy. As shown in Fig. 9c, the Pt-GCE rinsed with dry acetonitrile indicated weak absorption related to the  $[Me_3PrN][Tf_2N]$  RTIL. The surface area of the RTIL-modified Pt-GCE was estimated by using CO stripping voltammetry, like an original Pt-GCE described above. Figure 13 indicates cyclic voltammograms recorded at the RTIL-modified Pt-GCE on which CO was absorbed. There is a no CO stripping wave, but is a reduction wave for hydrogen evolution. It implies that the RTIL-modified Pt-GCE is electrochemically active without CO poisoning. As expected, RTIL-modified Pt-GCE with CO poisoning reduced oxygen electrochemically (Fig. 14a). Voltammograms recorded at different initial potentials,



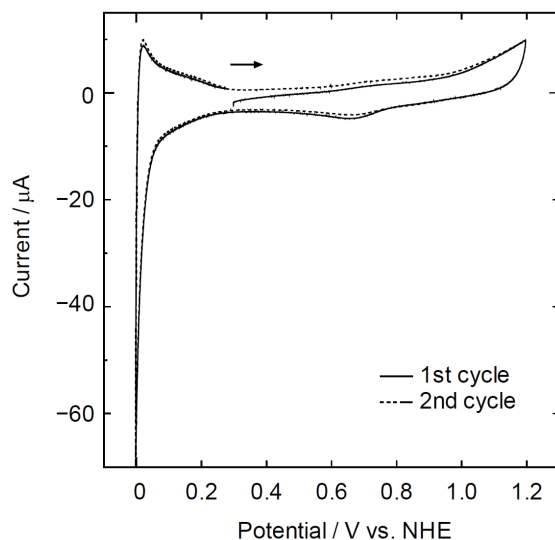


Fig. 13. Cyclic voltammograms recorded at a RTIL-modified Pt-GCE, on which CO monolayer was absorbed. The heat temperature for the Pt-GCE preparation was 573 K. The electrolyte was 0.5 M  $\text{H}_2\text{SO}_4$  aqueous solution at 298 K. The scan rate was  $10 \text{ mV s}^{-1}$ .

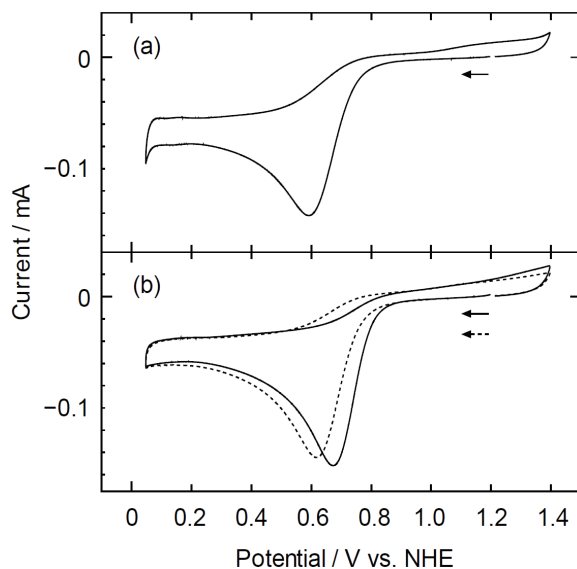


Fig. 14. Cyclic voltammograms recorded at (a) a RTIL-modified Pt-GCE with CO poisoning and (b) (—) a RTIL-modified Pt-GCE and (---) an original Pt-GCE in  $\text{O}_2$ -saturated 0.5 M  $\text{H}_2\text{SO}_4$  aqueous solution at 298 K. The heat temperature for the Pt-GCE preparation was 573 K. The scan rate was  $10 \text{ mV s}^{-1}$ . The Pt nanoparticles were prepared by RTIL-magnetron sputtering method.

e.g., +0.70 V, also showed a remarkably-similar oxygen reduction wave. In fact, a number of groups report an effective interaction between RTIL and metal nanoparticles (Dupont & Scholten, 2010; Torimoto et al., 2010). Probably the interaction prevents CO adsorption onto the Pt nanoparticles. Catalytic activity of the RTIL-modified Pt-GCE without CO poisoning toward ORR was investigated by cyclic voltammetry (Fig. 14b). This RTIL-modified electrode showed better catalytic ability than an original Pt-GCE. The reason is not clear but the high activity would be due to the high oxygen solubility in the RTIL (Tsuda & Hussey, 2009). Using  $[\text{Me}_3\text{PrN}][\text{Tf}_2\text{N}]$  RTIL as a solvent and a material, we succeeded in fabrication of a novel electrode, which has both  $\text{O}_2$  reduction catalytic ability and anti-CO poisoning nature.

## 5. Concluding remarks

RTIL is the first liquid that works well as reaction media even under vacuum condition. To apply RTIL science to the vacuum technology likely contributes to further development of science and technology, although modern vacuum technology already supports our comfortable daily lives. Especially we believe nanoparticle preparation by the use of the cutting-edge technology that combines RTIL and vacuum condition will be a future key technology in energy device and photonics material because even base metal, alloy, and semiconductor nanoparticles can be yielded by the technology without difficulty.

## 6. References

- Abedin, S. Z. E., Pölleth, M., Meiss, S. A., Janek, J. & Endres, F. (2007). Ionic Liquids as green electrolytes for the electrodeposition nanomaterials, *Green Chem.* 9: 549-553.
- Baba, K., Kaneko, T. & Hatakeyama, R. (2009). Efficient Synthesis of Gold Nanoparticles Using Ion Irradiation in Gas-Liquid Interfacial Plasmas, *Appl. Phys. Lett.* 2: 035006-1/3.
- Behar, D., Gonzalez, C. & Neta, P. (2001). Reaction Kinetics in Ionic Liquids: Pulse Radiolysis Studies of 1-Butyl-3-methylimidazolium Salts, *J. Phys. Chem. A* 105: 7607-7614.
- Bossé, É., Berthon, L., Zorz, N., Monget, J., Berthon, C., Bisel, I., Legand, S. & Moisy, P. (2008). Stability of  $[\text{MeBu}_3\text{N}][\text{Tf}_2\text{N}]$  under gamma irradiation, *Dalton Trans.*, 924-931.
- Brettholle, M., Höfft, O., Klarhöfer, L., Mathes, S., Maus-Friedrichs, W., Abedin, S. Z. E., Krischok, S., Janek, J. & Endres, F. (2010). Plasma electrochemistry in ionic liquids: deposition of copper nanoparticles, *Phys. Chem. Chem. Phys.* 12: 1750-1755.
- Cooper, E. I. & O'Sullivan, E. J. M. (1992). New, Stable, Ambient-Temperature Molten Salts, in Gale, R. J., Blomgren, G. & Kojima, H., *Proceedings of the Eighth International Symposium on Molten Salts*, The Electrochemical Society, Inc., Pennington, NJ, PV92-16, pp. 386-396.
- Dupont, J. & Scholten, J. D. (2010). On the structural and surface properties of transition-metal nanoparticles in ionic liquids, *Chem. Soc. Rev.* 39: 1780-1804.
- Grodzowski, J. & Neta, P. (2002). Reaction Kinetics in the Ionic Liquid Methyltributylammonium Bis(Trifluoromethylsulfonyl)imide. Pulse Radiolysis Study of  $\cdot\text{CF}_3$  Radical Reactions, *J. Phys. Chem. A* 106: 5468-5473.
- Hatakeyama, Y., Okamoto, M., Torimoto, T., Kuwabata, S. & Nishikawa, K. (2009). Small-Angle X-ray Scattering Study of Au Nanoparticles Dispersed in the Ionic Liquids 1-Alkyl-3-methylimidazolium Tetrafluoroborate, *J. Phys. Chem. C* 113: 3917-3922.

- Hatakeyama, Y., Takahashi, S. & Nishikawa, K. (2010). Can Temperature Control the Size of Au Nanoparticles Prepared in Ionic Liquids by the Sputter Deposition Technique?, *J. Phys. Chem. C* 114: 11098-11102.
- Imanishi, A., Tamura, M. & Kuwabata, S. (2009). Formation of Au nanoparticles in an ionic liquid by electron beam irradiation, *Chem. Commun.* 1775-1777.
- Kameyama, T., Ohno, Y., Kurimoto, T., Okazaki, K., Uematsu, T., Kuwabata, S. & Torimoto, T. (2010). Size control and immobilization of gold nanoparticles stabilized in an ionic liquid on glass substrates for plasmonic applications, *Phys. Chem. Chem. Phys.* 12: 1804-1811.
- Kaneko, T., Baba, K., Harada, T. & Hatakeyama, R. (2009). Novel Gas-Liquid Interfacial Plasmas for Synthesis of Metal Nanoparticles, *Plasma Process. Polym.* 6: 713-718.
- Khatr, O. P., Adachi, K., Murase, K., Okazaki, K., Torimoto, T., Tanaka, N., Kuwabata, S. & Sugimura, H. (2008). Self-Assembly of Ionic Liquid (BMI-PF<sub>6</sub>)-Stabilized Gold Nanoparticles on a Silicon Surface: Chemical and Structural Aspects, *Langmuir* 24: 7785-7792.
- Koel, M. (ed.), (2009). *Ionic Liquids in Chemical Analysis*, CRC Press, Boca Raton.
- Kuwabata, S., Tsuda, T. & Torimoto, T. (2010). Room-Temperature Ionic Liquid as New Medium for Material Production and Analyses under Vacuum Conditions, *J. Phys. Chem. Lett.* 1: 3177-3188.
- Li, F., Li, F. Song, J., Song, J., Han, D. & L. Niu. (2009). Green synthesis of highly stable platinum nanoparticles stabilized by amino-terminated ionic liquid and its electrocatalysts for dioxygen reduction and methanol oxidation, *Electrochem. Commun.* 11: 351-354.
- Meiss, S. A., Rohnke, M., Kienle, L., Abedin, S. Z. E., Endres, F. & Janek, J. (2007). Employing Plasmas as Gaseous Electrodes at the Free Surface of Ionic Liquids: Deposition of Nanocrystalline Silver Particles, *ChemPhysChem* 8: 50-53.
- Okazaki, K., Kiyama, T., Hirahara, K., Tanaka, N., Kuwabata, S. & Torimoto, T. (2008). Single-step synthesis of gold-silver alloy nanoparticles in ionic liquids by a sputter deposition technique, *Chem. Commun.* 691-693.
- Okazaki, K., Kiyama, T., Suzuki, T., Kuwabata, S. & Torimoto, T. (2009). Thermally Induced Self-assembly of Gold Nanoparticles Sputter-deposited in Ionic Liquids on Highly Ordered Pyrolytic Graphite Surfaces, *Chem. Lett.* 38: 330-331.
- Prondzinski, N. v., Cybinska, J. & Mudring, A.-V. (2010). Easy access to ultra long-time stable, luminescent europium(II) fluoride nanoparticles in ionic liquids, *Chem. Commun.* 46: 4393-4395.
- Richter, K., Birkner, A. & Mudring, A.-V. (2010). Stabilizer-Free Metal Nanoparticles and Metal-Metal Oxide Nanocomposite with Long-Term Stability Prepared by Physical Vapor Deposition into Ionic Liquids, *Angew. Chem. Int. Ed.* 49: 2431-2435.
- Shishino, Y., Yonezawa, T., Kawai, K. & Nishihara, H. (in press). Molten matrix sputtering synthesis of water-soluble luminescent Au nanoparticles with a large Stokes shift, *Chem. Commun.*
- Shkrob, I. A. & Wishart, J. F. (2009). Charge Trapping in Imidazolium Ionic Liquids, *J. Phys. Chem. B* 113: 5582-5592.
- Stafford, G. R. & Hussey, C. L. (2002). Electrodeposition of Transition Metal-Aluminum Alloys from Chloroaluminate Molten Salts, in Alkire, R. C. & Kolb, D. M. (eds.), *Advances in Electrochemical Science and Engineering* Vol. 7, Wiley-VCH, Weinheim, pp. 275-347.
- Suzuki, T., Okazaki, K., Kiyama, T., Kuwabata, S. & Torimoto, T. (2009). A Facile Synthesis of AuAg Alloy Nanoparticles Using a Chemical Reaction Induced by Sputter Deposition of Metal onto Ionic Liquids, *Electrochemistry* 77: 636-638.

- Suzuki, T., Okazaki, K., Suzuki, S., Shibayama, T., Kuwabata, S. & Torimoto, T. (2010). Nanosize-Controlled Syntheses of Indium Metal Particles and Hollow Indium Oxide Particles via the Sputter Deposition Technique in Ionic Liquids, *Chem. Mater.* 22: 3283-3287.
- Torimoto, T., Okazaki, K., Kiyama, T., Hirahara, K., Tanaka, N. & Kuwabata, S. (2006). Sputter deposition onto ionic liquids: Simple and clean synthesis of highly dispersed ultrafine metal nanoparticles, *Appl. Phys. Lett.* 89: 243117/1-3.
- Torimoto, T., Tsuda, T., Okazaki, K. & Kuwabata S. (2010). New Frontiers in Materials Science Opened by Ionic Liquid, *Adv. Mater.*, 22: 1196-1221.
- Tsuda, T., Hussey, C. L. & Stafford, G. R. (2007). Progress in Surface Finishing with Lewis Acidic Room-Temperature Chloroaluminate Ionic Liquids, *ECS Trans.*, 3(35): 217-231.
- Tsuda, T. & Hussey, C. L. (2009). Electrochemistry of Room-Temperature Ionic Liquids and Melts, in White, R. E. (ed.), *Modern Aspects of Electrochemistry Vol. 45*, Springer Science+Business Media, New York, pp. 63-174.
- Tsuda, T., Seino, S. & Kuwabata, S. (2009a). Gold nanoparticles prepared with a room-temperature ionic liquid-irradiation method, *Chem. Commun.* 6792-6794.
- Tsuda, T., Kurihara, T., Hoshino, Y., Kiyama, T., Okazaki, K., Torimoto, T. & Kuwabata, S. (2009b). Electrocatalytic Activity of Platinum Nanoparticles Synthesized by Room-Temperature Ionic Liquid-Sputtering Method, *Electrochemistry* 77: 693-695.
- Tsuda, T., Sakamoto, T., Nose, T., Seino, S., Imanishi, A., Uematsu, T., & Kuwabata, S. (2010a). Irradiation-Induced Metal Nanoparticles in Room-Temperature Ionic Liquid, *ECS Trans.* 33(7): 543-554.
- Tsuda, T., Yoshii, K., Torimoto, T. & Kuwabata, S. (2010b). Oxygen reduction catalytic ability of platinum nanoparticles prepared by room-temperature ionic liquid-sputtering method, *J. Power Sources*, 195: 5980-5985.
- Wang, Z., Zhang, Q., Kuehner, D., Ivaska, A. & Niu, L. (2008). Green synthesis of 1-2 nm gold nanoparticles stabilized by amine-terminated ionic liquid and their electrocatalytic activity in oxygen reduction, *Green Chem.* 10: 907-909.
- Wasserscheid, P. & Welton, T. (eds.), (2003). *Ionic Liquids in Synthesis*, Wiley-VCH, Weinheim.
- Wender, H., Oliveira, L. F. de, Migowski, P., Feil, A. F., Lissner, E., Precht, M. H. G., Teixeira, S. R. & Dupont, J. (2010). Ionic Liquid Surface Composition Controls the Size of Gold Nanoparticles Prepared by Sputtering Deposition, *J. Phys. Chem. C* 114: 11764-11768.
- Wilkes, J. S., Levitsky, J. A., Wilson, R. A. & Hussey C. L. (1982). Dialkylimidazolium Chloroaluminate Melts: A New Class of Room-Temperature Ionic Liquids for Electrochemistry, Spectroscopy, and Synthesis, *Inorg. Chem.* 21: 1263-1264.
- Wilkes, J. S. & Zaworotko, M. J. (1992). Air and Water Stable 1-Ethyl-3-methylimidazolium Based Ionic Liquids, *J. Chem. Soc., Chem. Commun.* 965-967.
- Wu, B., Hu, D., Kuang, Y., Liu, B., Zhang, X. & Chen, J. (2009). Functionalization of Carbon Nanotubes by an Ionic-Liquid Polymer: Dispersion of Pt and PtRu Nanoparticles on Carbon Nanotubes and Their Electrocatalytic Oxidation of Methanol, *Angew. Chem. Int. Ed.* 48: 4751-4754.
- Yu, P., Yan, J., Zhao, H., Su, L., Zhang, J. & Mao, L. (2008). Rational Functionalization of Carbon Nanotube/Ionic Liquid Bucky Gel with Dual Tailor-Made Electrocatalysts for Four-Electron Reduction of Oxygen, *J. Phys. Chem. C* 112: 2177-2182.
- Zhao, Z. W., Guo, Z. P., Ding, J., Wexler, D., Ma, Z. F., Zhang, D. Y. & Liu, H. K. (2006). Novel ionic liquid supported synthesis of platinum-based electrocatalysts on multiwalled carbon nanotubes, *Electrochem. Commun.* 8: 245-250.

## **Part 4**

### **Academic Technologies (New Technological Approaches)**



# Perspectives of Ionic Liquids Applications for Clean Oilfield Technologies

Rafael Martínez-Palou and Patricia Flores Sánchez

*Instituto Mexicano del Petróleo. Eje Central Lázaro Cárdenas 152. 07730, México, D.F.  
México*

## 1. Introduction

Ionic liquids (ILs) are gaining wide recognition as potential environmental solvents due to their unique properties (Wasserscheid & Keim, 2004, Martínez-Palou, 2007, Martínez-Palou, 2010) and their applications in Organic Synthesis (Wasserscheid & Welton, 2008, Martínez-Palou, 2006), catalysis (Gu et al., 2009, Toma et al., 2009, Olivier-Bourbigou, 2010), biocatalysis (Muginova et al., 2010, Moniruzzaman et al., 2010), in separation (Han & Row 2010), extraction (Poole & Poole, 2010) and dissolution processes (Torimoto et al., 2010, Zakrzewska et al., 2010), nanomaterials synthesis (Li et al., 2008), polymerization reactions (Srivastava, et al., 2009, Lu et al., 2009) and electrochemistry (McFarlane et al. 2010, Ohno & Fukumoto, 2008). ILs are an excellent alternative to substitute volatile organic solvents in more environmental friendly technologies, also known as “green technologies” (Rogers & Seddon, 2002) since their very low vapor pressures, their thermal and chemical stability, their ability to act as catalysts, and their non-flammability and non-corrosive properties which decreases the risk of worker exposure and the loss of solvent to the atmosphere.

Petroleum industry is one of the most important industry in the world and in the last decades it has enter in a continuous process of modernization and transition for becoming to a more clean and “green industry” around the world. This industry present typical operational and old technological problems, like corrosion, emulsions formation (oil/water and water/oil), asphaltenes flocculation during oil production and processing, contamination of hydrocarbons feeds and other which need new and more efficient solutions (Speight, 2009).

For their versatility and properties, ILs have a wide range of potential applications for chemical industry and especially for petroleum industry, as have been demonstrate with the increased number of papers about the evaluation of ILs for applications in areas as improvement of petroleum properties for their exploration, exploitation and transportation, elimination of toxic substances from fuels (sulfurated, nitrogenated and aromatics compounds), develop of new “green” additives with application as corrosion inhibitors, demulsifier and desalting agents, and several applications of the ILs as catalysts and solvents for petrochemical processes. ILs have also been explored in membranes technologies for selective separation of gases, liquids fuels and contaminants, and in another alternative fuels technologies like biofuels and fuel cells.

In this chapter, some of the most important advances about the study of ILs for potential oilfield applications are reviewed.

## 2. Ionic Liquids. Generalities

### 2.1 Definition

An ionic liquid (IL) is a salt in the liquid state. In our contexts, the term has been restricted to salts whose melting point is below of 100 °C. To a difference of a molten salt characterized by high-melting, highly viscous and very corrosive medium, ILs are already liquid at low temperatures (< 100 °C) and have relatively low viscosity, with exceptional properties for application as solvents to substitute high toxic and volatile organic solvents (Wasserscheid & Keim, 2004).

ILs are formed with a large organic cations, that can be symmetric or assymetric one. The asymmetry lowers the lattice energy, and hence the melting point, of the resulting ionic medium. Invariably the cation is organic (heterocyclic or acyclic) and the anion can be a halogen ("first generation ILs"), inorganic (i.e.  $[\text{BF}_4]^-$ ,  $[\text{PF}_6]^-$ ,  $[\text{SbF}_6]^-$ ,  $[\text{AlCl}_4]^-$ ,  $[\text{FeCl}_4]^-$ ,  $[\text{AuCl}_4]^-$ ,  $[\text{InCl}_4]^-$ ,  $[\text{NO}_3]^-$ ,  $[\text{NO}_2]^-$ ,  $[\text{SO}_4]^-$ ,  $[\text{SCN}]^-$ ) or organic (i.e.  $[\text{AcO}]^-$ ,  $[\text{N}(\text{OTf})_2]^-$ ,  $[\text{CF}_3\text{CO}_2]^-$ ,  $[\text{CF}_3\text{SO}_3]^-$ ,  $[\text{PhCOO}]^-$ ,  $[\text{C}(\text{CN})_2]^-$ ,  $[\text{RSO}_4]^-$ ,  $[\text{OTs}]^-$ ). In some cases, even the anions are relatively large and play a role in lowering the melting point. The composition and properties of the ILs depend on the cation and anion combinations. Some typical structures for the cation (i.e. 1, imidazolium, 2, pyridinium, 3, isoquinolinium, 4, ammonium, 5, phosphonium, 6, sulfonium)-type for ILs are showed in Figure 1. Where, R, R', R'' and R''' are essentially alkyl and sometime aryl, and alkyl chains.

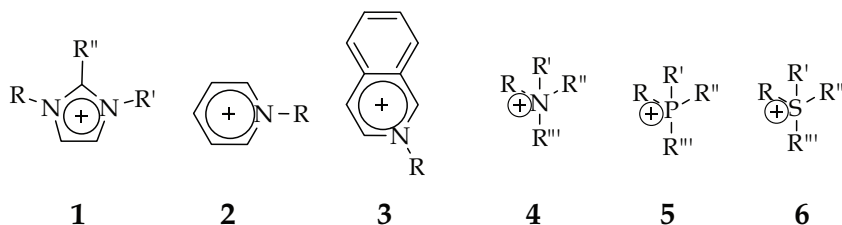


Fig. 1. Typical structures for ILs cations

### 2.2 Ionic Liquids synthesis

The first step in the synthesis of ILs is the quaternization of a nitrogenated heterocycle, like imidazole, pyridine, isoquinoline or tertiary amine or phosphane for example, to form the cation. Generally, the quaternization is carried out by alkylation reaction using an alkyl halide. The IL obtained after this step is known as "first generation ILs".

In the second step, the desire the anion could be introduced by anionic exchange or metathesis reaction using the corresponding acid (HY) or metallic salt (MeY).

The reaction time in each step depend on the reactivity of the involved reagents, but in general the first step is carried out in several hours by conventional heating ( $\Delta$ ), but the reaction time can be reduced considerably using non-conventional energy sources as ultrasound ())) or microwave irradiation (MW) (Martínez-Palou, 2010).

A general scheme for the synthesis of imidazolium type ILs from imidazole is presented in Figure 2.



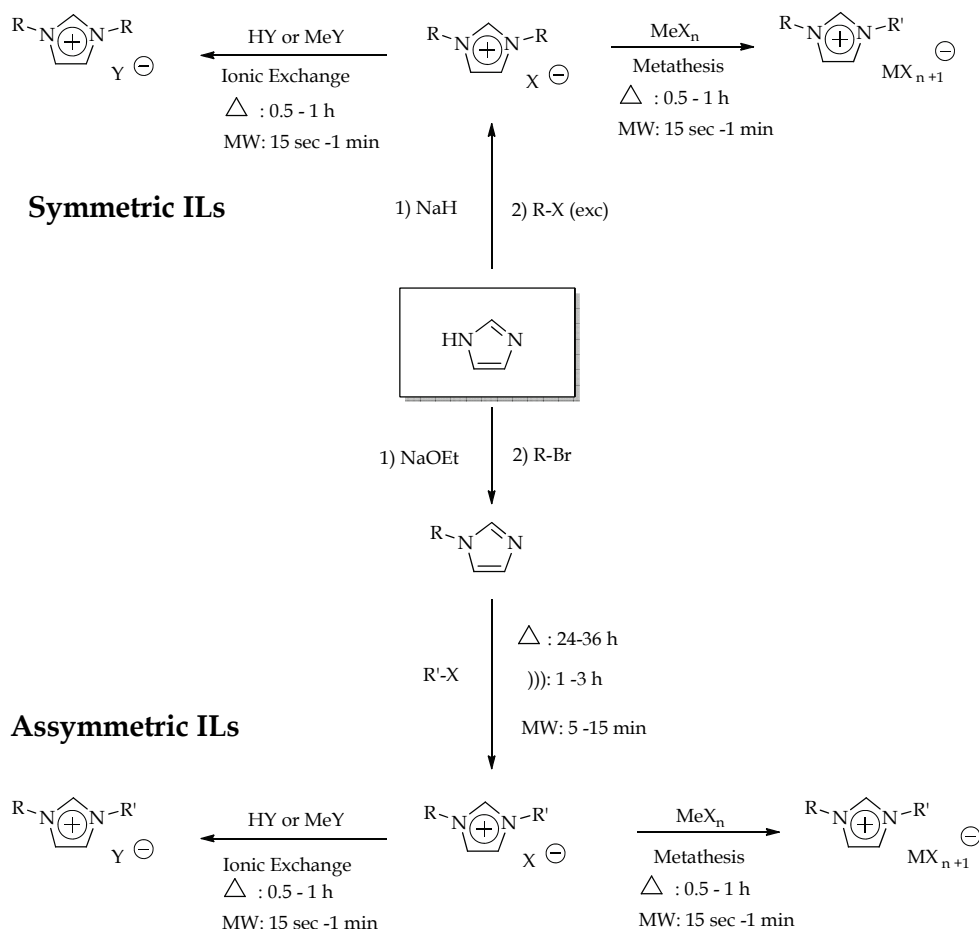


Fig. 2. General scheme of synthesis of imidazolium type ILs

### 2.3 Physicochemical properties

The physical and chemical properties of ILs can be fine-tuned by changing the structure of the cations and anions. The most important properties of ILs that are converted them in very attractive compounds are the following:

- **Extremely low vapor pressure.** To a difference of the classical organic solvents, ILs are known to have a negligible vapor pressure below their decomposition temperature. This is the main reason because ILs are considered environmental friendly solvents.
- **Thermal Stability:** The thermal stability of ILs is limited by the strength of their heteroatom-carbon and their heteroatom-hydrogen bonds, respectively. The nature of the ILs, containing organic cations, restricts upper stability temperatures, pyrolysis generally occurs between 350-450 °C. In most cases, decomposition occurs with complete mass loss and volatilization of the component fragments. The onset of thermal

decomposition calculated from fast thermogravimetric analysis (TGA) indicates high thermal stability for many ILs, generally higher than 350 °C.

- **Solubility:** ILs can be tailored to be immiscible with water or with certain organic solvents. Many ILs possess the ability to dissolve a wide range of inorganic and organic compounds. This is important for dissolving combinations of reagents into the same phase. Hydrophilicity/hydrophobicity properties depend significantly to the structure of the cations and anions.
- **Electrochemical Stability.** ILs often have wide electrochemical potential windows, they have reasonably good electrical conductivity. The electrochemical window of an IL is influenced by the stability of the cation against electrochemical reduction-processes and the stability of the anion against oxidation-processes. ILs exhibit broad range of conductivities from 0.1 to 20 mS cm<sup>-1</sup>. In general the higher conductivities are found for imidazolium-based ILs.
- **Non-flammability.** ILs are safe for hanging, because ILs are non-volatile and consequently non-flammable at ambient and higher temperatures, however ILs can be combustibles.
- **Catalytic properties.** The catalytic properties in organic and inorganic synthesis have been widely described (Olivier-Bourbigou et al., 2010) and many efforts have been carried out toward understanding the origin of effects of ILs on catalysis (Lee et al., 2010). In this chapter, some examples with potential application to oilfield will be discussed. In addition, biocatalytic transformations in ILs have been performed using a range of different enzymes and some whole cell preparations, mainly in biphasic aqueous systems using hydrophobic dialkylimidazolium ILs.

### 3. Ionic liquids as extractants

Clean fuels processing and production has become an important subject of environmental research area worldwide. Dramatic changes occurred in many countries concerning the regulations for fuel qualities in the past decade and the US Environmental Protection Agency (EPA) has applied new regulations, and government regulations in many countries call for the production and use of more environmentally friendly transportation fuels (Rogers & Seddon, 2002).

Compared to conventional volatile organic solvents, the use of ILs for extraction has a number of advantages determined by their properties. ILs are miscible with substances having very wide range of polarities and can simultaneously dissolve organic and inorganic substances (Huddleston et al., 1998, Zhao et al., 2005).

These features of ILs offer numerous opportunities for modification of existing and for the development of new extraction processes. In some cases, such processes would be impossible with conventional solvents because of their limited liquid range or miscibility and low boiling point and toxicities.

#### 3.1 Desulfurization of light oil using ionic liquids

Recently, a high emphasis has been placed on the deep desulphurization of oil products because hydrocarbon combustion releases SO<sub>x</sub>; which are responsible of acid rain, air contamination and ozone consumption. Environmental regulations have been modified to allow that lower levels of sulfured compounds to be ejected to the atmosphere. Industrially,

the removal of organosulfur and organonitrogen compounds in fuel oils is being carried out by means of a simultaneous hydrodesulfurization (HDS) and hydrodenitrogenation (HDN) process at around 350 °C using catalysts based on CoMo or NiMo, which involves the C-S and C-N bond cleavage to produce H<sub>2</sub>S and NH<sub>3</sub>, respectively (Zaczeplinski, 1996, Kabe et al., 1999; Ferrari et al., 2001; Caeiro, et al., 2007).

Deep desulfurization of diesel fuels is particularly challenging due to the difficulty of reduce aromatic sulfur compounds, particularly 4,6-dialkyldibenzothiophenes, using conventional hydrodesulfurization processes (HDS). The HDS process is normally only effective for removing organosulfur compounds of aliphatic and alicyclic types. The aromatic sulfur molecules including thiophenes, dibenzothiophenes (DBT), and their alkylated derivatives are very difficult to convert to H<sub>2</sub>S through HDS.

New processes and nonhydrodesulfurization technologies for production ultra-low sulfur clean oils have been studied to remove sulfur from the different cuts in the refinery industry (Babich, & Moulijn, 2003, Song, 2003, Brunet et al., 2005, Ito & Veen, 2006, Ann et al., 2007, Stanislaus et al., 2010).

One alternative called extractive desulfurization (EDS) seems very attractive for this purpose because of its low energy cost, the elimination of hydrogen usage, the retaining of the chemical structures of fuels and no requirements of special equipment.

In this sense, the first published paper described the extractive properties of sulfur-containing compounds (SCs) by liquid-liquid extraction employing ILs was described by Bosmann and coworkers (Bosmann et al., 2001). In this work, a serie of ILs with properties for removing SCs from a model solution (500 ppm of dibenzothiophene in *n*-dodecane) were described, however, deep desulfurization (higher than 90% of sulfur removed) were obtained only when Lewis acid ILs containing tetrachloroaluminates, particularly [BMIM]Cl/AlCl<sub>3</sub>. (0.35/0.65).

Anion effect was also evaluated employing the same cation ([BMIM]) working at the same experimental conditions. The alkylsulfate anions shows the best extractive properties between the neutral ILs. On the other hand, the effect of the *N*-alkyl chain also play an important role in the performance of these compounds, increasing the extractive properties from *n*-C2 to *n*-C8.

Finally the authors tested the efficiency of the best three ILs prototypes in a multistage desulfurization experiment using a real predesulfurized diesel oil sample (without additives, sulfur content: 375 ppm) at 60 °C with mass ratio oil/IL = 5/1 and 15 minutes of reaction time. Lewis acid ILs showed the best performance after four extraction steps (Table 1).

Extraction stage	[BMIM]Cl/AlCl <sub>3</sub>	[HN(C <sub>6</sub> H <sub>11</sub> )Et <sub>2</sub> ]MeSO <sub>3</sub> / [HNBu <sub>3</sub> ] MeSO <sub>3</sub> (1/1)	[BMIM]Octylsulfate
1	41.3	12.0	14.7
2	57.3	20.0	25.3
3	65.3	28.0	30.6
4	80.0	36.0	37.3

Table 1. Percentage of total sulfur remotion in multistage desulfurization of predesulfurized diesel sample with ILs.

The same authors studied newly the desulfurization by extraction with similar Lewis acids and halogen-free ILs. In this paper, the influence of S-species and S-concentration on extraction with halogen-free ILs, cross solubility of oil in the IL and vice versa, extraction of N-compounds, continuous extraction in a mixer-settler system, possibilities of regeneration of S-loaded ILs and the possible scenarios for the integration of this technology in the existing refinery network were studied. The results show the selective extraction properties of ILs, especially with regard to those S-compounds, which are hard to remove by HDS, e. g. dibenzothiophene derivatives present in middle distillates like diesel oil. The application of mild process conditions (ambient pressure and temperature) and the fact that no hydrogen is needed are additional advantages compared to HDS. Very promising ILs are [BMIM][O<sub>2</sub>SO<sub>4</sub>] and [EMIM][EtSO<sub>4</sub>], as they are halogen-free and available from relatively cheap starting materials (Eßer et al., 2004).

In 2004, Bowing and Jess studied the kinetic and continuous reactor design aspects for scaled synthesis of [EMIM]EtSO<sub>4</sub>, one of the most promising halogen-free ILs for sulfur extraction. Compared to batch reactors, the hold-up is by a factor of 1000 lower, which is particularly advantageous for toxic reactants (here diethyl sulfate). The results are beyond synthesis of [EMIM][EtSO<sub>4</sub>] instructive for other ILs, and probably also for other exothermic reactions with a temperature limit (Bowing and Jess, 2007).

Many other papers have been published about the desulfurization of oils by liquid-liquid extraction using ILs that is presented in the Table 2.

Reference	ILs evaluated	Conditions of desulfurization	Observations
(Zhang & Zhang, 2002)	[EMIM]BF <sub>4</sub> , [BMIM]BF <sub>4</sub> , [EMIM]PF <sub>6</sub>	Ratio IL/gasoline, 1/2, 15 minutes, rt	[EMIM]BF <sub>4</sub> : 17% of sulfur removal for low sulfur gasoline (240 ppm) and 11% for high sulfur gasoline (820 ppm). Using [BMIM]PF <sub>6</sub> : 29% and 13% of sulfur removal were obtained for the same samples.
(Zhang et al., 2004)	[EMIM]BF <sub>4</sub> , [BMIM]PF <sub>6</sub> , [BMIM]BF <sub>4</sub> Me <sub>3</sub> NHCl/AlCl <sub>3</sub>	Ratio IL/gasoline, 1/5, 30 minutes, rt	Sulfur removal of 11-14% for [BMIM]BF <sub>4</sub> , 15% for Me <sub>3</sub> NHCl/AlCl <sub>3</sub> (2/1) and 20% for Me <sub>3</sub> NHCl/AlCl <sub>3</sub> (1.5/1)
(Huang et al., 2004)	[BMIM]CuCl (1:2)	Ratio IL/gasoline, 1/5, 30 minutes, rt	23% of sulfur removal for model oil and 16-37% for gasolines with different sulfur contents (196-950 ppm). The extraction increase when sulfur content decrease.
(Nie et al., 2006)	[MMIM][DMP] [EMIM][DEP] [BMIM][DBP] DMP: dimethyl phosphate; DEP: dimethylphosphate and DBP: dibutyl phosphate	K <sub>N</sub> was determined by 1) A known weight IL and gasoline were mixed. 2) A known amount of S-concentrated IL was added and stirred for 15 min at rt. 3) 10 min for phase splitting and settling.	K <sub>N</sub> for each phosphoric IL and S-component (namely, 3-MT, BT, and DBT) is virtually a constant irrespective of the S-content in gasoline. K <sub>N</sub> was between 0.94-1.81.

Reference	ILs evaluated	Conditions of desulfurization	Observations
(Alonso et al., 2007)	[C <sub>8</sub> MIM][BF <sub>4</sub> ]	Mass ratio IL:model gasoline (MD) (1:1). MD: 28 wt% of n-hexane, 28 wt% cyclohexane, 28 wt% i-octane, 10 wt% toluene, 3 wt% thiophene and 3 wt% DBT, stirring 2 h at 298 K, 4 h settle down and analyzed by GC.	Thiophene distribution ratio ( $\beta$ ), and solvent selectivity (S) were determined to calculate solvent extraction capacity for ternary systems involved in desulfurization.
(Nie et al., 2007)	[MMIM][DMP] [EMIM][DEP] [BMIM][DBP]	1) 5996 ppm S content by dissolving DBT in MIM was prepared. 2) A known weight of S-free solvent and fuel oil is mixed under vigorous stirring. 3) A known amount of S-concentrated solvent was added to the above biphasic mixture, magnetically stirred for 15 min at rt.	$K_N$ values were measured between straight-run fuel oil and N-ethylimidazole, N-methylimidazole and its mixture with a dialkylphosphate IL, viz. [EMIM][DEP] or [BMIM][DBP]. The results indicate that both EIM and MIM have excellent EDS performance with $K_N$ above 3.1 for dibenzothiophene.
(Mochizuki et al., 2008)	[MMIM]MeSO <sub>4</sub> [EMIM]EtSO <sub>4</sub> [EMM]MeSO <sub>4</sub> [EEIM]EtSO <sub>4</sub> [BMIM]MeSO <sub>4</sub> [BEIM]EtSO <sub>4</sub>	The model fuel was prepared from DBT and <i>n</i> -dodecane. The ILs were mixed with the model fuel in a certain ratio and stirred for a certain time interval at rt. A GC-MS was used to determine S-content.	When the mass ratio of the IL/model fuel was 1/1, DBT was successfully extracted using [EMIM] MeSO <sub>4</sub> and [MMIM]MeSO <sub>4</sub> with yields of 40 and 70%, respectively, after one round of extraction.
(Schmidt, 2008)	[BMIM]AlCl <sub>4</sub>	The fuels were dried prior to use with activated 13X molecular sieve. Each fuel was then added to freshly prepared IL in an initial volume ratio of 1/6 (10 mL of IL/60 mL of fuel). The two-phase mixture was stirred for 5 min at rt.	High level of S and N removal (90-95%) were obtained after dried the fuel with molecular sieves. In spite of water was first removed, in all cases, the dark green IL turned black immediately when it contacted the fuels, indicating IL decomposition of the Lewis acid ILs.
(Gao, et al., 2008)	[BPy][BF <sub>4</sub> ] [HPy][BF <sub>4</sub> ] [OPy][BF <sub>4</sub> ]	The mass ratios of ILs to model diesel or diesel fuel were 1:1 or 1:3. The ILs were added to the model	The extractive performance using pyridinium-based ILs followed the order [BPy][BF <sub>4</sub> ] < [HPy][BF <sub>4</sub> ] < [OPy][BF <sub>4</sub> ], and selectivity of

Reference	ILs evaluated	Conditions of desulfurization	Observations
	B: Butyl, H: hexyl and O: octyl.	diesel or diesel fuel, magnetically stirred for 15 min at rt to reach thermodynamic equilibrium, and then allowed to settle for 5 min to obtain phase splitting and settling.	SCs followed the order thiophene < benzothiophene < dibenzothiophene. Sulfur extraction was only 46.7% and 36.7% after three time extractions with [OPy][BF <sub>4</sub> ] and [HPy][BF <sub>4</sub> ], respectively.
(Ko et al., 2008)	[BDMIIm]Cl/FeCl <sub>3</sub> [HDMIIm]Cl/FeCl <sub>3</sub> [HMIIm]Cl/FeCl <sub>3</sub> [HHIIm]Cl/FeCl <sub>3</sub>	The extraction was conducted at rt with the model oil containing 5000 ppm of DBT and 20000 ppm of <i>n</i> -octane as an internal standard in <i>n</i> -heptane. Weight ratio of model oil/IL 1/5 with molar ratio of FeCl <sub>3</sub> /[BDMIIm]Cl of 1, 2 and 5. Diesel oil with 1180 ppm of S was also used.	[BDMIIm]Cl/FeCl <sub>3</sub> and [BDMIIm]Cl/FeCl <sub>3</sub> in ratio higher than 2 (Lewis acidic ILs) shows quantitative extraction of SCs in model and real oil.
(Jiang et al., 2008)	[EMIM][DMP] [EEIM][DEP] [BEIM][DBP]	A straight-run gasoline was used. Before experiment, a concentrated IL solution with known S-content in mg(S) kg(IL) was prepared using gravimetric method by dissolving a definite amount of 3-MT, BT or DBT in a known quantities of IL, which was used as S-source in the following extraction experiments. K <sub>N</sub> was calculated.	For each S-component studied, the K <sub>N</sub> between IL and gasoline followed the order of [BEIM][DBP] > [EEIM][DEP] > [EMIM][DMP], and for a specified IL, the sulfur partition coefficient always followed the order of DBT > BT > 3-MT. The K <sub>N</sub> was significantly lower than that obtained with Lewis acidic IL containing AlCl <sub>3</sub> . A study for recovering of used ILs was made.
(Liu et al., 2008)	[BMIM][BF <sub>4</sub> ] [BMIM][PF <sub>6</sub> ] [BSAMIM]HSO <sub>4</sub> [BSAPy]HSO <sub>4</sub> [BSAEt <sub>3</sub> N]HSO <sub>4</sub> [BSAMIM]PTSA [BSAMIM]PTS PTSA: <i>p</i> -toluene sulfonic acid; PTS: <i>p</i> -toluene-sulfonate; BSA:	Extraction experiments were carried out at 60°C, mass ratio model oil/IL 4/1; extraction time 15 min; initial sulfur content, 500 ppmw. Effect of the extraction time, ratio gasoline/IL and regeneration of Sulfur-Loaded ILs was also studied.	1-(4-sulfonic acid) butyl-3-methyl-imidazolium hydrogen sulphate (52%) and 1-(4-sulfonic acid) butyl-3-methyl-imidazolium <i>p</i> -toluene-sulfonate (50%) were the best extractants.

Reference	ILs evaluated	Conditions of desulfurization	Observations
	4-butylsulfonic acid		
(Gao, et al., 2009)	3-MePy-based ILs	Experiments were conducted in a 50 mL flask. The mass ratios of ILs to model diesel or diesel fuel were 1:1 or 1:3. The ILs were added to the model diesel or diesel fuel, magnetically stirred for 15 min at room temperature to reach thermodynamic equilibrium, and then allowed to settle for 5 min to obtain phase splitting and settling.	The extractive performance followed the order of $[C8MPy][BF_4] > [C6MPy][BF_4] > [C4MPy][BF_4]$ . For real diesel (97 ppm), 60 % of sulfur removed was obtained after 3 steps of extraction at ratio 1:1 with $[C8MPy][BF_4]$ .
(Gao, et al., 2009)	$[BMIM]FeCl_4$	The mass ratios of ILs to model diesel or diesel fuel were 1:3. The ILs were added into model diesel or diesel fuel, magnetically stirred for 15 min at room temperature to reach thermodynamic equilibrium, and then laid aside for 5 min for phase splitting and settling.	40% of sulfur was removed after three extraction at 1:1 ratio at rt.

Table 2. Papers describing desulfurization of oils by liquid-liquid extraction using ILs.

Theoretical studies of desulfurization by ILs have also been carried out. Zhou, Mao and Zhang employing ab initio calculations using thiophene as model sulfur-containing compound and two ILs,  $[BMIM][PF_6]$  and  $[BMIM][BF_4]$ , according with the experimental results obtained by the same research group (Zhang and Zhang, 2002, Zhang et al., 2004, Su, et al., 2004).

The results showed that the interactions of thiophene with the anion and cation of the ILs mainly depends on electrostatic attractions. The absorption capacity of thiophene in the ILs is strongly dependent on the structure and property of the anion and the compactness between the cation and the anion of the ILs. For  $[BMIM][PF_6]$ , due to the strong electron donation of phosphor atom to fluorine atoms, the fluorine atoms in  $PF_6^-$  possess a relatively high negative charge and  $PF_6^-$  can also provide more native charged fluorine atoms to thiophene molecules compared with the  $BF_4^-$ . Moreover, the compactness degree of  $[BMIM]PF_6$  is lower than that of  $[BMIM]BF_4$ , which allows a facile restructuring of the IL in the process of thiophene dissolution (Zhou, et al., 2008).

Holbrey et al. studied the influence of structural aspects of the ILs in their performance as extractant of SCs. With varying classes (imidazolium, pyridinium, and pyrrolidinium) and a

range of anion types using liquid-liquid partition studies and QSAR (quantitative structure-activity relationship) analysis. The partition ratio of dibenzothiophene to the ILs showed a clear variation with cation class (dimethylpyridinium > methylpyridinium > pyridinium approximate to imidazolium approximate to pyrrolidinium), with much less significant variation with anion type. Polyaromatic quinolinium-based ILs showed even greater extraction potential, but were compromised by higher melting points (Holbrey et al., 2008). Very recently, a screening of ILs for the extraction of SCs with ILs employing for the first time a real sample of natural gasoline (highly volatile liquid recovered from natural gas and whose vapor pressure is between those of condensates and liquefied natural gas) was published. Desulfurizations with ILs have been focused on gasoline and diesel coming from FCC units.

In this study, the effect of the molecular structure of 75 ILs on the desulfurization efficiency of natural gasoline with high sulfur content was evaluated. Analysis indicated that anion played a more important role than cation on the desulphurization process. ILs based on halogen-ferrates and halogen-aluminates displayed the highest efficiency in sulfur removal, this becomes highly improved when there is an excess of metallic salt (Lewis acid ILs). Additionally, a method to recovery, regeneration and reuse of the water sensitive tetrachloroferrate ILs simple method to recover of the precursor halogenated IL was developed. A theory for predicting the ability of metallic ILs to remove SCs from NG, based on the ratio of the ionic charge to the atomic radius, is proposed.

In contrast to the results obtained by Holbrey et al., this study showed that under most drastic experimental conditions of evaluation (real system containing many hydrocarbons and more than 15 SCs). The extracting properties of an IL containing a  $\text{NTf}_2^-$  anion was very poor, yet any ILs containing an organic anion displayed good performance as sulfur removal. Only for Lewis acid ILs containing an anion with Fe, Al or Mo, extractions higher than 90% of SC were obtained. In these cases, the anion played the most important role on the IL efficiency (Likhanova et al., 2010). For this work, a Density Functional Theory study of the interaction between the most abundant SC in the studied sample of NG (ethanethiol) and Fe-containing ILs was studied.

The excellent performance of  $[\text{BMIM}][\text{FeCl}_4]$  to remove sulfur compounds from natural gasoline when exists an excess of  $\text{FeCl}_3$  was explain because the mixture contains  $\text{Fe}_2\text{Cl}_7^-$  anions, whose Fe-Cl-Fe bonds are larger and less strength than those in Fe-Cl of  $\text{FeCl}_4^-$  anions, being the former bonds actives for ethanethiol chemisorption. Molecular orbitals and atomic charges revealed the high desulfurization performance could be due to a donation-backdonation Dewar-Chatt-Duncanson-like model mechanism among sulfur of ethanethiol molecules and the metallic centers of  $\text{Fe}_2\text{Cl}_7^-$  anions, and this mechanism is promoted because of the symmetry relationship among molecular orbital of ethanethiol HOMO and the atomic  $d_{xy}$ -type orbital on Fe sites in  $\text{Fe}_2\text{Cl}_7^-$  LUMO (Martínez-Magadán et al., 2010).

### 3.2 Oxidative desulfurization of fuels using ionic liquids

The oxidative desulfurization (ODS) is another alternative of fuel desulfurization by liquid-liquid extraction, widely studied in the last years. This procedure consist in the oxidation of SCs to sulfoxides and sulfones or SCs are extracted from fuels and then oxidized in the extractant with the object of increasing their polarity and to make the liquid-liquid



extraction more efficient to remove SCs. Due to the short reaction time at ambient conditions, high efficiency, and selectivity, ODS combined with extraction, process known as is considered to be one of the most promising alternative processes to HDS for desulfurization of fuel. The oxidation process can be carried out without or with catalyst. In some case the ILs act as solvent for extraction but also as catalyst. One of its catalytic roles is to decompose hydrogen peroxide to form hydroxyl radicals.

The ODS system is more complicated process that the extraction of SCs in one step without oxidation, however with the former the efficiency of extraction generally increase considerably with the same IL at the same ratio, especially for water stable ILs.

Different ODS processes have used different oxidants such as molecular oxygen (Lu et al., 2007),  $\text{H}_2\text{O}_2$  in combination with polyoxometalate (Gao et al., 2006, Huang et al., 2007, Al-Shahrani et al. 2007), and acetic acid (Liu et al., 2009), ozone (Zaykina et al., 2004) and *tert*-butylhydroperoxide (Ishihara et al., 2005).

The extraction of oxidized SCs can be carried out using conventional volatile and toxic organic solvents, or using a combination of catalytic oxidation and extraction with ILs is regarded to the "green desulfurization system".

Lo, Yang & Wei (Lo et al., 2003) reported in 2003 the first procedure of ODS using ILs as extractant. In this paper tetradecane doped with DBT was used as model light oil for the investigation of sulfur removal. The ILs [BMIM]PF<sub>6</sub> and [BMIM]BF<sub>4</sub>, which are immiscible with light oils, were selected as solvents for the liquid-liquid extraction systems. DBT was extracted from the model light oils and oxidized in the ionic-liquid phase. The desulfurization system ( $\text{H}_2\text{O}_2$ -acetic acid/[BMIM]PF<sub>6</sub>). The oxidation of dibenzothiophene in [BMIM]PF<sub>6</sub> resulted in a high oxidation rate and the desulfurization process was more efficient than those using the same ILs as sulfur extractant without previous oxidation (Figure 3).

In a one-pot operation, the SCs in the light oils were extracted into ILs and then S-oxidized ( $\text{H}_2\text{O}_2$ -AcOH) to form the corresponding sulfones at 70 °C. The sulfur content of unoxidized light oil was 7370 and 7480 ppm in the presence of [BMIM]PF<sub>6</sub> and [BMIM]BF<sub>4</sub>, respectively; after 10 h of oxidation and extraction and ratio IL:hydrocarbon of 1:1. The sulfur content was reduced to 1300 and 3640 ppm, respectively. Thus, for a combination of oxidation and extraction with ILs, the use of [BMIM]BF<sub>4</sub> and [BMIM]PF<sub>6</sub> increased the desulfurization yields from 7 to 55% and 8 to 84%, respectively.

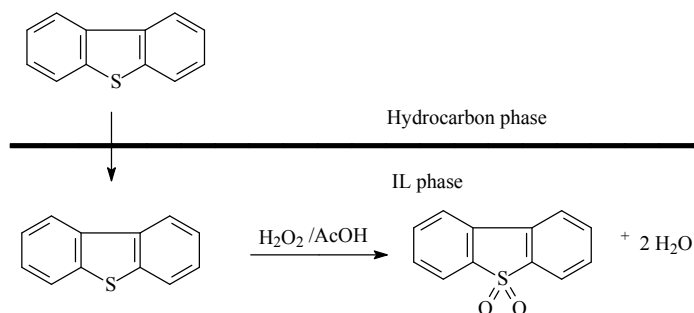


Fig. 3. ODS process using ILs as extractants.

When Brønsted acidic ILs 1-hexyl-3-methylimidazolium tetrafluoroborate [HMIM]BF<sub>4</sub> (Lu et al., 2007) and *N*-methyl-pyrrolidonium tetrafluoroborate [HNMP]BF<sub>4</sub> (Zhao et al., 2007) were used for desulfurization in the presence of H<sub>2</sub>O<sub>2</sub>, sulfur compounds can be deeply removed due to formation of hydroxyl radicals. For [HMIM]BF<sub>4</sub> the DBT remotion was 93% when a mixture of 3.2 mL of model oil and 5.0 mL of the IL were stirring at 90 °C during 6 h. In the case of [HNMP]BF<sub>4</sub> the efficiency of sulfur extraction was 99.4% for fuel diesel (total sulfur: 3240 ppm) at ratio of 1:1 and 2 h of reaction time at 60 °C. The IL was recycled 7 times without a significant decrease in desulfurization.

Some other published papers describing ODS procedures employing ILs are summarized in Table 3.

Reference	IL/catalyst/oxidizing agent	Conditions of desulfurization	Observations
(Huang et al., 2007)	Octadecyl-(STAB), cetyl-(CTAB), and tetradecyl-(TTAB), and dodecyl-(DTAB)/Phospho-tungstic acid (TPA)/30% H <sub>2</sub> O <sub>2</sub> .	DBT (500 ppm) in alkane. A certain amount of STAB and 0.06 g of TPA were added under vigorous stirring. 1 mL of 30% H <sub>2</sub> O <sub>2</sub> was dropped in and the oxidation reaction was started. Concentrations of the model sulfur compound in alkane were analyzed by HP-GC.	A conceptual model was established in the DBT oxidation process based on the interaction between TPA and STAB. It is suggested that the mass transfer of DBT from the organic media toward the interface, rather than the oxidized TPA phase transfer step, may be rate limiting.
(Zhu et al., 2007)	[BMIM]BF <sub>4</sub> or [OMIM]BF <sub>4</sub> or [BMIM]PF <sub>6</sub> or [OMIM]PF <sub>6</sub> /H <sub>2</sub> O <sub>2</sub> /WO(O <sub>2</sub> ) <sub>2</sub> .Phen.H <sub>2</sub> O	Model oil was prepared by dissolving DBT in <i>n</i> -octane to give solutions with a sulfur content 1000 ppm, (complex I) [WO(O <sub>2</sub> ) <sub>2</sub> .Phen.H <sub>2</sub> O], (complex II) [MoO(O <sub>2</sub> ) <sub>2</sub> .Phen]. The reaction conditions were as follows: <i>T</i> = 70 °C, <i>t</i> = 3 h, model oil = 5 mL, IL = 2 mL, [ <i>n</i> (DBT)/ <i>n</i> (catalyst) = 25], [ <i>n</i> (H <sub>2</sub> O <sub>2</sub> )/ <i>n</i> (DBT) = 10].	The ODS with 30 wt % H <sub>2</sub> O <sub>2</sub> in IL, model oil was 30.0-63.0%. While H <sub>2</sub> O <sub>2</sub> and catalyst were introduced together, the removal of sulfur increased sharply. In the case of the system containing H <sub>2</sub> O <sub>2</sub> , WO(O <sub>2</sub> ) <sub>2</sub> .Phen.H <sub>2</sub> O and [BMIM]BF <sub>4</sub> , extraction and catalytic oxidation increased the sulfur removal to 98.6%. However, the ODS for WO(O <sub>2</sub> ) <sub>2</sub> .Phen.H <sub>2</sub> O/H <sub>2</sub> O <sub>2</sub> was only 50.3% of sulfur removal in the absence of IL.
(Chan et al, 2008)	[BMIM]PF <sub>6</sub> /K <sub>2</sub> O-AcOH or [BMIM]PF <sub>6</sub> /H <sub>2</sub> O <sub>2</sub> -AcOH. K <sub>2</sub> O is a superoxide.	Experiments were carried out using, model gasoline, Diesel and fuel oil. IL was employed as PTC in ratio hydrocarbon/IL (2:1) solutions, once prepared, was continuously stirred with a	Using potassium superoxide as oxidant very similar desulfurization efficiencies in both model compounds and real diesel samples was achieved, with a significantly lower sulfur/oxidant ratio. In

Reference	IL/catalyst/oxidizing agent	Conditions of desulfurization	Observations
		magnetic stirrer in a 70 °C water bath and the oil and acid/IL phases were separated by a centrifuge. The oil phase was mixed with alumina powder for sulfone adsorption, and the sulfur content in the oil phase was measured.	comparison with H <sub>2</sub> O <sub>2</sub> potassium superoxide is safe and stable even in high purity. Less mass and less volume is required when using potassium superoxide as an oxidant, thus shipping, storage requirement, and volume of the reactor can be reduced significantly.
Cheng & Yen, 2008)	[BMIM]MeSO <sub>4</sub> /H <sub>2</sub> O <sub>2</sub> -trifluoroacetic acid	5 g of 500 ppm of model compounds of sulfides in mineral oil or <i>n</i> -dodecane is mixed with 5 g of 30% H <sub>2</sub> O <sub>2</sub> and 1.5 g of 20% trifluoroacetic acid and 0.3 g of tetraoctylammonium fluoride is introduced. The total ILs, [BMIM]MeSO <sub>4</sub> , are 5 g hydrocarbon/IL (1:1) The mixture was heated to 50 °C and under ultrasound for 10 min with subsequent stirring for 170 min.	In this work ultrasound-assisted oxidative desulfurization (UAOD) was employed to accelerate the oxidation process. The newly UAOD process was also used for desulfurization of Navy diesel (F-76) with a sulfur concentration of 4220 ppm. The overall sulfur removal was 100%.
(He et al., 2008)	[BMIM]BF <sub>4</sub> /Three peroxophosphomolybdates Q <sub>3</sub> {PO <sub>4</sub> [MoO(O <sub>2</sub> ) <sub>2</sub> ]} / H <sub>2</sub> O <sub>2</sub> where Q: [(C <sub>4</sub> H <sub>9</sub> ) <sub>4</sub> N] <sup>+</sup> , [C <sub>14</sub> H <sub>29</sub> N(CH <sub>3</sub> ) <sub>3</sub> ] <sup>+</sup> and [C <sub>16</sub> H <sub>33</sub> NC <sub>5</sub> H <sub>5</sub> ] <sup>+</sup>	The ODS experiments of the model oil (1000 of sulfur ppm as DBT in <i>n</i> -octane) were carried out with 0.00156 mmol of catalyst [ <i>n</i> (DBT)/ <i>n</i> (catalyst) = 100], 0.032 mL of 30 wt % H <sub>2</sub> O <sub>2</sub> [ <i>n</i> (H <sub>2</sub> O <sub>2</sub> )/ <i>n</i> (DBT) = 2] and the extracting solvent with IL (1 mL) was dissolved in the flask and then 5 mL of model oil (S = 1000 ppm) was added. The resulting mixture was stirred vigorously and heated to 70 °C in oil bath.	The S content in the model oil decreased from 1000 to 8 ppm, which was superior to the solvent extraction with ILs. The reactivity of sulfur compounds in the ECODS system decreased in the order of DBT > 4,6-DMDBT > BT. The catalyst with the short alkyl chain exhibited higher catalytic activity than that with the long alkyl chain. The deep desulfurization system containing [(C <sub>4</sub> H <sub>9</sub> ) <sub>4</sub> N] <sub>3</sub> {PO <sub>4</sub> [MoO(O <sub>2</sub> ) <sub>2</sub> ]} <sub>4</sub> , H <sub>2</sub> O <sub>2</sub> , and [BMIM]BF <sub>4</sub> can be recycled four times without significant loss of activity.

Reference	IL/catalyst/oxidizing agent	Conditions of desulfurization	Observations
Zhu et al., (2008)	[BMIM]BF <sub>4</sub> , [OMIM]BF <sub>4</sub> , [BMIM]PF <sub>6</sub> , [OMIM]PF <sub>6</sub> , [BMIM]TA and [OMIM]TA doped with the catalyst (such as Na <sub>2</sub> MoO <sub>4</sub> ·2H <sub>2</sub> O, H <sub>2</sub> MoO <sub>4</sub> , (NH <sub>4</sub> ) <sub>6</sub> Mo <sub>7</sub> O <sub>24</sub> ·4H <sub>2</sub> O, H <sub>3</sub> PMo <sub>12</sub> O <sub>40</sub> ·13H <sub>2</sub> O, (NH <sub>4</sub> ) <sub>3</sub> PMo <sub>12</sub> O <sub>40</sub> ·7H <sub>2</sub> O and Na <sub>3</sub> PMo <sub>12</sub> O <sub>40</sub> ·7H <sub>2</sub> O/H <sub>2</sub> O <sub>2</sub>	Model oil was prepared by dissolving DBT, BT and 4, 6-DMDBT in <i>n</i> -octane to give a corresponding sulfur content of 1000, 1000 and 500 ppm. The mixture, containing 5 mL of model oil, 0.064 mL of 30 wt% H <sub>2</sub> O <sub>2</sub> [ $n(\text{H}_2\text{O}_2)/n(\text{DBT}) = 4$ ], 1 mL of IL and catalyst [ $n(\text{S})/n(\text{Mo}) = 20$ ], was stirred vigorously at 70 °C for 3 h. The upper phase (model oil) was withdrawn and analyzed by GC-FID.	The S-removal of DBT containing model oil in [bmim]BF <sub>4</sub> could reach 99.0% at 70 °C for 3 h, which was the remarkable advantage of this process over the desulfurization by mere solvent extraction with IL or catalytic oxidation without IL. Moreover, the catalysts hardly dissolved in oil. The catalytic oxidation system containing Na <sub>2</sub> MoO <sub>4</sub> ·2H <sub>2</sub> O, H <sub>2</sub> O <sub>2</sub> and [bmim]BF <sub>4</sub> could be recycled five times without a significant decrease in activity and oxidized sulfur could be reclaimed by centrifugation.
(Xu et al., 2009)	[BMIM]BF <sub>4</sub> /V <sub>2</sub> O <sub>5</sub> , 30wt% H <sub>2</sub> O <sub>2</sub>	Experimental conditions: model oil = 5 mL, IL = 1 mL, [ $n(\text{DBT})/n(\text{V}_2\text{O}_5) = 20$ ], [ $n(\text{H}_2\text{O}_2)/n(\text{DBT}) = 6$ ], T = 30 °C, t = 4 h	In the described experimental conditions, 98.7 % of sulfur removal was obtained for model gasoline. [BMIM]BF <sub>4</sub> can be recycled seven times without a significant decrease in activity.
(Li et al., 2009)	[BMIM]BF <sub>4</sub> , [BMIM]PF <sub>6</sub> , [OMIM]BF <sub>4</sub> and [OMIM]PF <sub>6</sub> / H <sub>3</sub> PW <sub>12</sub> O <sub>40</sub> ·14H <sub>2</sub> O/ H <sub>2</sub> O <sub>2</sub>	The extraction and catalytic ODS was carried out with 5 mL of model oil, 0.048 mL of 30 wt % H <sub>2</sub> O <sub>2</sub> [ $n(\text{H}_2\text{O}_2)/n(\text{DBT}) = 3$ ], 1 mL of IL, and catalyst [ $n(\text{DBT})/n(\text{HPW}) = 100$ ], 30°C for 1 h .	At room temperature and short reaction time a commercially available H <sub>3</sub> PW <sub>12</sub> O <sub>40</sub> ·14H <sub>2</sub> O combined with H <sub>2</sub> O <sub>2</sub> and ILs [BMIM]BF <sub>4</sub> , [BMIM]PF <sub>6</sub> , [OMIM]BF <sub>4</sub> , and [OMIM]PF <sub>6</sub> is effective for removing DBT, 4,6-DMDBT, and BT.
(Kuhlman et al., 2009)	Several imidazolium phosphate IL were tested. Supported ILs phases (SILP) materials were also evaluated.	Dibenzothiophene/dodecane and butylmercaptan/ decane mixtures were used as model systems. Single-stage extractions reduced the sulfur content from 500 ppm to 200 ppm. In multistage extractions the sulfur content could be lowered to less than 10 ppm within seven stages.	SILP materials, obtained by dispersing the IL as a thin film on highly porous silica, reducing the sulfur content to less than 100 ppm in one stage. Multistage extraction with these SILP materials reduced the sulfur level to 50 ppm in the second stage. The SILP technology offers very

Reference	IL/catalyst/oxidizing agent	Conditions of desulfurization	Observations
		Regeneration of the IL was achieved by distillation or re-extraction procedures.	efficient utilization of ILs and allows application of the simple packed-bed column extraction technique.
(Seeberger & Jess, 2010)	[EMIM]DEP/ <i>n</i> -dodecane containing dibenzothiophene sulfone and real pre-desulfurized and completely oxidized Diesel	The efficiency of the extraction of S-compounds increases if the S-species are previously oxidized to the corresponding sulfoxides and sulfones. IL regeneration was also studied. Model oils containing single sulfones as well as real pre-oxidized diesel oils were investigated.	The evaporation of water from the IL is the crucial step with regards to the energy consumption of the process. The energy demand is comparable to classical HDS, if a multi-stage evaporation is used.

Table 3. Papers describing oxidative desulfurization of oils using ionic liquids.

Additional to the cited works, several other papers have been recently published about ODS using ILs as solvents (Lissner et al, 2009 Zhang et al., 2009), as catalysts (Li et al., 2009, Zhao et al., 2009, Gao et al., 2010) and in processes involving catalytic (b Li et al., 2009, Conte et al., 2009, Chao et al., 2010) and photochemical oxidation (Zhao et al., 2008).

Deep desulfurization processes using ILs without (Bosmann et al., 2003, Likhanova et al., 2009, Martínez-Palou et al., 2010, Guzmán et al., 2010) and with oxidating agent (Schoonover & Roger, 2006, Cheng, 2009) have also been patented, as such as, a method for the recovery of Lewis acid ILs after sulfur extraction (Guzmán et al., 2010).

In our considerations, in spite of the advances in the researches about the liquid-liquid extractions of SCs employing ILs, since the practical point of view, the industrial implementation of these technologies presents the following limitations:

- Many ILs show extractive properties of hydrocarbon contaminants (sulfurated and nitrogenated compounds), however much of these compounds required several extraction cycles for "quantitative" remotion of contaminants, even when in some cases a 1:1 ratio (IL/hydrocarbons) is required, it is, their extractive properties are very poor.
- The Nernst partition coefficient ( $K_N$ ) favors extraction of most aromatic components of the fuel oil and this can be a limitation of the extractive method.
- In many cases, the studies have been carried out with model feeds under laboratory scale. These obtained results are far from those under real conditions. The results should be validated at higher scale and with real samples.
- The most efficient ILs for desulfurization are water sensitive, Lewis acid ILs, which can be used in only one extraction cycle because they suffer decomposition after being used.
- In these extractive processes volumetric lost of hydrocarbons are produced, due to is difficult to achieve a exhaustive separation between phases, partial hydrocarbon dissolution in the ILs and because to a difference of HDS, in these extractive processes, the carbon and hydrogen atoms contained in the SCs are separated from the hydrocarbons feeds.
- The efficiency of the extraction of SCs for ODS procedures is high, however the synthetic process for the preparation of several efficient catalysts are generally

complicated and these catalysts are not commercially available. Very high volume of the oxidant and additional equipments are required.

Very recently, Kulkarni and Afonso published a critical review about deep desulfurization of diesel fuels using ILs where some additional references of this topic can be found (Kulkarni & Afonso, 2010).

### 3.3 Denitrogenation of gasolines

Another extractive process for increasing the efficiency of HDS process is the removal of nitrogenated compounds before the charges will be introduced in the HDS process to obtain ultralow sulfur hydrocarbons. It is well known that the selective removal of nitrogen compounds from the feeds before HDS strongly enhanced the further deep desulfurization, and increase the catalyst time of life because nitrogen compounds in the fuel and  $\text{NH}_3$  produced from them during hydrocarbon reforming process are poisons to the catalysts in hydrocarbon process and fuel cells; thus, the development of new approaches to reduce the nitrogen content in transportation fuel oils in order to meet the need of ultra-clean fuels for environmental protection and  $\text{H}_2$  production. (Laredo et al., 2001 and 2003).

The applications of ILs as extractants of *N*-containing compounds have also been studied for several researchers. Eßer et al. and Zhang et al., described for the first time in 2004, the ability of some ILs to remove nitrogenated compounds from hydrocarbons (Eßer et al., 2004, Zhang et al., 2004). Eßer et al. determined a high partition coefficient ( $K_N$ ) of 34  $\text{mg(N) kg(IL)}^{-1}/\text{mg(N) kg(oil)}^{-1}$  for an experiment with model oil containing 1000 ppm of *N* as indole in *n*-dodecane using  $[\text{BMIM}][\text{OCSO}_4]$ , while  $K_N$  were 0.7 and 2.9 for piperidine and pyridine, respectively.

Zhang et al. evaluated the adsorption capacities of *N*-containing saturated and non-saturated heterocyclic compounds and probed the extractive removal of both organonitrogen and organosulfur compounds for a model fuel (MF) consisted of *n*- $\text{C}_{12}$  with either DBT, pyridine, or piperidine, the IL removed 12% S (DBT) in *n*- $\text{C}_{12}$ , 45% N (pyridine) in *n*- $\text{C}_{12}$ , and 9% N (piperidine) in *n*- $\text{C}_{12}$  using  $[\text{BMIM}]\text{BF}_4$  (ratio IL/MF: 1/5). The amount removed from each model fuel is much less than the absorption capacity for the corresponding pure model compound by the ionic liquid, reflecting a partitioning of the model compounds in both the ionic liquid and the dodecane phases. The most effective extraction was the pyridine whose is fully miscible in the IL.

On the contrary of *S*-containing compounds, *N*-containing compounds can be very efficiently removed with chloride base-ILs (Fist generation ILs), which can be obtained in one-step synthesis, as have been demonstrated by Xie et al. (Xie et al. 2008 a and b)

In 2008, Xie et al. synthesized and evaluated four ILs with different carbon chain length and saturation of *N*-substituent groups: 1-butyl-3-methylimidazolium chloride ( $\text{BMIMCl}$ ), 1-allyl-3-methylimidazolium chloride ( $\text{AlMIMCl}$ ), 1-benzyl-3-methylimidazolium chloride ( $\text{BzMIMCl}$ ) and 1-octyl-3-methylimidazolium chloride ( $\text{OcMIMCl}$ ). The distribution coefficient of carbazole (CAR) and dibenzothiophene (DBT) between the ILs phase and the model fuel phase and the extraction selectivity of the ILs for CAR and DBT were determined using a dibenzothiophene and carbazole solution in toluene and *n*-decane as a model fuel. The results show that CAR has higher distribution coefficient than DBT in these ILs phases. The CAR distribution coefficients in  $\text{BMIMCl}$  and  $\text{AlMIMCl}$  are 46 and 14, and the selectivity of CAR/DBT is 125 and 38, respectively (c Xie et al., 2008).

Huh, et al reported on the use of Zn-containing imidazolium-based ILs bearing an alkylsulfate anion for the extraction of nitrogen compounds present in hydrocarbon mixtures at room temperature. The denitrogenation process was studied using a model oil containing 5000 ppm of quinoline and 20000 ppm of *n*-octane as internal standard in *n*-heptane. The performance of dialkylimidazolium alkyl sulfate IL for the extraction of basic nitrogen compounds, such as quinoline and acridine, was significantly improved up to more than 2 times.

Theoretical investigation on the interactions of  $\text{ZnCl}_2(\text{EtSO}_4)^-$  and  $\text{EtSO}_4^-$  with quinoline and indole were carried out at the B3LYP level of theory using Gaussian 03. Computational studies show that active Zn-containing anionic species, such as  $[\text{EMIm}]\text{ZnCl}_2(\text{EtSO}_4)$  and  $[\text{EMIm}]\text{ZnCl}(\text{EtSO}_4)_2$ , can be generated from the interaction of  $\text{ZnCl}_2$  with  $[\text{EMIm}]\text{EtSO}_4$ , and thus, the extraction of quinoline can be facilitated through the coordination of quinoline to the Zn center. The bonding mode of ethylsulfate ligand in  $\text{ZnCl}_2(\text{EtSO}_4)^-$  is changed from bidentate to monodentate for the coordination of quinoline, thereby retaining a tetrahedral environment around Zn.

The regeneration and reuse of the ILs was also investigated. Diethyl ether was found to be an efficient back extractant for the regeneration of  $[\text{EMIm}]\text{EtSO}_4\text{-ZnCl}_2$ , used for the denitrogenation of quinoline from the model oil, and to recover trapped quinoline in the IL (Huh et al., 2009).

Another strategy for separation of organic nitrogen compounds was by means supported liquid membranes based on 1-alkyl-3-methylimidazolium and quaternary ammonium salts ILs. Matsumoto et al. in 2006 showed the potential of these membranes for the separation process of organic nitrogen compounds and heptane. The organic nitrogen compounds selectively permeated the membranes.

The main difficult for this strategy is that when nitrogenated compounds are absent in the fuel HDS catalyst might start to deeply hydrogenate the feed, with the consequent high hydrogen consumption (Prins, 2001).

### 3.4 Separation of aliphatic/aromatic hydrocarbons

Aromatic compounds are other important contaminants in hydrocarbons mixture products. The feed stream of naphtha crackers may contain up to 25% aromatic hydrocarbons, which must be removed. In general these compounds are very toxic by inhalation and their evaporation into the atmosphere produce detrimental effects on the environment and human health. The presence of aromatic compounds in the feed to the cracker also has a negative influence on the thermal efficiency and tends to foul the radiation sections and the Transfer Line Exchangers.

The separation of these environmental pollutants (benzene, toluene, ethyl benzene and xylenes) from aliphatic hydrocarbon mixtures is challenging since these hydrocarbons have boiling points in a close range and several combinations form azeotropes.

The conventional processes for the separation of these aromatic/aliphatic hydrocarbon mixtures are liquid extraction, when the aromatic range is 20–65 wt.%, extractive distillation for 65–90 wt.% of aromatics and azeotropic distillation for more than 90 wt.% of aromatic content. Typical solvents used for the extraction are polar components such as sulfolane (Choi et al., 2002), *N*-methyl pyrrolidone (NMP) (Krishna et al., 1987), ethylene glycols (Al-Sahhaf et al., 2003) and propylene carbonate (Ali et al., 2003). A step of distillation for separating the extraction solvent is required.

For their negligible vapor pressure and low toxicity, ILs are, in theory, an excellent alternative for being used for the extraction of aromatic compounds by means an environmental friendly procedure and where the distillation step is not required. In 2001, Azko Novel patented a procedure for the extraction of an aromatic compound from an aliphatic phase using ILs (Shyu et al, 2001). To this point many papers have been published about studies of liquid-liquid equilibrium in mixtures of aliphatic and aromatic hydrocarbons (Letcher et al., 2003, Letcher et al., 2005) and in the last years spanish researchers have focused in these equilibria and in physicochemical aspects of two ternary systems comprising aliphatic/aromatic/ILs compounds (a-e. González et al., 2010, a- b. Pereiro et al., 2009, a-c. Arce et al., 2009, a-b. Arce, 2008, Alonso, 2008, a-b. García et al., 2008, García et al., 2010, a-b. Pereira, et al., 2010).

In 2005, Meindersma et al., found that several ILs are suitable for extraction of toluene from toluene/heptane mixtures. The toluene/heptane selectivities at 40 °C and 75 °C with ILs like [MeBuPy]BF<sub>4</sub>, [MeBuPy]CH<sub>3</sub>SO<sub>4</sub>, [BMIM]BF<sub>4</sub> (40 °C) and [EMIM]Tosylate (75 °C), are a factor of 1.5-2.5 higher compared to those obtained with sulfolane ( $S_{\text{tol/hept}} = 30.9$ ,  $D_{\text{tol}} = 0.31$  at 40 °C), which is the most industrially used solvent for the extraction of aromatic hydrocarbons from a mixed aromatic/aliphatic hydrocarbon stream, being [MeBuPy]BF<sub>4</sub> the most suitable, because of a combination of a high toluene distribution coefficient ( $D_{\text{tol}} = 0.44$ ) and a high toluene/heptane selectivity ( $S_{\text{tol/hept}} = 53.6$ ). Therefore, with [MeBuPy]BF<sub>4</sub> also extraction experiments with other aromatic/aliphatic combinations (benzene/*n*-hexane, ethylbenzene/*n*-octane and *m*-xylene/*n*-octane) were carried out, obtaining similar selectivities (Meindersma et al., 2005).

Also Meindersma & Haan presented a conceptual process design for the separation of aliphatic/aromatic hydrocarbons, in which the authors concluded that ILs which show a high aromatic distribution coefficient,  $D_{\text{arom}} = 0.6$  m/m, with a reasonable aromatic/aliphatic selectivity,  $S_{\text{arom/alif}} = 40$ , could reduce the investment costs of the aromatic/aliphatic separation to about M€ 25 to 30 and the annual costs to M€ 16 to 17 respect to total investment costs in the typically applied sulfolane extraction process (Meindersma & de Haan, 2007).

In 2006, Domanska et al. published a paper about the liquid-liquid equilibria in binary mixtures that contain a room-temperature IL and an organic solvents as [MMIM][CH<sub>3</sub>SO<sub>4</sub>], or [BMIM][CH<sub>3</sub>SO<sub>4</sub>] with an aliphatic hydrocarbon (*n*-pentane, or *n*-hexane, or *n*-heptane, or *n*-octane, or *n*-decane), or a cyclohydrocarbon (cyclohexane, or cycloheptane), or an aromatic hydrocarbon (benzene, or toluene, or ethylbenzene, or propylbenzene, or *o*-xylene, or *m*-xylene, or *p*-xylene) measured at normal pressure by a dynamic method from 270 K to the boiling point of the solvent and liquidus curves were predicted by the COSMO-RS method. For [MMIM][CH<sub>3</sub>SO<sub>4</sub>], the COSMO-RS results correspond. According with their results the solubilities of [MMIM][CH<sub>3</sub>SO<sub>4</sub>] and [MMIM][CH<sub>3</sub>SO<sub>4</sub>] in alkanes, cycloalkanes and aromatic hydrocarbons decrease with an increase of the molecular weight of the solvent and the differences of the solubilities in *o*-, *m*-, and *p*-xylene are not significant. By increasing the alkyl chain length on the cation, the upper critical solution temperature, UCST decreased in all solvents except in *n*-alkanes (Domanska et al., 2006).

In 2007, Cassol et al., found that the selectivity on the extraction of a specific aromatic compound is influenced by anion volume, hydrogen bond strength between the anion and the imidazolium cation and the length of the 1-methyl-3-alkylimidazolium alkyl side chain. The interaction of alkylbenzenes and sulfur heterocycles with the IL is preferentially through CH- $\pi$  hydrogen bonds and the quantity of these aromatics in the IL phase decreases with the



increase of the steric hindrance imposed by the substituents on the aromatic nucleus. Competitive extraction experiments suggest that benzene, pyridine and dibenzothiophene do not compete for the same hydrogen bond sites of the IL (Cassol et al., 2007).

The more relevant structural aspects of ILs (González et al., 2009 and a. González et al., 2010, Pereiro & Rodríguez, 2010), effect of the chain length of the aromatic ring (b. González et al., 2010), effect of the size of aliphatic hydrocarbons (c. González et al., 2010), and isomer effects (Arce et al., 2010) for their performance as aromatic extractants have been studied.

Very recently, a systematic study about the influence of structure of ILs on selectivity and capacity for aromatic/aliphatic hydrocarbons separation problem and *n*-hexane/hex-1-ene separation problem were reviewed. Analysis of cation and anion structure of the ILs and effect of the temperature on the selectivity and the capacity for aliphatics/aromatics and *n*-hexane/hex-1-ene separation problems was made. ILs based on imidazolium, pyridinium, pyrrolidinium, sulfonium, phosphonium and ammonium cations were taken into consideration. Analysis was made on the basis on activity coefficients at infinite dilution because this parameter is helpful for characterizing the behaviour of liquid mixtures, estimation of mutual solubilities, fitting the excess molar energy ( $G^E$ ) model parameters (e.g. Wilson, NRTL, UNIQUAC), predicting the existence of an azeotrope, analytical chromatography, calculation of Henry constant and partition coefficients, development of thermodynamic models based on the group contribution methods such as mod. UNIFAC. All the data utilized in this work were obtained from published literature available at the end of September 2009 and analysed by means a linear regression. According with the results the highest values of selectivity show ILs with less aliphatic character of the anion and the cation, e.g. based on following cations [MMIM]<sup>+</sup>, [EMIM]<sup>+</sup>, [ePy]<sup>+</sup>, [Et<sub>3</sub>S]<sup>+</sup> and with -CN group in the structure, like [CN-C<sub>3</sub>MM]<sup>+</sup>. Unfortunately always when the IL reveals high values of the selectivity, the capacity takes low values. The highest values of capacity have [NTf<sub>2</sub>]<sup>-</sup> and [FeCl<sub>4</sub>]<sup>-</sup> anions. As was shown most of ILs with high values of both selectivity and capacity is based on [NTf<sub>2</sub>]<sup>-</sup> anion. Details of specific structures and correlations of the ILs can be reviewed in this reference (Marciniak, 2010).

### 3.5 Removal of naphthenic acids from crude oil

Naphthenic acids are mixture of several cyclopentyl and cyclohexyl carboxylic acids, which are natural constituents in many petroleum sources. The main fraction contains carboxylic acids with a carbon backbone of 9 to 20 carbons. The naphtha fraction of the crude oil is oxidized and yields naphthenic acid. The composition differs with the crude oil composition and the conditions during refining and oxidation (Walter et al., 2002).

The presence of naphthenic acids in crude oil has a great influence tend to cause operational problems on petroleum refiners, such as foaming in the desalter or other units and carrying cations through the desalting process, which can cause deactivation of catalysts and corrosion problems.

Typically naphthenic acids are effectively removed from crude fractions by aqueous base washing (Varadaraj & Savage, 2000, Sartori et al., 2000), but serious emulsion problems are presented.

Chinese researchers proposed in 2008 a novel method to separate naphthenic acids from highly acidic crude oil by forming ILs. In this method, the basic character of imidazole heterocycle is utilized to prepare Brønsted ILs by acid-base reaction between imidazole and

naphthenic acids to form naphthenates ILs (Figure 4). Reagent recovery and naphthenic acids refining were also proposed (Shi et al., 2008).

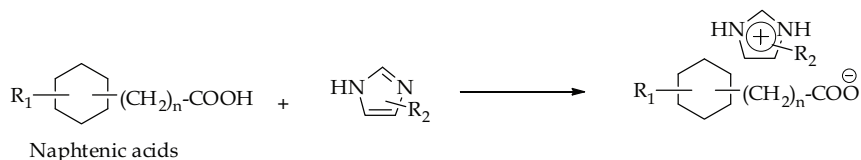


Fig. 4. ILs formation by acid-base reaction between naphtenic acids and alkylimidazole.

The effect of different imidazole derivatives and polar solvents were evaluated. The acid-removal rate was influenced by the 2-methylimidazole content, reagent/oil ratio, reaction time, and reaction temperature, all of which had a positive effect on the acid-removal rate. The reagent/oil ratio had a negative effect on the oil yield rate. High-purity naphthenic acids could be obtained in this process.

## 4. Ionic liquids in membrane technologies

### 4.1 Ionic liquids in membranes for selective gases separation

In Petroleum Industry several liquids and gases separations are highly required for gases purifications. Membrane technology can offer a competitive way of the off-gas treatment when the membrane able to work in the conditions of the power plant stack will be developed (Zhao et al., 2008), but maybe the main limitation of this process is the membrane stability especially at high temperatures due to solvent depletion through evaporation and long-term membrane performance.

By their very low vapor pressure, temperature stability, non-flammability and non-corrosively, ILs appear as an excellent alternative for membranes technology.

Efficiently separating CO<sub>2</sub> from H<sub>2</sub> is one of the key steps in the environmentally responsible uses of fossil fuel for energy production. Amines treatment is currently being used for separating CO<sub>2</sub> (Blauwhoff et al., 1984). This process is expensive due to high energy consumption at desorption stage and loss of the amine during the treatment and amine recovery (Rao & Rbin, 2002).

During the present century, a big number of studies have been performed to explore the prospects of ILs for gases separation and for founding the best prototypes for CO<sub>2</sub> capture (Bates et al., 2002, Baltus et al., 2004, Baltus et al., 2005, Shiflett & Yokozeki, 2005, Jacquemin et al., 2006, Hou & Baltus, 2007, . Schilderman et al., 2007, Yokozeki & Shiflett, 2007, Sánchez et al., 2007, Ventura et al., 2008, Shin and Lee, 2008, Shin et al., 2008, Li et al., 2008, Camper et al., 2008, Palgunadi et al., 2009, Soriano et al., 2008, Soriano et al., 2009, Condemarin & Scovazzo, 2009, Heintz et al., 2009, a, b. Carvalho et al., 2009, Kuleman et al., 2010, Shokouhi et al., 2010) and also several discoveries have been patented (Brennecke & Maginn, 2002 and 2003, Davis Jr., 2004, Chinn et al., 2006, Yu et al., 2008).

Oleffin/paraffin separation is other very important separation process in refineries. Propane produced in refinery operations often contains substantial amounts of propylene. Propylene may cause problems through engine and injector deposits when propane is used as a motor fuel. Also, propylene is capable of polymerizing in storage, fuel lines, or vaporizers, and thus may cause plugging by gum deposits. In this case the traditional separation technologies involving distillation (low-temperature and extractive distillation) and catalytic

hydrogenation (Bryan et al., 2004). Both processes are both energy and capital intensive because of the similarity in volatilities between olefins and their corresponding paraffins and by the high demand of hydrogen required in the case of the catalytical hydrogenation process. One of the most interesting strategies in membrane technologies are the Supported Liquid Membranes (SLMs). The first paper describing the application of ILs for SLMs was published in 1995 using quaternary ammonium salt hydrates (tetramethylammonium fluoride tetrahydrate,  $[(\text{CH}_3)_4\text{N}]\text{F} \cdot 4\text{H}_2\text{O}$ , or tetraethylammonium acetate tetrahydrate,  $[(\text{C}_2\text{H}_5)_4\text{N}]\text{CH}_3\text{CO}_2 \cdot 4\text{H}_2\text{O}$ , immobilized in films of Celgard 3401® (Quinn et al., 1995) and from this beginning a number of papers have increase exponentially in the following years until the present.

SLMs are porous membranes with the pores saturated with a solvent mixture. SLMs suffer significant solvent loss due to volatilization when conventional solvents are employed as supported liquid. The used of ILs as the immobilized phase within the pores of the membranes is the improving in the membrane stability and their performance do not depend of the water presence (a. Scovazzo et al., 2009). Supported ionic liquid membranes (SILMs) increase the efficiency and selectivity of gas separation respect to non-supported liquid membranes because the higher area of contact IL-gases.

Studies in SILMs are principally focused in  $\text{CO}_2$  capture especially from methane or nitrogen (For excellent recent reviews see: Hasib-ur-Rahman et al., 2010 and Bara et al., 2010) but also have been proposed for sulphur dioxide, carbon monoxide and hydrogen and olefin/paraffin, and water (dehydration) separation.

Several research group have proposed predictive correlations for gas solubilities in ILs (Camper et al., 2005, Kilaru et al., 2008, Kilaru & Scovazzo, 2008, Zhang et al., 2008, Carlisle et al., 2008, Sprunger et al., 2008, Lei et al., 2009) and gas diffusivities in ILs (Morgan et al., 2005, Camper et al., 2006, Hou & Baltus, 2007, Ferguson & Scovazzo, 2007, Condemarin & Scovazzo, 2009) based on their physico-chemistry properties.

In Table 4 several papers describing the applications of SILMs for gas separation are presented.

Reference	Selective separation studied	IL(s)/support(s) employed	Experimental Conditions	Observations
(Lee et al., 2006)	$\text{H}_2\text{S}/\text{CH}_4$ , $\text{CO}_2/\text{CH}_4$	ILs into poly(vinylidene fluoride)(PVDF) matrix.	Three types of feed gas ( $\text{CO}_2$ , $\text{H}_2\text{S}$ and $\text{CH}_4$ ) were permeated, at permeate pressure below 2 mbar, through the new SILMs using GPA-60 at feed $P = 2\text{--}5$ bar and $T = 35\text{--}65$ °C.	The membranes had excellent stability under sever operating conditions. The novel SILMs exhibited very high $\text{H}_2\text{S}$ , $\text{CO}_2$ permeability and $\text{H}_2\text{S}/\text{CH}_4$ and $\text{CO}_2/\text{CH}_4$ selectivities.
(Zhang et al., 2006)	$\text{CO}_2$ absorption	Tetrabutylphosphonium amino acid $[\text{P}(\text{C}_4)_4][\text{AA}]$ , where	$[\text{P}(\text{C}_4)_4][\text{AA}]$ was loaded in the porous silica ge by	No changes in absorption capacity and kinetics were found after four

Reference	Selective separation studied	IL(s)/support(s) employed	Experimental Conditions	Observations
		AA are amino acids, including glycine, L-alanine, L- $\beta$ -alanine, L-serine, and L-lysine/porous silica.	dopping method to enhance the absorption rate. CO <sub>2</sub> absorbed was determined by an analytical balance after absorption equilibrium in dry atmosphere (chemisorption of CO <sub>2</sub> ).	cycles of absorption/desorption. The CO <sub>2</sub> absorption capacity at equilibrium was 50 mol% of the ILs. In the presence of water (1 wt%), the ILs could absorb equimolar amounts of CO <sub>2</sub> . The CO <sub>2</sub> absorption in IL supported on silica is fast and reversible.
(Myers et al., 2008)	CO <sub>2</sub> /H <sub>2</sub>	bis(trifluoromethylsulfonyl)imide ([H <sub>2</sub> NC <sub>3</sub> H <sub>6</sub> mim][Tf <sub>2</sub> N])/cross-linked nylon	30 mL/min of feed (CO <sub>2</sub> (19.95 mole%), H <sub>2</sub> (20.01 mole%) and Argon (balance). 6-10 mL/min Ar passed of the permeate side of the membrane. Total pressure of 108 kPa for the feed.	Amine-functionalized IL based facilitated transport membrane with a selectivity maximum at 85°C.
(Huang et al., 2008)	Olefin/paraffin	[Ag(olefin) <sup>+</sup> Tf <sub>2</sub> N <sup>-</sup> ], olefin: 1-hexene, 1-pentene and isoprene, and Silver(I)/N,N-Dimethylbenzoamide [Ag(DMBA) <sub>2</sub> <sup>+</sup> Tf <sub>2</sub> N <sup>-</sup> ]/microporous alumina.	Experiments were carried out with IL membranes prepared by dropping 0.5 mL of IL on the top of the microporous alumina support and using a stainless steel permeation cell at 23 °C with an olefin/paraffin mixed gas. The feed pressure was 212 kPa.	[Ag(olefin) <sup>+</sup> Tf <sub>2</sub> N <sup>-</sup> ] and [Ag(DMBA) <sub>2</sub> <sup>+</sup> Tf <sub>2</sub> N <sup>-</sup> ] ILs exhibit excellent performance for olefin/paraffin separation. These ILs provided high permeability and good selectivity. The reversible interaction of olefins and silver ions in the [Ag(olefin) <sup>+</sup> Tf <sub>2</sub> N <sup>-</sup> ] was demonstrated.
(Kang et al., 2008)	Olefin/Paraffin (propylene/propane	[BMIM <sup>+</sup> BF <sub>4</sub> <sup>-</sup> ], [BMIM <sup>+</sup> Tf <sub>2</sub> N <sup>-</sup> ], and [BMIM <sup>+</sup> NO <sub>3</sub> <sup>-</sup> ] were employed to control	The ILs/Ag composite membranes were prepared by	The effect of ILs on the formation of a partial positive charge on the surface of silver

Reference	Selective separation studied	IL(s)/support(s) employed	Experimental Conditions	Observations
	mixtures)	the positive charge density of the surface of silver nanoparticles.	dispersing Ag nanopowder in ILs. For fabrication of the separation membranes, the mixed solution was coated onto polyester microporous membrane supports (Osmonics Inc., pore 0.1 $\mu\text{m}$ ) using an RK Control Coater. Gas flow rates were measured with a mass flow meter.	nanoparticle and its subsequent effect on facilitated olefin transport were investigated. A better separation performance for olefin/paraffin mixtures was observed with a higher positive charge density of the silver nanoparticles. It was therefore concluded that facilitated olefin transport was a direct consequence of the surface positive charge of the silver nanoparticles induced by ILs.
(Jiang et al., 2007)	SO <sub>2</sub> separation from	[EMIM]BF <sub>4</sub> [BMIM]BF <sub>4</sub> [BMIM]PF <sub>6</sub> [HMIM]BF <sub>4</sub> ([BMIM][Tf <sub>2</sub> N]/hydrophilic polyethersulfone	The SO <sub>2</sub> solubility in ILs in this study was also measured. The simulated flue gases were a mixture of N <sub>2</sub> and SO <sub>2</sub> with a SO <sub>2</sub> content of 8 % by volume at ambient pressure and at 40.0 °C. The gas stream was bubbled through about 3.5 g of IL and the flow rate was about 50 mL min <sup>-1</sup> .	The experimental results show that the SILMs not only offer very good permeability of SO <sub>2</sub> but also provide ideal SO <sub>2</sub> /CH <sub>4</sub> and SO <sub>2</sub> /N <sub>2</sub> selectivities up to 144 and 223, respectively. When compared to CO <sub>2</sub> in the tested SILMs, there is also over an order of magnitude increase in the permeability and selectivity of SO <sub>2</sub> .
(b. Scovazzo, 2009)	H <sub>2</sub> O/CH <sub>4</sub>	[EMIM][Tf <sub>2</sub> N], 1-ethyl-3-methylimidazolium dicyanamide ([EMIM]DCA), [EMIM]BF <sub>4</sub> and butyltrimethylammonium bis(trifluoromethanesulfonyl)-	Two procedures to investigate membrane performance changes due to H <sub>2</sub> O or CH <sub>4</sub> absorption were applied. The first procedure used nominal feed	SILMs have larger permeability coefficients that are constant with relative humidity. The initial evaluation of SILMs for dehumidification is that they are potentially competitive with polymer

Reference	Selective separation studied	IL(s)/support(s) employed	Experimental Conditions	Observations
		amide ([N(4)111][Tf <sub>2</sub> N])/hydrophilic polyethersulfone (PES)	absolute pressures of 1 bar (15 psi) and 2 bar (29.4 psi) of nitrogen. The procedure tested a series of feed relative humidities (rHs) from 0% to >90% at both nominal feed pressures. The second used nominal feed absolute pressures of 1 bar and 2 bar of methane for the [Tf <sub>2</sub> N]-membranes.	membranes. Water permeance does not change with relative humidity (rH). Methane permeance increases with increasing rH with the [Tf <sub>2</sub> N]-membranes having an increase of 20% and the water miscible [BF <sub>4</sub> ]-membrane having an increase of 110%.
(Park et al., 2009)	CO <sub>2</sub> /CH <sub>4</sub> , H <sub>2</sub> S/CH <sub>4</sub>	[BMIM]BF <sub>4</sub> /PVDF (poly vinylidene fluorolide)	Three types of feed gas (CO <sub>2</sub> , H <sub>2</sub> S and CH <sub>4</sub> ) were permeated, at permeate pressure below 2 mbar, through the new SILMs using GPA-60 at feed P = 2-5 bar and T = 35-65 °C.	The permeability coefficients of CO <sub>2</sub> and H <sub>2</sub> S were found to be considerably high at 30–180 and 160–1100 barrer, respectively. Moreover, the selectivity of CO <sub>2</sub> /CH <sub>4</sub> and H <sub>2</sub> S/CH <sub>4</sub> were found to be 25–45 and 130–260, respectively.
(Raeissi & Peters, 2009)	CO <sub>2</sub> /H <sub>2</sub>	1-alkyl-3-methylimidazolium bis(trifluoromethylsulfonyl)imide: [EMIM]NTf <sub>2</sub> , [BMIM]NTf <sub>2</sub>	Binary phase behaviour experiments were carried out Cailletet apparatus, which allows the measurement of phase equilibrium according to the synthetic method within temperatures and pressures up to 450 K and 15 MPa,	The experimental results indicated that CO <sub>2</sub> solubility is strongly dependent on temperature and pressure, decreasing with temperature and probably having an economically optimum mid-range pressure. Methane and carbon monoxide solubilities in [BMIM][Tf <sub>2</sub> N] fall in between those of H <sub>2</sub> and

Reference	Selective separation studied	IL(s)/support(s) employed	Experimental Conditions	Observations
			respectively.	CO <sub>2</sub> , and they have a linear relationship with pressure.
(b. Scovazzo et al., 2009)	CO <sub>2</sub> /CH <sub>4</sub> CO <sub>2</sub> /N <sub>2</sub>	[EMIM][BF <sub>4</sub> ], [EMIM][dca], [EMIM][CF <sub>3</sub> SO <sub>3</sub> ], [EMIM][Tf <sub>2</sub> N], and [BMIM][BETI].	Mixed-gas permeances and selectivities for the gas pairs CO <sub>2</sub> /CH <sub>4</sub> and CO <sub>2</sub> /N <sub>2</sub> using continuous flows of the mixed gases at various CO <sub>2</sub> concentrations (up to 2 bars of CO <sub>2</sub> partial pressure).	Three showed attractive mixed-gas selectivity combined with CO <sub>2</sub> -permeability for CO <sub>2</sub> /CH <sub>4</sub> separations. In addition, one of the tested membranes is, economically viable for CO <sub>2</sub> capture from flue gas.
(Shishatskiy et al., 2010)	CO <sub>2</sub> /N <sub>2</sub> , CO <sub>2</sub> /H <sub>2</sub>	Ammonium compounds obtained by reaction of (3-Aminopropyl)triethoxysilane, glycidyltrimethylammonium chloride in molar ratio of 1:1 (1N <sup>+</sup> ) and 1:2 (2N <sup>+</sup> ), blends with PEBAX® MH 1657, and products form hydrolysis of 1N <sup>+</sup> and 2N <sup>+</sup> in the presence of TEOS as co-monomer.	The diffusion, permeability and solubility of pure H <sub>2</sub> , He, N <sub>2</sub> , O <sub>2</sub> and CO <sub>2</sub> in dry membrane samples were measured at feed pressures 0.3–1.7 bar and temperatures 10–120 °C using a constant volume/variable pressure. The transport parameters of the same membranes in wet environment were determined on the constant volume/variable pressure, where feed gas stream was humidified to the water partial pressure close to the dew point at 23 and 60 °C.	1N <sup>+</sup> and 12N <sup>+</sup> in the form of blends with PEBAX® MH 1657 showed high CO <sub>2</sub> solubility coefficients and high CO <sub>2</sub> /N <sub>2</sub> (up to 1500) and CO <sub>2</sub> /H <sub>2</sub> (up to 1350) solubility selectivity. At low temperatures CO <sub>2</sub> was irreversibly absorbed in the quaternary ammonium compound and was released only at temperatures higher than 60 °C. Co-hydrolysis with TEOS at 60 °C was found to be an additional transition point giving for H <sub>2</sub> , N <sub>2</sub> , O <sub>2</sub> and CO <sub>2</sub> break on the solubility coefficient Arrhenius plots.

Reference	Selective separation studied	IL(s)/support(s) employed	Experimental Conditions	Observations
Simons et al., 2010	CO <sub>2</sub> /CH <sub>4</sub>	The polymerizable styrene-based 1-[(4-ethenyl phenyl) methyl]-3-alkyl-imidazolium bis (trifluoromethane) sulfonamide IL monomers with three different lengths of the alkyl substituent (methyl, n-butyl or n-hexyl)	The separation performance of the poly(IL) membranes was investigated with a temperature-controlled high pressure gas permeation setup using a constant volume-variable pressure method. A constant feed pressure was applied and during the measurement, the permeate side was kept under vacuum.	As opposed to regular glassy polymers, poly(ILs) do not show a minimum in permeation rates for CO <sub>2</sub> : the permeability increases continuously with increasing feed pressure. Non-plasticizing methane shows a pressure independent permeability.

Table 4. Papers describing the applications of supported ILs membranes for gas separation.

In 2009 Scovazzo published a significant paper where literature data obtained using the proposed model to predict gas solubility and gas permeability was summarized, along with adding new data, on the SILMs membranes permeabilities and selectivities for the gas pairs: CO<sub>2</sub>/N<sub>2</sub>, CO<sub>2</sub>/CH<sub>4</sub>, O<sub>2</sub>/N<sub>2</sub>, ethylene/ethane, propylene/propane, 1-butene/butane, and 1,3-butadiene/butane, with the object as to serve as guide for future researches in this area.

The data analysis predicts a maximum CO<sub>2</sub>-permeability for SILMs and an upper bound for permeability selectivity vs. CO<sub>2</sub>-permeability with respect to the CO<sub>2</sub>/N<sub>2</sub> and CO<sub>2</sub>/CH<sub>4</sub> separations. The analysis recommends a number of future investigations including studies into SILMs cast from ILs with smaller molar volumes.

According with Scovazzo's analysis, for CO<sub>2</sub>-separations, there are two critical ILs properties that effect SILM performance: molar volume and viscosity. The permeability selectivity is a function of IL molar volume while the CO<sub>2</sub>-permeability is a function of viscosity.

In the context of olefin/paraffin separations, the preliminary data is encouraging when considering the use of facilitated transport via silver carriers. Since IL-solvent/solvent interactions dominate interminating the overall SILM performance, past attempts at enhancing solute/solvent interactions via the addition of functional groups to the ILs have not produced SILMs with better separation performance compared to the unfunctionalized ILs. Future research into functionalized ILs needs to consider the changes to the dominant solvent/solvent interactions and not just the solute/solvent interactions (c. Scovazzo, 2009). Cserjesi and Belafi-Bako have published several papers about ILs membranes, especially for gas separations, which are discussed in details in other chapter of this book.



ILs with appropriated structure can polymerize via the cation and/or anion, forming solid films. This sence, several polyILs have also show a good performace for CO<sub>2</sub> capture (a-d.Tang et al., 2005, Hu et al., 2006, Bara et al., 2007, a, b. Bara et al., 2008, Tang et al., 2009). As example Bara et al. in 2008, after several works in developing polyILs for gas separation membranes, in 2008 published a paper about a second-generation of functionalized polyILs using imidazolium-based monomers containing either a polar, oligo(ethylene glycol) substituent and alkyl-terminated nitrile groups (C<sub>n</sub>CN) on the cation of imidazolium-based ILs, which contribute can have pronounced effects on gas separations in polymer membranes for improving CO<sub>2</sub> selectivity. Membranes were prepared via the photopolymerization of IL monomers with additional cross-linker (divinylbenzene) on porous supports. The nature of the polar substituent was significant impacts on the permeability of CO<sub>2</sub>, N<sub>2</sub> and CH<sub>4</sub>. OEG functionalities, when included in polyILs, produced membranes that were several times more permeable than those with C<sub>n</sub>CN functional groups. OEG-functionalized poly(ILs) exhibited CO<sub>2</sub> permeabilities on par with polyILs with *n*-alkyl groups, but with improved CO<sub>2</sub>/N<sub>2</sub> selectivities that exceeded the "upper bound" of the "Robeson Plot". CO<sub>2</sub>/CH<sub>4</sub> separation was also enhanced in each of these second-generation polyILs (c. Bara et al., 2008).

The nature of the polar substituent was significant impacts on the permeability of CO<sub>2</sub>, N<sub>2</sub> and CH<sub>4</sub>. OEG functionalities, when included in polyILs, produced membranes that were several times more permeable than those with C<sub>n</sub>CN functional groups. OEG-functionalized polyILs exhibited CO<sub>2</sub> permeabilities on par with polyILs with *n*-alkyl groups, but with improved CO<sub>2</sub>/N<sub>2</sub> selectivities that exceeded the "upper bound" of the "Robeson Plot". CO<sub>2</sub>/CH<sub>4</sub> separation was also enhanced in each of these second-generation polyILs.

## 4.2 Ionic liquids in selective liquid separations

ILs membranes are also being studied for the selective separation of liquids. Investigations on aliphatic/aromatic hydrocarbons, sulfur and nitrogen compounds separations have been carried out and will be presented in this section.

As was commented before the separation of benzene and cyclohexane is one of the most challenging processes in the chemical industry.

Because the characteristics of ILs are high surface tension and a lack of detectable vapor pressure, with the advantages of minimum loss of membrane liquid take place by the dissolution/dispersion effect, as well as by evaporation.

Pervaporation is a physical process that involves the separation of two or more components across a membrane by differing rates of diffusion through a thin polymer and an evaporative phase change comparable to a simple flash step. A concentrate and vapor pressure gradient is used to allow one component to preferentially permeate across the membrane. A vacuum applied to the permeate side is coupled with the immediate condensation of the permeated vapors. Pervaporation is considered a forward looking and modern membrane process for separation of various liquids or vapour mixtures.

Pervaporation, in its simplest form, is an energy efficient combination of membrane permeation and evaporation. It's considered an attractive alternative to other separation methods for a variety of processes (Smitha et al., 2004).

The potential of ILs in SILMs for pervaporation of solutes from aqueous mixtures was first demonstrated for Schaefer and coworkers (Schaefer et al., 2001), and Izák and coworkers (Izák et al., 2005, 2006 and 2009), however until now few paper about pervaporations using SILMs with potential applied in oilfield have been published.

With the object of prevent the loss of membrane liquids, Wang, Feng & Peng proposed a novel approach of SILMs in which vapor permeation with an IL filling-type supported liquid membrane replaces solvent extraction. The molecular diffusion coefficient is higher in ILs than in polymers, and the latter are often chosen as dense materials for the separation of organic liquids. According with the authors unlike solvent extraction, only a small amount of liquid is used to form SLMs, and the use of expensive ILs becomes economically possible. In this paper [BMIM][PF<sub>6</sub>] was studied as a membrane liquid for the separation of toluene/cyclohexane mixture, as a representative of aromatic and aliphatic hydrocarbons and the dehydration of aqueous 1-propanol and aqueous ethanol mixtures was also investigated with vapor permeation through SILMs.

A porous flat membrane made of poly(vinylidene fluoride) (PVDF) with a molecular weight cutoff of 150 kDa was used as the substrate to prepare de SILM. The affinity between the [MMIM][PF<sub>6</sub>] IL and the hydrophobic PVDF membrane resulted in a strong capillary force to hold the ionic liquid, so that the membrane liquid is stable even when the SLM is used under high-vacuum conditions.

For the separation of toluene/cyclohexane mixtures for a 550-h test, the permeation rate was determined by the aromatic component, and the separation factor reached 15-25 at 40 °C. Owing to the low organic solvent composition in the feed, the fluxes of the organic compounds were relatively small. When the same SLM was used for the dehydrations of aqueous 1-propanol and of aqueous ethanol, water was found to be the preferential permeation component (Wang et al., 2009).

In 2007, the application of the bulk liquid membrane technique is investigated for separation of toluene from *n*-heptane, using different imidazolium ILs (1-methyl-3-octyl imidazolium chloride, 1-ethyl-3-methyl-imidazolium ethyl sulfate, 1-methylimidazole hydrogen sulfate and 1H-imidazolium, 1-ethyl-4,5-dihydro-3-(2-hydroxyethyl)-2-(8-heptadecenyl) ethyl sulfate). Using silver ion as a carrier in membrane phase, batch wise extraction experiments were also carried out and the permeation rate and separation factor were determined by varying the operating parameters: the contact time, concentration of Ag<sup>+</sup>, stirring effect, initial feed phase concentration and temperature.

This study demonstrates that the use of [OMIM]Cl as a membrane solvent enables the bulk liquid membrane operation to be used for the separation of toluene from *n*-heptane. Although the permeation rates through the membrane based on [OMIM]Cl is low, the selectivity of toluene is high enough for the separation of toluene from *n*-heptane. Facilitated transport of toluene is also demonstrated using [OMIM]Cl membrane containing Ag<sup>+</sup> as the carrier. It has been found that Ag<sup>+</sup> concentration, stirring speed, initial toluene concentration in feed phase and temperature have a strong effect on permeation rate and separation factor (Chakraborty & Bart, 2007).

Matsumoto et al. have investigated the SILMs for selective separations since 2005 (Matsumoto, et al., 2005). In 2009, this group studied the vapor permeation of benzene/cyclohexane through SILMs based on 1-alkyl-3-methylimidazolium and quaternary ammonium salts. In this paper, the effects of ILs and the benzene fraction in the feed on the permeation flux and separation factor, and the stability of the SILMs was studied, founding that the sorption step mainly affected the separation factor depending on the hydrophilicity of the IL. The ammonium type IL *N,N*-diethyl-*N*-methyl-*N*-(2-methoxyethyl) ammonium tetrafluoroborate showed the highest selectivity of 47.1 for the mixed solution, gave the highest separation factor, 185 for 53 wt.% benzene and 950 for 11 wt.% benzene for the VP, which are superior to the previously reported values obtained by

pervaporation and the SILM was very stable after work over 1 month in steady flux without lot in their selectivity (Matsumoto et al., 2009).

Matsumoto and coworkers have begin to explored the application of SILMs for the selective permeation of organosulfur and nitrogenated compounds. They preliminary studies had demonstrated that SILMs has a good potential for the separation process of organic nitrogen and sulfur compounds from the fuels (Matsumoto et al., 2006 and 2007).

#### 4.3 Ionic liquids in membranes for fuel cells

Liquid-fuelled solid-polymer-electrolyte fuel cells are very promising as electrochemical power sources and have drawn immense attention as high-efficiency and low-emission power sources, for application in portable devices and automotive applications (Li, 2006). Fuel cells are an alternative power sources that could be a future substitutes of the hydrocarbons as energy source.

The performance of a polymer electrolyte membrane (PEM) fuel cell is significantly affected by liquid water generated at the cathode catalyst layer (CCL) potentially causing water flooding of cathode; while the ionic conductivity of PEM is directly proportional to its water content. Therefore, it is essential to maintain a delicate water balance, which requires a good understanding of the liquid water transport in the PEM fuel cells.

At present, the most commonly used humidified perfluorinated ionomer membranes, represented by Nafion, are limited to being used at temperatures lower than 100 °C because of the evaporation of water, which results in a rapid loss of conductivity. Nafion membranes are limited for practical application due to their high cost and high fuel crossover (Adjemian et al., 2002).

The ionic conductivity of PEM is significantly dependent on the membrane hydration. Inadequate membrane hydration results in high electrical resistance as well as the formation of dry and hot spots leading to membrane failure. The electroosmotic transport occurs due to the proton transport. Proton migrations drag water along with it from the anode side to the cathode side that can eventually reduce the membrane hydration and block the active reaction site in the CCL. Water transport process in a PEM fuel cell is a complex phenomenon, hence it is essential to make a delicate water balance for better and optimum fuel cell performance, and prevent material degradation (Das et al., 2010).

The operation of PEM at temperature higher 100 °C is receiving much attention because it could enhance reaction kinetics at both electrodes, improve the carbon monoxide tolerance of the platinum catalyst at the anode, and simplify heat and water managements of the fuel cells.

Many effort have been carried out in developing another polymeric membranes different than Nafion membranes with better performance and low cost and to enhance the water retention (Tezuka et al., 2006, Di Vona et al., 2008, Kim & Jo, 2010), and more resistant materials and with higher thermal stability, like inorganic/polymeric membranes have been evaluated (Triphathi & Shahi, 2008, Okamoto et al., 2010, Umeda et al., 2010, Pereira et al., 2010).

ILs are an interesting alternative for this purpose, due to their negligible vapor pressure, high thermal stability, and ionic conductivity ILs can increase the membrane hydration at higher temperatures and anhydrous proton conduction.

In principle, there are mainly two methods to prepare IL-based polymer electrolytes: one is doping of polymers with a selected IL (Ye et al., 2008, Subianto et al., 2009, Padilha et al.,

2010, Che et al., 2010), and another approach is via *in situ* polymerization of polymerizable monomers in an IL solvent (Susan et al., 2005).

With the main object to delay the release of the IL component, which may affect the long-term stability of the membranes, organic-inorganic composite membranes have been studied (Fericola et al., 2008, a-b. Lakshminarayana et al., 2010).

Yu et al. reported for the first time the preparation and polymerization of microemulsions that contain IL polar cores dispersed in polymerizable oil comprising surfactant-stabilized IL nanodomains.

They demonstrated the effectiveness of this method with methyl methacrylate, vinyl acetate, and *N,N*-dimethylacrylamide instead of styrene as a polymerizable oil to prepare the microemulsions containing IL polar cores, using a long acryloyloxy functionalized imidazolium type-IL (MAUM-Br). Phase diagrams show that all of these [Bmim][BF<sub>4</sub>]/vinyl monomer systems can form transparent and stable microemulsions when MAUM-Br (Figure 5) was used as surfactants.

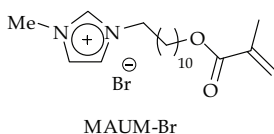


Fig. 5. Polymerizable surfactant used to prepare proton conducting membranes via the polymerization of microemulsions.

Polymerization of these IL-based microemulsions yielded free-standing, flexible, and transparent polymer electrolytes even though the resulting vinyl polymers are incompatible with IL cores. The obtained IL/polymer composites show high conductivity at both room temperature and elevated temperature (Yu et al., 2008).

In 2009, the same research group published the second paper in proton conducting membranes via the polymerization of microemulsions containing nanostructured Protic ILs (PILs) networks. PILs nanostructures formed in the precursor microemulsions could be preserved in the resultant polymeric matrix without macroscopic phase separation, even if the produced vinyl polymers are incompatible with PIL cores.

PLIs were synthesized by mixing of an imidazole derivative with equivalent molar amount of trifluoromethanesulfonic acid using newly the polymerizable surfactant MAUM-Br (Figure 6).

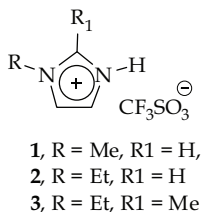


Fig. 6. Protic ILs employed to prepared proton conducting membranes via the polymerization of microemulsions.

These PIL-based polymer membranes have quite a good thermal stability, chemical stability, tunability, and good mechanical properties. Under nonhumidifying conditions, PIL-based

membranes show a conductivity up to the order of  $1 \times 10^{-1}$  S/cm at 160 °C, due to the well-connected PIL nanochannels preserved in the membrane (Yan et al., 2009).

## 5. Another applications

### 5.1 Ionic liquids as corrosion inhibitors

The use of corrosion inhibitors (CIs) constitutes one of the most economical way to mitigate the corrosion rate and to protect metal surface against corrosion and preserve industrial facilities (Sastri, 2008, Revie & Uhlig, 2008). The role of inhibitors added in low concentrations to corrosive media, is to delay the reaction of the metal with the corrosive species in the medium. The CIs act by adsorption of ions or molecules onto the metal surface. They generally reduce the corrosion rate by blocking of the anodic and/or cathodic reaction.

The treatment of mild steel corrosion through organic compounds has resulted in considerable savings to the oil industry. Several families of organic compounds, i.e. fatty amides (Olivares-Xometl et al., 2006 and 2008), pyridines (Abd El-Maksoud & Fouda, 2005, Ergun et al., 2008, Noor, 2009), imidazolines (García et al., 2004, Martínez-Palou et al., 2004, Olivares-Xometl et al., 2009, Liu et al., 2009) and other 1,3-azoles (Likhanova et al., 2007, Popova et al., 2007, Antonijevic et al., 2009) have showed excellent performance as CIs; however, the majority of these compounds are toxic and they are not in according with the environmental protection standards. By this reason, in the last years big efforts have been made by the researchers on this area to develop new environmental friendly CIs (Muthukumar et al., 2007).

ILs present a property structure suitable to absorb on metal surfaces and some compounds of the family had probed that they can form a protective coating over different metal surface again corrosive mediums as aqueous HCl [a-b. Zhang & Hua, 2009, Ashassi-Sorkhabi & Es'haghi, 2009) and H<sub>2</sub>SO<sub>4</sub> (Perez-Navarrete et al., 2010, Morad et al., 2008, Saleh & Atias, 2010).

Likhanova et al. have published recently a paper about the inhibitory action of 1,3-dioctadecylimidazolium bromide (ImDC<sub>18</sub>Br) and *N*-octadecylpyridinium bromide (PyC<sub>18</sub>Br) in 1 M H<sub>2</sub>SO<sub>4</sub> on mild steel at room temperature was investigated. The effect of the concentration of inhibitor compounds was investigated by electrochemical tests, whereas the surface analysis techniques were performed at 100 ppm for both compounds. In the case of ImDC<sub>18</sub>Br, corrosion products were additionally studied by X-ray diffraction and Mössbauer spectroscopy. The results revealed that ILs act as corrosion inhibitors with 82–88% at 100 ppm to protect the mild steel corrosion in the aqueous solution of sulfuric acid; their efficiencies are increased with the inhibitor concentration in the range 10–100 ppm. ImDC<sub>18</sub>Br provided a better inhibition effect than PyC<sub>18</sub>Br, which may be attributed to the larger esteric body of ImDC<sub>18</sub>Br in comparison to PyC<sub>18</sub>Br, which results in a higher surface coverage area during the chemical adsorption process. These compounds affected both anodic and cathodic reactions so they are classified as mixed type inhibitors. Chemisorption of these inhibitors on the mild steel surface followed the Langmuir's isotherm. SEM-EDX, XRD and Mössbauer analysis indicated the presence of carbon species and iron sulfates in the presence of ILs; whereas corrosion products such as iron oxyhydroxides were present in the absence of the ILs (Likhanova et al., 2010).

The same research group have submitted recently a paper en where five imidazolium-type ILs containing N1-insaturred chain and N3-long alkyl saturated chains as cation and bromide as anion were synthesized and evaluated as CIs for acid environment (Table 1). Weight loss test and electrochemical polarization technique were used to test the inhibitory properties of these compounds against AISI 1018 carbon steel corrosion in acidic media. These ILs showed inhibitory properties and the inhibition depends on the long chain size linked to N3, as was also evidenced by SEM/EDS and AFM images (Figure 7) (Guzmán-Lucero et al., 2010).

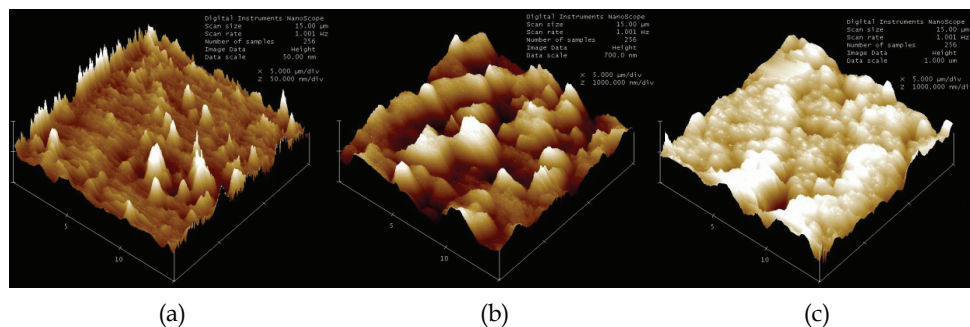


Fig. 7. Three-dimensional AFM images (at *data scale* = 50.0 nm) of (a) coupon after polish, (b) coupon after a 6 hour immersion in the corrosive media without inhibitor (at *data scale* = 700.0 nm), (c) coupon after a 6 hour immersion in the corrosive media containing 6 ppm of IL4 (at *data scale* = 1.0  $\mu\text{m}$ ).

ILs have also been employed to prepare a protective aluminium thin layer on carbon steel surface by electroreduction and electrodeposition of 1-butyl-3methyl-imidazolium chloroaluminate ( $\text{AlCl}_3/[\text{BMIM}]\text{Cl}$ ) (Caporali et al., 2008, Yue et al., 2009).

## 5.2 Ionic liquids as demulsifier agents

Crude oil containing brine generally results in the formation of stable water-in-oil (W/O) emulsions when turbulent mixing conditions are encountered during the transportation process. The dispersion of water droplets in oil is facilitated by the presence of interfacial active agents in the crude oil such as asphaltenes, waxes, resins and naphthenic acid (Schramm, 1992). The quantity of these natural emulsifiers is more abundant in heavy than in light crude oils and, thus, the formation of more stable emulsions in heavy crude oils (Kokal, 2005).

The crude oils should be desalted and dewatered before refining because salts produce enormous corrosion problems, they are poison for the catalysts in refining and reduce the efficiency of energy exchanging, and increase the oilflow resistance and even obstruct the pipes.

The process of desalting in Oil Refining Process usually involves addition 1–20% (w.) of wash water to the crude oil, mixing to form a W/O emulsion and then subjecting the emulsion to electrostatic demulsification or hydrocyclone treatment (Goyal, 1993, Varadaraj et al., 2001). Most crude oils that contain asphaltenes and naphthenic acids, especially heavy crude oils form marine environments trend to form stable W/O emulsions, which are complex scattered systems (Kumar et al., 2001).

Chemical demulsification by adding surfactant demulsifiers is still one of the most frequently applied industrial method to break the crude oil emulsions (Sjöblom et al., 2001). This process can be very difficult and non-efficient to demulsify W/O emulsions of heavy viscous crude oils, and it takes a long time.

Commercial demulsifiers are polymeric surfactants such as block copolymers of polyoxyethylene (EO) and polyoxypropylene (OP) (**1**) or alkylphenol-formaldehyde resins (**2**), or blends of different surface-active compounds and polyfunctionalized amines with EO/PO copolymer (**3**, Figure 8) (Kokal, 2005).

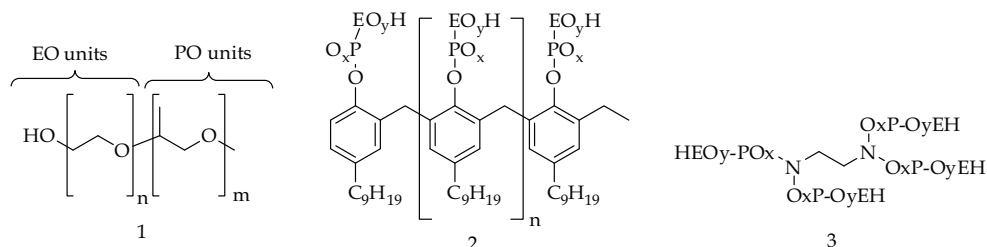


Fig. 8. Demulsifiers to break W/O emulsions.

The application of microwave irradiation to break a W/O emulsion was described for the first time in 1995 (Fang, 1995) and in the last decade has been studied by several research groups (Xia et al., 2002, a-b. Xia et al., 2004, a-c. Nour and Yunus, 2006, Fortuny et al., 2007). Recently, ILs were described as demulsifier agents for W/O emulsions. In this 2010 paper ten amphiphilic ILs were synthesized and evaluated as demulsification agents employing three emulsion of Mexican crude oils (medium: 29.59°API, heavy: 21.27 and ultra-heavy, 9.88°API). The ILs studied can act as demulsifiers in medium crude oils and, in some cases, in heavy crude oils at 1000 ppm after 10 hours of heating at 80°C. W/O emulsion from ultra-heavy crude oil was broken only by Trioctylmethylammonium chloride and its performance dramatically increased when it was carried out in conjunction with microwave irradiation (Guzmán-Lucero et al., 2010).

Lemos et al., investigated the role of two type of ILs ([OMIM]BF<sub>4</sub> and [OMIM]PF<sub>6</sub>) as demulsifier agents of high stable W/O emulsions in conjunction with microwave irradiation. The stable emulsion was prepared from a Brazilian crude oil (23.3° API) and distilled water or brine solutions ([NaCl] = 50 g.dm<sup>-3</sup>). The microwave experiments were always much faster and efficient than under conventional heating; however, Black test without ILs have not produce water separation, while the simultaneous use of ILs under microwave heating allows the demulsification with higher efficiency at shorter time (Lemos et al., 2010).

### 5.3 Ionic liquids-assisted biodiesel synthesis

Biodiesel is a mixture of fatty acid methyl esters (FAMES) which are produced from a broad range of crude oil materials, such as vegetable oil, animal fats, and waste oil, via transesterification of triglycerides with methanol or ethanol. Biodiesel has been regarded as a promising fuel to be able to partly substitute for conventional fossil diesel since it is obtained from renewable sources and for their environmental friendly properties like biodegradability and very low toxicity, lower particulate emissions and increased lubricity and provides a means to recycle CO<sub>2</sub> (Kim & Dale, 2005, Ryan et al., 2006).

The traditional route to perform the transesterification of triglycerides from vegetal oils, animal fats with an alcohol under homogeneous chemical catalysis at around 80 °C using a base (usually NaOH or KOH) or acid (generally H<sub>2</sub>SO<sub>4</sub>) as catalyst, but the application of these synthetic methods present environment problems such as corrosion and emulsification formation, difficulties to separate the catalyst from the final product and the generation of toxic effluents associated with these methodologies (Antolín et al., 2002). Some alternative to minimize these problems have recently been investigated, such as heterogeneous catalysts, enzymatic catalysis, application of organic bases, supercritical fluids, biphasic and multiphasic systems (Helwani et al., 2009).

The ILs could have several applications for biodiesel synthesis as described in Figure 9.

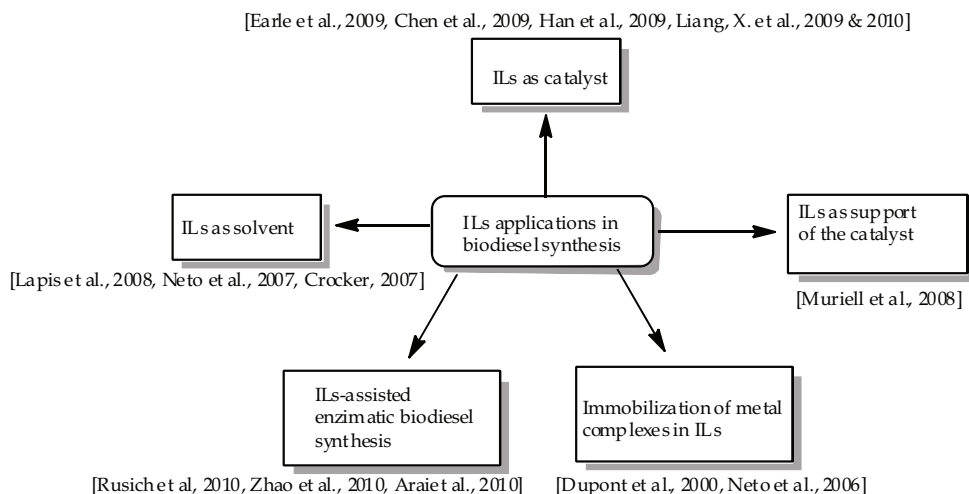


Fig. 9. Applications of ILs in biodiesel synthesis.

Wu et al. showed that some ILs could act as very efficient catalyst for the green synthesis of biodiesel. In this paper the transesterification of cottonseed oil with methanol to biodiesel was carried out in the presence of various Brønsted acidic ILs catalysts. 1-(4-Sulfonic acid)butylpyridinium hydrogen sulfate showed the best catalytic performance, confirmed that the catalytic activity of the ILs is dependent on its Brønsted acidic strength. Increased Brønsted acidity gave improved catalytic activity. Compared with conventional liquid and solid acid catalysts, ILs exhibit many outstanding advantages, such as high catalytic activity, excellent stability, easy product isolation, and environmental benefits. Brønsted acidic ILs have potential application in the production of biodiesel (Wu et al., 2006 and 2007). After this work, some other papers describing the catalytic effect of the ILs have been published as was described in Figure 9.

The catalysis of ammonium-based protic and Brønsted ILs for biodiesel synthesis under microwave dielectric heating has been investigated. Ammonium-based ILs. According with



the results, biodiesel can be obtained very fast and with high purity using these ILs. The application of microwave dielectric heating in conjunction with ILs as catalyst not only reduces considerably reaction time and simplifies the reaction handling, but also permits the access to an environmental friendly procedure for biodiesel production (Flores et al., 2010). In addition to the known application of ILs as solvent for chemically catalyzed transesterification, ILs can act as a solvent in enzymatic synthesis to enhance the dissolving of reactants and as an immobilization agent for enzymes, such as lipase. The IL forms a strong ionic matrix, therefore creating an adequate microenvironment for the catalyst to remain active.

Ha et al. screened several types of ILs in a lipase-catalyzed transesterification reaction using soybean oil and methanol. Results indicated that the use of hydrophobic ILs, yielded higher percent conversions as compared to solvent-free systems (Ha et al., 2007).

Very recently Ha et al. studied the continuous production and *in situ* separation of biodiesel using ILs through immobilized *Candida antarctica* lipase-catalyzed methanolysis of soybean oil. A screening of twenty three ILs was carried out, obtaining the best results with [EMIM]TfO after 12 hours at 50 °C. The production yield of 80% was eight times higher compared to the conventional solvent-free system (Ha et al., 2010).

Ruzzi and Bassi introduced the use of methyl acetate as the acyl acceptor in the place of the more commonly used methanol due to the negative effects methanol and the glycerol by-product has on lipase enzyme activity. The results of this research indicated that biodiesel was successfully produced, with an 80% overall biodiesel yield in the presence of [BMIM]PF<sub>6</sub>, at a 1:1 ratio (v/v) to the amount of oil and the addition of IL facilitated the separation of the methyl esters from the triacetyl glycerol by-product (a. Ruzich & Bassi, 2010).

The same authors, had investigated different reactor configurations for biodiesel production from triolein. These included shake flask or 500 mL jacketed conical reactors with two different configurations. Recycling and reuse of the lipase and IL was also examined, as well as the separation of products (b. Ruzich & Bassi, 2010).

Bioethanol is also a biofuel with high perspectives of wide application as non-fossil fuel, since it has a high octane and their use reduces the green house gas emission. Bioethanol can be produced from cellulosic materials. Pretreatment of cellulosic materials is a prerequisite to facilitate the release of sugars from a lignocellulosic biomass prior to fermentation recovery of bio-digestible cellulose from a lignocellulosic byproduct. Recently, some pretreatment methods have been tried with ILs which has showed a considerable increase in hydrolysis rate respect with the process without ILs and to develop an efficient process to recovery of bio-digestible cellulose from a lignocellulosic byproduct (Clark et al., 2009, Nguyen et al., 2010, Jones & Vasudevan, 2010, Bose et al., 2010, Yang et al., 2010, Simmons et al., 2010).

#### 5.4 Ionic liquids as catalyst of alkylation gasolines

One of the most important reactions in the petroleum industry is the isoparaffin-olefin alkylation for producing alkylated gasoline with a high content of isooctane (Albright, 2009). This process is industrially carried out employing an acid catalyst, in most of the cases sulfuric or hydrofluoric acid, because the reaction is quick, clean and with high yield of alkylated gasoline (Olah & Molnar, 1995). The general reaction to obtain alkylated gasolines is showed in Figure 10.

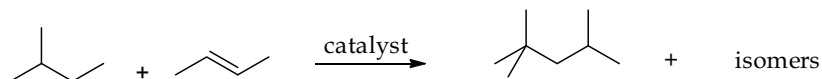


Fig. 10. Scheme of isoparaffin-olefin alkylation reaction.

Alkylated gasoline is a high-quality product from oil industry. The alkylate contains no olefins or aromatics but consists exclusively of isoalkanes. It has a low vapor pressure and a high octane number. In several time this gasoline contains fluoride traces due to inefficient catalyst remotion (Corma & Martínez, 1993).

The HF is a good and cheap catalyst for isobutene alkylation, however its use caused significant concern because its high vapors pressure and tendency to form aerosol. The fluoride anion is highly toxic and ecological problems are generated when fluoride is not completely removed after the alkylation reaction (Weitkamp & Traa, 1999).

Many efforts have been made to introduce new developments relating to established technologies and properly new technologies (Hommelt, 2001) and other catalysts have been evaluated as alternative for this process, such as solid materials like zeolites and Lewis and Brønsted acid in different solid supports (Feller et al., 2003, Feller et al., 2004, Feller & Lercher, 2004, Platon & Thomson, 2005, Thompson & Ginosar, 2005, Guzmán et al., 2006), heteropolyacids (Zhao et al., 2000) and Nafion silica nanocomposite (Kumar et al., 2006, a-b, Shen et al., 2010).

ILs being environmentally benign reaction media, open up exciting challenges and opportunities to clean catalytic processes. Since 1994, Chauvin et al. suggested the idea of employ Lewis acidic ILs as an alternative catalyst for alkylation reaction (Chauvin et al., 1994), but after this first effort several paper describing the application of supported and non-supported ILs catalysts have been published (Huang et al., 2004, Yoo et al., 2004, Kumar et al., 2006, Zhang et al., 2007, Tang et al., 2009).

Frech Petroleum Institute has applied acidic chloroaluminates ILs for the alkylation of isobutane with 2-butene or ethylene in a continuous-flow pilot plant operation, showing that [pyridine,HCl]/AlCl<sub>3</sub> (1:2 molar ratio) was the best catalyst in the case of ethylene. The reaction can be run at room temperature and provides good quality alkylate (2,3-dimethylbutane is the major product) over a period of 300 h with a Motor Octane Number (MON) of 90-94 and a research octane number (RON) of 98-101. In the case of butenes, a lower temperature and a fine tuning of the ILs acidity are required to avoid cracking reactions and heavy by-product formation. The continuous butene alkylation has been performed for more than 500 h with no loss of activity and stable selectivity (80-90% isooctanes are obtained containing more than 90% trimethylpentanes (TMP); MON = 90-95; RON = 95-98) (Olivier-Bourbigou, 2005).

Chinese researchers from Petrochina and China University of Petroleum, developed a very efficient process called "Ionokylation" for gasoline alkylation using a mixture of chloroaluminate-IL with CuCl as catalyst. The process was compared with the typical processes catalyzed by HF and H<sub>2</sub>SO<sub>4</sub> showing significant advantages and higher RON, MON and trimethylpentanes content was obtained. Ionikylation was probed at pilot plant scale demonstrated the high stability of this catalyst through 8 months ageing test before 60 days of operation. The alkylation reaction was performed at 15 °C and 0.4 MPa. During the pilot test period, olefin conversion was more than 99%. The C8 yield in alkylate gasoline was higher than 95% and the yield of TMP was 90%.

Another interesting alternative of new environmentally safe for isobutane-olefin alkylation was developed by Olah et al. They developed an immobilized liquid and solid modified HF catalysts. Being ionic complexes of amines and anhydrous HF, the IL compositions are efficient media and HF equivalent catalysts for alkylations. They decrease the volatility of anhydrous HF and as a result, HF release to the atmosphere in case of accidents is decreased allowing easy neutralization. The handling, use, recycling and regeneration of the catalysts are convenient. Both the liquid and solid polymer based poly(hydrogen fluoride) catalysts (Figure 11) in a ratio 22:1 of HF:pyridine can be advantageously applied in alkylation process representing environmentally benign and safer conditions readily adaptable to the existing refinery alkylation units (Olah et al., 2005).

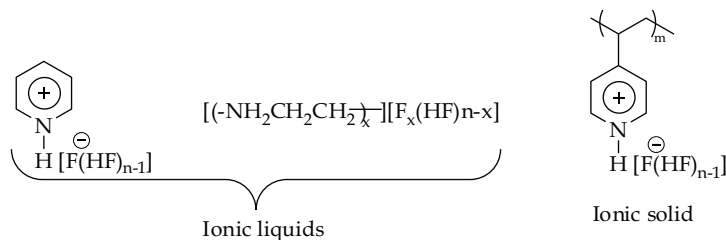


Fig. 11. Structure of liquid and solid polymer based poly(hydrogen fluoride) studied by Olah et al.

More recently the catalytic performance of 1-n-octyl-3-methylimidazolium bromide aluminium chloride ( $[OMIM]Br-AlCl_3$ ) based ILs was investigated for the alkylation of isobutane and 2-butene. The acidity of the IL was modified by addition of water, acid cation exchange resins or 1-(4-sulfobutyl)-3-methylimidazolium hydrogensulfate  $[(HO_3SBu)MIM]HSO_4$ . The activity, selectivity and deactivation behaviour with and without additives were studied in order to find the best catalytic composition. According to their results, the  $[OMIM]Br/AlCl_3$ /Amberlyst-15 resin (surface acid concentration: 0.11 meq.) catalyst yielded trimethylpentanes (up to 64%) and thus a high RON up to 96, higher than that with  $H_2SO_4$  as the alkylation catalyst. Thus, the approach to control the Brønsted acidity by forming superacidic IL species or superacidic species in ILs *via* protic additives is promising. In all cases, the products were separated simply by decantation, and thus the catalyst can be reused. Moreover, the formation of acid soluble heavy hydrocarbons is minimised (Thi et al., 2009).

### 5.5 Ionic liquids in other catalytic processes

ILs have been explored as solvents and catalysts in different petrochemical processes. Several examples of catalysis in both, homogeneous and biphasic reactions using supported ILs have been published. In Table 3, some recent results described in the scientific literature are shown.

Recently Olivier-Bourbigou published an excellent review about ILs as solvent and catalysts for chemical industry, including petrochemical processes where these topics are discussed in details (Olivier-Bourbigou, 2010).

Reference	ILs employed	Application	Observations
(Atkins et al., 2002)	Chloroaluminate ILs as liquid acid catalyst	Ethylbenzene production. Alkylation of benzene with ethylene	This biphasic alternatives led to the use of chloroaluminate ILs based on imidazolium cation (ex: [EMI][Cl]/AlCl <sub>3</sub> or [HNMe <sub>3</sub> ][Cl]/AlCl <sub>3</sub> in a 1:2 molar ratio). In a very detailed study based on bench-scale experiments.
(Olivier-Bourbigou & Lecocq, 2003)	Chloroaluminate ILs and Ni(COD)(2) with a Brønsted acid ILs	Biphasic ethylene oligomerization or butene and higher olefins dimerization (Difasol™ process).	These solvents stabilize and activate nickel catalysts, even without ligand, and greatly enhance the reaction activity. The presence of a diimine ligand allows the production of C <sub>4</sub> -C <sub>6</sub> linear olefins with improved alpha-selectivities.
(Zubin et al., 2007)	Three type of Chloroaluminate ILs from hydrochloride of Et <sub>3</sub> N, BuPy and BMIM as cation were evaluated as acid catalyst	Olefin reduction in FCC gasoline	The olefin content was reduced in more than 30% after 30 minutes under mild conditions in a ratio IL/oil of 20/100 (w/w).
(Lecocq & Olivier-Bourbigou, 2007)	Chloroaluminate ILs	Biphasic Ni-Catalyzed Ethylene Oligomerization in ILs	Chloroaluminate ILs are highly active catalysts either for the biphasic ethylene oligomerization or for polymerization depending on the bulkiness of the diimine ligand. The activation of Ni(0) with a Brønsted acid in different non-chloroaluminate ILs is also reported. The nickel catalysts are immobilized and stabilized in the ILs and can be recycled.
(Schmidt et al., 2008)	N-butyl-N-methylimidazolium tetrachloroaluminate on silica	Olefins disproportionation	Acidic ILs absorbed on silica could potentially catalyze disproportionation reactions more selectively at more favorable conditions.

Reference	ILs employed	Application	Observations
			At low temperatures, silica-supported ILs disproportionated $iC_5$ attaining up to 65 wt % feed conversion. The optimal temperature operating window was narrow between 80 and 130 °C.
(Magna et al., 2009)	The Brønsted acidity level was evaluated for ILs by means UV: [BMIM] similar to [BHIM] similar to [HNEt <sub>3</sub> ]), whereas changing the nature of the anion of the ionic liquid may lead to very different acidities ([SbF <sub>6</sub> ] > [PF <sub>6</sub> ] > [BF <sub>4</sub> ] > [NTf <sub>2</sub> ] > [OTf]).	Selective Isobutene Dimerization	By an adequate choice of the IL, selectivity for isobutene dimers can reach 88 wt% (at 70% isobutene conversion) with possible recycling of the catalytic system without loss of activity and selectivity. The "acidity scale" was tentatively compared with an "activity scale" obtained for the dimerization of isobutene into isooctenes.
(Gilbert et al., 2009)	EtAlCl <sub>2</sub> /AlCl <sub>3</sub>	Olefine dimerization by Difasol™ process, a biphasic analogue of the Dimersol-X™ process	The Difasol™ process produces mixtures of low branched octenes which are good starting materials for isononanol production (intermediates in the plasticizer industry). The reaction takes place with nickel catalyst precursor using chloroaluminate ILs, acting as both solvent and co-catalyst. The best results were obtained from [BMIM][Cl]/AlCl <sub>3</sub> /EtAlCl <sub>2</sub> (1:1.2:0.11) mixtures.

Table 5. Application of ILs in other catalytic processes.

### 5.6 Ionic liquids as hypergolic fuels

A mixture of two compounds (fuel-oxidizer) is called hypergolic when the propellants ignite spontaneously on contact. The terms "hypergolic propellant" are often used to mean the most common propellant combination, hydrazine/dinitrogen tetroxide or similar. Hypergolic rockets do not need an ignition system.

Hydrazine and its derivatives such as monomethylhydrazine and unsymmetrical dimethyl hydrazine have been extensively studied as hypergolic fuel, but these substances are highly

toxics, corrosives and difficult to handles. For these reasons, it is desirable to replace hydrazine derivatives with greener hypergolic fuels.

The design and synthesis of ILs based on energetic materials provide a powerful methodology in the development of a new type of hypergolic fuel. A variety of multinitrogenated ILs have showed good candidates as hypergolic fuels such as, methylated derivatives of hydrazinium azides (Hammerl et al., 2001), Urotropinium salts with nitrogenated conter ions (Fraenk et al., 2002), triazolium and tetrazolium-based ILs (Galvez-Ruiz et al., 2005, Singh et al., 2006), ILs containing azide and dicyanamide anions (a-c. Schneider et al., 2008,), ILs containing 2,2-dialkyltriazanium cation (Gao et al., 2009), nitrocyanamide derivatives (He et al., 2010), *N,N*-Dimethylhydrazinium (a. Zhang et al., 2010).

Joo et al., have also synthesized new azide-functionalized ILs like II and III by metathesis reaction from bis(2-azidoethyl)dimethylammonium iodide (I) as candidates to replace the highly toxic hydrazine and its hypergolic derivatives (Figure 11). The relationship between their structures and melting points, thermal stabilities, densities, standard enthalpies of formation, and specific impulse was determined. The high heat of formation of the azide functional group can be used for fine-tuning the energy content, and thus the performance of the hypergolic ILs (Joo et al., 2010).

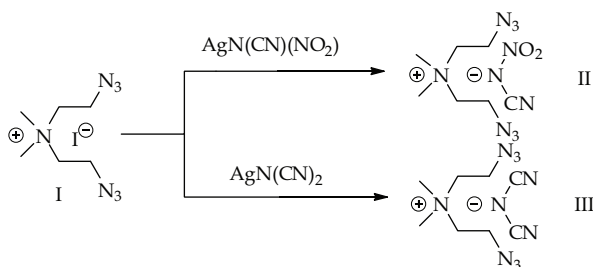


Fig. 11. New azide-functionalized hypergolic ILs.

The interesting properties of the hypergolic ILs have motivated a theoretical studies based on Density Functional Theory (Gao et al., 2007, b. Zhang et al., 2010). Heats of formation coupled with densities can be used further for predicting the detonation pressures and velocities and specific impulses of energetic salts for the rational design of hypergolic ILs.

## 6. Conclusions y future perspectives

Evidently ILs shows very attractive properties for their application in Petroleum Industry and in renewable energy sources. From this stands ILs have a good chance of becoming the process of choice in the future for different application; however, in many cases a long way is necessary to road for utilizing these technologies in industrial scale.

From an academic point of view, many applications using ILs results very attractive; however, in practice such results are difficult to apply for many reasons, such as economy, product disponibility, ILs stability, lost of activity during recycling and additional equipments required.

Several factors have made it difficult to introduce a new technology because new equipments and significant process engine changes are required and also because the economically competitive new technology has not been demonstrated. No matter how environmentally friendly or safe a new technology may be, it has to be economically competitive as well as reliable.

For the industrial use of ILs, some major issues must be addressed such as IL synthesis scale-up, purity, stability, toxicity, recycling, disposal and price and may constitute barriers to IL process commercialisation. The IL price must be related to the process performance and to overall economy.

## 7. References

- Abd El-Maksoud, S. A. & Fouda, A. S. (2005). Some pyridine derivatives as corrosion inhibitors for carbon steel in acidic medium. *Mat. Chem. Phys.*, 93, 84-90, ISSN 0254-0584.
- Adjemian, K. T.; Lee, S. J.; Srinivasan, S.; Benziger, J. & Bocarsly, A. B. (2002). Silicon oxide Nafion composite membranes for proton-exchange membrane fuel cell operation at 80-140 degrees C. *J. Electrochem. Soc.*, 149, A 256- 261, ISSN 0013-4651.
- Albright, L. F. (2009). Present and future alkylation processes in refineries. *Ind. Eng. Chem. Res.*, 48, 1409-1413, ISSN 0888-5885.
- Ali, S. H.; Lababidi, H. M. S.; Merchant, S. Q. & Fahim, M. A. (2003). Extraction of aromatics from naphtha reformates using propylene carbonate. *Fluid Phase Equilib.* 214, 25-38, ISSN 0378-3812.
- Alonso, L.; Arce, A.; Francisco, M. & Soto, A. (2008) Liquid-liquid equilibria for [C(8)mim][NTf<sub>2</sub>] + thiophene + 2,2,4-trimethylpentane or plus toluene. *J. Chem. Eng. Data*, 53, 1750-1755, ISSN 1520-5134.
- Alonso, L.; Arce, A.; Francisco, M.; Rodriguez, O. & Soto, A. (2007). Gasoline desulfurization using extraction with [C8mim][BF<sub>4</sub>] ionic liquid. *AIChE*, 53, 3108-3115, ISSN 1547-5905.
- AlSahhaf, T. A. & Kapetanovic, E. (1996). Liquid-liquid equilibria for the system naphtha reformat-dimethyl sulphoxide. *Fluid Phase Equilib.* 118, 271-285, ISSN 0378-3812.
- Al-Shahrani, F.; Xiao, T. C.; Llewellyn, S. A.; Barri, S.; Jiang, Z.; Shi, H. H.; Martinie, G. & Green, M. L. H. (2007). Desulfurization of diesel via the H<sub>2</sub>O<sub>2</sub> oxidation of aromatic sulfides to sulfones using a tungstate catalyst. *Appl. Catal. B.*, 73, 311-316, ISSN 0926-3373.
- An, G. J.; Zhou, T. N.; Chai, Y. M.; Zhang, J. C.; Liu, Y. Q. & Liu, C. G. (2007). Nonhydrodesulfurization technologies of light oil. *Prog. Chem.*, 19, 1331-1344, ISSN 1005-281X.
- Antolín, G.; Tinaut, F. V.; Briceño, Y.; Castaño, V. & Pérez, C. (2002). Ramírez, A. I. Optimization of biodiesel production by sunflower oil transesterification. *Bioresour. Technol.*, 83, 111-114, ISSN 0960-8524.
- Antonijevic, M. M.; Milic, S. M. & Petrovic, M. B. (2009). Films formed on copper surface in chloride media in the presence of azoles. *Corros. Sci.*, 51, 1228-1237, ISSN 0010-938X.

- Arai, S.; Nakashima, K.; Tanino, T.; Ogino, C.; Kondo, A.; Fukuda, H. (2010). Production of biodiesel fuel from soybean oil catalyzed by fungus whole-cell biocatalysts in ionic liquids. *Enzyme Microbiol. Technol.*, 46, 51-55.
- Arce, A.; Earle M. J.; Rodríguez H, Seddon, K. R. & Soto, A. (2010). Isomer effect in the separation of octane and xylenes using the ionic liquid 1-ethyl-3-methylimidazolium bis((trifluoromethyl)sulfonyl)amide. *Fluid Phase Equilib.*, 294, 180-186, ISSN 0378-3812.
- a) Arce, A.; Earle, M. J.; Katdare, S. P.; Rodríguez, H. & Seddon, K. R. (2008). Application of mutually immiscible ionic liquids to the separation of aromatic and aliphatic hydrocarbons by liquid extraction: a preliminary approach, *Phys. Chem. Chem. Phys.*, 10, 2538-2542, ISSN 1463-9076.
- Arce, A.; Earle, M. J.; Rodríguez, H. & Seddon, K. R. (2007). Separation of aromatic hydrocarbons from alkanes using the ionic liquid 1-ethyl-3-methylimidazolium bis((trifluoromethyl)sulfonyl)amide, *Green Chem.*, 9, 70-74, ISSN 1463-9270.
- b) Arce, A.; Earle, M. J.; Rodríguez, H.; Seddon, K. R. & Soto, A. (2008). 1-Ethyl-3-methylimidazolium bis((trifluoromethyl)sulfonyl)amide as solvent for the separation of aromatic and aliphatic hydrocarbons by liquid extraction - extension to C-7- and C-8-fractions. *Green Chem.*, 10, 1294-1300, ISSN 1463-9270.
- c) Arce, A; Soto, A; Ortega, J. & Sabater, G. (2008). Viscosities and volumetric properties of binary and ternary mixtures of tris(2-hydroxyethyl) methylammonium methylsulfate plus water plus ethanol at 298.15 K. *J. Chem. Eng. Data*, 53, 770-775, ISSN 1520-5134.
- a) Arce, A.; Soto, A.; Ortega, J. & Sabater, G. (2009). Mixing properties of tris(2-hydroxyethyl)methylammonium methylsulfate, water, and methanol at 298.15 K. Data treatment using several correlation equations. *J. Chem. Thermodyn.*, 41, 235-242, ISSN 0021-9614.
- b) Arce, A; Earle, M. J.; Rodríguez, H.; Seddon, K. & Soto, A. (2009). Bis((trifluoromethyl)sulfonyl)amide ionic liquids as solvents for the extraction of aromatic hydrocarbons from their mixtures with alkanes: effect of the nature of the cation. *Green Chem.*, 11, 365-372, ISSN 1463-9270.
- Ashassi-Sorkhabi, H. & Es'haghi, M. (2009). Corrosion inhibition of mild steel in acidic media by [BMIm]Br Ionic liquid. *Mater. Chem. Phys.*, 114, 267-271, ISSN 0254-0584.
- Atkins, M. P.; Bowlas, C.; Ellis, B.; Hubert, F.; Rubatto, A. & Wasserscheid, P. (2002). In: Rogers, R. D. Seddon, K. R. & Volkov, S. Editors, *Green Industrial Applications of Ionic Liquids*, Kluwer Academic Publishers, ISBN 1402011377, Dordrecht, 49-66.
- a) Bara, J. E.; Hatakeyama, E. S.; Gin, D. L. & Noble, R. D. (2008). Improving CO<sub>2</sub> permeability in polymerized room-temperature ionic liquid gas separation membranes through the formation of a solid composite with a room-temperature ionic liquid. *Polym. Adv. Technol.*, 19, 1415-1420, ISSN 1042-7147.
- b) Bara, J. E.; Gin, D. L. & Noble, R. D. (2008). Effect of anion on gas separation performance of polymer-room-temperature ionic liquid composite membranes, *Ind. Eng. Chem. Res.*, 47, 9919-9924, ISSN 0888-5885.



- c) Bara, J. E.; Gabriel, C. J. & Hatakeyama, E. S. (2008). Improving CO<sub>2</sub> selectivity in polymerized room-temperature ionic liquid gas separation membranes through incorporation of polar substituents. *J. Membr. Sci.* 321, 3–7, ISSN 0376-7388.
- Babich, I. V. & Moulijn, J. A. (2003). Science and technologies of novel processes for deep desulfurization of oil refinery streams: a review. *Fuel*, 82, 607-631, ISSN 0016-2361.
- Baltus, R. E.; Counce, R. M.; Culbertson, B. H.; Luo, H.; DePaoli, D.W.; Dai, S. & Duckworth, D. C. (2005). Examination of the potential of ionic liquids for gas separations. *Sep. Sci. Technol.*, 40, 525–541, ISSN 1520-5754.
- Baltus, R. E.; Culbertson, B. H.; Dai, S.; Luo, H. & DePaoli, D. W. (2004). Low-pressure solubility of carbon dioxide in room-temperature ionic liquids measured with a quartz crystal microbalance. *J. Phys. Chem. B* 108, 721–727, ISSN 0022-3654.
- Bara, J. E.; Camper, D. E.; Gin, D. L. & Noble, R. D. (2010). Room-Temperature Ionic Liquids and Composite Materials: Platform Technologies for CO<sub>2</sub> Capture. *Acc. Chem. Res.* 43, 152-159, ISSN 1520-4898.
- Bara, J. E.; Lessmann, S.; Gabriel, C. J.; Hatakeyama, E. S.; Noble, R. D. & Gin, D. L. (2007). Synthesis and performance of polymerizable room-temperature ionic liquids as gas separation membranes. *Ind. Eng. Chem. Res.* 46, 5397–5404. ISSN 0888-5885.
- Bates, E. D.; Mayton, R. D.; Ntai, I. & Davis, J. H. (2002). CO<sub>2</sub> capture by a task-specific ionic liquid. *J. Am. Chem. Soc.*, 124, 926–927, ISSN 0002-7863.
- Blauwhoff, P. M. M.; Versteeg, G. F. & van Swaaij, W. P. M. (1984). A study on the reaction between CO<sub>2</sub> and alkanolamines in aqueous solutions. *Chem. Eng. Sci.*, 39, 207-225, ISSN 0009-2509.
- Bose, S.; Armstrong, D. W. & Petrich, J. W. (2010). Enzyme-Catalyzed Hydrolysis of Cellulose in Ionic Liquids: A Green Approach Toward the Production of Biofuels. *J. Phys. Chem. B*, 114, 8221-8227, ISSN 1089-5647.
- Bosmann, A.; Datsevich, L.; Jess, A.; Lauter, A.; Schmitz, C. & Wasserscheid, P. (2001). Deep desulfurization of Diesel fuel by extraction with ionic liquids. *Chem. Commun.* 2494-2495, ISSN 1364-548X.
- Bosmann, A.; Datsevich, L.; Jess, A.; Lauter, A.; Schmitz, C. & Wasseerscheid, P. (2003). WO Patent 03/037835 A2.
- Bowing, A. G. & Jess, A. (2007). Kinetics and reactor design aspects of the synthesis of ionic Liquids-Experimental and theoretical studies for ethylmethylimidazole ethylsulfate. *Chem. Eng. Sci.*, 62, 1760-1769, ISSN 0009-2509.
- Brunet, S.; Mey, D.; Perot, G.; Bouchy, C. & Diehl, F. (2005). On the hydrodesulfurization of FCC gasoline: a review. *Appl. Catal. A* 278, 143-172, ISSN 0926-3373.
- Bryan, P. F. (2004). Removal of Propylene from Fuel-Grade Propane. *Sep. Purif. Rev.*, 33, 157-182, ISSN 1542-2119.
- Caeiro, G.; Costa, A. F.; Cerqueira, H. S.; Magnoux, P.; Lopes, J. M.; Matias, P. & Ribeiro, F. R. (2007). Nitrogen poisoning effect on the catalytic cracking of gasoil. *Appl. Catal.*, A 320, 8–15, ISSN 0926-3373.
- Camper, D.; Bara, J. E.; Gin, D. L. & Noble, R. D. (2008). Room-temperature ionic liquid-amine solutions: tunable solvents for efficient and reversible capture of CO<sub>2</sub>. *Ind. Eng. Chem. Res.* 47, 8496–8498, ISSN 0888-5885.

- Camper, D.; Becker, C.; Koval, C. & Noble, R. (2005). Low pressure hydrocarbon solubility in room temperature ionic liquids containing imidazolium rings interpreted using regular solution theory, *Ind. Eng. Chem. Res.*, 44, 1928–1933, ISSN 0888-5885.
- Camper, D.; Becker, C.; Koval, C. & Noble, R. (2006). Diffusion and solubility measurements in room temperature ionic liquids, *Ind. Eng. Chem. Res.*, 45, 445–450, ISSN 0888-5885.
- Caporali, S.; Fossati, A.; Lavacchi, A.; Perissi, I.; Tolstogouzm, A. & Bardi, U. (2008). Aluminium electroplated from ionic liquids as protective coating against steel corrosion. *Corros. Sci.*, 50, 534-539, ISSN 0010-938X.
- Clark, J. D. (1972). Ignition; Rutgers University Press, ISBN 978-0813507255, New Brunswick, NJ.
- Carlisle, T. K.; Bara, J. E.; Gabriel, J. C.; Noble, R. D. & Gin, D. L. (2008). Interpretation of CO<sub>2</sub> solubility and selectivity in nitrile-functionalized room-temperature ionic liquids using a group contribution approach. *Ind. Eng. Chem. Res.*, 47, 7005–7012, ISSN 0888-5885.
- Carvalho, P. J.; Álvarez, V. H.; Marrucho, I. M.; Aznar, M. & Coutinho, J. A. P. (2009). High pressure phase behavior of carbon dioxide in 1-butyl-3-methylimidazolium bis(trifluoromethylsulfonyl)imide and 1-butyl-3-methylimidazolium dicyanamide ionic liquids, *J. Supercrit. Fluids*, 50, 105–111, ISSN 0896-8446.
- Carvalho, P. J.; Álvarez, V. H.; Schröder, B.; Gil, A. M.; Marrucho, I. M.; Aznar, M.; Santos, L. M. N. B. F.; & Coutinho, J. A. P. (2009). Specific solvation interactions of CO<sub>2</sub> on acetate and trifluoroacetate imidazolium based ionic liquids at high pressures, *J. Phys. Chem. B*, 113, 6803–6812, ISSN 0022-3654.
- Cassol, C.; Umpierre, A. P.; Ebeling, G.; Ferrera, B.; Chiaro, S. S. X. & Dupont, J. (2007). On the extraction of aromatic compounds from hydrocarbons by imidazolium ionic liquids. *Int. J. Mol. Sci.*, 8, 593-605, ISSN 1422-0067.
- Chakraborty, M. & Bart, H. J. (2007). Highly selective and efficient transport of toluene in bulk ionic liquid membranes containing Ag<sup>+</sup> as carrier. *Fuel Process. Technol.*, 88, 43-49, ISSN 0378-3820.
- Chan, N. Y.; Lin, T. Y. & Yen, T. F. (2008). Superoxides: Alternative oxidants for the oxidative desulfurization process. *Energy Fuels*, 22, 3326-3328, ISSN 0887-0624.
- Chao, Y.; Li, H.; Zhu, W.; Zhu, G. & Yan, Y. (2010). Deep Oxidative Desulfurization of Dibenzothiophene in Simulated Diesel with Tungstate and H<sub>2</sub>O<sub>2</sub> in Ionic Liquids. *Petrol. Sci. Eng.*, 28, 1243-1249, ISSN 0920-4105.
- Chauvin, Y.; Hirschauer, A. & Olivier, H. (1994). Alkylation of isobutane with 2-butene using 1-butyl-3-methylimidazolium chloride–aluminium chloride molten salts as catalysts. *J. Mol. Catal.*, 92, 155-165, ISSN 1381-1169.
- Che, Q.; He, R.; Yang, J.; Feng, L. & Savinell, R. F. (2010). Phosphoric acid doped high temperature proton exchange membranes based on sulfonated polyetheretherketone incorporated with ionic liquids. *Electrochem. Commun.*, 12, 647-649, ISSN 1388-2481.
- Chen, X.; Liu, C.; Wang, J. & Li, Y. (2009). Progress in Application of Ionic Liquids to the Synthesis of Biodiesel. *Chinese J. Org. Chem.*, 29, 128-134, ISSN 0253-2786.
- Cheng, S. (2009). US Pat. 2009236266-A1.

- Cheng, S. S. & Yen, T. F. (2008). Use of Ionic Liquids as Phase-Transfer Catalysis for Deep Oxygenative Desulfurization. *Energy Fuels* 22, 1400-1401, ISSN 0887-0624.
- Chinn, D.; Vu, D. Q.; Driver, M. S. & Boudreau, L. C. (2006). US Pat. 20060251558A1.
- Choi, Y. J.; Cho, K.W.; Cho, B.W. & Yeo, Y.-K. (2002). Optimization of the sulfolane extraction plant based on modeling and simulation. *Ind. Eng. Chem. Res.*, 41, 5504-5509, ISSN 0888-5885.
- Clark, J. H.; Deswarte, F. E. I.; & Farmer, T. J. (2009). The integration of green chemistry into future biorefineries. *Biofuel Bioprod. Bior.*, 3, 72-90, ISSN 1932-104X.
- Condemarin, R. & Scovazzo, P. (2009). Gas permeabilities, solubilities, diffusivities, and diffusivity correlations for ammonium-based room temperature ionic liquids with comparison to imidazolium and phosphonium RTIL data. *Chem. Eng. J.*, 147, 51-57, ISSN 1385-8947.
- Condemarin, R. & Scovazzo, P. (2009). Gas permeabilities, solubilities, diffusivities, and diffusivity correlations for ammonium-based room temperature ionic liquids with comparison to imidazolium and phosphonium RTIL data. *Chem. Eng. J.*, 147, 51-57, ISSN 1385-8947.
- Consorti, C. S.; Aydos G. L. P.; Ebeling, G. & Dupont, J. (2009). Multiphase catalytic isomerisation of linoleic acid by transition metal complexes in ionic liquids. *Appl. Catal. A*, 371, 114-120, ISSN 0926-860X.
- Conte, V.; Fabbianesi, F.; Floris, B.; Galloni, P.; Sordi, D.; Arends, I. W. C. E.; Bonchio, M.; Rehder, D. & Bogdal, D. (2009). Vanadium-catalyzed, microwave-assisted oxidations with H<sub>2</sub>O<sub>2</sub> in ionic liquids. *Pure Appl. Chem.*, 81, 1265-1277, ISSN 0033-4545.
- Corma, A. & Martínez, A. (1993). Chemistry, Catalysis and processes for isoparaffin-olefin alkylation-Actual situation and future trends. *Catal. Rev.*, 35, 483-570, ISSN 0161-4940.
- Crocker, W. (2007). Ionic liquids on tap. *J. Mat. Chem.*, 17, T41-T41, ISSN 0959-9428.
- Das, P. K.; Li, X. & Liu, Z.-S. (2010). Analysis of liquid water transport in cathode catalyst layer of PEM fuel cells. *Int. J. Membr. Sci.*, 35, 2403-2416, ISSN 0376-7388.
- Di Vona, M. L.; Sgreccia, E.; Licoccia, S.; Khadhraoui, M.; Denoyel, R.; Knauth, P. (2008). Composite proton-conducting hybrid polymers: Water sorption isotherms and mechanical properties of blends of sulfonated PEEK and substituted PPSU *Chem. Mater.*, 20, 4327- 4334, ISSN 0897-4756.
- Domanska, U.; Pobudkowska, A. & Eckert, F. (2006). Liquid-liquid equilibria in the binary systems (1,3-dimethylimidazolium, or 1-butyl-3-methylimidazolium methylsulfate plus hydrocarbons). *Green Chem.*, 8, 268-276, ISSN 1463-9270.
- Dupont, J.; Consorti, C. S. & Spencer, J. (2000). Room temperature molten salts: Neoteric "green" solvents for chemical reactions and processes. *J. Braz. Chem. Soc.*, 11, 337-344, ISSN 0103-5053.
- Earle, M. J.; Plechkova, N. V. & Seddon, K. R. (2009). Green synthesis of biodiesel using ionic liquids. *Pure Appl. Chem.*, 81, 2045-2057, ISSN 0033-4545.
- Ergun, Ü.; Yüzer, D. & Emregül, K. C. (2008). The inhibitory effect of bis-2,6-(3,5-dimethylpyrazolyl)pyridine on the corrosion behaviour of mild steel in HCl solution. *Mat. Chem. Phys.*, 109, 492-499, ISSN 0254-0584.

- Eßer, J.; Wasserscheid, P. & Jess, A. (2004). Deep desulfurization of oil refinery streams by extraction with ionic liquids. *Green Chem.*, 6, 316-322, ISSN 1463-9270.
- Fang, C. S. & Lai, P. M. J. (1995). Microwave-heating and separation of water-in-oil emulsion. *Microwave Power Electromagn. Energy*, 30, 46-57, ISSN 0832-7823.
- Feller, A. & Lercher, J. A. (2004). Chemistry and technology of isobutane/alkene alkylation catalyzed by liquid and solid acids. *Adv. Catal.*, 48, 229-295, ISSN 0360-0564.
- Feller, A.; Barth, J. O.; Guzmán, A.; Zuazo, I. & Lercher, J. A. (2003). Deactivation pathways in zeolite-catalyzed isobutane/butene alkylation. *J. Catal.*, 220, 192-206, ISSN 00021-9517.
- Feller, A.; Guzmán, A.; Zuazo, I. & Lercher, J. A. (2004). On the mechanism of catalyzed isobutane/butene alkylation by zeolites. *J. Catal.*, 224, 80-93, ISSN 00021-9517.
- Ferguson, L. & Scovazzo, P. (2007). Solubility, diffusivity, and permeability of gases in phosphonium-based room temperature ionic liquids: data and correlations, *Ind. Eng. Chem. Res.*, 46, 1369-1374, ISSN 0888-5885.
- Fernicola, A.; Panero, S. & Scrosati, B. (2008). Proton-conducting membranes based on protic ionic liquids. *J. Power Sources*, 178, 591- 595, ISSN 0378-7753.
- Ferrari, M.; Maggi, R.; Delmon, B. & Grange, P. (2001). Influences of the hydrogen sulfide partial pressure and of a nitrogen compound on the hydrodeoxygenation activity of a CoMo/carbon catalyst. *J. Catal.*, 198, 47-55, ISSN 00021-9517.
- Flores, P.; Likhanova, N.; Olivares-Xomelt, O.; Martínez, M.; Martínez-Palou, R. (2010). Microwave-assisted Biodiesel Synthesis using Ionic Liquids as Catalysts. *Fuel*, Submitted, ISSN, 0016-2361.
- Fortuny, M.; Oliveira, C. B. Z.; Melo, R. L.; Nele, M.; Coutinho, R. C. C. & Santos, A. F. (2007). Effect of salinity, temperature, water content, and pH on the microwave demulsification of crude oil emulsions. *Energy Fuels*, 21, 1358-1364, ISSN 0887-0624.
- Fraenk, A. H. G.; Karaghiosoff, W.; Klapötke, T. M.; Nöth, H.; Sprött, J.; Suter, M.; Vogt, M. & Warchhold, M. (2002). Synthesis, Characterization, and Crystal Structures of Various Energetic Urotropinium Salts with Azide, Nitrate, Dinitramide and Azotetrazolate Counter Ions. *Z. Anorg. Allg. Chem.*, 628, 2901-2906, ISSN 00442313.
- Galvez-Ruiz, J. C.; Holl, G.; Karaghiosoff, K.; Klapötke, T. M.; Löhnwitz, K.; Mayer, P.; Nöth, H.; Polborn, K.; Rohbogner, C. J.; Suter, M. & Weigand, J. J. (2005). Derivatives of 1,5-diamino-1H-tetrazole: A new family of energetic heterocyclic-based salts. *Inorg. Chem.*, 44, 4237-4253, ISSN 0020-1669.
- Gamba, M.; Lapis, A. A. M. & Dupont, J. (2008). Supported ionic liquid enzymatic catalysis for the production of biodiesel. *Adv. Synth. Catal.*, 350, 160-164, ISSN 1615-4169.
- Gao, H.; Guo, C.; Xing, J.; Zhao, J. & Liu, H. (2010). Extraction and oxidative desulfurization of diesel fuel catalyzed by a Brønsted acidic ionic liquid at room temperature. *Green Chem.*, 12, 1220-1224, ISSN 1463-9270.
- Gao, H.; Joo, Y.-H.; Twamley, B.; Zhou, Z. & Shreeve, J. M. (2009). Hypergolic Ionic Liquids with the 2,2-Dialkyltriazanium Cation. *Angew. Chem. Int. Ed.*, 48, 2792-2795, ISSN 1433-7851.
- Gao, H.; Li, Y.; Wu, Y.; Luo, M.; Li, Q.; Xing, J. & Liu, H. (2009). Extractive Desulfurization of Fuel Using 3-Methylpyridinium-Based Ionic Liquids. *Energy Fuels*, 23, 2690-2694, ISSN 0887-0624.

- Gao, H.; Luo, M.; Xing, J.; Wu, Y.; Li, Y.; Li, W.; Liu, Q. & Liu, H. (2008). Desulfurization of Fuel by Extraction with Pyridinium-Based Ionic Liquids. *Ind. Eng. Chem. Res.*, 47, 8384-8388, ISSN 0888-5885.
- Gao, H.; Xing, J. M.; Li, Y.G.; Li, W L.; Liu, Q. F. & Liu, H. Z. (2009). Desulfurization of Fuel by Extraction with Lewis-Acidic Ionic Liquids. *Sep. Sci. Technol.*, 44, 971-982, ISSN 1520-5754.
- Gao, H.; Ye, C.; Piekarski, C. M. & Shreeve, J. M. (2007). Computational Characterization of Energetic Salts. *J. Phys. Chem. C*, 111, 10718-10731, ISSN 1932-7447.
- Gao, J. B.; Wang, S. G.; Jiang, Z. X.; Lu, H. Y.; Yang, Y. X.; Jing, F. & Li, C. (2006). Deep desulfurization from fuel oil via selective oxidation using an amphiphilic peroxotungsten catalyst assembled in emulsion droplets. *J. Mol. Catal. A*, 258, 261-266, ISSN 1381-1169.
- García, E.; Cruz, J.; Martínez-Palou, R.; Genesca, J. & García-Ochoa, E. (2004). Experimental and theoretical study of 1-(2-ethylamino)-2-methylimidazoline as an inhibitor of carbon steel corrosion in acid media. *J. Electroanal. Chem.*, 566, 111-121, ISSN 0022-0728.
- García, J.; García, S.; Fernández, A.; Torrecilla, J. S.;Oliet, M. & Rodríguez, F. (2009). Liquid-liquid equilibria for {hexane plus benzene+1-ethyl-3-methylimidazolium ethylsulfate} at (298.2, 313.2 and 328.2) K. *Fluid Phase Equilib.*, 282, 117-120, ISSN 0378-3812.
- García, J.; Fernández, A.; Torrecilla, J. S.; Oliet, M. & Rodríguez, F. (2010). Liquid-liquid equilibria for {hexane plus benzene + 1-ethyl-3-methylimidazolium ethylsulfate} at (298.2, 313.2 and 328.2) K. *Fluid Phase Equilib.* 282, 117-120, ISSN 0378-3812.
- García, J.; Fernández, A.; Torrecilla, J. S.; Oliet, M. & Rodríguez, F. (2010). (Liquid plus liquid) equilibria in the binary systems (aliphatic, or aromatic hydrocarbons+1-ethyl-3-methylimidazolium ethylsulfate, or 1-butyl-3-methylimidazolium methylsulfate ionic liquids). *J. Chem. Thermodyn.*, 42, 144-150, ISSN 0021-9614.
- García, J.; García, S.; Torrecilla, J. S.; Oliet, M. & Rodríguez, F. (2010). Separation of toluene and heptane by liquid-liquid extraction using z-methyl-N-butylpyridinium tetrafluoroborate isomers (z=2, 3, or 4) at T=313.2 K. *J. Chem. Thermodyn.* 42, 1004-1008, ISSN 0021-9614.
- Gilbert, B.; Olivier-Bourbigou, H. & Favre, F. (2007). Chloroaluminate Ionic Liquids: from their Structural Properties to their Applications in Process Intensification. *Oil Gas Technol.*, 62, 745-759, ISSN 1294-4475.
- González, E. J.; Calvar, N.; González, B. & Domínguez, A. (2009). (Liquid plus liquid) equilibria for ternary mixtures of (alkane plus benzene plus [EMPy] [ESO4]) at several temperatures and atmospheric pressure. *J. Chem. Thermodyn.*, 41, 1215-1221, ISSN 0021-9614.
- a) González, E. J.; Calvar, N.; González, B. & Domínguez, A. (2010). Liquid-Liquid Equilibrium for Ternary Mixtures of Hexane plus Aromatic Compounds plus [EMPy][EtSO<sub>4</sub>] at T=298.15 K. *J. Chem. Eng. Data*, 55, 633-638, ISSN 1520-5134.
- b) González, E. J.; Calvar, N.; Canosa, J. & Domínguez, A. (2010). Effect of the Chain Length on the Aromatic Ring in the Separation of Aromatic Compounds from Methylcyclohexane Using the Ionic Liquid 1-Ethyl-3-methylpyridinium Ethylsulfate. *J. Chem. Eng. Data*, 55, 2289-2293, ISSN 1520-5134.

- c) González, E. J.; Calvar, N.; González, B.; Domínguez, A. (2010). Separation of toluene from alkanes using 1-ethyl-3-methylpyridinium ethylsulfate ionic liquid at  $T = 298.15$  K and atmospheric pressure. *J. Chem. Thermodyn.*, 42, 742-747, ISSN 0021-9614.
- d) González, E. J.; Calvar, N.; González, B. & Domínguez, A. (2010). Separation of benzene from alkanes using 1-ethyl-3-methylpyridinium ethylsulfate ionic liquid at several temperatures and atmospheric pressure: Effect of the size of the aliphatic hydrocarbons. *J. Chem. Thermodyn.*, 42, 104-109, ISSN 0021-9614.
- Goyal, S. K.; Mosby, J. F. & Treadman II, J. E. (1993). US Pat. 5219471.
- Gu, Y. L. & Li, G. X. (2009). Ionic Liquid-base Catalysis with Solids: State of the Art *Adv. Synth. Catal.* 351, 817-847, ISSN 1615-4169.
- Guzmán, A.; Zuazo, I.; Feller, A.; Olindo, R.; Sievers, C. & Lercher, J. A. (2006). Influence of the activation temperature on the physicochemical properties and catalytic activity of La-X zeolites for isobutane/cis-2-butene alkylation. *Micropor. Mesopor. Mat.*, 97, 49-57, ISSN 1387-1811.
- Guzmán, D.; Likhanova, N. V.; Flores, E. A. & Martínez-Palou, R. (2009). Patent Pending (Resgistration No. MX/E/2010/014597).
- Guzmán-Lucero, D.; Flores, P.; Rojo, T. & Martínez-Palou, R. (2010). Ionic Liquids as Demulsifiers of Water-in-Crude Oil Emulsions: Study of the Microwave Effect. *Energy Fuels*, 24, 3610-3615, ISSN 0887-0624.
- Guzmán-Lucero, D.; Olivares-Xometl, O.; Martínez-Palou, R.; Likhanova, N. V. & Garibay-Febles, V. (2010). Amphiphilic Ionic Liquids as Corrosion Inhibitor for Acid Environment. *J. Appl. Electrochem.*, submitted, ISSN 1572-8838.
- Ha, S. H.; Lan, M. N.; Lee, S. H.; Hwang, S. M. & Koo, Y.-M. (2007). Lipase-catalyzed biodiesel production from soybean oil in ionic liquids. *Enzyme Microb. Technol.*, 41, 480-483, ISSN 0141-0229.
- Ha, S. H.; Mai, N. L. & Koo, Y. M. (2010). Continuous production and in situ separation of fatty acid ester in ionic liquids. *Enzyme Microbiol. Technol.*, 47, 6-10, ISSN 0141-0229.
- Hammerl, A.; Holl, G.; Höbler, K.; Kapötke, T. M. & Mayer, P. (2001). Methylated Derivatives of Hydrazinium Azide. *Eur. J. Inorg. Chem.*, 755-760, ISSN 1434-1948.
- Han, D. & Row, K. H. (2010). Recent Applications of Ionic Liquids in Separation Technology. *Molecules*, 15, 2405-2426, ISSN 1420-3049.
- Han, M.; Yi, W.; Wu, Q.; Liu, Y.; Hong, Y. & Wang, D. (2009). Preparation of biodiesel from waste oils catalyzed by a Bronsted acidic ionic liquid. *Biores. Technol.*, 100, 2308-2310, ISSN 0960-8524.
- Hasib-ur-Rahman, M.; Sijaj, M. & Larachi, F. (2010). Ionic liquids for CO<sub>2</sub> capture-Development and progress. *Chem. Eng. Proc.*, 49, 313-322, ISSN 0255-2701.
- He, L.; Li, H.; Zhu, W.; Guo, J.; Jiang, X.; Lu, J.; Yan, Y. (2008). Deep oxidative desulfurization of fuels using peroxophosphomolybdate catalysts in ionic liquids. *Ind. Eng. Chem. Res.*, 47, 6890-6895, ISSN 6890-6895.
- He, L.; Tao, G. H.; Parrish, D. A. & Shreeve, J. M. (2010). Nitrocyanamide-Based Ionic Liquids and Their Potential Applications as Hypergolic Fuels. *Chem. Eur. J.*, 16, 5736-5743, ISSN 0947-6539.
- Heintz, Y. J.; Sehabiague, L.; Morsi, B. I.; Jones, K. L.; Luebke, D. R. & Pennline, H. W. (2009). Hydrogen sulfide and carbon dioxide removal from dry fuel gas streams

- using an ionic liquid as a physical solvent, *Energy Fuels*, 23, 4822–4830, ISSN 0887-0624.
- Helwani, Z.; Othman, M. R.; Aziz, N.; Fernando, W. J. N.; Kim, J. (2009). Technologies for production of biodiesel focusing on green catalytic techniques: A review. *Fuel*, 90, 1502–1514, ISSN 0016-2361.
- Holbrey, J. D.; Lopez-Martin, I.; Rothenberg, G.; Seddon, K. R.; Silvero, G. & Zheng, X. (2008). Desulfurisation of oils using ionic liquids: selection of cationic and anionic components to enhance extraction efficiency. *Green Chem.*, 10, 87–92, ISSN 1463-9270.
- Hommeltoft, S. I. (2001). Isobutane alkylation: Recent developments and future perspectives. *Appl. Catal. A*, 221, 421–428, ISSN 0926-860X.
- Hou, Y. & Baltus, R. E. (2007). Experimental measurement of the solubility and diffusivity of CO<sub>2</sub> in room-temperature ionic liquids using a transient thin-liquid-film method, *Ind. Eng. Chem. Res.*, 46, 8166–8175, ISSN 0888-5885.
- Hu, X.; Tang, J.; Blasig, A.; Shen, Y. & Radosz, M. (2006). CO<sub>2</sub> permeability, diffusivity and solubility in polyethylene glycol-grafted polyionic membranes and their CO<sub>2</sub> selectivity relative to methane and nitrogen, *J. Membr. Sci.*, 281, 130–138, ISSN 0376-7388.
- Huang, D.; Zhai, Z.; Lu, Y. C.; Yang, L. M. & Luo, G. S. (2007). Optimization of composition of a directly combined catalyst in dibenzothiophene oxidation for deep desulfurization. *Ind. Eng. Chem. Res.* 46, 1447–1451, ISSN 0888-5885.
- Huang, C. P.; Chen, B. H.; Zhang, J.; Liu, Z. C.; Li, Y. X. (2004). Desulfurization of gasoline by extraction with new ionic liquids. *Energy Fuels*, 18, 1862–1864, ISSN 0887-0624.
- Huang, C.; Liu, Z.; Xu, C.; Chen B. & Liu, Y. (2004). Effects of additives on the properties of chloroaluminate ionic liquids catalyst for alkylation of isobutane and butene *Appl. Catal. A*, 277, 41–43, ISSN 0926-860X.
- Huang, D.; Zhai, Z.; Lu, Y. C.; Yang, L. M. & Luo, G. S. (2007). Optimization of composition of a directly combined catalyst in dibenzothiophene oxidation for deep desulfurization. *Ind. Eng. Chem. Res.*, 46, 1447–1451, ISSN 0888-5885.
- Huang, J.; Luo, H.; Liang, C.; Jiang D. & Dai, S. (2008). Advanced liquid membranes based on novel ionic liquids for selective separation of olefin/paraffin via olefin-facilitated transport, *Ind. Eng. Chem. Res.*, 47, 881–888, ISSN 0888-5885.
- Huddleston, J. G.; Willauer, H. D.; Swatloski, R. P.; Visser, A. E. & Rogers, R. D. (1998). Room temperature ionic liquids as novel media for ‘clean’ liquid-liquid extraction. *Chem. Commun.*, 1765–1766, ISSN 1364-548X.
- Huh, E. S.; Zazybin, A.; Palgunadi, J.; Ahn, S. & Hong, J. (2009). Zn-Containing Ionic Liquids for the Extractive Denitrogenation of a Model Oil: A Mechanistic Consideration. *Energy Fuels*, 23, 3032–3038, ISSN 0887-0624.
- Ishihara, A.; Wang, D. H.; Dumeignil, F.; Amano, H.; Qian, E. W. & Kabe, T. (2005). Oxidative desulfurization and denitrogenation of a light gas oil using an oxidation/adsorption continuous flow process. *Appl. Catal. A: Gen.*, 279, 279–287, ISSN 0926-860X.
-

- Ito, E. & van Veen, J. A. R. (2006). On novel processes for removing sulphur from refinery streams. *Catal. Today*, 116, 446-460, ISSN 0920-5861.
- Izak, P.; Friess, K.; Hynek, V.; Ruth, W.; Fei, Z.; Dyson, J. P. & Kragl, U. (2009). Separation properties of supported ionic liquid-polydimethylsiloxane membrane in pervaporation process. *Desalination*, 241, 182-187, ISSN 0011-9164.
- Izak, P.; Kockerling, M. & Kragl, U. (2006). Stability and selectivity of a multiphase membrane, consisting of dimethylpolysiloxane on an ionic liquid, used in the separation of solutes from aqueous mixtures by pervaporation. *Green Chem.*, 8, 947-948, ISSN 1463-9270.
- Izak, P.; Mateus, N. M. M.; Afonso, C. A. M. & Crespo, J. G. (2005). Enhanced esterification conversion in a room temperature ionic liquid by integrated water removal with pervaporation. *Sep. Purif. Technol.*, 41, 141-145, ISSN 1383-5866.
- Brennecke, J. F. & Maginn, E. J. (2002). US Pat. 20020189444.
- Brennecke, J. F. & Maginn, E. J. (2003). US Pat. 20036579343.
- Davis Jr., J. H. (2004). US Pat. 20040035293A1.
- Jacquemin, J.; Gomes, M. F. C.; Husson, P. & Majer, V. (2006). Solubility of carbon dioxide, ethane, methane, oxygen, nitrogen, hydrogen, argon, and carbon monoxide in 1-butyl-3-methylimidazolium tetrafluoroborate between temperatures 283 K and 343 K and at pressures close to atmospheric, *J. Chem. Thermodyn.* 38, 490-502, ISSN 0021-9614.
- Jiang, X.; Nie, Y.; Li, C. & Wang, Z. (2008). Imidazolium-based alkylphosphate ionic liquids - A potential solvent for extractive desulfurization of fuel. *Fuel* 87, 79-84, ISSN 0016-2361.
- Jiang, Y.; Zhou, Z.; Jiao, Z.; Li, L.; Wu, Y. & Zhang, Z. (2007). SO<sub>2</sub> gas separation using supported ionic liquid membrane, *J. Phys. Chem. B*, 111, 5058-5061, ISSN 0022-3654.
- Jones, P. O. & Vasudevan, P. T. (2010). Cellulose hydrolysis by immobilized *Trichoderma reesei* cellulase. *Biotechnol. Lett.*, 32, 103-106, ISSN 0141-5492.
- Joo, Y. H.; Gao, H. X.; Zhang, Y. Q. & Shreeve, J. M. (2010). Inorganic or Organic Azide-Containing Hypergolic Ionic Liquids. *Inorg. Chem.*, 49, 3282-3288, ISSN 0020-1669.
- Kabe, T.; Ishihara, A. & Qian, W. (1999). *Hydrodesulfurization and Hydrodenitrogenation: Chemistry and Engineering*. Wiley-VCH, ASIN B00069XB9C, Weinheim.
- Kang, S. W.; Lee, D. H.; Park, J. H.; Char, K.; Kim, J. H.; Won, J. & Kang, Y. S. (2008). Effect of the polarity of silver nanoparticles induced by ionic liquids on facilitated transport for the separation of propylene/propane mixtures. *J. Membr. Sci.*, 322, 281-285, ISSN 0376-7388.
- Kilaru, P. & Scovazzo, P. (2008). Correlations of low pressure carbon dioxide and alkenes solubilities in imidazolium-, phosphonium-, and ammonium-based room temperature ionic liquids. Part II. Using activation energy of viscosity, *Ind. Eng. Chem. Res.*, 47, 910-919, ISSN 0888-5885.
- Kilaru, P.; Condemarin, R. & Scovazzo, P. (2008). Correlations of low pressure carbon dioxide and alkenes solubilities in imidazolium-, phosphonium-, and ammonium-based room temperature ionic liquids. Part I: using surface tension, *Ind. Eng. Chem. Res.*, 47, 900-909, ISSN 0888-5885.



- Kim, S. & Dale, B. E. (2005). Life cycle assessment of various cropping systems utilized for producing biofuels: Bioethanol and biodiesel. *Biomass Bioenergy*, 29, 426-439, ISSN 0961-9534.
- Kim, T. A. & Jo, W. H. (2010). Synthesis of Nonfluorinated Amphiphilic Rod-Coil Block Copolymer and Its Application to Proton Exchange Membranes. *Chem. Mat.*, 22, 3646-3652, ISSN 0897-4756.
- Ko, N. H.; Lee, J. S.; Huh, E. S.; Lee, H.; Jung, K. D.; Kim, H. S. & Cheong, M. (2008) Extractive Desulfurization Using Fe-Containing Ionic Liquids. *Energy Fuels*, 22, 1687-1690, ISSN 0887-0624.
- Kokal, S. (2005). Crude Oil Emulsion. Petroleum and Engineering Handbook. Society of Petroleum Engineering, Richardson, Texas. ISBN 1555631088.
- Kokal, S. (2005). Crude-oil emulsions: A state-of-the-art review. *SPE Production & Facilities*, 20, 5-13. ISSN 1064-668X.
- Krishna, R.; Goswami, A.N.; Nanoti, S.M.; Rawat, B.S.; Khana, M.K. & Dobhal, J. (1987). Extraction of aromatics from 63-69°C naphtha fraction for food grade hexane production using sulfolane and NMP as solvent. *Indian J. Technol.* 25, 602-606, ISSN 0019-5669.
- Kuhlmann, E.; Marco, H.; Jess, A. & Wasserscheid, P. (2009). Ionic Liquids in Refinery Desulfurization: Comparison between Biphasic and Supported Ionic Liquid Phase Suspension Processes. *Chemsuschem*, 2, 969-977, ISSN 1864-5631.
- Kulkarni, P. S.; & Afonso, C. A. M. (2010). Deep desulfurization of diesel fuel using ionic liquids: current status and future challenges. *Green Chem.*, 12, 1139-1149, ISSN 1463-9270.
- Kumar, K.; Nikolon, A. D. & Wasan, D. T. (2001). Mechanisms of stabilization of water-in-crude-oil emulsion, *Ind. Eng. Chem. Res.*, 40, 3009-3014, ISSN 0888-5885.
- Kumar, P.; Vermeiren, W.; Dath, J.-P. & Hoelderich, W. F. (2006). Alkylation of Raffinate II and isobutane on naflon silica nanocomposite for the production of isooctane. *Energy Fuels*, 20, 481-487, ISSN 0887-0624.
- Kumar, P.; Vermeiren, W.; Dath, J.-P. & Hoelderich, W. F. (2006). Production of alkylated gasoline using ionic liquids and immobilized ionic liquids *Appl. Catal. A*, 304, 131-141, ISSN 0926-860X.
- Kumelan, J.; Kamps, A. P.-S. & Maurer, G. (2010). Solubility of the single gases carbon dioxide and hydrogen in the ionic liquid [bmpy][Tf<sub>2</sub>N]. *J. Chem. Eng. Data*, 55, 165-172, ISSN 1520-5134.
- Lapis, A. A. M.; de Oliveira, L. F.; Neto, B. A. D.; Dupont, J. (2008). Ionic Liquid Supported Acid/Base-Catalyzed Production of Biodiesel. *Chemsuschem.*, 1, 759-762.
- a) Lakshminarayana, G. & Nogami, M. (2010). Proton conducting organic-inorganic composite membranes under anhydrous conditions synthesized from tetraethoxysilane/methyltriethoxysilane/trimethyl phosphate and 1-butyl-3-methylimidazolium tetrafluoroborate. *Solid State Ionics*, 181, 760-766, ISSN 0167-2738.
- b) Lakshminarayana, G.; Tripathi, V. S.; Tiwari, I. & Nogami, M. (2010). Anhydrous proton-conducting organic-inorganic hybrid membranes synthesized from tetramethoxysilane/methyltrimethoxysilane/diisopropyl phosphite and ionic liquid. *Ionics*, 16, 385-395, ISSN 0947-7047.

- a) Laredo, G. C.; De los Reyes, J. A.; Cano, J. L. & Castillo, J. J. (2001). Inhibition effects of nitrogen compounds on the hydrodesulfurization of dibenzothiophene, *Appl. Catal. A*, 207, 103-112, ISSN 0926-860X.
- b) Laredo, G. C.; Altamirano, E. & De los Reyes, J. A. (2003). Inhibition effects of nitrogen compounds on the hydrodesulfurization of dibenzothiophene: Part 2, *Appl. Catal. A*, 243, 207-214, ISSN 0926-860X.
- Lecocq, V. & Olivier-Bourbigou, H. (2007). Biphasic Ni-catalyzed ethylene oligomerization in ionic liquids. *Oil Gas Technol.*, 62, 761-773, ISSN 1294-4475.
- Lee, J.; Shin, J.; Chun, Y.; Jang, H.; Song, C. & Lee, S. (2010). Toward Understanding the Origin of Positive Effects of Ionic Liquids on Catalysis. *Acc. Chem. Res.*, 43, 985-994, ISSN. 1520-4898.
- Lee, S.; Kim, B.; Lee, E.; Park, Y. & Lee, J. (2006). The removal of acid gases from crude natural gas by using novel supported liquid membranes. *Desalination*, 200, 21-22, ISSN 0011-9164.
- Lei, Z.; Zhang, J.; Li, Q. & Chen, B. (2009). UNIFAC model for ionic liquids. *Ind. Eng. Chem. Res.*, 48, 2697-2704, ISSN 0888-5885.
- Lemos, R. C. B.; da Silva, E. A.; dos Santos, A.; Guimares, R. C. L.; Ferrerira, B. M. S.; Guarnieri, R. A.; Dariva, C.; Franceschi, E.; Santos, A. F. & Fortuny, M. (2010). Demulsification of Water-in-Crude Oil Emulsions Using Ionic Liquids and Microwave Irradiation. *Energy Fuels*, 24, 4439-4444, ISSN 0887-0624.
- Letcher, T. M. & Reddy, P. (2005). Ternary (liquid + liquid) equilibria for mixtures of 1-hexyl-3-methylimidazolium (tetrafluoroborate or hexafluoroborate)+ benzene+an alkane at  $T=298.2$  K and  $p=0.1$  MPa, *J. Chem. Thermodyn.* 37, 415-421, ISSN 0021-9614.
- Letcher, T. M.; Deenadayalu, N.; Soko, B.; Ramjugernath, D. & Naicker, P. K. (2003). Ternary liquid-liquid equilibria for mixtures of 1-methyl-3-octylimidazolium chloride + an alkanol + an alkane at 298.2 K and 1 bar. *J. Chem. Eng. Data*, 48, 904-907, ISSN 1520-5134.
- Leung, D. Y. C.; Wu, X.; Leung, M. K. H. (2010). A review on biodiesel production using catalyzed transesterification. *Appl. Energy*, 87, 1083-1095.
- a) Li, H.; He, L.; Lu, J.; Zhu, W.; Jiang, X.; Wang, Y. & Yan, Y. (2009). Deep Oxidative Desulfurization of Fuels Catalyzed by Phosphotungstic Acid in Ionic Liquids at Room Temperature. *Energy Fuels*, 23, 1354-1357, ISSN 0887-0624.
- b) Li, H.; Jiang, X.; Zhu, W.; Lu, J.; Shu, H. & Yan, Y. (2009). Deep Oxidative Desulfurization of Fuel Oils Catalyzed by Decatungstates in the Ionic Liquid of [Bmim]PF<sub>6</sub>. *Ind. Eng. Chem. Res.*, 48, 9034-9039, ISSN 0888-5885.
- c) Li, H.; Zhu, W.; Wang, Y.; Zhang, J.; Lu, J. & Yan, Y. S. (2009). Deep oxidative desulfurization of fuels in redox ionic liquids based on iron chloride. *Green Chem.*, 11, 810-815, ISSN 1463-9270.
- Li, X. (2006). *Principles of fuel cells*. Taylor & Francis, ISBN 1591690226, New York.
- Li, X.; Hou, M.; Zhang, Z.; Han, B.; Yang, G.; Wang, X. & Zou, L. (2008). Absorption of CO<sub>2</sub> by ionic liquid/polyethylene glycol mixture and the thermodynamic parameters, *Green Chem.* 10, 879-884, ISSN1463-9270.
- Li, Z. G.; Jia, Z.; Luan, Y. X. & Mu, T. (2008). Ionic Liquids for synthesis of inorganic nanomaterials. *Curr. Opin. Solid St. M.*, 12, 1-8, ISSN 1359-0286.

- Liang, X. & Yang, J. (2010). Synthesis of a novel multi -SO<sub>3</sub>H functionalized ionic liquid and its catalytic activities for biodiesel synthesis. *Green Chem.*, 12, 201-204, , ISSN 1463-9270.
- Liang, X.; Gong, G.; Wu, H.; Yang, J. (2009). Highly efficient procedure for the synthesis of biodiesel from soybean oil using chloroaluminate ionic liquid as catalyst. *Fuel*, 88, 613-616, ISSN 0016-2361.
- Likhanova, N. V.; Dominguez-Aguilar, M. A.; Olivares-Xometl, O.; Nava-Entzana, N.; Arce, E. & Dorante, H. (2010). The effect of ionic liquids with imidazolium and pyridinium cations on the corrosion inhibition of mild steel in acidic environment. *Corr. Sci.*, 52, 2088-2097, ISSN 0010-938X.
- Likhanova, N. V.; Martínez-Palou, R. & Palomeque, J. F. (2009). Ger. Pat. 10 2009 039 176.2.
- Likhanova, N. V.; Martínez-Palou, R. & Palomeque, J. F. (2009). US Pat. Appl. 00288992 A1.
- Likhanova, N. V.; Martínez-Palou, R.; Veloz, M. A.; Matías, D. J.; Reyes-Cruz, V. E. & Olivares-Xometl, O. (2007). Microwave-assisted synthesis of 2-(2-pyridyl)azoles. Study of their corrosion inhibiting properties. *J. Het. Chem.*, 44, 145-153, ISSN 0022-152X.
- Likhanova, N.; Guzmán, D.; Flores, E.; Palomeque, J.; Domínguez, M. A.; García, P. & Martínez-Palou, R. (2010). *Mol. Divers.*, in press, DOI: 10.1007/s11030-009-9217-x.
- Lissner, E.; de Souza, W. F.; Ferrera, B. & Dupont, J. (2009). Oxidative Desulfurization of Fuels with Task-Especific Ionic Liquids. *Chemsuschem*, 2, 962-964, ISSN 1864-5631.
- Liu, D.; J. Gui, J.; Song, L.; Zhang, X. & Sun, Z. (2008). Deep Desulfurization of Diesel Fuel by Extraction with Task-Specific Ionic Liquids. *Petroleum Sci.Technol.*, 26, 973-982, ISSN 1091-6466.
- Liu, F.G.; Du, M.; Zhang, J. & Qiu, M. (2009). Electrochemical behavior of Q235 steel in saltwater saturated with carbon dioxide based on new imidazoline derivative inhibitor. *Corr. Sci.*, 2009, 51, 102-109, ISSN 0010-938X.
- Liu, G. Z.; Cao, Y. B.; Jiang, R. P. Wang, L.; Zhang, X. W. & Li, Z. T. (2009). Oxidative Desulfurization of Jet Fuels and Its Impact on Thermal-Oxidative Stability. *Energy Fuels* 23, 5978-5985. ISSN 0887-0624.
- Lo, W. H.; Yang, H. Y. & Wei, G. T. (2003). One-pot desulfurization of light oils by chemical oxidation and solvent extraction with room temperature ionic liquids *Green Chem.*, 5, 639-642, ISSN 1463-9270.
- Lu, L.; Cheng, S. F.; Gao, J. B.; Gao, G. H. & He, M. Y. (2007). Deep oxidative desulfurization of fuels catalyzed by ionic liquid in the presence of H<sub>2</sub>O<sub>2</sub>. *Energy Fuels*, 21, 383-384, ISSN 0887-0624.
- Lu, H.; Gao, J.; Jiang, Z.; Yang, Y.; Song, B.; Li, C. (2007). Oxidative desulfurization of dibenzothiophene with molecular oxygen using emulsion catalysis. *Chem. Commun.*, 150-152, ISSN 1364-548X.
- Lu, J. M.; Yan, F. & Texter, J. (2009). Advanced applications of ionic liquids in polymer science. *Progress Polym. Sci.* 34, 431-448, ISSN 0079-6700.
- MacFarlane, D. R.; Pringle, J. M.; Howlett, P. C. & Forsyth, M. (2010). Ionic liquids and reactions at the electrochemical interface. *Phys. Chem. Chem. Phys.*, 12, 1659-1669, ISSN 1463-9076.

- Magna, L.; Bilde, J.; Olivier-Bourbigou, H.; Robert, T. & Gilbert, B. (2009). About the Acidity-Catalytic Activity Relationship in Ionic Liquids: Application to the Selective Isobutene Dimerization. *Oil Gas Technol.*, 64, 669-679, ISSN 1294-4475.
- Marciniak, A. (2010). Influence of cation and anion structure of the ionic liquid on extraction processes based on activity coefficients at infinite dilution. A review. *Fluid Phase Equilib.*, 294, 213-233, ISSN 0378-3812.
- Martínez-Magadán, J. M.; Oviedo-Roa, R.; García, P. & Martínez-Palou, R. (2010) DFT Study of the Interaction between Ethanthiol and Fe-containing Ionic Liquids for Desulfurization of Natural Gasoline. *Fuel Process. Tech.* Submitted.
- Martínez-Palou, R. (2006). *Química en Microondas*. (E-book). CEM Publishing, ISBN 0972222921, Matthew, NC, 131-154.
- Martínez-Palou, R. (2007). Ionic liquids and Microwave-assisted Organic Synthesis. A "Green" and Synergic Couple. *J. Mex. Chem. Soc.*, 51, 252-264, ISSN 1870-249X.
- Martínez-Palou, R. (2010). Microwave-assisted synthesis using ionic liquids. *Mol. Divers.*, 14, 3-25, ISSN 1381-1991.
- Martínez-Palou, R.; Likhanova, N.; Flores, E. A. & Guzmán, D. (2010). US Patent US/2010/0051509 A1. Appl. No.12548917.
- Martínez-Palou, R.; Rivera, J.; Zepeda, L. G.; Rodríguez, A. N.; Hernández, M. A.; Marín-Cruz, J. & Estrada, A. Evaluation of corrosion inhibitors synthesized from fatty acids and fatty alcohols isolated from sugar cane wax. *Corrosion*, 60, 465-470. ISSN 0010-9312.
- Matsumoto, M.; Inomoto, Y. & Kondo, K. (2005). Selective Separation of Aromatic Hydrocarbons through Supported Liquid Membranes Based on Ionic Liquids. *J. Membr. Sci.*, 246, 77-81, ISSN 0376-7388.
- Matsumoto, M.; Mikami, M. & Kondo, K. (2006). Separation of organic nitrogen compounds by supported liquid membranes based on ionic liquids. *J. Japan Petrol. Inst.*, 5, 256-261, ISSN 1346-8804
- Matsumoto, M.; Mikami, M. & Kondo, K. (2006). Separation of organic nitrogen compounds by supported liquid membranes based on ionic liquids. *J. Japan Petrol. Inst.* 49, 256-261, ISSN 1346-8804.
- Matsumoto, M.; Mikami, M. & Kondo, K. (2007). Selective Permeation of Organic Sulfur and Nitrogen Compounds in Model Mixtures of Petroleum Fraction through Supported Ionic Liquid Membranes. *J. Chem. Eng. Japan*, 40, 1007-1010, ISSN 0021-9592.
- Matsumoto, M.; Ueba, K. T. & Kondo, K. (2009). Vapor permeation of hydrocarbons through supported liquid membranes based on ionic liquids. *Desalination*, 241, 365-371, ISSN 0011-9164.
- Meindersma, G. W. & de Haan, A. B. (2007). Conceptual process design for Aromatic/Aliphatic Separation with Ionic Liquids. *Proceedings of European Congress of Chemical Engineering (ECCE-6)*. Copenhagen, 16-20 September 2007.
- Meindersma, G. W.; Podt, A. J. G.; de Haan, A. B. (2005). Selection of ionic liquids for the extraction of aromatic hydrocarbons from aromatic/aliphatic mixtures. *Fuel Proc. Technol.*, 87, 59-70, ISSN 0378-3820.
- Mochizuki, Y. & Sugawara, K. (2008). Removal of Organic Sulfur from Hydrocarbon Resources Using Ionic Liquids. *Energy Fuels*, 22, 3303-3307, ISSN 0887-0624.

- Moniruzzaman, M.; Nakashima, K.; Kamiya, N. & Goto, M. (2010). Recent advances of enzymatic reactions in ionic liquids. *Biochem. Eng. J.*, 48, 295-314, ISSN 1369-703X.
- Morad, M. S.; Hermas, A. A.; Obaid, A. Y. & Qusti, A. H. (2008). Evaluation of some bipyridinium dihalides as inhibitors for low carbon steel corrosion in sulfuric acid solution. *J. Appl. Electrochem.*, 38, 1301-1311, ISSN 1572-8838.
- Morgan, D.; Ferguson, L. & Scovazzo, P. (2005). Diffusivity of gases in room temperature ionic liquids: data and correlation obtained using a lag-time technique. *Ind. Eng. Chem. Res.*, 44, 4815-4823, ISSN 0888-5885.
- Muginova, S. V.; Galimova, A. Z.; Polyakov, A. E. & Shekhovtsova, T. N. (2010). Ionic Liquids in enzymatic catalysis and biochemical methods of analysis: Capabilities and prospects. *J. Anal. Chem.*, 65, 331-351, ISSN 1061-9348.
- Muthukumar, N.; Maruthamuthu, S. & Palaniswamy, N. (2007). Green inhibitors for petroleum product pipelines. *Electrochemistry*, 75, 50-53, ISSN. 1344-3542.
- Myers, C.; Pennline, H.; Luebke, D.; Ilconich, J.; Dixon, J. K.; Maginn, E. J. & Brennecke, J. F. (2008). High temperature separation of carbon dioxide/hydrogen mixtures using facilitated supported ionic liquid membranes. *J. Membr. Sci.*, 322, 28-31, ISSN 0376-7388.
- Neto, B. A. D.; Alves, M. B.; Lapis, A. A. M.; Nachtigall, F. M.; Eberlin, M. N.; Dupont, J.; Suárez, P. A. Z. (2007). 1-n-Butyl-3-methylimidazolium tetrachloro-indate (BMI center dot InCl<sub>4</sub>) as a media for the synthesis of biodiesel from vegetable oils. *J. Catal.*, 249, 154-161.
- Nguyen, T. A. D.; Kim, K-R.; Han, S. J.; Cho, H. Y.; Kim, J. W.; Park, S. M.; Park, J. H. & Sim, S. J. (2010). Pretreatment of rice straw with ammonia and ionic liquid for lignocellulose conversion to fermentable sugars. *Biores. Technol.*, 101, 7432-7438, ISSN 0960-8524.
- Nie, Y.; Li, C. X. M. & Wang, Z. H. (2007). Extractive desulfurization of fuel oil using alkylimidazole and its mixture with dialkylphosphate ionic liquids. *Ind Eng Chem Res.*, 46, 5108-5112, ISSN 0888-5885.
- Nie, Y.; Li, C. X. M.; Sun, A. J.; Meng, H. & Wang, Z. H. (2006). Extractive desulfurization of gasoline using imidazolium-based phosphoric ionic liquids. *Energy Fuels*, 20, 2083-2087, ISSN 0887-0624.
- Noor, E. A. (2009). Evaluation of inhibitive action of some quaternary N-heterocyclic compounds on the corrosion of Al-Cu alloy in hydrochloric acid. *Mat. Chem. Phys.*, 114, 533-541, ISSN 0254-0584.
- a) Nour, A.H. & Yunus, R. M. (2006). Stability and Demulsification of Water-in-Crude Oil (w/o) Emulsions Via Microwave Heating. *J. Appl. Sci.*, 6, 1698-1702, ISSN 1812-5654.
- b) Nour, A.H. & Yunus, R. M. (2006). A Continuous Microwave Heating of Water-in-Oil Emulsions: An Experimental Study. *J. Appl. Sci.*, 6, 1868-1872, ISSN 1812-5654.
- c) Nour, A.H. & Yunus, R. M. (2006). A Comparative Study on Emulsion Demulsification by Microwave Radiation and Conventional Heating. *J. Appl. Sci.*, 6, 2307-2311, ISSN 1812-5654.
- Ohno, H. & Fukumoto, K. (2008). Progress in ionic liquids for electrochemical reaction matrices. *Electrochemistry*, 76, 16-23, ISSN. 1344-3542.

- Okamoto, K.; Yaguchi, K.; Yamamoto, H.; Chen, Endo, N.; Higa, M. & Kita, H. (2010). Sulfonated polyimide hybrid membranes for polymer electrolyte fuel cell applications. *J. Power Sources*, 195, 5856-586, ISSN 0378-7753.
- Olah, G. A. & Molnar, A. (2003). *Hydrocarbon Chemistry*, Wiley, ISBN 0471417823, New York.
- Olah, G. A.; Mathew, T.; Geoppert, A.; Török, B.; Bucsi, I.; Li, X.-Y.; Wang, Q.; Martinez, E. R.; Batamack, P.; Aniszfeld, R. & Pakash, G. K. S. (2005). Ionic liquid and solid HF equivalent amine-poly(hydrogen fluoride) complexes effecting efficient environmentally friendly isobutane-isobutylene alkylation. *J. Am. Chem. Soc.*, 127, 5964-5969, ISSN 0002-7863.
- Olivares-Xometl, O.; Likhanova, N. V.; Domínguez-Aguilar, M. A.; Arce, E.; Dorante, H. & Arellanes-Lozada, P. (2008). Synthesis and corrosion inhibition of alpha-amino acids alkylamides for mild steel in acidic environment. *Mat. Chem. Phys.* 110, 344-351, ISSN 0254-0584.
- Olivares-Xometl, O.; Likhanova, N. V.; Gómez, B.; Navarrete, J.; Llanos-Serrano, M. E.; Arce, E. & Hallen, J. M. (2006). Electrochemical and XPS studies of decylamides of alpha-amino acids adsorption on carbon steel in acidic environment. *Appl. Surf. Sci.*, 252, 2894-2909, ISSN 0169-4332.
- Olivares-Xometl, O.; Likhanova, N.V.; Martínez-Palou, R. & Dominguez-Aguilar, M. A. (2009). Electrochemistry and XPS study of an imidazoline as corrosion inhibitor of mild steel in an acidic environment. *Mat. Corros.* 60, 14-21, ISSN 0947-5117.
- Olivier-Bourbigou, H. & Lecocq, V. (2003). Ionic liquids as new solvents and catalysts for petrochemical and refining processes. In *Science and Technology in Catalysis*. Anpo, M.; Onaka, M. & Yamashita, H. (Eds.) Book Series: Studies in surface science and catalysis 145, 55-60, Elsevier Science B.V., ISBN 0444513493, Amsterdam.
- Olivier-Bourbigou, H.; Magna, L. & Morvan, D. (2010). Ionic liquids and catalysis: Recent progress from knowledge to applications. *Appl. Catal. A.*, 373, 1-56, ISSN. 0926-860X.
- Padilha, J. C.; Basso, J.; da Trindade, L. G.; Martini, E. M. A.; de Souza, M. O. & de Souza, R. F. (2010). Ionic liquids in proton exchange membrane fuel cells: Efficient systems for energy generation *J. power Source*, 195, 6483-6485, ISSN 0378-7753.
- Palgunadi, J.; Kang, J. E.; Nguyen, D. Q.; Kim, J. H.; Min, B. K.; Lee, S. D.; Kim, H. & Kim, H. S. (2009). Solubility of CO<sub>2</sub> in dialkylimidazolium dialkylphosphate ionic liquids. *Thermochim. Acta*, 494, 94-98, ISSN 0040-6031.
- Park, Y.-I. ; Kim, B.-S.; Byun, Y.-H.; Lee, S.-H.; Lee, E.-W. & Lee, J.-M. (2009). Preparation of supported ionic liquid membranes (SILMs) for the removal of acidic gases from crude natural gas, *Desalination*, 236, 342-348, ISSN 0011-9164.
- Pereira, F.; Valle, K.; Belleville, P.; Morin, A.; Lambert, S.; Sanchez, C. (2008). Advanced mesostructured hybrid silica-nafion membranes for high-performance PEM fuel cell. *Chem. Mater.*, 20, 1710-1718, ISSN 0897-4756.
- Pereiro, A. B. & Rodríguez, A. (2010). An Ionic Liquid Proposed as Solvent in Aromatic Hydrocarbon Separation by Liquid Extraction. *AIChE*, 56, 381-386, ISSN 1547-5905.
- Perez-Navarrete, J. B.; Olivares-Xometl, C. O. & Likhanova, N. V. (2010). Adsorption and corrosion inhibition of amphiphilic compounds on steel pipeline grade API 5L X52 in sulphuric acid 1 M. *J. Appl. Electrochem.*, 40, 1605-1617, ISSN 1572-8838.

- Platon, A. & Thomson, W. (2005). Solid acid characteristics and isobutane/butene alkylation. *Appl. Catal. A*, 282, 93-100, ISSN 0926-860X.
- Poole, C. F. & Poole, S. K. (2010). Extraction of organic compounds with room temperature ionic liquids. *J. Chromatog. A*, 1217, 2268-2286, ISSN 0021-9673.
- Popova, A.; Christov, M. & Zwetanova, A. (2007). Effect of the molecular structure on the inhibitor properties of azoles on mild steel corrosion in 1 M hydrochloric acid. *Corros. Sci.*, 49, 2131-2143, ISSN 0010-938X.
- Prins, R. (2001). Catalytic Hydrodenitrogenation. *Adv. Catal.*, 46, 399-464, ISSN 0360-0564.
- Quinn, R.; Appleby, J. B. & Pez, G. P. (1995). New facilitated transport membranes for the separation of carbon dioxide from hydrogen and methane, *J. Membr. Sci.* 104, 139-146, ISSN 0376-7388.
- Raeissi, R. & Peters, C. J. (2009). A potential ionic liquid for CO<sub>2</sub>-separating gas membranes: selection and gas solubility studies, *Green Chem.* 11, 185-192, ISSN 1463-9270.
- Rao, A. B. & Rubin, E. S. (2002). A technical, economic and environmental assessment of amine-based CO<sub>2</sub> capture technology for power plant green gas control. *Environ. Sci. Technol.*, 36, 4467-4475. ISSN 0013-936X.
- Revie, W. & Uhlig, H. H. (2008). Corrosion and corrosion control: an introduction to corrosion science and engineering. Wiley-Interscience, ISBN 0471732796, New York.
- Rogers, R. D. & Seddon, K. R (Eds.). (2002). *Ionic Liquids: Industrial Applications for Green Chemistry*. ACS, ISSN 1463-9270. Boston.
- Rogers, R. D. & Seddon, K. R. (Eds.). (2003). *Ionic Liquids as Green Solvent: Progress and Prospects*. ACS, ISSN 1463-9270. Boston.
- Rudzinski, W. E.; Oehlers, L. & Zhang, Y. (2002). Tandem Mass Spectrometric Characterization of Commercial Naphthenic Acids and a Maya Crude Oil. *Energy Fuels*, 16, 1178-1185, ISSN 0887-0624.
- a) Ruzich, N. I. & Bassi, A. (2010). Investigation of enzymatic biodiesel production using ionic liquid as a co-solvent. *Can. J. Chem. Eng.*, 88, 277-282, ISSN 1385-8947.
- b) Ruzich, N. I. & Bassi, A. (2010). Investigation of Lipase-Catalyzed Biodiesel Production Using Ionic Liquid [BMIM][PF<sub>6</sub>] as a co-solvent in 500 mL Jacketed Conical and Shake Flask Reactors Using Triolein or Waste Canola Oil as Substrates. *Energy Fuels*, 24, 3214-3222, ISSN 0887-0624.
- Ryan, L.; Convery, F.; Ferreira, S. (2006). Stimulating the use of biofuels in the European Union: Implications for climate change policy. *Energy Policy*, 34, 3184-3194, ISSN 0301-4215.
- Saleh, M. M. & Atia, A. A. (2006). Effects of structure of the ionic head of cationic surfactant on its inhibition of acid corrosion of mild steel. *J. Appl. Electrochem.*, 36, 899-905, ISSN 1572-8838.
- Sánchez, L. M. G.; Meindersma, G. W. & de Haan, A. B. (2007). Solvent properties of functionalized ionic liquids for CO<sub>2</sub> absorption, *Chem. Eng. Res. Des.*, 85, 31-39, ISSN 0263-8762.
- Sartori, G.; Savage, D. W.; Ballinger, B. H. (2000). U.S. Patent 6,121,411.
- Sastri, V. S. (1998) Corrosion Inhibitors Principles and Applications. John Wiley & Sons, ISBN 0471976083, New York.

- Schäfer, T.; Rodriguez, C. M.; Afonso, C. A. M., Crespo, J. G. (2001). Selective recovery of solutes from ionic liquids by pervaporation-a novel approach for purification and green processing. *Chem. Commun.*, 1622-1623, ISSN 1364-548X.
- Schilderman, A. M.; Raeissi, S. & Peters, J. C. (2007). Solubility of carbon dioxide in the ionic liquid 1-ethyl-3-methylimidazolium bis(trifluoromethylsulfonyl)imide, *Fluid Phase Equilib.* 260, 19-22, ISSN 0378-3812.
- Schmidt, R. (2008). [bmim]AlCl<sub>4</sub> Ionic Liquid for Deep Desulfurization of Real Fuel. *Energy Fuels*, 22, 1774-1778, ISSN 0887-0624.
- a) Schneider, S.; Hawkins, T.; Rosander, M.; Mills, J.; Brand, A.; Hudgens, L.; Warmoth, G. & Vij, A. (2008). Liquid azide salts. *Inorg. Chem.*, 47, 3617-3624, ISSN 0020-1669.
- b) Schneider, S.; Hawkins, T.; Rosander, M.; Mills, J.; Vaghjani, G. & Chambreau, S. (2008). Liquid Azide Salts and Their Reactions with Common Oxidizers IRFNA and N<sub>2</sub>O<sub>4</sub>. *Inorg. Chem.*, 47, 6082-6089, ISSN 0020-1669.
- c) Schneider, S.; Hawkins, T.; Rosander, M.; Vaghjani, G.; Chambreau, S. & Drake, G. (2008). Ionic liquid as hypergolic fuels. *Energy Fuels*, 22, 2871-2872, ISSN 0887-0624.
- Schoonover, S. & Roger, E. (2006). US Pat. 7001504.
- Schramm, L. L. (1992). Petroleum Emulsion. In: Schramm, L. L. (Ed.), *Emulsion Fundamentals and Applications in the Petroleum Industry*. American Chemical Society, ISSN 0841220069, Washington DC., p. 1-45.
- Schmidt, R.; Welch, M. B.; Anderson, R. L.; Sardashti, M. & Randolph, B. B. (2008). Disproportionation of Light Paraffins. *Energy Fuels*, 22, 1812-1823, ISSN 0887-0624.
- a) Scovazzo, P. (2009). Testing and evaluation of room temperature ionic liquid (RTIL) membranes for gas dehumidification. *J. Membr. Sci.*, 355, 7-17, ISSN 0376-7388.
- b) Scovazzo, P. (2009). Determination of the upper limits, benchmarks, and critical properties for gas separations using stabilized room temperature ionic liquid membranes (SILMs) for the purpose of guiding future research. *J. Membr. Sci.*, 343, 199-211, ISSN 0376-7388.
- a) Scovazzo, P.; Havard, D.; McShea, M.; Mixon, S. & Morgan, D. (2009). Long-term, continuous mixed-gas dry fed CO<sub>2</sub>/CH<sub>4</sub> and CO<sub>2</sub>/N<sub>2</sub> separation performance and selectivities for room temperature ionic liquid membranes. *J. Membr. Sci.*, 327, 41-48, ISSN 0376-7388.
- b) Scovazzo, P.; Havard, D.; McShea, M.; Mixon, S. & Morgan, D. (2009). Long-term, continuous mixed-gas dry fed CO<sub>2</sub>/CH<sub>4</sub> and CO<sub>2</sub>/N<sub>2</sub> separation performance and selectivities for room temperature ionic liquid membranes, *J. Membr. Sci.* 327, 41-48, ISSN 0376-7388.
- Seeberger, A. & Jess, A. (2010). Desulfurization of diesel oil by selective oxidation and extraction of sulfur compounds by ionic liquids-a contribution to a competitive process design. *Green Chem.*, 12, 602-608, ISSN 1463-9270.
- Shen W, Gu Y, Xu HL, Che, R. C.; Dube, D. & Kaliaguine, S. (2010). Alkylation of Isobutane/1-Butene on Methyl-Modified Nafion/SBA-16 Materials. *Ind. Eng. Chem. Res.*, 49, 7201-7209, ISSN 0888-5885.
- Shen, W.; Gu, Y.; Xu, H. L.; Dube, D. & Kaliaguine, S. (2010). Alkylation of isobutane/1-butene on methyl-modified Nafion/SBA-15 materials. *Appl. Catal. A.*, 377, 1-8, ISSN 0926-860X.



- Shi, L. J.; Shen, B. X. & Wang, G. Q. (2008). Removal of Naphthenic Acids from Beijiag Crude Oil by Forming Ionic Liquids. *Energy Fuels*, 22, 4177-4181, ISSN 0887-0624.
- Shiflett, M. B. & Yokozeki, A. (2005). Solubilities and diffusivities of carbon dioxide in ionic liquids: [BMIM][PF<sub>6</sub>] and [BMIM][BF<sub>4</sub>]. *Ind. Eng. Chem. Res.*, 44, 4453-4464, ISSN 0888-5885.
- Shin, E. & Lee, B. (2008). High-pressure phase behavior of carbon dioxide with ionic liquids: 1-alkyl-3-methylimidazolium trifluoromethanesulfonate, *J. Chem. Eng. Data*, 53, 2728-2734, ISSN 1520-5134.
- Shin, E.; Lee, B. & Limb, J. S. (2008). High-pressure solubilities of carbon dioxide in ionic liquids: 1-alkyl-3-methylimidazolium bis(trifluoromethylsulfonyl)imide. *J. Supercrit. Fluids*, 45, 282-292, ISSN 0896-8446.
- Shishatskiya, S.; Pauls, J. R.; Nunes, S.-P.; Peinemann, K.-V. (2010). Quaternary ammonium membrane materials for CO<sub>2</sub> separation. *J. Membr. Sci.*, 359, 44-53, ISSN 0376-7388.
- Shokouhi, M.; Adibi, M.; Jalili, A. H.; Hosseini-Jenab, M. & Mehdizadeh, A. (2010). Solubility and diffusion of H<sub>2</sub>S and CO<sub>2</sub> in the ionic liquid 1-(2-hydroxyethyl)-3-methylimidazolium tetrafluoroborate. *J. Chem. Eng. Data*, 55, 1663-1668, ISSN 1520-5134.
- Shyu, L.; Zhang, Z. & Zhang, Q. (2001). Process for the extraction of an aromatic compound from an aliphatic phase using a non-neutral ionic liquid, PCT Int. Appl. WO 2001/40150 A1, 07-06-2001.
- Simmons, B. A.; Singh, S.; Holmes, B. M. & Blanch, H.W. (2010). Ionic Liquid Pretreatment. *Chem. Eng. Prog.*, 106, 50-55, ISSN 0255-2701.
- Simons, K.; Nijmeijer, K.; Bara, J. E.; Noble, R. D. & Wessling, M. (2010). How do polymerized room-temperature ionic liquid membranes plasticize during high pressure CO<sub>2</sub> permeation? *J. Membr. Sci.*, 360, 202-209, ISSN 0376-7388.
- Singh, R. P.; Verma, R. D.; Meshri, D. T. & Shreeve, J. M. (2006). Energetic nitrogen-rich salts and ionic liquids. *Angew. Chem. Int. Ed.*, 26, 3584-3601, ISSN 1433-7851.
- Sjöblom, J.; Johnsen, E. E.; Westvik, A.; Ese, M. H.; Djuve, J.; Auflem, I. H.; Kallevik, H. (2001). In: Sjöblom, J. (Ed.), *Encyclopedic Handbook of Emulsion Technology*, Marcel Dekker, ISBN 8247-0454, New York, 595-620.
- Slavcheva E.; Shone B. & Turnbull A. (1999). Review of naphthenic acid corrosion in oilrefining. *British Corrosion J.* 34, 125-131, ISSN 0007-0599.
- Smitha, B., Suhanya, D.; Sridhar, S. & Ramakrishna, M. (2004). Separation of organic-organic mixtures by pervaporation - a review. *J. Memb. Sci.*, 241, 1-21, ISSN 0376-7388.
- Song, C. S. (2003). An overview of new approaches to deep desulfurization for ultra-clean gasoline, diesel fuel and jet fuel. *Catal Today*, 86, 211-263, ISSN 0920-5861.
- Soriano, A. N.; Doma Jr., B. T. & Li, M.-H. (2008). Solubility of carbon dioxide in 1-ethyl-3-methylimidazolium 2-(2-methoxyethoxy) ethylsulfate, *J. Chem. Thermodyn.*, 40, 1654-1660, ISSN 0021-9614.
- Soriano, A. N.; Doma Jr., B. T. & Li, M.-H. (2009). Carbon dioxide solubility in 1-ethyl-3-methylimidazolium trifluoromethanesulfonate, *J. Chem. Thermodyn.*, 41, 525-529, ISSN 0021-9614.
- Speight, J. G. (2009). *Encyclopedia of Hydrocarbon Fuel Science and Technology*. Marcel Dekker, Inc, ISBN 0470195169, New York.

- Sprunger, L. M. A.; Proctor, W.E. Acree Jr. & Abraham, M. H. (2008). LFER correlations for room temperature ionic liquids: separation of equation coefficients into individual cation-specific and anion-specific contributions. *Fluid Phase Equilibr.* 265, 104–111, ISSN 0378-3812.
- Srivastava, N. & Tiwari, T. (2009). New trends in polymer electrolytes: a review. *E-Polymers*. Article Number: 146, ISSN 1618-7229.
- Stanislaus, A.; Marafi, A. & Rana, M. S. (2010). Recent advances in the science and technology of ultra low sulfur diesel (ULSD) production. *Catal Today*, 153, 1-68, ISSN 0920-5861.
- Su, B. M.; Zhang, S. G. & Zhang, Z. C. (2004). Structural elucidation of thiophene interaction with ionic liquids by multinuclear NMR spectroscopy. *J. Phys. Chem. B*, 108, 19510-19517, ISSN 0022-3654.
- Subianto, S.; Mistry, M. K.; Choudhury, N. R.; Dutta, N. K. & Knott, R. (2009). Composite Polymer Electrolyte Containing Ionic Liquid and Functionalized Polyhedral Oligomeric Silsesquioxanes for Anhydrous PEM Applications *ACS Appl. Mater. Interfaces*, 1, 1173–1182, ISSN 1944-8244.
- Susan, M. A.; Kaneko, T.; Noda, A. & Watanabe, M. (2005). Ion gels prepared by in situ radical polymerization of vinyl monomers in an ionic liquid and their characterization as polymer electrolytes. *J. Am. Chem. Soc.*, 127, 4976-4983, ISSN 0002-7863.
- Tang, J.; Shen, Y.; Radosz, M. & Sun, W. (2009). Isothermal carbon dioxide sorption in poly(ionic liquid)s. *Ind. Eng. Chem. Res.*, 48, 9113–9118, ISSN 0888-5885.
- a) Tang, J.; Tang, H.; Sun, W.; Radosz, M. & Shen, Y. (2005). Poly(ionic liquid)s as new materials for CO<sub>2</sub> absorption, *J. Polym. Sci. Polym. Chem.*, 43, 5477–5489, ISSN 1099-0488.
- b) Tang, J.; Tang, H.; Sun, W.; Plancher, H.; Radosz, M. & Shen, Y. (2005). Poly(ionic liquid)s: a new material with enhanced and fast CO<sub>2</sub> absorption, *Chem. Commun.*, 3325–3327, ISSN 1364-548X.
- c) Tang, J.; Sun, W.; Tang, H.; Radosz, M. & Shen, Y. (2005). Enhanced CO<sub>2</sub> absorption of poly(ionic liquid)s, *Macromolecules*, 38, 2037–2039, ISSN 1521-3935.
- d) Tang, J.; Tang, H.; Sun, W.; Radosz, M. & Shen, Y. (2005). Low-pressure CO<sub>2</sub> sorption in ammonium-based poly(ionic liquid)s. *Polymer* 46, 12460–12467, ISSN 0032-3896.
- Tang, S. W.; Scurto, A. M. & Subramaniam, B. (2009). Improved 1-butene/isobutane alkylation with acidic ionic liquids and tunable acid/ionic liquid mixtures. *J. Catal.*, 268, 243-250, ISSN 0021-9517.
- Tezuka, T.; Tadanaga, K.; Hayashi, A.; Tatsumisago, M. (2006). Inorganic-organic hybrid membranes with anhydrous proton conduction prepared from 3-aminopropyltriethoxysilane and sulfuric acid by the sol-gel method. *J. Am. Chem. Soc.*, 128, 16470–16471, ISSN 0002-7863.
- Thi, L. T. B.; Korth, W.; Aschauer, S. & Jess, A. (2009). Alkylation of isobutane with 2-butene using ionic liquids as catalyst. *Green Chem.*, 11, 1961-1967, , ISSN 1463-9270.
- Thompson, D. N.; Ginosar, D. M. & Burch, K. C. (2005). Regeneration of a deactivated USY alkylation catalyst using supercritical isobutane. *Appl. Catal. A*, 279, 109-116, ISSN 0926-860X.

- Toma, S.; Meciarova, M. & Sebesta, R. (2009). Are Ionic Liquids Suitable Media for Organocatalytic Reactions? *Eur. J. Org. Chem.*, 321-327, ISSN 1434-193X.
- Torimoto, T.; Tsuda, T.; Okazaki, K. & Kuwabata, S. (2010). New Frontiers in Materials Science Opened by Ionic Liquids. *Adv. Mat.*, 22, 1196-1222, ISSN 1521-4095.
- Tripathi, P. & Shahi, V. K. (2008). Functionalized Organic-Inorganic Nanostructured *N-p*-Carboxy Benzyl Chitosan-Silica-PVA Hybrid Polyelectrolyte Complex as Proton Exchange Membrane for DMFC Applications. *J. Phys. Chem. B.*, 112, 15678-15690, ISSN 0022-3654, ISSN 0378-7753.
- Umeda, J.; Suzuki, M.; Kato, M.; Moriya, M.; Sakamoto, W.; Yogo, T. (2010). Proton conductive inorganic-organic hybrid membranes functionalized with phosphonic acid for polymer electrolyte fuel cell. *J. Power Sources*, 195, 5882-5888, ISSN 0378-7753.
- Varadaraj, R.; Savage, D. W. & Brons, C. H. (2001). Chemical demulsifier for desalting heavy crude. US 6,168,702 B1.
- Varadaraj, R.; Savage, D. W. (2000). U.S. Patent 6,030,523.
- Ventura, S. P. M.; Pauly, J.; Daridon, J. L.; da Silva, J. A. L.; Marrucho, I. M.; Dias, A.M.A. & Coutinho, J. A. P. (2008). High pressure solubility data of carbon dioxide in (tri-isobutyl(methyl)phosphonium tosylate + water) systems. *J. Chem. Thermodyn.*, 40, 1187-1192, ISSN 0021-9614.
- Wang, B.; Wu, J. L. & Peng, Y. (2008). Stability and Selectivity of Supported Liquid Membranes with Ionic Liquids for the Separation of Organic Liquids by Vapor Permeation. *Ind. Eng. Chem. Res.*, 47, 8355-8360, ISSN 0888-5885.
- Wasserscheid, P & Keim, W. (Eds.). (2004). *Ionic Liquids in Synthesis*, Wiley-VCH, ISBN 1 978-3-527-31239-9, Weinheim.
- Weitkamp, J. & Traa, Y. (1999). Isobutane/butene alkylation on solid catalysts. Where do we stand? *Catal. Today*, 49, 193-199, ISSN 0920-5861.
- Wu, Q.; Chen, He.; Han, M.; Wang, D. & Wang, J. (2007). Transesterification of Cottonseed Oil Catalyzed by Brønsted Acidic Ionic Liquids. *Ind. Eng. Chem. Res.*, 46, 7955-7960, ISSN 0888-5885.
- Wu, Q.; Chen, He.; Han, M.; Wang, D.; Wang, J. & Jin, Y. (2006). Transesterification of cottonseed oil to biodiesel catalyzed by highly active ionic liquids. *Chinese J. Catal.*, 27, 294-296.
- Xia, L. X.; Lu, S. W. & Cao, G. Y. (2002). Demulsification of emulsions exploited by enhanced oil recovery system. *Sep. Sci. Technol.*, 37, 3407-3420, ISSN 1520-5754.
- a) Xia, L. X.; Lu, S. W. & Cao, G. Y. (2004). Stability and demulsification of emulsions stabilized by asphaltenes or resins. *J. Colloid Interface Sci.*, 271, 504-506, ISSN 0021-9797.
- b) Xia, L. X.; Lu, S. W. & Cao, G. Y. (2004). Salt-assisted microwave demulsification. *Chem. Eng. Commun.*, 191, 1053-1063, ISSN 0098-6445.
- a) Xie, L.-L.; Favre-Reguillon, A.; Wang, X.-X.; Fu, X.; Pellet-Rostaing, S.; Toussaint, G.; Geantet, C.; Vrinat, M.; Lemaire, M. (2008). Selective extraction of neutral nitrogen compounds found in diesel feed by 1-butyl-3-methyl-imidazolium chloride. *Green Chem.*, 10, 524-531, ISSN 1463-9270.
- b) Xie, L.-L.; Favre-Reguillon, A.; Pellet-Rostaing, S.; Wang, X.-X.; Fu, X.; Estager, J.; Vrinat, M. & Lemaire, M. (2008). Selective Extraction and Identification of Neutral

- Nitrogen Compounds Contained in Straight-Run Diesel Feed Using Chloride Based Ionic Liquid. *Ind. Eng. Chem. Res.*, 47, 8801-8807, ISSN 0888-5885.
- c) Xie, L.-L.; Chen X.; Wang X.; Fu, X.; Favre-Reguillon, A.; Pellet-Rostaing, S. & Lemaire, M. (2008). Removal of N-compounds from diesel fuel by using chloridized imidazole based ionic liquids. *Chinese J. Inorg. Chem.*, 24, 919-925, ISSN 1001-4861.
- Xu, D.; Zhu, W.; Li, H.; Zhang, J.; Zou, F.; Shi, F. & Yan, Y. Oxidative Desulfurization of Fuels Catalyzed by V<sub>2</sub>O<sub>5</sub> in Ionic Liquids at Room Temperature. (2009). *Energy Fuels*, 23, 5929-5933, ISSN 0887-0624.
- Yan, F.; Yu, S.; Zhang, X.; Qiu, L.; Chu, F.; You, J. & Lu, J. (2009). Enhanced Proton Conduction in Polymer Electrolyte Membranes as Synthesized by Polymerization of Protic Ionic Liquid-Based Microemulsions. *Chem. Mater.*, 21, 1480- 1484, ISSN 0897-4756.
- Yang, F.; Li, L. Z.; Li, Q.; Tan, W.; Liu, W. & Xian, M. (2010). Enhancement of enzymatic in situ saccharification of cellulose in aqueous-ionic liquid media by ultrasonic intensification. *Carboh. Polym.*, 81, 311-316, ISSN 0144-8617.
- Ye, H.; Huang, J.; Xu, J.; Kodiweera, N.; Jayakody, J. & Greenbaum, S. (2008). New membranes based on ionic liquids for PEM fuel cells at elevated temperatures. *J. Power Sources*, 178, 651-660, ISSN 0378-7753.
- Yokozeki, A. & Shiflett, M. B. (2007). Hydrogen purification using room-temperature ionic liquids, *Appl. Energy*, 84, 351-361, ISSN 0306-2619.
- Yoo, K.; Nambodiri, V.V.; Verma, R. S. & Smirniotis, P. G. (2004). Ionic liquid-catalyzed alkylation of isobutane with 2-butene. *J. Catal.*, 204, 511-519, ISSN 0021-9517.
- Yu, S.; Yan, F.; Zhang, X.; You, J.; Wu, P.; Lu, J.; Xu, Q.; Xia, X. & Ma, G. (2008). Polymerization of Ionic Liquid-Based Microemulsions: A Versatile Method for the Synthesis of Polymer Electrolytes. *Macromolecules*, 41, 3389-3392, ISSN 1521-3935.
- Yu, T.; Weiss, R. G.; Yamada, T. & George, M. (2008). Eur. Pat. Appl. WO2008094846A1.
- Yue, G. K.; Lu, X. M.; Zhu, Y. L.; Xiang, X. P. & Zhang, S. J. (2009). Surface morphology, crystal structure and orientation of aluminium coatings electrodeposited on mild steel in ionic liquid. *Chem. Eng. J.*, 147, 79-86, ISSN 1385-8947.
- Zaczeplinski, S. (1996) Exxon Diesel Oil Deep Desulfurization (DODD). In: Meyer R. A. (Ed.) Handbook of Petroleum Refining Processes, McGraw-Hill, ASIN B000OFMB12, New York, Chapter 8.7.
- Zakrzewska, M. E.; Bogel-Lukasik, E. & Bogel-Lukasik, R. (2010). Solubility of Carbohydrates in Ionic Liquids. *Energy Fuels* 24, 737-745, ISSN 0887-0624.
- Zaykina, R. F.; Zaykin, Y. A.; Yagudin, S. G. & Fahrudinov, I. M. (2004). Specific approaches to radiation processing of high-sulfuric oil. *Radiat. Phys. Chem.*, 71, 467-470, ISSN 0253-570X.
- Zhang, J.; Huang, C.; Chen, B.; Ren, P. J. & Pu, M. (2007). Isobutane/2-butene alkylation catalyzed by chloroaluminate ionic liquids in the presence of aromatic additives. *J. Catal.*, 249, 261-268, ISSN 0021-9517.
- Zhang, J.; Zhang, S.; Dong, K.; Zhang, Y.; Shen, Y. & Lv, X. (2006). Supported absorption of CO<sub>2</sub> by tetrabutylphosphonium amino acid ionic liquids. *Chem. Eur. J.*, 12, 4021-4026, ISSN 0947-6539.

- Zhang, J.; Zhu, W.; Li, H.; Jiang, L.; Jiang, Y.; Huang, W.; Yan, Y. (2009). Deep oxidative desulfurization of fuels by Fenton-like reagent in ionic liquids. *Green Chem.*, 11, 1801-1807, ISSN 1463-9270.
- Zhang, S. G. & Zhang, Z. C. (2002). Novel properties of ionic liquids in selective sulfur removal from fuels at room temperature. *Green Chem.*, 4, 376-379, ISSN 1463-9270.
- Zhang, S. G.; Zhang, Q. L. & Zhang, Z. C. Extractive desulfurization and denitrogenation of fuels using ionic liquids. *Ind. Eng. Chem. Res.* 43, 614-622, ISSN 0888-5885.
- Zhang, X.; Liu, Z. & Wang, W. (2008). Screening of ionic liquids to capture CO<sub>2</sub> by COSMORS and experiments, *AIChE J.* 54, 2717-2728, ISSN 1547-5905.
- a) Zhang, Y. Q.; Gao, H.; Guo, Y.; Joo, Y. H. & Shreeve, J. M. (2010). Hypergolic N,N-Dimethylhydrazinium Ionic Liquids. *Chem. Eur. J.*, 16, 3114-3120, ISSN 0947-6539.
- b) Zhang, X.; Zhu, W.; Wei, T.; Zhang, C. & Xiao, H. (2010). Densities, Heats of Formation, Energetic Properties, and Thermodynamics of Formation of Energetic Nitrogen-Rich Salts Containing Substituted Protonated and Methylated Tetrazole Cations: A Computational Study. *J. Phys. Chem. C.*, 114, 13142-13152, ISSN 1520-6106.
- a) Zhang Q. B. & Hua, Y. X. (2009). Corrosion inhibition of mild steel by alkylimidazolium ionic liquids in hydrochloric acid. *Electrochim. Acta*, 54, 1881-1887, ISSN 0013-4686.
- b) Zhang Q. B. & Hua, Y. X. (2009). Corrosion inhibition of aluminum in hydrochloric acid solution by alkylimidazolium ionic liquids. *Mat. Chem. Phys.*, 119, 57-64, ISSN 0254-0584.
- Zhao, D. S.; Liu, R.; Wang, J. L. & Liu, B. (2008). Photochemical oxidation-ionic liquid extraction coupling technique in deep desulphurization of light oil. *Energy Fuels*, 22, 1100-1103, ISSN 0887-0624.
- Zhao, D.; Wang, J. & Zhou, E. (2007). Oxidative desulfurization of diesel fuel using a Bronsted acid room temperature ionic liquid in the presence of H<sub>2</sub>O<sub>2</sub>. *Green Chem.* 9, 1219-1222, ISSN 1463-9270.
- Zhao, D.; Wang, Y. & Duan, E. (2009). Oxidative Desulfurization of Fuel Oil by Pyridinium-Based Ionic Liquids. *Molecules*, 14, 4351-4357, ISSN 1420-3049.
- Zhao, H.; Xia, S. & Ma, P. (2005). Use of ionic liquid as 'green' solvent for extraction. *J. Chem. Technol. Biotechnol.*, 80, 1089-1096, ISSN 0268-2575.
- Zhao, L.; Riensche, E.; Menzer, R.; Blum, L. & Stolten, D. (2008). A parametric study of CO<sub>2</sub>/N<sub>2</sub> gas separation membrane processes for post-combustion capture. *J. Membr. Sci.*, 325, 284-294, ISSN 0376-7388.
- a) Zhao, H.; Song, Z. Y.; Olubajo, O. & Cowins, J. V. (2010). New Ether-Functionalized Ionic Liquids for Lipase-Catalyzed Synthesis of Biodiesel. *Appl. Biochem. Biotech.*, 162, 13-23.
- b) Zhao, H.; Song, Z. Y.; Olubajo, O.; Cowins, J. V. (2010). High transesterification activities of immobilized proteases in new ether-functionalized ionic liquids. *Biotech. Lett.*, 32, 1109-1116.
- Zhao, Z.; Sun, W.; Yang, X.; Ye, X. & Wu, Y. (2000). Study of the catalytic behaviors of concentrated heteropolyacid solution. I. A novel catalyst for isobutane alkylation with butenes. *Catal. Lett.*, 65, 115-121, ISSN 1011-372X.
- Zhou, J. X.; Mao, J. B. & Zhang, S. G. (2008). Ab initio calculation of the interaction between thiophene and ionic liquids. *Fuel Proc. Technol.*, 89, 1456-1460, ISSN 0378-3820.

- Zhu, W.; Li, H.; Jiang, X.; Yan, Y.; Lu, J. & Xia, J. (2007). Oxidative Desulfurization of Fuels Catalyzed by Peroxotungsten and Peroxomolybdenum Complexes in Ionic Liquids. *Energy Fuels*, 21, 2514-2516. ISSN 0887-0624.
- Zubin, C.; Shuyun, M. & Wei, M. (2007). Synthesis of chloroaluminate ionic liquids and use for olefin reduction in FCC gasoline. *Petrol. Sci. Technol.*, 25, 1173-1184, ISSN. 1091-6466.

# Ionic Liquid Based Electrolytes for Dye-Sensitized Solar Cells

Chuan-Pei Lee, Po-Yen Chen and Kuo-Chuan Ho

*National Taiwan University*

*Taiwan*

## 1. Introduction

### 1.1 New type of solar cell: dye-sensitized solar cells (DSSCs)

The rising price of fossil fuels, together with their rapid depletion and the pollution caused by their combustion, is forcing us to find sources of clean renewable energy. Fortunately, the supply of energy from the sun to the earth is gigantic, i.e.,  $3 \times 10^{24}$  joule a year or about ten thousand times more than what mankind consumes currently. This means that only 0.1% of the earth's surface with solar cells with an efficiency of 10% would suffice to satisfy our current needs (Hamakawa, 2004; Grätzel, 2001). Therefore, solar power is considered to be one of the best sustainable energies for future generations. There are already a number of terrestrial applications where photovoltaic devices provide a viable means of power generation. Photovoltaic devices are based on the concept of charge separation at an interface of two materials of different conduction mechanism. To date photovoltaics has been dominated by solid-state junction devices, usually in silicon, crystalline or amorphous, and profiting from the experience and material availability resulting from the semiconductor industry. However, the expensive and energy-intensive high-temperature and high-vacuum processes is needed for the silicon based solar cells. Therefore, the dominance of the photovoltaic field by such kind of inorganic solid-state junction devices is now being challenged by the emergence of a third generation of solar cell based on interpenetrating network structures, such as dye-sensitized solar cells (DSSCs) (Grätzel, 2001; O'Regan *et al.*, 1991).

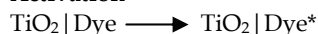
DSSCs have been extensively investigated since O'Regan and Grätzel reported a 7.1% solar energy conversion efficiency in 1991 (O'Regan *et al.*, 1991). DSSCs offer particular promise as an efficient, low cost alternative to Si semiconductor photovoltaic devices and represent a specific type of photoelectrochemical cell. The advantages of DSSCs are that they do not rely on expensive or energy-intensive processing methods and can be printed on flexible substrates using roll-to-roll methods. Instead of using a single crystal semiconductor, DSSCs rely on a thin mesoporous film (10-15  $\mu\text{m}$  thick) of nanocrystals of a metal oxide, most often  $\text{TiO}_2$ , which is sensitized to visible light with a molecular light absorber. The sensitized nanoparticles are combined with a redox active electrolyte solution and counter electrode to produce a regenerative photoelectrochemical cell. By using the traditional liquid electrolyte, the DSSC has achieved an 11.5% efficiency record (Chen *et al.*, 2009), encouraging the surge to explore new organic materials for the conversion of solar to electric power. However, presence of liquid electrolytes in traditional DSSCs has some problems such as a less long-

term stability and a need for hermetic sealing due to the leakage and evaporation of the organic solvent (Chen *et al.*, 2010; Lee *et al.*, 2010a & 2010b). In this review, we pay particular attention on the recent development of quasi-solid-state and all-solid-state DSSCs using ionic liquid (IL) electrolytes. The problems researchers have encountered and the prospects of DSSCs are also discussed.

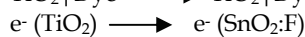
## 1.2 The structure and operational principle for DSSCs

A schematic presentation of the structure of a DSSC is given in Fig. 1. A typical DSSC is composed of two sheets of glass coated with a transparent conductive oxide layer. One of the glass plates (the working electrode) is covered with a film of small dye-sensitized semiconductor particles; The large surface area of the nanoparticles, which is as much as a factor of 1,000 greater than the geometric area of the film, allows a monolayer of surface-bound dye to absorb nearly all of the incident sunlight in the region of the spectrum where the dye absorbs. The other glass plate (the counter-electrode (CE)) is coated with a catalyst. Two electrodes are sandwiched together and the electrolyte, typically containing the iodide/triiodide ( $I^-/I_3^-$ ) redox couple in an organic solvent, fills the gap between them. The basic sequence of events in a DSSC is as follows:

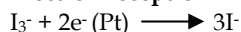
### Activation



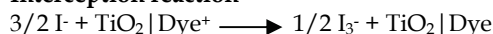
### Electron injection



### Electron reception



### Interception reaction



Upon absorption of light, an electron is injected from a metal-to-ligand charge transfer excited state of the dye into the conduction band of the metal oxide. The rate of this electron injection reaction is ultrafast, typically occurring on the order of hundreds of femtoseconds to tens of picoseconds. The injected electron percolates through the  $\text{TiO}_2$  film, and is thought to move by a “hopping” mechanism and is driven by a chemical diffusion gradient (rather than an electric field), and is collected at a transparent conductive substrate of fluorine doped tin oxide glass ( $\text{SnO}_2:\text{F}$ ), on which the  $\text{TiO}_2$  film is printed. After passing through an external circuit, the electron is reintroduced into the solar cell at the platinum counter electrode, where triiodide is reduced to iodide. The iodide then regenerates the oxidized dye, thereby completing the circuit with no net chemical change.

## 1.3 The application of ionic liquids (ILs) in DSSCs

DSSCs are among the most extensively investigated devices that provide a high light-to-electric energy conversion yield. The electrolyte is one of key components for dye-sensitized solar cells and its properties have much effect on the conversion efficiency and stability of



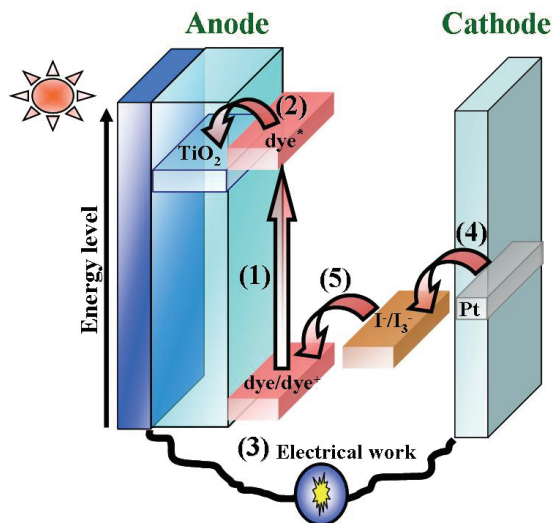


Fig. 1. Schematic diagram of structure and function of a typical  $\text{TiO}_2$  based dye-sensitized solar cell.

the solar cells. One of the critical components of DSSCs is the electrolyte containing a  $\text{I}^-/\text{I}_3^-$  redox couple that mediates the dye regeneration process. Alkylimidazolium iodides are frequently employed as the electrolyte because they can improve the photovoltaic performance of such devices (Kambe *et al.*, 2002; Kubo *et al.*, 2003). Alkylimidazolium cation may be adsorbed on the surface of semiconductor film to form the Helmholtz layer, which restricted the contact of triiodide and semiconductor films ( $\text{TiO}_2$ ), for the recombination between triiodide and electron in the conduction band of semiconductor. As the result, the fill factor and conversion efficiency of the solar cells were improved. On the other hand, the high solubility of alkyl imidazolium cation in organic solvent and the high activity of iodide increased the light harvesting efficiency and photocurrent as well as the stability of the sensitizer. The highest efficiency record of DSSC was obtained based on organic solvent electrolyte, especially the highly volatile organic solvent electrolyte due to the efficient infiltration of organic electrolyte in nanocrystalline films. However, the DSSCs based on organic electrolyte have the disadvantages such as less long-term stability, difficulty in robust sealing and leakage of electrolyte due to the volatility of organic solvent. In order to develop the DSSCs for outdoor use, we have to overcome the technological problems mentioned above. For this purpose, ILs have been considered as one of the alternative electrolytes for DSSCs and other electrochemical devices for replacing organic solvent because of their good chemical and thermal stability, negligible vapor pressure, nonflammability, wide electrochemical window, and high ionic conductivity (Fredlake *et al.*, 2004; Pringle *et al.*, 2002). Notably, 1-propyl-3-methylimidazolium iodide (PMII), an IL at room temperature with a viscosity of 880 cP, is by far the most commonly used in solvent-free ILs based electrolyte (PMII provides both iodide sources and solvents of electrolytes for DSSCs). Recently, many imidazolium salts with functional groups have been reported, and some functionalized imidazolium iodide salts have been evaluated as electrolytes in DSSCs with some success (Kambe *et al.*, 2002; Kubo *et al.*, 2003). Figure 2 summarizes the structure

and viscosity of some alkylimidazolium cations-based room temperature ionic liquids (RTILs) (Kong *et al.*, 2007).

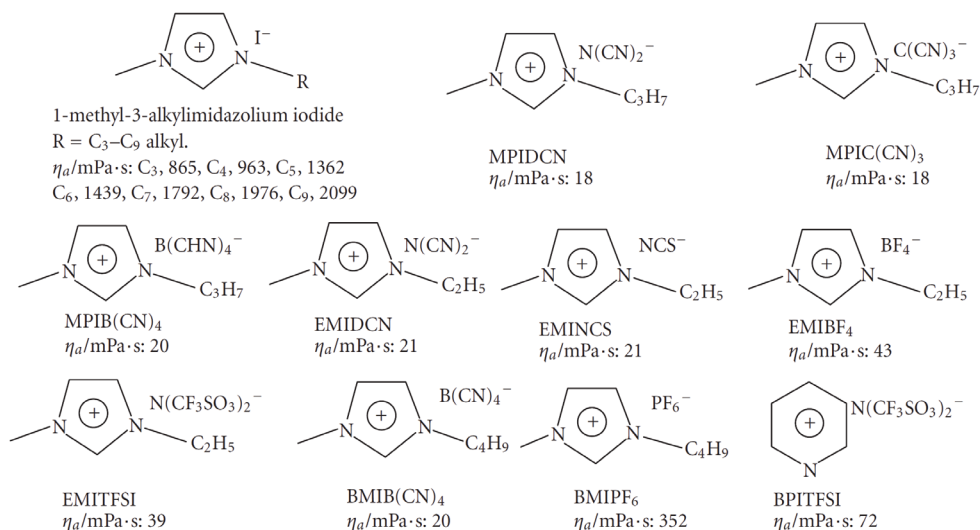


Fig. 2. Structure and the viscosity of several alkylimidazolium cations based RTILs (Kong *et al.*, 2007).

Here we scrutinize the recent advances on DSSCs using different electrolytes incorporating ILs. The IL employed in DSSC can be classified as follows: (a) a quasi-solid-state DSSC with IL served as both the source of iodide and the solvent themselves (system A: quasi-solid-state electrolyte with ILs), (b) a near-solid-state DSSC with an ionic liquid electrolyte containing nanoparticles (system B: near solid-state electrolyte with nanoparticles solidified ILs) and (c) an all-solid-state DSSC with ionic liquid crystals (system C). These electrolytes are progressively viscous enabling increased stability.

#### 1.4 Challenges

The significant limitation of DSSCs to date has been the relatively low number of choices for the electrolyte. For one, the redox couple  $I^-/I_3^-$  has proven to be quite unique: no other redox couples have been found to date that result in better cell performance, and only one gives comparable overall conversion efficiencies (Wang *et al.*, 2004b). Secondly, the use of liquid electrolyte is not ideal for commercial applications (especially the common use of acetonitrile derivatives as the solvent), due to problems with sealing, volatility, and toxicity. Therefore, solidification and quasi-solidification of DSSCs have been intensely studied with various approaches, such as using of p-type inorganic semiconductors (Kumara *et al.*, 2002; Perera *et al.*, 2003), organic hole conducting materials (Bach *et al.*, 1998; Krüger *et al.*, 2001; Krüger *et al.*, 2002), ionic gel electrolytes having a polymer or a gelator (Kubo *et al.*, 2001; Kubo *et al.*, 2002; Wu *et al.*, 2007; Ying *et al.*, 2008), and of ionic liquid electrolytes containing dispersed nano-components (Lee *et al.*, 2009a). A solid-state device has several advantages, but short of that, a gel, polymeric, or aqueous electrolyte would present a substantial improvement. However, no viable alternative to the use of a volatile organic solvent has

been found to date. Besides, imperfect filling of the dye-adsorbed porous  $\text{TiO}_2$  film by p-type inorganic semiconductors or polymers has resulted in poor efficiency for the cells. Moreover, the carrier diffusion length was limited in the case of conducting polymers due to their low conductivity.

## 2. Reviews and motivations

IL electrolytes were developed in recent year in view of the disadvantage of organic solvent electrolyte for DSSCs. Compared with traditional organic solvent electrolyte, ILs offer many advantages, such as good chemical and thermal stability, negligible vapor pressure, nonflammability, high ionic conductivity, and wide electrochemical window. Thus, ILs have been intensively pursued as alternative electrolytes for DSSCs and other electrochemical devices. In the past few years, IL electrolytes were developed rapidly. Kubo *et al.* (Kubo *et al.*, 2002) investigated the physical and physiochemical properties of 1-alkyl-3-methylimidazolium iodides (alkyl chain: C3–C9). They found that the viscosity of the ILs increases with increasing alkyl chain length because of van der Waals forces. The conductivity of the ILs decreases with increasing viscosity since the diffusion of ions in a liquid depends on its viscosity. The electrolyte with 1-hexyl-3-methylimidazolium iodide gave the highest photoelectric conversion efficiency. Among these ionic liquids, alkylimidazolium-based ILs provide both iodide sources and solvents of electrolytes for DSSCs. The counterions in the alkylimidazolium based ionic liquid included  $\text{I}^-$ ,  $\text{N}(\text{CN})_2^-$ ,  $\text{B}(\text{CN})_4^-$ ,  $(\text{CF}_3\text{COO})_2\text{N}^-$ ,  $\text{BF}_4^-$ ,  $\text{PF}_6^-$ ,  $\text{NCS}^-$ , and so forth. However, 1-alkyl-3-methylimidazolium iodides are viscous liquid, whose viscosity is much higher than that of organic solvent based liquid electrolyte (viscosities for ACN and MPN are 0.37 cP and 1.60 cP, respectively), the transport of  $\text{I}_3^-$  in the electrolyte is very slow, thus limiting the current density and the cell efficiency. To improve the mobility of redox couple in the electrolyte and the photovoltaic performance, various ionic liquids with low viscosity were developed (Fei *et al.*, 2006). Grätzel group reported the DSSCs based on low-viscosity ionic liquid and PMII mixture (Wang *et al.*, 2003b; Wang *et al.*, 2004a; Kuang *et al.*, 2006; Kuang *et al.*, 2007). Besides alkylimidazolium cation, alkylpyridinium salt and trialkylmethylsulfonium-salt-based ILs were developed for electrolytes. Paulsson *et al.* (Paulsson *et al.*, 2003) obtained 3.7% photoelectric conversion efficiency for solar cells based on  $(\text{Bu}_2\text{Me})\text{SI}$  ionic liquid containing 1% iodine. Kawano *et al.* (Kawano *et al.*, 2004) reported 2% conversion efficiency in alkylpyridiniumcation-based IL. Wang *et al.* (Wang *et al.*, 2004b) achieved 7.5% efficiency in solvent-free EMISeCN-based IL containing  $\text{SeCN}^-/(\text{SeCN})_3^-$  electrolyte, which is comparable with  $\text{I}^-/\text{I}_3^-$  redox couple. However, the rareness of selenium and high costs has limited its application in DSSCs. Zhao *et al.* (Zhao *et al.*, 2008) reported a solid-state DSSC utilizing imidazolium-type ionic crystal as transfer layer, and obtained a good cell efficiency of 3.1% under one sun irradiation by adopting 1-methyl-3-propylimidazolium tetrafluoroborate as a crystal growth inhibitor, lithium bis-trifluoro-methanesulfonylimide as a charge transport enhancer, and 4-tert-butylpyridine (TBP) as a carrier recombination inhibitor. As shown in their work, the cell efficiency remained 60% of the initial value after 30 days at room temperature. Besides, Ikeda *et al.* (Ikeda *et al.*, 2005) also constructed a solid-state DSSC with a poly(N-vinyl-carbazole) hole transporter mediated by an alkali iodide. They reached a cell efficiency of 2.0% under one sun irradiation, but without the incorporation of volatile components (TBP, iodine) in their devices. On their further study (Ikeda *et al.*, 2006), a clay-like conductive composite which contained only polyaniline-

loaded carbon black (PACB) particles and an ethyleneoxide-substituted imidazolium iodide was used as composite electrolyte; the corresponding quasi-solid-state DSSC showed a cell efficiency of 3.48% under one sun irradiation. Besides, a new class of solid-state ionic conductor with a carbazole-imidazolium cation was synthesized by Midya *et al.* and investigated for application in all-solid-state DSSCs (Midya *et al.*, 2010). This kind of solid-state electrolyte containing the designed solid-state ionic conductor and iodine provide dual channels for hole/triiodide transportation, giving rise to a conversion efficiency of 2.85% under one sun irradiation.

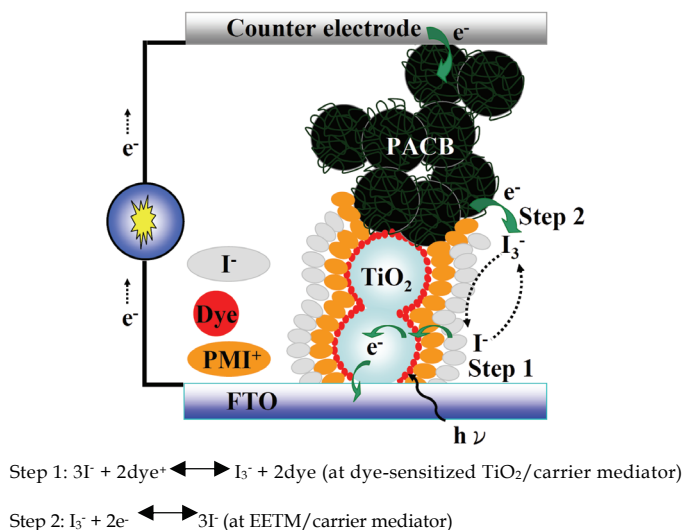


Fig. 3. The charge-transport process in a DSSC with a quasi-solid-state composite electrolyte containing an IL and PACB (Lee *et al.*, 2010a).

In the following discussions, our previous works are classified into three systems and reviewed to cover ILs-based DSSCs with good durability. In the first one (system A) (Lee *et al.*, 2009b), we compared the physicochemical properties of different structures of ILs such as 1-alkyl-3-methylimidazolium tetrafluoroborate containing various alkyl side chain lengths (alkyl chains used having the chemical formula  $\text{C}_n\text{H}_{2n+1}$ , where  $n=2, 4, 6, 8$ ), and 1-butyl-3-methylimidazolium salts containing various anions such as  $\text{BF}_4^-$ ,  $\text{PF}_6^-$  and  $\text{SO}_3\text{CF}_3^-$  on the cell performance at room temperature. An electrochemical impedance spectra (EIS) technique is also used to analyze the charge transport resistances in DSSCs, and further fit the data in Nyquist plot and calculate the exact time constant of the electrons in DSSCs, so as to understand the effect of various ILs in DSSCs. In the second system (system B) (Lee *et al.*, 2010a), we developed a quasi-solid-state DSSC with a non-volatile composite electrolyte, comprising PACB and the IL, PMII, without adding iodine. The structure of the DSSC with this kind of non-volatile composite electrolyte is shown in Figure 3. A higher cell efficiency could be achieved with the same composite electrolyte with the addition of EMISCN (1-ethyl-3-methylimidazolium thiocyanate). It is expected that PACB could form an extended electron transfer material (EETM) to reduce the diffusion length for  $\text{I}^-$  and  $\text{I}_3^-$  ions in the electrolyte, and also simultaneously serves as a charge-transporter and a catalyst for  $\text{I}_3^-$ .

reduction. Thus ultimately an iodine-free, cost-effective, efficient, and durable quasi-solid-state DSSC could be fabricated. Besides, iodine-free electrolyte is desirable for flexible metal-based DSSCs where a metal substrate, such as titanium is prone to corrosion by iodine. For the third one (system C) (Lee *et al.*, 2010b), we reported the fabrication of an all-solid-state DSSC with a hybrid SWCNT-binary charge transfer intermediate (CTI), consisting of single wall carbon nanotubes (SWCNT), EMII and PMII, without the addition of iodine and TBP. It is expected that the SWCNTs in the composite electrolyte serves simultaneously as the filler for physical gelation of electrolyte and as the catalyst for electrochemical reduction of  $I_3^-$ . Moreover, we utilized 1-methyl-3-propylimidazolium iodine (PMII), which acts simultaneously as a co-charge transfer intermediate and crystal growth inhibitor, to further improve the cell efficiency. The advantage of this device with respect to the hybrid SWCNT-binary CTI lies also in the fact that both ionic liquids and the carbon materials were considered to be stable materials (Fig. 4) and be environmentally friendly. Thus, this kind of composite electrolyte is suitable for application in DSSCs.

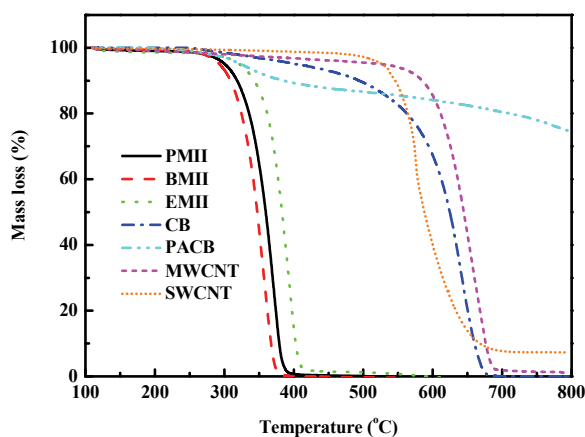


Fig. 4. Thermogravimetric traces of all components in the composite electrolyte (Lee *et al.*, 2010a & 2010b).

### 3. Experimental

#### 3.1 Chemicals and instruments

Both the key chemicals and instruments used for systems A, B, and C are partially listed here. Tert-butyl alcohol (tBA, 96%), 4-tert-butylpyridine (TBP, 99.5%), 1-ethyl-3-methylimidazolium tetrafluoroborate (EMIBF<sub>4</sub>), 1-butyl-3-methylimidazolium tetrafluoroborate (BMIBF<sub>4</sub>), 1-hexyl-3-methylimidazolium tetrafluoroborate (HMIBF<sub>4</sub>), 1-octyl-3-methylimidazolium tetrafluoroborate (OMIBF<sub>4</sub>), 1-butyl-3-methylimidazolium hexafluorophosphate (BMIPF<sub>6</sub>), and 1-butyl-3-methylimidazolium trifluoromethanesulfonate (BMISO<sub>3</sub>CF<sub>3</sub>) were obtained from Acros and used without further purification. The N3 dye, N719 dye and Surlyn® (SX1170-25) spacer were purchased from Solaronix (Solaronix S.A., Aubonne, Switzerland). Lithium iodide (LiI, synthetical grade), iodine (I<sub>2</sub>), poly(ethylene glycol) (PEG, M.W. 20,000), 1-methyl-3-propyl imidazolium iodide (PMII), and 1-buty-3-methylimidazolium iodide (BMII) were obtained from Merck; 1-ethyl-3-methylimidazolium

iodide (EMII) was obtained from TCI (Tokyo Chemical Industry Co., Ltd.); 1-ethyl-3-methylimidazolium thiocyanate (EMISCN), titanium (IV) isopropoxide (TTIP, 98%), acetonitrile (ACN, 99.99%), acetylacetone (AA, 99.5%), ethanol (99.5%), and isopropyl alcohol (IPA, 99.5%) were obtained from Aldrich. The polyaniline-loaded carbon black (PACB), which was supplied from Sigma-Aldrich Inc., contained 20 wt% of polyaniline emeraldine salt (half oxidized and hydrogenated polyaniline doped with organic sulfonic acid). The single wall carbon nanotubes (SWCNTs, >90%, specific surface area: >300 m<sup>2</sup> g<sup>-1</sup>, diameter: 2nm, length: 5~15  $\mu$ m) were supplied from Sciencetech Corporation (Taipei, Taiwan). The thermal stability of each component in the composite electrolyte was characterized by a thermogravimetric analyzer (TGA, TGA-7, Perkin-Elmer). The differential scanning calorimetric (DSC, Q20, TA instruments) was used to observe the variations of the binary CTI with various compositions. The morphology of the film was obtained using a field emission scanning electron microscopy (FEI ultra-high resolution FE-SEM with low vacuum mode, Nova NanoSEM 230). The thickness of TiO<sub>2</sub> film was determined using a surface profilometer (Sloan Dektak 3030). The surface of the DSSC was illuminated by a class A quality solar simulator (PEC-L11, AM1.5G, Peccell Technologies, Inc., Japan). The incident light intensity (100 mW cm<sup>-2</sup>) was calibrated with a standard Si cell (PECSI01, Peccell Technologies, Inc.). The photoelectrochemical characteristics of the DSSC were recorded with a potentiostat/galvanostat (PGSTAT 30, Autolab, Eco-Chemie, the Netherlands). EIS data were obtained by the above-mentioned potentiostat/galvanostat equipped with an FRA2 module under a constant light illumination of 100 mW cm<sup>-2</sup>. The frequency range explored was 10 mHz to 65 kHz. The applied bias voltage and ac amplitude were set at the open-circuit voltage of the DSSCs and 10 mV, respectively, between the counter electrode and the FTO-TiO<sub>2</sub>-dye working electrode, starting from the short-circuit condition. The impedance spectra were analyzed by an equivalent circuit model (Han *et al.*, 2004; Han *et al.*, 2006).

### 3.2 Fabrication of DSSCs

The schematic diagram for the fabrication of DSSCs is presented in Fig. 5. The succinct fabrication processes are presented below. A fluorine-doped SnO<sub>2</sub> conducting glass (FTO, 15  $\Omega$  sq<sup>-1</sup>, Solaronix S.A., Aubonne, Switzerland) was first cleaned with a neutral cleaner, and then washed with DI-water, acetone, and IPA, sequentially. The conducting surface of the FTO was treated with a solution of TTIP (0.084 g) in ethanol (10 ml) for obtaining a good mechanical contact between the conducting glass and TiO<sub>2</sub> film. A 10  $\mu$ m-thick film of TiO<sub>2</sub> was coated by doctor blade method onto the treated conducting glass and a portion of 0.4×0.4 cm<sup>2</sup> was selected as the active area by removing the side portions by scraping. The TiO<sub>2</sub> film was gradually heated to 500 °C in an oxygen atmosphere, and subsequently sintered at that temperature for 30 min. After sintering at 500 °C and cooling to 80 °C, the TiO<sub>2</sub> electrode was immersed in a 3×10<sup>-4</sup> M solution of dye (N3 or N719) in ACN and tBA (in the volume ratio of 1:1) at room temperature for 24 h. After dye-adsorption, a 25  $\mu$ m-thick Surlyn<sup>®</sup> spacer was put on the dye-sensitized TiO<sub>2</sub> electrode and attached by heating. The electrolyte was then coated onto the dye-sensitized TiO<sub>2</sub> film. The dye-sensitized TiO<sub>2</sub> electrode with the electrolyte was assembled with a platinum-sputtered conducting glass electrode (ITO, 7  $\Omega$  sq<sup>-1</sup>, Ritek), and the edges were sealed by UV glue (Optocast 3410 40K GEN2, Alexander Jewels Co., LTD.). As for the organic solvent electrolyte, a mixture of 0.1 M LiI, 0.6 M PMII, 0.05 M I<sub>2</sub>, and 0.5 M TBP in gamma-butyrolactone (GBL, Fluka) was used.

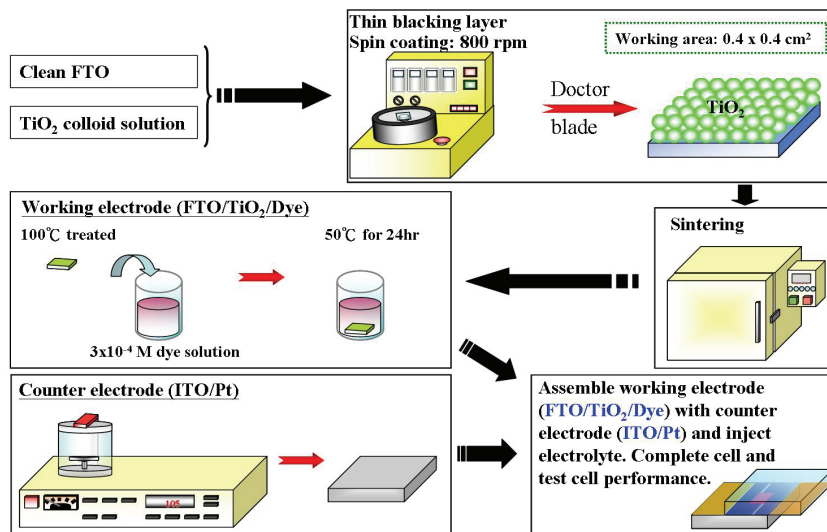


Fig. 5. Schematic diagram for the fabrication processes of DSSCs.

### 3.3 Preparation of quasi-solid-state electrolytes with ILs (system A)

The bi-IL electrolytes are obtained by mixing BMII with EMIBF<sub>4</sub>, BMIBF<sub>4</sub>, HMIBF<sub>4</sub>, OMIBF<sub>4</sub>, BMIPF<sub>6</sub>, or BMISO<sub>3</sub>CF<sub>3</sub> (13:7, v/v), respectively, followed by addition of 0.2 M I<sub>2</sub> and 0.5 M TBP. The prepared electrolytes were injected into the gap between the electrodes by capillarity, and the injecting process was kept at 80 °C because the viscosity of the IL electrolyte at 80 °C was low enough to penetrate into the space.

### 3.4 Preparation of near-solid-state electrolytes with nanoparticles solidified ILs (system B)

The composite electrolyte (Fig. 6) was prepared by mixing a solid powder of PACB or carbon black (CB, Alfa Aesar, 99.9%, *ca.* 42 nm) and one of the ILs mentioned above in a weight ratio of 1:8. Carbon black, owing to its larger size than the pore size of TiO<sub>2</sub> film (about 15-25 nm), is not expected to infiltrate into the film. At the same time, ACN was added to the composite to improve the mixing condition, and the contents were moved to a vacuum oven to obtain a well-mixed composite electrolyte. The composite electrolyte was then coated onto the dye-sensitized TiO<sub>2</sub> film at 80 °C to ensure that the IL can penetrate well into the porous structure.

### 3.5 Preparation of all-solid-state electrolytes with IL crystals (system C)

The hybrid SWCNT-binary CTIs were prepared by mixing the solid powder (SWCNTs) and the binary ILs (PMII and EMII) mentioned above in a weight ratio of 1:9. At the same time, ACN was added to the composite to improve the mixing, and was removed on a hot plate at a temperature of 90 °C. The hybrid SWCNT-binary CTI was then put onto the dye-sensitized TiO<sub>2</sub> film at 90 °C to ensure that the ILs can penetrate well into the porous structure and remove the residual ACN. From Fig. 7a, it shows that EMII and PMII have different colors, namely, bright yellow and deep brown, respectively. With the increase of addition of PMII

into EMII (0 to 80 wt%) the binary CTI (EMII mix with PMII) turns uniformly into brown color. Besides, the binary CTI (EMII/PMII = 40/60) with the addition of SWCNTs still has a solid-like form in an oven at 75 °C (Fig. 7b).

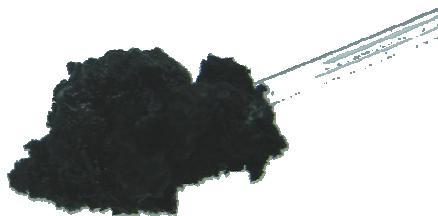


Fig. 6. The photograph of the composite electrolyte prepared with PACB and ILs (Lee *et al.*, 2010a).

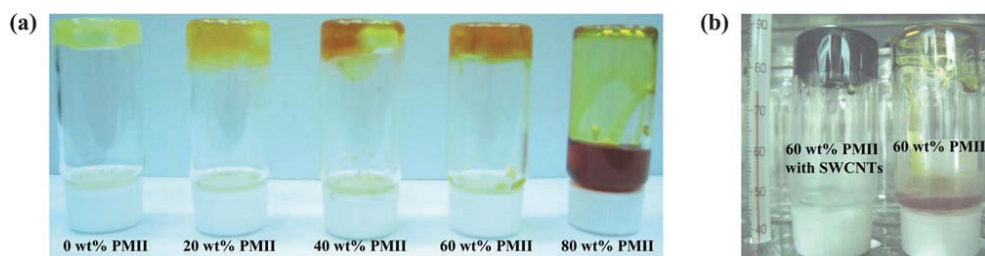


Fig. 7. (a) The pictures of the binary CTI with different weight percents of PMII. (b) The pictures of the binary CTI containing 60 wt% PMII with or without SWCNTs at 75 °C (Lee *et al.*, 2010b).

#### 4. Results and discussions of system A

In system A, steady-state voltammograms for  $I^-/I_3^-$  in 1-alkyl-3-methylimidazolium tetrafluoroborate with various lengths of side chain ( $C=2, 4, 6, 8$ ) and BMI<sup>+</sup> with different anions are performed and the calculated apparent diffusivity ( $D_{app}$ ) are shown in Table 1.

ILs	$D_{app}(I^-)$ ( $\text{cm}^2 \text{s}^{-1}$ )	$D_{app}(I_3^-)$ ( $\text{cm}^2 \text{s}^{-1}$ )	$J_{sc}$ ( $\text{mA cm}^{-2}$ )	$V_{OC}$ (V)	$\eta$ (%)	FF	$R_{diff}$ (ohm)	$\tau_n$ (ms) <sup>a</sup>
EMIBF <sub>4</sub>	$4.40 \times 10^{-7}$	$2.01 \times 10^{-7}$	7.78	0.647	2.98	0.60	45.2	12.3
BMIBF <sub>4</sub>	$3.64 \times 10^{-7}$	$1.36 \times 10^{-7}$	7.77	0.651	3.02	0.59	58.1	12.5
HMIBF <sub>4</sub>	$2.98 \times 10^{-7}$	$1.04 \times 10^{-7}$	7.51	0.643	2.81	0.58	63.4	14.4
OMIBF <sub>4</sub>	$2.71 \times 10^{-7}$	$1.02 \times 10^{-7}$	7.46	0.651	2.57	0.53	70.3	22.9
BMIPF <sub>6</sub>	$3.18 \times 10^{-7}$	$1.20 \times 10^{-7}$	6.76	0.649	2.61	0.60	60.2	12.7
BMISO <sub>3</sub> CF <sub>3</sub>	$3.58 \times 10^{-7}$	$1.31 \times 10^{-7}$	10.18	0.657	4.11	0.62	57.5	20.1

<sup>a</sup> The values of  $\tau_n$  were calculated from the fitting data of EIS measurements.

Table 1. The photovoltaic and EIS parameters of the DSSCs based on bi-ionic liquids with various side chain lengths and anions. The ionic diffusion coefficients were calculated from the limiting currents measured by a 10  $\mu\text{m}$  radius Pt ultramicroelectrode (Lee *et al.*, 2009b).



The result shows that the  $D_{app}$  of  $I^-$  and  $I_3^-$  decrease from  $4.40 \times 10^{-7}$  to  $2.71 \times 10^{-7}$   $\text{cm}^2 \text{s}^{-1}$  and  $2.01 \times 10^{-7}$  to  $1.02 \times 10^{-7}$   $\text{cm}^2 \text{s}^{-1}$ , respectively, by increasing the side chain length of ILs from C2 to C8. On the other hand,  $\text{BMI}^+$  containing  $\text{BF}_4^-$  has higher  $D_{app}$  than  $\text{PF}_6^-$  or  $\text{SO}_3\text{CF}_3^-$ . The  $D_{app}$  results show an inverse trend to the viscosity of the ILs. The photovoltaic characteristic parameters of DSSCs based on different ILs are also listed in Table 1. The DSSC containing

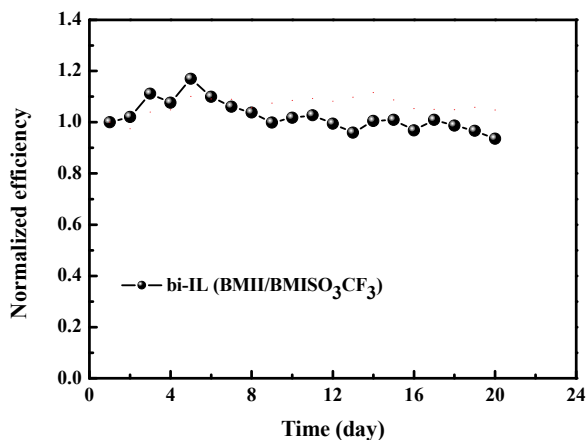


Fig. 8. The durability tests of the DSSCs based on bi-ILs ( $\text{BMII}/\text{BMISO}_3\text{CF}_3$ ) (Lee *et al.*, 2010b).

$\text{EMIBF}_4$  has higher current density and conversion efficiency than other chain lengths due to higher  $D_{app}$  of  $I^-$  and  $I_3^-$ . The charge transport in DSSCs was determined by the transport of  $I^-/I_3^-$  in the IL electrolytes, thus the decreased fill factor ( $FF$ ) and cell conversion efficiency with the increase of the side chain length of IL is resulted from the increased viscosity for longer chain length. The equivalent circuit employed for the curves fitted the impedance spectra of the DSSCs are also shown in Table 1. The  $R_{diff}$  increased with the increase in the side chain length, and the similar trend has been observed with the  $D_{app}$  also. Meanwhile, the time constant ( $\tau_n$ ) of electron in  $\text{TiO}_2$  film increases from 12.3 to 22.9 ms with the increase in side chain length from C2 to C8. This result is similar to the previously reported results by Kubo *et al.* (Kubo *et al.*, 2002), where the electron lifetimes increase with increasing of side chain length of imidazolium iodides from C3 to C9. Thus, it was found that the DSSC containing C7-imidazolium iodides has the best conversion efficiency due to the combination effects of the electron lifetime in  $\text{TiO}_2$  electrode and the electrolyte viscosity (Kubo *et al.*, 2002). In our system, as listed in Table 1, the DSSC containing  $\text{EMIBF}_4$  has higher current density than other longer side chain lengths. Meanwhile, the  $FF$  significantly decreased with the increase in side chain length, which was due to the increase in ions diffusion resistance and the lower electron transfer at the counter electrode. It is supported via the high-frequency (103–105 Hz) peaks in the Bode phase plot, shifting to lower frequency with increasing of side chain length (not shown here). Consequently, the electron lifetime in  $\text{TiO}_2$  electrode and the viscosity of electrolyte are the two main factors on the cell performances of DSSCs with bi-IL electrolyte systems. As to the effect of anions of ionic liquids on DSSCs, the time constants of the  $\text{BMIBF}_4$ ,  $\text{BMIPF}_6$  and  $\text{BMISO}_3\text{CF}_3$  based DSSCs are found to be 12.5, 12.7 and 20.1 ms, respectively, as shown in Table 1. Thus, the DSSC

containing  $\text{BMISO}_3\text{CF}_3$  has longer electron lifetime, which resulted in the best cell performance, in which the short-circuit current density ( $J_{sc}$ ), open-circuit voltage ( $V_{oc}$ ), conversion efficiency ( $\eta$ ) and  $FF$  were  $10.18 \text{ mA cm}^{-2}$ ,  $0.657 \text{ V}$ ,  $4.11\%$  and  $0.62$ , respectively, as listed in Table 1. As shown in Fig. 8, the at-rest long-term stability of DSSCs with  $\text{BMISO}_3\text{CF}_3$  gives slight decay (smaller than  $5\%$ ) after being stored for more than  $576 \text{ h}$ .

References	Composition	Dye	$\eta(\%)$	Stability
Wang <i>et al.</i> , 2003b	Binary ILs (PMII/EMIDCN) with $\text{I}^-/\text{I}_3^-$	Z907	6.60	N/A
Wang <i>et al.</i> , 2004a	Binary ILs (PMII/EMINCS) with $\text{I}^-/\text{I}_3^-$	Z907	7.00	N/A
Wang <i>et al.</i> , 2004b	IL with $\text{SeCN}^-/(\text{SeCN})_3^-$ , Iodine-free	Z907	7.50	N/A
Kuang <i>et al.</i> , 2004b	Binary ILs (PMII/EMIB(CN) $_4$ ) with $\text{I}^-/\text{I}_3^-$	K77	7.60	1,000 h light-soaking at $60^\circ\text{C}$ , decay $9\%$
Jhong <i>et al.</i> , 2009	Binary ILs (PMII/G.Cl) with $\text{I}^-/\text{I}_3^-$	D149	3.88	N/A
Lee <i>et al.</i> , 2009b (system A)	Binary ILs (BMII/BMISO $_3\text{CF}_3$ ) with $\text{I}^-/\text{I}_3^-$	N3	4.11	576 h at-rest at $25^\circ\text{C}$ , decay $< 5\%$

Table 2. Partial literatures reported on the quasi-solid-state DSSCs with ILs electrolytes.

Table 2 is a partial list of the quasi-solid-state DSSCs reported in literatures based on IL electrolytes. Normally, the conversion efficiency obtained with ILs at full solar irradiation ( $\text{AM } 1.5$ ,  $100 \text{ mW cm}^{-2}$ ) have been markedly lower than those achieved with organic solvent based electrolytes, only recently efficiencies of  $5\sim 6\%$  were achieved for DSSCs with pure ILs electrolyte (Wang *et al.*, 2002; Wang *et al.*, 2003a). Wang *et al.* (Wang *et al.*, 2003b) first prepared a binary-ILs electrolyte that consisted of PMII, EMIDCN, and LiI in a device to obtain a cell with an efficiency of  $6.6\%$  at full solar irradiation. However, their subsequent research showed that the presence of EMIDCN in the bi-ILs electrolyte led to an instability of the cells under visible light soaking. Hence, they used a new ILs electrolyte composed of PMII and EMINCS and a cell efficiency of  $7.00\%$  was obtained (Wang *et al.*, 2004a). In addition, they also developed an iodine-free  $\text{SeCN}^-/(\text{SeCN})_3^-$  based IL electrolyte by incorporation of a new, low viscosity IL EMISecN, and a high efficiency of  $7.5\%$  was achieved (Wang *et al.*, 2004b). For the first time an alternative redox couple has been identified that can rival or even exceed the performance of the iodide/triiodide couple at full sunlight. Kuang *et al.* reported on a new record of  $7.6\%$  cell efficiency under full sunlight irradiation using a EMIB(CN) $_4$  based binary-ILs electrolyte in combination with the high-molar-extinction-coefficient sensitizer K77 (Kuang *et al.*, 2004b). The cell with EMIB(CN) $_4$  based binary-ILs electrolyte maintained more than  $90\%$  of their initial efficiency under light-soaking at  $60^\circ\text{C}$  for  $1000 \text{ h}$ . Jhong *et al.* utilized a quaternary ammonium salt-derivative IL, called G. Cl, which is a eutectic mixture of glycerol and choline iodide as electrolyte for DSSCs, and a cell efficiency of  $3.88\%$  was achieved (Jhong *et al.*, 2009).

## 5. Results and discussions of system B

In system B, two ILs, BMII and PMII with different viscosities, were used as charge carrier mediators of the DSSCs. Table 3 (Case 2) shows that the cell efficiency of PMII/CB device is 4.38% ( $J_{SC}$ : 8.89 mA cm<sup>-2</sup>,  $V_{OC}$ : 726 mV,  $FF$ : 0.68), which is higher than that of BMII/CB device with an efficiency of 3.68% ( $J_{SC}$ : 8.04 mA cm<sup>-2</sup>,  $V_{OC}$ : 724 mV,  $FF$ : 0.63). As shown in Fig. 9a, PMII/CB cell has smaller  $R_{ct2}$  than BMII/CB cell, because PMII has lower viscosity than BMII (Pringle *et al.*, 2002; Fredlake *et al.*, 2004). In order to study the role of CB, ILs/CB composite electrolytes were replaced with the corresponding two bare ILs, i.e., with BMII and PMII. It can be seen in Table 3 (Case 1) that the cell efficiencies in both cases are much smaller than 1%, due to significant decrease in both  $J_{SC}$  and  $FF$ . Through the EIS analysis for pure ILs (Fig. 9b), the Warburg diffusion resistances ( $R_{diff}$ ) for I<sup>-</sup> and I<sub>3</sub><sup>-</sup> ions and the resistances of the charge-transfer at the counter electrodes ( $R_{ct1}$ ) have increased by about 2.5 and 5 times, respectively, as compared to the corresponding values from Fig. 9a. From these observations, it is more clear that the presence of CB as the extended electron transfer material (EETM) facilitates the electron transfer from the counter electrode to I<sub>3</sub><sup>-</sup> ions; a shorter length for I<sub>3</sub><sup>-</sup> ions and thereby for I<sup>-</sup> ions is created which enables the redox couple to work more efficiently than they would in the absence of the carbon material. From the literature reported by Ikeda *et al.* (Ikeda *et al.*, 2006), we found that the incorporation of I<sub>2</sub> is not necessary as shown in Table 4, and even detrimental in our case (Lee *et al.*, 2010a). This suggests that the iodide anion based IL can provide sufficient I<sup>-</sup> for the regeneration of the oxidized dye under illumination; I<sup>-</sup> in turn oxidizes to I<sub>3</sub><sup>-</sup>, which can be reduced back to I<sup>-</sup> at the EETM. Increasing the content of I<sub>2</sub> can increase concentration of polyiodides in the porous dye-coated TiO<sub>2</sub> matrix. It can facilitate recombination of injected conduction band electrons with polyiodides, and increase the dark current (Lee *et al.*, 2010a). Furthermore, increasing I<sub>2</sub> content also leads to enhanced light absorption even in the visible range by the carrier mediator existing in the porous dye-coated TiO<sub>2</sub> matrix. This decreases the light-harvesting of dye molecules (Wang *et al.*, 2006). Therefore, both  $V_{OC}$  and  $J_{SC}$  show decreases with the increases in the wt% of I<sub>2</sub> for this system. When CB was replaced with PACB, the highest cell efficiency of 5.81% was obtained. The results are shown in Table 3 (Case 3). A smaller interfacial resistance was obtained for the DSSC with PMII/PACB composite electrolyte than that for the cell with PMII/CB (Lee *et al.*, 2010a). According to a recent

Electrolyte	$V_{OC}$ (mV)	$J_{SC}$ (mA cm <sup>-2</sup> )	$\eta$ (%)	$FF$
Case 1 (Bare ILs)				
BMII	740	1.10	0.3	0.37
PMII	726	2.17	0.6	0.38
Case 2 (ILs/CB composite electrolytes)				
BMII/CB	724	8.04	3.68	0.63
PMII/CB	726	8.89	4.38	0.68
Case 3 (PMII/PACB composite electrolyte)				
PMII/PACB	737	12.20	5.81	0.65

Table 3. Photovoltaic parameters of the DSSCs with different composite electrolytes and with bare IL electrolytes, measured at 100 mWcm<sup>-2</sup> light intensity (Lee *et al.*, 2010a).

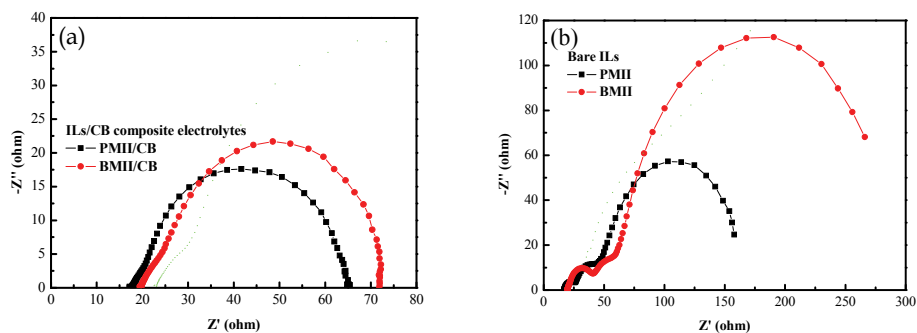


Fig. 9. EIS of the DSSCs with (a) PMII/CB and BMII/CB electrolytes (b) pure IL electrolytes, measured at  $100 \text{ mW cm}^{-2}$  light intensity under open-circuit voltage (Lee *et al.*, 2010a).

Iodine content (%)	$J_{SC}$ ( $\text{mA cm}^{-2}$ )	$V_{OC}$ (V)	$FF$	$\eta$ (%)
0	12.8	0.58	0.47	3.48
1.2	10.0	0.55	0.48	2.76
2.4	9.99	0.53	0.50	2.68
3.6	8.79	0.52	0.53	2.47
14	6.88	0.50	0.55	1.87

Table 4. Photoelectric performances of dye- $\text{TiO}_2$ /PACB-EOI/FTO solid-state dye-sensitized photocells measured under simulated solar irradiation of 1 sun (AM1.5) and influence of the content of  $\text{I}_2$  (wt%) added in the PACB-EOI layer on the cell performance (Ikeda *et al.*, 2006).

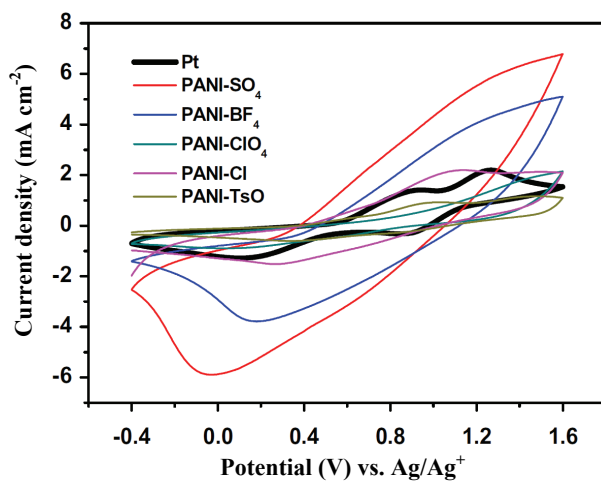


Fig. 10. CVs of electropolymerized-PANI with  $400 \text{ mC cm}^{-2}$  doped by different counterions and Pt CEs in  $10 \text{ mM LiI}$ ,  $1 \text{ mM I}_2$ , and  $0.1 \text{ M LiClO}_4$  acetonitrile solution (Li *et al.*, 2009).

report by Li (Li *et al.*, 2009), polyaniline shows high reduction current for the reduction of  $I_3^-$  (Fig. 10). Based on this report, it is inferred that more charge-transfer paths were formed between PMII and the polymer chains of PACB than those between the PMII and bare CB. This can be the reason for the better performance of the cell with PACB than that with CB. Interestingly, the devices using bare ITO as counter electrode still exhibit cell efficiencies of 3.65% and 2.67% for PMII/PACB and PMII/CB, respectively (Lee *et al.*, 2010a). Therefore, the significance of these carbon materials (PACB or CB) as catalysts in the form of EETM for the reduction of  $I_3^-$  ions to  $I^-$  ions at the counter electrode was univocally established from the fact that an efficiency as high as 3.65% could be achieved for the DSSC using bare ITO glass as the counter electrode. Thus it is established through the above observations that the carbon material in the composite electrolyte serves simultaneously as a charge transporter in the electrolyte and as a catalyst for electrochemical reduction of  $I_3^-$  ions. To increase the efficiency further, the low-viscosity IL, EMISCN (25 cP at 21°C), was added into PMII (900 cP at 20 °C) to form a binary ionic liquid (bi-IL). With a volume ratio of 35/65 for EMISCN/PMII, a cell efficiency of 6.15% was achieved, indicating the beneficial effect of EMISCN (Chen *et al.*, 2010). The enhancement in the efficiency of the DSSC with EMISCN, with reference to the efficiency of the best cell without this IL (5.81%) is attributed to the less viscous nature of the EMISCN, which provides better penetration of the composite electrolyte into  $TiO_2$  and also better conductivity of the electrolyte for  $I^-$  and  $I_3^-$  ions. Figure 11 shows the durability of the cell with the PACB-bi-IL composite electrolyte at 70 °C. The DSSC with the PACB-bi-IL composite electrolyte shows an extraordinary durability even at 70 °C. The cell with organic liquid electrolyte lost its efficiency virtually in no time. Thus, these results proved beyond doubt that the durability of the DSSC with PACB-bi-IL composite electrolyte is far superior to that of a cell with organic liquid electrolyte.

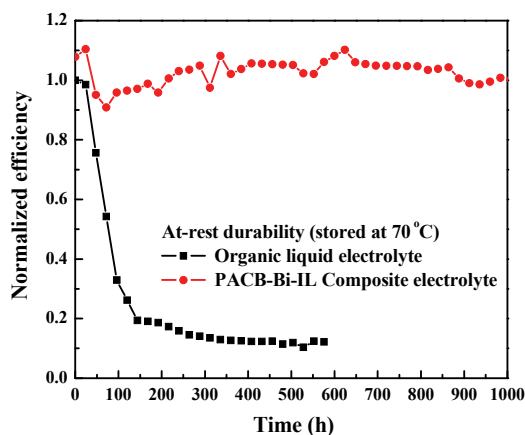


Fig. 11. At-rest durabilities of DSSCs stored at 70 °C, one with PACB-bi-IL composite electrolyte and the other with an organic liquid electrolyte (Chen *et al.*, 2010).

Table 5 is a partial list of the near-solid-state DSSCs reported in literatures with nanoparticles solidified ILs electrolytes. Hsui *et al.* prepared ionic gel electrolytes by

dispersing carbon materials (MWCNT, SWCNT, carbon black, carbon fiber and graphite) and  $\text{TiO}_2$  nanoparticles into binary ILs electrolytes for DSSCs and obtained the best cell efficiency of 5.00% when the  $\text{TiO}_2$  nanoparticles were incorporated (Hsui *et al.*, 2004). Ikeda *et al.* investigated a clay-like conductive composite electrolyte comprising polyaniline-loaded carbon black particles and an ethyleneoxide-substituted imidazolium iodide as shown in Fig. 12. The composite electrolyte was sandwiched between dye-sensitized porous  $\text{TiO}_2$  and counter electrode to form a near-solid-state DSSC, which achieved a cell efficiency of 3.48% at full sunlight irradiation without the addition of iodine (Ikeda *et al.*, 2006). Katakabe *et al.* demonstrated that the exchange-reaction-based diffusion and the interfacial charge-transfer rates of an iodide/triiodide redox couple in an ionic liquid were enhanced by the addition of  $\text{SiO}_2$  nanoparticles, although the composites successively became gels and solids with increasing nanoparticle content. Because of this acceleration of the charge transport and the interfacial charge-transfer rates, dye-sensitized solar cells using the

References	Composition	Dye	$\eta$ (%)	Stability
Hsui <i>et al.</i> , 2004	Binary ILs (EMII/EMITFSI) with $\text{I}^-/\text{I}_3^-$ , Addition of $\text{TiO}_2$	N3	5.00	N/A
Ikeda <i>et al.</i> , 2006	EOI with SWCNTs, Iodine-free	N719	3.48	N/A
Katakabe <i>et al.</i> , 2007	Binary ILs (EMII/G.Cl) with $\text{I}^-/\text{I}_3^-$ , Addition of $\text{SiO}_2$	N719	3.70	N/A
Chen <i>et al.</i> , 2010 (system B)	Binary ILs (PMII/EMISCN) with $\text{I}^-/\text{I}_3^-$ , Iodine-free	N719	6.15	1,000 h at-rest at 70 °C, no decay

Table 5. Partial literatures reported on the near-solid-state DSSCs with nanoparticles solidified ILs electrolytes.

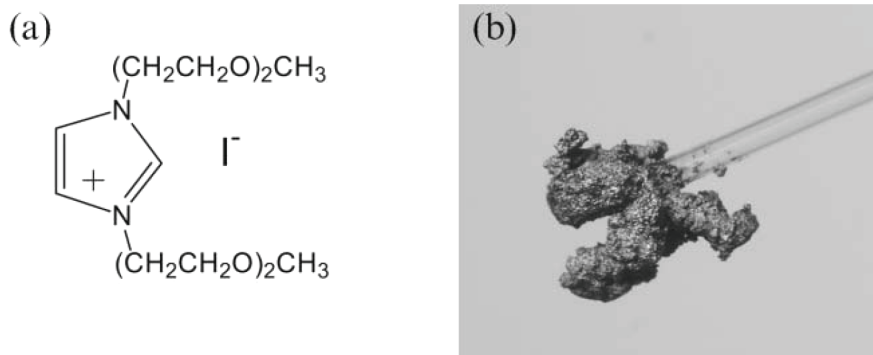


Fig. 12. (a) Molecular structure of the ethylene oxide-type ionic liquid iodide, EOI; (b) clay-like highly viscous, black paste of polyaniline-carbon black (PACB)-EOI composite (Ikeda *et al.*, 2006).

composite electrolytes achieved high conversion efficiencies of 3.70%, comparable to those using the pure or neat ionic liquid electrolyte (Katakabe *et al.*, 2007). In system B (Chen *et al.*, 2010), the near-solid-state DSSC with a non-volatile composite electrolyte, comprising PACB and the ionic liquid, PMII, without adding iodine showed a power conversion efficiency of 5.81%. A higher efficiency of 6.15% was achieved with the same composite electrolyte with the addition of EMISCN, the highest for any iodine-free quasi-solid-state DSSC. Besides, system B showed an unfailing stability at 70 °C, while the cell with liquid electrolyte lost its performance almost immediately. Thus, an iodine-free, cost-effective, efficient, and durable quasi-solid-state DSSC was realized.

## 6. Results and discussions of system C

Table 6 shows the photovoltaic parameters of the DSSCs using EMII as CTI with or without the incorporation of SWCNTs. A higher efficiency (1.88%) all-solid-state DSSC with this hybrid SWCNT-EMII was obtained as compared to that containing a bare EMII (0.41%). From EIS analysis, hybrid SWCNT-EMII cell has both smaller  $R_{ct2}$  and  $R_{diff}$  than those of a bare EMII cell. From this analysis, it is clear that the presence of SWCNTs as the EETM facilitates electron transfer from the counter electrode to  $I_3^-$  ions; a shorter diffusion length for  $I_3^-$  ions and thereby for  $I^-$  ions created, which enables the redox couple to work more efficiently than they would in the absence of SWCNTs. Moreover, it was found that incorporation of  $I_2$  is not necessary to drive the device. To further improve the cell efficiency, PMII was used; PMII acts simultaneously as CTI and a crystal growth inhibitor. Besides, the binary CTI exhibits a solid-like form when the content of PMII is increased to a weight percent of 60%, and a smoother surface morphology of the binary CTI is observed in this case as compared to that without the addition of PMII (Fig. 13). It is known that ionic crystallization would prevent the filling of solid-state electrolyte into the  $TiO_2$  porous structure and result in a decrease in photoelectrochemical responses of the device. Therefore, the inhibition of the crystal growth is expected to improve the cell performance for the all- solid-state DSSCs (Kumara *et al.*, 2002; Perera *et al.*, 2003). From DSC scans (Fig. 14), the melting point ( $T_m$ ) of the binary CTI decreases with the increase in the content of PMII. At a 60 weight percent of PMII, the melting point reaches 35 °C, which is already close to the room temperature. Table 7 shows that the cell efficiency increases with the increase in the content of PMII, and a cell efficiency of 3.49% was achieved at a weight ratio of 40/60 (EMII/PMII). From the EIS analysis, smaller  $R_{ct2}$  and  $R_{diff}$  are observed for the all-solid-state DSSCs containing hybrid SWCNT-binary CTI, as compared to the case without adding PMII; in consistency with our explanation that the presence of PMII leads to less

CTI layer	$J_{sc}$ (mA cm <sup>-2</sup> )	$V_{OC}$ (mV)	$\eta$ (%)	FF	$R_{ct2}$ (ohm)	$R_{diff}$ (ohm)
Bare EMII	1.11	652	0.41	0.56	685	-
SWCNTs-EMII	5.09	680	1.88	0.54	121	371

Table 6. The photovoltaic parameters of the DSSCs using EMII as CTI with or without the incorporation of SWCNTs (Lee *et al.*, 2010b).

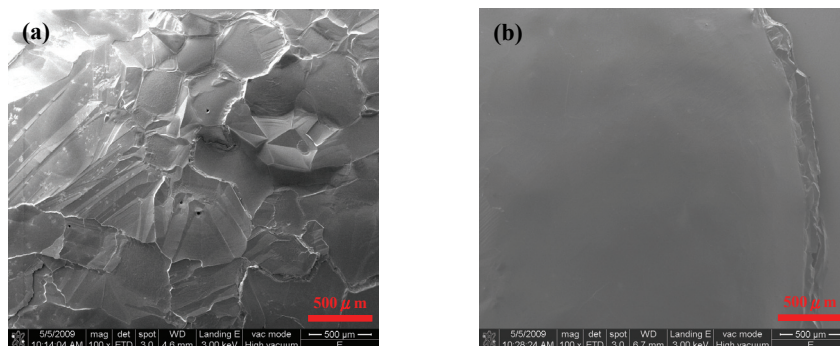


Fig. 13. SEM images of (a) bare EMII and (b) co-CTI, both after recrystallization by treating at 90 °C; EMII/PMII: 40/60 (weight ratio) (Lee *et al.*, 2010b).

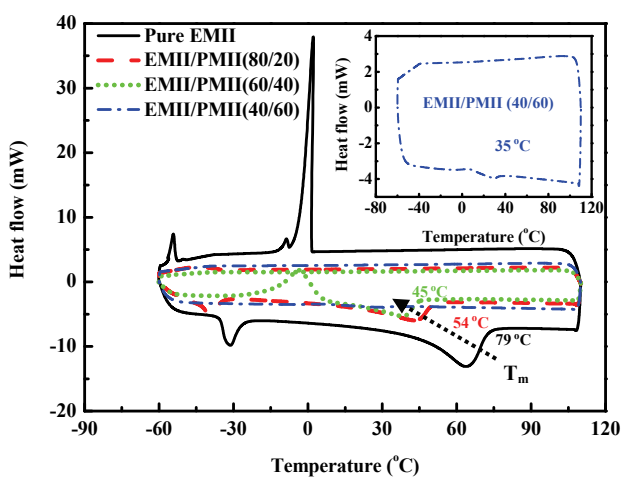


Fig. 14. DSC traces of binary CTI with different weight percents of PMII. The inset shows the magnified picture of the binary CTI with 60 wt% PMII (Lee *et al.*, 2010b).

EMII/PMII	$J_{SC}$ (mA cm <sup>-2</sup> )	$V_{OC}$ (mV)	$\eta$ (%)	$FF$	$R_{ct2}$ (ohm)	$R_{diff}$ (ohm)
100 : 0	5.09	680	1.88	0.54	121	371
80 : 20	5.32	706	2.23	0.59	81	167
60 : 40	6.70	716	3.01	0.62	75	84
40 : 60	8.07	716	3.49	0.61	59	68

Table 7. Photovoltaic performance parameters of the DSSCs with hybrid SWCNT-EMII, incorporating various amounts of PMII (wt%), measured at 100 mW cm<sup>-2</sup> (Lee *et al.*, 2010b).



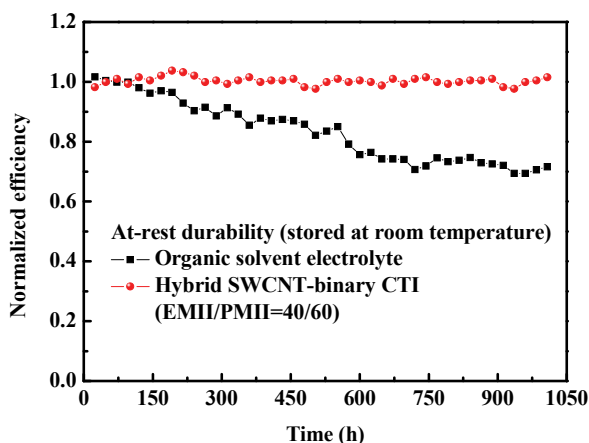


Fig. 15. The normalized efficiencies of DSSCs based on both hybrid SWCNT-binary CTI (EMII/PMII=40/60) and organic solvent electrolyte, respectively (Lee *et al.*, 2010b).

crystallization nature of the binary CTI, which penetrates deeper into the  $\text{TiO}_2$  and enhances the cell performance. Figure 15 shows the at-rest durability data of the DSSCs with hybrid SWCNT-binary CTI and organic liquid electrolyte. The proposed all-solid-state DSSCs showed excellent durability when compared with that of the cell with organic liquid electrolyte. It is noticed that the overall cell efficiency of the solid-state DSSC has increased about 1.5%, the overall cell efficiency of the DSSC with organic liquid electrolyte has decreased about 30% after more than 1,000 h, despite the fact that the boiling point of the organic solvent, GBL is 204 °C.

Table 8 is a partial list of the all-solid-state DSSCs obtained from the literatures. Ikeda *et al.* (Ikeda *et al.*, 2005) constructed an all-solid-state DSSC with a poly(*N*-vinyl-carbazole) (PVK) hole transporter mediated by an alkali iodide as illustrated in Fig. 16. They reached a cell efficiency of 2.0% under one sun irradiation, but without the incorporation of volatile

References	Composition	Dye	$\eta$ (%)	Stability
Ikeda <i>et al.</i> , 2005	PVK/alkali iodide/graphite with $\text{I}^-/\text{I}_3^-$ , Iodine-free	N719	2.00	N/A
Zhao <i>et al.</i> , 2008	IL crystal (MH-II) with $\text{I}^-/\text{I}_3^-$ and $\text{MPBF}_4$	N3	3.10	30 days at-rest at 25 °C, decay 40%
Midya <i>et al.</i> , 2010	IL crystal (SD) with $\text{I}^-/\text{I}_3^-$ and $\text{EMIB}(\text{CN})_4$	N719	2.85	N/A
Lee <i>et al.</i> , 2010b (system C)	IL crystal (EMII) with SWCNT and PMII, Iodine-free	N719	3.49	1,000 h at-rest at 25 °C, no decay

Table 8. Partial literatures reported on the all-solid-state DSSCs.

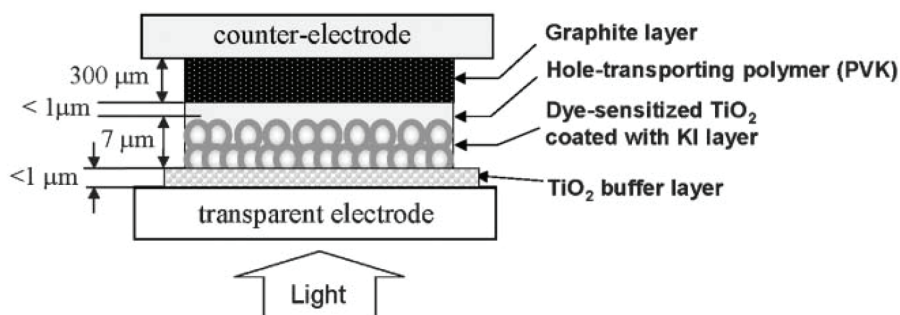


Fig. 16. Schematic structure of a solid-state dye-sensitized solar cell using PVK as a hole-transporting layer. (Ikeda *et al.*, 2005).

components (TBP,  $I_2$ ) in their devices. Zhao *et al.* (Zhao *et al.*, 2008) reported a solid-state DSSC utilizing imidazolium-type ionic crystal as transfer layer, and obtained a good cell efficiency of 3.1% under one sun irradiation by adopting 1-methyl-3-propylimidazolium tetra-fluoroborate as a crystal growth inhibitor, lithium bis-trifluoromethanesulfonylimide as a charge transport enhancer, and 4-*tert*-butylpyridine (TBP) as a carrier recombination inhibitor. As shown in their work (Fig. 17), the cell efficiency remained 60% of the initial value after 30 days at room temperature. Besides, a new class of solid-state ionic conductor based on a carbazole-imidazolium cation structure (Fig. 18) was synthesized by Midya *et al.* and investigated for application in all-solid-state DSSCs (Midya *et al.*, 2010). This kind of solid-state electrolyte containing the designed solid-state ionic conductor and iodine provide dual channels for hole/triiodide transportation (Fig. 19),

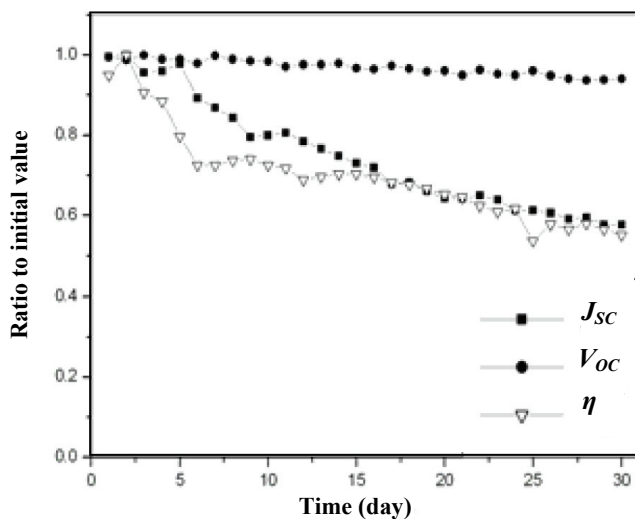


Fig. 17. The stability data of  $V_{oc}$  (●),  $J_{sc}$  (■),  $\eta$  (▽) for an all-solid-state DSSC (Zhao *et al.*, 2008).

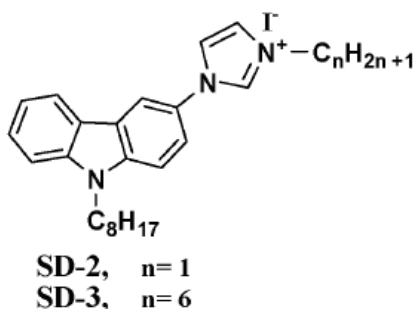


Fig. 18. The molecular structure of solid-state ionic conductor (Midya *et al.*, 2010).

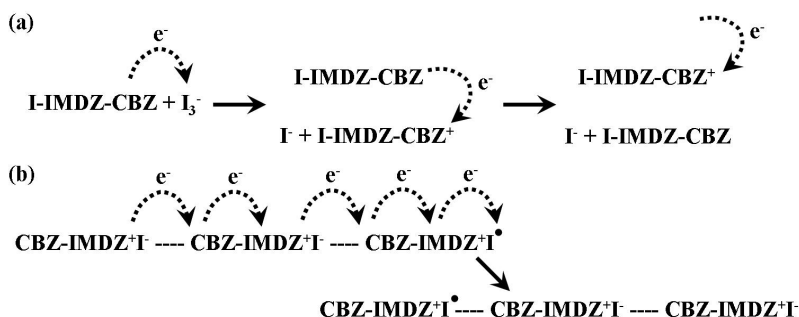


Fig. 19. Schematic illustration of the mechanisms of (a) hole hopping and (b) iodine radical transport through CBZ-IMDZ-I solid-state ionic conductors (Midya *et al.*, 2010).

giving rise to a conversion efficiency of 2.85% under one sun irradiation. System C proved that the all-solid-state DSSC with a hybrid SWCNT-binary CTI should avoid the problem of leakage or evaporation for traditional DSSCs and also provide the useful technique for fabrication of the DSSCs without losing their intrinsic performances. Most importantly, this system provides a unique approach to prepare all-solid-state CTI with organic ionic salts having relatively lower melting points ( $<100^\circ\text{C}$ ) in contrast to inorganic ionic salts mentioned in literature (Ikeda *et al.*, 2005), which normally having melting points higher than *ca.*  $300^\circ\text{C}$ . This approach in system C has advantage in that CTI can be filled in the porous  $\text{TiO}_2$  matrix under relatively low heating temperature (says,  $90^\circ\text{C}$ ). Another novel concept is also introduced, i.e., the melting point of the CTI is controlled through the adjustment of the composition of the binary CTI; this precludes a molecular design for organic ionic salts (Zhao *et al.*, 2008). At the same time, the charge transport is enhanced and both the carrier recombination and the crystallization of CTI is reduced through the incorporation of hybrid SWCNT-binary CTI, and without the incorporation of any volatile component (TBP, iodine etc). The all-solid-state DSSC in this schystem shows one of the best cell efficiencies, considering those reported in the literatures (Ikeda *et al.*, 2005; Zhao *et al.*, 2008).

## 7. Conclusions and future works

In this chapter, we first review general progress on IL-based electrolytes for DSSCs. The selected researches cover IL electrolytes for DSSCs published during 2002~2010. Efficiencies of 5~6% were initially achieved for DSSCs with pure ILs electrolyte proposed by Wang *et al.* (Wang *et al.*, 2002; Wang *et al.*, 2003a). They (Wang *et al.*, 2003b) firstly prepared a binary-ILs electrolyte (PMII/EMIDCN) and obtained a cell with an improved efficiency of 6.6%. They also used new binary-ILs electrolyte composed of PMII and EMINCS and a cell efficiency of 7.00% was obtained (Wang *et al.*, 2004a). Further, they developed an iodine-free SeCN<sup>-</sup>/(SeCN)<sub>3</sub><sup>-</sup> based IL electrolyte by incorporation of a new, low viscosity IL EMISCN, and a high efficiency of 7.5% was achieved (Wang *et al.*, 2004b) for the first time. Kuang *et al.* reported on a record of 7.6% cell efficiency using a EMIB(CN)<sub>4</sub> based binary-ILs electrolyte in combination with the high molar extinction coefficient sensitizer K77 (Kuang *et al.*, 2004b). Hsui *et al.* prepared a binary IL electrolyte by dispersing TiO<sub>2</sub> nanoparticles for DSSCs and obtained a cell efficiency of 5.00% (Hsui *et al.*, 2004). Ikeda *et al.* investigated a clay-like conductive composite electrolyte (EOI/PACB) for DSSCs, which achieved a cell efficiency of 3.48% without the addition of iodine (Ikeda *et al.*, 2006). Zhao *et al.* (Zhao *et al.*, 2008) reported a solid-state DSSC utilizing imidazolium-type ionic crystal (MH-II) as transfer layer, and obtained a good cell efficiency of 3.1%. Besides, a new class of solid-state ionic conductor (SD) based on a carbazole-imidazolium cation structure was synthesized and investigated for application in all-solid-state DSSCs with a conversion efficiency of 2.85%.

We then focus on the IL electrolytes developed in our group for DSSCs and categorize them into three systems, namely, quasi-solid-state (system A), near-solid-state (system B), and all-solid-state (system C). In system A, among the discussed bi-ILs electrolytes, the DSSC containing BMISO<sub>3</sub>CF<sub>3</sub> achieved the best cell efficiency of 4.11%. The at-rest long-term stability of DSSCs with BMISO<sub>3</sub>CF<sub>3</sub> shows slight decay (lower than 5%) after being stored for more than 576 h. In system B, the near-solid-state DSSC with a non-volatile composite electrolyte, comprising PACB and the ionic liquid, PMII, without added iodine, showed a power conversion efficiency of 5.81%. A higher efficiency of 6.18% was achieved with the same composite electrolyte with the addition of EMISCN, the highest value for any iodine-free near-solid-state DSSC. At 70 °C the near-solid-state DSSC showed an unfailing stability (more than 1,000 h). In system C, efficient all-solid-state DSSC was developed using a hybrid SWCNT-binary CTI (EMII/PMII) without the addition of iodine and TBP, and achieved a high efficiency (3.49%). The DSSC with the hybrid SWCNT-binary CTI showed an excellent durability at room temperature for 1,000 h.

Nowadays, most quasi-solid state DSSCs with ionic liquid electrolyte achieved relatively low cell efficiency as compared to the traditional DSSCs with liquid electrolyte. Despite the former system possessed superior long-term stability than that of the latter, the cell efficiency indeed needs to be further improved. Thereby, the recent challenge in ILs based quasi-solid state DSSCs is on how to lower the viscosity of the ILs and to enhance the diffusion rate of the redox couples. This matter would be a key issue for future study.

## 8. References

- Bach, U.; Lupo, D.; Comte, P.; Moser, J. E.; Weissörtel, F.; Salbeck, J.; Spreizer, H.; & Grätzel, M. (1998). Solid-state dye-sensitized mesoporous TiO<sub>2</sub> solar cells with high photon-to-electron conversion efficiencies. *Nature*, 395, 1998, 583-585.

- Chen, C. Y.; Wang, M. J.; Lee, Y.; Pootrakulchote, N.; Alibabaei, L.; Ngoc-le, C.-ha.; Decoppet, J.-D.; Tsai, J. H.; Grätzel, C.; Wu, C. G.; Zakeeruddin, S. M. & Grätzel, M. (2009). Highly efficient light-harvesting ruthenium sensitizer for thin-film dye-sensitized solar cells. *ACS NANO*, 3, 2009, 3103-3109.
- Chen, P. Y.; Lee, C. P.; Vittal, R. & Ho, K. C. (2010). A quasi solid-state dye-sensitized solar cell containing binary ionic liquid and polyaniline-loaded carbon black. *Journal of Power Sources*, 195, 2010, 3933-3938.
- Fei, Z.; Kuang, D.; Zhao, D.; Klein, C.; Ang, W. H.; Zakeeruddin, S. M.; Grätzel, M. & Dyson, P. J. (2006). A supercooled imidazolium iodide ionic liquid as a low-viscosity electrolyte for dye-sensitized solar cells. *Inorganic Chemistry*, 45, 2006, 10407-10409.
- Fredlake, C. P.; Crosthwaite, J. M.; Hert, D. G.; Aki, S. N. V. K. & Brennecke, J. F. (2004). Thermophysical properties of imidazolium-based ionic liquids. *Journal of Chemical & Engineering Data*, 49, 2004, 954-964.
- Grätzel, M. (2001). Photoelectrochemical cells. *Nature*, 414, 2001, 338-344.
- Hamakawa, Y. (2004). Thin-film solar cells: next generation photovoltaics and its applications. Springer-verlag, Germany, 2004.
- Han, L.; Koide, N.; Chiba, Y.; Islam, A. & Mitate, T. (2006). Modeling of an equivalent circuit for dye-sensitized solar cells: improvement of efficiency of dye-sensitized solar cells by reducing internal resistance, *Comptes Rendus Chimie*, 9, 2006, 645-651.
- Han, L.; Koide, N.; Chiba, Y. & Mitate, T. (2004). Modeling of an equivalent circuit for dye-sensitized solar cells. *Applied Physics Letters*, 84, 2004, 2433-2435.
- Ikeda, N. & Miyasaka, T. (2005). A solid-state dye-sensitized photovoltaic cell with a poly(N-vinyl-carbazole) hole transporter mediated by an alkali iodide. *Chemical Communications*, 2005, 1886-1888.
- Ikeda, N.; Teshima, K. & Miyasaka, T. (2006). Conductive polymer-carbon-imidazolium composite: a simple means for constructing solid-state dye-sensitized solar cells. *Chemical Communications*, 2006, 1733-1735.
- Jhong, H. U.; Wong, D. S.-H.; Wan, C. C.; Wang, Y. Y. & Wei T. C. (2009). A novel deep eutectic solvent-based ionic liquid used as electrolyte for dye-sensitized solar cells. *Electrochemistry Communications*, 11, 2009, 209-211.
- Kambe, S.; Nakade, S.; Kitamura, T.; Wada, Y. & Yanagida, S. (2002). Influence of the electrolytes on electron transport in mesoporous TiO<sub>2</sub>-electrolyte systems. *Journal of Physical Chemistry B*, 106, 2002, 2967-2972.
- Katakabe, T.; Kawano, R. & Watababe, M. (2007). Acceleration of redox diffusion and charge-transfer rates in an ionic liquid with nanoparticle addition. *Electrochemical and Solid-state Letters*, 10, 2007, F23-F25.
- Kawano, R.; Matsui, H.; Matsuyama, C.; Sato, A.; Susan, M. A. B. H.; Tanabe, N. & Watababe, M. (2004). High performance dye-sensitized solar cells using ionic liquids as their electrolytes. *Journal of Photochemistry and Photobiology A*, 164, 2004, 87-92.
- Krüger, J.; Plass, R. & Grätzel, M. (2002). Improvement of the photovoltaic performance of solid-state dye-sensitized device by silver complexation of the sensitizer cis-bis(4,4'-

- dicarboxy-2,2'-bipyridine)-bis(isothiocyanato) ruthenium(II). *Applied Physics Letters*, 81, 2002, 367-369.
- Krüger, J.; Plass, R.; Cevey, L.; Piccirelli, M. & Grätzel, M. (2001). High efficiency solid-state photovoltaic device due to inhibition of interface charge recombination. *Applied Physics Letters*, 79, 2001, 2085-2087.
- Kuang, D.; Klein, C.; Zhang, Z.; Ito, S.; Moser, J.-E.; Zakeeruddin, S. M. & Grätzel, M. (2007). Stable, high-efficiency ionic-liquid-based mesoscopic dye-sensitized solar cells. *Small*, 3, 2007, 2094-2102.
- Kuang, D.; Wang, P.; Ito, S.; Zakeeruddin, S. M. & Grätzel, M. (2006). Stable mesoscopic dye-sensitized solar cells based on tetracyanoborate ionic liquid electrolyte. *Journal of the American Chemical Society*, 128, 2006, 7732-7733.
- Kubo, W.; Kambe, S.; Nakade, S.; Kitamura, T.; Hanabusa, K.; Wada, Y. & Yanagida, S. (2003). Photocurrent-determining processes in quasi-solid-state dye-sensitized solar cells using ionic gel electrolytes. *Journal of Physical Chemistry B*, 107, 2003, 4374-4381.
- Kubo, W.; Kitamura, T.; Hanabusa, K.; Wada, Y. & Yanagida, S. (2002). Quasi-solid-state dye-sensitized solar cells using room temperature molten salts and a low molecular weight gelator. *Chemical Communications*, 2002, 374-375.
- Kubo, W.; Murakoshi, K.; Kitamura, T.; Yoshida, S.; Haruki, M.; Hanabusa, K.; Shirai, H.; Wada, Y. & Yanagida, S. (2001). Quasi-solid-state dye-sensitized TiO<sub>2</sub> solar cells: effective charge transport in mesoporous space filled with gel electrolytes containing iodide and iodine. *Journal of Physical Chemistry B*, 105, 2001, 12809-12815.
- Kumara, G. R. A.; Konno, A.; Shiratshchi, K.; Tsukahara, J. & Tennakone, K. (2002). Dye-sensitized solid-state solar cells: use of crystal growth inhibitors for deposition of the hole collector. *Chemistry of Materials*, 14, 2002, 954-955.
- Lee, C. P.; Chen, P. Y.; Vittal, R. & Ho, K. C. (2010a). Iodine-free high efficient quasi solid-state dye-sensitized solar cell containing ionic liquid and polyaniline-loaded carbon black. *Journal of Materials Chemistry*, 20, 2010, 2356-2361.
- Lee, C. P.; Lin, L. Y.; Chen, P. Y.; Vittal, R. & Ho, K. C. (2010b). All-solid-state dye-sensitized solar cells incorporating SWCNTs and crystal growth inhibitor. *Journal of Materials Chemistry*, 20, 2010, 3619-3625.
- Lee, C. P.; Lee, K. M.; Chen, P. Y. & Ho, K. C. (2009a). On the addition of conducting ceramic nanoparticles in solvent-free ionic liquid electrolyte for dye-sensitized solar cells. *Solar Energy Materials & Solar Cells*, 93, 2009, 1411-1416.
- Lee, K. M.; Chen, P. Y.; Lee, C. P. & Ho, K. C. (2009b). Binary room-temperature ionic liquids based electrolytes solidified with SiO<sub>2</sub> nanoparticles for dye-sensitized solar cells. *Journal of Power Sources*, 190, 2009, 573-577.
- Li, Z.; Ye, B.; Hu, X.; Ma, X.; Zhang, X. & Deng, Y. (2009). Facile electropolymerized-PANI as counter electrode for low cost dye-sensitized solar cell. *Electrochemistry Communications*, 11, 2009, 1768-1771.
- Midya, A.; Xie, Z.; Yang, J.-X.; Chen, Z.-K.; Blackwood, D. J.; Wang, J.; Adams, S. & Loh, K. P. (2010). A new class of solid state ionic conductors for application in all solid state dye sensitized solar cells. *Chemical Communications*, 46, 2010, 2091-2093.

- O' Regan, B. & Grätzel, M. (1991). A low-cost, high-efficiency solar cell based on dye-sensitized colloidal  $\text{TiO}_2$  films. *Nature*, 353, 1991, 737-740.
- Paulsson, H.; Hagfeldt, A. & Kloo, L. (2003). Molten and solid trialkylsulfonium iodides and their polyiodides as electrolytes in dye-sensitized nanocrystalline solar cells. *Journal of Physical Chemistry B*, 107, 2003, 13665-13670.
- Pringle, J. M.; Golding, J. C.; Forsyth, M. G.; Deacon, B.; Forsyth, M. & MacFarlane, D. R. 2002. Physical trends and structural features in organic salts of the thiocyanate anion. *Journal of Materials Chemistry*, 12, 2002, 3475-3480.
- Perera, V. P. S.; Pitigala, P. K. D. D. P.; Jayaweera, P. V. V.; Bandaranayake, K. M. P. & Tennakone, K. (2003). Dye-sensitized solid-state photovoltaic cells based on dye multilayer semiconductor nanostructures. *Journal of Physical Chemistry B*, 107, 2003, 13758-13761.
- Usui, H.; Matsui, H.; Tanabe, N. & Yanagida, S. (2004). Improved dye-sensitized solar cells using ionic nanocomposite gel electrolytes. *Journal of Photochemistry and Photobiology A: Chemistry*, 164, 2004, 97-101.
- Wang, H.; Liu, X.; Wang, Z.; Li, H.; Li, D.; Meng, Q. & Chen, L. (2006). Effect of iodine addition on solid-state electrolyte  $\text{LiI}/3\text{-Hydroxypropionitrile}$  (1:4) for Dye-Sensitized Solar Cells. *Journal of Physical Chemistry B*, 110, 2006, 5970-5974.
- Wang, P.; Zakeeruddin, S. M.; Comte, P.; Exnar, I. & Grätzel, M. (2003a). Gelation of ionic liquid-based electrolytes with silica nanoparticles for quasi-solid-state dye-sensitized solar cells. *Journal of the American Chemical Society*, 125, 2003, 1166-1167.
- Wang, P.; Zakeeruddin, S. M.; Exnar, I. & Grätzel, M. (2002). High efficiency dye-sensitized nanocrystalline solar cells based on ionic liquid polymer gel electrolyte. *Chemical Communications*, 2002, 2972-2973.
- Wang, P.; Zakeeruddin, S. M.; Humphry-Baker, R. & Grätzel, M. (2004a). A binary ionic liquid electrolyte to achieve  $\geq 7\%$  power conversion efficiencies in dye-sensitized solar cells. *Chemistry of Materials*, 16, 2004, 2694-2696.
- Wang, P.; Zakeeruddin, S. M.; Moser, J.-E.; Humphry-Baker, R. & Grätzel, M. (2004b). A solvent-free,  $\text{SeCN}^-/(\text{SeCN})_3^-$  based ionic liquid electrolyte for high-efficiency dye-sensitized nanocrystalline solar cells. *Journal of the American Chemical Society*, 126, 2004, 7164-7165.
- Wang, P.; Zakeeruddin, S. M.; Moser, J.-E. & Grätzel, M. (2003b). A new ionic liquid electrolyte enhances the conversion efficiency of dye-sensitized solar cells. *Journal of Physical Chemistry B*, 107, 2003, 13280-13285.
- Wu, J.; Hao, S.; Lan, Z.; Lin, J.; Huang, M.; Huang, Y.; Fang, L.; Yin, S. & Sato, T. (2007). A thermoplastic gel electrolyte for stable quasi-solid-state dye-sensitized solar cells. *Advanced Functional Materials*, 17, 2007, 2645-2652.
- Ying, Y.; Zhou, C. H.; Xu, S.; Hu, H.; Chen, B. L.; Zhang, J.; Wu, S. J.; Liu, W. & Zhao, X. Z. (2008). Improved stability of quasi-solid-state dye-sensitized solar cell based on poly (ethylene oxide)-poly (vinylidene fluoride) polymer-blend electrolytes. *Journal of Power Sources*, 185, 2008, 1492-1498.

- Zhao, Y.; Zhai, J.; He, J.; Chen, X.; Chen, L.; Zhang, L.; Tian, Y.; Jiang, L. & Zhu, D. (2008). High-performance all-solid-state dye-sensitized solar cells utilizing imidazolium-type ionic crystal as charge transfer layer. *Chemistry of Materials*, 20, 2008, 6022-6028.



# Quaternary Ammonium and Phosphonium Ionic Liquids in Chemical and Environmental Engineering

Anja Stojanovic, Cornelia Morgenbesser, Daniel Kogelnig,  
Regina Krachler and Bernhard K. Keppler  
*University of Vienna, Institute of Inorganic Chemistry,  
Währinger Straße 42, 1090 Vienna,  
Austria*

## 1. Introduction

Quaternary ammonium salts (quats) are an economically advantageous class of industrial compounds. They have surface-active properties, possess anti-microbial activity and are known to be bioactive (Boethling & Lynch, 1992; Juergensen et al., 2000). Contrary, reports regarding low melting tetraalkylphosphonium salts were relatively rare in the literature during the last decades (Bradaric et al., 2003).

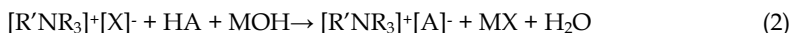
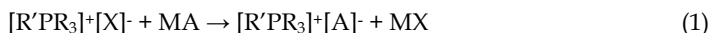
Although ILs based on quaternary ammonium cations have been known and produced for years, and also numerous phosphonium based ILs have been produced even in ton-scale, these groups of ionic liquids have been more or less “neglected” in the literature comparing to their imidazolium or pyridinium based counterparts. However, during the last decade significant work has been done, pointing out the advantages and broad application spectrum of these types of ionic liquids. Their improved thermal and chemical stability in comparison to e.g. pyridinium and imidazolium based ILs, their unique miscibility behaviour and solvating properties advances their use in specific applications (Rogers et al., 2002; Plechkova & Seddon, 2007; Chowdhury et al., 2007; Wasserscheid & Welton, 2008). Several ILs based on these classes of cations are already commercially available and have been successfully applied as phase-transfer catalysts, solvents, lubricants, gas capture agents, coating materials, or chemical sensors (Bradaric et al., 2003; Weng et al., 2006; Pernak et al., 2006; Yuan et al., 2007; Fraser & MacFarlane, 2009; Werner et al., 2010).

Tricaprylmethylammonium chloride (trade name Aliquat® 336), produced in ton-scale by Henkel, is nowadays widely used as metal extraction agent, phase transfer catalyst, surfactant, or antistatic agent. In contrast, trihexyl(tetradecyl)phosphonium chloride (trade name Cyphos® IL 101) was developed by Cytec Industries as a thermally stable phase transfer catalyst (Bradaric et al., 2003). Due to the relatively simple preparation route, Cyphos® IL 101 is produced in ton-scale and therefore represents a fairly cheap IL. Hence, due to their commercial availability and low prices, both Aliquat® 336 and Cyphos® IL 101 can be used themselves or represent favorable precursors for a series of ionic liquids. The goal of this chapter is to give some insight into the fascinating and fast-growing field of

these groups of ILs - especially based on cations of the cost-saving precursors Aliquat® 336 and Cyphos® IL 101 - concerning the field of chemical and environmental engineering.

## 2. Synthesis of ammonium- and phosphonium-based ionic liquids

Aliquat® 336 ([A336][Cl]) is prepared by methylation of a mixture of trioctyl/decyl amine (Alamine® 336, Cognis Corp.), whereas Cyphos® IL 101 ([P<sub>6,6,6,14</sub>][Cl]) is produced by Cytec Ind. in a quaternization reaction of trihexylphosphine with 1-chlorotetradecane (Robertson, 2001; Bradaric et al., 2003). A subsequent anion-exchange reaction between the quaternary ammonium/phosphonium halide and acid or salt (see Eqns. (1) and (2); R, R' = alkyl; X = halogen; M = alkali metal; A = desired anion) with corresponding anions leads to the desired ionic liquid (Bradaric et al., 2003; Mikkola et al., 2006a; Kogelnig et al., 2008; Fraser & MacFarlane, 2009).



However, the cation generation by alkylation reaction with halides and the following anion exchange often results in ILs comprising halide impurities, which results in alteration of their physico-chemical properties (Seddon et al., 2000). As chloride impurities are for example known to act as “catalytic poison”, ILs with halide contamination are unsuitable for catalytic reactions (Davies et al., 2004). To overcome the drawback of halide impurities, many literature protocols deal with synthetical approaches in which dialkylsulfates, carbonates, trialkylphosphates, alkyltosylates, methane sulfonates or fluorinated esters are used as alkylating reagents (Bradaric et al., 2003; Seddon et al., 2001; Kalb, 2005). However, since the main focus of this chapter lies on Aliquat® 336 and Cyphos® IL 101 based ionic liquids, different metathesis routes including these two commercially available ILs as precursors will be cited. Mikkola and co-workers (2006a) introduced the “new family” of ILs based on Aliquat® 336 as cation source by conducting a simple metathesis route utilizing appropriate sodium, potassium, or ammonium salts as anion source (see Eqn. 1). The authors obtained a series of hydrophobic ILs containing common anions like [PF<sub>6</sub>]<sup>-</sup>, [BF<sub>4</sub>]<sup>-</sup>, phosphate, nitrate or bis(trifluoromethylsulfonyl)imide ([Tf<sub>2</sub>N]<sup>-</sup>), but with a residual chloride content ranging between 0 and 6 wt%. On the other hand, the use of economically favorable Aliquat® 336 as a precursor may even justify the subsequent use of an anion exchanger in order to remove the residual chloride content, if necessary for specific applications. A well-established example of Eqn. (2) within the IL-community is the preparation of different phosphonium phosphinates (Robertson & Seddon, 2002). Trihexyl(tetradecyl)phosphonium bis(2,4,4-trimethylpentyl)phosphinate (trade name Cyphos® IL 104) is commercially produced following this route (see Figure 1a, Bradaric et al., 2003). We also have shown recently (Kogelnig et al., 2008) that the simple deprotonation-metathesis route (Eqn. 1) under inert conditions leads to Aliquat-based ILs with sufficient purity (residual chloride contents between <0.1 and 0.8 wt%) for selected applications (see Figure 1b).

The slightly modified synthesis route (Stojanovic et al., 2010) could also be applied for the preparation of both ammonium- and phosphonium-based ILs containing functionalized anions like thiosalicylate, 2-(methylthio)benzoate, or phenyl(thio)acetate. All prepared ILs exhibited chloride contents below 0.9 wt%. However, due to the significantly high viscosities of the obtained ILs (up to 5242 mPas), the use of appropriate organic solvents was

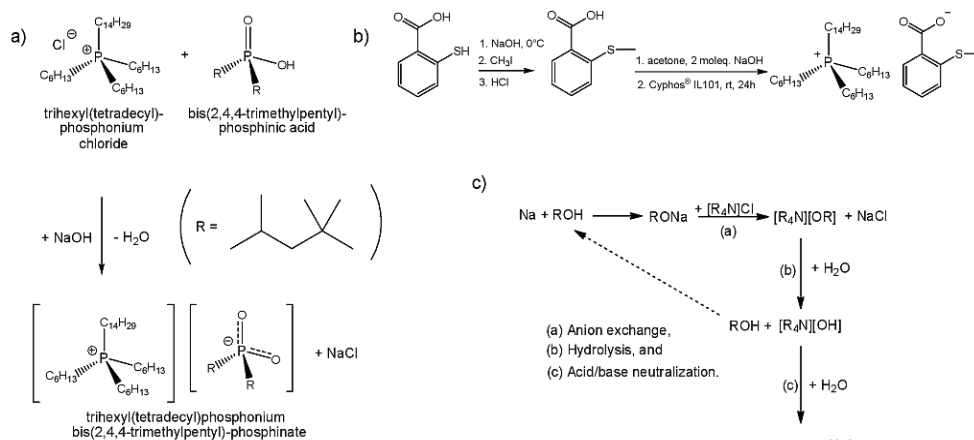


Fig. 1. a) Synthesis of Cyphos® IL 104 (redrawn from Bradaric et al., 2003) b) Synthesis of [P<sub>6,6,6,14</sub>] 2-methylthiobenzoate, [P<sub>6,6,6,14</sub>][MTBA] (redrawn from Stojanovic et al., 2010) c) Acid/base neutralization synthesis route (redrawn from Sun et al., 2010a)

inevitable to minimize loss of yield, which makes the preparation process in general more expensive and wasteful, limiting the industrial production of ILs. Sun et al. (2010a) recently presented a relatively simple preparation strategy which may alleviate industrial manufacturing of ammonium based ILs. Following the acid/base neutralization route shown in Figure 1c, the authors gained the IL tricaprylmethylammonium nitrate, [A336][NO<sub>3</sub>], exhibiting a chloride content significantly lower than the same IL prepared via the conventional anion metathesis route. Although the obtained IL still contains a measurable amount of chloride, the described synthetic route may be attractive for large scale preparation since its reactants are cheap and easily available in contrast to halide-free intermediates.

### 3. Features of ammonium- and phosphonium-based ionic liquids

By now, numerous ILs based on both the Aliquat® 336 and the [P<sub>6,6,6,14</sub>] cation have been prepared using one of the synthesis routes described above. Several selected examples of common anions are presented in Figure 2.

The differences in physico-chemical properties of ammonium and phosphonium ILs begin with their stability towards degradation under various conditions, which differs clearly (Karodia et al., 1998; Wolff et al., 2000). Although both can decompose at elevated temperatures, phosphonium salts are generally more stable as their ammonium analogs (Wolff et al., 2000; Bradaric et al., 2003). Whereas ammonium salts undergo facile Hofmann- or  $\beta$ -eliminations in the presence of base (Hanhart & Ingold, 1927; Ingold & Vass, 1928), their phosphonium analogs decompose to tertiary phosphine oxide and alkane under alkaline conditions. Although the decomposition temperature of ILs depends strongly on the choice of anion, in most cases thermogravimetric analysis (TGA) of phosphonium ILs reveals a dynamic thermal stability even above 300°C (Bradaric et al., 2003; Fraser & MacFarlane, 2009). In contrast, corresponding ammonium-based ILs decompose at approximately 100°C lower temperatures. The enhanced thermal stability of phosphonium

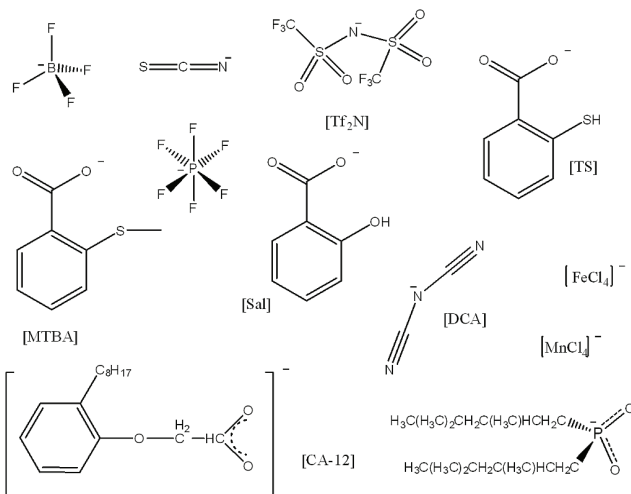


Fig. 2. Selected anions of phosphonium- and ammonium-based ILs

ILs play a crucial role when applied as solvents or catalysts for different reactions at high temperatures, or if the reaction products should be distilled from the ionic liquid at high temperatures. In general, the viscosity of Aliquat® 336-based ILs is significantly higher than that of  $[\text{P}_{6,6,6,14}]$  based ILs, but also strongly depends on the choice of anion. For example, the exchange of the chloride anion with thiosalicylate leads to an increase in viscosity, whereas the anion exchange with 2-(methylthio)benzoate leads to an increase in viscosity for the Aliquat® 336-based IL and to a decrease in viscosity for the corresponding phosphonium-based IL (Stojanovic et al., 2010). However, due to the strong temperature dependence, viscosities diminish extremely at temperatures typical for industrial applications (e.g. 70–100°C) (Bradaric et al., 2003; Kulkarni et al., 2007a; Stojanovic et al., 2010). Furthermore, phosphonium ILs generally depict higher electronic polarizabilities than their ammonium counterparts, indicating a difference in their solvation behaviour (Tariq et al., 2009; Stojanovic et al., 2010), whereas similarities can be found concerning the density. Both IL families exhibit densities ranging from 0.7 to 1.2 g cm<sup>-3</sup> with common values < 1 g cm<sup>-3</sup>. However, it is important to note that a reliable set of data regarding physico-chemical parameters of ammonium and phosphonium ILs is still missing, which limits their potential widespread industrial application (Atkins et al., 2004). On the other hand, even the available data sets should be considered carefully, since the properties of ILs strongly depend on their purity.

Besides an efficient and commercially favorable synthetic route, the determination of the purity level of obtained ILs accompanied with their purification plays a crucial role for their widespread use. Although the high-purity of ILs needs not to be achieved in every case, several authors observed negative effects of halide and water impurities on the rate and/or selectivity of reactions carried out in ionic liquids, on their catalytic performance as well as on their properties (Carmichael et al., 1999; Seddon et al., 2000; Gallo et al., 2002; Davies et al., 2004; Stark et al., 2006). From the engineering point of view, the presence of halide impurities in ILs can influence the choice of constitutional materials due to the corrosiveness of these anions. On the other hand, the presence of residual acid in ILs may have an impact on their performance in catalytic and separation processes (Werner et al., 2010). It also has been shown recently that the presence of impurities in ILs unambiguously narrows their apparent

electrochemical window, making the use of ultra high-purity ILs in electrochemical applications necessary (Buzzeeo et al., 2004). Besides conventional methods like NMR, IR, ESI-MS, UV- spectroscopy, Karl-Fischer titration for the determination of water content, or elemental analysis, only a few analytical methods are dealing with the characterization of ammonium and phosphonium ILs. The absence of chromophoric UV-active groups in the Aliquat® 336 and Cyphos® IL 101 cations makes the conventional RP-HPLC with UV-detection unsuitable for these compounds, requesting more sophisticated coupling methods. Moreover, several difficulties arise in the course of the analysis of Aliquat® 336-based ILs as the cation depicts a mixture of quaternary ammonium cations with different alkyl chain lengths rather than a well-defined pure compound. This property makes the quantification of the Aliquat® 336 mix and hence all of its products more complicated. Lee et al. (1981) identified Aliquat® 336 as a mixture of quaternary ammonium cations with C<sub>6</sub>, C<sub>8</sub> and C<sub>10</sub> alkyl chain lengths applying gas chromatography. The distinct composition of the Aliquat® 336 mix was confirmed and quantitatively determined via Electro Spray Mass Spectrometry (ESMS), and revealed following mass percentages of different chloride components in Aliquat® 336: 3.7 ± 0.7 % of methyl(n-hexyl)di(n-octyl)ammonium (A336<sup>+</sup><sub>C23</sub>), 21.7 ± 1.5 % of methyltri(n-octyl)ammonium (A336<sup>+</sup><sub>C25</sub>), 32.8 ± 2.3 % of methyl di(n-octyl)(n-decyl)ammonium (A336<sup>+</sup><sub>C27</sub>), 18.4 ± 1.3 % of methyl(n-octyl)di(n-decyl)ammonium (A336<sup>+</sup><sub>C29</sub>), and 3.5 ± 0.2 % of methyltri(n-decyl)ammonium (A336<sup>+</sup><sub>C31</sub>) (Argiropoulos et al., 1998b). Recently, we developed an adequate, cost-saving and fast method for the purity determination of ammonium- and phosphonium-based ILs (Stojanovic et al., 2008), applying Reversed Phase High Performance Liquid Chromatography (RP-HPLC) with a serially coupled UV detector and a mass sensitive charged aerosol detector (CAD). This combination allows a simultaneous quantitative determination of non-chromophoric aliphatic cationic species and their aromatic, UV-active anionic counterparts. Further, a unified calibration can be applied with a single standard. Most notably, the resulting calibration function can be used for all other compounds or impurities for which no standards are available – which is particularly suitable for mixtures like Aliquat® 336. As it can be seen in Figure 3, all five components of the Aliquat® 336 cation could be efficiently separated and accurately quantified using an optimized step-gradient method, confirming the results obtained by ESI-MS measurements. The developed method was validated according to the ICH-guidelines ([www.ich.org](http://www.ich.org)) and successfully applied for the determination of molar ratios of ionic components of a series of Aliquat® 336- and Cyphos® IL 101-based ILs containing different aromatic anions.

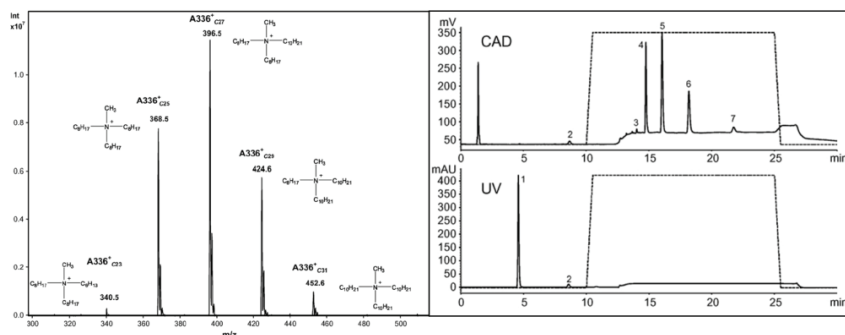


Fig. 3. ESI-MS spectrum of Aliquat® 336 (left) and chromatogram of IL [A336][TS] (taken from Stojanovic et al., 2008, Copyright © 2008 Elsevier B. V.)

#### 4. Ammonium- and phosphonium-based ionic liquids in extraction processes

Due to the hydrophobicity of Aliquat® 336- and [P<sub>6,6,6,14</sub>]-based ILs the formation of liquid-liquid biphasic systems with aqueous phases can be realized, making them suitable for such extraction processes. On the other hand, due to their polar nature many ILs show a pronounced miscibility gap with common apolar organic solvents. From the engineering point of view a severe drawback of ILs compared to conventional solvents is based on their high viscosity, requesting changes in the hydrodynamic design of extraction columns (Meindersma et al, 2007). However, very little is known about the behaviour of ammonium and phosphonium ILs in biphasic systems, e.g. about coalescence phenomena or micelle formation etc. (Werner et al., 2010).

##### 4.1 ILs as extracting agents for heavy metals

Already in the 1960's Seeley & Crouse highlighted the enhanced performance of Aliquat® 336 as liquid ion-exchanger for the removal of different metal species from hydrochloric acid solutions compared to conventionally used amine extractants like Alamine® 336 or Amberlite LA-1 (Seeley & Crouse, 1966). Since then Aliquat® 336 has been evaluated as extracting agent (in most cases dissolved in an appropriate organic solvent) for different metals from acidic aqueous solutions (e.g. Cd(II), Fe(III), Pt(II) and Hg(II) from hydrochloric acid solutions; El-Wakil et al., 1982; Hoh et al., 1985; de Mendonça Fábrega & Borges Mansur, 2007). Nayl (2010) presented a successful separation of Co(II) and Ni(II) from acidic sulfate solutions using Aliquat® 336 dissolved in kerosene. Further, Aliquat® 336 could be efficiently applied for the recovery of Co and Ni from spent Ni-MH batteries (Nayl, 2010). Aliquat® 336 dissolved in kerosene was also applied for the effective separation of Pt(IV) from Rh(III) from acidic chloride solutions (Lee et al., 2009). As Aliquat® 336 was first applied as extractant in the mining industry, it is not surprising that numerous studies are dealing with the evaluation of its extraction ability towards uranium, thorium and several lanthanides (e.g. Atanassova & Dukov, 2004; El-Nadi et al., 2005; Ali et al., 2007). In general, the extraction mechanism with Aliquat® 336 is based on the anion exchange/ion association of metal chloride/sulfate species; it therefore strongly depends on the composition of the aqueous phase (formation of different metal species) and pH (see Eqns. 4 and 5). Hence, effective metal stripping is mostly easily achieved by variation of pH, or via an efficient complexing agent like thiourea. In contrast, Cyphos® IL 101 has only recently been investigated as potential new IL extracting agent dissolved in toluene for the elimination of zinc and palladium from aqueous phases (Regel-Rosocka, 2009; Cieszyńska et al., 2007). Alguacil and co-workers (2010) investigated the transport of Cr (VI) through a pseudo-emulsion membrane from a feeding to an appropriate stripping phase using Cyphos® IL 101 as metal carrier. Additionally, we have investigated the separation of iron(III) and nickel(II) from hydrochloric acid solution (6 M HCl) with Cyphos® IL 101 dissolved in chloroform (Kogelnig et al., 2010a). The efficient back extraction was achieved with 0.5 M HCl solution. The conducted bulk liquid membrane (BLM) experiments as well as kinetic model data elucidated the transport mechanism as a combination of anion exchange and ion association (see Eqns. 4 and 5).



However, the application of Aliquat® 336 and Cyphos® IL 101 in liquid/liquid extraction processes has several disadvantages. Firstly, due to the high viscosity of ILs the use of organic solvents is inevitable, influencing both price and “greenness” of the process. Secondly, the extraction mechanism is based on anion exchange and hence strongly dependent on the composition of the aqueous phase. Further, the potential leachability of both IL and organic solvent in the aqueous phase may pose an additional environmental risk. Therefore, in order to overcome these drawbacks, two different approaches have been developed during the last years: 1) Avoiding of liquid/liquid extraction and hence increasing of the stability of the extracting agent may be achieved by immobilization of ILs onto different solid materials or via embedment of ILs into different matrices. However, the main challenge regarding these approaches is to attain the favorable performance of “liquid” ionic liquids. 2) In order to avoid anion exchange and to enhance the extracting ability, it is possible to combine favorable properties of quaternary ammonium and phosphonium cations like hydrophobicity and thermal stability with different functionalized anions containing functional moieties known for their affinity towards selected metals, and forming task specific ionic liquids (TSILs) as metal scavengers. Generally, problems connected with solvent extraction, like inhibition of phase separation and product recovery by formation of difficult-to-separate emulsions, high consumption of organic reagents, solvent loss or shortcomings due to the flooding and loading in conventional column reactors may be overcome by so-called non dispersive solvent extraction (Gabelman & Hwang, 1999). Thereby hollow fiber membranes or so-called “supported liquid membranes” (SLMs), which consist of a porous polymeric (organic or inorganic) material whose pores are impregnated or in contact with an extractant or carrier, are used. Hollow fiber membranes impregnated with Aliquat® 336 as efficient ionic carrier were evaluated for removal of different metal species, e.g. cobalt(III), rhodium(III), or chromium(VI), from an aqueous feeding phase to an adequate stripping phase (Fontàs et al., 2000; Kao & Juang, 2005; Güell et al., 2008). The hollow fiber liquid membrane using Aliquat® 336 (35% v/v) as extractant and 0.5 M NaOH as stripping solution was successfully applied for the removal of arsenic ions in waste water from a gas separation plant. The extraction efficiency of Aliquat® 336 was thereby remarkably higher compared with other evaluated extractants (Cyanex® 923, tri-*n*-butylphosphate (TBP), bis(2, 4, 4-trimethylpentyl) dithiophosphinic acid (Cyanex® 301), tri-*n*-octylamine (TOA); Pancharoen et al., 2009). Myasoedova et al. (2008) evaluated different solid supports (polyacetonitrile, Amberlite XAD-7, hyper cross linked polystyrene or multi walled carbon nanotubes) with  $[P_{6,6,6,14}][Cl]$ ,  $[P_{6,6,6,14}][PF_6]$ , and  $[P_{6,6,6,14}][BF_4]$  as solid-phase extractants for Pt(IV), U(VI) and Pu(IV) from acid solutions, achieving the best performance with polyacrylonitrile impregnated with Cyphos® IL 101. Next to SLMs, polymer inclusion membranes (PIMs) were evaluated as solid supports for ILs. In contrast to SLMs, PIMs consist of a high molecular weight polymer to provide mechanical strength, a plasticizer to provide elasticity and a carrier molecule for facilitating the selective transport of the analytes (Nghiem et al., 2006). Polyvinyl chloride (PVC) and cellulose triacetate (CTA) are the most commonly used polymers for the preparation of PIMs, since they are able to embed carrier molecules and inhibit their leaching. It is also noteworthy that the mechanical properties of PIMs are quite similar to those of filtration membranes (Nghiem et al., 2006). Rahman and co-workers (2005) have shown that ionic liquids could be used both as a carrier as well as a stable plasticizer for PIMs. Until now, predominantly Aliquat® 336 has been evaluated as carrier for the extraction of different metal species (e.g. Au(III) (Argiropoulos et al., 1998a), Cd(II), Cu(II)

(Wang et al., 2000), Co(II) (Blitz-Raith et al., 2007), Pd(II) (Kolev et al., 2000), and Zn(II) (Juang et al., 2004)). Another interesting approach for the immobilization of ILs is the encapsulation of liquid extractants in polystyrene microcapsules. Yang et al. (2005) investigated the uptake of Cd(II), Cr(III), and Zn(II) from hydrochloric acid solutions by Aliquat® 336 encapsulated in polystyrene particles. The encapsulated extractant displayed high stability over a wide pH-range and the microcapsules could be successfully regenerated and reused several times, hence justifying their relatively extensive preparation. Furthermore, Guibal et al. (2009) selected another approach by choosing different biological materials such as alginate as "green" materials for encapsulation or immobilization of extractants. The prepared alginate particles were evaluated as efficient metal sorbents for Au(II), Hg(II), Pd(II), Pt(VI), or Bi(III) from hydrochloric acid solutions. The disadvantages of the method, however, still originate from the competition of metal ions capable of forming chloride complexes and the limitations associated with slow mass transfer when using dried resins.

A further approach regarding the advancement of metal uptake ability of ILs is the use of task specific ionic liquids as extracting agents. By anchoring different functional groups onto the anion, it is possible to combine the hydrophobicity of ammonium and phosphonium cations with the affinity of the functional group towards selected metal species, and hence enhancing both efficiency and selectivity of the extracting agent. For example, an ionic liquid based on the trioctylmethylammonium cation with thiosalicylate as anion, prepared via a halide free synthesis route, is commercially available and has been evaluated as extracting agent for heavy metals (e.g. Hg(II), Cu(II), or Pb(II)) from aqueous solutions with high distribution coefficients (Kalb, 2005; Kalb et al., 2006).

By a simple anion exchange of the chloride anion of Aliquat® 336 with a salicylate anion, Egorov et al. (2008, 2010) prepared a TSIL suitable for the extraction of Cu(II) and Fe(III) from aqueous solutions. During the last years we have prepared a series of hydrophobic ionic liquids based on Aliquat® 336- and  $[P_{6,6,6,14}]$  cations with functionalized aromatic anions (see Figure 2, Kogelnig et al., 2008; Stojanovic et al., 2010). The newly prepared IL tricaprylmethylammonium thiosalicylate,  $[A336][TS]$ , could be evaluated as highly effective extracting agent for Cd(II) from a natural river water matrix with a distribution coefficient  $>10^4$  (Kogelnig et al., 2008). The investigated IL exhibited high selectivity towards cadmium in the presence of naturally occurring alkali and earth alkali metals ( $K^+$ ,  $Na^+$ ,  $Ca^{2+}$ , and  $Mg^{2+}$ ). The same IL was efficiently applied for the removal of uranium traces from natural mineral water (Srncik et al., 2009). The selectivity of  $[A336][TS]$  towards alkali and earth alkali metals and a subsequent successful stripping of uranium with 2 M  $HNO_3$  makes this IL suitable as possible preconcentration agent for uranium for its subsequent analytical determination in natural waters. Further, thiol- and thioether functionalized ILs ( $[A336][TS]$ ,  $[P_{6,6,6,14}][TS]$ ,  $[A336][MTBA]$ , and  $[P_{6,6,6,14}][MTBA]$ ) seem to be suitable for the extraction of Pt(II) from aqueous solutions (see Figure 4, Stojanovic et al., 2010). The incorporation of aromatic anions significantly increased the stability of the investigated ILs in the aqueous phase, whereby ILs containing  $[MTBA]$  exhibited an extremely high stability with a leaching of the anion in the aqueous phase of max. 0.2 wt.%. Interestingly, the change from ammonium to phosphonium cations for methylthiobenzoate and thiosalicylate functionalized ILs resulted in different platinum uptake (see Figure 4). Whereas the highest uptake of Pt(II) was achieved with  $[P_{6,6,6,14}][MTBA]$ , only 40% of Pt(II) could be extracted with the ammonium analog. Therefore, also the physico-chemical properties of TSILs have to be considered in order to determine distinct reaction mechanisms, as the presence of a functional group is obviously not the sole factor influencing the extracting ability of TSILs.



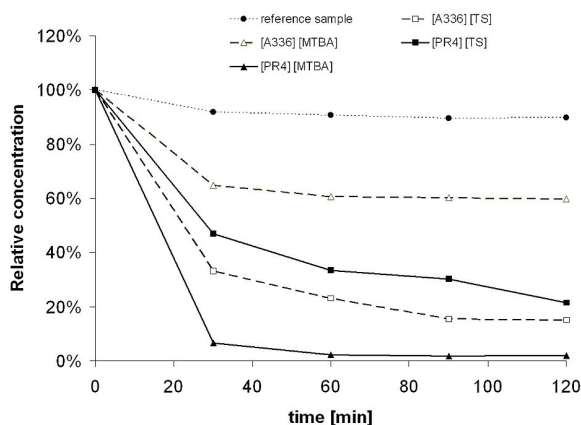


Fig. 4. Extraction efficiency of [A336][TS], [A336][MTBA], [PR<sub>4</sub>][TS], and [PR<sub>4</sub>][MTBA] for platinum(II) (Stojanovic et al., 2010, Copyright © CSIRO 2010)

A different concept of enhancing the extraction efficiency focuses on so-called bifunctional ionic liquids (bif-ILs). The idea behind this concept is the synergetic effect on the solvent extraction by combination of two extractants. An excellent example is given by the IL [P<sub>6,6,6,14</sub>][bis(2,4,4-trimethylpentyl)phosphinate] (trade name Cyphos® IL 104), as displayed in Figure 1a. In this case the synergetic effect on the solvent extraction is achieved by combination of Cyphos® IL 101 and bis(2,4,4-trimethylpentyl)phosphonic acid, which is known as excellent solvent for the extraction of cobalt and nickel from both hydrochloride and sulfate acidic solutions (Rickelton et al., 1984; Danesi et al., 1985), and is currently used to produce more than a half of the western world's cobalt (Rickelton & Robertson, 1982; Robertson, 1983; Rickelton et al., 1984). Sun et al. (2010b) investigated the separation of cobalt and nickel by synergetic extraction with the Aliquat® 336-based bifunctional IL [A336][CA-12] (see Figure 5). Their results indicated that the extraction abilities of the tricaprylylmethylammonium cation ([A336]<sup>+</sup>) and the sec-octylphenoxy acetic acid group ([CA-12]<sup>-</sup>) can be remarkably enhanced by combining them in a corresponding IL. The same authors also investigated the synergetic effect of different bifunctional ILs (see Figure 2) for the extraction of europium and other rare earth elements from hydrochloric and nitric acid media (Sun et al., 2010a). On the other hand, Liu et al. (2010) evaluated the bif-IL

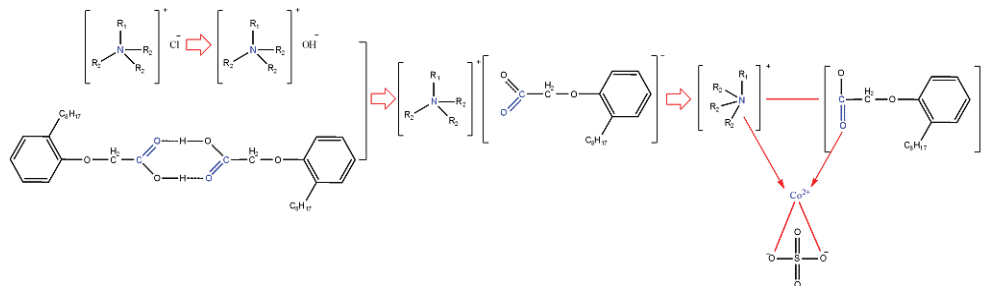


Fig. 5. Extraction of cobalt with the ionic liquid [A336][CA-12] (redrawn from Sun et al., 2010b)

Cyphos® IL 104, together with soybean oil methyl ester (SBME, biodiesel) as delutant, as extractant for rare earth elements from aqueous solutions. They achieved both enhanced extracting efficiency due to the presence of the bif-ILE and a diminished loss of IL due to the use of biodiesel as solvent.

In summary, the removal of heavy metals from aqueous solutions using phosphonium- and ammonium-based ILs both as anion exchanger and as functionalized TSILs depicts a field of extensive research and promising results. However, from the engineering and economic point of view, extensive research is needed regarding a complete recovery of the ionic liquid and the full isolation of the extracted metal from the loaded ionic liquid. Furthermore, the question of ILs' stability in aqueous phases and subsequently their possible toxicity towards the aquatic environment still needs more attention.

#### 4.2 Other separation processes with ammonium- and phosphonium-based ILs

Kulkarni et al. (2007b) investigated the absorption capacity of a series of Aliquat® 336-based ILs (see Figure 2) towards organic vapors (1,4-benzodioxane, biphenyl, xylene, and methanol) and received promising results with the ILs [A336][Tf<sub>2</sub>N] and [A336][DCA]. However, although both ILs showed remarkable absorption capacity, none of the tested ILs was able to provide sufficient selectivity regarding different organic solutes (see Figure 6). A possible solution may be a combination of different ILs in order to achieve the desired selectivity. The absorbed organic solutes were recovered by desorption under vacuum and preconcentrated by steam condensation. Compared to the relatively slow absorption process, the organic vapors could be desorbed very fast (<12h). The recycled ILs were also successfully reused. The same research group investigated the IL [A336][DCA] as capturing agent for dioxins from the vapor phase (Kulkarni et al., 2008), whereby the investigated IL absorbed 15.6 % by weight of dibenzo-p-dioxin in equilibrium. Due to the high thermal stability of ammonium ILs, dioxin was easily desorbed by vacuum distillation at 100°C, and the IL could be further reused.

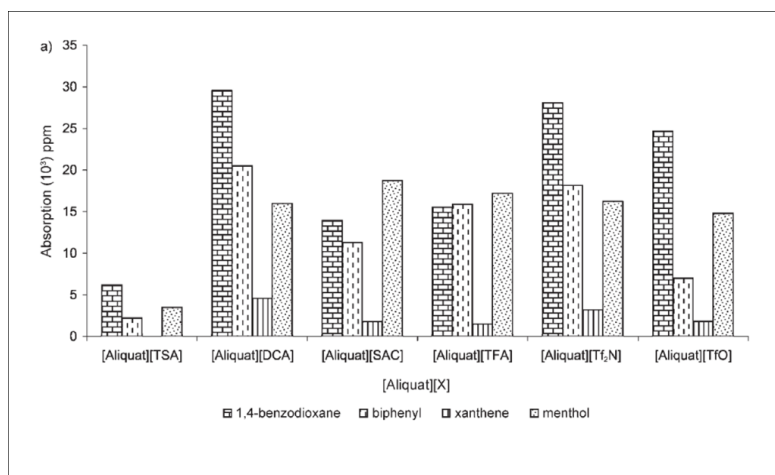


Fig. 6. Extraction efficiency of Aliquat® 336-based ILs for organic vapors (taken from Kulkarni et al., 2007b, Copyright© Wiley-VCH Verlag GmbH&Co. KGaA)

Furthermore, Egorov et al. (2008) investigated the extraction of eleven aromatic compounds (phenols and aromatic amines) from aqueous phases with the Aliquat® 336-based IL tricaprylylmethylammonium salicylate, [A336][Sal] (see Figure 2). The best results were achieved for nitrophenols and naphthols, showing even better absorption capacities as common imidazolium-based ILs over the investigated pH-range. Recently, Aliquat® 336 and Cyphos® IL 101 were also evaluated as solvents for carboxylates and their extraction from aqueous phase (Rosatella et al., 2009). Whereas a large quantity of disaccharide mixtures was extracted, no satisfying extraction of monosaccharide mixtures was obtained. Further, the highly hydrophobic IL trihexyl(tetradecyl)phosphonium tris(pentafluoroethyl)trifluorophosphate, [PH<sub>3</sub>T][FAP], was evaluated as extraction agent for polycyclic aromatic hydrocarbons from the aqueous phase via single drop microextraction. Extremely high enrichment factors (680-2145) were achieved for compounds with high molecular weights and fused rings (Yao et al., 2009). On the other hand, Cyphos® IL 104 could be efficiently embedded in polysulfone resins and evaluated for the extraction of phenol from aqueous solutions. Prepared polysulfone resins exhibit remarkable mechanical stability and possess extremely high extractant loading capacity (0.83-0.88 cm<sup>3</sup>g<sup>-1</sup>) (Van den Berg et al., 2009). Due to the favorable features of polysulfone encapsulated ILs, this could be an interesting approach regarding the application of ILs in separation processes.

Another interesting application field is the removal of carboxylic acids from aqueous solutions. Both Aliquat® 336 and Cyphos® IL 101 have been investigated concerning their extracting ability for several acids, e.g. lactic, levulinic, glutaric, or amino acids (e.g. Uddin et al., 1990; Bora & Dutta, 1998; Kyuchoukov et al., 2005; Harington & Hossain, 2008; Hossain & Maisuria, 2008; Uslu & Kırbaslar, 2009; Pehlivanoglu et al., 2010). As an outstanding example the extraction of lactic acid with the bifunctionalized IL Cyphos® IL 104, should be mentioned. In contrast to distribution factors of about 1, which could be reached with trialkylamines (e.g. trioctylamine) as classical lactic acid solvents, distribution factors above 40 could be reached with Cyphos® IL 104. The assumed extraction mechanism suggests the coordination of lactic acid (LA) to the IL under formation of complexes (LAH)<sub>p</sub>(IL)(H<sub>2</sub>O)<sub>2</sub> (with p ranging from 1-3). The uptake of LA by Cyphos® IL 104 is directly connected with the water uptake of the IL, including the formation of reverse micelles in the IL and inclusion of water into hydrated complexes of lactic acid (Marták & Schlosser, 2007).

## 5. Applications as catalysts and solvents in organic synthesis

Since the pioneering work of Mąkosza, Brändström, and Starks (Mąkosza & Serafinowa, 1965; Brändström & Gustavilii, 1969; Starks, 1971), quaternary ammonium and phosphonium salts have been used as phase transfer catalysts in liquid/liquid biphasic systems. Bender et al. (2010) evaluated a series of ILs including Aliquat® 336 as phase transfer catalysts for the etherification reaction of 1-octanol with 1-chlorobutane. The conversions ranged from 87-96% with Aliquat® 336 catalysts. Whereas the use of Aliquat 336 as a phase transfer catalyst is widespread and extensively investigated (e.g. Baidossi et al., 1997; Villa et al., 2003; Rup et al., 2009), phosphonium ILs have only recently been investigated for this application. Yadav & Tekale (2010) evaluated the ILs [P<sub>6,6,6,14</sub>][Cl], [P<sub>6,6,6,14</sub>][Br], [P<sub>6,6,6,14</sub>][decanoate], and [P<sub>6,6,6,14</sub>][PF<sub>6</sub>] as phase transfer catalysts for selective *O*-alkylation of 2-naphthol. Thereby, the reactivity of ILs was strongly dependent on the anion attached to the phosphonium cation following the order Br<sup>-</sup> > Cl<sup>-</sup> > hexafluorophosphate >

decanoate, corresponding to the order of nucleophilicity for the anions. Hence,  $[P_{6,6,6,14}][Br]$  was chosen as most reactive catalyst. It depicted a good catalytic performance in the solid-liquid phase transfer catalyzed synthesis of p-nitrodiphenyl ether, leading to 100% selectivity towards the desired product (Yadav & Motirale, 2008).

Though Aliquat® 336 represents a widely used, economically favorable phase transfer catalyst with remarkable performance, the main drawback is its chemical and thermal stability. This could be overcome by the use of more stable phosphonium ILs, hence more fundamental research should be done in this direction.

Regarding the environmental pressure to reduce waste and to reuse material in terms of "green chemistry", one of the most problematic areas to create environmentally friendly solutions is the field of solution phase chemistry (Rogers et al., 2002; Fraser & MacFarlane, 2009). Phosphonium- and ammonium-based ILs may play a role in these efforts, as described in following selected examples (Fraser & MacFarlane, 2009).

The Heck cross-coupling reaction is a common reaction for the formation of carbon-carbon bonds between alkenes and organic halides (Heck & Nolley, 1972). Kaufmann et al. (1996) applied a phosphonium-based IL, trihexyl(tetradecylphosphonium) bromide ( $[P_{6,6,6,14}][Br]$ , trade name Cyphos® IL 162) as recyclable medium for the palladium-mediated Heck coupling of aryl halides with acrylate esters (see Figure 7) for the first time. Although relatively high yields were obtained, the reaction temperature was rather high (100°C) and more activated aryl halides were strongly favored. In contrast, the use of Cyphos® IL 101 seems more applicable for Heck coupling reactions of deactivated and sterically demanding aryl halides (see Figure 7). The reaction was conducted under moderate conditions (at 50°C within 2h), resulting in sufficiently high yields (Gerritsma et al., 2004). Further evaluation of different  $[P_{6,6,6,14}]$ -based ILs revealed the dominant role of the chosen anion on the yield of the reaction. Whereas ILs with chloride and decanoate anions seem to be suitable for high yield Heck reactions,  $[PF_6]^-$  and  $[BF_4]^-$  containing ILs resulted in significantly lower yields (Gerritsma et al., 2004). On the other hand, Aliquat® 336 was successfully applied as reaction media for the palladium-catalyzed hydroxycarbonylation of aryl halides and benzyl chloride derivatives (Mizushima et al., 2004), as its presence significantly enhanced the hydroxycarbonylation reaction. Furthermore, the catalyst in the IL phase could be easily recycled after extraction of the products with water.

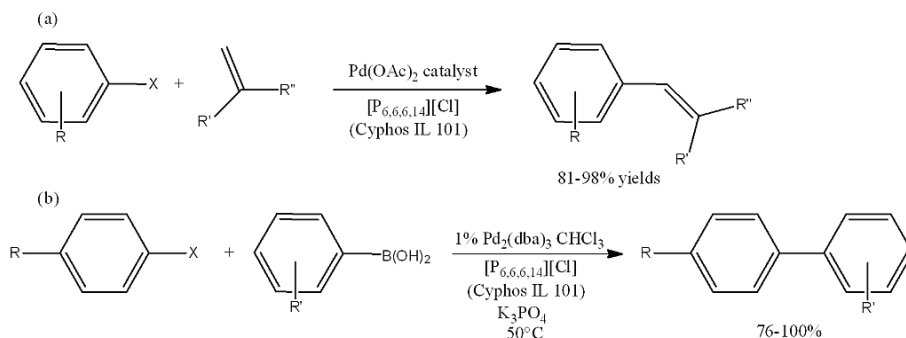


Fig. 7. (a)  $[P_{6,6,6,14}][Cl]$  ionic liquids reported as solvents in the Heck coupling reaction (redrawn from Fraser & MacFarlane, 2009). (b) Suzuki coupling carried out in a phosphonium ionic liquid (redrawn from Fraser & MacFarlane, 2009).

Several research groups investigated multiphase systems made by hydrogen, an aqueous phase, isooctane, Aliquat® 336 as phase transfer agent and a heterogeneous catalyst (e.g. Pd/C, Pt/C, Raney-Ni). These systems allow a variety of reduction reactions to be conducted under mild conditions ( $T = 50^{\circ}\text{C}$ ,  $p(\text{H}_2) = 1 \text{ atm}$ ), ranging from hydrodehalogenation of aryl halides (Tundo et al., 2001; Marques et al., 1994, 1995), hydrogenolysis of hydroxyls (Marques et al., 1995) up to aromatic hydrogenation (Marques et al., 1995; Selva et al., 1998). Perosa et al. (2002) for example studied the multiphase hydrogenolysis of benzyl methyl ether with different catalytic systems. It is noteworthy to mention that the relatively inexpensive Raney-Ni system is effective for debenzylolation under such conditions while simpler systems require Pd/C as catalyst. This methodology enables difficult transformations to be carried out under mild conditions, using a less expensive catalytic system and allowing easy catalyst recovery and reuse. The same working group observed a tenfold acceleration of a Heck coupling of aryl iodides with electron poor olefins using a triphasic system containing Aliquat® 336 and Pd/C as catalyst (Perosa et al., 2004).

Another interesting example is the use of ILs in Suzuki cross-coupling reactions (carbon-carbon bond formation between an  $\text{sp}^3$  carbon or non- $\beta$ -hydride containing electrophile and a boronic acid derivative; Miyaura & Suzuki, 1995). Cyphos® IL 101 has been recently reported as an extremely successful medium for such types of reaction (see Figure 7, McNulty et al., 2002). The palladium catalyst ( $\text{Pd}_2(\text{dba})_3\text{CHCl}_3$ ) was dissolved in the IL, forming a stable solution in absence of oxygen, and hence could also be effectively recycled after solvent extraction of reaction products. The Suzuki reactions in Cyphos® IL 101 were efficient even under moderate conditions ( $50\text{--}70^{\circ}\text{C}$ ), whereas the use of imidazolium-based ILs in contrast requires elevated temperatures (up to  $110^{\circ}\text{C}$ ) (Mathews et al., 2000).

In general, ILs are also regarded as favorable solvents for Diels-Alder reactions, producing good to high yields (Welton, 1999). Janus & Stefaniak (2008) reported that Diels-Alder reactions carried out in the phosphonium IL  $[\text{P}_{6,6,6,14}][\text{Tf}_2\text{N}]$  under presence of catalysts occurs smoothly, in short time and with high yield and high stereoselectivity. Further advantages of the reaction originate from the good solubility of catalysts belonging to the group of metal chlorides, triflates, and bis-triflimides in  $[\text{P}_{6,6,6,14}][\text{Tf}_2\text{N}]$  and - due to the high thermal stability of the IL - from the easy separation of the product via distillation. Several authors have been investigating the use of phosphonium-based ILs as media for strong base mediated reactions such as Grignard reactions (Ramnial et al., 2005; Law et al., 2006; Fraser & MacFarlane, 2009). Ramnial et al. (2008) investigated the ILs Cyphos® IL 101 and trihexyl(tetradecyl)phosphonium decanoate,  $[\text{P}_{6,6,6,14}][\text{C}_9\text{H}_{19}\text{COO}]$ , as solvents for bases such as Grignard reagents, isocyanides, Wittig reagents (phosphoranes), and N-heterocyclic carbenes. The authors illustrated that ILs can be used for generating N-heterocyclic carbenes and their metal complexes and as solvent medium for the generation of Wittig reagents. The reactivity of Cyphos® IL 101 in Grignard reagent solutions with tetrahydrofuran-to-IL ratio of 1:3 was tested by the addition of anhydrous bromine resulting in the exclusive formation of bromobenzene. Furthermore, Cyphos® IL 101 seems to be stable in basic Grignard reagents solutions, since even after one month no deprotonation was observed (Ramnial et al., 2008). It should also be noted that the use of phosphonium-based ILs facilitates the separation of the product due to the formation of three-phasic systems of some IL/water/hexane combinations. This may reduce the use of ethereal solvents in this class of reactions and hence lead to a general "greening" of Grignard chemistry (Ramnial et al., 2005; Fraser & MacFarlane, 2009). However, phosphonium-based ILs may also undergo

deprotonation in the presence of strong base, similarly to the C-H activation of imidazolium based ILs (Fraser & MacFarlane, 2009). Tseng et al. (2007) clearly indicated that the  $\alpha$ -protons of  $[P_{6,6,6,14}]$  ions, although shielded, are still accessible to small bases such as OH<sup>-</sup>. However, this exchange does not seem to produce a significant impact on the acidity of the cation.

Another promising field of phosphonium and ammonium ILs comprises the metal based ionic liquids. Following the idea of Hayashi and co-workers (Hayashi & Hamaguchi, 2004; Hayashi et al., 2006; Okuno & Hamaguchi, 2006). Del Sesto et al. (2008) prepared a set of transition metal based  $[P_{6,6,6,14}]$ -ILs. The simple reaction of Cyphos® IL 101 with FeCl<sub>3</sub>, CoCl<sub>3</sub>, MnCl<sub>2</sub> or GdCl<sub>3</sub> yields the corresponding ILs. All prepared ILs exhibited paramagnetic behavior as a sole property of ILs, and hence a series of hydrophobic, magnetic ILs was prepared. We have recently shown that the reaction of Aliquat® 336 with FeCl<sub>3</sub> leads to the corresponding paramagnetic IL tricaprylmethylammonium tetrachloroferrate,  $[A336][FeCl_4]$  (Kogelnig et al., 2010b). The development of magnetic ILs opens a new field of possible applications (e.g. as catalysts, Bica and Gaertner, 2006; Nguyen et al., 2008).

One more aspect is worth mentioning regarding possible applications of ammonium and phosphonium ILs in environmental and chemical engineering: the environmental impact. Although ILs were often described as new „environmental benign“ and „green“ compounds due to their low (often immeasurable) vapor pressure and non-inflammability, many new ILs have shown to be toxic (e.g.) to aquatic organisms, or even explosive (Pham et al., 2010; Gao et al., 2009). In general, very little is known about the toxicity of ammonium and phosphonium ILs. Frade et al. (2009) investigated the toxicity of selected ILs in a human colon carcinoma cell line (CaCo-2). The evaluated Aliquat® 336-based ILs  $[A336][Cl]/[FeCl_4]/[TFA]/[TfO]$  are very toxic and can not be regarded as candidates for greener solvents. Interestingly, whereas  $[P_{6,6,6,14}][Cl]/[FeCl_4]$  were also very toxic, the dicyanamide ([DCA]) anion led to a considerable decrease in toxicity. Kumar & Molhotra (2009) investigated the potential anti-cancer activity and cytotoxicity of selected ammonium- and phosphonium-based ILs. Cyphos® IL 101 may also be regarded as toxic in aquatic environment, exhibiting much higher ecotoxicity compared with common organic solvents (Wells & Coombe, 2006). The activity and cytotoxicity of investigated ILs were strongly influenced by alkyl chain length of and alkyl substitution on the cations. In general, phosphonium ILs were more active and less cytotoxic compared with ammonium ILs. Hence, ammonium and phosphonium ILs should not be a priori regarded as „green“ solvents, and their behavior and environmental impact has to be extensively studied.

## 6. Conclusions

Ammonium and phosphonium ionic liquids undoubtedly represent a promising group of ILs. However, as it can be seen in examples presented in previous sections, many of the discussed applications and concepts are still in the early stage of development (with the exception of several widespread applications of Aliquat® 336, of course). This can be attributed mainly to the circumstance that ammonium- and phosphonium-based ILs have just recently gained attention both in the ionic liquid and engineering community. Hence most of the examples presented in the literature still deal with concept research. On the other hand the development of engineering applications of ILs generally requires a reliable and broad spectrum of knowledge concerning the nature of the IL itself and of relevant aspects regarding the attended application. At current stage of research much more information concerning fundamental IL properties and behavior is needed. In the further

stage of development aspects like efficiency of the recycling process, ionic liquid recovery and reusability, or the degree of ionic liquid degradation with time needs to be considered. Further, the toxicity and environmental impact of this group of ILs needs to be extensively studied as both Aliquat® 336 and Cyphos® IL 101 can not be regarded as “green” solvents.

## 7. References

- Alguacil, F. J., Alonso, M., Lopez, F. A. & Lopez-Delgado, A. (2010). Pseudo-emulsion membrane strip dispersion (PEMSD) pertraction of chromium(VI) using Cyphos IL 101 ionic liquid as carrier. *Environmental Science and Technology*, in press, DOI: 10.1021/es101302b
- Ali, A. M. I., El-Nadi, Y. A., Daoud, J. A. & Aly, H. F. (2007). Recovery of thorium (IV) from leached monazite solutions using counter-current extraction. *International Journal of Mineral Processing*, 81, 4, 217-223, ISSN: 0301-7516
- Argiropoulos, G., Cattrall, R. W., Hamilton, I. C., Kolev, S. D. & Paimin, R. (1998a). The study of a membrane for extracting gold(III) from hydrochloric acid solutions. *Journal of Membrane Science*, 138, 2, 279-285, ISSN: 0376-7388
- Argiropoulos, G., Cattrall, R. W., Hamilton, I. C. & Paimin, R. (1998b). Determination of the quaternary ammonium ion components of Aliquat 336 by electrospray mass spectrometry. *Analytica Chimica Acta*, 360, 1-3, 167-169, ISSN: 0003-2670
- Atkins, M.P., Davey, P., Fitzwater, G., Rouher, O., Seddon, K.R. & Swindall, J. (2004). *Ionic Liquids: A Map for Industrial Innovation*. Report Q001, January 2004, QUILL, Belfast
- Atanassova, M. & Dukov, I. L. (2004). Synergistic solvent extraction and separation of trivalent lanthanide metals with mixtures of 4-benzoyl-3-methyl-1-phenyl-2-pyrazolin-5-one and Aliquat 336. *Separation and Purification Technology*, 40, 2, 171-176, ISSN: 1383-5866
- Baidossi, W., Lahav, M. & Blum, J. (1997). Hydration of alkynes by a  $\text{PtCl}_4\text{-CO}$  catalyst. *Journal of Organic Chemistry*, 62, 3, 669-672, ISSN: 0022-3263
- Bender, J., Jepkens, D. & Hüskens, H. (2010). Ionic liquids as phase-transfer catalysts: Etherification reaction of 1-Octanol with 1-Chlorobutane. *Organic Process Research & Development*, 14, 3, 716-721, ISSN: 1083-6160
- Bica, K. & Gaertner, P. (2006). An iron containing ionic liquid as recyclable catalyst for aryl Grignard cross-coupling of alkyl halides. *Organic Letters*, 8, 4, 733-735, ISSN: 1523-7060
- Blitz-Raith, A. H., Paimin, R., Cattrall, R. W. & Kolev, S. D. (2007). Separation of cobalt(II) from nickel(II) by solid-phase extraction into Aliquat 336 chloride immobilized in poly(vinyl chloride). *Talanta*, 71, 1, 419-423, ISSN: 0039-9140
- Boethling, R. S. & Lynch, D. G. (1992). Quaternary ammonium surfactants, In: *The Handbook of Environmental Chemistry*, Oude, N. T. (Ed.), 3, 144-177, Springer, ISSN 1867-979X, Berlin, Germany
- Bora, M. M. & Dutta, N. N. (1998). Extraction of 7-aminocephalosporanic acid with secondary, tertiary, and quaternary amines. *Journal of Chemical and Engineering Data*, 43, 3, 318-324, ISSN: 0021-9568

- Bradaric, C. J., Downard, A., Kennedy, C., Robertson, A. J. & Zhou, Y. (2003). Industrial preparation of phosphonium ionic liquids. *Green Chemistry*, 5, 2, 143-152, ISSN: 1463-9262
- Brändström, A. & Gustavii, K. (1969). Ion pair extraction in preparative organic chemistry. *Acta Chemica Scandinavica*, 23, 4, 1215-1218, ISSN: 0001-5393
- Buzzeo, M. C., Evans, R. G. & Compton, R. G. (2004). Non-haloaluminate room-temperature ionic liquids in electrochemistry - a review. *ChemPhysChem*, 5, 8, 1106-1120, ISSN: 1439-4235
- Carmichael, A. J., Earle, M. J., Holbrey, J. D., McCormac, P. B. & Seddon, K. R. (1999). The Heck reaction in ionic liquids: A multiphasic catalyst system. *Organic Letters*, 1, 7, 997-1000, ISSN: 1523-7060
- Chowdhury, S., Mohan, R. S. & Scott, J. L. (2007). Reactivity of ionic liquids. *Tetrahedron*, 63, 11, 2363-2389, ISSN: 0040-4020
- Cieszyńska, A., Regel-Rosocka, M. & Wiśniewski, M. (2007). Extraction of palladium(II) ions from chloride solutions with phosphonium ionic liquid Cyphos® IL 101. *Polish Journal of Chemical Technology*, 9, 2, 99-101, ISSN: 1509-8117
- Danesi, P. R., Reichley-Yinger, L., Mason, G., Kaplan, L., Horwitz, E. P. & Diamond, H. (1985). Selectivity-structure trends in the extraction of cobalt(II) and nickel(II) by dialkyl phosphoric, alkyl alkylphosphonic, and dialkylphosphinic acids. *Solvent Extraction and Ion Exchange*, 3, 4, 135-452, ISSN: 0736-6399
- Davies, D. L., Kandola, S. K. & Patel, R. K. (2004). Asymmetric cyclopropanation in ionic liquids: effect of anion and impurities. *Tetrahedron: Asymmetry*, 15, 1, 77-80, ISSN: 0957-4166
- Del Sesto, R. E., McCleskey, T. M., Burrell, A. K., Baker, G. A., Thompson, J. D., Scott, B. L., Wilkes, J. S. & Williams, P. (2008). Structure and magnetic behavior of transition metal based ionic liquids. *Chemical Communications*, 447-449, ISSN: 1359-7345
- De Mendonça Fábrega, F. & Borges Mansur, M. (2007). Liquid-liquid extraction of mercury(II) from hydrochloric acid solutions by Aliquat 336. *Hydrometallurgy*, 87, 3-4, 83-90, ISSN: 0304-386X
- Egorov, V. M., Smirnova, S. V. & Pletnev, I. V. (2008). Highly efficient extraction of phenols and aromatic amines into novel ionic liquids incorporating quaternary ammonium cation. *Separation and Purification Technology*, 63, 3, 710-715, ISSN: 1383-5866
- Egorov, V. M., Djigailo, D. I., Momotenko, D. S., Chernyshov, D. V., Torocheshnikova, I. I., Smirnova, S. V. & Pletnev, I. V. (2010). Task-specific ionic liquid trioctylmethylammonium salicylate as extraction solvent for transition metal ions. *Talanta*, 80, 3, 1177-1182, ISSN: 0039-9140
- El-Nadi, Y. A., Daoud, J. A. & Aly, H. F. (2005). Modified leaching and extraction of uranium from hydrous oxide cake of Egyptian monazite. *International Journal of Mineral Processing*, 76, 1-2, 101-110, ISSN: 0301-7516
- El-Wakil, A. M., Farag, A. B. & Ez-Eldin, A. K. (1982). Liquid-liquid extraction of iron(III), cobalt(II), nickel(II) and cadmium(II) from aqueous halide media with Aliquat 336. *Fresenius' Zeitschrift für Analytische Chemie*, 311, 5, 522-526, ISSN: 0016-1152



- Fontàs, C., Palet, C., Salvado, V. & Hidalgo, M. (2000). A hollow fiber supported liquid membrane based on Aliquat 336 as a carrier for rhodium(III) transport and preconcentration. *Journal of Membrane Science*, 178, 1-2, 131-139, ISSN: 0376-7388
- Frade, R. F. M., Rosatella, A. A., Marques, C. S., Branco, L. C., Kulkarni, P. S., Mateus, N. M. M., Afonso, C. A. M. & Duarte, C. M. M. (2009). Toxicological evaluation on human colon carcinoma cell line (CaCo-2) of ionic liquids based on imidazolium, guanidinium, ammonium, phosphonium, pyridinium and pyrrolidinium cations. *Green Chemistry*, 11, 10, 1660-1665, ISSN: 1463-9262
- Fraser K. J. & MacFarlane D. R. (2009). Phosphonium-based ionic liquids: An overview. *Australian Journal of Chemistry*, 62, 4, 309-321, ISSN: 0004-9425
- Gabelman, A. & Hwang, S.-T. (1999). Hollow fiber membrane contactors. *Journal of Membrane Science*, 159, 1-2, 61-106, ISSN: 0376-7388
- Gallo, V., Mastrolilli, P., Nobile, C. F., Romanazzi, G. & Suranna, G. P. (2002). How does the presence of impurities change the performance of catalytic systems in ionic liquids? A case study: the Michael addition of acetylacetone to methyl vinyl ketone. *Journal of the Chemical Society, Dalton Transactions*, 23, 4339-4342, ISSN: 1472-7773
- Gao, H., Joo, Y.-H., Twamley, B., Zhou, Z. & Shreeve, J. M. (2009). Hypergolic ionic liquids with the 2,2-dialkyltriazanium cation. *Angewandte Chemie, International Edition*, 48, 15, 2792-2795, ISSN: 1433-7851
- Gerritsma, D. A., Robertson, A., McNulty, J. & Capretta, A. (2004). Heck reactions of aryl halides in phosphonium salt ionic liquids: library screening and applications. *Tetrahedron Letters*, 45, 41, 7629-7631, ISSN: 0040-4039
- Güell, R., Antico, E., Salvado, V. & Fontàs, C. (2008). Efficient hollow fiber supported liquid membrane system for the removal and preconcentration of Cr(VI) at trace levels. *Separation and Purification Technology*, 62, 2, 389-393, ISSN: 1383-5866
- Guibal, E., Vincent, T. & Jouannin, C. (2009). Immobilization of extractants in biopolymer capsules for the synthesis of new resins: a focus on the encapsulation of tetraalkyl phosphonium ionic liquids. *Journal of Materials Chemistry*, 19, 45, 8515-8527, ISSN: 0959-9428
- Hanhart, W. & Ingold, C. K. (1927). Nature of the alternating effect in carbon chains. XVIII. Mechanism of exhaustive methylation and its relation to anomalous hydrolysis. *Journal of the Chemical Society*, 997-1020, ISSN: 0368-1769
- Harington, T. & Hossain, Md. M. (2008). Extraction of lactic acid into sunflower oil and its recovery into an aqueous solution. *Desalination*, 218, 1-3, 287-296, ISSN: 0011-9164
- Hayashi, S. & Hamaguchi, H. (2004). Discovery of a magnetic ionic liquid [bmim]FeCl<sub>4</sub>. *Chemistry Letters*, 33, 12, 1590-1591, ISSN: 00366-7022
- Hayashi, S., Saha, S. & Hamaguchi, H. (2006). A new class of magnetic fluids: bmim[FeCl<sub>4</sub>] and nbmim[FeCl<sub>4</sub>] ionic liquids. *IEEE Transactions on Magnetics*, 42, 1, 12-14, ISSN: 0018-9464
- Heck, R. F. & Nolley, J. P. Jr. (1972). Palladium-catalyzed vinylic substitution reactions with aryl, benzyl, and styryl halides. *Journal of Organic Chemistry*, 37, 14, 2320-2322, ISSN: 0022-3263

- Hoh, Y. C., Chuang, W. S. & Yueh, P. S. (1985). The extraction of platinum from platinum(II) chloride solution by a quaternary ammonium compound. *Journal of Chemical Technology and Biotechnology, Chemical Technology*, 35A, 1, 41-47, ISSN: 0264-3413
- Hossain, Md. M. & Maisuria, J. L. (2008). Effects of organic phase, fermentation media, and operating conditions on lactic acid extraction. *Biotechnology Progress*, 24, 3, 757-765, ISSN: 8156-7938
- <http://www.ich.org>
- <http://www.cognis.com>
- Ingold, C. K. & Vass, C. C. N. (1928). The influence of poles and polar linkings on the course pursued by elimination reactions II. The mechanism of exhaustive methylation. *Journal of the Chemical Society*, 3125-3127, ISSN: 0368-1769
- Janus, E. & Stefaniak, W. (2008). The Diels-Alder reaction in phosphonium ionic liquid catalysed by metal chlorides, triflates and triflimides. *Catalysis Letters*, 124, 1-2, 105-110, ISSN: 1011-372X
- Juang, R.-S., Kao, H.-C. & Wu, W.-H. (2004). Analysis of liquid membrane extraction of binary Zn(II) and Cd(II) from chloride media with Aliquat 336 based on thermodynamic equilibrium models. *Journal of Membrane Science*, 228, 2, 169-177, ISSN: 0376-7388
- Juergensen, L., Busnarda, J., Caux, P. Y. & Kent, R. A. (2000). Fate, behaviour, and aquatic toxicity of the fungicide DDAC in the Canadian environment. *Environmental Toxicology*, 15, 3, 174-200, ISSN: 1520-4081
- Kalb, R. S. (2005). Method for producing ionic liquids, ionic solids or mixtures thereof. WO 2005 021484.
- Kalb, R. S., Krachler, R. & Keppler, B. K. (2006). Determination of heavy metal polluted process water, waste water and filter cake with high performance. *Chemical Industry and Environment V*, Volume I, W. Höflinger (Ed.), EMChIE, Vienna, Austria.
- Kao, H.-C. & Juang, R.-S. (2005). Kinetic analysis of non-dispersive solvent extraction of concentrated Co(II) from chloride solutions with Aliquat 336: Significance of the knowledge of reaction equilibrium. *Journal of Membrane Science*, 264, 1-2, 104-112, ISSN: 0376-7388
- Karodia, N., Guise, S., Newlands, C. & Andersen, J. (1998). Clean catalysis with ionic solvents - phosphonium tosylates for hydroformylation. *Chemical Communications*, 21, 2341-2342, ISSN: 1359-7345
- Kaufmann, D. E., Nouroozian, M. & Henze, H. (1996). Molten salts as an efficient medium for palladium-catalyzed C-C coupling reactions. *Synlett*, 11, 1091-1092, ISSN: 0936-5214
- Kogelnig, D., Stojanovic, A., Galanski, M., Grössl, M., Jirsa, F., Krachler, R. & Keppler, B. K. (2008). Greener synthesis of new ammonium ionic liquids and their potential as extracting agents. *Tetrahedron Letters*, 49, 17, 2782-2785, ISSN: 0040-4039
- Kogelnig, D., Stojanovic, A., Jirsa, F., Körner, W., Krachler, R. & Keppler, B. K. (2010a). Transport and separation of iron(III) from nickel(II) with the ionic liquid trihexyl(tetradecyl)phosphonium chloride. *Separation and Purification Technology*, 72, 1, 56-60, ISSN: 1383-5866

- Kogelnig, D., Stojanovic, A., Kammer, F. v. d., Terzieff, P., Galanski, M., Krachler, R. & Keppler, B. K. (2010b). Tricaprylylmethylammonium tetrachloroferrate ionic liquid: magnetic- and aggregation behavior. *Inorganic Chemistry Communications*, 13, 12, 1485-1488, ISSN: 1387-7003
- Kolev, S. D., Sakai, Y., Cattrall, R. W., Paimin, R. & Potter, I. D. (2000). Theoretical and experimental study of palladium(II) extraction from hydrochloric acid solutions into Aliquat 336/PVC membranes. *Analytica Chimica Acta*, 413, 1-2, 241-246, ISSN: 0003-2670
- Kulkarni, P. S., Branco, L. C., Crespo, J. G., Nunes, M. C., Raymundo, A. & Afonso, C. A. M. (2007a). Comparison of physicochemical properties of new ionic liquids based on imidazolium, quaternary ammonium, and guanidinium cations. *Chemistry – A European Journal*, 13, 30, 8478-8488, ISSN: 0947-6539
- Kulkarni, P. S., Branco, L. C., Crespo, J. G. & Afonso, C. A. M. (2007b). A comparative study on absorption and selectivity of organic vapors by using ionic liquids based on imidazolium, quaternary ammonium, and guanidinium cations. *Chemistry – A European Journal*, 13, 30, 8470-8477, ISSN: 0947-6539
- Kulkarni, P. S., Branco, L. C., Crespo, J. G. & Afonso, C. A. M. (2008). Capture of dioxins by ionic liquids. *Environmental Science & Technology*, 42, 7, 2570-2574, ISSN: 0013-936X
- Kumar, V. & Malhotra, S. V. (2009). Study on the potential anti-cancer activity of phosphonium and ammonium-based ionic liquids. *Bioorganic & Medicinal Chemistry Letters*, 19, 16, 4643-4646, ISSN: 0960-894X
- Kyuchoukov, G., Yankov, D., Albet, J. & Molinier, J. (2005). Mechanism of lactic acid extraction with quaternary ammonium chloride (Aliquat 336). *Industrial & Engineering Chemistry Research*, 44, 15, 5733-5739, ISSN: 6534-6538
- Law, M. C., Wong, K.-Y. & Chan, T. H. (2006). Grignard reagents in ionic liquids. *Chemical Communications*, 23, 2457-2459, ISSN: 1359-7345
- Lee, G. L., Cattrall, R. W., Daud, H. & Smith, J. F. (1981). The analysis of aliquat-336 by gas chromatography. *Analytica Chimica Acta*, 123, 213-220, ISSN: 0003-2670
- Lee, J.-Y., Kumar, R. J., Kim, J.-S., Kim, D.-J. & Yoon, H.-S. (2009). Extraction and separation of Pt(IV)/Rh(III) from acidic chloride solutions using Aliquat 336. *Journal of Industrial and Engineering Chemistry*, 15, 3, 359-364, ISSN: 1226-086X
- Liu, Y., Zhu, L., Sun, X. & Chen, L. (2010). Toward greener separations of rare earths: bifunctional ionic liquid extractants in biodiesel. *AIChE Journal*, 56, 9, 2338-2346, ISSN: 0001-1541
- Mąkosza, M. & Serafinowa, B. (1965). Reactions of organic anions. Part I. Catalytic ethylation of phenylacetone nitrile in aqueous medium. *Roczniki Chemii*, 39, 9, 1223-1231, ISSN: 0035-7677
- Marques, C. A., Selva, M. & Tundo, P. (1994). Facile hydrodehalogenation with H<sub>2</sub> and Pd/C catalyst under multiphase conditions 2. Selectivity and kinetics. *Journal of Organic Chemistry*, 59, 14, 3830-3837, ISSN: 0022-3263
- Marques, C. A., Selva, M. & Tundo, P. (1995). Facile hydrohalogenation with H<sub>2</sub> and Pd/C catalyst under multiphase conditions 3. Selective removal of halogen from functionalized aryl ketones. 4. Aryl halide-promoted reduction of benzyl alcohols to alkanes. *Journal of Organic Chemistry*, 60, 8, 2430-2435, ISSN: 0022-3263

- Marták, J. & Schlosser, S. (2007). Extraction of lactic acid by phosphonium ionic liquids. *Separation and Purification Technology*, 57, 3, 483-494, ISSN: 1383-5866
- Mathews, C. J., Smith, P. J. & Welton, T. (2000). Palladium catalyzed Suzuki cross-coupling reactions in ambient temperature ionic liquids. *Chemical Communications*, 14, 1249-1250, ISSN: 1359-7345
- McNulty, J., Capretta, A., Wilson, J., Dyck, J., Adjabeng, G. & Robertson, A. (2002). Suzuki cross-coupling reactions of aryl halides in phosphonium salt ionic liquid under mild conditions. *Chemical Communications*, 17, 1986-1987, ISSN : 1359-7345
- Meindersma, G. W., Galán Sánchez, L. M., Hansmeier, A. R. & de Haan, A. B. (2007). Application of task-specific ionic liquids for intensified separations. *Monatshefte für Chemie*, 138, 11, 1125-1136, ISSN: 0026-9247
- Mikkola, J.-P., Virtanen, P. & Sjöholm, R. (2006a). Aliquat 336®—a versatile and affordable cation source for an entirely new family of hydrophobic ionic liquids. *Green Chemistry*, 8, 250-255, ISSN: 1463-9262
- Mizushima, E., Hayashi, T. & Tanaka, M. (2004). Environmentally benign carbonylation reaction: palladium-catalyzed hydroxycarbonylation of aryl halides and benzyl chloride derivatives in ionic liquid media. *Topics in Catalysis*, 29, 3-4, ISSN: 1022-5528
- Miyaura, N. & Suzuki, A. (1995). Palladium-catalyzed cross-coupling reactions of organoboron compounds. *Chemical Reviews*, 95, 7, 2457-2483, ISSN: 0009-2665
- Myasoedova, G. V., Molochnikova, N. P., Mokhodoeva, O. B. & Myasoedov, B. F. (2008). Application of ionic liquids for solid-phase extraction of trace elements. *Analytical Sciences*, 24, 10, 1351-1353, ISSN: 0910-6340
- Nayl, A. A. (2010). Extraction and separation of Co(II) and Ni(II) from acidic sulfate solutions using Aliquat 336. *Journal of Hazardous Materials*, 173, 1-3, 223-230, ISSN: 0304-3894
- Nghiem, L. D., Mornane, P., Potter, I. D., Perera, J. M., Cattrall, R. W. & Kolev, S. D. (2006). Extraction and transport of metal ions and small organic compounds using polymer inclusion membranes (PIMs). *Journal of Membrane Science*, 281, 1+2, 7-41, ISSN: 0376-7388
- Nguyen, M. D., Nguyen, L. V., Jeon, E. H., Kim, J. H., Cheong, M., Kim, H. S. & Lee, J. S. (2008). Fe-containing ionic liquids as catalysts for the dimerization of bicycle[2.2.1]hepta-2,5-diene. *Journal of Catalysis*, 258, 1, 5-13, ISSN: 0021-9517
- Okuno, M., Hamaguchi, H. & Hayashi, S. (2006). Magnetic manipulation of materials in a magnetic ionic liquid. *Applied Physics Letters*, 89, 13, 132506/1-2, ISSN: 0003-6951
- Pancharoen, U., Poonkum, W. & Lothongkum, A.W. (2009). Treatment of arsenic ions from produced water through hollow fiber supported liquid membrane. *Journal of Alloys and Compounds*, 482, 1-2, 328-334, ISSN: 0925-8388
- Pernak, J., Smiglak, M., Griffin, S. T., Hough, W. L., Wilson, T. B., Pernak, A., Zabielska-Matejuk, J., Fojutowski, A., Kita, K. & Rogers, R. D. (2006). Long alkyl chain quaternary ammonium-based ionic liquids and potential applications. *Green Chemistry*, 8, 9, 798 - 806, ISSN: 1463-9262
- Perosa, A., Tundo, P. & Zinovyev, S. (2002). Mild catalytic multiphase hydrogenolysis of benzyl ethers. *Green Chemistry*, 4, 5, 492-494, ISSN: 1463-9262

- Perosa, A., Tundo, P., Selva, M., Zinovyev, S. & Testa, A. (2004). Heck reaction catalyzed by Pd/C, in a triphasic-organic/Aliquat 336/aqueous-solvent system. *Organic & Biomolecular Chemistry*, 2, 15, 2249-2252, ISSN: 1477-0520
- Pehlivanoglu, N., Uslu, H. & Kirbaşlar, S. I. (2010). Extractive separation of glutaric acid by Aliquat 336 in different solvents. *Journal of Chemical & Engineering Data*, 55, 9, 2970-2973, ISSN: 0021-9568
- Pham, T. P. T., Cho, C.-W. & Yun, Y.-S. (2010). Environmental fate and toxicity of ionic liquids: a review. *Water Research*, 44, 2, 352-372, ISSN: 0043-1354
- Plechkova, N. V. & Seddon, K. R. (2007) Ionic liquids: "Designer" solvents for green chemistry, In *Methods and Reagents for Green Chemistry*, Perosa, A., Zecchini, F. (Eds.), 105-130, John Wiley Sons, ISBN: 978-0-471-75400-8, NewYork
- Rahman, M., Shoff, H. W. & Brazel, C. S. (2005). Ionic liquids as alternative plasticizers for poly(vinyl chloride): flexibility and stability in thermal, leaching, and UV environments. In *Ionic Liquids in Polymer Systems*, Brazel, C. S. & Rogers, R. D. (Eds.), 103-118, American Chemical Society, ISBN: 9780841239364
- Ramnial, T., Ino, D. D. & Clyburne, A. C. (2005). Phosphonium ionic liquids as reaction media for strong bases. *Chemical Communications*, 3, 325-327, ISSN: 1359-7345
- Ramnial, T., Taylor, S. A., Bender, M. L., Gorodetsky, B., Lee, P. T. K., Dickie, D. A., McCollum, B. M., Pye, C. C., Walsby, C. J. & Clyburne, J. A. C. (2008). Carbon-centered strong bases in phosphonium ionic liquids. *Journal of Organic Chemistry*, 73, 3, 801-812, ISSN: 0022-3263
- Regel-Rosocka, M. (2009). Extractive removal of zinc(II) from chloride liquors with phosphonium ionic liquids/toluene mixtures as novel extractants. *Separation and Purification Technology*, 66, 1, 19-24, ISSN: 1383-5866
- Rickelton, W. A. & Robertson, A. J. (1982). US Patent 4 353 883
- Rickelton, W. A., Flett, D. S. & West, D. W. (1984). Cobalt-nickel separation by solvent extraction with bis(2,4,4 trimethylpentyl)phosphinic acid. *Solvent Extraction and Ion Exchange*, 2, 6, 815-838, ISSN: 0736-6299
- Robertson, A. J. (Cytec Industries) (2001). Phosphonium salts. WO 01/87900
- Robertson, A. J. (1983). Process for the preparation of highly purified, dialkyl phosphinic acids. US 4 374 780, WO/2006/047545A2
- Robertson, A. L. & Seddon, K. R. (Cytec Industries) (2002). Phosphonium phosphinate compounds and their preparation, WO 02/079212 A1
- Rogers, R. D., Seddon, K. R. & Volkov, S. (Eds.) (2002). Green industrial applications of ionic liquids. Kluwer Academic Publishers, ISBN: 1-4020-1136-9, Netherlands
- Rosatella, A. A., Branco, L. C. & Afonso, C. A. M. (2009). Studies on dissolution of carbohydrates in ionic liquids and extraction from aqueous phase. *Green Chemistry*, 11, 9, 1406-1413, ISSN: 1463-9262
- Rup, S., Zimmermann, F., Meux, E., Schneider, M., Sindt, M. & Oget, N. (2009). The ultrasound-assisted oxidative scission of monoenoic fatty acids by ruthenium tetroxide catalysis: Influence of the mixture of solvents. *Ultrasonics Sonochemistry*, 16, 2, 266-272, ISSN: 1350-4177

- Seddon, K. R., Stark, A. & Torres, M.-J. (2000). Influence of chloride, water, and organic solvents on the physical properties of ionic liquids. *Pure and Applied Chemistry*, 72, 12, 2275-2287, ISSN: 0033-4545
- Seddon, K. R., Carmichael, A. & Earle, M. J. (2001). Process for preparing ambient temperature ionic liquids, WO 01/40146 A1
- Seeley, F. G. & Crouse, D. J. (1966). Extraction of metals from chloride solutions with amines. *Journal of Chemical & Engineering Data*, 11, 3, 424-429, ISSN: 0021-9568
- Selva, M., Tundo, P. & Perosa, A. (1998). Hydrodehalogenation of halogenated aryl ketones under multiphase conditions 5. Chemoselectivity toward aryl alcohols over a Pt/C catalyst. *Journal of Organic Chemistry*, 63, 10, 3266-3271, ISSN: 0022-3263
- Srncik, M., Kogelnig, D., Stojanovic, A., Körner, W., Krachler, R. & Wallner, G. (2009). Uranium extraction from aqueous solutions by ionic liquids. *Applied Radiation and Isotopes*, 67, 12, 2146-2149, ISSN: 0969-8043
- Stark, A., Ajam, M., Green, M., Raubenheimer, H. G., Ranwell, A. & Ondruschka, B. (2006). Metathesis of 1-octene in ionic liquids and other solvents: effects of substrate solubility, solvent polarity and impurities. *Advanced Synthesis & Catalysis*, 348, 14, 1934-1941, ISSN: 1615-4150
- Starks, C. M. (1971). Phase-transfer catalysis I. Heterogeneous reactions involving anion transfer by quaternary ammonium and phosphonium salts. *Journal of the American Chemical Society*, 93, 1, 195-199, ISSN: 0002-7863
- Stojanovic, A., Lämmerhofer, M., Kogelnig, D., Schiesel, S., Sturm, M., Galanski, M., Krachler, R., Keppler, B. K. & Lindner, W. (2008). Analysis of quaternary ammonium and phosphonium ionic liquids by reversed-phase high-performance liquid chromatography with charged aerosol detection and unified calibration. *Journal of Chromatography A*, 1209, 1-2, 179 - 187, ISSN: 0021-9673
- Stojanovic, A., Kogelnig, D., Fischer, L., Hann, S., Galanski, M., Grössl, M., Krachler, R. & Keppler, B. K. (2010). Phosphonium and ammonium ionic liquids with aromatic anions: Synthesis, properties, and platinum extraction. *Australian Journal of Chemistry*, 63, 3, 511-524, ISSN: 0004-9425
- Sun, X., Ji, Y., Chen, J. & Li, D. (2010a). An engineering - purpose preparation strategy for ammonium -type ionic liquid with high purity. *AIChE Journal*, 56, 989-996, ISSN: 0001-1541
- Sun, X., Ji, Y., Zhang, L., Chen, J. & Li, D. (2010b). Separation of cobalt and nickel using inner synergistic extraction from bifunctional ionic liquid extractant (Bif-ILE). *Journal of Hazardous Materials*, 181, 1-3, 447-452, ISSN: 0304-3894
- Tariq, M., Forte, P. A. S., Costa Gomes, M. F., Canongia Lopes, J. N. & Rebelo, L. P. N. (2009). Densities and refractive indices of imidazolium- and phosphonium-based ionic liquids: Effect of temperature, alkyl chain length, and anion. *Journal of Chemical Thermodynamics*, 41, 6, 790-798, ISSN: 0021-9614
- Tseng, M.-C., Kan, H.-C. & Chu, Y.-H. (2007). Reactivity of trihexyl(tetradecyl)phosphonium chloride, a room temperature phosphonium ionic liquid. *Tetrahedron Letters*, 48, 52, 9085-9089, ISSN: 0040-4039

- Tundo, P., Perosa, A., Selva, M. & Zinovyev, S. S. (2001). A mild catalytic detoxification method for PCDDs and PCDFs. *Applied Catalysis B: Environmental*, 32, L1-L7, ISSN: 0926-3373
- Uddin, M. S., Hidajat, K., Lim, B.-G. & Ching, C.-B. (1990). Interfacial mass transfer in extraction of amino acid by Aliquat 336 in organic phase. *Journal of Chemical Technology and Biotechnology*, 48, 4, 415-426, ISSN: 0268-2575
- Uslu, H. & Kirbaşlar, I. S. (2009). Investigation of phase equilibria of levulinic acid distribution between aqueous phase to organic phase by Aliquat 336 in different modifiers. *Journal of Chemical Thermodynamics*, 41, 9, 1042-1048, ISSN: 0021-9614
- Van den Berg, C., Roelands, C. P. M., Bussmann, P., Goetheer, E. L. V., Verdoes, D. & van der Wielen, L. A. M. (2009). Preparation and analysis of high capacity polysulfone capsules. *Reactive & Functional Polymers*, 69, 10, 766-770, ISSN: 1381-5148
- Villa, C., Mariani, E., Loupy, A., Grippo, C., Grossi, G. C. & Bargagna, A. (2003). Solvent-free reactions as green chemistry procedures for the synthesis of cosmetic fatty esters. *Green Chemistry*, 5, 5, 623-626, ISSN: 1463-9262
- Wang, L., Paimin, R., Cattrall, R. W., Shen, W. & Kolev, S. D. (2000). The extraction of cadmium(II) and copper(II) from hydrochloric acid solutions using an Aliquat 336/PVC membrane. *Journal of Membrane Science*, 176, 1, 105-111, ISSN: 0376-7388
- Wasserscheid, P. & Welton, T. (2008). *Ionic Liquids in Synthesis*, second edition, Wiley-VCH, ISBN 978-3-527-31239-9, Weinheim, Germany
- Welton, T. (1999). Room-temperature ionic liquids. Solvents for synthesis and catalysis. *Chemical Reviews*, 99, 8, 2071-2083, ISSN: 0009-2665
- Wells, A. S. & Coombe, V. T. (2006). On the freshwater ecotoxicity and biodegradation properties of some common ionic liquids. *Organic Process Research & Development*, 10, 4, 794-798, ISSN: 1083-6160
- Weng, J., Wang, C., Li, H. & Wang, Y. (2006). Novel quaternary ammonium ionic liquids and their use as dual solvent-catalysts in a hydrolytic reaction. *Green Chemistry*, 8, 1, 96-99, ISSN: 1463-9262
- Werner S., Haumann, M. & Wasserscheid, P. (2010). Ionic liquids in chemical engineering, *Annual Review of Chemical and Biomolecular Engineering*, 1, 203-230, ISSN: 1947-5438
- Wolff, M. O., Alexander, K. M. & Belder, G. (2000). Uses of quaternary phosphonium compounds in phase transfer catalysis. *Chimica Oggi*, 18, 1/2, 29-32, ISSN: 0392-839X
- Yadav, G. D. & Motirale, B. G. (2008). Ionic liquid as catalyst for solid-liquid phase transfer catalyzed synthesis of p-nitrodiphenyl ether. *Industrial & Engineering Chemistry Research*, 47, 23, 9081-9089, ISSN: 0888-5885
- Yadav, G. D. & Tekale, S. P. (2010). Selective O-alkylation of 2-naphtol using phosphonium-based ionic liquid as the phase transfer catalyst. *Organic Process Research & Development*, 14, 3, 722-727, ISSN: 1083-6160
- Yang, W. W., Luo, G. S. & Gong, X. C. (2005). Extraction and separation of metal ions by a column packed with polystyrene microcapsules containing Aliquat 336. *Separation and Purification Technology*, 43, 2, 175-182, ISSN: 1383-5866
- Yao, C., Pitner, W. R. & Anderson, J. L. (2009). Ionic liquids containing the tris(pentafluoroethyl)trifluorophosphate anion: a new class of highly selective and

ultra hydrophobic solvents for the extraction of polycyclic aromatic hydrocarbons using single drop microextraction. *Analytical Chemistry*, 81, 12, 5054-5063, ISSN: 0003-2700

Yuan, X. L., Zhang, S. J. & Lu, X. M. (2007). Hydroxyl ammonium ionic liquids: synthesis, properties, and solubility of SO<sub>2</sub>. *Journal of Chemical & Engineering Data*, 52, 2, 596-599, ISSN: 0021-9568



# Ionic Liquids within Microfluidic Devices

Marina Cvjetko<sup>1</sup> and Polona Žnidaršič-Plazl<sup>2</sup>

<sup>1</sup>*Faculty of Food Technology and Biotechnology, University of Zagreb,*

<sup>2</sup>*Faculty of Chemistry and Chemical Technology, University of Ljubljana,*

<sup>1</sup>*Croatia*

<sup>2</sup>*Slovenia*

## 1. Introduction

In past decade, the use of ionic liquids as the replacement for conventional molecular solvents in organic reactions has tremendously increased, both in academia as well as in industry. Features that make ionic liquids attractive for use in organic synthesis in general and catalytic processes in particular include their insignificant vapor pressure (even at elevated temperatures), great dissolving power for a wide range of otherwise sparingly soluble compounds, non-flammability, and thermal, chemical and electrochemical stability. Another important feature of these liquids is the possibility of tuning their physical and chemical properties by varying the nature of an anion and/or a cation in order to improve their miscibility with water or organic solvents, to increase extraction capacity or to enhance enzyme stability/activity when used as media for biocatalytic reactions. The number of possible chemical structures is extremely high, and it enables to tailor the best ionic liquid for a specific application (Park & Kazlauskas, 2003; Yang & Pan, 2005).

Recently, ionic liquids were found to be much more than just green solvents. They might be used also as additives in new materials, as well as in a variety of (bio)chemical catalytic reactions, where they could act as supports for catalyst immobilization or even as catalysts (Gorman, 2001).

The production of ionic liquids in high purity, which is essential for their application, is a special challenge due to the extreme heat release during the alkylation step leading to low product quality. Insufficient mixing in conventional batch synthesis procedures represents a major problem for large-scale production. Besides, additional purification processes required to obtain ionic liquids with satisfying purity significantly increase overall production costs, leading to limited potential for industrial application. Therefore there is a great demand for the development of alternative processes of ionic liquids synthesis as well as for their application.

Implementation of microstructured devices offers a promising solution to this type of challenge due to several advantages leading to process intensification, which was already impressively demonstrated in many chemical and biochemical processes (Hessel et al., 2004a; Pohar & Plazl, 2009). Microfluidic systems are also an extremely efficient tool for the rapid screening of (bio)catalysts and for biocatalytic process design and analysis as well. In recent years, a successful application of enzymatic microreactors has been reported, mainly in chemical analysis and kinetic studies (Urban et al., 2006). Their use as components of

integrated systems, often termed lab-on-a-chip, or in micro total analysis ( $\mu$ TAS) for analysis of biomolecules, is growing every year. However, the implementation of enzymatic microreactors into industrial-scale synthesis is relatively scarce (Žnidaršič-Plazl & Plazl, 2009). Furthermore, the potential for the use of ionic liquids in enzymatic reactions as well as for product isolation within microstructured devices is not yet exploited.

The present work aims to provide a literature review of the implementation of microreactor technology into the synthesis of ionic liquids, into (bio)catalyzed production of commercially important chemical compounds with ionic liquids as sustainable solvents, as well as in downstream processing with ionic liquids.

## 2. Advantages of microfluidic devices

Microreactor technology has uncovered new scientific solutions and challenges in a broad range of areas, from the electronic industry, chemical industry, medical technology, biotechnology, to fuel production and processing, environmental protection, and process safety (Ehrfeld et al., 2000). It is based on continuous flow chemistry through microchannels with a typical height or width of less than 1 mm. Besides continuous way of operation, the use of parallel microreactor modules provides access to kilogram or even ton quantities, thus making the technology also suitable for large-scale, commercial production (Pavlou, 2009). The concept of numbering-up avoids bottlenecks usually present at scaling up and yet very short time is needed for transferring a process in a microreactor from research on the lab scale to pilot and production scale.

Due to significantly higher surface-to-volume ratios and superior heat exchange properties compared to conventional reactions system, these micro- or submillimeter devices are extremely efficient tools for existing (bio)chemical synthesis and downstream processing. The implementation of microstructured devices into these processes offers great reaction selectivity, improved kinetics and overall yields, minimal reagent and solvent volumes, easy process control and automation to improve operator safety and reduce human errors, and improved sustainability with reduced waste at low energy consumption. The small hold-up and the large specific transport rates result in extremely short response times, providing a favorable basis for efficient process control (Jähnisch et al., 2004; Hessel et al, 2004a). Due to increased process intensification and possibility of numbering up offered by microreactor technology, more traditional pilot-scale reactor systems and pilot plant systems may be replaced, at least in some cases, by smaller, faster responding, more flexible mini-plants with reduced capital and operating costs (Mills et al., 2007; Pohar & Plazl, 2009).

## 3. Synthesis of ionic liquids within microreactors

High purity of ionic liquids and overall production costs are crucial factor for their application in the industry. Therefore, a lot of effort was put into overcoming the difficulties regarding the preparation of ionic liquids. In order to understand the need for alternative synthesis of ionic liquids, the problems of conventional batch synthesis will be briefly discussed.

### 3.1 Problems associated with the preparation of ionic liquid

Ionic liquids could be prepared in one-step reaction, although usually two consecutive steps are employed: the formation of the salt with the desired cation, followed by the reaction for

anion exchange (metathesis). The majority of the ionic liquids are prepared *via* alkylation of a nitrogen containing heterocycle, such as 1-substituted imidazole, followed by salt metathesis (Figure 1). Alkyl halides (chloroalkanes, bromoalkanes, and iodoalkanes) are widely used as alkylating agents in a quaternization reaction, since they are cheap and easily available. Metathesis step is usually achieved by addition of the alkali salt of the desired anion (with precipitation of the alkali halide salt).

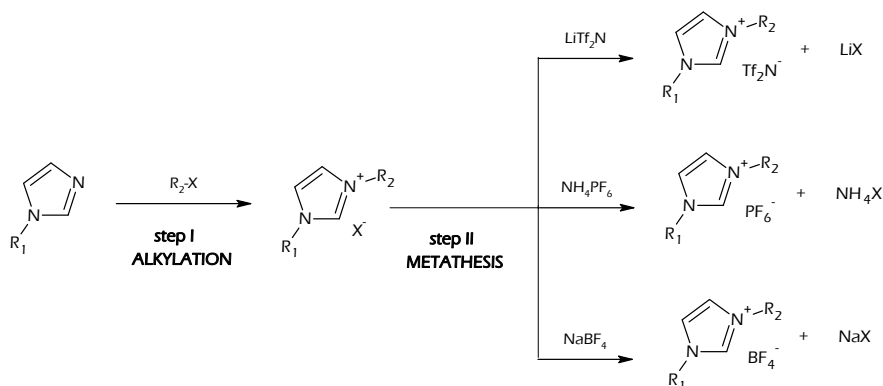


Fig. 1. Standard route to 1-alkyl-3-methylimidazolium-based ionic liquids.

At first sight, batch alkylation is a simple reaction: the amine and the desired alkyl halide are mixed and the reaction mixture is heated, typically in an inert atmosphere ( $N_2$  or Ar). In batch alkylation many difficulties arise due to long reaction times (up to 72 h) at relatively high temperature, depending on the reactivity of the alkyl halide. Conventional batch-synthesis procedures fail to yield products with purities higher than about 96%. Due to incomplete conversion in standard batch procedure, intensive purification steps are needed (Gonzales et al., 2009). Purification cannot be achieved by simple distillation methods used for conventional organic solvents due to high boiling points of these compounds ( $>300^\circ C$ ), but rather it requires the use of harmful organic solvents such as acetonitrile, ethyl acetate or tetrahydrofuran, which is contrary to green chemistry principles. Non-conventional techniques such as irradiation with microwaves (Loupy, 2006) and power ultrasound (Cravotto & Cintas, 2006), have been intensively studied and have considerably improved ionic liquid synthesis by cutting down reaction times and improving yields.

Ideally, ionic liquids should be colorless (at least in the absence of functional groups), clear, odorless and free flowing liquids (Dyson & Geldbach, 2005). The formation of »hot spots«, caused by poor mixing, can have detrimental effect on the quality of the obtained ionic liquid, manifested by the product colorization (Bowing & Jess, 2005). Löb et al. (2007) demonstrated that even a dropwise addition of alkylating agent to the bulky amine in a lab-scale batch vessel gave rise of a local temperature of the mixture up to  $150^\circ C$ . The chemical entities of the coloring matter are still not clear, but several authors agree that imidazolium species participate in the creation of colored compound, either by its polymerization or decomposing at high temperature (Renken et al., 2007). Therefore, in order to improve the purity of ionic liquids, an efficient removal of released reaction heat is crucial. To avoid reaction mixture overheating, solvents such as 1,1,1-trichloroethane, ethyl acetate, acetonitrile or toluene are usually used in the reaction. On the other hand, application of

solvents leads to very long processing time and introduces unwanted environmentally harmful compounds (Waterkamp et al., 2009; Hu et al., 2010).

The use of microreactors in ionic liquid synthesis is therefore a very promising alternative, mainly due to the very effective mixing and temperature control, corresponding to reaction control, leading to high-quality, (near)colorless products at shorter reaction times (without the necessity of subsequent purification steps), and higher space-time-yields (Hessel et al., 2005; Waterkamp et al., 2009).

### 3.2 Design of the microstructured reactors for ionic liquids synthesis

Microfluidic devices allow for processing small volumes ( $10^{-9}$  to  $10^{-12}$  m<sup>3</sup>) of fluid within channels and are compatible with continuous flow mode of operation (Fernandes, 2010). Hence, the use of microscale devices in preparation of ionic liquids is potentially as 'green' as chemical synthesis can be; as reagents are quantitatively converted into the final product, no solvents are needed for synthesis or purification and absolutely no waste is generated (Ehrfeld et al, 2000). Wilms et al. (2009) reported that less than 1 % of impurities, mostly unreacted starting material, are present in ionic liquids synthesized within microfluidic devices. Hu et al. (2010) showed that microchannel reaction system is also suitable for the kinetic study of fast reactions with high heat release and/or a viscous system, such as alkylation of imidazolium species.

In Figure 2, a general scheme for a continuous ionic liquid production in a microreactor is presented. The core part of the microscale production set-up is a micromixer in which amine and alkylating agent are rapidly mixed, linked to the reaction tube.

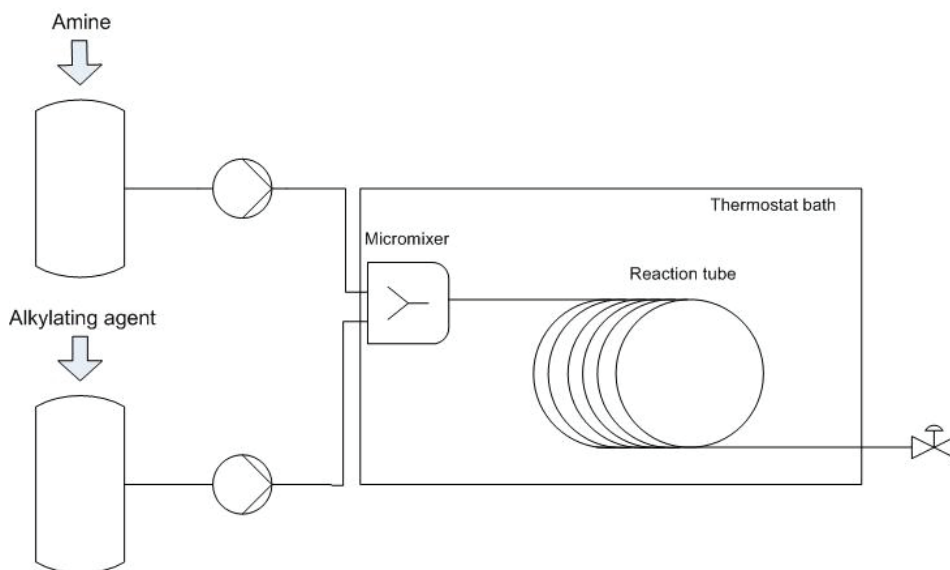


Fig. 2. General scheme of an experimental set-up for ionic liquid synthesis comprising of a micromixer and a (micro)tubular reactor.

The reactants are pump driven into capillaries that are usually heated to reaction temperature, mixed in the micromixer and then directly guided into temperature regulated

section of the reaction section. Since residence times in the micromixers are in the range of milliseconds, very small conversions are achieved, and therefore no significant temperature increase is observed in this section (Löb et al., 2007). The reaction mainly takes place in the following tubular reactor with diameters of less than 1 mm, or in a millimeter or even in a centimeter scale (Hessel et al., 2004b). The necessary residence time for the reaction can be adjusted by changing the flow rate and/or the length of the reaction tube. The capacity of the reactor system can be increased by simply numbering up of the system, allowing to achieve even multikilograms of ionic liquids per day (Wilms et al., 2009).

Due to the fact that the physical dimensions of the flow structures in microfluidic systems are in the micro-scale, the Reynolds numbers characterizing fluid-flow in microfluidic systems are well below the critical value for turbulence and the flow regime is, consequently, laminar (Pohar & Plazl, 2008). Therefore, micromixers in microfluidic systems rely on molecular diffusion. In general, micromixers used for ionic liquid synthesis are designed in such a way that their internal flow geometries reduce diffusion distances. Some examples of micromixers used for ionic liquid synthesis are shown in Figure 3.

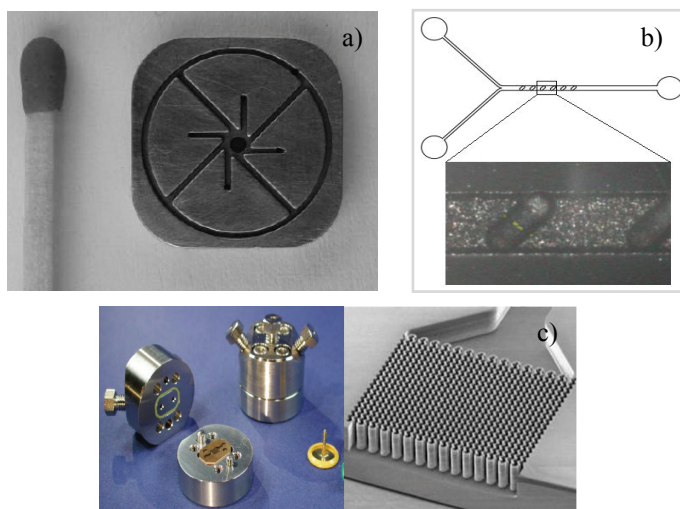


Fig. 3. Different micromixer designs: a) Vortex-type micromixer (Adapted from Waterkamp et al. (2007). Reproduced by permission of the Royal Society of Chemistry; b) Slanted groove micromixer (Sabotin et al., 2010); c) SIMM-V2 micromixer (Adapted from Hu et al., 2010). Reproduced by permission of Elsevier)

Due to the problems regarding overheating and temperature control during ionic liquid synthesis, a lot of effort was put into designing of an efficient system for temperature control. The simplest temperature control could be achieved by embedding the whole reactor system in thermostat bath (Ranken et al., 2007; Löb et al., 2007; Wilms et al., 2009; Hu et al., 2010). Große et al. (2007) investigated the cooling efficiency of simple and low-cost adiabatic microreactor with product recycle (loop reactor). The recycle stream in this reactor was externally cooled by a heat exchanger and returned into the reactor. The loop reactor was inherent safe (no runaway) and the mixing temperature of recycle stream and fresh feed could be simply regulated by recycle ratio. In order to make this system applicable, high

conversion of reactants was needed, e.g. to avoid an expensive post-treatment of the ionic liquid to remove unconverted reactants. Another efficient system for passive heat removal was presented by Löwe et al. (2009). A heat pipe system, which transfers thermal energy by evaporation and condensation of a thermal fluid, provided a very efficient passive cooling without using cooling liquids (e.g. water) or other materials which can have an impact on ecology and wasting energy. Additionally, implementation of such heat pipes could contribute to cost reduction. The first prototype of plate stack microstructured heat exchanger was reported by Löb and his coworkers (Löb et al., 2007). The heat exchanger consisted of a stack of wet chemically etched plates with microchannel arrays. A microchannel array for the reaction mixture was surrounded by two microchannel arrays for the heat exchanger fluid. Imidazolium-based ionic liquid obtained with this prototype was almost colourless.

### 3.3 Benefits of the ionic liquid synthesis within microfluidic devices

In recent years, a number of articles have been published in which successful implementation of microreactor technology into ionic liquid synthesis was reported. Obtained ionic liquids were of high quality and, in certain process conditions, reaction times were reduced down to minutes as opposed to conventional batch systems in which reaction time was measured in hours, even days (Waterkamp et al., 2007; Renken et al., 2007). Waterkamp et al. (2007) presented a way to intensify the solvent-free synthesis of 1-butyl-3-methylimidazolium bromide ([BMIM]Br) from 1-methylimidazole (MeIm) and 1-bromobutane (BrBu), using a continuously operating microreactor system consisted of a vortex-type micromixer (0.45 mm channel width) followed by series of three tubes with increasing inner diameter (2–6 mm). Each part of a tube was 6 m in length with total reaction volume of 306 mL, allowing the production rate of 9.3 kg [BMIM]Br per day. In this reactor system, the strongly exothermic alkylation could be thermally controlled even at elevated temperatures, leading to high reaction rates in a solvent-free modus. The degree of process intensification achieved resulted in a more than twentyfold increase of the space–time–yield compared to the conventional batch process. In the experiment, a conversion of 95% could be obtained after 38 min at 85 °C. By the proposed simulation, the residence time demand could be reduced down to 10 min at wall temperatures of 105 °C, leading to space–time–yield of 6.1 kg h<sup>-1</sup> L<sup>-1</sup>.

Ranken et al. (2007) developed a first prototype of multiscale reactor system for the solvent-free synthesis of ethylmethylimidazolium ethylsulfate ([EMIM][EtSO<sub>4</sub>]) *via* alkylation of *N*-methylimidazole with diethylsulfate (Figure 4). A microstructured reactor for efficient mixing of the reactants was the main part of the setup, followed by the section consisted of two tubular capillary reactors with diameters in the range of several millimeters. Microstructured reactor was composed of a stack of plates with parallel rectangular microchannels (1 mm wide and 0.65 mm high, 125 mm in length) with total inner volume of 10.8 cm<sup>3</sup>. Compared to capillary reactors operating at two different temperature levels, the space time was reduced from 4 h down to 4.6 min. With this system the performance of the reaction could be increased by a factor of 50. The throughput of the reactor system can be increased by simply numbering up of the system.

The limitation of a conventional batch process and the potential of continuous alkylation of 1-methylimidazole in microreactor rig with a micromixer followed by a capillary as residence time section were studied by Löb et al. (2007). A production rate of 0.2 l h<sup>-1</sup> of

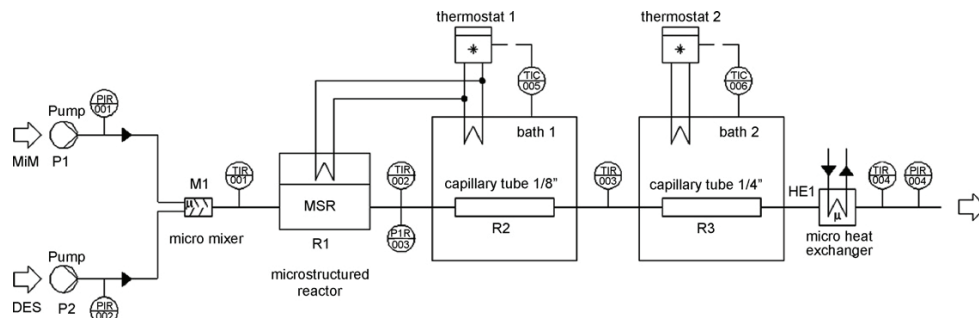


Fig. 4. Scheme of the experimental setup for [EMIM][EtSO<sub>4</sub>] synthesis. Adapted from Renken et al. (2007). Reproduced by permission of Elsevier.

almost colorless ionic liquid could be reached in a microreactor rig with a reactor inner volume of only 7.5 mL. Therewith a reduction of reaction time from some hours for the current batch process to only 2.2 min was conducted.

Waterkamp and his group also tested the influence of reaction temperature and flow rate on the colorization of the product in solvent free synthesis of 1-butyl-3-methylimidazolium bromide ([BMIM]Br) in capillary reactor. By using microreactor technology they have studied to which extent intensified mass transfer can be used as a tool to control side product formation in the form of colored impurities. It was concluded that temperature and flow rate at which the alkylation is governed both influence the product colorization. The temperature increase (at identical flow rate), as well as flow rate decrease (at identical temperature) led to more intensive colorization. This effect was explained by enhanced transport velocity of 1-methylimidazole from the product phase to the alkylating agent phase, leading to higher overall rate of the main reaction and reducing the contact time of the 1-methylimidazole with itself. Even at harsh temperature conditions, meaning a reaction temperature of 145 °C, a lowly colored ionic liquid could be produced by increasing the flow velocity (Waterkamp et al., 2009).

Even though there are numerous reports regarding the batch laboratory-scale synthesis of ionic liquids using microwave irradiation under solvent-free conditions, only few articles regarding microwave-assisted microreactor processing ( $\mu^2$ ) were published on this topic. Minrath et al. (2008) investigated the synthesis of 1-methyl-3-hexylimidazolium bromide under different continuous procedures, using the micro-wave irradiation. A micromixer-tubular ( $d < 0.5$  mm) reactor was used to perform the reaction with microwave heating. As a result it can be turned out that a low microwave energy-supply, partially less than 50 W, and a short residence time of approx. 10 min led to high conversion and selectivity of the targeted product. Also at higher microwave energies ( $> 200$ W), the residence time could be shortened to less than 2 min.

An interesting novel and cheaper method for ionic liquid synthesis by modified Radziszewski reaction was recently published by Zimmermann et al. (2010). They demonstrated that water-soluble 1,3-dialkylimidazolium-based ionic liquids could be produced in high yields and purities, starting from available and relatively cheap precursors - monoalkylamines, glyoxal, formaldehyde, and mineral or organic acids (Figure 5). The synthesis of 1,3-dibutylimidazolium acetate ([dBIM][OAc]) and 1,3-dibutylimidazolium chloride ([dBIM]Cl) was achieved by continuous production in a microreactor. The solution

of formaldehyde and acid (HCl, HOAc) was mixed with *n*-butylamine within micromixer (internal volume 0.06 mL), and directed into the residence time unit. After passing through residence time unit, the reaction mixture was brought in contact with glyoxal in a second mixer and reacted in a second residence time unit. All sections of the set-up were under pressure and temperature control. In comparison to the modified Radziszewski reaction in batch mode, the reaction times were reduced by factor 3 and 6 for [dBIM]Cl and [dBIM][OAc], respectively, while the yields increased slightly.

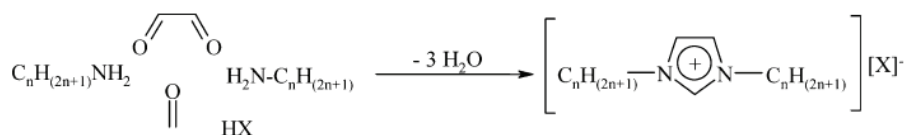


Fig. 5. Modified Radziszewski reaction. Adapted from Zimermann et al. (2010). Reproduced by permission of the American Chemical Society.

#### 4. (Bio)catalysis in ionic liquids within microfluidic devices

Ionic liquids have been employed as the reaction media for a wide range of (bio)catalytic processes, as catalysts or as (bio)catalyst-supports. These modern solvents have been shown to possess a significant effect on the stabilization of charged intermediates in chemical catalytic processes, as well as on enzymes' stability. Some ionic liquids have been shown to be by far the best non-aqueous media for biocatalytic processes due to their positive influences on enzyme stability and activity, as well as on the enantioselectivity of the reactions catalyzed by them (Park & Kazlauskas, 2003). When the right ionic liquid is chosen for a given reaction, it can lead not only to enhanced selectivity, yield or reaction rate, but it also improves the result of the work-up, from product separation (extraction/distillation) to recycling of the system ionic liquid/(bio)catalysts (Dyson et al, 2003; Pârvulescu & Hardacre, 2007; van Rantwijk & Sheldon, 2007). Separation of products from ionic liquid and ionic liquid recovery can be accomplished by distillation of product (if the product is sufficiently volatile), extraction with supercritical CO<sub>2</sub>, or simple phase separation (if the product is immiscible in the ionic liquid) (Cornils, 1999).

Implementation of microreactor technology, together with the use of ionic liquids as a replacement for conventional organic solvents, into (bio)catalysis could be a significant alternative to conventional (bio)catalytic processes, considering advantages of both approaches. Tailor-made concept of environmentally friendly ionic liquids to improve their properties for certain catalyzed reaction (enzyme activity/stability, solubility of the substrates, stabilization of charged intermediates), together with the benefits of high-throughput reaction optimization, should be considered as a new promising "symbiosis" for the production of commercially important chemicals.

##### 4.1 Chemical catalysis

Ionic liquids have been thoroughly investigated as (co)solvents in most types of catalytic reactions such as rhodium and ruthenium catalyzed hydrogen addition and rearrangement reactions (Chauvin et al., 1995; Dyson et al., 1999), C-C and C-O cleavage reactions (Green et al., 2000; Song et al., 2000), and C-C or C-heteroatom coupling reactions (Earle et al., 1999; Zulfigar & Kitazume, 2000). In these reaction systems, ionic liquids can be used as solvent or



both solvent and catalyst in monophasic systems. In biphasic systems, ionic liquid can be used as a phase for embedding catalyst while substrate/product remains dissolved in a second phase. Moreover, the anion of the ionic liquid can also act as ligand for the homogeneous catalysis, both in monophasic and biphasic systems (Sheldon, 2001). Even though the monophasic catalysis poses a lot of advantages (e.g. availability of the reagents to the catalyst), catalysis in biphasic mode is becoming very popular due to easy separation of substrate/product and catalyst recovery (Welton, 1999). Disadvantage of traditional aqueous-organic biphasic systems is low solubility of the catalyst and/or organic substrates in water, causing low reaction rates. When used in place of water, ionic liquids can form ionic liquid-organic solvent systems without suffering from these limitations (Zhao et al., 2002).

Applications of microreactors to biphasic catalytic reactions constitute a topic of interest. The benefits of having an exceedingly high surface-to-volume ratio and efficient mass-transfer in microchannels have led many researchers to study continuous flow systems using microreactors for catalytic reactions. The excellent mass transfer characteristics within and between the catalyst carrier phase and reaction medium, together with the minimal catalytic pore diffusion resistances at the micrometer scale, make such biphasic catalysis an attractive alternative to conventional catalysis operation (Wießmeier, 1996; Rahman et al., 2006).

Several authors reported on successful Pd-catalyzed cross coupling reactions in ionic liquids within a microfluidic devices, such as Sonogashira reactions (Fukuyama et al., 2002; Rahman et al., 2006) and Mizoroki-Heck reactions (Liu et al., 2004). Fukuyama and his group conducted the first example of a homogeneous metal-catalyzed reaction in a microreactor (Figure 6). The  $\text{PdCl}_2(\text{PPh}_3)_2$ -catalyzed Sonogashira coupling of terminal alkynes with aryl or vinyl halides in 1-butyl-3-methylimidazolium hexafluorophosphate ( $[\text{BMIM}][\text{PF}_6]$ ) as the reaction medium and catalyst-support in the absence of a copper salt was successfully performed, in good to high yields. Sonogashira coupling is typically carried out in organic solvents, such as toluene, tetrahydrofuran, and dimethylsulfoxide, with a palladium catalyst, a copper (I) cocatalyst, and stoichiometric amount of amine base. The advantage of ionic liquid as a reaction media was in terms of catalyst recycling, since the organic products could be readily separated from the transition metal catalysts dissolved in the ionic liquids by simple extraction with a conventional organic solvent. Reaction was also performed in a microflow system in conjunction with a micromixer having interdigitated channels (0.04 mm width and 0.2 mm depth) to ensure the continuous production of acetylenic compounds. The coupling product diphenylacetylene was formed and was easily isolated from the mixture by extraction with hexane/water (93% yield). The resulting ionic liquid containing the Pd catalyst could be successfully reused for several times with only a slight loss in its activity (Fukuyama et al., 2002).

Another successful application of  $[\text{BMIM}][\text{PF}_6]$  ionic liquid supported catalytic microflow reactions for Pd-catalyzed carbonylative Sonogashira coupling of aryl iodides and phenylacetylene was reported by Rahman et al. (2006). Ionic liquid containing Pd catalysts, CO and the substrates were mixed successively, in different micromixers (channel diameter = 1 and 0.40 mm), and then pumped as a multiphase (ionic liquid-substrate-CO) into heated capillary tube reactor acting as a residence time unit ( $V=14.1$  mL). It was found that Pd-catalyzed production of solely the acetylenic ketones in ionic liquids, when conducted in conjunction with a microreactor, preceded efficiently with superior selectivity and higher yields compared to the conventional batch system, even at low CO pressures. Authors suggested that this improvement in selectivity and yield was the result of a large interfacial

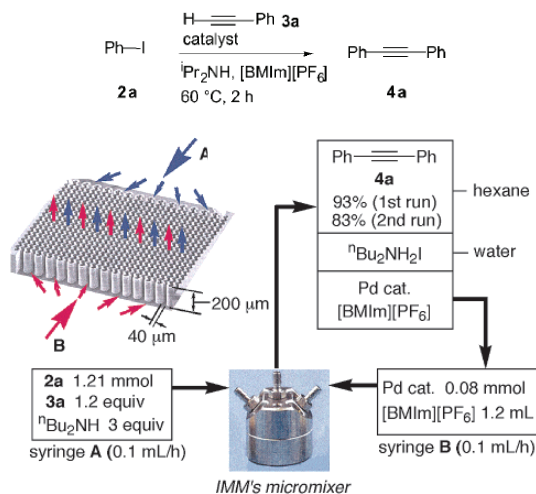


Fig. 6. Sonogashira reaction in a microflow system. Iodobenzene (2a), phenylacetylene (3a) and amine base were mixed in the micromixer. The coupling product (4a) was formed and was easily isolated by extraction with hexane/water. Adapted from Fukuyama et al. (2002). Reproduced by permission of the American Chemical Society.

area-to-volume ratio or efficient CO diffusion through ionic liquid in microflow system that couldn't be obtained in standard batch reactor.

An example of a microflow continuous palladium-catalyzed Mizoroki-Heck coupling between iodobenzene with butyl acrylate, in combination with continuous microextraction/catalyst recycling was reported by Liu and coworkers (Liu et al., 2004). Their reaction was catalyzed by a  $[\text{Pd}(\text{PPh}_3)\text{Cl}_2(\text{BMIM})]$  carbene complex, which was immobilized in the low-viscosity ionic liquid 1-butyl-3-methylimidazolium bis(trifluoromethylsulfonyl)imide ( $[\text{BMIM}][(\text{CF}_3\text{SO}_2)_2\text{N}]$ ). Using automated microflow apparatus (Figure 7), iodobenzene, butyl acrylate, and tripropylamine were introduced from one inlet of the micromixer (channel width 0.1 mm, inner volume 2 mL), and the ionic liquid containing the Pd catalyst was introduced from the other inlet. Two solutions were mixed in the microreactor and were pumped into the temperature controlled residence time unit.

The ionic liquid solution exiting from the microflow reaction apparatus was introduced into a T-shaped static micromixer (channel diameter 0.3 mm), where the ammonium salt (byproduct) was washed by mixing with aqueous solution of NaOH. The mixture was then mixed by another T-shaped static micromixer, where hexane was introduced to extract the product. On standing in the Y-shaped glass flask, the resulting mixture separated into three phases, a hexane layer containing the product and tripropylamine, an aqueous layer containing the inorganic salt, and the ionic liquid layer containing the Pd catalyst. The ionic liquid in the bottom layer was pumped back to container for recycling the Pd catalyst. The coupling product, butyl cinnamate, was produced in an overall yield of 80% (115.3 g, 10 g  $\text{h}^{-1}$ ). With an originally developed microextraction/catalyst recycling system, the ionic liquid containing Pd catalyst could be continuously recycled to provide a total of 115.3 g (80%, 10 g  $\text{h}^{-1}$ ).

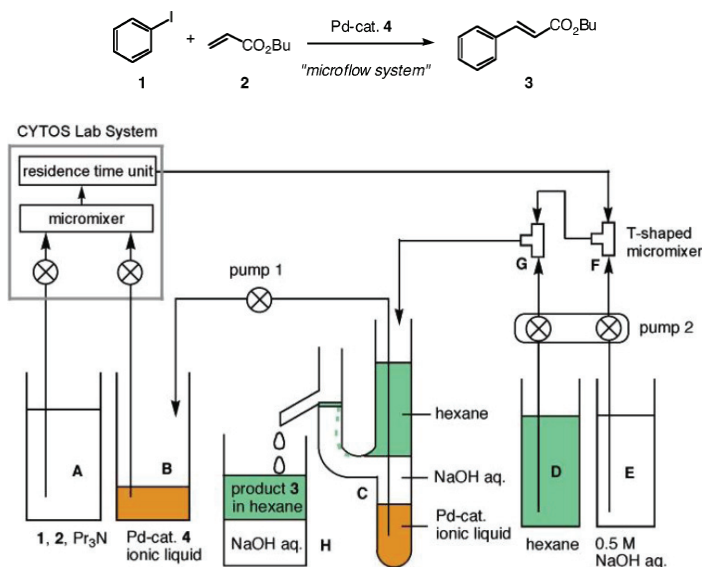


Fig. 7. Detailed continuous workup process of coupling between iodobenzene with butyl acrylate with flow workup/catalyst recycling system. Adapted from Liu et al. (2004). Reproduced by permission of the American Chemical Society.

The first study of the epoxidation of cyclohexene in a silicon-based microreactor was reported by Basheer et al. (2006). Due to a low solubility of cyclohexene in the phosphate buffer reaction media, ionic liquid 1-butyl-3-methylimidazolium tetrafluoroborate ([BMIM][BF<sub>4</sub>]) was introduced (0.5 % v/v) to the buffer solution. The performance of four various types of catalysts such as Schiff-base and reduced Schiff-base complexes of Cu(II) and Mn(II) complexes were investigated. The T-shaped microfluidic channel was filled with phosphate buffer solution of ionic liquid and 5 % of the Schiff catalysts. The reactant was introduced to the microchannel, driven by a difference in the electric potential between the inlet and the outlet of the microchannel. Catalytic activity and yields were found to be relatively high for the Cu (II) complexes as compared with those obtained with conventional bulk scale epoxidation.

Recently, ionic liquid was employed in a structured catalytic wall microreactor suitable for highly exothermic heterogeneous gas/solid reactions (Kiwi-Minsker et al., 2010). Pd<sup>0</sup>-nanoparticles embedded in an ionic liquid and deposited on activated carbon fibers with high specific surface area were used as a structured catalyst. The system allowed flowing of the reaction mixture through an empty micro-slit above the structured catalyst placed along the wall of the reactor (Figure 8). Selective acetylene hydrogenation was tested as a model of highly exothermic reaction with temperature sensitive catalyst. The temperature was easily controlled without hot spot formation, confirming the efficient heat exchange in the microreactor. The reaction performance was optimized by varying flow rates and temperatures. The selectivity of ~70% was obtained at conversion of 96.5% under steady-state conditions at 200 °C without any catalyst deactivation over 10 h on stream.

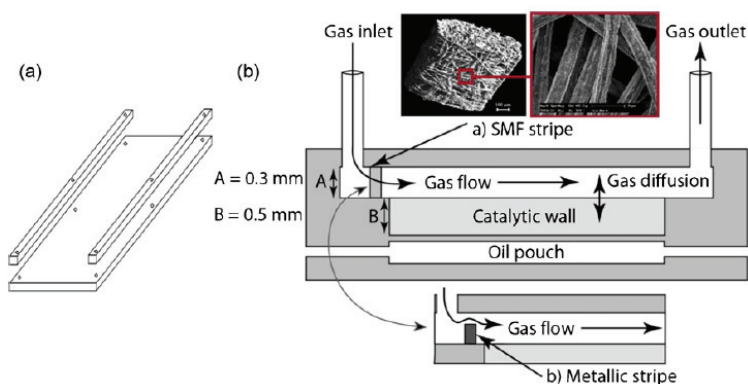


Fig. 8. a) 3D representation of the aluminum plates fixing the ionic liquid-supported catalyst, b) 2D scheme of the structured catalytic wall microreactor. Adapted from Kiwi-Minsker et al. (2010). Reproduced by permission of Elsevier.

#### 4.2 Biocatalysis

Enzymatic microreactors are becoming a useful tool for organic synthesis, together with chemical analysis and kinetic studies of catalytic reactors (Urban et al., 2006; Fernandes, 2009). Additionally, these systems have the potential for introduction into industrial-scale synthesis. From the aspect of the use of ionic liquids as reaction media within microreactors, the ability of external numbering-up is of great importance, due to high viscosity of ionic liquids and problems regarding mass and heat transfer in large scale bioreactors. This mode of scaling up provides good adjustability and control over the process, due to repetition of the fluidic path while the transport properties and hydrodynamics are preserved (Hessel et al., 2004a). Biocatalytic synthesis in microreactors is still a relatively new field and most examples therefore describe the proof of concept with known enzymatic transformations. However, because of the advantages that have been clearly demonstrated, biocatalytic microreactors are also expected to be used for explorative research purposes.

An example of highly efficient *Candida antarctica* lipase B-catalyzed synthesis of isoamyl acetate in 1-butyl-3-methylpyridinium dicyanamide ([BMPYR][dca])/n-heptane two-phase system within continuously operated glass microreactor was recently published (Pohar et al., 2009). The microreactor had one outlet and three separate  $\psi$ -shaped inlet channels, one for the inflow of ionic liquid phase with dissolved enzyme and isoamyl alcohol, the other for ionic liquid with dissolved acetic anhydride together with aqueous enzyme solution, and the third for the inflow of n-heptane. Furthermore, a 3 m long polytetrafluoroethylene tube with the inner diameter of 0.245 mm was fitted at the exit of the glass part of the microreactor to provide longer residence times for the reaction. A [BMPYR][dca]/n-heptane biphasic system within microfluidic system was found to be highly efficient as it showed an almost three-fold increase in the reaction rate as compared to an intensively mixed batch operation, resulting in far better productivity than any, reported so far. This was mainly a consequence of efficient reaction-diffusion dynamics in the microchannel system, where the developed flow pattern comprising of intense emulsification provided a large interfacial area for the reaction and simultaneous product extraction (Figure 9).

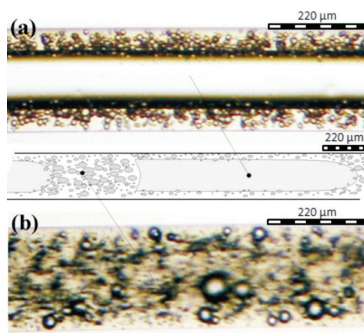


Fig. 9. Schematic presentation with photographic details of the developed flow pattern within the major part of the microreactor. (a) A long slug of *n*-heptane with concave tail surrounded with small droplets of *n*-heptane and (b) fine dispersion between the two neighboring *n*-heptane slugs. Adapted from Pohar et al. (2009). Reproduced by permission of the American Chemical Society.

A functional, easily assembled, operated and cleaned microbioreactor packed with immobilized *Candida antarctica* lipase B (Novozyme 435) was recently developed by Pohar et al. (2010). So far, microbioreactor was used for studying continuous mode ester synthesis within bis(trifluoromethylsulfonyl)imide - based ionic liquid media. Ionic liquid containing substrates was pumped into the microbioreactor at various flow rates, and at the outlet of the reactor the product was collected and analyzed. With fully adjustable length, width and depth, the developed packed bed microbioreactor was proven to be a very successful and versatile tooling for biocatalytic reactions such as isoamyl acetate or butyl butyrate synthesis (Cvjetko et al, 2010; Pohar et al., 2010).

## 5. Downstream processing employing ionic liquids within microfluidic devices

The quality of any industrial product is highly dependent on the correct selection of downstream processes and purification methods. Also, downstream processing costs might require the majority of the total production costs. The short molecular diffusion distance in miniaturized devices and the large specific interface allow very efficient separation. Since microchannel devices provide better control of process conditions, improved safety, and speed to market from laboratory development to commercial manufacturing, these devices are extremely useful for purification of reagents, solvents, intermediates, or final products (Žnidaršič-Plazl & Plazl, 2007). Microfluidic technology also allows the design and operation of analytical devices for high-throughput application such as selective separation and analysis of biomolecules and chemicals (Sato et al., 2003). Furthermore, the integration of reaction with *in situ* product isolation within microchannel system has already been proved to substantially increase productivity of (bio)catalyzed processes (Cauwenberg et al.; 1999, Huh et al., 2006; Pohar et al., 2009)

The two-phase characteristics of ionic liquid-organic solvent system also pave the way for the use in microreactors. Extraction of products at the micro scale by the implementation of ionic liquids gives rise to the possibility of the convenient separation of synthetic goods, plastics and metals. Besides, ionic liquids offer the specificity required to separate similar

compounds from each other (Wasserscheid & Eichmann, 2001). Several authors reported on the use of ionic liquids for extraction of biomolecules (Pei et al., 2009; Ge et al., 2010; Tomé et al., 2010), aromatic compound (Meindersma et al., 2005; Zhou et al., 2009), metals (Wei et al., 2003; Germani et al., 2007; Yoon et al., 2010; Egorov et al., 2010), and organic compounds (Marták & Schlosser, 2007; Simoni et al., 2010). The use of ionic liquids for enantioselective extraction was studied as well (Huh et al., 2006; Tang et al., 2010).

At the time, rare cases of simultaneous reaction/extraction in two-phase systems containing ionic liquids within microfluidic devices confirm the potential for further prosperity of this field. Huh et al. (2006) were the first to investigate the possibility of ionic liquid-supported microfluidic separation using enzymatic reaction. In general, the three-phase (water/ionic liquid/water) flow in the microchannel was formed by controlling the flow rate of the ionic liquid phase (Figure 10). The feeding phase consisted of ethanol, racemic ibuprofen, buffer and *Candida rugosa* lipase (CRL) that catalyzed esterification of (*S*)-ibuprofen rather than (*R*)-ibuprofen. By combining lipase-catalyzed reaction and fast selective transport of (*S*)-ibuprofen through 1-hexyl-3-methylimidazolium hexafluorophosphate ([BMIM][PF<sub>6</sub>]) membrane, a successful enantioselective separation of (*S*)-ibuprofen from racemic mixture was achieved. In receiving phase, *Porcine pancreas* lipase (PPL) catalyzed ester hydrolysis to produce starting ester, (*S*)-ibuprofen, and ethanol. The high efficiency of this microfluidic device was the consequence of the large area between the aqueous phase and the ionic liquid phase compared to the conventional bulk processes. Therefore, this microfluidic device with the ionic liquid phase could become suitable portable system with decreased reagent requirements for the selective and rapid separation of biologically functional molecules from the racemic mixtures.

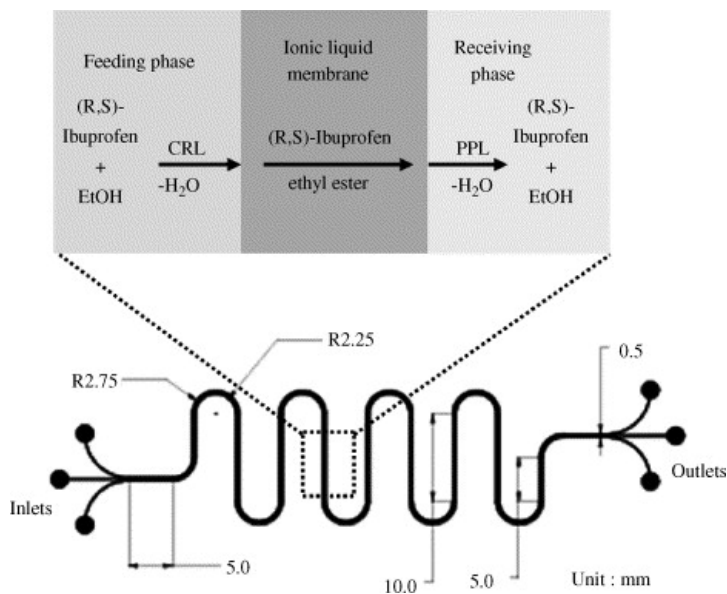


Fig. 10. Schematic drawing of the microfluidic channel and the enantioselective transport of (*S*)-ibuprofen through the ionic liquid in the microfluidic device. Adapted from Huh et al. (2006). Reproduced with permission. Copyright Elsevier, 2006.

A successful lipase-catalyzed synthesis of isoamyl acetate in ionic liquid/*n*-heptane two-phase system, presented in the previous section (Pohar et al., 2009), also based on the integration of synthesis and product recovery within microfluidic device. Since the majority of the product was accumulated in *n*-heptane, while enzyme stayed suspended in [BMPYR][dca], which was separated from *n*-heptane at the exit from the microchannel, this modus provided the efficient simultaneous product separation and ionic liquid/enzyme recycling.

Recently, an integrated system consisting of a microbioreactor packed with immobilized *Candida antarctica* lipase B and a miniaturized separator was developed for performing biocatalytic reactions in a continuous mode (Pohar et al., 2010). In order to isolate the product from the ionic liquid media after the reaction in a microbioreactor, a miniaturized continuous evaporator was designed. Since ionic liquids have a very high boiling point compared to solutes (substrates/products), they could be effectively removed with evaporation within the microchannel. The use of a continuous microevaporator was shown to be highly effective for the isolation of a product (butyl butyrate) from the chosen ionic liquid, as well as for the cleaning of ionic liquid, which could be further reused (Pohar et al., 2010).

## 6. References

- Basheer, C., Vetrichelvan, M., Suresh, V., Lee, H. K. (2006). Ionic-liquid supported oxidation reactions in a silicon-based microreactor. *Tetrah. Lett.*, 47, 6, (February 2006) 957-961, ISSN 0040-4039
- Böwing, A. G. & Jess, A. (2005). Kinetics of single- and two-phase synthesis of the ionic liquid 1-butyl-3-methylimidazolium chloride. *Green Chem.*, 7, 4, (March 2005) 230-235, ISSN 1463-9262
- Cauwenberg, V., Vergossen, P., Stankiewicz, A., Kierkels, H. (1999). Integration of reaction and separation in manufacturing of pharmaceuticals: Membrane-mediated production of *S*-ibuprofen. *Chem. Eng. Sci.* 54, 10, (May 1999) 1473-1477, ISSN 0009-2509
- Chauvin, Y., Mussmann, L., Olivier, H. (1996). A novel class of versatile solvents for two-phase catalysis: hydrogenation, isomerization, and hydroformylation of alkenes catalyzed by rhodium complexes in liquid 1,3-dialkylimidazolium salts. *Angew. Chem. Int. Ed. Engl.* 34, 23-24, (January 1996) 2698-2700, ISSN 0570-0833
- Cornils, B. (1999). Bulk and fine chemicals via aqueous biphasic catalysis. *J. Mol. Catal. A*, 143, 1-3, (July 1999) 1-10, ISSN 1381-1169
- Cravotto, G., Cintas, P. (2006). Power ultrasound in organic synthesis: moving cavitation chemistry from academia to innovative and large-scale applications. *Chem. Soc. Rev.*, 35, 2, (October 2005) 180-196, ISSN 1460-4744
- Cvjetko, M., Vorkapić-Furač, J., Pohar, A., Žnidaršič-Plazl, P. (2010). Synthesis of ionic liquids and their use as solvents for biocatalysis in microreactors. *Proceedings of the International thematic conference "Implementation of microreactor technology into biotechnology"*, September 29-30, 2010, Ljubljana, Slovenia, Faculty of Chemistry and Chemical Technology, Ljubljana: ISBN 978-961-6756-20-4

- Dyson, P. J., Ellis, D. J., Parker, D. G., Welton, T. (1999). Arene hydrogenation in a room temperature ionic liquid using a ruthenium cluster catalyst. *Chem. Commun.*, 25-26. ISSN 1359-7345
- Dyson, P. J., Ellis, D. J., Henderson, W., Laurenczy, G. (2003). A comparison of ruthenium-catalysed arene hydrogenation reactions in water and 1-alkyl-3-methylimidazolium tetrafluoroborate ionic liquids. *Adv. Synth. Catal.*, 345, 1-2, (January 2003) 216-221, ISSN 1615-4150
- Dyson, P. J., Geldbach, T. J. (2005). *Metal catalysed reactions in ionic liquids, in catalysis by metal complexes*, volume 29, Springer, ISBN-10 1-4020-3915-8, Dordrecht, the Netherlands.
- Earle, M.J., McCormack, P.B., Seddon, K.R. (1999). The first high yield green route to a pharmaceutical in a room temperature ionic liquid. *Green Chem.*, 2, 6, (October 2000) 261-262, ISSN 1463-9262
- Egorov, V. M., Djigailo, D. I., Momotenko, D. S., Chernyshov, D. V., Torocheshnikova, I. I., Smirnova, S. V., Pletnev, I. V. (2010). Task-specific ionic liquid trioctylmethylammonium salicylate as extraction solvent for transition metal ions. *Talanta*, 80, 3, (January 2010) 1177-1182, ISSN 0039-9140
- Ehrfeld W., Hessel V., Löwe H. (2000). *Microreactors: new technology for modern chemistry*, Wiley-VCH, ISBN 978-3-527-29590-6, Weinheim, Germany.
- Fernandes, P. (2010). Miniaturization in biocatalysis. *Int. J. Mol. Sci.*, 11, 3, (March 2010) 858-879, ISSN 1422-0067
- Fukuyama, T., Shinmen, M., Nishitani, S., Sato, M., Ryu, I. (2002). A copper-free Sonogashira coupling reaction in ionic liquids and its application to a microflow system for efficient catalyst recycling. *Org. Lett.*, 2002, 4, 10, (April 2002) 1691-1694, ISSN 1523-7060
- Ge, L., Wang, X., Tan, S. N., Tsai, H. H., Yong, Y. W. H., Hua, L. (2010). A novel method of protein extraction from yeast using ionic liquid solution, *Talanta*, 81, 4-5, (June 2010) 1861-1864, ISSN 0039-9140
- Germani, R., Mancini, M. V., Savelli, G., Spreti, N. (2007). Mercury extraction by ionic liquids: temperature and alkyl chain length effect. *Tetrahedron Lett.*, 48, 10, (March 2007) 1767-1769, ISSN 0040-4039
- Gonzales, M. A., Ciszewski, J. T. (2009). High conversion, solvent Free, continuous synthesis of imidazolium ionic liquids in spinning tube-in-tube reactors. *Org. Process Res. Dev.*, 13, 1, (December 2008) 64-66, ISSN 1083-6160
- Gorman, J. (2001). Faster, better, cleaner? New liquids take aim at old-fashioned chemistry. *Sci. News*, 160, 10, (September 2001), 156-158, ISSN 1016-1503
- Green, L., Hemeon, I., Singer, R.D. (2000). 1-Ethyl-3-methylimidazolium halogenoaluminate ionic liquids as reaction media for the acylative cleavage of ethers. *Tetrahedron Lett.*, 41, 9, (February 2000) 1343-1346, ISSN 0040-4039
- Hessel, V., Löwe, H., Schönfeld, F. (2004b). Micromixers—a review on passive and active mixing principles. *Chem. Eng. Sci.*, 60, 8-9, (April-May 2005) 2479-2501, ISSN 0009-2509
- Hessel, V., Hardt, S., Loewe, H. (2004a). *Chemical Micro Process Engineering - Fundamentals, Modelling and Reactions*, Wiley-VCH, ISBN 3-527-30741-9, Mainz, Germany
- Hessel, V., Löb, P., Löwe, H. (2005). Development of microstructured reactors to enable chemistry rather than subduing chemistry around the reactor - potentials of



- microstructured reactors for organic synthesis. *Curr. Org. Chem.*, 9, 8, (May 2005) 765-787, ISSN 1385-2728
- Hu, S., Wang, A., Löwe, H., Li, X., Wang, Y., Li, C., Yang, D. (2010). Kinetic study of ionic liquid synthesis in a microchannel reactor. *Chem Eng J.*, 162, 1, (August 2010) 350-354, ISSN 1385-8947
- Huh, Y. S., Jun, Y., Hongb, Y. K., Honga, W. H., Kima, D. H. (2006). Microfluidic separation of (S)-ibuprofen using enzymatic reaction. *J. Mol. Catal. B: Enzym.*, 43, 1-4, (December 2006), 96-101, ISSN 1381-1177
- Jähnisch, K., Hessel, V., Löwe, H., Baerns, M. (2004). Chemistry in microstructured reactors. *Angew. Chem. Int. Ed.*, 43, 4, (January 2004) 406-446, ISSN 1433-7851
- Kiwi-Minsker, L., Ruta, M., Eslanloo-Pereira, T., Bromley, B. (2010). Structured catalytic wall microreactor for efficient performance of exothermic reactions. *Chem. Eng. Process.*, 49, 9, (September 2010) 973-978, ISSN 0255-2701
- Liu, S., Fukuyama, T., Sato, M., Ryu, I. (2004). Continuous microflow synthesis of butyl cinnamate by a Mizoroki-Heck reaction using a low-viscosity ionic liquid as the recycling reaction medium. *Org. Proc. Res. Dev.*, 8, 3, (April 2004) 477-481, ISSN 1083-6160
- Löb, P., Hessel, V., Balon-burger, M., Hang, T., Illg, T., Menges, G., Hofmann, C., Krtschil, U., Uerdingen, M. (2007). Ionic Liquid synthesis in continuous microreactor using multiscale approach, *Proceedings of the 1<sup>st</sup> international congress on green process engineering*, pp. 1-9, 2-910239-68-3, Toulouse, France, 24-26 april 2007, Ed. SFGP, Paris, France
- Loupy, A. (2006). *Microwaves in organic synthesis*; Wiley-VCH, ISBN 9783527601776, Weinheim, Germany.
- Lowe, H., Axinte, R. D., Breuch, D., Hofmann, C. (2009). Heat pipe controlled synthesis of ionic liquids in microstructured reactors. *Chem. Eng. Jour.*, 155, 1-2, (December 2009) 545-550, ISSN 1385-8947
- Marták, J., Schlosser, Š. (2007). Extraction of lactic acid by phosphonium ionic liquids. *Sep. Purif. Technol.*, 57, 3, (November 2007), 483-494, ISSN 1383-5866
- Meindersma, G. W., Podt, A., de Han, A. B. (2005). Selection of ionic liquids for the extraction of aromatic hydrocarbons from aromatic/aliphatic mixtures. *Fuel Process. Technol.*, 87, 1, (December 2005) 59-70, ISSN 0378-3820
- Mills, P. L., Quiram, D. J., Ryley, J. F. (2007). Microreactor technology and process miniaturization for catalytic reactions. A perspective on recent developments and emerging technologies. *Chem. Eng. Sci.*, 62, 24, (December 2007) 6992-7010, ISSN 0009-2509
- Minrath, I., Beck, M., Pitton, D., Zankl, F., Loewe, H.  $\mu^2$  - Microwave assisted microreactor processing: synthesis of ionic liquids, *Proceedings of the "10<sup>th</sup> International Conference on Microreaction Technology, IMRET 10"*, 06 -10 April, 2008, New Orleans, LU.
- Park, S., Kazlauskas, R. J. (2003). Biocatalysis in ionic liquids-advantages beyond green technology. *Curr. Opin. Biotechnol.*, 2, 14, (August 2003) 432-437, ISSN 0958-1669
- Părvulescu, V. I., Hardacre, C. (2007). Catalysis in ionic liquids. *Chem. Rev.*, 107, 6, ISSN 2615-2665
- Pavlou, F. (2009). Microreactor technology: Is the industry ready for it yet? *Pharm. Tech. Europe*, 21, 10, (October 2009) ISSN 0164-6826

- Pei, Y., Wang, J., Wu, K., Xiaopeng, X., Lu, X. (2009). Ionic liquid-based aqueous two-phase extraction of selected proteins. *Sep. Purif. Technol.*, 64, 3, (January 2009) 288-295, ISSN 1383-5866
- Pohar, A., Plazl, I. (2008) Laminar to turbulent transition and heat transfer in a microreactor : mathematical modeling and experiments. *Ind. Eng. Chem. Res.*, 47, 19, (August 2008) 7447-7455, ISSN 0888-5885.
- Pohar, A., Plazl, I. (2009). Process intensification through microreactor application. *Chem. Biochem. Eng. Q.*, 23, 4, (December 2009) 537-544, ISSN 0352-9568
- Pohar, A., Plazl, I., Žnidaršič-Plazl P. (2009). Lipase-catalyzed synthesis of isoamyl acetate in an ionic liquid/*n*-heptane two-phase system at the microreactor scale. *Lab Chip*, 9, 23, (December 2009) 3385 - 3390, ISSN 1473-0189
- Pohar, A., Žnidaršič-Plazl, P., Plazl, I. (2010). Integrated process of transesterification within a microchannel system. *Proceedings of the International thematic conference "Implementation of microreactor technology into biotechnology"*, September 29-30, 2010, Ljubljana, Slovenia, Faculty of Chemistry and Chemical Technology, Ljubljana: ISBN 978-961-6756-20-4
- Poole, C. F., Pool, S. K. (2010) Extraction of organic compounds with room temperature ionic liquids. *J. Chrom. A*, 1217, 16, (April 2010) 2268-2286, ISSN 0021-9673
- Rahman, T., Fukuyama, T., Kamata, N., Sato, M., Ryu, I. (2006). Low pressure Pd-catalyzed carbonylation in an ionic liquid using a multiphase microflow system. *Chem. Commun.*, 21, (June 2006) 236-2238, ISSN 4995-4997
- Renken, A., Hessel, V., Löb, P., Miszczuk, R., Uerdingen, M. & Kiwi-Minsker, L. (2007). Ionic liquid synthesis in a microstructured reactor for process intensification. *Chem. Eng. Process.*, 46, 9, (September 2007) 840-845, ISSN 0255-2701
- Sabotin, I., Tristo, G., Bissacco, G., Junkar, M., Valentinčič, J. (2010). Staggered Herringbone Mixer designed for micro EDM milling. *Proceedings of the International thematic conference "Implementation of microreactor technology into biotechnology"*, September 29-30, 2010, Ljubljana, Slovenia, Faculty of Chemistry and Chemical Technology, Ljubljana: ISBN 978-961-6756-20-4
- Sato, K., Hibara, A., Tokeshi, M., Hisamoto, H., Kitamori, T. (2003). Microchip-based chemical and biochemical analysis systems. *Adv. Drug Deliv. Rev.*, 55, 3, (February 2003) 379-391, ISSN 0169-409X
- Sheldon, R. (2001). Catalytic reactions in ionic liquids. *Chem. Comm.*, 23, (December 2001) 2399-2407, ISSN 4995-4997
- Simoni, L. D., Chapeaux, A., Brennecke, J. F., Stadtherr, M. A. (2010). Extraction of biofuels and biofeedstocks from aqueous solutions using ionic liquids. *Comput. Chem. Eng.*, 34, 9, (September 2010) 1406-1412, ISSN 0098-1354
- Song, C.E., Oh, C. R., Roh, E.J., Choo, D.J. (2000). Cr(salen) catalysed asymmetric ring opening reactions of epoxides in room temperature ionic liquids. *Chem. Commun.*, 32, 1, (January 2001) 1743-1744, ISSN 1359-7345
- Tang, F., Zhang, Q., Ren, D., Nie, Z., Liu, Q., Yao, S. (2010). Functional amino acid ionic liquids as solvent and selector in chiral extraction. *J. Chrom. A*, 1217, 28, 9, (July 2010) 4669-4674, ISSN 0021-9673
- Tomé, L. I. N., Catambas, V. R., Teles, A. R. R., Freire, M. G., Marrucho, I. M., Coutinho, J. A. P. (2010). Tryptophan extraction using hydrophobic ionic liquids. *Sep. Purif. Technol.*, 72, 2, (April 2010) 167-173, ISSN 1383-5866

- Urban, P. L., Goodall, D. M. & Bruce N. C. (2006). Enzymatic microreactors in chemical analysis and kinetic studies. *Biotech. Adv.*, 24, 1, (January-February 2006), 42-57, ISSN 0734-9750
- van Rantwijk, F.; Sheldon, R. A. (2007). Biocatalysis in ionic liquids. *Chem. Rev.*, 107, 6, (June 2007) 2757-2785, ISSN 0010-8545
- Wasserscheid, P., Eichmann, M. (2001). Selective dimerisation of 1-butene in biphasic mode using buffered chloroaluminate ionic liquid solvents - Design and application of a continuous loop reactor. *Catal. Today*, 66, 2-4, (March 2001) 309-316, ISSN 0920-5861
- Waterkamp, D. A., Heiland, A., Schlüter, A., Sauvageau, J. C., Beyersdorff, T., Thöming, J. (2007). Synthesis of ionic liquids in micro-reactors – a process intensification study. *Green Chem.*, 9, (June 2007) 1084 – 1090, ISSN 1463-9270
- Waterkamp, D., Engelbert, M., Thöming, J. (2009). On the effect of enhanced mass transfer on side reactions in capillary microreactors during high-temperature synthesis of an ionic liquid. *Chem. Eng. Technol.* 32, 11, (November 2009) 1717-1723, ISSN 1521-4125
- Wei, G.-T., Yang, Z., Chen, C.-J. (2003). Room temperature ionic liquid as a novel medium for liquid/liquid extraction of metal ions. *Anal. Chim. Acta*, 488, 2, (July 2003) 183-192, ISSN 0003-2670
- Welton, T. (1999). Room-temperature ionic liquids. Solvents for synthesis and catalysis. *Chem. Rev.*, 99, (July 1999) 2071-2083, ISSN 0009-2665
- Wießmeier, G., Hönicke, D. (1996). Heterogeneously catalyzed gas-phase hydrogenation of cis,trans,trans-1,5,9-cyclododecatriene on palladium catalysts having regular pore systems. *Ind. Eng. Chem. Res.*, 35, 12, (December 1996) 4412-4416, ISSN 0888-5885
- Wilms, D., Klos, J., Kilbinger, A.F.M., Löwe, H., Frey, H. (2009). Ionic liquids on the demand in continuous flow. *Org. Proc. Res. Dev.*, 13, 12, (December 1996) 961-964, 0888-5885
- Yang, Z., Pan, W. (2005). Ionic liquids: green solvents for nonaqueous biocatalysis, *Enzyme and Microb. Technol.*, 37, 1, (June 2005) 19-28, ISSN 0141-0229
- Yoon, S. Y., Lee, J. G., Tajima H., Yamasaki, A., Kiyono, F., Nakazato, T., Tao, H. (2010). Extraction of lanthanide ions from aqueous solution by bis(2-ethylhexyl)phosphoric acid with room-temperature ionic liquids. *J. Ind. Eng. Chem.*, 16, 3, (May 2010) 350-354, ISSN 1226-086X
- Zhao, D., Wu, M., Kou, Y., Min, E. (2002). Ionic liquids: applications in catalysis. *Catal. Today*, 74, 1-2, 157-189, ISSN 0920-5861
- Zhou, Q., Zhang, X., Xiao, J. (2009). Ultrasound-assisted ionic liquid dispersive liquid-phase micro-extraction: A novel approach for the sensitive determination of aromatic amines in water samples. *J. Chrom. A*, 1216, 20, (May 2009) 4361-4365, ISSN 1570-0232
- Žnidaršič-Plazl, P., Plazl, I. (2007). Steroid extraction in a microchannel system - mathematical modelling and experiments. *Lab Chip*, 7, 7, (July 2007) 883-889, ISSN 1473-0189
- Žnidaršič-Plazl, P., Plazl, I. (2009). Modelling and experimental studies on lipase-catalyzed isoamyl acetate synthesis in a microreactor. *Process Biochem.*, 44, 10, (October 2009) 1115-1121, ISSN 1359-5113
- Zimmermann, J., Ondruschka, B., Stark, A. (2010). Efficient synthesis of 1,3-dialkylimidazolium-based ionic liquids: The modified continuous Radziszewski

reaction in a microreactor setup. *Org. Process Res. Dev.*, 14, 5, (August 2010) 1102–1109, ISSN 1083-6160

Zulfiqar, F., Kitazume, T. (2000). One-pot aza-Diels–Alder reactions in ionic liquids. *Green Chem.*, 2, 137-139, (June 2000) 1463-9262, ISSN 1463-9262

# Ionic Liquids: Methods of Degradation and Recovery

E.M. Siedlecka<sup>1</sup>, M. Czerwicka<sup>1</sup>, J. Neumann<sup>2</sup>, P. Stepnowski<sup>1</sup>,  
J.F. Fernández<sup>2</sup> and J. Thöming<sup>2</sup>

<sup>1</sup>*Faculty of Chemistry, University of Gdańsk, ul. Sobieskiego 18, 80-952 Gdańsk*

<sup>2</sup>*UFT - Center of Environmental Research and Sustainable Technology, University of  
Bremen, Leobener Straße, D-28359 Bremen,*

<sup>1</sup>*Poland*

<sup>2</sup>*Germany*

## 1. Introduction

In recent years ionic liquids (ILs) have attracted considerable attention owing to their potential use in a diversified range of applications. It is believed that ILs can successfully replace volatile organic media in a wide range of chemical processes. They have been studied and applied in organometallic catalysis, organocatalysis and biocatalysis, where they provide unique reaction media offering better selectivity, faster rates and greater catalyst or enzyme stability in comparison to conventional solvents (Buszewski & Studzińska, 2008; Dupont et al., 2002; Liu et al., 2010; Mathews et al., 2000; Minami, 2009; Welton, 1999). The applications of ILs also include areas such as electrochemical transformation, fuel cells, solar cells, sensors and nanochemistry. They are emerging as lubricants, modifiers of mobile and stationary phases in the separation sciences, and are candidates for the dissolution of cellulose, starch and wood (Wassersheid & Welton, 2003).

ILs are characterized by properties such as negligible vapour pressure and non-flammability under ambient conditions, high thermal conductivity, a wide electrochemical window and high polarity. They also have the ability to dissolve a wide diversity of materials, including salts, fats, proteins, amino acids, surfactants, sugars, polysaccharides and organic solvents. However, the most important attribute of ILs is the possibility of designing their properties to order. Thanks to the enormous number of cation and anion combinations, ILs can possess a wide spectrum of physical and chemical properties (solubility, polarity, viscosity or solvent miscibility), and they are already recognized by the chemical industry as new, target-oriented reaction media.

The properties of ILs can be used for developing new processes that are technologically, environmentally and economically advantageous. Listed benefits include the possibilities of reusing and relatively easily recovering ILs, which effectively reduces the amount of waste generated during technological operations. It is, however, important to remember that ILs are still quite expensive media, and their recycling after regeneration or recovery makes such a technology economically all the more justified. Among available technologies, conventional processes such as distillation, membrane separation and extraction can be

applied (Fernandez et al., 2010). Distillation in mild conditions may be the first choice for the separation of volatile products owing to the negligible vapour pressure of ILs. For separating non-volatile products, extraction and membrane processes such as nanofiltration and evaporation can be used. The operations to recover ILs from aqueous solutions described in this chapter are classified as phase addition (for example, salting-out), force field (gravity settling) and barrier (membrane separation).

Since the recovery of ILs on a large industrial scale will consume a great amount of energy, or if they are to be recovered from very dilute solutions where either investment or operational costs can be so high that they make the recovery operation not feasible, effective treatment is needed prior to the final application. Most ILs are not readily biodegradable, so advanced oxidation processes (AOPs) are frequently suggested as effective processes (Siedlecka et al., 2010; Stolte et al., 2010). The AOPs used for IL degradation, as well as a few examples of biological degradation and adsorption removal processes, are described in this chapter. The possibilities of reducing the amount of industrial waste containing ILs as well as potential sources of environmental release are illustrated in Figure 1.

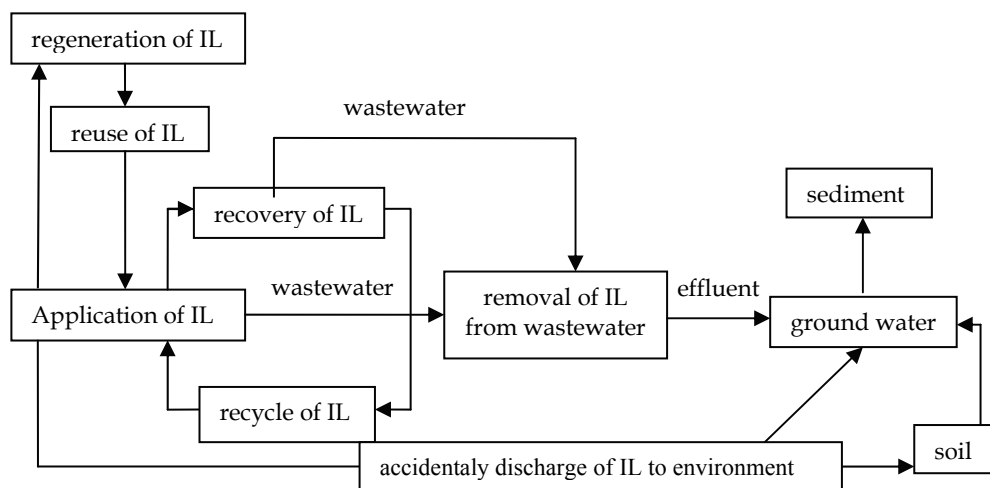


Fig. 1. Reduction of wastes containing ionic liquids in industrial applications, and potential sources of ILs released to the environment.

The non-measurable vapour pressure is a reason why ILs are frequently uncritically regarded as inherently environmentally friendly compounds. The loss of ILs is low, so a potential source of air pollution or inhalation is eliminated. Nevertheless, if one does classify ILs as “green” chemicals, questions such toxicity and persistence in the environment must also be addressed. The application of ILs on an industrial scale may pose an environmental hazard as a result of their transport, storage, technical breakdown, discharge in wastewaters etc. Therefore, in order to responsibly apply ILs in industrial processes, investigations of their fate and behaviour in the relevant environmental compartments (degradation, sorption etc.) and a proper risk assessment of ILs in the soil and aquatic environment (toxicity) must be undertaken and taken into consideration. The biodegradability of ILs, their toxicity and sorption in the environment are also briefly discussed in this chapter.

## 2. Behaviour of ionic liquids in water

Knowledge of the impact of structural variations of ionic liquids on their solubilities in water is of significance in relation to future applications, selecting the appropriate wastewater treatment process, and understanding their environmental fate. The loss of ILs into the aqueous phase may be an important factor in estimating the costs of recycling and water treatment.

Studies on the behavior of ILs in water have been taken by some research groups. Studies in which the cation and/or anion were changed were carried out by Freire et al. (Freire et al., 2007; Freire et al., 2008). They demonstrate unequivocally that the size of ILs, hydrophobicity and hydrogen bonding ability of both cation and anion are the most important factor regarding the solubility of ILs in water. However the nature of the anions largely determines the behaviour of IL-water mixture (Freire et al., 2008). Furthermore, ILs possessing long aliphatic substituents have been reported to undergo micellization (Anouti et al., 2009, Jungnickel et al., 2008, Łuczak et al., 2008; Łuczak et al., 2009). The formation of micelles in aquatic solution is due to the nature of the ions making up the ILs, which generally contain hydrophobic and hydrophilic domains. Hence the aggregation tendency of surfactant-like ILs is dependent on the relative size of these domains (Łuczak et al., 2008, Sirieux-Plener et al., 2004) – the larger the hydrophobic domain, the greater the tendency to aggregate. Moreover, this tendency to aggregate increases in the presence of inorganic entities (Rickert et al., 2007), which is of significance for industrial wastewater treatment.

Several examples of IL hydrolysis are described in the literature. It is mainly the anions used in ILs that undergo hydrolysis – when reacting with water they generate mineral acids, e.g. sulphuric acid, phosphoric acid and hydrofluoric acid (Islam & Ohsaka, 2008, Swatłowski, 2003). Hydrolysis of ILs can cause corrosion by these acids: it has been reported that carbon steel and stainless steel are corroded as a result of the dilution of ILs in water. A negative effect is exerted by anions such as tosylate, dimethylphosphate, hexafluorophosphate etc. (Uerdingen et al., 2005). Therefore, investigations into the recovery and removal of ILs from wastewaters and the environmental fate of ILs should take the influence of both cation and anion species into consideration.

## 3. Recovery operations of ionic liquids

According to the waste hierarchy developed by the European Union Directive 2008/98/EC (European Union, 2008), the effort priorities for dealing with spent material are expressed as “Re-duce, Re-use, Re-cycle”. This means that only minimum amounts of substances should be used in a process. If possible, the substance should then be reused and reincorporated into the system and eventually recovered from the waste stream. Different operations are required in order to comply with the regulations.

Regeneration is often necessary if a substance cannot be reused directly. For the recycling of waste, recovery operations are applicable. Removal operations are then the final step to prevent a negative impact on the environment or human health when the final waste is disposed of.

This procedure is also valid for ILs, not just for legislative reasons, but also because of their relatively high production costs. However, the continual reuse of ILs will lead to a concentration of contaminants. Regeneration can then enhance the reusability of the IL and prolong its lifetime by separating it from the suspected contaminant. This was the first operation to be used and developed. An overview is given in Fernandez et al. (2010).

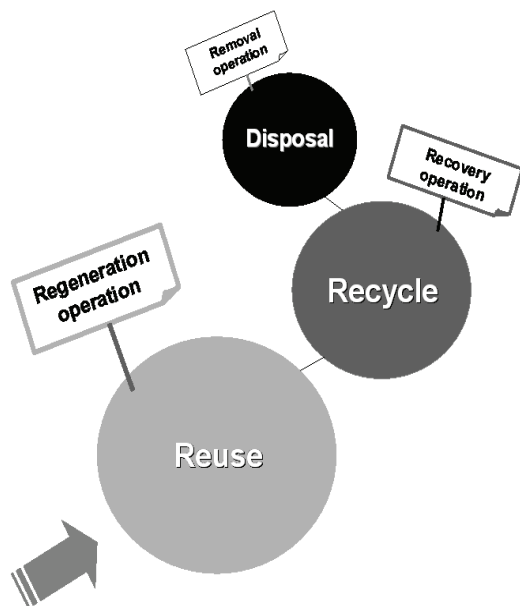


Fig. 2. Scheme of the effort priorities for dealing with spent ionic liquids. The spheres starting with “reuse” are the overall treatment purposes requiring different technical operations (in rectangles).

However, these regeneration processes are limited to the threshold concentration of contaminants that make ILs unusable for a given purpose and turns them into IL waste. Recovery operations of IL waste are then of special interest.

In view of the physicochemical properties and applications of ILs, the recovery of IL wastes focuses mostly on wastewater streams. ILs adsorbed on solid surfaces can also enter the waste stream; but most solid waste is treated thermally, and IL recovery from such waste has not yet been undertaken.

Wastewater streams containing ILs are of concern when it comes to environmental aspects on the one hand, e.g. (eco)toxicity and biodegradability, and technical aspects on the other hand, e.g. operating costs for replenishing ILs lost from a process. The amounts of ILs that can be expected in wastewater streams are roughly equivalent to their solubilities. Even though hydrophobic ILs are poorly soluble in water, concentrations in water can be relatively high. In this case, attempts should be made either to replace the IL used with a less soluble substance or to develop processes to recover them from wastewater, preferably in a closed system where recovery can be carefully controlled (McFarlane et al., 2005).

In this chapter the recovery operations of ILs from aqueous solutions are explained and classified by their separation mechanism: (1) phase addition, (2) force field and (3) barrier.

### 3.1 Recovery by phase addition

Simple salting-out processes have been investigated for separating ILs from water. Distillation, as applied to regeneration (Mathews et al., 2000), has not yet been applied to recovery, probably because of the low IL concentration in wastewater in contrast to the regeneration of spent ILs contaminated with water.



The principle of salting out is relatively simple, although its mechanism is not completely known, yet. To salt out an IL from an aqueous solution, an electrolyte is added as a solid or as a saturated aqueous solution. The electrolyte withdraws some of the water present, forming a second phase that can be removed by decantation; the energy penalty incurred by the evaporation of the water is thus avoided. As the electrolyte used as the mass-separation agent is not usually recoverable, its cost is an important factor to be taken into account. An example has been given by Gutowski et al. (2003) of how this recovery operation works in practice: a homogeneous mixture of 1-butyl-3-methylimidazolium chloride and water is turned into a biphasic system when a concentrated solution of potassium phosphate is added: (1) the upper phase – rich in IL; (2) the lower phase – rich in potassium phosphate. Further studies on the recovery of ILs by the addition of other kosmotropic salts and carbon dioxide were reported and reviewed by Fernandez et al. (2010). There is, however, still a lack of information on which to base a definition of these phase systems before they can be implemented in new technologies (Bridges et al., 2007).

### 3.2 Recovery using a force field

The standard use of a force field for the recovery of ILs is gravity settling, e.g. enhanced by a centrifugal contactor. It has been applied with success to a dispersion of a hydrophobic IL with common salt and with water (Birdwell et al., 2006).

When IL cations such as 1-butyl-3-methylimidazolium are coupled with an iron-containing anion, e.g. tetrachloridoferrate, they show a strong magnetic response, which can be used for their recovery (Hayashi & Hamaguchi, 2004; Lee et al., 2007). A magnetic field is thereby induced on a biphasic system consisting of an IL-rich phase and water-rich phase, which can then be separated easily. Together with other methods, e.g. ultracentrifugation, separation could possibly be improved, although this might be impracticable in an industrial situation.

### 3.3 Recovery using a barrier

Besides the separation of ILs and water by phase addition and force field, membrane filtration has been studied as a promising technology. The first report on the application of nanofiltration to separate mixtures containing ILs was published in 2003 by Kröckel et al. Retentions of ILs of up to 82% and 95% were obtained for 1-butyl-3-methylimidazolium tetrafluoroborate and 1-butyl-3-methylimidazolium sulphate, respectively, using commercial Desal membranes. In a more recent study, lower retention values of only 60% for 1-butyl-3-methylimidazolium tetrafluoroborate and 67% for 1-butyl-3-methylimidazolium bromide as maximum values were obtained (Wu et al., 2009). Own experiences, published in 2008 by Fernández et al., are reaching up to 99 % of ILs retention from aqueous solutions. This means that depending on the initial concentration of the IL in waste water the residual concentrations could still be too high for biological processes during waste water treatment why the removal of ILs from waste water is then of great importance. In general, the use of membrane technology for IL recovery is regarded as advantageous in comparison to the other two separation methods described. In membrane technology no auxiliary substance as required for phase addition needs to be added, and it can be applied to a variety of ILs, whereas separation by force field is limited to magnetic ILs.

Although membrane technology is an important step towards the effective recovery of ILs from waste water, not all technological potentials have been fully tapped and research has so far been based mainly on phase separation, barrier and forced field technologies. Further

research is still going on to reduce IL waste. However, if ILs are not reusable and recoverable any more, the removal of ILs can be applied as the final treatment step. Though the last step in a series of treatment steps, it needs to be considered, because no infinitely applicable regeneration and recovery techniques are available at the moment; up till now, every product has eventually become waste.

## 4. Removal of ILs

### 4.1 Physicochemical removal

Adsorption is an important technology that is widely used to remove organic pollutants from water. The effectiveness of sorption depends fundamentally on the characteristics of the substance to be adsorbed and on the type of adsorbent. In addition, operational requirements may lead to contact times that are too short to ensure equilibration.

Adsorbents such as activated carbon (Palomar et al., 2009), ion-exchange resin, activated sludge and fermentation waste (Vijayaraghavan et al., 2009) have all been used to remove ILs from aqueous solutions. The ion-exchange resin exhibits the best sorption efficiency (98%) but the process is relatively slow (180 min.). Activated carbon gives a faster rate of sorption (15 min.), but the affinity of ILs for this sorbent is much poorer compared to ion-exchange resin. Adsorption on activated sludge and fermentation waste is insignificant (Vijayaraghavan et al., 2009).

The affinity of ILs for activated carbon is the result of diverse intermolecular interactions (polar,  $\pi$ - $\pi$ , van der Waals and hydrogen bonding). Ion exchange is minimal at acidic and neutral pH, but is significantly enhanced at basic pH values, where deprotonation and the generation of negatively charged functional groups takes place on the carbon surface (Vijayaraghavan et al., 2009). There is a rise in the adsorption capacity of activated carbon as imidazolium-based ILs are composed of hydrophobic cations (1-methyl-3-octyl-imidazolium and 1-hexyl-3-methylimidazolium cations) and/or hydrophobic anions (bis[(trifluoromethyl)sulfonyl]amide, hexafluorophosphate) (Palomar et al., 2009). The role of van der Waals interactions between the non-polar groups of the cation and the organic matter has also been investigated using soil and sediments (Beaulieu et al., 2008; Matzke et al., 2009; Mrozik et al., 2008a; Mrozik et al., 2008b; Stepnowski, 2005; Stepnowski et al., 2007; Studzińska et al., 2009). Physical adsorption phenomena have been effectively used for the immobilization of hydrophobic ILs on other solid supports (Liu et al., 2010).

The results obtained on different activated carbons demonstrate that adsorbent porosity is also an important factor in IL sorption. The higher average pore diameter in activated carbon facilitates the comparatively easy diffusion of ILs into the pore structure, enhancing its sorption (Vijayaraghavan et al., 2009).

### 4.2 Degradation methods

It is known that ILs are thermally, electrochemically and chemically relatively stable (Siedlecka et al., 2010), but they will eventually decompose during technological operations. In recent years numerous investigations have been carried out into IL toxicity and biodegradability (Bailey et al., 2008; Bernot et al., 2005a; Bernot et al., 2005b; Docherty et al., 2006; Gathergood et al., 2004; Gathergood et al., 2006; Gathergood & Scammells, 2002; Garcia et al., 2005; Latała et al., 2005; Latała et al., 2009a; Latała et al., 2009b; Latała et al., 2010; Pernak et al., 2003; Pham et al., 2010; Renke et al., 2003; Składanowski et al., 2005; Stasiewicz et al., 2008; Stepnowski et al., 2004; Stock et al., 2005; Stolte et al., 2008; Swatłowski et al., 2004).

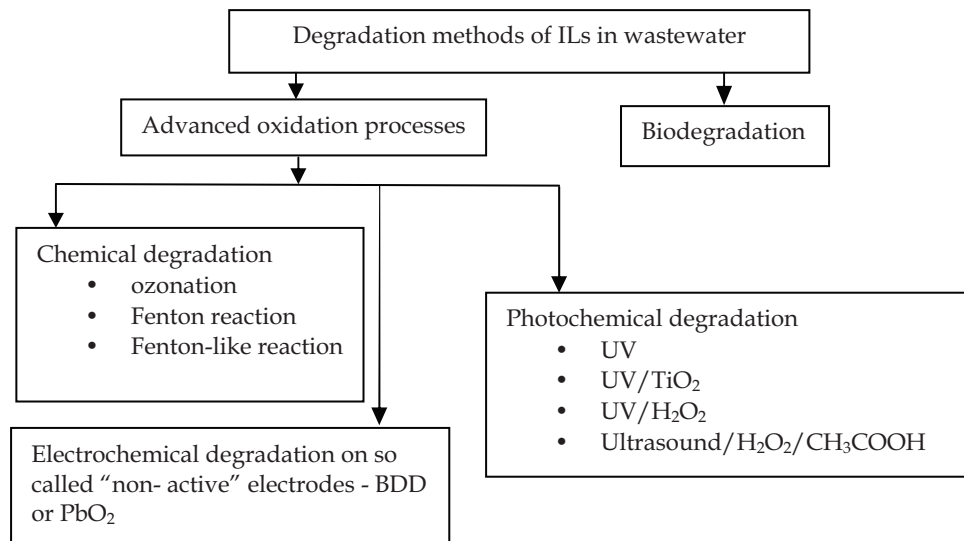


Fig. 3. ILs degradation methods proposed in literature

However, the toxicity and environmental resistance of their decomposition products is totally unknown. For this reason, chemical, photochemical or electrochemical oxidation have been put forward as processes for removing from wastewater both non-recoverable ILs and their degradation products (Czerwicka et al., 2009; Li et al., 2007; Pernak & Branicka, 2004; Siedlecka et al., 2008; Stepnowski & Zalewska, 2005; Stolte et al., 2008) (Fig.2.). Biological wastewater treatment is regarded as environmentally very friendly, and some examples of this process are given in this chapter.

#### 4.2.1 Chemical degradation

The chemical oxidation of aqueous solutions of ILs has been investigated. Information is available on ozonation (Pernak & Branicka, 2004), the Fenton reaction and Fenton-like reactions (Siedlecka et al., 2008a; Siedlecka et al., 2008b; Siedlecka et al., 2009).

Ozonation of 1-(alkoxymethyl)-3-hydroxypyridinium, 1-(alkoxythiomethyl)-3-hydroxypyridinium and 1-(alkoxymethyl)-3-(dimethylamino)pyridinium chlorides was found to be rapid and effective. In this process small amounts of decomposition products were generated, with the drop in pH indicating that some of them could be organic acids. Additionally, the ozonation products of 1-(tetradecyloxy)methylpyridinium chlorides substituted by a hydroxyl group in position 3 or 5 or containing a dimethylamino group in position 3, demonstrated no bacteriostatic or mycostatic effects. (Pernak & Branicka, 2004). These authors conclude that the products formed are less harmful than parent pyridinium compounds. The fact that pyridinium ILs without a hydroxyl group substituted at the pyridinium head group do not lend themselves to ozonation confirms that ozone itself is a highly selective oxidant (Hoigne et al., 1989).

In Fenton ( $\text{H}_2\text{O}_2/\text{Fe}^{2+}$ ) and Fenton-like ( $\text{H}_2\text{O}_2/\text{Fe}^{2+}$ ) systems the hydroxyl radical ( $\bullet\text{OH}$ ) with a very strong oxidative potential ( $E_0=+2,8\text{V}$ ) degrades non-biodegradable and recalcitrant organic pollutants. In contrast to ozone, the hydroxyl radical is a non-selective oxidant. Furthermore, the modification of Fenton-like reactions by the addition of a large dose of  $\text{H}_2\text{O}_2$  promotes a series of propagation reactions that produce a perhydroxyl radical, a superoxide anion, and a peroxide anion in addition to the hydroxyl radical (Walling, 1975). These radicals can lead to different pathways of IL degradation, products and display different transformation kinetics (Siedlecka et al., 2009; Siedlecka & Stepnowski, 2009). Fenton and Fenton-like systems are very effective in the degradation of 1-alkyl-3-methylimidazolium ILs. It was demonstrated that the efficiency of oxidation is structurally dependent. The lengthening of the alkyl chain from four to eight carbons in the 1-alkyl-3-methylimidazolium cation significantly lowered the rate of degradation (Siedlecka & Stepnowski, 2009). A comparative study of three 1-butyl-3-methylimidazolium salts leads to the conclusion that anions can inhibit degradation by competition with cations for hydroxyl radicals, or by undergoing complex reactions with ferric and ferrous ions (Siedlecka et al., 2009). Moreover, the 1-butyl-3-methylimidazolium cation degradation rate was retarded with the lengthening of the alkyl chain in the perfluorocarboxylic anions present in a solution of 1-butyl-3-methylimidazolium chloride (Siedlecka et al., 2009). A high dose of  $\text{H}_2\text{O}_2$  in a Fenton-like system accelerates the degradation of imidazolium-based ILs, especially 1-butyl-3-methylimidazolium chloride, but slows down the degradation of 1-butyl-3-methylpyridinium chloride. The authors conclude that increasing the  $\text{H}_2\text{O}_2$  dose in Fenton-like systems changes the mechanism of IL degradation (Siedlecka et al., 2008a; Siedlecka et al., 2008b; Siedlecka & Stepnowski, 2009).

Analysis of mixtures oxidized by Fenton-like systems shows that mono-, di- and amino-carboxylic acids are probably degradation products. Effective degradation of the imidazolium ring is achieved only for 1-butyl-3-methylimidazolium chloride (Siedlecka et al., 2008b; Siedlecka & Stepnowski, 2009).  $^1\text{H}$ -NMR spectra and GC-MS results showed that radical attack is non-specific, with any one of the carbon atoms in the ring and the alkyl chain being susceptible to attack. The products with some hydroxyl groups substituted at different sites in the parent compounds are rather unstable and decomposed by two pathways: the first is oxidative ring opening, the second is cleavage of the N-C bond in the N-alkyl side chain. Unfortunately, all these chemical degradation investigations were limited to imidazolium-based ILs, where a great number of pyridinium-, pyrrolidinium-, phosphonium- or ammonium-based ILs are commercially available.

It seems that a hybrid system consisting of a Fenton-like process and a biological stage should be considered for IL degradation, thereby accelerating the mineralization of ILs. Therefore, systematic investigations of the toxicity and biodegradability of post-oxidation mixtures should be conducted.

#### 4.2.2 Photochemical degradation

In one of the first studies, Stepnowski & Zaleska compared the effectiveness of three methods: UV photodegradation, UV photolysis of hydrogen peroxide, and photocatalysis on UV-irradiated  $\text{TiO}_2$ . For these investigations imidazolium ILs with different alkyl chain length were chosen (1-butyl-, 1-hexyl-3-methylimidazolium, 1-methyl-3-octylimidazolium, 1-ethyl-3-ethylimidazolium chloride or tetrafluoroborate, methyl imidazole as reference). The stability of these compounds with respect to all the photodegradation methods used

appeared to be structure-related. The process that was most effective with all the compounds was oxidation based on the UV/H<sub>2</sub>O<sub>2</sub> system, the degradation efficiency decreasing in the order: 1-butyl-3-methylimidazolium < 1-hexyl-3-methylimidazolium < 1-methyl-3-octylimidazolium < 1-ethyl-3-ethylimidazolium cations. The 1-ethyl-3-ethylimidazolium cation turned out to be the most stable compound, although in the case of direct photolysis, the octyl- and hexyl- alkyl side chain cations were the least degradable (Stepnowski & Zaleska, 2005). For confirmation of the results, the AOP degradation products had to be identified. For these investigations 1-ethyl-, 1-butyl-, 1-hexyl-3-methylimidazolium and 1-methyl-3-octylimidazolium chlorides were treated with the UV/H<sub>2</sub>O<sub>2</sub> system. Identification was based on LC-MS/MS measurements. It was found that modification (at least in the first stage of oxidation) occurred in the imidazolium ring, not in the alkyl chain of the molecule. The longer the alkylated cation, the greater the probability of oxidation of the alkyl chain (Czerwica et al., 2009). The results tallied with those obtained using a Fenton-like system (Siedlecka et al., 2008b) or after biodegradation (Stolte et al., 2008). Nevertheless, the toxicity and biodegradability of the degradation products still need to be analysed. The major objective of the work of Morawski et al. was to investigate photocatalysis as a method of degrading different types of ILs (imidazolium, ammonium, phosphonium, pyridinium). For that purpose those authors used UV light in the presence of TiO<sub>2</sub>. They concluded that the lower the molar mass, the greater the IL stability, and also that degradability depends upon the cation and anion, although to different degrees. Phosphonium ILs were shown to be the most susceptible to this type of degradation (Morawski et al., 2005).

Itakura et al. studied the efficacy of the photocatalytic decomposition of ILs using platinized TiO<sub>2</sub> (Pt/TiO<sub>2</sub>) and bare TiO<sub>2</sub>, but unlike other authors, they also took anion degradation into account. They tested three ILs: 1-ethyl-3-methylimidazolium bromide, 1-ethyl-3-methylimidazolium hexafluorophosphate, 1-butyl-3-methylimidazolium tetrafluoroborate. There was no significant difference between the degradation efficiencies obtained with TiO<sub>2</sub> or Pt/TiO<sub>2</sub>. It appears to be a perfect method for cation degradation, but it is unsuitable for anions. To degrade these (especially hexafluorophosphate and tetrafluoroborate), another method was needed: hydrothermal treatment with Ca(OH)<sub>2</sub> mineralizer could serve this purpose (Itakura et al., 2009).

Katoh & Takahashi studied photochemical degradation under pulsed laser irradiation in order to examine the decomposition behaviour of 1-methyl-3-butylimidazolium bis[(trifluoromethyl)sulphonyl]amide and iodide. They concluded that the excited state 1-butyl-3-methylimidazolium cation ([BMIM<sup>+</sup>]) underwent degradation efficiently and suggested that the neutral 1-butyl-3-methylimidazolium radical ([BMIM]•) was relatively stable (Katoh & Takahashi, 2009). The majority of studies have looked at the photodegradation of imidazolium-based ILs. Nevertheless, there is some information on the photochemical transformations of pyridinium salts, which could be a good starting point for later IL degradation studies (Damiano et al., 2007).

It seemed interesting to use the ultrasonic chemical oxidative degradation method proposed for 1,3-dialkylimidazolium ILs with different anions (chloride, bromide, hexafluorophosphate and tetrafluoroborate). The oxidative decomposition of ILs was carried out in aqueous hydrogen peroxide/acetic acid assisted by ultrasonic chemical irradiation. Li et al. in 2007 achieved a high efficiency of degradation (93% after 12h, and 99% after 72h). The degradation products were monitored using GC-MS. They demonstrated that hydrogen atoms in the imidazolium ring are oxidized first, and that fragmentation leads to ring

opening. This is in agreement with the results obtained by other authors (Czerwicka et al., 2009; Li et al., 2007). They also found that there was no significant influence of either alkyl chain length or anion type on the degradation pathway. The high degree of degradation augurs well for this method (Li et al., 2007). Also the direct influence of sonification on pure imidazolium based ILs decomposition was analysed. The first sign of degradation was the darkening of their colour to an amber shade. It was shown that ultrasonic treatment led to the decomposition of organic ILs. GC-MS, IR spectroscopy, and NMR spectroscopy were used for monitoring the degradation process (Oxley et al., 2003).

#### 4.2.3 Electrochemical degradation

ILs are thought to be electrochemically stable. They possess large electrochemical potential windows from 2V to 6V, but these data are the result of rather short cyclic voltammetry experiments (Galiński et al., 2006). It has been demonstrated that different reaction products can be found when longer electrolysis experiments are performed (Kroon et al., 2006). The differences in the electrochemical stabilities of ILs results from the presence of impurities. In the presence of water the potential window of ILs narrows dramatically (Islam & Ohsata, 2008; Welton, 1999). Moreover, some reactions, e.g. the generation of a superoxide ion or a hydroxide radical, which limits the chemical stability of ILs, may be affected by the presence of water in ILs (Barnes et al., 2008).

Therefore, a very promising disposal strategy for toxic and recalcitrant ILs in aqueous solutions is electrolysis using “non-active” anodes such as boron-doped diamond (BDD) or PbO<sub>2</sub>. These anodes have the ability to generate quasi-free hydroxyl radicals during the electrolysis of water, which are capable of efficiently oxidizing ILs. The electrochemical oxidation of imidazolium ILs was carried out for the first time by Stolte et al. in 2008. Almost complete degradation of 1-butyl-3-methylimidazolium chloride was achieved on a bipolar BDD anode. The positively charged imidazolium core, responsible for the non-biodegradability of imidazolium-based ILs, was completely destroyed after 4h of electrolysis. In addition, the biodegradability improved in comparison to that of the parent compound solution (Stolte et al., 2008). Further investigations carried out by our research group indicate that another “non-active” anode – PbO<sub>2</sub> – also successfully degrades imidazolium- and pyridinium-based ILs (data not published).

#### 4.2.4 Other degradation methods

Thermal degradation could be an alternative method for degrading ILs, in spite of their excellent thermal stability. Very promising is the fact that, despite their tolerance to short-term high temperature treatment, longer exposure to such temperatures could induce decomposition. Kroon et al. predicted the susceptibility of ILs to thermal degradation on the basis of quantum chemical calculations. These authors stated that long-term thermal stability depends on the cation type (imidazolium and phosphonium cations were found to be the most stable), that the effect of alkyl chain length is not significant, and that highly proton-abstracting anions (halides) are more susceptible, whereas poorly proton-abstracting ones like bis[(trifluoromethyl)sulphonyl]amide are more resistant to high temperature decomposition (Kroon et al., 2007). These conclusions are comparable with published experimental data. The thermal degradation of some ILs is relatively easy, for example, that of a water-HAN (80 wt. %, hydroxylammonium nitrate) mixture. The experiment was performed using a dynamic reactor with mass spectrometry. The critical temperature had

earlier been established as 120°C, but in this study a temperature of 200°C was used, at which NO, NO<sub>2</sub>, N<sub>2</sub>O, N<sub>2</sub> or O<sub>2</sub> were produced (Amariei et al., 2007). The thermal decomposition behaviour of readily investigated imidazolium-based ILs was studied by Ohtani et al. The thermal degradation products of 1-alkyl-3-methylimidazolium ILs (with trifluoromethylsulphonate, hexafluorophosphate and tetrafluoroborate, chloride, or bromide anions) were detected with Py-GC coupled to different analysers (FID, Nr-ECD, NPD, MS). It was concluded that in the case of halides, the corresponding haloalkanes and 1-alkylimidazoles were mainly formed, that from ILs containing the tetrafluoroborate anion, the corresponding alkenes with smaller amounts of haloalkanes and 1-alkylimidazoles were formed, that from 1-butyl-3-methylimidazolium trifluoromethylsulphonate, butene, 1-methyl- and 1-butylimidazole, a few haloalkanes and CF<sub>3</sub>H and SO<sub>2</sub> were formed, that in the case of the hexafluorophosphate anion, the products were similar to those obtained from the tetrafluoroborate anion (additionally some phosphorus-containing compounds were observed), and that the imidazole ring decomposed very little under the experimental conditions at around 550°C (Ohtani et al., 2008).

The high-temperature decomposition of some ILs could be very dangerous. The problem lies in the degradation products of, for example, cyano-containing ILs. Wooster et al. examined the thermal degradation of different ILs with dicyanamide or tricyanomethide anions using pyrolysis + GC-MS. They showed that under the influence of temperature products were formed whose structure was strongly dependent on cation type. They found that polymerization occurred in the case of cyano-containing anions and *N*-based cations (*N*-butyl, *N*-methyl-pyrrolidinium, *N*-methyl, *N*-propyl-pyrrolidinium), whereas the presence of the phosphonium cation (trihexyltetradecylphosphonium) led to complete decomposition to volatile compounds (Wooster et al., 2006). All investigations involving the thermal decomposition of ILs need to be supplemented by mass spectrometric analysis of the degradation products in order to identify these products and to evaluate their toxicity. On the other hand, if we take into consideration the matrix and the examples just mentioned, thermal degradation does not appear to be a very suitable method for decomposing ILs from wastewater.

There are rather few investigations covering the complete degradation of ILs, that is, both cation and anion. Itakura et al. reported that a combination of two methods was needed to achieve success. They investigated the combination of hydrothermal mineralization (HM) and photocatalytic degradation (PD) to decompose 1-ethyl-3-methylimidazolium bromide or hexafluorophosphate and 1-butyl-3-methylimidazolium tetrafluoroborate. As already mentioned, PD did not decompose the anions to a sufficient extent. On the other hand, hydrothermal treatment used on its own did not completely degrade the cations either. Only the combination of both methods led to the detoxification of water contaminated by the ILs being tested (Itakura et al., 2009).

### 4.3 Biological methods

The use of living organisms, especially microorganisms, for degrading ILs seems a natural and obvious approach, one that appears at least potentially to be more friendly to the environment. The results of primary biodegradation (using bacteria) studies using different IL cations were very interesting. 27 ILs with different head groups (e.g. imidazolium, pyridinium) and side chains were tested. LC-MS was used to identify the primary biodegradation products. It was shown that the more toxic ILs with longer side-chains were more susceptible to biodegradation. It was found that lipophilicity was the factor

responsible for the increasing tendency towards toxicity and biodegradability, but unfortunately it creates a conflict of interests in looking for biological degradable ILs (Stolte et al. 2008). Markiewicz et al. showed that a level of 0.2mM 1-methyl-3-octylimidazolium chloride is the terminal concentration threshold for primary biodegradation. Higher concentrations led to sorption onto the sewage sludge flocs, although inhibition of cell function as a consequence of decreased dehydrogenase activity was observed (Markiewicz et al., 2009). This indicates that the toxicity of ILs towards activated-sludge microorganisms should be taken into consideration. To predict this effect quantitative structure-property relationship modelling could be helpful (Couling et al., 2006). Besides bacteria, fungi can also be used for IL degradation. To this end, Esquivel-Viveros et al. tested *Fusarium* sp., and demonstrated that 1-butyl-3-methylimidazolium hexafluorophosphate could be degraded by these fungi. The results were obtained using a membrane-accelerated biofilm reactor as well as tests on Petri dishes and in Erlenmeyer flasks (Esquivel-Viveros et al., 2009). Minimal or zero degradation of 1-butyl-3-methylimidazolium-based ILs was confirmed by Gathergood and co-workers ((Garcia et al., 2005; Gathergood et al., 2004; Gathergood et al., 2006).

Comparative studies have also been carried out regarding the differences between the biodegradabilities of various ILs. The biodegradability of ILs containing imidazolium and pyridinium cations by an activated sludge microbial community were investigated by Docherty et al. and Pham et al. (Docherty et al., 2007; Pham et al., 2007). They came to the same conclusions, namely, that alkylpyridinium ILs are more rapidly biodegraded than imidazolium ILs. It was also found that ILs with a pyridinium head group are less toxic (Pham et al., 2007) and that the longer the alkyl chain, the faster the biodegradation (Docherty et al., 2007). Only one of all the tested ILs – 3-methyl-1-octylpyridinium bromide – fitted the criteria for DOC Die-Away, and could be designated as readily biodegradable (Docherty et al., 2007). Excellent biodegradability is also shown by pyridinium cations bearing an ester containing a substituent at positions 1 or 3 (Stolte et al., 2008).

From the toxicity point of view, the identification of products formed during biodegradation is very important, because the toxic effect could interrupt the biodegradation process. For this purpose, Pham et al. first studied the biodegradation pathway of 1-butyl-3-methylpyridinium bromide, including the identification by LC-MS of the metabolites formed. They found two pathways of degradation, one leading to 1-(2-hydroxybutyl)-3-methylpyridinium and the other to 1-(2-hydroxyethyl)-3-methylpyridinium (Pham et al., 2009). Unlike Pham et al., however, Docherty et al. found 1-butyl-3-methylpyridinium bromide to be very poorly biodegradable: responsible for this was the different IL concentration, another parameter to be taken into account when testing (Docherty et al., 2007; Pham et al., 2009). Apart from imidazolium- and pyridinium-based ILs, alkylammonium salts were also tested in the context of biodegradation in activated sludge. The problem is that many quaternary ammonium salts possess biocidal properties. Nishiyama et al. found the salt form of trimethylamine, dimethylamine and methylamine as a result of biodegradation in the presence of activated sludge. They noticed that the biochemical oxygen consumption needed for the degradation of alkylammonium salts with long alkyl chains could reduce the antimicrobial activity. Despite this, however, the removal of dissolved organic matter was almost complete (Nishiyama et al., 1995). The influence of UV/H<sub>2</sub>O<sub>2</sub> peroxidation on the biodegradability of quaternary ammonium salts was also tested. Adams et al. found this pretreatment to be very effective only in the case of alkyl dimethylbenzyl ammonium chlorides, whereas with dioctyldimethyl ammonium



chloride there was no significant influence on biodegradability (Adams et al., 2000). It was shown that perfluorinated IL ions were more susceptible to biodegradation than halides (Gathergood & Scammells, 2002). Garcia et al. investigated the influence of imidazolium-based IL anions on their biodegradation. They found that the octyl sulphate anion was better biodegradable than hexafluorophosphate, bromide, tetrafluoroborate, and bis[(trifluoromethyl)sulphonyl]amide (Garcia et al., 2005). This was in agreement with the results of Gathergood et al. (Gathergood et al., 2006) but contradicted the results obtained in the same research group by Hartjani et al. These authors tested pyridinium ILs and did not find any significant influence of the octyl sulphate anion on IL biodegradability (Hartjani et al., 2008). It could be concluded that the anion on its own influences the biodegradability of ILs to a minimal degree, but if combined with some other cations may alter the susceptibility to biodegradation (Stolte et al., 2010). The results of comprehensive IL biodegradability studies are collated in several valuable papers and reviews (Gathergood et al., 2004; Garcia et al., 2005; Gathergood et al., 2006; Coleman & Gathergood, 2010; Stolte et al., 2010).

## 5. The fate and degradation of ILs in the environment

So far, the majority of ILs have been used in research laboratories, but before long they are going to be utilized in industry. Because of their potential toxicity, their behaviour and possibility to degradation in the environment are very important factors in risk assessments concerning their introduction as new industrial chemicals on to the market. Non-volatile ILs will inevitably pollute the soil, sediments and ground waters as a result of accidental spills, leaching of landfill sites or via effluents. Therefore, the sorption, biodegradability and (eco)toxicity of ILs play a very important role in their environmental fate.

Sorption has a critical effect on the transport, reactivity and bioavailability of organic compounds in the environment. Up till now, sorption studies have focused mainly on imidazolium-based salts. Several experiments have examined sorption to a variety of soils and sediments, indicating that these compounds are relatively strongly adsorbed (Matzke et al., 2009; Mrozik et al., 2009; Stepnowski, 2005; Stepnowski et al., 2007). The sorption ability and mobility of ILs in soil have been investigated in two ways: by batch testing or column leaching experiments. Using batch tests, the interactions of ILs involved in sorption, the strength of these interactions and the sorption capacity were studied on selected soils. The column leaching experiments investigated both the sorption and transport of ILs (Studziński et al., 2009). All the studies confirmed that the sorption mechanism is a combination of electrostatic interaction and physical sorption. However, the major type of interaction between soil and ILs is electrostatic. The highly negatively charged moieties on the surfaces of particles, e.g. of clay minerals, or on ionized carboxylic functional groups in biomolecules, are able to interact with the positively charged head group of ILs. However, van der Waals forces also play a significant role in sorption process. The content of clay, and to a small extent that of organic matter, elevates the sorption capacity of ILs in soil (Matzke et al., 2009; Stepnowski et al., 2007).

Lipophilicity and the side chain length of ILs are the main factors determining the rate of their transport through the soil matrix. Elongating the alkyl chain increases affinity for soil or sediment. Further, double layer sorption has been observed in the more hydrophobic, long-chain ILs. In contrast, the presence of a hydroxyl group in the alkyl chain causes the sorption ability of these ILs to be relatively poor (Mrozik et al., 2009).

Desorption of ILs is inversely correlated with sorption strength: strongly bound long-chain ILs are desorbed to a lesser extent than short-chain ones (Matzke et al., 2009; Stepnowski et al., 2007). This means that the transport of ILs in the environment will be strongly related to their hydrophilicity. Hydrophobic ILs in aquatic systems will be attenuated by sediments. In contrast, more mobile, hydrophilic contaminants released into the environment are likely to enter aquatic ecosystems. However, the anions present in the aqueous phase, with which certain cations form ion pairs, also affect phase transfer (Matzke et al., 2009; Stepnowski et al., 2007).

The presence of ILs in ground water will have an influence on living organisms, from bacteria to human beings. Therefore, the tests that investigate IL toxicity towards microorganisms, cells and animals, as well as their inhibitory effects upon enzymes, are of particular interest. IL toxicity towards aquatic organisms – *Lemna minor* (Larson et al., 2008), algae (Latała et al., 2005), the fresh water crustacean *Daphnia magna* (Bernot et al., 2005a), the fresh water snail *Physa acuta* (Bernot et al., 2005b), the zebra fish *Danio rerio* (Pretti et al., 2006) and the reef sponge (Kelman et al., 2001) – are discussed in detail by Pharm et al. (Pham et al., 2010). The results suggest that toxicity is correlated with the hydrophobicity of pyridinium-, imidazolium- and quaternary ammonium-based ILs. Moreover, pyridinium and imidazolium cations containing nitrogen-bearing rings are more toxic than quaternary ammonium cations (Couling et al., 2006).

The toxic effects of ILs on microorganisms in particular would limit their biodegradability. Studies analysing the biodegradability of ILs were reviewed in the previous chapter (Coleman & Gathergood, 2010; Gathergood et al., 2004; Gathergood et al., 2006; Garcia et al., 2005; Romero et al., 2008; Stolte et al., 2008).

Imidazolium-based ILs can also be partially degraded in aerobic aqueous solution inoculated with soil-bacteria (Kumar et al., 2006). Analysed by GC-MS, the breakdown products found after the 12-day degradation of 1-butyl-3-methylimidazolium tetrafluoroborate, degradation were  $m/z=97$  and  $m/z=124$ .

The poor biodegradability and (eco)toxicity of some ILs are reasons why we should prevent leakages of ILs to the environment by searching for effective means of removing and recovering them from wastewater and minimizing their presence in waste streams.

## 6. Conclusion

ILs are a very promising class of organic solvent, potentially useful in many different areas of the chemical industry. However, in view of their toxicity and poor biodegradability, they have so far played a marginal role in commercial technologies. We therefore need to look for such a technology using ILs that fulfils the criteria for a sustainable process. One of the aims of sustainable processes is the minimization of waste – in the case of ILs, this can be achieved by regenerating and recycling them after having been used in various processes, operations that extend their whole life cycle. More attention must therefore be paid to the recovery of ILs from wastewaters. Investigations should focus on searching for quick, simple, cost acceptable and effective methods. At the same time, there should be progress in wastewater treatment: advanced oxidative processes appear promising in this respect. However, oxidation studies have been carried out only with aqueous solutions of ILs, which are a much simpler matrix than an industrial effluent. In addition, more information on the transformation pathways during chemical, photochemical, electrochemical and biochemical

degradation processes is needed. The biodegradability and toxicity of the post-oxidation products of ILs are still unknown.

Regardless of the application, method of recovery and restoration of ILs, to the system, some of these compounds will sooner or later get into the environment as a result of uncontrolled leakage. The discharge of ILs into environment may cause soil and groundwater contamination. Therefore, the risk to human health and living organisms should be precisely assessed before ILs are used by industry. The growing number of studies of the biodegradability and (eco)toxicity of ILs indicates that they will probably be the first class of chemicals to have been thoroughly investigated from the ecological point of view prior to their application on an industrial scale. The study of the fate and behaviour of chemicals used by industry should be a basic criterion of environmental friendly processes. Additionally, this knowledge and the possibility of designing IL properties by changing the cation and/or anion, makes it possible to select less toxic and more biodegradable ILs for application.

## 7. Acknowledgments

Financial support was provided by Polish Ministry of Research and Higher Education under grant N N523 42 3737, BW 8270-5-0465-0, DS 8270-4-0093-10.

## 8. References

- Adams, C.D. & Kuzhikannil, J.J. (2000). Effects of UV/H<sub>2</sub>O<sub>2</sub> preoxidation on the aerobic biodegradability of quaternary amine surfactants. *Wat. Res.*, 34, 668-672, ISSN 0043-1354
- Amariei, D.; Courthéoux, L.; Rossignol, S. & Kappenstein, C. (2007). Catalytic and thermal decomposition of ionic liquid monopropellants using a dynamic reactor. Comparison of powder and sphere-shaped catalysts. *Chem. Eng. Process.*, 40, 165-174, ISSN 0255-2701
- Anouti, M.; Jones, J.; Jacquemin, J.; Caillon-Caravanier, M. & Lemordant, D. (2009). Aggregation behavior in water of new imidazolium and pyridinium alkylcarboxylates protic ionic liquids. *J. Coll. Inter. Scie.*, 340, 104-111, ISSN 0021-9797
- Barnes, A.S.; Rogers, E.I.; Streeter, I.; Aldous, L.; Hardacre, Ch.; Wildgoose, G.G.; Compton, R.G. (2008). Unusual voltammetry of the reduction of O<sub>2</sub> in [C<sub>4</sub>dmm][N(Tf)<sub>2</sub>] reveals a strong interaction of O<sub>2</sub>•<sup>-</sup> with the [C<sub>4</sub>dmm]<sup>+</sup> cation. *J. Phys. Chem. C*, 112, 13709-13715, ISSN 1932-7447
- Bailey, M.M.; Townsend, M.B.; Jernigan, P.L.; Sturdivant, J.; Hough-Troutman, W.L.; Rasco, J.F.; Swatoski, R.P.; Rogers R.D. & Hood R.D. (2008). Developmental toxicity assessment of the ionic liquid 1-butyl-3-methylimidazolium chloride in CD-1 mice. *Green Chem.*, 10, 1213-1217, ISSN 1463-9262
- Beaulieu, J.J.; Tank, J.L. & Kopacz, M. (2008). Sorption of imidazolium-based ionic liquids to aquatic sediments. *Chemosphere*, 70, 1320-1328, ISSN 0045-6535
- Bernot, R.J.; Brueske, M.A.; Evans-White, M.A. & Lamberti, G.A. (2005a). Acute and chronic toxicity of imidazolium-based ionic liquids on *Daphnia magna*. *Environ. Toxicol. Chem.*, 24, 87-92, ISSN 0730-7268

- Bernot, R.J.; Kennedy, E.E. & Lamberti, G.A. (2005b). Effects of ionic liquids on the survival, movement, and feeding behavior of the freshwater snail, *Physa acuta*. *Environ. Toxicol. Chem.*, 24, 1759–1765, ISSN 0730-7268
- Birdwell, J.F.; McFarlane, J.; Hunt, R.D.; Luo, H. & DePaoli, D.W. (2006). Separation of ionic liquid dispersions in centrifugal solvent extraction contactors. *Sep. Sci. Technol.*, 41, 2205–2223, ISSN 0149-6395
- Bridges, N.J.; Gutowski, K.E. & Rogers, R.D. (2007). Investig contemporaneous lyation of aqueous biphasic systems formed from solutions of chaotropic salts with kosmotropic salts (salt-salt ABS). *Green Chem.*, 9, 177–183, ISSN 1463-9262
- Buszewski, B. & Studzińska, S. (2008). A Review of ionic liquids in chromatographic and electromigration techniques. *Chromatographia*, 68, 1–10, ISSN 0009-5893
- Coleman, D. & Gathergood N. (2010). Biodegradation studies of ionic liquids. *Chem. Soc. Rev.*, 39, 600–637, ISSN 0306-0012
- Couling, D.J.; Bernot, R.J.; Docherty, K.M.; Dixon, J.K. & Maginn, E.J. (2006). Assessing the factors responsible for ionic liquid toxicity to aquatic organisms via quantitative structure–property relationship modeling. *Green Chem.*, 8, 82–90, ISSN 1463-9262
- Czerwicka, M.; Stolte, S.; Müller, A.; Siedlecka, E.M.; Gołębiowski, M.; Kumirska, J. & Stepnowski, P. (2009). Identification of ionic liquid breakdown products in an advanced oxidation system. *J. Hazard. Mater.*, 171, 478–483, ISSN 0304-3894
- Damiano, T.; Morton, D. & Nelson, A. (2007). Photochemical transformation of pyridinium salts: mechanistic studies and applications in synthesis. *Org. Biomol. Chem.*, 5, 2735–2752, ISSN 1477-0520
- Docherty, K.; Hebbeler, S.Z. & Kulpa Jr., C.F. (2006). An assessment of ionic liquid mutagenicity using the Ames Test. *Green Chem.*, 8, 560–567, ISSN 1463-9262
- Docherty, K.M.; Dixon, J.K. & Kulpa Jr, C.F. (2007). Biodegradability of imidazolium and pyridinium ionic liquids by an activated sludge microbial community. *Biodegradation*, 18, 481–493, ISSN 0923-9820,
- Dupont, J.; de Souza, R.F. & Suarez, P.A.Z. (2002). Ionic liquid (molten salt) phase organometallic catalysis. *Chem.Rev.*, 102, 3667–3692, ISSN 0009-2665
- Esquivel-Viveros, A.; Ponce-Vargas, F.; Esponda-Aguilar, P.; Prado-Barragán, L.A.; Gutiérrez-Rojas, M.; Lye, G.J. & Huerta-Ochoa, S. (2009). Biodegradation of [bmim][PF<sub>6</sub>] using *Fusarium* sp. *Revista Mexicana de Ingeniería Química*, 8, 163–168, ISSN 1665-2738
- European Union (2008). Directive 2008/98/EC of the European Parliament and of the Council of 19 November 2008 on waste and repealing certain Directives. *Official Journal of the European Communities*, 51(L312), 3–30
- Fernández, J.F.; Chilyumova, E.; Waterkamp, D. & Thöming, J. (2008). Ionic liquid recovery from aqueous solutions by cross-flow nanofiltration. *Proc. 10<sup>th</sup> World Filtration Congress*, Vol. II, 528–532.
- Fernández, J.F., Neumann, J. & Thöming, J. (2010). Regeneration, Recovery and Removal of Ionic Liquids. *Curr. Org. Chem* – in press, ISSN 1385-2728
- Freire, M.G.; Santos, L.M.N.B.F.; Fernandez A.M.; Coutinho, J.A.P. & Marrecho, I.M. (2007). An overview of the mutual solubility of water-imidazolium-based ionic liquids systems. *Fluid Phase Equilib.*, 261, 449–454, ISSN 0378-3812

- Freire, M.G.; Ventura, S.P.M.; Santos, L.M.N.B.F.; Marrucho, I.M. & Coutinho, J.A.P. (2008). Evaluation of COSMO-RS for the prediction of LLE and VLE of water and ionic liquids binary systems. *Fluid Phase Equilibr.*, 268, 74-84, ISSN 0378-3812
- Galiński, M.; Lewandowski, A. & Stepniak, I. (2006). Ionic liquids as electrolytes. *Electrochim. Acta*, 5567-5580, ISSN 0013-4686
- Garcia, M.T.; Gathergood, N. & Scammells, P.J. (2005). Biodegradable ionic liquids: Part II. Effect of the anion and toxicology. *Green Chem.*, 7, 9-14, ISSN: 1463-9262
- Gathergood, N. & Scammells, P.J. (2002). Design and Preparation of Room-Temperature Ionic Liquids Containing Biodegradable Side Chains. *Aust. J. Chem.*, 55, 9, 557-560, ISSN 0004-9425
- Gathergood, N.; Garcia, M.T. & Scammells, P.J. (2004). Biodegradable ionic liquids: Part I. Concept, preliminary targets and evaluation. *Green Chem.*, 6, 166-175, ISSN 1463-9262
- Gathergood, N.; Scammells, P.J. & Garcia, M.T. (2006). Biodegradable ionic liquids: Part III. The first readily biodegradable ionic liquids. *Green Chem.*, 8, 156-160, ISSN 1463-9262
- Gutowski, K.E.; Broker, G.A.; Willauer, H.D.; Huddleston, J.G.; Swatloski, R.P.; Holbrey, J.D. & Rogers, R.D. (2003). Controlling the aqueous miscibility of ionic liquids: aqueous biphasic systems of water-miscible ionic liquids and water-structuring salts for recycle, metathesis, and separations. *J. Am. Chem. Soc.*, 125, 6632-6633, ISSN 0002-7863
- Harjani, J.R.; Singer, R.D.; Garcia, M.T. & Scammells, P.J. (2008). The design and synthesis of biodegradable pyridinium ionic liquids. *Green Chem.*, 10, 436-438, ISSN: 1463-9262
- Hayashi, S. & Hamaguchi, H. (2004). Discovery of a magnetic ionic liquid [bmim]FeCl<sub>4</sub>. *Chem. Lett.*, 33, 1590-1591, ISSN 0366-7022
- Hoigne, J. (1989). Chemistry of aqueous ozone and transformation of pollutants by ozonation and advanced oxidation processes. In: Hrubec, J. (Ed.), *The Handbook of Environmental Chemistry*. Springer-Verlag, Berlin Heidelberg, 83-141, ISBN 1867-979X
- Islam, M.M. & Ohsako, T. (2008). Roles of ion pairing on electroreduction of dioxygen in imidazolium-cation-based room-temperature ionic liquid. *J. Phys. Chem. C*, 112, 1269-1275, ISSN 1932-7447
- Itakura, T.; Hirata, K.; Aoki, M.; Sasai, R.; Yoshida, H. & Itoh, H. (2009). Decomposition and removal of ionic liquid in aqueous solution by hydrothermal and photocatalytic treatment. *Environ. Chem. Lett.*, 7, 343-345, ISSN 1610-3653
- Jungnickel, Ch.; Łuczak J.; Ranke J.; Fernández J.F.; Müller A. & Thöming J. (2008). Micelle formation of imidazolium ionic liquids in aqueous solution *Colloid Surface A*, 316, 278-284 ISSN 0927-7757
- Katoh, R. & Takahashi, K. (2009). Photo-degradation of imidazolium ionic liquids. *Radiat. Phys. Chem.*, 78, 1126-1128, ISSN 0969-806X
- Kelman, D.; Kashman, Y.; Rosenberg, E.; Ilan, M.; Ifrach, I. & Loya, Y. (2001). Antimicrobial activity of the reef sponge *Amphimedon viridis* from the Red Sea: evidence for selective toxicity. *Aquat. Microb. Ecol.*, 24, 9-16, ISSN 0948-3055

- Kröckel, J. & Kragl, U. (2003). Nanofiltration for the separation of non-volatile products from solutions containing ionic liquids. *Chem. Eng. Technol.*, 26, 1166-1168, ISSN 0930-7516
- Kroon, M.C.; Buijs, W.; Peters, C.J. & Witkamp, G.J. (2006). Decomposition of ionic liquids in electrochemical processing. *Green Chem.*, 8, 241-245, ISSN 1463-9262
- Kroon, M.C.; Buijs, W.; Peters, C.J. & Witkamp, G.-J. (2007). Quantum chemical aided prediction of the thermal decomposition mechanisms and temperatures of ionic liquids. *Thermochim. Acta*, 465, 40-47, ISSN 0040-6031
- Kumar, S.; Ruth, W.; Sprenger, B. & Kragl, U. (2006). On the biodegradation of ionic liquid 1-butyl-3-methylimidazolium tetrafluoroborate. *Chim. Oggi*, 24, 24-26 ISSN 0392-839X
- Larson, J.H.; Frost, P.C. & Lamberti, G.A. (2008). Variable toxicity of ionic liquid-forming chemicals to Lemna minor and the influence of dissolved organic matter. *Environ. Toxicol. Chem.*, 27, 676-681, ISSN 0730-7268
- Latała, A.; Stepnowski, P.; Nędzi, M. & Mrozik, W. (2005). Marine toxicity assessment of imidazolium ionic liquids: acute effects on the Baltic algae *Oocystis submarina* and *Cyclotella meneghiniana*. *Aqua. Toxicol.*, 73, 91-98, ISSN 0166-445X
- Latała, A.; Nędzi, M. & Stepnowski, P. (2009a). Toxicity of imidazolium and pyridinium based ionic liquids towards algae. *Bacillaria paxillifer* (a microphytobenthic diatom) and *Phormidium amphibium* (a cyanobacterium). *Green Chem.*, 11, 1371-1376, ISSN 1463-9262
- Latała, A.; Nędzi, M. & Stepnowski, P. (2009b). Toxicity of imidazolium and pyridinium based ionic liquids towards algae. *Chlorella vulgaris*, *Oocystis submarina* (phytoplankton green algae) and *Cyclotella meneghiniana*, *Skeletonema marinoi* (diatoms). *Green Chem.*, 11, 580-588, ISSN 1463-9262
- Latała, A.; Nędzi, M. & Stepnowski, P. (2010). Toxicity of imidazolium ionic liquids towards algae. Influence of salinity variations. *Green Chem.*, 12, 60-64, ISSN 1463-9262
- Lee, S.H.; Ha, S.H.; You, C.Y. & Koo, Y.M. (2007). Recovery of magnetic ionic liquid [bmim]FeCl<sub>4</sub> using electromagnet. *Korean J. Chem. Eng.*, 24, 436-437, ISSN 0256-1115
- Li, X.; Zhao, J.; Li, Q.; Wang, L. & Tsang, S.C. (2007). Ultrasonic chemical oxidative degradation of 1,3-dialkylimidazolium ionic liquids and their mechanistic elucidation. *Dalton Trans.*, 19, 1875-1880, ISSN 1477-9226
- Liu, Y.; Zhang, S.; Yuang, J.; Shi, L. & Zheng, L. (2010). Dispersion of multiwalled carbon nanotubes by ionic liquid-type Gemini imidazolium surfactants in aqueous solution. *Colloids and Surfaces A: Physicichem. Eng. Aspects* 359, 66-70, ISSN: 0927-7757
- Łuczak J., Hupka J., Thöming J., Jungnickel, Ch., (2008). Self-organization of imidazolium ionic liquids in aqueous solution, *Colloids Surface A.*, 329, 125-133, ISSN 0927-7757
- Łuczak, J., Jungnickel, Ch.; Joskowska M., Thöming J., Hupka J. (2009). Thermodynamics of micellization of imidazolium ionic liquids in aqueous solutions. *Journal of Colloid and Interface Science*, 336, 111-116, ISSN 0021-9797
- Markiewicz, M.; Jungnickel, C.; Markowska, A.; Szczepaniak, U.; Paszkiewicz, M. & Hupka, J. (2009). 1-Methyl-3-octylimidazolium Chloride-Sorption and Primary Biodegradation Analysis In Activated Sewage Sludge. *Molecules*, 14, 4396-4405, ISSN 1420-3049

- Mathews, C.J.; Smith, P.J.; Welton & T. Palladium (2000). Catalysed Suzuki cross-coupling reactions in ambient temperature ionic liquids. *Chem. Commun.*, 14, 1249-1250, ISSN 1359-7345
- Matzke, M.; Thiele, K.; Müller, A. & Filser, J. (2009). Sorption and desorption of imidazolium based ionic liquids in different soil types. *Chemosphere*, 74 ,568-574, ISSN 0045-6535
- McFarlane, J.; Ridenour, W.B.; Luo, H.; Hunt, R.D. & DePaoli, D.W. (2005). Room temperature ionic liquids for separating organics from produced water. *Sep. Sci. Technol.*, 40, 1245-1265, ISSN 0149-6395
- Minami, I. (2009). Ionic liquids in tribology. *Molecules*, 14, 2286-2305, ISSN: 1420-3049
- Morawski, A.W.; Janus, M.; Goc-Maciejewska, I.; Syguda, A. & Pernak, J. (2005). Decomposition of Ionic Liquids by Photocatalysis. *Polish J. Chem.*, 79, 1929-1935, ISSN 0137-5083
- Mrozik, W.; Jungnickel, Ch.; Skup, M.; Urbaszek, P. & Stepnowski, P. (2008a). Determination of the adsorption mechanism of imidazolium-type ionic liquids onto kaolinite: implications for their fate and transport in the soil environment. *Environ Chem.*, 5, 299-306, ISSN 1448-2517
- Mrozik, W.; Nichthauser, J. & Stepnowski, P. (2008b). Prediction of the adsorption coefficients for imidazolium ionic liquids in soils using cyanopropyl stationary phase. *Pol. J. Environ. Stud.*, 17, 383-388, ISSN 1230-1485
- Mrozik, W.; Jungnickel, Ch.; Ciborowski, T.; Pitner, W.R.; Kumirska, J.; Kaczyński, Z. & Stepnowski, P. (2009). Predicting mobility of alkylimidazolium ionic liquids in soils. *J. Soils Sediments*, 9, 237-245, ISSN 1439-0108
- Nishiyama, N.; Toshima, Y. & Ikeda, Y. (1995). Biodegradation of alkyltrimethylammonium salts in activated sludge. *Chemosphere*, 30, 593-603, ISSN 0045-6535,
- Ohtani, H.; Ishimura, S.; & Kumai, M. (2008). Thermal decomposition behaviors of imidazolium-type ionic liquids studied by pyrolysis-gas chromatography. *Anal. Sci.*, 24, 1335-1340, ISSN 0910-6340
- Oxley, J.D.; Prozorow, T. & Suslick, K.S. (2003). Sonochemistry and Sonoluminescence of Room-Temperature Ionic Liquids. *J. Am. Chem. Soc.*, 125, 37, 11138-11139, ISSN 0002-7863
- Palomar, J.; Lemus, J.; Gilarranz, M.A. & Rodriguez, J.J. (2009). Adsorption of ionic liquids from aqueous effluents by activated carbon. *Carbon*, 47, 1846-1856, ISSN: 0008-6223
- Pernak, J.; Sobaszekiewicz, K. & Mirska, I. (2003). Anti-microbial activities of ionic liquids. *Green Chem.*, 5, 52-56, ISSN 1463-9262
- Pernak, J. & Branicka, M. (2004). Synthesis and aqueous ozonation of some pyridinium salts with alkoxyethyl and alkylthiomethyl hydrophobic groups. *Ind. Eng. Chem. Res.*, 43, 1966-1974, ISSN 0888-5885
- Pham, T. P. T.; Cho, C.-W. & Yun, Y.-S. (2007). Ecotoxicological Effects and Biodegradability of Ionic Liquids Associated with Imidazolium and Pyridinium Cations. *Applied Chemistry*, 11, 105-108
- Pham, T. P. T.; Cho, C.-W.; Jeon, C.-O.; Chung, Y.-J.; Lee, M.-W. & Yun, Y.-S. (2009). Identification of Metabolites Involved in the Biodegradation of the Ionic Liquid 1-

- Butyl-3-methylpyridinium Bromide by Activated Sludge Microorganisms. *Environ. Sci. Technol.*, 43, 516-521, ISSN 0013-936X
- Pham, T. P. T.; Cho, Ch.-W.; Yun, Y.-S. (2010). Environmental fate and toxicity of ionic liquids: A review. *Wat. Res.*, 44, 352-372, ISSN 0043-135
- Pretti, C.; Chiappe, C.; Pieraccini, D.; Gregori, M.; Abramo, F.; Monni, G. & Intorre, L. (2006). Acute toxicity of ionic liquids to the zebrafish (*Danio rerio*). *Green Chem.*, 8, 238-240, ISSN 1463-9262
- Ranke, J.; Mölter, K.; Stock, F.; Bottin-Weber, U.; Poczbott, J.; Hoffmann, J.; Ondruschka, B.; Filser, J. & Jastorff, B. (2003). Biological effects of imidazolium ionic liquids in acute (*Vibrio fischeri*) and WST1 cell viability assays. *Ecotox. Environ. Safety*, 28, 396-404, ISSN 0147-6513
- Rickert, P. G.; Stępiński, D. C.; Rausch, D. J.; Bergeron, R. M.; Jakab, S. & Dietz, M.L. (2007). Solute-induced dissolution of hydrophobic ionic liquids in water. *Talanta*, 72, 315-320, ISSN 0039-9140
- Romero, A.; Santos, A.; Tojo, J. & Rodríguez, A. (2008). Toxicity and biodegradability of imidazolium ionic liquids. *J. Hazard. Mater.*, 151, 268-273, ISSN 0304-3894
- Siedlecka, E.M.; Gołbiowski, M.; Kumirska, J. & Stepnowski, P. (2008a). Identification of 1-butyl-3-methylimidazolium chloride degradation products formed in Fe(III)/H<sub>2</sub>O<sub>2</sub> oxidation system. *Chem. Anal. (Warsaw)*, 53, 943-951, ISSN 0009-2223
- Siedlecka, E.M.; Mroziński, W.; Kaczyński, Z. & Stepnowski, P. (2008b). Degradation of 1-butyl-3-methylimidazolium chloride ionic liquid in a Fenton-like system. *J. Hazard. Mater.*, 154, 893-900, ISSN 0304-3894
- Siedlecka, E.M.; Gołbiowski, M.; Kaczyński, Z.; Czupryniak, J.; Ossowski, T. & Stepnowski, P. (2009). Degradation of ionic liquids by Fenton reaction; the effect of anions as counter and background ions. *Appl. Cat. B: Environmental*, 91, 573-579, ISSN 0926-3373
- Siedlecka, E.M. & Stepnowski, P. (2009). The effect of alkyl chain length on the degradation of alkylimidazolium- and pyridinium-type ionic liquids in a Fenton-like system. *Environ. Sci. Pollut. Res.*, 16, 453-458, ISSN 0944-1344
- Siedlecka, E.M.; Czerwica, M.; Stolte, S.; Stepnowski, P.; (2010). Stability of Ionic Liquids in Application Conditions. *Curr. Org. Chem* - in press, ISSN: 1385-2728
- Siriex-Plener, J.; Gaillon, L. & Letellier, P. (2004). Behaviour of a binary solvent mixture constituted by the amphiphilic ionic liquid 1-decyl-3-methylimidazolium bromide and water. Potentiometric and conductometric studies. *Talanta*, 63, 979- 986, ISSN 0039-9140
- Składanowski, A.C.; Stepnowski, P.; Kleszczyński, K. & Dmochowska, B. (2005). AMP deaminase in vitro inhibition by xenobiotics. A potential molecular method for risk assessment of synthetic nitro- and polycyclic musks, imidazolium ionic liquids and N-glucopyranosyl ammonium salts. *Environ. Toxicol. Pharmacol.*, 19, 291-296, ISSN:1382-6689
- Stasiewicz, M.; Mulkiewicz, E.; Tomczak-Wandzel, R.; Kurmirska, J.; Siedlecka, E.M.; Gołbiowski, M.; Gajdus, J.; Czerwica, M. & Stepnowski, P. (2008). Assessing toxicity and biodegradation of novel, environmentally benign ionic liquids (1-



- alkoxymethyl-3-hydroxypyridinium chloride, saccharine and acesulfamates) on cellular and molecular level. *Ecotox. Environ. Saf.*, 71, 157–165, ISSN 0147-6513
- Stepnowski, P.; Skladanowski, A.C.; Ludwiczak, A. & Łączyńska, E. (2004). Evaluating the Cytotoxicity of Ionic Liquids Using Human Cell Line HeLa. *Human Exp. Toxicol.*, 23, 513-517, ISSN 0960-3271
- Stepnowski, P. & Zaleska, A. (2005). Comparison of different advanced oxidation processes for degradation of room temperature ionic liquids. *Photochem. Photobiol.*, 170, 45-50, ISSN 0031-8655
- Stepnowski, P. (2005). Preliminary assessment of the sorption of some alkyl imidazolium cations as used in ionic liquids to soils and sediments. *Aust. J. Chem.*, 58, 170-173, ISSN: 0004-9425
- Stepnowski, P.; Mrozik, W. & Nichthauser, J. (2007). Adsorption of alkylimidazolium and alkylpyridinium ionic liquids onto natural soils. *Environ. Sci. Technol.*, 41, 511-516, ISSN 0013-936X
- Stock, F.; Hoffman, J.; Ranke, J.; Stormann, R.; Ondruschka, B. & Jastorff, B. (2005). Effects of ionic liquids on the acetylcholinesterase - a structure-activity relationship consideration. *Green Chem.*, 6, 286-290, ISSN 1463-9262
- Stolte, S.; Abdulkarim, S.; Arning, J.; Blomeyer-Nienstedt, A.-K.; Bottin-Weber, U.; Matzke, M.; Ranke, J.; Jastorff, B. & Thöming, J. (2008). Primary biodegradation of ionic liquid cations, identification of degradation products of 1-methyl-3-octylimidazoliumchloride and electrochemical wastewater treatment of poorly biodegradable compounds. *Green Chem.*, 10, 214-224, ISSN 1463-9262
- Stolte, S.; Steudte, S.; Igartua, A. & Stepnowski, P. (2010). The biodegradation of ionic liquids - the view from a chemical structure perspective. *Curr. Org. Chem.* - in press, ISSN 1385-2728
- Studzińska, S.; Kowalkowski, T. & Buszewski, B. (2009). Study of ionic liquid cations transport in soil. *J. Hazard. Mater.*, 168, 1542-1547, ISSN 0304-3894
- Swatloski, R.P.; Holbrey, J.D. & Rogers, R.D. (2003). Ionic liquids are not always green: hydrolysis of 1-butyl-3-methylimidazolium hexafluorophosphate. *Green Chem.*, 5, 361-363, ISSN 1463-9262
- Swatloski, R.P.; Holbrey, J.D.; Memon, S.B.; Caldwell, G.A.; Caldwell, K.A. & Rogers, R.D. (2004). Using *Caenorhabditis elegans* to probe toxicity of 1-alkyl-3-methylimidazolium chloride based ionic liquids. *Chem. Commun.*, 6, 668-669.
- Uerdingen, M.; Treber, C.; Balser, M.; Schmitt, G. & Werner, Ch. (2005). Corrosion behavior of ionic liquids. *Green Chem.*, 7, 321-325, ISSN 1463-9262
- Vijayaraghavan, K.; Pham, T.P.T.; Cho, C.-W.; Won, S.W.; Choi, S. B.; Mao, J.; Kim, S.; Kim, Y.-R.; Chung, B.W. & Yun, Y.-S. (2009). An assessment on the interaction of a hydrophilic ionic liquid with different sorbents. *Ind. Eng. Chem. Res.*, 48, 7283-7288, ISSN 0888-5885
- Walling, C. (1975). Fenton's reagent revisited. *Acc. Chem. Res.*, 8, 125-131, ISSN 0001-4842
- Wasscheid P. & Welton T. (2003). Some liquids in synthesis, Wiley-VCH, Weinheim
- Welton, T. (1999). Room temperature ionic liquids. Solvents for synthesis and catalysis. *Chem. Rev.*, 99, 2071-2083, ISSN 0009-2665

- Wooster, T.J.; Johanson, K.M.; Fraser, K.J.; MacFarlane, D.R. & Scott, J.L. (2006). Thermal degradation of cyano containing ionic liquids. *Green Chem.*, 8, 691-696, ISSN 1463-9262
- Wu, B.; Zhang, Y.M. & Wang, H.P. (2009). Non-equilibrium thermodynamic analysis of transport properties in the nanofiltration of ionic liquid-water solutions. *Molecules*, 14, 1781-1788, ISSN 1420-3049

# Progress in Paramagnetic Ionic Liquids

Yukihiro Yoshida and Gunzi Saito

*Meijo University*

*Japan*

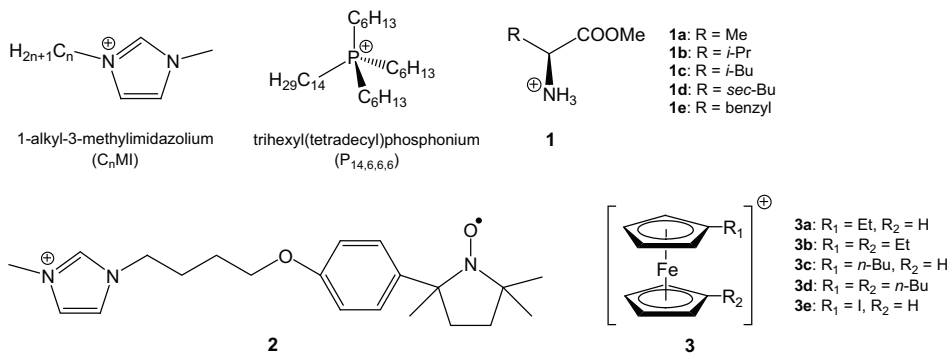
## 1. Introduction

Ionic liquids are entirely composed of ions as the name implies, and melt below room temperature (RT) or 100 °C. The ionic character means the extraordinary high ion density (i.e., the order of a molarity), and thus results in the negligible vapor pressure (i.e., wide liquid temperature region and negligible flammability) and high ionic conductivity. Such special fascinations attract considerable attention of researchers in many fields, as promising greener alternatives to the volatile molecular solvents for many areas of synthetic, separation, and electrochemical applications (Wasserscheid & Keim, 2000; Dupont et al., 2002; Buzzeeo et al., 2004; Armand et al., 2009; Yoshida & Saito, 2010). Although ionic liquids have been known for nearly a century (Walden, 1914; Gabriel & Weiner, 1888), efforts in exploring new and more versatile ionic liquids have only recently been devoted, after the discovery of the first water- and air-stable RT ionic liquids formed with 1-ethyl-3-methylimidazolium ( $C_2MI$ ; Scheme 1) cation reported by Wilkes and Zaworotko (Wilkes & Zaworotko, 1992), and Cooper and O'Sullivan (Cooper & O'Sullivan, 1992), in 1992. The majority of existing ionic liquids is composed of organic quaternary cations (e.g., 1,3-dialkylimidazolium, *N*-alkylpyridinium, and tetraalkylphosphonium) and inorganic small anions (e.g.,  $BF_4^-$ ,  $PF_6^-$ , and  $AlCl_4^-$ ), for which monovalent ions are favorable for stabilizing the liquid state because of the depressed interionic Coulomb interactions. In general, cations are responsible for reducing the melting point, and therefore, low-symmetrical hetero cations with well-delocalized charge and/or long alkyl group(s) have been used.

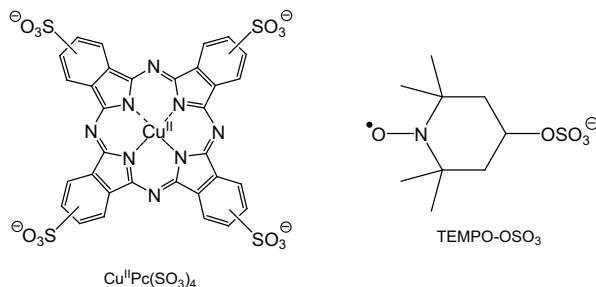
On the other hand, the selection of anions can readily tailor the liquid properties and introduce the desired functionalities. For example, the combination with  $PF_6^-$  and  $(CF_3SO_2)_2N^-$  (bis(trifluoromethanesulfonyl)amide;  $Tf_2N^-$ ) anions gives the hydrophobic ionic liquids (Bonhôte et al., 1996; Suarez et al., 1998), and  $CH_3COO^-$  and  $EtOSO_3^-$  anions stabilize the liquid state even at low temperatures (Wilkes & Zaworotko, 1992; Holbrey et al., 2002; Borra et al., 2007). These properties could find a range of synthetic and separation applications. In relation,  $HCOO^-$  and  $(MeO)(R)PO_2^-$  ( $R = H, Me, MeO$ ) anions give ionic liquids, which can solubilize cellulose (Fukaya et al., 2006; Fukaya et al., 2008).  $BF_4^-$ ,  $Tf_2N^-$  and  $(FSO_2)_2N^-$  anions give ionic liquids with a wide electrochemical window, which opens the applicative way for electrolytes of capacitors, lithium ion batteries, field-effect transistors, and electrodeposition (Bonhôte et al., 1996; Fuller et al., 1997; Sato et al., 2004; Zein El Abedin et al., 2005; Matsumoto et al., 2006; Ono et al., 2009). Highly conducting ionic liquids formed with  $N(CN)_2^-$ ,  $C(CN)_3^-$ , and  $B(CN)_4^-$  anions have served as electrolytes for dye-sensitized solar cells (MacFarlane et al., 2001; Wang et al., 2003; Yoshida et al., 2004; Kawano et al., 2004; Wang et al., 2005; Kuang et al., 2006; Yoshida et al., 2007a; Yoshida et al., 2007b).

Recently, a new class of functional ionic liquids, in which chemically synthesized organic or metal complex ions are largely responsible for the functionality, is starting to attract interest, and some reviews on catalytic, pharmaceutical and energetic properties have been published (Fei et al., 2006; Singh et al., 2006; Hough & Rogers, 2007; Smiglak et al., 2007). Such component ions allow the fine and dual tuning of liquid properties of the resulting ionic liquids, by the chemical modification of both cation and anion. In this review, we focus on developments of the functional ionic liquids, especially composed of magneto-active inorganic and organic ions.

### Cations



### Anions



Scheme 1. Component ions in this chapter.

## 2. Magneto-active anions

### 2.1 Inorganic anions containing iron

In most cases, a certain functionality of anions can be passed to the resulting ionic liquid when the interionic interaction has little impact on the functionality. Magneto-active metal complex anions, such as  $Fe^{III}X_4^-$  (X: Cl, Br) (Yoshida et al., 2005a; Yoshida et al., 2005b; Yoshida & Saito, 2006; Del Sesto et al., 2008; Li et al., 2009),  $Mn^{II}X_4^{2-}$  (X: Cl, Br) (Del Sesto et al., 2008; Pitula & Mudring, 2010),  $Mn^{II}(Tf_2N)_3^-$  (Pitula & Mudring, 2010),  $Co^{II}X_4^{2-}$  (X: Cl, NCS, NCSe, N(CN)<sub>2</sub>) (Del Sesto et al., 2005; Del Sesto et al., 2008; Peppel et al., 2010),  $Gd^{III}Cl_6^{3-}$  (Del Sesto et al., 2008), and  $Dy^{III}(SCN)_{8-x}(H_2O)_x^{(5-x)-}$  (x: 0–2) (Mallick et al., 2008) anions, have been known to form

paramagnetic RT ionic liquids, by pairing with organic quaternary cations. Paramagnetic ionic liquids, whose magnetic properties were given in the literatures, are listed in Table 1. Many of them can be obtained simply by mixing the halide salt and neutral metal halide; for example, dark brown ionic liquids  $[C_nMI][FeCl_4]$  are formed by mixing exactly equimolar crystalline  $[C_nMI]Cl$  and  $FeCl_3$  under inert atmosphere at RT (Yoshida et al., 2005b). This procedure dispenses with the need for reaction solvent and ion exchange process.

Cation	Anion	$T_m$ (°C)	$\mu_{eff}$ ( $\mu_B$ ) <sup>c</sup>	References
$C_2MI$ (+1)	<b>Fe<sup>III</sup>Cl<sub>4</sub></b> (-1)	18	5.83	Yoshida et al., 2005b
$C_4MI$ (+1)	<b>Fe<sup>III</sup>Cl<sub>4</sub></b> (-1)	-88 ( $T_g$ )	5.80	Yoshida & Saito, 2006
$C_6MI$ (+1)	<b>Fe<sup>III</sup>Cl<sub>4</sub></b> (-1)	-86 ( $T_g$ )	5.85	Yoshida & Saito, 2006
$C_8MI$ (+1)	<b>Fe<sup>III</sup>Cl<sub>4</sub></b> (-1)	-84 ( $T_g$ )	5.85	Yoshida & Saito, 2006
$C_{10}MI$ (+1)	<b>Fe<sup>III</sup>Cl<sub>4</sub></b> (-1)	-81 ( $T_g$ )	5.66	Del Sesto et al., 2008
$P_{14,6,6,6}$ (+1)	<b>Fe<sup>III</sup>Cl<sub>4</sub></b> (-1)	-71 ( $T_g$ )	5.89	Del Sesto et al., 2008
1a (+1)	<b>Fe<sup>III</sup>Cl<sub>4</sub></b> (-1)	-48 ( $T_g$ )	5.59	Li et al., 2009
1b (+1)	<b>Fe<sup>III</sup>Cl<sub>4</sub></b> (-1)	-45 ( $T_g$ )	5.56	Li et al., 2009
1d (+1)	<b>Fe<sup>III</sup>Cl<sub>4</sub></b> (-1)	-41 ( $T_g$ )	5.52	Li et al., 2009
1e (+1)	<b>Fe<sup>III</sup>Cl<sub>4</sub></b> (-1)	-31 ( $T_g$ )	5.66	Li et al., 2009
$C_4MI$ (+1)	<b>Fe<sup>III</sup>Br<sub>4</sub></b> (-1)	-83 ( $T_g$ )	5.73	Yoshida & Saito, 2006
$C_6MI$ (+1)	<b>Fe<sup>III</sup>Br<sub>4</sub></b> (-1)	-82 ( $T_g$ )	5.75	Yoshida & Saito, 2006
$C_8MI$ (+1)	<b>Fe<sup>III</sup>Br<sub>4</sub></b> (-1)	-81 ( $T_g$ )	5.84	Yoshida & Saito, 2006
$P_{14,6,6,6}$ (+1)	<b>Mn<sup>II</sup>Cl<sub>4</sub></b> (-2)	-69 ( $T_g$ )	5.81	Del Sesto et al., 2008
$C_4MI$ (+1)	<b>Mn<sup>II</sup>Br<sub>4</sub></b> (-2)	< RT <sup>b</sup>	5.84	Del Sesto et al., 2008
$P_{14,6,6,6}$ (+1)	<b>Co<sup>II</sup>Cl<sub>4</sub></b> (-2)	-68 ( $T_g$ )	4.45	Del Sesto et al., 2008
$P_{14,6,6,6}$ (+1)	<b>Co<sup>II</sup>[N(CN)<sub>2</sub>]<sub>4</sub></b> (-2)	-70 ( $T_g$ )	4.23 <sup>d</sup>	Del Sesto et al., 2005
$C_4MI$ (+1)	<b>Co<sup>II</sup>(NCS)<sub>4</sub></b> (-2)	-61 ( $T_g$ )	4.40	Peppel et al., 2010
$P_{14,6,6,6}$ (+1)	<b>Co<sup>II</sup>(NCS)<sub>4</sub></b> (-2)	-72 ( $T_g$ )	4.06	Del Sesto et al., 2008
$P_{14,6,6,6}$ (+1)	<b>Gd<sup>III</sup>Cl<sub>6</sub></b> (-3)	< RT	7.86	Del Sesto et al., 2008
$C_6MI$ (+1)	<b>Dy<sup>III</sup>(NCS)<sub>6</sub>(H<sub>2</sub>O)<sub>2</sub></b> (-3)	-56 ( $T_g$ )	10.4	Mallick et al., 2008
$C_6MI$ (+1)	<b>Dy<sup>III</sup>(NCS)<sub>7</sub>(H<sub>2</sub>O)</b> (-4)	-58 ( $T_g$ )	10.6	Mallick et al., 2008
$C_6MI$ (+1)	<b>Dy<sup>III</sup>(NCS)<sub>8</sub></b> (-5)	-60 ( $T_g$ )	10.4	Mallick et al., 2008
$C_4MI$ (+1)	<b>TEMPO-OSO<sub>3</sub></b> (-1)	-27 ( $T_g$ )	1.73	Yoshida et al., 2007c
$C_6MI$ (+1)	<b>TEMPO-OSO<sub>3</sub></b> (-1)	-27 ( $T_g$ )	1.68	Yoshida et al., 2007c
$C_8MI$ (+1)	<b>TEMPO-OSO<sub>3</sub></b> (-1)	-31 ( $T_g$ )	1.61	Yoshida et al., 2007c
$P_{14,6,6,6}$ (+1)	<b>Co<sup>II</sup>(DBSQ)<sub>2</sub>(bpy(COO)<sub>2</sub>)</b> (-2)	-11 ( $T_g$ )	3.60	Yoshida et al., 2009
<b>2</b> (+1)	<b>Tf<sub>2</sub>N</b> (-1)	-37 ( $T_g$ )	1.75	Uchida et al., 2009
<b>2</b> (+1)	<b>BF<sub>4</sub></b> (-1)	-32 ( $T_g$ )	1.75	Uchida et al., 2009
<b>2</b> (+1)	<b>PF<sub>6</sub></b> (-1)	-22 ( $T_g$ )	1.69	Uchida et al., 2009
<b>3a</b> (+1)	<b>Tf<sub>2</sub>N</b> (-1)	3.8	2.33	Inagaki & Mochida, 2010
<b>3b</b> (+1)	<b>Tf<sub>2</sub>N</b> (-1)	1.0	2.17	Inagaki & Mochida, 2010

<sup>a</sup> Numbers in parentheses are valences of ions. Bold ions are responsible for the magnetic behavior.  $T_m$ : melting temperature,  $T_g$ : glass transition temperature,  $\mu_{eff}$ : effective magnetic moment.

<sup>b</sup> In a more recent paper (Pitula & Mudring, 2010),  $T_g$  = -50 °C and  $T_m$  = 44 °C.

<sup>c</sup> Measured at RT (25–27 °C).

<sup>d</sup> Private communication from Dr. Del Sesto.

Table 1. Characteristics of paramagnetic RT ionic liquids<sup>a</sup>

Effective magnetic moments ( $\mu_{\text{eff}}$ ), represented by  $g[S(S+1)]^{1/2}\mu_{\text{B}}$ , of  $[\text{C}_n\text{MI}][\text{FeCl}_4]$  were estimated to be the range of 5.66–5.89  $\mu_{\text{B}}$  at 25 °C, which are close to that expected for a paramagnetic  $S = 5/2$  high-spin on  $\text{Fe}^{\text{III}}$  ions (spin-only value: 5.92  $\mu_{\text{B}}$ ). The temperature dependency simply follows the Curie law in their liquid region, whereas their solid states at low temperatures show the pronounced deviation from the Curie law due to the antiferromagnetic interactions (Figure 1). In particular,  $[\text{C}_0\text{MI}][\text{FeCl}_4]$ ,  $[\text{C}_2\text{MI}][\text{FeCl}_4]$ , and  $[\text{C}_2\text{MI}][\text{FeBr}_4]$  exhibited long-range antiferromagnetic ordering at 9.5, 4.2, and 12.5 K, respectively (Yoshida et al., 2005b; Yoshida & Saito, 2006).

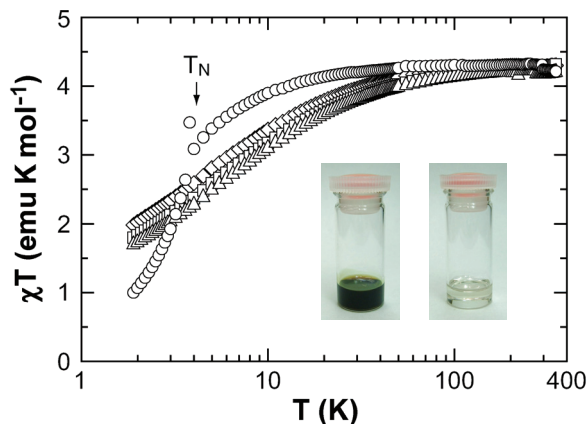


Fig. 1. Temperature dependence of the product of static susceptibility and temperature ( $\chi T$ ) for  $[\text{C}_n\text{MI}][\text{FeCl}_4]$  in an applied field of 100 Oe on heating process ( $\circ$ :  $n = 2$ ,  $\Delta$ :  $n = 4$ ,  $\square$ :  $n = 6$ , and  $\diamond$ :  $n = 8$ ). An arrow indicates the Néel temperature ( $T_N$ ). The inset is the photographs of  $[\text{C}_2\text{MI}][\text{FeCl}_4]$  (left) and  $[\text{C}_2\text{MI}][\text{GaCl}_4]$  (right) (Yoshida et al., 2005b).

Among the paramagnetic ionic liquids,  $[\text{C}_2\text{MI}][\text{FeCl}_4]$  having a melting point ( $T_m$ ) of 18 °C has the highest ionic conductivity of  $2.0 \times 10^{-2} \text{ S cm}^{-1}$  and lowest viscosity of 18 cP at 25 °C (Yoshida et al., 2005b). These values are comparable to those of  $[\text{C}_2\text{MI}][\text{Ga}^{\text{III}}\text{Cl}_4]$  with non-magnetic  $\text{Ga}^{\text{III}}\text{Cl}_4$  anion ( $2.2 \times 10^{-2} \text{ S cm}^{-1}$  and 16 cP at 25 °C) (Yoshida et al., 2005b). It appears that the small size and monovalency of both component ions, as well as the charge-delocalized low-symmetrical  $\text{C}_2\text{MI}$  cation, are factors governing the high ion diffusivity.  $[\text{C}_0\text{MI}][\text{FeCl}_4]$  containing smaller  $\text{C}_0\text{MI}$  cation is not in liquid state but crystalline solid at RT ( $T_m = 103$  °C), and the  $\text{C}_2\text{MI}$  salt with  $\text{Fe}^{\text{II}}\text{Cl}_4$  dianion,  $[\text{C}_2\text{MI}]_2[\text{Fe}^{\text{II}}\text{Cl}_4]$ , is also in solid state at RT ( $T_m = 86$  °C). The crystalline solid  $[\text{C}_2\text{MI}]_2[\text{Fe}^{\text{II}}\text{Cl}_4]$ , whose crystal structure was determined by a synchrotron X-ray powder diffraction measurement (Yoshida et al., 2005b), is isostructural to the reported  $[\text{C}_2\text{MI}]_2[\text{Co}^{\text{II}}\text{Cl}_4]$  ( $T_m = 100$ – $102$  °C) and  $[\text{C}_2\text{MI}]_2[\text{Ni}^{\text{II}}\text{Cl}_4]$  ( $T_m = 92$ – $93$  °C) (Hitchcock et al., 1993). As seen in Figure 2, each  $\text{C}_2\text{MI}$  cation is connected with three  $\text{Fe}^{\text{II}}\text{Cl}_4$  dianions through hydrogen bonding type interactions. The shortest distance was found for  $\text{C}(2)\text{--H}\cdots\text{Cl}$  (3.261 Å), presumably associated with the high acidic character of the 2-hydrogen.

Dual functionalities, namely the paramagnetism and chiral discrimination ability, were recently realized by the combination with the chiral protonated L-amino acid methyl esters (**1**; Scheme 1) (Li et al., 2009). Their RT magnetic moments (5.52–5.66  $\mu_{\text{B}}$ ) are comparable to those of  $[\text{C}_n\text{MI}][\text{FeCl}_4]$ , and the salt composed of phenylalanine-derivative **1e** shows a

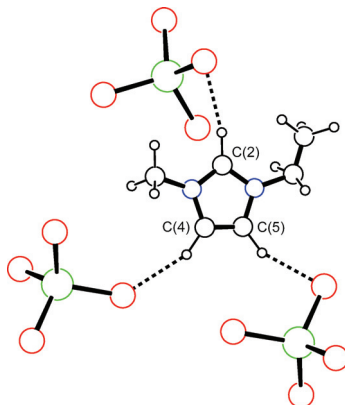


Fig. 2. Interionic contacts between  $C_2MI$  cation and  $Fe^{III}Cl_4$  dianion in  $[C_2MI]_2[FeCl_4]$ . Short  $C-H \cdots Cl$  contacts are shown by dashed lines. The crystal structure was determined by a synchrotron X-ray powder diffraction measurement (Yoshida et al., 2005b).

positive circular dichroism band at 218 nm with a maximum of  $2.4 \times 10^{-2}$  deg. Luminescence study using several chiral analytes revealed that the salt composed of alanine-derivative **1a** has a chiral discrimination ability. Future works may be to synchronize the dual functionalities, such as chiral extraction and enrichment of chiral compounds by applying the magnetic field.

As seen in Figure 3, the ionic conductivity and viscosity are under the control of the alkyl chain length of  $C_nMI$  cations and on the sort of halide of  $Fe^{III}X_4$  anions (Yoshida & Saito, 2006). The elongation of alkyl chain results in the increased ion size and interionic van der Waals interactions, both of which modify the ion diffusivity in the unfavorable direction. Replacing the chloride to bromide also results in the significant decrease in ion diffusivity, possibly due to the increased ion size and interionic interactions. The replacement leads to the slight decrease in  $\mu_{eff}$ , as a consequence of the lower ligand field strength  $\Delta$  in  $FeBr_4$  anion as  $\mu_{eff} = \mu_0(1 - 2\lambda/\Delta)$ , where  $\mu_0$  is the spin-only value and  $\lambda$  is the spin-orbit coupling constant at  $FeX_4$  anions.

Ionic liquids whose magnetic properties extend far beyond that of the existing ones may be those with the pronounced response to the external stimuli and with the pronounced magnetic interactions including long-range magnetic ordering. The former type of ionic liquids will be described later. For the latter, it seems that the combination of magneto-active cations and anions or the use of multinuclear metal complex (metal cluster) ions is effective to enhance the magnetic interactions. Although not strictly an "ionic" liquid, the extreme example may be the successful preparation of superparamagnetic liquid, in which maghemite ( $\gamma\text{-Fe}_2\text{O}_3$ ) nanoparticles with 4 nm in diameter are chemically modified by silyl-containing quaternary cations (Bourlinos et al., 2005). The dark brown liquid may be regarded as a new type of magnetic fluid, namely solvent-free colloidal dispersion of nanoparticles. Magnetorheological fluids, whose rheological behavior can be controlled by the applied magnetic field, were obtained by dispersing 25 wt% micrometer-sized magnetite ( $Fe_3O_4$ ;  $< 5 \mu m$ ) particles in ionic liquids (Guerrero-Sanchez et al., 2007). The use of  $[C_4MI][PF_6]$  leads to a colloidal dispersion that is remarkably stable against aggregation over a period of 2 months.

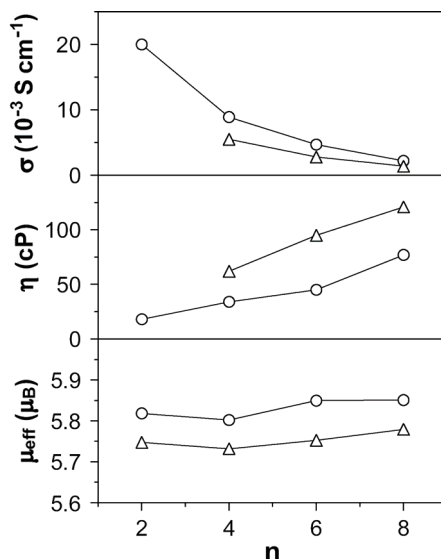


Fig. 3. Dependence of ionic conductivity ( $\sigma$ ), viscosity ( $\eta$ ), and effective magnetic moment ( $\mu_{\text{eff}}$ ) on alkyl chain length in the  $C_n\text{MI}$  cations for  $[C_n\text{MI}][\text{FeCl}_4]$  (○) and  $[C_n\text{MI}][\text{FeBr}_4]$  (Δ) salts (Yoshida et al., 2005b; Yoshida & Saito, 2006).

## 2.2 Inorganic anions containing other transition metals

For the divalent anions such as  $\text{Co}^{\text{II}}\text{Cl}_4^{2-}$ , twice molar amount of halide salts of exceptionally bulky monocations such as trihexyl(tetradecyl)phosphonium ( $\text{P}_{14,6,6,6}$ ; Scheme 1) would be necessary to realize RT ionic liquids such as  $[\text{P}_{14,6,6,6}]_2[\text{CoCl}_4]$  (glass transition  $T_g = -68^\circ\text{C}$ ) (Del Sesto et al., 2008). Its analogous  $[\text{C}_2\text{MI}]_2[\text{CoCl}_4]$  is in solid state at RT, and shows a melting event at  $100\text{--}102^\circ\text{C}$  (Hitchcock et al., 1993). Keeping the cation invariant ( $\text{C}_4\text{MI}$ ), however, the replacement of chloride of  $\text{Co}^{\text{II}}\text{Cl}_4$  dianions ( $T_m = 62^\circ\text{C}$ ) (Zhong et al., 2007) by bulky bromide ( $T_m = 45^\circ\text{C}$ ) (Kozlova et al., 2009) and isothiocyanate ( $T_g = -61^\circ\text{C}$ ) (Peppel et al., 2010) steadily stabilizes the liquid state. Notably,  $[\text{C}_2\text{MI}]_2[\text{Co}(\text{NCS})_4]$  ( $T_g = -62^\circ\text{C}$ ) shows a relatively high ionic conductivity ( $4.0 \times 10^{-3} \text{ S cm}^{-1}$  at  $25^\circ\text{C}$ ) and low viscosity (145 cP at  $25^\circ\text{C}$ ) despite the divalency of anions (Peppel et al., 2010). Based on the Pearson's HSAB concept, the softness of the ligand NCS, when compared with halides, may relate to the high fluidity as a consequence of the depressed interionic Coulomb interactions with the hard hydrogen atoms of  $C_n\text{MI}$  cations.

Very recently, Pitula and Mudring reported absorption and luminescent properties of a series of manganese(II)-containing ionic liquids  $[C_n\text{MI}]_2[\text{Mn}^{\text{II}}\text{X}_4]$  (X: Cl, Br) and  $[C_n\text{MI}][\text{Mn}^{\text{II}}(\text{Tf}_2\text{N})_3]$ , though no magnetic data (Pitula & Mudring, 2010).  $[C_n\text{MI}]_2[\text{MnX}_4]$  with a tetrahedral  $\text{Mn}^{\text{II}}$  coordination show a yellow-greenish emission, whereas  $[C_n\text{MI}][\text{Mn}(\text{Tf}_2\text{N})_3]$  with an octahedral  $\text{Mn}^{\text{II}}$  coordination show a reddish emission at RT. The colorations derive mainly from the predominant emission band at around 520 nm for the former and at around 590 nm for the latter, both of which are readily assigned to the intramolecular  ${}^4\text{T}_1(\text{G}) \rightarrow {}^6\text{A}_1$  transition on  $\text{Mn}^{\text{II}}$  ions.

Ionic liquids formed with metal complex anions have been used as green solvents for catalysis. For example,  $[\text{C}_4\text{MI}][\text{Co}^{\text{III}}(\text{CO})_4]$  is active for the catalytic debromination of 2-



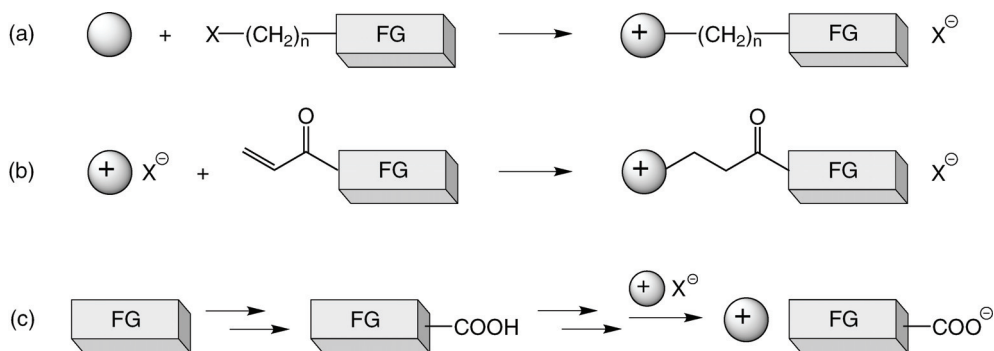
bromoketones in the presence of NaOH (Brown et al., 2001), and  $[\text{C}_4\text{MI}][\text{Cr}^{\text{VI}}\text{ClO}_3]$  and  $[\text{C}_4\text{MI}]_2[\text{Mo}^{\text{VI}}(\text{NCS})_4\text{O}_2]$  are active for the catalytic oxidation of alcohol (Noguera et al., 2005).

### 2.3 Inorganic anions containing rare-earth metals

Only two ionic liquids containing rare-earth metals,  $[\text{P}_{14,6,6,6}]_3[\text{Gd}^{\text{III}}\text{Cl}_6]$  (Del Sesto et al., 2008) and  $[\text{C}_6\text{MI}]_{5-x}[\text{Dy}^{\text{III}}(\text{NCS})_{8-x}(\text{H}_2\text{O})_x]$  ( $x$ : 0–2) (Mallick et al., 2008), have been magnetically-studied, although a series of  $[\text{C}_4\text{MI}]_4[\text{RE}(\text{NCS})_{8-x}(\text{H}_2\text{O})_x]$  (RE: Y, La, Pr, Nd, Sm, Eu, Gd, Tb, Ho, Er, Yb;  $x$ : 1, 2) were prepared and their miscibility and absorption properties were investigated by Nockemann et al. (Nockemann et al., 2006). Magnetic moments of  $[\text{C}_6\text{MI}]_{5-x}[\text{Dy}^{\text{III}}(\text{NCS})_{8-x}(\text{H}_2\text{O})_x]$  were estimated to be  $10.4\text{--}10.6\mu_{\text{B}}$  at  $25^\circ\text{C}$ , which resemble closely that expected for a paramagnetic high-spin on  $\text{Dy}^{\text{III}}$  ions with  $f^9$  electrons ( $10.65\mu_{\text{B}}$ ). In addition,  $[\text{C}_6\text{MI}]_{5-x}[\text{Dy}^{\text{III}}(\text{NCS})_{8-x}(\text{H}_2\text{O})_x]$  show a yellow emission in the liquid state (Mallick et al., 2008). The coloration derives mainly from the predominant emission band at around 575 nm, which is readily assigned to the intramolecular  ${}^4\text{F}_{9/2} \rightarrow {}^6\text{H}_{13/2}$  transition on  $\text{Dy}^{\text{III}}$  ions. The observed monoexponential intensity decay with a lifetime of  $24\text{--}48\ \mu\text{s}$  gives evidence of single  $\text{Dy}^{\text{III}}$  species in these ionic liquids.

### 2.4 Organic and metal complex anions

Davis introduced some complimentary strategies for the synthesis of functional ionic liquids, by the inclusion of functional group (FG) to the cationic skeleton, in his review (Davis, 2004). The called “task-specific ionic liquids” have been synthesized, for example, by *N*-alkylation of alkyl halides covalently linked to FG with appropriate Lewis bases (e.g., imidazole, amine, phosphine, and sulfide; Scheme 2a), accompanied by the anion metathesis to realize ionic liquids. One of other strategies is to use Michael reaction of alkyl vinyl ketones linked to FG with tertiary cations, as in Scheme 2b (Wasserscheid et al., 2003). It is noteworthy that this facile one-pot reaction dispenses with the need for a further anion metathesis step and are free from halide-containing by-product.



Scheme 2. Schematic synthetic routes of functional ionic liquids by (a) *N*-alkylation reaction (Davis, 2004) and (b) Michael addition reaction (Wasserscheid et al., 2003) to form ionic liquids of functional cations, and (c) the addition of acidic group to form ionic liquids of functional anion. A blank sphere represents a Lewis base such as imidazole, amine, phosphine, and sulfide, while a sphere with a plus sign represents the corresponding cation.

Similarly, functional ionic liquids can be realized by the use of anions, in which an acidic group such as carboxyl and sulfonate is covalently linked to the neutral functional molecule. We note that the molecular makeup, namely a neutral moiety linked to an acidic group, reminds us of amino acids, which offered 20 kinds of ionic liquids formed with  $C_2MI$  cation (Fukumoto et al., 2005). The acid form of anions is transformed to the target ionic liquids by combining conventional liquid-forming counter cations as in Scheme 2c. In this approach, the serious obstacle in some cases is the difficulty of the chemical inclusion of the acidic group to the functional molecule. In other words, if the acid form can be realized whatever the synthetic route is used to access, one can anticipate the realization of ionic liquids composed of functional anions with the acidic group. However, such ionic liquids are fraught with drawbacks of their high viscosity, mainly caused by the confined negative charge to the acidic group and the presence of bulky FG.

The  $P_{14,6,6,6}$  salt made by combining  $Cu^{II}Pc(SO_3)_4^{4-}$  (copper phthalocyanine-tetrasulfonate; Scheme 1) anion, reported by Del Sesto and Wilkes in 2005, may be regarded as the first paramagnetic ionic liquid ( $T_g = -41\text{ }^\circ\text{C}$ ) composed of anion with acidic groups (Del Sesto et al., 2005). The highly viscous ionic liquid is anticipated to have an  $S = 1/2$  spin on central  $Cu^{II}$  ions, although there is no magnetic evaluation in the paper. However, this is not the synthesis of the component ions but the proper choice of the ions, since commercially available  $CuPc(SO_3Na)_4$  was utilized as precursor. Our first step was to design and synthesize the component anions with a special functionality and then combine them with proper counter cations to form ionic liquids. Thus, the nascent strategy has been to search for functional molecules that can chemically introduce the acidic group in the facile synthetic route.

In 2007, our own group reported the first metal-free paramagnetic ionic liquids, by the inclusion of a sulfate group to a neutral 2,2,6,6-tetramethyl-1-piperidinyloxy (TEMPO) radical moiety (Scheme 1) (Yoshida et al., 2007c). Whereas the  $C_2MI$  salt is reddish crystalline solid with  $T_m = 57\text{ }^\circ\text{C}$ , the salts with  $n = 4, 6$ , and  $8$  are reddish highly viscous liquids ( $> 400\text{ cP}$  even at  $70\text{ }^\circ\text{C}$ ; see the inset of Figure 4). As mentioned above, the confined

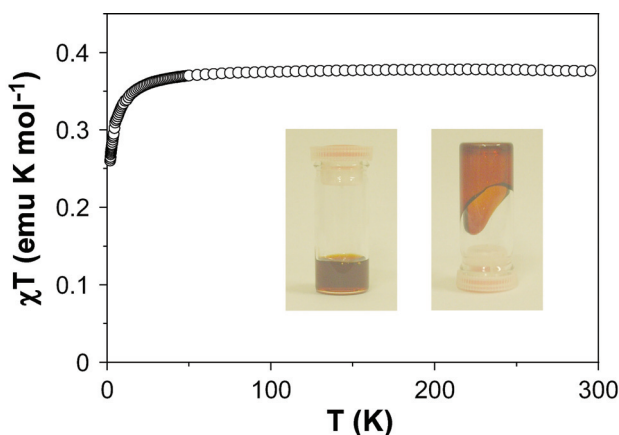
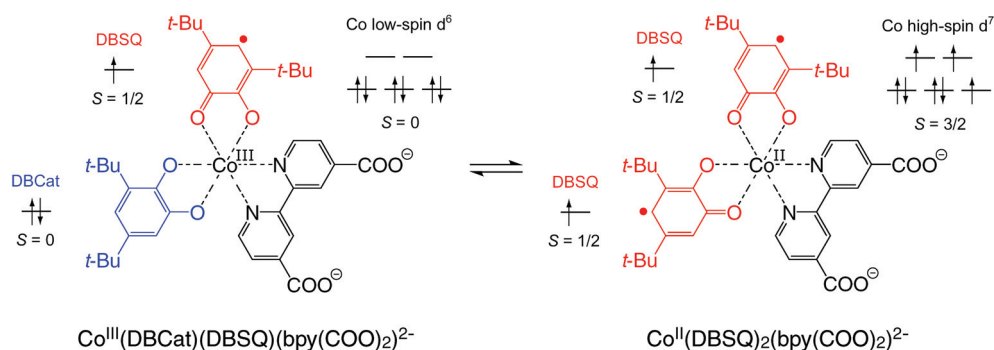


Fig. 4. Temperature dependence of the product of static susceptibility and temperature ( $\chi T$ ) for  $[C_4MI][TEMPO-OSO_3]$  in an applied field of 1 kOe on heating process. The inset is the photographs of  $[C_4MI][TEMPO-OSO_3]$  (Yoshida et al., 2007c).

negative charge on a sulfate group, which leads to the significant interionic Coulomb interactions, would be a factor governing the high viscosity. These ionic liquids show Curie-like behavior in their liquid region. The RT magnetic moments were estimated as values in the range of  $1.61\text{--}1.72\mu_B$  (Figure 4), which resemble closely that expected for a paramagnetic  $S = 1/2$  spin (spin-only value:  $1.73\mu_B$ ) on nitroxyl radical.

Our strategy, that introduces the acidic group to functional molecules to form functional ionic liquids, can be used to access the next stage of ionic liquids, namely the liquids that can modify the physical properties by applying external stimuli, e.g., temperature, pressure, electric field, and light irradiation. The selection criteria for the functional molecules includes that the functionality can work without having interionic interactions and even at high temperature (at least RT), and also that the molecules can introduce the acidic group in the facile synthetic route. We chose to utilize the cobalt bis(dioxolene) complex as FG, which has been known to exhibit the valence tautomerism (VT) by the intramolecular interconvert between low-spin  $\text{Co}^{\text{III}}$  ( $S = 0$ ) system with a radical 3,5-di-*tert*-butyl-1,2-semiquinonate monoanion ( $\text{DBSQ}^{\cdot-}$ ) and a closed-shell 3,5-di-*tert*-butyl-1,2-catechol dianion ( $\text{DBCat}^{2-}$ ) ligands and high-spin  $\text{Co}^{\text{II}}$  ( $S = 3/2$ ) system with two  $\text{DBSQ}^{\cdot-}$  ligands (Scheme 3) (Pierpont, 2001). Such phase equilibrium has potential applicability for molecular devices such as information storage and switches, and could be driven by either temperature change or light irradiation. Considering the fact that the VT behavior has been observed in the diluted solution (Pierpont, 2001), it appears that the intermolecular interaction is not indispensable for the appearance of the equilibrium.

We combined the cobalt bis(dioxolene) unit with 2,2'-bipyridine (bpy) having two carboxylate groups at 4-positions, to realize an ionic liquid showing valence-tautomeric behavior. The dark green liquid  $[\text{P}_{14,6,6,6}]_2[\text{Co}^{\text{III}}(\text{DBSQ})_2(\text{bpy}(\text{COO})_2)]$  is highly viscous ( $> 10^3$  cP) and shows a glass transition at  $-11^\circ\text{C}$  (Yoshida et al., 2009). The ionic conductivity is determined to be  $1.0 \times 10^{-6}$  S  $\text{cm}^{-1}$  at  $27^\circ\text{C}$  and follows the Arrhenius law with an activation energy of 0.625 eV in the whole measured temperature range ( $27\text{--}77^\circ\text{C}$ ). The RT  $\sigma$  value is much lower than that of  $[\text{P}_{14,6,6,6}]\text{Cl}$  ( $8.9 \times 10^{-6}$  S  $\text{cm}^{-1}$  at  $27^\circ\text{C}$ ) apparently due to the bulky dianions.



Scheme 3. Valence tautomeric bistability of cobalt bis(dioxolene) complex (Pierpont, 2001; Yoshida et al., 2009).

Figure 5a shows the electronic absorption spectrum at  $-173^\circ\text{C}$ , which is reminiscent of that of crystalline solid  $\text{Co}^{\text{III}}(\text{DBCat})(\text{DBSQ})(\text{bpy})$  (Pierpont, 2001). At low temperatures, an absorption band characteristic of a ligand to metal charge transfer (LMCT) from DBCat ligand to central cobalt was observed at around 610 nm. As the temperature increases from 7

to 47 °C, the intensity of the 610 nm band apparently decreases whereas a band at around 740 nm increases in intensity (Figure 5b). Since the 740 nm band is associated with a metal to ligand charge transfer (MLCT) from the central cobalt to DBSQ ligand, this spectral change indicates that the present salt exhibits a VT equilibrium in the liquid state at around RT. The presence of isosbestic point (ca. 670 nm) would confirm two different species in equilibrium. As expected, a low-energy band (ca. 2400 nm), which is ascribed to mixed valence intervalence charge transfer from the DBCat to DBSQ ligands (ligand-to-ligand charge transfer; LLCT), gradually decreases in intensity with increasing temperature (Figure 5c). The  $\mu_{\text{eff}}$  value at 2 K ( $1.40\mu_{\text{B}}$ ) falls into the range of values expected for the  $S = 1/2$  unpaired spin (spin-only value:  $1.73\mu_{\text{B}}$ ). With increasing temperature, it exhibits a gradual increase up to ca. 10 °C through the glass transition. As seen in Figure 6, there is an upturn of  $\mu_{\text{eff}}$  above 10 °C, which then begins to approach the value expected for an uncorrelated three-spin system with  $S = 1/2, 1/2$ , and  $3/2$  (spin-only value:  $4.58\mu_{\text{B}}$ ) without magnetic saturation. Such temperature dependency is rather different from that of polycrystalline VT complex  $\text{Co}(\text{DBSQ})_2(\text{bpy})$  (Pierpont, 2001), but reminds us of that of the colloidal suspension of nanoparticles composed of VT coordination polymer  $\text{Co}^{\text{II}}(\text{DBSQ})_2(\text{bix})$ , where bix is 1,4-bis(imidazol-1-ylmethyl)benzene (Imaz et al., 2008). It should be noted that the observed VT behavior has little impact on the ion diffusivity, since no anomaly was observed for ion conduction in this temperature region.

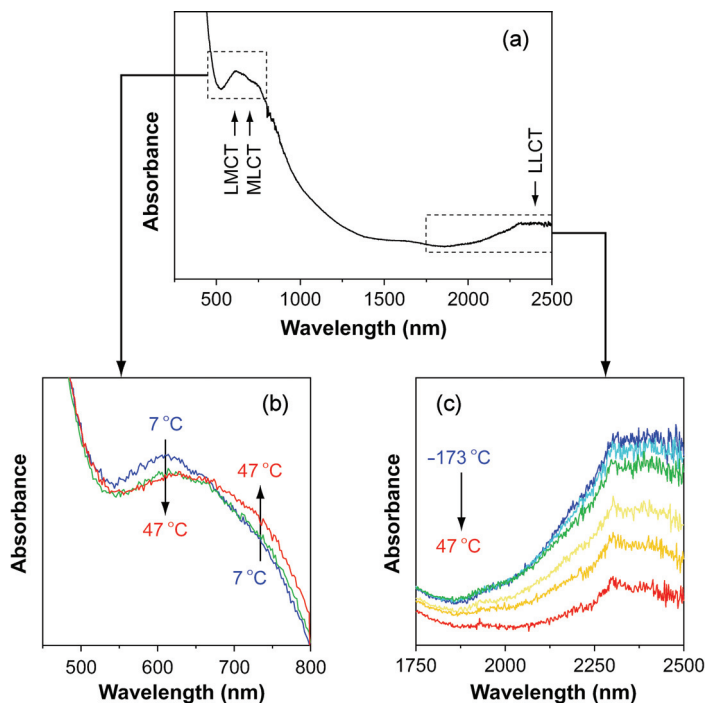


Fig. 5. (a) Electronic absorption spectrum of  $[\text{P}_{14,6,6,6}]_2[\text{Co}(\text{DBSQ})_2(\text{bpy}(\text{COO})_2)]$  at -173 °C. Temperature dependence of the spectra (b) in the high-energy region (7, 27, 47 °C) and (c) in the low-energy region (-173, -73, -13, 7, 27, 47 °C) (Yoshida et al., 2009).

The use of chelate complex anions is preferred due to a huge variety of chemically tunable organic ligands, which allow the fine tuning of ligand  $\pi$  orbital levels and thus charge transfer between the central metal and ligands. The modification of electronic structures exerts a drastic effect on physical properties such as magnetic (e.g., spin and charge states, and spin polarization) and emission (e.g., lifetime, emission energy, and quantum efficiency) properties. We would note that the “bidentate ligand ionic liquid”  $[P_{14,6,6,6}]_2[bpy(COO)_2]$  is a useful tool to synthesize ionic liquids containing chelate complex anions, in a combinatorial fashion, especially  $Fe^{II}$ ,  $Mn^{II}$ ,  $Ru^{II}$ , and  $Ir^{III}$  metal complexes. Such functional ionic liquids can be envisaged to become a grown area because of the enormous accumulated knowledge of complex chemistry from both fundamental and practical aspects.

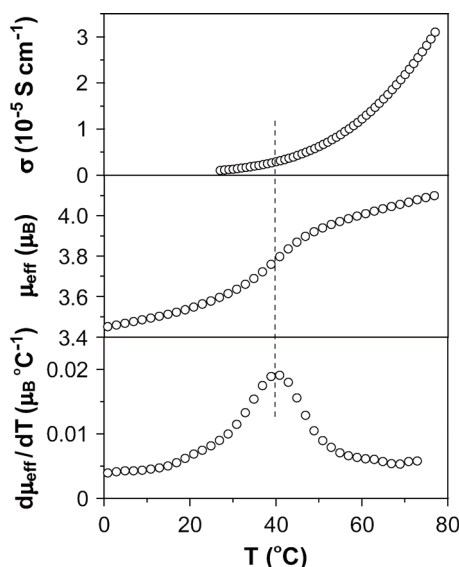


Fig. 6. Temperature dependence of ionic conductivity ( $\sigma$ ), effective magnetic moment ( $\mu_{\text{eff}}$ ), and its derivative  $d\mu_{\text{eff}}/dT$  of  $[P_{14,6,6,6}]_2[Co(DBSQ)_2(bpy(COO)_2)]$ . A vertical dotted line indicates the equilibrium temperature (Yoshida et al., 2009).

### 3. Magneto-active cations

Metal-free paramagnetic ionic liquids, in which a chiral pyrrolidin-1-yloxy (PROXYL) radical moiety is included in the component cation (**2**; Scheme 1), were reported by Tamura and his coworkers in 2009 (Uchida et al., 2009). It is apparent that this approach falls into the category as in Scheme 2a. The RT magnetic moments were estimated to be  $1.69\text{--}1.75\mu_B$  as expected from a paramagnetic  $S = 1/2$  spin on nitroxyl radical. Notably, the  $Tf_2N$  salt is more fluidic ( $7.2 \times 10^{-4} \text{ S cm}^{-1}$  and 84 cP at 70 °C) than  $[C_nMI][TEMPO\text{-}OSO_3]$  ( $2.0 \times 10^{-4} \text{ S cm}^{-1}$  and 568 cP at 70 °C for  $n = 4$ ), presumably associated with the well-delocalized charge on the  $Tf_2N$  anions.

In a more recent study, Inagaki and Mochida reported a series of paramagnetic ionic liquids by making use of a new breed of component cations (**3**; Scheme 1) (Inagaki & Mochida, 2010). In the ferrocenium cations, negatively-charged cyclopentadienyl rings would inhibit

the attractive Coulomb interactions between the positively-charged central iron and counter anions. Moreover, it seems that the thermal motion of the substituents as well as the low symmetry in the cations stabilizes the liquid state, since the pristine ferrocenium ( $R_1 = R_2 = H$ ) and methyl-substituted ferrocenium ( $R_1 = Me, R_2 = H$  or  $R_1 = R_2 = Me$ ) cations give salts with  $T_m$  higher than 100 °C. Among the ferrocenium-based ionic liquids, the salt combining **3a** with  $Tf_2N$  anion ( $T_m = 24.5$  °C) is highly fluidic (26.6 cP at 25 °C). The RT magnetic moments of the salts combining **3b** and **3d** with  $Tf_2N$  were estimated to be  $2.33\mu_B$  and  $2.17\mu_B$ , respectively, which lie in the range of typical ferrocenium salts (Kahn, 1993).

#### 4. Conclusion

In this review, the known range of paramagnetic ionic liquids has been discussed concerning the choice and chemical synthesis of magneto-active ions. The selection of small-sized and monovalence  $C_2MI$  cation and  $Fe^{III}Cl_4$  anion gives the most fluidic paramagnetic  $[C_2MI][Fe^{III}Cl_4]$ . Metal complex anion containing soft pseudo-halides gives relatively fluidic ionic liquids  $[C_nMI]_2[Co^{II}(NCS)_4]$  despite the divalency of the anion. By the chemical inclusion of acidic group to the neutral magneto-active molecules, metal-free paramagnetic ionic liquids  $[C_nMI][TEMPO-OSO_3]$  and a valence-tautomeric ionic liquid  $[P_{14,6,6,6}]_2[Co^{II}(DBSQ)_2(bpy(COO)_2)]$  have been realized. Imidazolium cation covalently linked to PROXYL radical moiety, also gives a new type of metal-free paramagnetic ionic liquids.

Ionic liquids whose functionality is inherited from the component ions will increasingly come to be attracting attentions, because of a vast number of the potential functional molecules that can introduce the acidic group and develop their functionality without having interionic interactions. The development of smart ionic liquids whose external-field-responsivity extends far beyond that of existing ones has also been an active area of research are also anticipated to be strong growth in the field of ionic liquids. Future works are also to develop a special functionality for each ion and then combine them to realize ionic liquids having cooperative functionalities.

#### 5. References

- Armand, M.; Endres, F.; MacFarlane, D. R.; Ohno, H. & Scrosati, B. (2009). Ionic-liquid materials for the electrochemical challenges of the future. *Nat. Mat.*, 8, 621–629
- Bonhôte, P.; Dias, A. -P.; Armand, M.; Papageorgiou, N.; Kalyanasundaram, K. & Grätzel, M. (1996). Hydrophobic, highly conductive ambient-temperature molten salts. *Inorg. Chem.*, 35, 1168–1178
- Borra, E. F.; Seddiki, O.; Angel, R.; Eisenstein, D.; Hickson, P.; Seddon, K. R. & Worden, S. P. (2007). Deposition of metal films on an ionic liquid as a basis for a lunar telescope. *Nature*, 447, 979–981
- Bourlinos, A. B.; Herrera, R.; Chalkias, N.; Jiang, D. D.; Zhang, Q.; Archer, L. A. & Giannelis, E. P. (2005). Surface-functionalized nanoparticles with liquid-like behavior. *Adv. Mater.*, 17, 234–237
- Brown, R. J. C.; Dyson, P. J.; Ellis, D. J. & Welton, T. (2001). 1-Butyl-3-methylimidazolium cobalt tetracarbonyl  $[bmim][Co(CO)_4]$ : a catalytically active organometallic ionic liquid. *Chem. Commun.*, 1862–1863

- Buzzeo, M. C.; Evans, R. G. & Compton, R. G. (2004). Non-haloaluminate room-temperature ionic liquids in electrochemistry –a review. *ChemPhysChem*, 5, 1106–1120
- Cooper, E. I. & O'Sullivan, E. J. M. (1992). New, stable, ambient-temperature molten salts. *Proc. -Electrochem. Soc.*, 92-16, 386–396
- Davis, Jr., J. H. (2004). Task-specific ionic liquids. *Chem. Lett.*, 33, 1072–1077
- Del Sesto, R. E.; Corley, C.; Robertson, A. & Wilkes, J. S. (2005). Tetraalkylphosphonium-based ionic liquids. *J. Organomet. Chem.*, 690, 2536–2542
- Del Sesto, R. E.; McCleskey, T. M.; Burrell, A. K.; Baker, G. A.; Thompson, J. D.; Scott, B. L.; Wilkes, J. S. & Williams, P. (2008). Structure and magnetic behavior of transition metal based ionic liquids. *Chem. Commun.*, 447–449
- Dupont, J.; de Souza, R. F. & Suarez, P. A. Z. (2002). Ionic liquid (molten salt) phase organometallic catalysis. *Chem. Rev.*, 102, 3667–3692
- Fei, Z.; Geldbach, T. J.; Zhao, D. & Dyson, P. J. (2006). From dysfunction to bis-function: on the design and applications of functionalised ionic liquids. *Chem. Eur. J.*, 12, 2122–2130
- Fukaya, Y.; Sugimoto, A. & Ohno, H. (2006). Superior solubility of polysaccharides in low viscosity, polar, and halogen-free 1,3-dialkylimidazolium formates. *Biomacromolecules*, 7, 3295–3297
- Fukaya, Y.; Hayashi, K.; Wada, M. & Ohno, H. (2008). Cellulose dissolution with polar ionic liquids under mild conditions: required factors for anions. *Green Chem.*, 10, 44–46
- Fukumoto, K.; Yoshizawa, M. & Ohno, H. (2005). Room temperature ionic liquids from 20 natural amino acids. *J. Am. Chem. Soc.*, 127, 2398–2399
- Fuller, J.; Carlin, R. T. & Osteryoung, R. A. (1997). The room temperature ionic liquid 1-ethyl-3-methylimidazolium tetrafluoroborate: electrochemical couples and physical properties. *J. Electrochem. Soc.*, 144, 3881–3886
- Gabriel, S. & Weiner, J. (1888). Ueber einige Abkömmlinge des Propylamins. *Ber.*, 21, 2669–2679
- Guerrero-Sanchez, C.; Lara-Ceniceros, T.; Jimenez-Regalado, E.; Raşa, M. & Schubert, U. S. (2007). Magnetorheological fluids based on ionic liquids. *Adv. Mater.*, 19, 1740–1747
- Hitchcock, P. B.; Seddon, K. R. & Welton, T. (1993). Hydrogen-bond acceptor abilities of tetrachlorometalate(II) complexes in ionic liquids. *J. Chem. Soc., Dalton Trans.*, 2639–2643
- Holbrey, J. D.; Reichert, W. M.; Swatloski, R. P.; Broker, G. A.; Pitner, W. R.; Seddon, K. R. & Rogers, R. D. (2002). Efficient, halide free synthesis of new, low cost ionic liquids: 1,3-dialkylimidazolium salts containing methyl- and ethyl-sulfate anions. *Green Chem.*, 4, 407–413
- Hough, W. L. & Rogers, R. D. (2007). Ionic liquids then and now: from solvents to materials to active pharmaceutical ingredients. *Bull. Chem. Soc. Jpn.*, 80, 2262–2269
- Imaz, I.; Maspocho, D.; Rodríguez-Blanco, C.; Pérez-Falcón, J. M.; Campo, J. & Ruiz-Molina, D. (2008). Valence-tautomeric metal-organic nanoparticles. *Angew. Chem. Int. Ed.*, 47, 1857–1860
- Inagaki, T. & Mochida, T. (2010). Metallocenium ionic liquids. *Chem. Lett.*, 39, 572–573
- Kahn, O. (1993). *Molecular Magnetism*, Wiley-VCH, New York
- Kawano, R.; Matsui, H.; Matsuyama, C.; Sato, A.; Susan, M. A. B. H.; Tanabe, N. & Watanabe, M. (2004). High performance dye-sensitized solar cells using ionic liquids as their electrolytes. *J. Photochem. Photobiol. A*, 164, 87–92

- Kozlova, S. A.; Verevkin, S. P.; Heintz, A.; Peppel, T. & Köckerling, M. (2009). Paramagnetic ionic liquid 1-butyl-3-methylimidazolium tetrabromidocobaltate(II): activity coefficients at infinite dilution of organic solutes and crystal structure. *J. Chem. Eng. Data*, 54, 1524–1528
- Kuang, D.; Wang, P.; Ito, S.; Zakeeruddin, S. M. & Grätzel, M. (2006). Stable mesoscopic dye-sensitized solar cells based on tetracyanoborate ionic liquid electrolyte. *J. Am. Chem. Soc.*, 128, 7732–7733
- Li, M.; De Rooy, S. L.; Bwambok, D. K.; El-Zahab, B.; DiTusa, J. F. & Warner, I. M. (2009). Magnetic chiral ionic liquids derived from amino acids. *Chem. Commun.*, 6922–6924
- MacFarlane, D. R.; Golding, J.; Forsyth, S.; Forsyth, M. & Deacon, G. B. (2001). Low viscosity ionic liquids based on organic salts of the dicyanamide anion. *Chem. Commun.*, 1430–1431
- Mallick, B.; Balke, B.; Felser, C. & Mudring, A.-V. (2008). Dysprosium room-temperature ionic liquids with strong luminescence and response to magnetic fields. *Angew. Chem. Int. Ed.*, 47, 7635–7638
- Matsumoto, H.; Sakaebe, H.; Tatsumi, K.; Kikuta, M.; Ishiko, E. & Kono, M. (2006). Fast cycling of Li/LiCoO<sub>2</sub> cell with low-viscosity ionic liquids based on bis(fluorosulfonyl)imide [FSI]<sup>-</sup>. *J. Power Sources*, 160, 1308–1313
- Nockemann, P.; Thijs, B.; Postelmans, N.; Van Hecke, K.; Van Meervelt, L. & Binnemans, K. (2006). Anionic rare-earth thiocyanate complexes as building blocks for low-melting metal-containing ionic liquids. *J. Am. Chem. Soc.*, 128, 13658–13659
- Noguera, G.; Mostany, J.; Agrifoglio, G. & Dorta, R. (2005). Room temperature liquid salts of Cr and Mo as self-supported oxidants. *Adv. Synth. Catal.*, 347, 231–234
- Ono, S.; Miwa, K.; Seki, S. & Takeya, J. (2009). A comparative study of organic single-crystal transistors gated with various ionic-liquid electrolytes. *Appl. Phys. Lett.*, 94, 063301/1–3
- Peppel, T.; Köckerling, M.; Geppert-Rybczyńska, M.; Ralys, R. V.; Lehmann, J. K.; Verevkin, S. P. & Heintz, A. (2010). Low-viscosity paramagnetic ionic liquids with doubly charged [Co(NCS)<sub>4</sub>]<sup>2-</sup> ions. *Angew. Chem. Int. Ed.*, in press
- Pierpont, C. G. (2001). Studies on charge distribution and valence tautomerism in transition metal complexes of catecholate and semiquinonate ligands. *Coord. Chem. Rev.*, 216–217, 99–125
- Pitula, S. & Mudring, A.-V. (2010). Synthesis, structure, and physico-optical properties of manganate(II)-based ionic liquids. *Chem. Eur. J.*, 16, 3355–3365
- Sato, T.; Masuda, G. & Takagi, K. (2004). Electrochemical properties of novel ionic liquids for electric double layer capacitor applications. *Electrochim. Acta*, 49, 3603–3611
- Singh, R. P.; Verma, R. D.; Meshri, D. T. & Shreeve, J. M. (2006). Energetic nitrogen-rich salts and ionic liquids. *Angew. Chem. Int. Ed.*, 45, 3584–3601
- Smiglak, M.; Metlen, A. & Rogers, R. D. (2007). The second evolution of ionic liquids: from solvents and separations to advanced materials –energetic examples from the ionic liquid cookbook. *Acc. Chem. Res.*, 40, 1182–1192
- Suarez, P. A. Z.; Einloft, S.; Dullius, J. E. L.; de Souza, R. F. & Dupont, J. (1998). Synthesis and physical-chemical properties of ionic liquids based on 1-n-butyl-3-methylimidazolium cation. *J. Chim. Phys.*, 95, 1626–1639



- Uchida, Y.; Oki, S.; Tamura, R.; Sakaguchi, T.; Suzuki, K.; Ishibashi, K. & Yamauchi, J. (2009). Electric, electrochemical and magnetic properties of novel ionic liquid nitroxides, and their use as an EPR spin probe. *J. Mater. Chem.*, 19, 6877–6881
- Yoshida, Y.; Muroi, K.; Otsuka, A.; Saito, G.; Takahashi, M. & Yoko, T. (2004). 1-Ethyl-3-methylimidazolium based ionic liquids containing cyano groups: synthesis, characterization and crystal structure. *Inorg. Chem.*, 43, 1458–1462
- Yoshida, Y.; Fujii, J.; Muroi, K.; Otsuka, A.; Saito, G.; Takahashi, M. & Yoko, T. (2005a). Highly conducting ionic liquids based on 1-ethyl-3-methylimidazolium cation. *Synth. Met.*, 153, 421–424
- Yoshida, Y.; Otsuka, A.; Saito, G.; Natsume, S.; Nishibori, E.; Takata, M.; Sakata, M.; Takahashi, M. & Yoko, T. (2005b). Conducting and magnetic properties of 1-ethyl-3-methylimidazolium (EMI) salts containing paramagnetic irons: liquid  $[\text{EMI}][\text{Fe}^{\text{III}}\text{Cl}_4]$  and solid  $[\text{EMI}]_2[\text{Fe}^{\text{III}}\text{Cl}_4]$ . *Bull. Chem. Soc. Jpn.*, 78, 1921–1928
- Yoshida, Y. & Saito, G. (2006). Influence of structural variations in 1-alkyl-3-methylimidazolium cation and tetrahalogenoferrate(III) anion on physical properties of the paramagnetic ionic liquids. *J. Mater. Chem.*, 16, 1254–1262
- Yoshida, Y.; Baba, O. & Saito, G. (2007a). Ionic liquids based on dicyanamide anion: influence of structural variations in cationic structures on ionic conductivity. *J. Phys. Chem. B*, 111, 4742–4749
- Yoshida, Y.; Baba, O.; Larriba, C. & Saito, G. (2007b). Imidazolium-based ionic liquids formed with dicyanamide anion: influence of cationic structure on ionic conductivity. *J. Phys. Chem. B*, 111, 12204–12210
- Yoshida, Y.; Tanaka, H. & Saito, G. (2007c). Organic paramagnetic ionic liquids based on anion containing 2,2,6,6-tetramethyl-1-piperidinyloxy radical moiety. *Chem. Lett.*, 36, 1096–1097
- Yoshida, Y.; Tanaka, H.; Saito, G.; Ouahab, L.; Yoshida, H. & Sato, N. (2009). Valence-tautomeric ionic liquid composed of cobalt bis(dioxolene) complex dianion. *Inorg. Chem.*, 48, 9989–9991
- Yoshida, Y. & Saito, G. (2010). Design of functional ionic liquids using magneto- and luminescent-active anions. *Phys. Chem. Chem. Phys.*, 12, 1675–1684
- Walden, P. (1914). Ueber die Molekulargrösse und elektrische Leitfähigkeit einiger geschmolzenen Salze. *Bull. Acad. Imper. Sci. (St. Petersburg)*, 8, 405–422
- Wang, P.; Zakeeruddin, S. M.; Moser, J.-E. & Grätzel, M. (2003). A new ionic liquid electrolyte enhances the conversion efficiency of dye-sensitized solar cells. *J. Phys. Chem. B*, 107, 13280–13285
- Wang, P.; Wenger, B.; Humphry-Baker, R.; Moser, J.-E.; Teuscher, J.; Kántlehner, W.; Mezger, J.; Stoyanov, E. V.; Zakeeruddin, S. M. & Grätzel, M. (2005). Charge separation and efficient light energy conversion in sensitized mesoscopic solar cells based on binary ionic liquids. *J. Am. Chem. Soc.*, 127, 6850–6856
- Wasserscheid, P. & Keim, W. (2000). Ionic liquids –new “solutions” for transition metal catalysis. *Angew Chem. Int. Ed.*, 39, 3772–3789
- Wasserscheid, P.; Driepen-Hölscher, B.; van Hal, R.; Steffens, H. C. & Zimmermann, J. (2003). New, functionalized ionic liquids from Michael-type reactions –a chance for combinatorial ionic liquid development. *Chem. Commun.*, 2038–2039
- Wilkes, J. S. & Zaworotko, M. J. (1992). Air and water stable 1-ethyl-3-methylimidazolium based ionic liquids. *J. Chem. Soc., Chem. Commun.*, 965–966

- Zein El Abedin, S.; Moustafa, E. M.; Hempelmann, R.; Natter, H. & Endres, F. (2005). Additive free electrodeposition of nanocrystalline aluminium in a water and air stable ionic liquid. *Electrochem. Commun.*, 7, 1111-1116
- Zhong, C.; Sasaki, T.; Jimbo-Kobayashi, A.; Fujiwara, E.; Kobayashi, A.; Tada, M. & Iwasawa, Y. (2007). Syntheses, structures, and properties of a series of metal ion-containing dialkylimidazolium ionic liquids. *Bull. Chem. Soc. Jpn.*, 80, 2365-2374